Guidelines for the use of flow cytometry and cell sorting in immunological studies (second edition)

Andrea Cossarizza*[1], Hyun-Dong Chang*[2], Andreas Radbruch*[2], Andreas Acs[3], Dieter Adam[4],
Sabine Adam-Klages[13], William W. Agace[5,6], Nima Aghaeepour[323], Mübeccel Akdis[7],
Matthieu Allez[8], Larissa Nogueira Almeida[9], Giorgia Alvisi[10], Graham Anderson[11],
Immanuel Andrä[12], Francesco Annunziato[70], Achille Anselmo[65], Petra Bacher[4,14],
Cosima T. Baldari[15], Sudipto Bari[319,320], Vincenzo Barnaba[16,17,18], Joana Barros-Martins[19],
Luca Battistini[20], Wolfgang Bauer[21], Sabine Baumgart[2], Nicole Baumgarth[22], Dirk Baumjohann[23],
Bianka Baying[24], Mary Bebawy[25], Burkhard Becher[135,268], Wolfgang Beisker[27], Vladimir Benes[24],
Rudi Beyaert[29], Alfonso Blanco[30], Dominic A. Boardman[31,32], Christian Bogdan[33,34],
Jessica G. Borger[35], Giovanna Borsellino[36], Philip E. Boulais[37,38], Jolene A. Bradford[39],
Dirk Brenner[40,41,324], Ryan R. Brinkman[43,337], Anna E. S. Brooks[44], Dirk H. Busch[12,45,46],
Martin Büscher[47], Timothy P. Bushnell[48], Federica Calzetti[49], Garth Cameron[50],
Ilenia Cammarata[16], Xuetao Cao[51], Susanna L. Cardell[52], Stefano Casola[53], Marco A. Cassatella[49],
Andrea Cavani[54], Antonio Celada[55], Lucienne Chatenoud[56], Pratip K. Chattopadhyay[57],
Sue Chow[58], Eleni Christakou[59,60], Luka Čičin-Šain[61], Mario Clerici[62,63,64], Federico S. Colombo[65],
Laura Cook[32,66], Anne Cooke[67], Andrea M. Cooper[68], Alexandra J. Corbett[50], Antonio Cosma[69],
Lorenzo Cosmi[70], Pierre G. Coulie[71], Ana Cumano[72], Ljiljana Cvetkovic[73], Van Duc Dang[2],
Chantip Dang-Heine[74], Martin S. Davey[75,332], Derek Davies[254], Sara De Biasi[76], Genny Del Zotto[77],
Gelo Victoriano Dela Cruz[78], Michael Delacher[79,330], Silvia Della Bella[28], Paolo Dellabona[80],
Günnur Deniz[81], Mark Dessing[82], James P. Di Santo[263,264], Andreas Diefenbach[2,83,84],
Francesco Dieli[85], Andreas Dolf[86], Thomas Dörner[2,87], Regine J. Dress[100], Diana Dudziak[333],
Michael Dustin[88], Charles-Antoine Dutertre[89,100], Friederike Ebner[90], Sidonia B. G. Eckle[50],
Matthias Edinger[79,91], Pascale Eede[92], Götz R.A. Ehrhardt[93], Marcus Eich[94], Pablo Engel[95],
Britta Engelhardt[96], Anna Erdei[97], Charlotte Esser[98], Bart Everts[99], Maximilien Evrard[100],
Christine S. Falk[101], Todd A. Fehniger[102], Mar Felipo-Benavent[103], Helen Ferry[104],
Markus Feuerer[79,330], Andrew Filby[105], Kata Filkor[106], Simon Fillatreau[107], Marie Follo[108,109],
Irmgard Förster[110], John Foster[111], Gemma A. Foulds[112], Britta Frehse[9], Paul S. Frenette[37,38,113],
Stefan Frischbutter[2,114], Wolfgang Fritzsche[115], David W. Galbraith[116,117], Anastasia Gangaev[118],
Natalio Garbi[119], Brice Gaudilliere[120], Ricardo T. Gazzinelli[121,122], Jens Geginat[123],
Wilhelm Gerner[124,125], Nicholas A. Gherardin[50], Kamran Ghoreschi[126], Lara Gibellini[76],
Florent Ginhoux[100,127,331], Keisuke Goda[26,128,129], Dale I. Godfrey[50], Christoph Goettlinger[130],
Jose M. González-Navajas[131,132], Carl S. Goodyear[209], Andrea Gori[133], Jane L. Grogan[134],
Daryl Grummitt[111], Andreas Grützkau[2], Claudia Haftmann[135], Jonas Hahn[136],
Hamida Hammad[137], Günter Hämmerling[138], Leo Hansmann[84,139,140], Goran Hansson[141],
Christopher M. Harpur[142], Susanne Hartmann[90], Andrea Hauser[91], Anja E. Hauser[2,143,144],
David L. Haviland[145], David Hedley[58], Daniela C. Hernández[2,146], Guadalupe Herrera[147],

Correspondence: Prof. Andrea Cossarizza and Dr. Hyun-Dong Chang
e-mail: andrea.cossarizza@unimore.it; chang@drfz.de

*joint first author

Martin Herrmann[136], Christoph Hess[148,149], Thomas Höfer[150], Petra Hoffmann[79,91],
Kristin Hogquist[151], Tristan Holland[119], Thomas Höllt[322,328], Rikard Holmdahl[152],
Pleun Hombrink[250,285], Jessica P. Houston[153], Bimba F. Hoyer[154], Bo Huang[156],
Fang-Ping Huang[155], Johanna E. Huber[23], Jochen Huehn[157], Michael Hundemer[158],
Christopher A. Hunter[159], William Y. K. Hwang[318,320,321], Anna Iannone[160], Florian Ingelfinger[135],
Sabine M Ivison[31,32], Hans-Martin Jäck[73], Peter K. Jani[2,161], Beatriz Jávega[162], Stipan Jonjic[163],
Toralf Kaiser[2], Tomas Kalina[164], Thomas Kamradt[165], Stefan H. E. Kaufmann[161],
Baerbel Keller[166,167], Steven L. C. Ketelaars[118], Ahad Khalilnezhad[100,168], Srijit Khan[93],
Jan Kisielow[169], Paul Klenerman[104], Jasmin Knopf[136], Hui-Fern Koay[50], Katja Kobow[170],
Jay K. Kolls[171], Wan Ting Kong[100], Manfred Kopf[169], Thomas Korn[172], Katharina Kriegsmann[158],
Hendy Kristyanto[173], Thomas Kroneis[174], Andreas Krueger[175], Jenny Kühne[101], Christian Kukat[176],
Désirée Kunkel[177,178], Heike Kunze-Schumacher[175], Tomohiro Kurosaki[179], Christian Kurts[119],
Pia Kvistborg[118], Immanuel Kwok[100,180], Jonathan Landry[24], Olivier Lantz[181], Paola Lanuti[182],
Francesca LaRosa[62,64], Agnès Lehuen[183], Salomé LeibundGut-Landmann[184], Michael D. Leipold[185],
Leslie Y.T. Leung[93], Megan K. Levings[31,32,186], Andreia C. Lino[2,87], Francesco Liotta[70],
Virginia Litwin[187], Yanling Liu[93], Hans-Gustaf Ljunggren[213], Michael Lohoff[188],
Giovanna Lombardi[189], Lilly Lopez[190], Miguel López-Botet[191], Amy E. Lovett-Racke[192],
Erik Lubberts[193], Herve Luche[194], Burkhard Ludewig[195], Enrico Lugli[10,65], Sebastian Lunemann[196],
Holden T. Maecker[197], Laura Maggi[70], Orla Maguire[198], Florian Mair[199], Kerstin H. Mair[124,125],
Alberto Mantovani[200,201], Rudolf A. Manz[9], Aaron J. Marshall[202], Alicia Martínez-Romero[203],
Glòria Martrus[196], Ivana Marventano[62,64], Wlodzimierz Maslinski[204], Giuseppe Matarese[205],
Anna Vittoria Mattioli[76,336], Christian Maueröder[206,207], Alessio Mazzoni[70], James McCluskey[50],
Mairi McGrath[2], Helen M. McGuire[208], Iain B. McInnes[209], Henrik E. Mei[2], Fritz Melchers[2,161],
Susanne Melzer[210], Dirk Mielenz[73], Stephen D. Miller[211], Kingston H.G. Mills[212],
Hans Minderman[198], Jenny Mjösberg[213,214], Jonni Moore[215], Barry Moran[212], Lorenzo Moretta[216],
Tim R. Mosmann[239], Susann Müller[217], Gabriele Multhoff[218,219], Luis Enrique Muñoz[136],
Christian Münz[135,268], Toshinori Nakayama[220], Milena Nasi[76], Katrin Neumann[221],
Lai Guan Ng[100,168,180,222,223], Antonia Niedobitek[2], Sussan Nourshargh[224], Gabriel Núñez[225],
José-Enrique O'Connor[162], Aaron Ochel[221], Anna Oja[285], Diana Ordonez[226], Alberto Orfao[227],
Eva Orlowski-Oliver[228], Wenjun Ouyang[229], Annette Oxenius[230], Raghavendra Palankar[231],
Isabel Panse[2], Kovit Pattanapanyasat[232], Malte Paulsen[226], Dinko Pavlinic[24], Livius Penter[140],
Pärt Peterson[233], Christian Peth[47], Jordi Petriz[253], Federica Piancone[62,64], Winfried F. Pickl[234],
Silvia Piconese[16,18], Marcello Pinti[235], A. Graham Pockley[112,236],
Malgorzata Justyna Podolska[136,237], Zhiyong Poon[318], Katharina Pracht[73], Immo Prinz[19],
Carlo E. M. Pucillo[238], Sally A. Quataert[239], Linda Quatrini[216], Kylie M. Quinn[240,241],
Helena Radbruch[92], Tim R. D. J. Radstake[242], Susann Rahmig[243], Hans-Peter Rahn[245],
Bartek Rajwa[246], Gevitha Ravichandran[221], Yotam Raz[247], Jonathan A. Rebhahn[239],
Diether Recktenwald[248], Dorothea Reimer[73], Caetano Reis e Sousa[249],
Ester B.M. Remmerswaal[250,251], Lisa Richter[252], Laura G. Rico[253], Andy Riddell[254],
Aja M. Rieger[255], J. Paul Robinson[256], Chiara Romagnani[2,146], Anna Rubartelli[257],
Jürgen Ruland[258], Armin Saalmüller[124], Yvan Saeys[325,326], Takashi Saito[259], Shimon Sakaguchi[179],
Francisco Sala-de-Oyanguren[260], Yvonne Samstag[261], Sharon Sanderson[262], Inga Sandrock[19],
Angela Santoni[265], Ramon Bellmàs Sanz[101], Marina Saresella[62,64], Catherine Sautes-Fridman[266],
Birgit Sawitzki[267], Linda Schadt[135,268], Alexander Scheffold[4], Hans U. Scherer[173],
Matthias Schiemann[12], Frank A. Schildberg[269], Esther Schimisky[270], Andreas Schlitzer[271],
Josephine Schlosser[90], Stephan Schmid[272], Steffen Schmitt[273], Kilian Schober[12],
Daniel Schraivogel[274], Wolfgang Schuh[73], Thomas Schüler[275], Reiner Schulte[276],

Axel Ronald Schulz[2], Sebastian R. Schulz[73], Cristiano Scottá[189], Daniel Scott-Algara[277], David P. Sester[278], T. Vincent Shankey[279], Bruno Silva-Santos[280], Anna Katharina Simon[88], Katarzyna M. Sitnik[61], Silvano Sozzani[281], Daniel E. Speiser[282], Josef Spidlen[42], Anders Stahlberg[283], Alan M. Stall[284], Natalie Stanley[323], Regina Stark[250,285], Christina Stehle[2,146], Tobit Steinmetz[73], Hannes Stockinger[286], Yousuke Takahama[287], Kiyoshi Takeda[179], Leonard Tan[100,168], Attila Tárnok[288,289,329], Gisa Tiegs[221], Gergely Toldi[106], Julia Tornack[2,290], Elisabetta Traggiai[291], Mohamed Trebak[292], Timothy I.M. Tree[59,60], Joe Trotter[284], John Trowsdale[67], Maria Tsoumakidou[293], Henning Ulrich[294], Sophia Urbanczyk[73], Willem van de Veen[7,295], Maries van den Broek[135,268], Edwin van der Pol[296], Sofie Van Gassen[325,326], Gert Van Isterdael[297], René A.W. van Lier[285], Marc Veldhoen[280], Salvador Vento-Asturias[119], Paulo Vieira[72], David Voehringer[298], Hans-Dieter Volk[299], Anouk von Borstel[75,332], Konrad von Volkmann[300], Ari Waisman[301], Rachael V. Walker[302], Paul K. Wallace[303], Sa A. Wang[305], Xin M. Wang[304], Michael D. Ward[39], Kirsten A Ward-Hartstonge[31], Klaus Warnatz[166,167], Gary Warnes[306], Sarah Warth[178], Claudia Waskow[243,244], James V. Watson[307], Carsten Watzl[308], Leonie Wegener[47], Thomas Weisenburger[3], Annika Wiedemann[2,87], Jürgen Wienands[309], Anneke Wilharm[19], Robert John Wilkinson[310,311,312], Gerald Willimsky[313], James B. Wing[179], Rieke Winkelmann[4], Thomas H. Winkler[3], Oliver F. Wirz[7], Alicia Wong[100], Peter Wurst[314], Jennie H. M. Yang[59,60], Juhao Yang[157], Maria Yazdanbakhsh[99], Liping Yu[315], Alice Yue[327], Hanlin Zhang[88], Yi Zhao[316], Susanne Maria Ziegler[196], Christina Zielinski[45,334,335], Jakob Zimmermann[317] and Arturo Zychlinsky[161]

[1] Department of Medical and Surgical Sciences for Children and Adults, Univ. of Modena and Reggio Emilia School of Medicine, Modena, Italy

[2] Deutsches Rheuma-Forschungszentrum (DRFZ), an Institute of the Leibniz Association, Berlin, Germany

[3] Department of Biology, Nikolaus-Fiebiger-Center for Molecular Medicine, Friedrich-Alexander-University Erlangen-Nuremberg, Erlangen, Germany

[4] Institut für Immunologie, Christian-Albrechts-Universität zu Kiel, Kiel, Germany

[5] Mucosal Immunology group, Department of Health Technology, Technical University of Denmark, Kgs. Lyngby, Denmark

[6] Immunology Section, Lund University, Lund, Sweden

[7] Swiss Institute of Allergy and Asthma Research (SIAF), University of Zurich, Davos, Switzerland

[8] Université de Paris, Institut de Recherche Saint-Louis, INSERM U1160, and Gastroenterology Department, Hôpital Saint-Louis – APHP, Paris, France

[9] Institute for Systemic Inflammation Research, University of Luebeck, Luebeck, Germany

[10] Laboratory of Translational Immunology, Humanitas Clinical and Research Center, Rozzano, Italy

[11] University of Birmingham, Birmingham, UK

[12] Institut für Medizinische Mikrobiologie, Immunologie und Hygiene, Technische Universität München, Munich, Germany

[13] Institut für Transfusionsmedizin, Universitätsklinik Schleswig-Holstein, Kiel, Germany

[14] Institut für Klinische Molekularbiologie, Christian-Albrechts Universität zu Kiel, Germany

[15] Department of Life Sciences, University of Siena, Siena, Italy

[16] Dipartimento di Medicina Interna e Specialità Mediche, Sapienza Università di Roma, Rome, Italy

[17] Center for Life Nano Science@Sapienza, Istituto Italiano di Tecnologia, Rome, Italy

[18] Istituto Pasteur - Fondazione Cenci Bolognetti, Rome, Italy

[19] Institute of Immunology, Hannover Medical School, Hannover, Germany

[20] IRCCS Fondazione Santa Lucia, Rome, Italy

[21] Division of Immunology, Allergy and Infectious Diseases, Department of Dermatology, Medical University of Vienna, Vienna, Austria

[22] Center for Comparative Medicine & Dept. Pathology, Microbiology & Immunology, University of California, Davis, CA, USA

[23] Institute for Immunology, Faculty of Medicine, Biomedical Center, LMU Munich, Planegg-Martinsried, Germany

[24] Genomics Core Facility, European Molecular Biology Laboratory (EMBL), Heidelberg, Germany

[25] Discipline of Pharmacy, Graduate School of Health, The University of Technology Sydney, Sydney, NSW, Australia

[26] Department of Bioengineering, University of California, Los Angeles, California, USA

[27] Flow Cytometry Laboratory, Institute of Molecular Toxicology and Pharmacology, Helmholtz Zentrum München, German Research Center for Environmental Health, München, Germany

[28] Department of Medical Biotechnologies and Translational Medicine, University of Milan, Milan, Italy

[29] Department of Biomedical Molecular Biology, Center for Inflammation Research, Ghent University - VIB, Ghent, Belgium

[30] Flow Cytometry Core Technologies, UCD Conway Institute, University College Dublin, Dublin, Ireland

[31] Department of Surgery, The University of British Columbia, Vancouver, Canada

[32] BC Children's Hospital Research Institute, Vancouver, Canada

[33] Mikrobiologisches Institut - Klinische Mikrobiologie, Immunologie und Hygiene, Universitätsklinikum Erlangen, Erlangen, Germany

[34] Friedrich-Alexander-Universität (FAU) Erlangen-Nürnberg and Medical Immunology Campus Erlangen, Erlangen, Germany

[35] Department of Immunology and Pathology, Monash University, Melbourne, Victoria, Australia

[36] Neuroimmunology and Flow Cytometry Units, Fondazione Santa Lucia IRCCS, Rome, Italy

[37] Department of Cell Biology, Albert Einstein College of Medicine, Bronx, NY, USA

[38] The Ruth L. and David S. Gottesman Institute for Stem Cell and Regenerative Medicine Research, Bronx, New York, USA

[39] Thermo Fisher Scientific, Eugene, Oregon, USA

[40] Luxembourg Institute of Health, Department of Infection and Immunity, Experimental and Molecular Immunology, Esch-sur-Alzette, Luxembourg

[41] Odense University Hospital, Odense Research Center for Anaphylaxis, University of Southern Denmark, Department of Dermatology and Allergy Center, Odense, Denmark

[42] BD Life Sciences, Ashland, OR, USA

[43] Department of Medical Genetics, University of British Columbia, Vancouver, BC, Canada

[44] University of Auckland, School of Biological Sciences, Maurice Wilkins Center, Auckland, New Zealand

[45] German Center for Infection Research (DZIF), Munich, Germany

[46] Focus Group "Clinical Cell Processing and Purification", Institute for Advanced Study, Technische Universität München, Munich, Germany

[47] Biophysics, R&D Engineering, Miltenyi Biotec GmbH, Bergisch Gladbach, Germany

[48] Department of Pediatrics and Shared Resource Laboratories, University of Rochester Medical Center, Rochester, NY, USA

[49] University of Verona, Department of Medicine, Section of General Pathology, Verona, Italy

[50] Department of Microbiology and Immunology, Peter Doherty Institute for Infection and Immunity, University of Melbourne, Parkville, Victoria, Australia

[51] National Key Laboratory of Medical Immunology, Nankai University, Tianjin, China

[52] Department of Microbiology and Immunology, University of Gothenburg, Gothenburg, Sweden

[53] The FIRC Institute of Molecular Oncology (FOM), Milan, Italy

[54] National Institute for Health, Migration and Poverty (INMP), Rome, Italy

[55] Macrophage Biology Group, School of Biology, University of Barcelona, Barcelona, Spain

[56] Université Paris Descartes, Institut National de la Santé et de la Recherche Médicale, Paris, France

[57] Isaac and Laura Perlmutter Cancer Center, NYU-Langone Medical Center, New York, USA

[58] Divsion of Medical Oncology and Hematology, Princess Margaret Hospital, Toronto, Ontario, Canada

[59] Department of Immunobiology, School of Immunology and Microbial Sciences, King's College London, UK

[60] National Institutes of Health Research Biomedical Research Centre at Guy's and St. Thomas' National Health Service, Foundation Trust and King's College London, UK

[61] Department of Vaccinology and Applied Microbiology, Helmholtz Centre for Infection Research, Braunschweig, Germany

[62] IRCCS Fondazione Don Carlo Gnocchi, Milan, Italy

[63] Department of Physiopathology and Transplants, University of Milan, Milan, Italy

[64] Milan Center for Neuroscience, University of Milano-Bicocca, Milan, Italy

[65] Flow Cytometry Core, Humanitas Clinical and Research Center, Milan, Italy

[66] Department of Medicine, The University of British Columbia, Vancouver, Canada

[67] Department of Pathology, University of Cambridge, Cambridge, UK

[68] Department of Respiratory Sciences, University of Leicester, Leicester, UK

[69] National Cytometry Platform, Luxembourg Institute of Health, Department of Infection and Immunity, Esch-sur-Alzette, Luxembourg

[70] Department of Experimental and Clinical Medicine, University of Florence, Florence, Italy

[71] de Duve Institute, Université catholique de Louvain, Brussels, Belgium

[72] Unit Lymphopoiesis, Department of Immunology, Institut Pasteur, Paris, France

[73] Division of Molecular Immunology, Nikolaus-Fiebiger-Center, Dept. of Internal Medicine III, University of Erlangen-Nuremberg, Erlangen, Germany

[74] Clinical Research Unit, Berlin Institute of Health (BIH), Charite Universitätsmedizin Berlin, Berlin, Germany

[75] Infection and Immunity Program and Department of Biochemistry and Molecular Biology, Biomedicine Discovery Institute, Monash University, Clayton, Victoria, Australia

[76] Department of Surgery, Medicine, Dentistry and Morphological Sciences, Univ. of Modena and Reggio Emilia, Modena, Italy

[77] IRCCS Istituto Giannina Gaslini, Genova, Italy

[78] Novo Nordisk Foundation Center for Stem Cell Biology – DanStem, University of Copenhagen, Copenhagen, Denmark

[79] Regensburg Center for Interventional Immunology (RCI), Regensburg, Germany

[80] Division of Immunology, Transplantation and Infectious Diseases, San Raffaele Scientific Institute, Milan, Italy

[81] Istanbul University, Aziz Sancar Institute of Experimental Medicine, Department of Immunology, Istanbul, Turkey

[82] Sony Europe Ltd, Weybridge, UK

[83] Charité - Universitätsmedizin Berlin, Laboratory of Innate Immunity, Department of Microbiology, Infectious Diseases and Immunology, Berlin, Germany

[84] Berlin Institute of Health (BIH), Berlin, Germany

[85] University of Palermo, Central Laboratory of Advanced Diagnosis and Biomedical Research, Department of Biomedicine, Neurosciences and Advanced Diagnostics, Palermo, Italy

[86] Flow Cytometry Core Facility, Institute of Experimental Immunology, University of Bonn, Bonn, Germany

[87] Dept. Medicine/Rheumatology and Clinical Immunology, Charité Universitätsmedizin Berlin, Germany

[88] Kennedy Institute of Rheumatology, University of Oxford, Oxford, UK

[89] Program in Emerging Infectious Disease, Duke-NUS Medical School, Singapore

[90] Institute of Immunology, Centre for Infection Medicine, Department of Veterinary Medicine, Freie Universität Berlin, Germany

[91] Department of Internal Medicine III, University Hospital Regensburg, Germany

[92] Charité – Universitätsmedizin Berlin, corporate member of Freie Universität Berlin, Humboldt-Universität zu Berlin, and Berlin Institute of Health, Department of Neuropathology, Germany

[93] Department of Immunology, University of Toronto, Toronto, ON, Canada

[94] Heidelberg Institute for Stem Cell Technology and Experimental Medicine (HI-STEM gGmbH), Heidelberg, Germany

[95] University of Barcelona, Faculty of Medicine and Health Sciences, Department of Biomedical Sciences, Barcelona, Spain

[96] Theodor Kocher Institute, University of Bern, Bern, Switzerland

[97] Department of Immunology, University L. Eotvos, Budapest, Hungary

[98] Leibniz Research Institute for Environmental Medicine, Düsseldorf, Germany

[99] Department of Parasitology, Leiden University Medical Center, Leiden, The Netherlands

[100] Singapore Immunology Network (SIgN), A*STAR (Agency for Science, Technology and Research), Biopolis, Singapore

[101] Institute of Transplant Immunology, Hannover Medical School, MHH, Hannover, Germany

[102] Division of Oncology, Washington University School of Medicine, St. Louis, MO, USA

[103] Laboratory of Cytomics, Joint Research Unit CIPF-UVEG, Principe Felipe Research Center, Valencia, Spain

[104] Experimental Medicine Division, Nuffield Department of Medicine, University of Oxford, Oxford, UK

[105] The Flow Cytometry Core Facility, Faculty of Medical Sciences, Newcastle University, Newcastle upon Tyne, UK

[106] MDQuest Ltd., Szeged, Hungary

[107] Institut Necker-Enfants Malades, Université Paris Descartes Sorbonne Paris Cité, Faculté de Médecine, AP-HP, Hôpital Necker Enfants Malades, INSERM U1151-CNRS UMR 8253, Paris, France

[108] Department of Medicine I, Medical Center - University of Freiburg, Faculty of Medicine, University of Freiburg, Freiburg, Germany

[109] Universitaetsklinikum FreiburgLighthouse Core Facility, Zentrum für Translationale Zellforschung, Klinik für Innere Medizin I, Freiburg, Germany

[110] Immunology and Environment, LIMES Institute, University of Bonn, Bonn, Germany

[111] Owl Biomedical Inc., Santa Barbara, USA

[112] John van Geest Cancer Research Centre, Nottingham Trent University, Nottingham, UK

[113] Department of Medicine, Albert Einstein College of Medicine, Bronx, NY, USA

[114] Charité – Universitätsmedizin Berlin, corporate member of Freie Universität Berlin, Humboldt-Universität zu Berlin, and Berlin Institute of Health, Department of Dermatology, Venereology and Allergology

[115] Nanobiophotonics Department, Leibniz Institute of Photonic Technology (IPHT), Jena, Germany

[116] School of Plant Sciences and Bio5 Institute, University of Arizona, Tucson, USA

[117] Honorary Dean of Life Sciences, Henan University, Kaifeng, China

[118] Division of Molecular Oncology and Immunology, the Netherlands Cancer Institute, Amsterdam, The Netherlands

[119] Institute of Experimental Immunology, University of Bonn, Germany

[120] Stanford Department of Anesthesiology, Perioperative and Pain Medicine, Stanford University School of Medicine, CA, USA

[121] Fundação Oswaldo Cruz - Minas, Laboratory of Immunopatology, Belo Horizonte, MG, Brazil

[122] Department of Mecicine, University of Massachusetts Medical School, Worcester, MA, USA

[123] INGM - Fondazione Istituto Nazionale di Genetica Molecolare "Ronmeo ed Enrica Invernizzi", Milan, Italy

[124] Institute of Immunology, Department of Pathobiology, University of Veterinary Medicine Vienna, Austria

[125] Christian Doppler Laboratory for Optimized Prediction of Vaccination Success in Pigs, Institute of Immunology, Department of Pathobiology, University of Veterinary Medicine Vienna, Austria

[126] Department of Dermatology, Venereology and Allergology, Charité - Universitätsmedizin Berlin, Berlin, Germany

[127] Translational Immunology Institute, SingHealth Duke-NUS Academic Medical Centre, Singapore

[128] Department of Chemistry, University of Tokyo, Tokyo, Japan

[129] Institute of Technological Sciences, Wuhan University, Wuhan, China

[130] Institut für Genetik, Universität zu Köln, Köln, Germany

[131] Alicante Institute for Health and Biomedical Research (ISABIAL), Alicante, Spain

[132] Networked Biomedical Research Center for Hepatic and Digestive Diseases (CIBERehd), Madrid, Spain

[133] Fondazione IRCCS Ca' Granda, Ospedale Maggiore Policlinico, University of Milan

[134] Cancer Immunology Research, Genentech, South San Francisco, CA, USA

[135] Institute of Experimental Immunology, University of Zurich, Zurich, Switzerland

[136] Friedrich-Alexander-University Erlangen-Nürnberg (FAU), Department of Medicine 3, Rheumatology and Immunology, Universitätsklinikum Erlangen, Erlangen

[137] Department of Internal Medicine and Pediatrics, Faculty of Medicine and Health Sciences, Zwijnaarde, Belgium

[138] German Cancer Research Center (DKFZ), Heidelberg, Germany

[139] German Cancer Consortium (DKTK), partner site Berlin, Berlin, Germany

[140] Department of Hematology, Oncology, and Tumor Immunology, Charité – Universitätsmedizin Berlin, Campus Virchow Klinikum, Berlin, Germany

[141] Department of Medicine and Center for Molecular Medicine at Karolinska University Hospital, Solna, Sweden

[142] Murdoch Children's Research Institute, Parkville, Victoria, Australia

[143] Charité – Universitätsmedizin Berlin, corporate member of Freie Universität Berlin, Humboldt-Universität zu Berlin

[144] Department of Rheumatology and Clinical Immunology, Berlin Institute of Health, Berlin, Germany

[145] Flow Cytometry, Houston Methodist Hospital Research Institute, Houston, TX, USA

[146] Charité - Universitätsmedizin Berlin, Medical Department I, Division of Gastroenterology, Infectiology and Rheumatology, Berlin, Germany

[147] Cytometry Service, Incliva Foundation. Clinic Hospital and Faculty of Medicine, University of Valencia, Valencia, Spain

[148] Immunobiology Laboratory, Department of Biomedicine, University and University Hospital Basel, Basel, Switzerland

[149] Cambridge Institute of Therapeutic Immunology & Infectious Disease, Jeffrey Cheah Biomedical Centre, University of Cambridge, Cambridge, UK

[150] German Cancer Research Center (DKFZ), Division of Theoretical Systems Biology, Heidelberg, Germany

[151] Center for Immunology, University of Minnesota, Minneapolis, MN, USA

[152] Karolinska Institutet Biomedicum, Solna, Sweden

[153] Department of Chemical & Materials Engineering, New Mexico State University, Las Cruces, NM, USA

[154] Rheumatologie/Klinische Immunologie, Klinik für Innere Medizin I und Exzellenzzentrum Entzündungsmedizin, Universitätsklinikum Schleswig-Holstein, Kiel, Germany

[155] Institute for Advanced Study (IAS), Shenzhen University, Shenzhen, China

[156] Department of Immunology & National Key Laboratory of Medical Molecular Biology, Institute of Basic Medical Sciences, Chinese Academy of Medical Sciences (CAMS) & Peking Union Medical College, Beijing, China

[157] Experimental Immunology, Helmholtz Centre for Infection Research, Braunschweig, Germany

[158] Department of Hematology, Oncology and Rheumatology, University Heidelberg, Heidelberg, Germany

[159] Department of Pathobiology, School of Veterinary Medicine, University of Pennsylvania, Philadelphia, PA, USA

[160] Department of Diagnostic Medicine, Clinical and Public Health, Univ. of Modena and Reggio Emilia, Modena, Italy

[161] Max Planck Institute for Infection Biology, Berlin, Germany

[162] Laboratory of Cytomics, Joint Research Unit CIPF-UVEG, Department of Biochemistry and Molecular Biology, University of Valencia, Valencia, Spain

[163] Department of Histology and Embryology/Center for Proteomics, Faculty of Medicine, University of Rijeka, Rijeka, Croatia

[164] Department of Paediatric Haematology and Oncology, Second Faculty of Medicine, Charles University, Prague, Czech Republic

[165] Jena University Hospital, Institute of Immunology, Jena, Germany

[166] Department of Rheumatology and Clinical Immunology, Medical Center - University of Freiburg, Faculty of Medicine, University of Freiburg, Freiburg, Germany

[167] Center for Chronic Immunodeficiency, Medical Center - University of Freiburg, Faculty of Medicine, University of Freiburg, Freiburg, Germany

[168] Department of Microbiology and Immunology, Yong Loo Lin School of Medicine, National University of Singapore, Singapore

[169] Institute of Molecular Health Sciences, ETH Zurich, Zürich, Switzerland

[170] Department of Neuropathology, Universitätsklinikum Erlangen, Germany

[171] John W Deming Endowed Chair in Internal Medicine, Center for Translational Research in Infection and Inflammation Tulane School of Medicine, New Orleans, LA, USA

[172] Department of Neurology, Technical University of Munich, Munich, Germany

[173] Department of Rheumatology, Leiden University Medical Center, Leiden, The Netherlands

[174] Division of Cell Biology, Histology & Embryology, Gottfried Schatz Research Center, Medical University of Graz, Graz, Austria

[175] Institute for Molecular Medicine, Goethe University Frankfurt, Frankfurt am Main, Germany

[176] FACS & Imaging Core Facility, Max Planck Institute for Biology of Ageing, Cologne, Germany

[177] Flow & Mass Cytometry Core Facility, Charité - Universitätsmedizin Berlin and Berlin Institute of Health, Berlin, Germany

[178] BCRT Flow Cytometry Lab, Berlin-Brandenburg Center for Regenerative Therapies, Charité - Universitätsmedizin Berlin

[179] WPI Immunology Frontier Research Center, Osaka University, Osaka, Japan

[180] School of Biological Sciences, Nanyang Technological University, Singapore

[181] INSERM U932, PSL University, Institut Curie, Paris, France

[182] Department of Medicine and Aging Sciences, Centre on Aging Sciences and Translational Medicine (Ce.S.I.-Me.T.), University "G. d'Annunzio" of Chieti-Pescara, Chieti, Italy

[183] Institut Cochin, CNRS8104, INSERM1016, Department of Endocrinology, Metabolism and Diabetes, Université de Paris, Paris, France

[184] Section of Immunology, Vetsuisse Faculty, University of Zurich, Zurich, Switzerland

[185] The Human Immune Monitoring Center (HIMC), Institute for Immunity, Transplantation and Infection, Stanford University School of Medicine, CA, USA

[186] School of Biomedical Engineering, The University of British Columbia, Vancouver, Canada

[187] Caprion Biosciences, ImmuneCarta, Montréal, Quebec, Canada

[188] Inst. f. Med. Mikrobiology and Hospital Hygiene, University of Marburg, Germany

[189] King's College London, "Peter Gorer" Department of Immunobiology, London, UK

[190] Beckman Coulter, Inc, Miami, FL, USA

[191] IMIM(Hospital de Mar Medical Research Institute), University Pompeu Fabra, Barcelona, Spain

[192] Department of Microbial Infection and Immunity, Ohio State University, Columbus, OH, USA

[193] Department of Rheumatology, Erasmus MC, University Medical Center Rotterdam, Rotterdam, The Netherlands

[194] Centre d'Immunophénomique - CIPHE (PHENOMIN), Aix Marseille Université (UMS3367), Inserm (US012), CNRS (UMS3367), Marseille, France

[195] Institute of Immunobiology, Kantonsspital St.Gallen, St. Gallen, Switzerland

[196] Department of Virus Immunology, Heinrich Pette Institute, Leibniz Institute for Experimental Virology, Hamburg, Germany

[197] Institute for Immunity, Transplantation, and Infection, Stanford University School of Medicine, Stanford, CA, USA

[198] Flow and Image Cytometry Shared Resource, Roswell Park Comprehensive Cancer Center, Buffalo, NY, USA

[199] Fred Hutchinson Cancer Research Center, Vaccine and Infectious Disease Division, Seattle, WA, USA

[200] Istituto Clinico Humanitas IRCCS and Humanitas University, Pieve Emanuele, Milan, Italy

[201] William Harvey Research Institute, Queen Mary University, London, United Kingdom

[202] Department of Immunology, Rady Faculty of Health Sciences, University of Manitoba, Winnipeg, MB, Canada

[203] Cytomics Technological Service, Principe Felipe Research Center, Valencia, Spain

[204] National Institute of Geriatrics, Rheumatology and Rehabilitation, Department of Pathophysiology and Immunology, Warsaw, Poland

[205] Treg Cell Lab, Dipartimento di Medicina Molecolare e Biotecologie Mediche, Università di Napoli Federico II and Istituto per l'Endocrinologia e l'Oncologia Sperimentale, Consiglio Nazionale delle Ricerche (IEOS-CNR), Napoli, Italy

[206] Cell Clearance in Health and Disease Lab, VIB Center for Inflammation Research, Ghent, Belgium

[207] Department of Biomedical Molecular Biology, Ghent University, Ghent, Belgium

[208] Ramaciotti Facility for Human Systems Biology, and Discipline of Pathology, The University of Sydney, Camperdown, Australia

[209] Institute of Infection Immunity and Inflammation, College of Medical Veterinary and Life Sciences, University of Glasgow, Glasgow Biomedical Research Centre, Glasgow, UK

[210] Clinical Trial Center Leipzig, University Leipzig, Leipzig, Germany

[211] Interdepartmental Immunobiology Center, Dept. of Microbiology-Immunology, Northwestern Univ. Medical School, Chicago, IL, USA

[212] Trinity College Dublin, School of Biochemistry and Immunology, Trinity Biomedical Sciences Institute, Dublin, Ireland

[213] Center for Infectious Medicine, Department of Medicine Huddinge, ANA Futura, Karolinska Institutet, Stockholm, Sweden

[214] Department of Clinical and Experimental Medine, Linköping University, Linköping, Sweden

[215] Abramson Cancer Center Flow Cytometry and Cell Sorting Shared Resource, Perelman School of Medicine at the University of Pennsylvania, Philadelphia, PA, USA

[216] Department of Immunology, IRCCS Bambino Gesu Children's Hospital, Rome, Italy

[217] Centre for Environmental Research - UFZ, Department Environmental Microbiology, Leipzig, Germany

[218] Institute for Innovative Radiotherapy (iRT), Experimental Immune Biology, Helmholtz Zentrum München, Neuherberg, Germany

[219] Radiation Immuno-Oncology Group, Center for Translational Cancer Research Technische Universität München (TranslaTUM), Klinikum rechts der Isar, Munich, Germany

[220] Department of Immunology, Graduate School of Medicine, Chiba University, Chiba city, Chiba, Japan

[221] Institute of Experimental Immunology and Hepatology, University Medical Center Hamburg-Eppendorf, Hamburg, Germany

[222] Discipline of Dermatology, University of Sydney, Sydney, New South Wales, Australia

[223] State Key Laboratory of Experimental Hematology, Institute of Hematology, Chinese Academy of Medical Sciences & Peking Union Medical College, Tianjin, China

[224] Barts and The London School of Medicine and Dentistry, Queen Mary University of London, UK

[225] Department of Pathology and Rogel Cancer Center, the University of Michigan, Ann Arbor, Michigan, USA

[226] Flow Cytometry Core Facility, European Molecular Biology Laboratory (EMBL), Heidelberg, Germany

[227] Department of Medicine, Cancer Research Centre (IBMCC-CSIC/USAL), Cytometry Service, University of Salamanca, CIBERONC and Institute for Biomedical Research of Salamanca (IBSAL), Salamanca, Spain

[228] Burnet Institute, AMREP Flow Cytometry Core Facility, Melbourne, Victoria, Australia

[229] Inflammation and Oncology, Research, Amgen Inc, South San Francisco, USA

[230] ETH Zurich, Institute of Microbiology, Zurich, Switzerland

[231] Department of Transfusion Medicine, Institute of Immunology and Transfusion Medicine, University Medicine Greifswald, Greifswald, Germany

[232] Center of Excellence for Flow Cytometry, Department of Research and Development, Faculty of Medicine Siriraj Hospital, Mahidol University, Bangkok, Thailand

[233] Institute of Biomedicine and Translational Medicine, University of Tartu, Tartu, Estonia

[234] Institute of Immunology, Center for Pathophysiology, Infectiology and Immunology, Medical University of Vienna, Vienna, Austria

[235] Department of Life Sciences, University of Modena and Reggio Emilia, Modena, Italy

[236] Chromocyte Limited, Electric Works, Sheffield, UK

[237] Department for Internal Medicine 3, Institute for Rheumatology and Immunology, AG Munoz, Universitätsklinikum Erlangen, Erlangen, Germany

[238] Department of Immunology, University of Udine, Udine, Italy

[239] David H. Smith Center for Vaccine Biology and Immunology, University of Rochester Medical Center, Rochester, NY, USA

[240] School of Biomedical and Health Sciences, RMIT University, Bundoora, Victoria, Australia

[241] Department of Biochemistry and Molecular Biology, Monash University, Clayton, Victoria, Australia

[242] Department of Rheumatology and Clinical Immunology, University Medical Center Utrecht, Utrecht University, Utrecht, The Netherlands

[243] Regeneration in Hematopoiesis, Leibniz-Institute on Aging, Fritz-Lipmann-Institute (FLI), Jena, Germany

[244] Faculty of Biological Sciences, Friedrich Schiller University Jena, Jena, Germany

[245] Preparative Flow Cytometry, Max-Delbrück-Centrum für Molekulare Medizin, Berlin, Germany

[246] Bindley Biosciences Center, Purdue University, West Lafayette, IN, USA

[247] Department of Internal Medicine, Groene Hart Hospital, Gouda, The Netherlands

[248] Desatoya LLC, Reno, NV, USA

[249] Immunobiology Laboratory, The Francis Crick Institute, London, UK

[250] Department of Experimental Immunology, Amsterdam Infection and Immunity Institute, Amsterdam UMC, University of Amsterdam, Amsterdam, The Netherlands

[251] Renal Transplant Unit, Division of Internal Medicine, Academic Medical Centre, Amsterdam UMC, University of Amsterdam, Amsterdam, The Netherlands

[252] Core Facility Flow Cytometry, Biomedical Center, Ludwig-Maximilians-University Munich, Germany

[253] Functional Cytomics Group, Josep Carreras Leukaemia Research Institute, Campus ICO-Germans Trias i Pujol, Universitat Autònoma de Barcelona, UAB, Badalona, Spain

[254] Flow Cytometry Scientific Technology Platform, The Francis Crick Institute, London, UK

[255] Department of Medical Microbiology and Immunology, University of Alberta, Alberta, Canada

[256] Purdue University Cytometry Laboratories, Purdue University, West Lafayette, IN, USA

[257] Cell Biology Unit, IRCCS Ospedale Policlinico San Martino, Genova, Italy

[258] Institut für Klinische Chemie und Pathobiochemie, Fakultät für Medizin, Technische Universität München, München, Germany

[259] RIKEN Center for Integrative Medical Sciences, Yokohama, Japan

[260] Flow Cytometry Facility, Ludwig Cancer Institute, Faculty of Medicine and Biology, University of Lausanne, Epalinges, Switzerland

[261] Heidelberg University, Institute of Immunology, Section of Molecular Immunology, Heidelberg, Germany

[262] Translational Immunology Laboratory, NIHR BRC, University of Oxford, Kennedy Institute of Rheumatology, Oxford, UK

[263] Innate Immunty Unit, Department of Immunology, Institut Pasteur, Paris, France

[264] Institut Pasteur, Inserm U1223, Paris, France

[265] Department of Molecular Medicine, Sapienza University of Rome, IRCCS, Neuromed, Pozzilli, Italy

[266] Centre de Recherches des Cordeliers, Equipe Cancer et Immunité anti-tumorale, Paris, France

[267] Charité – Universitätsmedizin Berlin, and Berlin Institute of Health, Institute of Medical Immunology, Berlin, Germany

[268] Comprehensive Cancer Center Zurich, Switzerland

[269] Clinic for Orthopedics and Trauma Surgery, University Hospital Bonn, Bonn, Germany

[270] R&D Reagents, Miltenyi Biotec GmbH, Bergisch Gladbach, Germany

[271] Quantitative Systems Biology, Life & Medical Sciences Institute, University of Bonn, Bonn, Germany

[272] Internal Medicine I, University Hospital Regensburg, Germany

[273] Flow Cytometry Core Facility, German Cancer Research Centre (DKFZ), Heidelberg, Germany

[274] Genome Biology Unit, European Molecular Biology Laboratory (EMBL), Heidelberg, Germany

[275] Institute of Molecular and Clinical Immunology, Otto-von-Guericke University, Magdeburg, Germany

[276] University of Cambridge, Cambridge Institute for Medical Research, Cambridge, UK

[277] Institut Pasteur, Cellular Lymphocytes Biology, Immunology Departement, Paris, France

[278] TRI Flow Cytometry Suite (TRI.fcs), Translational Research Institute, Wooloongabba, QLD, Australia

[279] AsedaSciences, West Lafayette, IN, USA

[280] Instituto de Medicina Molecular João Lobo Antunes, Faculdade de Medicina, Universidade de Lisboa, Portugal

[281] Dept. Molecular Translational Medicine, University of Brescia, Brescia, Italy

[282] Department of Oncology, University of Lausanne and CHUV, Epalinges, Switzerland

[283] Lundberg Laboratory for Cancer, Department of Pathology, Sahlgrenska Academy at University of Gothenburg, Gothenburg, Sweden

[284] BD Life Sciences, San Diego, CA, USA

[285] Department of Hematopoiesis, Sanquin Research and Landsteiner Laboratory, Amsterdam UMC, University of Amsterdam, Amsterdam, The Netherlands

[286] Institute for Hygiene and Applied Immunology, Center for Pathophysiology, Infectiology and Immunology, Medical University of Vienna, Vienna, Austria

[287] National Institutes of Health, Bethesda, MD, USA

[288] Departement for Therapy Validation, Fraunhofer Institute for Cell Therapy and Immunology IZI, Leipzig, Germany

[289] Institute for Medical Informatics, Statistics and Epidemiology (IMISE), University of Leipzig, Leipzig, Germany

[290] BioGenes GmbH, Berlin, Germany

[291] Novartis Biologics Center, Mechanistic Immunology Unit, Novartis Institute for Biomedical Research, NIBR, Basel, Switzerland

[292] Department of Cellular and Molecular Physiology, Penn State University College of Medicine, PA, United States

[293] Institute of Bioinnovation, BSRC Alexander Fleming, Vari, Greece

[294] Department of Biochemistry, Institute of Chemistry, University of São Paulo, São Paulo, SP, Brazil

[295] Christine Kühne Center for Allergy Research and Education (CK-CARE), Davos, Switzerland

[296] Vesicle Observation Center; Biomedical Engineering & Physics; Laboratory Experimental Clinical Chemistry; Amsterdam University Medical Centers, Location AMC, The Netherlands

[297] VIB Flow Core, VIB Center for Inflammation Research, Ghent, Belgium

[298] Department of Infection Biology, University Hospital Erlangen, Friedrich-Alexander University Erlangen-Nuremberg (FAU), Erlangen, Germany

[299] BIH Center for Regenerative Therapies (BCRT) Charité Universitätsmedizin Berlin and Berlin Institute of Health, Core Unit ImmunoCheck

[300] A·P·E-Applied Physics & Electronics, Berlin, Germany

[301] Institute for Molecular Medicine, University Medical Center of the Johannes Gutenberg University of Mainz, Mainz, Germany

[302] Flow Cytometry Facility, Babraham Institute, Cambridge, UK

[303] Roswell Park Comprehensive Cancer Center, Elm and Carlton Streets, Buffalo, NY, USA

[304] The Scientific Platforms, the Westmead Institute for Medical Research, the Westmead Research Hub, Westmead, New South Wales, Australia

[305] Dept of Hematopathology, The University of Texas MD Anderson Cancer Center, Houston, TX, USA

[306] Flow Cytometry Core Facility, Blizard Institute, Queen Mary London University, London, UK

[307] Medinfomatics Ltd., West Drayton, Middlesex, UK

[308] Department for Immunology, Leibniz Research Centre for Working Environment and Human Factors at TU Dortmund (IfADo), Dortmund, Germany

[309] Institute for Cellular & Molecular Immunology, University Medical Center Göttingen, Göttingen, Germany

[310] Department of Infectious Disease, Imperial College London, UK

[311] Wellcome Centre for Infectious Diseases Research in Africa and Department of Medicine, Institute of Infectious Disease and Molecular Medicine, University of Cape Town, Republic of South Africa

[312] Tuberculosis Laboratory, The Francis Crick Institute, London, UK

[313] Cooperation Unit for Experimental and Translational Cancer Immunology, Institute of Immunology (Charité - Universitätsmedizin Berlin) and German Cancer Research Center (DKFZ), Berlin, Germany

[314] University Bonn, Medical Faculty, Bonn, Germany

[315] BD Biosciences, San Jose, CA, USA

[316] Department of Rheumatology and Immunology, West China Hospital, Sichuan University, Chengdu, Sichuan, China

[317] Maurice Müller Laboratories (Department of Biomedical Research), Universitätsklinik für Viszerale Chirurgie und Medizin Inselspital, University of Bern, Bern, Switzerland

[318] Department of Hematology, Singapore General Hospital, Singapore

[319] Division of Medical Sciences, National Cancer Centre Singapore, Singapore

[320] Cancer & Stem Cell Biology, Duke-NUS Medical School, Singapore

[321] Executive Offices, National Cancer Centre Singapore, Singapore

[322] Leiden Computational Biology Center, Leiden University Medical Center, Leiden, The Netherlands

[323] Departments of Anesthesiology, Pain and Perioperative Medicine; Biomedical Data Sciences; and Pediatrics, Stanford University, Stanford, CA, USA

[324] Luxembourg Centre for Systems Biomedicine (LCSB), University of Luxembourg, Belvaux, Luxembourg

[325] Data Mining and Modeling for Biomedicine, VIB-UGent Center for Inflammation Research, Ghent, Belgium

[326] Department of Applied Mathematics, Computer Science and Statistics, Ghent University, Ghent, Belgium

[327] School of Computing Science, Simon Fraser University, Burnaby, Canada

[328] Computer Graphics and Visualization, Department of Intelligent Systems, TU Delft, Delft, The Netherlands

[329] Department of Precision Instruments, Tsinghua University, Beijing, China

[330] Chair for Immunology, University Regensburg, Germany

[331] Shanghai Institute of Immunology, Department of Immunology and Microbiology, Shanghai Jiao Tong University School of Medicine, Shanghai, China

[332] Australian Research Council Centre of Excellence in Advanced Molecular Imaging, Monash University, Clayton, Victoria, Australia

[333] Department of Dermatology, Laboratory of Dendritic Cell Biology, Friedrich-Alexander Universität Erlangen-Nürnberg (FAU), University Hospital Erlangen, Erlangen, Germany

[334] Institute of Virology, Technical University of Munich, Munich, Germany

[335] TranslaTUM, Technical University of Munich, Munich, Germany

[336] Lab of Clinical and Experimental Immunology, Humanitas Clinical and Research Center, Rozzano, Milan, Italy

[337] Terry Fox Laboratory, BC Cancer, Vancouver, BC, Canada

Contents

Andrea Cossarizza et al.

Abstract

These guidelines are a consensus work of a considerable number of members of the immunology and flow cytometry community. They provide the theory and key practical aspects of flow cytometry enabling immunologists to avoid the common errors that often undermine immunological data. Notably, there are comprehensive sections of all major immune cell types with helpful Tables detailing phenotypes in murine and human cells. The latest flow cytometry techniques and applications are also described, featuring examples of the data that can be generated and, importantly, how the data can be analysed. Furthermore, there are sections detailing tips, tricks and pitfalls to avoid, all written and peer-reviewed by leading experts in the field, making this an essential research companion.

Additional supporting information may be found online in the Supporting Information section at the end of the article.

Note: In order to make the guidelines as beneficial as possible to the scientific community, if you wish to refer to a specific section when referring to these guidelines, please ensure to use the Chapter and Section information. For example: ... as noted in section VII.11 of [1] ...

1. Cossarizza, A., Chang, H. D., Radbruch, A., Acs, A., Adam, A., Adam-Klages, S., Agace, W. et al., Guidelines for the use of flow cytometry and cell sorting in immunological studies Eur. J. Immunol. 2019. **49**: 1457–1973.

Introduction

Continuing my theme of the marriage between immunology and cytometry noted in my Introduction to the previous version of these Guidelines [1], long relationships always have periods in which the partners have contrasting feelings for each other, and may eventually divorce; however, this does not seem to be the case for immunology and cytometry, disciplines that continue with a very stable and incredibly productive marriage, as witnessed by the enormous number of publications in almost all areas of the immunology discipline that we all love. It is indeed almost impossible to count the original papers, reviews, abstracts, and meeting communications, and talks in which an immunologist, from undergraduate students to Nobel laureates, has measured a parameter of interest at the single cell, organelle, or even molecular level using one of the sophisticated cytometric technologies that we are discussing here.

Unfortunately, measuring what happens in a biological system, starting from the single cell level (that is, 'cyto' for cell, 'metry' for measure) is not as simple as it seems, and can lead to results that are not always optimal. In most cases, flow cytometry is relatively easy to use, and often even a brief training—if not the simple reading of a bench manual or a rapid glance over a protocol—enables a researcher to use a flow cytometer and start producing data. As we have already pointed out in ref. [1], paradoxically, this is a main weakness of cytometry. Indeed, a well-trained cytometrist can often identify in published papers experimental aspects or data that must be improved, if not fully redone. The importance of adequate controls, correct compensation, clean and well monitored sorting strategies, correct data analysis, presentation, and interpretation, and the description of the methods used cannot be stressed enough.

It is for these reasons, a few years ago, following enthusiastic discussions at the European Congress of Immunology held in Vienna, September 2015, and under the guidance of Professor Andreas Radbruch (at that time Chair of the Executive Committee of the *European Journal of Immunology* (*EJI*) and currently EFIS President), that the Editorial Team of the *European Journal of Immunology* felt that it was worthwhile to offer our community guidelines for the correct use of cytometric techniques in the field of immunology. For this, we were able to put together a large team of renowned experts who prepared a first collection of protocols of interest for our community.

In the previous version of the guidelines, which was authored by 236 scientists from 194 institutions spread across the world, we focused on core aspects including advice and best practice regarding how to study complex cell phenotypes, the type or amount of molecules produced or secreted after stimulation by the cell population of interest, signaling processes, differentiation, proliferation, cell death, cytotoxic activities, cell–cell interactions, the functionality of organelles such as mitochondria, the different types of response induced against tumours, transcription factor activity, quantification of soluble molecules, drug uptake, and rare events, not forgetting the parts related to the choice of reagents, the preparation and/or storage of the cells under analysis, the overall experimental plan, and last but not least, the analysis of data.

But a good scientist knows that all efforts, including those collected in extensive guidelines like ours, can and must be improved. Accordingly, we asked for feedback on the published guidelines and received critical comments, new ideas, and suggestions for this new version, and here we are! In this updated version, we have tried to ameliorate and update several parts and the reader will find more standardized sections that should make it easier to navigate throughout the text that now features novel tips and pitfalls to avoid. Importantly the phenotyping sections are clearly divided into human and murine sections, again to help the reader find the section most relevant to their work.

There are also several new or expanded sections, with the phenotyping section covering all the major cell types including, for example, dendritic cells and their subsets, unconventional T cells, such as gamma delta, NKT or MAIT cells, B cells, and beyond, as well as sections covering the functional aspects of regulatory T cells and recently described assays on antigen specific cells. There is also the identification and characterization of bone marrow and cord blood neutrophils, plus liver cells and brain/neural cells are actors that play a crucial role in the economy of the immune system and can now be analyzed by cytometric assays. Soluble molecules have received particular attention with cytokine-producing cell sorting with secretion assays, as well as the quantification of soluble cytokines with cytometric bead arrays, are now described. A discussion regarding single cell genomics and cytometry is also present, along with novel cytometric views on the microbiota, methods to detect inflammasome assembly and activation in immune cells, and assays related to multidrug resistance.

The importance of the optimal organization of a laboratory is self-evident, and clearly highlighted in the new sections that describe how to perform flow cytometry under GLP/GMP conditions, how to set up and maintain a core facility, including housekeeping/shared resource lab management, as well as covering the importance of sample banking and high-throughput screening methods.

There is no need to underline how fundamental and complex data analysis is, especially when we are coping with polychromatic and high dimensional flow cytometry, and are able to detect dozens of antigens in a cell—not to mention mass cytometry. As an aside, who will be the first to measure 100 parameters in a single cell by using a cytometric assay? Thus, new sections are now present that discuss neuronal networks, dimensionality reduction, methods for clustering and creating trajectories, and integration of cytometric data into multi-omics analysis among others. We would like to stress once again that today the limit for asking critical questions is our creativity, and certainly not the instruments, the technology, or the bioinformatics approach that we can use in our experiments.

The following three points have already been flagged in the previous version of the Guidelines but we would nonetheless like to remind our readers that, first, "FACS" (fluorescence activated cell sorting) should only be used for Becton Dickinson (BD) technologies as it is a BD trademark (FACS™); the more general term

"flow cytometry" (for the pure analysis of the cells of interest) or "flow cytometry cell sorting" (obviously, if one sorts cells) should be used to be company agnostic and correct. Second, CD mAbs and not anti-CD mAbs (in other words, CD1 mAb and not anti-CD1 mAb for example) should be used. This is because the CD nomenclature is primarily a system to cluster/characterize mAbs and it was only later accepted to use this system to also describe the respective CD molecules. Third, although the Guidelines are as comprehensive as possible, there are naturally limitations, e.g., only a subset of antibodies and antigens are shown and, at times, only certain reagents/companies are used as examples, and others work in the same excellent manner.

In conclusion, we would like to thank the people who played a major role in ensuring that Andreas Radbruch's and Andrea Cossarizza's vision became a reality. These are Hyun-Dong Chang and Ute Hoffman, both at the DRFZ (Berlin), and Karen Chu, former Associate Editor, who were instrumental in getting the first version of the guidelines in place. For the revision, Nadja Bakocevic (Associate Editor), Sylvia Heider (Editorial Assistant), Cate Livingstone (Managing Editor), and Laura Soto-Vazquez (Associate Editor) of the *European Journal of Immunology*, together with Hyun-Dong Chang and Ute Hoffman, worked tirelessly together with the authors and those providing feedback to ensure that this revised version is a significant improvement. It is a job that is never done as, due to time limits, some suggestions could not be incorporated but we feel that this version will continue to provide invaluable advice for the immunology community.

I Cytometry equipment

1 Fluidic system of a flow cytometer

1.1 *Purposes of the fluidic system of a flow cytometer*

To accurately measure optical properties of cells with a flow cytometer, cells have to pass through the uniformly bright center of focused laser beams. Light collection optics is focused on the intersection point of cells with the laser beams to pick up fluorescence and scattered light from cells. This is the sensing zone of a flow cytometer, here, the measurements of cell parameters are taken. In stream-in-air cell sorters, the sensing zone is located around 0.3 mm under the nozzle tip, in other cytometers it is located inside a cuvette.

One purpose of the fluidic system is to move the cells one by one precisely through the sensing region in a liquid stream in such a way that each cell is illuminated by the same amount of light from the lasers.

In cytometers with sort capabilities or cell sorters, the fluidic system has to establish a stable break off from the liquid stream in small uniform droplets. Droplets containing the cells of interest can be charged and deflected in an electric field for sorting.

This kind of cell sorting technique was invented by Mack J. Fulwyler in 1965 at Los Alamos National Laboratory [2].
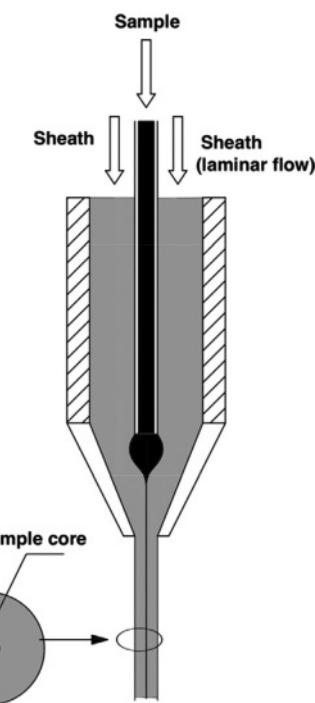
Figure 1. Sample core after hydrodynamic focussing by laminar sheath flow in a flow chamber.

Mack Fulwyler needed a machine for testing the performance of Coulter counters, so the first particle separator was used for sorting of particles with different Coulter volumes. Len Herzenberg was interested in a machine that could sort living cells on the basis of fluorescence, he got the design plans of the particle separator from Mack Fulwyler and found a little group at Stanford University to build the first FACS in the late 1960s (see the video Inventing the Cell Sorter, Herzenberg Lab, https://www.youtube.com/watch?v=Ro8P3w9BPhg).

1.2 *Hydrodynamic focusing*

For precise positioning of cells in a liquid jet, the hydrodynamic focusing technique is used in most cytometers and cell counters [3].

The cells in suspension are injected by a thin tubing in a laminar flow of a sheath fluid that enters from a wide tubing into a narrow tubing or small orifice. The sheath flow speeds up when it enters the narrow tubing and the diameter of sheath and sample flow (sample core) is decreased (Fig. 1). Crosland-Taylor described this technique first in Nature 1953 [4] and used it in a device for counting small particles suspended in a fluid. Some years before in 1947, F.T. Gucker used a similar technique for detecting bacteria in a laminar sheath stream of air [5].

The hydrodynamic focusing takes place in the so-called flow chamber or flow cell of a cytometer. A detailed description of an optimized flow chamber for a stream-in-air cell sorter can be found in the patent applications from Gerrit van den Engh [6, 7]) and
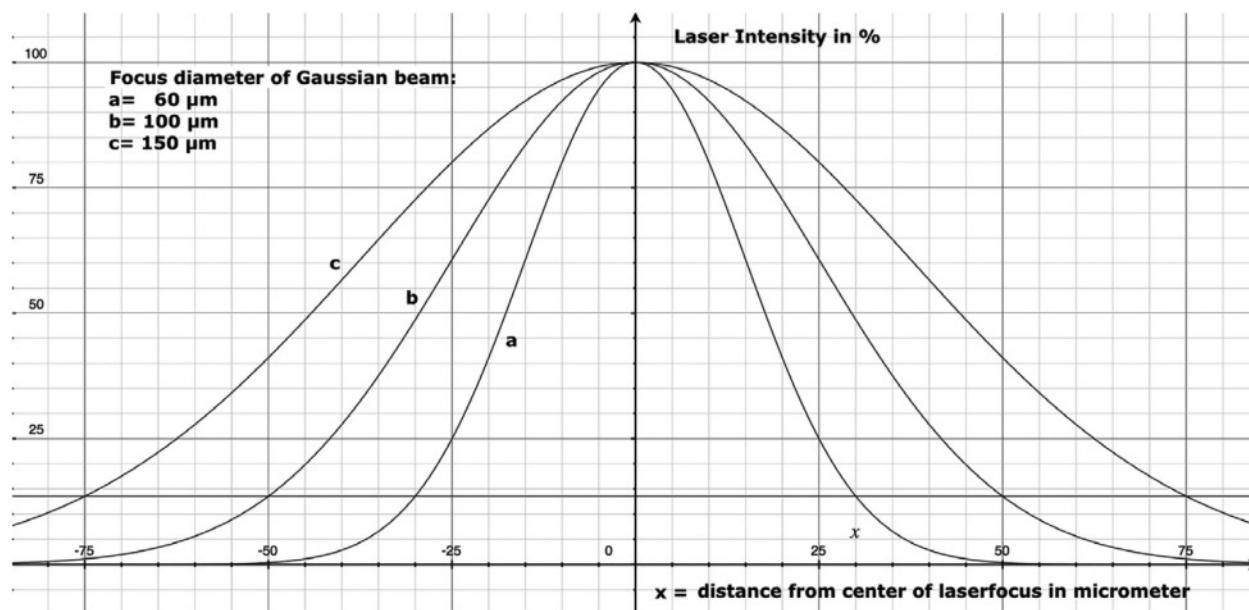
Figure 2. Intensity profile of a focus spot of a gaussian laser beam. Note: if a cell is out of the center of the laser focus by 10 μm (20 μm sample core), laser intensity goes down about 5% with a 60 μm diameter laser focus.

a flow chamber of a cuvette system is found in another patent application from BD [8].

In addition to flow chambers for laser based cytometers, flow chambers with hydrodynamic focusing for cytometers with an arc lamp light source were developed. These early cytometers were based on a standard fluorescence microscope with epi- fluorescence setup. Here, the same microscope lens is used to bring excitation light to the cells and take fluorescence emission from the cells. Excitation and emission light is separated by a dichroic mirror and special filters. With an immersion microscope lens of high numerical aperture, a stabilized arc lamp and optimized staining protocol, and DNA histograms with coefficient of variations (CVs) lower than 1% (0.50–0.7%) were achieved [9, 10].

With the hydrodynamic focusing technique, cells can be aligned to a precision of one micrometer. With high sample flow rates the sample core is increased, however, and cells in the sample core can move out of the focus center of the laser. Thus, not all cells get the same amount of laser illumination. This means that the accuracy of measurements is lost.

To avoid loss of measurement precision when the sample core increases and to maintain laser intensity, cytometers use elliptical laser focus spots. Typical sizes of focus spot are 60–150 μm horizontally and 5–20 μm vertically. Recently, beam shaping optics for flat top focused laser beams were introduced in flow cytometers by the manufacturer. The intensity profile of a Gaussian laser beam with 60, 100, and 150 μm focus diameters is shown in Fig. 2.

An approximation of the sample core diameter d in micrometers is given in ref. [11] as follows:

$d = 1.13 * 1000 * \sqrt[2]{u/nv}$ with $u =$ particle measurement rate in particle per second, $n =$ particle concentration in particle/mL, and $v =$ jet velocity in m/s.

An approximation of the jet velocity is given by

$$v = 3,7 * \sqrt[2]{\text{delta P}}$$

with v in m/s and delta P, the sheath pressure drop at the nozzle in psi (in practice around the pressure on the sheath container minus 1 to 3 psi pressure drop on tubings and sterile filter).

The approximation of the sample core diameter calculation shows that for a ten times lower sample concentration a more than three times bigger sample core diameter is necessary to keep the particle measurement rate.

For the sheath fluid, PBS (phosphate buffered saline) filtered through a 0.22 or 0.1 μm filter is often used. The sheath fluid should be compatible with cells or species that have to be sorted.

1.3 Acoustic focusing of particles in a liquid stream

An acoustic focusing technology was developed by Gregory Kaduchak and co-workers at the Los Alamos National Laboratory in 2001 and introduced to flow cytometry [12, 13]. Recently, the acoustic focusing technique was implemented into a flow cytometer to support hydrodynamic focusing. This technique helps to increase measurement precision in particular if wide sample cores are used. According to the manufacturer, cytometers with acoustic-assisted hydrodynamic focusing can run samples with low concentrations of cells up to ten times faster as compared with cytometers without and still maintain the precision of the measurements. The fundamentals of acoustic cytometry are given in ref. [14].
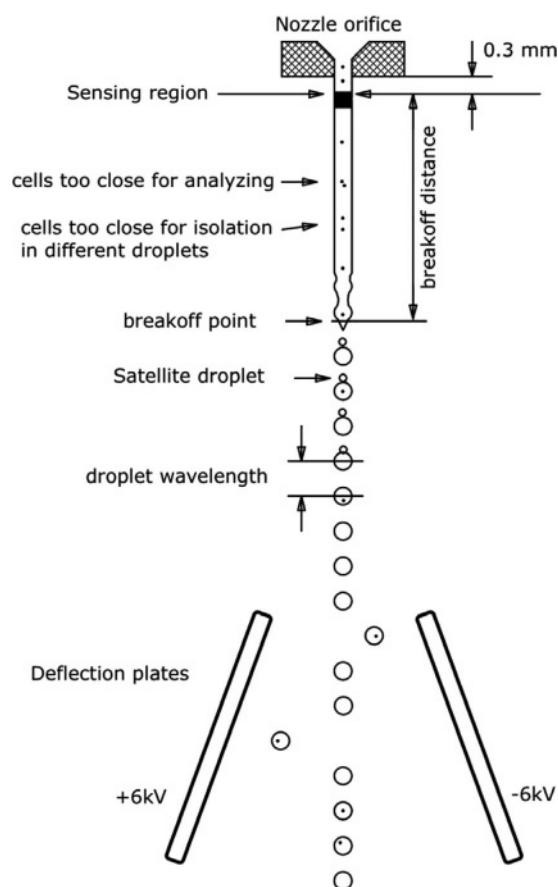
Figure 3. Liquid stream of a jet in air sensing cell sorter. Depending of abort settings of the cell sorter, cells that are too close together are aborted from sorting. Reproduced with permission from ref. [16].

1.4 *Droplet generation of a cell sorter*

Based on the invention from Richard Sweet [15], droplet formation of the liquid jet of a cell sorter is stabilized by vibrations of an ultrasonic transducer.

Little disturbances on the surface of the liquid jet at the exit of the nozzle orifice are generated by the transducer. The disturbances grow exponentially and lead to break up of the jet in little droplets [3, 11]. A cell of interest that should be sorted is measured at the sensing zone and moves down the stream to the breakoff point. During the separation of the droplet with the cell in it from the intact liquid jet, a voltage pulse is given to the liquid jet. So electrons are caught with the cell in a droplet and cannot go back when the droplet is separated from the liquid stream and the voltage pulse is shut off. The droplet with the cell is charged and can be deflected in a static electric field of two deflection plates for sorting (Fig. 3).

It is important for the sorting process that the cell of interest is at the right place when a voltage pulse is given to the liquid jet to charge a droplet. The delay from the measurements of cell parameters to the charging pulse is determined by the cell sorter operator or by the cell sorter electronics. This is done with the help of fluorescent beads and a laser beam under the deflection plates. The

laser beam illuminates the streams of deflected and undeflected droplets. The fluorescent beads are sorted all in one direction, and with a camera, the fluorescence in the droplet streams is observed on a monitor. During observation of the fluorescent spots the drop delay is changed so that the brightness of the fluorescence of the deflected droplet stream is maximized and the brightness of the fluorescence of the un-deflected droplet stream is minimized. The distance from the sensing zone to the break off point is controlled by a microscope and held constant.

The delay setting is fixed during sorting and in general the break off distance is kept constant by the operator. If the velocity of the liquid jet is constant during sorting the sorting works fine, but in practice this is not always the case. Small changes of sheath pressure, for example, due to partial clogging of the sheath filter can alter jet velocity during sorting. Petersen and van den Engh have examined the problem and showed how little variations of sheath pressure can disturb the sorting process and how the operator can handle it [17]. Toralf Kaiser examined how temperature changes of sheath fluid alters sorting performance and gives a solution for stabilizing sheath fluid temperature [18]).

A schematic of a typical fluid system of a cell stream-in-air sorter is shown in Fig. 4.

2 Optics and electronics

2.1 *Introduction*

From a technical point of view, a flow cytometer is a light detection device capable of detecting photons of different wavelengths over a high dynamic range. In order to achieve a high dynamic range, the optics, signal detection, and processing units must be carefully designed.

2.2 *Optics*

2.2.1 Lenses.   In flow cytometers, lenses are used to collect light emitted from the cell of interest, i.e., due to their spatial resolution they collect light only from the point of interest. Furthermore, they are used to make the collected light parallel in order to direct it through the optical bench to the detectors. A flow cytometer employs collection and collimation lenses. Collection lenses (convex lenses) are used to focus the light from the interrogation point either to the end of an optical fiber or directly to a collimation lens (e.g., aspheric condenser lenses). Some instruments use optical fibers to route the detected light to detectors, which are installed in an octagon. In this case, a collimation lens is installed at the other end of the fiber to ensure that all light is routed parallel through the octagon. Inside the octagon another collimation lens is placed in front of each detector to focus the parallel light onto the photocathode. In instruments without fiber optics the parallel light is routed through the optical bench and then focused onto the photocathode by a collimation lens.
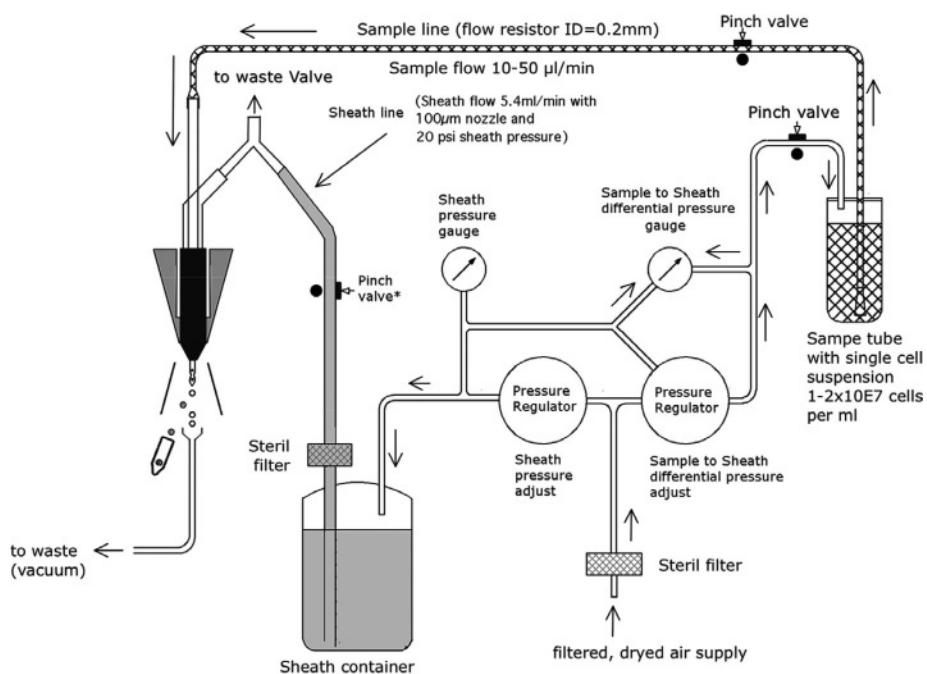
Figure 4. Schematics of fluidics of a jet in air sensing cell sorter.

2.2.2 Optical filter. The photodetectors used in flow cytometers are spectrally broadband and therefore unable to generate a signal exclusively from specific wavelengths and thus specific markers. To add specificity, optical filters and dichroic mirrors are used in a well defined manner to route the light to the detectors. Optical filters are designed as band pass (BP), long pass (LP), or short pass (SP) filters, and are mostly installed in front of the light detectors. The common property of the filters is that they transmit light only within a spectral range. An LP filter transmits light below a certain wavelength. For example, a LP of 660 nm will transmit all light above 660 nm. In contrast, SP filters will pass short wavelengths and block longer ones. A BP filter transmits light in a certain wavelength range. For example, if the BP is named as 660/20, this means that light between 650 and 670 nm will pass through the filter. Dichroic mirrors are also used to allocate light to a specific detector based on wavelength. Like optical filters, dichroic mirrors are separated in LP and SP versions. To achieve maximum sensitivity, dichroic LPs are installed closer to the light source (flow cell) to first direct long-wave photons onto the light detector. Due to aging, quality of coating, and contamination, the actual parameter of an optical filter or dichroic mirror can differ from the technical description. Therefore, it is recommended to check the transmission spectra of new filters provided by the manufacturer and always keep filters dust free. Sometimes mirrors (usually silver mirrors) are used in the optical bench of a flow cytometer in order to deflect light for geometrical or constructive reasons. These filters are >99% reflective over a wide range of wavelengths.

2.2.3 Dispersing elements. Recently, commercial cytometers have become available which use spatially dispersing elements instead of or in combination with optical filters in order to deflect light wavelength specific to a detector array. The rationale behind this is the measurement of the entire emission spectra of a cell (see section I.3 Flow cytometry, including flow cytometry cell sorting). A dispersing element can be a dispersive prism or a grating. Prisms have a higher light efficiency over gratings and they are not sensitive for polarized light. This maybe the reason why they are employed in the spectral flow cytometer from Sony. A dispersing element is installed between the interrogation point and a detector array.

2.2.4 Laser. Lasers employed for flow cytometers are mainly solid-state, continuous wave lasers. Such lasers have a small footprint and a typical output power range from 20 to 100 mW. Lasers are coherent light sources that allow a high photon density at the illumination point, and therefore an efficient energy transfer to the fluorochrome.

2.3 Electronics

As a flow cytometer measures the biological information of a particle (e.g., a cell) via photons, this light needs to be converted to electrons and processed by an amplifier, filter, analog to digital converter (ADC), and baseline restorer in order to visualize and store the biological information of the cells or other particles. In this section, the main components of cytometer electronics are briefly described.
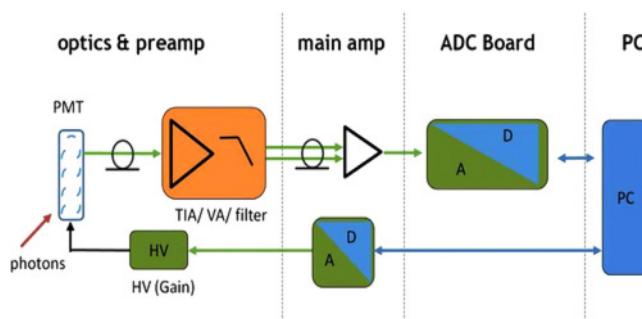
Figure 5. Typical electronic signal processing of a flow cytometer. The signal coming from a PMT or photo diode is amplified by a preamp and a main amp. The analogue signals are then digitized by an ADC board. A personal computer (PC) is used for further data processing and HV controlling.

2.3.1 Detectors. From a technical point of view, the detection of cell related light is difficult due to (i) the low light level, (ii) the high analysis rate, and (iii) the high dynamic range of the light level. Photomultiplier tubes (PMTs) meet these requirements and are therefore employed in almost all flow cytometers. PMTs are vacuum tubes containing a photocathode, electron focusing electrodes, and a series of dynodes for electron multiplication. The photocathode converts photons to photoelectrons that are then multiplied by a series of dynodes driven by a high voltage (Fig. 5). Photocathodes of PMTs employed in flow cytometers are made from bialkali material that determines the spectral quantum efficiency η of the PMT, which is the ratio of emitted electrons to incident photons. The quantum efficiency of the photocathode is always $0 < \eta < 1$ and is a function of the light quantum energy ($h \times f$). A typical PMT (R9220, Hamamatsu) of a cytometer has a quantum efficiency $\eta = 0.2$ at 500 nm and $\eta = 0.09$ at 700 nm, which is a reduction in sensitivity of about 7 dB. This means that the detection of PE-Cy7 is always less sensitive as the detection of FITC, for example. In many applications, PMTs are increasingly being replaced, e.g., by avalanche photodiodes due to their higher quantum efficiency. However, in flow cytometry, only one commercial instrument (CytoFlex, Beckman Coulter, Aurora and Norther lights, Cytek) employs APDs in order to improve the sensitivity for wavelengths > 700 nm [19].

2.3.2 Amplifier and signal processing. Amplifiers in a flow cytometer can be grouped as pre- and main amplifiers. Pre-amplifiers are either voltage (VA) or transimpedance (TIA) amplifiers that are used to amplify the voltage amplitude of a PMT (VA) or to convert a signal current of a photodiode to a voltage (TIA). Furthermore, pre-amplifiers perform operations, such as:

- impedance matching,
- filtering and pulse shaping,
- and bandwidth limiting.

All amplifiers in a cytometer are analogue hardware devices which must be very well designed for optimal signal to noise ratios (SNRs). In a typical cytometer such amplifiers have an SNR of >86 dB. Once the signals are processed by the pre-amplifiers, the main amplifier moves the signal level to a suitable range for the ADC (Fig. 5).

In modern cytometers, the conversion of the continuous analog voltage signal into discrete digital values is done by ADCs that are defined by their sampling frequency and sample resolution. The required dynamic detection range (DNR) of a flow cytometer can be defined as the intensity range of stained and unstained cells, for example. A stained cell can be 10 000 times brighter than an unstained cell that gives a DNR of 4 log or 80 dB (DNR[dB]=20log(10^4)). The DNR of an ideal ADC is given by: DNR = 6.02*N + 1.76 dB [20].

This means that in theory, an ADC with $N = 14$ bit will have a DNR of 86.04 dB. In practice, the effective number of bits of an ADC is, due to noise and distortion of the circuit, some decibels below the theoretical value (e.g., the ADC AD9240AS of the BD Diva electronic has 78.5 dB [21]). This limits the dynamic range to less than 4 decades and, more importantly, shrinks the resolution of dim signals.

The sampling frequency of the AD9240AS is 10 MHz that results in 30 samples per measured pulse of a high speed cell sorter (pulse length = 3 μs). This results in a peak detection error of 1–2% [22]. Modern ADCs have a resolution of 16 bit and a sampling frequency of 250 MHz which allows the design of flow cytometers with dynamic range of >4 decades and a peak detection error of <0.1%.

In the digital domain, the signals are processed by filters, baseline restorer, pulse height, pulse width algorithms, and trigger (see Section I.3). Filtering is done to smooth the raw PMT signal in order to improve the SNR. The resulting signal consists of an unwanted DC part due to laser scatter light and electronic noise (among others) and a specific AC part. Hence, the DC part is subtracted by baseline restorers to increase the SNR and the DNR of the cytometer. The baseline restorer attempts to keep the baseline at zero. In practice, however, baseline restoring is not perfect and can lead to negative values on the histogram axis or introduce a slight distortion of low signals and therefore to an increased CV of dim signals. After baseline restoring, the pulse parameters (height, width, and area) are extracted and converted into a *.fcs file.

Taken together, the analogue and digital components of a flow cytometer in combination with the baseline and pulse shaping algorithms need to be well adjusted in order to maximize SNR and DNR.

3 Flow cytometry, including flow cytometry cell sorting

3.1 *Convention, or fluorescence-activated flow cytometry and sorting*

Since the invention of the first prototype of a Fluorescence Activated Cell Sorter in 1968 at Stanford University, the technology has become a powerful tool to analyze and sort individual

cells based on their functional status. Moreover, flow cytometry provides a robust statistic of thousands of individual cells and can detect rare events at a frequency below 10^{-4} cells. The sample uptake by the instrument can be done from tubes or multi-well plates at an acquisition rate of thousands of cells/s. In a typical cytometer, the sensitivity decreases with increasing flow rate due to the increasing diameter of the cell stream within the flow cell. Alternatively, the AttuneNXT (ThermoFisher) uses acoustic-assisted hydrodynamic focusing, which helps keeping the core stream tight and therefore gives accurate results even at a much higher sample throughput. Furthermore, the serial acquisition of multiple cell samples can be automated by using high-throughput platforms (HyperCyt®).

Today, instruments are available designed to detect up to 27 different bio-markers on an individual cell. Typically these markers are fluorescently tagged antibodies, molecular sensors, as well as genetically encoded reporters. For instance, the FACSymphony™ (Becton Dickinson) is technically capable of detecting up to 50 parameters of an individual cell. In practice, this high number of parameters is not achievable because at the moment the range of appropriate fluorescent dyes is limited.

Technical limitations regarding the maximum number of detectable markers are also given by the overlap of the emission spectra of the different fluorescent tags, since each fluorescence detection channel is correlated to a biological marker. To overcome this, fluorescent tags became available that have different excitation wavelengths. Currently, up to seven lasers with emission wavelengths from 325 to 808 nm are used in order to achieve a high flexibility in the choice of the fluorescent tags. Furthermore, tunable lasers are used for special applications like fluorescent life time measurements (FLIMs).

Flow cytometers use either PMTs or avalanche diodes to convert the emitted or scattered light into amplified electrical pulses that are processed by appropriate electronics to extract information like pulse height, area, length, and time. The electronics of the cytometer consist basically of a preamp circuit, baseline restoration circuit, and an ADC. In most modern cytometers, the data post-processing (i.e., pulse integration, compensation, log-transformation) and data analysis is done in a computer by software. All components together must have a low noise level (i.e., a high SNR) to achieve high instrument sensitivity (Q) and low background (B) detection.

Avalanche diodes have better detection efficiency in long wavelengths and thus a better SNR in that range over PMTs. Furthermore, they open new possibilities for the application of fluorescent tags with long-wave emission spectra. Avalanche diodes are implemented in the CytoFLEX (Beckman Coulter) cytometer. Within this instrument, the emitted fluorescence light is divided by a wavelength division multiplexer (WDM) through a series of band pass filters and integrated optics, onto an array of avalanche diodes that enables a high sensitivity in the detection of, e.g., PE-Cy7.

Avalanche diodes or PMTs itself are light detectors that are unsuitable for wavelength detection, hence, the fluorescent light needs to be filtered by optical filters and mirrors. These filters must be carefully chosen because a multiparameter experiment, i.e., an experiment in which multiple parameters (markers) are analyzed, requires that multiple fluorophores are used simultaneously; a consequence of this is spectral overlap or spillover (see Section II.1 Compensation).

Conventional flow cytometers circumvent this problem by compensation (see Section II.1 Compensation) in order to accurately correlate the physical light properties with the biological properties of the cell. Following this, the data are analyzed in a multivariate fashion in combination with a hierarchical gating strategy (see Section VII.1 Data analysis).

It is essential to adapt the combination of fluorescent tags to the given optical, laser, and electronic setup of the instrument to minimize spillover, increase Q, and lower B signals. For instance, by choosing the right concentration of a certain reagent (see Section III.2 Titration: Determining optimal reagent concentration), the fluorochrome related B can be optimized such that it contributes ideally nothing to the B given by the instrument. This can help to increase the separation (the distance between the means) between a blank and a fluorescent population that is a function of Q and B. Thus, it requires the characterization of Q and B of the used instrument.

Mostly polystyrene particles (beads) are used for this purpose in combination with software based protocols implemented in the instruments, e.g., MACS®Quant, Fortessa, Yeti, Cytoflex to name just a few. Beads are small particles and so to say "cell dummies" of well-defined fluorescent intensity and sizes that also can be used for PMT voltage optimization, compensation setup, cell counting, scale calibration, and so on.

Scale calibration is an especially useful approach to measure absolute values (e.g., number of binding antibodies, amount of fluorescent molecules or photoelectrons) instead of relative mean fluorescent intensities (MFIs), which leads to quantitative flow cytometry (see Section VII). Beside beads, scale calibration can also be achieved by using LED light pulses. Recently, the quantiFlash™ (APE) tool has become available that provides ultra stable LED light pulses. Furthermore, by using this tool, instruments can be compared within or between labs regarding their Q and B values.

Up to this point, analytical cytometers have been described but cells can, in addition, be sorted based on specific marker expression for downstream analysis (molecular biology, sequencing, etc.) or cell culture (see Section II).

3.2 Spectral flow cytometry: Principles and evolution

For spectral flow cytometry, the "one detector, one marker" paradigm is changed. After excitation (Fig. 6A), the complete emitted light of a marker (Fig. 6B) is spectrally dispersed either by refraction within a prism or by diffraction within a grating (Fig. 6C) over a highly sensitive photo detector array (Fig. 6D). Gratings are susceptible for polarized light. As polarization occurs frequently in flow cytometry [23], the total efficiency of a grating may be reduced. In fact, prisms are better suited for spectral light dispersion because they have a better
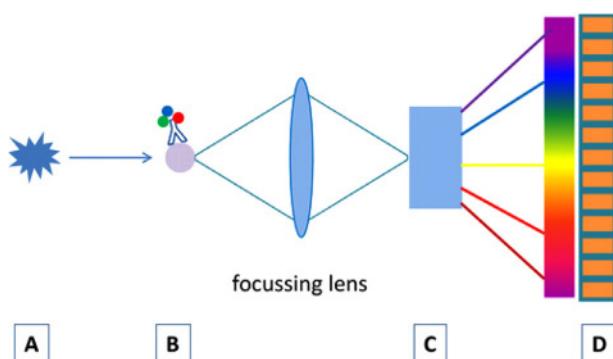
Figure 6. Principle of a spectral flow cytometer. (A) Excitation light source (laser), (B) labeled cell, (C) dispersing element, (D) multichannel light detector (CCD or multichannel PMT).

light transmission and are also stable for polarized light. Unfortunately, the dispersion of a prism is not linear with regard to the wavelength, which makes it difficult to use linear detector arrays such as multianode PMTs [24].

As mentioned above, multianode PMTs or charge-coupled devices (CCDs) can be used as detector arrays. CCDs have a high quantum efficiency of 80–90% in the visible range (500–800 nm) and a relative long readout time that limits the acquisition rate. On the other hand, this in combination with high spectral resolution allows the spectral detection of Raman scattering, which is a characteristic spectrum of molecular vibrations, much narrower than fluorescence spectra. This allows the application of new biological markers, such as surface enhanced Raman scattering tags or near infrared fluorescent dyes [25, 26].

Spectral flow cytometry was introduced in 1979 [27], when the cytometric measurement of FITC- and PI-labeled mouse cells was demonstrated using a video camera tube as a detector. More recently, Robinson et al. developed a single cell spectral flow cytometer based on a grating and PMT array [28–31]. This instrument created single cell spectra and demonstrated a spectral flow cytometer based on a 32-channel PMT array detector using a holographic grating and showed the detection and analysis of labeled lymphocytes and microspheres in hyperspectral space. Goddard et al. [32] employed a grating spectrograph attached to an intensified CCD for measuring microspheres and cells. This spectrograph was implemented in the optical pathway of a conventional flow cytometer and was able to take spectra of single cells and microspheres as well as to discriminate free versus bound propidium iodide.

The first commercially available spectral flow cytometer, the SP6800, was developed by Sony [33]. This instrument employs a prism array to disperse the collected light over a 32-channel multianode PMT. Moreover, the instrument is equipped with three lasers (405, 488, and 638 nm), which allow for full spectral detection of the resulting emission spectra. The measured spectra from single cells are subsequently unmixed by using reference spectra of all used dyes and the autofluorescence spectrum. Least Square Fitting algorithms are used to calculate the most accurate fit for all reference spectra, leading to an accurate determination of which

dyes are present on each cell and at which intensity. Using this method, a complete fluorescence emission is used instead of only a small portion of emitted light entering a dedicated detector through a specific set of mirrors and optical filters. This is a major advantage over conventional flow cytometry, in which light that is lost outside of the optical filters also contaminates other channels with unwanted light that has to be corrected by a subtractive method (see Section II.1 Compensation). Since dyes frequently used in flow cytometry have rather broad emission spectra and large spectral overlaps, spectral unmixing can help mitigate this problem. Therefore, applications for spectral flow cytometry are similar to those performed on conventional flow cytometers with the additional benefit of spectral unmixing, which allows spectrally overlapping dyes to be measured, and auto-fluorescence subtraction to be included. Moreover, control of reagents (especially tandem dyes) is paramount with the increased need for standardization. Given that spectral flow cytometry shows full spectrum unbiased data, quality control is more or less integrated.

In this fashion, spectral flow cytometers are designed to measure the biological information across multiple detection channels, where the optical configuration can be fixed for all experiments, giving the added benefit of instrument stability, sensitivity [34], and easier standardization across instruments, aided by the lack of individual PMTs and individual optical filters and mirrors.

II Setup—Instrument setup and quality control

1 Compensation

1.1 *Introduction*

In flow cytometry, fluorescence spillover (i.e., which can be overcome by compensation) is probably the single greatest source of frustration for the scientist and cause of bad data. Correctly compensating for spillover is critical to accurately identify populations in multicolor flow experiments. Errors in compensation for one fluorochrome can be propagated into other detectors resulting in erroneous "virtual" positive populations or errors in population percentages due to incorrect gating. Mastering fluorescence spillover is much like chess, the rules are simple, but becoming a skilled practitioner can take some effort. Here, the basic concepts of fluorescence spillover are reviewed and some simple principles to follow in order to maximize data quality are provided, while debunking some of the myths that surround this field. For further information on this subject, readers are referred to the following references: [35–38]. In addition, a guide as to the Minimum Information about a Flow Cytometry experiment has been developed and vetted by the International Society for the Advancement of Cytometry (ISAC) [39]. This includes recommendations for ways to document compensation of complex panels.
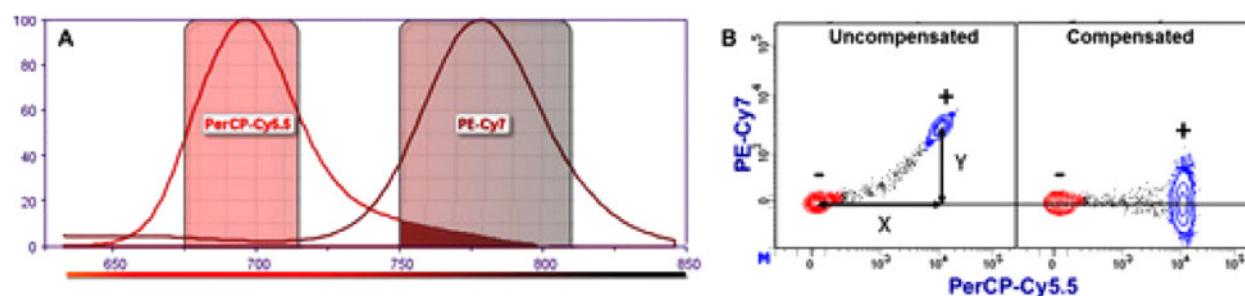
Figure 7. Spillover and compensation: (A) the emission spectra of PerCP-Cy5.5 and PE-Cy7. (B) Peripheral blood lymphocytes stained with PerCP-Cy5.5 CD4 mAb. The MdFI is shown for the PerCP-Cy5.5 and PE-Cy7 detectors without (left) and with (right) compensation.

1.2 Principle of spillover and compensation

Fluorescence spillover is the amount of signal, measured in median fluorescence intensity (MdFI), that a fluorochrome emits in a secondary detector specific for a different fluorochrome (Fig. 7A shows the fluorochrome PerCP-Cy5.5 is spilling into the PE-Cy7 detector [dark red]). This is equivalent to a background in that detector. We can calculate a spillover value (SOV) of PerCP-Cy5.5 into PE-Cy7 as Y/X × 100% (Fig. 7B, left). Compensation is the mathematical process used in all flow cytometers and software in which these SOVs are used to determine a compensation matrix that effectively subtracts/corrects background due to spillover in all detectors (Fig. 7B, right).

The accuracy of this correction is totally dependent upon the accuracy of the SOVs determined from the appropriate single-color compensation controls. In Fig. 7B, the spillover is correct when the MdFI [PE-Cy7] of the PerCP-Cy5.5 positive (+) population is equal to the MdFI [PE-Cy7] of the PerCP-Cy5.5 negative (–) population. With a few exceptions, the mathematical calculation of SOVs is the same for all cytometers and flow cytometry software packages.

1.3 Measuring SOVs/compensation controls

On all cytometers, SOVs should be determined using single-color compensation controls. Most errors in calculating SOVs are due to the use of inappropriate compensation controls. A compensation control should consist of a positively stained population and a negative or unstained population. The positive and negative populations do not need to be run in the same tube. Cytometer and software protocols will specify what combinations can be used. It is never good practice to try to run two controls in the same tube, for example, using FITC CD4 mAb and PE CD19 mAb. This makes the assumption that there is absolutely no antibody bound to the "negative" cells, which is typically not the case.

Many software packages from flow cytometer manufactures and third party companies have an "auto-compensation" feature. While these can be very powerful, they are based on automated gating algorithms in which the software identifies the positive and negative populations. These gates may not always be appropriate. It is recommended that for new controls the user confirm that the software is providing correct gates and results.

In general, correct SOVs can be obtained by following four simple principles for single-color compensation controls:

1. The fluorescence spectrum of the compensation control fluorochrome-conjugated reagent should be identical to the reagent used in the experiment. More specifically, the fluorochrome should be identical not similar. For example, even though Alexa Fluor® 488 and FITC are spectrally very similar, an Alexa Fluor® 488 compensation control cannot be used for a FITC reagent or vice versa. Other examples are allophycocyanin (APC)/Alexa Fluor® 647 and APC-Cy7/ APC-H7.
   This principle is especially critical for tandem reagents (e.g., PE-Cy7, APC-Cy7) where there can be significant spectral differences from lot to lot, which can lead to differences in the SOV [40]. In such cases, it is recommended that users run individual single-color, lot-specific compensation controls.

2. The autofluoresence of the positive and negative populations must be equivalent. The spillover calculation assumes that any difference in the MdFI of the spillover detector (e.g., Y in Fig. 7A, left) is due to the presence of the fluorochrome measured by the primary detector. If the autofluoresence differs, then part of the MdFI in the spillover detector will be due to the difference in autofluoresence and not the fluorochrome itself. An example is shown in Table 1. In measuring the SOV of FITC into PE when similarly autofluorescent positive and negative cells are used, the calculated SOV is 27%; however, incorrectly using beads for the negative population results in an SOV of 22%, a 5% error.
   This also applies to cell types. Cell lines and untransformed lymphocytes should not be used for the same control. If a stained cell line is used as a positive control, the same unstained cell line should be used as a negative control. It is similar with cell subsets, for example, if lymphocytes are analyzed, lymphocytes, and not monocytes, should be used as both the positive and negative control. Some software programs allow a universal negative population (e.g., unstained lymphocytes); however, this is acceptable only as long as all analyzed samples are exclusively lymphocytes.
   Myth: the SOV depends upon the type and autofluoresence of the cells you are analyzing. False. The SOV is only a function of the fluorochrome. When correctly measured,

the SOV is independent of the cell type(s) in the biological sample.

3. The positive population should be as bright as possible.

As noted earlier, the SOV is equal to the slope of the MdFI of the two detectors (Fig. 8, dashed line). The actual SOV is not a function of the brightness of the positive population but is the same all across the dynamic range. A truly correct SOV will provide correct compensation whether it is derived from a bright or dim positive population (Fig. 8, Correct SOV). When calculating a slope, the most accurate measurement (i.e., SOV) is obtained when the two data points obtained are apart as far as possible. This is especially important for low spillover values such as PE-Cy7 into PE.

However, we rarely get "perfect" SOVs, and the impact of any errors in the SOV are magnified as the MdFI of the primary detector increases as shown in Fig. 8. In this example, if there is a 1% under compensation error in the SOV (Fig. 8; red line), it would have a minimal impact on a dim population. In this example, in an MdFI of 10^3 in FL1, the error would be 10 MdFI in FL2, not noticeable. However, if the FL1 MdFI is 10^5, the MdFI error in FL2 would be 1000 and this would incorrectly look like a new positive population.

Myth: For spillover to be correct, it is required that the compensation control positive population needs to be as bright as your sample. Partly False.

To restate the message here, you want to get the most accurate slope/SOV possible. Therefore as noted in the title, it is good practice to have the positive control population as bright as possible, preferably close to your sample MdFI (static or activated). However, for spillover to be correct, it is *not* required that the compensation control positive population needs to be as bright as your sample. In some cases, the positive population of compensation beads may not be as bright as your sample. This does not mean it is not a valid compensation control. In general, if the positive population is approximately equivalent to CD4, you will get good results. There is one major caveat to this statement. For all measurements, it is critical that the positive population is in the linear range of the detector. Outside of this range, the corrected data will be inaccurate. Most cytometer manufacturers provide linearity information for their instruments.

4. Collect enough events to obtain meaningful accurate SOVs.

As a rule of thumb, collect at least 5000 events for both your negative and positive population. Again this is to ensure the accuracy of the measurements, especially for low SOVs.

1.4 *Compensation controls*

Compensation controls typically fall into two categories: (i) stained cells; (ii) beads, these are seen as either (i) directly fluorochrome-coated or (ii) anti-Ig capture beads and are available from a number of sources. Each of these controls has advantages and disadvantages. In a given multicolor experiment, compensation controls can be mixed and matched including all three types.
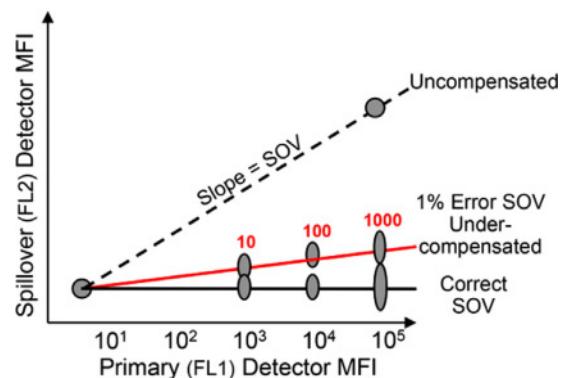
Figure 8. Brightness of positive population.

Table 1. The consequences of using positive and negative populations with differing autofluoresence: Lymphocytes were stained with diluted FITC CD4 mAb. The MdFI of the CD4$^+$ [Cells (+), unstained [Cells (–)] cells and unstained beads [Beads (–)] were measured in the FITC and PE detectors. SOVs were calculated using positive and negative cells or positive cells and negative beads

	Fluorescence (MdFI)		
	FITC	PE	SOV
Cells (+)	3 135	903	n/a
Cells (–)	95	78	27%
Beads (–)	107	228	22%

That is beads (positive and negative) can be used to compensate Fluorochrome A, and cells (positive and negative) to compensate Fluorochrome B. The key is to follow the second principle and not mix and match different control types within the same single color fluorescent control.

1.4.1 Stained cells. The advantage of using stained cells is that these controls most closely replicate what is happening in the assay tube. The disadvantage is that you may have to use precious biological material. In particular, if you need a tandem, lot-specific control for a specific CD marker, splitting the sample to generate such a control decreases the number of cells available for analysis. This may therefore require the use of even more of the biological sample at the outset.

1.4.2 Beads. The advantage of beads is that no biological material is required and they are easy to prepare and use. Following the manufacturer's protocols, for many fluorochromes, beads provide sufficiently accurate SOVs. The disadvantage is that these beads are a surrogate for cells and may not in all cases provide a perfect match to cells. This can result in discernible and reproducible differences in the SOVs obtained from the exact same reagent measured on beads versus cells. Where different SOVs are obtained, the cells must be considered the biologically relevant gold standard.

Compensation controls using fluorochrome-coated and anti-Ig capture beads are available from a variety of sources. Some are
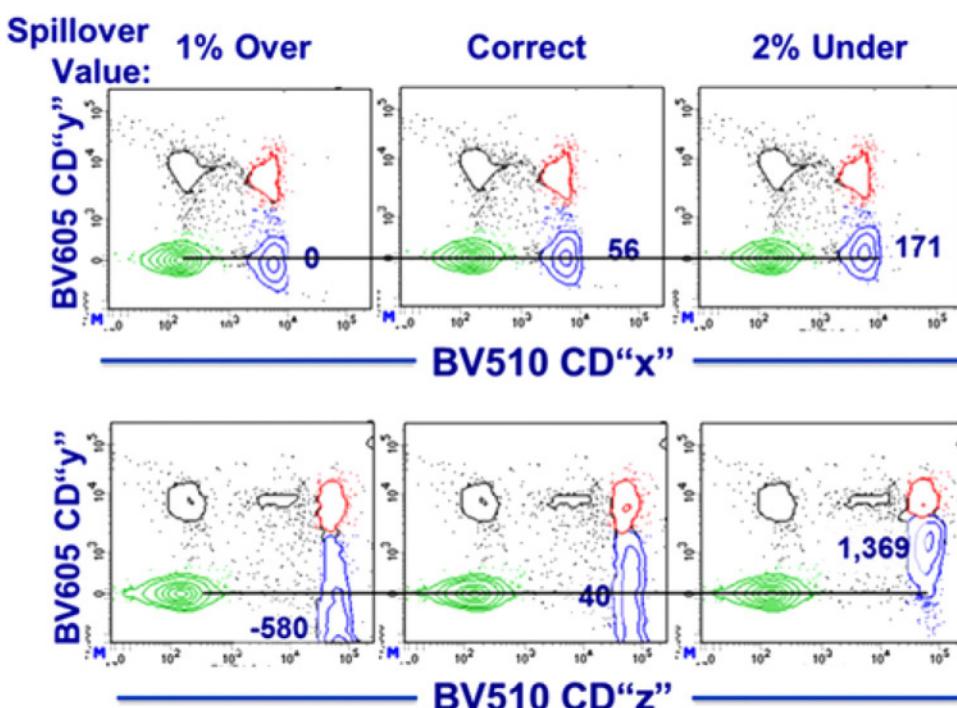
Figure 9. Accuracy for SOV: The figure shows two different assays in which lysed whole blood was stained with the same fluorochromes: BD Horizon™ Brilliant Violet 510 (BV510) and BD Horizon™ Brilliant Violet 605 (BV605). Both assays used the same BV605 reagent. In the top panels, the BV510 positive population was dim while in the bottom panels the BV510 positive population is very bright. For each assay, the SOVs were determined and the correct spillover was applied (Middle panels). For the left panels, the BV510→BV605 SOV was increased by 1% (overcompensated) and compensation applied. For the right panels, the BV510→BV605 SOV was decreased by 2% (undercompensated) and compensation applied.

used as stand-alone controls, some are integrated into software packages. However, when used for 10–18 color instruments, differences in SOVs can be seen in all of these beads when comparing the SOVs obtained with the beads to the SOVs obtained with the gold standard of cells. These differences can vary from manufacturer to manufacturer. For example, the beads from Manufacturer A may be more accurate than the beads from Manufacturer B when calculating the SOV of Fluorochrome X into Y, while the beads from Manufacturer B may be better for calculating the SOV of Fluorochrome Y into Z. SOV differences between beads and cells can be as large as 5–10%.

Compensation beads are a powerful tool for making the process of determining SOVs fast and easy and should be used where appropriate. However, it is important to use them with reasonable caution. The best laboratory practice to ensure accurate compensation when using beads is to pretest any new reagent on both beads and cells to ensure that they are providing you with SOVs equivalent to your stained assay samples. For example, if you are using a new fluorochrome or a new lot of a tandem, run a quick test staining both cells and beads; calculate the SOVs from both. If the SOVs are effectively equivalent then you can be comfortable using the beads as controls for all future assays. However, if there are significant differences, you may need to use cells as your controls or try a different bead. Finally, in such a test, you may want to treat the cells and beads as you would in your assay, e.g., if your assay includes a fix/perm step, you can include this in your control staining. Fix/Perm buffers can sometimes, but not always, alter the SOV of your fluorochromes.

1.5 What are "good" SOVs?

This is really a question that cannot be definitively answered. There is great deal of misunderstanding regarding what SOVs actually mean in terms of a multicolor flow cytometer and the experiments run on them. First and foremost, SOVs are empirically determined mathematical values that are used by flow cytometry software to correct for the background due to fluorescence. While these values are related to fluorescence spillover, they *are not* direct absolute measurements of the fluorescence spillover of one fluorochrome into another detector. SOVs are based upon median fluorescence measurements, which are gain (i.e., PMT voltage) dependent. That means that when you change the PMT voltage on a detector, the SOVs associated with that detector will change. However, the actual spillover of fluorescence from one detector into another is unchanged. So you cannot ask "Why is the SOV on my instrument different than the lab next door?" without knowing the PMT voltages. The single most important fact to remember is "Changing the PMT voltage on an instrument will change the SOVs but it has absolutely no impact on the actual florescence spillover and its associated spread and *does not* affect the quality of the data."

1.6 What is "good enough" accuracy for SOVs?

Using the right compensation controls under the right conditions will maximize the accuracy of your spillover values. Still, no matter which controls are used, it is likely that there will be some error in some of the SOV measurements you make. This brings up the final question of what SOV accuracy is good enough to provide you quality data. The honest answer is that "it depends." It depends upon the design of your assay, the fluorochromes used, and the density of the antigens being analyzed. Any error in the final data is directly proportional to both the error in the SOV measurement and the brightness (MdFI) of the population being analyzed. This is demonstrated in Fig. 9. In the assay represented in the top panels, the Brilliant Violet^{TM} (BV) 510 positive population is somewhat duller (MdFI $\sim$6000). In this situation, small ($\pm$2%) errors in the BV510 into BV605 detector do not significantly affect the error in the MdFI in the BV605 detector ($\sim\pm$100).

The situation in the assay shown in the bottom panels is quite different. The BV510 positive population is quite bright (MdFI $\sim$68 000). Identical errors (i.e., $\pm$2%) in the BV510 $\rightarrow$ BV605 SOV results in truly BV605 negative populations appearing to be positive (BV605 MdFI errors of $\pm$1300). The MdFI error in the spillover detector (here BV605) = the MdFI of the population in the primary detector (BV510) $\times$ the %error in the SOV. Therefore, an "acceptable" error in the SOV for one assay (e.g., the top panels) may be quite unacceptable for another (the bottom panels). This is again why it is important to pretest your compensation controls to better understand and manage any potential errors that can impact the quality of the final assay.

In conclusion, with an understanding of the concepts of compensation/fluorescence spillover and following a simple set of principles when using compensation controls, it should be relatively easy to obtain and present high quality multicolor flow cytometry data.

2 Maintenance

Flow cytometric experiments produce relative data and they are strictly dependent on the actual context of measurement (e.g., sample quality, reagent quality, or instrument performance). To get comparable results over time, each single step of a flow cytometry experiment needs to be controlled. This section focuses on the instrument side and discusses important (preventive as well as some reactive) steps in maintaining flow cytometric instruments to ensure a constant quality level of measurement. Even if several tips and tricks are mentioned, this section can only offer a basic selection of possibilities and options. For some maintenance steps, you need to have additional experience. In case of doubt, consult the technical support of the respective company.

2.1 Introduction

The signals generated by flow cytometric instruments are determined by many different factors, such as optical layout (laser and laser power, optical filter), sheath fluid, room climate, and so on. It is therefore a prerequisite to "know" the performance of the respective system at a certain time point. By using appropriate controls and standards, it is possible to define the original status of instrument performance and track it over time. This can be performed in different ways and depends upon the type of instrument (analyzer, cell sorter), the instrumental layout (number of lasers, high-throughput system (HTS)) and the type of measurement one wants to conduct (e.g., screening, diagnostic, qualitative vs. quantitative or volumetric tests). Due to an increasing diversity of available flow cytometers on the market, there is no common routine of conducting maintenance and also the time frames and maintenance intervals may vary from one instrument type to the other. While most of the manufacturers offer service contracts for their systems, the experienced user can do several things to prevent potential damage and maintain or restore the instrument's original level of performance. Be aware that for some steps during maintenance (e.g., laser alignment) additional precautions (e.g., wearing laser safety goggles) are necessary to accommodate for an altered hazardous potential (optical (high energy laser), biological, or electrical (high voltage)) compared to normal instrument operation. Those interventions should only be done by service engineers or specially trained users with the necessary risk assessment and personal protection equipment in place.

Maintaining a flow cytometer means retrieving information about the actual status of an instrument and comparing it to the original (ideal) situation. It should be ensured that the data have been collected under comparable conditions such as comparable laser warm up time (between 15 and 30 min), fluidic setup (using a primed system and choosing the same flow speed: low, medium, high), and event-rate. If the performance check fails, one needs to know how to bring it back to the original level (if possible). Below several options detailing how to check the performance of a flow cytometric instrument and what can be done as preventive mainentance procedures are described (summarized in Table 2).

2.2 Maintaining optical devices

Maintenance starts with cleaning the instrument. To prevent danger from laser radiation or electrical hazards, this can be done without switching on the cytometer. For example, it is necessary to remove dust from the ventilation systems to allow effective air-cooling of lasers and power supplies as well as from optical filters (BP, SP, and LP), (dichroic) mirrors, and prisms of the optical path. Dust will impair the laser-alignment and sensitivity of fluorescence signals by generating additional background and loss of fluorescence signals. These parts can be cleaned with unsoiled pressurized air (e.g., as used for electronic parts or computers) and more resistant dust can be carefully removed with cotton swaps or dust free paper wipes (moistened with a drop of pure methanol (e.g., those used in microscopy) as methanol will evaporate without leaving residues on the optics). How often these types of preventive maintenance have to be performed strictly depends on the environmental conditions and are sometimes included in

Table 2. Summary of options how to check the performance of a flow cytometric instrument and what can be done as a preventive procedure

System	Component	Observation/read out	Reason/maintenance	Frequency of checking
Optics	Laser/ LED/light source	Measured decline of power output	Exchange light source	As required
		High %rCVs (performance test failed)	Realign Optic	As required
		Weak or shifting signals	Laser Delay	Routinely
	Filter/beam Splitter	Performance fail	Wrong BP-filter	As required
			Ageing	Seldom
	PMT/diode/detector	Impaired Scatter or Fluorescence signals	Dust	Frequently
		When loss of sensitivity is observed	Sensitivity	Routinely
		Weak separation of dim populations	Linearity (define Min. Volt and Max. Volt to know the linear detection range of each detector)	After initial installation or changing components
Fluidics	Saline-Filter	Weak or no signals	Venting	Routinely
	Tubing/SIP	Unexpected scatter signals/high background	Replacement	Every 6 month
		High carry over between samples	Cleaning	After usage
		Unwanted dead cell staining for the sample	Bleaching	After usage of DNA-Dyes
	Flow cell/cuvette	No signals/Clog	Sonicate or exchange	As required
		Unexpected scatter signals/high background	Priming	As required
			Cleaning inside	As required
			Storage over night	After usage
	Pressure system	Unstable flow	Cleaning or replace sealing, if leaky	As required
	Bal Seal	No signals/sample tube is filling up	Replacement	Every 6 month
	Volumetric pump	Wrong cell counting	Replace tubing	As required/ bi-monthly
	Sheath tank		Refill	Routinely
	Waste TANK		Cleaning	2-3 times/ year
			Empty and Cleaning	Routinely
	HTS	Carry over between samples	Cleaning	After usage
		Stop during operation	Alignment	As required
Computer/ Software	Database	System is slowing down	Backup/Size control	Usage dependent
	Hard drive	System is slowing down	Defragmentation	Monthly
	Keyboard/mouse	Under special Biosafety conditions	Cleaning	After usage
Cell Sorting	Deflection plates	Spray in drop deflection	Cleaning	Routinely
	Camera optics	Additional scattering signals	Cleaning	Routinely
	ACDU	Poor plating efficiency	Adjustment	In front of sort
	Drop delay	Poor Yield, lower purity	Adjustment	In front of sort
	Nozzle	Unstable droplet break off	Cleaning or degas Sheath	As required
		Leakage	Exchange	Upon failure
		Unsterile sorting	Cleaning	As required
	Cuvette/flow cell	Additional background/lower sensitivity	Remove dust and salt	As required
	Cooling system	Bacterial growth in water bath	Cleaning and replacing water	1-2 times/year

Table 3. Summary of some critical parameters defining the optical performance of a flow cytometer

Parameter	A measure for …	Recommended Value
SD_{EN}	… electronical noise	as low as possible
%rCV	… Laser alignment	as low as possible
Q_r	… Detector efficiency	as high as possible
B_r	… the channel background	as low as possible
Signal to Noise ratio	… sensitivity of Detector	as high as possible

maintenance contracts of the vendors. Many flow cytometers' lasers are directed via glass fibers to the detection site and, therefore, are relative stable over time in their alignment. Other machines are equipped with fixed optical benches, making repetitive laser- and filter-alignment nearly obsolete. But in any case, it is important to check (or "know") the instrument status prior to the measurement.

The Cytometer Setup and Tracking (CS&T) module from Becton Dickinson (BD), available since software version DIVA 6.0, is an example, how instrument performance can be monitored over time (BD Cytometer Setup and Tracking Application Guide V3.0, [41]). The combination of software and the use of standardized beads make possible to retrieve critical parameters in one run. After installation through a service engineer or exchange of components (e.g., lasers, filters, or PMTs), the status of the instrument is documented in a so-called "baseline." A lot of information (not all of it is listed here) about the linear range of each PMT (important for proper measurement and compensation (see Chapter II Section 1.3 Measuring SOVs/compensation controls), electronic noise and background (B_r, SD_{EN}), detector efficiency (Q_r), as well as sensitivity (Peak ratio between negative and positive population) and quality of laser alignment (%rCV) is stored in this file. All the introduced values are summarized in Table 3 with a very brief explanation and are described in much greater detail elsewhere [42–51].

In a second step, the instrument performance can be tracked and compared to the baseline values by running the same lot of standard-beads at different time points. The software module is then reporting every observed change. In Fig. 10A, a typical result of a CS&T performance check is shown. A wrong BP filter in front of the PMT-detector resulted in a lower signal. As a consequence, the system needed a higher PMT-voltage (ΔV) to reach the defined target value for this particular channel. The change in ΔV was larger than the accepted range (which is as default value in CS&T ≤ 50 V) and instrument performance failed with notice to the user (red cross). On flow cytometers without a CS&T-option, a similar result can be achieved by using nearly any kind of standardized particles (e.g., Rainbow Beads, 6- or 8-Peak Beads, Calibrite®, CS&T Beads [41] or other fluorescent-labeled Beads). Instead of a "baseline," one has to generate a system-specific calibration containing all the fluorescent channels and parameters including a fluorescence channel of each available laser versus

time. At already suggested time-points, one is measuring the beads under defined settings and save this result as a (instrument specific) "standard." Future measurements with the same kind of beads (consider and document potential lot to lot variations over time) and the same instrument settings (see Chapter IV, Section 2.1) will allow a comparison to the first "standard" measurement and monitors changes in instrument performance. In Fig. 10B, a result for the same situation as described for the CS&T-option is shown. With the correct BP filter (510/50), the beads are falling inside the target values (positive peak of the blue curve is inside the brackets), whereas with a wrong BP filter (610/20), the instrument performance fails (red curve).

Having this kind of information for all parameters at various timepoints (every day or week) will give a good overview of the performance of the system. Tracking at least one fluorescent channel per laser over time gives additional information about the stream stability and indicates if air bubbles inside the system are causing problems. Displaying these plots during an experiment may help to reveal problems with sticky or unfiltered samples.

Beside the target channels, also the shape and width of the peaks are of importance and can indicate for instance a laser misalignment. As shown in Fig. 11A, the peak of the positive beads is still inside the defined target area, but the width (%rCV) is twice as big as the corresponding measurement during the standard performance (Fig. 11B). After realigning the laser, the shape of the peak and the %rCV value are again in the expected range.

The selected examples illustrate, that tracking an instrument performance is possible in different ways (8-Peak Beads, CS&T or fluorescent labeled beads, etc.) as long as one knows where to look at and to what instrument specific "standard" an actual result has to be compared to. As noted earlier, there are several additional parameters, which can be tracked (e.g., laser delay and area scaling factors), but with a correct standard setup, most of them can be accessed via appropriate bead measurements.

2.3 Maintaining the fluidic system

2.3.1 Sheath filters. The fluidic system of most flow cytometers is assembled with parts that need to be maintained on a regular basis. One has to ensure that the fluidic lines and filters are free of air bubbles. Entrapped air compresses differently than sheath fluid and can cause unstable ("dancing") fluorescence signals due to incorrect time calculation of the incoming signals. The more lasers a machine has, the less tolerant the system is against air bubbles or unstable compressed air supply. Sheath or saline filters therefore have to be vented on a daily basis and replaced every 6 months (most commonly suggested time interval by manufacturers). In machines without extra sheath supply (e.g., Guava EasyCyte, Partec/ Sysmex, Accuri etc.), air in the system will cause false values for volumetric cell counting or will lead to empty fcs-files without any measured event.
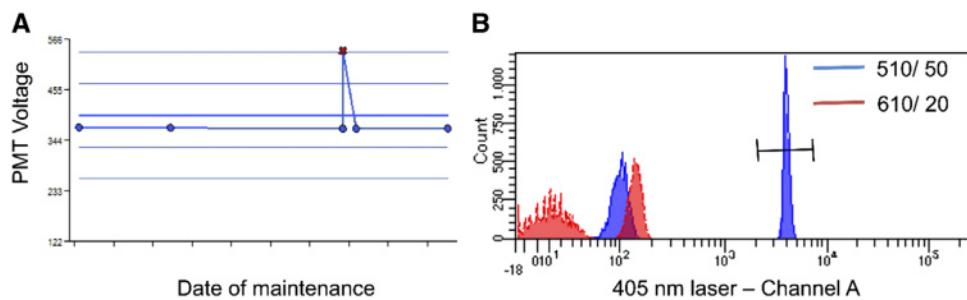
Figure 10. Examples for performance tracking with and without a CS&T module [130]. (A) A Levey-Jennings chart of a weekly measured performance for one parameter (out of 10) is shown. The cross in red indicates a failure in the performance check (a higher PMT-Voltage is needed to reach the target values of the beads, which corresponds to a loss of sensitivity). After checking and changing the band-pass filter in front of the corresponding PMT, the performance is measured again and is compared to the previous situation (blue dots). With the correct band-pass filter installed, the performance of the PMT is back to the previous level. The graph is taken from a CS&T-Cytometer Performance Report of a BD FAC-SCanto II equipped with 3 lasers. (B) The histogram of channel A of the violet 405 nm laser shows the corresponding measurement to the situation described above in (a) and is taken from a self-defined, instrument-specific calibration worksheet. The blue population represents the "standard" setup (with a 510/50 band-pass filter in front of the PMT of channel A, where the beads are reaching the respective target values (brackets). The red curve shows a measurement with a 610/20 nm band-pass filter instead. The beads are clearly outside the target values and the positive and negative populations are barely separated from each other. This is an example, how one can easily track basic instrument performance without having a separate software module available.

2.3.2 Sheath tanks.

Sheath tanks, especially when they are pressurized, have to be refilled and checked for leakiness on a frequent basis. Bal seals have to be replaced before they lose integrity. The consequences are similar to those described above for entrapped air bubbles. An additional consequence in cell sorters is an unstable droplet breakoff point, which is critically dependent on a constant and stable pressure (especially for nozzle sizes above 85 μm, see also Chapter I Section 1.4 Droplet generation of a cell sorter). Degasing Sheath tanks before usage can therefore improve the stability of the droplet formation in cell sorters.

To ensure sterile cell sorting, one has to clean/autoclave the sheath tanks on a regular basis. This goes in line with cleaning the sample injection port (SIP) and the sample tubing (see Table 2, Fluidics). Some machines offer semi-automated start-up and shut-down protocols, as well as cleaning routines one can run after a defined period of time or on demand [52]. In general, there are at least four basic protocols to maintain a fluidic system, depending on the intention of the cleaning:

- sterilization/decontamination,
- avoid crystallization for long-term storage (e.g., overnight),
- unclogging,
- and bleaching (get rid of cross-contaminating dyes).

2.3.3 Fluidic lines, SIP, and HTS.

For long-term storage, such as an overnight shutdown or prior to maintenance through a service engineer, most labs run a decontamination protocol followed by a wash cycle before they switch off the instrument (or hand it over to a service technician). The most commonly used solutions to decontaminate a flow cytometer are 1% sodium hypochlorite or 70–80% Ethanol. But freshly prepared 1% hydrogen peroxide can also be used. Distilled or deionized water is ideal for washing out the cleaning solution. To keep a machine in a "dormant"/unused state for a longer period of time (weeks/month), one could dry the tanks and system tubing completely after the cleaning process or flush all lines and tanks with distilled or deionized water (containing some preserving agents to prevent bacterial and fungal
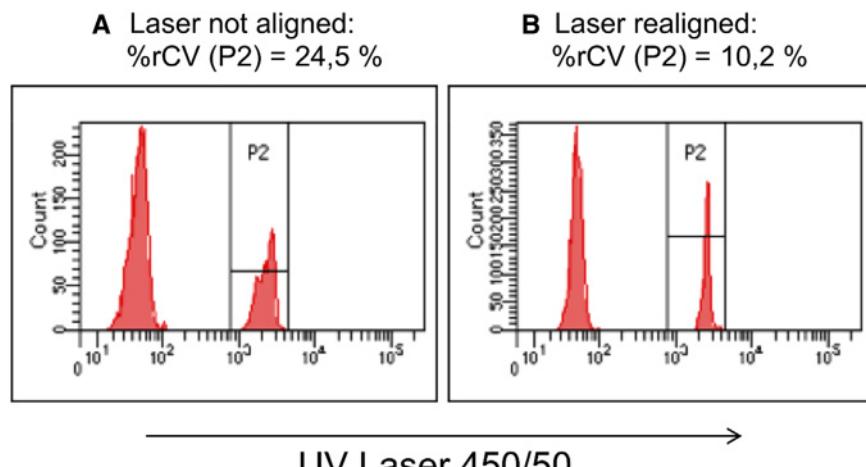
Figure 11. How one can detect suboptimal alignment of lasers. Both histograms display a negative and positive bead population in the 450/50 channel of the UV-Laser of a BD FAC-SAria SORP cell sorter. Although the positive peak in (A) still falls into the defined target area (brackets = P2), the shape and %CV of the peak suggest a suboptimal alignment of the UV-Laser. After realignment the shape of the positive peak become narrower with only the half of the %CV. (B) Laser-alignment is optimal, when the lowest %CV values are reached.

contamination). When possible, a sample tube containing water can be left at the SIP. All this is to ensure that no salt crystal formation occurs, which could subsequently cause clogging, even if the SIP or tubing were to dry out.

Sticky or clumpy cells, which are either not properly filtered or used at too high a cell concentration, could block the orifice of an instrument. In some (mostly pump driven) instruments (e.g., BD Accuri, Merck/Millipore Guava EasyCyte) one can reverse the direction of the fluidics to push the blockage backwards out of the tubing. Running a (prewarmed) detergent (e.g., FACSRinse) through the system for several minutes, followed by filtered deionized water or PBS, can help to release the obstraction in clogged SIP and/or sample lines. In machines where one can easily access and remove the SIP, sonication (in clean water) of the tubing is also an option (e.g., Guava EasyCyte). As a last option, one could use thin wires to clean the SIP, working like a sweeper cleaning a chimney. If an optional HTS or Carousel Module is available, the washing steps are even more important and fluidic parts and tubing should be changed like recommended from the vendor. The usage of fluorescent dyes such as PI, DAPI, or Acridine Orange (AO), which are used to stain nucleic acids (e.g., live/dead, cell cycle, or RNA–DNA ratio) makes an additional cleaning step necessary (because the use of AO can cause a lot of trouble, there are different alternatives available for many applications in which AO is used [e.g., lysotracker, Syto® dyes, and Pyronin Y]). These dyes are often stained in excess to ensure a good staining profile. Due to their planar structure, they are sticky and can also adhere to the tubing. Therefore, a high likelihood of cross-contaminating samples between different users exists. Running a bleaching solution (e.g., 1% sodium hypochlorite) for 5–10 min will prevent this. To check for efficient cleaning, run an unstained cell sample and observe in a bivariate plot (fluorescence channel of the dye (e.g., PI) versus time) if background of these cells is increasing over time. In that case additional cleaning is necessary.

In all situations, one has to be careful with the use of aggressive/corrosive solutions and make sure that they are washed out/replaced by the respective sheath fluid or distilled water and are not left inside the flow cell for an extended period of time (e.g., overnight) [53], as this could damage the tubing and sealing and end up in leakiness of the system.

Some flow cytometers (e.g., Accuri C6, Guava Easycyte, Attune Nxt, MACS®Quant, and CyFlow) allow volumetric measurement, which enables counting and direct calculating of the cell number and concentration of a sample. A prerequisite for accurate cell counting is also an air bubble and particle free (filtered) sheath fluid and intact sample lines. Mechanical stress makes it necessary to replace the tubing at appropriate intervals (e.g., a bimonthly change of the peristaltic pump tubing is recommended for the BD Accuri C6 system [54]).

2.3.4 Flow Cell/Cuvette.   The flow cell is part of the fluidic and optical system of a flow cytometer and is therefore included when performing a cleaning as described above. Nevertheless, some instruments (e.g., BD FACSAria cell sorter, BD FACSCanto II)

provide separate automated cleaning procedures to improve performance. For most instruments (e.g., FACSCalibur, LSRII, and Fortessa), there are also manual cleaning options, which will require separate training.

2.4 *Computer and software*

Beside the above-described maintenance steps to ensure proper function of a flow cytometer, the computer and software need some attention. Defragmentation of the computer's hard drive and backups of the FCS-files should be scheduled in a frequent way (weekly/monthly, depending on the usage). Where the FCS-files are organized in databases, one should take care that the size of the database does not exceed recommended size limits (e.g., ≤45% of available disk space for the BD FACSDiva Software [55]). This will impair and slow down at a certain time point the performance of the entire system. Using the implemented Data Manager software on BD instruments (at least once per month) reduces the size of the database log file and is improving the overall performance and stability of the DIVA software.

Although most flow cytometers on the market are very robust and reliable, there are still many things that need to be controlled. Table 2 summarizes many common steps to consider during instrument maintenance. As already mentioned, it depends on the instrument and environmental setup which steps have to be done in which frequency and the focus might vary from laboratory to laboratory. Therefore, it is an overview and a suggestion of procedures, which should help to get the best results out of your flow data. In any case of doubt, contact the reference guidelines and/or service engineers of your vendor to prevent damage from your system and to keep it in a good condition.

3 PMT voltage optimization

Correctly setting PMT voltage gains is essential to optimize signals and improve the resolution of dim populations. The aim is to bring signal out of the low end of the scale, which is dominated by electronic noise that will obscure dim events, without pushing bright events off the top of the scale.

Historically, many cytometry users set voltages by eye, often by placing an unstained population in the first decades of a log scale. However, this method is potentially problematic, particularly in channels with inherently low autofluorescence, such as those in the red spectrum. Alternatively, while it is possible to set voltages using stained cells on a per experiment basis this is time-consuming, uses valuable samples and lacks reproducibility. As a result, standardized methods to optimize voltages are required.

Due to their ability to provide consistent signals, fluorescent bead-based methods are an important step in PMT setup. Several approaches can be used. On BD instruments Cytometer setup and tracking (CS&T), an automated bead-based method is available [41]. In this case, CS&T beads are used in an automated fashion to obtain an initial baseline voltage optimization based on setting the
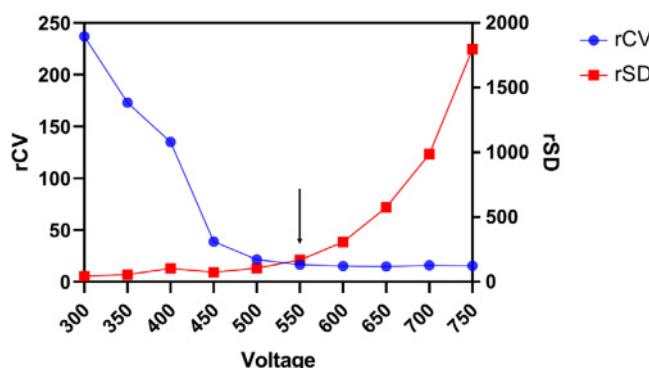
Figure 12. Voltage walk displaying rCV and rSD of the second peak of sperotech 8 peak rainbow calibration particles. The arrow indicates the point of minimal PMT voltage.

MdFI of dim beads to 10 times the robust standard deviation of the electronic noise (rSDen), essentially ensuring that electronic noise only contributes 10% or less of the signal. This allows setting of reproducible voltages in reference to a bead standard, but does not guarantee that the voltages are optimal for the biological samples being used in a particular experiment.

An alternative is a voltage walk approach in which a range of voltages are applied to beads to determine the point at which separation of an unstained and dim bead population is maximal, while also ensuring that the separation of highly stained bead populations is not altered. The level of separation can be determined via ratios such as M2 (separation of dimmest peak = MFI of the lowest positive peak/90th percentile of the negative bead) and M5 (separation of brightest peak) [48] or via calculation of the stain index [56]. A variant of this approach is the peak 2 method which also applies a voltage walk to a bead set containing a dim population [57]. This is used to find the point at which the robust CV (rCV) of the second peak, the dimmest positive population, is not reduced by further voltage increases. The rCV of dim particles directly corresponds to the resolution sensitivity [58]. This point also coincides with the point at which the standard deviation begins to increase (Figure 12). A disadvantage here is that the exact point to choose is subjective and differing bead sets may have differing levels of separation of the peak 2 beads, affecting sensitivity.

While bead-based methods are effective at determining minimal voltage requirements and tracking reproducibility, some further optimization may be required to determine optimal settings for particular biological samples. In some cases, it may be found that the minimum voltage determined by beads causes highly stained cells to be off scale or above the linear maximum. In this case, it is essential to reduce the voltage in order to obtain reliable results from these cells since data outside the linear range will result in compensation errors. If this occurs regularly, switching to a dimmer fluorochrome for the highly stained marker or adjusting staining protocols may be a better solution to preserve resolution of dim populations for this channel. Another source of variation in optimal PMT voltages is the difference in the level of autofluorescence in a cell population and the calibration beads.

One method to deal with this is to use the BD application settings [59]. To ensure that electronic noise does not have a major influence on the resolution of dim populations, unstained cells can be run and the PMT gain adjusted until the population has an rSDen of 2.5 times baseline. This will effectively balance the autofluorescence of the population on the outer edge of the electronic noise meaning that dim signals should be resolvable and define the minimal acceptable voltage. BD application settings are able to save these cell population optimized values in reference to CS&T baseline values so that they can be automatically adjusted in reference to any ΔPMT between CS&T baseline and CS&T daily performance checks. On non-BD instruments, it is also possible to carry out these daily adjustments if the electronic noise of the instrument has been determined by the user or by using a voltage walk approach to define optimal separation distances of measured populations and then saving these values in reference to a corresponding MdFI of a bead population at the same voltage [48].

In summary, the goal of PMT voltage optimization is to initially determine the settings with optimal sensitivity and then reproduce them on a daily basis. It is important to note that the aim is not to reuse the same voltage value but rather to optimize the voltage each time to ensure the same signal. While multiple methods are available, most conform to a similar basic structure: 1) initial setup using a control population (normally a bead control) to determine reproducible minimum voltage requirements; 2) validation and if needed, further optimization of settings for relevant biological samples, to be saved in reference to the bead control; and 3) a daily check of the beads controls in order obtain the desired reference values and thus the optimal voltage. Importantly, while steps 1 and 2 may be initially time-consuming, baseline settings determined in this way should be robust for an instrument as long as it does not undergo significant configuration changes. Once this baseline is set, a relatively brief daily performance check can be used to ensure reproducibility and maintain optimal performance.

III Before you start: Reagent and sample preparation, experimental design

1 Controls: Determining positivity by eliminating false positives

1.1 *Introduction*

For antibodies, the desired way of binding is the specific binding of the antibody, i.e., via its antigen-binding site, to its antigen. However, antibodies can bind in another manner to cells, also deemed as "specific," by interaction with that cell's endogenous Fc receptors. A third possible interaction between antibodies and antigens is "nonspecific," and occurs through ionic and hydrophobic interactions between the two molecules ("stickiness"). It is of critical importance to exclude the latter two to be able to reliably

quantify antigen expression by immunofluorescence. Therefore, proper controls are essential in flow cytometry to determine background fluorescence and/or background staining, to distinguish false positivity from true staining and to quantitate "true" positivity as such. Antibodies, the most widely used staining reagents in flow cytometry, can bind a cell in many different manners.

1.2 Fluorescence spreading into the channel of interest: Fluorescence minus one controls

The first step in establishing what a positive signal should look like is to obtain a reference for the natural or background levels, autofluorescence, in that particular detection channel. For this purpose, a sample without the staining of interest should be acquired. In the case of multiparameter staining, this should be the fluorescence minus one (FMO) control. In the FMO control, all antibody conjugates in the experiment are included except the one that is controlled for. The FMO control provides a measure of the spread of fluorescence from the other staining parameters into the channel of interest, and is required to accurately determine the threshold for positive staining [60]. It does not, however, provide any measure of nonspecific binding.

1.3 Specificity of reagent for staining target: Biological controls

There are several methods to control for the specificity of antibody-mediated immunofluorescent staining, each of which confers varying degree of confidence. The most reliable, but often also the most difficult to obtain, control is a negative control consisting of cells that do not express the marker of interest. The negative control should be as similar as possible to the experimental sample to exclude differences due to autofluorescence, size, "stickiness," and so on. Such a negative control could be represented by using cell lines that do not usually express the marker of interest, and comparing these against cell lines engineered for ectopic overexpression of the marker, or by comparison to cells genetically deficient for the marker of interest, both of which provide excellent controls for establishing staining protocols and for testing staining specificity. Depending on the nature of the marker of interest, the comparison to activated versus non-activated cells may be suitable if markers dependent on activation are analyzed, although one has to consider that activation may also change properties of the cell, such as its size and shape, which may also increase the inherent autofluorescence or unspecific staining. The use of internal controls, by staining additional markers to identify cells not expressing the marker of interest within the same sample, e.g., using CD8^{+} T cells as a negative control for CD4^{+} T-cell-specific markers, or CD19^{+} B cells when examining CD3^{+} T cell-specific markers, should also be considered.

1.4 Specificity of reagent for staining target: Blocking and isotype controls

In cases where biological negative controls are not available or difficult to come by, blocking controls can also provide an excellent measure of unspecific binding. Specific binding is blockable, i.e., loss of staining by the fluorescently labeled antibody after the addition of either excess soluble antigen or unlabeled antibody, both of which block the specific interaction of the staining antibody with its cognate antigen. Unlabeled blocking antibody must recognize the same antigenic epitope with comparable affinity of the labeled antibody whose specificity has to be verified. Ideally the same antibody clone should be used. Any positive signals still detected despite the use of blocking controls indicate that unspecific binding due to ionic and hydrophobic interactions of the antibody or the fluorochrome has occurred. When using these controls, however, one has to be aware that blocking controls do not exclude cross-reactivity of the staining antibody to other antigens. Normal human serum (10% in PBS with an optional addition of 0.5% BSA) can be used to block the binding of labeled antibodies to FcγR when human cells (particularly B cells or myeloid cells, i.e., monocytes, dendritic cells, and macrophages) are analyzed.

Probably the most widely used staining control, the isotype control, is of limited use in determining the threshold of positivity/level of background fluorescence due to unspecific binding. The rationale behind using isotype controls is the assumption that unspecific staining is due to the isotype of the antibody. As a matter of fact, positive staining with isotype controls may be an indication that antibodies bind via Fc receptors to the cell. In that case, Fc receptor blocking reagents should be used to prevent such an interaction [61]. However, isotype controls are by nature different reagents than the staining antibody, with a different amino acid composition in the variable region, different numbers of fluorochromes bound to the antibody, and different concentrations, and, thus, have different "unspecific" binding properties. Therefore, a negative staining with the isotype control does not infer that the staining one observes with the experimental antibody is specific.

2 Titration: Determining optimal reagent concentration

Before any experiment, it is good practice to validate and optimize the reagents used. In flow cytometry, these reagents are generally specific antibodies used to detect and quantify proteins on single cells. Using too much or too little of the staining reagent will result in increased unspecific staining, decreased SNR, decreased sensitivity, lack of linearity between level of expression and staining intensity, and increased experimental costs. Thus, it cannot be stressed enough that determining the optimal concentration of antibodies for your experiment is of utmost importance. The optimal concentration or "titer" of an antibody or any other staining reagent has to be determined empirically for target and your staining condition (i.e., staining time and temperature), and for
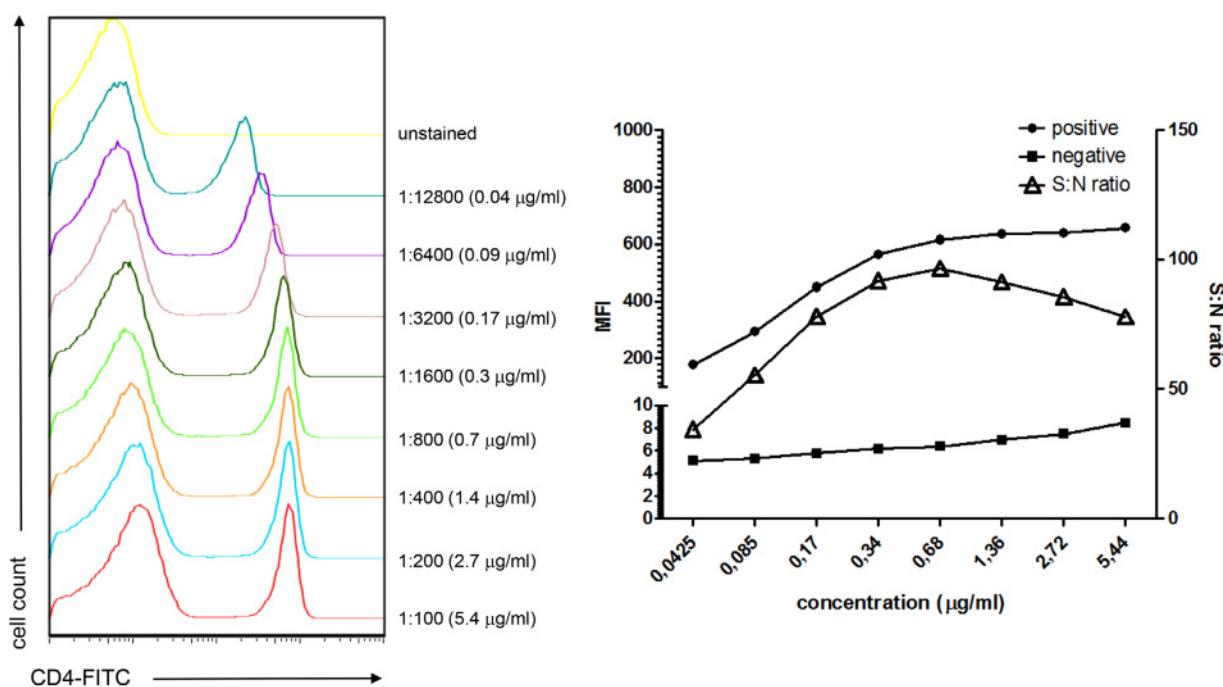
Figure 13. Titration of a CD4 mAb (clone GK1.5) conjugated to FITC and titrated on murine splenocytes. The antibody was titrated in 1:2 dilution steps starting from a 1:100 dilution (5.4 µg/mL) up to 1:12 800 (0.04 µg/mL). (A) Histograms of the stained samples are shown. (B) MFI of the positive and negative populations (left axis) and SNR between the positive and negative populations (right axis) are plotted. Best separating titer for this particular antibody was determined to be 0.7 µg/mL (1:800 dilution).

every new batch of staining reagent for that matter. Live cells may have a different staining optimum than fixed cells, proteins stained on the cell surface different than the same protein stained intracellularly. As it is very improbable that commercial reagents have been tested on your particular experimental conditions, they should also always be titrated rather than being used at the manufacturer's recommended titer or concentration.

To determine the optimal titer for the staining antibody it is recommended to make a serial dilution of the antibody. If it is not known from which concentration to start from, a generic starting point is 10 µg/mL of antibody, which is then serially diluted 1:2 for six to eight dilution steps. The number of cells used for the titration should be orientated toward the number of cells being stained in the actual experiment. However, while the number of cells affects the staining quality, staining tends to be quite robust within quite a large density range, e.g., 10^5–5×10^6 cells. Once titrated, an antibody concentration generally gives comparable staining quality within a ten- to 50-fold range of cell concentrations. If cell concentrations are increased by more than that, it is usually sufficient to increase antibody concentrations by two- to threefold, or to make a quick two to three step titration.

Once a titration series has been made, there are several ways to evaluate the data to determine the optimal titer. The simplest method is to calculate the ratio of the MFI of the positive population (stained by the CD4 mAb) to the MFI of the negative population, i.e., the SNR (Fig. 13A and B). It should be taken into consideration that the applied gates for the negative and positive

population will have to be adjusted for each sample in the titration series. The titer for the best separation will be the one with the highest SNR (Fig. 13B), i.e., in this case 0.68 µg/mL or a 1:800 dilution of the original antibody stock.

One can also consider the lowest antibody concentration that gives near maximum signal. This will be the concentration at which staining is saturating and most robust toward changes in cell number, staining time, and temperature. Other methods to assess optimal staining by determining the staining index are described here [62]:

Additional aspects to consider are

1. When using antibodies, it is the concentration of the antibody which is the critical parameter, i.e., when upscaling an experiment to stain in a bigger volume, increase the amount of antibody correspondingly to keep the concentration the same.
2. When titrating an antibody, make sure you have a population that does not express the antigen of interest; this helps to correctly assess background staining. If there are no "negative" cells in the population, consider spiking in cells.
3. Once an optimal titer has been determined, indicate the concentration of the staining antibody for optimal staining, and not the dilution factor, when it comes to publishing your results.
4. If possible, use counterstains to identify subsets of cells that coexpress or do not coexpress the marker you are titrating for.

This will help determine/confirm the specificity of the titrated antibody.

3 Preparation of single-cell suspensions

3.1 *Introduction*

The fluidic nature of counting in flow cytometry requires single-cell suspensions. If cells from either solid tissue or an adherent cell culture have to be analyzed, a disintegration of the tissue or the cell layer into single cells is an absolute prerequisite for any flow analysis.

Techniques for the disaggregation of tissue into single cells are very old with most of the basic protocols being from the 1980s or 1990s. Since flow cytometry was first developed, it has always been of great importance to measure cells not only from a suspension culture but also from adherent cell cultures or from solid tissue. In particular, in tumor research, disaggregation of the tissue has to be done carefully for the application of flow cytometry. Nonetheless, despite all the protocols and even some automatic disaggregation systems, disaggregation is still a process that has to be optimized specifically for each tissue in order to get the best possible results. A high degree of standardization can be maintained in the cytometric laboratory using automatic processing machines from industrial companies. For non-automated protocols, companies provide a large variety of special enzymes and protocols for enzymatic digestion.

The protocol for cell preparation depends strongly on the cellular properties that are under study. These staining targets could either be markers on the cell surface, in the cell plasma, or in the nucleus. Alternatively, it could be DNA or RNA extracted from each cell after cell sorting.

With similar techniques, subcellular components such as nuclei, chromosomes, and mitochondria can be extracted either directly from the tissue or after disintegration.

The two main principles for dissociation of a tissue or an adherent cell culture into single cells are mechanical or enzymatic dissociation; however, the effect of the enzymes on each protein of interest needs to be determined, e.g., some cell surface proteins are cleaved by collagenase. Also note, just as a reminder, if unknown clinical material is to be analyzed, biological safety regulations have to be maintained.

3.2 *Mechanical disintegration*

From a tissue (e.g., solid tumors), a sufficient number of cells have to be extracted by applying mechanical forces. The tissue is generally placed into a Petri dish containing some growth medium and held by forceps. Using a scalpel, the tissue is then scraped and minced, as long as it takes until cells are released. The solution is then filtered to remove large tissue pieces and very gently centrifuged. The resulting pellet is resuspended in growth medium afterward.

3.3 *Enzymatic digestion*

For enzymatic digestion, very often trypsin and collagenase Type II are used. In addition, other commonly used enzymes include papain, elastase, pronase, hyaluronidase, and Dispase®. If the degree of ploidy has to be determined, as in the case of tissue from solid tumors, DNase I should be added to the cocktail to remove DNA from non-intact cells. The tissue is incubated in the enzyme solution, usually at 37°C for some time. This is followed by removing the enzymatic cocktail by centrifugation and resuspending the cells in medium.

It is advised after dissociation by either mechanical or enzymatic methods to determine the number of cells and their viability. An easy way of determining viability is to use a dye exclusion test with the classical Trypan blue test in a hemocytometer by visual microscopic inspection being the "gold standard." Use of either this test, or other dye exclusion tests with fluorescing dyes that can be assessed by flow cytometry are helpful to perform. Further information on establishing/controlling for viability is covered later in this article (Section III.4 Dead cell exclusion, cell viability, and sample freezing). After viability has been established, the cell suspension can be used directly for flow cytometric analysis or stored after fixation or freezing for later measurement.

In many published protocols, both mechanical and enzymatic methods of generating single-cell suspensions from original material are commonly combined and modified appropriately to give the best results in term of cell yield, cell viability, and integrity of aneuploid populations. A good representation of all kinds of cells in the sample after tissue dissociation is always aimed for; however, it can never be taken for granted that it is 100% and that the proportion of different cell types in the final sample resembles exactly their proportions in the tissue. Furthermore, the physiological state of the generated cell suspension may be different from that in the starting material.

3.4 *Special disaggregation techniques*

Two special disaggregation techniques deserve a mention and these are nuclei from paraffin-embedded tissue and nuclei and chromosome isolation.

3.4.1 Nuclei from paraffin-embedded tissue. The preparation of samples from paraffin-embedded sections for flow cytometry requires a different protocol from those described above. In clinical research, the flow cytometric analysis of cells from a paraffin-embedded section can be required, especially if backward screening of patients needs to be performed. Preparations of cell nuclei from paraffin sections are possible. In principle, a section cut from the paraffin block has to be dewaxed using a solvent such as xylene, followed by treatment with ethanol and water for rehydration. However, this can be a very lengthy procedure. Thereafter, DNA staining of the isolated nuclei with intercalating dyes can give reasonably good DNA histograms.

3.4.2 Nuclei and chromosome isolation. Pure cell nuclei and/or micronuclei can be isolated directly from most tissues and the protocols used for nuclei preparation for cells in suspension can be adopted. Excellent results from adherent cell cultures are possible even without using trypsination. The tissue is first treated with salt solutions containing a detergent and RNase. This is followed by treatment with an acidic sucrose solution. In this way, the cytoplasm is destroyed and nuclei are released [63]. In a very similar way, whole chromosomes can be isolated from metaphase cells and their DNA content can be measured with high precision. Even single chromosomes can be sorted based on their difference in DNA content.

3.5 Ensuring a single-cell suspension/removing oversized aggregates after extraction

For all disaggregation methods described, it is essential to ensure a single-cell suspension and to remove oversized aggregates after extraction. To do so, the suspensions should be filtered through a simple mesh (~30 to 50 μm) or a cell strainer to remove larger aggregates, which otherwise can clog the flow cytometer's nozzle or channel.

3.6 General comments

Once a protocol for a certain cell type and experiment has been developed, it is strongly recommended to always proceed in a highly standardized way. Automatic systems with high reproducibility provide mechanical as well as enzymatic tissue disaggregation in a more or less automatic process and may be advantageous in the routine cytometric laboratory. For a typical solid tissue, the cell yield is about 10^7 cells/mg material and it should be possible to achieve >50% viability in the isolated cells. What should not be underestimated, however, is the probability of perturbing cell surface structures and epitopes or disrupting the cell, which could occur in solid tissue disaggregation. In some cases, cell clumping, dramatically reducing the cellular yield, can be a big obstacle for a productive flow analysis.

Many protocols for tissue dissociation and cell isolation use a combination of the above procedures as one technique on its own may not deliver a high cell yield and cell viability. Alternative methods such as aspiration may also be used [64]. A successful protocol depends in general on the personal experience in the laboratory. It is also highly dependent on the amount of available tissue(s), the nature of the tissue, and the planned use of the material.

4 Dead cell exclusion, cell viability, and sample freezing

4.1 Exclude dead cells

The cell type and the isolation procedure from dissociated tissues or liquid samples will influence cellular integrity and viability. In principle, dead cells will increase background signals either caused by a general increase in autofluorescence or by an increased behavior to bind antibodies in a low-affinity and unspecific manner. Therefore, dead cells should be labeled by high affinity DNA stains such as PI, DAPI, or 7- ADD (7-amino-actinomycin D), so that they can be excluded by appropriate gating from further analysis (see live/dead discrimination see Section III.4 and Section V.2). In general, fluorochromes for discrimination of living and dead cells can be differentiated between those that passively integrate in the DNA of plasma membrane-permeable dead cells or those that were actively transported into living cells only. However, these probes are not applicable for intracellular analyses, since all cells have to be fixed and permeabilized before staining. For these purposes, fixable dead cell stains are available that bind to amines of proteins. These probes are available in a wide range of different fluorescence colors, and samples are to be stained first before applying the fixation and permeabilization protocol. An extensive overview of life/dead cell discrimination based on dye exclusion can be found in ref. [65].

4.2 DNA-binding dyes

The principle of identifying dead cells using DNA binding dyes is based on the concept that these dyes are impermeable to the plasma membrane and so cannot enter viable cells having intact membranes. Viable cells will exclude these dyes and therefore exhibit little to no fluorescence. Cell viability can therefore be assessed by incubating samples with a DNA dye such as PI or 7-AAD; dead cells will stain positively for either of these two nuclear dyes. It is important to be aware that dyes such as PI and 7-AAD can be taken up into viable cells over time, and so these stains should be added immediately (~10 min) prior to analysis, and the staining protocol should be standardized across the experiments. It is also important to note that DNA binding dyes cannot be used on fixed or permeabilized cells such as those that would be used in studies interrogating the expression of intracellular "targets" using intracellular flow cytometry.

For the analysis, a data acquisition region is placed around the positively stained cells, and color-eventing or "back gating" on the PI+ or 7-AAD+ cells present is used to identify most, but not all, dead cells as exhibiting lower FSC and higher SSC than viable cells. Although it is possible to gate around the viable cell population on the basis of their light scatter profile and use this for all subsequent samples, even if these samples do not include a viability indicator, by far the best method for excluding dead cells from data analysis is to use a vital DNA dye in all samples. Although common dyes used in multicolor analyses include PI, 7-AAD, TOPRO-3, pyronin Y(G) (PY(G)), and SYTOX, a plethora of options are now available from a range of commercial suppliers. A note of caution is that the broad emission spectrum of 7-AAD (600–750 nm at 20% normalized emission maximum) can result in a significant level of spectral overlap into other detectors and exclude its use in the context of other fluorochromes such as PE-Cy5, PerCP, and PerCP-

Cy5.5 in large multi-parameter panels. Furthermore, it is quite a "dim" (low quantum efficiency) fluorescent molecule when compared to PI, which is very "bright." However, the minimal spectral overlap between 7-AAD emission and that of fluorochromes such as FITC and PE can be useful in some instances. One will also need a compensation control for these dyes, and this could be generated by staining cells that have been heat treated (70°C, 30 min), or by leaving cells in isotonic saline without nutrition overnight.

Although these approaches use one of the fluorescent detection channels and thereby reduce the number of other parameters that can be interrogated, the issue of viability is an important one and the integrity of the experimental data and their interpretation should not be compromised by not including a viability stain in all experiments. The far-red viability dye DRAQ7TM (Biostatus Ltd., UK) is another viability dye that can be used in similar settings to PI and 7-AAD and allows the identification or exclusion of apoptotic, damaged, or dead cells. A particularly useful feature of DRAQ7TM is that its dual excitation using blue (488 nm) and red (633/638 nm) lasers and its emission at 650–800 nm allows multibeam excitation and the exclusion of dead (DRAQ7+) cells without "consuming" what could be a vital, and much needed, additional fluorescent channel [66, 67]. The advantages of the classical DNA-binding dyes are that this is a well-established approach that involves a short incubation at the end of the staining procedure, and that the reagents are of low cost. However, they are limited in their spectral (excitation, emission) characteristics and a significant disadvantage is that they are not suitable for experiments that are interrogating intracellular expression of relevant antigens that require fixation and permeabilization. A typical staining protocol involves the following:

1. Add 500 µL of cell suspension ($1–2 \times 10^6$ cells—unfixed) to a 12×75 mm polystyrene tube.
2. Add nuclear staining compound dissolved in PBS [PI: 5 µL, 200 µg/mL, 7-AAD: 4 µL, 250 µg/mL, TO-PRO-3: 4 µL, 250 µg/mL, or PY(G): 5 µL, 200 µg/mL] to tube.
3. Incubate cells on ice for at least 5 min.
4. Analyze cells by flow cytometry.

4.3 Protein-binding dyes

In some instances, the aim of the analysis will be to determine and compare the expression of intracellular molecules/proteins, in which case cells must be fixed and permeabilized in order to allow the probes and antibodies to enter the cells. The use of DNA binding dyes is inappropriate in these circumstances. In these instances, the use of dyes binding to the amine groups of proteins (amine-binding dyes), not DNA, is recommended.

The identification of nonviable cells under such circumstances can be achieved using products having varied fluorescence spectral properties such as the LIVE/DEAD‿ fixable range of products from Life Technologies, the eFluor™ fixable dyes from eBioscience, BioLegend's Zombie range of fixable dyes, Tonbo biosciences' Ghost Dyes™, and the Fixation and Dead Cell Discrimi-

nation Kit from Miltenyi Biotec. These dyes covalently react with protein so that the discrimination is completely preserved following fixation of the sample. It should be noted that these dyes are membrane impermeable and so will be internalized only by nonviable cells. However, the level of fluorescence emitted by viable cells (with which the dye has had access to only a few amines on the cell surface), and nonviable cells (in which the dye has had access to many more amines intracellularly) will be clearly distinguishable. A word of caution: it is crucial to ensure that staining protocols are performed in the absence of proteins in the staining buffer, to which the dye will bind. Experiments can be compensated using commercial amine-reactive beads or labeled and unlabeled cells.

4.4 Vital dyes

A third category of reagent that can be used for determining cell viability and cell death are the vital dyes. These dyes indicate viability by emitting fluorescence in response to metabolic activity in cells. Cellular esterases cleave the acetomethoxy group to yield calcein inside metabolically active cells. "Free" calcein binds intracellular calcium and fluoresces brightly green. Calcein AM dyes can be passively loaded into adherent and non-adherent cells. These cell-permeable esterase substrates serve as viability probes that measure both enzymatic activity, which is required to activate their fluorescence, and cell membrane integrity, which is required for intracellular retention of their fluorescent products. Available with blue, violet, and green fluorescence, these dyes are ideal for short-term staining (signals can be measured within 5 min, but once the AM group is cleaved, it can be actively transported out of the cell within a few hours) of live cells and can be used in multiplexed flow cytometry experiments. However, as the fluorescence generated by these dyes is driven by the presence of metabolic activity, it is not easy to include them in staining protocols that require fixation and permeabilization.

4.5 Dye-free approaches

As a sub-optimal alternative to the use of fluorescent stains, the light scatter properties of dying cells and cells undergoing apoptosis change and these can be detected by flow cytometry based on forward and side light scatter (FSc, SSc) properties. However, the nature of these changes and their detection will depend on the cells and the optical design of the instrument being used. Apoptotic or dying cells can therefore be identified without any staining by FSC and SSC parameters only. Reardon et al. [68] have extensively compared the use of light scatter- and fluorescence-based approaches for monitoring viability after freezing. Cells can also be stained for apoptotic markers (e.g., cleaved caspase-3 or cleaved-PARP). This works well for cells that are directly collected from growth culture or in vivo, as cells in these situations commonly die by apoptosis. These markers will not work for cells that die by necrosis, but such cells are more likely to have abnormal scatter.

4.6 Freezing cell samples

The freezing of cell samples offers the advantage of being able to monitor responses over a prolonged period and to manage longitudinal studies involving many patients and/or healthy donors/controls. Freezing of cells is also used when including samples taken at multiple sites and having them analyzed at a central laboratory. Freezing, therefore, facilitates the logistics of measurement, such as when only a few samples per day are to be analyzed and the simultaneous analysis of samples that have been collected at different times reduces the potential impact of experimental and analytical variabilities that can be introduced. Of course, all of these should be minimized by establishing standard operating procedures for the experimental set up and flow cytometric analyses and undertaking robust and regular quality control processes for the instrument.

However, even if precautions are taken, freezing cells inevitably influences cellular biology and key parameters that are likely to be a key element of the study such as viability, immunological capacity and responsiveness, and ability to be expanded in vitro. The properties of thawed cells might be significantly different to their freshly isolated counterparts. These potential issues and limitations therefore need to be taken into consideration. Whenever possible, one should determine the effect of freezing and thawing on the key biological and immunological readouts before embarking on an experimental program that stores frozen samples.

Maintaining the highest level of viability requires cells to be frozen in a cryoprotective solution. DMSO is a commonly used solution that, when used at a concentration between 5 and 10% v/v in an appropriate medium, retains a high level of viability after storage. One technical point to consider is that the best recovery is achieved with a gradual freezing process, i.e., lowering the temperature of the cells by 1 to 2°C/min. This procedure is intentionally slow in order to prevent the formation of ice crystals and cell rupture. Higher concentrations of DMSO (up to 10% v/v) allows faster freezing and has been shown to deliver 85% post-thaw viability, with some variability between different types of leukemia. Automatic freezing techniques using temperature-controlled setups have been developed for the routine cytometry laboratory. In these systems, the cell samples are slowly moved down a tank of liquid nitrogen by a motor-driven spindle. Commercially available cell freezers are the most suitable appliances for this process. However, manual methods have been widely reported to give adequate results.

The thawing process is as important as the freezing one and must be done very rapidly, with active thawing being preferential to a passive one. Active thawing and other steps in the thawing process have been evaluated for leukocytes by Hønge et al. [69]. It should be appreciated that different cell types respond differently to thawing, and this needs to be taken into consideration during experimental design. As an example, Alsayed et al. [70] reported that myeloid leukemia cells recovered better than lymphoid leukemia cells. Immunophenotyping is an important and frequently used method in risk assessment and post-

therapy follow-up in the clinical laboratory that requires a high degree of standardization and post-thaw viability tests in order to ensure that results are accurate and robust.

It is also possible to fix live cells and then freeze them. This is not appropriate for any setting where the cells need to be analyzed for function after thawing, if the main issue is one of logistics, fixing, and then freezing works well. One can use the Smart Tube System (Smart Tube Inc), or the fixing protocol published by Chow et al. [71].

5 Cell fixation and permeabilization for flow cytometric analyses

5.1 Introduction

The analysis of intracellular targets using flow cytometry (intracellular cytometry) presents a number of technical challenges that are not generally encountered in the measurement of cell surface epitopes, or in the measurement of dye uptake/processing (e.g., Calcein AM) in viable cells. In general, cells (in suspension) must be first "fixed" to preserve and maintain both the structure and location of target epitopes, then "permeabilized" to allow probe (e.g., antibodies) access—ideally to all cellular compartments (cytoplasm, mitochondria, ribosomes, nucleus, etc.).

In general, cell fixation is accomplished by the use of either crosslinking fixatives (e.g., formaldehyde, glutaraldehyde), or low molecular weight alcohols (methanol, ethanol), which generally act to "coagulate" proteins. Formaldehyde has the advantage of generally maintaining the overall conformation of the native protein. However, since formaldehyde generates multiple reactive sites on peptides, polysaccharides, and lipids, crosslinking can hide or sequester epitopes such that they are not freely accessible to antibody probes after fixation. An additional benefit of formaldehyde fixation in the study of posttranslational protein modifications (e.g., phosphorylation, methylation, acetylation, ubiquitination, etc.) is that formaldehyde appears to both "fix" the modification of target amino acids (serine, threonine, tyrosine), and also inhibits the degradation of these targets in living cells (e.g., phosphatase removal of phosphorylations, demethylase removal of methylations, and so on). In contrast, alcohol fixation generally results in poor detection of some (phospho-, and potentially other protein) modifications.

5.2 Fixation of whole blood specimens

Studies in the field of immunology frequently utilize peripheral blood, lymph node, or bone marrow cells, often with a preliminary purification step (Ficoll–Hypaque, hypotonic lysis, ammonium chloride) to remove red blood cells. In addition, preliminary purification techniques can remove potential target cell populations (e.g., loss of blasts using Ficoll–Hypaque). In this section, we will first cover fixation and permeabilization techniques for samples containing red blood cells, and subsequently cover fixa-

tion and permeabilization techniques for isolated cell populations (tissue culture cells, isolated lymphocytes, monocytes, etc.)

Following fixation, cell permeabilization is performed in order to gain access to the cell interior. This can be accomplished using either detergents (e.g., Triton X-100, NP-40) or saponifiers (e.g., Saponin), or with low molecular weight alcohols (methanol or ethanol). A complete discussion of the advantages and disadvantages of different approaches/reagents is beyond the scope of this guideline, but also see Chapter V section 15. Here, we focus on a fixation and permeabilization technique developed for use with clinical samples (whole blood, bone marrow) [71]. We set out to develop a technique that would allow the direct addition of fixative to clinical samples (to immediately "fix" phospho-epitopes and prevent dissociation of signaling inhibitors out of cells, which can result in rapid reversal of their inhibition). However, the addition of fixative directly to whole blood presented the problem of how to remove RBCs after fixation. We discovered that the addition of Triton X-100 at the appropriate concentration and time directly to the sample (still containing formaldehyde) achieved RBC lysis and WBC fixation without any significant loss of WBC populations. As a cautionary note, it is important that the incubation times are strictly followed.

As shown in Fig. 14, whole blood from a healthy human fixed using the formaldehyde/Triton X-100 technique shows three major populations using FSC versus SSC (lower panel). Here, the location of the monocyte population (blue) is determined using CD14. The separation of lymphocytes from monocytes by light scatter alone is sufficient to identify both populations; and as shown in the figure, the use of CD14 provides a good resolution of these cell types. The resolution of lymphocytes from cellular debris using light scatter alone, however, is problematic. The lysis of RBCs generates a significant amount of debris that overlaps with lymphocytes in light scatter measurement. However, as shown in Fig. 14 (top panel), staining the sample with CD45 allows clear resolution of CD45-positive/negative lymphocytes from CD45-positive/negative debris. The data shown here were generated after a single wash following the RBC lysis step. Use of additional washes at this point reduces debris significantly for most samples.

5.3 Materials

5.3.1 Staining whole human blood.

1. Fresh human whole blood (5–10 mL) collected in anticoagulant (K_2EDTA or sodium heparin).
2. Formaldehyde, 10% (methanol-free). Store at room temperature in the dark. Use within 6 months.
3. Triton X-100 detergent (e.g., Surfact-Amps[TM] X-100, Thermo Fisher). Prepare working solution by diluting 116 μL 10% aqueous Triton X-100 solution with 10 mL 1× PBS. Store stock and working solutions at room temperature. Working solution is stable for 1 month.
4. PBS, calcium- and magnesium-free, pH 7.4.
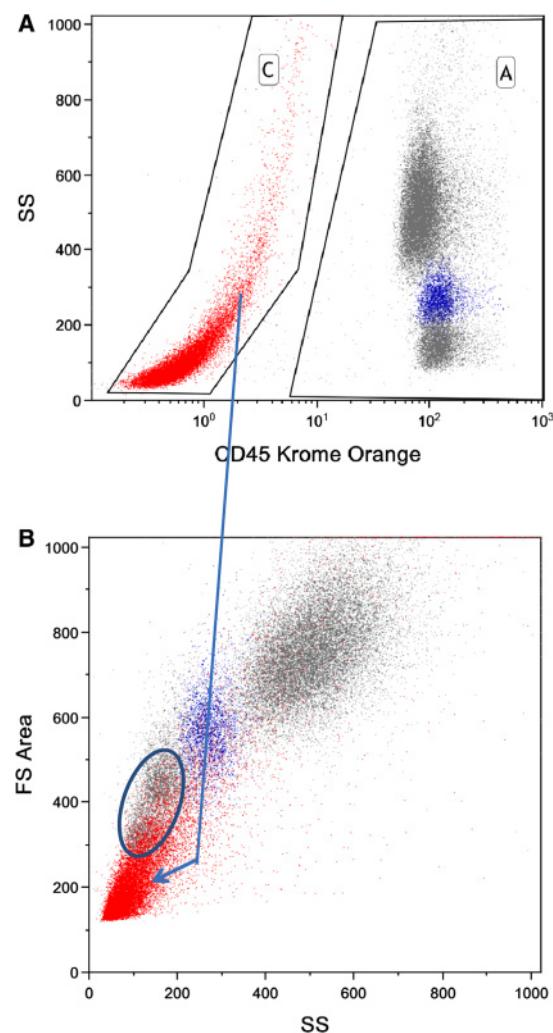
Figure 14. Human whole blood fixed with formaldehyde and permeabilized with TX-100. White blood cell populations were identified using CD14-PE-Cy7 and CD45-Krome Orange. Debris (red) is identified using CD45 versus SS (top panel—region C). Identification of peripheral blood monocytes (shown in blue in both panels) was accomplished using CD-14-PE-Cy7 (not shown).

5. Wash buffer—PBS/5% BSA (preferably protease-free BSA if also using for antibody dilutions).
6. Methanol—100% reagent grade, dilute to 50 or 80% with NaCl (final concentration 0.9%), store at –20°C; use at 4°C.

5.3.2 Procedure: Whole blood fixation and permeabilization.

1. Place anti-coagulated whole blood sample at 37°C and allow temperature to equilibrate.
2. For 100 μL whole blood sample, add 65 μL 10% formaldehyde, and immediately vortex. Incubate at room temperature (∼24°C) for exactly 10 min.
3. After exactly 10 min of incubation in formaldehyde at room temperature, add 1 mL of room temperature Triton working solution, vortex, and place in 37°C bath and set timer for 15 min.

4. Add 1 mL of cold (4°C) wash buffer and vortex. Centrifuge at 500 × g for 4 min.

5. Inspect tube for complete RBC lysis (rust red pellet, clear red supernatant—not turbid). If RBC lysis is incomplete, resuspend pellet in 1 mL Triton working solution at 37°C for an additional 15 min.

6. Remove supernatant, and wash pellet thrice using cold wash buffer (centrifuge at 500 × g).

7. For methanol treatment, slowly add 1 mL 4°C methanol solution (50 or 80% depending on target epitope) to the washed cell pellet while vortexing pellet. Incubate in ice for 10 min.

8. Centrifuge (500 × g) and wash pellet twice using 2 mL cold wash buffer.

9. After final centrifugation, carefully remove as much supernatant fluid as possible. Resuspend pellet by vortexing. Add antibody cocktail, incubate and wash twice with cold wash buffer.

10. Resuspend cell pellet in 0.5 mL wash buffer and analyze immediately on flow cytometer. For intracellular epitopes that degrade, or for samples that need to be analyzed more than 6 h after resuspension, resuspend in 0.1% paraformaldehyde in PBS. Store at 4°C in the dark until analysis.

5.4 Effect of methanol on epitope staining

Some intracellular or intranuclear epitopes remain poorly accessible to antibody probes after fixation and permeabilization using the formaldehyde–Triton technique described above. This is likely a limitation of all similar aldehyde–detergent (only) fixation and permeabilization techniques. In our experience, phospho-STAT proteins are largely undetected after this type of processing. However, treatment of the fixed and permeabilized cells with cold (4°C) methanol for 5–10 min "unmasks" these epitopes [71], although care must be taken to validate the effects of methanol treatment particularly when used post-staining and when using tandem dyes as described below. As shown in Fig. 15, treatment of fixed and permeabilized whole blood (activated using GM-CSF) with up to 50% cold methanol has minimal impact on the quality of P-STAT5 staining (same signal intensity for 50% methanol or untreated sample indicating almost no P-STAT5 staining, not shown). However, treatment with 80% cold methanol produces a significantly stronger P-STAT5 signal. The impact of treatment with methanol at both 50% (top) and 80% (bottom) concentrations on P-ERK and P-S6 staining (ribosomal S6 protein) is also shown in Fig. 15. Here, methanol treatment has minimal effect on the P-ERK signal intensity and reduces the P-S6 signal by about 20%. It is therefore important, when first developing and optimizing fixation and permeabilization for new cytoplasmic epitopes, to determine the impact of methanol treatment on all target epitopes that will be measured in the assay.

While methanol "unmasking" is important for the evaluation of some phospho-epitopes, it also has the effect of decreasing (or eliminating) the immunoreactivity of other important epitopes used to detect specific cell populations. In our experience, this is of
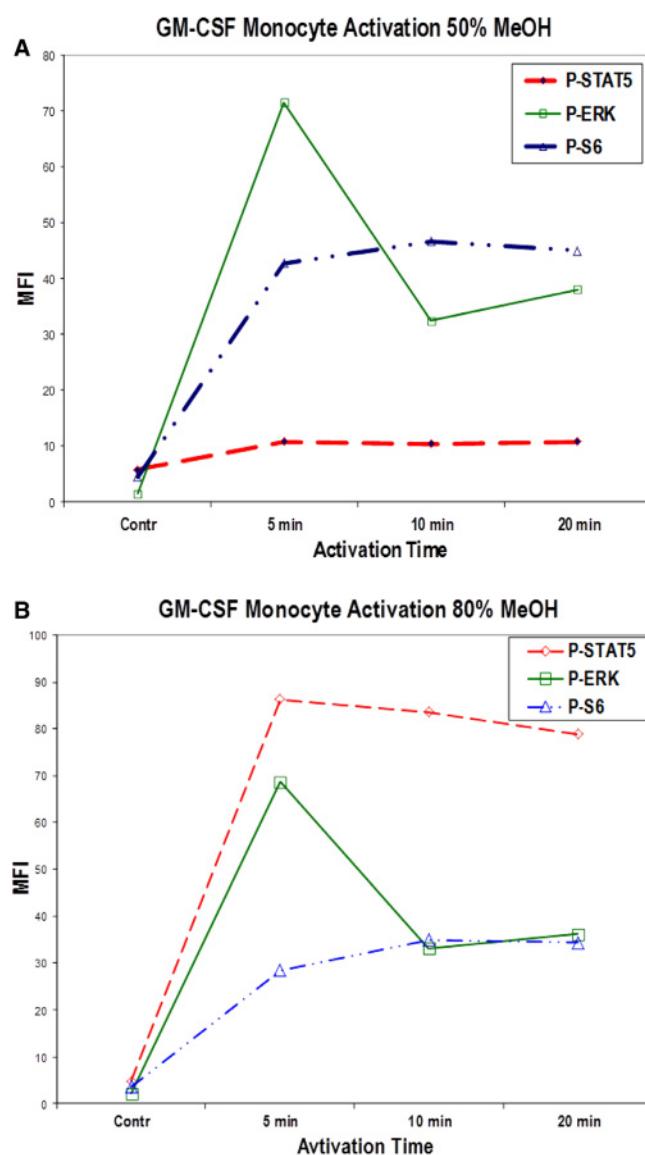
Figure 15. Impact of methanol concentration on P-STAT5 immunoreactivity in peripheral blood monocytes activated in vitro using GM-CSF. Whole blood from a normal donor was treated with GM-CSF for up to 20 min in vitro at 37°C. One part of the fixed and permeabilized samples was treated with 50% methanol (A) and the other with 80% methanol (B) at 4°C. After washing, all samples were stained with (·◇·) P-STAT5, (·□·) P-ERK, and (·△·) P-S6.

particular importance in the analysis of some myeloid–monocyte markers in human blood or bone marrow (CD14, CD33, CD64), and of less importance for stem-cell or progenitor cell markers (CD34, CD117). See ref. [72, 73] for details regarding cell surface CD markers that we have tested, which are effected by methanol treatment.

In the example illustrated in Fig. 16, we have compared the signal strength obtained when staining whole blood CD14-positive monocytes using either 50 or 80% cold methanol. In addition, in this study, cell surface CD14 was stained with a tandem dye
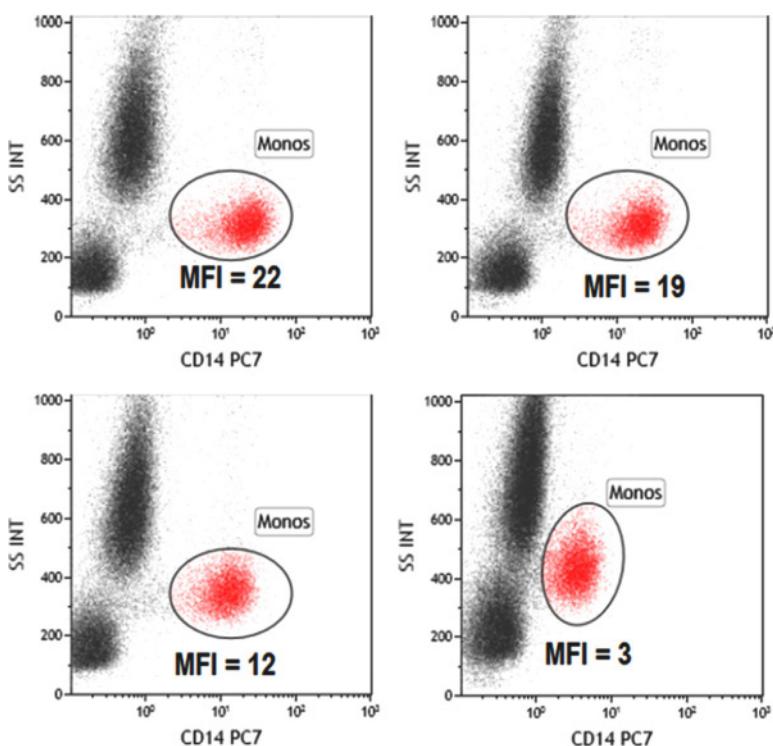
Figure 16. Effect of methanol treatment on CD14 staining of human peripheral blood monocytes. Whole blood samples from one individual were stained with CD-14-PE-Cy7 before (left panels) or after (right panels) fixation and permeabilization. Samples were treated with either 50% (top panels) or 80% (lower panels) methanol. See text for details.

(PE-Cy7) either before fixation and permeabilization (and prior to cold methanol treatment), or after fixation, permeabilization, and cold methanol treatment. Looking at the impact of 50% methanol treatment (upper panels), comparing the CD14 fluorescence intensity for monocytes labeled before or after fix-perm and methanol, the MFIs are very similar for cells labeled before or after fixation and subsequent treatment. In contrast, when considering the impact of pre- or post-fixation staining as shown in the lower panels, cells labeled with CD14 after fix-perm and 80% methanol (lower right panel) show a significant reduction in CD14 staining intensity (compared with that of cells stained after 50% cold methanol, top right). While cells stained with CD14 mAb before fix-perm and 80% cold methanol treatment (bottom left) show a fourfold higher MFI than cells stained after, they still show a 50–60% loss in CD14 staining intensity (relative to unfixed whole blood). Together, these data support the concept that the CD14 epitope detected by the antibody used here (BCI clone RMO52) is not affected significantly by treatment with 50% cold methanol, but is affected following 80% cold methanol. In addition, these data show that the antibody-conjugate is also impacted by 80% cold methanol (MFI is lower for cells stained following fix-perm and 80% methanol treatment). These data should reinforce the concept that all of the details of fixation–permeabilization and methanol treatment need to be validated for the complete set of antibody conjugates used for a new experiment. For more information regarding the use of pre- or post-staining peripheral blood in relation to intracellular and CD epitopes, see ref. [74]. This technique [74] has been utilized to stain both cell surface and intracellular epitopes for the analysis of MAP Kinase, STAT, and

ribosomal S6 signal transduction pathways in human bone marrow samples [72, 73].

5.5 Fixation and permeabilization for non-adherent tissue culture cell preparations

Routine fixation and permeabilization of tissue culture cells (anchorage-independent cell lines) is accomplished using formaldehyde fixation followed by permeabilization of cytoplasmic and nuclear membranes using absolute methanol. Although we routinely stain both cell surface and cytoplasmic or nuclear epitopes simultaneously, it is also possible to stain cell surface epitopes with some antibody conjugates prior to fixation and permeabilization [74]. This approach is particularly useful for cell surface markers that are altered (e.g., CD19) or destroyed (e.g. CD14, CD15, CD64) by fixation using alcohol treatment alone.

5.5.1 Determining optimal formaldehyde fixative concentration. Optimal detection of phospho-epitopes appears to be influenced by the formaldehyde concentration used to fix different types of cells. As shown in Fig. 17, P-STAT5 in K562 cells is optimally detected following treatment with 0.05 to ~0.4% formaldehyde (37°C for 10 min). Since the degree of potential epitope cross-linking/fixation is proportional to the formaldehyde concentration, incubation time, and temperature, all three of these variables should be controlled and performed identically each time. As shown in Fig. 17 at higher final formaldehyde concentrations, the P-STAT5 signal decreases, likely from overfixation,
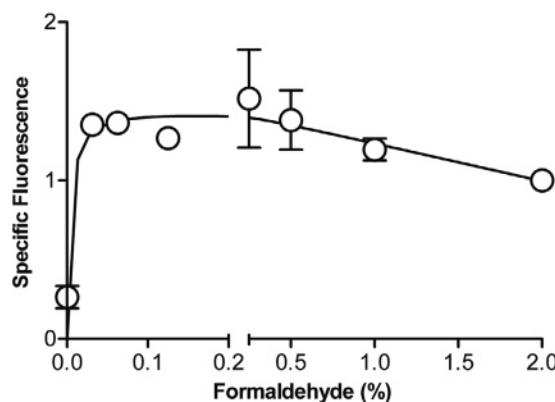
Figure 17. Effect of formaldehyde concentration on P-STAT5 immunoreactivity in K562 cells (reproduced from ref. [75] with permission). Cells were fixed at 37°C for 10 min using increasing final concentrations of formaldehyde, permeabilized, and stained with anti-P-STAT5-PE as described.

and limitation of phospho-epitope accessibility by antibody conjugates [75]. As also shown in Fig. 17, treatment with absolute methanol alone (no formaldehyde: first data point) results in a background level of signal.

5.5.2 Routine fixation, permeabilization, and antibody staining for non-adherent cultured cell preparations. For fixation and permeabilization of non-adherent tissue culture cells, we add the optimal formaldehyde concentration directly to sub-confluent cells (ideally re-fed 12–24 h prior to harvest) in tissue culture media (routinely containing 15–20% FBS), and return cells to the 37°C tissue culture incubator for 10 min. Cells are then centrifuged (400 × g for 10 min), and resuspended using a vortex mixer (note: cells are clumped at this point and require vigorous treatment with vortex to achieve resuspension of all cells). While vortexing, absolute methanol (stored at –20°C) is added with ~1 mL absolute methanol per 10^7 cells being added. At this point, the cells can be stored in a well-sealed container at –20°C for several weeks with no significant decrease in the detection of phospho-epitopes (epitopes tested thus far).

For staining of intracellular epitopes, place $3–5 × 10^6$ cells into each tube (we routinely perform staining of tissue culture cells in 1.2 mL microfuge tubes). Centrifuge tubes (for refrigerated microfuge, use 10 000 rpm for 12 s), carefully aspirate off supernatant, and resuspend the cell pellet in 1 mL cold (4°C) wash buffer (Dulbecco's PBS/5% FCS or Dulbecco's PBS/5% protease-free BSA) while vortexing. Place tube on ice for 5 min to allow buffer to equilibrate and remove residual alcohol. Centrifuge as above. Repeat and wash twice with cold wash buffer.

Carefully remove supernatant following the last centrifugation step, and resuspend cells in 100 μL of antibody conjugate (or antibody conjugate mixture). It is important that each antibody used is titrated to ensure optimal SNR. Incubate cells with antibody (or antibodies) on ice (4°C) in the dark (if using photosensitive conjugates) for 30 min.

Resuspend cells in 0.5 mL cold wash buffer for flow cytometry analysis (if cells are to be analyzed within 1–2 h). If cells will not be analyzed within 1–2 h, centrifuge the washed cells, and resuspend the cell pellet in cold PBS/0.1% paraformaldehyde. Cells post-fixed in 0.1% paraformaldehyde and stored at 4°C (dark) are stable (light scatter and phospho-epitope detection) for at least 24 h. It should be noted that the signal intensity of some phospho-epitopes start to decrease significantly within minutes of the final resuspension in cold wash buffer (e.g., P-S6). For these epitopes, it is strongly recommended to immediately place the cells in PBS/0.1% formaldehyde, which significantly decreases the rate of signal loss.
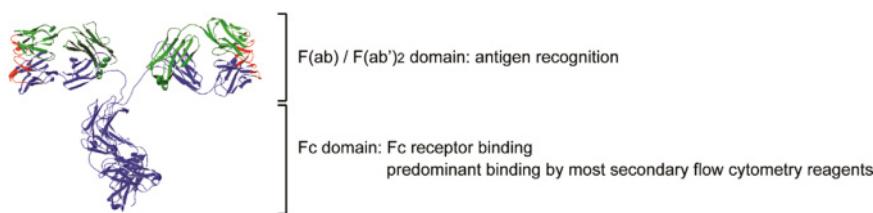
6 Variable lymphocyte receptor antibodies

6.1 *Overview*

Variable lymphocyte receptor antibodies of the evolutionarily distant jawless sea lamprey are structurally distinct from Igs of jawed vertebrates. They recognize antigens with a high degree of specificity and can be utilized in various biomedical research applications in which their unique antigen recognition characteristics complement conventional antibody panels. In this section, we provide a protocol for the use of these novel reagents in multicolor flow cytometry applications.

6.2 *Introduction*

The recently identified variable lymphocyte receptor (VLR) antigen receptors of jawless vertebrates have contributed greatly to our understanding of the evolution of the adaptive immune system [76]. Three VLR genes (VLRA, VLRB, and VLRC) have been described that are assembled by a gene conversion-like mechanism, and are expressed by cells reminiscent of αβ T cells, B cells, and γδ T cells, respectively, with VLRB being secreted in the form of disulfide-linked decameric complexes. Conventional antibodies utilize the Ig domain as the basic structural unit and are generated by recombination of the variable (V), diversity (D), and joining (J) gene segments for the antibody heavy chain and the V and J gene segments of the antibody light chain. As illustrated in Fig. 18, the resulting antibody consists of an F(ab)/F(ab')2 domain that engages the antigen primarily via interactions mediated by residues located in the complementarity determining regions (CDR) 1, 2, and 3 whereas the Fc domain allows for the communication with various cells of the immune system to elicit biological responses. The ability of antibodies to recognize their antigens with a very high degree of specificity and to label these reagents with fluorescent dyes makes antibodies the key component of most flow cytometric applications. Unlike conventional antibodies, VLR antibodies utilize the leucine-rich repeat (LRR) as a basic structural unit [77]; the resulting gene product assumes a solenoid shape (Fig. 19A), wherein the corresponding antigen interacts with residues located at the inner concave surface, and

Figure 18. Structural characteristics of Igs. Ribbon diagram of a mouse monoclonal IgG antibody consisting of two identical heavy and light chain proteins, respectively. Antibody heavy chain residues are indicated in blue and light chain residues in green. Amino acid residues encoding the CDR1, 2, and 3 regions are shown in red. (Image was generated using the Swiss PDB viewer and PDB accession number 1IGT).

with a variable loop structure protruding from the capping C-terminal LRR unit [78, 79]. VLR antibodies have become a novel class of highly specific biomedical research tools, by virtue of the vast VLR antibody repertoire. Interestingly, VLR antibodies appear to be particularly suited for the specific recognition of posttranslational protein modifications. Several monoclonal VLR antibodies recognizing carbohydrate moieties were described [80, 81] and recently our group reported the isolation of a monoclonal VLR antibody recognizing the HLA-I antigen in a tyrosine sulfation-dependent manner specifically on human memory B cells and plasma cells, a binding pattern distinct from those of any described conventional antibody [82]. The distinctive antigen recognition characteristics of these VLR antibodies indicate that the unique origins and protein architecture of VLR antibodies may permit binding to antigens that conventional antibodies may not readily recognize because of tolerogenic and/or structural constraints. An established protocol harnesses the expansive repertoire to generate antigen-specific monoclonal VLR antibodies with ready applicability in standard laboratory techniques such as flow cytometry and ELISAs [83].

Several research groups have used monoclonal VLR antibodies, either unmodified or engineered as Fc fusion proteins for purification using protein A/G columns and detection with a variety of commercially available reagents recognizing the IgG Fc domain. Alternatively, purification is also readily performed using Ni-columns targeting an engineered 6xHis epitope tag followed by detection of the VLR antibody with reagents specific for the incorporated HA-epitope tag (Fig. 19B). Here, we describe a protocol for use of VLR antibodies in multicolor flow cytometry analyses of human PBMCs in combination with conventional, directly labeled monoclonal antibodies. Depending on the type of VLR antibody used and the expression levels of the targeted antigen, a two-layer or three-layer staining approach can be used (see below for

protocol). The use of monoclonal VLR antibodies with engineered epitope tags or VLR-Fc fusion proteins permit a more efficient two-layer staining approach. The use of unmodified monoclonal VLR antibodies or experiments targeting antigens expressed at low levels require a three-layer staining approach since the established anti-VLRB monoclonal antibody 4C4 cannot be readily modified with common labeling systems that target primary amines. Several positive and negative control reagents for VLR-based experiments have been described [83, 85].

6.3 Experimental workflow and acquisition

6.3.1 Reagents.

* Fluorescently labeled anti-epitope tag or Fc-specific reagents are available from several commercial sources.
* Monoclonal mouse anti-VLRB clone 4C4 [86]. Note that this antibody is reactive with an epitope in the stalk region of all VLRB molecules, and it displays impaired antigen-binding characteristics following modification with amine-reactive dyes.
* Negative control monoclonal VLR4 antibody (specific for the BclA antigen of the exosporium of *B. anthracis* [83]).
* Positive control VLR32 antibody (specific for human CD5) [87] or VLRB MM3 antibody (specific for human CD38 on plasma cells) [85]. Suitable cell lines for testing of positive controls are the Jurkat T-cell leukemia and the Daudi Burkitt's lymphoma, respectively.

6.3.2 Two-layer staining approach.

* Incubate PBMC with monoclonal VLR antibody in PBS/0.5 BSA for 25 min on ice (v = 40 µL).
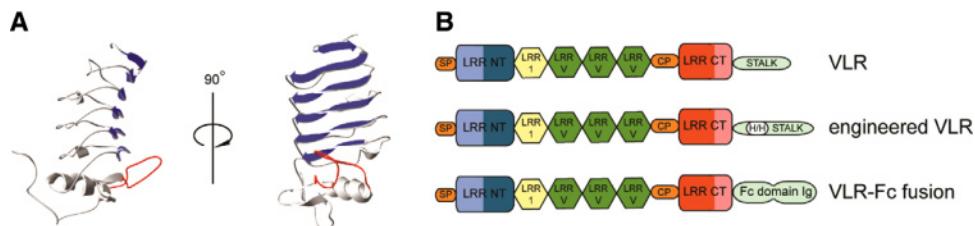
Figure 19. Structural characteristics of VLR antibodies. (A) Ribbon diagram of the antigen-binding units of a monoclonal VLR antibody. Parallel β-sheets lining the concave antigen-binding surface are shown in blue and a variable loop structure involved in antigen binding is depicted in red. The invariant stalk region necessary for multimerization of the secreted VLR antibody was omitted (Model was generated using the Protein Model Portal Algorithm [84]). (B) Structural characteristics of VLR antibodies. Individual VLRB units consist of a signal peptide, N-terminal LRR (LRR-NT), LRR-1, up to nine variable LRRv units, a connecting peptide, C-terminal capping LRR (LRR-CT) and the invariable stalk region and can be modified by inclusion of engineered 6xHis and HA-epitope tags or Fc-fusion sequences.

* Wash with PBS/0.5% BSA.
* Resuspend cells in antibody cocktail containing fluorescently labeled lineage-specific conventional monoclonal antibodies and fluorescently labeled anti-epitope tag antibodies (or anti-Fc antibodies if VLR-Fc fusion proteins are used), incubate for 15 min on ice.
* Wash twice with PBS/0.5% BSA.
* Resuspend in PBS/0.5% BSA/1 µg/mL PI and analyze by flow cytometry.

6.3.3 Three-layer staining approach.

* Incubate PBMC with monoclonal VLR antibody in PBS/0.5% BSA for 25 min on ice (v = 40 µL).
* Wash with PBS/0.5% BSA.
* Resuspend cells in PBS/0.5% BSA, add anti-VLRB clone 4C4 at a concentration of 1 µg/mL and incubate for 15 min on ice (v = 40 µL).
* Wash with PBS/0.5% BSA.
* Resuspend cells in PBS/0.5% BSA, add fluorescently labeled goat anti-mouse reagent (typically at a 1:300 dilution), incubate for 15 min on ice (v = 40 µL).
* Wash with PBS/0.5% BSA.
* Resuspend cells in PBS/0.5% BSA/5% normal mouse serum, incubate for 10 min on ice. (Blocking step, see "Pitfalls" below)
* Add antibody cocktail containing fluorescently labeled lineage-specific conventional mAbs, continue incubation for 15 min on ice.
* Wash twice with PBS/0.5% BSA.
* Resuspend in PBS/0.5% BSA/1 µg/mL PI and analyze by flow cytometry.

As is the case with all conventional antibodies, monoclonal VLR reagents must be titrated prior to use and 2 µg/mL serves well as a starting point. While background signals with the negative control VLR4 are not typically observed, negative control stains lacking any VLR antibody, in addition to negative controls or the various conventional antibodies, should be routinely included.

6.4 Pitfalls

Potential omission of blocking step in three-layer staining approach. This blocking step is important to prevent binding of directly labeled antibodies from the next incubation step to potentially unoccupied binding sites of the goat anti-mouse reagent from the previous step.

7 New antibody reagents

As discussed earlier in this chapter, the determination of specific binding of antibodies to antigens and Fcγ receptors as well as nonspecific antibody binding to cells can be difficult. Furthermore, the critical role of antibodies and their limitations are known and published [88]. Therefore, to improve the data reliability in these respects, further advanced technologies are desirable and various antibody products with improved characteristics are available. A few of them are discussed here.

Miltenyi Biotec developed the REAfinity antibodies. These are recombinant antibodies, which are engineered by cloning of the antibody-binding region of mouse or rat mAbs with the human IgG1 Fc region. The construct is expressed in a mammalian cell line under standardized conditions. To eliminate any binding of the recombinant antibodies to the Fcγ receptors, the Fc region of the antibody is mutated suggesting that no blocking of the Fcγ receptor binding sites on the target cell surface is necessary. Since all recombinant antibodies are derived from human IgG1, the same isotype control antibody can be used to prove that there is no binding of any REAfinity antibody to the Fcγ receptors on target cells. Additional advantages are proposed to be a very high antibody purity and a very good lot-to-lot consistency due to the standardized antibody expression by the used cell lines. Other companies, such as Enzo Lifesciences, provide recombinant antibodies as well.

Another type of antibodies without any reactivity to mammalian Fcγ receptors is the chicken IgY [89], making it an alternative to be considered for improving data accuracy. One more possibility to reduce error sources, when analyzing cells with high multiparameter panels, is the use of the Duraclone system provided by Beckman Coulter. These are pre-formulated antibody panels, which are unitized and dry, allowing an easy work flow, since no pipetting and antibody mixing is necessary. To perform the staining, the cell suspension (e.g., a sample of whole blood) needs to be added to the lyophilized antibody mixture. Due to that standardization, a reduced staining variability can be expected. Additionally, the panel does not need to be developed, in contrast leading to a reduced flexibility, although drop-in markers are provided. Solutions to stain samples for compensation are included in the available kits.

Another technology to be mentioned here, because it allows a huge flexibility (especially if a primary conjugated antibody fluorochrome combination is not available) is the Zenon labeling system by Thermo Fisher Scientific. It consists of Fab fragments conjugated with fluorochromes, which target the Fc region of primary, non-conjugated antibodies. The creation of that complex can be performed with very small amounts and it is very fast. It needs only some minutes, although remaining unbound Fab fragments should be captured afterward by addition of nonspecific IgG. Also, the ratio between the Fab fragments and the primary antibody needs to be titrated to obtain the desired degree of binding and therefore the staining intensity. After staining the cells, a fixation based on aldehydes might be beneficial to preserve the staining and to prevent the transfer of Zenon labels from one antibody to another one. Since the Zenon labeled antibodies are significant bigger than directly labeled primary antibodies, there might be limitations when using them especially for intracellular staining.

It should be noted that this section should not be understood as an advertisement to specific products. Rather it is an incomplete selection of some materials on the market to get an overview about different systems. Other related or comparable products, which are not discussed here, are offered by various companies. Nevertheless, the discussed materials might help improving the data quality. However, irrespectively which of the discussed techniques are used, the researcher needs to gain an impression if the used material will indeed help to create more accurate results. Furthermore, the same controls, as stated above, should be considered to ensure the reliability of the obtained data.

Figure 20. In cell sorting experiments one often needs to find a compromise between purity, yield, and time, which cannot be optimized all at the same time.

IV Cell sorting

1 Pre-enrichment of low abundant cell populations prior to acquisition/cell sorting

1.1 *Introduction*

One of the major advantages of flow cytometry is the capability to measure multiple parameters per cell with a speed of several thousand cells per second. This allows the measurement and detection of rare cell populations with frequencies below one in one million cells ($1/1 \times 10^6$). But even with this relatively high number of cells analyzed per second, a lot of time is required to acquire a significant number of rare cells for statistical analysis. Assuming a frequency of one cell of interest per 1×10^6 cells in a given sample, one would need to acquire a minimum of 1×10^9 cells to have at least 10^3 cells of interest at the end of acquisition. The average acquisition speed of many flow cytometric analyzers, at which they will detect and acquire all incoming signals without significant loss due to coincident or electronic aborts, is around 10^4 cells/s. It would therefore take more than 24 h to acquire enough of the described sample in order to reach the 1000 cells of interest.

While this time calculation is basically true for many available flow cytometric analyzers, for cell sorting, the time calculation is different. Here, additional parameters come into focus. In common flow cytometers that hydrodynamically focus the cells in front of the laser intersection point (point of fluorescence detection, see Chapter I Section 1.2 Hydrodynamic focusing), the speed of the carrier stream is given by the system and only the volume of sample running through per time can be adjusted by the user. In contrast, the fluidic of most cell sorters is more variable and allows adjustments of speed and flow-through volumes at various steps (both on the sample and instrument side). In many cell sorting experiments, there is a demand to maximize both the yield and purity of the sorted cells and minimize the time you need to run your cells through a machine. Yield and purity influence each other and are both dependent on the speed (cells running through a sorter per second) and the frequency of cells of interest (see Chapter IV, Section 2.1). Unfortunately, they cannot be max-

imized both at the same time. The less abundant a cell population is, the lower the speed of sorting has to be, in order to ensure a high yield with an acceptable purity (>95%). If you speed up (increase the number of cells running through the machine per time), your yield will drop significantly (up to 50% in some cases) or alternatively, the purity is sacrificed for a higher yield obtained in a shorter period of time (see Fig. 20). Therefore, sorting 1000 rare cells with high purity could last twice as long as the acquisition only (the relation between speed, frequency of cells, yield, and purity are discussed in more detail in Chapter IV, Section 2.1). This crude calculation only accounts for the time needed for acquisition and cell sorting; not counted is the time already invested in preparing and staining the cells (see, e.g., Chapter III, Section 3).
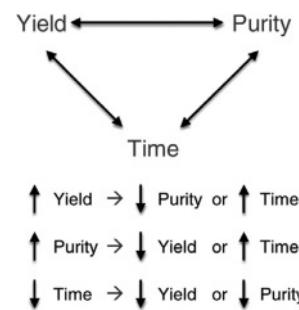
Given that flow cytometry as a method allows the identification and quantification of individual cells within a given population and given that in cell sorting this decision takes even more time, thereby slowing down the process, it is obvious that enumeration/evaluation of every single event especially of samples with large cell numbers prior to sorting is not a practicable way to go about analysis and sorting of rare cell populations. How then can we achieve acceptable work times and make it possible to analyze those rare cell populations?

We need a reduction in workload, meaning a reduction of the amount of cells that need to be measured in the flow cytometer. One way to overcome this situation is to get rid of as many "unwanted" cells as possible prior to acquisition, in the form of pre-enrichment. Cells can be separated from each other in many different ways and some methods of pre-enriching rare cells before flow cytometric analysis are discussed below. Because same pre-enriching techniques can be used as stand-alone bulk sorting approaches, the following section complements the subsequent chapter about parallel cell sorting. Requirements and pitfalls analysing rare cells are discussed in Chapter V, Section 1.

In general, we can distinguish methods based on physical properties (such as density and size) or using immunological features (antibodies coated to beads or magnetic particles) as discussed in the following two sections.

1.2 Pre-enrichment by physical properties

Physical properties of cells may be exploited to enrich them. For instance, monocytes, macrophages, and dendritic cells within a mixed cellular population adhere to plastic and are in general adherent within the first 2 h of being incubated on a Petri dish. Cells other than macrophages and dendritic cells can be removed and washed off with the supernatant. After longer incubation periods (≈20 h), dendritic cells start detaching from the plastic again. With this method, an enrichment of up to 70% could be reached for dendritic cells. This method is used in the process of generating and isolating dendritic cells out of monocytes and macrophages derived from blood or bone marrow [90, 91].

Another simple method to eliminate unwanted events is the lysis of red blood cells (see also Chapter IV, Section 2.5 and Fig. 22B), which are a common "contaminating element" in tissue preparations. In contrast to nucleated cells, erythrocytes burst upon brief exposure (<60 s) to a hypotonic medium (e.g., erythrocyte lysis buffer: 155 mM NH4Cl; 10 mM KHCO3; 100 mM EDTA). Remember that human and mouse erythrocytes differ in size and ability to resist hypotonic shock over time. Various buffers and protocols are available, which differ in temperature and exposure time, affecting lysis outcome. It is therefore necessary to adapt the lysing protocol to the experimental conditions ([92–94] and Chapter IV, Section 2.5).

Peripheral PBMCs can be enriched by density gradient centrifugation using Ficoll®. This biological inert polysaccharide allows the separation of PBMCs from plasma, granulocytes, and erythrocytes based on their cellular density (Fig. 21) (see also Section IV.2: Parallel cell sorting: 1.3.1 Ficoll-Paque™, Lymphoprep™).

While many users report a lower recovery (up to 10–15%) in the absolute numbers of target cells after density gradient centrifugation, they profit from faster operational times in downstream assays and lowered costs, because fewer (staining) reagents in less buffer are needed for the significantly reduced total cell numbers. In functional assays, e.g., antigen presentation or proliferation assays and transplantation (e.g., hematopoietic stem cell transplantation to reconstitute bone marrow and blood formation in irradiated mice), a higher cell viability and reconstitution frequency is reported when Ficoll-enriched cells were used, as compared to preparations without preenrichment via density gradients.

Elutriation [95–97] is another method of separating cells based on their size, which uses centrifugal forces. The technique is also called counter flow centrifugation and makes use of a modified elutriator rotor containing a separation chamber with which one can gently separate a large variety of cells from different tissues and specimens. The cells are separated in this chamber mainly based on their different sizes by the opposing action of the centrifugal field generated by the rotation of the rotor and the liquid flow inside the chamber (Fig. 21; centripetal, means in direction to the rotor axis (counter flow)). Because the separation is not dependent on a specific density gradient, this method is compatible with a wide set of media. Another big advantage is high viability and low activation of the cells, making it an interesting tool in a clinical environment [98].

1.3 Pre-enrichment by immunological properties

Although pre-enrichment methods based on physical properties (such as size, density, etc.) are straightforward, they do not allow for functional or biological discrimination of sub-populations, e.g. discrimination between T and B lymphocytes. To do so, immunological separation methods, which make use of antibodies to reach the specificity and cell population of interest, could be used.

One of the first methods established (in the early 1970s) is antibody-mediated complement lysis of unwanted cells. The cells (e.g. erythrocytes or T cells in a mixed lymphocyte pool) that you want to eliminate are detected and opsonized with specific antibodies (at the beginning serum from immunized animals were used, nowadays one can also use mAbs against the antigen of interest). Soluble parts from the complement C system are added to the cell suspension, bind to the antibody-tagged cells, and lyse them [99, 100]. There are more "classical" methods to enrich different immune cell subpopulations, some of which are still in use. These methods are summarized elsewhere [101] and are only mentioned to complete the overview. In the meantime, a variety of easier and more efficient techniques have become available. These techniques combine the advantages of beads and antibodies.

To enrich or deplete subpopulations out of a heterogeneous cell population, one can use beads coupled with mAbs against antigens expressed on the cells of interest that bind to the antigens forming larger aggregates. These cell-bead aggregates can now be easily separated from the unbound cells in the solution by passing the bead/cell-mixture over a mesh (Fig. 21). Cells that are bound to beads would not pass through the mesh, and are thus enriched on the mesh surface, whereas all other cells are smaller than the mesh-size and flow through. After filtration through the mesh, the antibody-coupled beads can be detached from the cells to allow the cells to be further analyzed. Using varying sizes of mesh and beads make sequential separations possible. For example, the pluriBead® technology allows cell enrichment as well as depletion of specific subpopulations [102]. Advantages and disadvantages of that technology are further discussed in Chapter IV Section 2.2.1.1.

The most commonly used methods for pre-enrichment of subpopulations are based on beads passing a magnetic field. A variety of companies offer different solutions for enrichment or depletion of cell populations. One system of immunological pre-enrichment employing magnetic fields is the MACS® Bead-Technology [103].
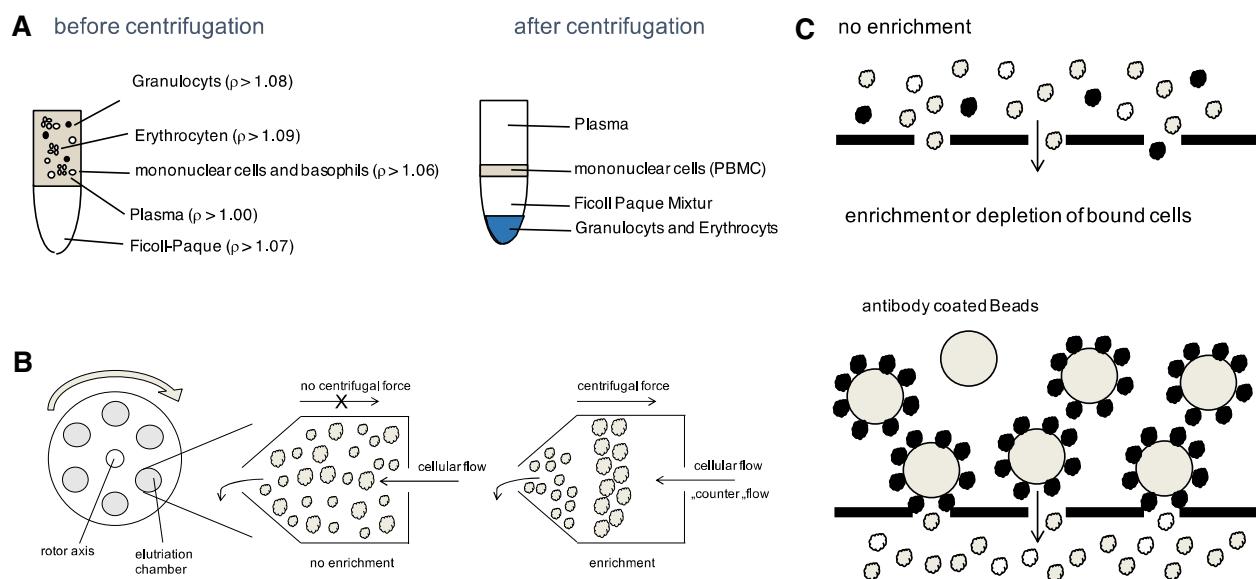
Figure 21. This figure shows a summary of discussed enrichment methods. (A) The separation of different cell types with a Ficoll® density gradient is shown. (B) Once one applies a centrifugal force in an elutriation chamber, cells will stop passing through and start separating along a density gradient built inside the chamber. The equilibrium formed depends on the speed of the cellular flow, the amount of applied centrifugal force, and the viscosity of the medium used. This is the reason why elutriation is compatible with a wide range of cell types and carrier media. (C) Target cells (black) can form aggregates with antibody-labeled beads and If you add beads that are coated with specific antibodies against your target cells (black) to the cell suspension, the target cells will form aggregates with the beads. These aggregates are held back on the top of the mesh while the rest of the cell suspension is passing through. With this method one can either deplete or enrich for a specific cell population. Combining different mesh and bead sizes is allowing for a serial enrichment of target cells.

1.4 Magnetic pre-enrichment for high-resolution detection and analysis of rare cell populations

For the detection and analysis of cell subsets that are detectable only in very low frequencies (<0.1%), appropriate pre-enrichment strategies, as detailed in the sections "Pre-enrichment by physical properties" and "Pre-enrichment by immunological properties," may help improve gating resolution for the cell population of interest. Typical applications are the detection of hematopoietic stem cells [104], CTCs [105], dendritic cells [106], or lymphocyte subsets, such as antigen-specific T cells [107]. As one of the most commonly used pre-enrichment technologies immunomagnetic positive and negative selection strategies have been established (this has been exemplified in the context of detecting antigen-specific T cells (Chapter V Section17.5.3, Fig. 67). Magnetic pre-enrichment is a unique tool to improve resolution of cell populations, e.g., via isolation of weakly labeled cells to achieve separation of "overlapping" populations, depletion of irrelevant cells, or enrichment of rare cells (Fig. 24). As described above for mesh-filtration based enrichment, the concept is based on the attachment of small, inert, supra-magnetic particles to mAbs specific for antigens on the target cell population.

Cells labeled to these antibody–bead conjugates are then separated via a column containing a ferromagnetic matrix. By applying a magnetic field to the matrix, the beads stick to the matrix inside the column and the bead-carrying cells are held back from

passing through (Fig. 22C). Unlabeled cells can pass through the matrix and are collected in the flow-through (Fig. 22D). To elute the trapped cells from the column, the magnetic field is simply removed. The MACS® technology therefore enables different strategies for positive enrichment or depletion of cells. MACS® beads are comparable small and offer the advantage of not interfering (too much) with downstream assays (see also Chapter V, Section 18.5). In contrast to cell sorting, up-scaling the cell numbers does not significantly increase processing times. For some cell types (e.g., CD4$^+$ T cells or B cells), a high enough purity can be achieved such that further enrichment is not necessary (of course this is dependent on the quality needed for the downstream assay, e.g., RNA/DNA purification). Solutions using magnetic beads other than MACS® beads are also available for cell separation (e.g., Dynal® Beads [108] or BD iMag^{TM} [109]). The beads in these kits are generally larger than the MACS® beads and do not require a separate matrix to retain the cells in the magnetic field. The disadvantage of using these systems is that, for many downstream assays, it is necessary to detach the beads from the cells to avoid interference with the system.

To pre-enrich your cells, you can choose a protocol from a variety of different techniques, which separate your cells based on their physical and/or immunological properties. Pre-enrichment could be useful to cut down the processing time of your experiment, increase the quality of downstream assays, or to reduce the amount of reagents needed.
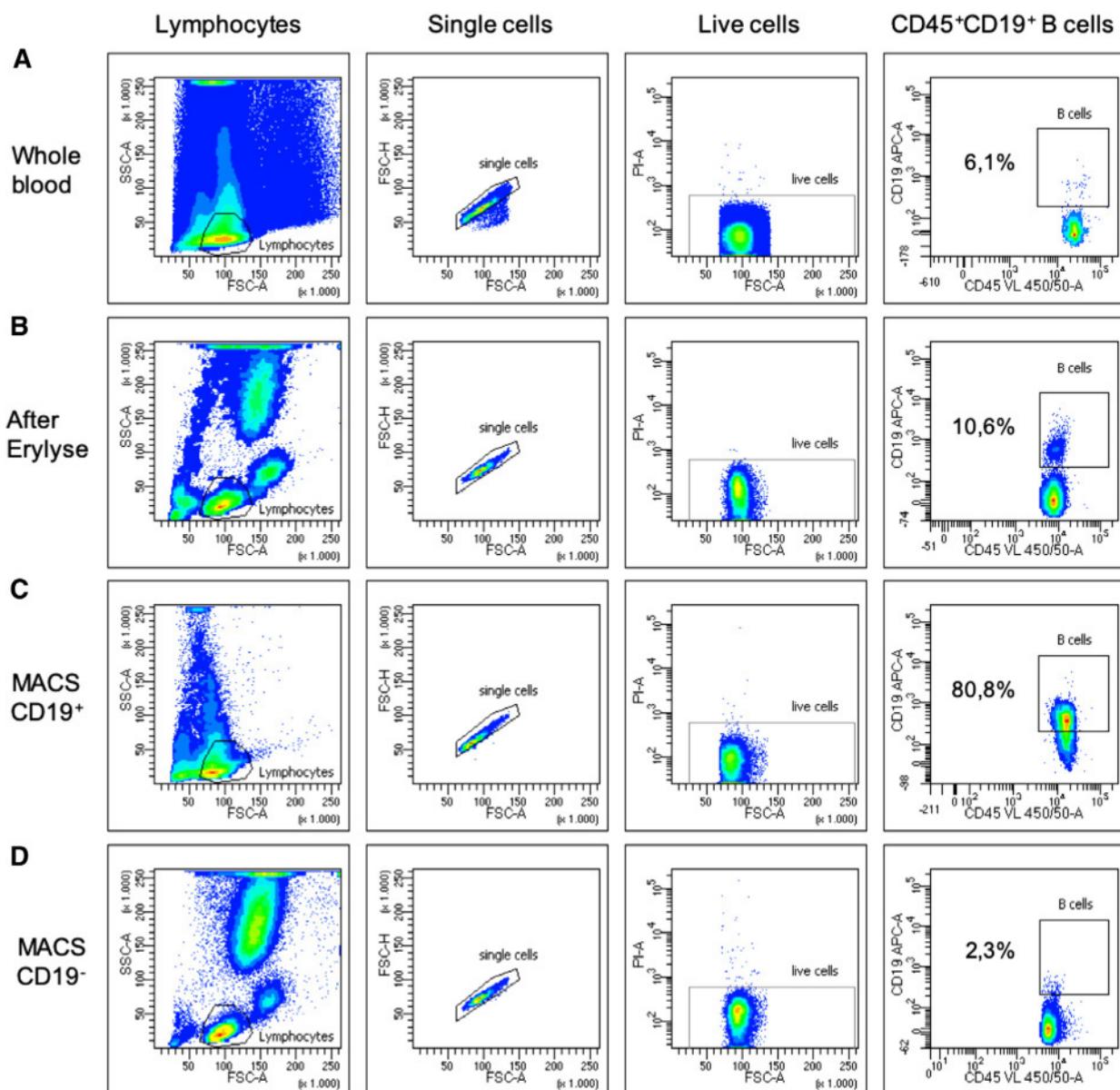
Figure 22. Enrichment of human B cells out of whole blood stained for CD45 BV421 and CD19 APC. (A) Staining prior enrichment. (B) Staining after lysis of erythrocytes with Lysing-buffer. (C) Staining after CD19$^+$ MACS® enrichment. (D) Staining of the CD19$^-$ fraction (MACS® flow through).

2 Parallel cell sorting

2.1 Introduction and general considerations

Parallel or bulk cell sorting is generally used to isolate a large number of cells in a batch mode, often as a pre-enrichment step before a single-cell sort (see Section IV.1 "Pre-enrichment of low abundant cell populations prior to acquisition/cell sorting"). Parallel sorting uses parameters such as cell size, density, magnetic, or electrical properties. Affinity binding reagents (e.g., antibodies) for specific cell subsets can be used to change specific properties, e.g., magnetism or density to achieve an antigen-specific bulk sort.

General considerations: Bulk cell sorting from a cell mixture can be done by many methods, each one having different advantages and challenges. The main variable parameters to be considered are specificity, yield, purity, viability, and functionality. Moreover, speed, cost, and consumables for equipment must be also taken into account. The importance of the different functional parameters will depend on the specific experimental goals, e.g., very high purity may be essential in many cases, while yield may be less important, because sufficient material is available. Instrumentation features depend on the specific needs and the experience of the user(s). Figure 23 illustrates the various parameters needed in deciding on a sorting strategy or method. Not always can all
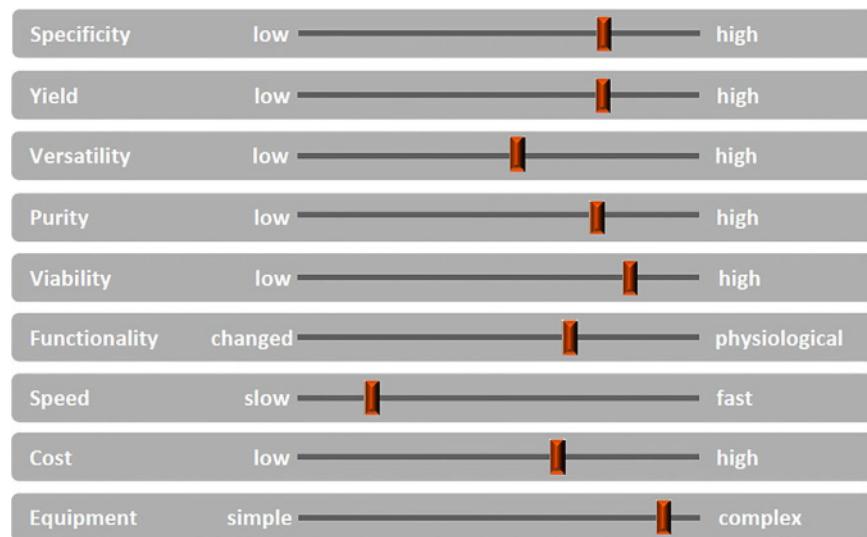
Figure 23. Check-list: Parameters for selecting a sorting method. The parameters that affect cell sorting and therefore must be prioritized when choosing a sorting strategy are shown. Starting from the available material (amount, fragility), they range from the mundane cost aspect to practical and methodological concerns such as the available time, to the important experimental approaches regarding what yield, purity, or versatility is needed for down-stream applications. Optimization of one parameter may downgrade another parameter, e.g., a high purity may be at the expense of a high yield or speed, or unchanged functionality of the cells may not allow direct positive selection.

parameters be set at optimal levels simultaneously. For cell isolations, where multiparameter sorting is not needed, but where speed is of essence, e.g., because high numbers of cells must be sorted, bulk cell sorting is preferred.

Flow cytometry cell sorting, where cells are sorted one-by-one, is the gold standard for multiparameter cell sorting. This procedure yields very high specificity according to one or several surface markers, which are made visible by fluorescence-labeled antibodies. The limitation is mainly the number of cells that can be sorted during a work-day. Pre-enrichment for subsequent flow cytometry cell sorting is another important application of bulk sorting and should always be considered, especially when the wanted cells are comparatively rare. First, because it reduces time of the cell

Cell "yield" is the fraction of wanted cells in the original mixture that could be recovered alive after the sorting procedure.

To quantitatively evaluate sorting performance, several calculations can be performed. The purity, i.e., fraction of positive cells in the sorted fraction, can be expressed as the ratio of positive cells and the sum of positive and negative cells. Then, using the measured purity and yield, the yield for nontarget particles, the negYieldFraction (Fraction = Percentage/100), in the target sample after sorting can be calculated. This provides a helpful metric when optimizing a sorting technology. Ideally this number will be zero, when 100% purity is achieved in the separation. The negYieldFraction, a measure for how many unwanted cells are found in the sorted sample, can be calculated by re-arranging the equation:

$$\text{Purity Fraction} = \frac{\text{posFraction} * \text{posYieldFraction}}{\text{posFraction} * \text{posYieldFraction} + \text{negFraction} * \text{negYieldFraction}}$$

to obtain

$$\text{negYieldFraction} = \frac{\text{posFraction} * \text{posYieldFraction} * (1.0/\text{PurityFraction} - 1.0)}{1.0 - \text{posFraction}}.$$

sort, and second because it helps to improve gating quality by eliminating potential fluorescence overlap between stained and unstained cells (Fig. 24). An overview of cell sorting technologies and applications can be found in ref. [110]

Bulk cell sorting can either use any cell surface marker for distinction, or use distinct physical properties of cells, such as density differences (Ficoll[TM] isolation), size, plastic adherence, phagocytic capacity (macrophage enrichment), or sensitivity to hypotonicity (erythrocyte lysis). Keeping track of cell numbers, viability, and analyzing the sorted cells before, during, and after any separation is good routine in order to determine cell yield and cell purity, and to detect any unreasonable cell losses or damages.

Another approach for the evaluation of bulk sorting performance is described in ref. [111], where it only uses fractions of cells in the original and positive fraction and does not need information about the yield of the positive (wanted) population. The enrichment factor Fe in ref. [111] is the inverse of the negYieldFraction, if the yield of positive cells is 100%. At lower yields, there are small differences between the two metrics. Table 4 provides an example showing that final purity values alone are not a good measure for sorting performance (rows 4 and 5 in Table 4), even though it may be the important measure for biological activity.

Figure 24. Improvement of population discrimination after pre-enrichment. Cytometer histograms of unwanted (gray lines) and wanted (solid green) populations. (A) A large excess of an unwanted population may create substantial overlap with the target population, making it impossible to achieve a good single cell sort. (B) After a pre-enrichment bulk sort, which removes most of the unwanted population a good discrimination between the two populations can be achieved.

Table 4. Example of sort performance metrics. The values for purity, yield, and the fraction of positive cells in the original sample are measured and the negative logarithm of negYieldFraction, –log(Y–) (the underlying equations are detailed in the text (IV.2.1) and the logarithm of Fe [111] are calculated

Purity (%)	Yield (%)	Orig (%)	-log(Y-)	Log(Fe)
95	100	50	1.28	1.28
95	90	50	1.32	1.28
95	10	50	2.28	1.28
99	90	1	4.04	3.99
95.6	90	0.1	4.38	4.34

2.2 Antibody based bulk cell sorting

Physical properties of cells can be changed by the reaction with specially tagged affinity reagents like antibody conjugates with magnetic particles. In this way, specific subsets can be isolated with bulk sorting methods.

2.2.1 Magnetic beads coupled to antibodies. This technique uses the force of magnetism to sort out cells according to specific cell surface markers. Several commercial systems are available, which use either inorganic superparamagnetic or ferromagnetic materials embedded in polystyrene beads or in a matrix such as dextran, or coated with graphene [112]. Beads in sizes from tens of nanometers up to several times the size of a typical mammalian cell are available for bulk cell sorting. The bead-size is not disclosed by all companies. Cells are incubated with the beads and then drawn to a magnet of appropriate strength either in a column, tube, or 96-well plate. Nanometer sized beads require high field strength and field gradients, generally achieved in columns or microfluidic channels with optimized ferromagnetic structures. Unwanted cells are poured off or eluted. In negative selection strategies, all unwanted cells are labeled, leaving the wanted ones untouched for downstream applications or a second round of selection by another surface marker. Several bead or affinity reagent chemistries allow the detachment from the cells if needed. The bulk sorting method hinges on the quality of the antibodies used, and the density of the surface markers on the cells. Cells with a low density surface marker expression may be more difficult to sort. Rare cell sorting is possible, albeit it may require several rounds of sorting and intensive washing to remove nonmagnetic cells. Bulk sorting with beads, especially with large beads, cannot distinguish between high and low expression of a given antigen on the cells.

Selection of a good antibody is crucial for successful sorting, as is the concentration of beads in the labeling step. Nonspecific binding associated with antibodies clustered on beads has to be addressed with some reagents and cell types. Nowadays, many kits for sorting a range of cell types in various species are commercially available. Custom-made beads may be a choice as well, and are offered by some companies. Conjugation of antibodies to magnetic beads in your own laboratory or the use of avidin beads with second-step labeling with biotinylated antibodies is another option.

Advantages: Fast, high cell numbers, specific, positive, and negative selection possible.

Pitfalls: No distinction of antigen density in sorting with larger beads (some nanometer-sized colloidal beads show some differences in magnetic retention in some systems [113]); activation of cells by bead attachment is possible (must be excluded for individual downstream applications). Temperature and duration for binding must be considered (in the context of phagocytosis, decreasing possibility of nonspecific binding, capping, or efficient binding kinetics). Note: the sort quality must always be analyzed to detect possible cell losses and impurities. Also the cell viability can be influenced by buffers or bead sizes.

Selected manufacturers: miltenyibiotec.com, Sepmag.eu, stemcell.com, thermofisher.com, turbobeads.com, cd-bioparticles.com, biolegend.com

2.2.1.1 Nonmagnetic beads coupled to antibodies. Nonmagnetic beads coupled to antibodies (pluribeads®) use strainers to fish out cells, attached to large polystyrene beads. The method is based on the size-enlargement of cells as the beads are larger than cells. Specificity is achieved by the antibodies and, again, the quality of the antibodies is important. As beads vary in size, several cell subsets can be sorted out of a mixture by using different sized beads for different antibodies. A potential advantage is that the size of the beads may prevent phagocytic uptake. Beads can be detached by a special buffer, and sequential sorting is possible.

Advantages: Fast, high cell numbers, specific, positive, and negative selection possible.

Pitfalls: Generally no distinction of antigen density in sorting; activation of cells by bead attachment/detachment procedure is possible (must be excluded for individual downstream applications); nonspecific binding (the sort quality must be analyzed to detect possible cell losses and impurities). Temperature and duration for binding must be considered (in the context of

phagocytosis, decreasing possibility of nonspecific binding, capping, or efficient binding kinetics).

Selected manufacturer: pluriselect.com

2.3 Methods based on density differences

Cells, organelles, parasites, and so on have different densities, and their density differences can be used for cell separation [114, 115].

*2.3.1 Ficoll-Paque*TM*, Lymphoprep*TM. Ficoll-Paque™ contains Ficoll™, a highly branched polysaccharide, and metrizoate. LymphoPrep™ replaces the latter with sodium diatrizoate. Sideby-side comparisons of the gradient media have previously been done [116]. They have low viscosity, are nontoxic, and can be prepared for different densities. Ready-made solutions are also commercially available. Ficoll-Paque™ gradients are frequently used to separate peripheral PBMCs versus granulocytes/erythrocytes from whole blood. Efficient removal of dead cells from a mixture is possible as well (note of caution: this procedure is stressful for the living cells). When separating blood, the upper fraction contains both lymphocytes and other mononuclear cells. Addition of iohexol, a nonionic X-ray contrast agent, to the gradient medium can remove monocytes as well [116]. Nycoprep™ and OptiPrep™ are gradient solutions without Ficoll™, based on a tri-iodinated derivative of benzoic acid with three aliphatic, highly hydrophilic side chains or on iodixanol, respectively. They thus are not based on a polysaccharide net [117]. From the granulocyte/erythrocyte mix, neutrophil granulocytes can be isolated further by dextran sedimentation [118, 119], and erythrocytes lysed by hypotonic shock (see Chapter IV, section 2.5).

Advantage: Easy to use, little equipment needed.

Pitfalls: Density for similar cells between species can differ (e.g., for mouse, horse, and human lymphocytes [120]); erythrocytes and granulocytes can become captured in the upper layer, if the gradient is overloaded or the blood was frozen. Centrifugation must be done at room temperature and with the centrifuge brakes turned off. The step of overlayering blood on the gradient is time consuming and must be done with care. Various commercially available systems such as SepMate™ exist to aid in this, including prepared Ficoll-gradients in containers to draw blood. Loss of cells and recontamination when harvesting them from the gradient surface is possible. Cell activation can be an issue, e.g., when isolating neutrophils [118].

Selected manufacturers: gelifesciences.com, http://www.stemcell.com/en/Products/Popular-Product-Lines/SepMate.aspx

Percoll: A second density separation medium is Percoll, made from colloidal nanosized silica particles coated with polyvinylpyrrolidone [121]. Percoll is nontoxic and has a low viscosity, so cells can be centrifuged at low centrifugal forces. Isoosmotic gradients of densities between 1.0 and 1.3 g/mL can be formed by layering solutions of different percentages of Percoll in a tube. Cells of differing densities collect at the different interfaces and can be taken off. Colored density marker beads made

of Sephadex™ are helpful to visualize the density borders in the gradients.

Advantage: Versatile, as several cell types separate in the different layers in one tube.

Pitfalls: See Ficoll-Paque™; cell activation can be an issue and must be considered.

2.4 Methods based on cell size

Size differences of cells of interest, e.g., erythrocytes, platelets, leukocytes, or circulating tumor cells (CTCs) in blood, can also be used for separation.

2.4.1 Filters. Membrane filters are applied in sample de-bulking as they can separate particles or molecules based on size. The pore size enables larger cells to be retained on the membrane and smaller cells to pass through. For example, leukocytes (mean diameter 8–10 μm) can be isolated from erythrocytes (6–8 μm but disc shaped) by flowing whole blood through a membrane filter; back flushing will recover the captured white blood cells. However, classical filter membranes do not have homogeneous and precisely controlled pore sizes, so the resolving power of this separation is limited and, due to the material of the filter, the recovery of white blood cells may be inefficient.

Another separation method based on cell size that targets red blood cells and platelets specifically uses microfibrated silicon chips. These feature homogeneously etched slots of a certain size designed to let erythrocytes pass through under a certain pressure while retaining leukocytes on the surface of the chip. The leukocytes can then be recovered by elution. Early evaluation of this technology has demonstrated 98.6 ± 4.4% recovery of leukocytes without bias to any leukocyte subpopulation and 99% removal of erythrocytes. The enriched leukocytes have over 95% viability [122].

Mesh-size based catching of cells from adipose tissue directly in culture has been demonstrated using various filter materials [123].

Advantages: Easy to use and little equipment is needed.

Pitfalls: Throughput of the filters is limited by surface area and overload may result in reduced purity and recovery of leukocytes. So far the commercial devices can only handle up to 2 mL of whole blood, which is sufficient for some cell analysis assays but not enough for blood transplantation and cell therapy applications. The recovery of leukocytes is sensitive to the pressure applied—pushing with higher pressure and higher flow rate may result in decreased recovery.

Selected manufacturer: avivabio.com (for microchip devices)

2.4.2 Deterministic lateral displacement. A method of bulk sorting currently under development is based on cell size. There are several publications reporting a microfluidic device that separates particles and cells with high resolution [124] and is able to not only fractionate whole blood components by their sizes [125] but to also isolate CTCs from whole blood [126]. Recent work describes improvements for the routine use of the technology for

rare cell enrichment [127], for the isolation of leukocytes from whole blood [128], and for cell washing for cellular therapy applications [129]. The micro-fabricated silicon device consists of a matrix of obstacles, and the gap and the size of the obstacles are precisely controlled. When the particle mixture is introduced to the device, the laminar flow goes through the arrays of obstacles and the smaller particles will follow the streamlines and the larger particles will be "bumped" by the obstacles and deflected into a different flow stream. Multiple sections of an obstacle matrix with varying gap sizes can be built in one device so that multiple sized particles can be isolated because each sized particle will follow its own determined path flowing through the device. In theory, there should be no throughput limitation of the technology as it is a continuous flow system; however, some surface treatment of the device may be needed to avoid cell adhesion. The device has little tolerance to clogging, air bubbles, or cell aggregates, as changes in the fluid flow profile alter the particle travel path and deflect the flow streams possibly resulting in decreased purity and/or recovery.

Advantages: High resolution, continuous separation, and having the potential to be high throughput, high resolution size discrimination with high purity of cell populations with non-overlapping sizes.

Pitfalls: Clogging with samples with cell aggregates.

Manufacturer: Contact gpbscientific.com for quote for custom fabrication.

2.4.3 Acoustic particle sorting. Particles exposed to an acoustic field are known to move in response to an applied acoustic radiation force. Numerous researchers have investigated the effect of acoustic waves on cells and particles in aqueous solution. The force exerted on a particle by an acoustic field can be described by the following equation:

$$Fx \sim r3K\,\Phi\sin(2\pi x/\lambda)$$

where *r* is particle radius, *K* is a constant proportional to density of medium and particle, φ is the acoustic contrast factor (proportional to density and compressibility), and *x* is the distance from the pressure node in the direction of the wave [130]. Thus, acoustic focusing can be used to separate and position particles based on size, density, and deformability. The ultrasonic standing wave is generated by a piezoelectric transducer and resonance vibration of the microfluidic device made in silicon or glass. The channel width is designed to match half a wave length resonance of 2 MHz in order to have larger cells "focused" in the middle of the channel. [131]) demonstrated the removal of platelets from peripheral blood progenitor cell product on a microfluidic device in which an acoustic standing wave is generated in the fluidic channel. The acoustic pressure pushes leukocytes to the pressure node located at the center of the channel and leaves platelets at the side stream going to a waste outlet. Size is a dominant parameter for acoustic cell sorting but not the only parameter as shown in the equation above. For example, separation of leukocytes from erythrocytes in whole blood is not easily done on an acoustic device as erythro-

cytes, although having a smaller diameter, move to the acoustic energy node along with leukocytes as the erythrocytes have a higher density. Recently, optimization of the technology has been achieved and the preparation of mononuclear cells from diluted peripheral blood has been reported [132].

Advantages: Continuous flow—no throughput limitation, label free.

Pitfalls: The cell moving trajectory in the flow channel is determined by both the acoustic pressure and the shear pressure so the flow rate and channel configuration need to be well controlled otherwise the separation efficiency will suffer. Due to the heterogeneous nature of cells in biological sample and the multiparameter physics of acoustic separation, separations have to be optimized for specific samples.

Manufacturer: acousort.com

2.5 Erythrocyte lysis

Enucleated erythrocytes are more susceptible to hypotonic shock than nucleated cells (see also Chapter IV, Section 1.2). Either a low isotonic Tris/NH_4Cl buffer for several minutes at room temperature or 37°C, or pure water for several seconds will lyse erythrocytes in cell mixtures. The latter method is particularly useful for blood, which contains approximately 1000 times more erythrocytes than leukocytes. Several other cell lysis solutions are available commercially as well [92, 93].

2.6 A historical note

The methods described in Chapter IV, Sections 2.2–2.5 have superseded older methods to specifically isolate cells, such as panning on antibody-coated plastic dishes [133], nylon–wool based isolation of T cells, or sheep red blood cell rosetting followed by a Ficoll gradient [134, 135]. The latter is still commercially available under the name RosetteSep[TM] for specific uses, in particular for the removal of unwanted cells from blood and can be considered a protocol still in use. These older methods are not discussed here, but they are summarized in ref. [101].

3 Serial cell sorting

3.1 Cell sorting by flow cytometry

Successful cell sorting by flow cytometry often requires that more attention be paid to sample preparation than is typically done when preparing samples for analysis only. When sorting, the often-challenging objective is to not only separate some sample fraction in a timely manner such that the sorted output is a pure viable fraction, but also that the sorted cells be functionally capable, that they expand well in culture or perhaps be competent to perform in some other subsequent assay (e.g., produce cytokines or

some other vital cellular function). Another requisite for good cell sorting is to have a proper single-cell suspension, ensuring a desirable sample behavior in flow where good doublet discrimination can be performed with minimal conflict aborts during the sort. How to best achieve good sample behavior and maximize performance?

3.1.1 Choice of buffers.   The most commonly used media/buffers for processing mammalian cells were designed to work at 1 atmosphere pressure either on a laboratory bench or within a CO_2 incubator, yet inside the sample chamber of most cell sorters the pressure can often exceed 2 to 4 atmospheres depending on the conditions and nozzle size chosen for the sort. Sample buffers that historically tend to perform well for sorting such as Dulbecco's PBS or HBSS (minus Ca^{++} and Mg^{++}), both with 10 to 25 mM HEPES and protein (usually 1 to 2% heat inactivated serum or BSA), and more recently BD FACS^{TM} Pre-Sort Buffer plus from 0.2 to 2% protein (application dependent) are recommended. Bicarbonate media buffers such as Roswell Park Memorial Institute (RPMI) or DMEM usually do not make the best candidates for sample sort buffers or sort collection buffers since they (i) are a different buffer type than the cytometer's sheath buffer (bicarbonate vs. phosphate), and (ii) by design require 5% CO_2 to maintain physiological pH, and (iii) usually contain divalent cations (Ca^{2+} and Mg^{2+}) plus phenol (very fluorescent). If a bicarbonate media is used, one should be wary and use either Ca^{++} or Mg^{++} minus formulas without phenol or mitigate the undesirable divalent cation side effects for sorting (making the cells "sticky") by adding ~1 mM EDTA in addition to 25 mM HEPES and protein. HEPES buffered bicarbonate media has been reported to be light sensitive [136].

3.1.2 Considerations for adherent cells and cells isolated from solid tissues.   In preparing adherent cell lines for sorting a common pitfall is often within the protocol to remove the cells from a dish using trypsin or trypsin-EDTA and subsequently inactivate the trypsin by adding back culture media containing a significant amount of serum. This step is designed to stop the proteolytic activity of the trypsin and make the cells "sticky" to easily adhere to a plastic dish when passaging the cells. The opposite is desired for cell sorting by flow cytometry, the sample should not be "sticky" with a tendency to adhere to plastic. As a result, good flow cytometry cell sorting protocols for adherent cells will typically either inactivate the trypsin with soybean trypsin inhibitor or use one of the many available nonenzymatic cell disassociation buffers (e.g., Accutase^{TM}); in either case, if the cells grow in media with serum, the culture should be gently rinsed twice with Dulbecco's PBS before disassociating and removing the cells from their substrate. Some cell types, when disassociated with nonenzymatic disassociation buffers that rely on chelating agents, may show decreased viability as compared to trypsin disassociation [137]. If there is any doubt, a few simple pilot experiments designed to determine the best preparation method for the specific cells in question is often a

very good investment toward successful sorting, since things like EDTA can affect certain cell types [138].

Similarly, isolating cells from any primary tissue for flow cytometry cell sorting can be very challenging, care should be taken to ensure the chosen protocol is optimized and tested to not only provide the intended cells (e.g., regarding isolated dendritic cells from spleen different protocols can enrich for different phenotypes) but helps coerce the cells into a well-behaved single-cell suspension. The highest quality reagents should be used, especially when using proteolytic enzymes such as collagenase, pronase, dispase, or trypsin since small amounts of contaminants can have serious undesirable effects resulting in poor sample performance. Collagenase is dependent on calcium for activation, for example, and other divalent cations may be activators (Zn^{++}) or inhibitors (Mg^{++}) [139], and care should be taken to ensure any additive endotoxin levels are as low as possible.

3.1.3 Stickiness to plastic: A menace of cell sorting.   When performing bulk sorts and collecting a sorted fraction into a plastic tube, it is usually best to precoat the tube with serum leaving some at the bottom, or if desired, additionally seed the tube with a small volume of the sample buffer containing 2 to 10% serum. Adding unbuffered bicarbonate media to the collection tube and sorting on top of it runs the risk of high pH conditions causing undesirable salts to form while the phosphate and bicarbonate buffers mix with the cells present, thereby reducing cell viability. When performing single-cell sorts into a microtiter plate, any media pre-added to the wells should be HEPES buffered and conditioned beforehand if possible. Additionally, when sorting onto/into small targets such as microtiter plate wells extra care should be taken to ensure the accuracy of the deflected drops during the sort by choosing an appropriate nozzle size to minimize the effects of cells on drop breakoff [140] (choose a nozzle at least five to six times the cell diameter as verified under a microscope).

3.1.4 Cell concentrations and sorting rates.   Once prepared, the sample should have a final cell concentration that allows the desired event rate to be achieved with only a modest differential pressure on the sample. Increasing the sample rate significantly by simply forcing more through the system is not recommended. The sample should be filtered just prior to being loaded onto the sorter to help ensure no clumps are present and further disperse any weakly adhered cells. After filtering the sample through a Nitex nylon monofilament mesh with an appropriate pore size (30–50 μm depending on cell size), any samples that tend to dynamically re-aggregate during a sort are best dealt with by installing an in-line nylon sample filter of the same pore size to help prevent clogs. Generally, since the theoretical sorting efficiency of a single cell preparation is that of a homogeneous Poisson process [141], the operational efficiency of the sorter may be estimated by

$$Efficiency = e^{-\left(rate \times (1.0 - fraction) \times \frac{drop\_packet}{frequency}\right)}$$

where rate is total events/s, fraction is percent being sorted, drop packet is the number of drops including any additional temporal purity mask, and frequency is the drop rate in drops/s. Normalizing to sorter drop frequency, this means when sorting a fraction that is 10% of the total at an event rate of one cell to every four to five drops, it can be expected to sort with an efficiency of 80 to 85% when using a single drop sort.

3.1.5 Purity and doublets. If, after optimizing the sorter during setup, suddenly the application sorting efficiency is low (higher than expected conflict abort rate), it is indicative that the sample is not a monodisperse cell suspension, that cells are likely "sticky," adhering to one another during entrainment and not arriving into the sensing zone as a homogeneous Poisson process. This is a very common scenario with many cell preparations, especially adherent and primary cells, and often the sorter performance is blamed for what is a behavior intrinsic to the sample. Much of the time this can be significantly mitigated by reexamination of the sample preparation protocol to discover what might be improved to help coerce the cells into a well-behaved single-cell suspension. This often involves the addition of EDTA or DNase etc. to the sample sort buffer.

Whenever a sorted sample using a purity sort mode (where system-defined spatial-temporal drop zones in the stream are examined logically for potential contaminants for each sort event) is not as highly sorted as desired, the most common reasons are that either the classification scheme for single cells is not robust enough and hidden passenger cells are occasionally sorted, or that there are particles in the stream that are disturbing the droplet breakoff stability and, as a result, the wrong drops will occasionally appear in the collection tube, or a combination of the two. Sorters certainly cannot read the operator's mind and will attempt to do exactly what they are set up to do so, if a positive selection from the sorter suffers from disappointing purity, one simple performance check is enough to sort a completely negative cell fraction for comparison. If that sorted negative fraction is 99% pure or higher, yet the positive fraction is only 80 to 95% pure, then the likely cause is undetected "doublets" due to an insufficiently constrained single-cell gating strategy. In many flow systems, doublets tend to align with the doublet figure's major axis in line with the partially developed laminar flow and the pulse width becomes a very useful parameter to help distinguish singlets from doublets. Other systems, such as the BD FACSAria™ family that use fully developed laminar flow in their fluidics design can have those same doublet figures rotate off axis after entrainment in flow such that forward scatter (FSC) pulse width alone will not detect enough doublets, and in such cases using both FSC and side scatter (SSC) looking at plots of Height versus Width (or Height versus Area—but that usually leaves less screen real estate for drawing gates) will help reveal many more doublets, boosting the purity to a more acceptable level with careful gating. Figure 25 (reproduced with permission from ref. [142]) is an example of such a strategy where pulse geometry gates on both FSC and SSC detect an additional 9% of doublets that would pass through a standard scatter gate.

Matching nozzle size to particle size is key, and the general rule of thumb is that the nozzle should be four to five times that of the particles for bulk sorting and five to six times that of the particles for plate deposition where accuracy is more critical. Ensure that the actual cell size is what you expect it to be when choosing a nozzle, and whenever there is doubt it is very useful to quickly compare to known bead size standards by simply putting small drops of each on a microscope slide and checking, not only the size(s) within the sample but also the quality as the amount of debris should be low, the number of single cells high, and clumps/aggregates should be the rare exception rather than the rule. Electrostatic cell sorters tend to perform very well with monodisperse samples and struggle with poorly dispersed ones so, as with many other applications, sample preparation can be the limiting or enabling step. The International Society for the Advancement of Cytometry (ISAC) Cell Sorter Biosafety Standards were published in 2014 by the ISAC Biosafety Committee [143], and related information is readily available and is a highly recommended reading before embarking on any series of cell sorting experiments including:

1. The ISAC web site (http://isac-net.org) Resources for Cytometrists → Biosafety
2. CYTO University (ISAC's on-line portal for cytometry education) http://cytou.peachnewmedia.com → Course: Flow Cytometry Biosafety

3.1.6 Gating Strategies. Most real-world sort samples are a complex mixture of cells in various states and contain varying amounts of debris and dead cells; identifying and sorting the cells of interest while excluding unwanted populations and debris is done by "gating" the sample using selected features and some number of graphical gate regions combined with Boolean logic. This can become complex in high dimensional experiments where it is now possible to sort cells based on over 30 dimensions on some instruments (such as BD FACSymphony™). Any classical gating strategies used to phenotypically identify the cells may not be the most effective or even possible to use for the purposes of sorting, especially if the number of gates is high or the population of interest is identified through a variety of clustering methods or a dimensionality reduction technique such as tSNE [144] or UMAP [145]. Algorithms such as GateFinder [146], Hypergate [147], and Hyper-Finder [148] tackle this problem where analytical methods or data projections are unavailable in the cell sorter by treating the identified population of interest as a training set, and computationally determine an optimal feature set and gating strategy by using data dimensions that do exist in hardware to sort the population. These algorithms objectively optimize feature selection and gate efficacy by means of an F1 measure, the harmonic mean of precision (purity) and recall (yield) at each gate step. Since the real-time sort decisions within the sorter are done extremely rapidly within onboard electronics, it is always desirable to find a gating strategy that is efficient and uses as few gates as possible. When population analysis and identification is by computational
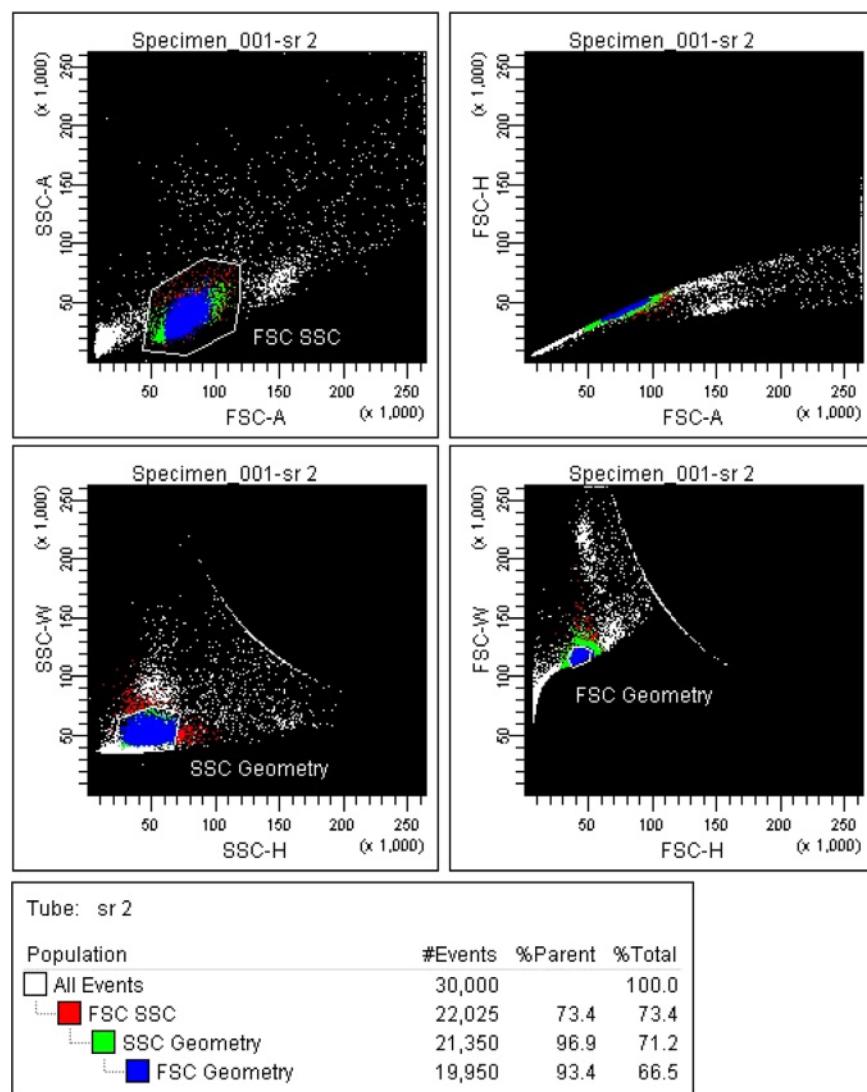
Figure 25. PBMC Sort. A PBMC sort on a BD FACSAriaTM where by adding both FSC and SSC Height versus Width plots and carefully gating on singlets an additional 9% of likely doublets are removed (reproduced with permission from ref. [142]).

methods, then creating a set of optimal sort gates by means of an appropriate optimizing algorithm becomes necessary.

3.1.7 Prevention of cell sedimentation. Long-term sorting often leads to sedimentation of the cells. The sedimentation rate of cells in a fluid depends on their physical properties such as density, cell size, cell shape, viscosity of the surrounding medium, and gravity [149]. In addition, the effective density of a cell is also affected by its water content, and thus the sedimentation rate is not a constant property for an individual cell type [149, 150].

Sedimentation of cells can be avoided by shaking or rotating the sample tube, or stirring with the sample line inside the cell sorter (BD FACS [151]). Rotating unidirectionally is not very effective since the sedimentation is delayed but not prevented. For example, the threshold rate of human leukocytes decreases to 80% after 30 min of cell sorting and then to 50% after an additional 15 min. Moreover, the constant rotation of the tube, especially if cells stick between the lower end of the sample line and the

tube bottom, acts like a "cell crasher." A more effective and gentle treatment is achieved by shaking or pipetting the cell suspension. Another possibility is the use of Surface Acoustic Waves (SAW) to keep the cells in a homogeneous suspension. SAWs are generated on the surface of a piezoelectric crystal by applying a high-frequency electrical signal to specially formed pairs of electrodes deposited on the crystal [152]. By use of a coupling fluid (e.g., water) between the crystal and the sample tube, the SAWs are conducted to the sample via the tube bottom. This allows a mechanical and gentle resuspending of the sample by acoustic streaming. This approach is specific in that it uses low amplitudes and high frequencies and is therefore not detrimental for living cells and can be implemented in a cell sorter (e.g., BD FACSAria™) [153].

Furthermore, the sedimentation of cells can be controlled by using isopycnic (i.e., equal or constant density) media [154]. This can be achieved by using various reagents, e.g., Percoll®, Ficoll®, HBSS, Nychodenz®, Xanthan Gum [149, 154, 155]. For example, a 60% Percoll solution results in a media density of 1.07 g/cm³, which is equal to the density of human lymphocytes but
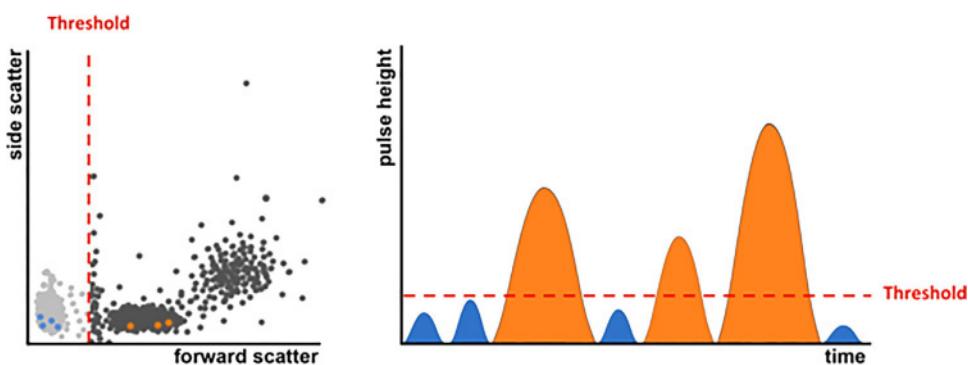
Figure 26. The threshold value defines a signal intensity, in one or more parameters, above which the cytometer starts to recognize an event. All other events will be invisible to the instrument's electronics. A particle passing the laser beam emits a certain amount of light over time. The threshold is set on the height of the signal that is emitted by each particle. On the left-hand side a dotplot with the forward scatter as the trigger parameter is shown. Only particles with a signal higher than this threshold value are recognized by the software as an event and shown in the dotplot (black and orange dots). The dots in on the left side of the threshold value (grey and blue dots) are not included in the data file.

different from that of human erythrocytes (1.10 g/cm³). However, in practice the sedimentation rate of both cell types is decreased or stopped and therefore sedimentation is drastically minimized. The toxicity of the final buffer should be tested by leaving cells in the buffer overnight at 4°C and the resultant cell viability should not be below 80%.

3.1.8 Trigger and threshold. To facilitate the discrimination of particles of interest from background events, it is useful to define a minimal signal value, the threshold value, which a particle passing the optics of a flow cytometer must reach to be actually recognized as an event. The threshold value defines the signal intensity above which the cytometer starts to recognize an event and therefore limits the number of events coming from background signal (Fig. 26). Every event showing a lower signal than the threshold defined will not be processed by the cytometer electronic and will not be represented in the data file. Therefore, it is advisable to look for a leading parameter (i.e., a parameter with a clear discriminator for the population of interest) as the trigger parameter, and predefine a threshold value. This fact is important to consider when it comes to cell sorting. Because the instrument ignores events below the threshold, they are not being included in the process of the sort decision. Consequently, sorted fractions can get contaminated due to the fact that these "invisible" particles are in fact still part of the sample. When the droplets are formed these particles can end up inside or in the neighboring drop of a target cell because the settings of the sorting mask are ignored, resulting in a contamination of the sorted fractions. It is therefore recommendable to use the minimal threshold value possible for identifying the required population.

The default setting of the trigger parameter on most instruments is set to forward light scatter. Alternatively, a fluorescence parameter can be used for triggering. The discrimination of small particles, e.g., platelets, erythrocytes, or extracellular vesicles, is often more specific when the threshold can be set on a fluorescent signal (e.g., a common surface marker or even autofluorescence that clearly defines the target population) as background

discrimination in FSC and SSC is often difficult. A combination of several threshold parameters can also be used to set the threshold more strictly. In this case, the event must meet the value of multiple thresholds to be processed by the flow cytometer. Such a threshold combination is often used when the expected signal of a particle is quite close to the background noise of the trigger channel. As threshold levels are applied to pulse height (H), it is advisable to set threshold values while viewing pulse height [24], especially if the trigger parameter might be a fluorescence parameter where signal levels are low and the main contributor to area is pulse width (*W*). For many cytometers, pulse height and width are not collected by default and have to be chosen in the instrument setting beforehand.

3.2 *Microfluidic*

Recently, microfluidic devices have entered the arena of flow cytometry and, in particular, cell sorting devices [156–159]. As these devices also utilize sequential sorting and similar fluorescence detection technologies to identify the cells of interest, best practices for microfluidic devices have a lot in common with those applicable to droplet sorters. This is especially true for considerations regarding sample preparation, such as choosing the right marker panel or appropriate buffer selection as discussed above (See Chapter IV Cell sorting). While sequential sorting technologies have a lot in common, there are also some major differences and knowing and understanding these differences is key to successful application. One of the biggest differences is that droplet sorters are typically operated in resonance [160], whereas many microfluidic sorters are operated purely on demand [158, 161, 162]. To explain further, operated in resonance means that the drop generating nozzle is running in resonant mode, stably generating a constant stream of drops. This way, drop volume and spacing is fixed and cells are randomly "positioned" inside the drops. This contrasts with many microfluidic sorters, where the displaced volume can be fine-tuned in size (volume)

and time/space (centering the target cells). Although the enabling principles vary, the sorting effect is mainly generated by displacing a certain volume [161, 163]. Given that the sort-timing is precise and correct, this volume defines expected purities and yields of target cells. In an ideal system, target cells and nontarget cells are totally uncorrelated and thus follow a Poisson distribution [164]. In the case of a "yield sort," where all target cell candidates are to be sorted independently of the nontarget cells nearby, the expected yield is 100% by definition. The expected purity can be calculated as follows: Let λ_T be the average number of target cells per displaced volume, then the relative number of sort-actuations is defined by $N_{\lambda T} = e^{-\lambda T}$. For each displaced volume, there is a chance to catch a nontarget cell, defined by λ_N, the average number of nontarget cells per displaced volume. With this, the expected purity P can be calculated to be

$$P = \frac{1}{1 + \lambda_N \, e^{-\lambda_T}}.$$

On the other hand, in case of a "purity sort," every time a second cell is in close proximity to a target cell, the potential displacement will be inhibited. Thus, the theoretical purity is 100%, whereas the expected yield decreases. In this case, the yield calculation is simply the likelihood of having a single cell within the displaced volume:

$$Y = \frac{(\lambda_N + \lambda_T)^1}{(\lambda_N + \lambda_T)\,1!} \; e^{(-\lambda_N - \lambda_T)} = e^{(-\lambda_N - \lambda_T)}$$

Besides the obvious close formal relationship between the two formulas, it is worth noting that the expected yield in a purity sort is solely determined by the total cell frequency ($\lambda_N + \lambda_T$) and not by the target/nontarget ratio, whereas the expected purity in yield sorts is strongly dependent on the target cell frequency. In order to give a practical example, these two figures are here calculated for a virtual sorting device assuming that the microfluidic sorter:

1. has a sample flow rate of 4 mL/h and does not require a sheath to be operated.
2. is able to redirect 100% of the sample stream into the target cell reservoir for 50 µs and then instantly return the flow back to the nonsorted fraction.

Table 5. Expected purities, yields and processing times for different starting cell concentrations

Total cells/mL	10^6	10^7	10^8
Purity in Yield Sort [%]	96	69	18
Yield in Purity Sort [%]	96	64	11
Time to process 10^9 cells	309	31	3:05

3. uses a sample with 10^6 total cells/mL with 0.1% target cells.

This translates to a flow of 1.1 µL/s and cell detection frequency of 1.1×10^3 total cells/s. Since in this example 0.1% of all cells are target cells, the target cell frequency is 1/s; resulting in an average time of 1 000 000 µs between target cells and 900 µs between any two cells. Given that the sorting volume displacement is done in 50 µs, λ_T and λ_N can be calculated as:

$$\lambda_T = \frac{50 \ \mu s}{1.000.000 \ \mu s} = 0.00005$$

$$\lambda_N = \frac{50 \ \mu s}{900 \ \mu s} = 0.056$$

Thus, the expected purity in a yield sort would be

$$P = \frac{100\%}{1 + 0.056 \, e^{-0,00005}} = 96\%$$

Similarly, the expected yield in a purity sort would be

$$Y = 100\% \cdot e^{(-0.05605)} = 96\%$$

Using the same calculation for 1×10^7 total cells/mL and 1×10^8 total cells/mL, generates the data presented in Table 5. The key observation here is that, even though the resulting purity in the above yield sort example is limited, especially when processing input material with a concentration of 1×10^8 total cells/mL (Table 5), the enrichment from 0.1 to 18% purity is still 180-fold. This opens up the opportunity to utilize a sequential sorting strategy, where a fast yield sort is followed by a purity sort. When starting the experiment with the higher frequency yield sort from the above example, the first pass would have theoretically yielded an 18% pure target cell fraction being processed with a rate of
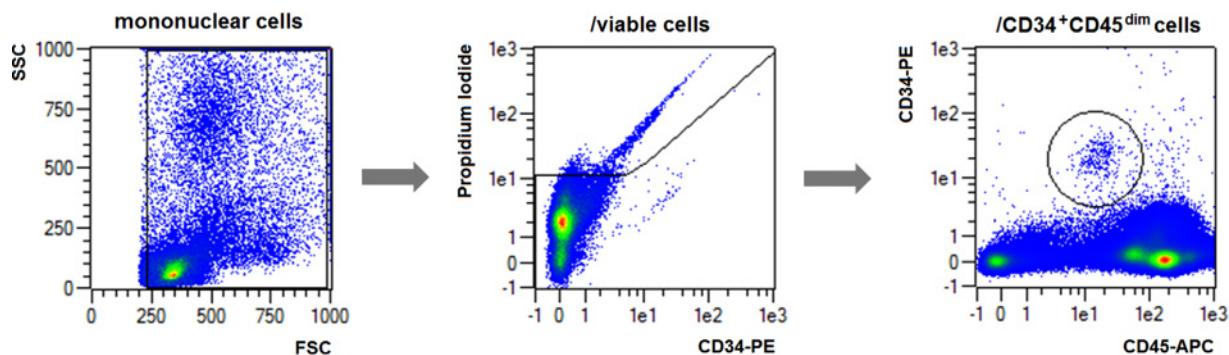
Figure 27. Staining pattern and gating strategy for a CD34$^+$ enrichment. The cells are stained with CD34-Pe and CD45-APC. For analysis purposes only, PI was added for post analysis only.
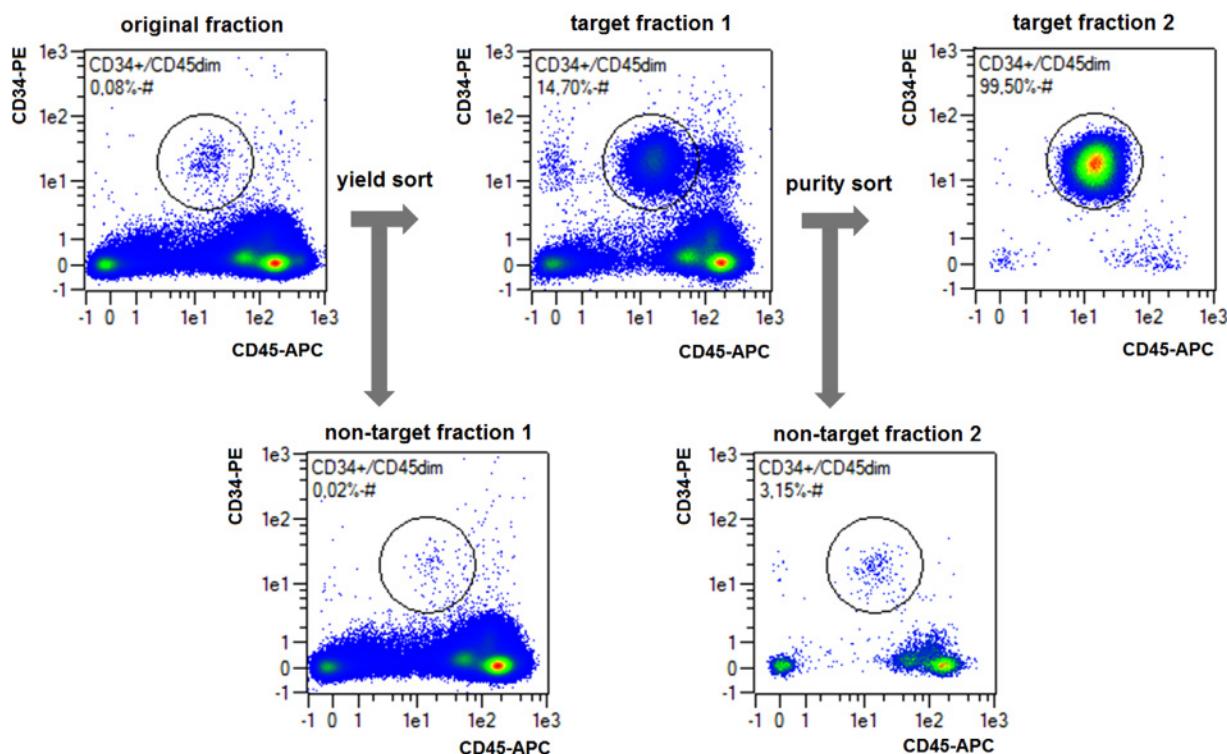
Figure 28. Result of a sequential sorting process. 109 total cells have been processed sequentially in 5 h to a final purity greater than 99%. Overall 280 000 target cells have been harvested from 800 000 target cells starting material, resulting in an overall yield of approximately 35%.

roughly 100 000 cells/s. If re-suspended again in the original volume, the second pass is processed with a total cell count very close to the one in the first example and would have yielded the target cells in a greater than 99% pure fraction. The above is demonstrated with a microfluidic sorter using a MEMS sorting chip in a completely closed cartridge performing a CD34$^+$ cell enrichment from a nonmobilized donor. As seen in Fig. 27, the staining pattern and gating strategy is straightforward. The target cell frequency was determined to be 0.08% and the total concentration was chosen so that the 10^9 total cells were suspended in 10 mL solution. From there, a yield sort was carried out, with a flow rate of 4 mL/h. The resulting cell processing rate was 110 000 total cells/s. With a target frequency of 0.08%, approximately 90 sorting actuations per second were expected. The enriched cells were then re-suspended in 10 mL solution and processed a second time for purity. The results are shown in Fig. 28. As a result of this sequential sorting strategy, with an overall sorting time investment of only 5 h, a result was achieved equaling a typical 20 h single-pass sort.

Since microchip sorting devices are particularly powerful in sorting cells gently due to the absence of high shear forces or electrostatic charges, they are ideally suited to follow such a sequential sorting approach. The rarer the target cell population or the higher the total cell count, the more advantageous this method becomes.

4 Collecting cells

4.1 Introduction

Even if a cell sorter is well adjusted, i.e., the instrument is able to deflect the right drop with the cell of interest at the right moment, it is still possible that the drop does not hit the collection vessel, due to issues regarding the relationship between cell size, nozzle size, sheath fluid temperature, and pressure stability. This results in a low sort yield and sometimes low purity. Optimal collection efficiency therefore depends on the setup of the cell sorter as well as the position and properties of the sample collection tubes.

4.2 Cell sorter-specific parameters

For a cell sort with high purity and yield an optimal gating strategy and detector setup is mandatory. Often, the discrimination between stained and unstained cell populations is problematic if they have a high overlap. In "dim" populations (i.e., low signal intensity, e.g., due to low marker expression or weak fluorochrome) the distribution of the cell events is dominated by the photon counting statistic of the PMTs and the background light and electronic noise of the detection channel. In other words,

when the light intensity emitted from a single cell is measured by a PMT, the specific signal has an additive part of a constant amount of nonspecific signal (coming from the background light, electronic noise, etc.). Thus, when a specific cell signal decreases, the nonspecific part remains stable and more and more dominates the entire signal and hence the distribution of the population. Consequently, the relative position of a cell inside a dim population is dominated by the background signal. This can lead to low cell recovery if gates are not well adjusted. Proper staining controls such as FMO [165] controls instead of unstained/single stained cells are very helpful to find the real boundaries of cell populations (see Section III.1: Controls: Determining positivity be eliminating false negatives). Furthermore, an optimal SNR by choosing the required PMT gain is essential for good population discrimination and optimal cell recovery [48].

Modern cell sorters can sort up to six cell populations simultaneously in collection devices equipped with tubes (e.g., Falcon® 5–50 mL round buttom tubes, 1–2 mL microcentrifuge tubes). Depositions of single cells in multi-well culture plates or onto slides, are also possible. Droplet sorters allow drops to be charged on different charge levels either positively or negatively, which allows drops to be deflected either to the left, far left or to right, far right. Deflection streams containing populations with the highest number of events to be sorted should be placed close to the center stream (i.e., left or right), since the focusing of the deflection streams is often better if their deflection is low. This minimizes the risk of cross contamination between the collection tubes.

Furthermore, the position of the deflection stream should be monitored during the sort process. This can be achieved by using the AccuDrop™ technology (BD FACSAria user's guide [151]) that consists of a red diode laser for side stream illumination, a filter block, and a camera mounted in the back of the sort chamber. The camera provides an image of the deflection streams with the intercept points of the laser beam. This allows the user the monitoring of the deflection stream quality in terms of position, focusing, and stability. Some sorters allow the monitoring of the break-off point using a camera and control the amplitude of the drop drive frequency depending on the camera image. This keeps the break-off point in a stable position by increasing or decreasing the amount of drop drive energy to the stream. This is a useful approach as long as the viscosity, density, and pressure of the sheath fluid is stable. If not, the cell recovery decreases even if the position of the break-off point is stable. Rapid temperature fluctuations of the sheath fluid of 1–2 K inside or next to the nozzle can become critical for cell recovery as well as for the side stream focusing. Therefore, good air conditioning or a sheath cooling [18] a device is highly recommended.

The side stream position for cells sorting in multi-well plates is essential and needs to be verified by test sorting of the target cells because the final drop positioning is often slightly different for beads or other cells. For single-cell sorting of 384-well plates, a plate cooling device is recommended to avoid evaporation of the cell media.

4.3 *Sample collection tubes*

The collection tubes can differ in terms of material as well as size. Polypropylene tubes are preferable over polystyrene tubes because the cells adhere less to the tube wall. Polystyrene tubes may build up the charge of the deflected drops on their surface. This can generate cross-contamination between collection tubes due to "jumping drops" caused by repulsion of incoming drops but can be prevented by using a grounded wire connected to a bent injection needle hung over the side of tube, such that the needle is in the fluid [154]. Different tubes sizes can be combined in a specific tube holder depending on the flexibility of the cell sorter. Moreover, a custom made tube holder became available recently as 3D print file [166].

The size of the collection vessel should fit to the expected volume of the sorted cell suspension and is correlated to the drop size and therefore to size of the nozzle. For example, 4×10^6 cells fill approximately a 5 mL Falcon® tube (12×75 mm), when using a 70 µm nozzle. The same amount of cells would require five 5 mL tubes when a 100 µm nozzle is used. Especially for long-term sorts, these correlations should be concerned, in order to prepare enough collection tubes beforehand. On the other hand, there is a high risk that cells may not be recovered in the collection tube if the tube size is much higher than the expected sample volume.

Collection tubes should be coated with proteins to avoid that the sorted cells stick to the tube wall as this results in reduced recovery and viability. This can be done by filling the tubes with 10% FCS 30 min before sorting or incubated overnight at 4°C with 10% BSA. As a general rule, the collection tubes should be prefilled with a small volume of media optimized for the cells of interest. This prevents the dehydration of the sorted cells and keeps the cells under optimal conditions to ensure their viability [167].

5 Flow-Cytometric Cell Sorting under GMP Conditions

5.1 *Introduction*

Flow cytometric cell sorting is a versatile and well-established research tool to isolate cells in high purity and speed. Multiparameter sorting permits the identification and isolation of specific cell subpopulations based on qualitative and/or quantitative antigen expression as well as on positive and negative selection criteria within a single selection procedure. With the advent of numerous cell therapy approaches for clinical applications, mainly driven by the success of chimeric-antigen-receptor-modified (CAR) T cells [168], interest in the clinical use of flow cytometric sorting is rising. Yet, cytometry-based cell sorting under good manufacturing practice (GMP) conditions is not yet available in a ready-to-use format and custom-made solutions pose a major challenge as stringent rules and regulations must be obeyed. The authors of this section established GMP-compliant and approved flow-sorting technologies and protocols adhering to European guidelines and regulations for the isolation of regulatory T cell subpopulations to

generate homogeneous cell products for the treatment of patients with graft-versus-host disease [169] within clinical trials. Based on their experience, a "list to consider" for researchers envisaging the implementation of flow sorting for medicinal products is provided, but not an "easy to use recipe," as manufacturing rules are complex and vary for each product depending on cell source, applied reagents, manufacturing process, cell specifications, (inter-) national and regional regulations, and various other issues pinpointed in this section. Thus, the first issue to clarify when flow-sorting is envisaged for the production of medicines is the clinical need and benefit as compared to established and/or approved alternative cell enrichment technologies, taking into account the efforts and implementation costs for GMP-compatible flow cytometric sorting.

5.2 GMP: Regulatory Requirements and Product Classification

When cellular products are supposed to be administered to patients, strict requirements have to be obeyed including international, national, and regional laws, rules, and regulations. For pharmaceutical manufacturing, GMP principles have highest priority and adherence to these guidelines is inspected by regulatory agencies during the manufacturing authorization process and regularly thereafter. GMP rules shall ensure high quality and batch to batch consistency for pharmaceutical products to prevent harm of patients caused by deviations during drug manufacturing. In contrast to the United States, full GMP-adherence is required within the European Union (EU) even for phase-I clinical trials [170], including cell therapy studies. Main areas covered by these GMP-regulations include detailed prerequisites concerning (i) quality management system, (ii) personnel, (iii) facility and equipment, (iv) documentation, (v) manufacturing, (vi) quality control, (vii) external suppliers, (viii) complaints and callbacks, and (ix) self-inspections.

The regulatory landscape in Europe is complex and became even more so since the category "advanced therapy medicinal products" (ATMP) was introduced by the European Commission (EC) in 2008 to discriminate unmanipulated blood products and tissues from gene therapy-, somatic cell therapy-, and tissue engineered medicinal products. ATMPs are medicinal products *"containing cells or tissues that have been subject to substantial manipulation so that biological characteristics [. . .] have been altered".* They *"have properties [. . .] to treat, prevent or diagnose a disease through the pharmacological, immunological or metabolic action of its cells or tissues"* [171–173]. "Substantial manipulation" in this context is defined in Annex I to regulation (EC) No 1394/2007 [174] where those manipulations are listed that are not considered substantial (e.g., cutting, grinding, centrifugation) and thus do not result in classification of a product as ATMP (then regulated as conventional blood, tissue, or cell products). Thus, flow cytometric cell sorting itself does not lead to classification as ATMP, unless additional cell manipulations before (e.g., gene transduction) or after cytometric sorting (e.g., in vitro stimulation or expansion)

are performed. In such cases, ATMP-specific GMP rules installed in 05/2018 by the European Commission must be obeyed [171].

5.3 Facility and Equipment

GMP rules concerning facility and equipment focus on controlled manufacturing conditions to ensure final product quality with a particular focus on the prevention of (cross-) contaminations (e.g., by particles or microbial agents). Thus, the facility and equipment must be qualified for the intended purpose and environmental conditions during manufacturing must be tightly monitored (e.g., controlled air flow and pressure, temperature, humidity, environmental particles, sterility, and so on). Based on thorough risk analyses and embedded in a detailed quality management system, qualification of the facility and all equipment (such as a flow-cytometric cell sorter) is performed in a stepwise fashion with particular attention on the intended performance and the inherent risks of a manufacturing process:

Design qualification (DQ): Documented verification that the proposed design of the facilities, systems, and equipment is suitable for the intended purpose. Thus, an upfront description of the intended use and definition of quality criteria for a manufacturing equipment (and/or the whole facility) is required and defined in "user requirement specification" (URS) documents.

Installation qualification (IQ): Documented proof that the URS are met by the equipment after its installation at the manufacturing site.

Operation qualification (OQ): Documented proof that the equipment is suited for the intended purpose and meets all predefined quality criteria when in operation.

Process qualification (PQ): Documented proof that the equipment is suited for the intended purpose within the whole manufacturing process of a pharmacologic agent.

During cell sorting with a stream in air cytometer the cells are exposed to the environment. Even instruments using cuvette flow cells contain open handling steps where the cells are exposed to the environment, therefore both techniques require clean room conditions class A (laminar air flow hood) in a class B room. The classification of clean room conditions in Europe is based on the maximal permitted airborne particle numbers as described in Annex 1 to part I of the European GMP guidelines (Table 6).

As no commercially available cell sorter is designed to meet these criteria, we cooperated with a cytometer manufacturer and a laminar air flow provider specialized in manufacturing equipment for the pharmaceutical industry and installed the cell separation chamber of the sorter in a custom-made laminar air flow bench qualified to meet class A clean room conditions while all auxiliary equipment potentially emitting particles (due to their air cooling systems) are contained in a separate air-filtered (in- and outlet) cabinet (Figure 29).

For cell therapy medicinal products batch to batch cross-contamination by cells, infectious agents or subcellular components (e.g., RNA or DNA) must be omitted and aseptic conditions are required. With conventional flow-cytometric cell sorters vali-

Table 6. Maximum permitted airborne particle concentration for each cleanroom grade (modified after EU GMP Guidelines Annex 1). Annex 1 to the EU GMP Guidelines defines the maximum permitted number of particles equal to or greater than 5.0 μm/m^3 as 20, corresponding to an ISO classification of 4.8. ISO class 5 would permit 29 particles equal to or greater than 5.0 μm per m^3. ISO = EN ISO 14644. Other clean room definitions apply to the US and other non-EU countries

Maximum permitted number of particles/m^3 equal to or greater than the tabulated size

Clean room grade		At rest		Clean room grade		In operation	
Annex 1	ISO	0.5 μm	5.0 μm	Annex 1	ISO	0.5 μm	5.0 μm
A	5/4.8	3520	20	A	5/4.8	3520	20
B	5	3520	29	B	7	352 000	2900
C	7	352 000	2900	C	8	3 520 000	29 000
D	8	3 520 000	29,000	D	–	Not defined	Not defined

dation of line clearance is almost impossible as it must be proven for each potential microbial contaminant (bacteria, fungi, viruses, endotoxins) and the test systems themselves for sterility testing have to be validated. To circumvent these problems, we use a sorter permitting the exchange of the whole fluidics system after production of each batch that is then replaced with a new sterile (γ-irradiated) single-use kit. Some providers currently develop new sorters that use mechanical valves or air pulses in closed systems for fluorescence-based cell separation that may significantly facilitate GMP-compatible flow sorting in the future.

5.4 Raw Materials

For the manufacturing of cell-based medicinal products a variety of raw materials are required. Hardly any of these raw materials, e.g., fluorescence-labeled antibodies for sorting, are covered by a pharmacopoeia or have ever been used for production of a medicinal product before. Since they come into direct contact with the cells, they are classified as critical for the safety, purity and potency of the final product. Therefore, in-house specifications, considering all potential risks, have to be provided if no reference to pharmacopoeial monographs can be made. Minimal requirements for quality control of critical raw materials are identity, biological activity/potency, toxicity, content, purity, sterility and microbial safety (including mycoplasma where applicable), viral safety, risk

of transmissible spongiform encephalopathies (where applicable), and stability. As these quality criteria reach back at least two generations (thus, definition of environment, equipment, and quality standards during the production of the respective materials), it is pivotal to ensure their highest possible quality for cell manufacturing. Since hardly any GMP-compliant (fluorescent-labeled) antibodies for flow-sorting are currently commercially available, they have to be custom-made by a qualified manufacturer.

5.5 Process validation, quality control, and product release

Process validation usually has to be performed prospectively with production of at least three batches. However, it is accepted by most authorities that process validation of investigational medicinal products (IMP; for clinical trials) cannot be as complete as for authorized (marketed) medicinal products. Guidance on process validation is provided by the European Medicines Agency (Guideline [175]) and the U.S. Food and Drug Administration (Guidance for Industry [176]). During process validation not only predefined final release criteria have to be examined, but also process-related impurities. These may originate from the cells (e.g., proteins, DNA), cell culture media (e.g., antibiotics, media supplements), or downstream processing equipment (e.g., columns). Most often they originate from raw materials for cell processing, e.g., cytokines, antibodies, serum, culture media, chemicals,
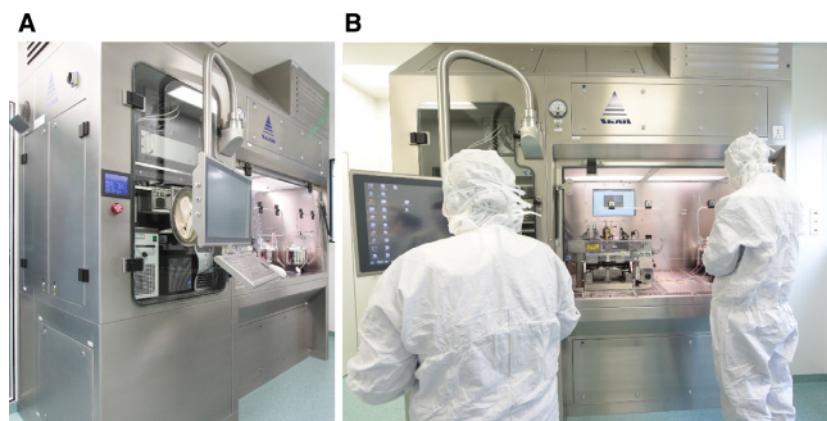
Figure 29. Custom-made GMP-compliant flow cytometric cell sorter (A) with auxiliary equipment cabinet (left) and laminar air flow hood (right) containing the sort chamber and (B) the sort unit in operation (safety-cabinet-enclosed sort unit seen between the two operators).

enzymes, and nucleic acids for genetic modifications. Since at least some of these substances (e.g., cytokines and stimulatory or sort-antibodies) may have an influence on the therapeutic cell product and/or may put a patient at risk even if administered in residual amounts (e.g., immunogenicity of antibodies, in vivo activity of cytokines), their presence in the final cell product has to be evaluated (ICH Q6B) [177]. Based on the potential risk, strategies for the determination of impurities may be arithmetical (calculation of residual amounts based on starting concentration and dilution factors or washing efficacy) or analytical (quantitative or limit test for impurities in the final product). While the arithmetical approach may be suited and accepted for impurities with low risk profile, evaluation of a particular impurity may be necessary or requested by the authorities for every batch if substances are suspected to bear a significant risk for the recipient (e.g., biologically active antibodies, toxic fluorochromes). Since standardized methods for the analysis of impurities are usually not available, respective test systems have to be designed and validated individually in advance (proving the appropriateness of an assay with respect to sensitivity, specificity, accuracy, precision, detection limit, range and limits of quantitation, robustness, and repeatability) [178], which is at least laborious and time consuming.

A successfully validated manufacturing process is a prerequisite to receive a manufacturing license by the respective authorities for cell therapy medicinal products that are either applied within clinical trials (separate clinical trial approval required) or as authorized medicinal products. In Europe, each cellular product for clinical use must be released by a qualified person who is responsible for the GMP-compliant manufacturing and final quality of the product. Predefined quality and release criteria typically include parameters such as volume, cell numbers, cell concentration, viability, identity, purity, potency, cellular contaminants, sterility, endotoxins, mycoplasma negativity, visual control, and eventually impurities (e.g., for sort-antibodies). Almost all assay systems for these quality controls (including flow cytometry-based tests) have to be developed individually and specifically for a given cell product and require validation (same criteria as described above) during the development of the manufacturing process to ensure their adequacy.

5.6 Final Remarks

The huge advantages of multi-parameter flow cytometric cell sorting with its speed and flexibility in a research environment thus far do not apply to GMP-compatible sorting. The high demands on the quality of auxiliary and raw materials and on the environmental conditions as well as stringent quality assurance measures and controls require a precisely structured and long-term preparation phase for each cell manufacturing process that cannot easily be changed once established. Thus, product characteristics and manufacturing tools and methods for an envisaged clinical cell product must be defined in detail in preclinical testing and be robust enough to justify the implementation of an expensive and strenuous manufacturing process involving flow cytometry.

Most importantly, the clinical benefit and advancement has to be considered in comparison to established and comparably "easy to use" cell enrichment technologies. Yet, once established it is satisfying to witness that cell purities easily exceeding 95% are regularly achieved with GMP-compatible flow sorting, which may be relevant in certain clinical situations such as GvHD therapy. The increasing interest of clinicians in cell therapy may motivate equipment and reagent manufactures to invest in financial and intellectual resources for the development of GMP-compatible flow sorting equipment and to provide a broader range of suited sort reagents in the near future.

V Biological applications

1 Rare cells: General rules

1.1 Introduction

Rare cell populations are of growing importance in several fields, from basic research to translational medicine and diagnostics. In several clinical settings, rare cell counts provide valuable information on the status and stage of the patient's disease. Some examples are rare CTCs in the peripheral blood, tumor stem cells, circulating endothelial cells, hematopoietic progenitor cells and their subpopulations, and fetal cells in maternal circulation. Interesting applications of rare cell analysis include the detection of metastatic breast cancer cells [179] or neuroblastoma cells infiltrating the bone marrow [180], monitoring of minimal residual disease [181, 182], detection of stem cells and rare HIV-infected cells in peripheral blood [183], antigen specific T cells, invariant natural killer T (iNKT) cells, and analysis of mutation frequencies in genetic toxicology [184]. Moreover, polyfunctional assays, such as the Ag-induced production of different cytokines by T lymphocytes, are often performed, and these raise the problem of finding rare cells within these T-cell populations as well. In this section, the main issues of this topic will be discussed, including the amount of biological material required, the use of pre-enriched populations, the number of markers to use and cells to acquire, the importance of excluding doublets and the use of a DUMP channel.

1.2 Optimization

Studying rare cells requires attention, optimal methodologies in all phases, including collection of biological samples, well-defined controls, and adequate use of software and hardware [185]. The term "rare" generally refers to events with a frequency of 0.01% or less, although the record claimed in the literature has long stood at one cell in 10 million for tumor cells spiked in the peripheral blood [186, 187]. For this, the acquisition of a large number of events (see Section V.1.2.3: Number of acquired events) and a high SNR (see Section V.1.2.5: Thresholds, gating, and DUMP channel) are the most relevant aspects.

1.2.1 The quantity of the biological material.   On the basis of the estimated frequency of the rare cells under investigation, it is crucial to calculate how much biological material is required. For example, if the endpoint of the experiment is to enumerate rare cell populations present in the cerebrospinal fluid (CSF), considering that only a few milliliter can be obtained from a patient, it is logical that all the CSF has to be used. If blood is the biological matrix of interest, the rare cell population of interest and the pathology of the patient should be considered in depth. Should the endpoint of the study be the evaluation of cytokine production after in vitro stimulation by cells such as iNKT cells in patients with HIV infection, some pre-analytical considerations should be taken into account. For example, iNKT cells are extremely rare among peripheral PBMCs (0.01–1%), and in order to define this population several markers must be used, including those for recognizing CD3, CD4, CD8, invariant TCR, as well as those for cell viability and several cytokines such as TNF-α, IFN-γ, IL-4, and IL-17 could be of interest, meaning that nine markers are required. HIV$^+$ patients who do not take antiretroviral therapy are obviously severely immunocompromised, and have a low number of CD3$^+$ T lymphocytes. Thus, the amount of blood required to detect a reasonable number of rare cells (according to Poisson statistics) can be as much as 50 mL of blood, since either resting or stimulated cells have to be analyzed [188].

1.2.2 Enrichment and choice of markers.   On the basis of the experimental endpoint(s) (e.g., phenotyping, functional assays), the rare population may be enriched or not, and the number of markers that are needed to unambiguously identify a rare cell population needs to be defined. For example, the accurate quantification of circulating endothelial cells and their progenitors, shown in Fig. 30, is a matter of debate. Several studies have been published, but no consensus has thus far been reached on either the markers that should be used to identify these cells, or on the necessity of a pre-analytical enrichment (by density gradient, buffy coat, and/or magnetic enrichment). The enrichment, however, can have negative effects if rare cells are lost, or these effects may be positive, if unwanted cells are removed [189–193]. Unfortunately, quite often, the lack of well standardized methods influences the decision regarding the number of markers, which are necessary for the identification of the population of interest. Depending on the technical characteristics of the flow cytometers, which have a varying number of fluorescence channels and the speed of acquisition, the most important marker allowing the identification and characterization of such populations should be decided. For example, in the case of iNKT cells, the Vα24Jα18 invariant TCR allows the unique identification of these cells. Having done that, the marker panel has to be built following a general rule that the brightest fluorochrome has to be used for the weakest expressed marker. Finally, attention should be paid to compensation, and acquisition of FMO controls, which is covered in more detail in Section II.1: Compensation and Section III.1: Controls: Determining positivity by eliminating false positives.

1.2.3 Number of acquired events.   Concerning the number of events that need to be acquired, it is recommended to use Poisson statistics, which defines the probability that a given number of events will occur in a fixed interval of time/space, assuming these events would occur with a known average rate and independently of the time elapsed from the previous event [194]. Therefore, Poisson statistics are applied to count randomly distributed cells in a certain volume. Let us consider a general case of enumerating a total of N events, of which R meet a certain criterion (i.e., they are positive, P). In this case, a proportion of P events is defined as $P = R/N$. The probability of any single event to be positive is obviously $0 \leq P \leq 1$, and this is related to the random manner in which cells are selected for analysis. As with all statistical distributions, the variance, Var, is a fundamental parameter, and is defined as: $\text{Var}(R) = NP(1 - P)$. The SD is the square root of the variance, and the CV is the SD equal to 1/square root of Var [195]. These equations can be used to examine some practical situations. Let us consider a phenotype analysis of human PBMCs stained with a mAb for detection of B cells (e.g., CD19 mAb). In healthy individuals, 10% of the cells can be positive, so that: $P = 0.1$ and $P(1 - P) = 0.09$. Good experimental practice suggests to keep CV below 5%; thus, acquiring even 5000 events could be sufficient, because the CV is 0.047 (i.e., in percentage, 4.71%). Using a number of cells such as 10 000, the CV becomes 3.33%. However, should positive events be less frequent, a higher number of events must be acquired. Table 7 reports an example for events whose frequency is 0.01%, as often occurs studying antigen-specific T cells.

This is clearly the ideal methodology. However, real life is different from theory, and very often the final number of events cannot be high enough to satisfy this golden rule. For example, we can consider the case in which one million peripheral T cells are stimulated with an antigen that activates less than 0.1% of them, namely 100 cells in one million. Nowadays, by polychromatic flow cytometry, T-cell activation can be analyzed by evaluating the polyfunctionality of these cells, and protocols have been developed that can identify in a relatively easy manner four or even five functions per cell. Thus, among responding cells, up to 32 populations can exist, likely with a different frequency, and each subpopulation contains a few cells that are completely absent in the control, unstimulated sample. Can we consider such cells positive, even if their number is much lower than that indicated by a strict statistical approach? A pivotal paper by Mario Roederer, an opinion leader in this field, gives us very useful and clear suggestions [196]. Indeed, if alternative explanations for the presence of such positive events can be excluded (i.e., if there is no noise due to dead cells or fragments, and if cell activation is really due to the antigen used in vitro and not to a pre-activation in vivo of T cells), the events can be considered positive, irrespective of their number. Thus, there is no reason to fix a threshold for the number of events below which any frequency must be considered "negative" [196]. In this case, "positivity" can be determined after comparison of the measurement against a set of control samples, among which the adequate negative controls, using standard statistical tools to compare the frequencies. For example, assuming that from the technical point of view the experiment is well performed, if T
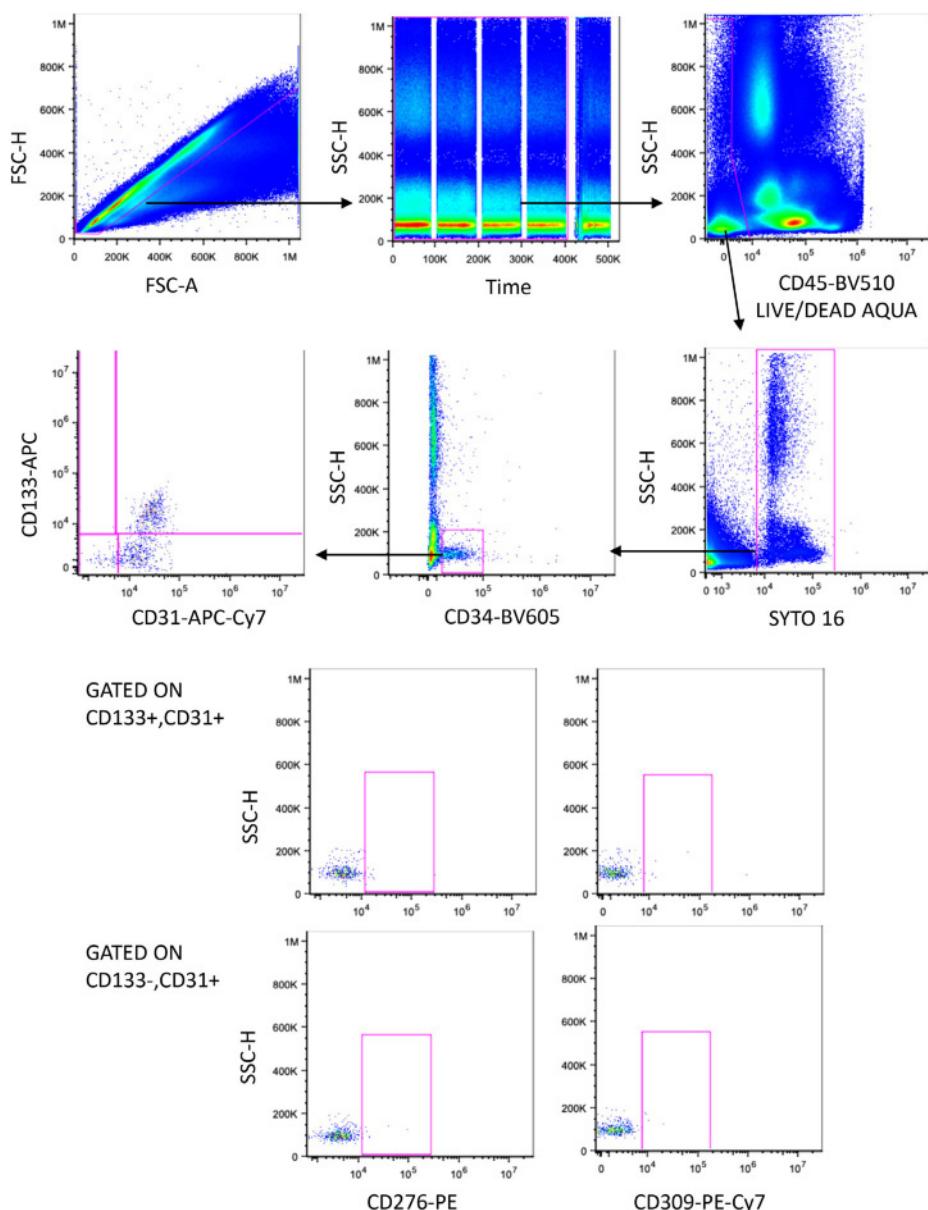
Figure 30. An example of a gating stategy for rare cells. Gating stategy used to identify circulating endothelial cells (CECs) and their precursors (EPCs) among peripheral blood leukocytes. (A) Debris and aggregates were eliminated using FSC-Area versus FSC-Height, (B) possible clogs were removed using the parameter Time versus SSC. (C) A DUMP channel was used to remove CD45^{+} cells and dead cells from the analysis. (D) Nucleated cells were identified based on Syto16 positivity. (E) Stem cells were identified according to CD34 positivity, (F) EPCs (CD133^{+}, CD31^{+}) and CECs (CD133^{−}, CD31^{+}) were identified. The expression of CD276, also named B7-H3 (G, I), and CD309 (H, J), also named VEGFR-2 or KDR, was evaluated in each subpopulation. In this example, more than 10 million events were initially acquired in order to enumerate a population that, according to the literature, is always represented less than 0.1%.

cells from "n" unvaccinated controls show no activation after the stimulation with the adequate peptides, while T cells from "n" vaccinated individuals do, even extremely low frequencies can be taken as positive. The same logics can be applied in thousands of other cases, assuming that the relative controls are well chosen.

1.2.4 Sample concentration and flow rate. Because it is crucial to acquire a high(er) numbers of events for detection of rare cell population, sample concentration and flow rate are critical parameters, which can typically shorten acquisition time. However, care must be taken that increasing the flow rate results in an increase of coincidence, and thus higher CV, if flow cytometers use

Table 7. Example to calculate the number of acquired events for a rare cell population representing 0.01%

Acquired events(N)	10 000	500 000	1 000 000	4 010 000	10 000 000	20 000 000
Positive (R)	1	50	100	401	1000	2000
Proportion (P)	0.0001	0.0001	0.0001	0.0001	0.0001	0.0001
Variance (Var)	0.9	49.99	100.0	400.1	999.9	1999.80
Standard deviation (SD)	0.9	7.07	10.00	20.02	31.62	44.72
Coefficient of Variation (CV)	100.00	14.14	10.00	4.99	3.16	2.24

hydrodynamic focusing (which is the system used at present in most commercially available flow cytometers).

1.2.5 Thresholds, gating, and DUMP channel.   A threshold should be fixed in order to distinguish the signal (using fluorescence or scatter) required to define the population of interest from the noise/background (see Section V.2: Trigger, thresholds, and live gating). Hence, maximizing the SNR of the cells of interest is mandatory. Gates should be drawn to exclude dead cells, identified by viability marker, doublets/aggregates/debris, and all the unwanted cell populations from the analysis, and a "DUMP" channel containing antibodies that identify cells of no interest is highly recommended. Moreover, using a dot plot with the parameter "time" versus that of interest allows to remove the event bursts caused by clogs or other transient problems during the acquisition. The instrument should be kept clean, and it is essential to wash the instrument between acquisitions of different samples in order to minimize sample contamination, which could cause the detection of false positive events.

1.3 *Data analysis*

Finally, data analysis requires adequate software and powerful hardware (more than 8 GB RAM or higher), because acquired data file tend to be huge, depending on how many events and parameters have been acquired (e.g., ten colors and two scatters in 10 million events are indeed a good test for your computer). To minimize the file size, parameters that are not really needed can be unselected, and a fluorescence/scatter threshold trigger can be used. Data analysis will be covered in greater detail in Sections VII.1–2: Data analysis: An overview, Data analysis—Automated analysis: Automated flow cytometry cell population identification and visualization, and Statistics for flow cytometry. In conclusion, flow cytometry is at present the most potent technology to address rare cell analysis, and the so called "next generation" instruments with very high speed and sensitivity are already allowing an easy detection and analysis of such cells.

2 Organisms, cells, organelles, chromosomes, and extracellular vesicles

2.1 *Overview*

Flow cytometry allows information about the structural and chemical characteristics of particles to be measured. Although the most common applications of flow cytometry use single mammalian cells, it is also applicable to studies of bacteria, yeast, and viruses as well as whole organisms such as nematodes and *Drosophila*. Conversely, parts of cells such as isolated nuclei, chromosomes, organelles, or extracellular vesicles may also be examined.

2.2 *Organisms*

Model systems are used to study molecular biology, developmental biology, and neurology and an example of this is the use of *Caenorhabditis elegans* (*C. elegans*). These organisms are around 1 mm in length, can be cultivated in large numbers, and have a short life cycle that makes them ideal for studying many areas of developmental biology. Particles of this size are not able to pass through the injection port and flow cell of most cytometers so specifically designed analyzers and sorters are available to identify and separate these organisms [197]. These large particle sorters can also be used for analyzing and sorting groups of cells such as imaginal discs, pancreatic islets, or embryoid bodies [198, 199].

2.3 *Cells*

Flow cytometry is perfectly suited for cells that are naturally in suspension, e.g., blood but any multicellular system (cell lines, tissue samples, whole organisms) may be made into single cell suspensions using a variety of mechanical and enzymatic techniques. In all cases, there is a balance between creating a good single cell suspension and keeping cell viability high. It is always important to make sure that measurement exclude dead cells as these will show increased autofluorescence and may bind antibodies and probes non-specifically. Exclusion of dead cells may be achieved by adding a viability dye—either a DNA binding dye such as DAPI or Propidium Iodide or an amine-reactive dye, which will bind to proteins [200, 201]. Any part of a cell may be labeled with a fluorescent probe but it is important to remember that flow cytometry gives whole cell information, there is no localization of the fluorescence nor any idea about its distribution within the cell. To determine the location of fluorescence, an imaging technique is needed, e.g., fluorescence or confocal microscopy or imaging flow cytometry [202].

2.4 *Nuclei*

Sometimes only the DNA or a nuclear protein is of interest and in these cases, cell nuclei can be produced that often will have less nonspecific binding and therefore a cleaner background. Production of nuclei from cells can be achieved in unfixed samples by treating cells with a detergent, e.g., 0.1% Triton-X100, which will lyse cells and release nuclei [203]. Or in fixed samples, cells may be treated with an enzyme such as pepsin that will digest the cytoplasm and again release nuclei [204]. Isolated nuclei will often give a better CV (coefficient of variation, a measure of data spread) than whole cells, making it easier to discern cell cycle phases.

2.5 *Cell organelles*

Cell organelles within whole cells can be specifically identified by staining them with fluorescent dyes. These dyes

may be fluorochrome-labeled antibodies or fluorescent probes. Autophagosomes may be identified by staining with LC3 antibody [205], whereas mitochondria can be stained with Mito-Tracker dyes [206]; lysosomes, endoplasmic reticulum, and Golgi can also be identified [207]. Care must be taken with many dyes that are organelle-specific as the staining time and concentration will be very cell-type dependent and these factors may need to be determined empirically. Also important when analyzing organelles are controls; not just a negative control to assess background fluorescence but also a positive control to ensure that staining is successful as the majority of these assays involve unfixed samples. Also important is building in a kinetic element to experiments, i.e., looking at time points following treatment or stimulation.

Cell signaling events are often studied in immunological cells and a common way to do this is to monitor changes in calcium levels that result from the binding of antibodies to surface receptors. There are several fluorescent dyes available that can monitor calcium levels such as Indo-1, Fluo-4, and Fura Red [208]. Indo-1 is a UV-excited dye that precludes its use in many common flow cytometers but it does have the advantage that it uses a ratio of the bound to unbound calcium signal and is therefore independent of cell size and variability in dye loading.

If cell organelles are to be analyzed, in some cases it is better to digest the organelle from the cell. It is possible to isolate mitochondria, endocytic vesicles, and endoplasmic reticulum by several methods generally using tissue homogenization [209]. Such treatment will inevitably lead to some cell loss and a sample that will have a considerable amount of debris. However, the selection of dyes combined with light scatter characteristics can allow specific organelles to be identified. Although isolated organelles can often result in cleaner staining, the smaller the particle the more problems there will be with co-incident events, i.e., when more than one event is being measured in the flow cell of the cytometer. Both in analysis and sorting, the use of light scatter and fluorescence is needed to delineate true particles from background.

2.6 Chromosomes

Although interphase chromosomes cannot be delineated by standard flow cytometry, chromosomes at metaphase may be identified and isolated and this is important in genomic analysis in many animal and plant species [210]. Cell division is blocked during metaphase using a drug such as colcemid, chromosomes are isolated following rupture of the cells in a detergent solution and are stained with two DNA binding dyes that have different base-pair specificities [211]. In this way, chromosomes may be separated on size and base-pair ratio, Chromomycin A3 (G-C binding) and Hoechst 33258 (A-T binding) is the preferred pair of DNA dyes. This is an extremely powerful technique but is not widespread as the dyes used require nonstandard excitation wavelengths (355 and 457 nm) and high-powered lasers that are not widely available. However, chromosome analysis and sorting is also possible using standard benchtop analyzers or sorters [212]. Sample preparation, staining buffer, and cytometer setup are all critical in chromosome analysis.

2.7 Extracellular vesicles

A growth area in cytometric analysis in recent years has been the detection of small particles that encompass exosomes, microparticles, microvesicles, and cell-derived microparticles (including platelets, endothelial, and leukocyte microparticles). Microvesicles are defined as being 100–1000 nm in size [213] compared with exosomes, which are <100 nm [214], which can lead to challenges with detecting them using a flow cytometer. Most modern cytometers will have a detection limit in terms of the size of the particle that will be governed by the optical configuration of the cytometer. Light scatter is traditionally generated by using a 488 nm laser but it can be detected from any laser wavelength given the correct optical filters [215]. In general, microvesicles will be identified and detected by a combination of light scatter (side scatter, or right angle light scatter is preferred to forward scatter) and fluorescence. Vesicles mostly consist of a lipid membrane plus cytosolic contents that may include cellular organelles, therefore, labeling the lipids, specific membrane proteins, or specific organelles is the best approach. This can be an amine reactive dye such as carboxyfluorescein succinimidyl ester [216], a specific lipid binding protein such as fluorescently-labeled annexin V [217] or mitochondria-binding dyes such as MitoTracker [218]. As the size of the particles is smaller than the diameter of the lasers used in the flow cytometer, there are the same considerations of co-incidence as with isolated organelles. As well as in conventional flow cytometry, exosomes and microvesicles can also be studied using other cytometric technologies such as imaging flow cytometry [219]. See Chapter V Section 2.7 Extracellular vesicles for more detailed information.

3 Mitochondria

Mitochondria are essential mediators of cell metabolism, being producers and targets of reactive oxygen species (ROS), regulators of ATP levels and calcium homeostasis, and hubs of the biosynthetic pathways involved in the synthesis of amino acids, lipids, and nucleotides [220]. Mitochondria are present in all cells, including those that rely mostly on glycolysis rather than on oxidative phosphorylation for ATP synthesis. They are very heterogeneous in size, shape, and number, depending on the metabolic requirement of the cells, the underlying tissue, and several other factors. Given their crucial role in cellular and organismal functions, it is not surprising that mitochondrial (mt) dysfunctions have been observed in a number of genetic and nongenetic diseases, as well as in cancer and aging [221]. In the vast majority of cases, distinctive features of mt dysfunction include changes in mtmP, mt mass, and redox potential.

Flow cytometry allows the rapid monitoring of all these parameters in intact cells, avoiding artifacts associated with mt isolation and/or permeabilization, and offering the benefits to work in a

Table 8. Main fluorescent probes used to stain mitochondria in intact, living cells

Full name	Short name	Abs (nm)	Em (nm)	Fixable
Mitochondrial membrane potential				
3,3'-Dihexyloxacarbocyanine iodide	$DiOC_6$	484	501	No
Rhodamine 123	Rh123	507	529	No
5,5',6,6'-Tetrachloro-1,1',3,3'-tetraethyl-benzimidazolcarbocyanine	JC-1	514	529/590	No
3,3'-Dimethyl-αlpha-naphthox-acarbocyanine iodide	JC-9	522	535/635	No
Tetramethylrhodamine ethyl ester	TMRE	549	574	No
Tetramethylrhodamine methyl ester	TMRM	548	573	No
MitoTracker Red CMXRos		578	599	Yes
Mitochondrial mass				
Nonyl Acridine Orange	NAO	495	519	No
Mito ID Red		558	690	Yes
Mitotraker Green FM		489	517	No
Mitotraker Deep Red 633		644	665	Yes
MitoTracker Red 580		581	644	No
Mitochondrial reactive oxygen species				
MitoSOX Red mitochondrial superoxide indicator	MitoSOX	510	580	
Mitochondria Peroxy Yellow-1	MitoPY-1	510	528/540	

Abs, absorbance; nm, nanometers.

preserved cellular environment [222]. A number of mt-specific fluorescent probes have been developed, which can be used to measure mtmP, mt mass, and intra-mt ROS (Table 8) [223].

mtmP is the main component of the proton-motive force, which is established by protons pumped from the mt matrix to the inter-membrane space, and combines the mtmP to the mt pH gradient. This potential varies according to the status of mitochondria, it is related to their capacity to synthetize ATP, and is a common indicator of cell health. According to the Nernst equation [224], the mt matrix is negative, thus indicating that hyperpolarized or depolarized mitochondria present a more or less negative mt matrix, respectively. Dyes for measuring mtmP are typically lipophilic cationic compounds, i.e., positively charged molecules that can cross membranes without binding them, and accumulate in the mt matrix in direct proportion to mtmP. Hyperpolarized mitochondria accumulate more dye, whereas depolarized mitochondria accumulate less dye. When mtmP is assessed by flow cytometry, two major recommendations have to be taken into account. First, dye concentration should be carefully titrated. High dye concentrations lead to fluorescence quenching, which generates artifacts and misleading results. Even if quenching threshold varies depending on the dye, concentrations in the range 1–30 nM should be low enough to avoid unwanted quenching phenomena [225]. Second, functional controls must be used to ensure that changes in the dye signal are interpreted properly and are not caused by other parallel changes, including those in mt mass. Appropriate controls are represented by:

1. carbonyl cyanide-4-(trifluoromethoxy)phenylhydrazone (FCCP), carbonyl cyanide m chlorophenyl hydrazine (CCCP), and valinomycin, which are uncouplers;
2. oligomycin, an ATP synthase inhibitor;
3. and nigericin, a K^+/H^+ ionophore.

While FCCP, CCCP, valinomycin, and oligomycin induce depolarization, nigericin induces hyperpolarization.

A list of the main fluorochromes used to assay mtmP in living cells is shown in Table 8. Among them, 3,3'-dihexyloxacarbocyanine iodide ($DiOC_6$) has been extensively used in flow cytometric studies [226]. However, $DiOC_6$ activity as NADH inhibitor, together with its toxicity toward mt respiration, strongly limits the use of this probe [227, 2258]. Similarly to $DiOC_6$, rhodamine 123 (Rh123) was initially used in several studies [228]. However, Rh123 enters easily into the cells and rapidly equilibrates, but is not well retained. In addition, in certain conditions, Rh123 binding to mitochondria can be independent of mitochondrial energy status, and this further restricts its use [229, 2258]. Conversely, tetramethylrhodamine ethyl ester (TMRE) and tetramethylrhodamine methyl ester (TMRM) are widely used to probe mtmP by flow cytometry [230, 231]. These dyes are nontoxic, specifically stain polarized mitochondria, and do not display quenching effects [231]. They should be used at relatively low concentrations, and the analysis can be performed immediately after staining, even in the absence of wash steps. Upon excitation at 488 nm, TMRE and TMRM emits at 574 nm. As monochromatic dyes, the MdFI relative to the proper channel should be measured for TMRE and TMRM. Typically, an unstained sample (also known as "blank") should be prepared, in order to set the levels of background fluorescence, and subtract this background fluorescence to fluorescence of the stained sample. When assayed by TMRE or TMRM, changes in mtmP are thus evaluated as changes in MdFI of a given sample (Fig. 31).

Carbocyanine dyes, especially 5,5',6,6'-tetrachloro-1,1',3,3'-tetraethyl-benzimidazol-carbocyanine (JC-1), are considered the most reliable probes for the detection of mtmP. JC-1 has poly-chromatic fluorescence emission spectra, and allows a ratiometric semi-quantitative assessment of mt polarization [232, 233]. In the
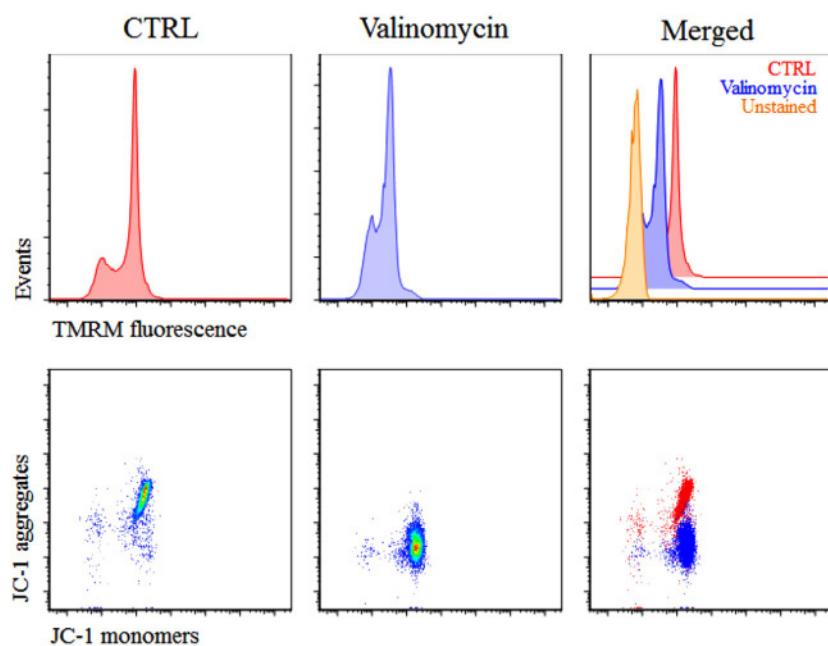
Figure 31. TMRM and JC-1 staining of CD4$^+$ T cells. The K$^+$ ionophore valinomycin depolarizes mitochondria of CD4$^+$ T cells, as revealed by the decrease in TMRM fluorescence, and by the decreased fluorescence of JC-1 aggregates and increased fluorescence of JC-1 monomers. Untreated cells (CTRL) are shown in left panels. For TMRM, unstained sample is also shown in right panel. Dot plot combining untreated sample and valinomycin-treated sample is also reported (lower right panel).

monomeric state, it emits a green fluorescence (529 nm), whereas in the aggregate state, which is highly dependent upon mtmP, it emits an orange-red fluorescence (>590 nm), well detectable in healthy cells. In the presence of compounds that cause a collapse in mtmP, JC-1 becomes monomer. This means that while in healthy cells both green and orange-red fluorescence are expected, cells with depolarized mitochondria display only green fluorescence [234]. Considering the shift in fluorescence due to mtmP changes, the best way to display results is that of indicating the percentage of cells with high or low mtmP, rather than the ratio between green and orange-red fluorescence. Since 1993, JC-1 has been reported as a reliable membrane potential indicator for several cell types and assay conditions [232, 235, 236], and its compatibility with other fluorescent probes has also been demonstrated in the design of multicolor panels [237, 238]. However, the sensitivity of JC-1 toward hydrogen peroxide, its photosensitivity, and the slow rate of equilibration between monomers and aggregates, could partially limit its use. Other dyes, similar to JC-1, are also available but are scarcely used. JC-9 is characterized by polychromatic fluorescence emission, with excitation at 522 nm, and emission at 535 or 635 nm, in the monomeric or aggregate forms, respectively. The green fluorescence of JC-9, characterized by a different chemical structure respect to JC-1, is essentially invariant with membrane potential, whereas the red fluorescence is significantly increased at hyperpolarized membrane potentials. JC-10 is excited at 490 nm, and emits at 520 nm (monomeric form) or 590 nm (aggregated form). Compared to JC-1, JC-10 is characterized by higher water solubility and diffuses out of mitochondria in apoptotic and necrotic cells.

Mitochondrial mass can be monitored by using dyes able to bind specific mt components regardless of mt polarization status. For this reason, the amount of fluorescence is directly proportional to mt content. Mito ID and nonyl acridine orange (NAO) bind to cardiolipin in the inner mt membrane, whereas MitoTracker dyes react with the thiol groups of cysteine residues present in mt proteins [239, 240]. Some of these dyes, including MitoTracker deep red 633, also form covalent bonds with mt proteins, thus allowing fixation after cell staining. As described for TMRE and TMRM, the MdFI relative to the proper channel should be measured for MitoTracker dyes, and the MdFI of the unstained sample should be subtracted to the MdFI of the stained one (Fig. 32).

Regarding mt ROS, two fluorescent probes, i.e., MitoSOX red mitochondrial superoxide indicator (MitoSOX) and mitochondria peroxy yellow-1 (mitoPY1), have been recently developed to stain specifically anion superoxide and hydrogen peroxide in mitochondria, respectively [241–243]. MitoSOX is the mitochondria-targeted form of hydroethidine. It accumulates into mitochondria depending on mtmP, and it emits fluorescence upon oxidation and binding to mitochondrial DNA [244]. As already reported for other probes, when using MitoSOX and mitoPY1, preparing adequate positive and negative controls is crucial to fully validate the presence of mt H$_2$O$_2$ in biological systems. Antimycin A or doxorubicin are best-suited positive controls for MitoSOX staining, whereas exogenous H$_2$O$_2$ or other molecules that increase the fluorescence signal of the probe represent proper positive controls for mitoPY1. Negative controls for MitoSOX staining are cell-permeable superoxide dismutase mimetics or mt uncouplers, depending on the cell type. Additional controls can be represented by antioxidants, such as N-acetylcysteine, or other specific scavengers that highly reduce free radical production [245]. MitoSOX and mitoPY1 have been tested by flow cytometry for selective quantification of mt anion superoxide and mt hydrogen peroxide in keratinocytes, endothelial cells, fibroblasts, several cancer cell lines, among others [246–249]. The possible simultaneous use of MitoSOX and mitoPY1 in the same panel for the analysis of mt ROS in living cells has also been reported (Fig. 33; [246]).
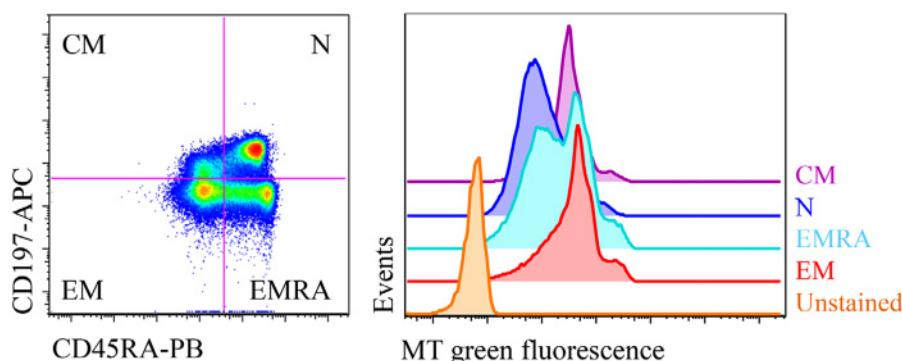
Figure 32. MitoTracker Green staining of different subsets of CD8^{+} T cells. Different CD8^{+} T-cell subsets, i.e., central memory (CM), naïve (N), effector memory (EM), and terminally differentiated effector memory (EMRA) were identified according to the expression of CD45RA and CD197. Among them, the use of MitoTracker Green (MT Green) allows to determine mt mass, which is clearly different among cell subsets.

Flow cytometry is undoubtedly a useful tool to assay mt functions in biological samples. Protocols to assay mt parameters can be applied to several cell models, and are relatively fast, as the time required to complete staining and data analysis (even in the case of multicolor panels) rarely exceeds 3 h. In addition, the analysis of several thousands of cells in a few minutes allows accurate measurements. Nevertheless, as a general rule, the use of more than one probe, as well as the use of complementary methods to assess changes in mt membrane potential or mt mass, is strongly recommended.

4 Extracellular vesicles

4.1 Overview

Body fluids contain cell-derived extracellular vesicles (EVs), which can suppress and enhance the immune system and contribute to the development of systemic autoimmune disease. To investigate the role of EVs in immunology, flow cytometry (FCM) is the technology of choice for determining the concentration of EVs expressing certain antigens. However, because EVs are substantially smaller and dimmer than cells, EV detection and data interpretation are challenging, leading to misconceptions. For example, on the one hand, it is often overlooked that FCM does not detect the entire size range of EVs. On the other hand, it is often incorrectly thought that FCM is incapable of detecting EVs smaller than the wavelength of light. The aim of this section is to briefly address some common misconceptions of EV FCM and to provide recommendations to prevent potential artifacts arising from sample preparation, staining, assay protocol, and data analysis.

4.2 Introduction

Blood and other body fluids contain cell-derived extracellular vesicles (EVs), which is the umbrella term for all types of cell-derived vesicles including microvesicles and exosomes. Figure 34A shows a transmission electron microscopy (TEM) image of EVs, which can be seen as subcellular cargo containers transporting biomolecules, such as transmembrane receptors and genetic information, to tar-

get cells. From an immunological perspective, EVs are interesting because EVs transport ligands that can suppress the immune system, enhance the immune response by antigen presentation, and contribute to the development of systemic autoimmune disease [250]. See also Chapter V Section 2 Organisms, cells, organelles, chromosomes, and extracellular vesicles.

4.3 EV analyses by flow cytometry

EV FCM is particularly useful to determine the number concentration of certain EV types in (body) fluids. However, the small size of EVs complicates FCM analyses. Figure 34B shows a size distribution of EVs from human urine based on TEM and resistive pulse sensing. General properties of an EV size distribution are a smallest diameter of 50 nm, a peak below 400 nm, and a decreasing concentration with increasing diameter for EVs larger than the peak diameter [251, 255–257]. Thus, most EVs are smaller than the illumination wavelength (λ) typically used in FCM. A general misconception is that EVs smaller than the illumination wavelength cannot be detected by FCM. According to the Rayleigh criterion, EVs smaller than roughly half the illumination wavelength cannot be distinguished by classical light microscopy [258]. However, even the smallest EVs do scatter light of longer wavelengths and can be detected by FCM, provided that single EVs are illuminated and the flow cytometer has nanoparticle sensitivity. In practice, most flow cytometers do not have nanoparticle sensitivity: a recent standardization study showed that only six of 46 tested flow cytometers in the field were able to detect EVs as small as 300 nm [259].

To explain how the size of EVs affect their light scattering intensity, Fig. 34C shows the FSC measured by FCM (A60-Micro, Apogee Flow Systems, UK) versus the diameter of platelet-derived EVs and platelets exposing integrin β_3 (CD61) from human plasma and, for comparison, of polystyrene particles. The diameters of EVs, platelets, and polystyrene particles were obtained from the FCM scatter ratio [253], literature values [254], and specifications of the manufacturer, respectively. Please notice that the scattering intensity of EVs rapidly decreases for small diameters [251, 258, 260, 261] and is substantially lower compared to platelets and similar-sized polystyrene particles [260, 261]. The low scattering
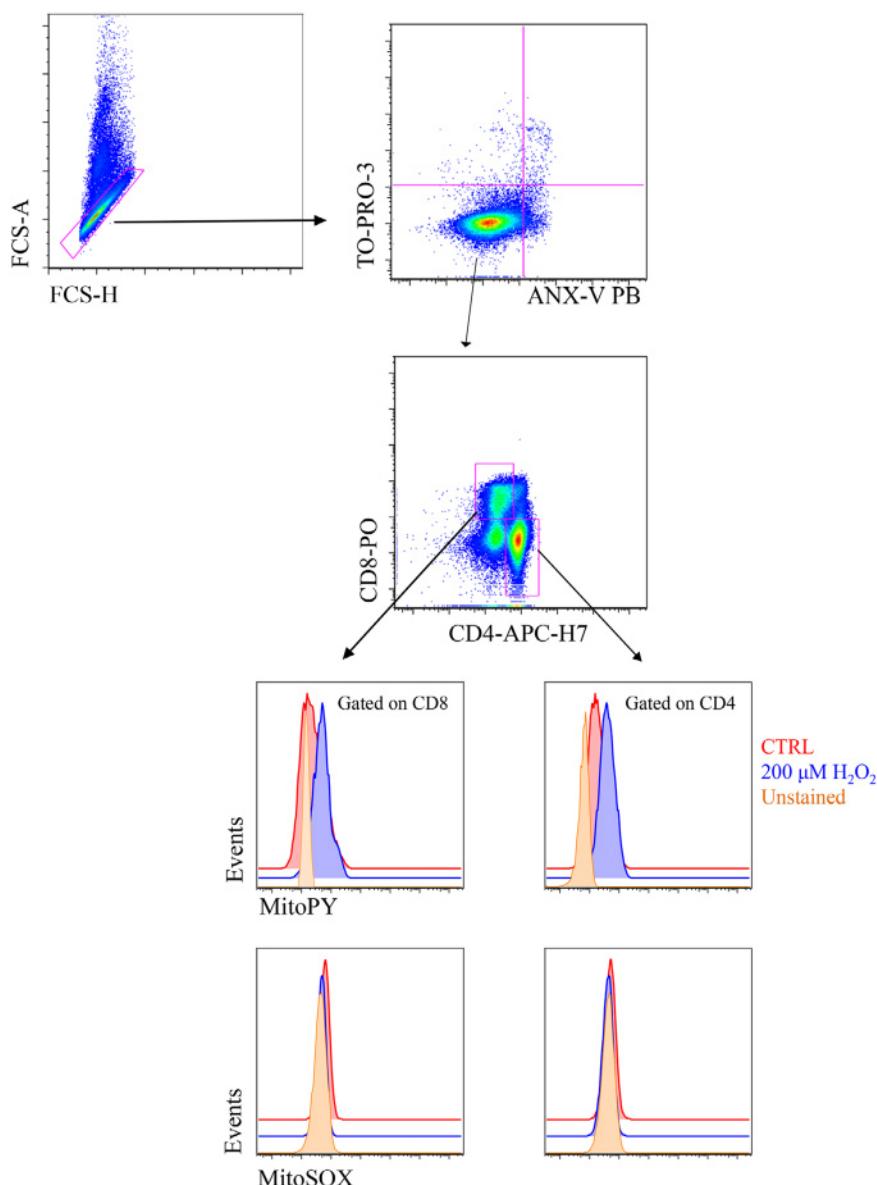
Figure 33. MitoSOX Mitochondrial Red superoxide indicator and Mitochondria Peroxy Yellow-1 staining of different subsets of CD8$^+$ T cells. Doublets were excluded from the analysis of PBMCs by using FCS-A and FSC-H (upper left panel); viable cells were selected according to negativity for annexin-V (ANX-V) Pacific Blue conjugate and TO-PRO-3 iodide (upper right panel). Then, CD4$^+$ or CD8$^+$ T lymphocytes were selected on the basis of positivity for a CD4$^-$ APC-H7 mAb or a CD8-PO mAb respectively. Among these, fluorescence intensity of MitoSOX Mitochondrial Red Superoxide Indicator (MitoSOX) and Mitochondria Peroxy Yellow-1 (mitoPY) was analyzed.

efficiency of EVs implies that a flow cytometer cannot detect EVs as small as the smallest detectable polystyrene beads.

The small size of EVs also results in low fluorescence intensities. Figure 34D shows the fluorescence intensity versus diameter of EVs and platelets labeled with APC CD61 mAb. The parabolic curve indicates that EVs and platelets have a similar surface density of CD61. However, because the surface area scales quadratically with the particle diameter, EVs have much less antigens available to bind APC CD61 mAb than platelets and therefore emit less fluorescence. The complex size distribution combined with low scatter and fluorescence intensities imply that signals from EVs are close to and/or below the detection limit of FCM. Hence, a flow cytometer with the dynamic range to detect all EVs in biological samples does currently not exist.

The difficulty of EV FCM is recognized by the EV Flow Cytometry Working Group (evflowcytometry.org), which consists of experts from the International Society for Extracellular Vesicles (ISEV), International Society for Advancement of Cytometry (ISAC), and International Society on Thrombosis and Haemostasis (ISTH). At present, the working group is compiling a series of consensus manuscripts, which will become a framework that is consistent with the MIFlowCyt guidelines [39]. A preliminary outcome is that a general step-by-step protocol for EV FCM does not exist yet, because the optimal procedures depend on the research question, the sample studied, and the flow cytometer used. The steps below are therefore recommendations for EV FCM experiments with references to articles with detailed protocols and examples. This section does not cover imaging FCM, flow sorters, or mass cytometry. Based on new insights and reaching consensus in the rapidly evolving EV research field, however, current recommendations will likely become subject to change.
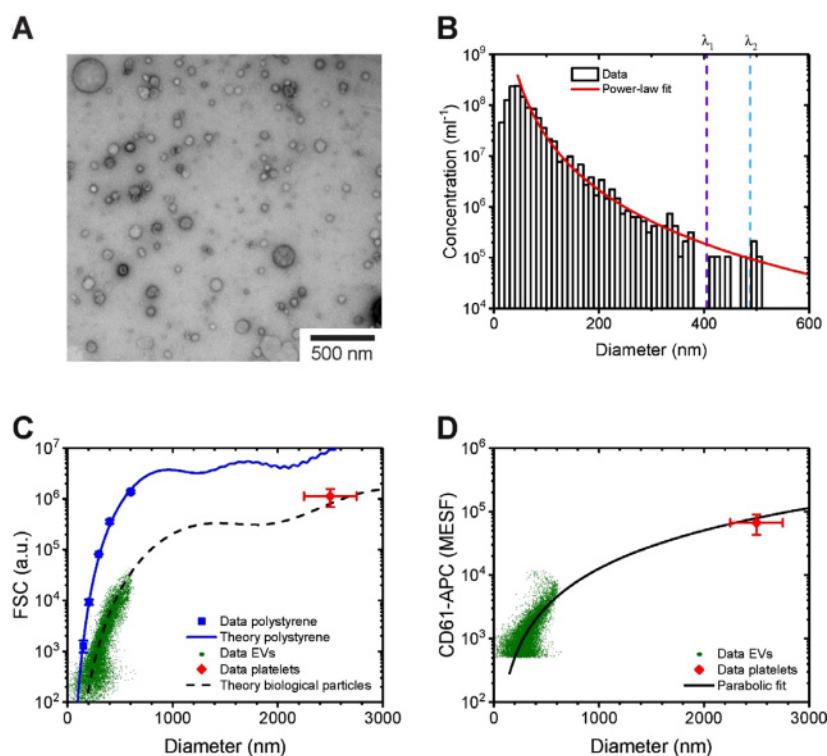
Figure 34. Flow cytometry (FCM) detection of extracellular vesicles (EVs). (A) Transmission electron microscopy (TEM) image of EVs from human urine after one freeze–thaw cycle [251]. (B) Size distribution of EVs from human urine by TEM [251]. Please note that all graphs have logarithmically scaled vertical axes. The size distribution has a maximum and follows a power-law distribution for larger EVs. For comparison, λ_1 and λ_2 (dashed lines) indicate illumination wavelengths typically used in FCM. (C) Forward scatter (FSC) versus diameter for EVs and platelets exposing integrin β_3 (CD61$^+$) from human blood plasma and polystyrene particles measured (symbols) by FCM (A60-Micro, Apogee Flow Systems, UK) and calculated (lines) with Mie theory (Rosetta Calibration, Exometry, the Netherlands) [252]. The diameters of EVs, platelets, and polystyrene particles were obtained from the FCM scatter ratio [253], literature values [254], and specifications of the manufacturer, respectively. Polystyrene particles were modeled as solid spheres with a refractive index (RI) of 1.633, whereas EVs and platelets were modeled as concentric spheres having a shell with a thickness of 4 nm and an RI of 1.48 and a core with an RI of 1.38. FSC increases with increasing diameter and refractive index and scatter of polystyrene particles cannot be directly related to the scatter and diameter of EVs. (D) CD61-APC versus diameter for EVs and platelets exposing CD61$^+$. The parabolic fit describes CD61-APC expression of EVs and platelets ($R^2 = 0.59$), meaning that EVs and platelets have a similar density of CD61. In (C) and (D), the EV diameter was determined by the FCM scatter ratio [253], whereas the platelet diameter was obtained from the literature [254].

4.4 Step-by-step sample preparation

4.4.1 Collection, isolation, and storage. Because cells may still release EVs after collection of a (body) fluid, unprocessed fluids are unstable EV samples [262, 263]. To obtain stable EV samples, it is common practice to collect the fluid, remove cells, and freeze EV-containing aliquots. However, each pre-analytical step will impact the concentration and composition of EVs. The optimal protocol depends on the research question, the type of (body) fluid, the type of the EVs of interest, and the used flow cytometer. To limit the scope and emphasize differences between pre-analytical variables involved in cell and EV FCM, we will summarize considerations involved in collection and isolation of EVs from human blood for characterization by FCM. The considerations are based on ISEV guidelines [264], ISTH guidelines [265], and methodological guidelines to study EVs [262]. Considerations for other fluids, such as urine [266] and saliva [267] can be found in the literature [263].

4.4.2 Collection. Collect blood from overnight fasting subjects with a 21-gauge needle and avoid prolonged use of a tourniquet [268–271]. Collect blood in plastic tubes at room temperature and discard the first 2–3 mL of collected blood [272, 273]. Omit hemolyzed blood samples or interpret results with care [264]. The recommended anticoagulant for FCM analyses is citrate (0.109 mol/L final concentration) [265]. During transport, minimize vibrations and keep the tubes in a vertical position. Minimize and standardize the time interval between collection and removal of cells.

4.4.3 Isolation. When preparing serum, EVs are released during the clot formation [262]. Therefore, plasma is usually preferred over serum and serum that is used as culture medium should be EV-free. To prepare plasma from blood, current guidelines recommend to apply two subsequent centrifugation steps of 2500 × g for 15 min at room temperature [265]. Use the lowest or no deceleration, and do not collect the 5 mm of plasma above the buffy coat.

Quantify the number of residual platelets in the platelet-depleted plasma. To improve reproducibility, report centrifugation conditions, including deceleration, rotor type, speed, temperature, time, tube type, and volumes in the tubes [274].

A misconception about EV FCM is the use of additional high-speed and ultracentrifugation steps to isolate and concentrate EVs of different size (e.g., microvesicles and exosomes). Separating EVs of different sizes is unnecessary because the size of EVs can be determined by FCM based on scatter or fluorescence signals [252, 253, 275]. Concentrating EVs is unnecessary for all EV samples that require dilution upon FCM analysis. A centrifugation washing step or size exclusion chromatography, however, may be useful to decrease the concentration of lipoprotein particles, which overlap in size with EVs, soluble proteins, and unbound reagents [276]. The presence of these non-EV particles may cause artifacts, which will be discussed in the next sections about staining and swarm detection.

4.4.4 Storage. Although the stability of EVs during a freeze–thaw cycle and storage warrants further investigation [263], freezing is the most common method to store EVs. Use vials with a rubber ring and screw lid to minimize cryo-precipitation and to prevent formation of ice crystals. Snap-freeze aliquots in liquid nitrogen [277], store aliquots at or below −80°C, and thaw aliquots at 37°C [278–280].

4.5 Staining

EVs can be stained with labels available for cells, such as antibodies (Abs; Chapter III, Section 1.1 Controls: Determining positivity by eliminating false positives), membrane dyes, and fluorescent dyes that are used to stain nucleic acids (see V.6 DNA synthesis, cell cycle, and proliferation). EV staining, however, involves different problems and choices and requires more controls than cell staining. For example, if a flow cytometer detects smaller and thus more EVs with fluorescence triggering compared to scatter triggering, EVs are preferably stained with a generic EV marker, such as lactadherin. However, generic EV markers that specifically detect all and exclusively EVs do not exist [281].

When designing experiments for polychromatic FCM, Ab-conjugated fluorochromes should be carefully selected. Preferably, use fluorochromes that (i) are readily conjugated to Abs, (ii) have high associated fluorescence intensities ("bright"), and (iii) exhibit little spectral overlap with other fluorochromes [282, 283]. The use of bright fluorophores increases the SNR of EVs with low antigen exposure (Fig. 34D), whereas spectral overlap should be reduced because compensation of spectral spill-over is complicated by low signal levels and unstable autofluorescence levels. The aforementioned restrictions on fluorochromes limit the number of Abs that can be simultaneously measured in typical EV FCM experiments. To increase specificity, phallotoxin can be used to differentiate between intact EVs and nonspecific binding of mAb conjugates to damaged membrane fragments [284].

Similar to cell analysis, it is good practice to titrate reagents to find the optimal Ab concentration (see III.2 Titration: Determining optimal reagent concentration). To prevent that Ab-aggregates are artifactually counted as EVs, remove Ab-aggregates by centrifugation at 19 000 × g for 5 minutes before staining. After staining, reduce the concentration of unbound reagents by washing, size exclusion chromatography, or dilution to reduce sample related noise and thus increase the SNR.

4.6 Assay protocol

4.6.1 Swarm detection. Before optimizing the acquisition settings, it is important to realize that in most FCM measurements, only a part of the EVs exceed the detection limit [251, 260]. Due to the complex size distribution of EVs (Fig. 34B), however, the fraction of EVs below the detection limit may outnumber EVs exceeding the detection limit. Consequently, EVs below the detection limit may contribute to the measured signal or even exceed the trigger threshold (see Chapter IV, Section Cell sorting). This special form of coincidence detection is named swarm detection [260, 285]. Serial dilutions can be used to find the optimal dilution and minimize the effect of swarm detection. The measured number concentration versus dilution should give a linear decrease and a consistent median fluorescence and scatter intensity.

4.6.2 Acquisition settings. The optimal acquisition settings differ between flow cytometers. Select settings that lead to the highest sensitivity, and thus detection of the dimmest EVs, while avoiding background noise and swarm detection. In general, use the highest illumination power, use the shortest illumination wavelength for scatter detection, select the lowest flow rate, and optimize detector voltages and thresholds (See Chapter IV, Section Cell sorting) [57]. The choice whether to trigger on scatter or fluorescence depends on the flow cytometer [281, 286–288]. Regarding scatter, SSC is generally more sensitive than FSC, particularly for instruments equipped with a photodiode at FSC [260, 289].

4.6.3 Controls. To verify what events are truly EVs, controls are needed, such as buffer only control, reagents in buffer control, unstained sample control, blocking and isotype control alone or in addition to the related FMO control, serial dilutions, detergent treatment, and sample analyses by techniques complementary to FCM [57].

The buffer only control involves periodic measurements of buffer to address sources of noise and monitor the stability of background counts. The reagents in buffer control involves the addition of reagents to the buffer at the same concentration as used in the experiment, and to confirm the absence of events caused by the reagents [216, 281, 290]. The unstained sample control (see also Chapter V, Section 3 Mitochondria) involves a measurement of unstained EVs and may assist in determining aut-

ofluorescence levels and setting gates. Blocking and isotype controls can be used to differentiate between specific and nonspecific binding of Abs (Chapter III, Section 1.4 Specificity of reagent for staining target: Blocking and isotype controls), but not to set gates or to correct counts for nonspecificity. Isotype controls should be used from the same manufacturer and at the same concentration as the respective Ab [291]. In an FMO control, which is used for experiments with multiple Abs, one reagent is left out or added to the isotype control to determine the fluorescent gate for that reagent (Chapter III, Section 1.2 Fluorescence spreading into the channel of interest: FMO controls).

Serial dilutions can minimize the effect of swarm detection, as discussed before. Detergent treatment involves the lysis of EVs by addition of detergent to check whether events that are supposed to be EVs disappear. Results of detergent treatment should be interpreted with care, because other particles than EVs may lyse as well [292] and change in scattering properties due to a refractive index change of the medium [293]. For FCM, data from complementary techniques are useful for experimental design. For example, the size distribution and concentration measured by resistive pulse sensing may be used to determine the optimal dilution and prevent swarm detection, whereas surface plasmon resonance imaging or a western blot may be used to confirm the presence of certain antigens.

4.6.4 Calibrations. FCM provides data in arbitrary units. To improve data interpretation and enable data comparison, fluorescence signals can be calibrated in units of molecules of equivalent soluble fluorophore (MESF) or equivalent reference fluorophore (ERF) [294–296] and scatter signals can be calibrated in units of nm^2 [252, 259, 260, 297]. Do not use the scatter intensity of two sizes of polystyrene particles to set gates for two reasons. First, polystyrene particles scatter light much more efficiently than similar-sized EVs (Fig. 34C), which may lead to data misinterpretation. For example, an earlier proposed gating strategy based on the scatter intensities of 500 nm and 900 nm polystyrene particles [298, 299] leads to the inclusion of platelets, membrane fragments, and perhaps erythrocyte ghosts [255] instead of the envisioned EVs [260]. Second, a gate based on two polystyrene particles selects different EV sizes at different flow cytometers and therefore is not suitable for the purpose of data comparison [259].

Statements about the number concentration of EVs also require calibration of the flow rate, especially because the actual flow rate may be 50% lower or 100% higher than the set flow rate [259]. The flow rate can be estimated using commercial reference particles with a specified concentration, by mass discharge measurements [259], or by a calibrated flow rate sensor.

4.7 Materials

Materials required for collection, isolation, storage, and staining depend on the experiment. Generally, use a clean, filtered buffer and measure the buffer to confirm cleanness. Preferably, the flow

cytometer is able to detect the scatter intensity of at least 200 nm polystyrene particles and a fluorescence intensity of at least 1000 MESF (see also Fig. 34C and D). For comparison, one of the most sensitive flow instruments for EV detection today can detect single ~20 nm polystyrene particles and a single PE molecule [300].

4.8 Data analysis

Most data analyses steps can be done with software capable of reading FCM data, creating histograms and scatter plots and applying gates. Preferably, start with the aforementioned calibrations of the scatter and fluorescence detectors to obtain data with units that are understandable and comparable. Use the aforementioned controls to exclude swarm detection and define gates. Count the number of EVs within the gate during a measurement and use the calibrated flow rate to relate counts to number concentration. Because only a part of the EVs can be detected [251, 260], the reported number concentration should be accompanied with the range wherein the EVs are detected. For example, in Fig. 34D we measured a concentration of 4.4×10^8 CD61$^+$ EVs/mL with an APC intensity between 5.0×10^2 and 11.7×10^3 MESF.

Because the size, scatter intensity, and fluorescence intensity distributions of EVs are often asymmetrical, the use of statistical parameters such as mean, median, and SD should be used with care. To describe the shape of an EV distribution, it is generally more appropriate to use a mathematical function. For example, EV size distributions can often be described with a power-law function (Fig. 34B), log-normal function, or exponential decay.

New, sophisticated procedures exist to derive the diameter of EVs from scatter or fluorescence signals. For example, Exometry offers a commercial kit and the National Institute of Health offers free software [301] to determine the EV diameter from a single scatter detector. The information from two scatter detectors can be combined to determine the refractive index, which can be used for label-free differentiation between EVs and lipoprotein particles [253].

To ensure reproducibility, all details involved in sample collection, isolation, storage, staining, data acquisition, controls, calibrations, and data analyses such as gating (Chapter VII, Section 3 Analysis presentation and publication (MIFlowCyt)) should be reported. Graphs should have clear axes labels and calibrated scales and reported values of the fluorescence intensity and scattering intensity preferably have comparable units. Data sharing via public repositories is highly recommended (See Chapter VII, Section 4 Data repositories: Sharing your data).

4.9 Pitfalls

- Detecting artifacts, such as swarm detection and background noise, instead of single EVs.
- Using the scatter intensity of two sizes of polystyrene particles to gate EVs.

- Providing the concentration of EVs without reporting the dynamic range of the detector(s) in standardized, comparable units.
- Using high-speed and ultracentrifugation steps to isolate and concentrate EVs of different size (e.g., microvesicles and exosomes) upon FCM analyses.

4.10 *Top tricks*

- Realize that FCM measures only a part of all EVs in the sample.
- Quantify which EVs the flow cytometer can measure and map out related artifacts.
- Use controls to verify detection of the envisioned, single EVs.
- Report (1) the research question and hypotheses, (2) all details of the protocol required to reproduce the data, and (3) data values in standardized, comparable units.

5 Surface parameters

5.1 *Overview*

This section focuses on the handling of suspension cells and cells obtained enzymatically from tissue samples for the detection of cell surface molecules. Although this is the most commonly used application in flow and mass cytometry, some pitfalls during sample handling, staining, and data analysis can occur, which will be discussed here.

5.2 *Introduction*

Surface molecules comprise membrane proteins, such as receptors, enzymes, ion channels, adhesion, and transporter molecules, lipids, or polysaccharides but also external ligands, either specifically loaded onto their specific receptors, e.g., cytokines or Abs or nonspecifically attached to the cell surface (reviewed in ref. [302]). These molecules are easily accessible by FCM and do not typically require special preparation of cells, such as fixation or permeabilization. Most surface markers, in particular those known as lineage markers, are also expressed at reasonable density allowing clear-cut discrimination between positively and negatively stained cells.

In principle, surface molecules can be detected with different types of labels in a range of affinities, such as Abs, receptor ligands, lectins for the detection of glycan structures, annexin V for the detection of phosphatidylserine at the outer membrane of apoptotic cells (see Chapter V Section 7: Measuring cell death mechanisms) and complex multivalent reagents, e.g., for increased binding avidity, e.g., MHC/peptide-tetramers (see Chapter V Sections 17.3-17.5: Antigen-specific T-cell cytometry), which in general are chemically conjugated to fluorescent reporter molecules.

5.3 *Minimize artifacts by minimal cell manipulation*

If possible, surface molecules should be stained on live cells to avoid any kind of antigen denaturation possibly introduced by pre-treatment steps, such as cell fixation or cell permeabilization, to clearly differentiate between intra- and extracellular localization. For combined intracellular (see also Chapter V Section 14 Intracellular parameters) and surface staining, surface markers should be stained first, followed by fixation and permeabilization before staining for intracellular antigens. Defined reagents such as recombinant Abs [303] with reduced "nonspecific" interactions should be used whenever possible (see also Chapter III Section 1, Controls: Determining positivity by eliminating false positives) especially when cells do express high or low affinity Ig Fc receptors, such as CD64 or CD32. Unspecific, Fc receptor-mediated binding of immunoglobulins can be suppressed by incubating cells in the presence of blocking reagents, such as purified Igs.

In contrast to blood cells or cells from liquid exudates, primary cells located in tissues often require an enzymatic pretreatment for tissue dissociation to finally obtain cells in suspension (see Chapter III Section 3). But during this procedure antigenicity of surface proteins can be also affected. Therefore, depending from the tissue type and cells of interest, conditions for enzymatic digestions have to be carefully established. In general, there are a variety of enzymes available, such as elastase, hyaluronidase, dispase, and different types of collagenases. They differ in their digestive characteristics and, therefore, incubation time, temperature, and concentration of enzymes have to be optimized with respect to cell viability, cell yield, and preservation of antigens that will be investigated by FCM. In the case of very sensitive antigens, which are destroyed during tissue digestion, isolated cells may be cultured over night to allow re-expression of affected cell surface proteins. Principally, cells obtained after enzymatically tissue digestion are much more stressed than suspension cells and therefore, require the identification of dead cells and their exclusion from the analysis as described in Chapter III, Section 4: Dead cell exclusion, cell viability, and sample freezing. As described there, dead cells will increase background signals due to a general increase in autofluorescence or due to the increased unspecific binding of staining reagents.

A very detailed protocol to isolate thymic epithelial cells is given by Jain and Gray [304] and for human skin mast cells by Grützkau et al. [305]. Moreover, *The tissue dissociation guide* from Worthington summarizes all aspects of tissue dissociation in a very comprehensive way (Worthington Biochemical Corporation Tissue Dissociation Guide [306]).

Although flow cytometric analyses should ideally be performed with fresh samples, there are several possibilities to stabilize cells or blood samples before preparation for FCM (see also Chapter III, Section 3: Preparation of single-cell suspensions; Section 4: Dead cell exclusion, cell viability, and sample freezing; and Section 5: Cell fixation and permeabilization for flow cytometry). Short-term preservation of blood for up to 24 h by Ficoll 70 kDa is mainly aiming at inhibiting blood settling-induced stress that is caused by RBC aggregation [307]. For long-term storage, the

cryopreservation of PBMCs is another option. But it should to be kept in mind that some surface molecules, like CD62L or chemokine receptors in general, can be negatively affected by this procedure. In addition, some cell types may be more sensitive to this type of treatment, which has to be determined individually for each cell population of interest.

In addition, there are several commercial reagents available, that can be used for long-term storage of blood samples, such as TransFix (CYTOMARK, Caltag Medsystems, Buckingham, UK), Cyto-Chex BCT (Streck, Omaha, US) and Smart Tube (Smart Tube, San Carlos, CA) [308]. The latter one even allows analyzing frozen blood samples after appropriate treatment without losing granulocytes.

But for all these stabilizing protocols, it is strongly recommended that they have thoroughly been validated for the surface markers of interest.

Live cells may be sensitive to prolonged in vitro handling procedures or may actively internalize surface molecules or shed them from the surface, e.g., after labeling with Abs. This can be avoided by gentle treatment, e.g., careful pipetting, short handling time, low temperature (on ice), or addition of sodium azide to the staining buffers, which blocks active shedding/internalization. After staining, cells should be immediately analyzed or strictly be kept on ice and in the dark to avoid photobleaching.

For the detection and analysis of cell subsets that are detectable only in very low frequencies (<0.1%), appropriate pre-enrichment strategies may help to improve gating resolution for the cell population of interest (see Chapter IV Section 1: Pre-enrichment of low abundant cell populations prior to acquisition/cell sorting).

5.4 *Transient surface markers*

Some markers are only transiently expressed on the cell surface and thus may escape detection. This can be caused by different mechanisms, such as ectodomain shedding [309] or rapid internalization and subsequent endocytic recycling [310]. Cytokine receptors especially behave in a very sensitive manner during sample preparation and thus different results may be obtained by analyzing whole blood after hypoosmotic lysis of erythrocytes or enrichment of PBMCs after Ficoll density gradient centrifugation [311]. Moreover, incubation temperature and time for Ab staining have to be carefully adjusted for each particular Ab. For instance, chemokine receptors are often stained rather at room temperature than at 4°C to ensure highest sensitivity of receptor detection [310]. Another example is the identification of antigen-specific T cells by the detection of CD154 (CD40-ligand), which is transported to the cell surface only upon T-cell activation and is then rapidly internalized after binding to its receptor (see Chapter V Section 17.3: Antigen-specific T-cell cytometry). A final example is the rapid downregulation of the CD3/TCR complex upon TCR/CD3-ligation [312]. In principle, depending on the marker investigated internalization can be prevented by pharmacological or Ab blockade as shown for the chemokine receptor CCR5 by Müller et al. [313] or alternatively the antigen has to

be continuously stained during culture or by intra-cytoplasmic staining.

5.5 *Genuine membrane molecules versus membrane adsorption*

Not all molecules detected on the cell surface are genuine surface molecules but may have been passively adsorbed to the cell surface or exchanged by an intercellular transfer of membrane patches. This might lead to significant artifacts and is particularly relevant for cells from cell cultures and for cells getting in close contact with each other, e.g., within cell pellets following centrifugation. On the other hand, it can be caused by alternative peptide/protein transfer mechanisms, such as trogocytosis, extracellular vesicle-mediated transfer between cells (i.e., through exosomes or microvesicles, see also Chapter V Section 2 Organisms, cells, organelles, chromosomes and extracellular vesicles) or tunneling nanotubes, which may allow an intercellular transfer of preformed MHC class I and class II molecules in the immunological synapse [314]. Principally, unspecific adsorption may be reduced by short processing times and low temperature, addition of Ca^{2+} chelators (EDTA) or neutral "blocking" proteins such as BSA to all staining buffers and by repetitive washing steps, or even short treatment with high salt or low pH. Passive adsorption can also be tested for by incubation with the relevant molecule, block of transport to the cell surface (e.g., brefeldin A for activation-induced molecules) or by the use of purified cell populations to prevent cross-feeding. However, if the results remain insensitive to these treatments, they have to be confirmed by alternative analysis methods, e.g., fluorescence microscopy (to determine spatial distribution on the cell surface), RNA-analysis, transgenic expression of the molecule of interest in cell lines, and so on.

Adsorption of molecules to the cell surface can also actively be exploited for staining of surface receptors with the specific ligands, such as chemokines [315], cytokines, soluble ligands/Fc-fusion proteins, if suitable Abs are not available.

5.6 *Quantitative considerations*

Quantification of surface marker expression on particular cell types can be principally done in two ways: (i) calculation of relative frequencies as percent positive cells expressing a particular surface protein or a combination of several ones according to a threshold determined by an isotope or FMO control; (ii) quantification of absolute cell numbers per sample volume; and (iii) calculation of the strength of protein expression on a particular cell type considering fluorescence intensity as given by the mean, geometric mean, or median value of fluorescence intensity (see Chapter III Section 1: Controls determining positivity by eliminating false positives; and Chapter VII Section 2: Statistics for flow cytometry). The decision whether to calculate relative frequencies, absolute cell numbers for a given sample volume or both depends

on the scientific question, e.g., to discriminate between an apparent decrease of a particular cell population probably caused by an increase of other cell populations or by a real decline probably caused by an increased rate of cell death. Principally, frequencies are useful when asking for a percentage of activated cells within a given population (e.g., percentage of CD69-positive CD4 cells) while reporting data in absolute cell counts (i.e., 1×10^6 CD4 cells/µL blood) will be essential in many settings, e.g., to address questions of emigration or immigration of immune cells from or in the peripheral blood circulation.

To analyze the activation of cells not only the percentage of activated cells is of interest but also the magnitude of activation marker expression, e.g., CD69, CD25, or HLA-DR, is important and can be given by the fluorescence intensity. In quantitative FCM, fluorescence-labeled beads are used, which are commercially available from several vendors, such as Calibrites from BD or calibration beads from BioCytex or Quantum^{TM} MESF kits from Bangs laboratories. These beads not only allow a standardized detection of fluorescence intensity units as needed for diagnostic applications but may be also used to assess the detection threshold, resolution, and linearity of the relevant detector. For quantitative comparison of surface marker expression, it should be kept in mind that the surface increases with the square of the cell diameter, i.e., the same marker density results in much brighter signals. Thus, changes in cell size, e.g., upon cellular activation, have to be considered for selection of the proper controls.

6 DNA synthesis, cell cycle, and proliferation

Cell cycle analysis was one of the very first applications for which FCM was used, and has since been used in a large range of different settings such as interrogating the biology of cancer, drug development, and toxicology studies [316]. In mammals, non-dividing cells in the G_0 phase enter the G_1 phase when they are preparing for division. The G_1 phase does not result in an increase in DNA, but does involve the synthesis of proteins that are required for subsequent progression. DNA synthesis occurs when cells enter the synthetic (S) phase of the cell cycle, in which they will remain until the DNA content has doubled, at which time they will enter the G_2 phase and undergo mitosis. Cells in G_0 and G_1 therefore contain the same amount of DNA and will exhibit the same fluorescent properties when stained with a DNA-binding dye. In contrast, the fluorescent intensity of cells moving through S Phase will progressively increase as their DNA content increases until they have twice the amount of DNA than cells in G_0 when they reach the G_2 and M Phases.

6.1 *DNA synthesis and cell cycle analysis*

The determination of DNA synthesis and cell cycle analysis involves the use of fluorescent dyes that bind to DNA, of which there are many (e.g., PI, Hoechst stains, TO-PRO-3, SYTOX, acridine orange, pyronin Y, 7-AAD, DAPI, DRAQ5^{TM}, and DRAQ7^{TM}).

The selection of the dye to be used will be dependent on the instrument that is available and the spectral parameters that it can detect. One should also be aware of the binding characteristics of the dyes and their preference for base pairs. The compatibility of an instrument for a dye will be dictated by the wavelength of the lasers that are available, and the optical characteristics of the filters with which each laser is associated. This highlights the issue of understanding your instrument and its capabilities, as without this understanding it will not be possible to design and deliver valid experimental data. The investigator should consult the manufacturer's instruction manual for specific information regarding the operation and capabilities of their FCM platform. Online FCM resources (see Useful resources below) provide a repository of key information and tools for informing and facilitating good experimental design, and for improving FCM practice.

Another consideration relates to whether there is a need to analyze viable or fixed cells, and whether to only fix or fix and permeabilize samples. Given that permeabilization can remove intracellular components, this approach can give more definite peaks on the fluorescent histograms. Crosslinking agents such as formaldehyde lower dye binding because of chromatin crosslinking. Although dehydrating fixatives such as methanol and ethanol can also be used, at high concentrations, these can cause cell clumping due to protein coagulation. Dehydrating fixatives can also negatively impact on fluorescent dyes if DNA is being stained in association with surface marker staining for the expression of antigenic determinants, as many protein-based fluorescent molecules are sensitive to the dehydrating effects of the alcohols. One should also be aware that signals from Green Fluorescent Protein, mCherry, and Cerulean can be destroyed by alcohol treatment. The addition of permeabilizing detergents to disrupt the plasma membrane such as Triton, NP-40, and saponin can improve access of the DNA dye. Another issue to consider is that the concentration of the DNA dye must be sufficient so that it binds in proportion to the amount of the DNA in the cell. It is therefore essential to determine the DNA profiles that are generated at different concentrations and incubation times for a defined cell number and identify the approach, which generates the lowest CV, but in the absence of any cytotoxic effect (i.e., check the viability of cell populations and the influence of the dye thereupon). One should also remember that some dyes (PI, for example) will bind to both DNA and RNA. In such instances, it is necessary to include a ribonuclease (RNAse) in the staining buffer, otherwise the fluorescence histograms that are generated will be sub-optimal as they will include a signal from the RNA. A typical experimental protocol using PI for staining and generating a typical staining profile (Fig. 35) will involve the following:

1. Fix cells that have been harvested and washed in PBS in 70% v/v ethanol. Adding the ethanol dropwise to the cell pellet while vortexing will ensure that all cells are fixed and will minimize clumping.
2. Fix cells for 30 min at 4°C, after which wash cells twice in PBS ($850 \times g$). Be careful to avoid cell loss when discarding the supernatants.
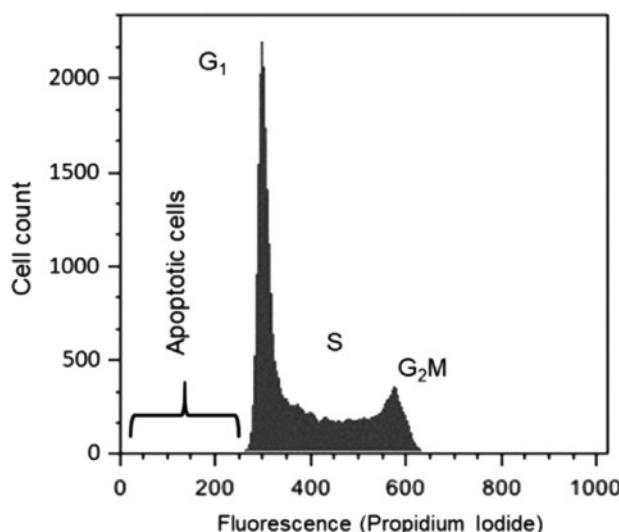
Figure 35. Representative DNA fluorescence histogram of PI-stained cells. Isolated cells are fixed and stained as described above, and their fluorescence determined on a linear fluorescence scale. The presence of a sub-G_1 peak can be used to indicate the presence of cells undergoing apoptosis (See Apoptosis: Measurement of apoptosis).

3. Treat cells with RNAse (50 μL, 100 μg/mL) in order to ensure that only DNA is stained.
4. Add PI (200 μL PI, 50 μg/mL stock solution) immediately before analyzing.

The "quality" of the DNA histogram that is generated is typically indicated by the appearance and CV (data spread) of the G_0/G_1 peak, which must be as low as possible (Fig. 35). Factors that can influence this element of the data acquisition include the flow rate (which must be low) and laser alignment and hydrodynamic focusing (both of which should always be optimized as part of the routine maintenance and quality control procedures that are stipulated by the instrument and calibration bead manufacturers). It is essential to maximize the electronic signal intensity and minimize variability of the measurement of the beads in order to achieve accurate DNA measurements. The precise definition of "low," "medium," and "high" flow rate will depend on the instrument and its configuration. It is better to run a more concentrated sample at a slower flow rate, than a diluted sample at a higher flow rate.

Although it would appear obvious, it is crucial that the presence of cell aggregates or doublets is minimized, and that these are excluded from the analysis. Doublets or cells going through the cytometer together can mimic cells in the G_2/M phase. Such problems can be avoided by employing good experimental techniques for the preparation of samples and filtering samples before the analysis [316] (see Chapter III, Section 3: Preparation of single cell suspensions). The analysis gate can be set to acquire data on singlet cells by acquiring data using a "Pulse/Cell Width" versus "Pulse/Cell Area" plot or "Pulse/Cell Height" versus "Pulse/Cell Area," which can be set using the instrument software (Fig. 36). This approach allows doublets and aggregates to be easily iden-

tified and excluded from the analysis. As with all experiments, controls should be included. Chicken and trout erythrocytes have been proposed as internal standards for analysis of DNA content by cytometry in order to control and maintain consistency in the staining and measurement approaches. However, it should be noted that the ploidy of DNA in fish can also vary, and so it is important to be aware of ploidy when using cells as a standard [317].

It is also crucial to exclude nonviable cells from any analysis, as the presence of these can introduce heterogeneity into the datasets that are generated. Although DNA analysis, by its nature, requires that cells are fixed and therefore nonviable, it is possible to stain cells using nonfixable dyes (protein-binding dyes) prior to their fixation for DNA staining. Details on these approaches are provided in the relevant section (see Chapter III Section 4.2: DNA-binding dyes).

A typical instrument setup and sample acquisition could use the following sequential series of plots, and 10 000–20 000 relevant (*NOT* total) events should be collected:

- FSC versus SSC plot to identify relevant cell population(s)
- "Pulse Width" versus "Pulse Area" plot or "Pulse Height" versus "Pulse Area" plots (to exclude doublets)
- Live/Dead versus FSC (to exclude dead cells)
- DNA stain (e.g., PI) versus FSC (to monitor instrument performance)
- DNA histogram (using a linear scale)

A typical analysis could use the following sequential series of plots:

- "Pulse Width" versus "Pulse Area" plot, or "Pulse Height" versus "Pulse Area" plots (to exclude doublets)
- Live/dead versus PI (to exclude dead cells)
- FSC versus SSC plot (to exclude unusual-looking populations)
- DNA histogram (using a linear scale)

The placement of markers on the G_1, S, and G_2 peaks for the analysis of cell cycle profiles can be subjective, as a consequence of which the analysis and interpretation of cell cycle analysis data now involve a number of mathematical models, all of which attempt to deconvolute the peaks and provide a more objective approach. Specialized programs such as ModFit LT™ from Verity Software House (http://www.vsh.com/products/mflt/mfFeatures.asp) and Multicycle AV™ from Phoenix Flow Systems (http://www.phnxflow.com/MultiCycle.stand.alone.html) have been designed for this purpose.

Although cell cycle analysis is a powerful tool, it requires a great deal of optimization for the data to be robust, interpretable, and meaningful. Furthermore, although cell cycle analysis provides information on the proliferation of cells, other approaches must be used if you are wanting to quantify how many times cells have replicated (see part 7.2 Proliferation).
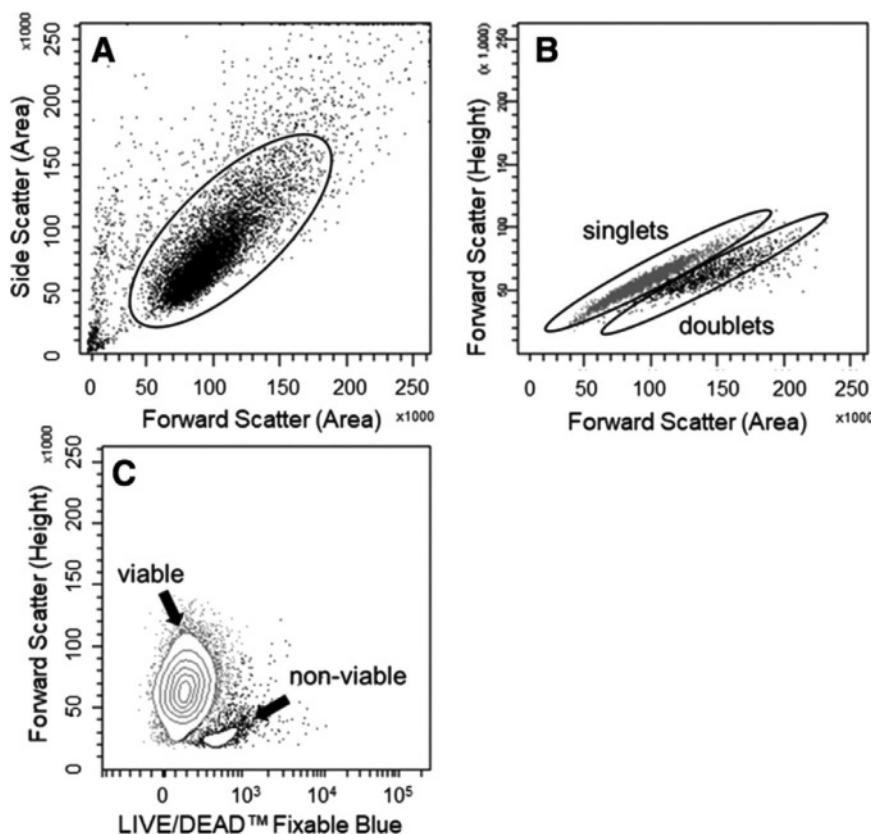
Figure 36. Identification of single cell populations for analysis using FCM. Cultured tumor cells were harvested, washed, and stained [316]. (A) Tumor cells are identified on an FSC versus SSC plot and gated to exclude debris, which is found in the lower left corner. (B) Single cells can be separated from cell aggregates by analyzing cell height and area (upper right)—single cells will show as a correlated line, with any clumped cells below. (C) Viable cell populations can be identified using viability stains such as the LIVE/DEAD® fixable range of products from Life Technologies, the eFluor® fixable dyes from eBioscience, BioLegend's Zombie range of fixable dyes, Tonbo biosciences' Ghost Dyes™, and the Fixation and Dead Cell Discrimination Kit from Miltenyi Biotec, as described in Chapter III Section 4 Dead cell exclusion, cell viability, and sample freezing. Reproduced with permission from ref. [316].

6.2 Proliferation

The analysis of cell proliferation is at the core of many biological studies and is typically used for cell growth and differentiation studies, and for the evaluation of toxicity and therapeutic responses to stimulators and inhibitors in a variety of settings. Cell proliferation can be determined on the basis of direct cell counting, on the basis of DNA synthesis (using an approach that typically involves measuring the uptake of ^{3}H-thymidine), or by measuring metabolic activity such as mt dehydrogenase activity using colorimetric assays such as the MTT (3-(4,5-dimethythiazol-2-yl)-2,5-diphenyl tetrazolium bromide) assay. For the latter, cells are incubated with MTT, and the yellow MTT is converted into an insoluble purple formazan product by mt succinate dehydrogenase. The product is solubilized and level of proliferation determined by measuring the absorbance of the medium with a spectrophotometer. An alternative colorimetric approach uses the [3-(4,5-dimethylthiazol-2-yl)-5-(3-carboxymethoxyphenyl)-2-

(4-sulfophenyl)-2H-tetrazolium] tetrazolium salt that results in a soluble, rather than an insoluble, formazan product. Although these approaches are effective, their common disadvantage is that they provide a measure of proliferation in the bulk population, and do not provide insight into the proliferative responses of cell subpopulations. The multiparameter capabilities of FCM offers a number of options for studying cellular proliferation in complex settings, and the majority of the approaches involve the measurement of nucleotide incorporation or dye dilution. The approach that needs to be used will very much depend on the experimental setting (Table 9)

6.3 DNA synthesis—Nucleotide incorporation

Analogous to the measurement of proliferation based on ^{3}H-thymidine incorporation, cell division can be monitored by FCM using 5-bromo-2'-deoxyuridine (BrdU), a synthetic nucleoside
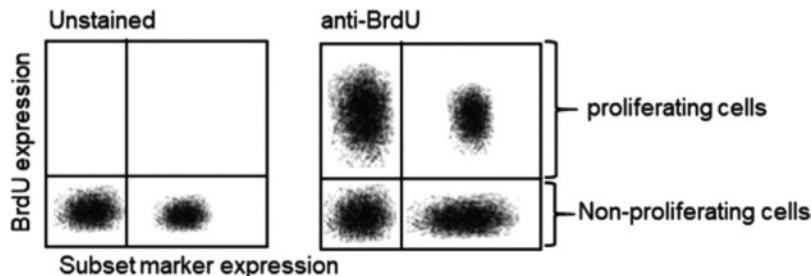
Figure 37. Schematic representation of fluorescent dot plot for the flow cytometric analysis of cell proliferation based on BrDU incorporation. Human PBMCs have been labeled with BrDU and a phenotypic marker, with unlabeled cells acting as the control. The total viable cell population was used for the analysis.

Table 9. Approaches for determining cell proliferation

Nucleotide incorporation/ dye dilution	Determination of cell divisions
BrdU	1–2
BrdU/Hoechst/PI (quenching) technique	3–4
Dye dilution	>4

BrdU, 5-Bromo-2′-deoxyuridine

analogue of thymidine. For this, BrdU is incorporated into the newly synthesized DNA of replicating cells (during the S phase of the cell cycle), and its incorporation detected using conjugated Abs specific for BrdU, which are widely available from a number of commercial sources. Binding of the Ab requires denaturation of the DNA, usually by exposing the cells to acid or heat. The measurement of BrdU is typically undertaken in conjunction with viability dyes and/or DNA stains for cell cycle analysis.

Although appearing to be a straightforward assay, sample preparation and DNA denaturation for BrdU-based measurements of cell division must be performed carefully, as too little treatment will result in a low signal and too much treatment will influence the DNA and the signal that is generated. Samples need to be washed well (at least three times), as any residual acid will denature the detecting Ab. Furthermore, BrdU is labile even at 4°C and so must be used fresh. A typical experimental protocol producing a typical staining profile (Fig. 37) involves the following:

1. Incubate cells with BrdU (~10 μM) for 30–60 min
2. Fix harvested and pelleted cells by suspending in ice-cold 70% v/v ethanol at 4°C for at least 30 min (samples can be left for up to 7 days).
3. Pellet cells, wash in PBS and incubate for 30 min at room temperature (RT) (with occasional mixing) in freshly prepared 2 M HCl.
4. Wash cells twice in PBS, and then in PBS-Tween (PBS containing 0.1% w/v BSA and 0.2% v/v Tween 20, pH 7.4).
5. Add an appropriate amount of anti-BrdU mAb (conjugated/unconjugated), as determined by titration experiments, to the cell pellet and incubate samples at RT for 20 min in the dark (BrdU is photo-unstable).
6. Wash samples twice in PBS-Tween and, if an unconjugated mAb has been used, incubate samples with an appropriate secondary Ab at RT for 20–30 minutes.
7. After washing in PBS, incubate cell pellets with RNAse (50 μL, 100 mg/ml) for 15 min at RT or 37°C.
8. Add an appropriate volume of the required viability stain (e.g., PI, 200 μL, 50 mg/mL).
9. Analyze the viable cell populations(s) by FCM, collecting a minimum of 10 000 relevant events per sample.

An alternative to BrdU is the modified nucleoside, EdU (5-ethynyl-2′-deoxyuridine). Assays such as the Molecular Probes™ Click-iT™ EdU cell proliferation assay are based on the labeling of proliferating cells with a bright, photostable Alexa Fluor® dye in a
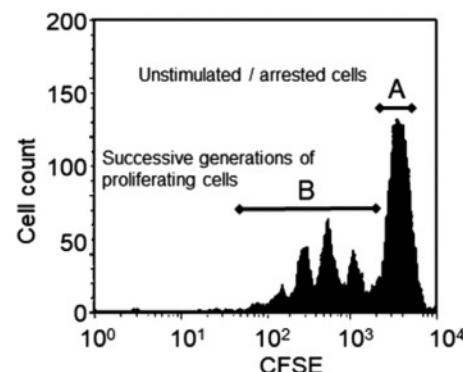
Figure 38. Schematic fluorescence histogram depicting a progressive decline in the fluorescent intensity of proliferating cells stained with CFSE. For the assays, 10^6 isolated cells (e.g., human PBMCs) are incubated with CFSE (~5 mM final concentration) at room temperature for 8 min, at which time the reaction is blocked by the addition of FBS (2% v/v final concentration). Cells are washed in PBS containing 2% v/v FBS, after which they are stimulated. The fluorescence of the stimulated cells is then measured at appropriate time-points using FCM. (A) The bright/strong, undiluted fluorescent signal of nonproliferating/arrested cells. (B) The (serially) diluted fluorescence intensity of cell populations from successive generations of proliferated cells.

fast, highly specific click reaction. Unlike BrdU assays, EdU assays are not Ab -based and therefore do not require DNA denaturation for the detection of the incorporated nucleoside. Click-iT™ EdU can also easily be multiplexed with fluorescent proteins like R-PE, R-PE tandems, and green fluorescent protein. Only a mild fixation and detergent permeabilization is sufficient for the small molecule-based Click-iT™ EdU detection reagent to gain access to the DNA. A typical experimental protocol producing a typical staining profile and improved DNA histograms has previously been reported [318, 319].

6.4 Dye dilution

The essence of dye dilution approaches is that cells are labeled with fluorescent dyes that intercalate into the cells such that the dye is approximately equally distributed between the two daughter cells following division. As the cell divides, the dye is diluted out and by counting the peaks (or modeling the pattern) the number of original dividing cells can be calculated (Fig. 38).

As originally described in 1994 by Lyons and Parish [320], cells were stained with the protein-binding, amino-reactive dye carboxyfluorescein succinimidyl ester (*CFSE*). One limitation of CFSE is that there is a proliferation-independent loss of fluorescence in the first 24–36 h, and therefore, this must be considered during the analysis and interpretation of the data. Although alternatives for which there is no loss of signaling after labeling include membrane-labeling lipophilic dyes that include the PKH2 (green), PKH67 (green), PKH26 (orange), and CellVue™ claret (far red) dyes from Sigma–Aldrich, these are more suitable for cell tracking experiments. More suitable for dye dilution studies are protein-binding dyes such as the CellTrace™ range from

Molecular Probes®, the eFluor® Cell Proliferation dyes from eBioscience, the BD Horizon™ dyes from BD Biosciences and the Tag-it Violet™ Proliferation and Cell Tracking Dye from BioLegend. If cells require fixing, then it is important to avoid organic solvents when using membrane dyes. It is also important to use the correct dilution of dyes, as they can have adverse effects on cell viability and function. Use the highest concentration that does not induce such negative effects for a given cell number. Protocols for the staining and analysis approaches can be accessed from the many suppliers of the reagents that are being used.

As with all experiments, it is essential to include the relevant negative and positive controls. Moreover, once the instrument settings have been optimized, it is important to place unstimulated cells at the highest decade on the fluorescence plot. Nonviable cells should be excluded, as they lose the dye as they enter apoptosis. Doublets should be excluded as a doublet of two cells in the G_0/G_1 phase would exhibit the same fluorescence intensity on a DNA stain as a single cell in the G_2/M phase. G_0/G_1 doublets would therefore create false positive results for G_2/M cells [321]. Furthermore, a doublet formed between a positive and negative cell would be seen as being positive during a cell sort, as a consequence of which the sort would be contaminated with negative cells. The presence of doublets would also cause problems for DNA content/ploidy analyses and could lead to misinterpretation of double positives during immunophenotyping studies, in that a double positive cell could in fact be a mixed doublet of two individually positive cells.

Useful Resources

- BitesizeBio Flow Cytometry Channel (http://bitesizebio.com/category/technical-channels/flow-cytometry)
- Chromocyte Limited: Resource for FCM and cell-based assays (www.chromocyte.com)
- European Society for Clinical Cell Analysis (ESCCA, www.escca.eu)
- Expert Cytometry: Flow cytometry training (www.expertcytometry.com)
- International Society for Advancement of Cytometry (ISAC, http://isac-net.org)
- Purdue University Cytometry Laboratories (www.cyto.purdue.edu)

7 Measuring cell death mechanisms

7.1 Apoptosis: Measurement of apoptosis

The above approaches for identifying the induction and presence of cell death are based on the loss or maintenance of membrane integrity, and thereby reflect cellular necrosis. They provide little insight into the nature of that cell death. In instances where the induction of cell death is a primary endpoint of the experiment, interrogating changes in the plasma membrane provides an opportunity to generate insight into the mechanisms that are involved. By far the most common approach is to determine the induction

of apoptosis (programmed cell death). Apoptosis is a tightly controlled and programmed pattern of cell death that is required for the maintenance of normal cell growth and development. Defective apoptosis can result in abnormal development and pathogenesis. Understanding cell death mechanism(s) is important, as the mode of cell death (necrosis vs. apoptosis) can influence the pro- and anti-inflammatory responses that cell death can induce. The importance of this area was recognized by the award of the 2002 Nobel Prize in Physiology or Medicine to Sydney Brenner, H. Robert Horvitz, and John E. Sulston "for their discoveries concerning genetic regulation of organ development and programmed cell death."

During early apoptosis, phosphatidylserine (PS) is translocated from the cytosolic side of the intact plasma membrane to the extracellular surface. Early apoptotic cells cannot therefore be reliably identified using approaches that are based on membrane permeability. Annexin V belongs to a family of proteins consisting of over 160 members, and has high affinity, specificity, and sensitivity for PS. Thus, the binding of annexin V to cells can be used as a marker of early apoptosis [322]. In order to rule out "leaky" necrotic cells, annexin V staining must always be used in conjunction with reagents that determine the integrity of the cell membrane, such as PI or 7-AAD. Of course, such assays cannot be performed using fixed cells.

Although the protocols for such assays are relatively straightforward, they should be undertaken according to the instructions provided by the supplier of the reagents. This is especially important in the case of Annexin V binding, as all Annexin family members share the same characteristics of Ca^{2+}-dependent binding to negatively charged phospholipid surfaces. It is essential that the correct staining buffers are used, as changing or variations in Ca^{2+} ion concentrations can have dramatic effects on the staining profiles. Furthermore, the binding of Annexin V to PS is reversible, and so samples must be analyzed as soon as possible (typically 1–3 h after labeling), using a consistent and reproducible protocol. A typical experimental protocol producing a typical staining profile (Fig. 39; [323, 324]) involves the following:

1. Wash cells (1×10^5) in Annexin V Binding Buffer (PBS containing 10% v/v FCS, 1.0 mM $MgCl_2$, and 2.5 mM $CaCl_2$);
2. Pellet cells (5 min, $400 \times g$), remove the supernatant, either by decanting or vacuum aspiration and resuspend cells in 100 μL of Annexin V Binding Buffer;
3. Incubate cells with an appropriate volume (e.g., 5 μL) of fluorescently-conjugated Annexin V (e.g., Alexa Fluor™647-Annexin V, Biolegend), vortex mix in order to ensure even distribution of the stain) for 15 min at room temperature while protected from light;
4. Wash cells in Annexin V Binding Buffer and resuspend cells in 250 μL fresh buffer;
5. Transfer cells to 12 × 75mm polypropylene tubes, stored on ice protected from light before being analyzed by flow cytometry;
6. Immediately prior to analysis, add DNA-binding dye (PI: 5 μL, 200 μg/mL, 7-AAD: 4 μL, 250 μg/mL] to allow identification, and exclusion, of any nonviable cells.
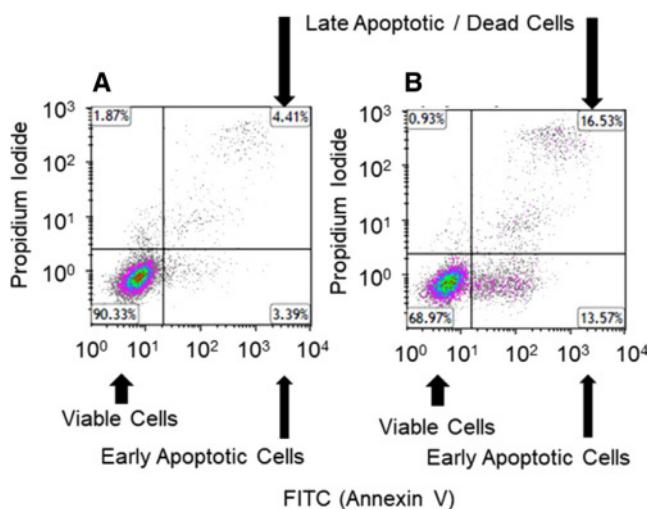
Figure 39. Identifying healthy and apoptotic cells based on Annexin V staining. The human prostate cancer cell line LNCap was seeded into six-well plates and allowed to adhere overnight. The following day, cells were left untreated (A) or incubated for 6 h with 4 µg/mL human recombinant granzyme B [323, 324] (B). After the incubation period, cells were harvested and processed as described above, with 10^5 cells being stained with Alexa-Fluor® 647 Annexin V (following the manufacturer's instructions) and PI (final concentration 1 µg/mL). Cells were analyzed on a Beckman Coulter Gallios™ flow cytometer. Plotting Annexin V binding on the *x*-axis of a 2D dot/density plot and PI/7-AAD on the *y*-axis enables the identification of healthy (Annexin V^{negative}PI/7-AAD^{negative}, bottom left quadrant), apoptotic (Annexin V^{positive}PI/7-AAD^{negative}, bottom right quadrant) and late apoptotic/dead (Annexin V^{positive}PI/7-AAD^{positive}, top right quadrant) cells. The cells incubated in the presence of granzyme B showed induction of apoptosis and increased cell death.

Although Annexin V staining is probably the most commonly used approach used for determining apoptosis, others can be used. For instance, the terminal deoxynucleotidyltransferase (TdT)-mediated dUTP nick end labeling (TUNEL) method involves labeling the ends of DNA breaks with dUTP using TdT. These labeled breaks can then be detected using an anti-BrdU antibody. In this case, fixation is required. However, given that this approach depends on DNA damage rather than staining actual components of the apoptotic pathway, it can be insensitive. Another alternative to the Annexin V assay is the Violet Ratiometric Membrane Asymmetry Probe, F2N12S from ThermoFisher. This probe is excitable at 405 nm and detects variations in surface charge associated with PS flipping. Viable cells produce an orange emission that shifts to green with apoptosis, resulting in a decreased orange/green emission ratio.

The later stages of apoptosis involve chromatin condensation and DNA fragmentation, a consequence of which is that the nuclei of apoptotic cells become smaller than those of viable cells and display higher fluorescence when labeled with dyes such as UV excited Hoechst 33342 (which is available from a number of suppliers and is also excited at 405 nm) or 405 nm-excited Vybrant™ DyeCycle™ Violet stains (ThermoFisher). When paired with an impermeable dead cell stain, it is possible to distinguish live, apoptotic, and necrotic cell populations using such chromatin condensation assays.

The loss of mitochondrial membrane potential is another hallmark of early apoptosis [325]. In cells undergoing apoptosis, the mitochondria will release cytochrome C and the apoptosis inducing factor—both of which are necessary for caspase activation (yet another critical step in apoptosis). It is also possible to assess apoptosis based on mitochondrial membrane polarization using fluorescent dyes such as JC-1 (5,5ʹ,6,6ʹ-tetrachloro- 1,1ʹ,3,3ʹ-tetraethyl-benzimidazol-carbocyanine) or JC-10 that can be obtained from a number of different suppliers. As the mitochondrial potential is lost during apoptosis, the emission shifts from red to green, thereby resulting in a decreased red/green fluorescence ratio. The principle of this approach is that the dye accumulates in healthy mitochondria, in which it is present as a multimer. Upon disruption of the mitochondrial membrane, the dye is released, and changes color due to it transforming into a monomer in the cytoplasm.

DiIC1(5) (1,1ʹ,3,3,3ʹ,3ʹ-hexamethylindocarbocyanine iodide) is another positively charged dye that accumulates in active mitochondria. It is excited at 635 nm and is read in the APC channel (peak emission 658 nm). The fluorescence intensity of DiIC1(5) decreases as membrane potential is lost. MitoTracker Red CMXRos is another useful mitochondrial probe that is optimally excited at 561 nm, and to a lesser extent 488 nm, and read in the phycoerythrin (PE) channel (peak emission 599 nm). CMXRos also shows a decrease of fluorescence as membrane potential is lost.

A key issue to be aware of is that the sample preparation process can all lead to preferential loss of apoptotic cells during sample preparation (i.e., prolonged trypsinization, mechanical or enzymatic disaggregation from tissues, centrifugation steps). It is therefore important to collect cells that have been released into the media when experimenting with adherent cell cultures. Density gradient separation of cells can also selectively deplete apoptotic cells due to differing relative densities.

7.2 Apoptosis: Caspase activation

A distinctive feature of the early stages of apoptosis is the activation of caspase enzymes. The caspases constitute a family of aspartate-specific cysteine proteases that cleave protein substrates at specific amino acid residues. This triggers a sequence of cleavage events, including the cleavage of other caspases, and generates a caspase signaling cascade that leads to apoptosis. In mammals, the "initiator" caspases-2, -8, -9, -10, and -12 are closely coupled to upstream, pro-apoptotic signals, and cleave and activate downstream effector or "executioner" caspases-3, -6, and -7 that modify the proteins that ultimately drive apoptosis [326, 327]. In most cases, caspase activation is one of the earliest measurable markers of the apoptotic cascade, and precedes the induction of cell permeability, DNA fragmentation, cytoskeletal collapse, and the "flipping" of PS. The pivotal and early involvement of mitochondria and caspases in cell death events has prompted the development of several assays that can be applied alone, or in conjunction with assays for detecting other aspects of the cell death process [325, 328]. Several commercial suppliers provide validated assays for the detection of apoptosis based on caspase activation.
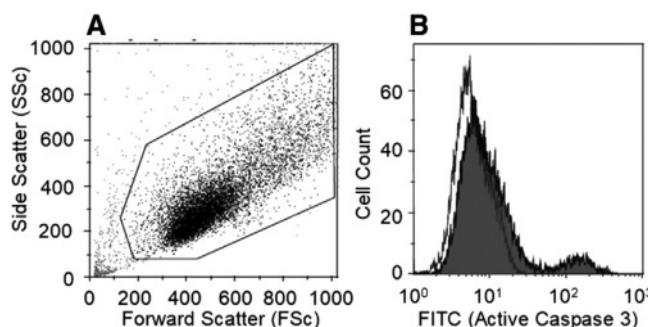
Figure 40. Identifying healthy and apoptotic cells based on the expression of activated caspase-3. The human breast cancer cell line MDA-MB-231 was seeded into six-well plates and allowed to adhere overnight. The next day, cells were left untreated or incubated for 24 h with the topoisomerase I inhibitor camptothecin (4 μg/mL, induces apoptosis). After the incubation period, cells were harvested and stained using the FITC active caspase-3 apoptosis kit (BD Biosciences) following the manufacturer's instructions and analyzed on a BD Biosciences LSRII flow cytometer. Cells were identified using FSc and SSc measurements (A) and the expression of active caspase-3 determined on the basis of FITC fluorescence (B; control sample shown on open histogram and camptothecin treated shown on grey histogram).The cells incubated in the presence of camptothecin showed activation of caspase-3

Caspase activation assays can involve the intracellular staining of cell populations using mAbs that are specific for the activated forms of the relevant caspase (Fig. 40), or can employ small inhibitor peptides conjugated to a fluorophore that specifically target the active site of the chosen caspase.

As an example, the CellEvent™ Caspase-3/7 Green Detection Reagent from ThermoFisher is a cell-permeable reagent consisting of a four-amino acid peptide (DEVD) conjugated to a nucleic acid-binding dye. The activation of caspase-3 and caspase-7 proteins enables them to cleave the caspase 3/7 recognition sequence, which is encoded in the DEVD peptide. Cleavage of the recognition sequence and binding of DNA by the reagent labels the apoptotic cells with a bright, fluorogenic signal that has absorption/emission maxima of 511/533 nm. When used together with the SYTOX™ AADvanced™ Dead Cell Stain, apoptotic cells can be easily discriminated from live and necrotic cells.

Caspase activity can also be determined using the PhiPhiLux™ system, which employs a nonfluorescent substrate for the enzyme that yields a fluorescent product if the enzyme is active. The PhiPhiLux™ caspase substrates are cell permeable, demonstrate relatively good caspase specificity, possess high SNRs between their uncleaved and cleaved forms, and have fluorescence spectral properties that are compatible with other fluorescent probes. Apo-Stat (R&D Systems) identifies and quantifies caspase activity in apoptotic cells by irreversibly labeling cells with a cell permeable, FITC-conjugated pan-caspase inhibitor (ApoStat). Any unbound reagent diffuses out of the cell and is washed away, with an increased fluorescence being indicative of caspase activity. The CaspGLOW™ staining system detects active caspase-9 in mammalian cells using FITC-conjugated LEHD-fluoromethyl ketone, a specific inhibitor of caspase-9, which is cell permeable and irreversibly binds to the active enzyme.

Another approach involves the use of a fluorescently labeled inhibitor peptide that binds to the active site of the caspase or FLICA™—Fluorescent-Labeled Inhibitor Caspase. FLICA™ probe based assays, which are available from a number of suppliers, are composed of an affinity peptide inhibitor sequence, a fluoromethyl ketone moiety that facilitates an irreversible binding event with the activated caspase enzyme, and a fluorescent tag reporter. The FLICA™ are therefore retained in apoptotic cells, but not in non-apoptotic cells following washing. Necrotic and late apoptotic cells can be concurrently identified in green FLICA™-labeled cells using red fluorescent dyes such as PI or 7-AAD, or the far red dye DRAQ7™. The ability to measure three apoptotic phenotypes in a single assay provides a powerful and comprehensive view of the apoptotic process, applicable to both suspension cells by traditional flow cytometry.

The approach selected for measuring cell viability, cell death, and apoptosis will very much depend on the experimental question, the supplier of the reagents, and the analysis of the strengths and weaknesses for each assay. Conventional internet searches will readily identify the plethora of kits and approaches that can be used for measuring caspase activation.

Useful resources.

See the "Useful resources" in DNA synthesis, cell cycle, and proliferation

7.3 Necroptosis

7.3.1 Overview. Necroptosis is a form of cell death defined by phosphorylation of the proteins mixed-lineage kinase domain-like (MLKL) and receptor-interacting serine/threonine protein kinase 3 (RIPK3), induction of the RIPK3/MLKL complex, oligomerization of MLKL, and membrane translocation of MLKL. Currently, none of these biomarkers can be directly and unequivocally determined by FCM, which may make a section on necroptosis in these guidelines seem foolhardy; however, once necroptosis has been validated by, e.g., Western blot identification of the necroptosis-specific biomarkers, FCM can be used for analysis of cells treated under the same necroptosis-inducing conditions. Here, we discuss current and future options to detect necroptosis by FCM. We also present an easy and straightforward example protocol using differences in DNA fragmentation to discriminate necroptosis from apoptosis as a potential application of FCM to cell death assessment, although it should be noted that this method still requires that necroptosis be validated by alternative methods.

7.3.2 Introduction. By definition of the Nomenclature Committee on Cell Death, necroptosis is "a type of regulated cell death triggered by perturbations of extracellular or intracellular homeostasis that critically depends on MLKL, RIPK3, and (at least in some settings) on the kinase activity of RIPK1" [329]. In contrast to apoptosis, necroptosis culminates in the rupture of the cell membrane and is associated with the release of intracellular danger-associated molecular patterns (DAMPs) and a strong

inflammatory phenotype. As a consequence, necroptotic cell death has been linked to diseases such as kidney and cardiac injury, Alzheimer's disease, atherosclerosis, rheumatoid arthritis, sepsis, stroke, and cancer [330, 331]. Physiologically, necroptosis contributes to immunosurveillance through the stimulation of innate and adaptive immune responses that target malignant and infectious threats [330, 332]. Furthermore, necroptosis ensures the elimination of potentially defective organisms before parturition, thereby contributing to developmental safeguard programs, and is involved in the maintenance of adult T-cell homeostasis [333].

At the molecular level, all triggers of necroptosis (such as death receptors, pathogen recognition receptors, or the receptor for type I IFNs) invariably induce the activation of RIPK3. This is accomplished via proteins that contain an RIP homotypic interaction motif (RHIM), i.e., RIPK1, TRIF, or DAI. The RHIM-mediated interaction of RIPK1, TRIF, or DAI with RIPK3 causes oligomerization, activation, and phosphorylation of RIPK3 at S227 (in humans) or S232 (in mice). Phosphorylated RIPK3 subsequently binds to the second essential core protein of necroptosis, MLKL, and phosphorylates MLKL at T357/S358 (in humans) or S345 (in mice). This results in oligomerization, translocation, and probably insertion of MLKL into the plasma membrane where it elicits rupture of the plasma membrane [332]. Inhibitors of necroptosis can prevent this process, e.g., necrostatin-1s (RIPK1 inhibitor), GSK'840, GSK'843, GSK'872 (RIPK3 inhibitors), or necrosulfonamide (targets human, but not mouse MLKL) [334], and sometimes can even switch necroptotic cell death back to apoptosis, although this switch mainly applies to the RIPK3 inhibitors [335]. Of note, caspase-8 has been identified as a physiologic negative regulator of necroptosis, supposedly by cleaving and inactivating RIPK1 [336], RIPK3 [337], and the deubiquitinase CYLD [338]. As a consequence, interference with the enzymatic activity of caspase-8, e.g., by the broad-spectrum caspase inhibitors benzyloxycarbonyl-Val-Ala-Asp(OMe)-fluoromethylketone (zVAD-fmk), Q-VD-OPh, or Emricasan, will not only inhibit apoptosis, but concurrently also enhance necroptosis [331]. As a side note, although mitochondria and ROS have been implicated in necroptosis [339], they are not essential components [340] and a failure to detect ROS by FCM does not necessarily rule out necroptosis. Therefore, we do not further discuss the flow cytometric measurement of mitochondrially derived ROS and mitochondrial dysfunction here.

At present, the only factors common and specific for all triggers of necroptosis are phosphorylation of MLKL and RIPK3, formation of the RIPK3/MLKL complex, oligomerization of MLKL, and membrane translocation of MLKL [341]. Therefore, any FCM protocol aiming to deliver definite proof of necroptosis would have to unequivocally demonstrate the appearance of one or more of these biomarkers. Unfortunately, none of currently available protocols fulfills this requirement. To detect phosphorylation of MLKL and RIPK3, the current method of choice is Western blot with Abs that recognize phospho-T357/S358 or phospho-S345 in humans or mouse MLKL and phospho-S227 or phospho-S232 in humans or mouse RIPK3 [342]. The direct analysis of RIPK3 and MLKL phosphorylation status by FCM may become an option in the future, e.g., by adaptation of the BD Phosflow™ protocol. This

will, however, require appropriate Abs for detection of pMLKL and pRIPK3 under near-native conditions (i.e., intracellular staining, see Chapter III: "Before you start: Reagent and sample preparation, experimental design", Section 5: "Cell fixation and permeabilization for flow cytometric analyses"), which, to the best of our knowledge, are currently not available. Likewise, formation of the RIPK3/MLKL complex is generally determined by immunoprecipitation analyses, proof of MLKL oligomerization requires separation of the oligomers on nonreducing gels followed by Western blot analyses, and evidence for membrane translocation of MLKL is best obtained by immunostaining analyses or cell fractionation followed by Western blots [341] rather than by flow cytometric assays.

Nevertheless, once it has been established by one or more of the above assays that a particular treatment indeed induces necroptosis in a specific cell system, FCM can serve as an easy and fast method to detect and quantify the death of cells subjected to the same treatment. Today, FCM is routinely used by hundreds of laboratories worldwide to assess loss of membrane integrity after treatment with necroptotic stimuli. The protocol is usually identical to that used to detect apoptotic cells (see Chapter V: "Biological Applications," Section 7.1 "Apoptosis: Measurement of apoptosis"), except that the cells are treated under conditions that prevent apoptosis, e.g., in the presence of zVAD-fmk. Notably, by inhibiting caspase-8, zVAD-fmk will not only block apoptosis but concurrently enhance necroptosis. Furthermore, parallel staining for PS externalization can be omitted since studies have recently demonstrated that PS externalization can no longer be regarded as a reliable marker to differentiate between apoptosis and necroptosis because PS is also externalized in necroptotic cells prior to loss of membrane integrity [343, 344]. Instead, parallel measurements of samples additionally treated with inhibitors of necroptosis (e.g., necrostatin-1s, GSK'840, GSK'843, GSK'872, or necrosulfonamide) or flow cytometric exclusion of apoptotic caspase-3 activity (e.g., via the BD FITC Active Caspase-3 Apoptosis Kit) can ensure that cells positive for stains such as PI, 7-AAD, or DRAQ7 (i.e., showing loss of membrane integrity) are indeed necroptotic.

In addition to this straightforward approach, further protocols have been developed to assess necroptosis by FCM but they, like those noted above, have caveats. Lee and co-workers have recently described the simultaneous flow cytometric immunophenotyping of necroptosis, apoptosis, and RIPK1-dependent apoptosis, employing fluorescently tagged Abs that target RIPK3 and active caspase-3 in combination with a fixable live dead fluorescent dye [345]. This assay scores cells that show upregulation of RIPK3 as necroptotic; however, Moriwaki et al. have recently shown that RIPK3 has necroptosis- and kinase-independent functions in promoting reparative cytokine expression in tissue repair [346] and, therefore, detecting upregulation of RIPK3 by itself is not unequivocal evidence for necroptosis. Pietkiewicz et al. [347] have developed an approach that uses a combination of imaging flow cytometry with classical Annexin V/PI staining. Their protocol uses image-based analysis of nuclear morphology to differentiate between secondary necrotic/late apoptotic and necroptotic cells, a distinction that cannot be achieved by mere flow cytometric measurement
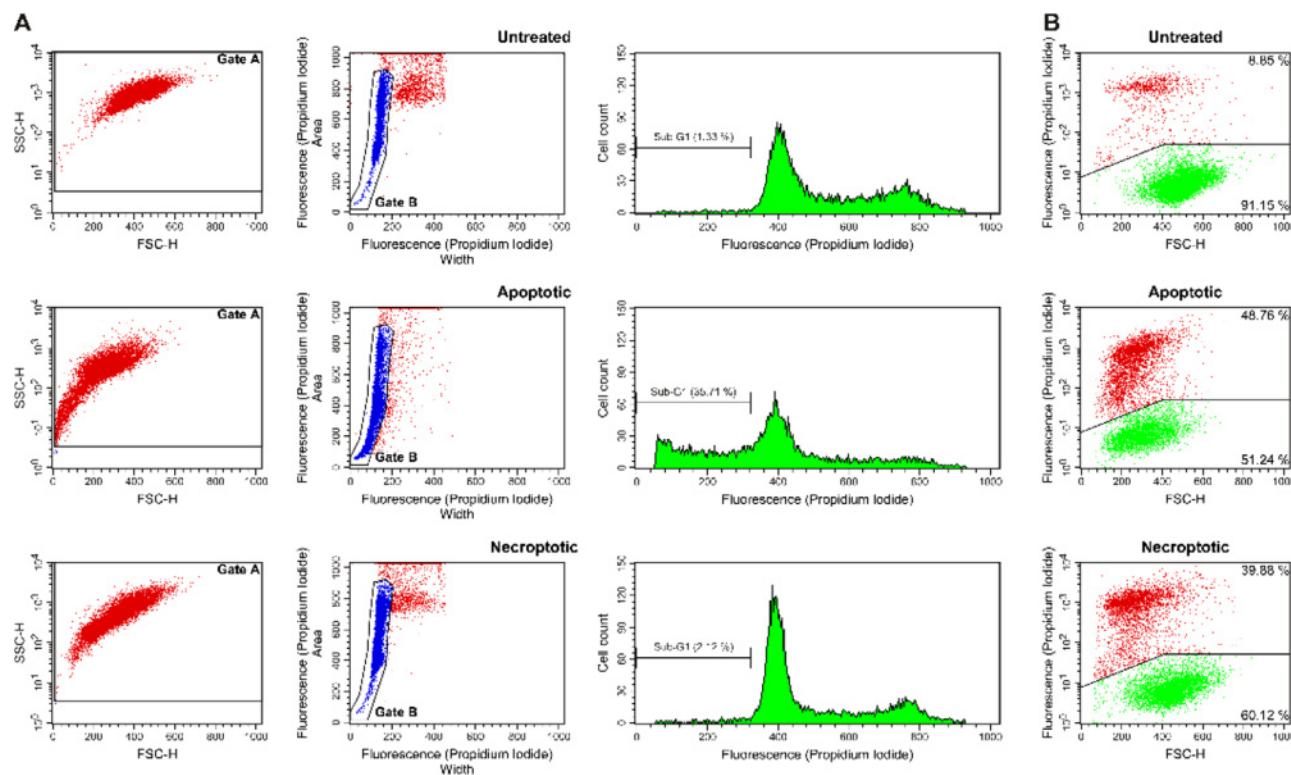
Figure 41. (A) BxPC-3 pancreatic adenocarcinoma cells were left untreated (top) or stimulated to elicit apoptosis (middle) or necroptosis (bottom). The left panels show dot plots of cell size (FSC-H) versus granularity (SSC-H) (relevant cell populations gated as gate A). The middle panels show dot plots of Pulse Width versus Pulse Area of the PI fluorescence channel to gate for singlets (gate B). The right panels depict the respective cell cycle profiles, with percentages of hypodiploid (sub-G1) cells indicated. (B) BxPC-3 cells were treated as in A and analyzed for loss of membrane integrity by PI staining. The percentages of PI-negative and PI-positive cells are indicated in the lower and upper right corners of the dot plots.

of PS exposure and loss of membrane integrity [343, 347]. The comparison of the morphology of ANX-V/PI double positive cells using imaging flow cytometry [347] or the difference in kinetics of ANX-V exposure using live microscopy [343] could be used in the future to differentiate apoptosis and necroptosis. However, not every laboratory has access to an imaging flow cytometer limiting the applicability of this approach.

We detail below an easy and straightforward protocol to detect necroptosis by conventional FCM, although this still needs the validation step of an alternative method for necroptosis confirmation. This protocol takes advantage of the fact that the DNA fragmentation caused by caspase activation in apoptotic cells does not occur in necroptotic cells [348]. Therefore, necroptosis and apoptosis can be discriminated via simple cell cycle analysis (i.e., detection of the fraction of hypodiploid (sub-G1) cells, see also Chapter V: "Biological Applications," Section 6.1: "DNA synthesis and cell cycle analysis"). Necroptotic, in contrast to apoptotic, cells do not show DNA fragmentation as detected in the cell cycle profile as sub-G1 cells (Fig. 41A). In parallel, PI staining can be used to verify loss of membrane integrity (Fig. 41B). We want to stress that although the protocol below is given for a specific setting ((TNF-related apoptosis-inducing ligand (TRAIL)-induced necroptosis in human BxPC-3 pancreatic adenocarcinoma cells), it can easily be adapted to any cell line/type and treatment that elicits necroptosis.

The protocol for cell cycle staining described here is an alternative protocol that we have applied successfully for other cell types revealing a satisfactory resolution of the cell cycle profile [349–351]. However, we point out that an incubation of at least 24 h at –20°C after the addition of 100% v/v ethanol or using a final concentration of 70% v/v instead of 50% v/v ethanol may improve the resolution of the cell cycle profiles if required.

7.3.3 Step-by-step sample preparation and assay protocol.

1. Seed 1×10^5 BxPC-3 cells in 12-well plates in 1 mL RPMI 1640 medium supplemented with 10% v/v FBS, 2 mM L-glutamine, 1 mM sodium pyruvate, and 50 μg/mL each of streptomycin and penicillin. Prepare two wells for each condition that you want to analyze. Prepare an additional well per condition for conventional analysis of loss of membrane integrity (step 20).

2. Let the cells grow for 24 h at 37°C in a humidified incubator containing 5% v/v CO_2.

3. Remove the old medium.

4. For induction of necroptosis, pre-incubate the cells for 30 min at 37°C in 1 mL of fresh medium that contains 20 μM zVAD-fmk and 0.5 μM homoharringtonine (a patient-approved drug that sensitizes cancer cells for necroptosis [352]). Cycloheximide can be used instead. Optimal concentrations must be

determined for each cell system. For induction of apoptosis, omit zVAD-fmk.

5. Add 100 ng/mL *Killer*TRAIL^{TM} and incubate the cells for 16 h at 37°C.

6. Transfer the medium together with any detached cells into Falcon® 5 mL polystyrene round bottom test tubes that are placed on ice. Pool the two wells that you have set up for the same condition in step 1.

7. Wash the wells with 300 μL PBS, pool into the same 5 mL tube.

8. Add 300 μL StemPro^{TM} Accutase^{TM} Cell Dissociation Reagent to each well, incubate for 10–15 min at 37°C to detach all remaining cells and pool everything into the same 5 mL tube.

9. Repeat step 7.

10. Collect the cells by centrifugation at 4°C (5 min, 400 x *g*), wash twice with cold PBS.

11. Resuspend the cells in 500 μL cold PBS/5 mM EDTA.

12. Fix the cells by dropwise addition of 500 μL 100% v/v ethanol while vortexing.

13. Incubate at room temperature for 30 min (or >24 h at –20°C to get the best resolution if required).

14. Collect the cells by centrifugation at 4°C (5 min, 560 x *g*). Be careful to avoid cell loss.

15. Resuspend the cells in 200 μl cold PBS/5 mM EDTA.

16. Add RNase A to a final concentration of 40 μg/mL.

17. Incubate for 30 min at room temperature.

18. Add 200 μL PI (50 μg/mL in PBS/5 mM EDTA stock solution) and stain for 30 min at 4°C.

19. Measure your cells in a suitable flow cytometer, such as the BD FACSCalibur^{TM}.

20. To additionally verify that loss of membrane integrity, i.e., necroptotic or apoptotic cell death has occurred, process the third well from step 1 as outlined above for steps 2–10. After step 10, resuspend the cells in 100 μL cold PBS/5 mM EDTA, add 100 μL PI (4 μg/mL in PBS/5 mM EDTA stock solution) and immediately measure your cells in a suitable flow cytometer, such as the BD FACSCalibur^{TM}.

7.3.4 Materials.

- BxPC-3 pancreatic adenocarcinoma cell line: ATCC® CRL-1687^{TM}, American Type Culture Collection, Manassas, VA, USA.
- Twelve-well plates: CELLSTAR® Cell Culture Multiwell Plates, catalog no. 665180, Greiner Bio-One, Frickenhausen, Germany.
- RPMI 1640 medium: catalog no. 52400, ThermoFisher Scientific, Dreieich, Germany.
- Fetal bovine serum: catalog no. 10270, ThermoFisher Scientific, Dreieich, Germany
- L-Glutamine: catalog no. K 0202, Merck, Berlin, Germany
- Sodium pyruvate: catalog no. 11360, ThermoFisher Scientific, Dreieich, Germany
- Penicillin/streptomycin: catalog no. A 2212, Merck, Berlin, Germany
- zVAD-fmk: catalog no. 4026865, Bachem, Weil am Rhein, Germany

- Homoharringtonine: catalog no. sc-202652, Santa Cruz, Heidelberg, Germany
- KillerTRAIL^{TM}: catalog no. ALX-201-123, Enzo, Lörrach, Germany
- Falcon® 12 x 75 mm, 5mL polystyrene round bottom test tubes: catalog no. 352054, Corning, Wiesbaden, Germany
- StemPro^{TM} Accutase^{TM} Cell Dissociation Reagent: catalog no. A1110501, ThermoFisher Scientific, Dreieich, Germany
- RNase A: catalog no. 19101, Qiagen, Hilden, Germany
- PI: catalog no. P4170, Merck, Darmstadt, Germany
- BD FACSCalibur^{TM} Flow Cytometer: BD Biosciences, Heidelberg, Germany
- BD CellQuest^{TM} Pro software: BD Biosciences, Heidelberg, Germany

7.3.5 Data analysis.   The data can be acquired using the acquisition software provided with the flow cytometer, e.g., the BD CellQuest^{TM} Pro software. Analysis can be done with either the software used for data acquisition or with any suitable FCM data analysis software.

Data acquisition for cell cycle analysis is described in detail in Chapter V: "Biological Applications," Section 6.1: "DNA synthesis and cell cycle analysis." Briefly, PI as DNA-binding dye is excited at 488 nm (blue laser) and emits at a maximum wavelength of 617 nm. Thus, PI fluorescence can either be detected using a BP filter 585/42 (FL2 channel of the FACSCalibur flow cytometer) or using a 670 nm LP filter (FL3 channel of the FACSCalibur flow cytometer) or a 695/40 BP filter. Instrument settings have to be set for the PI fluorescence channel on linear fluorescence scale and the threshold should be set on the same channel with a low value such as 20. For sample acquisition and analysis, three sequential plots are needed: dot plot 1: FSC-H versus SSC-H to gate for relevant cell population(s) (gate A); dot plot 2: Pulse Width versus Pulse Area of the PI fluorescence channel set on gate A to exclude doublets and to gate singlets as gate B; histogram 1: Pulse Area of the PI fluorescence channel gated on gate B. In total, 10 000–20 000 events in gate B should be collected. A typical result is shown in Fig. 41A. Dot plots 1 are depicted at the left, dot plots 2 in the middle, the respective histograms are shown at the right. In the histograms, a marker is placed on sub-G1 cells displaying lower staining intensity than the cell cycle profile, indicating apoptotic cells with fragmented and therefore lost DNA. In the dot plots, you can see a shift of the cell population to smaller and less granular cells as typical sign for cell death in both apoptotic as well as necroptotic cells.

Using DNA-binding dyes for quantification of dead cells is described in Chapter III: "Before you start: reagent and sample preparation, experimental design," Section 4.2: "DNA-binding dyes." For data acquisition using PI as the DNA-binding dye, instrument settings have to be set for the used PI fluorescence channel on logarithmic scale and the threshold should be set on FSC to exclude debris and small cell fragments. For sample acquisition and analysis, two sequential plots are needed; dot plot 1: FSC-H versus SSC-H to gate for relevant cell population(s) (gate A),

thereby excluding debris and small cellular fragments; dot plot 2: FSC-H versus the respective PI channel set on gate A. In total, 10 000–20 000 events in gate A should be collected. A typical result is shown in Fig. 41B using the same cells and stimulations as used for Fig. 41A. The percentages of PI-negative and PI-positive cells are indicated in the respective dot plot 2. A similar increase in the amount of PI-positive cells is detected in apoptotic as well as necroptotic samples. In summary, the two cell death modes, apoptosis and necroptosis, can be distinguished by cell cycle analysis, while quantification of cell death can be achieved by the simple method of PI staining.

7.3.6 Pitfalls/Top tricks. Please see Chapter V: "Biological Applications," Section 7.4: "Pyroptosis."

7.4 Pyroptosis

7.4.1 Overview. Cell death by pyroptosis critically depends on cleavage of gasdermin proteins by inflammatory caspases, followed by oligomerization and membrane translocation of the gasdermin N-terminal fragment. At present, FCM cannot directly track these events and the only definitive proof of pyroptosis is, e.g., by Western blot to detect cleavage of the protein gasdermin D (GSDMD). Yet, pyroptotic cells can be detected indirectly by FCM once pyroptosis has been confirmed. In this section, we present the currently available options to assess pyroptosis by FCM. In addition, we provide an example protocol to detect activation of inflammatory caspases as an indirect indicator for pyroptosis, noting that this method still requires that pyroptosis be validated by alternative methods but its inclusion in these guidelines is to indicate the potential application of FCM to a variety of cell death mechanisms.

7.4.2 Introduction. The Nomenclature Committee on Cell Death defines pyroptosis "as a form of regulated cell death that critically depends on the formation of plasma membrane pores by members of the gasdermin protein family, often (but not always) as a consequence of inflammatory caspase activation" [329]. Pyroptosis is a variant of regulated cell death that combines features of both apoptosis and necroptosis. Similar to apoptosis, pyroptotic cell death depends on caspase activation. On the other hand, rupture of the cell membrane and the release of DAMPs are features shared with necroptosis, classifying pyroptosis as an intensely inflammatory from of regulated cell death [353]. Pyroptosis occurs in response to microbial infection and has a critical role in immunity against intracellular pathogens [354]. Pyroptosis disrupts infected cells and thereby causes the release of intracellular pathogens, making them accessible to killing and phagocytosis by neutrophils. The concurrent release of DAMPs and of the inflammatory cytokines IL-1β and IL-18 recruits additional immune cells, ensuring a robust inflammatory response of both the innate and the adaptive immune system [353, 355]. However, pyroptosis can also drive pathogenic inflammation, i.e., in lethal septic shock [353, 356]. Pyroptosis is mostly observed in professional phagocytes, but can also occur in other cell types [357]. Triggers of pyroptosis encompass bacteria and viruses as well as their products, i.e., LPS and viral DNA [358].

The key molecular event in pyroptosis is caspase-mediated cleavage of GSDMD. Different from apoptosis, the relevant caspases belong to the inflammatory, not the apoptotic subtype (i.e., caspases-1, -4, and -5 in humans, and caspases-1 and -11 in mice) [354, 357]. As an exception, the apoptotic caspase caspase-3 can also induce pyroptosis by cleavage of the GSDMD-related protein gasdermin E [332]. GSDMD-dependent pyroptosis can be triggered by two pathways, the canonical or the noncanonical pathway. In the canonical pathway, cellular stressors such as bacterial or viral pathogen signatures are recognized by pattern-recognition receptors. Together with the adapter protein ASC, these pattern-recognition receptors form complexes ("inflammasomes"), which recruit and activate caspase-1. In the noncanonical pathway, human caspases-4 and -5 or mouse caspase-11 are directly activated by cytosolic LPS from Gram-negative bacteria [332, 354]. In both pathways, caspase activation results in cleavage of GSDMD and release of its N-terminal domain (GSDMD-N). GSDMD-N then inserts into the plasma membrane of the cell (or into the bacterial plasma membrane) and causes membrane rupture and pyroptotic cell death [332, 354].

Given that cleavage of GSDMD as well as membrane translocation and oligomerization of GSDMD-N are the only definitive biomarkers for pyroptosis, the options for direct flow cytometric detection of pyroptosis are as equally limited as for necroptosis (see Chapter V: "Biological Applications," Section 7.3 "Necroptosis"). At present, the best method to detect cleavage of GSDMD into the 31-kDa GSDMD-N fragment is Western blot using GSDMD-N-specific Abs. Membrane translocation of GSDMD-N can be shown via cell fractionation with subsequent Western blot or via immunostaining, and oligomerization of GSDMD-N can be confirmed by nonreducing gel electrophoresis and Western blot.

Although direct flow cytometric detection of these biomarkers is not possible at present, the above assays can be performed to initially ensure that pyroptosis is induced by a specific treatment condition. Subsequently, FCM can be utilized to routinely detect pyroptotic loss of membrane integrity in identically stimulated cells (PI staining, see also Chapter III: "Before you start: reagent and sample preparation, experimental design," Section 4.2: "DNA-binding dyes." and Chapter V: "Biological Applications," Section 7.3 "Necroptosis"). As a further limitation, parallel control measurements of samples additionally treated with pyroptosis inhibitors are not possible because inhibitors that directly and specifically target GSDMD-N are currently not commercially available. As a workaround, cells can be treated with VX-765, an inhibitor of caspase-1, or with MCC950, an inhibitor of NLRP3 inflammasome activation, although inhibition of caspase-1 or the inflammasome may elicit cellular responses beyond inhibition of pyroptosis.

Alternatively, it is possible to employ FCM to detect inflammasome formation as an indirect indicator for canonical pyroptosis induction. Normally, the inflammasome component ASC is dif-

fusely distributed within the cell, but relocates to a dense speck in the cytosol within minutes of inflammasome activation. Sester and colleagues have employed FCM to monitor ASC redistribution in primary macrophages and monocytes, detecting changes in fluorescence peak height and width of immunostained or fluorescently tagged ASC as detailed in ref. [359].

A separate approach to assess pyroptosis by FCM exploits the fact that pyroptosis depends on the activation of inflammatory caspases. Upon addition of a green, cell permeant FLICA[TM] reagent such as fluorescein-6-carbonyl-Tyr-Val-Ala-DL-Asp(OMe)-fluoromethylketone (FAM-YVAD-fmk), activated caspases-1, -4, and -5 covalently and irreversible bind to FAM-YVAD-fmk and become accessible to quantification by FCM as an indirect measure for the initiation of pyroptosis. Below, we outline a protocol to quantify the activation of caspases-1, -4, and -5 in nigericin-treated pyroptotic human BxPC3 pancreatic adenocarcinoma cells (a cell line for which pyroptosis has been demonstrated [360]) by conventional FCM (Fig. 42A), or to simultaneously confirm loss of membrane integrity by PI staining (Fig. 42B). Although representing a specific example, the protocol can easily be modified for any treatment that triggers pyroptosis in a particular cell line. It should be re-stated that this method needs to be used in conjunction with alternative validation of pyroptosis.

7.4.3 Step-by-step sample preparation and assay protocol.

1. Seed 1 x 10^5 BxPC3 pancreatic adenocarcinoma cells in 12-well plates in 1 mL RPMI 1640 medium supplemented with 10% v/v FBS, 2 mM L-glutamine, 1 mM sodium pyruvate, and 50 µg/mL each of streptomycin and penicillin. Prepare three wells for each condition that you want to analyze.
2. Let the cells grow for 24 h at 37°C in a humidified incubator containing 5% v/v CO_2.
3. Reconstitute the lyophilized nigericin contained in the Pyroptosis/Caspase-1 Assay Kit with 100 µL DMSO, yielding a 5 mM stock solution. The stock solution can be stored at –20°C for 1 year, provided that it is protected from light and thawed maximally two times.
4. Dilute the nigericin stock solution with sterile ultrapure water to a working concentration of 500 µM immediately before use.
5. Remove the old medium from the cells.
6. To initiate pyroptosis, preincubate the cells for 1 h at 37°C in 300 µL of fresh medium that contains 20 µM nigericin (optimal concentrations must be determined for each cell system).
7. Reconstitute a vial with lyophilized FLICA[TM] contained in the Pyroptosis/Caspase-1 Assay Kit with 50 µL DMSO, yielding a 150–300× stock solution. The stock solution can be stored at –20°C for 6 months, provided that it is protected from light and thawed maximally two times.
8. Dilute the FLICA[TM] stock solution 1:5 with sterile PBS to a 30–60× working solution and immediately add the working solution to the cells in two wells of each condition at a final concentration of 1–2×.
9. Incubate the cells for 48 h at 37°C, protected from light.

10. Dilute 10× Cellular Wash Buffer contained in the Pyroptosis/Caspase-1 Assay Kit to 1× with ultrapure water.
11. Transfer the medium together with any detached cells into Falcon® 5 mL polystyrene round bottom test tubes that are placed on ice.
12. Add 300 µL 1x Cellular Wash Buffer to each well, incubate for 10 min at 37°C (this allows any unbound FLICA[TM] to diffuse out of the cells). Remove the Wash Buffer and transfer into the 5 mL tube from step 11.
13. Repeat step 12 twice.
14. Add 300 µL StemPro[TM] Accutase[TM] Cell Dissociation Reagent to each well, incubate for 10–15 min at 37°C to detach all remaining cells and transfer everything into new Falcon® 5 mL polystyrene round bottom test tubes.
15. Wash the wells with 300 µL 1× Cellular Wash Buffer, transfer everything into the 5 mL tubes from step 14.
16. Centrifuge the 5 mL tubes from step 13 and from step 15 at 4°C (5 min, 400 × g) to collect all cells.
17. Discard the supernatants and wash the cells twice with cold 1× Cellular Wash Buffer. Be careful to avoid cell loss.
18. Resuspend and combine the cells from the two corresponding tubes from steps 13 and 15 in a total of 300 µL cold 1× Cellular Wash Buffer and place on ice.
19. For single-color analysis or for a single-color compensation control (caspase-1 activity), measure the cells (from the first well treated with FLICA[TM]) by FCM within 4 h or fix for analysis within 16 h by adding Fixative contained in the Pyroptosis/Caspase-1 Assay Kit at a v/v ratio of 1:5. Store your samples protected from light and at 4°C. For dual-color analyses (caspase-1 activity and loss of membrane integrity), add 2 µg/mL PI to the cells from the second well treated with FLICA[TM] and analyze immediately as such assays cannot be performed using fixed cells. For a single-color compensation control (loss of membrane integrity), use the cells from the third well (not treated with FLICA[TM]), add 2 µg/mL PI and analyze immediately.
20. Measure your cells in a suitable flow cytometer, such as the BD FACSCalibur[TM].

7.4.4 Materials.

- BxPC-3 pancreatic adenocarcinoma cell line: ATCC® CRL-1687[TM], American Type Culture Collection, Manassas, VA, USA.
- Twelve-well plates: CELLSTAR® Cell Culture Multiwell Plates, catalog no. 665180, Greiner Bio-One, Frickenhausen, Germany.
- RPMI 1640 medium: catalog no. 52400, ThermoFisher Scientific, Dreieich, Germany.
- FBS: catalog no. 10270, ThermoFisher Scientific, Dreieich, Germany.
- L-Glutamine: catalog no. K 0202, Merck, Berlin, Germany.
- Sodium pyruvate: catalog no. 11360, ThermoFisher Scientific, Dreieich, Germany.
- Penicillin/streptomycin: catalog no. A 2212, Merck, Berlin, Germany.
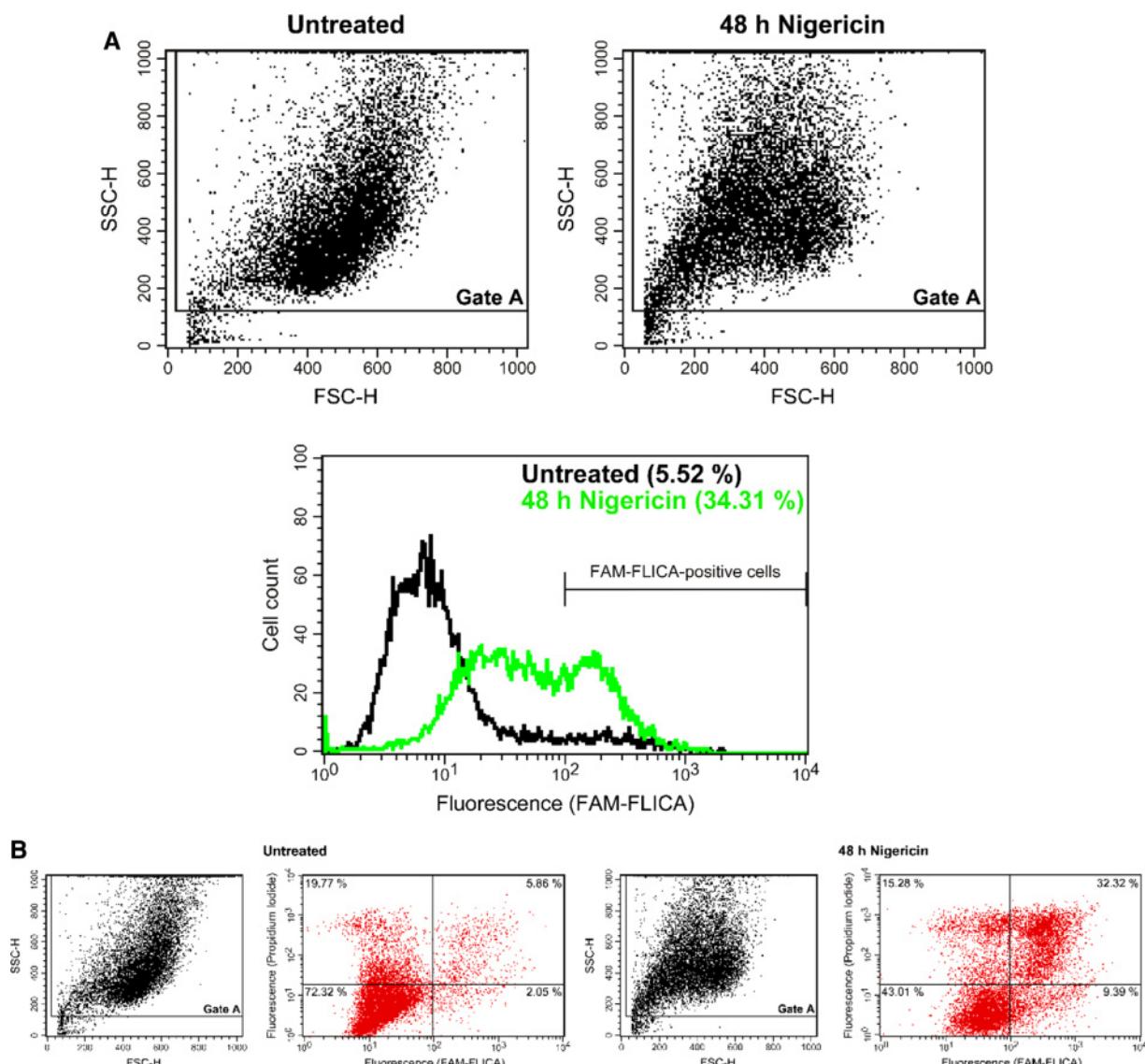
Figure 42. (A) Single-parameter analysis of BxPC-3 cells left untreated or treated with nigericin for 48 h and analyzed for caspase-1 activity by FAM-FLICA staining (48 h were determined in previous experiments as optimal to achieve the best separation between the FAM-FLICA-positive and the FAM-FLICA-negative population). FSC-H versus SSC-H dot plot is depicted on top, the respective histogram is presented at the bottom. The percentages of FAM-FLICA-positive cells in untreated and nigericin-stimulated cells are indicated in the upper right corner of the histogram. (B) Dual parameter analysis of BxPC-3 pancreatic adenocarcinoma cells either untreated for 48 h or stimulated with nigericin for 48 h to induce pyroptosis (cells are from the same experiment as shown in (A) but from a parallel stimulation). For each sample (untreated and treated cells) FSC-H versus SSC-H dot plots are shown on the left and PI versus FAM-FLICA on the right. The compensation gating is not shown. This flow cytometric analysis also needs pyroptosis to be validated by methods such as Western blot.

- Pyroptosis/Caspase-1 Assay Kit containing nigericin, FAM-YVAD-fmk, Cellular Wash Buffer and Fixative, catalog no. 9146, ImmunoChemistry Technologies, Bloomington, MN, USA.
- Falcon® 12 × 75mm, 5 mL polystyrene round bottom test tubes: catalog no. 352054, Corning, Wiesbaden, Germany.
- StemPro™ Accutase™ Cell Dissociation Reagent: catalog no. A1110501, ThermoFisher Scientific, Dreieich, Germany.
- PI: catalog no. P4170, Merck, Darmstadt, Germany.
- BD FACSCalibur™ Flow Cytometer: BD Biosciences, Heidelberg, Germany.

- BD CellQuest™ Pro software: BD Biosciences, Heidelberg, Germany.

7.4.5 Data analysis. Data can be acquired using the acquisition software provided with the flow cytometer, for example, the BD CellQuest™ Pro software. Analysis can be done with either the software used for data acquisition or with any suitable FCM data analysis software. For data analysis, follow the manual provided with the Pyroptosis/Caspase-1 Assay Kit. The FAM-FLICA reagent is excited at 488 nm (blue laser) and has a peak emission at

515–535 nm. Thus, FAM-FLICA fluorescence can be detected using a BP filter 530/30 (FL1 channel of the FACSCalibur flow cytometer). For single-staining, instrument settings have to be set for the FAM-FLICA fluorescence channel on logarithmic fluorescence scale and the threshold should be set on FSC to exclude small cellular fragments and debris. For sample acquisition and analysis, two sequential plots are needed: an FSC-H versus SSC-H dot plot to gate on the population of interest (gate A) and a histogram plot with the log FAM-FLICA fluorescence on the *x*-axis versus the number of cells on the *y*-axis set on gate A. Adjust the voltage of the FAM-FLICA fluorescence channel, if necessary, to ensure that fluorescence is on scale and caspase-negative (FAM-FLICA^{-}) cells appear within the lower log fluorescence output decades of the *x*-axis. Caspase-positive (FAM-FLICA^{+}) cells will appear as a shoulder or as a separate peak shifted to the right side of the negative peak. A typical result demonstrating a histogram overlay of negative and positive cells is shown in Fig. 42A. The gate is set on FAM-FLICA-positive cells and their percentages in untreated and nigericin-stimulated cells are indicated in the upper right corner of the histogram.

For dual-color analyses using additionally PI as DNA-binding dye, first run each single-color untreated control. PI is excited at 488 nm (blue laser) and emits at a maximum wavelength of 617 nm. Thus, PI fluorescence can either be detected using a BP filter 585/42 (FL2 channel of the FACSCalibur flow cytometer) or using a 670 nm LP filter (FL3 channel of the FACSCalibur flow cytometer) or a 695/40 BP filter. To determine the correct instrument settings, use the single-color untreated cells and analyze two dot plots, FAM-FLICA-fluorescence versus FSC-H and PI fluorescence versus FSC-H (use a logarithmic fluorescence scale for both channels) set on gate A. Adjust the voltages for both fluorescence channels so that PI- or FAM-FLICA-negative cells appear in the lower log fluorescence output decades. For compensation, use the single-color nigericin-treated cells as compensation controls (see Chapter II: "Setup: Instrument setup and quality control," Section 1: "Compensation").

For sample acquisition and analysis, the following gating steps are required. First, FSC-H versus SSC-H to gate for the relevant cell population(s) (gate A). Second, FAM-FLICA-fluorescence versus PI fluorescence set on gate A is used to quantify double-negative cells (healthy), single-FAM-FLICA-positive cells (containing activated caspase-1 without signs of pyroptosis), single-PI-positive cells (undergoing cell death independently of caspase-1) and double-positive cells (undergoing pyroptosis). In total, 10 000–20 000 events in gate A should be collected. A typical result is shown in Fig. 42B.

7.4.6 Pitfalls/Top tricks. When studying necroptosis, to obtain credible results, it is imperative that your cells are mycoplasma-negative because mycoplasma express large amounts of nucleases [361], and you will detect false-positive DNA fragmentation in necroptotic cells if cells are contaminated. Also, using NIH3T3 cells may be problematic as various sublines exist that differ in

their disposition to undergo necroptosis with or without caspase inhibition [362], thus possibly leading to mixed cell death mechanisms. However, in our proposed protocol, cell cycle staining showing fragmented DNA as sub-G1 cells would clearly reveal such a mixed cell death mechanism by demonstrating more PI-positive cells (general cell death) than sub-G1 cells (purely apoptosis).

When studying pyroptosis, protect samples containing FAM-YVAD-FMK from light. Also, the optimal time-point to achieve the best separation between the FAM-FLICA-positive and the FAM-FLICA negative population has to be determined individually for each cell line. In dual-color analyses for pyroptosis, more PI-positive cells may be detected than in single-color PI analyses due to the more extensive washing and handling of the cells. As an additional point to take note of, binding of FLICA reagents to their target sequence is generally not as caspase-specific as originally thought because of the FMK group reactivity with thiol groups of intracellular proteins that become available upon caspase cleavage [363]. Nevertheless, and despite this apparent lack of absolute specificity, FLICA probes have consistently shown themselves to be highly reliable reporters of caspase activation [364] and the assay presented here has been successfully used to detect caspase-1 activation in recent studies [365, 366].

It is recommended to consult Chapter III: "Before you start: Reagent and sample preparation, experimental design," Section 4.2: "DNA-binding dyes," Chapter V: "Biological Applications," Sections 6.1: "DNA synthesis and cell cycle analysis," Section 7.1: "Apoptosis: Measurement of apoptosis," and Section 7.2: "Apoptosis: Caspase activation" as well as the manual of the Pyroptosis/Caspase-1 Assay Kit for additional information regarding cell death measurement.

As a general pitfall, it has to be pointed out that the protocols described to analyze either necroptosis or pyroptosis by FCM are not specific for the mode of cell death. The lack of DNA fragmentation as detected by cell cycle analysis merely excludes apoptosis but does not discriminate between different modes of cell death leading to membrane rupture without caspase activation. Therefore, the occurrence of necroptosis or pyroptosis has to be validated by alternative methods, i.e., when analyzing a new cell system, you will have to make sure that your treatment indeed induces the cell death mode under investigation, either necroptosis, e.g., by Western blot for phosphorylation of RIPK3 and/or MLKL [352, 367], or pyroptosis by Western blot to detect cleavage of GSDMD. Western blot analysis, however, is at best semi-quantitative, because all cells are analyzed as a single population. In contrast, FCM yields a quantitative result as it analyses each cell within the sample separately and therefore provides additional information.

A reasonable way to enhance the specificity of the flow cytometric assays described here would be the use of inhibitors while stimulating the cells that are specific for necroptosis (necrostatin-1s, GSK'840, GSK'843, GSK'872, or necrosulfonamide) or pyroptosis (VX-765 and MCC950), although the pyroptosis inhibitors may affect other cell processes and complicate the interpretation.

8 Phagocytosis

8.1 *Overview*

Phagocytes are essential components of the first defensive line of the innate immune system. Professional phagocytes include neutrophilic and eosinopilic granulocytes, monocytes, dendritic cells, tissue-resident macrophages (e.g, alveolar macrophages, marginal zone and metallophilic splenic macrophages, Kupffer cells of the liver, intestinal macrophages, osteoclasts, and microglia of the brain) and macrophages derived from monocytes during inflammatory processes [368]. Phagocytosis is, indeed, one of the most ancient and evolutionarily conserved functions of immunity [369].

Ingesting and killing of microorganisms involves intrinsic functions of phagocytes as well as complex interactions between phagocytes, pathogens, and plasma factors such as opsonins. Deficiencies in these functions or interactions are associated with increased susceptibility to infection. Phagocytosis as part of the antimicrobial immune defense involves sequentially chemotactic migration of the phagocytes, recognition of pathogen determinants, ingestion of microorganisms, and finally, destruction by oxygen-dependent (e.g., "oxidative burst" of the phagocyte NADPH oxidase [Phox], NO production by the type 2 or inducible nitric oxide synthase [NOS2, iNOS]) and oxygen-independent mechanisms (e.g., acidification and protease activities, antimicrobial peptides) [368].

It is important to note that the interaction with extracellular or intracellular pathogens may lead to the apoptotic death of phagocytes [370]. On the other hand, phagocyte recognition of apoptotic cells helps clearance of senescent, stressed, damaged, or altered cells of the body from tissues. Phagocytosis of apoptotic cells prevents the release of cell components that might otherwise trigger inflammatory response [371]. Phagoptosis is a form of cell death caused by primary phagocytosis and destruction of viable cells. Phagoptosis mediates turnover of erythrocytes, neutrophils and other cells, and thus is one of the main forms of cell death in the body. Phagoptosis is triggered by exposure of "eat-me" signals (such as phosphatidylserine or calreticulin) and/or loss of "don't-eat-me" signals (such as CD47) on the plasma membrane of viable cells, causing their phagocytosis by phagocytes. Live cells may modify the expression of such signals as a result of cell stress, damage, activation, or senescence [372].

Also of interest is the study of phagocytic ingestion of synthetic nanoparticles in the range of 1–100 nm. These particles are increasingly used in industrial and commercial products [373].

8.2 *Flow cytometric assays of phagocytosis: Fundamentals and general applications*

FCM has been used for many years to study phagocytosis [374–380]. Although frequent applications include the clinical study of human immunodeficiencies and septic conditions [381], phagocytosis assays also serve veterinary [382] and environmental settings [383] as well as a growing multiplicity of other experimental settings.

In classical FCM phagocytosis assays, phagocytes are incubated at 37°C with fluorescent target particles pre-opsonized with an appropriate dilution of serum. Phagocytosis is measured as the mean fluorescence of effector cells and/or the percentages of fluorochrome-positive phagocytes, or serum dilutions at which a defined endpoint value is calculated. These techniques have intrinsic drawbacks, such as quenching of fluorescence upon internalization, the difficulty to distinguish between adherent and internalized bacteria in most cases, or a failure to determine Ab-mediated phagocytosis [374–380].

Phagocytosis studies benefit from the unique integration of functional and phenotypic information provided by FCM and the large availability of phagocytic cell types and targets (both natural and synthetic) that are suitable for the technical capabilities of FCM [374–380]. In many cases, FCM assays of phagocytosis are available as commercial kits, and may include simultaneous assessment of other functional aspects or consequences of phagocytosis, typically the oxidative burst [381] or apoptosis [381, 384].

8.3 *Critical points in the pre-analytical and analytical phases of assays*

8.3.1 Phagocytic cell types and sample preparation. FCM assays of phagocytosis and other phagocytic-related functions can be performed on a large variety of primary phagocytic cells, including but not restricted to peripheral blood monocytes and neutrophils from humans (Fig. 43) [381], rats [385], dogs [386], cats [387], cows [388], or cetaceans (Fig. 44) [383], human dendritic cells [389], human peritoneal [390] or monocyte-derived macrophages [391], peritoneal- or bone-marrow murine macrophages [392], and coelomocytes from earthworms [393]. In addition, several established cell lines with phagocytic capacity can be used for experimental studies, typically the human monocytic cell lines U937 and THP-1, or the murine macrophage cell lines J774A.1 and RAW 264.7 [394].

When using whole blood samples, heparin is often the anticoagulant of choice, as both EDTA and citrate bind divalent cations and thereby can interfere with phagocytosis processes and oxidative burst (e.g., see ref. [395–397]). All classical anticoagulants negatively affect complement activity and opsonophagocytosis [398]. Anticoagulated blood samples should be processed within 4 h of collection. Prolonged storage may lead to abnormal results. Specimens should typically be maintained at 18–22°C, and temperatures below 10°C and above 30°C must be avoided if possible when using whole blood. If cryo-preserved blood cells are used for assay, it is essential to thaw and use the cells rapidly. Neutrophils are particularly fragile. Myeloid cells can be activated by endotoxins, excessive agitation, or repeated centrifugations, resulting in cell death. Endotoxin-free polypropylene tubes should be used. Cell clumping after standing at room temperature can be avoided by using the cells promptly or by adding DNase to the cell suspension [377].
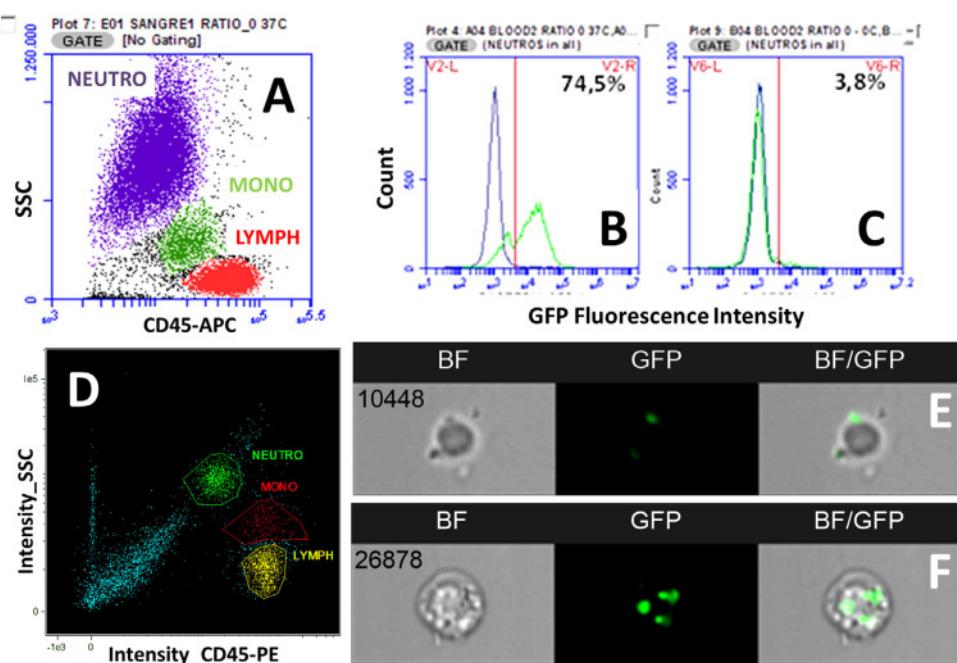
Figure 43. Representative examples of strategies to differentiate between attached and internalized fluorescent bacteria in whole-blood phagocytosis assays by conventional flow cytometry (A–C) and imaging flow cytometry (D–F). In both assays, whole-blood samples anticoagulated with heparin were stained with CD45-APC (A) or CD45-PE (D) Ab and incubated for 30 min at 37°C (B) or at 4°C (C) with a suspension of *Escherichia coli* (ATCC 11775) transformed by electroporation with a plasmid containing the GFP gene (pMEK91 GFP). The ratio of bacteria to leukocytes was 1:4. Then, samples were lysed with BD FACS Lysing Solution, put on ice and analyzed immediately in a BD Accuri C6 conventional flow cytometer (A–C) or in an Amnis ImageStream 100 multispectral imaging flow cytometer (D–F), both using a 488 nm blue laser. Graphs B and C show the intensity of GFP fluorescence emission in granulocytes distinguished by higher granularity (SSC) and lower CD45 expression (purple-colored events in graph A) after incubation of whole blood with GFP-expressing *E. coli* at 37°C (graph B) or at 4°C (graph C). Comparison of B and C shows the difference between granulocytes with adherent and/or internalized bacteria (74.5% of the population after incubation at 37°C) and granulocytes with only adherent bacteria (3.8% of the population after incubation at 4°C). Graph (D) shows the features of the main leukocyte populations identified on an imaging flow cytometer by their light scatter under darkfield illumination (intensity_SSC) and the expression CD45 (intensity_CD45-PE). Composite graphs (E) and (F) show the intracellular localization of GFP bacteria in single cells of the granulocyte subpopulation (gated on NEUTRO, graph D) after incubation of whole blood with GFP-expressing *E. coli* at 37°C. Merged images (BF/GFP) from the brightfield illumination channel (BF) and the green fluorescence channel (GFP) allow distinguishing cells with external bacteria (graph E) from cells with internalized bacteria (graph F). Numbers on the BF image in (E) and (F) composites indicate the sequential number of the event in the sample run.

Human PBMCs and neutrophils can be isolated by using different classical procedures, with dextran sedimentation preferable for neutrophil purification and gradient centrifugation by Histopaque 1077 for monocyte enrichment [399]. In addition, magnetic separation can be used successfully to isolate functional primary phagocytic cells based upon immunophenotypic myeloid cell determinants [91]. Human monocytes are often cultured in serum-free or serum-supplemented media to create macrophages or dendritic cells [91].

8.3.2 Phagocytosis targets. A multiplicity of fluorescent biological and synthetic micro- or nanoparticles can be used as suitable targets for phagocytosis with FCM assays, reflecting, on the one hand, the different roles and clinical failures of phagocytosis, and on the other hand, the diversity of plasma membrane receptors that mediate phagocytic recognition of microbes, apoptotic cells, or synthetic particles [368].

The best biological targets are live microorganisms, including pathogenic and nonpathogenic bacteria and yeast. Because of their hazardous nature, pathogens can be inactivated by different means. However, inactivation by heat killing (e.g., boiling) may result in loss of cell wall components, which are extremely important for phagocyte recognition, thus potentially reducing phagocytosis [400]. Inactivation by fixation with 4% paraformaldehyde may preserve some pathogen-associated determinants and improves recognition [401]. Another typical target for phagocytosis assays are zymosan particles, prepared from the cell wall of *Saccharomyces cerevisiae* and consisting of protein-carbohydrate complexes [376–378, 402]. FCM assays of phagocytosis can use fluorescent microbeads of different optical properties, chemical composition, and diameter that may be, in addition, coupled with components relevant for receptor-mediated particle recognition [377].

Since physiological phagocytosis occurs mainly after binding of opsonized particles to receptors of the constant fragment of immunoglobulins (Fc) or complement receptors expressed on phagocytes, it may be essential to ensure opsonization of phagocytosis targets. Engagement of phagocyte Fc receptors is achieved by pre-incubation of targets with appropriate sera or IgG solutions, as well as by coating of fluorescent beads with IgG Abs. In this
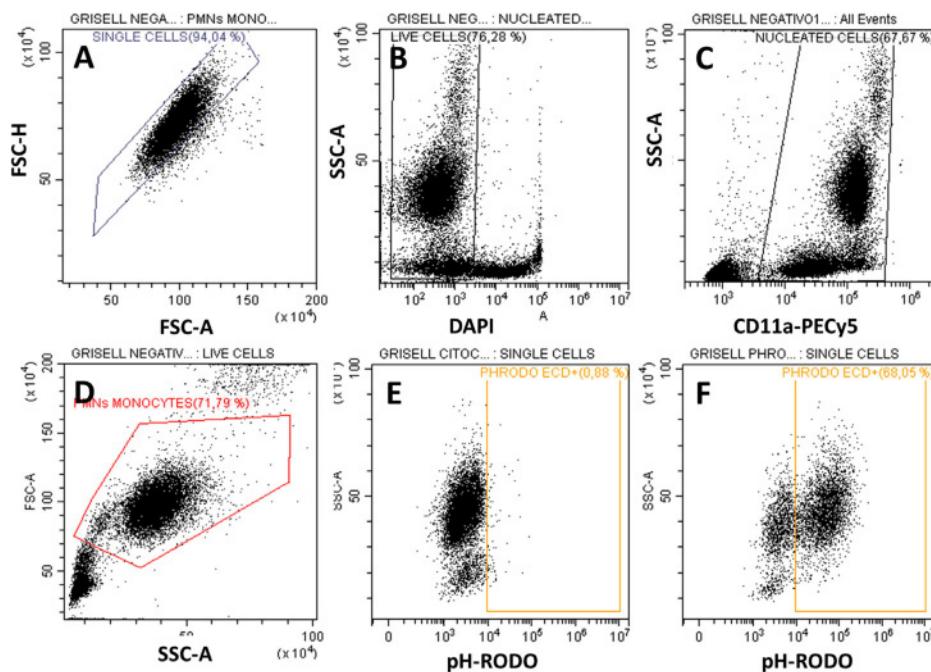
Figure 44. A representative example of flow cytometric assay of phagocytosis in whole blood of Bottlenose dolphin (*Tursiops truncatus*) using pHrodo Red *E. coli* BioParticles. The assay was performed following the protocol described in the text. Data were obtained in a CytoFlex flow cytometer (Beckman Coulter). Graph (A): Doublet exclusion based on FSC-A versus FSC-H features. Graph (B): Selection of live cells based on exclusion of DAPI dye. Graph (C): Identification of leukocytes based on staining with CD11a-PECy5 Ab. Graph (D): Morphological features of live blood cells, showing the populations of phagocytic cells (monocytes and polymorphonuclear neutrophils) where ingestion of pHrodo Red *E. coli* BioParticles should be expected. Graph (E): Fluorescence intensity of pHrodo Red *E. coli* BioParticles in the negative control tube, showing the low level of *E. coli* ingestion in the sample treated with Cytochalasin A. Graph (F): Fluorescence intensity of pHrodo Red *E. coli* BioParticles in the assay tube, showing the high level of *E. coli* BioParticles ingestion by phagocytic cells from the blood of a healthy dolphin.

aspect, whole-blood assays of phagocytosis have the advantage of not requiring additional steps of target opsonization.

As rates of phagocytosis are highly dependent on the target-to-cell ratio, accurate counting of targets and effector phagocytes and the use of a suitable ratio is important [402]. Target: effector ratios ranging from 1:1 [402] to 260:1 [403] have been applied in different assay settings. Similarly, the determination of the duration of the assay must take into account the difference of phagocytosis kinetics between synthetic and natural targets, as well as among different types of biological targets. One-hour incubation is usually sufficient and typically, phagocytosis assays require incubation times of 15–30 min [404].

8.3.3 Fluorescent labeling of targets. There are several convenient commercial sources of fluorescently conjugated biological and synthetic particles [379]. In some cases, such particles are components of assay kits that can be used in conventional FCM using a suitable laser. For custom labeling of targets, the most common fluorescent labels are incorporated as N-hydroxysuccinimide esters, which react covalently with –NH2 groups [379]. Fluorescein derivatives (e.g., fluorescein, dicarboxyfluorescein, Oregon Green, dihydrodichlorofluorescein) have been popular, but their fluorescence is quenched in the acidic compartments of phagocytes and, moreover, their emission wavelength overlaps markedly with green autofluorescence, which is especially present in macrophages and monocytes [405]. Other fluorophores such as Alexa Fluor, BODIPY FL, tetramethylrhodamine, and Texas Red have stable, intense emission over a broad pH range (pH 4–9). Most interestingly, pHrodo, a new series of probes with green or red fluorescence emission increasing with decreasing pH has been recently developed [379, 406]. Fluorescent protein-expressing *E. coli* strains are also suitable for FCM assays [407–409].

8.3.4 Identification of live subpopulations of phagocytic cells by light scatter and surface immunophenotype. The nucleated phagocytes in whole blood assays may be distinguished from debris and from smaller targets (microorganisms and fluorescent beads) by gating on the granulocyte and monocyte populations using FSC and SSC properties [377, 379]. As phagocytosis may lead to degranulation and even apoptosis of phagocytes, especially neutrophils, it is recommended to include at least a viability marker and eventually appropriate immunophenotypic markers (for human cells, e.g., CD45, CD14, CD13, CD15, CD16, CD11b) [410]. It is worth mentioning that the lymphocyte population in whole blood assays may often serve as an internal negative control of nonphagocytic cells. In FCM assays using homogeneous phagocytic populations (e.g., U937, TPH-1, RAW264.7 cell lines) and small targets, it is recommended to include viability markers, in order to exclude nonspecific attachment of targets to dead or dying phagocytic cells. In those specialized assays, in which target cells (e.g., apoptotic cells, infected erythrocytes) may have similar size as phagocyte effectors, it is recommended to separately label effectors and/or targets with appropriate tracking dyes [403, 411].

In all cases, phagocytosis assays involving immunophenotyping with multicolor cytometry should include the appropriate controls for fluorescence compensation (single-stained tubes) and gating (FMO controls). This is further discussed in Chapter II, Section 1, Compensation.

8.3.5 Distinguishing non-internalized from internalized particles.

In order to accurately assess the phagocytosis process, it is mandatory to demonstrate that the particles are in fact ingested as opposed to coincident with the phagocyte in the laser-illuminated volume or adherent to the cell surface.

While coincidence of phagocytes and targets can be minimized by running diluted samples at slower flow rates, quantification of internalized particles as opposed to surface adherent particles may be approached by different strategies:

1. Comparing the cell-associated fluorescence intensity in conditions avoiding (negative controls) or allowing particle internalization. Negative controls of this type should include cells incubated without fluorescent targets (which allows for the detection of autofluorescence) and cells and targets co-incubated at 4°C (Fig. 43) or in the presence of inhibitors of cytoskeleton rearrangement, such as the most commonly used cytochalasins (Fig. 44), or other inhibitors of phagocyte function, such as N-ethylmaleimide [404].
2. Using targets labeled with a dye that is sensitive to quenching agents. FITC or Calcofluor White can be quenched by trypan blue and crystal violet [377–379], while Sytox Green is quenched by PI [400]. In this approach, extra washing steps are necessary to remove the quenching dye, thus increasing assay time and making the assay prone to artifacts and cell loss.
3. Using fluorescent targets emitting fluorescence at different wavelengths at neutral or acidic pH. Probes of this type include the pHRodo series, and the Eos-FP fluorescent protein. pHRodo dye can be used for the labeling of targets, as it reacts with the primary amino groups on the particle to yield a covalently linked pH probe, which increases fluorescence emission as the pH of its environment becomes more acidic. Due to the low pH of the phagolysosome, phagocytized targets can be quantified without interference of adherent particles [379, 406, 412, 413]. The optimal absorption and fluorescence emission maxima of the pHrodo Green dye and its conjugates are approximately 509 nm and 533 nm, respectively, while pHrodo Red excites at 560 nm and emits at 585 nm. Both pHrodo Green and pHrodo Red can also be excited with the 488 nm argon-ion laser installed on most flow cytometers (Fig. 44).

    Eos-FP can be transfected into infectious microorganisms. After UV-irradiation of bacteria, peptide cleavage in Eos-FP occurs and the transfected bacteria emit green (≈516 nm) and orange (≈581 nm) fluorescent light at 488 nm excitation. Orange fluorescence is sensitive to acidic pH, and the phagocytosed bacteria stop emitting orange fluorescent light as soon as the phagosomes fuse with lysosomes. The green fluorescence is maintained in the phagolysosome until bacterial degradation is completed [408].
4. Applying imaging FCM. This novel technique of cytometry combines the statistical power and fluorescence sensitivity of standard FCM with the spatial resolution and quantitative morphology of digital microscopy, as it is based on the cap-

ture of images of particles in flow and subsequent pixel-based image analysis of objects [413]. Imaging FCM allows defining the intracellular localization of fluorescent targets in phagocytes, thus ruling out the need of quenching or blocking steps (Fig. 43) [414–416].

8.3.6 Assessing or quantifying phagocytosis kinetics and capacity.
The simplest calculation is the proportion of phagocytosing cells within the evaluated population, defined as the percentage of gated cells with target fluorescence, present in the appropriate gate(s), established by morphological, viability, and immunophenotypic criteria [377], as seen in Fig. 44.

Regarding the quantification of ingested fluorescent targets, calculation may be relatively straightforward if pH-independent fluorescent particles (biological or synthetic) are used. The mean number of particles ingested per effector cell can be calculated by dividing the MFI of the cell population by the fluorescence of a single, extracellular target [417]. When using targets labeled with pH-dependent dyes, however, this calculation is inaccurate and must be modified by subtracting the number of free targets per phagocyte from the initial number of targets per phagocyte [377, 378].

An interesting parameter to quantify phagocytosis capacity is the phagocytosis product (PP) parameter [377]. PP is defined as the percentage of phagocytosing cells multiplied by the number of targets per phagocytosing cell. PP reflects that the total elimination of targets from a given assay preparation depends both of the percentage of phagocytosing cells and the number of targets ingested by each effector cell [377].

8.4 A general protocol for assesing phagocytosis in whole-blood samples using pHrodo Red E.coli BioParticles

8.4.1 Overview.   This assay is suitable to determine phagocytic activity in whole blood samples based on the use of pHrodo *E. coli* Red BioParticles, which undergo a strong increase in fluorescence when the surrounding pH becomes more acidic during the ingestion phase of phagocytosis process. Labeling of whole blood samples with appropriate pan-leukocytic markers, such as CD45 or CD11a (Fig. 44), easily allows excluding easily erythrocytes and platelets. Using species-specific phagocyte markers allows to evaluate phagocytosis of pHrodo BioParticles by granulocytes in multiple species [418]. By adding a suitable fluorogenic substrate of ROS such as Dihydrorhodamine 123 (DHR123), this protocol allows the simultaneous examination of phagocytosis and oxidative burst.

CD11a clone HI111 reacts with human, rhesus, cynomolgus, or baboon monkey, dog, and rabbit. Moreover, it has been shown in our laboratory to crossreact with some cetaceans and pinnipedes. Thus, in addition to human studies, this protocol has been successfully applied to evaluate ingestion of *E. coli* and respiratory burst in whole-blood samples of dolphins (Fig. 44), Beluga whales, and walruses.

8.4.2 Step-by-step sample preparation and assay protocol.

1. Prepare three tubes and label appropriately for:
   - autofluorescence control
   - cytochalasin A (negative control)
   - pHrodo Red *E.coli* BioParticles
2. Dispense 50 μL heparinized whole blood into each tube.
3. Dispense 10 μL CD11a PE-Cy5 antibody into each tube and incubate at room temperature for 15 min in the dark.
4. Place all the tubes on ice for 10 min.
5. Dispense 2 μL 400 μM cytochalasin A into the cytochalasin A negative control tube and incubate 30 min at 37°C in a CO_2 incubator.
6. After that, dispense into:
   - negative control tube: 10 μL PBS.
   - cytochalasin A negative control tube: 10 μL pHrodo Red *E. coli* BioParticles stock solution.
   - pHrodo Red E.coli BioParticles tube: 10 μL pHrodo Red *E. coli* BioParticles stock solution.
7. Incubate the tubes at 37°C for 15 min in a CO_2 incubator.
8. Place the tubes on ice for 5 min.
9. Add 500 μL of lysing solution into all tubes, vortex 1 s, and incubate for 10–20 min at room temperature and in the dark.
10. Centrifuge the tubes at $200 \times g$ for 5 min.
11. Remove the supernatant and wash all the tubes with 3 mL PBS.
12. Centrifuge the tubes at $200 \times g$ for 5 min.
13. Remove the supernatant and resuspend the pellet in 300 μL RPMI 1640 Medium.
14. Add 1 μL of DAPI stock solution previously to flow cytometry acquisition.
15. Analyze samples in a flow cytometer having blue (488 nm) and violet (405 nm) laser lines.

8.4.3 Materials.

- Fresh whole blood (1 mL) collected in heparinized tubes.
- Versalyse lysing solution: Store between 18 and 25°C (Beckman Coulter, Ref: A09777).
- PBS pH 7.4: store between 15 and 30°C (Gibco, Thermofisher Scientific, Ref: 10010015).
- RPMI 1640 medium (1×) + GlutaMAX (Gibco, Ref: 61870-010), supplemented with 10% of FBS (Gibco, Ref: 26140-079) and 1% penicillin/streptomycin (Gibco, Ref: 15140-122). Store between 2 and 8°C.
- Cytochalasin A: 10 mM in DMSO. Aliquoted and store at –20°C (ENZO, Ref: ALX-380-057-M001).
- CD11a-PE-Cy5 mouse anti-human mAb, Clone HI111. Store between 2 and 8°C (BD Biosciences, Ref: 551131).
- pHrodo Red *E. coli* BioParticles conjugate for phagocytosis: 1 mg/mL in PBS. Aliquote and store at -20°C (ThermoFisher Scientific, Ref: P 35361).
- DAPI: 1 mg/mL in demineralized water. Aliquote and store at -20°C (Sigma, Ref: D9542).

9 Autophagy

9.1 *Overview*

Autophagy is a cellular catabolic pathway tightly regulated for homeostasis maintenance and remodeling. During autophagy, cellular debris and other cargo is delivered by autophagosomes to lysosomes for degradation and recycling. LC3-II, which localizes to autophagosomes, is a widely used autophagy marker. In this section, quantitative measurement of autophagy focusing on FCM staining of LC3-II will be discussed.

9.2 *Introduction*

Autophagy is a lysosome-based catabolic pathway for the degradation and turnover of cytoplasmic constituents. Stressors, such as nutrient starvation and hypoxia, are potent autophagy inducers. To maintain cellular homeostasis, cellular debris is removed by constitutive (basal) autophagy. Autophagy generates metabolites, which are reused as sources of energy or synthesis of new macromolecules. It is known to be an important player in the regulation of proliferation, cell growth, remodeling, and differentiation in a number of systems [419]. There are three main types of autophagy in mammalian cells: chaperone-mediated autophagy [420], microautophagy [421], and macroautophagy [419]. The techniques described in this section detect macroautophagy that hereafter will be referred to as autophagy.

Autophagy is tightly regulated by complex signaling pathways including mTORC1, AMPK, class I PI3K complex, AKT, ULK1 complex, and class III PI3K complex. Close to 40 core autophagy genes have been identified that mediate the completion of a double-membrane autophagosome, which engulfs unwanted cytosolic material such as aged and damaged organelles, protein aggregates, or pathogens. Subsequent fusion of the autophagosome to the lysosome enables degradation of the cargo (Fig. 45). Autophagy related genes (ATGs) were originally identified in yeast, but most of these are evolutionarily conserved in higher organisms such as mammals [422]. A key player often used to quantify autophagy is the ATG8-family member MAP1LC3B (LC3). During autophagosome elongation, the cytosolic protein LC3-I is lipidated by conjugation to phosphatidylethanolamine to become LC3-II, and thereby inserted into the membrane of the growing autophagosome.

Autophagic flux (i.e., flow through the autophagy pathway) is used to measure autophagic activity. One such approach is to measure the rate of protein breakdown by autophagy by arresting the autophagic degradation at a given point and recording the time-dependent accumulation of representative autophagic cargoes. The most common way to induce this block is to inhibit lysosomal proteolysis, thus, increasing levels of autophagosomes and the autophagosome marker LC3-II, which can be measured. Many compounds are known to block the autophagic flux [424] such as chloroquine, which primarily inhibits autophagosome–
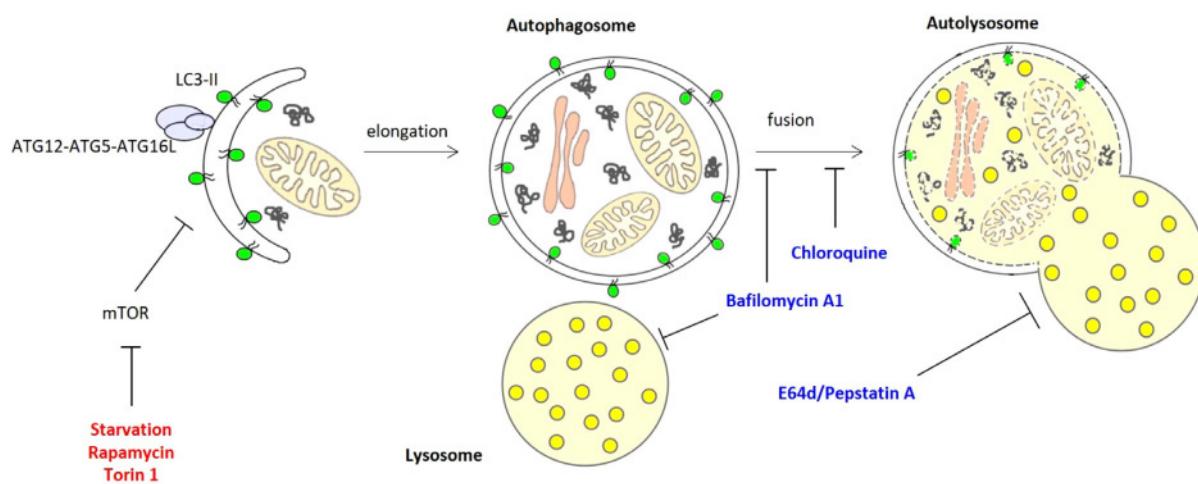
Figure 45. Autophagy pathway (modified and reproduced with permission from ref. [423]). In the first step of autophagy, a double-membraned vesicle is formed, which elongates to form an autophagosome (left). During the elongation step, the cytosolic protein LC3-I is lipidated to become LC3-II, which is inserted into the membrane of the growing autophagosome. The autophagosome closes, engulfing bulk cytoplasmic material to be degraded (middle). The autophagosome then fuses with a lysosome to breakdown the autophagy vesicle and its contents (right). Autophagy inducers are shown in RED, and autophagic flux inhibitors are shown in BLUE.

lysosome fusion [425], and bafilomycin A1 (BafA), which inhibits both lysosomal acidification (thus inhibits lysosomal hydrolase activity) and autophagosome–lysosome fusion [426]. Both are common inhibitors used to measure autophagic flux (Fig. 45).

9.3 Flow cytometry autophagy assays

In recent years, autophagy has been successfully measured with commonly used techniques such as Western blot and microscopy [427]. However, these assays have their limitations since a certain number of cells are needed or cell sorting is required to measure autophagy in a specific cell type within a mixed cell population. More recently, novel techniques for FCM and imaging FCM have opened up new possibilities in the field of autophagy. Not only can primary cells be analyzed, these techniques also allow a higher throughput and the possibility to measure multiple parameters simultaneously. As the available Abs to LC3 do not discriminate between its lipidated and non-lipidated forms, these techniques rely on detecting punctate LC3 visible by imaging or removing the non-lipidated form prior to staining [428].

Detection of fused autophagosomes also relies on the identification of lysosomes, as required for the Amnis® ImageStream autophagy assay described later. Lysosomes are acidic organelles that can be identified by pH sensors. One example of such reagents are the LysoTracker probes (ThermoFisher Scientific), which are selective for acidic organelles. They must be used at low concentrations (usually 50 nM) and incubation time should be restricted to 1–5 min before imaging, otherwise they induce an increase in lysosomal pH. They can, however, be fixed with aldehydes, but the autofluorescence or non-specific staining as mentioned by the manufacturer, means their specificity for quantifying lysosomes by FCM will depend on the cell type. However, Lysotracker has had

some success in flow assays with cells showing an increase in signal after treatment with chloroquine [429]. LysoSensor pH indicators (ThermoFisher Scientific) are similar, but exhibit a pH-dependent increase in fluorescence intensity upon acidification. They have the same issue of increasing lysosomal pH with longer incubation times and nonspecific staining when used for FCM. Lyso-ID (Enzo) is another acidic organelle-selective dye but does not increase lysosomal pH over time lending itself to short- and long-term tracking of lysosomes. An alternative are lysosome-specific Abs, such as against the LAMP family members. Anti-LAMP1 staining was shown to give the same results when compared to Lyso-ID in the autophagy imaging FCM assay discussed later in this guideline [430].

Autophagy FCM assays include:

1. Amnis® ImageStream autophagy assay. Imaging FCM allows quantification of endogenous LC3 puncta while detecting surface markers. To detect autolysosomes, the co-localization between LC3 and lysosomes using a bright detail similarity analysis feature can be used [430–432] (See Chapter VIII, Section Imaging FCM for general introduction to ImageStream).

2. Cyto-ID® Autophagy detection kit (Enzo)

   This is a proprietary dye that stains autophagic vesicles. Version 2.0 of the kit has been developed in 2015 with better performance in signal intensity and photostability compared to the old version. Both versions seem to stain autophagic vesicles in a pH-dependent manner, as blocking lysosomal acidification by bafilomycin A1 significantly compromises the staining signal. In contrast, chloroquine that blocks autophagosome–lysosome fusion is compatible with the kit as shown by the manufacturer. The staining is simple and direct (see protocol provided by the manufacturer). However, the data is difficult to interpret as the manufacturer does not state the mechanism on which the staining is based.

3. FlowCellect Autophagy LC3 kit (Merck Millipore). Selective cell membrane permeabilization with mild detergents allows discrimination between cytosolic non-lipidated LC3-I from membrane bound LC3-II by washing out the soluble cytosolic form. This is our first choice to measure autophagy in primary cells. Selective detection of endogenous LC3-II by FCM provides many advantages to investigate autophagy in primary cells including lower cell numbers, detection of surface markers, and other parameters at the same time and it is significantly quicker than the ImageStream autophagy assay. This assay was first reported by Eng et al. [428], and can also be performed with common laboratory chemicals and anti-LC3 Abs. Optimization might be required for different conditions and primary cells.

9.4 Step-by-step sample preparation (FlowCellect Autophagy LC3 kit, adapted from the manufacturer's protocol)

1. Collect tissues and homogenize into single cell suspension.
2. Culture cells at 37°C in appropriate medium (RPMI 1640 with 10% FBS for human or murine hematopoietic cells) containing autophagic flux inhibitors (e.g., 10 nM bafilomycin A1) or vehicle for 2 h. Treatment time and doses may need to be titrated for different cell types.
3. Transfer the cells to tubes or plates for staining.
4. Stain cells with fixable Live/Dead staining (e.g., ThermoFisher, BioLegend) and Fc block in PBS in dark at 4°C for 20 min. Wash cells by topping up with PBS-0.1% BSA and spin down.
5. Stain cells with surface markers in PBS-0.1% BSA in the dark at 4°C for 20 min. Wash by topping up with 1× Assay Buffer (provided with kit) and spin down.
   Note: Usually (4) and (5) can be combined together for one-step surface marker staining in PBS without significantly compromising the staining quality. Wash by topping up with 1× Assay Buffer.
6. Add 1× Autophagy Reagent B (provided with kit) to the cell pellet, resuspend by pipetting up and down, and immediately spin down. This step washes away cytosolic LC3-I.
7. Stain cells with FITC-conjugated anti-LC3 antibody (20×, dilute in 1× Assay Buffer) in the dark at 4°C for 30 min. Wash by topping up with 1× Assay Buffer and spin down.
8. Wash once more with 1× Assay Buffer to remove the remaining unbound antibody.
9. Fix cells with 2% paraformaldehyde dissolved in PBS in the dark at room temperature for 10 min. Wash by topping up with PBS and spin down.
10. Resuspend cells in PBS and analyze by FCM.

9.5 Materials

FlowCellect Autophagy LC3 Antibody-based Assay Kit (Merck Millipore), PBS, cell culture medium, autophagic flux inhibitor (e.g., bafilomycin A1 or chloroquine), Live/Dead fixable dead cell stains, Fc Block, Abs for cell surface staining, BSA, and paraformaldehyde.

9.6 Data analysis

A rough idea of autophagic flux can be directly obtained from LC3-II histograms (Fig. 46A and B). After compensation and gating on the cell population of interest, the geometric mean of LC3-II fluorescence intensity can be determined. Autophagy is a complex cellular process and more accurate assessment requires quantification and calculation. Therefore, different aspects of the autophagic flux are determined by the following calculations:

1. Basal LC3-II levels alone are a direct measurement of the number of autophagosomes (Fig. 46C). Their increase indicates either increased autophagosome formation or blocked lysosomal degradation, or both.
2. BafA minus basal LC3-II calculates the amount of LC3-II being degraded during the period of BafA treatment, which is the net autophagic flux (Fig. 46D).
3. (BafA minus basal)/ basal LC3-II is a modified version of autophagic flux measurement, which normalizes the net autophagic flux to basal LC3-II levels, eliminating variation in basal LC3-II (including tissue-specific variation and cell size) and thereby quantifying the efficiency of autophagy (Fig. 46E).

The combination of these different ways of quantification will gain a comprehensive analysis of autophagy occurring within the cell. To confirm autophagy levels found by LC3-II, we recommend to also measure other autophagy-related processes such as lysosomal function and mass, degradation of autophagy adaptor proteins (e.g., p62), other proteins expressed on autophagosomes (e.g., WIPI2), and signaling molecules (e.g., phosphorylation status of mTOR and ULK1) by FCM, microscopy, and Western blot.

9.7 Pitfalls

The autophagy levels in different types of primary cells under different conditions vary a lot. Often, only small changes after autophagy inducing or inhibiting treatments are being observed in comparison to cell lines. Many commonly used autophagy inducers such as rapamycin, torin 1, or starvation do not cause large differences in autophagy levels in naïve immune cells according to our unpublished data. Typically in immune cells, cell-specific stimulations such as through the TCR, BCR, TLR, or cytokine receptors are the strongest and the most reliable (Table 10) [433]. Generally, it is wise to test a wide panel of inducers and inhibitors in a time course to find the best read out. Notably, when using any compounds to induce autophagy, the vehicle needs to be considered. For example, DMSO is known to induce autophagy [434] and therefore should be avoided if possible or used at minimum concentrations for a short period. As usual, it is necessary to include vehicle-treated controls in all experiments as any mild stress might induce autophagy.
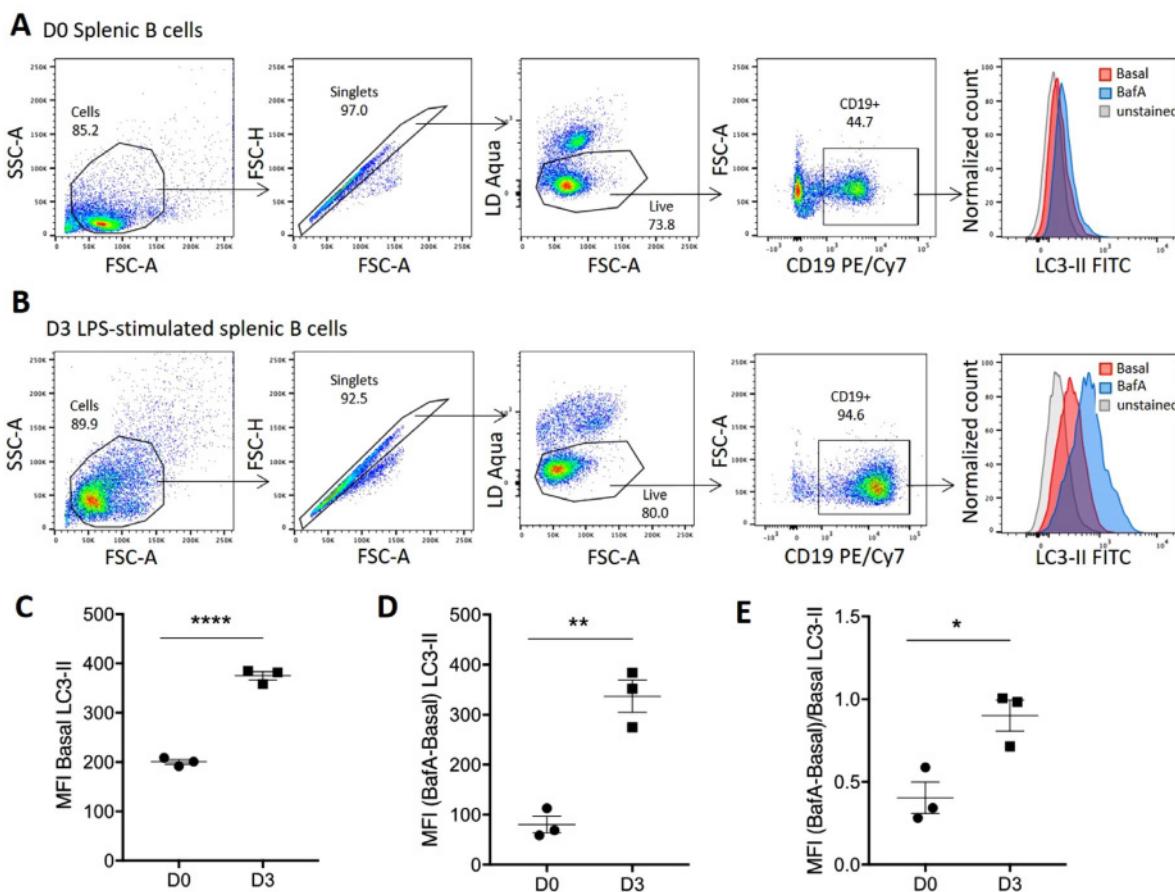
Figure 46. An example of autophagy induction and flux measurement with the FlowCellect LC3 kit in murine B cells. (A) Unstimulated murine splenocytes were cultured with 10 nM Bafilomycin A1 (BafA) or Vehicle (Basal) for 2 h. LC3-II expression was quantified by FCM. (B) Purified murine B cells were stimulated with 10 μg/mL LPS for 3 days and treated with BafA as in (A) during the last 2 h before harvest. LC3-II expression was measured by FCM. (C–E) The quantification of basal LC3-II levels (MFI Basal LC3-II) (C), net autophagic flux (MFI (BafA-Basal) LC3-II) (D), and normalized autophagic flux (MFI (BafA-Basal)/Basal LC3-II) (E) are shown. Data are represented as mean ± SEM. Student's t-test. $^{*}P \leq 0.05$, $^{**}P \leq 0.01$, $^{****}P \leq 0.0001$.

Table 10. Autophagy inducers for human primary immune cells. Treatments that successfully induce autophagy after 24 h[a]

Primary cell type	Autophagy inducer
T cells	αCD3/CD28 (highest after 4 days)
B cells	IgM, megaCD40L
Monocytes	LPS, IFN-γ
Macrophages	LPS, IFN-γ

[a] This is not an exhaustive list and kinetic experiments have not been performed.

One also needs to be aware of off-target effects of compounds used to modulate autophagy. Some may require specific concentrations or incubation times [424]. For example, 3-MA (inhibiting class III PI3K Vps34 in autophagy pathway) is of low potency, requiring it to be used at ∼10 mM to block autophagosome formation. At this concentration, it can also affect other kinases including class I PI3K, p38MAPK, or c-Jun kinase, therefore affecting many cellular processes [435]. For this reason, 3-MA is not our primary choice to inhibit autophagy. Bafilomycin A1 is widely used in many

laboratories but in primary cells, we recommend to use at a low concentrations for <4 h, otherwise it is toxic. It also needs to be noted that bafilomycin A may inhibit the proteasome, endocytic trafficking, and other cellular processes [436].

There are several drawbacks of the FlowCellect Autophagy LC3 kit. The LC3-II staining is incompatible with other intracellular staining because it requires the wash-out of cytosolic proteins. As permeabilization and fixation are required for the assay, live-cell sorting cannot be performed. Moreover, autophagy induction involves conversion of LC3-I to LC3-II, and thereby the ratio of LC3-II to LC3-I is another way to quantify autophagy induction. Yet the current protocol of LC3 kit cannot be used to measure LC3-I. Generally speaking, every technique has its own advantages and limitations. It is important to choose the best one for the experimental question, and ideally combine several techniques.

9.8 Top tricks

Being a stress response, autophagy can be nonspecifically induced by many insults. Therefore first keeping live cells at low

temperatures during sample preparation at all times (except for the cell culture step) helps to minimize these unwanted effects on autophagy. Second, for adherent cells, care must be taken when preparing single cell suspensions. The detachment requires disruption and injury of the plasma membrane, which can induce autophagy. For some cells, we found Accutase® induced less autophagy when compared to scraping or trypsinization.

Finally, the LC3 kit assay involves multiple washing steps. Accumulative cell loss during each centrifugation may eventually lead to a very low yield of cells. To maximize the sample recovery, 96-well V-bottom plates are recommended over U-bottom plates.

10 Reactive oxygen species production with minimal sample perturbation

10.1 *Overview*

FCM enables the detection of ROS in live cells. However, RBC lysis and sample manipulation can result in incomplete lysis of erythrocytes or in unwanted damage to leukocytes. This sample manipulation can cause both cellular depletion and artifactual activation and may result in inaccurate measurements of ROS, especially in those cases where target cells are the minority. No-lyse no-wash protocols reduce sample handling, are simple and fast, and perhaps most importantly, they can minimize sample preparation and consequent artifacts relevant to the biology of increasingly important assays that target fragile cell subsets and or combine live cell function with cell phenotype. In order to mimic physiological conditions, this method takes advantage of classic methods that are widely used in FCM and is applicable for both murine and to human cord blood, peripheral blood, and bone marrow specimens. Examples provided in this section are from human PBMCs.

10.2 *Introduction*

ROS have been shown to be associated with oxidative stress [437]. Toxic, oxygen free radicals contribute to aging [438], apoptosis [439, 440], and pathological processes [441] in many clinical disorders, such as cardiac dysfunction and myocyte injury [442, 443]. More recently, ROS have also been shown to be involved in signaling processes [444–450], having a role as signaling molecules that generate specificity in ROS homeostasis.

ROS are generated during mitochondrial oxidative phosphorylation or after interaction of myeloid immune cells with xenobiotic compounds [447], and their rate of production increases under hypoxia or after inhibition of mitochondrial respiration [451, 452]. The term ROS includes superoxide anion (O_2^-), hydrogen peroxide (H_2O_2), hydroxyl anion (OH^-), hypohalous acid anions (e.g. OCl^-, OBr^-), ozone, singlet oxygen, and so on [447]. ROS are formed by the incomplete reduction of oxygen. ROS are mainly free radicals that many times are not very

reactive and have a short half-life [446]. Oxygen-derived free radicals are molecular species with unpaired electrons [453] and are the product of multiple biological oxidation and reduction pathways [447].

Although ROS are generated during normal mitochondrial oxidative metabolism, they are also generated in cellular response to exogenous compounds, cytokines, and bacterial invasion [450, 454, 455]. ROS, including all highly reactive molecules that contain oxygen, are members of important mechanisms of protection against infections [456]. The family of NADPH oxidases (NOX), notably the phagocyte NADPH oxidase (NOX2), are a key source of ROS and are critical for the defense against infections with viral, bacterial, fungal, and parasitic pathogens [456–459]. However, as well as protecting against infection, ROS generation can result in cell and tissue damage, as a result of the interaction with cell membranes, nucleic acids, proteins, and enzymes [446, 460, 461]. Oxidative stress is a consequence of the excessive production of oxygen reactive species or a decrease in the antioxidant defense [462]. Oxidative stress causes cytotoxicity through structural and functional alterations, that result in the disruption of cell homeostasis [463].

One of the main sources of anion superoxide ($O_2^{\cdot-}$) during homeostatic conditions is the electron transport system of mitochondria. Anion superoxide is the first ROS to be produced after oxygen enters living cells and this radical may generate many other ROS of different reactivity. Superoxide is produced by one electron reduction of molecular oxygen, has a short half-life, low reactivity, and does not normally result in oxidative attack of polyunsaturated lipids and DNA. However, defects in superoxide dismutase (SOD), a powerful enzyme that catalyzes the dismutation of superoxide into O_2 and H_2O_2, can cause membrane damage due to spontaneous dismutation of O_2^- into H_2O_2, resulting in elevated levels of superoxide, which can lead to cell membrane damage because of the accumulation of this oxygen reactive species [464]. Its instability is related to the rapid $O_2^{\cdot-}$ dismutation reaction to hydrogen peroxide (H_2O_2) catalyzed by SOD [465].

Hydrogen peroxide is not a free radical but it can give rise to other ROS. Most ROS are free radicals that cause little damage due to their short half-life, but they are always reactive. H_2O_2 is much more stable and less reactive than superoxide anion. However, it can cause cell damage at lower concentrations when compared with O_2^- damage [466]. H_2O_2 is hydrosoluble and can diffuse across cells and reach distant targets to cause damage a long distance from its site of formation [466]. Hydrogen peroxide is formed by $O_2^{\cdot-}$ dismutation, catalyzed by SOD, and an unstable intermediate, hydroperoxyl radical [467]. However, dismutation can also be spontaneous or can be formed through direct oxygen reduction with participation of two electrons. Hydrogen peroxide can generate other ROS with enhanced reactivity, such as the hydroxyl radical ($OH^\cdot$) or the hypohalous acid anions [450, 466, 468]. The direct activity of H_2O_2 can damage cells by crosslinking sulfhydryl groups and oxidizing ketoacids, causing inactivation of enzymes and mutation of DNA and lipids [466]. Hydroxyl radical is highly reactive and toxic. With a relatively short half-life, hydroxyl radical can also react with many

biomolecules, including DNA, proteins, lipids, aminoacids, sugars, and metals [466].

Production of ROS by human monocytes was originally described using the NBT salt assay [469] or luminol-dependent chemiluminescence [470]. FCM is progressively replacing these assays [471] and has several advantages: it is rapid, sensitive, and multiparametric, and allows cell subpopulations to be studied [472]. However, in many of these cytofluorometric assays, samples are subjected to manipulation in the form of centrifugation, washing steps, erythrocyte lysis, and in some cases, fixation of cells or enrichment of the target cells by means of density gradients [473, 474]. This sample manipulation can cause both cellular depletion and artifactual activation and may result in inaccurate measurements, especially in those cases where target cells are the minority.

10.3 Step-by-step sample preparation and assay protocol

Ideally, cytofluorometric functional studies on oxidative burst should be performed in whole blood with minimal sample manipulation (stain, no-lyse, and no-wash) in order to mimic physiological conditions. We have tested different probes to detect ROS (V.9.4. Materials) in leukocyte cells (lymphocytes, monocytes and granulocytes) using no-lyse no-wash approaches (Figs. 47 and 48) and have developed different protocols and recommendations according to the reagent used (See also Chapter V Section 16: Assessing lymphocyte metabolism through functional dyes).

We have developed two no-lyse no-wash strategies for identifying leukocytes in whole human blood that can be used to analyze ROS production using FCM. Approach A (Fig. 47) uses a nucleic acid stain to label and discriminate nucleated cells from non-nucleated cells, avoiding anucleate mature RBCs. A fluorescence threshold is applied to the nucleic acid stain detector to eliminate the non-nucleated cells from detection by the cytometer during acquisition. Approach B uses a light scatter threshold (Fig. 48) and exploits the difference in light-absorbing properties between RBCs and leukocytes. RBCs contain hemoglobin, a molecule that readily absorbs violet laser (405 nm) light, whereas leukocytes and platelets/debris do not. This results in an unusual scatter pattern when analyzing human whole blood with both blue (488 nm) and violet (405 nm) SSC, which can be used to discriminate leukocytes from red blood cells by light scatter. Alternatively, red and violet SSC can also be used (Fig. 48).

The general step-by-step sample preparation is as follows:

1. Dilute 20–50 μL of EDTA anticoagulated fresh blood in 1 mL HBSS. Adjust the leukocyte concentration to approximately 5×10^5 cells/mL.
2. Prepare positive and negative controls. For positive controls, use *tert*-Butyl hydroperoxide 200 μM or PMA 1.63 μM. For negative controls, prepare a tube in the absence of any ROS inducing agent.
3. Add the desired ROS staining reagent:
   - Dihydrorhodamine 123 50nM

   - Total ROS Assay kit 1X
   - Cell ROX™ Deep Red/ Green/ Orange 500 nM
4. Add a nucleated cell staining reagent (e.g., Vybrant™ DyeCycle™ Violet (DCV) Stain 1 μM) to each tube if you want to perform approach A. To perform the approach B, this step is not required.
5. Incubate samples for 30 min, in a dedicated water bath at 37ºC, and invert tube samples gently every 5–10 min.
6. Mini-centrifuges are ideal for quick and easy spin down. Centrifuge the tubes shortly (10 s 16.1uf) and conserve the supernatant. Add 1.5 μg/mL 100 μL final volume of the desired Abs and incubate 20 min at room temperature.
7. Add the conserved supernatant and the viability dye (e.g., DRAQ7™ 3 μM) to discriminate necrotic cells. Incubate 10 min at room temperature.
8. Immediately analyze the samples in the flow cytometer. Run your isotype controls and adjust compensation properly prior to analyzing the stained sample (Section II.1: Compensation).

10.4 Materials

10.4.1 Reagents.

1. Hanks' Balanced Salt Solution (1×) (HBSS), w/o Ca & Mg, w/o Phenol Red (Capricorn Scientific GmbH, catalog no. HBSS-2A)
2. ROS reagents: Dihydrorhodamine 123 (DHR) (Thermo Fisher Scientific, catalog no. D23806), Total ROS Assay Kit 520nm (Thermo Fisher Scientific, catalog no. 88-5930-74), CellROX™ Deep Red Reagent (Thermo Fisher Scientific, catalog no. C10422), CellROX™ Orange Reagent (Thermo Fisher Scientific, catalog no. C10443), CellROX™ Green Reagent (Thermo Fisher Scientific, catalog no. C10444).
3. Induction reagents: PMA (Sigma–Aldrich® catalog no. P8139-1MG), *tert*-Butyl hydroperoxide solution, 70% solution in water (Thermo Fisher Scientific, catalog no. C10491).
4. Viability dye: DRAQ7™ (BioStatus, catalog no. DR70250)
5. Total nucleated cells dye: Vybrant™ DyeCycle™ Violet (DCV) Stain (Thermo Fisher Scientific, catalog no. V35003)
6. Abs: CyFlow™ CD3 APC-Cy7 (Sysmex, catalog no. AU20 8254), CyFlow™ CD11b PE-Cy7 (Sysmex, catalog no. CB652124), CyFlow™ CD14 PE (Sysmex, catalog no. BR806060), CyFlow™ CD33 APC (Sysmex, cat. no. AW821754)

10.4.2 Equipment.

1. Invitrogen™ Attune™ NxT flow cytometer (Thermo Fisher Scientific, catalog. no. A24858)
2. Invitrogen™ Attune™ No-Wash No-Lyse Filter Kit (Thermo Fisher Scientific, catalog no. 100022776)
3. Water bath set at 37ºC
4. Eppendorf® Microcentrifuge 5415D, with rotor F 45-25-11
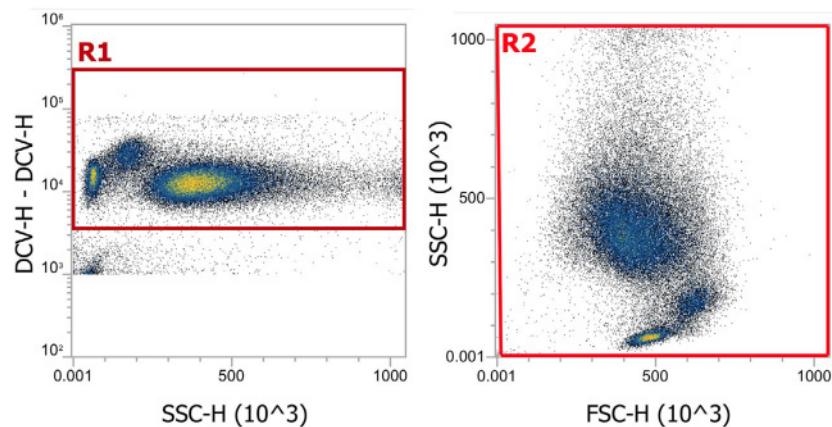
Figure 47. Identification of leukocytes in human whole blood using violet laser and Vybrant DyeCycle Violet stain on the Attune NxT Flow Cytometer. Leukocytes are outnumbered by red blood cells 700-fold in whole blood and generally require enrichment by RBC lysis or gradient centrifugation prior to analysis. This strategy exploits the use of Vybrant DyeCycle Violet stain (DCV), a low cytotoxicity permeable DNA-specific dye that can be used for DNA content cell cycle analysis and stem cell side population by FCM. DCV threshold levels were set empirically to exclude the large amounts of red blood cells that are found in unlysed whole blood. A proper threshold is shown in a SSC-H versus DCV-H dotplot (left). DCV can be excited with violet lasers and can be used for simultaneous staining with Abs. This protocol is ideally suited to study the numbers of nucleated cells in unlysed whole blood. Using a gate in this figure as the parent gate (R1), the three main leukocyte cell populations (R2) in human blood are identified using classic forward and side scatter plots (right).

10.5 *Data analysis*

Install the Attune NxT No-Wash No-Lyse Filter Kit (catalog no. 100022776) in the optical bench of the instrument. To use the filter kit, remove the 440/50 BP filter in VL1 slot 1 and place the 405/10 BP filter that is placed in the VL1 slot 1 in slot 1. Remove the 495 Dichroic LP (DLP) filter in a lot A the 415DLP. The Blank filter in slot 1A is switched with the 417LP filter in slot 0. SSC was detected using both blue laser (488/10 BP) and violet laser (405/10 BP filters) (Fig. 49).

Labeled and diluted blood samples were run on the cytometer with a sample input rate of 100 μL/min. DCV fluorescent threshold levels were set empirically using a V-SSC versus DCV dual parameter plot to eliminate from detection the large amounts of red blood cells that are found in unlysed whole blood. A proper threshold is shown in Fig. 47A. In this example, the DCV threshold values on the Attune NxT are set at 0.3×1000, and this setting also excludes from analysis non-nucleated cells and debris. This value is adjusted while acquiring data and observing the position of the DCV+ cells

on the bivariate dot plots such that all the nucleated blood cells are on scale with the least amount of debris appearing in these plots. Other specimens, such as marrow or cord blood may appear with different scatter properties and minor variations in fluorescence intensities. A rectangular gate R1 was drawn to enclose the DCV-positive cells, and subsequent bivariate plots were generated based on this gate.

10.6 *Pitfalls*

At higher sample concentrations/sample input rates, erythrocytes are frequently coincident with leukocytes, but leukocytes are very rarely coincident with each other. Height parameters are more accurate than area due to contributions to the area from these erythrocytes, when no-lyse no-wash methods are used. Relationships between extinction pulse widths, peak heights, and integrals, tend to be different for symmetric and asymmetric cells, and for single particles and doublets or multiplets, making the
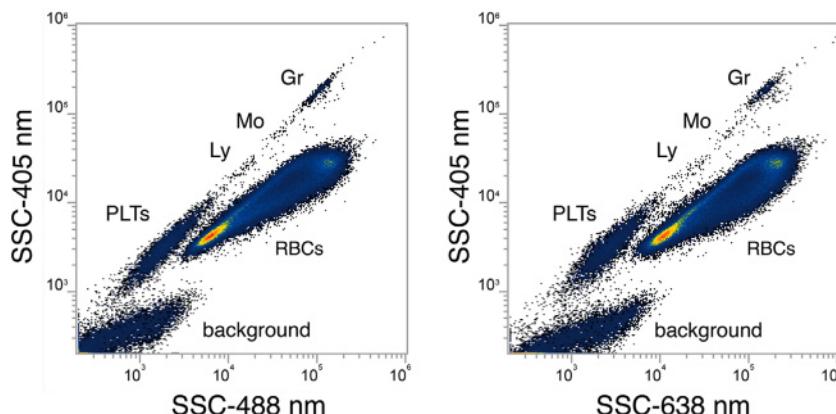
Figure 48. Identification of leukocytes in human whole blood using violet side scatter on the flow cytometer. Resolution of leukocytes from red blood cells in whole blood is improved by incorporating violet 405 nm side scatter. Using both violet and blue side scatter (left) or both violet and red side scatter (right), allows identification of leukocytes in whole blood. Using a gate in this figure as the parent gate, the three main leukocyte cell populations in human blood can be identified using classic forward and side scatter plots (PLTs, platelets; Ly,: lymphocytes; Mo, monocytes; Gr, granulocytes; RBCs, red blood cells).
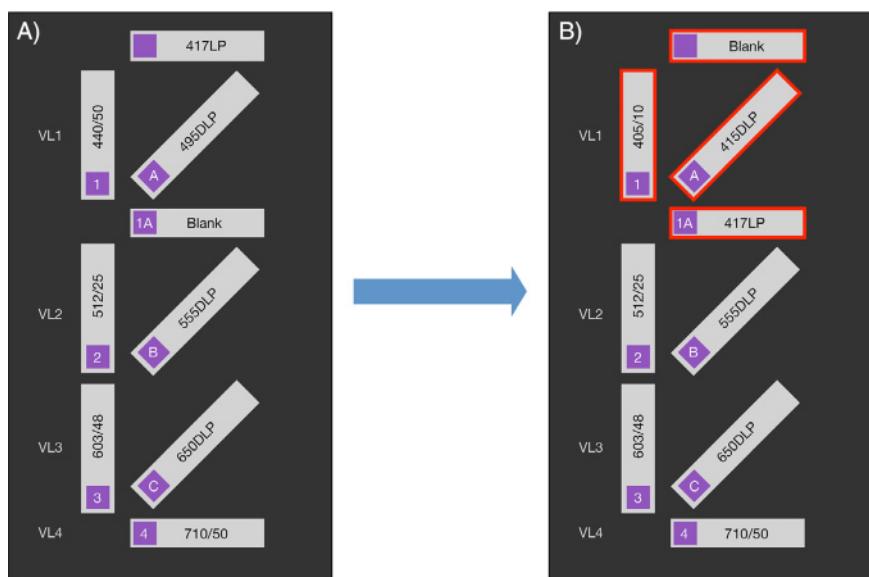
Figure 49. Use of the Attune NxT No-Wash No-Lyse Filter Kit. The standard configuration for the 405 nm violet laser optical filter block is shown in (A) and the same optical filter block using the No-Wash No-Lyse Filter Kit shown in (B), with changes outlined in red. To use the filter kit, remove the 440/50 BP filter in VL1 slot 1 and place the 405/10 BP filter that is placed in the VL1 slot 1in slot 1. Remove the 495 Dichroic Longpass (DLP) filter in a lot A the 415DLP. The Blank filter in slot 1A is switched with the 417LP filter in slot 0.

discrimination of pathological large cells from doublets and/or aggregates difficult. The more conventional way of dealing with doublets is based on scatter signals. However, fluorescent triggering using DNA viable stains may increase single-cell discrimination. Moreover, fluorescence thresholding is typically required at higher sample concentrations needed for large numbers of cells per sample. Specific DNA fluorescent labeling can be used to rise above RBC background through fluorescence thresholding, even using lyse no-wash methods. Scatter for fluorescence parameters chosen for thresholds in a no-lyse no-wash assay should produce the highest separation possible from the background.

Important note: The influence of different blood anticoagulants on ROS production should not be ignored. Please take into account which anticoagulants can be used in combination with your kits and reagents. Dihydrorhodamine 123 flow cytometric method can be used either with EDTA or heparin, without the usual necessity of a preliminary search for artifacts.

10.7 Top tricks

In this approach, non-nucleated cells are detected by the instrument during acquisition, but excluded by gating during analysis. Care must be taken when using the method to keep event rates below instrument limitations for Poisson coincidence. RBC concentration in whole blood is on the order of 5 million cells/µL so whole blood must be properly diluted (1/100 or greater) to avoid instrument saturation.

Dead cells often give false positive results, as they tend to bind nonspecifically to many reagents. Therefore, removing dead cells from your FCM data is a critical step to help ensure accurate results and analysis. Different manufacturers market nonfixable cell viability assays for FCM to distinguish live and dead cell populations with more accuracy than FSC and SSC data. For more detail on this control aspect, see Section III.4: Dead cell exclusion, cell viability,

and sample freezing. For ROS production studies, different dyes can be used on a flow cytometer based on auto-oxidation, photo-chemical reactions, mitochondrial respiration, cytochrome P450, NADPH oxidase, and other enzymes. Most of these reagents are photostable fluorogenic probes that can also be detected by conventional fluorescence microscopy or high content imaging and screening. One of the most common cytofluorometric assays uses dihydrorhodamine 123, an uncharged and nonfluorescent ROS indicator that can passively diffuse across membranes where it is oxidized to cationic rhodamine 123, which then localizes in the mitochondria and exhibits green fluorescence [475].

As shown in Fig. 50, ROS production can be easily distinguished using these markers with a multi-laser FCM protocol using no color compensation. This simplicity makes these no-lyse no-wash strategies even more attractive as a better choice for phenotypic and functional measurements using freshly drawn blood samples [476].

10.8 Compensation guidelines

Single color compensation controls should be used with all multicolor experiments in FCM (See Chapter II Section 1: Compensation). Compensation controls need to be at least as bright as the sample they apply to. Ab capture beads are ideally suited for this. Background fluorescence should be the same for the positive and negative control populations for any given parameter. The compensation color must be matched to the experimental color. Match fluorophores by brightness (values from the stain index) to density of the antigens—try to match brightest fluorophores with lowest-expressed antigens (APC-CD33), and least bright fluorophores with highest-expressed antigens (PE-CD14). If multiple lasers (spatially separated) are present, spread fluorophores across the lasers to minimize spillover. Know your instrument configuration-pick fluorophores that work with your instru-
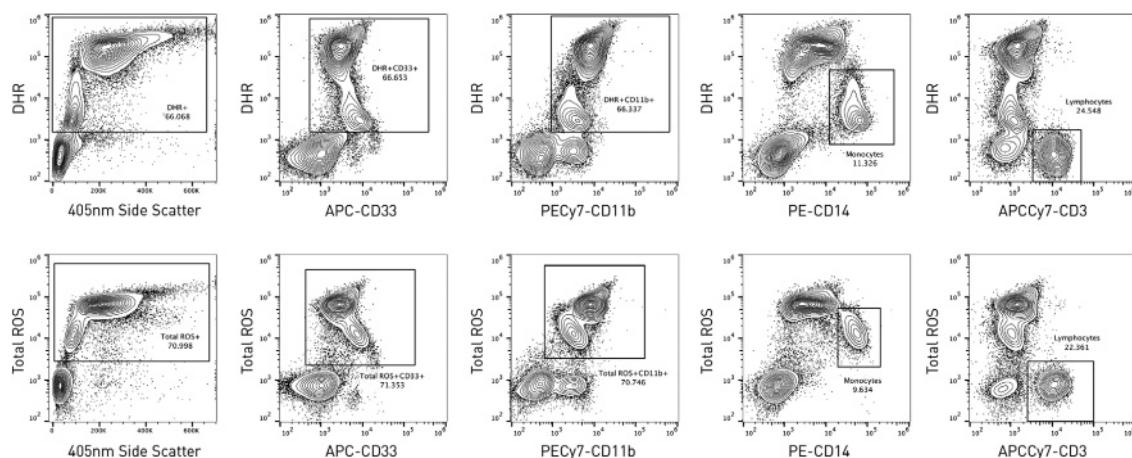
Figure 50. Reactive oxygen species production. Representative experiment of activated leukocytes in unlysed whole blood. Cells were stained with Vybrant DyeCycle Violet stain to discriminate nucleated cells from erythrocytes (excitation/emission (nm): 405/437), in combination with dihydrorhodamine (DHR) 123 or Total ROS 520 nm (excitation/emission (nm): 488/530) PE-CD14 (excitation/emission (nm): 561/578), APC-CD33 (Excitation/Emission (nm): 637/660), and 7-ADD (Excitation/Emission (nm): 488/647). A polygonal gate was drawn to enclose the DCV-positive cells, and subsequent bivariate plots were generated based on this gate. Cells were stimulated with PMA dissolved with DMSO and incubated in presence of DHR (upper row) or Total ROS (lower row) for 30 min at 37°C. Subsequently, cells were stained with DCV and PE-CD14, PECy7-CD11b, APC-CD33, and APCCy7-CD3 Abs for 20 min at room temperature. Following incubation, blood was diluted in HBSS and immediately analyzed on the flow cytometer. DRAQ7™ was added to discriminate necrotic cells (data not shown).

ment's optical configuration and design panels to maximize use of multilaser instruments. In order to have a statistically significant count of the target cells, a minimum of 50 000 DCV+ should be counted.

Despite limitations, no-lyse no-wash assays are simple and fast and perhaps most importantly, they can minimize sample manipulations and consequent artifacts relevant to the biology of increasingly important assays that target fragile cell subsets and or combine live cell function with cell phenotype. For more than 15 years, we have used these no-lyse no-wash methods for ROS production, but also for the detection of rare cells, as well as for cell sorting experiments [477]. ROS production should be studied using this simple and fast methodology, but also for rare cell detection (Chapter V Section 1: Rare cells—general rules), minimal residual disease studies or human hematopoetic progenitor cell counting.

11 Intracellular Ca^{2+} mobilization by means of Indo-1 AM

11.1 *Overview*

Ca^{2+} ions play an essential role as an intracellular messenger in nearly all cellular systems and regulate a multiplicity of cellular functions [478]. In this section, we focus on antigen receptor-mediated Ca^{2+} mobilization in naïve B-cells by means of Indo-1 AM. However, this method can be adapted to any other cell population, lymphocyte subpopulation, or cell line that can be triggered via any surface receptor that induces Ca^{2+} flux.

11.2 *Introduction*

In the immune system, Ca^{2+} mobilization induces many direct processes such as activation of platelets, degranulation of mast cells, or the killing of target cells by cytolytic T cells. It is also an essential component of the signaling cascades downstream of several receptors, including the B- and T-cell receptors, activating Fc receptors, and chemokine receptors, and has been shown to regulate the transcription of target genes and subsequently driving processes such as proliferation, and differentiation [479–482], suggesting that Ca^{2+} mobilization should be a consideration in many aspects of immunological research. In brief, in the case of antigen receptors, binding of the antigen initiates a signaling cascade leading to the generation of the second messenger IP$_3$. This binds to its receptor in the ER membrane after which Ca^{2+} is released from the ER into the cytoplasm. This release is the very transient internal store release (ISR) [483, 484]. Reduced Ca^{2+} levels in the ER are sensed by STIM1/2, leading to the opening of the Ca^{2+} release activated Ca^{2+} (CRAC) channels such as ORAI1 in the plasma cell membrane causing a more sustained store operated Ca^{2+} entry (SOCE) from the extracellular space into the cytoplasm (Feske et al.; [484]). Based on patch clamp methods, Ca^{2+} currents can be measured very precisely at the single cell level [485, 486].

Because this method is not feasible for many laboratories, determination of Ca^{2+} mobilization by means of the widely available FCM may represent an easy alternative, providing relative values of Ca^{2+} mobilization at the single cell level.

Indo-1 acetoxymethyl ester (AM) is a cell-permeant ratiometric Ca^{2+} indicator, used to determine intracellular Ca^{2+} mobilization at the single cell level [487]. The dye is excited at 355 nm and therefore requires a true UV laser. The Indo-1 AM emission peak at 475 nm in the absence of Ca^{2+} shifts to 400 nm upon binding of
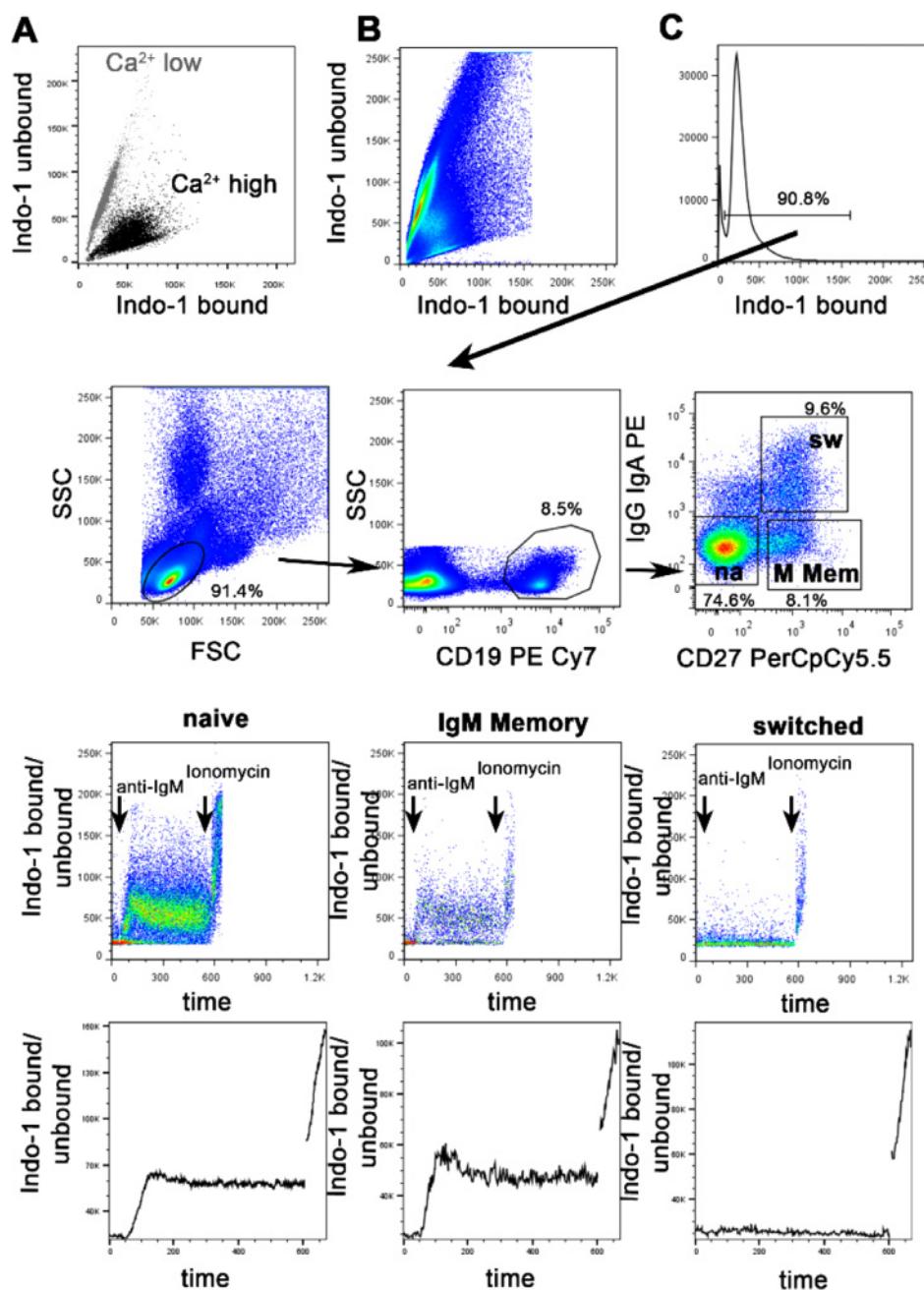
Figure 51. Measuring intracellular Ca^{2+} mobilization in human B cells in response to anti-IgM stimulation after labeling with Indo-1 AM. (A) The shift in Indo-1 bound to Indo-1 unbound at low intracellular Ca^{2+} concentrations (grey) and high intracellular Ca^{2+} concentrations (black). Ca^{2+} increase was induced in Indo-1-labeled PBMCs by addition of iono. (B) Setting of Indo-1 AM bound versus Indo-1 AM unbound on x-axis and y-axis, respectively. The PMTs should be adjusted so that unstimulated cells occur on a line about 45° to the y-axis. (C) Gating strategy for the analysis of Ca^{2+} mobilization in naïve (na), IgM memory (M Mem), and switched (sw) memory B cells after stimulation with anti-IgM. PBMCs were labeled with Indo-1 AM and stained with CD27, CD19, IgG, and IgA After gating on living Indo-1 bound cells, lymphocytes were determined. Gating of CD19+ B cells is followed by differentiation of IgG/IgA-/CD27- naïve (na) B cells, IgG/IgA-/CD27+ IgM Memory B cells (M Mem), and IgG/IgA+/CD27+ class switched memory B cells (sw). Dot plots of time versus ratio of Indo-1 bound/unbound (middle panels) and kinetics (lower panels) are shown for the three subpopulations. After baseline acquisition anti-IgM (arrow) was added inducing a shift of Indo-1 AM bound/unbound in IgM-expressing naïve and IgM Memory B cells whereas this ratio is at baseline levels in IgM-negative class switched memory B cells. After addition of iono the ratio of Indo-1 AM bound/unbound is rapidly increasing in all subsets. Data were acquired with a BD LSR Fortessa™ and analyzed by FlowJo™.

Ca^{2+} to cytosolic de-esterified Indo-1. Therefore, changes in the ratio of Ca^{2+}-bound Indo-1 signal at 475 nm to Ca^{2+}-unbound Indo-1 AM signal at 400 nm allow the immediate detection of alterations in intracellular Ca^{2+} concentration (Fig. 51A).

Alternative methods for detecting Ca^{2+} by FCM include methods involving the use of Fluo-3 or Fluo-4 [488, 489], either alone or in combination with Fura Red, taking advantage of excitation with a standard 488 nm laser [208, 490]. This avoids the necessity of the more costly UV laser required for excitation of Indo-1. Furthermore, Fura Red can also be used on its own taking advantage of differential excitation from the violet (405 nm) and green (561 nm) lasers, enabling ratiometric measurements

as for Indo-1 [491]. Ratiometric measurements have the added advantage of controlling internally for cell size and dye uptake. An excellent overview of the different dyes that can be used for Ca^{2+} analysis can be found at https://www.thermofisher.com/us/en/home/references/molecular-probes-the-handbook.html.

11.3 Step-by-step sample preparation

Isolation of peripheral blood mononuclear cells (PBMCs)

1. See Chapter III. Before you start: Reagent and sample preparation, experimental design; Section 4. Pre-enrichment of low

abundant cell populations prior to acquisition/cell sorting; Section 4.2 Pre-enrichment by physical properties

All steps of cell isolation should be performed at room temperature with buffers and media also at room temperature. If this is not possible, the cells should be allowed to equilibrate to room temperature for 30 min.

Loading:

1. Per measurement of Ca^{2+} mobilization in B cells 2×10^6 PBMCs are needed. Cells are adjusted to 10×10^6 PBMCs/mL RPMI/10% FCS. The respective amount of cells is loaded with 4.5 µM Indo-1 AM in the presence of 0.045% of the detergent Pluronic F-127 for 45 min at room temperature in the dark [492].
2. Mix the cell suspension during the loading procedure by dragging the sample tubes over a tube rack every 15 min.

Washing:

1. Wash twice with 5 mL RPMI/3% FCS ($300 \times g$, 5 min, at room temperature), remove supernatant.

Cell surface staining:

1. Add fluorescence-conjugated Abs (CD27, IgG, IgA, CD19).
2. Incubate for 15 min at room temperature in the dark.

Washing:

1. Wash with 4 mL RPMI/3% FCS, remove supernatant. Resuspend cells in 300 µL RPMI 10% FCS.

The sample measurement should be performed within the next 1–2 h.

Flow cytometer settings:

1. Display Indo-1 bound (FL12 405/10) and Indo-1 unbound (FL13 520/35, 445 LP) on a linear scale.
2. View Indo-1 unbound on the *y*-axis and Indo-1 bound on the *x*-axis. Adjust the PMT voltage so that the signals from unstimulated cells are located on a line about 45° to the *y*-axis (Fig. 51B).
3. A dot plot showing time on the *x*-axis versus the ratio of Indo-1 bound/unbound on the *y*-axis displays the kinetics of Ca^{2+} mobilization. Ensure that the baseline and the maximal peak upon stimulation (iono) are within the displayed range. If this is not the case, the PMTs must be adjusted.

Data acquisition:

Do not change the velocity of data acquisition during the measurement

1. Acquire the baseline for 30 s.
2. Remove the tube and add 10 µg/mL anti-IgM (do not stop data acquisition).

3. Acquire for an additional 4 min.
4. Add 1 µg/mL iono as a loading control (do not stop data acquisition). In the presence of Ca^{2+} in the medium and proper labeling of the cells with Indo-1 AM, all cells have to show a maximal increase in the intracellular Ca^{2+} concentration. Stop acquisition after an additional 90 s.
5. Wash the flow cytometer thoroughly before the next tube is loaded. Run fresh tubes of PBS twice for 1 min each (residual iono can directly induce Ca^{2+} mobilization in the subsequent sample).

To allow for comparison of different data sets the rate of sample flow, the time of baseline acquisition, time point of BCR stimulation and addition of iono must be kept constant between samples.

11.4 Materials

RPMI 1640		PAN Biotech
FCS		Biochrome
Indo-1 AM		Life Technologies
DMSO		Sigma
Pluronic F-127		Life Technologies
Ionomycin		Sigma
Fortessa BD equipped with a UV laser		BD Biosciences
Antibodies:		
CD19	PE-Cy7	Beckman Coulter
CD27	PerCp-Cy5.5	Biolegend
IgG	PE	BD Biosciences
IgA	PE	Southern Biotech
anti-IgM	UNLB	Southern Biotech

11.5 Data analysis

Depending on the required resolution of the information, data analysis can be performed by using standard acquisition software such as BD FACSDIVA™ (BD Biosciences, San Jose, CA) or similar. In addition, the analysis software programs FCS Express™ from De Novo Software (Glendale, CA), Flowlogic™ from Inivai Technologies (Victoria, Australia) and FlowJo™ (Treestar Inc., Ashland, OR) each offer a "kinetics" tool to analyze the acquired Ca^{2+} mobilization data. An example for anti-IgM-induced Ca^{2+} mobilization in human B-cell subpopulations when analyzed by Flowjo™ is shown in Fig. 51C. Prior to further gating, Indo-1 AM-negative cells must be excluded. Thereafter, the commonly used gating strategy including FSC/SSC, exclusion of doublets, and gating on the specifically stained subpopulations is performed. Looking at the respective B-cell subpopulations in a dot plot showing the ratio of Indo-1 AM bound/unbound versus time gives a better impression than merely looking at the kinetics function, since Ca^{2+} kinetics provide multiple read-out parameters. For example, the mean peak intensity and the time to peak, imply the early phases of Ca^{2+} mobilization, which in B cells is essential for

the induction of NF-κB and JNK [493]. In contrast, the decline represents the later phase, which is important for the activation of NFAT [479, 493]. Of note, the response of lymphocyte subpopulations is usually less homogeneous than, for example, those of cell lines. The percentages of responding cells can differ, and the non-responding population will strongly influence the read out, especially with regard to the mean values. We therefore advise you to perform an additional analysis of the parameters mentioned above, referring to the responding cells only, by setting the baseline as the threshold and excluding non-responding cells from further analysis.

11.6 Pitfalls

As with all functional assays, control samples that have ideally undergone the same pre-analytical steps as the test samples are required for Ca^{2+} mobilization studies. This is especially important when samples were shipped or previously frozen. The optimal temperature for the investigation of Ca^{2+} mobilization, as for all signaling studies, is 37°C. However, standard instruments are usually not equipped with a heatable acquisition chamber to maintain the samples at a constant temperature of 37°C during the measurement. Strong fluctuations in temperature during cell preparation and between the different experiments should be avoided, since this may influence the Ca^{2+} flux. Although most cell types are capable of inducing Ca^{2+} mobilization at room temperature (e.g., human lymphocyte subpopulations), some cell types are more sensitive and may require 37°C to run the assay. In most cases, pre-warming of the samples to 37°C improves Ca^{2+} mobilization, but subsequent cooling during the measurement may lead to changes of the Ca^{2+} baseline levels in some subpopulations and may thus render the analysis inaccurate. Therefore, we perform the entire process of loading, staining, washing, and measuring the cells at room temperature. Of note, during cell isolation or preparation (e.g., isolating PBMCs through Ficoll), labeling, and staining, the use of cold PBS and other media should also be avoided. Furthermore, mechanical force may induce Ca^{2+} flux. Therefore, carefully dragging the sample tubes over a tube rack to mix them during the entire procedure is better than vigorous shaking or vortexing of the cells.

It is important to make sure that the Abs used for cell surface staining do not themselves induce Ca^{2+} mobilization. This can be tested by adding the staining Ab to Indo-1 AM loaded cells and detecting the resulting Ca^{2+} levels. Since kinetics may vary, the period of acquisition for these tests should be for at least 10–15 min. If the Ca^{2+} baseline shifts in response to the staining Ab, that Ab should not be used. To test whether one of the staining Abs interferes with binding of the Ab used for stimulation, the measurement should be compared in the presence and absence of the respective cell surface Ab.

If datasets from different days have to be compared, it is recommended that you keep the times between loading, staining, and data acquisition constant for all of the samples.

The UV laser should be turned on at least 15 min beforehand to allow it to stabilize prior to use, since it is highly sensitive and more prone to fluctuation than other lasers. To ensure data reproducibility, it is also useful to wait a few seconds after loading the tube before recording the events. This will provide a better definition of the baseline. The flow rate should be kept constant throughout the measurement at low or intermediate rates. However, if the population of interest represents only a very small percentage of the acquired cells, it will be necessary to measure at higher speed in order to be able to record enough events/second for your analysis.

It is important to note that extracellular concentrations of Ca^{2+} will affect Ca^{2+} entry, with higher concentrations leading to higher entry, and other ions (e.g., Cl^-, Na^+, K^+) may also have an effect. The presence of serum may influence the availability of ions and other factors. The phosphate present in PBS may precipitate Ca^{2+}, also affecting extracellular Ca^{2+} levels. Depending on your experimental question, cell type and other conditions, RPMI with serum and/or PBS may not be optimal to use as the final buffer. Because of this, it may be helpful to make your own buffer, in which the concentrations of all ions are known. For washing your samples and the final measurement on the cytometer, it may help you to use HBSS solution without Ca^{2+} (Hanks solution), preferably self-made, and to supplement a portion of this with 2 mM Ca^{2+} on the day of the experiment.

11.7 Top tricks

11.7.1 Measuring different cell types and various subpopulations.
The protocol described above is in general applicable for the determination of Ca^{2+} mobilization in B cells, T cells, NK cells, granulocytes, monocytes, and also different cell lines. By adding surface markers to the Ab staining, a high resolution of the different subpopulations from peripheral blood as well as from lymphoid organs can be achieved. The stimuli have to be adjusted, according to the Ca^{2+} flux-inducing receptor. In primary human T cells CD3 mAb must be crosslinked. To analyze class switched B-cell populations in parallel, anti-Ig instead of anti-IgM should be used for antigen receptor stimulation. While Ca^{2+} levels are relatively similar in T and B cells, different cell types have different intracellular Ca^{2+} levels. The appropriate PMT settings for B cells would not necessarily fit those for granulocytes or cell lines, therefore PMTs should be reset accordingly.

For cell lines, it might be necessary to serum starve the cells prior to Ca^{2+} determination, therefore both loading and washing steps could occur in the absence of FCS, or in the presence of lower concentrations of FCS. Alternatively, lower concentrations of Indo-1 AM, shorter incubation times, and the omission of Pluronic F-127 can be tested, depending on the cell type and the precise application, leading to changes in the fluorescence intensity of the Indo-1.

11.7.2 Distinction between ISR and SOCE. Cell culture medium usually contains Ca^{2+}. To differentiate between ISR, from the ER into the cytoplasm, and SOCE, from the extracellular space into the cell, Ca^{2+}-containing medium has to be removed by washing and resuspending the cells in Ca^{2+}-free PBS or other Ca^{2+}-free buffers. Alternatively, EGTA, a chelator that is related to EDTA but preferentially binds Ca^{2+} ions, can be used. The transient ISR is detected after the appropriate stimulation, while subsequent addition of $CaCl_2$ during the measurement reveals the sustained SOCE.

12 mRNA

12.1 Overview

The quantification of transcripts (mRNA) is key to understanding the immediate response of cells to changes. Furthermore, measuring transcripts is a useful alternative when Abs for protein detection are not available. Several techniques have been traditionally developed to quantify mRNA, such as quantitative RT-PCR, Northern blot analysis, nuclease protection assays and fluorescence in situ hybridization but none of these methods allow complex high-throughput single-cell analysis. This section will introduce a novel FCM technique that enables simultaneous quantification of transcripts as wells as intracellular and surface proteins on a single-cell level [494–496].

12.2 Introduction

The immune system comprises many different cell types, each of them bearing specialized functions. The response of any cell can be detected first at the transcriptional level (mRNA) and subsequently at the level of proteins translated from the mRNAs. Until recently, the simultaneous detection of specific nucleic acid sequences in combination with proteins on a single-cell basis was restricted to microscopy, limiting the analysis to a few hundred cells. Fluorescence in situ hybridization is an example of such a method, although high-throughput acquisition is not applicable. Flow cytometric analysis of nucleic acids, especially RNA species, including mRNA, miRNA, long noncoding RNA (lncRNA), and viral RNA targets, allows the high-throughput acquisition of several million cells on a single-cell basis.

The PrimeFlow^TM RNA Assay (Invitrogen, ThermoFisher) uses branched DNA technology (bDNA) to quantify up to four RNA targets of interest by FCM. bDNA technology amplifies the reporter signal instead of the target; the latter is the case, for example, for RT-PCR. By building a tree-like structure for reporter signal amplification, the specificity and SNR of bDNA technology increases.

In principle, RNA sequence-specific probe sets consist of oligonucleotide pairs (20-40 per target) that hybridize to the target RNA sequence. The preamplifier, which forms the trunk

of the tree, directly hybridizes to adjacent oligonucleotide pairs. Subsequently, multiple amplifier molecules hybridize to a single preamplifier molecule, like the branches of the tree. Finally, multiple fluorescently-labeled probes bind to an amplifier molecule mimicking the leaves of the tree (Fig. 52). According to the manufacturer's instructions, an 8000–16 000-fold amplification of the transcript is achieved after optimal assay performance.

Currently, four fluorescent dyes that are detectable in different channels are available: Type 1/AF647, type 10/AF568, type 4/AF488, and type 6/AF750. Of those types, AF647 and AF568 give the strongest signal, and we recommend using those to detect RNAs with low or unknown expression. AF488 (medium-intensity signal) and AF750 (low-intensity signal) should be used for highly expressed RNA targets.

A main advantage of the PrimeFlow^TM RNA Assay is that proteins, such as lineage markers, intracellular proteins of interest, and mRNAs can be detected simultaneously. This will allow for the quantification of transcripts and protein in defined cell types on a single-cell level.

12.3 Step-by-step protocol

The PrimeFlow^TM RNA Assay can be performed in a conventional laboratory equipped with a CO_2 incubator, capable of stably maintaining 40°C, a refrigerated swinging bucket centrifuge, and a flow cytometer supplied with three lasers: blue (488 nm), yellow-green (561 nm), and red (633 nm or similar).

The assay can be performed in 1.5-mL Eppendorf tubes provided in the kit, or in 96-well V- or U-bottom plates. The step-by-step protocol in this version is based on using 96-well V-bottom plates. When using 1.5-mL Eppendorf tubes, the volumes have to be adjusted.

It is important that after all centrifugation and discarding steps, the residual volume in each well does not exceed 10 μL.

12.3.1 Single cell suspension preparation. For reliable results, it is crucial that the assay is performed with vital cells.

12.3.1.1 Cultured cells. Collect cells by centrifugation (suspension cells) or trypsinization (adherent cells). For cell lines, it is recommended using cells in the exponential growth phase.

12.3.1.2 Blood. It is recommended that blood is collected in a solution preventing coagulation and stored at room temperature to ensure best physiological conditions and high quality sample preparation. RBCs can be removed using a Ficoll- or Percoll-gradient purification step according to standard operating procedures (human), or by lysis as described below for tissues (mouse).
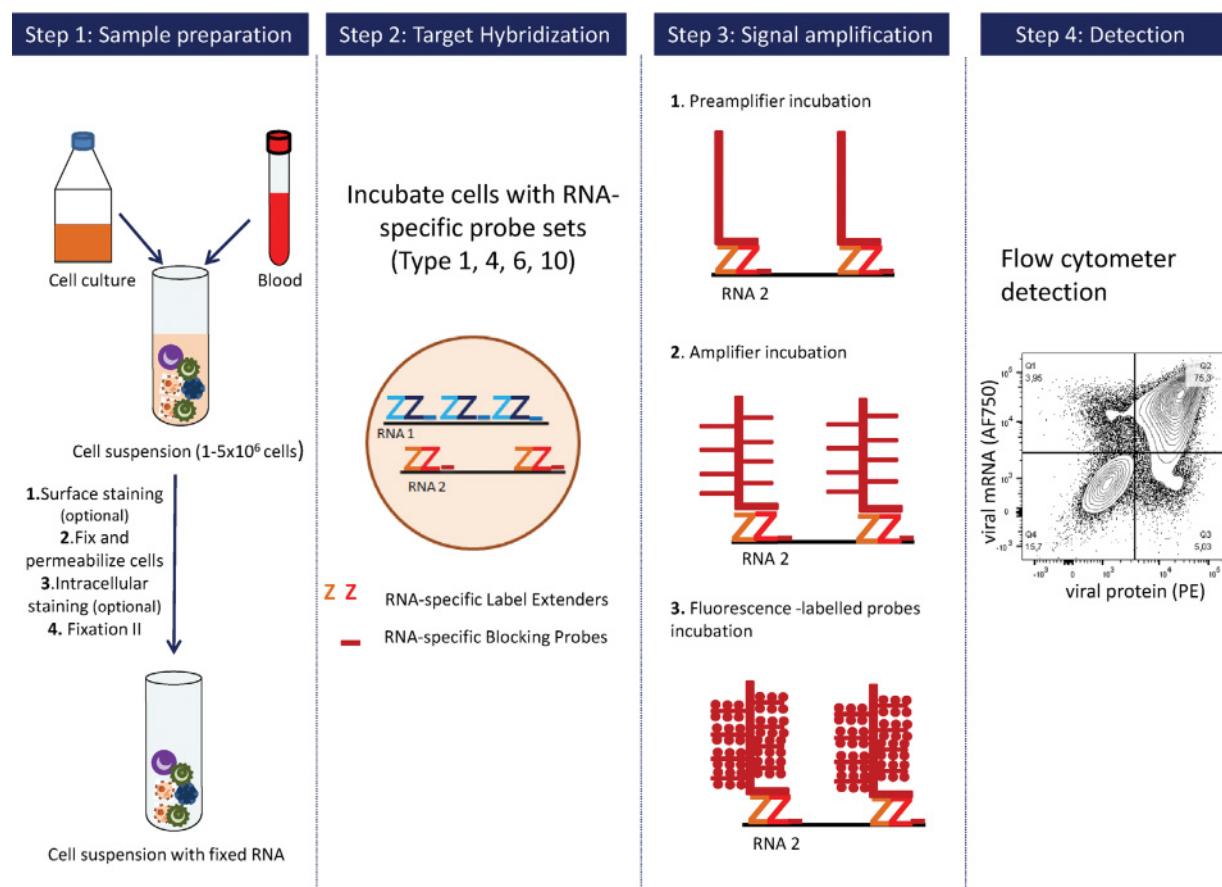
Figure 52. Schematic workflow for the quantification of transcripts by FCM using the PrimeFlow™ RNA Assay. Step 1: Single-cell suspensions are stained for surface and intracellular proteins according to standard protocols for FCM followed by a second fixation step. Step 2: Cells are incubated with mRNA-specific probe sets. Step 3: The signal of the mRNA-specific probes is amplified using different sets of amplifiers and probes. Step 4: The fluorescence of stained cells is measured using a flow cytometer and analyzed by suitable software after gating on live singlets. The example shows the expression of intracellular gagpol mRNA and surface p24 Gag protein of J89 cells that were latently infected with HIV-1 and activated with hTNF-α (10 ng/mL) for 40 h [495]. Steps 1–3 reproduced with permission from ThermoFisher Scientific © 2019.

12.3.1.3 Tissues (procedure is validated for murine tumors, lung, and liver). Collect resected tissues in RPMI supplemented with 10% FCS and cut into small pieces. Digest with 1 mg/mL collagenase IV (Bioconcept) at 37°C on a rotating device. After 45 min, add 2.6 µg/mL DNAseI (ThermoFisher) and continue digestion for additional 15 min at 37°C. Wash cells with 0.01 M EDTA in PBS by centrifugation at $350 \times g$ for 5 min. Lyse RBCs using RBC lysis buffer (17 mM Tris pH 7.2, 144 mM NH_4Cl) for 2 min. Wash cells with PBS and filter the cell suspension through a 70-µm filter to remove debris.

Be aware that collagenase treatment may affect the expression of certain cell surface antigens [497] and may be replaced by other methods for single-cell preparation from tissue include mechanical hashing and serial filtering [498]. Moreover, manipulation of tissues ex vivo may influence both the stability and composition of mRNA in the sample [499]. Because the influence of the tissue-processing method on the quality and quantity of individual proteins and transcripts cannot be predicted, we recommend including test runs or validation steps wherever possible.

12.3.1.4 Cell surface, intracellular staining, and target probe hybridization. The method described below is based on the manufacturer's protocol. All buffers included in the PrimeFlow™ RNA Assay kit are marked with an asterix (*). The notes are added by the authors based on their experience.

The following protocol is adapted for the use of 96-well U- or V-well plates. Please refer to the manufacturer's protocol for 1.5 mL tube protocol.

The washing buffer should be brought to room temperature before usage.

1. Prepare 2–5×10^6 cells in 100 µL of FCM buffer (PBS, 2% FCS) per well of a 96-well plate. Centrifuge at $500 \times g$ for 4 min at 4°C. Discard the supernatant by inverting the plate over the sink and blotting it on a paper towel.

Note 1: Please be aware that due to the high number of washing steps, approximately double the initial amount of cells in comparison to regular antibody staining should be used.

Note 2: Please note that target expression levels should be taken into consideration for defining the amount of starting material. The authors recommend to start with higher amounts of cells if the target mRNA, the target antigen, or target cell type are present in low frequency.

Note 3: The authors recommend a final concentration of 20 mM EDTA at pH 8.0 in the FCM buffer for tissue samples to ensure proper single cell disaggregation.

2 Surface stain cells with appropriate fluorophore-labeled Abs diluted in 100 µL FCM buffer for 30 min at 4°C.

Note: Include a fixable viability dye to exclude dead cells from the analysis. If a fixable viability dye is used, usually an FCS-free buffer for washing and staining must be used.

3 Centrifuge at 500 × g for 4 min at 4°C and discard the supernatant. Wash with 200 µL FCM buffer. Discard supernatant by careful aspiration or inverting and blotting.

4 Prepare Fixation Buffer 1*: Mix equal parts of Fixation Buffer 1A* and Fixation Buffer 1B* (by gently inverting 4 times). A total volume of 200 µL/sample is required.

Note: Prepare fresh. Avoid vortexing and shaking.

5 Centrifuge at 1000 × g for 4 min at 4°C, discard the supernatant, and resuspend cells in residual volume by pipetting (vortexing when using 1.5 mL tubes).

6 Add 200 µL of Fixation Buffer 1* to each well and mix gently by pipetting. Incubate for 30 min at 4°C.

7 Centrifuge at 1000 × g for 4 min at 4°C, discard the supernatant and suspend cells in residual volume by pipetting.

8 Prepare Permeabilization Buffer with RNase inhibitors*: Dilute Permeabilization Buffer* tenfold with RNAse-free water. Add RNase-inhibitor* at 1/100 ratio. The needed total volume throughout the assay per sample is 700 µL.

Note: Prepare fresh. Avoid vortexing and shaking. We recommend to prepare 10% more of the permeabilization buffer to account for the buffer foaminess and pipetting errors.

9 Add 200 µL of permeabilization buffer with RNase inhibitors* to each well and mix gently. Centrifuge at 1000 × g for 4 min at 4°C, discard the supernatant and resuspend cells in residual volume.

10 Repeat step 9.

11 (Optional) Stain cells intracellularly with the appropriate fluorophore-labeled Abs in 100 µL permeabilization buffer with RNase inhibitors* for 30 min at 4°C.

12 (Optional) Centrifuge at 1000 × g for 4 min at 4°C, discard the supernatant, and suspend cells in residual volume.

13 Repeat step 12.

14 Prepare Fixation Buffer 2*: Dilute Fixation Buffer 2* eightfold in Wash Buffer*. Volume per sample: 200 µL. Mix by inverting.

15 Add 200 µL Fixation Buffer 2* to each well and incubate for 1 h at room temperature in the dark.

Note: The protocol can be stopped at this step after adding Fixation Buffer 2. The cells can be incubated overnight in the dark at 4°C.*

16 Centrifuge at 1000 × g for 4 min at room temperature, discard the supernatant, and resuspend cells in residual volume.

17 Wash with 200 µL Wash Buffer*. Centrifuge at 1000 × g for 4 min at room temperature, discard the supernatant, and resuspend cells in residual volume.

18 Repeat step 16.

Note: The protocol can be stopped at this step. The cells can be stored in Wash Buffer with RNASe inhibitors* (1/100) overnight at 4°C in the dark.*

19 Thaw target probe sets at room temperature and pre-warm Target Probe Diluent* to 40°C in the incubator.

20 Prepare target probes: Dilute target probes 20-fold in Target Probe Diluent*. Volume per sample is 100 µL. Mix the solution by pipetting up and down.

Note 1: If you combine more than one target probe in a sample, make sure that the final volume is 100 µL.

Note 2: For detecting low-expressed mRNA targets, tenfold or fivefold dilutions of target probe dilutions might be helpful. Be aware to use the appropriate scrambled probes at the same concentration to control for unspecific binding.

21 Add 100 µL Wash Buffer* to each well. Add 100 µL of target probes to the cell suspension and mix by pipetting. Incubate the plate for 2 h at 40°C.

Note 1: A lid can be used instead of the plastic seal.

Note 2: To increase the signal, the incubation time can be prolonged to 3 h.

22 Centrifuge at 1000 × g for 4 min at room temperature, discard the supernatant, and suspend cells in residual volume.

23 Wash with 200 µL Wash Buffer*. Centrifuge at 1000 × g for 4 min at room temperature, discard the supernatant and suspend cells in residual volume.

24 Repeat step 22.

25 Prepare Wash Buffer* with 1/100 RNase-inhibitor*. Mix by inverting. Volume per sample: 100 µL.

Note: Prepare fresh. Avoid vortexing and shaking.

26 Add 100 µL Wash Buffer with RNase-inhibitors* to each well and mix by pipetting.

Note: For the manageability of the whole procedure, the manufacturer recommends to interrupt the procedure at this step and to keep the cells overnight in the dark at 4°C.

12.3.2 Signal amplification.

27 Pre-warm PreAmp Mix*, Amp Mix* and Label Probe Diluent* at 40°C (in the incubator).
28 Pre-warm samples and Wash Buffer* at room temperature in the dark.
29 Thaw Label Probes* on ice in the dark.
30 Add 100 µL of pre-warmed PreAmp Mix* directly into the cell suspension and pipet to mix. Incubate plate with lid for 1.5 h at 40°C.

Note: To increase the signal, up to 2 h incubation time can be performed.

31 Centrifuge at 1000 × g for 4 min at room temperature, discard the supernatant, and suspend cells in residual volume.
32 Wash with 200 µL Wash Buffer*. Centrifuge at 1000 × g for 4 min at room temperature, discard the supernatant, and suspend cells in residual volume.
33 Repeat step 31.
34 Add 100 µL Wash Buffer* to each well. Add 100 µL of Amp Mix* directly to the cell suspension and mix by pipetting. Incubate the plate with lid for 1.5 h at 40°C.

Note: To increase the signal, the incubation time can be prolonged to 2 h.

35 Centrifuge at 1000 × g for 4 min at room temperature, discard the supernatant, and suspend cells in residual volume.
36 Wash with 200 µL Wash Buffer*. Centrifuge at 1000 × g for 4 min at room temperature, discard the supernatant, and suspend cells in residual volume.
37 Repeat step 35.
38 Prepare Label Probes*: Dilute Label Probes* 100-fold in Label Probe Diluent*. Volume needed per sample is 100 µL.
39 Add 100 µL of Wash Buffer* to each well. Add 100 µL of Label Probes* directly to the cell suspension and mix by pipetting. Incubate plate with lid for 1 h at 40°C.

Note: To increase the signal, the incubation time can be prolonged to 2 h.

40 Centrifuge at 1000 × g for 4 min at room temperature, discard the supernatant, and suspend cells in residual volume.
41 Wash with 200 µL Wash Buffer*. Centrifuge at 1000 × g for 4 min at room temperature, discard the supernatant, and suspend cells in residual volume.
42 Repeat step 40.
43 Resuspend cells in 100 µL Storage Buffer* or FCM buffer. Transfer each sample to a polystyrene FCM tube and measure samples in a flow cytometer.

Note 1: You may keep the samples at 4°C for 3 days before analyzing. The manufacturer recommends storing the cells in IC Fixation Buffer at a ratio of 1/1 with the cell suspension.*

Note 2: For compensation of fluorophore-labeled Abs for surface staining, intracellular staining, and viability staining, we recommend using the provided UltraComp beads. For compensation of the fluorophore-labeled probes, the manufacturer recommends using the Compensation Kit* together with the UltraComp beads*. It is not recommended replacing the Compensation Kit* with other fluorophore-labeled Abs that are detected in the same BP filters. Alternatively, samples can be single-stained with house-keeping gene probes labeled in all four types and used as positive controls for compensation.*

12.4 Materials

The PrimeFlow™ RNA Assay kit (ThermoFisher, 88-18005-210) contains the following material: PrimeFlow™ RNA Fixation Buffer 1A (00-18100), PrimeFlow™ RNA Fixation Buffer 1B (00-18200), PrimeFlow™ RNA Permeabilization Buffer (10×) (00-18300), PrimeFlow™ RNA Fixation Buffer 2 (8×) (00-18400), PrimeFlow™ RNA Wash Buffer (00-19180), PrimeFlow™ RNA Target Probe Diluent (00-18185), PrimeFlow™ RNA PreAmp Mix (00-16000), PrimeFlow™ RNA Amp Mix (00-16001), PrimeFlow™ RNA Label Probe Diluent (00-19183), PrimeFlow™ RNA Storage Buffer (00-19178), PrimeFlow™ RNase Inhibitor (100×) (00-16002), PrimeFlow™ RNA Label Probes (100×) (00-16003), PrimeFlow™ Compensation Kit (88-17009), IC Fixation Buffer (00-8222), PrimeFlow™ RNA tubes (1.5-mL microcentrifuge tubes) (19197), and UltraComp eBeads™ Compensation Beads (Invitrogen, ThermoFisher 01-2222-42).

The following material is required, but not included in the kit:

RNA detection	Content
Target Probe Sets	Target mRNA of interest in preferred fluorophore, ThermoFisher
Media	Content
RPMI + FCS RNAse-free water	RPMI, 10% FCS
Buffer	Content
FCM buffer	PBS, 2% FCS
RBC lysis buffer	Cat. Number: 00-4300 (ThermoFisher)
Abs	
Surface staining Abs	Fluorophore-labeled Abs for surface antigens
Intracellular staining Abs	Fluorophore-labeled Abs for intracellular antigens
Viability dyes	Fixable viability dyes
Other material	
96-well plate	96-well V- or U-bottom polystyrene plate
FCM tube	Polystyrene FCM tube
Instruments	

Incubator	Incubator validated to maintain $40 \pm 1°C$
Centrifuge	Swinging bucket centrifuge, refrigeration to 4°C
Flow cytometer	Flow cytometer containing three lasers: blue (488 nm), yellow-green (561 nm) and red (633 nm). Excitation/ Emission maximum of probe sets: Type 1/AF647: Ex_{max}: 650 nm, Em_{max}: 655 nm, bandpass filter: 660/20 nm; type 10/AF568 (Ex_{max}: 578 nm, Em_{max}: 603 nm), bandpass filter: 610/20 nm; type 4/AF488 (Ex_{max}: 490 nm, Em_{max}: 525 nm), bandpass filter: 530/30 nm type 6/AF750 (Ex_{max}: 749 nm, Em_{max}: 775 nm), bandpass filter: 780/60 nm.

12.5 Controls and data analysis

It is recommended to include two negative controls to allow discrimination of false positive results: (i) a sample stained with the full Ab panel but without the probe (similar to a classical FMO control) and (ii) a scrambled probe (similar to an isotype control). Additionally, cells known to not express the target mRNA serve as a biological control. Background signals can be diminished by additional washing steps between different incubations, however this might lead to cell loss.

To control for correct performance of procedure, include a sample stained with the full Ab panel plus a probe for a housekeeping transcript.

If the target RNA is expressed at low level, increasing the signal may be desired. This can be achieved by longer incubation times of target probes, PreAmp Mix, Amp Mix, and label probe. In addition, increasing the amount of target probes during 3 h of incubation significantly increases the signal of the target RNA detection without increasing the background.

Acquired data can be analyzed with any software compatible with FCM files.

12.6 Pitfalls

Although the stability and the number of applications have improved, the technique still harbors some limitations. First, low expression of mRNA targets is the major pitfall, as rare expression events may not be detectable with this assay. Second, mutations as well as splicing variants of the target mRNA might result in signal reduction or even signal loss. Third, this protocol increases the autofluorescence of cells, which mostly affects FITC and PE channels.

Fourth, several available fluorochromes are not compatible with this assay. This mainly affects temperature-sensitive and tandem dyes such as PerCP, PerCP-Cyanine5.5, and PerCP-eFluor710. This restriction may hamper the design of large multicolor panels. It is recommended testing each Ab throughout the whole procedure to determine its suitability beforehand. Finally, phospho-specific Abs for intracellular staining that require a methanol-based fixation are not compatible with the PrimeFlow™ RNA Assay.

12.7 Top tricks

The top tricks to clearly obtain a reliable signal or to increase the signal for the target mRNAs are:

1. Careful design of the target probes: (i) Use a high number of target probes pro target mRNA, (ii) Use bright fluorescent target probes for mRNA with unknown or low-expression.
2. Increase the signal: (i) Increase incubation times of target probes, PreAmp, Amp, and Label Probes, (ii) Increase concentration of target probes.
3. Use a stable incubator and do not open the door during incubation times at 40°C. If available, monitor the temperature with a NIST calibrated thermometer.
4. Use all controls suggested and perform a meticulous compensation following the instructions above.
5. Use the RNA inhibitors included in the kit and work in a clean environment.
6. Contact the manufacturer in advance for panel design.

12.8 Conclusion

In conclusion, the PrimeFlow™ RNA Assay opens up new options for studying complex cellular interactions, short-term responses to stimuli, or expression of a certain marker on single-cell level, when specific Abs for the target proteins are not commercially available [494–496, 500, 501] Moreover, the simultaneous quantification of mRNA and protein allows the detailed study of cellular dynamics upon certain culture conditions. This assay also offers the possibility of high-throughput screening on a single-cell basis.

13 Transcription factors

13.1 Introduction

Cell functionality and differentiation are all controlled by transcription factors within cells that regulate gene expression. As these factors are generally proteins, they may be detected using an Ab directed against some specific epitope within the protein. In this way, detection of transcription factors is in essence no different from detecting proteins on the surface of the cell. However, as the proteins of interest will be located within the cell, either in the

cytoplasm, within a cellular sub-compartment or in the nucleus, cells must be permeable to allow access of the Ab to its binding site. As the factors need to be preserved in their sub-cellular location and in their physiological condition at the time of sampling, any fixation must be very rapid and pervasive.

Detection of transcription factors by FCM thus requires careful planning, with attention paid to several specific questions that will dictate the best protocols to follow. The most important of these questions is, "Will surface staining (i.e., phenotyping) be necessary to identify the cells of interest?"

The answer to this question is critical, as it will dictate the best way to prepare the cells, allowing the antigens access to the intracellular compartment and their target. It will also impact the choice of fluorochromes used because different fixation methods can have dramatic impact on the fluorescent molecules [502]. The two most common fixation reagents are alcohols and aldehydes, each having their strengths and drawbacks.

Alcohols, such as ethanol and methanol, or acetone, are dehydrating fixatives that both coagulate proteins (fixation) and create holes in the lipid membrane (permeabilization). Many of the cyclins and phospho-specific proteins are readily detectable post-alcohol fixation [503]. Unfortunately, alcohol fixation adversely affects fluorescent proteins such as GFP, which will be affected by alcohol fixation in such a way that it will no longer be fluorescent after conformational changes or may even leach out of the cell [504].

Alcohol fixation will also adversely affect commonly used fluorochromes including PE, PerCP, and APC, making these fluorochromes a poor choice for surface staining. Small cyclic ring fluors such as FITC, the Alexa Fluor®, and the cyanine dyes are more resistant to alcohol fixation. Surface markers may also be stained post-fixation if the protein structure, or at least the specific recognized sequence is unaltered by the chemical process of fixation. If no evidence is available, this may have to be determined empirically.

Aldehyde fixation is performed usually with formaldehyde in the range 1–4% [505]. Aldehydes are cross-linking fixatives so they lock protein structure in place by forming crosslinks between lysine residues, forming methylene bridges. This generally means Abs will still recognize their epitope. However, formaldehyde on its own is not a good permeabilizing agent and it would normally be combined with a detergent—this is the basis of many Fix and Perm kits that are on the market (although the exact composition of commercial kits is often not common knowledge due to Intellectual Property policies). A range of detergents is available such as Triton X-100, lysolecithin, Nonidet-P40, and saponin. The choice may depend on localization of the protein. Transcription factors tend to be nuclear and the use of a stronger detergent such as Triton X-100 (generally around 0.1%) is a good choice as it can permeabilize both the plasma and the nuclear membrane. Saponin on the other hand is not a good permeabilizing agent for nuclear factors due to its more "gentle" and reversible nature and has often seen more use in cytokine staining. However, it should

also be noted that cytokine staining is also compatible with detergents such as NP-40 (see also Chapter III Section 5: Cell fixation and permeabilization for flow cytometric analyses) [506].

It is important to note, as with any FCM protocol, the exclusion of dead cells is critical for analysis. Commonly used viability dyes such as PI or 7AAD rely on an intact membrane for differentiation of live versus dead cells (see Chapter III Section 4: Dead cell exclusion, cell viability, and sample freezing). When targeting intracellular markers by flow, the use of fixable amine-reactive dyes must be used (see also Chapter II Section 5: Cell fixation and permeabilization for flow cytometric analyses) [201]. These dyes still allow for the discrimination of dead and live cells from live even after the fixation and permeabilization processes.

As fixation chemically alters the cells, it will also change to some extent the autofluorescence of the cell. Changes in morphology may be seen as alterations in light scatter patterns in a flow cytometer. Again, alcohols will have a more dramatic effect. Conversely, alcohols do not cause, in general, a change in levels of background autofluorescence that may be important if a low level specific signal is expected. If an aldehyde is used, fixation should be brief and cells should be stored in a phosphate buffer prior to staining as aldehydes, especially glutaraldehyde, will cause an increase in autofluorescent background.

Reagent manufacturers each sell specific buffers and kits for staining of specific transcription factors, often with proprietary reagents, but these buffers have been designed to allow detection of nuclear antigens without comprising surface antigen detection. Some of these kits will have separate fixation and permeabilization steps, while others will be in a single solution. The choice of which kit or reagents to use is often dictated by the intracellular target, so reading of the technical specification of the given Ab is critical.

The location of the target may also influence the fluorochrome used to label the Ab. Fluorochromes such as PE, APC, and PerCP and their tandems are large proteins that add considerably to the molecular weight and size of the Ab. This means that to detect a nuclear protein, a harsher permeabilization/fixation regime may be needed, which may also lead to selective loss of small molecules from the cell. But it may also mean that the comparatively larger fluorochrome will restrict access of the Ab to the nucleus altogether.

In conclusion, there is not a universal protocol applicable to all transcription factors, which can be expressed in different cellular locations (see Table 11); the type of fixation, the length of fixation, the type of permeabilization, the choice of fluorochromes, and the staining protocol, including incubation times of Ab staining, must all be optimized. The principle advantage of FCM in this area is the ability to multiplex an assay, and by using multiple analytes be able to very specifically define subsets of interest—this will only be limited by the cytometer available. One downside of FCM is the lack of morphological information and inability to specifically localize the fluorescence within the cell. If this is important then imaging using either fluorescence microscopy, confocal microscopy, or imaging FCM should be considered.

Table 11. Most common transcription factors measured by FCM. For more information about them http://www.uniprot.org/uniprot/

Transcription factors	Cell type	Cellular location
AHR	Liver, Treg, and Th17 cells	Cytoplasm
Aiolos	B, T, and NK cells	Nucleus
AIRE	Dendritic cells, lymph node, lymphoid stromal cells, and monocytes	Perinuclear region (??)
BATF	B and T cells	Nucleus
Bcl-6	B cells and CD4$^+$ T follicular helper cells and memory T cells	Nucleus
β Catenin	Several non-immune tissues, B, T, and hematopoietic stem cells	Cytoplasm/nucleus
Blimp1	B, T, dendritic, and some NK cells	Cytoplasm
c-Maf	Neural, ocular, and hematopoietic systems	Nucleus
c-Rel	Treg, mature T cells	Cytoplasm/nucleus
E4BP4	NK, NKT, and dendritic cells	Nucleus
Egr1	B, T and myeloid cells	Cytoplasm/nucleus
Egr2	(B), T and NKT cells	Cytoplasm/nucleus
Eomesodermin/TBR2	NK and T cells	Nucleus
Eos	T cells and nervous system	Transmembrane
FoxJ1	Ciliated epithelial cells, naive B, and T cells	Nucleus
FoxP3	CD4$^+$CD25$^+$ regulatory T cells (Treg cells), and CD4$^+$CD25$^-$ cells	Cytoplasm/nucleus
Gata-3	Central nervous system, kidney, mammary glands, skin, and T cells	Nucleus
Helios/IKZF2	T and hematopoietic stem cells	Nucleus
IκB-zeta	Macrophages, monocytes, B and T cells	Nucleus
IRF4	Macrophages, B and T cells	Cytoplasm/nucleus
Nanog	Blastocyst, embryonic stem cells, and embryonic germ cells	Nucleus
NFkB	Almost all cell types	Cytoplasm/nucleus
NFAT	T cells	Cytoplasm/nucleus/ transmembrane
Notch1	Thymocytes, bone marrow hematopoietic stem cells, T and NK cells	Cytoplasm/Golgi/nucleus/ transmembrane
Notch2	Activated peripheral T cells, bone marrow and thymocytes,	Cytoplasm/Golgi/nucleus/ transmembrane
Notch3	CNS, some thymocyte subsets, vascular smooth muscle, and T cells	Cytoplasm/Golgi/nucleus/ transmembrane
Notch4	CD8$^+$ splenic dendritic cells, endothelial cells, and macrophages	Cytoplasm/Golgi/nucleus/ transmembrane
Nurr77	Thymocytes and T cell	Cytoplasm/nucleus
OCT3/4	Embryonic stem and induced pluripotent stem (iPS) cells	Nucleus
Pax5	Hematopoietic cells, B cells	Nucleus
PLZF	CD4 and CD8$^+$ T cells, gamma delta T cells and NK.	Cytoplasm/nucleus
RORγ	Heart, kidney, liver, lung, muscle, and CD4$^+$CD8$^+$ thymoycte cells	Nucleus
Runx1/AML1	Hematopoietic, myeloid, B and T cells	Cytoplasm/nucleus
Sox2	Embryonic stem cells and neural cells	Cytoplasm/nucleus
T-bet	B cells and CD4$^+$ T-cell lineage	Nucleus
ThPOK	Hematopoietic cells, skin, heart, smooth muscle, and liver, invariant natural killer T (iNKT) cells and gamma delta T cells	Nucleus
TOX	Thymocytes, T lymphocytes, NK cells, and lymphoid tissue-inducer (LTi) cells	Nucleus

13.2 Example of a generic protocol for an intranuclear antigen—pH3

13.2.1 Staining protocol (adapted from ref. [507]). Staining is done in a 96-well U- or V-bottom plate.

1. Count cells from culture/primary sample and resuspend at 10 million cells/mL, aliquot 100 µL/well (~10^6 viable cells per sample for staining). Spin down plate at 350 × *g* for a minimum of 3 min at room temperature. Flick SN and vortex plate to re-suspend. These will be the conditions for all wash steps.
2. Optional: Stain for Live/dead and surface markers prior to fixation. Follow manufacturer's recommendations for live/dead staining. Make up Ab cocktail in staining buffer at optimized dilutions. Add 100 µL per well per million cells and incubate for optimized time (1 h minimum).
3. Add 100 µL of Staining buffer per well and spin down as in step 2. Add 200 µL of fresh Staining buffer and spin down again.
4. Resuspend cells in 100 µL of PBS only and pipette up and down to ensure cells are fully in suspension. Then add 100 µL of 4% fixation buffer to final concentration of 2%. The pre-suspension in PBS minimizes the formation of cell clumps during the fixation process. Leave at room temperature for a minimum of 60 min.
5. Spin down cells and treat as in step 1.
6. Resuspend pellet in 100 µL of PERM buffer using a P200 pipette. Incubate tubes at room temperature for exactly 5 min (stagger addition of PERM buffer if needed).
7. Add 100 µL of Staining buffer to each well in staggered fashion to end permeabilization step. Spin down and process as in step 2.
8. Add 100 µL of primary Ab cocktail and mix in PBS + 2% FCS. Incubate at room temperature for optimized time (usually 1–2 h).
9. Add 100 µL of Staining buffer and spin down and process as in step 2. Repeat this wash step with 200 µL fresh Staining buffer.
10. If necessary, incubate cells with secondary Ab cocktail mix for the optimized time (usually a minimum of 30 min) at room temperature in the dark.
11. Wash the cells, as outlined in step 2, twice in fresh Staining buffer.

Final resuspend volume should be 200–400 µL of Staining buffer.

14 Intracellular parameters

FCM is a powerful tool to measure expression levels of proteins that can be found inside cells such as transcription factors, cytoskeletal components, and apoptosis regulators, or those that are usually secreted like cytokines and chemokines. However, whereas proteins from the former category are normally expressed constitutively, cytokine expression usually requires restimulation of the cell, as is the case for T cells, which express cytokines ~2–24 h after T-cell receptor engagement [508, 509]. However, some cell types, such as innate lymphoid cells, also express cytokines constitutively [510, 511]. To enable the intracellular detection of otherwise secreted proteins, secretion can be blocked by Brefeldin A or Monensin that block transport of vesicles from the ER to the Golgi or within the Golgi apparatus, respectively.

To activate cytokine expression, T cells can be stimulated in two ways: while cytokine expression in some memory T-cell subsets can be induced by cytokine signaling, such as IFN-γ which can be induced by IL-12 and IL-18 [512, 513], most T cells have to receive a T-cell receptor signal and a costimulatory stimulus. This can be achieved in a polyclonal way by agonistic Abs against CD3ε and CD28, coated to the surface of a culture vessel or in an antigen-dependent manner by the incubation with peptide-pulsed APCs. Alternatively, cells can be exposed to the chemicals phorbol 12-myristate 13-acetate (PMA) and ionomycin that mimic TCR signaling by activating protein kinase C/NFκB and calcineurin/NFAT pathways, respectively. The restimulation conditions have a strong impact on the cytokine expression results and should thus be chosen carefully:

1. PMA/iono is usually a stronger inducer of cytokine expression compared to CD3/CD28 stimulation. While it might be argued that this trigger is not physiological, it is very well suited to reveal the maximal cytokine expression potential of the T cells rather than their actual cytokine expression, e.g., in vivo at the time point of analysis.
2. For PMA/iono, the Ca^{2+} concentration of the medium can be critical: maximal cytokine expression requires 1.5 mM of Ca^{2+} as present for example in Iscove's modified Dulbecco's medium, but not in the routinely used medium RPMI 1640 (Fig. 53A) [514].
3. The cell concentration should not be too high as this will reduce cytokine expression. For PMA/iono stimulation, we have noticed decreased cytokine expression when using 1–5 × 10^7 cells/mL compared to 2 × 10^6 cells/mL (Fig. 53B).
4. Expression kinetics can be important. Using PMA/iono, maximal cytokine expression is achieved as early as 4 h following stimulation (Fig. 53C) [515].

For the detection of intracellular antigens, cells have to be fixed and permeabilized. Numerous protocols and reagent kits are available for fixation and permebilization, each optimized for the detection of certain antigens, such as cytokines, transcription factors, and so on. For cytokine detection, cells can be fixed after surface Ab staining with 1–4% formaldehyde [516], although in our experience the use of commercially available fixation kits can be beneficial for the integrity of the surface staining. Cells are then permeabilized with a mild detergent, e.g., saponin that builds complexes with cholesterol and hence forms holes in the cholesterol-rich plasma membrane but not in the cholesterol-poor nuclear membrane [517, 518]. It should be noted that restimulation of Th cells leads to internalization of CD3/TCR and CD4
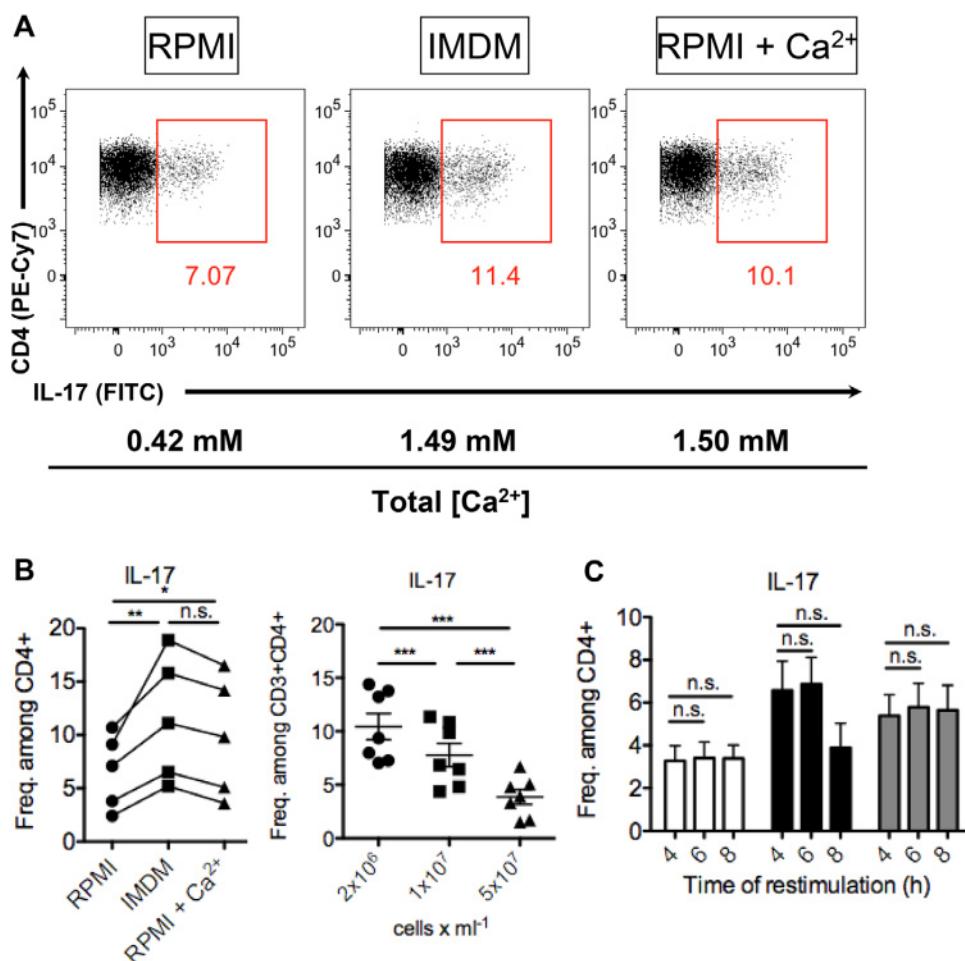
Figure 53. An example of intracellular cytokine detection. Shown are viable, single, CD3$^+$CD4$^+$ C57BL/6 WT Th cells from the inflamed colon of T-cell transfer-induced colitis. (A) Cells were restimulated for 4 h with PMA/iono (and Brefeldin A added after 1 h) in RPMI, IMDM, or CaCl$_2$-supplemented RPMI and stained for intracellular cytokine expression. (B) Frequency of IL-17$^+$ cells among colonic Th cells restimulated with PMA/iono at the indicated densities for $n = 7$ mice. (C) Frequency of IL-17$^+$ cells among colonic Th cells restimulated with PMA/iono for the indicated amount of time for $n = 4$ mice per group. $^*p < 0.05$, $^{**}p < 0.01$, and $^{***}p < 0.001$ by one-way ANOVA for repeated measurements and Tukey's post hoc test. Reproduced with permission from ref. [514].

proteins from the surface of the cell [519, 520]. It can thus be beneficial to stain these antigens following fixation and permeabilization to also detect the internalized molecules. To control for true positive cytokine staining, unstimulated cells, cells that have not been permeabilized, or endogenous negative control cells can be used.

Transcription factors can usually be stained directly, i.e., without prior acute restimulation, as they are normally expressed constitutively. Nevertheless, the expression levels of certain transcription factors might also change depending on the activation status of the cell (Fig. 54A). Following surface staining, cells are commonly fixed and permeabilized with commercially available kits for transcription factor staining, as saponin-mediated permeabilization is too weak to enable nuclear penetration of Abs. The optimal fixation time and condition may vary for each different transcription factor and among different cell types and should thus be established for the specific setting of interest (Fig. 54B). Using T cells from the inflamed gut of T-cell transfer colitis, we

have observed that overnight fixation impaired staining of the transcription factor eomesodermin, which was clearly detectable when fixing for only 1 h. In contrast, ROR-γt staining in these cells was comparable between the two fixation regimens. In contrast, for splenic T cells from the same model, overnight fixation resulted in an even better ROR-γt staining compared with fixation for 1 h. The topic of transcription factor staining is covered in more detail in Chapter V Section 13 Transcription factors.

As for any FCM application, optimal titration of Abs is instrumental for obtaining high quality results. Intracellular stainings tend to have a higher background due to the abundance of biologically active molecules inside of the cell. As transcription factors are rather rare proteins, they should be stained with bright fluorochromes when designing a panel. Most cytokines accumulate to high density within a cell during reactivation in the presence of secretion blockers and can hence be detected with less-bright fluorochromes. There are, however, also cytokines expressed at low levels and, thus, the panel design should be adjusted
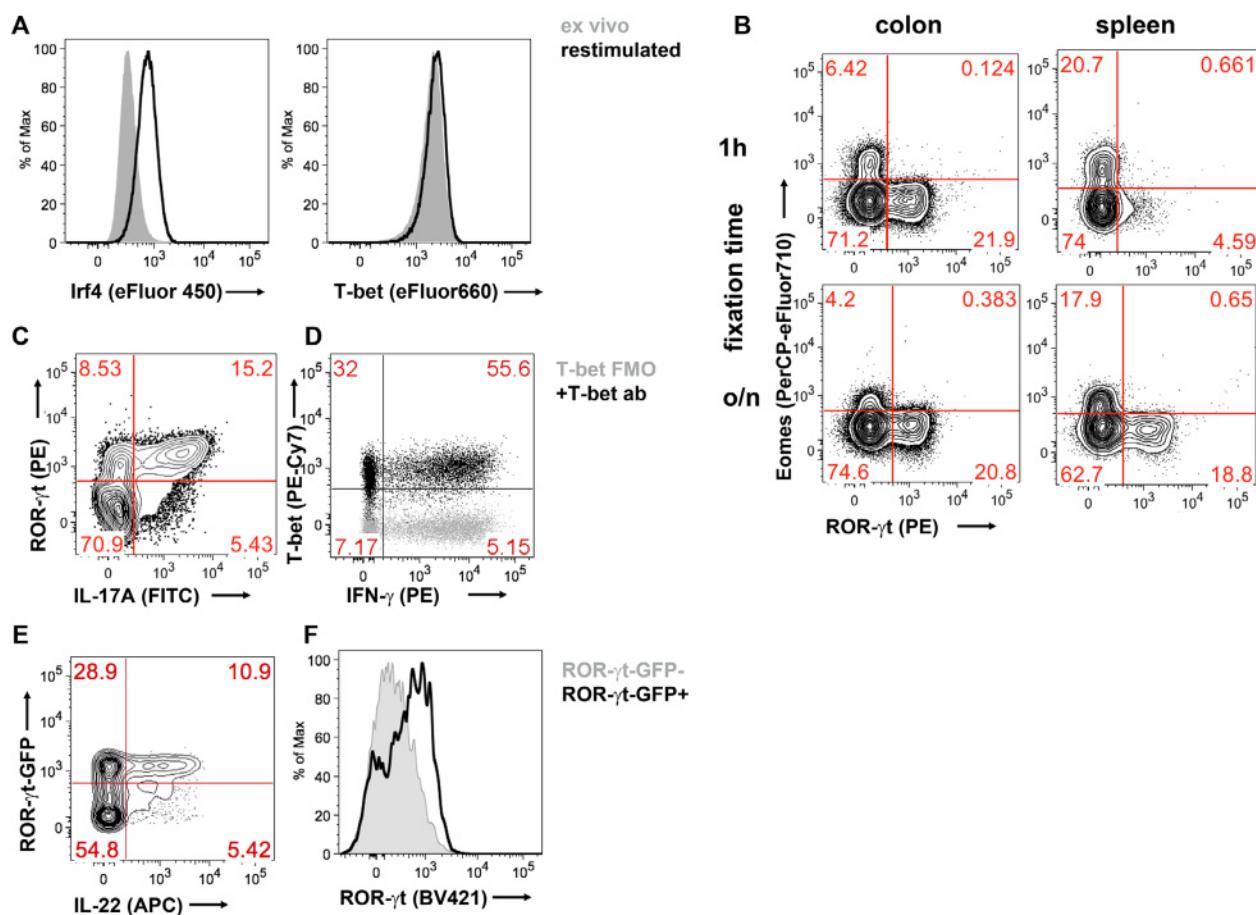
Figure 54. An example of intranuclear transcription factor detection. (A–D) Shown are viable, single, CD3⁺CD4⁺ C57BL/6 WT Th cells from the inflamed colon or the spleen of T cell transfer-induced colitis. (A) Transcription factor expression can depend on activation state of the cell: Interferon regulatory factor 4 (Irf4) and T-box expressed in T cells (T-bet) were stained directly ex vivo (grey shaded) or after 4 h restimulation with PMA/iono (black line). (B) Fixation time can positively or negatively influence staining quality of transcription factors: Eomesodermin (Eomes) and retinoic acid receptor-related orphan receptor gamma t (ROR-γt) were stained after 1 h or after overnight (o/n) fixation with the eBioscience Foxp3/transcription factor staining buffer set. (C–F) Transcription factor staining can be combined with cytokine staining or fluorescent reporter genes. (C and D) ROR-γt, T-bet, IFN-γ, and IL-17 were stained simultaneously with the eBioscience Foxp3 staining buffer set. (D) Black indicates the full staining and grey the FMO control for the T-bet antibody (ab). (E and F) Depicted are viable, single, CD45⁺B220⁻CD11b⁻F4/80⁻Gr-1⁻CD90⁺, TCRβ⁺, TCRγδ⁻ cells from the small intestine of C57BL/6 *Rorc*^GFP/+ reporter mice. (E) IL-22 was stained after 4 h of restimulation with PMA/iono and 5 μg/mL IL-23 with the Miltenyi Biotec inside stain kit. (F) ROR-γt stained directly ex vivo with the Miltenyi inside stain kit is depicted for ROR-γt⁻GFP⁻ (grey shaded) and ROR-γt⁻GFP⁺ cells (black line).

according to the expected results. Any intracellular staining panel should include a fixable viability dye to discriminate dead cells. This is especially important when analyzing cytokine expression, as the restimulation can induce apoptosis in a significant fraction of the cells while maintaining their FSC/SSC profile, thus making their distinction based on scatter parameters impossible. Fixable viability dyes are now broadly available and are commonly based on the unspecific binding of fluorochromes with an active chemical group, e.g., succinimidyl esters, to amino groups of cellular proteins. Thus, viable cells are poorly labeled through their surface proteins while dead cells with a permeable plasma membrane are labeled brightly through the binding to intracellular proteins.

For certain questions, a co-staining of transcription factors and cytokines can be required. While transcription factors are poorly detected following saponin-mediated permeabilization, several cytokines can be detected with the same protocol as transcrip-

tion factors, i.e. with commercially available transcription factor staining kits. We were able to stain IFN-γ, IL-17A, T-bet, and ROR-γt with a commercial transcription factor staining kit (Fig. 54C and D). However, other cytokines, such as IL-22, can hardly be detected using a transcription factor staining kit. In this case, iterative staining and fixation steps of first surface antigens, then cytokines, and ultimately transcription factors might provide a solution.

Many researchers want to stain intracellular antigens while maintaining the fluorescence of endogenous fluorescent proteins such as GFP. Using commercially available staining kits, GFP fluorescence is often lost, most likely due to the passive leakage of the protein outside of the cell. This can be prevented by a pre-fixation step with 0.5–2% formaldehyde prior to fixation/permeabilization with commercial kits [521, 522]. We have obtained good results for GFP/cytokine staining and for GFP/transcription factor stain-

ing using a commercial intracellular staining kit (Fig. 54E and F).

15 Measurement of signal transduction pathways by flow cytometry

15.1 Introduction

The large majority of proteins involved in the regulation of cell signaling, survival, and growth regulation are intracellular. This section covers the technical aspects of intracellular antigen staining for FCM, using activation and simultaneous monitoring of multiple pathways in human peripheral blood monocytes as a practical example. The approaches we use for cell fixation and permeabilization that optimize intracellular labeling while preserving light scatter and phenotypic markers are presented in the section on cell fixation and permeabilization (Chapter III Section 5: Cell fixation and premeabilization for flow cytometric analyses). Although more demanding than cell surface staining, mastery of intracellular cytometry enables the study of fundamental regulatory mechanisms of normal and abnormal cell biology, many of which remain underexplored.

Signaling pathways typically relay instructions from outside the cell to the nucleus, where an appropriate genetic program such as DNA synthesis or enhanced cell survival is executed in response to inputs from growth factors, cell–cell contacts, or ECM interactions. The biochemical basis of signal transduction involves the addition (by kinases) and removal (by phosphatases) of phosphate groups from the amino acids serine, threonine, and tyrosine that contain –OH side chains. Phosphorylation alters the charge distribution, hence the conformation, of proteins. Typically this activates the catalytic site of an enzyme, although some phosphorylations are inhibitory, inactivating the kinase function of the protein. Individual proteins involved in signal transduction are arranged in pathways, where an incoming phosphorylation activates the kinase activity, allowing it to pass the phosphorylation signal on to the next signaling element. There are other key cellular pathways that similarly result in different types of posttranslational protein modifications, including methylation, hydroxylation, acetylation, ubiquitination, and so on, and the basic fixation and permeabilizkation technique described in Chapter III Section 5: Cell fixation and permeabilization for flow cytometric analyses, has been used to study some of these [523].

Signal transduction is clearly a complex area of biology. Although it is likely that the major signaling pathways in mammalian cells have now been identified, basic research into how these are regulated and interconnected continues at a rapid pace. The complexity of signal transduction pathways allows for multiple activating and inhibitory inputs, and for networking between pathways. Considering that signal transduction is essential for the survival of multicellular organisms, this is to be expected.

Derangements in signal transduction are extremely common in human cancers, and appear to play a major role in the develop-ment and progression of both solid and hematological malignancies. Similarly, signal transduction pathways play a pivotal role in multiple aspects in both the development of the immune system, and in regulating responses to antigenic challenges.

15.2 Sample preparation for signal transduction analysis

The analysis of phospho-epitope expression in clinical samples (whole blood, bone marrow, body fluids) is complicated by the need to lyse RBCs, while at the same time preserving surface immunophenotypic markers as well as light scatter. For this, we have developed a technique that starts with fixation of the entire cell suspension, ensuring that phospho-epitopes are stabilized as soon as possible, followed by red cell lysis using Triton X-100 (Chapter III Section 5: Cell fixation and permeabilization for flow cytometric analyses). As discussed there, some epitopes (e.g., phosphorylated-STAT proteins) require an additional methanol "unmasking" step for optimization of their expression [75]. We have also used this technique for the analysis of signaling in bone marrow samples [72, 73].

15.3 Activation of signal transduction pathways regulating acute inflammatory responses

Like most signaling pathways, the MAPK pathways are arranged in cascades in which one member becomes catalytically active following phosphorylation by its upstream activating kinase. The activated upstream kinase is able to pass on the signal by phosphorylating its downstream substrate. This complexity allows multiple levels of feedback regulation, and interconnections involving pathways that are critical to the normal maintenance of tissues. There are three MAPK pathways that in mammals have very distinct functions, although they are highly conserved in evolution. The ERK pathway, often simply called the "MAPK pathway" is involved in growth factor stimulation, whereas the SAPK/JNK (Stress-Activated Protein Kinase/c-JUN N-terminal Kinase) and p38 MAPK pathways are more sensitive to other environmental cues including osmotic stress and heat shock.

In the innate immune response, the bacterial endotoxin LPS induces the activation of multiple signaling pathways ("pan-kinase" activation), which leads to an inflammatory response in monocytes.

As shown in Fig. 55, LPS activation of signaling pathways in peripheral blood monocytes is somewhat unique, in that it results in the activation of multiple signaling pathways, including all three major MAPKs, PI3K >AKT, and NFκB pathways. NFκB and MAPK activation induces the production of inflammatory and other cytokines. These pathways have widespread effects on cell function, which together coordinate the host response to acute bacterial infection.

Although the original canonical signaling maps indicated that LPS activates ERK in monocytes via the "classical" Ras>Raf pathway [524], in monocytes one pathway for LPS activation of ERK

LPS Activation of Multiple Signaling Pathways in Human Monocytes
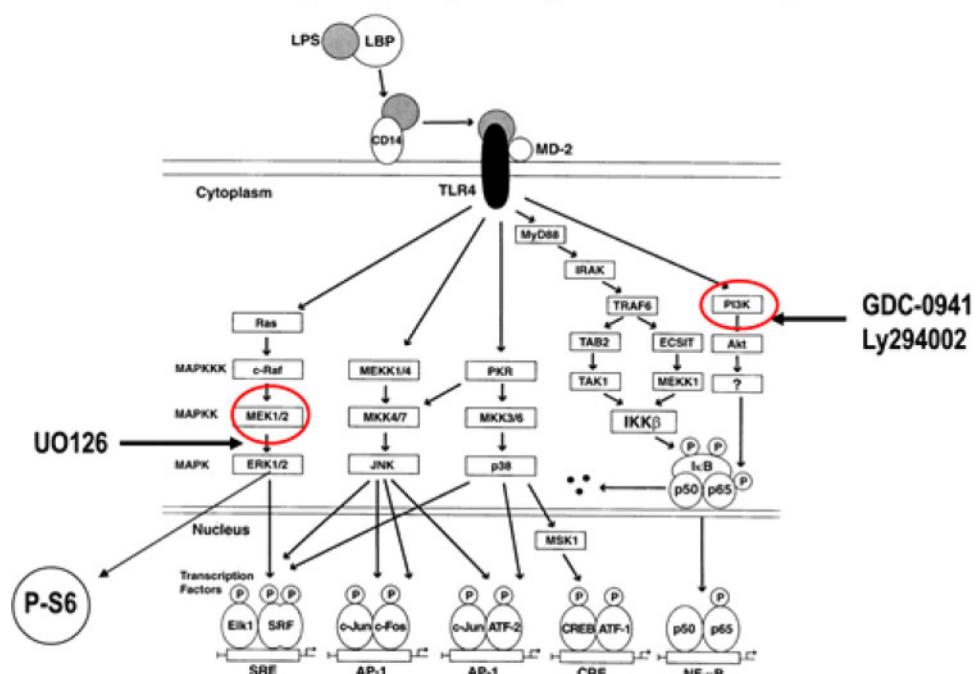
Figure 55. "Canonical" pathways for LPS activation of multiple signaling pathways in peripheral blood monocytes via TLR-4 (adapted from Guha and Mackman [524] and reproduced with permission). Inhibition of PI3K (right) by Ly294002 or GDC-0941) or of MEK 1/2 (left) by U0126 is also illustrated here. Also shown, in monocytes, activation of the ribosomal S6 protein is predominantly through activated ERK.

is via TPL-2, a MAPKKK, which is sequestered in one of the forms of IκB, is phosphorylated/activated by IKK, and released from the complex by proteasomal degradation of IκB. Phosphorylated TPL-2 subsequently phosphorylates/activates its downstream target, MEK 1/2, which then activates/phosphorylates ERK 1/2 [525]. Signaling pathways are complex, and a specific pattern or pathway seen in one type of cell does not predict the same pattern or pathway in all cells. Therefore, it may be important to study a broad set of specific signaling proteins/modifications for comprehensive understanding of signaling pathways in a specific cell type.

15.4 Kinetics

In studying the activation (and inactivation) of signaling pathways, it is critical to include multiple time-points within the experiment. For example, the phosphorylation of ERK in human bone marrow CD34$^+$ cells (at 37°C incubation) reaches a peak and returns to unstimulated cell levels in less than 10 min [72], indicating that the dephosphorylation of P-ERK occurs rapidly in this cell population.

15.5 Kinase and phosphatase inhibitors

Specific (or relatively specific) kinase inhibitors are very useful when analyzing pathways downstream from a signaling "node."

For example, U0126 binds to MEK1/2 and prevents it from phosphorylating (activating) its downstream partner ERK1/2 (see Fig. 55). Adding U0126 to a whole blood sample will block activation of ERK1/2 and activation of any downstream target such as ribosomal S6 protein (in monocytes). In addition, by comparing the level of a target phospho-epitope expressed in cells exposed to an inhibitor with that of untreated cells, it is possible to reveal background or constitutive levels of activation of a specific kinase and its downstream partners. In Fig. 56, whole blood was treated (here for 4 min) at 37°C with LPS alone, or with UO126 (MEK inhibitor) or with Ly294002 (PI3K inhibitor). In the presence of UO126, activation of both ERK 1/2 and the downstream S6 ribosomal protein are inhibited. Also shown here, the PI3K inhibitor Ly294002 (we have also used the more specific PI3K inhibitor GDC-0941 with similar results) likewise inhibits activation of both ERK 1/2 and S6 at this time point. Neither inhibitor changes the responses for p38 or SAPK/JNK, although PI3K inhibition does prevent AKT activation (see below). These results are consistent with a model in which ERK 1/2 can be activated (in human monocytes) via PI3k>AKT. However, a better understanding of the responses and inhibitions of specific pathways requires monitoring the responses to different stimuli over time.

As shown in Fig. 56, after appropriate inhibitor and LPS treatment, cells were fixed and permeabilized using formaldehyde/Triton X-100, and subsequently stained using antibodies to phospho-ERK 1/2 (p44/42 MAPK), phospho-S6 ribosomal protein, plus CD14 and CD45 to identify monocytes (not shown in figure) and eliminate debris from the analysis. Figure 56 demonstrates
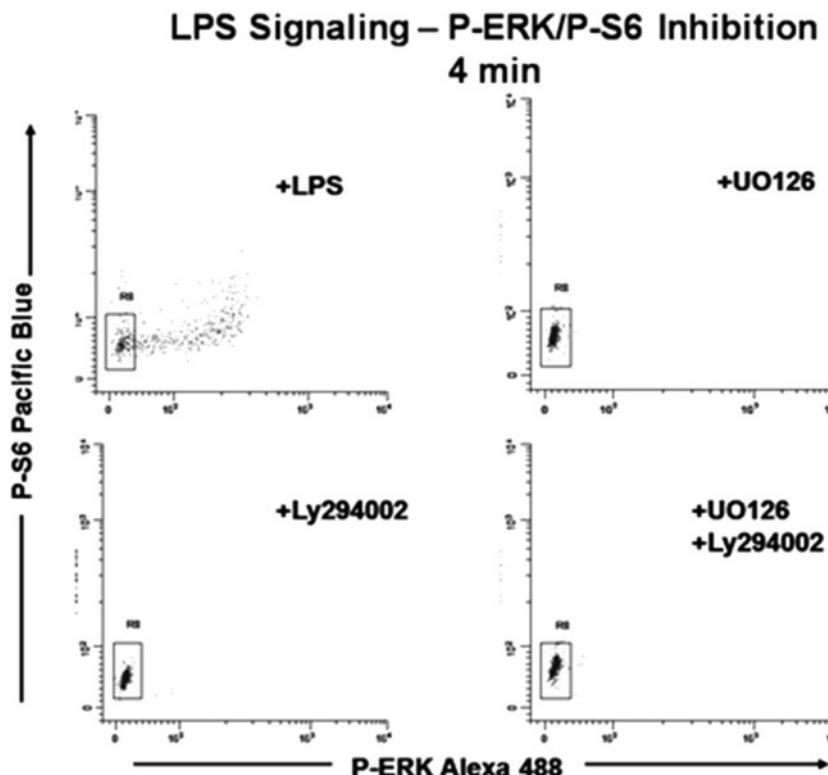
Figure 56. LPS activation of the ERK pathway in human peripheral blood monocytes. Samples were pre-incubated with the indicated inhibitors for 60 min at 37°C before the addition of LPS to all samples. After 4 min incubation with LPS, all samples were fixed using formaldehyde and permeabilized using Triton X-100 (see Chapter III Section 5: Cell fixation and permeabilization for flow cytometric analyses, for details on fixation and permeabilization steps). Only monocyte responses are shown here, based on CD45 and CD14 gating (not shown here).
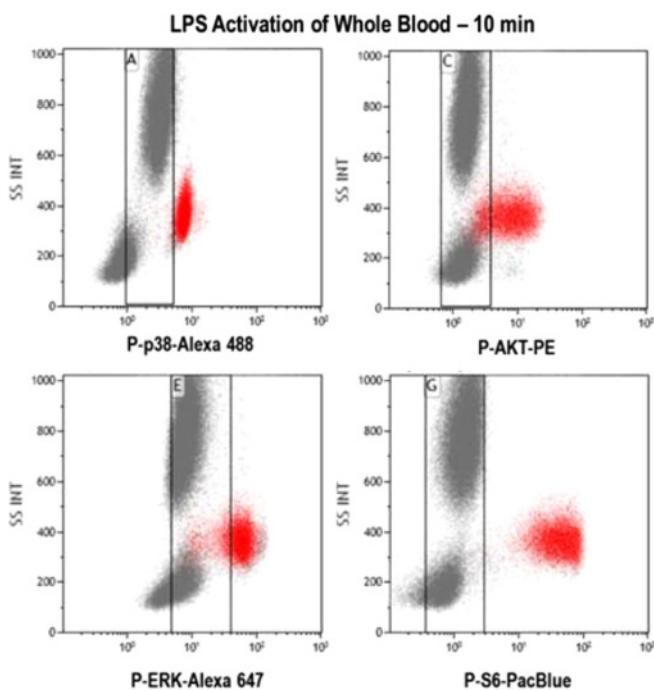
Figure 57. Simultaneous measurement of four different signaling targets. Human peripheral blood was incubated with LPS for 10 min at 37°C. Here, each of the measured phospho-epitopes is shown versus SSC, with the CD-14pos monocytes in red.

several key points mentioned above. LPS activates the ERK pathway rapidly, and only the monocytes showing maximal levels of ERK phosphorylation also show phosphorylation of S6 (top left). U0126 inhibition of ERK activation (top right) inhibits the activation of both ERK and S6. It should be noted that the "canonical" pathway usually shown in signaling documents indicates that S6 is activated by PI3K>AKT [526]. The data shown in Fig. 56 are consistent with the concept that activation of ribosomal S6 protein is via the ERK pathway in human peripheral blood monocytes, highlighting the need to carefully investigate the appropriate upstream activation pathways. Finally, both the activation of ERK and S6 are inhibited (at this time point) by the PI3 kinase inhibitor Ly294002, consistent with the concept that ERK activation in human peripheral blood monocytes can also be via AKT (not the "canonical" RAS>RAF pathway, bottom left) [524]. At first, these data seem inconsistent with the comment above that ERK activation in monocytes is via TPL-2 [525]. However, as shown below (Figure 58), there are two separate signaling pathways activating ERK, one through PI3K (early ERK activation), the other through NF-κB.

Signaling pathways (particularly phosphorylation/dephosphorylation) in normal cells are frequently activated and then rapidly inactivated. Inactivation of a kinase involves dephosphorylation of the target phosphorylated amino acid(s) by a phosphatase. One of the predictions of this model is that inactivation of a phosphatase should result in maintaining the effects of an activated kinase for longer time periods [527].

Inhibition of P-AKT and "early" P-ERK
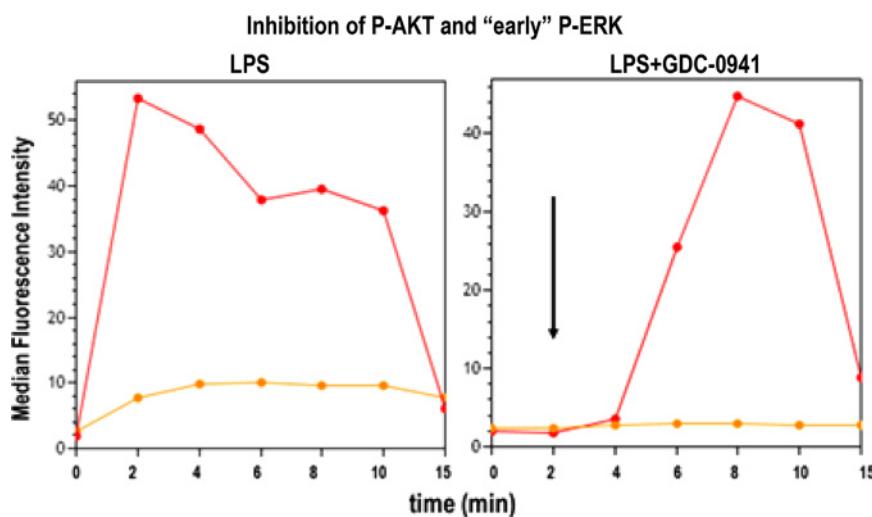
Figure 58. Kinetics of LPS activation of the AKT and ERK pathways in peripheral blood monocytes. Whole blood samples were pretreated with the PI3K inhibitor GDC-0941 (right panel), or vehicle controls (left panel), followed by activation with LPS for 0 to 15 min at 37°C. P-AKT (orange, lower line in both panels) and P-ERK (red, upper line in both panels). Note that in the GDC-0941 treated sample (right), the P-ERK peak seen in the untreated sample is missing (arrow, right panel).

15.6 Simultaneous monitoring of multiple signaling pathways in the context of response kinetics

The results shown above in Fig. 56 can be interpreted to indicate that both ERK and AKT pathways are activated by LPS. While this conclusion is correct, the use of different pathway inhibitors in conjunction with detailed kinetic analyses reveals important details of the specific pathways that are activated in human peripheral blood monocytes by LPS.

Using the same logic that is commonly used to understand complex biological systems (e.g., hematopoietic cell differentiation and lineage reconstruction in bone marrow), for simultaneous measurement of multiple signaling targets, we routinely measure multiple signaling targets in each sample. As in all complex immunophenotyping experiments, attention to details is essential in the design and execution of these types of experiments. For example, large fluorophores such as PE or APC should only be used for nuclear localizing target phospho-epitopes after running preliminary experiments to ensure the Ab-conjugate can get to the target. Similarly, tandem dyes (PE-Cy5) should be used with caution, with appropriate controls to ensure integrity of the tandem at the time of the assay.

As an illustration of simultaneous measurement of four different signaling targets, Fig. 57 demonstrates the whole blood analysis of LPS-stimulated human peripheral blood using CD14-PE-Cy7 to detect monocytes, plus P-p38 (MAPK)-Alexa Fluor® 488, P-AKT-PE, P-ERK- Alexa Fluor® 647, and P-S6-PacBlue.

These results demonstrate that the majority of monocytes (shown in red) are positive for all four phospho-epitopes at 10 min incubation with LPS. As also shown in Fig. 57, the analysis of each phospho-epitope response includes an evaluation using SSC, demonstrating that in this donor, only the monocytes show significant activation of these phospho-epitopes (in many donors, the granulocytes also show a positive P-p38 population following LPS activation, not seen here). However, the details of the individual signaling pathway responses can only be appreciated using

both multiple time points for LPS activation and the simultaneous use of specific pathway inhibitors. As shown in Fig. 58, looking at the kinetics of both P-ERK and P-AKT activation simultaneously over a 15 min period of LPS activation shows two different peaks of P-ERK expression (upper response in red in both panels): one extremely rapid, peaking at ~2–4 min (left panel), the second peaking at 8–10 min (at 37°C incubation). In most (though not all) normal human donors, we see both peaks, while in a minority of donors we only see the "later" P-ERK. In a sample pretreated with the PI3K inhibitor (here GDC-0941, right panel), only the "early" (2–4 min) P-ERK response is inhibited. In contrast, pretreatment with U0126 (as shown in Fig. 56) inhibits both the early and the late P-ERK peak, indicating that the first peak goes through PI3K, but requires P-MEK. The second peak of activation of P-ERK actually goes through IKK>IκB>TPL-2 [525]. Consistent with this concept, we have demonstrated that the "second" P-ERK peak is inhibited by proteasome inhibitors, such as MG-132 (inhibition of proteasomal destruction of IκB prevents the release of TPL-2, preventing it from activating MEK).

The kinetics of AKT activation (Fig. 58) demonstrate a peak at 4–8 min (left panel, lower response in orange) with a sustained response for the time period measured here. As shown in the right panel of Fig. 58, GDC-0941 causes complete inhibition of AKT activation, a useful internal control that strengthens the concept that the "early" ERK activation is through PI3K>AKT. These data also suggest that there is a constitutive activation of AKT in peripheral blood monocytes, which is inhibited by PI3K inhibitors (GDC-0941).

15.7 Sample protocol for LPS activation of human whole blood

This same approach can be used to study the impact of specific signaling pathway inhibitors to determine which downstream signaling pathways are affected. Overall, monitoring signal

transduction pathways in stimulated whole blood (and other similar types of samples) offers a unique way to test and validate Abs, specific agonists, or antagonists, using a relevant biological system. In addition, this approach can be used to monitor the activity of targeted therapies (inhibitors) in vivo, or to monitor the prior exposure of individuals to LPS/endotoxin [528].

15.8 Materials

1. 4.0–5.0 mL human whole blood collected into K_2EDTA or sodium heparin, stored at room temperature until tested. The blood sample must be used as soon as possible in order to preserve appropriate signaling capabilities. Sample testing should (ideally) begin within 1–4 h of collection.
2. Directly conjugated Abs to phospho-epitopes (e.g., Cell Signaling Technology, Danvers, MA) and cell surface-specific conjugates are necessary. We generally use multiple (generally 4) phospho-epitope specific Abs in each tube, using lower molecular weight fluorophores (e.g., Alexa Fluor® 488, or 647, Pacific Blue) for staining nuclear or ribosomal targets, and PE or APC for cytoplasmic targets. The same guidelines must be used here for the selection of fluorophore–Ab pairs for phospho as for other targets (e.g., use "bright" conjugates for non-abundant targets and "dim" conjugates with abundant targets).
   (a) CD14-PC7
   (b) CD45-KrO
   (c) P-ERK-Alexa Fluor® 647 [T202/Y204], also known as P-p44/42 MAPKP
   (d) P-S6-Pacific Blue [Ser235/236]
   (e) P-AKT-PE [Ser 473]
   (f) P-p38 MAPK-Alexa Fluor® 488

15.9 Reagents

1. LPS from *E. coli* 0127:B8; dilute to 50 µg/mL in PBS; store this working dilution at 4°C; stable for up to 6 months.
2. Triton X-100, 10% aqueous solution; prepare working solution by diluting 116 µL stock with 10 mL PBS; store stock and working solution at room temperature; working dilution is stable for 1 month.
3. Appropriate pathway inhibitors (e.g., U0126 MEK>ERK, GDC-0941 PI3K>AKT, bortezomib for proteasome inhibitor), as necessary.
4. Formaldehyde, 10% (methanol-free); store at room temperature in the dark.
5. Albumin solution from bovine serum; store at 4°C.
6. PBS (calcium- and magnesium-free).
7. Wash Buffer: 4% BSA in PBS; filtered through 0.22 µm sterile filter.
8. Deionized water (for Triton X-100 dilution)

15.10 Procedure: Whole blood fixation and permeabilization protocol for kinetics and use of inhibitors

Before starting this procedure, prepare an experiment worksheet to aid in the critical timing steps (see sample Worksheet presented in Table 12). The experiment described below is for time points of up to 10 min of LPS activation. LPS is added to the tube(s) with the longest incubation time first (here, 10 min), followed by staggered LPS addition for shorter incubation times. For experiments adding specific signaling pathway inhibitors (not outlined here), whole blood samples are incubated at 37°C with inhibitor(s) for an appropriate time (generally 30–60 min, depending on the specific inhibitor) before the addition of LPS.

1. Label the appropriate number of 75 mm polypropylene test tubes for the experiment. There will be one control tube for each cell surface Ab-conjugate, and appropriate control tubes for each phospho-epitope (remember that the compensation control for each phospho-epitope target should express maximal levels of each target).

   For phospho-epitopes requiring methanol treatment, have a 50% methanol solution ready for use in the freezer and right before use, remove from freezer and place into an ice bucket. See Chapter III Section 5: Cell fixation and permeabilization for flow cytometric analyses, for details.
2. Just before use, mix blood by inverting vacutainer tube several times, then transfer blood into a 50 mL conical tube. Mix blood while aliquoting samples into 75 mm tubes from Step 1.
3. Pipette 100 µL of blood sample into the bottom of each appropriately labeled tube. Use a cotton-tipped applicator to remove any blood from the side of the tube.
4. Add 100 ng LPS (2 µL of working dilution) to the first of the designated stimulation tubes and mix by shaking tube. Place that tube into the water bath and start a stopwatch. At the appropriate time interval, add LPS to the next tube, vortex and place it into the water bath. Continue for all tubes in the stimulation part of the experiment.
5. Continue to use the staggered start to place the 37°C "no LPS" control tube and the CD14-only tube into the water bath (last tubes to be placed into the 37°C water bath.
6. At the 10 min mark, remove the first tube in the timed sequence from the water bath and add 65 µL of 10% formaldehyde to the tube. Immediately mix well by shaking tube and place it into a tube rack. Continue adding 65 µL of formaldehyde to each tube in the timed sequence, mixing between each one. Note: This is a critical step. Formaldehyde stops the LPS activation and fixes the cell.
7. Incubate each tube for a total of 10 min at room temperature.
8. After exactly 10 min of incubation in formaldehyde at room temperature, pipette 1 mL of Triton X-100 solution into each tube at the appropriate time interval, vortex well, and return tube to rack. After Triton is added to the last tube, vortex all tubes, place into the 37°C bath, and set timer for 15 min.

Table 12. Worksheet for timed addition of reagents for 15 min (max) LPS activation of whole blood

Tube number	Tube label	Time of addition LPS	Time of addition Formaldehyde	Time of addition Triton X-100
1	LPS 15′	0:00	15:00	25:00
2	LPS 10′	5:10	15:10	25:10
3	LPS 8′	7:20	15:20	25:20
4	LPS 6′	9:30	15:30	25:30
5	LPS 4′	11:40	15:40	25:40
6	LPS 2′	13:50	15:50	25:50
7	Unstimulated control		16:00	26:00
8	CD14-PC7/CD45-KrO only		16:10	26:10
	Unstimulated control:	Vortex and put into 37°C water bath at 14:00		
	CD14-PC7/CD45-KrO only:	Vortex and put into 37°C water bath at 14:10		
	Blood samples:	100 µL		
	Addition of LPS:	2 µL of 50 µg/mL PBS; final concentration 100 ng per 100 µL blood		
	Addition of formaldehyde:	65 µL of 10% solution: final concentration 4%		
	Addition of 0.1% Triton X-100:	1 mL of 0.1% Triton X-100/PBS		

- After 15 min, inspect tubes for complete RBC lysis (clear nonturbid red color). If lysis is incomplete, continue incubation for a maximum of 15 additional min.
- If lysis is still incomplete, centrifuge, decant supernatant, loosen pellet by vortexing, resuspend with 1 mL of Triton working solution, and incubate in 37°C bath for up to 30 min to obtain maximal RBC lysis.

9. Remove tubes from the water bath, dab on paper towel to remove water from the bottom of the tubes and place in rack. Add 1 mL of cold (4°C) wash buffer (4% BSA/PBS) to each of the tubes, and then vortex all tubes well.
10. Centrifuge all tubes at 500 × g for 4 min. Remove supernatant. Vortex each tube to loosen pellet.
11. Resuspend pellet by adding 1 mL of cold (4°C) wash buffer (4% BSA/PBS) to each of the tubes, and then vortex all tubes well.
12. Centrifuge all tubes at 500 × g for 4 min. Remove supernatant. Vortex each tube well to loosen pellet
    - For phospho-epitopes that require 80% methanol treatment to "unmask" (e.g. P-STATs)
      - Add 1 mL of cold (4°C) 80% methanol while vortexing. NOTE: This is critical to reduce cell aggregation. Place the tube on ice.
      - After the last tube, set timer and incubate for 10 min.
      - At the end of the incubation, centrifuge all tubes at 500 × g for 4 min. Remove supernatant. Vortex each tube well to loosen up the pellet. Pipette 2 mL of cold (4°C) wash buffer (4% BSA/PBS) to each tube.
      - Centrifuge all tubes at 500 × g for 4 min.
      - Remove supernatant. Note: not necessary to loosen up the pellet before the addition of antibody cocktail

13. Add antibodies (concentrations and volumes previously defined) and cold wash buffer to a final volume of 100 µL. (Prepare a cocktail containing all desired Abs. This ensures that the Ab concentration for each tube is "identical.") All Abs should be diluted in PBS/4% BSA (protease free).
14. Incubate all tubes at room temperature for 30 min in the dark.
15. At the end of the incubation, add 2 mL of cold (4°C) wash buffer (4% BSA/PBS) to each tube.
16. Centrifuge all tubes at 500 × g for 4 min. Remove as much of the supernatant as possible, exercising care to preserve the cell pellet. Vortex each tube well to loosen up the pellet.
17. Resuspend the cells in 350 µL of 0.5% paraformaldehyde in PBS, and store at 4°C in the dark, until sample can be analyzed. Samples in 0.5% paraformaldehyde are stable for 24 h.

16 Assessing lymphocyte metabolism through functional dyes

16.1 *Overview*

The aim of this chapter is to provide rapid and simple protocols to measure lymphocyte metabolism by FCM. We briefly layout general pathways and the relevance of some selected pathways for lymphocyte biology before going into methodological detail. The focus is on measuring glucose and fatty acid uptake, mt membrane potential, mt mass, and ROS.

16.2 *Introduction*

Lymphocytes upregulate glycolysis and mt oxidative phosphorylation (OxPhos) during their activation [529]. Metabolic

reprogramming differs between B cells and T cells, and also within regulatory T-cell subsets [529]. For instance, naïve murine splenic CD4$^+$ T cells upregulate glycolysis as well as glucose uptake and reveal a strongly enhanced ratio of glycolysis versus OxPhos upon CD3/CD28 mAb stimulation. In contrast, B cells upregulate both glycolysis and OxPhos upon lipopolysaccharide or anti-B-cell receptor stimulation, and therefore maintain the glycolysis/OxPhos ratio of resting B cells [530]. Although OxPhos ensures efficient ATP production under aerobic conditions, mitochondria also contribute cytosolic biosynthetic precursors such as acetyl-CoA and pyrimidines. Moreover, mitochondria are responsible for the production of ROS and cell death by the intrinsic apoptosis pathway [220]. Glycolysis also takes place under aerobic conditions and can be actively induced to meet the cells' energy demand, for instance in cancer cells [531], and also in certain lymphocyte subtypes, such as activated T cells [529]. However, regulatory T cells or resting B cells preferentially rely on fatty acid (FA) oxidation by the mt respiratory chain [530, 532] and regulatory T cells obtain fatty acids exogenously [533]. During hypoxia, which is encountered by lymphocytes in the bone marrow and the thymus [534, 535], ROS production by complex III of the respiratory chain has been observed [536]. The three cellular ROS species are superoxide anions ($\cdot O^{2-}$) that are the precursors of hydrogen peroxide (H_2O_2), and hydroxyl radicals ($\cdot OH$). ROS at high levels can cause oxidative stress to cells by either directly inducing single- and double-stranded DNA breaks or by oxidizing amino acids in proteins, fatty acids, or enzymatic co-factors [537]. At low levels and under normoxic conditions, ROS represent important cellular signaling molecules; i.e., in stem cells, ROS act as second messenger to ensure cycling of the cells [537]. The ROS species involved in intracellular signaling is H_2O_2 as it has a long half-life and diffuses easily [537]. Numerous proteins are redox sensors. For instance, the oxidation of cysteine inactivates PTEN or Akt, which are critically involved in B cell development [537]. Bach2, a transcription factor involved in Ab class switch recombination, is also redox-sensitive [538]. Thus, metabolism may reflect the activation status and predict the fate of an immune cell. In fact, anergic B cells are metabolically less active than naïve B cells, and even less than hyperactive B cells from "B-cell activating factor of the TNF family (BAFF)"- transgenic mice [530]. These selective examples show that immune cell metabolism comprises glycolysis, mt activity and ROS, which intersect with signaling pathways. The gold standard to measure glycolytic and mt activities in real time is via extracellular flux analysis using a Seahorse^{TM} device. However, this experimental setup requires rapid access to such a device and a substantial number of cells (up to $\sim$2 x 10^6 per single experiment), which (i) might be difficult to achieve, especially when looking at rare lymphocyte subsets and (ii) may require time-consuming cell sorting beforehand. In addition, cell sorting over hours may alter metabolic phenotypes. To perform a quick first screen or to analyze complex and rare cell populations, such as bone marrow lymphocytes, without enrichment and purification, rapid flow cytometric techniques can provide first clues of whether a given treatment, genetic deletion or a cytokine alters glucose uptake, mt activity or generation of ROS.

16.3 Experimental Design

We describe here the use of cell permeable functional dyes to measure basic parameters such as: (i) glucose uptake (2- or 6-NBDG; 2- or 6-(N-(7-Nitrobenz-2-oxa-1,3-diazol-4-yl)Amino)-2-Deoxyglucose), (ii) fatty acid (FA) uptake (BoDipy-FA), (iii) mt mass (MitoTracker Green/Deep Red FM), (iv) mt membrane potential (mtmP) (TMRE; Tetramethylrhodamine), (v) ROS (DCFDA; 2'-7'-Dichlorodihydrofluorescein diacetate and CellROX) and mt ROS (MitoSOX). Our focus is on murine B cell analysis but all protocols can easily be adapted to the investigation of other cell types, for instance human cells. We found it feasible to choose one color for all dyes (for instance, FL1/green emission; 2- or 6-NBDG; MitoTracker Green FM, DCFDA) to analyze complex cell populations, such as bone marrow lymphocytes. Information on stock and working concentrations, solvents and commercial distrubutors for all dyes can be found in Table 13. This has the advantage that one single, titrated cocktail of fluorochrome-coupled Abs can be combined with each functional dye to analyze glucose uptake, mt mass, and ROS. Of course, the same strategy can be applied to use dyes with a different emission wavelength (MitoTracker Deep Red FM, TMRE, CellRox, MitoSOX). To separate functionally distinct B cell fractions in vitro, different MitoTracker dyes can be combined [538].

16.3.1 Measurement of glucose uptake.   The direct uptake of glucose into living cells can be monitored in vitro and in vivo by the fluorescent glucose analogs 2-NBDG or 6-NBDG. 6-NBDG is supposed to specifically reflect glucose uptake via the glucose transporter GLUT-1 [539], while 2-NBDG gets imported by all GLUT-family members [540]. The in vitro incubation of cultured cells or ex vivo prepared single cell suspensions with 2- or 6-NBDG requires glucose free medium and results in the uptake of NBDG instead of glucose. Thus, the increase in 6-NBDG fluorescence mirrors GLUT-1 activity. Freshly isolated murine splenic B cells show a higher uptake of 2- versus 6-NBDG (Fig. 59), likely reflecting the activity of glucose transporters other than only GLUT-1. By injecting 2- or 6-NBDG intravenously into mice, this glucose analogue can even be tracked under physiological conditions, reflecting more precisely natural glucose uptake activity of different cell populations, for instance plasma cells [541] (please consider this reference for a procedure). Both glucose analogues are detected in the same emission channel as GFP, what limits their use in combination with a wide range of GFP-reporter mice. However, this issue can be circumvented by using a spectral fluorescence analyzer. It has to be noted that this assay does not directly measure glycolysis, i.e., pyruvate or lactate production, as it is restricted to measuring specifically glucose up-take only.

16.3.2 Measurement of FA uptake.   The direct uptake of FA into living cells can be monitored in vitro and in vivo by fluorescently labeled FA, such as BoDipy-FA [542]. BoDipy-FA analogues undergo native-like transport and metabolism in cells making it effective as a tracer for lipid trafficking [543]. Increased sensitiv-

Table 13. Reagents (*some chemicals such as DCFDA can also be obtained from other suppliers)

Reagents

Dye/Ab	Supplier*	Solvent	(Stock) Working concentration	Storage	Staining medium
6-NBGD	(Life Technologies, #N23106)	dH$_2$O	(100 mM) 300 μM	–20°C	glucose-free DMEM
2-NBDG	Abcam (#ab146200)	dH$_2$O	(1mg/ml) 25μg/ml	–20°C	glucose-free DMEM
Bodipy-labeled FA	Thermo Fisher Palmitate (#D3821), C12 (#D3822, D3835)	MeOH	(2.5mM) 6-10 μM	–20°C	PBS containing 20 μM FA-free BSA
DCFDA	Thermo Fisher (#D399)	DMSO	(100 mM) 1 μM	–20°C	Optimem or RPMI1640
MitoTracker Green FM	Cell signalling (#9074S)	DMSO	(1mM) 5-10 nM	–20°C	Optimem or RPMI1640
MitoTracker Red FM	Thermo Fisher (#M22425)	DMSO	(1mM) 50-100 nM	–20°C	Optimem or RPMI1640
TMRE	Life Technologies (#T668)	MeOH or DMSO	(20 μM) 20nM	–20°C	Optimem or RPMI1640
CellROX Deep Red	Thermo Fisher (#C10422)	DMSO	(2.5 mM) 5-50μM	–20°C	Optimem or RPMI1640
MitoSOX Red	Thermo Fisher (#M36008)	DMSO	(5mM) 5μM	–20°C	(HBSS/Ca^{2+}/Mg^{2+})
Anti B220 PerCP/Cy5.5	eBioscience, clone RA3-6B2, #45045282	–	1:100	4°C	FCM buffer
Anti B220 Brilliant Violet 421	BioLegend, clone RA3-6B2, #103420	–	1:100	4°C	FCM buffer
Anti CD19 APC-Fire 750	BioLegend, clone 6D5, #115557	–	1:200	4°C	FCM buffer
Anti CD138 Brilliant Violet 421	BioLegend, clone 281-2, #142508	–	1:100	4°C	FCM buffer
Anti CD138 PE/Cy7	BioLegend, clone 281-2, #142514	–	1:1600	4°C	FCM buffer
Anti TACI/CD267 APC	eBioscience, eBio8F10-3, #17-5942-82	–	1:100	4°C	FCM buffer

ity can be reached by coupling FA to quantum dots [544]. The in vitro incubation of cultured cells or ex vivo prepared single cell suspensions with labeled FA requires FA-free medium.

16.3.3 Measurement of mt mass and activity. MitoTracker Green FM labels mt proteins via mildly thiol-reactive chloromethyl- moieties within the dye. MitoTracker Green FM diffuses through the plasma membrane and is supposed to be taken up by active mitochondria irrespective of their mtmP. In contrast, uptake of Mito Tracker Deep Red FM appears to be influenced by the mtmP of the cells [545]. However, there are also reports on a sensitivity of MitoTracker Green FM toward mtmP [545]. Once inside, Mito-Trackers cannot be removed from the cells again. Like other cell permeable dyes MitoTrackers are used to semi-quantify mt mass using standardized conditions for cell numbers, dye concentration, and incubation time. Increased MitoTracker FM staining can either signify more or larger mitochondria or even more structured mitochondria, i.e., increased protein content providing more reaction targets for the dye, and henceforth, refers to the total mt mass of

a cell. Like MitoTracker Deep Red FM, the lipophilic and cationic fluorescent dye TMRE specifically accumulates in mitochondria in relation to their mtmP at low concentrations. It has to be noted that loss of mtmP is a marker for early apoptotic cells [546]. Thus, care has to be taken to gate on viable cells if alterations of mtmP that are not related to apoptosis are to be analyzed by Mito-Tracker Deep Red FM or TMRE. Of course, loss of TMRE staining is useful to define early apoptotic cells. We provide an example of MitoTracker staining of bone marrow lymphocytes, revealing that there are two populations of plasma cells identified by MitoTracker fluorescence (Fig. 60). Gating on the MitoTracker^{high} cells reveals that those plasma cells (red dots) have a higher SSC compared to the MitoTracker^{low} cells (grey dots), whereas B cells exhibiting strong MitoTracker fluorescence do not (black dots vs. green dots). The physiological significance of this finding remains to be determined.

16.3.4 Measurement of ROS. In lymphocytes, the major sources of ROS are the two respiratory chain complexes I and III. The
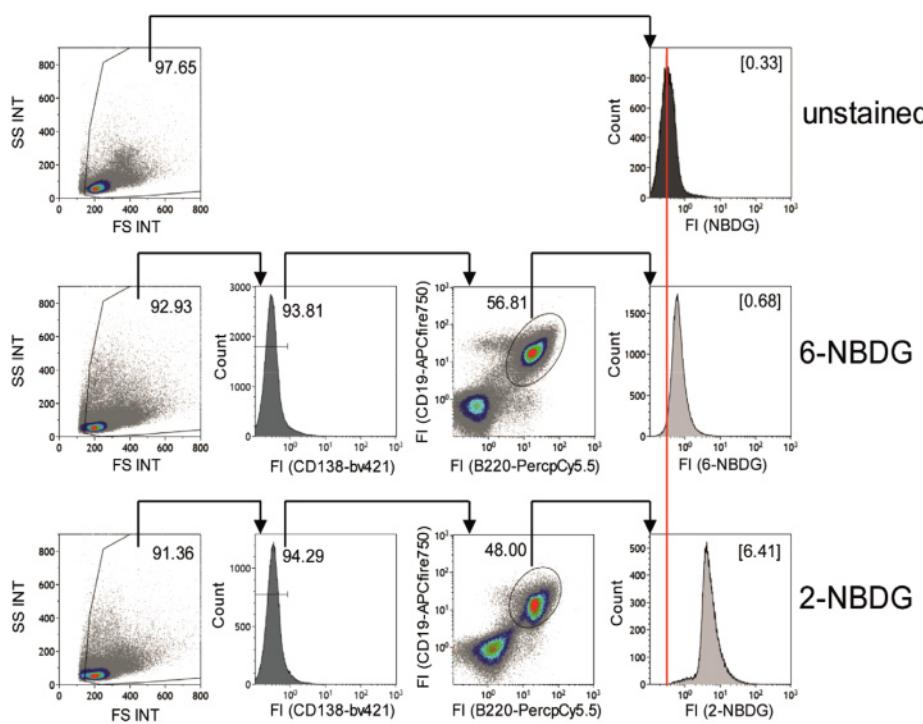
Figure 59. Glucose uptake activity of murine splenocytes. Splenic single cell suspensions from naïve C57BL/6-mice were incubated with or without (control) the glucose-derivates 2-NBDG or 6-NBDG in glucose-free RPMI1640 medium for 45 min (37°C, 5% CO_2). Then, cells were stained with fluorochrome-coupled antibodies directed against CD138 (Brilliant violet 421), B220 (PerCP/Cy5.5), and CD19 (APCFire) (in the dark; 20 min, 4°C). Viable cells were defined by FSC/SSC. B cells were defined as CD138⁻B220⁺CD19⁺ cells. Numbers indicate percentage gated cells, numbers in brackets indicate MFI. The red line indicates the main peak of the unstained, NBDG, negative fraction.

fluorogenic dye DCFDA or CM-H2DCFDA, a derivative with more effective cellular retention, detects cellular ROS. Inside a cell, DCFDA is first deacetylated but does not emit fluorescence until oxidized into DCF (2′,7′-dichlorofluorescein) by ROS. Of note, DCFDA is not specific for a particular ROS species [548] but exhibits a broad reactivity, particularly in the presence of other oxidizing enzymes and factors like Fe^{2+} [549, 550]. Alternatively, the CellROX Deep Red Reagent can be used for intracellular ROS measurement with the advantage that it is retained even after formaldehyde-based fixation methods [551]. To selectively detect mt superoxide the dye MitoSOX Red can be used. MitoSOX Red is selectively targeted to the mitochondria of viable cells and can only be oxidized by the short-lived superoxide ($\cdot O^{2-}$), but not by other ROS species [552].

Taken together, the results obtained with the methods described here can provide first indications of the very basal metabolic and oxidative status of a given cell population. They may nevertheless be helpful to decipher complex mechanisms, such as Ab class switch recombination [538].

16.3.5 Step-by-step sample preparation.   Cells and buffers

1. Desired single cell preparation.
2. Staining medium (in the case of lymphocytes): Opti-MEM/RPMI1640 without any additives or glucose-free DMEM or Hank's balanced salt solution with Ca^{2+} and Mg^{2+} (HBSS/Ca^{2+}/Mg^{2+}), or PBS containing 20 µM FA-free BSA.
3. FCM buffer (2% fetal calf serum in PBS, 0.02% NaN_3; for measurement of mtmP, NaN_3 should be omitted).

4. Abs for staining of surface antigens (Abs indicated in the table have been used to stain murine B- and plasma cells, Figs. 59 and 60).

16.3.6 Acquisition and analysis.

16.3.6.1 Glucose uptake: 2- or 6-NBDG.

1. Wash desired single cell suspension once with glucose-free DMEM/RPMI1640 and resuspend samples in the same glucose-free medium supplemented with 300 µM 6-NBDG or 25 µg/mL 2-NBDG for 30–45 min at 37°C, 7.5% CO_2/5% CO_2 (1–3 × 10^6/mL) in a reaction tube/dish.
2. Pellet cells and discard the supernatant.
3. Wash cells with 250–500 µL FCM buffer, if required stain for surface antigens with fluorochrome-coupled Abs on 4°C for 15–20 min in the dark.
4. Resuspend cells in 150–250 µL FCM buffer and analyze by FCM (Figure 59).

16.3.7 FA uptake: BoDipy-FA.

1. Wash desired single cell suspension with PBS and stain surface antigens with fluorochrome-coupled Abs in PBS/2% FA-free BSA.
2. Wash cells twice with PBS.
3. Resuspend cells in 6 µM BoDipy-FA (in PBS with 20 µM FA-free BSA) for 3 min at room temperature. Quench BoDipy-FA uptake by adding 4× volume of ice-cold PBS with 2% FBS and two washes.
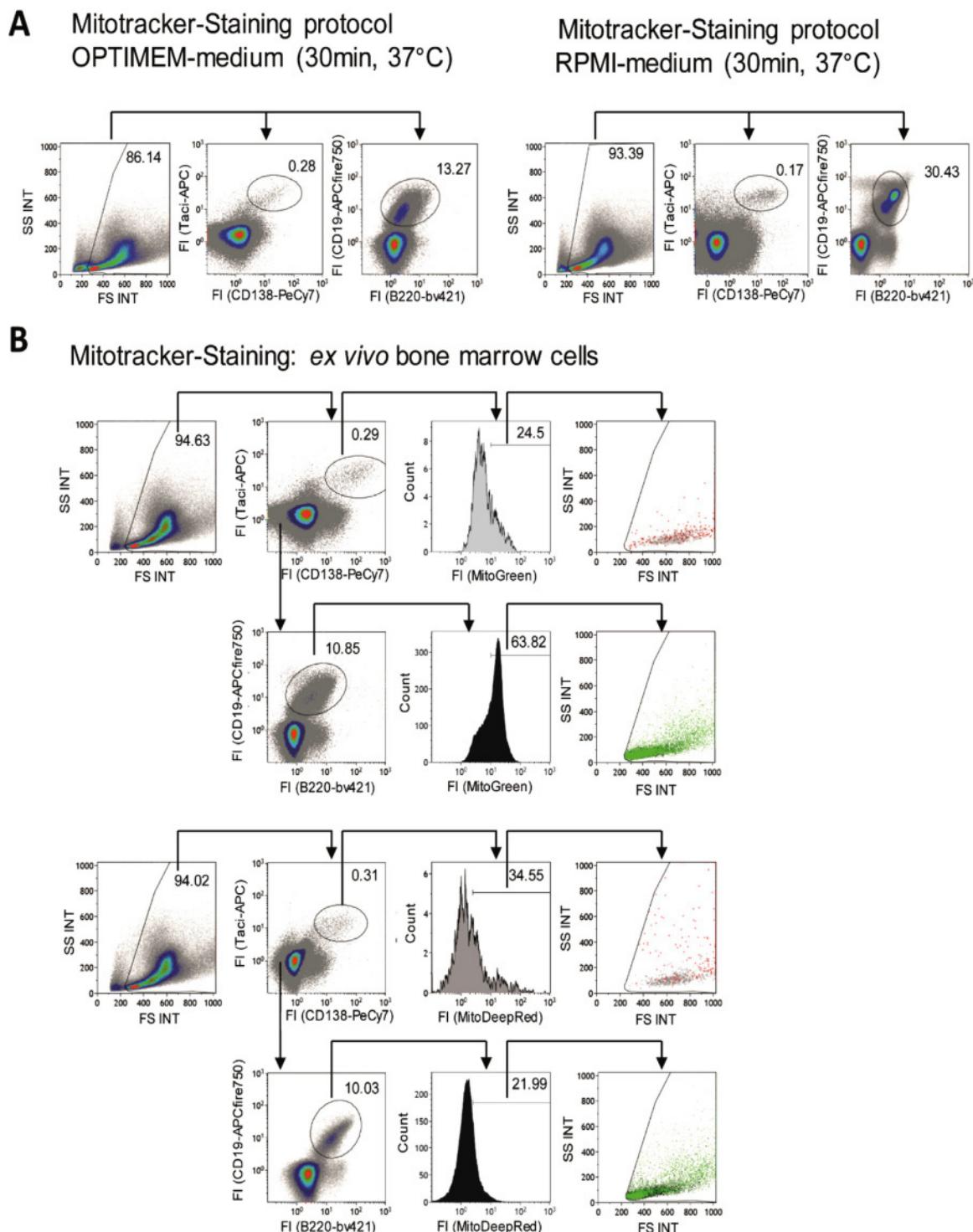
Figure 60. MitoTracker FM-staining of plasma cells in different media and buffers. Single cell bone marrow suspensions from femur and tibia of naïve C57BL/6 mice were prepared and incubated in serum-free medium with MitoTracker Green FM or MitoTracker Deep Red FM (37°C, 30 min, 5% CO_2). Suspensions were then stained with fluorochrome-coupled Abs against the surface markers CD138 (PE/Cy7), TACI (APC), B220 (Brilliant Violet 421), and CD19 (APCFire) [547] in the dark (20 min, 4°C) after incubation with MitoTracker FM. Viable cells were defined by FSC/SSC. Plasma cells were defined as CD138+TACI+-cells and B cells as B220+CD19+CD138-TACI- [547]. (A) Influence of medium (OPTIMEM or RPMI1640) on plasma cell staining. (B) Analysis of MitoTracker Green FM and MitoTracker Deep Red FM uptake in bone marrow plasma cells and B cells. Cells were re-gated on FSc and SSc. Plasma cells and B cells exhibiting a high MFI for MitoTracker Green FM or MitoTracker DeepRed FM are depicted in red or black whereas plasma cells and B cells exhibiting a low MFI for MitoTracker Green FM or MitoTracker DeepRed FM are depicted in grey or green, respectively. Numbers indicate percentage gated cells, numbers in brackets indicate MFI.

4. Optionally: block BoDipy-FA uptake by pre-incubation with 100 μM palmitic acid (Sigma–Aldrich) for 10 min at 37°C prior to BoDipy-FA addition.

5. Resuspend cells in 150–250 μL FCM buffer and analyze by FCM (Figure 59).

16.3.8 Mitotracker, ROS, and mtmP.

1. Resuspend cells at 1–3×10^6/mL in 100–300 μL medium without supplements (serum will cause unspecific MitoTracker staining); use RPMI1640 especially for analysis of NBDG uptake in plasma cells because OPTIMEM does not allow the optimal definition of CD138/TACI$^+$ plasma cells and CD19/B220$^+$ B cells (Fig. 60A).

2. Incubate the cell suspensions (working concentrations see 17.3) with MitoTracker Green FM (10–100 nM), MitoTracker DeepRed FM (1 nM), DCFDA (1 μM), TMRM (20 nM), Cell-ROX (5–50 μM), or MitoSOX (5 μM) in the same serum-free medium for 10-45 min (needs to be empirically determined for each cell type) in the respective incubator

3. Wash cells once in the same medium

4. Stain for surface antigens with fluorochrome-coupled Abs in serum-free medium for 20 min at 4°C in the dark

5. Wash cells with 250-–00 μL FCM buffer or resuspend in 250 μL of the same buffer and analyze by FCM.

6. To adjust the mt activity to the volume of the cells, normalize data to the cubic value of FSC pulse width (that is, [FSC pulse width]^3) of the different samples. Important note: In certain cytometric software, recording FSC pulse width may have to be activated before acquisition

16.4 Pitfalls

Care has to be taken in the choice of the right medium. For instance, RPMI1640 is a suitable medium to stain plasma cells (see Fig. 60). Another problem is, especially when measuring the organelle content of a cell, such as mitochondria, that fluorescence intensity correlates with cell size, which also concerns plasma cells. Therefore, we recommend to choose the MdFI (more robust against outliers) over MFI. Some conditions may require normalization of MdFI to cell volume by adjusting MdFI to FSC pulse width, which is the preferable parameter to evaluate cell size rather than the height or area of FSc or SSc [553]. For instance, large pre B cells that consume more glucose stain ~40% brighter with 6-NBDG but are also significantly larger than small pre B cells [554]. Normalization of 6-NBDG fluorescence to cell size within these very related cell populations ruled out staining artifacts [554].

Other critical issues are dye concentrations and incubation times. The specificity of dyes mirroring mtmP (TMRE, MitoTracker Deep Red FM, Mitotracker Green FM) can easily be verified by adding nano- to micromolar concentrations of the protonophore Carbonyl cyanide 3-chloro phenyl hydrazine (CCCP). By titrat-

ing CCCP, this assay can be used to test the stability of mtmP of different cell types or under different environmental or genetic conditions [555]. The highest possible signal for the mtmP can be obtained by adding oligomycin, which is an ATP-synthase inhibitor and leads to hyperpolarization of the mt membrane. Thus, CCCP and oligomycin can define the dynamic range of TMRE staining. As mentioned above, care has to be taken to gate on viable cells. Moreover, MitoTracker FM staining can be confounded by mtmP.

16.5 Top tricks

To validate the desired specificity and working concentration of dyes for ROS measurements, positive controls and negative controls can be included. For instance, we used the radical starter ammonium peroxodisulfate (APS; 0.001–0.1%) to assess the dynamic range of DCFDA. The oxidation of DCFDA can vice versa be blocked by the addition of vitamin C (mM Range) to the assay. For further reading on this issue we recommend ref. [548]. The specificity of FA uptake can be assessed by pre-incubation of the cells with unlabeled FA, such as palmitic acid [542].

17 T cell assays

17.1 Measurement of signal transduction pathways in human T cells

17.1.1 Overview. In this section, we describe how to investigate, in human T cells, the phosphorylation status of S6 ribosomal protein (pS6Ribo) as an indicator of PI3K-Akt-mTOR signaling pathway activation following TCR stimulation [556]. However, this protocol can be applied to other signaling pathways in T cells, for example, cytokine stimulation or costimulatory molecules triggering [557].

17.1.2 Introduction. T cell activation requires TCR engagement by peptide-MHC complex together with additional costimuli such as CD28 triggering by CD80/86 molecules expressed on APCs, as well as cytokine stimulation. Surface receptor stimulation is followed by intracellular events that rely mainly on the phosphorylation or de-phosphorilation of molecules involved in the signaling cascade. This is important to amplify and transmit the information originated by receptor stimulation. Signaling cascades are usually connected downstream of different surface receptors, thus leading to an intracellular integration of distinct signaling events. The final outcome is the activation or inhibition of specific transcription factors, and then the expression of a specific gene signature. The investigation of the phosphorylation status of intracellular mediators is a useful tool to understand step-by-step how the extracellular information is propagated inside the cell. By this way it is also possible to understand if any alteration is present in a given signaling pathway. (See also

Chapter V Section 15 – Measurement of signal transduction pathways by FCM).

17.1.3 Step-by-step sample preparation.

17.1.3.1 Mononuclear cells' recovery.

1. Collect whole blood in a tube coated with an anticoagulant.
2. Gently stratify 9 mL blood onto 6 mL Ficoll in a 15 mL tube.
3. Centrifuge at room temperature, $1500 \times g$ without break for 20 min.
4. Collect the ring between the phases, containing mononuclear cells, and transfer in a new 15 mL tube. Fill up the tube with PBS 7.2 and centrifuge $300 \times g$ for 7 min.
5. Discard the supernatant and resuspend cells in 15 mL PBS 7.2. Repeat the centrifugation step.
6. Resuspend cells in complete medium (RPMI+10% FBS) and count. At least 200 000 cells for each experimental condition are needed.

17.1.3.2 Cell stimulation.

1. Stain cells with mouse anti-human CD3 Ab (clone HIT3a, IgG2a, 5 μg/mL) and mouse anti-human CD28 antibody (clone CD28.2, IgG1, 5 μg/mL) in 50 μL of complete medium in a 1.5 mL Eppendorf tube. Incubate at 4°C for 5 min.
2. Cap primary Abs by adding 50 μL complete medium containing anti-mouse IgG1 and anti-mouse IgG2a. Final concentration of anti-mouse IgG1 and anti-mouse IgG-2a is 5 μg/mL. Incubate at 37°C for the kinetics experiment. We recommend the following kinetics: 0' (no stimulation), 10', 20', and 30'.
3. At each time point of the kinetics experiment, fill up the appropriate tube with cold PBS 7.2 and centrifuge at $300 \times g$ for 7 min at 4°C.
4. Discard the supernatant and resuspend cells in 250 μL of PBS 7.2. Add an equal amount (250 μL) of pre-warmed (37°C) BD Cytofix and incubate for 10' at 37°C.
5. Fill up the tube with 1 mL wash buffer (PBS 7.2 +BSA 0.5%) and centrifuge at $300 \times g$ for 7 min.
6. Resuspend cells in 500 μL wash buffer.
7. Centrifuge the tubes at $300 \times g$ for 7 min.
8. Discard the supernatant and resuspend cells in 500 μL pre-cooled (–20°C) BD Perm Buffer III. Incubate for 30' on ice.
9. Fill up the tubes with wash buffer and centrifuge $300 \times g$ for 7 min.
10. Discard the supernatant and stain cells with anti-human CD3-PB, anti-human CD4-PECy7, anti-human CD8-APCCy7, anti-human pS6Ribo (Ser235/236)-Alexa Fluor 488 for 20' at room temperature.
11. Fill up the tubes with wash buffer and centrifuge at $300 \times g$ for 7 min to remove unconjugated antibodies.
12. Discard the supernatant and resuspend in 500 μL wash buffer for FCM analysis

17.1.4 Materials.

1. Complete medium: RPMI+10% heat inactivated FBS
2. Wash buffer: PBS 7.2+0.5%BSA
3. PBS 7.2
4. Fixation buffer: BD Cytofix
5. Permeabilization buffer: BD Perm Buffer III
6. mouse anti-human CD3 Ab (BD, clone HIT3a, IgG2a)
7. mouse anti-human CD28 Ab (clone CD28.2 IgG1, 5μg/ml)
8. Goat anti-mouse IgG1
9. Goat anti-mouse IgG2a
10. anti-human CD3-PB (BD, clone UCHT1)
11. anti-human CD4-PECy7 (BD, clone SK3)
12. anti-human CD8-APCCy7 (BD, clone SK1)
13. anti-human pS6Ribo (Ser235/236)-Alexa Fluor 488 (Cell Signaling, clone 2F9)

17.1.5 Data analysis.
Data analysis can be performed via the identification of the percentage of cells that display the phosphorylated protein of interest (as in the Figure 61). However, sometimes two clear cell subsets (phosphorylated versus unphosphorylated) cannot be identified. In those cases, it is very useful to evaluate the MFI of the protein of interest.

17.1.6 Pitfalls.
In case of TCR signaling study, staining of surface CD3 requires the usage of an Ab clone distinct from that used for cell stimulation. The two Abs should not compete for the same epitope.

17.1.7 Top Tricks.
PI3K-Akt-mTOR activity lasts only several minutes following stimulation. Alterations of the signaling pathway can be observed either as a delayed/shorter kinetic of phosphorylation or as a reduced/increased magnitude of phosphorylation. For these reasons, we recommend to perform kinetics experiments rather than a single time point observation. The same can be applied either to STAT protein phosphorylation or other signaling cascades.

17.2 Measuring antigen specific T cell responses

17.2.1 Introduction.
T cells recognize their cognate antigen in the context of MHC molecules. Over 20 years ago, Davis and colleagues developed the technique to mimic the interaction between the T-cell receptor and the peptide (p)MHC complex in the laboratory [558]. Using fluorescently labeled pMHC multimers and FCM, antigen-specific T cells could be visualized and this has become a crucial tool in the analysis of antigen-specific T cell immunity in mouse and human.

The classical approach with pMHC multimer detection of antigen specific T cell populations is to have a specific pMHC complex coupled to a single fluorescent dye. The major drawback of this approach is the limited number of epitopes to which T cell reactivity can be detected in parallel. This limitation is given by the limited number of fluorochromes and detectors available for
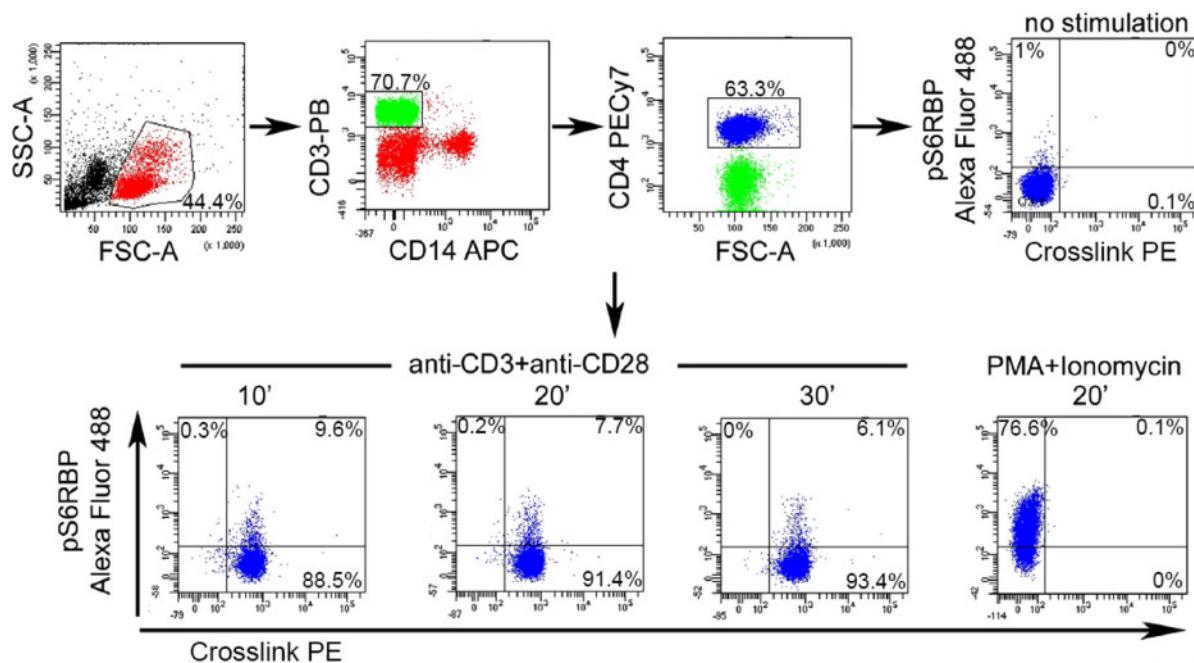
Figure 61. pS6ribo evaluation on PBMNC following TCR stimulation. Lymphocytes were gated based on physical parameters, then T cells were identified as CD3$^+$CD14$^-$. T helper cells were gated as CD4$^+$. pS6ribo was evaluated either on unstimulated cells or upon CD3 mAb and CD28 mAb stimulation for 10, 20, or 30 min. As a positive control of the procedure PBMNC were stimulated with PMA and Iono for 20 min. In this experiment CD3 mAb and CD28 mAb capping was performed by the addition of PE-conjugated anti-isotype mAbs (anti-mouse IgG1 and anti-mouse IgG2a). Thus, cells with an efficient crosslink can be detected as PE-positive.

the detection as well as limitations in the availability of patient material. Multiplexing strategies have been developed that greatly increase the number of T cell reactivities that can be detected in a single sample [559, 560].

The multiplexing strategy we employ is based on the generation of pMHC complexes with dual fluorochrome codes. Using this labeling approach, the number of unique codes that can be generated can be calculated using factorial operations. As an example, ten distinct fluorochromes yield 45 possible unique dual codes: (10 × 9)/(1 × 2) = 45. Additional approaches have been published including work from Newell et al., which uses all possible fluorochrome combinations instead of limiting to dual fluorochrome combinations [559].

An alternative method to identify antigen-specific T cells is through the use of isotope-labeled pMHC multimers, and time-of-flight cytometry [561]. However, this method destroys the cognate cells and does not allow further analysis. In the last couple of years, other high-throughput methods have made their debut, which are based on adding barcoded DNA oligos to pMHC multimers followed by sequencing to detect antigen-specific T cells. The cell mixture can be sequenced as a whole, or to reduce sequencing costs, if the pMHC multimers are labeled with fluorochromes, antigen-specific T cells can be isolated using FCM or anti-fluorochrome magnetic bead-conjugated Abs before sequencing. Using next generation sequencing, the cognate peptide is identified based on the DNA barcode, unique to the peptide [562–564]. According to the same principle, barcoded DNA oligos can also be attached to Abs, to detect and quantify surface pro-tein expression. In the end, proper use of DNA barcoded reagents allows simultaneous identification of the TCR sequence, transcriptome, surface protein expression, and peptide-specificity of T cells.

Besides the major benefit of increasing the number of specificities that can be screened for in a single sample, the other advantage of using multiplexing is the fact that the background signal is significantly reduced when using dual fluorochrome codes. This is due to the fact that the vast majority of background signal is detected in either one or more than two channels detecting fluorescent signal. As the false positive signal decreases, the sensitivity of the assay increases. This increase in sensitivity is accomplished using Boolean gating strategies including signal that is only dual fluorochrome positive. Using this gating strategy, we are currently working with a cutoff of 0.005% of total CD8$^+$ T cells and a minimum of ten recorded events. A triple fluorochrome labeling approach following the same principles, can in theory maintain the sensitivity of detectable T cell reactivities and further enhance complexity.

17.2.2 UV light-mediated peptide exchange. Peptide MHC complexes can be generated in vitro by placing the heavy- and β2m chain of the MHC allele together with the peptide of interest in optimized conditions allowing correct formation of the pMHC complex. As refolding the pMHC complexes is a time consuming and laborious process this approach is not optimal for generation of large numbers of different pMHC complexes.

To overcome this limitation, we developed a UV light-mediated peptide exchange method [565]. With this technology, the MHC complex is refolded using a peptide that includes a UV light-sensitive amino acid. Exposure to UV light results in degradation of the UV-sensitive peptide leading to the dissolution of the MHC complex. However, when this process takes place in the presence of a rescue peptide, this peptide can bind and stabilize the MHC complex, thereby giving rise to pMHC complexes with the peptides of choice. This UV-mediated exchange can be performed in a multi-well format, allowing the generation of thousands of unique pMHC complexes in parallel. Alternative methods for the high-throughput refolding of MHC molecules with peptides of choice include the use of temperature-labile peptides, periodate-cleavable peptides, azobenzene-containing peptides that may be cleaved by sodium dithionite, or the use of certain di-peptides that bind specifically to the F pocket of MHC class I molecules, catalyzing rapid exchange with peptides in the environment [566–569].

Multiple factors can influence the ligand exchange reaction. In case UV-cleavable peptides are used, it is crucial to keep the pMHC complexes in the dark as much as possible as they are light sensitive and as cool as possible as the pMHC complexes can be unstable at temperatures above 4°C. Furthermore, it is important that these protein-containing reactions are performed using polypropylene material. This is to avoid loss of protein through sticking to the plates/tubes. As the solubility of the peptide influences the ligand exchange, it is possible to add ligands that have a poor solubility in water from stocks in DMSO. It has been shown that the ligand exchange reactions proceed normally in conditions up to 10% DMSO [565].

After the peptide exchange, (biotinylated) pMHC complexes are multimerized by binding them to streptavidin-conjugated fluorochromes. For each peptide, a combination of two differently fluorescently labeled pMHC tetramers are produced using a stairway panel as illustrated in Fig. 62. For example, in one plate, pMHC tetramers are labeled according to the horizontal fluorochromes (Fig. 62, top) while in the other plate pMHC tetramers are labeled according to the vertical fluorochromes (Fig. 62, bottom). All fluorescently labeled pMHC multimers are then pooled together and added to the T cells of interest. Cognate T cells will be double-positive for the two fluorochromes to which the cognate pMHC complexes were added.

When selecting what fluorochromes are better suited to include in the making of the multimers, the main determinant is the configuration of the flow cytometer that will be used. Next is a consideration of brightness. In case the goal of using the technology is to detect viral responses, the brightness is of less concern compared to detecting T-cell responses against self-antigens. Nevertheless, it is advisable to select bright fluorochromes, and when using less bright fluorochromes to only combine them in the dual-codes with the fluorochromes that give a bright signal to ensure the antigen-specific T cell population is separated from the background.

Titrations of the pMHC complex:streptavidin-fluorochrome are crucial to ensure optimal SNR. After multimer formation, addition of D-biotin ensures any remaining free binding sites on the streptavidin-conjugated fluorochromes are blocked, thereby preventing the binding of unconjugated pMHC complexes to other fluorochromes when collecting the pMHC multimer collections prior to staining.

17.2.2.1 Staining and FCM. Following the multimer formation, multimers are collected, pooled together, and centrifuged to remove any aggregates before adding them to the T cells. Aggregates can easily be formed when using multiple multimers in a single staining, and can cause background issues in the staining. This is especially true when using rescue peptides that may not be able to bind sufficiently to stabilize the MHC complex. The addition of a 1% skim milk solution (in PBS) to the multimers after adding the streptavidin-conjugated fluorochrome can help to reduce the level of aggregates.

After centrifugation of the pooled multimers, T cells are stained with non-aggregated multimers for a maximum of 15 min at 37°C if the goal is to solely measure T cell responses, or for a maximum of 30 min at 4°C if the goal is to also sort out the cells for downstream transcriptional analyses. Staining at 37°C results in improved binding of the pMHC complexes due to pMHC–TCR dissociation being significantly delayed at this temperature [570]. After the pMHC staining, fluorochrome-conjugated Abs are used to stain (surface) proteins of choice. It is advised to pick and choose a certain fluorochrome, ideally with the same emission spectrum as the live/dead-marker, that is conjugated to Abs targeting cell surface markers unique to unwanted cells to act as a "dump-channel." These unwanted cell surface markers include CD4, CD14, CD16, and CD19, specific for (among others) T helper cells, monocytes, NK cells, macrophages, and B cells. The cells can be washed following standard FCM protocol after which they are ready for analysis.

To ensure that the T cell reactivities detected are indeed real, a confirmation is required in an independent experiment. For this purpose, it is recommended to make new reagents for the potential hits, change the fluorochrome code and to stain the other half of the sample tested. We have previously demonstrated that the reproducibility between these independent experiments is high (R^2=0.9638) [571].

On the basis of the high sensitivity and robustness, this is a highly suitable tool for the analysis of T cell responses in patient material. We have previously demonstrated the value of the technology to map T cell responses against shared antigens in large patient cohorts as well as T cell responses against mutated antigens on a patient-specific basis [571–574].

17.2.2.2 Example: Detection of neoantigen-specific T cell responses in an advanced melanoma patient. Based on DNA sequencing of resected tumor material and healthy PBMCs, tumor-specific variants were identified using exome sequencing. Based on the data, 2058 non-synonymous variants were detected. Candidate tumor-specific neo-epitopes were determined and annotated using an in-house epitope prediction pipeline that predicts which neo-epitopes are most likely expressed on the surface of tumor

Fluorochrome1	Fluorochrome2	Fluorochrome3	Fluorochrome4	Fluorochrome5	Fluorochrome6	Fluorochrome7	Fluorochrome8	
	Peptide 1	Peptide 2	Peptide 3	Peptide 4	Peptide 5	Peptide 6	Peptide 7	Fluorochrome1
		Peptide 8	Peptide 9	Peptide 10	Peptide 11	Peptide 12	Peptide 13	Fluorochrome2
			Peptide 14	Peptide 15	Peptide 16	Peptide 17	Peptide 18	Fluorochrome3
				Peptide 19	Peptide 20	Peptide 21	Peptide 22	Fluorochrome4
					Peptide 23	Peptide 24	Peptide 25	Fluorochrome5
						Peptide 26	Peptide 27	Fluorochrome6
							Peptide 28	Fluorochrome7
								Fluorochrome8

Fluorochrome1	Fluorochrome2	Fluorochrome3	Fluorochrome4	Fluorochrome5	Fluorochrome6	Fluorochrome7	Fluorochrome8	
	Peptide 1	Peptide 2	Peptide 3	Peptide 4	Peptide 5	Peptide 6	Peptide 7	Fluorochrome1
		Peptide 8	Peptide 9	Peptide 10	Peptide 11	Peptide 12	Peptide 13	Fluorochrome2
			Peptide 14	Peptide 15	Peptide 16	Peptide 17	Peptide 18	Fluorochrome3
				Peptide 19	Peptide 20	Peptide 21	Peptide 22	Fluorochrome4
					Peptide 23	Peptide 24	Peptide 25	Fluorochrome5
						Peptide 26	Peptide 27	Fluorochrome6
							Peptide 28	Fluorochrome7
								Fluorochrome8

Figure 62. An example of a combinatorial staircase giving 28 unique dual fluorochrome codes to 28 different peptides, allowing the detection of 28 different T cell responses in parallel.

cells based on the RNA expression level of the antigen, proteasomal processing, and binding of the peptide to the MHC. The prediction pipeline led to 1071 unique peptides of which 497 were used to generate pMHC complexes with the UV light-mediated peptide exchange method. pMHC complexes were formed with HLA-A*02:01, B*27:05 and B*40:01 monomers. Using 14 different streptavidin-conjugated fluorochromes for multimer formation, 75 dual color combinations were used in parallel per tube. This also included peptides predicted to bind more than one MHC. Using this setup, screening the PBMCs from this patient for 498 predicted neo-epitopes was possible in eight tubes with approximately one million cells per tube (20% CD8^{+} T cells). The extra eighth tube was included to avoid mixing peptides that were potentially cross-reactive for multiple TCRs. The analysis of the PBMCs revealed three confirmed neoantigen-specific T cell responses against neoantigens (Fig. 63).

17.3 Antigen-specific T-cell cytometry

17.3.1 Introduction. Antigen-specific T cells play a pivotal role in immune protection toward infection and cancer and are the cellular basis for specific immunotherapy. Antigen-specific T cells are also crucially involved in the pathophysiology of chronic inflammatory diseases, such as allergies, inflammatory bowel disease, or autoimmune diseases. Therefore, the direct visualization, quantification, and characterization of these cells have important diagnostic and therapeutic implications. pMHC molecules present antigenic peptide (epitopes) to T cells, which are recognized by specific binding of a suitable T-cell receptor (TCR), which is expressed in multiple identical copies (usually $>1 \times 10^5$ molecules) on the T-cell surface. CD8^{+} T cells recognize peptides presented by MHC class I, while CD4^{+} T cells recognize antigen via MHC class II molecules. Two main experimental approaches have been developed for the detection of antigen-specific T cells: function-independent methods such as staining with soluble MHC multimers, and function-

based assays (such as intracellular cytokine staining, ELISPOT, or cytokine capture technology). Their advantages and limitations are described below along with other aspects of antigen-specific T-cell cytometry.

17.4 MHC multimers

Function-independent antigen-specific T cell identification has the advantage that it can be applied directly to a sample ex vivo and does not rely on in vitro T cell activation, in contrast to many function-based assays. Compared to the broadly applied detection of antigens by mAbs, detection of TCR-ligand (=pMHC)-binding antigen-specific T cells has turned out to be challenging. This is mainly due to the relatively low binding affinity of TCR–pMHC monomer interactions, which does not allow using soluble (monomeric) pMHC for stable T cell staining. Altman and Davis addressed this problem by the development of so-called "MHC tetramers" [558]. The principle behind this approach is the multimerization of the natural TCR ligand, e.g., to tetrameric complexes, thereby increasing the binding avidity to surface-expressed TCRs. Dimerization of pMHC via immune globulin fusion proteins can be sufficient to detect antigen-specific T cells [575], but such pMHC dimers often fail to identify all antigen-reactive T cells present in a polyclonal population [576]. However, also pMHC tetramers might not label all epitope-reactive T cells, which could be due to very low affinity TCRs [577] or TCR/co-receptor down-regulation or variable surface distribution [578].

Reagents with different degrees of multimerization have been developed, as multimerization seemed to be relevant for stable and antigen-specific binding. Surprisingly, a direct comparison of MHC tetramers, pentamers, dextramers, octamers, and higher polymerization reagents has failed to show significantly improving binding properties with increasing degrees of multimerization [579]. It seems that an avidity gain with MHC trimers represents the crucial threshold to result in stable MHC multimer staining for most
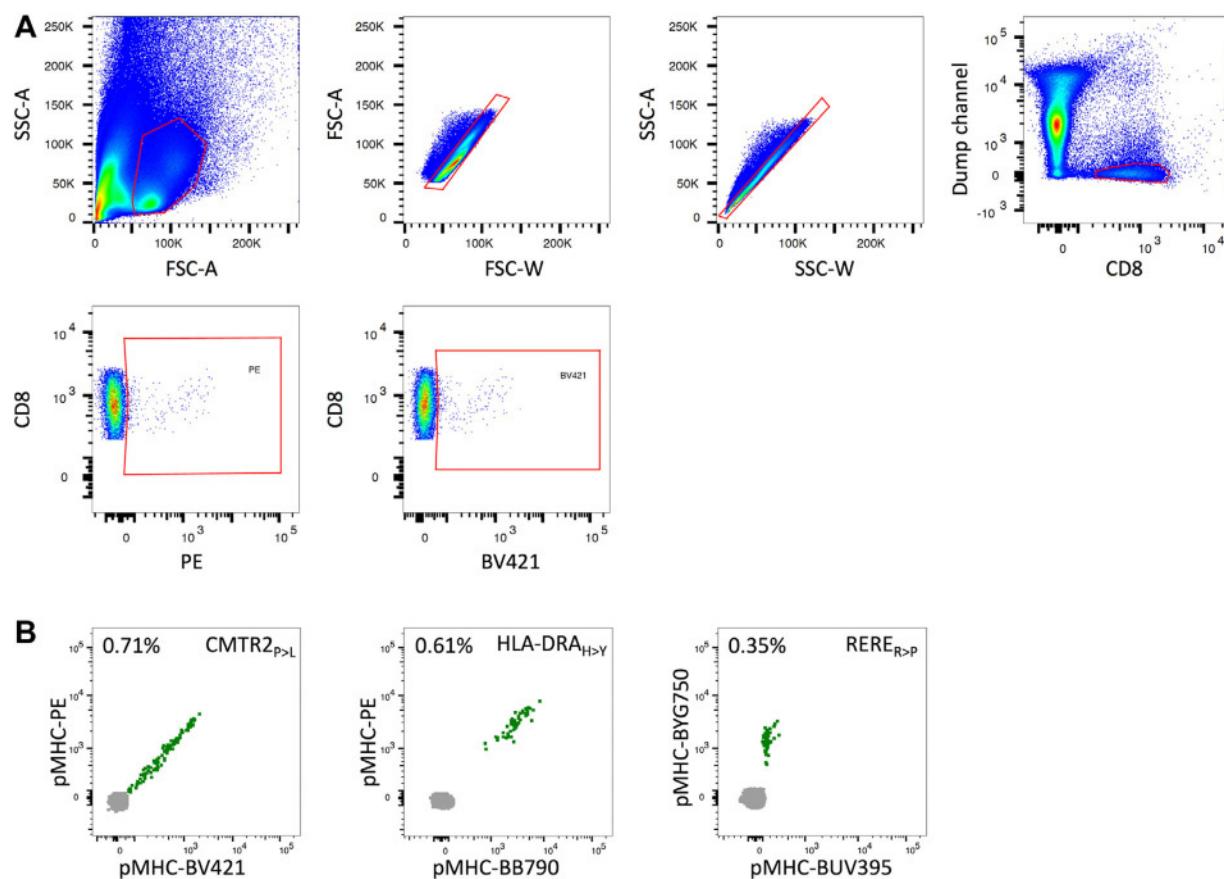
Figure 63. FCM analysis of PBMCs from a patient suffering from advanced melanoma. Dot plots show the gating strategy (A) used to identify live single CD8$^+$, PE$^+$, and BV421$^+$ cells. Fluorochrome$^+$ dot plots are made for all fluorochromes used, however to reduce the image size only gating for PE$^+$ and BV421$^+$ CD8$^+$ cells is shown here. The "Dump channel" consists of CD4$^+$, CD14$^+$, CD16$^+$, CD19$^+$ and dead cells. Dual (AND) boolean gating of fluorochrome$^+$ channels, combined with all the NOT gates of the other channels to get rid of the background, is done to identify neoantigen-specific CD8 T cell populations (B). The neoantigen-specific T cells are positioned in the diagonal of the upper right corner of the plot as they are positive for the two fluorochromes. The gating strategy shown in the upper panel is the one performed for the identification of the CMTR2 neoantigen-specific T cell population in the lower panel.

TCRs. This interpretation was based on the finding that also in conventional PE-conjugated MHC "tetramers," three of the four MHC molecules simultaneously take part in binding to surface-expressed TCRs, although they stain polyclonal T cell populations effectively with high staining intensity [580].

MHC tetramers are based on multimerization with biotinylated ligands and avidin/streptavidin (Fig. 64C, "non-reversible pMHC"). Conjugation with fluorochromes allows usage in FCM-based applications and conjugation with paramagnetic particles promotes combination with magnetic purification technologies [581, 582]. However, binding of TCR ligands can lead to T cell stimulation/activation and labeling-reagent internalization, as well as apoptosis and cell death [583–585]. Therefore, the reversible MHC Streptamer technology was developed, allowing removal of staining reagents from the cell surface after their application (Fig. 64C, "reversible pMHC") [586, 587]. This is achieved by targeted disruption of multimer complexes, leaving only MHC monomers that rapidly dissociate from the cell surface. With directly fluorochrome-labeled MHC molecules, the dissociation can be precisely measured and serves as an important

parameter for TCR avidity (Fig. 64C, "dye-conjugated reversible pMHC") [588, 589]. Reversible staining has been further transferred to low affinity Ab-derived Fab fragments (Fab Streptamer), extending the applicability of this labeling technology to virtually any surface antigen [590].

A large spectrum of MHC reagents is commercially available for the analysis of antigen-specific CD8$^+$ T cells. Assembly of pMHC monomers requires folding of MHC heavy chain and β_2 microglobulin in the presence of the antigenic peptide (Fig. 64A). For downstream biotinylation or fluorophore-conjugation, pMHC monomers need to carry a functionalization site. An Avi-tag, for example, enables BirA-mediated biotinylation for pMHC multimerization on a streptavidin backbone (as is the case for classical tetramers) [558]. Furthermore, solvent exposed cysteine residues have been used for fluorophore conjugation using maleimid chemistry [588, 591]. Reversibility of Streptamers (Fig. 64C, "reversible pMHC") is achieved through a Strep-tag, which allows stable multimerization on a streptactin (rather than streptavidin) backbone in a biotin-free manner [586]. Due to the higher binding affinity of d-biotin to the strep-tag, this multimeric complex can be
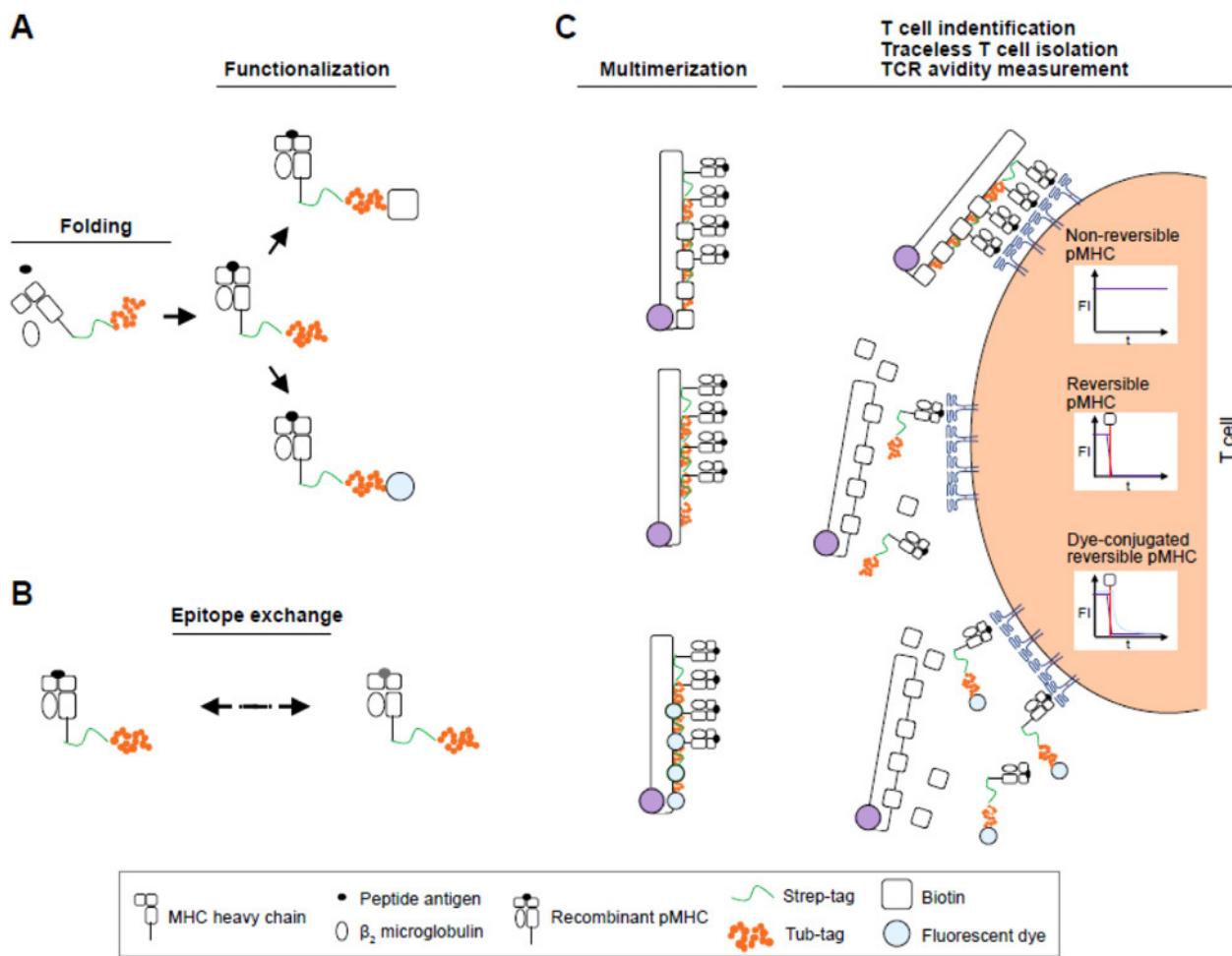
Figure 64. Production and usage of pMHC multimers. (A) pMHC monomer generation through folding and functionalization; (B) Epitope exchange technologies enable high-throughput generation of pMHC complexes for different antigen-specificities; (C) Different usage of nonreversible, reversible, and dye-conjugated reversible pMHC multimers.

disrupted through addition of D-biotin. As the affinity of monomeric pMHC complexes to the TCR is not high enough for stable binding, pMHC monomers consequently dissociate from the TCR (Fig. 64C, "reversible pMHC" and "dye-conjugated reversible pMHC").

In the past, therefore different pMHC production strategies were necessary depending on the pMHC reagent (reversible/non reversible; probe-conjugated/unconjugated) desired for a specific application. In order to streamline and standardize the production process, we have recently developed the so-called "FLEXamer technology," which allows flexible generation of pMHC reagents from a single precursor pMHC protein [592]. These FLEXamers possess a dual-tag consisting of a Strep-tag for reversibility and a Tub-tag for versatile functionalization with biotin, fluorophores, or other probes such as DNA oligos [562] (Fig. 64A).

In order to enable versatility also on the epitope level, a technology based on UV light-cleavable surrogate peptides has been developed (for more information also see Chapter V Section 17.2.2 UV light-mediated peptide exchange method) [565], but also dipeptides can be used for this purpose [569] (Fig. 64B). Further-

more, multiplexed staining of samples with different fluorescence-conjugated MHC multimers is possible and promotes simultaneous analysis or sorting for multiple epitope specificities (for more information also see Chapter V Section 17.5 Functional read-outs) [559, 560]. Combinatorial MHC multimer staining can also be used not only to combine and distinguish large numbers of different MHC molecules within the same sample, but also to increase staining sensitivity for the detection of rare cell populations. Cell incubation with two MHC multimers, which are specific for the same antigen but are conjugated to different fluorophores, results in double-staining of antigen-specific T-cell populations. This approach significantly reduces background staining (for more information also see Chapter V Section 17.5 Functional read-outs), which is fundamentally important to identify rare cell populations.

The pMHC multimer stainings shown in Fig. 65 summarize many of the above-introduced aspects. Figure 65 shows enhanced specificity through the use of two pMHC multimers, with the same pMHC but backbones with different fluorophores. The antigen-specific T cell population in Fig. 65 was stained with a non-reversible pMHC multimerized with streptavidin-PE and a
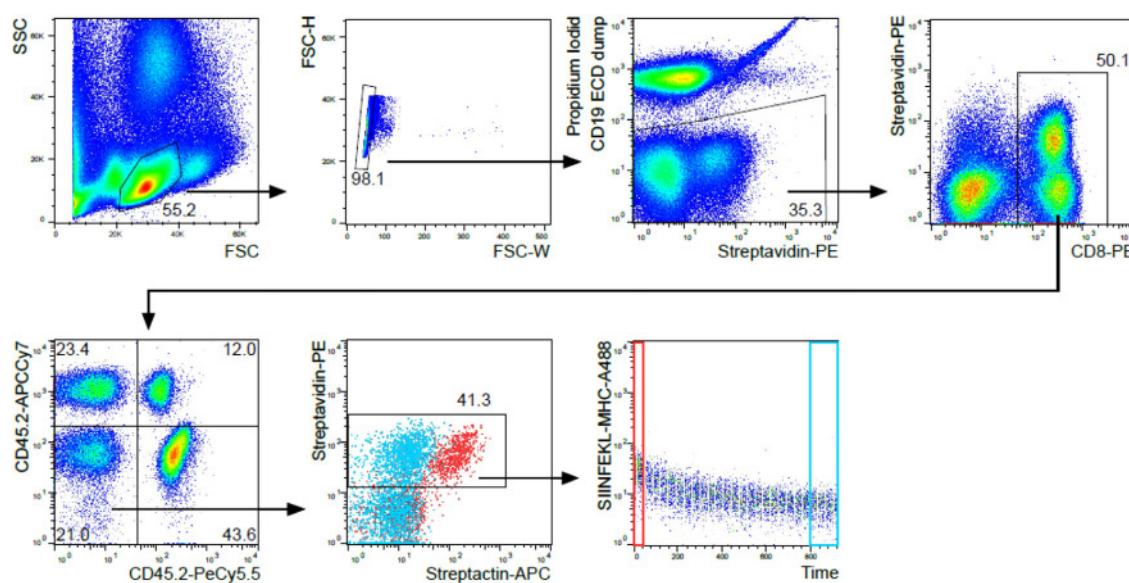
Figure 65. Versatile analysis of a murine H2-k^b/SIINFEKL-specific T cell population. Double staining with nonreversible pMHC multimerized with streptavidin-PE ("Tetramer") and reversible pMHC multimerized with streptactin-APC ("Streptamer") before (red) and after (blue) addition of D-biotin; dissociation of Alexa488-conjugated monomeric SIINFEKL-pMHC molecules over time after addition of D-biotin (outside red box); pregating on lymphocytes, singlets, living CD19$^-$, CD8$^+$ CD45-color coded T cells; gate of SIINFEKL-MHC-A488 additionally pregated on streptavidin-PE$^+$ T cells; CD45 color coding enables simultaneous analysis of multiple samples.

reversible ("Streptamer") pMHC multimerized on streptactin-APC. After the addition of D-biotin only the biotinylated pMHC multimer staining prevails (Fig. 65), demonstrating reversibility of Streptamer stainings. The breakup of Streptamer pMHC complexes is followed by dissociation of pMHC monomer from the TCR. Fluorophore conjugation of pMHC monomers thereby allows tracking of dissociation kinetics, and quantification of TCR-pMHC k$_{off}$-rates (Fig. 65). Continuous tracking of the dissociating pMHC monomers can still be linked to the antigen-specific population through gating on the population positive for the nonreversible pMHC. This emphasizes that not only the versatile nature of the different pMHC constructs themselves, but also their combinatorial usage, have made them become indispensable tools for in-depth T cell characterization.

Co-receptor (CD8 or CD4) interaction is often required for stable binding of MHC multimers. Therefore, parallel surface staining for CD8 or CD4 has to be controlled carefully to avoid artifacts by blocking (or sometimes even enhancement) of co-receptor binding. In order to control this problem, most staining protocols are based on an incubation period with MHC multimers alone before Ab reagents for co-receptors are added. An initial incubation with MHC multimer reagent alone for 25 min, followed by the addition of co-staining mAbs for further 20 min, has proven to be applicable to most MHC multimers in practice. In particular, when using PE-conjugated MHC multimers, background staining—especially coming from B cells and dead cells—can complicate the analysis. Therefore, implementation of a CD19 dump channel and live/dead discrimination has become standard for most MHC multimer staining protocols. By using covalently linkable DNA staining probes

(such as ethidium monoazide bromide (EMA)), it is also possible to combine live/dead discrimination with cell fixation [593].

Optimal MHC multimer concentrations have to be determined for each batch by using positive and negative controls, as done for all other cellular labels used in FCM. Besides reagent concentration, the duration of incubation time and staining temperature are crucial parameters for MHC multimer labeling. Since this technology relies on binding of the natural TCR ligand to the cell surface, at higher temperatures (above 10–15°C), signaling events and potential cell changes (e.g., up- or downregulation of cell surface markers, activation-induced cell death) can occur. Therefore, whenever possible, MHC class I multimer staining should be performed at low temperatures, i.e., 4°C. For reversible MHC multimer staining, cell labeling/sorting at low temperatures is essential, as reagent internalization would negatively interfere with its subsequent removal. In contrast, for most of the currently available MHC class II multimers, successful antigen-specific cell labeling is only possible at higher temperatures (usually at 37°C for ~1 h), since signal accumulation by reagent internalization seems to be required in this case [594, 595].

In addition to conventional experimental controls (single color-, compensation-, and FMO-controls), biological controls for MHC multimer staining are recommended to determine the degree of background staining (e.g., by MHC mismatch controls). General considerations regarding minimal numbers of positive events that have to be acquired and optimal gating strategy (FSC/SSC, singlets, live/dead discrimination, co receptor/multimer, etc.) are important to achieve meaningful and highly reproducible results. A detailed protocol for MHC multimer staining includ-

ing some examples for staining artifacts is described in Cellular Diagnostics—Karger 2009 [596].

For more information, including instructions for the development of MHC class I reagents, please visit our website http://www.mikrobio.med.tum.de/node/51.

17.5 *Functional read-outs*

As antigen-specific T-cells are rare, a major goal in antigen-specific cytometry is to analyze as much parameters as possible from each single antigen-specific T-cell. Recent advances in multicolor FCM have increased the number of markers that can be analyzed, but have also complicated the design and optimization of multicolor Ab panels, as well as the multidimensional analysis of such experiments. These important topics have been reviewed elsewhere [597–601] and are also discussed in Chapter IV. Section 9 - Key Concepts for the Design and Testing of Multicolor Panels and Chapter VI. Section 1–3 Evaluation/Data handling. In this section, we will focus on use of flow cytometric methods for the detection of antigen-specific T-cells following stimulation with an antigen.

Direct labeling of specific T-cells can be achieved by peptide/MHC(pMHC)-multimers (see Chapter V Section 17.4—MHC multimers). However, pMHC-multimers can only be generated for a limited number of predefined pMHC combinations, in particular for MHC class I peptides and CD8$^+$ T-cell analysis. In contrast, MHC class II multimers for identification of antigen-specific CD4$^+$ T-cells are still less well established. In addition, tetramer use is limited for complex antigens or antigens not fully characterized, e.g., microbes, tumors or autoantigens, and for the heterogeneous MHC background in humans. As an alternative, functional tests provide more flexibility, since they rely on T-cell stimulation by autologous APCs, which can process and present all types of antigens, peptides, proteins, or crude cellular extracts in the context of the physiological MHC background. Following in vitro antigen-stimulation, the antigen-induced T-cell response is analyzed as an indirect read-out indicating specific T cells, i.e., proliferation, activation-induced surface, or secreted molecules or cytotoxicity [602] (Figure 66).

17.5.1 *Selection of the right parameter: Minimal manipulation.*

Functional assays require stimulation, which may affect T-cell frequency, function, and phenotype [602]. Cellular proliferation as a result and readout of stimulation requires usually several days (typically 3–5 days) of stimulation (see also Chapter V Section 6—DNA synthesis, cell cycle, and proliferation) and introduces an unpredictable bias due to significant in vitro selection and "bystander" proliferation. Therefore, it is difficult to extrapolate from frequency and phenotype of cells after proliferation to the original sample, and proliferation-based assays should be used with caution for quantitative or qualitative T-cell analyses. Therefore, short stimulation times should be preferred; for instance, cytokines and rapid activation markers (e.g., CD154,

CD137, CD69) typically require only 5–12 h of stimulation before their levels are measurable intracellularly, on cell surfaces or in culture supernatants, ensuring minimal manipulation [602]. Furthermore, β2-integrin activation on activated T cells occurs even within minutes [603].

For antigen-specific stimulation experiments, it should also be considered that the source of material (whole blood; PBMCs; different tissues sources), as well as the treatment of the cell source (fresh or frozen material; resting periods before stimulation; culture medium), might have a profound influence on T-cell marker expression and the detection of antigen-specific T cell responses [514, 604–607]. In our hands, overnight resting (<16 h) at 37°C in the incubator of freshly isolated PBMCs has been proven to reduce background expression of activation markers and cytokines, while retaining responsiveness of antigen-specific CD4$^+$ Tcon and Treg, leading to an increased SNR for antigen-specific T-cell analyses (unpublished). However, in multicenter trials, cryopreservation of PBMCs is often unavoidable. Therefore, standardized procedures are needed to compare antigen-specific T-cell data from different laboratories [608, 609]. When analyzing and comparing antigen-specific T-cell responses from blood and tissue, also the presence of functional APCs with comparable processing and presenting capacity should be considered.

17.5.2 *Selection of the right parameter—Integrate all T-cell subsets.*

T cells are heterogeneous and cover a wide range of different phenotypical and functional subsets. Information about the frequency, differentiation stage (e.g., naive, memory), phenotype, and functional properties of antigen-specific T-cells is essential to gain a comprehensive picture about the immune response against a certain antigen and the immune status of an individual. As CD4$^+$ and CD8$^+$ T cells provide different functions, also different read-outs apply for the detection of antigen-specific CD4$^+$ and CD8$^+$ T cells (see Table 14).

In particular, CD4$^+$ T cells can acquire a highly diverse set of functional properties. Therefore, antigen-induced cytokine secretion is widely used as functional read-out for CD4$^+$ T cells. Cytokines can be detected on the cell surface by retention of the secreted cytokine on the surface of the secreting cells via a capture matrix [620, 621] or intracellular when cytokine secretion is inhibited by addition of secretion inhibitors like Brefeldin A or Monensin [622] (see also chapter V Section 14—Intracellular parameters, Chapter V Section 17.6 Live cytokine-producing cell sorting with secretion assay). Differences may apply with usage of different secretion inhibitors [608], for example, Monensin has been shown to only insufficiently inhibit TNF-α secretion [623]. Due to the heterogeneity of CD4$^+$ T-cells, ideally, the functional read-out should encompass all relevant T-cell types to obtain a complete picture of the immune status, i.e., all conventional T (Tcon) cells, i.e., naïve, all memory subsets as well as Foxp3$^+$ regulatory T (Treg) cells, which typically comprise 5–10% of all CD4$^+$ T-cells and are essential for tolerance. An alternative to individual cytokines, such as IFN-γ, which are often only expressed by a minor fraction of all antigen-specific CD4$^+$ T-cells [613, 614, 624],
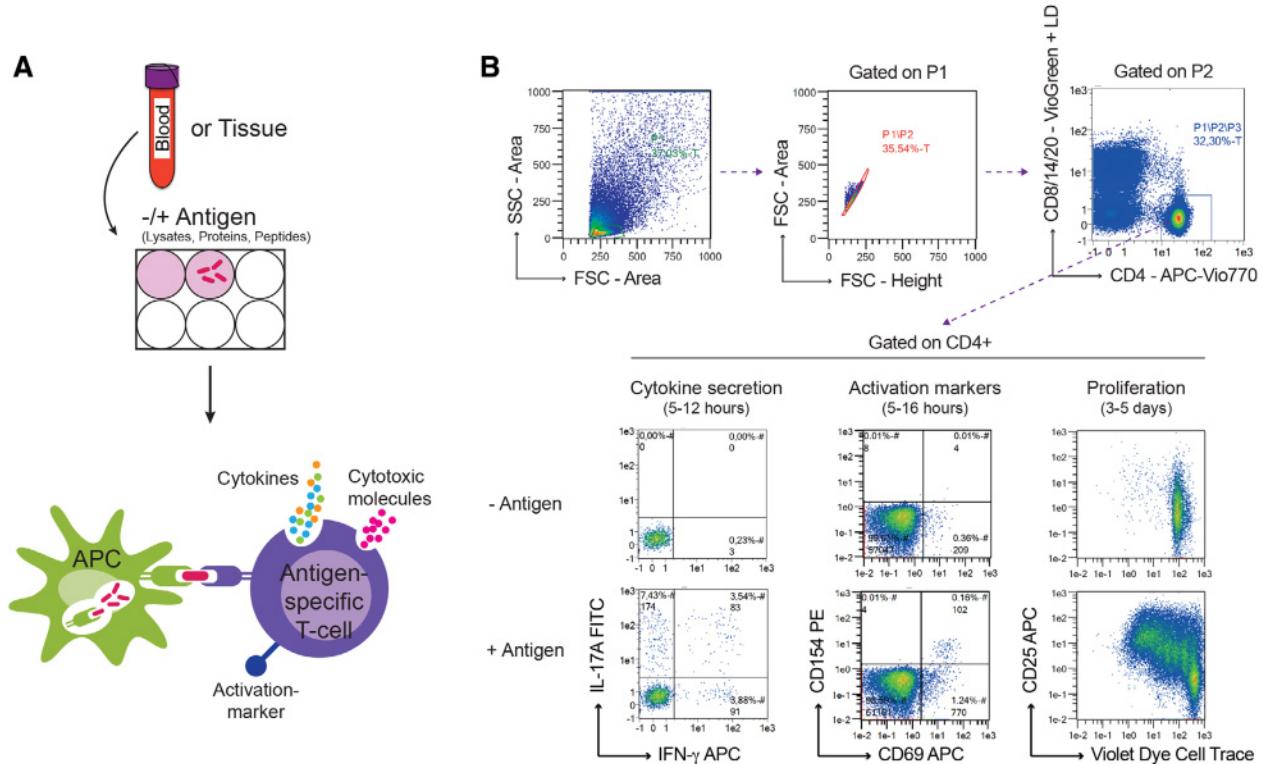
Figure 66. Principal of antigen-specific stimulation assays. (A) PBMCs or single cell suspensions from tissues are incubated with the antigen of interest or without antigen as negative control to determine background levels of the assay. If whole proteins are used for stimulation, the antigen has to be taken up by the autologous APCs of the cell source, processed and presented on MHC molecules. Peptides of a certain length can bind externally to MHC molecules. (B) The antigen-specific T-cells will start to secrete cytokines and/or cytotoxic molecules (5–12 h), express activation markers (5–16 h) and at later time points start to proliferate (3–5 days). For the different functions of T-cells, such as cytokine release, cytotoxicity, expression of activation markers, and proliferation single-cell flow-cytometric assays are available and for most technologies also selection markers on the cell surface are available allowing additional isolation of the specific cells.

and thus may ignore a significant fraction of specific T cells, are so called activation markers, that are upregulated on the T-cell surface upon specific T-cell receptor triggering. In contrast, the combination of the activation markers CD154 (CD40L; which is expressed on all Tcon subsets) and CD137 (4-1BB; which is expressed on Treg) following short-term (6 h) stimulation allows in parallel detection of naive and memory Tcon and Tregs reacting against the same antigen [615, 616, 624, 625].

For CD8^{+} T-cells, cytokines like TNF-α and IFN-γ are widely used, which are expressed by the majority of the antigen-activated CD8^{+} population. The activation marker CD137 is also expressed by CD8^{+} T-cells following stimulation for >12 h [618, 619, 626], but may also be induced due to bystander activation. Furthermore, for CD8^{+} T-cells detection of cytotoxic activity by staining for cytotoxic effector molecules (e.g., granzyme or perforin) can be used. In contrast to most other mediators, these molecules are found preformed in the cells and can be immediately released following antigen stimulation. An alternative approach for measuring cytotoxicity is the detection of CD107a, which is only present on the cell surface transiently following degranulation [627, 628] (see also Chapter V Section 17.8 Cytotoxicity).

A common drawback of these techniques is that they all rely on upregulation or de novo synthesis of the read-out markers, e.g.,

activation markers or cytokines, and therefore, require at least several hours of stimulation. Recently, a new approach for rapid identification of activated CD8^{+} T cells has been introduced, based on immediate changes of surface integrins that occur within minutes following antigen stimulation [603]. The authors made use of the fact that resting antigen-experienced T cells express high levels of membrane-bound β2-integrins [629, 630]. TCR activation leads to clustering of the membrane-bound integrins within seconds following stimulation, which can be detected by intercellular adhesion molecule 1 (ICAM-1)-multimers, that specifically bind to activated β2-integrins [603]. An advantage of the assay is the short stimulation time of only several minutes that allows the detection of functional (producing cytokines and/or expressing CD107a) CD8^{+} T cells. However, comparison with peptide MHC multimers showed that only a fraction of the peptide MHC multimer positive T cells stained positive for ICAM-1. Further analyses revealed that activated β2-integrins mark T cells with immediate, strong effector function, but, for example, miss nonfunctional antigen-specific cells. In addition, the protocol requires stimulation of low cell numbers in relatively high volumes (7.6 × 10^{5} PBMCs in 380 µL test), which limits the detection limit and makes it difficult to scale-up the assay for the detection of low-frequent antigen-specific T cells.

Table 14. Methods for the detection of antigen-specific T cells

Detection Method	Duration	Commonly used markers	Cell Type	Disadvantages
Proliferation	3–5 days		CD4$^+$ and CD8$^+$	Bystander proliferation may occur Selective outgrowth of single clones No direct quantification of specific cells Phenotypical and functional changes during long-term in vitro culture
Cytokine secretion	5–12 h (different cytokines may have different kinetics)	TNF-α	CD4$^+$ and CD8$^+$	Restricted to preselected cytokine producers; Non-cytokine producing Tcells (e.g. naïve, Treg) are neglected
		IFN-γ	CD4$^+$ and CD8$^+$	
		IL-2	CD4$^+$ and CD8$^+$	
		IL-4, IL-5, IL-9, IL-10, IL-13, IL-17A, IL-17F, IL-21, IL-22, GM-CSF, etc.	Mainly CD4$^+$	
		GARP/LAP/TGF-β	Treg	
Activation marker	5 h to several days (different activation markers have different kinetics)	CD69 (3 till 24 hours) [610]	CD4$^+$ and CD8$^+$	Sensitive to bystander activation
		CD25 (24 till <72 h) [610]	CD4$^+$ and CD8$^+$	Sensitive to bystander activation; late up-regulation; constitutively expressed by Treg
		HLA-DR (24 till <72 h) [610]	CD4$^+$ and CD8$^+$	Late up-regulation
		CD134 (OX-40) (48 till 72 h) [611, 612]	CD4$^+$ and CD8$^+$	Late up-regulation
		CD154 (CD40L) (6 till 16 hours) [613, 614]	Mainly CD4$^+$	Restricted to CD4$^+$ T cells; not expressed on Treg
		CD137 (4-1BB) (6 till 24 hours)	Treg (6h) [615–617] later also on CD4$^+$Tcon and CD8$^+$ [618, 619]	Detection Treg requires co-staining with CD154; On CD4$^+$ and CD8$^+$ Tcon sensitive to bystander activation
Cytotoxicity	1–6 h	Perforin	Mainly CD8$^+$	Restricted to preselected cytotoxic marker; non-cytotoxic T cells are neglected
		Granzyme A	Mainly CD8$^+$	
		Granzyme B	Mainly CD8$^+$	
		CD107a	Mainly CD8$^+$	
Activated integrins	4–120 min	(ICAM)-1 multimers that specifically bind to activated β2-integrins [603]	So far described for CD8$^+$	Restricted to a subset of cytokine secreting /cytotoxic memory T cells; non-functional antigen-specific T cells and naïve cells are neglected

17.5.3 Combination with magnetic enrichment of rare cells. Antigen-specific T-cells typically comprise <1% and often <0.1% of the total T-cell population [602]. Therefore, magnetic preselection of rare antigen-specific T-cells from large cell samples is frequently used to decrease background and improve optical resolution. Preselection increases the sensitivity for the detection of antigen-specific T-cells, i.e., frequencies down to 1 cell within 10^{-5}–10^{-6} and thus even detection of specific T cells within the naïve repertoire is possible [620, 624, 631–634]. Enrichment allows the collection of sufficient target cells for subsequent multiparameter analysis and resolution of small cell subsets. Magnetic enrichment may employ surface markers, e.g., tetramers, CD154,

CD137, ICAM-1-multimers, or secreted cytokines [602, 603, 620, 624, 631–634] (Figure 67).

17.5.4 Type of antigen. As for the functional read-out, there are differences between the antigens used for stimulation of CD4$^+$ and CD8$^+$ T-cells. CD4$^+$ T-cells recognize antigens that are presented via the exogenous pathway of antigen presentation on class II MHC molecules [636]. Accordingly, for CD4$^+$ T-cells, peptides, proteins, and even cellular extracts can be used for stimulation. Presentation of peptides from whole proteins depends on the processing activity of the available APCs, which may vary between cell sources (blood,
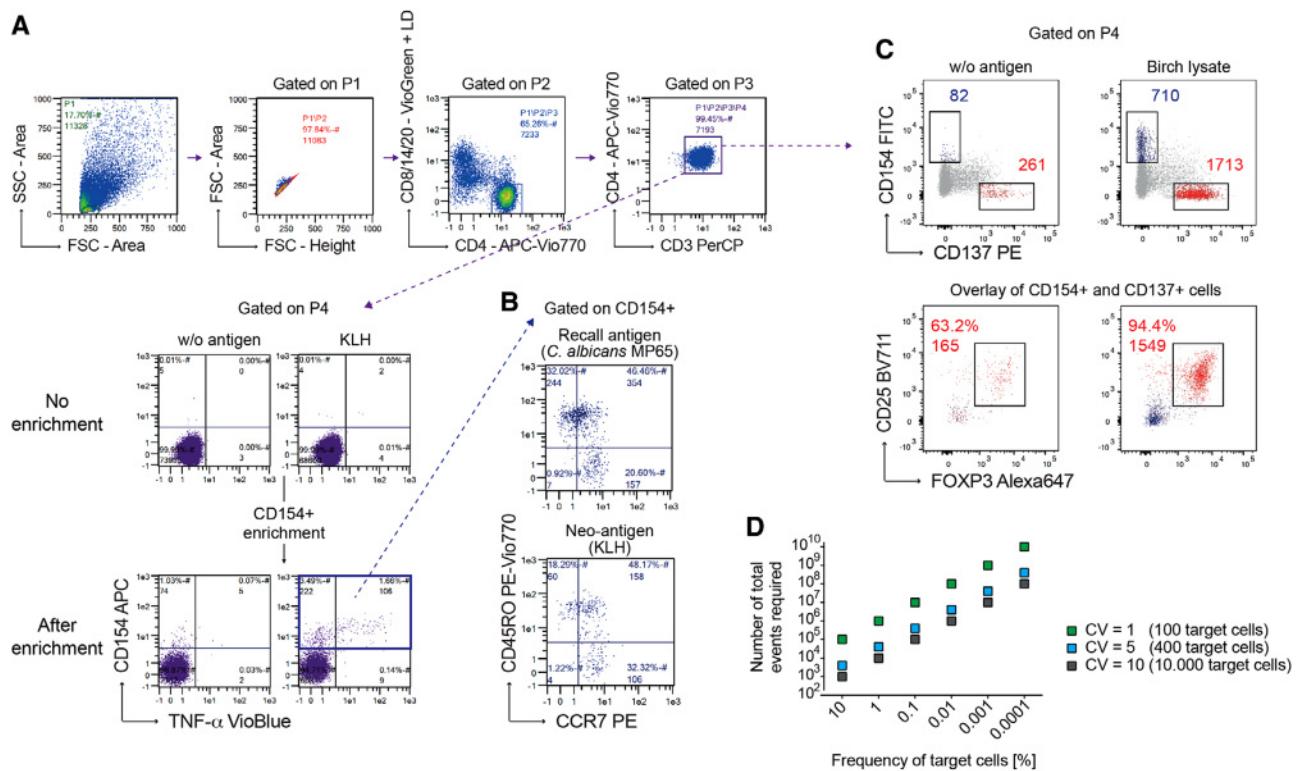
Figure 67. Enrichment of antigen-specific T-cells increases sensitivity for the detection of rare cells. (A) CD154 and TNF-α expression was analyzed on human CD4$^+$ T-cells without addition of an antigen and following stimulation wit the neo-antigen keyhole limpet hemocyanin (KLH). Cells are gated on CD4$^+$ T-cells and percentage and absolute numbers of CD154$^+$ cells after acquiring 5×10^5 PBMCs (upper plots) or obtained from 1×10^8 PBMCs after enrichment of CD154$^+$ cells (lower plots). (B) Phenotypic characterization of the enriched CD154$^+$CD4$^+$ T-cells to discriminated between CD45RO$^+$ memory cells and CD45RO$^-$CCR7$^+$ naive T-cells, following stimulation with a peptide pool of *C. albicans* MP65 as recall antigen or KLH as neoantigen. (C) Parallel detection of antigen-specific Tcons (CD154$^+$) and Tregs (CD137$^+$) following stimulation with birch pollen lysate and magnetic enrichment for CD154+ and CD137+ cells from 2×10^7 stimulated PBMC. Upper plots: cells are gated on CD4$^+$ T-cells and absolute cell counts of CD154$^+$ and CD137$^+$ cells with and without stimulation are indicated. Lower plots: Overlayed flow-cytometric analysis of birch-specific CD154$^+$ and CD137$^+$ cells. Numbers indicate percentages among CD137$^+$CD154$^-$ CD4$^+$ T-cells and absolute numbers of CD137$^+$CD25$^+$FOXP3$^+$ Treg. (D) To describe the precision of flow cytometry data, the CV can be calculated from the variance and the SD) For rare cell analysis, the approximations SD $= \sqrt{r}$ and CV [%] $= 100/\sqrt{r}$ can be used, where r is the number of positive events [635]. From CV [%] $= 100/\sqrt{r}$ follows r $= [100/CV]^2$. Using this approximation the number of total required events is illustrated depending on the frequency of target cells for different CVs.

(lymphoid-) organs) and donors. Antigen preparations containing potential innate immune signals (pathogen-associated molecular patterns) may cause bystander activation and specificity of the antigen-reactive T-cells has to be confirmed for each antigen (see also Section 17.5.5 Controls and statistical analyses).

In contrast, stimulation of CD8$^+$ T-cells with whole proteins is difficult, since MHC class I epitopes are not easily generated from endocytosed proteins that depends on cross presenting capacity of the APCs. Therefore, short synthetic peptides are preferable. The use of peptides as antigen stimulants is advantageous as peptides are instantly presented by all APCs expressing MHC molecules, including B cells or other nonclassical APCs. Peptides can be used individually or in pools, such pools being able to cover complete protein amino acid sequences (protein spanning peptide pools). The use of peptides of 15 amino acids length and 11 overlaps has proven very successful for both CD4$^+$ and CD8$^+$ T-cells [637, 638]. The use of 15mers is in conflict with the concept that the binding groove of class I MHC molecules can only accommodate a peptide of nine amino acids in length. Since approaches using

15mer peptides are successful, it is assumed that mechanisms exist that shorten these peptides in the extra cellular space (clipping or trimming) [639, 640].

17.5.5 Controls and statistical analyses. Standard controls for flow-cytometric multicolor analyses that apply here (single color, compensation, FMO-controls, exclusion of doublets and dead cells, as well as a dump channel) are described in Chapter III. Section 1. Controls—Determining positivity by eliminating false positives. However, special emphasis has to be given to elimination of background due to the low frequencies of antigen-specific T-cells, as noted above. A nonstimulated sample processed under identical conditions is absolutely required to determine background. Specificity should be verified for each pMHC-multimer and antigen, especially for preparations containing pathogen-associated molecular patterns, as well as for different cell sources (blood, tissue). Specificity can be determined, for example, by MHC blocking Abs, the use of fixed APCs (for processing dependent antigens) or

expansion of cell lines and single cell clones for confirmation of specificity by antigen re-stimulation [624].

Also, a positive control for the assay should be included, to determine functionality of the T-cells and APCs. Polyclonal stimulation can be achieved by, e.g., agonistic Abs against CD3 and CD28 or by stimulation with the chemicals PMA and Iono. However, these controls only apply for the T-cells and are independent of the presence of functional APCs. Alternatively, superantigens like Staphylococcus enterotoxin B (SEB) can be used, which crosslinks MHC molecules and specific Vβ regions of T-cell receptors. Thus, usage of SEB might be limited in samples with restricted Vβ repertoires. Since polyclonal stimuli are usually very strong, an antigen-specific control might represent a more physiological control, e.g., an antigen derived from an ubiquitous pathogen like *Candida albicans*, or standard vaccine like tetanus, to which typically all donors react [624].

When frequencies of antigen-specific T-cell are calculated, background values have to be subtracted from that of the antigen sample. Regarding statistical significance of rare event analyses, considerations have to be applied to determine the minimal number of events that have to be acquired for statistically relevant analyses. To describe the precision of flow-cytometry data, the CV can be calculated from the variance and the SD [635]. For example, for a CV of 5% at least 400 antigen-specific T-cells have to be acquired. If the antigen-specific cells occur with a frequency of 0.1%, at least 400 000 total events should be acquired. If the frequency of specific cells is just 0.01%, at least 4 000 000 have to be acquired, and so on. This illustrates that for many antigens, magnetic preselection of the rare antigen-specific T-cells from large cell samples is necessary to increase the sensitivity of the assay and obtain sufficient target cells for statistically relevant analyses (see also Chapter VII Section 2 Statistics for Flow cytometry).

For methods employing enrichment, the absolute count of target cells obtained from a certain input cell number has to be determined to calculate frequencies in the original sample. The frequency of positive cells after enrichment is not relevant for quantification. A minimal SNR and minimal number of events per input cell number has to be determined for each test system independently (see also Chapter V Section 1 Rare cells (general rules)).

17.5.6 Interpretation of results. Originally, specific T-cell analysis relied on the idea that antigen-specific memory-type T-cells can only be detected in antigen-experienced individuals. However, recent advances, in particular in the enrichment of rare cells, has allowed detection of rare specific T-cells even within the naïve repertoire [624, 633, 634, 641–644] (Fig. 67B). These analyses also showed that the memory compartment contains a significant fraction of specific T-cells against bona fide "neo-antigens," i.e., antigens not previously encountered by the immune system. This may result from specific (structurally related epitopes) or from statistical cross-reactivity, i.e., recognition of a neo-epitope by TCRs from a polyclonal repertoire [624, 642, 644]. Thus, the presence of memory-type T-cells does not per se imply that this results from a genuine antigen-specific immune response. Therefore, additional biological parameters have to be considered to determine the actual immune status: overall ratio between specific memory to naive and Treg cells, ratio of memory T-cells in the antigen-specific population versus the total T-cell population (is expected to be >1 in genuine memory responses), clonal composition of TCRs (deep sequencing), and affinity or functional avidity that can be estimated be restimulation of expanded antigen-specific clones or cell lines with decreasing antigen concentrations or via reversible MHC-multimers [589].

Taken together, antigen-specific cytometry allows combination with multiparametric single cell analysis tools for full resolution of the antigen-specific immune response.

17.6 Live cytokine-producing cell sorting with Cytokine Secretion Assay™

17.6.1 Overview. The aim of this section is to illustrate how to recover live human T cells depending on their capacity to produce specific cytokines. This technique can be applied to both identification and sorting of antigen specific cells, as well as polyclonal T cells with a common cytokine production profile.

17.6.2 Introduction. Following antigen recognition, T cells acquire effector properties that guarantee pathogen clearance. Cytokine secretion is one of the most effective properties of activated T cells as it orchestrates a functional immune response involving both cells of adaptive and innate immunity. Different pathogens evoke different cytokine responses; thus T cells can be functionally distinguished based on their cytokine profile. Indeed, there are at least three major types of cell-dependent immunity, classically defined as types 1–3 responses (see also Chapter VI Section 1.11 Human CD4 and CD8 T cells). Type 1 immunity defends from intracellular bacteria and viruses, involves Th1 and CTL T (Tc)1 cells and is orchestrated by the transcription factor Tbet with the production of IFN-γ. Type 2 immunity fights extracellular parasites and is mediated by Th2 and Tc2 cells, which express the transcription factor GATA3 and produce IL-4, IL-5, and IL-13. Finally, RORgt$^+$IL-17$^+$ Th17 and Tc17 cells mediate type 3 immunity, which protects from extracellular bacteria and fungi [645]. Despite these distinctions, it has been described more recently that distinct effector programs can coexist within the same cell. Indeed, cells simultaneously producing IFN-γ and IL-17 (Th1/17), IL-4, and IL-17 (Th2/17) and IFN-γ and IL-4 (Th1/2) have been identified [646–648]. Moreover, it has been demonstrated that a single pathogen can evoke functionally heterogeneous T cell responses [649]. In this complex scenario, the Cytokine Secretion Assay™ (Miltenyi Biotec) is a versatile tool that allows the identification and recovery of live antigen specific T cells based on their cytokine production profile. First, cells are shortly stimulated with antigen (see also Chapter V Section 17.5 Functional read-outs) or with polyclonal stimuli. Then, cells are labeled with the Catch

Reagent specific for the cytokine of interest. Catch Reagent is made up of two Abs linked for their Fc regions. One Ab is specific for the pan-leukocyte marker CD45 and allows binding to the leukocyte surface. The other Ab is specific for the cytokine of interest. Cells are then incubated again at 37°C to favor cytokine production. If a cell secretes the specific cytokine, it will bind to the catch reagent on the cell surface. The addition of a secondary fluorochrome-linked Ab, recognizing a distinct epitope of the cytokine from that of the catch reagent allows the detection of cytokine producing cells. The Cytokine Secretion Assay™ can be applied either on whole blood, PBMNC, or even directly on T cells when using polyclonal stimulation. Staining with lineage specific Abs allows the identification of a specific cell subset that is producing the cytokine, when working on whole blood or PBMNC [650] or on cells from biological fluids [651]. Live cytokine producing cells can then be recovered either by immunomagnetic or flow cytometric sorting (See also Chapter IV Section 1.4 Magnetic pre-enrichment for high-resolution detection and analysis of rare cell populations and Chapter IV Cell sorting).

17.6.3 Step-by-step sample preparation.

17.6.3.1 Starting material.
The protocol can be applied either on whole blood, PBMNC, or isolated T cells. Whole blood must be collected with anticoagulant sodium heparin. Since calcium is critical for lymphocyte activation, chelating anticoagulants cannot be used for blood collection. When working with PBMNC, fresh cells are preferred but cryopreserved cells can be also used.

17.6.3.2 Cell stimulation.

1. Wash cells at $300 \times g$ for 7 min.
2. Resuspend cells in RPMI 1640 supplemented with 5% human serum. Final cell concentration must be 10×10^6/mL.
3. Add the specific peptide/protein at the desired concentration. Always include a positive control (SEB, PMA/Ionomycin) and a negative control (no stimulus). The optimal positive control must be chosen based on the cytokine of interest. Incubation period ranges from 3 h in case of polyclonal stimuli to 6–16 h for proteins. Incubation must be performed at 37°C with 5% CO_2.
4. Following incubation, collect cells in a 15 mL polypropylene tube.

17.6.3.3 Cytokine Secretion Assay.

1. Prepare 100 mL cold buffer; 100 μL cold medium; 10 mL warm medium. Volumes are adjusted for up to 10×10^6 cells. Scale up for larger numbers. Do not reduce volumes if working with less than 10×10^6 cells.
2. Wash cells from previous step 4 with 10 mL cold buffer and spin down at $300 \times g$ for 7 min.

3. Resuspend up to 10×10^6 cells with 80 μL cold medium, then add 20 μL of catch reagent. Mix and incubate 5 min on ice.
4. Add warm (37°C) medium and dilute cells depending on the expected amount of cytokine-producing cells. Proper dilution is critical to prevent unspecific binding of secreted cytokines to close cells. If less than 5% cytokine producing cells are expected, add 10 mL of warm medium to achieve a final concentration of 10^6 cells/ml. If more than 5% cytokine producing cells are expected, add 100 mL of warm medium to a final concentration of $\leq 10^5$ cells/mL. Further dilution is required for expected frequencies of cytokine producing cells >20%.
5. Incubate cells 45 min at 37°C 5% CO_2 to allow cytokine secretion and binding to catch reagent. During this incubation period rotate tubes every 5 min or use MACSMix™ rotator to avoid cell to settle, thus leading to cytokine unspecific binding.
6. Following incubation put the tubes on ice. Spin down cells in a precooled centrifuge at $300 \times g$ for 7 min.
7. Wash cells with cold buffer to block cytokine secretion and repeat the centrifugation step.
8. Resuspend cells up to 10×10^6 cells with 80 μL cold medium, then add 20 μL of cytokine detection fluorochrome-conjugated Ab. Additional Abs can be added at this step to allow simultaneous detection of other markers. Mix and incubate 10 min on ice.
9. Wash cells with cold buffer and centrifuge at $300 \times g$ for 7 min.
10. Cells are now ready for FCM analysis or sorting. Always add PI to exclude dead cells from the analysis.

17.6.4 Materials.

- Buffer: PBS, pH 7.2, supplemented with 0.5% BSA and 2mM EDTA
- Medium: RPMI 1640 supplemented with 5% human serum. Do not use fetal cow serum or bovine serum to avoid unspecific stimulation.
- Peptide/Protein of interest
- PMA and Iono; Staphylococcal Enterotoxin B (SEB) for polyclonal stimulation
- PI for flow cytometric exclusion of dead cells

17.6.5 Data analysis. Data analysis requires the exclusion of doublets and dead cells using a live-dead marker. This is especially true if using cryopreserved cells instead of freshly isolated. As in Fig. 68, lineage markers allow the identification of the population of interest for the identification of cytokine producing cells.

17.6.6 Pitfalls. Dilution steps and continuous rotation during the incubation period are critical to avoid cytokine binding to nonproducing cells.
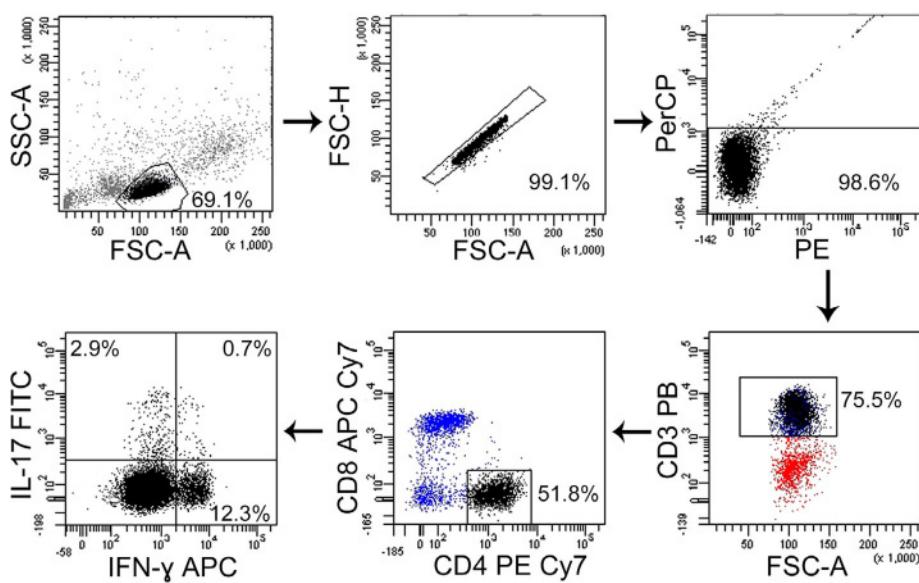
Figure 68. Cytokine secretion assay performed on PBMNC for the detection of IFN-γ and IL-17 producing T helper cells. Cells were stimulated with PMA/Iono. Lymphocytes were gated based on physical parameters, then doublets removed using FSC Height and Area (FSC-H and FSC-A, respectively). Dead cells were excluded as PerCP-positive and PE-positive following PI addition. T helper cells were then identified as CD3+ positive, CD4+, CD8−. IFN-γ and IL-17 expression were subsequently analyzed.

17.6.7 Top tricks. Secretion of two distinct cytokines can be evaluated simultaneously via combining cell staining with two distinct catch reagents and detection Abs. The only requirement is that detection Abs must be conjugated to distinct fluorochromes. Dilution factor during the incubation period must be calculated based on the expected higher percentage of cytokine producing cells.

17.7 Quantification of soluble cytokines with cytometric bead array

17.7.1 Overview. Cytokines are the main soluble proteins secreted by various cells of the immune system. These soluble factors play different roles in regulation of immune responses, since they influence migration, activation, and proliferation of various cell types, including tissue resident cells. Cytokines show commonly pleitropic features, exhibit redundant, and overlapping properties; they also mediate production or regulate function of other cytokines. The final effect on a specific cell type depends on the balance among multiple cytokines that again depends on their activity or concentration. Thus, an evaluation of an extended number of cytokines in biological fluids, rather than a single cytokine, may be an optimal strategy to better investigate various physiological and/or pathological settings. In this context, multiplex bead-based array described in this section is a valuable tool that allows simultaneous flow cytometry analysis of several analytes from a single sample using a small sample volume [556, 2218, 2249, 2251, 2253, 2255].

17.7.2 Introduction. Different methods have been developed to define cytokine concentration in biological fluids, and these are mainly based on competitive or sandwich principles. In these systems, antigens or Abs are labeled with an enzyme or a fluorescent, luminescent, or radioactive molecule. Historically, the classical method that belongs to this family is the ELISA, in which the targeted cytokine is sandwiched by two Abs specific for different epitopes of the same cytokine. In this method, the first Ab is linked to a plastic plate support and is defined as the "capture" Ab; instead, the second Ab is conjugated with the detection molecule and is defined as the "detector" Ab. ELISA is characterized by high specificity and sensitivity; however, it only allows detection of a single analyte and requires the use of a higher sample volume for each measurement.

The introduction of multiplex beads-based immunoassays significantly changed the approach for the quantification of cytokines and other soluble factors in biological fluids or culture supernatants. The principle of this method is the use of a specific Ab coated on microbeads that serve as a "solid" support as in the version of the ELISA technique. Microbeads can be detected by FCM instruments, based on their fluorescence. During the incubation with the sample, the analyte of interest will bind to the Ab–microbead complex. The addition of a fluorochrome-conjugated secondary Ab allows the detection of the analyte-microbead complex. Quantification is performed via referring to a standard curve, prepared with known scalar doses of protein concentration.

The combination of beads with different size and/or beads with different florescence intensity, represents the flexibility and the power of this method allowing to evaluate simultaneously up to 100 analytes in the same sample. Several kits for multiplex beads-based assay are available from different commercial vendors, each with specific properties, i.e., sample volume (generally ranging between 50 and 15 μL), assay duration (on average only a few hours, depending on the period of incubation and washing steps), the possibility to customize the combination of primary beads, and sensitivity of the test, which also depends on the range of the standard curve.

17.7.3 Step-by-step sample preparation. Here, we provide the detailed protocol of Cytometric Beads Array™ (CBA) from BDBioscience as an example. Specific protocols from other vendors must
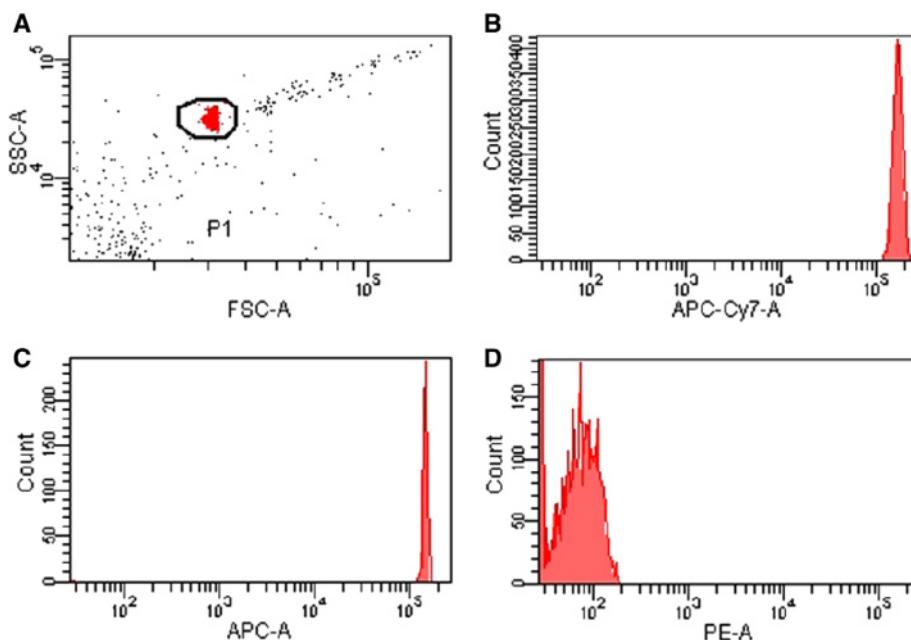
Figure 69. Flow cytometer setup for multiplex-bead based array. (A) FSC–SSC plot for the identification of beads based on their physical parameters. Histogram plots of APC-Cy7 (B) and ACP (C) channels showing that PMT voltages are optimally set to the highest visible MFI. By this way, it is possible to properly distinguish different types of beads used. Panel (D) represents histogram plot of PE channel (the fluorochrome bound to the secondary antibody) measured on unstained beads.

be followed according to the manufacturer's instructions. The BD CBA kit can detect: human, mouse, and rat soluble proteins, immunoglobulins, as well as cell signaling factors. BD CBA solutions are available in two formats to meet diverse needs. BD CBA Kits are preconfigured with routine panels, while BD CBA Flex Sets provide an open and configurable method of detection, so that researchers can design their own multiplex kit. Beads are coated with an Ab specific to the protein of interest; each bead in the array has a unique red fluorescence intensity so that different beads can be mixed and run simultaneously in a single tube. These beads are incubated with a small sample volume and then further incubated in the presence of a capture Ab tagged with the fluorochrome PE. At the same time, a curve of standard samples ranging from 10 to 2500 pg/mL, is performed to enable protein quantification.

1 Standard preparation

   1.1. Prepare the highest concentration of the standard curve for all analytes by pooling all the lyophilized standard spheres in a single 15 mL polypropylene tube. Add the appropriate amount of assay diluent following manufacturer's instructions.

   1.2. Mix well and wait 15 min at room temperature;

   1.3. Perform 1:2 serial dilutions in flow cytometric tubes adding the appropriate volume of assay diluent. Usually ten standard points are recommended including the 0 (zero) tube that contains only assay diluent.

2 Beads and sample preparation

   2.1. Calculate the number of total tubes of the experiment (including both standards and samples). For each tube, you need 1 μL of beads for each analyte. Prepare a sufficient volume of beads for all the tubes. Mix all beads specific for all analytes in a single tube.

   2.2. Add 500 μL of Wash Buffer from the kit.

   2.3. Centrifuge at $200 \times g$ for 5 min.

   2.4. Aspirate supernatant and resuspend in appropriate volume of Capture Beads Diluent to reach a final volume of 50 μL per tube of the experiment.
Use appropriate Capture Beads Diluent depending on the type of sample (serum, plasma, or culture supernatants)

   2.5. *Optional*. Depending on the type of experiment and expected protein concentration, perform appropriate sample dilution using assay diluent;

   2.6. Dispense 50 μL of standard or sample (or its appropriate dilution) in a tube;

   2.7. Add 50 μL of bead mix in each tube of standard or sample;

   2.8. Incubate 1 h at room temperature;

   2.9. Prepare the total mix of PE reagent containing the secondary Ab specific for each analyte included in the experiment, based on the number of total tubes to acquire (including both standards and samples), as reported in point 2.1;

   2.10. Add 50 μL of PE reagent in each tube of standard or sample;

   2.11. Incubate 2 h at room temperature;

   2.12. Wash each tube with 1 mL of Wash Buffer, centrifuge at $200 \times g$ for 5 min.

   2.13. Remove supernatants, then resuspend beads in 300 μL wash buffer and vortex before FCM acquisition.

3 Instrument setup

It is necessary to setup the instrument to correctly define the optimal voltage for different channels. First of all it necessary to set the FSC and SSC parameters to identify the bead population as singlets while excluding doublets (Fig. 69A). Subsequently, use compensation beads provided by the kit to set up
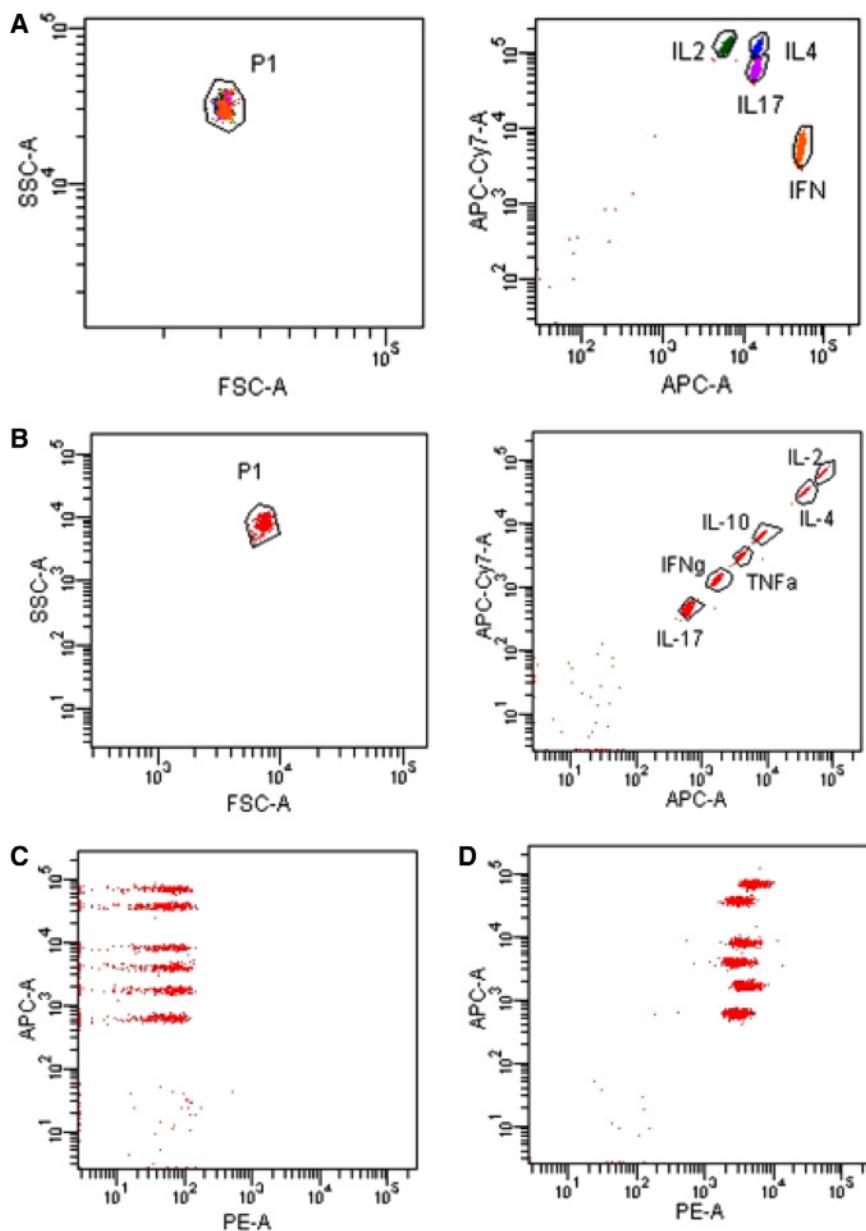
Figure 70. Quantification of human soluble cytokines with cytometric bead array (CBA) (A) Representative flow cytometry analysis of an experimental setting for evaluation of four different cytokines from culture supernatants of polyclonally stimulated human CD4+ T cells. The FSC/SSC plot allows identification of the total beads population; the APC-APC-Cy7 plot allows the identification of each bead corresponding to a specific analyte. Single beads are clustered based on the conjugation with different quantities of two different flurochromes. (B) Representative flow cytometric plots of an experiment for evaluation of six different cytokines from culture supernatants of polyclonally stimulated human CD4+ T cells. The FSC/SSC plot allows identification of the total bead population; the APC-APCCy7 plot allows identification of each bead corresponding to a specific analyte. Single beads are clustered based on their fluorescence intensity; in this case each bead population is conjugated with the same quantity of two different flurochromes used for its identification. (C and D) Representative flow cytometric plots of a standard curve from an experiment for measurement of six different cytokines, as reported in panel B: the "zero" tube in panel C (0 pg/mL) and the "top" tube in panel D (2500 pg/mL). Beads clusters are identified in APC (or APC-Cy7) channel and the different quantities of each analyte are defined by PE MFI.

the APC and APC-Cy7 voltages to reach the highest MFI (see Fig. 69B and C). This is of importance for proper identification of different beads, since they have different APC and APC-Cy7 emissions (Fig. 70A and B). Use the provided unstained beads to set up the minimum voltage of the PE channel (Fig. 69D).

4 Sample acquisition

4.1. Apply the final instrument setup obtained in the previous step to all samples within the same experiment;

4.2. Acquire the standard tubes from the lowest to the highest concentration (this sequence is important as the data analysis with the FCAP software will be easier, see below in section "data analysis");

4.3. Acquire each sample tube. In both standard and sample tubes it is important to record at least 300 events for each of the beads included in the mix.

17.7.4 Materials not included in the kit.

- Classic tubes for FCM
- 15 mL polypropylene tubes for preparation of standards solutions
- vortex, centrifuge, pipets, and tips

17.7.5 Data analysis. Data analysis is performed with FCAP Array software (available for Windows or MAC). Data generated for each acquired sample (including the standards) are exported from the acquisition software as .fcs files and then imported in the FCAP Array software. In the first step, it is necessary to select in the software menu the fluorescence of the beads (APC-APC Cy7 in this example) and that of the secondary Ab (PE in the

example) used in the experiment. Subsequently, the .fcs file of the first tube of the standard curve is imported into the software. Using this first .fcs file, the name of the specific target analyte to each bead cluster is assigned in the software. Next, the remaining .fcs files (both standards and samples) are imported, and the beads-recognition setting as set for the first imported file is applied to all fcs files. Standards should be distinguished from samples in a specific grid. For each sample it is possible to include the dilution factor, if applied (step 2.5). Using the MFI of the fluorochrome on the detector Ab (PE in this example) the software calculates the standard curve from .fcs files of the standard tubes. A specific standard curve is generated for each analyte. Unknown protein concentrations in sample .fcs files are then calculated by the software comparing the MFI of each bead cluster to the corresponding standard curve.

17.7.6 Pitfalls.

- Fluidic alteration during the acquisition of different samples can induce a wrong bead clusterization impairing the analysis by the FCAP software.
- Different dilution factors may be required to study different cytokines in the same sample. In case of preconfigured commercial kits, it is necessary to repeat the experiment with both diluted and undiluted samples. Instead, in case of customized experiments, it is possible to have separate kits so that cytokines with the same dilution factor are analyzed in the same experiment and separated from cytokines that require a distinct dilution.

17.7.7 Top tricks.

- Appropriate resuspension of standards, samples, and their dilutions are important to define the correct final concentration of the cytokines.
- Usually serum and plasma need higher dilution than culture supernatants but this depends on the type of analyzed cytokine as well as culture conditions of in vitro supernatants.
- Gently mix standards and tubes prior to acquisition, by pipetting. Do not use vortex. Use vortex only to resuspend beads before beads preparation (steps 2.1 and 2.5).
- Samples can be stored –30°C before evaluation; in this case, it is important to completely defrost samples and mix well before their dilution and/or usage.

17.8 Cytotoxicity

17.8.1 Overview.
Priming of naive pathogen- or tumor-reactive CD8$^+$ T lymphocytes (TN) occurs in secondary lymphoid organs (SLOs), where they undergo clonal expansion and differentiate into effector CD8$^+$ T (TE) lymphocytes (see also Chapter VI Section 1.1 Murine CD4 and CD8 T cells). In the course of their functional maturation, CD8$^+$ TE acquire the ability to leave SLOs, enter non-lymphoid organs (NLOs), produce inflammatory cytokines

and lyse target cells displaying cognate MHC class I-peptide complexes [652, 653]. Besides TE, immune activation also leads to the generation of long-lived memory T lymphocytes (TM), see also Chapter VI Section 1.4 Murine tissue resident memory T cells). CD8$^+$ T$_M$ can be found in SLOs and NLOs where they exert immediate effector functions upon secondary Ag contact [654, 655]. Peptide-specific target cell lysis is a cardinal feature of cytotoxic CD8$^+$ TE/TM (CTLs) [655, 656] and its quantification is a valuable means to track CD8$^+$ T cell responses. Here, we review methods to quantify cytotoxic function in vivo and ex vivo and present exemplary data using these assays to monitor cytotoxic activity of murine influenza-specific CTLs.

17.8.2 Introduction.
Traditionally, in vitro CTL assays relied on the detection of compounds released from dying target cells. For example, target cells loaded with radioactive sodium chromate lose their radioactive label as a result of CTL-mediated lysis. Hence, the amount of radioactivity in the supernatant of effector (CTL)/target cell co-cultures directly correlates with the lytic activity of the respective CTL population [657]. To achieve suitable effector-to-target cell (E:T) ratios of at least 50:1, high numbers of CTLs are required for this type of assay. This usually requires antigen-dependent CTL expansion in vitro, a process that may alter the composition and/or function of the starting CTL population.

In order to replace radioactive CTL assays, several FCM-based techniques were established in the past years. Their major aim is to visualize the biochemical processes involved in CTL-mediated target cell lysis.

CTLs induce target cell apoptosis via the Fas/Fas ligand pathway [658] or the release of cytotoxic granules containing perforin and granzymes [659]. Either pathway results in the activation of caspase-dependent target cell apoptosis. To visualize this process, cell-permeable fluorogenic caspase substrates were developed [660]. They consist of two fluorophores, which are linked by a caspase-sensitive peptide. Only upon caspase-dependent cleavage these substrates become activated and can be detected by FCM. Alternatively, target cell apoptosis can be visualized with the help of fluorochrome-labeled inhibitors of caspase (FLICA), which bind specifically to active caspases [661, 662]. Hence, in both cases fluorescence intensities correlate with CTL-dependent target cell destruction. However, similar to the chromium release assay, relatively high E:T ratios are required for these experimental approaches.

A more sensitive assay relies on the co-incubation of CTLs with a mixture of target cells consisting of at least two different populations. For this so-called fluorometric assessment of T lymphocyte antigen-specific lysis (FATAL) assay [663], the first target cell population is loaded with the MHC I-restricted peptide of interest and stained with one dye (e.g., PKH-26). The second population is loaded with an irrelevant peptide, stained with a different dye (e.g., CFSE) and serves as negative control [663]. Different concentrations of the same dye can be used to stain both target cell populations, which are discriminated based on their differential fluorescence intensities. Alternatively, amine-reactive dyes such as Cell Tracer Violet can be used, which are less prone to dye

transfer between cells observed with lipophilic dyes. The extent of CTL activity is determined by the relative numeric decrease of labeled target cells loaded with the desired peptide over nonspecific target cells after a period of time, usually 5 h. Significant advantages of this assay are its high sensitivity and favorable SNR due to negligible amounts of spontaneous tracer release, a common side effect of the chromium release assay. Due to these advantages, the FATAL assay is often well suited to directly measure CTL function ex vivo without prior expansion and at comparably low E:T ratios.

Target cells may be immune (e.g., splenocytes) or somatic cells (e.g., epithelial cells or fibroblasts) to more closely resemble the physiological CTL targets. CTLs can be purified from any organ of interest, either lymphoid or non-lymphoid. Depending on the research question, purification of total $CD8^+$ T cells, or antigen-specific $CD8^+$ T cells may be required. In the former case, the frequency of antigen-specific CTLs can be determined in parallel by MHC/peptide multimer staining to adjust E:T ratios for different tissue samples. Figure 71 shows an example of ex vivo cytotoxicity by influenza-specific CTLs isolated from the broncho-alveolar space of infected mice without the need of a prior sort for influenza-specific CTLs.

However, if the frequency of antigen-specific $CD8^+$ T cells is very low, it may be necessary to enrich them prior to the cytotoxicity assay. In this case, it is not advisable to sort antigen-specific $CD8^+$ T cells by means of TCR labeling (e.g., by MHC/peptide multimers) since this may alter their lytic function. If available, the use of congenically-marked TCR-transgenic (TCR^{tg}) CD8 T cells might be useful to circumvent this problem. This allows their marker-based, TCR-independent enrichment prior to the ex vivo CTL assay. Hence, direct ex vivo CTL assays have several advantages: (i) they are very sensitive, (ii) CTLs may be isolated from any organ, (iii) the type of target cell may be adapted to the nature of the experiment, and (iv) E:T ratios can be adjusted to compare different samples. However, it is important to note that the tissue microenvironment affects CTL activity [664]. Hence, the lytic potential of tissue-resident CTLs may differ from those purified for ex vivo CTL assays.

To circumvent this problem CTL activity can be measured in vivo [656, 665, 666]. Again, at least two target cell populations are required. One is labeled with the peptide of interest and e.g., a high concentration of a suitable dye such as CFSE ($CFSE^{hi}$ population). The control population is loaded with an irrelevant peptide and a tenfold lower concentration of CFSE ($CFSE^{lo}$ population). Equal numbers of $CFSE^{hi}$ and $CFSE^{lo}$ cells are co-injected into effector mice. After 4–18 h, SLO can be isolated to analyze single cell suspensions by FCM. Similar to the direct ex vivo assay described above, the relative loss of $CFSE^{hi}$ target cells over $CFSE^{lo}$ cells indicate the extent of CTL-mediated lysis. This method provides the most sensitive and physiological assessment of CTL activity. Figure 72 shows an example of influenza-specific CTL activity in lung-draining mediastinal LNs and nondraining distal LNs in mice undergoing flu infection.

In vivo CTL assays can also be used to determine the lytic potential of multiple CTL populations with different specificities at the same time. This requires the simultaneous use of more than two target cell populations. A simple method to achieve this goal is the use of splenocytes from homozygous $CD45.1^+/1^+$ and heterozygous $CD45.1^+/2^+$ congenic mice as target cells in $CD45.2^+/2^+$ effector mice. Using mAbs against CD45.1 and CD45.2, mixed $CD45.1^+$ target cells can be discriminated from host cells. Furthermore, the different target cell types can be distinguished based on their differential CD45.1/.2 expression and varying CFSE intensities.

17.8.3 Preparation of target cells. For in vivo CTL cytotoxicity assays, cell suspensions from the spleen are commonly used as target cells. For the experimental results shown in Fig. 72, a spleen cell suspension from naive mice was split in two equal groups. One group was labeled with 1 μM of the immunodominant IFV peptide $NP_{366-374}$ and the other group with an irrelevant peptide for 30 min at room temperature. Time and concentration may be changed depending on the affinity of the peptide for MHC class I. An equal volume of 0.2 μM Cell Proliferation Dye eFluor 670 (CPD-eF670) in protein-free RPMI was then added to the sample with the irrelevant peptide and immediately mixed. The other sample was labeled with a tenfold higher concentration of CPD-eF670. Samples were further incubated in the dark for 15 min at room temperature. Beyond this point, samples were maintained at 4°C at all times to prevent decay of H-2D^b/ $NP_{366-374}$ complexes. Samples were extensively washed in PBS containing 10% FCS to remove excess peptide and dye and counted in independent triplicates. An equal number of cells was mixed 1:1 and finally resuspended in PBS. The final concentration of cells to be injected into mice depends on several factors such as (i) the organ of final analysis (target cells migrate in higher numbers into the spleen compared to the lymph nodes); (ii) the amount of target organ available for analysis; (iii) the desired (expected) effector to target ratio. Typically, 2×10^6 or 5×10^6 of each target population is sufficient to analyze kill activity in spleen or lymph nodes, respectively. In the literature killing of $5–10 \times 10^6$ of each target cell population is typically monitored.

For in vitro or ex vivo cytoxicity assays, a wider range of target cell types may be used since effectors and target cells are incubated in vitro. Independently of this, however, the treatment and labeling of target cells is performed in a similar manner as described above.

17.8.4 Materials.

Product	Company
PBS	Gibco
RPMI	Gibco
FCS	Gibco
Peptides	Xaia peptides
Cell Proliferation Dye eFluor670	Thermofisher
Hoechst33258	Thermofisher
Propidium iodide	Sigma
BD FACSCantoII	BD Biosciences
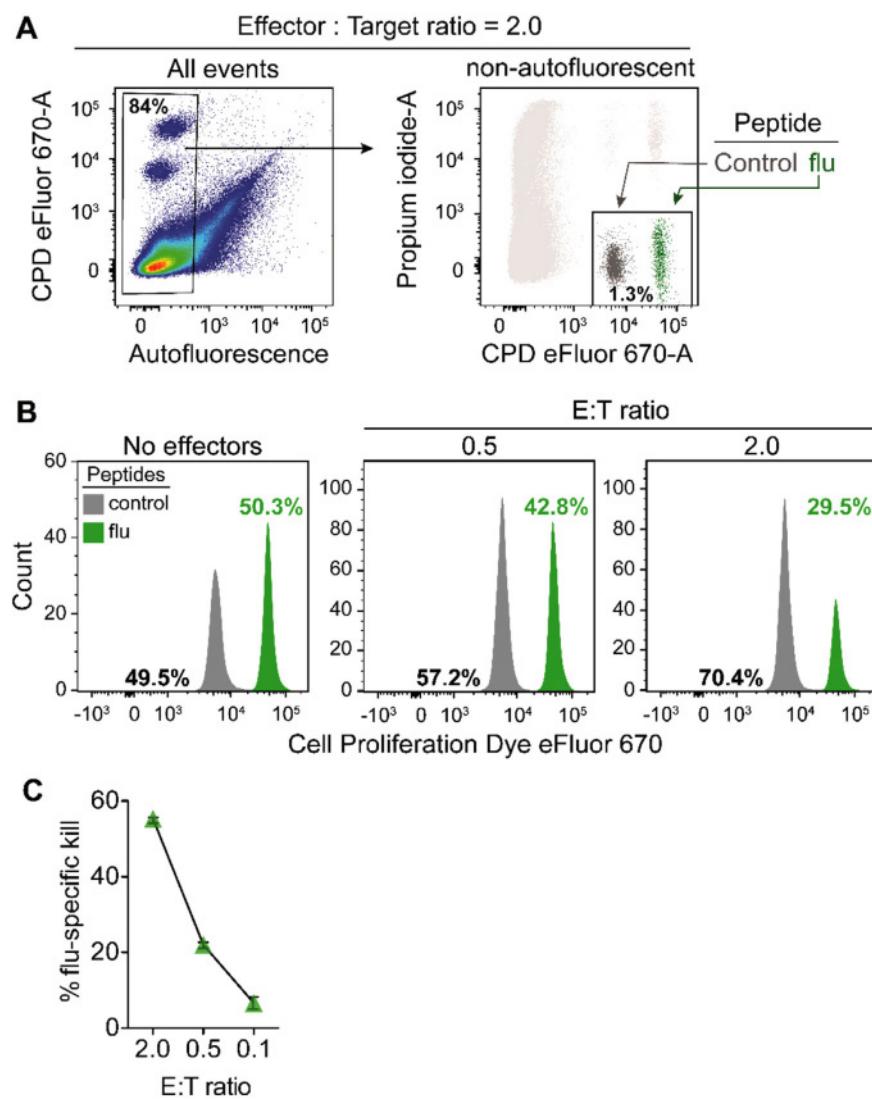
Figure 71. Quantification of *ex vivo* cytotoxicity by influenza-specific CTLs. Seven days after pulmonary infection with influenza A/WSN/33, untouched flu-specific murine CTLs in unfractionated bronchoalveolar lavage (Effectors, E) were incubated in vitro with a titrated number of target cells (T). Targets consisted of an equal mixture of spleen cells loaded with the MHC-I-binding influenza peptide $NP_{366-374}$ (flu) or an irrelevant MHC-I ligand (control). Flu peptide-loaded spleen cells were labeled with a higher concentration of Cell Proliferation Dye eFluor 670 than their control counterparts. Five hours later, the relative frequency of the remaining target cells was quantified by FCM. The exact frequency of flu-specific CTLs can be determined in parallel by staining with the corresponding MHC-I multimer. (A) Flow cytometric gating strategy to identify target cells. Shown are results for the Effector:Target ratio of 2. (B) Histograms showing the percentage for each target cell population at the end of the assay. (C) Quantification of technical duplicates shown in (B). The percentage of flu-specific kill was calculated as: $100 - [100 \times (T^{flu} / T^{control})_{with\ E} / (T^{flu} / T^{control})_{without\ E}]$.

17.8.5 Data analysis. Samples are processed for standard flow cytometric analysis. Specially, for in vivo cytotoxicity assays, it is necessary to acquire a relatively large number of events since the proportion of target cells among the total acquired population is very low, typically below 1–2%. The gating strategy for quantifying antigen-specific cytotoxic activity is illustrated in Figs. 71A and 72A for ex vivo and in vivo cytotoxicity assay, respectively. It is recommended that an "empty channel" is used to gate out autofluorescent cells. The degree of cytotoxic activity is determined by the relative decrease in the number of target cells displaying the specific epitope over those displaying an irrelevant epitope at the end of the assay time. To calculate the percentage of specific killing, the following formula can be used:

Ratio = (% control targets/% specific targets)

% specific lysis = 1 − (ratio negative control/ratio test group) × 100

17.8.6 Pitfalls. Although in vivo CTL assays offer obvious advantages, they are not suitable for all experimental systems. For example, the choice of target cells is limited. Most somatic cells, which are often the primary "natural" targets of viral infections, are trapped within the lung and liver vasculature soon after i.v. injection into mice. Thus, they are of limited use as target cells in vivo. The use of naive splenocytes as target cells may help to circumvent this problem. However, naive splenocytes usually do not enter NLOs effectively. Hence, the appropriate tissue tropism of the desired target cell type is a prerequisite for the successful application of the FCM-based in vivo kill assay. A disadvantage of in vivo CTL assays is the fact that E:T ratios cannot be adjusted. Hence, differences in lytic activity may result from differences in CTL numbers and/or the lytic potential of individual cells. The quantification of specific CTLs by MHC/peptide multimers in the respective target organs may be useful to judge
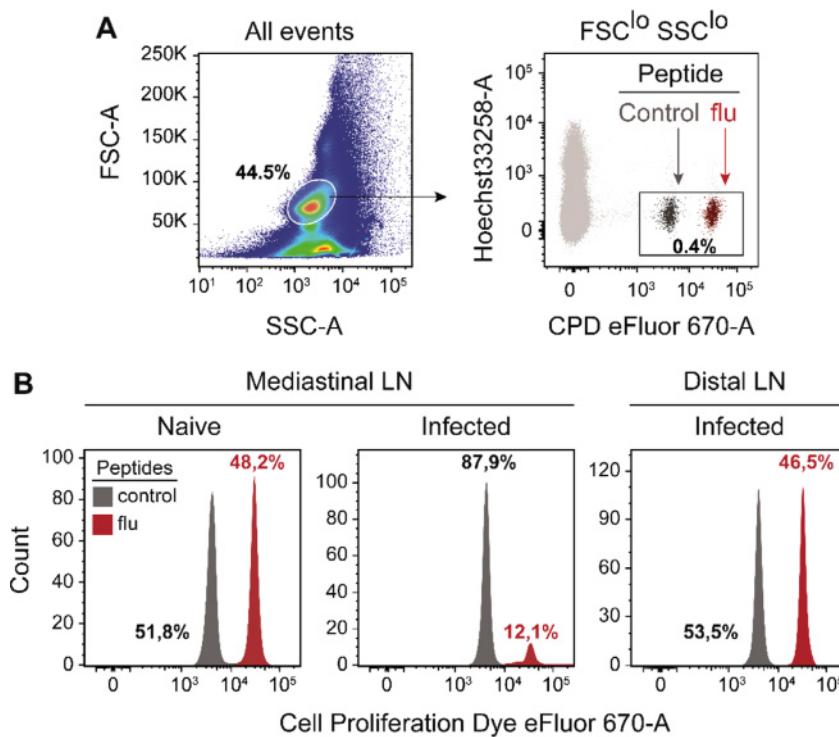
Figure 72. Quantification of *in vivo* cytotoxicity by influenza-specific CTLs. Seven days after pulmonary infection with influenza A/WSN/33, infected and naive mice received target cells intravenously. Targets consisted of an equal mixture of spleen cells loaded with an MHC-I-binding influenza peptide (flu) or an irrelevant MHC-I ligand (control). Flu peptide-loaded spleen cells were labeled with a higher concentration of Cell Proliferation Dye eFluor 670 than their control counterparts. Four hours later, target cells in lung-draining mediastinal LNs and non-draining inguinal (distal) LNs were quantified by flow cytometry. (A) Flow cytometric gating strategy to identify target cells in the indicated organs. (B) Representative histograms indicating the percentage of eqch target cell population at the end of the assay in the indicated organs.

whether differences in target cell lysis rely on differences in CTL number and/or function.

All assays described so far are suitable to quantify the lytic action of CTL populations. However, the lytic potential of individual CTLs cannot be judged. To approach this problem, Abs directed against, e.g., CD107a can be used. This molecule is present on the membrane of cytotoxic granules and becomes detectable on the cell surface of degranulating CTLs. CD107a levels correlate closely with the lytic potential of CTLs [627]. However, they can also be differentially regulated [667]. Precise imaging of the accumulation of CD107a, granzyme, and other molecules in the cytotoxic immune synapse between T cells and target cells can be performed by imaging FCM [668] (see also the section on Imaging FCM). mAbs directed against CD107a can be combined with FATAL assays, MHC/peptide multimers, or cytokine-specific Abs to determine multiple effector functions of individual antigen-specific CTLs by FCM [669, 670]. This method might be helpful to complement the ex vivo and in vivo CTL assays described above. However, it should be noted that, contrary to the degree of target cell lysis, the level of CD107a upregulation is most pronounced at low E:T ratios [669].

17.9 Treg suppression assays

17.9.1 Overview.   Regulatory T (Treg) cells are critical for the maintenance of immune homeostasis. However, since many of their markers are shared by activated T-cells, accurately defining Treg cells can be difficult by phenotype alone. One defining feature of Treg cells is that they are capable of suppressing the proliferation and activation of other cells both in vitro and in vivo. As a result, measurement of their in vitro suppressive capacity is an important part of defining and characterizing a putative Treg cell population. This chapter details several methods for the assessment of the suppressive function of polyclonal or antigen specific regulatory T-cells in mice or humans.

17.9.2 Introduction.   The ability to measure the capacity of Treg cells to prevent the proliferation of conventional CD4 and CD8 T-cells is an important factor in understanding their function. Tregs have been described to use a range of suppressive mechanisms with CTLA-4 dependent depletion of the co-stimulatory molecules CD80 and CD86 from the surface of antigen presenting cells known to have a critical role [671]. Several methods for the assessment of cellular proliferation by incorporation of radioactive isotopes or cells counting have been used to measure cellular proliferation and suppressive function. However, these assays have difficulty in determining which cells are proliferating and cannot give detailed information on the number of divisions undertaken by individual cells. More recently cytometry-based assays relying on staining a responder population with an amine-reactive fluorescent dyes such as CFSE and cell trace violet (CTV) that are diluted in a predictable manner during cell division has proven an effective method to measure cell proliferation. Utilizing this system, it is possible to add Treg cells to culture and observe the effects of varied ratios of Tregs on the proliferation of the responder population [672]. In addition to assays utilizing polyclonal stimuli such as CD3 mAb, the measurement of the suppression of human antigen-specific T cells in vitro provides information closer to the physiology. However, suppression assays using antigen-specific T cells is made difficult by the low frequency of T cells specific to a single antigen in the T cell repertoire in vivo. In addition, highly functional CD8$^+$ T effector cells, in contrast to their naïve coun-

Table 15. Materials for murine suppression assay

Reagent	Fluorochrome	Clone	Company	Catalog
LIVE/DEAD™ Fixable Near-IR Dead Cell Stain Kit	Near-IR dye	N/A	Invitrogen	L10119
CD4+ T Cell Isolation Kit, mouse	–	N/A	Miltenyi	130-104-454
Cell Trace™ CFSE Cell Proliferation Kit	CFSE	N/A	Invitrogen	C34554
Anti-B220*	APC-Cy7	RA3-6B2	BD	552094
Anti-CD11c	APC-Cy7	N418	Biolegend	117323
Anti-CD11b	APC-Cy7	M1/70	Biolegend	101225
Anti-GITR	PE-CY7	DTA-1	BD	558140
Anti-CD25	APC	PC65.5	eBioscience	17-0251-82
Anti-CD4	V500	RM4-5	BD	560782
Anti-CD3	AF700	14-A2	Biolegend	100216
Anti-CD3	N/A	145-2C11	BD	553057

terparts, can resist Treg cell suppression in vitro, and can display multiple molecular strategies (including cell cytotoxicity targeting Tregs) to counteract excessive Treg cell suppression [673, 674]. In doing so, they can preserve their effector functions, which can produce protective or detrimental effects depending on the context (e.g., infection recovery vs. autoimmunity). As a result, measurement of their in vitro killing capacity is important to discriminate the highly functional CD8+ T effector cells that are not susceptible to Treg cell suppression, from those dysfunctional that have lost the capacity to resist Treg cells, because they become exhausted in tumor or chronic infection settings. Here, we describe protocols allowing the measurement of human and murine Treg suppressive function in both a polyclonal manner and using a low number of antigen-specific CD8+ T cells, by selectively gating the latter with multimers of MHC class I molecules complexed with relevant antigenic peptides.

17.9.3 Polyclonal suppression assays.

17.9.3.1 Murine polyclonal suppression assay.   Step-by-step sample preparation (see Table 15 for reagents)

Single cell suspensions of lymph nodes or spleen of a Foxp3-GFP reporter mouse are subjected to negative selection of CD4 T-cells by magnetic beads (CD4+ T Cell Isolation Kit, Miltenyi Biotec).

Cells are then stained for 30 min at 4°C with Abs for CD3, CD4, CD25, and B220 and sorted on a BD Aria-II. Tregs are sorted as CD3+CD4+B220-Foxp3+CD25+ and confirmed to have a post sort purity of 90%+ (Fig. 73A). Conventional T (Tconv) cells are sorted as CD3+CD4+B220-Foxp3-CD25-. When a Foxp3 reporter mouse is not available CD25 and GITR can be used in its place (Fig. 73B).

CD4 Tconv are then stained with 1 μM CFSE for 10 min in serum free media at room temperature. Excess CFSE is then quenched by addition of media+10%FCS before washing three times.

A total of 1×10^4 Tconv cells per well are cultured with or without Treg cells at varied ratios (0:1, 1:1, 1:2, 1:4, 1:8 Treg:Tconv) for 3 days in the presence of 1×10^5 γ-irradiated CD4 depleted APCs (18.5Gy irradiated CD4 depleted splenocytes obtained by magnetic separation in step 1) and 1 μg/mL soluble CD3 mAb (Clone: 145-2C11) in 96-well U-bottomed plates, in RPMI media containing 10% FCS, 2-ME, L-glutamine and Penicillin/streptomycin with a final volume of 200 μL. In all cases the number of Tconv is fixed while the number of Tregs is changed to obtain the intended ratios.

At the end of the 3 day culture period, cells are then stained with CD4 mAb, CD25 mAb, and IR Live/Dead dye and data collected on a BD LSR Fortessa.

17.9.3.2 Human polyclonal suppression assay.   Step-by-step sample preparation (see Table 16 for reagents)

Initially PBMCs are isolated from fresh blood via Ficol–Paque centrifugation in Leucosep tubes. CD4 T-cells are enriched by negative selection of CD4 cells with magnetic beads (Miltenyi). Cells are stained with Abs for CD4, CD45RA, CD127, and CD25 for 30 min at 4°C.

Bulk Treg cells can be sorted as CD3+CD4+CD127loCD25+ (Fig. 73C). If finer fractionation of Treg cells is required, CD127loCD25+ cells can then be further separated into fraction I Naïve Tregs, fraction II effector Tregs and fraction III non-suppressive cells (Fig. 73C) [675]. It should be noted that while fraction III as a whole is mostly made up of Foxp3 expressing non-Treg cells it may contain 20–30% CXCR5+ effector Tfr, which are functionally suppressive Treg cells [676].

Naïve responder Tconv cells are sorted as CD25-CD45RA+CD4+CD3+ and then stained with 1 μM CFSE. A total of 1×10^4 Tconv cells are co-cultured with various ratios of Tregs cells (0:1, 1:1, 1:2, 1:4, 1:8 Treg:Tconv) and 1×10^5 γ-irradiated APC (18.5Gy irradiated CD4 depleted PBMCs obtained by magnetic separation in Step 1) and stimulated with 1 μg/mL soluble CD3 mAb (Clone: OKT3) for 4–5 days in 96-well round-bottom plates in RPMI medium containing 10% AB serum, 2-ME, L-glutamine, HEPES, and penicillin/streptomycin in a final volume of 200 μL. In all cases the number of Tconv and APC is fixed while the number of Tregs is changed to obtain the intended ratios.
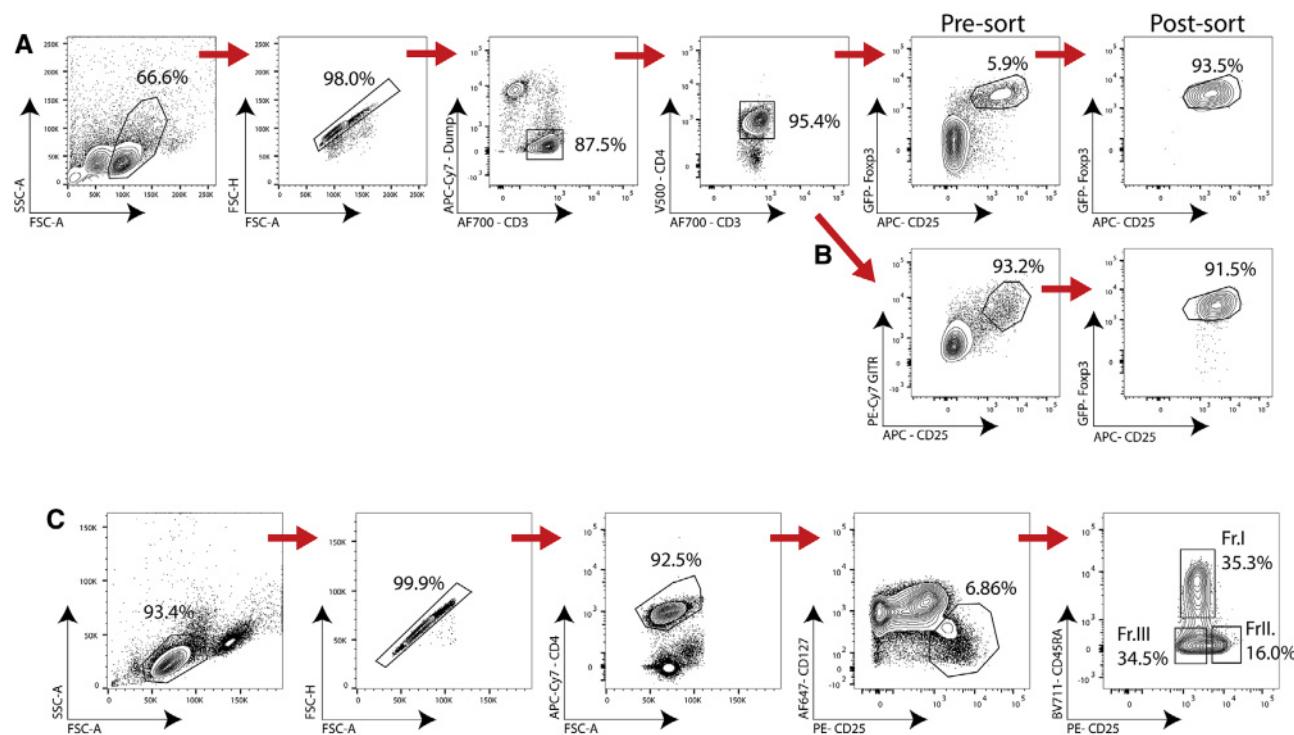
Figure 73. (A) Gating example of murine CD3$^+$CD4$^+$B220$^-$CD25$^+$Foxp3-GFP$^+$ Treg cells. (B) Alternative strategy if Foxp3 reporter is not available. (C) Gating example of human CD4$^+$CD25$^+$CD127^{lo}FOXP3$^+$ cells and further sub gating into fractions I (Naïve Tregs), II (effector Tregs), and III (Non-Tregs/Tfr). In this example, CD4 APC-Cy7 was used to avoid clash with CXCR5 BV421 but we would recommend CD4 V500 and IR live/dead when this is not the case.

After a culture period of 4–5 days cells were then stained with CD4, CD25 and IR Live/Dead dye and data collected on a BD LSR Fortessa.

17.9.4 Suppression assays and antigen-specific T cells.

17.9.4.1 Human suppression assay of antigen-specific T cells.
Step-by-step sample preparation

1. PBMCs are isolated from fresh heparinized blood by density gradient centrifugation with Lympholyte (Cedarlane, Burlington, Canada).

2. CD8$^+$ T cells are pre-enriched from PBMCs with the corresponding CD8$^+$ T Cell Isolation Kit (Miltenyi Biotec, Bergisch Gladbach, Germany) and then highly purified CD8$^+$ T naïve (TN; CCR7$^+$CD45RA$^+$) cells are enriched from CD8$^+$ T cells by magnetic bead-separation with the Naïve CD8$^+$ T Cell Isolation Kit (Miltenyi Biotec). The combination of highly purified CD8$^+$ T effector memory (EM; CCR7$^-$CD45RA$^-$) and effector memory RA$^+$ (EMRA; CCR7$^-$CD45RA$^+$) cell population is obtained by using the positive fraction after enrichment of TN cells. Treg cells are isolated from PBMCs with the CD4$^+$CD25$^+$ Regulatory T Cell Isolation Kit (Miltenyi Biotec) (Fig. 74). Each purified cell subset is used in the various experiments only when the

Table 16. Materials for human suppression assay

Reagent	Fluorochrome	Clone	Company	Catalog
LIVE/DEAD^{TM} Fixable Near-IR Dead Cell Stain Kit	Near-IR dye	N/A	Invitrogen	L10119
Ficoll-Paque PLUS	N/A	N/A	GE healthcare	17144003
CD4$^+$ T-cell isolation kit, human	N/A	N/A	Miltenyi	130-096-533
Leucosep^{TM} Centrifuge Tubes	N/A	N/A	Greiner Bio-One	227290
Anti-CD4	V500	RPA-T4	BD	560768
Anti-CD127	AF647	HIL-7R-M21	BD	558598
Anti-CD45RA	BV711	HI100	Biolegend	304138
Anti-CD25	PE	M-A251	BD	555432
Cell Trace^{TM} CFSE Cell Proliferation Kit	CFSE	N/A	Invitrogen	C34554
Anti-CD3	N/A	OKT3	BioLegend	317302
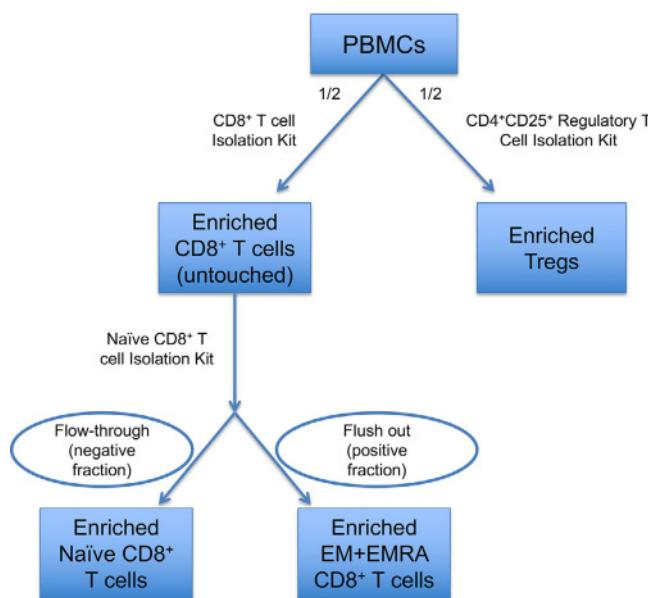
Figure 74. Flow chart illustrating steps of cell subsets isolation. A portion of PBMCs is used for enrichment of CD8+ T cells, another portion is used for enrichment of Tregs. The enriched CD8+ T cells fraction (untouched) is used for isolation of Naïve (negative fraction) and EM+EMRA (positive fraction) CD8+ T cells, with Naïve CD8+ T cell isolation kit.

purity of the corresponding cells is >96% and 90% for T cell populations and Treg cells, respectively (Fig. 75A and B).

3. Highly purified autologous CD8+ T cell subpopulations (isolated as described above) are labeled with 10 μM of CFSE (Thermo Fisher Scientific, Massachusetts, USA) for 15 min at 37°C in RPMI complete medium containing 10% FBS (up to 10×10^6 cells/mL). To quench the reaction, an isovolume of cold FBS is added and cells are washed twice.

4. Then, they (500 000–1×10^6/well) are co-cultured with both autologous γ-irradiated (70Gy) PBMCs as APCs (at a 1:1 ratio), which had previously been pulsed or not with 20 μg/mL of antigen or peptide(s) plus 1 μg/mL of CD28 mAb, and highly purified Treg cells, which had previously been stained with 5 μM of CellTrace Violet (Cell Proliferation Kit, Thermo Fisher Scientific) at different CD8+ T cell:Treg cell ratios (100:1, 10:1, 4:1, and 1:0), in RPMI complete medium containing 5% human serum AB, in 48-well plate (0.5–1 mL/well). The number of CD8+ T cells is changed while the number of Tregs is fixed. Cells are cultured for 7 days, and half of the medium is replaced with fresh medium containing 20 IU/mL of IL-2 at day 4.

5. Cells are stained with Fixable Viability Dye eFluor780 for exclusion of dead cells in PBS 30 min at room temperature. After washing, cells are incubated with the pool of APC-labeled-multimers of MHC class I molecules complexed with the relevant peptides, in PBS containing 2% FBS at room temperature for 10 min. Surface staining are performed incubating cells with labeled mAbs to CD8, CD4, CCR7, CD45RA, and with a cocktail of labeled mAbs to CD14, CD16, CD56, CD19, (dump channel was included for the exclusion of monocytes, NK cells,

and B cells, respectively) for 20 min at 4°C. After washing, cells are fixed and permeabilized using the FOXP3/Transcription Factor Staining Buffer Set (eBioscience, MA, USA) at 4°C for 30 min, washed, and then stained with mAbs to FOXP3 for 30 min at room temperature (Ab details reported in Table 17) (Fig. 76A and B). All the incubations are performed in the dark. In the representative experiments shown in Fig. 76, as multimers of MHC class I molecules, we used APC-labeled-HLA-A*0201 dextramers complexed with self-peptides (MYH9$_{478-486}$, MYH9$_{741-749}$, VIME$_{78-87}$, VIME$_{225-233}$, ACTB$_{266-274}$) (Immudex, Copenhagen, Denmark) to detect autoreactive CD8+ T cells in various forms of autoimmune diseases [673]. The percentage of Treg-mediated suppression is calculated using the following formula: %Treg suppression = (MFI CFSE-stained dextramer+ CD8+ T cells with Treg cells − MFI CFSE-stained dextramer+ CD8+ T cells without Treg cells)/(MFI CFSE-stained dextramer+ CD8+ T cells unstimulated − MFI CFSE-stained dextramer+ CD8+ T cells without Treg cells) × 100 (Figure 76C).

17.9.4.2 Human killing assay of Treg cells by antigen-specific CD8+ T effector cells.   Step-by-step sample preparation

1. Highly purified CD8+ T, TEM+EMRA (effectors), or TN cells are stained with 10 μM of CFSE and co-cultured with autologous γ-irradiated (70Gy)-PBMCs (1:1 ratio), which had previously been pulsed (or not) with 20 μg/mL of antigen or peptide(s) plus 1 μg/mL of CD28 mAb, and highly purified autologous or allogeneic target cells (purified T cells, Treg cells, or others), which had previously been stained with 5 μM of CellTrace Violet (CellTrace Cell Proliferation Kit).

2. CD8+ T cells and target cells are co-cultured (or not) at a ratio of 10:1 for 7 days in complete RPMI medium containing 5% human serum AB, as previously described; at day 3, half of the medium is replaced with fresh medium plus 20 IU/mL of IL-2.

3. To investigate the granzyme B (GZMB)-mediated killing effect of CD8+ TEM+EMRA on targets, the assays are performed in the presence of GZMB inhibitor (Santa Cruz Biotechnology, Dallas, TX) or NKG2D neutralizing Ab (R&D Systems, Minneapolis, MN). Specifically, target cells are treated (or not) with 20 μM of GZMB inhibitor for 1 h at 37°C, and CD8+ TEM+EMRA cells are treated with 1 μg/1×10^6 of NKG2D neutralizing Ab for 15 min at room temperature. Cells are stained with Fixable Viability Dye eFluor780, APC-labelled-HLA-A*0201 multimers complexed with the relevant peptides (previously described), labeled mAbs to CD8, CD4, CCR7, CD45RA and with a cocktail of labeled mAbs to CD14, CD16, CD56, CD19 (dump channel was included for the exclusion of monocytes, NK cells, and B cells, respectively) for 20 min at 4°C. After washing, cells are fixed and permeabilized for the subsequent intranuclear staining with mAb to FOXP3, as previously described (Ab details reported in Table 17; Fig. 77).

Table 17. Materials for human suppression assay of antigen-specific T cells

Reagent	Fluorochrome	Clone	Company	Catalog
Lympholyte	N/A	N/A	Cedarlane	CL5010
CD8$^+$ T Cell Isolation Kit	N/A	N/A	Miltenyi	130-096-495
Naïve CD8$^+$ T Cell Isolation Kit	N/A	N/A	Miltenyi	130-093-244
CD4$^+$CD25$^+$ Regulatory T Cell Isolation Kit	N/A	N/A	Milteny	130-091-301
CellTrace^{TM} CFSE Cell Proliferation Kit	CFSE	N/A	Thermo Fisher	C34554
CellTrace^{TM} Violet Cell Proliferation Kit	Violet	N/A	Thermo Fisher	C34571
FOXP3/Transcription Factor Staining Buffer Set	N/A	N/A	eBioscience	00-5523-00
Viability dye	eFluor780	–	eBioscience	65-0865-18
Anti-CD8	Vio-Green	BW135/80 Fab	Miltenyi	BW-1 35/80
Anti-CD8	Alexa-Fluor488	SK1	Biolegend	344716
Anti-CD8	BV-510	SK1	Biolegend	344732
Anti-CD45RA	BV-605	HI100	Biolegend	304133
Anti-CCR7	PerCP-Cy5.5	G043H7	Biolegend	353220
Anti-GZMB	Bv510	GB11	BD Biosciences	563388
Anti-NKG2D	PECF594	1D11	BD Biosciences	562498
Anti-FOXP3	PerCP-Cy5.5	PCH101	eBioscience	45-4776-42
Anti-CD14	APC-eFluor780	61D3	eBioscience	47-0149-42
Anti-CD16	APC-eFluor780	CB16	eBioscience	47-0168-42
Anti-CD56	APC-eFluor780	CMSSB	eBioscience	47-0567-42
Anti-CD19	APC-eFluor780	HIB19	eBioscience	47-0199-42
Anti-CD3	PE-Cy7	SK7	BioLegend	344816
Anti-CD3	APC	SK7	BioLegend	344812
Anti-CD40L	BV-421	24-31	BioLegend	310823
Annexin V	FITC		BioLegend	640906
PI			BioLegend	421301
Anti-CD4	Alexa-Fluor488	OKT4	eBioscience	53-0048-42

PI: Propidium Iodide

17.9.4.3 Materials.

17.9.5 Data Analysis. There are several possible approaches to analyzing proliferation data. A common approach is to place a gate based on the nondivided peak measuring the percentage of cells that have divided at least once. This method has the benefit of simplicity and is commonly used. However, this method is also insensitive as it fails to take into account the number of divisions undertaken by the dividing cells. For example, if two populations have 75% that have divided at least once but the first has most cells in the second peak and the second has most cells in the fourth peak, then this method will report the same result despite their being a clearly observable difference in proliferation.

Modeling of the peaks to calculate the total number of cell in each peak allows the use of more sensitive measurements such as division index (the average number of divisions by each cell) or proliferation index (the average number of divisions undertaken by each dividing cell) [677]. It should be noted that different software uses the terms division index and proliferation index with differing definitions, so they should always be clearly defined when used, the division index used here was calculated by FlowJo software. When both percentage divided and division index are used to measure proliferation in the same population, it may be seen that while the results are broadly similar, division index is

able to measure appreciable suppression at low Treg ratios that are less clearly different when using percentage divided (Fig. 78). In the assay calculating the percentage suppression of antigen-driven T cells (Fig. 76), the resulting T cell proliferation can be detectable by using the MFI of CFSE-stained T cells better than by using percentage of divided T cells or the division index. Indeed, because of the tiny number of T cells specific to a given epitope, they are less synchronous as compared with polyclonal T cells stimulated with CD3/CD28 mAb, in which the high number of proliferating cells allow to define peaks and to distinguish their generations (see Fig. 78) [677]. Furthermore, the different antigen-specific cell subsets (e.g., naïve or effector T cells) display a striking difference in their baseline proliferation (without Treg) (Figs. 76 and 79). Figure 79 shows the difference between percentage suppression calculated using percentage divided T cells (A), and percentage of suppression calculated using MFI CFSE (B) (as reported above and in Fig. 76C).

17.9.6 Pitfalls. Care must be taken with the timing of the assay to ensure that the cells do not proliferate to the extent that they completely lose the proliferation dye. This will both make it impossible to resolve any proliferation past this point but also risk mixing up the responder and suppressor populations that are often separated on the basis of the proliferation dye. To an extend inclusion
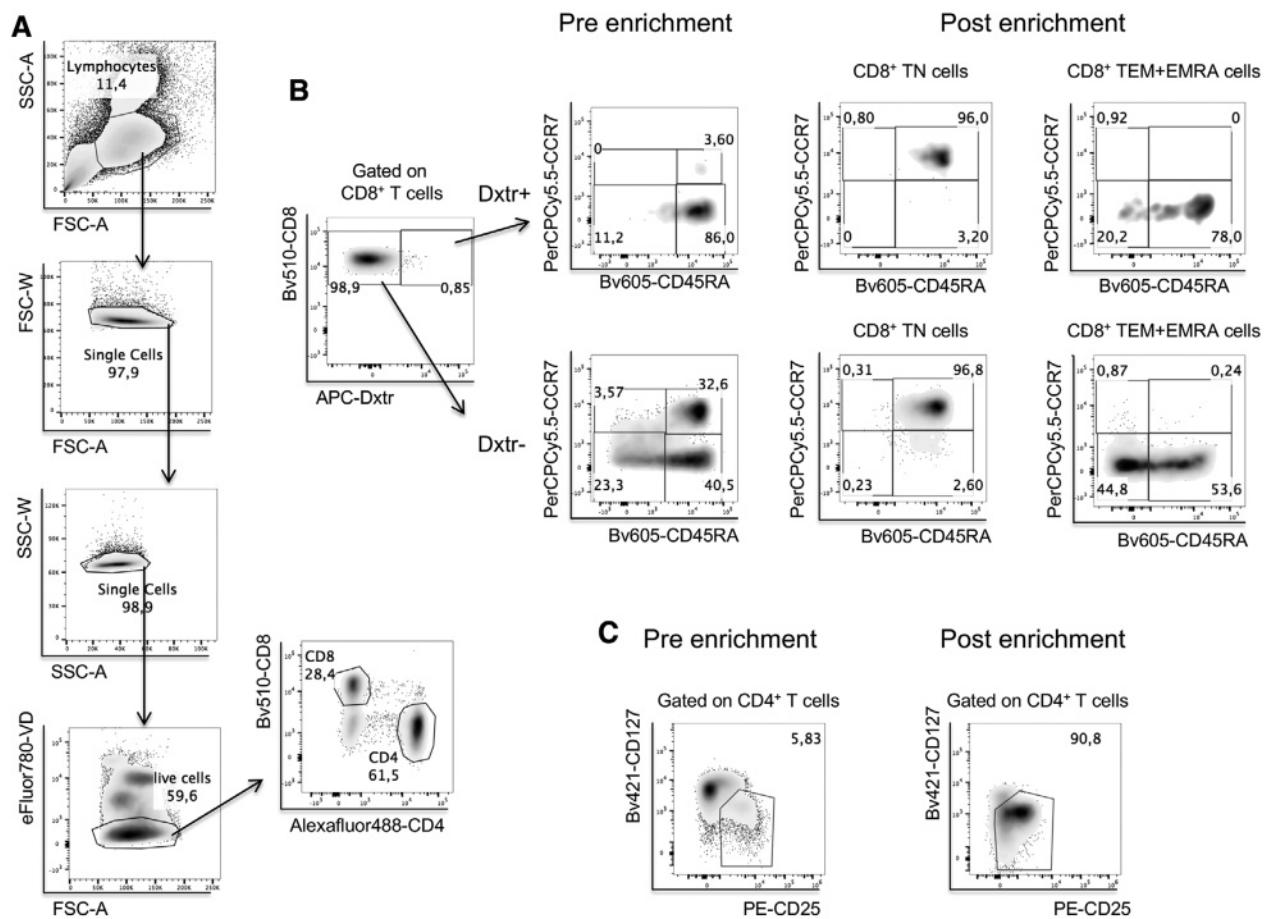
Figure 75. (A) Representative flow-cytometry (FC) analysis of the gating strategy applied for the identification of CD8$^+$ and CD4$^+$ T cells. Briefly, lymphocytes were first gated by the physical parameter Forward and Side scatter area (FSC-A and SSC-A) and doublets and debris were eliminated by plotting the width against the area of FSC and SSC parameters (FSC-W and SSC-W). Dead cells were excluded using viability dye (VD), and gating into live cells we identified CD8$^+$ and CD4$^+$ T cells. (B) Representative FC analysis of pre- and post-enrichment of naïve (N) or effector memory plus effector memory RA$^+$ (EM+EMRA) CD8$^+$ T cells, gated on (dextramer$^+$)-CD8$^+$ T cells (upper) or (dextramer$^-$)-CD8$^+$ T cells (lower). (C) Representative FC analysis of pre- and post-enrichment of Treg cells with magnetic beads.

of further stains such as CD25 and Foxp3 may help resolve populations but these may also be upregulated by proliferating Tconv cells. If this proves a problem for mice, this can be resolved by using congenic markers such as CD45.1 Tconv and CD45.2 Treg. CD8 T-cells can also be used as responders.

It should be remembered that suppressive function is not totally Treg exclusive. Activated non-Treg cells are capable of showing some CTLA-4 dependent suppressive function, although this is relatively weak in comparison to Treg cells. As a result, in some cases inclusion of known highly suppressive and non/lo-suppressive cells as control groups to allows placement of the cell population of interest on this scale.

To a large extent the APC dependent suppression assay measures CTLA-4 dependent suppressive function. However, this is context dependent, naïve CTLA-4 deficient Treg lack detectable suppressive function, while highly activated CTLA-4 deficient Tregs are suppressive due to upregulation of other suppressive molecules post-activation [671]. Another common variant of this

assay is to use CD3 mAb and CD28 mAb beads in place of APCs, this APC independent assay largely measures CTLA-4 independent suppressive function.

The use of CD3 in the sorting strategy (Fig. 73) runs the risk of causing pre-activation of the T-cells. We have not found this to be a problem, but if this is a concern CD3 can be omitted without a major change in the purity of the sorted cells.

As regards the killing assay of Treg cells by antigen-specific CD8$^+$ T effector cells, care must be taken to ensure that Treg cells do not display cytotoxicity activity, as suggested in older reports [678]. This risk can be ruled out by the evidence showing that: (i) highly purified peripheral Treg cells, as well as Treg cells infiltrating inflamed tissues, completely lack GZMs, in contrast to CD8$^+$ T effector cells; (ii) highly purified Treg cells are unable to kill antigen-specific CD8$^+$ T effector cells in cytotoxicity assays in vitro (see [673]). S. Koristka et al. proposed that the discrepancy with older reports [678] is due to the purity of Treg cells used in the assays [679].
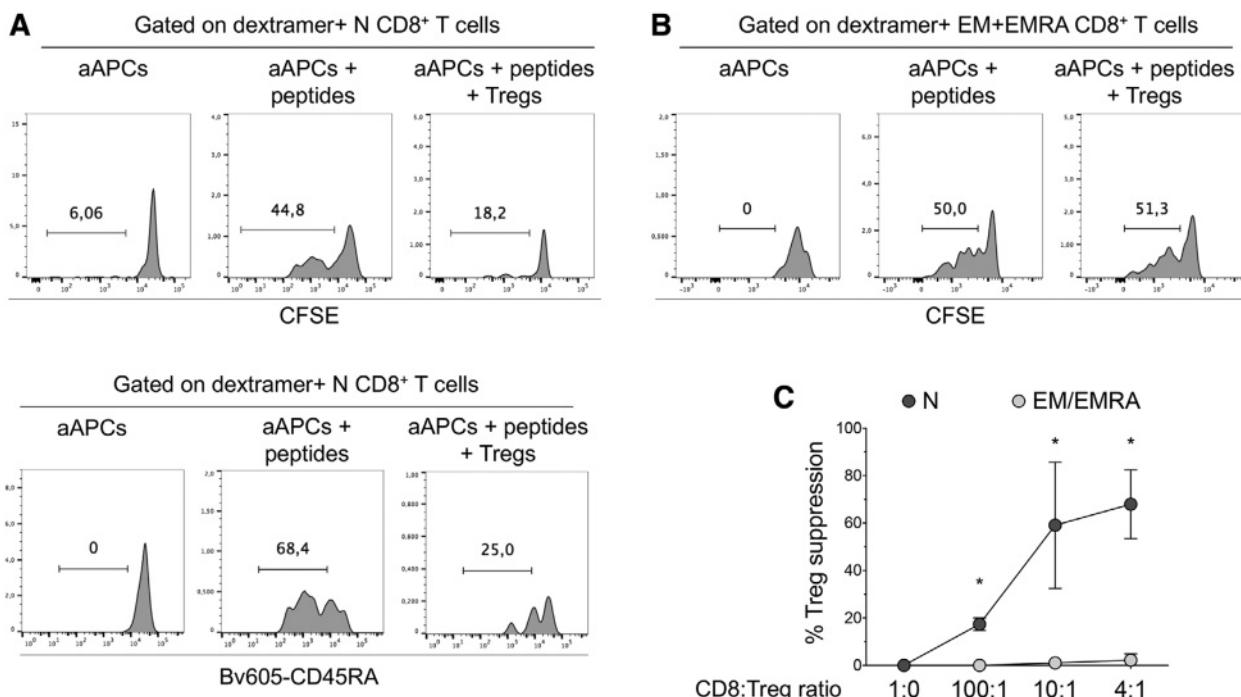
Figure 76. Representative histograms of purified CFSE-stained CD8$^+$ T (N) cells (A) or effector memory plus effector memory RA$^+$ (EM+EMRA) CD8$^+$ T cells (B) stimulated with autologous (a)APCs pulsed (or not) with 20 μg/mL of peptides (aAPCs + peptides) and co-cultured (or not) with Treg cells at a CD8:Treg ratio of 10:1 for 7 days. Histograms indicate the percentage of cell proliferation (as detected by CFSE dilution) and differentiation (as detected by CD45RA downregulation) in (dextramer$^+$)-CD8$^+$ T cells. (C) Mean values of four independent suppression assays at different CD8:Treg ratios. %Treg suppression = (MFI CFSE-stained dextramer$^+$ CD8$^+$ T cells with Treg cells – MFI CFSE-stained dextramer$^+$ CD8$^+$ T cells without Treg cells) / (MFI CFSE-stained dextramer$^+$ CD8$^+$ T cells unstimulated − MFI CFSE-stained dextramer$^+$ CD8$^+$ T cells without Treg cells) × 100. $^*P < 0.05$ one-way ANOVA with Tukey's multiple comparison test.

17.9.7 Top tricks. CFSE and CTV dyes can both be used and we have not observed clear differences in results between them. When a Foxp3-GFP reporter mouse is used, CTV may be the optimal choice to avoid mixing up signal from GFP and CFSE. However, when this is not the case and blue, yellow–green, and violet lasers are all available, we find that CFSE frees up the bright fluorochrome BV421 while the blue and Yellow–green lasers allow better separation of CFSE and PE than would be possible with just a blue laser. In some cases, high doses of CFSE can be toxic, and the effect in a particular setting should be defined empirically.

Choice of APCs: With optimization it is possible to use various cells as APCs. In the murine system, we have successfully used CD11c$^+$ DCs, B220$^+$ B-cells, and T-cell depleted splenocytes as APCs. For the human suppression assay, monocytes-derived DCs and T-cell depleted PBMCs have all proven effective. There is not necessarily one correct choice but some consideration should be given to which cell type is appropriate according to experiment in question.

Since dead cells are often nonrecoverable or excluded from analysis, counting the total number of recovered Tconv cells can also be useful to understand the dynamics of the suppression system. Cytometric counting beads can be used in order to accurately count the cells while collecting proliferation data.

Addition of exogenous IL-2: Particularly for humans some donors Tconv may proliferate poorly even in the absence of Tregs.

In this case, addition of a low dose of exogenous IL-2 in the range of 10-20 IU/mL may aid proliferation while also allowing clear suppression. Careful titration is needed as higher doses of IL-2 overwhelm Treg suppressive function.

The use of a pre-enrichment bead sorting is not essential but improves the purity of the sorted populations. This is more important when rare populations such as fraction I naïve Tregs are sorted.

18 Adoptive T and B cell transfer as a read-out for antigen-specific immune responses in mice

18.1 *Overview*

For over three decades now, adoptive transfer of TCR-transgenic (TCRtg) and BCR-transgenic (BCRtg) cells, followed by challenge with cognate antigen in various experimental settings such as immunization, infection, autoimmunity, and tumors, has proven to be an elegant tool to study antigen-specific immune responses in vivo. These experiments have generated a wealth of information on the activation requirements, kinetics, magnitude, and effector as well as memory responses of T and B cells. Importantly, adoptive transfer experiments continue fueling research in these areas. Here, we describe critical parameters for performing adop-
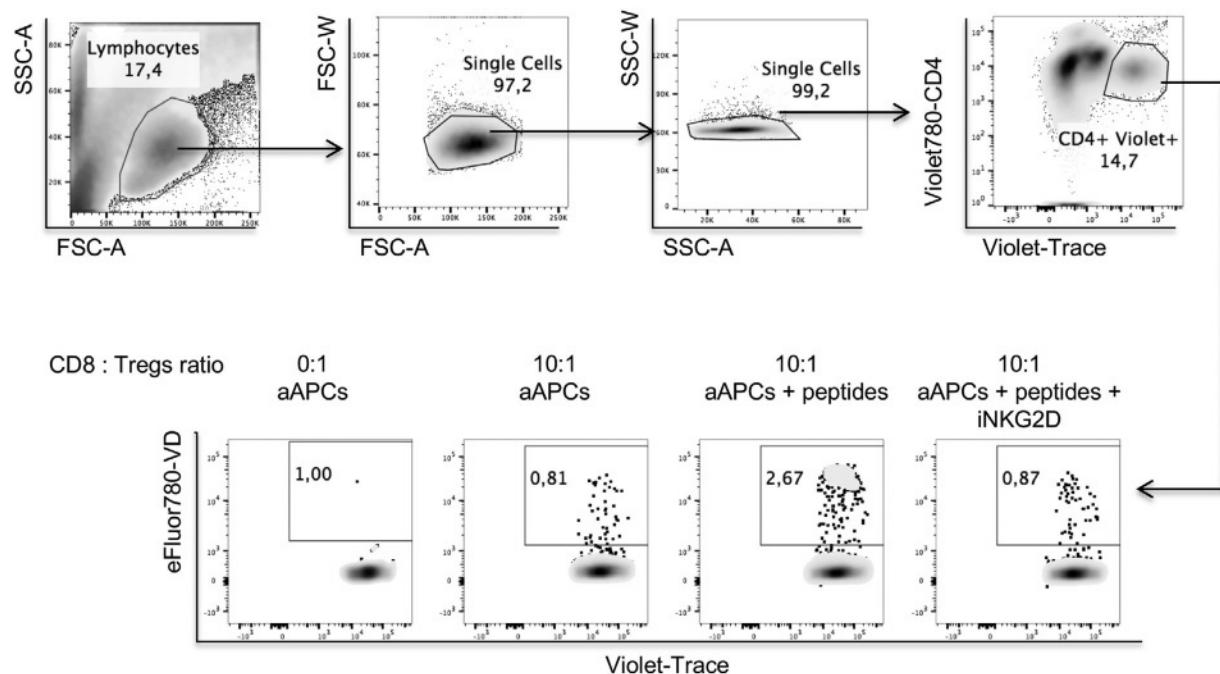
Figure 77. Representative FC analysis of dead Tregs, as detected by the percentage of VD$^+$ cells in Tregs, alone (0:1) or co-cultured with purified CD8$^+$ TEM + EMRA cells (10:1) and aAPCs stimulated or not with peptides in the presence or absence of iNKG2D.

tive transfer experiments with TCRtg and BCRtg cells and discuss advantages and disadvantages of these approaches in regards to study design and data interpretation.

18.2 Introduction

Experimental immunization or infection of mice is frequently used to study immune responses in vivo. Using various activation marker combinations, polyclonal T and B cell responses can be easily analyzed by FCM. Activated T cells can be identified in mice by staining for activation markers such as CD69 or CD44 (see Chapter V, Section 17.5). However, this generally does not provide information on the differentiation history or the antigen specificity of these cells. For the detection of antigen-specific CD8$^+$ or CD4$^+$ T cells in bulk cell populations, MHC multimers may be used in humans and mice (see Chapter V, Section 17.4). While each multimer covers one antigenic specificity, thereby allowing quantification of antigen-specific cells, functional and fate-mapping assays are rather limited. Complementary to this approach, TCRtg T cells have been widely used for studying antigen-specific T cell responses in many in vivo settings. The advantage of using TCRtg cells is the known specificity of these cells and their suitability for adoptive transfer experiments. Various TCRtg mouse lines have been described in the literature. Prominent examples for CD8$^+$ T cells include P14, which are specific for LCMV GP$_{33-41}$ peptide [680] or OT-I, which are specific for OVA$_{257-264}$ peptide [681]. Examples for CD4$^+$ T cells include SMARTA, which are specific for LCMV GP$_{61-80}$ peptide [682], and OT-II, which are specific for OVA$_{323-339}$ peptide [683]. All these lines are on the C57BL/6 background. DO11.10 mice, which are on the BALB/c background,

carry a TCRtg that also recognizes OVA$_{323-339}$ peptide [684]. For this mouse strain, a clonotypic Ab has been generated that allows detecting DO11.10 TCRtg cells without the need of additional markers such as congenes or fluorescent reporter alleles. TCRtg mice can also be used for inducing autoimmunity. For example, adoptively transferred P14 TCRtg cells can kill genetically engineered LCMV GP-expressing beta cells in the pancreas, thus causing diabetes [685]. Another example are 2D2 mice, in which 95% of CD4$^+$ T cells carry a TCR specific for MOG$_{35-55}$ peptide [686]. These cells can be used to track autoantigen-specific T helper cell responses in the CNS after MOG/CFA/PTX-induced active EAE. 2D2 cells can also be activated and transferred into secondary hosts, where they are sufficient to induce full-blown disease (passive EAE). While TCRtg mice usually harbor only very few Treg cells, if any, polyclonal Foxp3 reporter mice such as Foxp3-GFP may be used instead for isolation of GFP$^+$ polyclonal Treg and Tfr cells with unknown specificity for adoptive transfer experiments.

Similar to T cells, B cell responses can also be studied in detail using FCM. For example, activated B cells that differentiate into germinal center B cells downregulate surface IgD expression and instead express GL-7 and FAS or can be stained with the lectin PNA (see Chapter VI, Section 2.2). In addition, class-switched Ab isotypes can be measured by FCM. Since B cells recognize their cognate antigen directly through their BCR, antigen-fluorophore complexes can be used to identify antigen-specific B cells by FCM, e.g., 4-Hydroxy-3-nitrophenylacetyl (NP) hapten-specific B cells with NP-PE after NP-KLH immunization or hen egg lysozyme (HEL)-APC after HEL immunization. However, it is often advantageous to be able to track the fate of antigen-specific naïve B cells during the entire immune response following activation of these
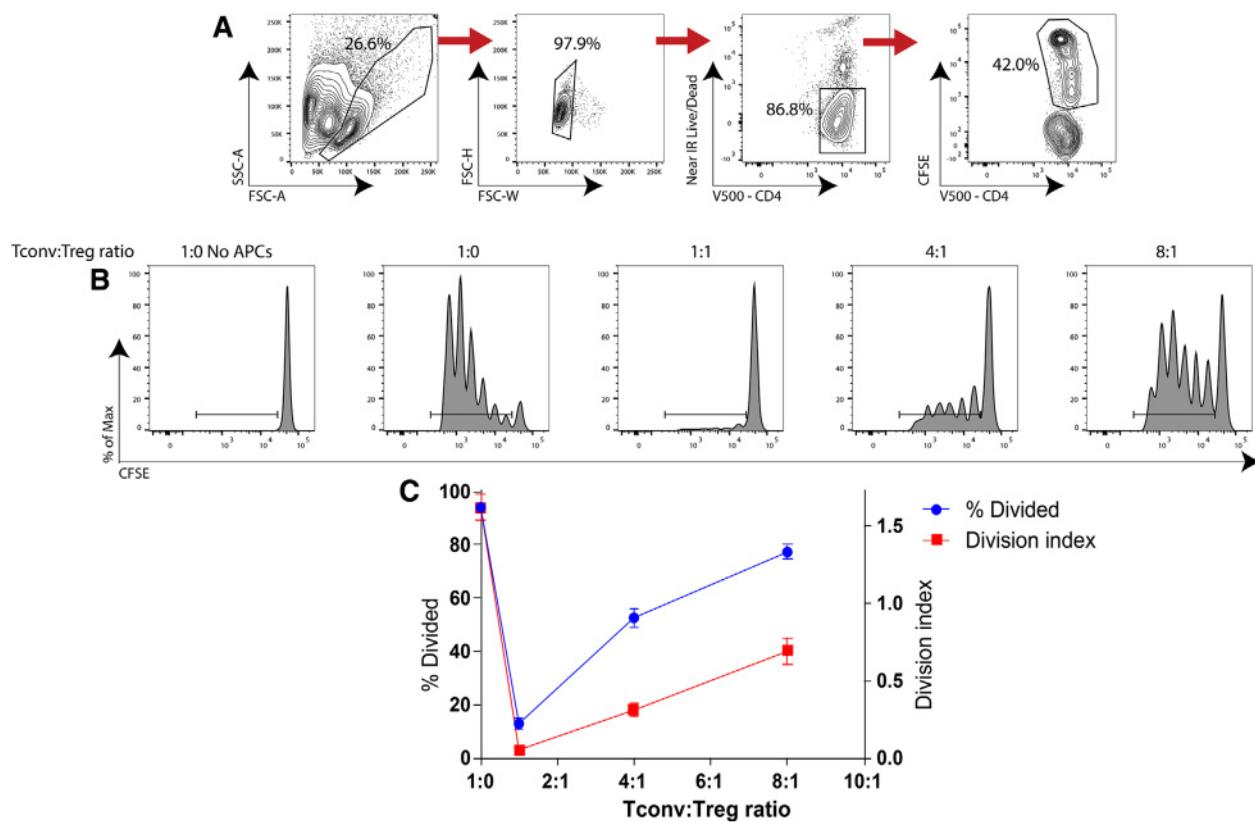
Figure 78. (A) Gating strategy for identification of responder cells in human polyclonal suppression assay. (B) Proliferation histograms of human Tconv cells cultured with various ratios of Treg cells, irradiated CD4⁻ splenocytes, and CD3 mAb for 3 days. (C) Summary data comparing percentage divided and division index of Tconv cells performed in duplicate. Division index is the average number of divisions by each cell as calculated in Flowjo Software.

cells. BCRtg B cells that can be used in adoptive transfer experiments are ideally suited for this purpose. Several BCRtg mouse lines have been described in the literature. Among them, HEL-specific MD4 [687], SWHEL [688], and Hy10 [689] mice as well as NP-specific B1-8 [690] mice have been used in various studies to dissect the contribution and kinetics of antigen-specific B cell responses in vivo.

To limit the precursor frequencies of antigen-specific TCRtg and BCRtg cells as much as possible to physiological levels, low numbers of purified naïve TCRtg or BCRtg cells should be transferred into wild-type recipients. For functional questions, these donor cells can be derived from control or knock-out backgrounds and are then being compared in separate or competitive adoptive transfers into wild-type mice. Alternatively, for examination of extrinsic factors important for T and B cell biology, TCRtg or BCRtg B cells can be transferred into hosts that lack certain genes (i.e., knock-out mice). In order to distinguish the transferred cells from host lymphocytes, it is advisable to intercross the TCRtg and BCRtg lines to different congenic alleles. Since wild-type C57BL/6 mice are CD45.2, TCRtg, and BCRtg cells that carry one or two alleles of the congene CD45.1 can be easily identified by FCM or immunofluorescence microscopy by staining with fluorescence-labeled Abs against CD45.1 and CD45.2. Using combinations of CD45.1 and CD45.1/2, it is even possible to perform competitive

co-transfers into CD45.2 wild-type C57BL/6 mice, e.g., comparing control and knockout TCRtg or BCRtg cells within the same host. For T cells, combinations of the congenic markers Thy1.2 (CD90.2, expressed by wild-type C57BL/6 mouse T cells) and Thy1.1 (CD90.1) have been regularly used as an alternative to the CD45.2/CD45.1 system. While CD45 is expressed by B cells, Thy1 is not. Alternatively, some BCRtg mice carry different Ig heavy chain (Igh) allotypes that can be used for identification instead. For example, MD4 and Hy10 BCRtg B cells are Igh^a, which is different as compared to the Igh^b background of wild-type C57BL/6 mice. This does not only allow for the identification of these cells by surface or intracellular staining of various Ig isotypes of Igh^a, but also secreted Abs derived from these cells, which are also of the Igh^a allotype and can be measured by ELISA. Another possibility is to cross TCRtg or BCRtg mouse lines to fluorescent reporter alleles, e.g., GFP, which can also be used for intravital two-photon microscopy studies. For short-term assays or for the assessment of cell proliferation in vivo for up to 3 to 4 days, naïve TCRtg or BCRtg cells can be labeled with CFSE, CTV or similar fluorescent dyes prior to adoptive transfer (see Chapter V, Section 18). BCRtg cells can also be co-transferred together with antigen-specific TCRtg cells to study the cooperation between antigen-specific B and T cells [691]. Examples include co-transfer of OVA-specific OT-II cells and NP-specific B1-8hi cells, followed by immunization with
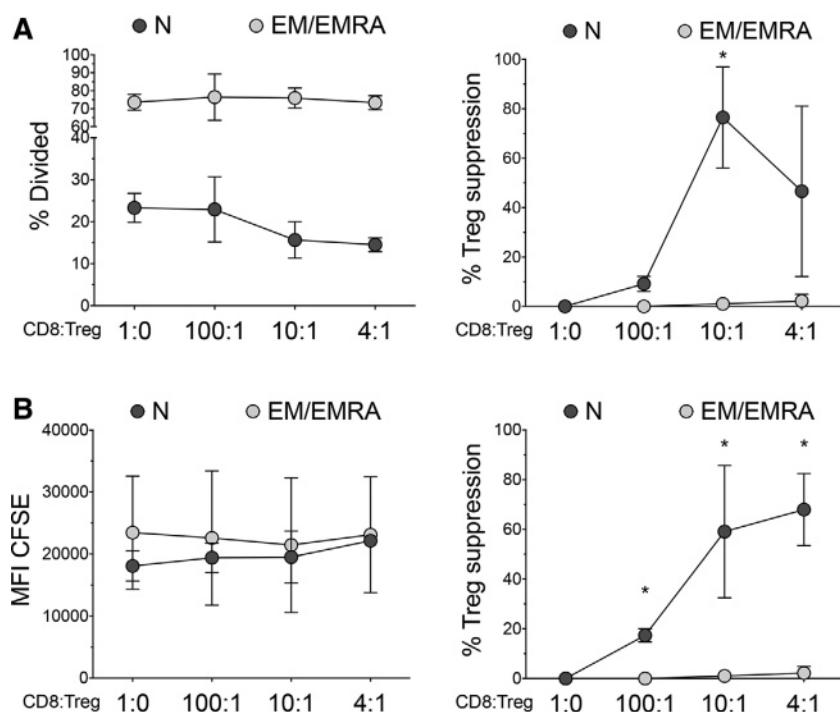
Figure 79. Comparison between different methods to analyze proliferation in suppression assay of antigen-specific T cells (as described in Figure 76); mean values of four independent experiments are reported. (A) Left panel shows % divided of N or EM+EMRA (dextramer$^+$)-CD8$^+$ T cells, at different CD8:Treg ratio. Right panel shows %Treg suppression calculated using % divided T cells (see formula reported in Fig. 76C). (B) Left panel shows MFI of CFSE of N or EM+EMRA (dextramer$^+$)-CD8$^+$ T cells, at different CD8:Treg ratio. Right panel shows %Treg suppression calculated using MFI of CFSE (see formula reported in Figure 76 C). *P < 0.05 one-way ANOVA with Tukey's multiple comparison test.

NP-OVA in adjuvants, e.g., alum. If 2D2 TCRtg mice are crossed to the BCRtg mouse line Th [692], in which approximately 20% of peripheral B cells are specific for MOG, these compound animals can be used as a model for spontaneous EAE development [693].

The following protocol provides a framework for adoptive transfer experiments with CD4$^+$ and CD8$^+$ TCRtg T cells as well as BCRtg B cells. The protocol can be easily modified and tailored to the specific question of interest. An example of how this protocol can be used for the assessment of CD4$^+$ T cell proliferation in vivo is shown in Figure 80.

18.3 Step-by-step sample preparation

1. Prepare single-cell suspensions from pooled spleen and lymph nodes of TCRtg or BCRtg donor mice of interest (see Chapter III, Section 3).
2. Enrich naïve T or B cells with magnetic beads (preferentially by negative selection) (see Chapter IV, Sections 1 and 2) and/or by cell sorting (see Chapter IV, Section 3). If the scope of the study is to analyze the fate of already differentiated cells (in vivo or in vitro generated), these cells may also be used for adoptive transfer experiments.
3. To track proliferation and expression kinetics of transferred cells, they can be optionally labeled with a cell proliferation dye (e.g., CFSE or CTV) prior to adoptive transfer (see Chapter V, Section 18).
4. Inject TCRtg or BCRtg cells into host mice (e.g., wild-type C57BL/6), usually per i.v. route. Keeping in mind to aim for the lowest feasible number of cells to be injected, adjust the required cell number to the characteristics of the specific TCRtg or BCRtg, to the immunization or infection model used, and

to the intended readout (e.g., short term vs. long-term) as the number of endogenous and transferred cells can strongly influence the outcome of the experiment [694, 695]. While typical cell numbers will range from hundreds to hundreds of thousands, even as few as one or ten transferred cells may be sufficient for certain experimental settings [634, 696]

5. Before challenging the transferred cells in the new host with the cognate antigen, allow the transferred cells to equilibrate in the host for a few hours to days.
6. Immunize or infect the recipient mice with the cognate antigen. For protein and peptide immunizations, it is usually required to mix the antigen with an adjuvant to elicit a strong response.
7. Analyze the adoptively transferred cells by FCM. To this end, prepare single cell suspensions of secondary lymphoid tissues or other tissues of interest (see Chapter III, Section 3) and stain the cells with appropriate combinations of fluorescence-labeled Abs for subsequent acquisition on a flow cytometer or cell sorter.

18.4 Pitfalls

While adoptive transfer experiments with TCRtg and BCRtg cells represent an elegant and powerful approach to study T and B cell responses in vivo, several important points need to be considered for generating valid and reproducible results:

Purity of adoptively transferred cells. Most often, naïve TCRtg or BCRtg cells are being used for adoptive transfer experiments. To purify naïve T cells from recipients, it is advisable to enrich naïve CD4$^+$ or CD8$^+$ T cells with magnetic bead-coupled Abs, preferentially using negative enrichment that yields untouched cells for downstream applications (see Chapter IV).
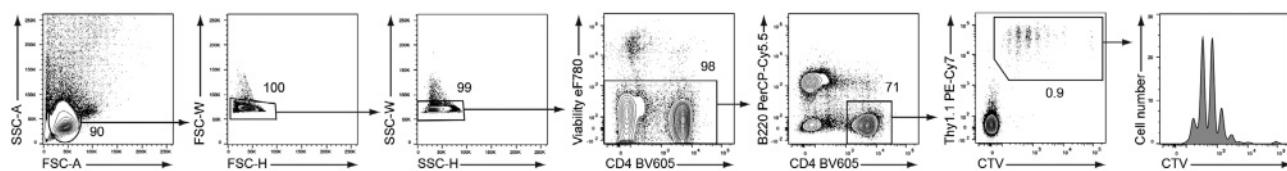
Figure 80. Gating strategy for the identification of CTV-labeled, Thy1.1$^+$ OT-II cells by FCM. Wild-type C57BL/6 mice were injected i.v. with 5x10^5 naïve OT-II TCRtg CD4$^+$ T cells. In this setting, such high numbers of naïve OT-II TCRtg CD4$^+$ T cells (in contrast to classical adoptive transfer experiments with typically less than 1–5 × 10^4 naïve OT-II cells per mouse) are required for recovering enough events for proper cell division analyses. One day later, recipient mice were immunized with 5 µg OVA and 2 µg LPS in the hock. Three and a half days later, draining popliteal lymph nodes were dissected, single-cell suspensions were prepared and the cell surface was stained with appropriate combinations of fluorescently labeled mAbs. Thereafter, samples were fixed and stained with the Foxp3 transcription factor staining set and samples were then acquired on a BD LSRFortessa. Single lymphocytes were first gated based on FSC/SSC characteristics. CD4$^+$ T cells were further gated to exclude dead cells and B cells, and finally with the congenic marker Thy1.1 and CTV to differentiate transferred OT-II cells from endogenous (Thy1.1$^-$) T cells of the recipient. The CTV profile of the identified OT-II cells is shown in the histogram. To reduce the overall size of the acquisition data file, 50 000 lymphocytes were acquired first and then only TCRtg Thy1.1$^+$ CD4$^+$ T cells were appended to the file.

Alternatively, or in addition, naïve cells can be further purified using cell sorting. In the case of T cells, naïve CD4$^+$ or CD8$^+$ T cells can be sorted as CD44$^{int/low}$CD62L^{hi} cells. CD25 can be included as well to exclude activated T cells and Treg cells among CD4$^+$ cells. The TCR should not be stained directly (e.g., CD3ε), as this may crosslink the TCR and activate the cells. Untouched resting B cells can be efficiently enriched using CD43 magnetic beads.

Precursor frequency. It is highly advisable to transfer as few TCRtg or BCRtg cells as possible. Endogenous antigen-specific precursor frequencies are usually very low (in the range of tenth to hundreds of T cells per mouse) [694]. Since TCRtg or BCRtg mice harbor millions of cells specific for the same antigen, it is tempting to also transfer hundreds of thousands or millions of these cells. However, since all these cells would compete with each other in the new host for the specific antigen after infection or immunization, such high precursor frequencies are unphysiological and results of these experiments need to be interpreted with care [634]. In addition, while most transferred TCRtg cells will die and disappear during the transfer procedure, only a small percentage (often less than 10%) of transferred cells will be eventually "parked" in the host. Nevertheless, under certain conditions, it can be required to transfer higher cell numbers in order to recover enough cells for analyses, e.g., in the case of proliferation experiments using CFSE or CTV, in which it is often difficult to recover enough cells that are within the first cell division(s) [697].

High affinity TCRs and BCRs. TCRtg and BCRtg cells often carry antigen receptors with very high affinities for the specific antigen, which may confound the conclusions derived from adoptive transfer experiments utilizing these cells. For example, the HEL-specific BCRs of MD4, SWHEL, and Hy10 BCRtg mouse lines bind HEL with extremely high affinity. To adapt for this problem, mutated HEL proteins and peptide sequences have been engineered that exhibit much lower binding affinities to these BCRs, thus providing a more physiological setting [698]. Alternatively, the HEL-related duck egg lysozyme, which exhibits lower binding affinity to these BCRs, has been used as well [689].

Rejection of transferred cells. Congenic markers or fluorescent proteins expressed by adoptively transferred cells can potentially facilitate rejection. While this may not be such a big issue for short-term experiments, long-term experiments require more careful planning and interpretation by taking this potential caveat into account. As an example, when transferred into CD45.2 hosts, heterozygous CD45.1/2 cells might be less prone to rejection than CD45.1 homozygous cells. The use of CD45.1/2 heterozygous hosts could provide an elegant solution to this problem, as CD45.1 and CD45.2 homozygous cells would be much less likely rejected in these mice. In addition, for critical issues, allelic marker combinations of CD45.1 and CD45.2 (or similar) may also be switched in complementary adoptive transfer experiments to test whether the same conclusions are reached. To further decrease the possibility of rejection, TCRtg and BCRtg mice should be bred on and/or regularly back-crossed to the same background strain of the host mice used in the adoptive transfer experiments. Another strategy for reducing the risk of GFP$^+$ cells being rejected after adoptive transfer is the use of host mice that express GFP under an endogenous promotor, thus rendering these hosts tolerant towards GFP.

Exclusion of dead and contaminating cells. It is imperative to carefully exclude dead cells as well as "sticky" cells. To exclude dead cells, which often show autofluorescence and unspecific binding of fluorescently labeled antibodies, a viability dye should be incorporated in the FCM staining panel (see Chapter III, Section 4). Similarly, it is advantageous to block unspecific binding by preincubation with rat or mouse serum (according to the primary antibodies used for FCM) and Fc receptor blocking reagents. Finally, a dump channel may be incorporated to exclude cells that are "sticky" and/or may share marker expression with the cell type of interest. Typical target antigens that could be used in a dump channel are CD11c, CD19 (if T cells are the cells of interest) or CD3 (if B cells are the cells of interest) and other lineage-defining markers [699]. It is of importance to ensure that the antigen used in a dump channel is not expressed by the cells of interest though.

TCRtg and BCRtg mice are often "leaky." This means that not all T and B cells are monoclonal and some polyclonal T cells have expanded that do not express the antigen-specific tg. The degree of T and B cells not carrying the TCRtg and BCRtg, respectively, varies considerably between the individual mouse lines. One possibility to generate true monoclonal TCRtg and BCRtg mice is to cross these mice onto Rag1- or Rag2-deficient backgrounds. This is particularly important if TCRtg T cells will be transferred into

lymphopenic hosts, e.g., Rag1, Rag2, TCRαβ or CD3ε knockout mice, as naïve polyclonal T cells will undergo considerable homeostatic proliferation and may even cause disease, such as IBD after transfer of naïve CD4$^+$ T cells into Rag1 knockout mice.

18.5 *Top tricks*

Pre-enrichment of target populations: Low numbers of transferred cells and/or poor expansion of these cells in the host may limit recovered cell numbers that can be analysed by FCM. To accommodate for this problem, pre-enrichment of the adoptively transferred cells may be used before acquisition on a flow cytometer/sorter. Similar to the techniques described in the "Purity of adoptively transferred cells" section above, congenic TCRtg and BCRtg cells can be pre-enriched from whole host spleen or lymph node tissues by labeling with magnetic beads coupled to monoclonal Abs against the respective congenic marker (e.g., CD45.1 or Thy1.1). Small bead sizes (e.g., Miltenyi MACS® or Stemcell Technologies) should be preferred over big bead sizes (Thermo Dynabeads) for this positive selection approach.

VI Flow cytometric phenotyping of cells across species and tissues

1 T cells and their subsets

1.1 *Murine CD4 and CD8 T cells*

1.1.1 Differences in flow cytometric analysis of murine and human T cells. FCM and cell sorting have been instrumental to understanding the fundamental principles of T cell differentiation. The analysis of human samples alongside complementary experimental animal models has given us great insights into thymic T cell selection, induction of T cell effector responses and the generation of long-lived T cell memory (See Chapter VI Section 1.11 Human CD4 and CD8 T cells). Mice are the primary animal model used to investigate T cell biology and, while many of the same mechanisms apply to the differentiation of T cells in humans and mice, there are some fundamental differences in the flow cytometric analysis of human and murine T cells.

One key difference is in the infection status of humans as compared to mice. The human immune system is challenged by a daily onslaught of microorganisms, pathogens, and foreign substances from the environment. This includes a vast and diverse range of potential antigen exposures, including non-persistent and persistent latent viruses, bacteria, vaccinations, neoplastically transformed cells, as well as the flora of our individual microbiota. These agents constantly trigger and shape the human immune system and, given that the average human lifespan is currently over 70 years in many countries, these exposures can perturb the immune system from its original naïve state over a substantial period of time. In contrast, most laboratory mice are used at 8–12 weeks after birth and are bred and maintained in clean facilities

under specific pathogen-free (SPF) conditions, with reduced exposure to foreign antigens and pathogens. Consequently, immune composition and immune cell phenotypes from adult SPF mice are more similar to that of neonatal, rather than adult, humans [700].

The use of murine models has enabled researchers to selectively induce disease states and study the T cell response longitudinally at defined synchronized time points. To a more limited degree, this is also possible in human clinical studies, for example, those that monitor the immune response following vaccination [701, 702] or primary infection after organ transplantation [703]. However, the tendency to study T cell responses longitudinally in mice has driven development of terminology that is distinct from those used in human T cell biology. For example, murine effector T cells are generally defined as transiently expanding T cells in the effector phase of an immune response, while in humans, effector T cells are generally present at any snapshot of analysis.

Finally, different immune compartments are generally more accessible in mice than in humans. Analysis of human T cells is largely confined to blood, whereas T cell analyses in murine models can access blood in addition to bone marrow and secondary lymphoid organs, including the thymus, lymph nodes, and spleen. Tissues, such as skin, intestine, and bone marrow, are also more readily available for analysis in mice and, accordingly, have given us distinct and unique insights into T cell biology.

1.2 *Murine Conventional αβ CD4 T cells*

1.2.1 Overview. CD4 T cells are central effector cells that crosstalk with many other components of the adaptive and innate immune system. Primed by signals they receive during development in the thymus and in the periphery, MHCII-restricted CD4 T cells specialize functionally. Tregs can suppress immune responses and balance between immune activation and tolerance (See also Chapter VI Section 1.6 Murine Foxp3$^+$ regulatory T cells). Conventional nonregulatory CD4 T cells contribute to the efficiency of many vaccines and are vital for the protection against many infections with bacteria, parasites, and fungi, but they can also mediate autoimmune diseases. This section focuses on conventional nonregulatory T cells and gives an overview of surface markers used to identify the diverse CD4 T cells subsets. Furthermore, we provide examples for the detection of transcription factors and effector functions of conventional CD4 T cells.

1.2.2 Conventional αβ CD4 T cells: Identification and surface markers. Conventional TCRαβCD4$^+$ T cells can be identified by gating on time, scatter parameters and exclusion of duplicates and dead cells to identify viable lymphocytes and gating on CD3ε$^+$ or TCRβ$^+$ cells and CD4$^+$CD8α$^-$ cells (Fig. 81). The use of CD3ε or TCRβ as selection markers is critical for the analysis of CD4 T cells to avoid inclusion of myeloid cell subsets that express low levels of CD4. Additional markers may be required in specific tissues to differentiate conventional CD4 T cells from other nonconventional T cell subsets, such as from CD4$^+$ NKT cells in the liver (See also Chapter VI Section 1.4 Murine tissue resident memory T cells). These
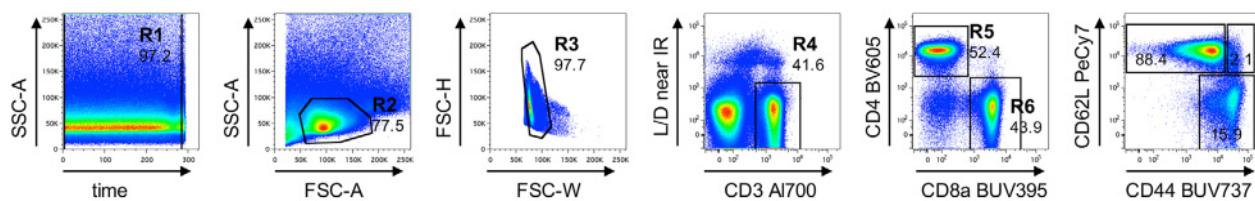
Figure 81. Murine CD4 and CD8 T cells. Sample gating tree for the identification of CD4 and CD8 T cell subsets from the spleen. Conventional CD4 and CD8 T cells can be identified by gating on time, lymphocytes according to FSC and SSC (R1, R2), exclusion of doublets (R3) and dead cells (R4) and gating on CD3ε$^+$ or TCRβ$^+$ cells (R4) and CD4$^+$CD8α$^-$ cells (R5).
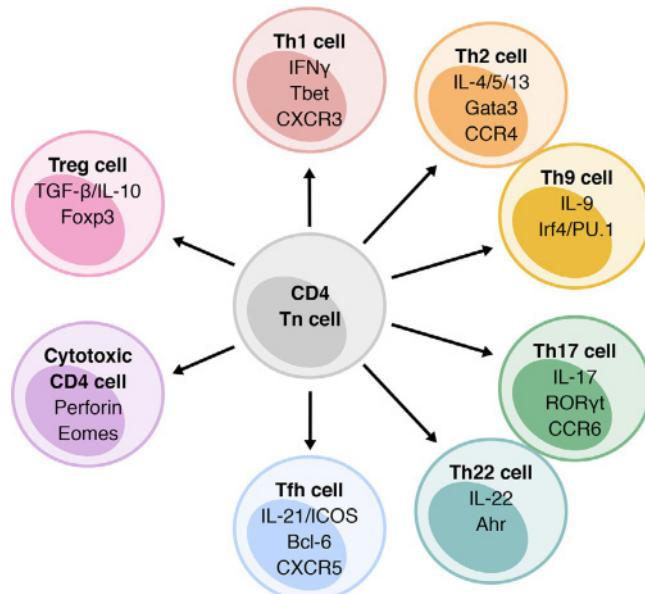
Figure 82. Schematic of murine CD4 T cell differentiation. An array of CD4 helper T cell subsets differentiate from CD4 Tn cells, including Th1, Th2, Th9, Th17, Th22, Tfh, Treg, and cytotoxic CD4 T cells. Molecules under each CD4 helper T cell subsets heading indicate the key effector cytokine/molecules, key transcription factor/s, and key chemokine receptors.
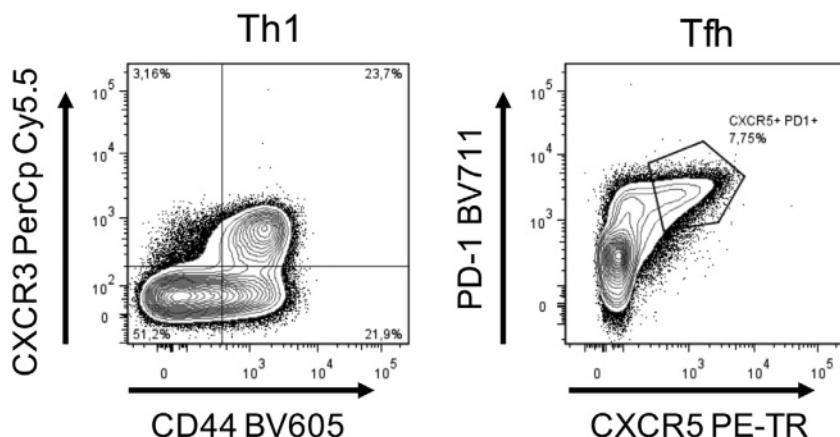
markers can be used in a "dump" gate to exclude myeloid lineages and nonconventional T cells.

CD4 T cell differentiation state is often defined by the expression of surface markers that correlate with the location of cells within the body. Mature CD4 naïve T (Tn) cells are CD44^{lo}CD62L^{hi} and enriched in the lymphoid tissues (Fig. 81). The L-selectin CD62L mediates attachment to endothelia and access to lymph nodes. Upon activation, CD4 T cells acquire CD44, which binds hyaluronan to promote access to peripheral tissues, and lose CD62L to become CD4 effector T (Teff) cells. Antigen-activated Teff populations expand and mediate pathogen clearance, then contract after pathogen resolution and form CD4 memory T (Tmem) populations. Two main circulating memory populations are central memory T (Tcm) cells, which are CD44^{hi}CD62L^{hi} and reside predominantly in the lymphoid tissue, and effector memory T (Tem) cells, which are CD44^{hi}CD62L^{lo} and circulate more through peripheral tissues (Fig. 81). Additionally, noncirculating tissue-resident T cells (Trm) are primarily present in barrier tissues (See also Chapter VI Section 1.4 Murine tissue resident memory T cells).

Pathogen-specific CD4 Teff (and Tmem) cells can be classified according to their phenotype and function into multiple T "helper" (Th) subsets; Th1, Th2, Th9, Th17, Th22, and T follicular helper (Tfh) cells (Fig. 82). These subsets are each equipped with a unique set of transcription factors, chemokine receptors, and effector molecules. However, recent research suggests that CD4 Th cell subsets are not separate lineages but a continuum of mixed functional capacities [704]. Alongside these conventional CD4 Th cell subsets, natural and induced T regulatory (Treg) cells have a predominant immunomodulatory phenotype with the ability to suppress autoreactive immune responses and promote resolution of active immune responses, by a variety of mechanisms (for more details See also Chapter VI Section 1.4 Murine tissue resident memory T cells).

CD4 Th cell subsets participate in a range of diverse and overlapping adaptive immune responses [705, 706]. Th1 cells are vital in the defense against intracellular infections, such as *Mycobacterium tuberculosis* and protozoa. Th2 cells protect against parasitic infections, including helminths, but also mediate much of the pathology associated with allergic reactions and correlate with asthma severity. Th17 cells, originally described in mice as being pathogenic in murine models of autoimmune disease [707, 708], have more recently been shown to protect against certain pathogens, including fungal infections [709]. Th9 and Th22 cells are relatively newly described subsets, which share some functional and developmental features with Th2 and Th17 cells, respectively. Tfh cells crosstalk with B cells to stimulate the production of high affinity Abs in germinal center reactions. Intriguingly, in certain infections such as influenza, unique populations of CD4 T cells can exhibit cytolytic capacity [710].

In CD4 Th cells, the expression of chemokine receptors is associated with skewing toward specific effector functions and migratory behavior. Rapid upregulation of CXCR3 facilitates the migration of Th1 cells to inflamed tissue sites along gradients of chemokines, such as CXCL9, CXCL10, and CXCL11 (Figs. 82 and 83) [711]. The specific interaction of CCR4 on Th2 cells with CCL17 and CCL22 is critical for movement of Tmem into the skin [712]. Th17 preferentially utilize CCR6, also expressed by Treg cells, for migration to mucosal tissues that are enriched for CCL20 [713]. Tfh cells express the chemokine receptor CXCR5, which is vital in the migration of Tfh cells from the T cell zone into B cell follicles within the spleen [714] (Figs. 82 and 83) and also express high levels of PD-1 and ICOS to facilitate B cell interactions (Figure 83).

Figure 83. Chemokine receptors for identification of murine CD4 subsets. Subsets of CD4 T cells can be identified based on the expression of chemokine receptors. CD4 T cells were gated on lymphocytes according to scatter parameters, live cells, dump negative (CD25, NKT tetramer, B220), and CD3+/ CD4+. Examples shown include Th1 cells that express the chemokine receptor CXCR3 and CD4+ Tfh cells that express PD1 and CXCR5.

1.2.3 CD4 T cells: transcription factors. The differentiation of specific CD4 Th cell lineages is induced by specific cytokine stimulation and is guided by master transcription factors (Figs. 82 and 84), which control the expression of downstream effector molecules. Priming of Th1 cells by IL-12 [715] and IFN-γ [716] results in expression of their master transcription factor T-bet [717] (Fig. 84), Th2 cell priming by IL-4 [718, 719] leads to expression of GATA-3 [720] and priming by IL-23, IL-6, and TGF-β drives RORγt expression in Th17 cells [721] (Fig. 84). Th22 cells are regulated by expression of the transcription factor Ahr [722, 723], while Th9 cells do not appear to be regulated by an individual transcription factor but rather a combination of factors, including IRF4 and PU.1 [722, 723]. Tfh cells are controlled by the transcription factor Bcl6 [724] (Figure 84) and the development of cytotoxic CD4 T cells can be mediated by the transcription of Eomes.

Transcription factors are mainly located intranuclearly and, to assess these by FCM, staining buffers are used that efficiently permeabilize the nucleus and enable intranuclear access of Abs. When no reliable Abs are available, reporter mice are a valuable tool for the flow cytometric analysis of transcription factor expression [725]. Additionally, the use of reporter constructs can also enable functional assays based on transcription factor expression that are not possible with fixed and permeabilized cells.

1.2.3.1 Step-by-step sample preparation protocol for staining of the transcription factor Bcl-6 and Tfh surface markers in CD4 T cells.

- Prepare single-cell suspensions of draining lymph nodes (LNs) and non-draining LNs in HBSS (or PBS) by standard procedures.
- Add 1–2 × 10^6 cells in 100 μL for each sample into 5 mL FCM tubes.
- Add 100 μL of 1:1000-diluted eFluor780 Fixable Viability Dye (eBioscience) in HBSS (or PBS) (no serum/protein, no azide).

  ○ Incubate for 10 min on ice.

- Wash cells with 2000 μL FCM buffer (2% FCS in PBS) and pellet cells at 500 × g for 5 min at 4°C and remove supernatant.
- Add 200 μL of blocking solution (1 μg/mL CD16/32 mAb, 2% normal mouse/rat serum in FCM buffer).

  ○ Incubate for 5 min on ice.

- Critical step: On top of the blocking solution, add 200 μL of 2×-diluted anti-CXCR5-biotin (clone 2G8, BD Biosciences, 1:50 final dilution).

  ○ Incubate for 30 min at 37°C, gently rolling at room temperature.
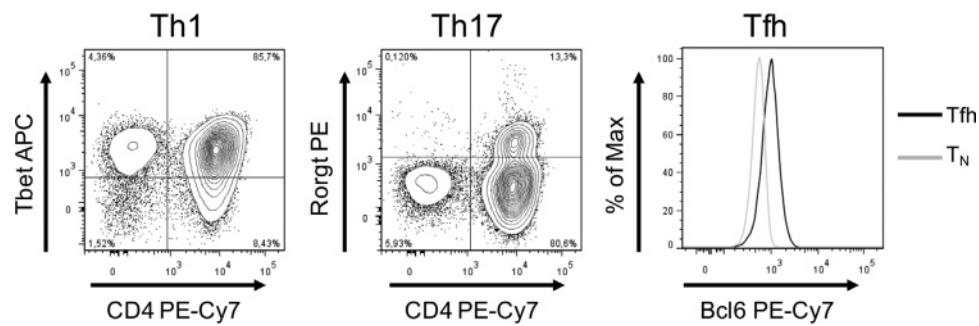
Figure 84. Transcription factors for identification of murine CD4 subsets. Subsets of CD4 T cells can be identified based on their expression of master transcription factors (TFs). Examples shown include Th1 cells identified by expression of T-bet, Th17 cells by RORγt, and CD4+ Tfh cells by Bcl6 expression. Live CD3+ cells are displayed for Th1 and Th17 cells both gated as shown in Fig. 81. For analysis of Bcl2 expression, within live CD3+/ CD4+ cells Tfh cells (CXCR5+/CD44 high) and naïve T cells (T_N CXCR5−/CD44 low) are displayed.

- Wash cells with 2000 μL FCM buffer (2% FCS in PBS) and pellet cells at 500 × *g* for 5 min at 4°C and remove supernatant.
- Transfer cells in 40 μL of primary Ab mix containing CD4-Pe mAb (clone RM4-5, BD Biosciences), anti-ICOS-APC (clone C398.4A, Biolegend), and anti-PD-1-PeCy7 (clone RMP1-30, Biolegend) to a 96-well round bottom plate.

  ○ Incubate for 20 min at 4°C

- Wash cells with 200 μL FCM buffer (2% FCS in PBS) and pellet cells at 500 × *g* for 5 min at 4°C and remove supernatant.
- Add 40 μL Streptavidin-PerCP (1:1000 final dilution) per well:

  ○ Incubate for 15 min on ice.

- Wash cells with 200 μL FCM buffer (2% FCS in PBS) and pellet cells at 500 × *g* for 5 min at 4°C and remove supernatant.
- Add 100 μL Fixation/Permeabilization buffer from the eBioscience FoxP3 staining buffer set per well:

  ○ Incubate for 15 min at room temperature.

- Add 100 μL Permeabilization buffer from the eBioscience FoxP3 staining set per well and pellet cells at 500 × *g* for 5 min at 4°C and remove supernatant.
- Wash 1× with 200 μL Permeabilization buffer and pellet cells at 500 × *g* for 5 min at 4°C and remove supernatant.
- Add 20 μL of blocking solution (1 μg/mL CD16/32 mAb, 2% normal mouse/rat serum in Permeabilization buffer).

  ○ Incubate for 5 min at room temperature.

- On top of the blocking solution, add 20 μL of 2×-diluted anti-Bcl6-PE (clone K112-91, BD Biosciences, 1:50 final dilution).

  ○ Incubate for 45 min at room temperature.

- Wash thrice with Permeabilization buffer and pellet cells at 500 × *g* for 5 min at 4°C.
- Resuspend cells in FCM buffer and analyze on a flow cytometer.

1.2.3.2 Materials.

- Single cell suspension containing T cells
- FCM buffer: PBS with 2% FCS
- Hank's Balanced Salt Solution (Gibco, catalog no. 14025092)
- FoxP3 staining set (eBioscience, catalog no. 00-5523-00)

1.2.3.3 Antibodies.

- anti-mouse CD16/32 (clone 2.4G2)
- anti-mouse CXCR5-biotin (BD Biosciences, catalog no. 551960, clone 2G8)
- anti-mouse CD4-Pe (BD Biosciences, catalog no. 553930, clone RM4-5)

- anti-human/mouse/rat ICOS-APC (Biolegend, catalog no.313510, clone C398.4A)
- anti-mouse PD-1-PeCy7 (Biolegend, catalog no. 109110, clone RMP1-30)
- Streptavidin-PerCP (1:1000 final dilution)
- anti-Bcl6-PE (BD Biosciences, catalog no. 561522, clone K112-91).
- eFluor780 Fixable Viability Dye (eBiosciences, 65-0865-18)

1.2.4 CD4 T cells: effector functions and antigen-specificity. Most memory CD4 T cells are quiescent in steady state. Consequently, analysis of CD4 Th cell functional capacity by FCM usually involves in vitro restimulation and subsequent effector protein profiling by intracellular staining. The hallmark cytokines for CD4 Th cell subsets are as follows; Th1 cells express IFN-γ [726], Th2 cells express IL-4, IL-5, and/or IL-13, Th17 cells express IL-17 [727], Th9 cells express IL-9, Th22 cells express IL-22, and Tfh cells express IL-21 (Fig. 85). Although yet to be fully characterized, cytotoxic CD4 T cells have been identified through the expression of cytolytic molecules such as perforin [710]. CD4 T cells also upregulate the expression of the co-stimulatory molecule CD40L after activation [614], which is crucial for their T helper functions [691, 728].

To unleash and detect their effector function CD4 T cells can be stimulated polyclonally using CD3ε mAb to drive TCR signaling or using the phorbol ester PMA together with Iono to bypass TCR signaling and activate protein kinase C. CD4 T cells can be stimulated in an antigen-specific manner with their cognate peptide presented by MHCII. Antigen can be provided in in vitro stimulation either as a purified short peptide containing the relevant epitope, or as more complex antigens; live or killed pathogens, pathogen lysates, full-length proteins, or long peptides, which are then processed into short peptides and directly presented on MHCII by professional APCs. Restimulation with more complex antigen therefore requires the presence of APCs and, as a result, whole splenocyte preparations or sorted CD4 T cells with addition of peptide-pulsed APCs should be used to assess responses to complex antigen. Additionally, synthetic MHCII dimers loaded with peptide can be generated and covalently linked to beads or coated onto plates for in vitro restimulation assays. After activation, T cells start to produce and/or secrete effector molecules including co-stimulatory surface molecules, cytokines, and chemokines (see also Chapter V Section 17.5 Functional Read-outs).

To identify cytokine production on single cell level and increase the signal, cells are treated with protein transport inhibitors such as brefeldin A (BrefA) or monensin during the stimulation to allow accumulation of cytokines and activation-associated surface molecules in responding T cells. Of note, when CD4 T cells are stimulated with complex antigen, protein transport inhibitors should be added after a delay (∼2 h) to permit sufficient processing of peptide, loading onto MHCII and surface export of peptide/MHCII complexes. In addition, as extended exposure of cells to these inhibitors can be toxic, it is optimal to limit exposure. The stimulation time depends on the kinetic of the detected cytokine,
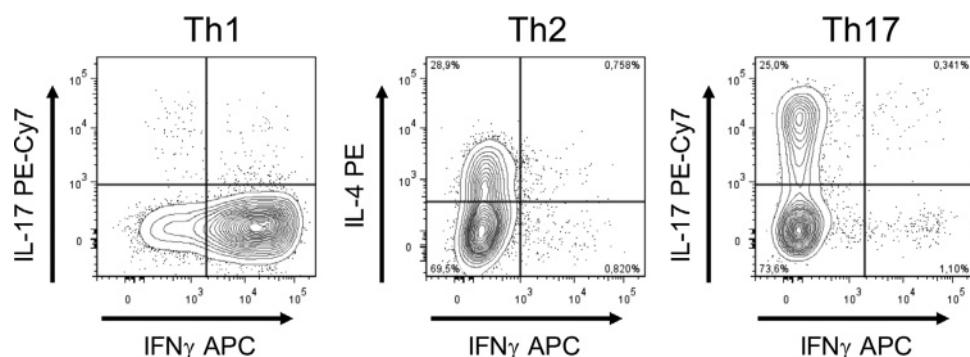
Figure 85. Effector molecules produced by murine CD4 T cells. CD4 helper T cell subsets produce distinct sets of cytokines. To analyze production of cytokines, in vitro generated Th-subsets were restimulated with PMA and Iono in the presence of BrefA. Examples shown include Th1 cells that produce IFN-γ, Th2 cells that produce IL-4 and Th17 cells that produce IL-17. All dot plots are gated on live CD4+ T cells as shown in Fig. 81.

but 4–6 h is usually sufficient to detect cytokines including IFN-γ and TNF by intracellular cytokine staining. Administration of monensin or BrefA to mice during an active immune response and analysis shortly after administration can be used to assess cytokine production directly ex vivo [729] (see also Chapter V Section 17.5 Functional Read-outs).

The detection of effector functions by FCM can be used to gain information about the properties of specific T cell subsets, but it is also utilized to enumerate antigen-specific CD4 T cells. To evaluate the total magnitude of an antigen-specific response using functional measures, an effector response should be selected that will be present in the majority of antigen-specific CD4 T cells following restimulation. A particularly useful marker for assessing total response magnitude for CD4 T cells is CD40L, as this marker is rapidly expressed on CD4 T cells after activation [730]. Unfortunately, it can be difficult to stain for CD40L, as it is transiently expressed on the cell surface and then rapidly secreted or internalized and degraded after interaction with its ligand, CD40. To circumvent this issue, cells can be either stained intracellularly for CD40L in the presence of BrefA or stimulated in vitro in the presence of both fluorescently labeled Ab against CD40L and blocking CD40 Ab [730]. Staining for CD40L in this way thereby permits evaluation of the majority of the antigen-specific CD4 T cell response.

The simultaneous detection of multiple activation markers or cytokines can aid the detection of low frequency responses, due to the decreased background. For the identification of live CD4 T cells producing a certain cytokine, a cytokine secretion assay can be used (see also Chapter V Section 17.6 Live cytokine-producing cell sorting with Cytokine Secretion Assay). In Chapter V Section 17.5 Functional Read-outs, additional information on antigen-specific T cell stimulation can be found.

Antigen-specific CD4 T cells can be detected indirectly using in vitro restimulation with defined antigens, but antigen-specific CD4 T cells can also be directly identified, analyzed, and tracked in mice using a number of methods. First, CD4 T cells specific for a given antigen can be detected by MHCII tetramers/multimers (see also Chapter V Section 17.4 MHC Multimers). Of note, tetramer staining can exhibit nonspecific binding and high background. To improve identification of low frequency tetramer+ T cells, stain-

ing with the same MHCII tetramer labeled with two different fluorophores can be used (see also Chapter V Section 17.4 MHC Multimers). Another strategy to track antigen-specific responses in vivo is to transfer congenically labeled or fluorescently labeled TCR transgenic T cells. Different transgenic mouse strains expressing TCRs specific for a number of antigens and derived from CD4 T cells have been developed, including ovalbumin (OT-II), LCMV glycoprotein (SMARTA), and malarial antigen (pBT-II). Allelic variants of the cell surface molecules CD90 (Thy-1) and CD45 (Ly-5) can be distinguished with selective Abs and allow tracking of adoptively transferred T cells in congenically distinct recipients. T cells can also be genetically modified to stably express fluorescent proteins, such as Green Fluorescent Protein (GFP), yellow (Y)FP, and red (R)FP, to track transferred cells or act as reporters for deletion or expression of genes in genetically modified mice. Fluorescent dyes, such as carboxyfluorescein succinimidyl ester (CFSE) and cell trace/tracker violet (CTV) (see Chapter V Section 18 Adoptive T cell transfers as a readout for Ag-specific immune responses), can be used to label cells, which are then transferred into hosts to track migration or cell division in vivo, although the fluorescent signal from these dyes is lost with protein turnover and so they can only be detected for a finite period. Functional indicators of antigen-specificity can also be used. Activated T cells that are actively dividing, can be identified in vivo or in vitro by uptake of Bromodeoxyuridine (BrdU) or by intranuclear staining with the proliferation-associated marker Ki-67.

1.3 Murine Conventional αβ CD8 T cells

1.3.1 Overview. MHCI-restricted CD8 T cells are one of the central effector cell populations of the adaptive immune system and contribute to protection against viruses, intracellular bacteria, and malignant cells. In this section, we provide examples how to identify conventional CD8 T cells and use surface markers to determine functionally distinct populations of CD8 T cells in steady state and during an immune response. Furthermore, we give an overview of methods that can be used to analyze transcription factors, track antigen-specific CD8 T cell responses, and measure CD8 T cell effector function.
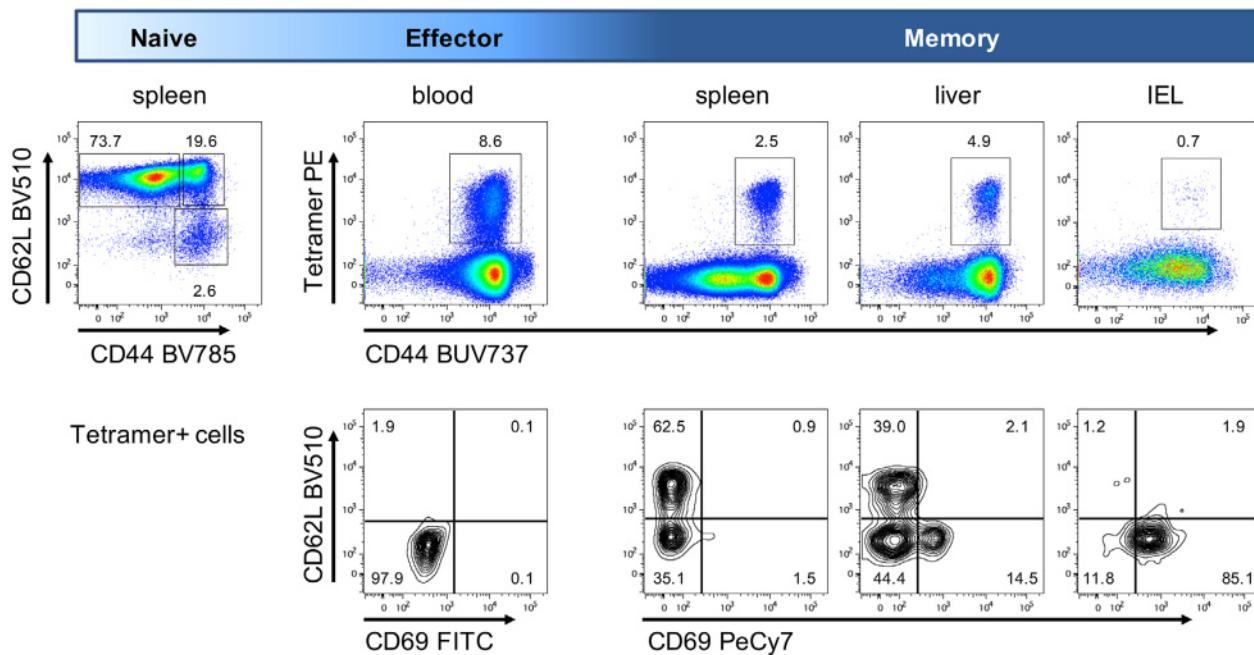
Figure 86. Discriminating murine CD8 T cell subsets. The expression of CD44, CD62L, and CD69 can be used to identify CD8 T cell populations in the different phases of the immune response. CD8 T cells displayed in the top row were gated as shown in Fig. 81. Naïve mice mainly contain naïve CD8 T cells. Pathogen-specific T cells can be identified using tetramer staining, here GP33-specific CD8 T cells after LCMV infection. During the effector phase (d8 post infection), the majority of LCMV-specific CD8 T cells upregulate CD44 and downregulate CD62L. In the memory phase (day 30+ post infection), T cells retain high expression of CD44 and can be divided in Tcm, Tem, and Trm using expression of CD62L and CD69, with distinct contribution of Tcm, Tem, and Trm in different tissues.

1.3.2 Conventional αβ CD8 T cells: Identification and surface markers. Conventional TCRαβ CD8$^+$ T cells can be identified by gating according to time, FSC and SSC, exclusion of doublets and dead cells, gating on CD3ε$^+$ or TCRβ$^+$ cells and finally gating on CD4$^-$CD8α$^+$ cells (Fig. 81). Gating on CD3ε$^+$ or TCRβ$^+$ T cells is useful to exclude myeloid cells or NK cells that express CD8α. Of note, this gating strategy can lead to the inclusion of unconventional T cells, such as intraepithelial lymphocytes (IELs), γδ T cells, NK T cells, and MAIT cells (see also Chapter VI Sections 1.7–1.10), as some of these cells express a CD8αα homodimer. These unconventional T cell populations can together comprise up to 50% of the CD8 T cell populations in some peripheral tissues, such as the small intestine. To avoid this misclassification, CD8β Abs should be included in gating strategies to exclude unconventional T cells that do not express this marker. The use of CD8β Abs can, however, reduce binding of MHCI tetramers and thereby limit the identification of antigen-specific CD8 T cells [731]. These factors should therefore be taken into consideration when identifying antigen-specific populations in tissues that are rich in unconventional T cells populations.

The differentiation state of CD8 T cells is defined by CD44 and CD62L expression (Figs. 81 and 86). Naïve CD8 T cells (Tn) are CD44loCD62Lhi. After infection or immunization, antigen-activated CD8 T cells upregulate expression of CD44 and lose CD62L during differentiation into CD8 Teff cells (CD44^{hi}CD62L^{lo}) (Fig. 86). The expression of additional surface markers during activation and expansion can be indicative of cellular fate in developing CD8 Teff cells. Two such markers are CD127, which

is the IL-7 receptor α chain that promotes T cell survival in the periphery, and KLRG1, which is upregulated with strong or sustained antigen encounter and regarded as a marker of terminal differentiation (Figure 87). Antigen-specific CD8 T cells derived from the effector phase of a response can express various combinations of CD127 and KLRG1, which define either short-lived effector cells (SLEC; CD127$^-$KLRG1$^+$), which are lost during the contraction phase of the immune response, or memory precursor effector cells (MPEC; CD127$^+$KLRG1$^-$), which are more likely to persist and contribute to memory populations [732, 733]. Of note, repeated antigenic stimulation, such as during live or prime boost vaccination, can drive accumulation of a CD127$^+$KLRG1$^+$ population [734], although their functionality and memory potential is not well defined.

After resolution of infection, the CD8 Teff cell population contracts and memory populations begin to form. Similar to CD4 T cells, CD8 Tmem cells are often defined as Tcm cells (CD44^{hi}CD62L^{hi}) and Tem cells (CD44^{hi}CD62L^{lo}), as well as tissue resident memory cells (Trm; CD44^{hi}CD62L^{lo}CD69^{hi}; see Chapter VI Section 1.4 Murine tissue resident memory T cells) (Figure 86). Additionally, the differential expression of the fractalkine receptor CX3CR1 can been used to identify CX3CR1^{int} peripheral memory T cells (Tpm), which have direct access to peripheral tissues for surveillance [735].

Of note, cytokine stimulation in the absence of antigen stimulation can upregulate memory markers in antigen-naïve CD8 T cells. These virtual memory CD8 T cells (Tvm; CD44^{hi} CD49d^{lo}) acquire CD44 expression in the periphery in response to IL-15
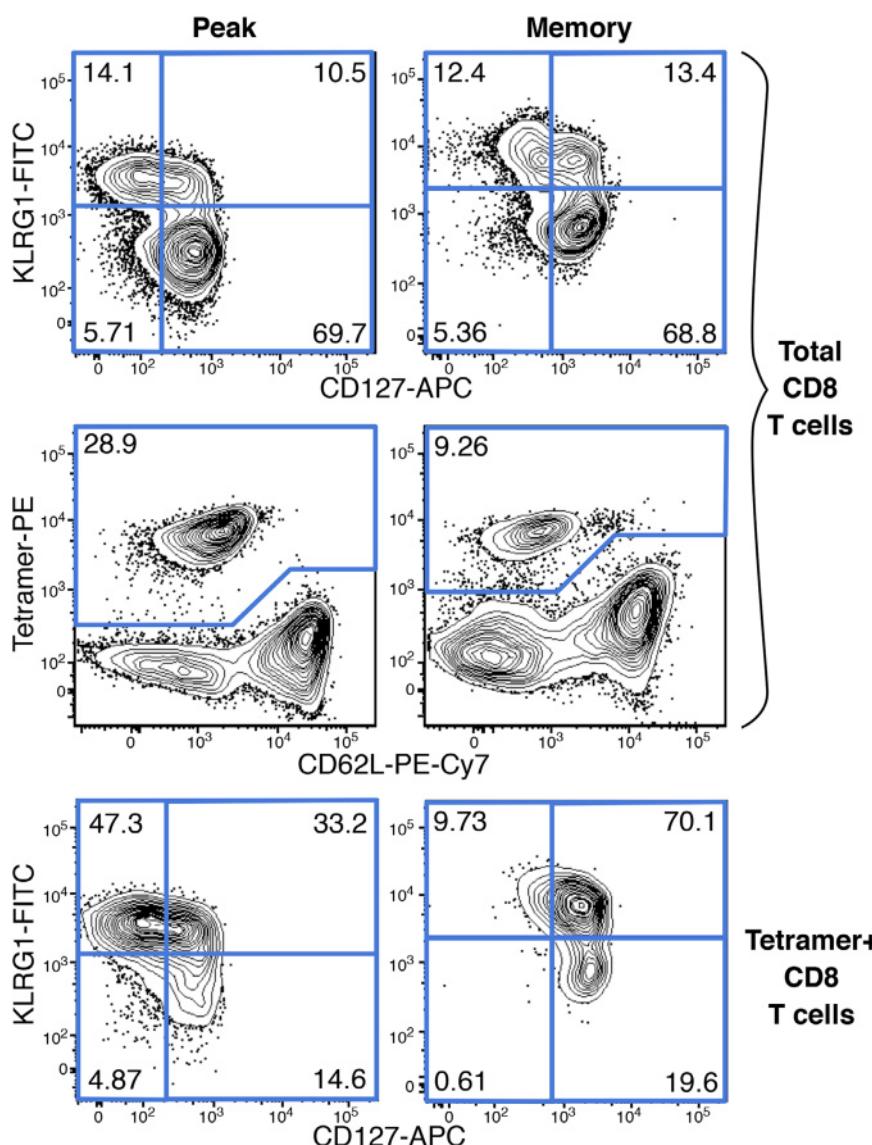
Figure 87. Delineating murine SLEC and MPEC populations. The expression of KLRG1 and CD127 can be used to differentiate SLECs (KLRG1$^+$CD127$^-$) from MPECs (KLRG1$^-$CD127$^+$). Plots are gated on CD8α^+ T cells as in Fig. 81 (total CD8 T cells, top two rows) and additionally on tetramer+ cells as in Fig. 86 (bottom row). Cells are derived from peripheral blood at the peak (day 27, left) or memory timepoint (day 230, right) post-vaccination with recombinant adenoviral vector expressing SIV-Gag as a target antigen.

stimulation but do not upregulate CD49d, a subunit of very-late activation antigen (VLA)-4 [736]. Other Tvm cell markers include high expression of Eomes, Bcl-2, CD122, and CD127. While Tvm cells are antigen-naïve, they are functionally distinct from CD8 Tn cells [737]. Crucially, Tvm cells are also CD62L^{hi}. As a result, CD44^{hi}CD62L^{hi}CD49d^{lo} Tvm cells are often included in gates for CD44^{hi}CD62L^{hi}CD49d^{hi} Tcm cells (Figure 88), when CD49d is not included in gating strategies or when a marker to identify antigen-specific Tcm cells, such as tetramer staining, is not used. Given the unique functional profile of Tvm cells, this has led to misattribution of Tvm cell qualities to the Tcm cell compartment [738]. Care should be taken to properly identify Tcm cells versus Tvm cells, especially during aging when virtual memory cells become more dominant (see also Chapter VI Section 1.5).

1.3.3 CD8 T cells: Transcription factors.   The differentiation of CD8 T cells from Tn into Teff, Tcm, Tem, and Trm cells is co-

ordinated by a network of transcription factors. Tn cells exhibit high expression of Bach2, which maintains naivety and multipotency [740]. After activation, some transcription factors favor Teff cell differentiation, such as Tbet, Id2, Blimp1, while others favor Tcm or Tem cell differentiation, such as Eomes, Bcl6, and Id3. Eomes in particular has been correlated with Tcm cell development [741] but it is also crucial in Tvm cell development [736]. Additionally, Blimp and Hobit (homolog of Blimp1 in T cells) mediate Trm generation [742]. To assess transcription factors by FCM, intranuclear staining is used (see also Chapter V Section 13 Transcription factors).

1.3.4 CD8 T cells: Effector functions and antigen specificity.   During activation, CD8 Tn cells start to express surface molecules and produce and secrete proteins that are necessary for their effector function. Directed killing of infected or malignant cells is the main effector function of activated CD8 Teff cells. This
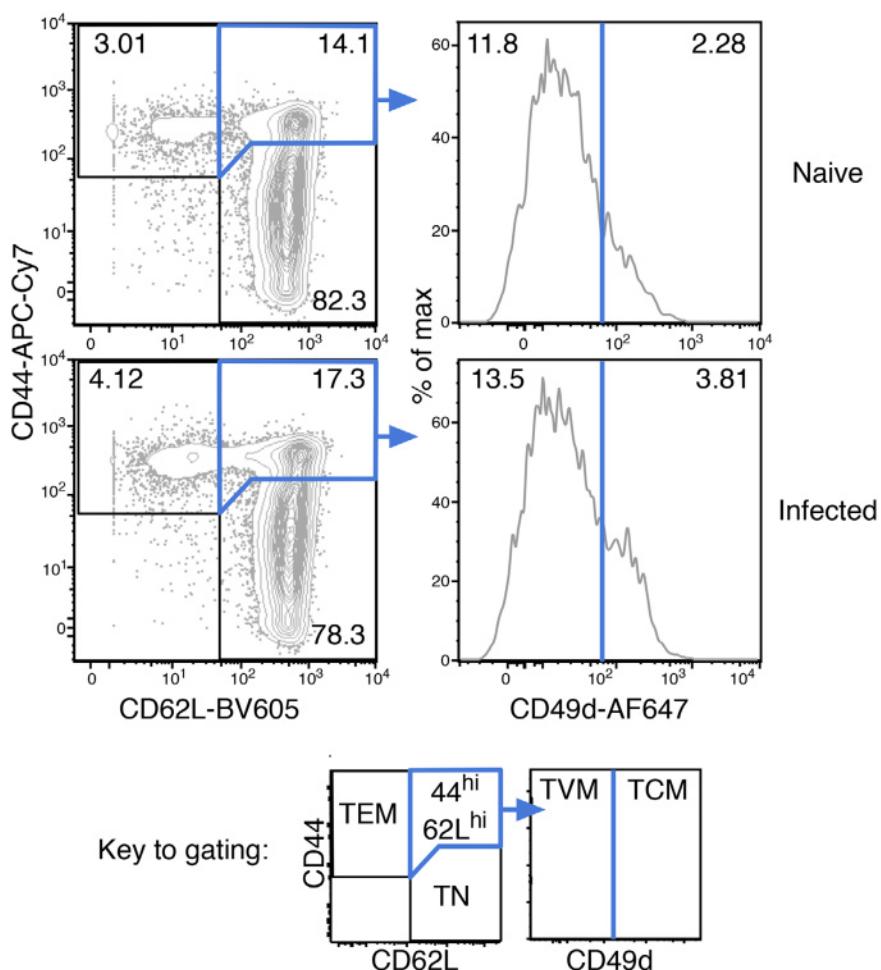
Figure 88. Discriminating murine Tcm cells from Tvm cells. The expression of CD44, CD62L, and CD49d can be used to differentiate antigen-experienced Tcm cells from antigen-inexperienced Tvm cells. Tcm cells are CD44hiCD62LhiCD49dhi while Tvm cells are CD44hiCD62LhiCD49dlo. Shown are splenocytes from 3-month-old naive or flu-infected (day 60 post-infection) C57BL/6 mice. Cells in contour plots are gated on singlets, lymphocytes, live, dump (B220, NK1.1, CD4, CD11c, CD11b, F4/80)-, CD8α+ T cells as given in Quinn et al. [739].

cytotoxicity is typically mediated by secretion of cytokines, such as IFN-γ and TNF, the release of cytotoxic granules containing granzymes and perforin, and/or surface expression of FasL, which can induce apoptosis of Fas expressing cells. Similar to CD4 T cells, different subsets of CD8 cytotoxic T (Tc) cells have been described, including Tc1, Tc2, Tc9, and Tc17 cells [743], and a subset of CD8 T cells has been observed that can mediate help via CD40L [744]. Some effector functions, such as constitutive Granzyme B expression, can be directly analyzed in resting Tmem, while most cytokines are only produced after reactivation.

To assess cytokine production quantitatively and qualitatively, intracellular cytokine staining is commonly used. Like CD4 T cells (See Chapter VI Section 1.2.4. CD4 T cells: effector functions and antigen-specificity), cytokine production in CD8 T cells is generally analyzed after in vitro restimulation, either polyclonally using PMA/Ionomycin or CD3/28 mAb, or in an antigen-specific manner using protein (i.e., purified protein, pathogen lysate, or live pathogen) or peptide. Of note, antigen-specific restimulation of CD8 T cells involves stimulating the cells with their cognate antigen presented on MHCI. While complex protein antigen can be used to efficiently stimulate CD4 T cells, cross-presentation of exogenous complex protein antigen on MHCI by APCs is a relatively inefficient process in vitro and is generally less suitable for restimulation of CD8 T cells. In contrast, short peptides are very efficiently loaded onto MHCI (and II) and restimulation with peptides that contain known epitopes is therefore an effective way to induce and assess CD8 T cell responses. Alternatively, cells directly infected with bacteria/virus or cell lines expressing MHCI-peptide conjugates, such as SAMBOK (MEC.B7.SigOVA) [745] or RMA-S, can be used to stimulate CD8 T cells, as these cells exhibit efficient presentation of peptide on MHCI.

During stimulation, cells will start to express cytokines and other effector molecules. To drive the accumulation of these molecules within the cell and increase the detection of secreted effector molecules, protein inhibitors like BrefA or monensin are used during the activation. These protein transport inhibitors are toxic; thus, it is optimal to limit the time of cell exposure. Typically, 4–6 h are used to accumulate cytokines like IFN-γ, IL-2, and TNF for detection by staining (Fig. 89a). In addition, BrefA or monensin can be administered to mice during an active immune response, with mice euthanized shortly after administration and immediate analysis of cytokine production directly *ex vivo* [729]. The advantage of this approach is that it allows measurement of cytokine production with in situ antigen presentation, which is more relevant to understanding immune priming in the lymph node and site of infection.
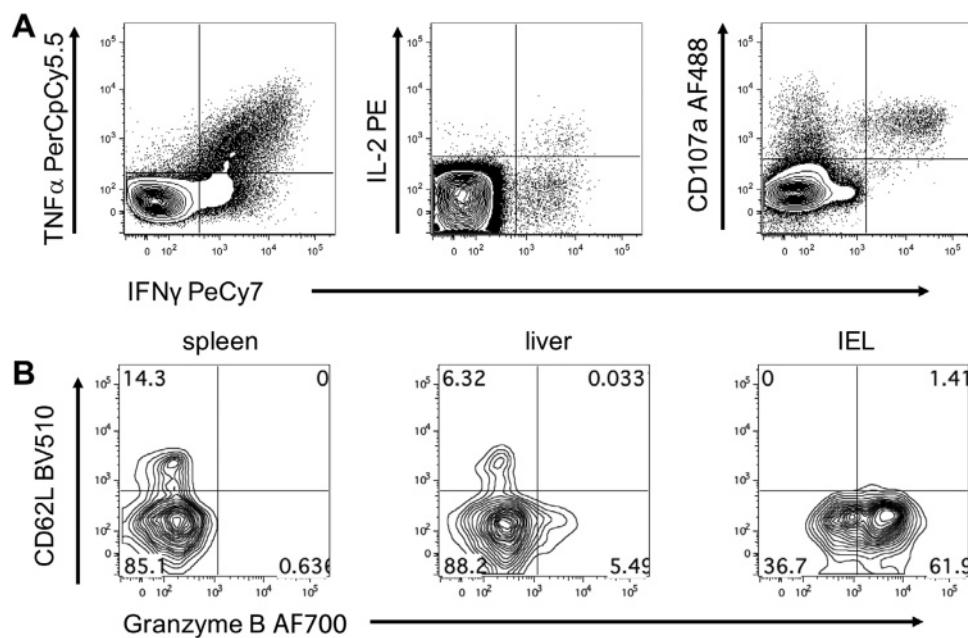
Figure 89. Effector molecules produced by murine CD8 T cells (A) Splenocytes of virus-immune mice were stimulated with peptide for 6 h in the presence of BrefA to identify virus-specific CD8 T cells based on their cytokine expression and degranulation using CD107a (gated on live CD8α⁺ T cells). (B) Virus-specific CD8 T cells from different tissues were stained Granzyme B (gated on CD8α⁺ T cells as in Figure 81, with identification of transferred OT1 CD8 T cells using congenic markers CD45.1 /CD45.2).

T cells can engage multiple effector mechanisms after activation. The simultaneous detection of multiple activation markers or cytokines can aid the detection of low frequency responses, due to decreased background (Fig. 89A), but it also permits the assessment of a characteristic known as poly- or multifunctionality. Multifunctionality refers to T cells that express more than one effector molecule or cytokine simultaneously upon stimulation and can be assessed through Boolean gating, processed with software called Pestle and visualized with software called SPICE. Alternatively, newer FlowJo plugins such as SPADE analysis and Cytobank, can facilitate analysis of multiparametric data.

Cytotoxic potential can be assessed directly ex vivo by intracellular staining for cytotoxic proteins such as granzyme B and perforin. CD8 Teff and some Tmem cells contain vesicles of preformed cytotoxic granules, including granzymes and perforin, that are detected via intracellular staining directly ex vivo without the need for stimulation (see protocol, Fig. 89B). This approach is optimal, as stimulation can cause CD8 T cell degranulation, which can lead to a reduction in the amount of granzyme B or perforin per cell and a loss of fluorescence intensity and staining resolution. Cytotoxic capacity can be directly assessed using in vitro or in vivo killing assays (see also Chapter V Section 17.8 Cytotoxicity). In these assays, fluorescently labeled target cells loaded with a target peptide are mixed at a 1:1 ratio with fluorescently labeled control cells loaded with an irrelevant peptide. The target/control mix is either co-incubated in vitro with antigen-specific CD8 T cells at varying ratios or administered intravenously to immune animals. A reduction in the relative frequency of target versus control cells acts as a measure of antigen-specific CD8 Teff cell cytotoxic capacity. Finally, degranulation capacity can also be assessed. When a

CD8 T cell is stimulated, cytotoxic granules can be released at the cell surface and lysosomal markers such as CD107a and -b become transiently accessible at the cell surface before being recycled. To stain these markers as a measure of degranulation, fluorescently labeled Abs for CD107a and -b are included during restimulation and monensin should be used to neutralize lysosomal pH and prevent protein degradation (Fig. 89A).

To identify, analyze, and track antigen-specific CD8 T cells in mice, a number of methods previously described in the section on CD4 Teff cell functions, can be used (see also Chapter VI Section 1.2.4 CD4 T cells: effector functions and antigen specificity). Briefly, antigen-specific CD8 T cells can be identified directly ex vivo using MHCI tetramers/multimers. CD8 Teff cells can be restimulated with cognate antigen and proliferation or cytokine production can be used to indirectly identify antigen-specific CD8 T cells. Antigen-specific CD8 T cell responses can also be tracked using transfer of congenically marked or fluorescently labeled TCR transgenic CD8 T cells from mouse strains such as OT-I, p14, and gBT-I and subsequent challenge with their cognate antigen. During an ongoing immune response, activation markers such as CD11a and CD49d [746], as well as markers of proliferation (BrdU or Ki67) can be used to directly identify antigen-experienced CD8 cells ex vivo.

1.3.5 Step-by-step sample preparation for detection of GrB in murine CD8 T cells.

- Transfer 1–5 × 10⁶ cells per sample to a 96-well V-bottom plate
- Pellet cells at 500 × *g* for 5 min at 4°C and remove supernatant.
- Resuspend cells in 50 μL surface stain Ab mix (in FCM buffer).

- Incubate at 4°C for 15–30 min.
- Wash with 150 µL of FCM buffer, and centrifuge for 5 min at 500 × g at 4°C and remove supernatant.
- Resuspend cells in 50 µL of freshly prepared Foxp3 Fixation/Permeabilization working solution prepared according to manufacturer's instructions.
- Incubate at 4°C for 30 min.
- Optional: wash in 150 µL FCM buffer, and pellet cells at 500 × g for 5 min at 4°C, remove supernatant, resuspend in 50 µL FCM buffer, and store overnight in fridge at 4°C.
- Add 150 µL 1× Foxp3 Perm/wash solution (prepared according to manufacturer's instructions), pellet cells at 500 × g for 5 min at 4°C and remove supernatant.
- Add intracellular Ab stain mix (in Foxp3 Perm/wash solution)
- Incubate at 4°C for 30 min.
- Add 150 µL 1× Foxp3 Perm/wash solution, and centrifuge at 500 × g for 5 min at 4°C and remove supernatant.
- Resuspend in FCM buffer for analysis on a flow cytometer.

1.3.6 Materials.

- Single cell suspension containing T cells (here material from LCMV immune mouse)

- eBioscience™ Foxp3 / Transcription Factor Staining Buffer Set (Thermo Fischer, Cat# 00-5523-00)
- FCM buffer: PBS with 2% FCS

1.3.7 Surface stain mix.

- Anti-murine CD8α BUV395 (BD, catalog no. 563786, clone 53–6.7, dilution 1:200)
- Anti-murine CD45.1 FITC (eBioscience, catalog no. 11-0453-82, clone A20, 1:200)
- Anti-murine CD45.2 eF450 (eBioscience, catalog no. 48-0454-82, clone 104, 1:200)
- Anti-murine CD62L BV510 (Biolegend, catalog no. 104441, clone MEL-14, 1:400)
- LIVE/DEAD™ Fixable Near-IR Dead Cell Stain Kit (Thermo Fischer, catalog no. L10119, 1:1000)
- Diluted in FCM buffer

1.3.8 Intracellular stain mix.

- Anti-human granzyme B AF700 (BD, catalog no. 561016, clone GB11, dilution 1:200) (this Ab is crossreactive with murine granzyme B)

1.3.9 Summary Table (Table 18).

Table 18. Molecules that discriminate subpopulations of conventional CD8αβ T cells (identified by expression of CD3 or TCRαβ, lack of TCRγδ and CD4, expression of CD8a and CD8b)

	TN	TEFF (SLEC)	TEFF (MPEC)	TVM	TCM	TEM	TRM
Surface markers							
CD44	lo	hi	Hi	hi	hi	hi	hi
CD62L	hi	lo	Lo	hi	hi	lo	lo
CD69	lo	int	Int	hi or lo	lo	lo	hi
CD103	hi or lo	hi or lo	hi or lo			lo	lo	hi or lo
CD25	lo	hi	hi	lo	lo	lo	
CXCR3	lo	hi	hi	hi	hi	hi	hi
CXCR6	lo	int	int			int	int	hi
CD127	hi	lo	hi				
KLRG1	lo	hi	lo				lo
CD49d	int	hi	hi	lo	hi	hi	hi
CD122	lo	lo	lo	hi	int	lo	
CD49a	lo	hi or lo	hi or lo			hi or lo	int	hi
Intracellular markers to be stained ex vivo							
Granzyme B	lo	hi	hi	int	lo	lo	int
Perforin	lo	hi	hi	int	lo	lo	int
Markers to be stained after restimulation							
IFN-g	lo	hi	hi	hi	hi	hi	Hi
TNF	lo	hi	hi	hi	hi	hi	hi
IL-2	lo	hi	hi	lo	hi	int	int
Intranuclear markers and transcription factors							
Bach2	hi	int	int	int	lo	lo	lo
Tbet	lo	hi	hi	hi	int	int	int
Bcl-2	lo	lo	lo	hi	int	int	
Eomes	lo	lo	lo	hi	int	int	int or lo
Hobit	lo				lo	lo	hi
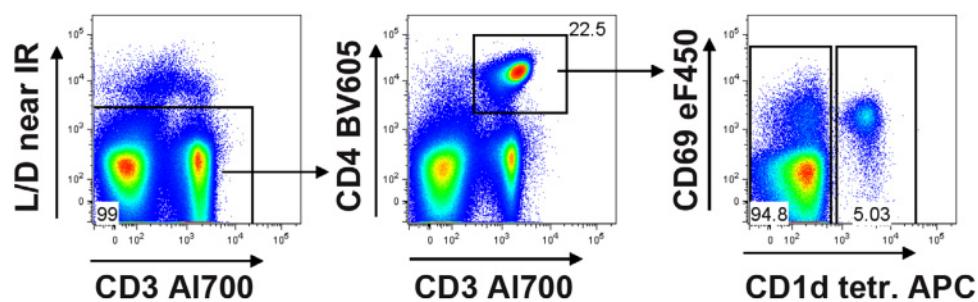
Figure 90. Unconventional and conventional murine T cells can have overlapping phenotypes. Splenocytes were gated on scatter parameters (see Figure 81), live, CD3$^+$/CD4$^+$ T cells. Staining with CD1d PBS-57 tetramer identifies NKT cells that mainly express CD69.

1.4 Murine tissue resident memory T cells

1.4.1 Overview. Tissue-resident memory T cells (Trm) cells are noncirculating T cells that form the first line of defense against reinfection in tissues [747, 748]. They are enriched in barrier tissues, such as the lung, skin, and intestine, but they are also present in internal organs, such as brain, liver, bone marrow, white adipose tissue, and lymphoid organs. The tissue residency phenotype was initially described for CD8 T cells, but analogous tissue residency programs for CD4 T cells and other lymphocyte populations are currently being defined [749].

1.4.2 Methods to identify and analyze tissue resident T cells. Most tissue resident T cells are located within a dense network of parenchymal cells and extracellular matrix. This cellular network needs to be dissociated to analyze the lymphocytes in a single-cell suspension by FCM. It is important to note that the isolation procedure of murine T cells from tissues can have a significant impact on cell viability and detected phenotype. Enzymes like collagenase and dispase, which are used to enzymatically dissociate tissue, can cleave off lineage-defining markers such as CD4 and CD8 [750]. Additionally, tissue dissociation not only causes sheer stress and destruction, but signals released during the dissociation of tissue can influence the phenotype, function, and viability of CD4 and CD8 T cells. For example, activation of the danger receptor P2RX7 by extracellular NAD or ATP, released by dying cells during processing, can lead to shedding of surface molecules such as CD62L and CD27, the masking of CD8β and the induction of cell death in susceptible cells like Treg, NKT, and Trm cells [751–753]. This is especially important when T cells are used in functional assays. As a result, the method of tissue dissociation should be carefully chosen and viability of cell preparations used in FCM should always be assessed.

In many peripheral tissues, unconventional T cells are increased and can even dominate (see also Chapter VI Sections 1.7-10), which is important to consider when identifying Trm cell populations. These unconventional T cells can have overlapping expression patterns with conventional TCRαβ CD4 and CD8 T cells for basic surface markers. For example, in liver and spleen, the CD3$^+$ CD4$^+$ gate is composed of both conventional TCRαβ CD4 T cells and a population of NKT cells with a tissue resident phenotype (Fig. 90). Similarly, in the small intestine, the CD3$^+$ CD8α$^+$ gate for intraepithelial lymphocytes (IELs) can include conventional TCRαβ CD8αβ T cells and CD8αα IELs and γδ T cells. Therefore, careful selection of the surface markers is key for the correct identification of target cells, particularly across tissues.

Their location and signals of the local microenvironment determine the expression profile of T cells. Accordingly, the physiologically quite diverse parenchyma of tissues can drive a tissue-specific phenotype Trm and expression of surface molecules might differ per organ [747]. CD69 is constitutively expressed by many Trm cells, it is functionally important for their residency and it is therefore a commonly used marker for Trm identification (Figs. 86 and 91). The chemokine receptor CXCR6 (Fig. 91), immunoglobulin CD101 and CD49a, the α-chain of the α1β1 integrin (VLA-1), are also highly expressed on Trm cells in many tissues. CD8 Trm cells in epithelial and neuronal tissues can also express CD103 (Fig. 91), which is the α-chain of the αEβ7 integrin [747]. CD103 is also expressed by a subset of CD8 Tn cells, which makes the use of CD44 or CD62L essential to discriminate between CD8 Trm and Tn cells. While the majority of Trm cells throughout different tissues constitutively express CD69, parabiosis and in vivo labeling experiments have highlighted that there are CD69$^-$ cells that reside long-term in tissues [754].

In vivo labeling offers an alternative way of Trm identification by providing information about the location of T cells. During in vivo labeling, fluorescently labeled Abs directed against CD4, CD8 or pan-T cell markers, such as CD90 and CD45, are injected intravenously shortly before tissue harvest [755]. This brief exposure labels leukocytes in circulation, which can be used to distinguish between the labeled cells in the vasculature of a tissue and unlabeled T cells located within the tissue itself. These unlabeled T cells are therefore enriched for Trm cells and this approach can be particularly important when working with highly vascularized tissue such as the lung.
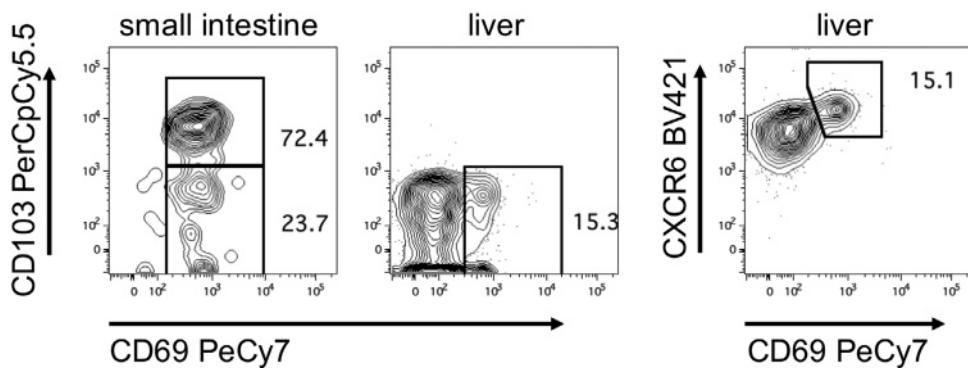
Figure 91. Identifying Trm cells. Expression of CD69, CD103, and CXCR6 can be used to identify Trm. Lymphocytes from different tissues of LCMV-immune mice (d30+ post infection) were isolated and LCMV-specific memory T cells identified as live, CD8α+, tetramer+ (see Figs. 81 and 84).

1.4.3 Step-by-step sample preparation for the analysis of Trm from the small intestine and the liver.

1.4.3.1 Isolation of intraepithelial lymphocytes from the small intestine.

- Remove small intestine and store in cold HBSS with 2% FCS (wash buffer)
- Cut intestine into three pieces and store in HBSS with wash buffer
- Clean each piece of intestine on a wet tissue soaked with wash buffer from fat, remove peyers patches, cut longitudinal and remove feces, keep intestine wet during the whole time
- Wash two times with 5 mL wash buffer (e.g., six-well plate)
- Cut into pieces of 1 cm and transfer to 10 mL wash buffer, vortex 10 s, pour over cell strainer, and collect tissue pieces, repeat twice
- Transfer tissue pieces to 20 mL EDTA solution (HBSS, 10% FCS, 5 mM EDTA, 1 mM DTT)
- Incubate 30 min at 37°C in water bath, vortexing every 10 min
- Filter over cell strainer and collect the flow through containing intraepithelial lymphocytes
- Remaining tissue pieces and be used for the isolation of lamina propria lymphocytes

1.4.3.2 Isolation of lymphocytes from the liver.

- Remove liver and store in cold PBS with 0.5% FCS
- Remove gall bladder and other connective tissue attached
- Mash liver over cell strainer with PBS with 0.5% FCS using the plunger of a 3 mL syringe

1.4.3.3 Enrichment of lymphocytes by gradient centrifugation.

- Pellet cells (500 × g, 5 min, 4°C)

- Resuspend cells in 5 mL 40% isotonic percoll and overlay to 3 mL 60% isotonic percoll in a 15 mL falcon
- Centrifuge 20 min at 800 × g, acceleration 5, deceleration 0 (no break)
- Remove top layer of fat and tissue cells
- Collect lymphocytes from the interphase
- Wash with PBS with 0.5% FCS

1.4.3.4 Staining of lymphocytes.

- Transfer up to 4 × 10^6 cells to FCM tubes or 96-well V-bottom plate
- Pellet cells (500 × g, 5 min, 4°C)
- Resuspend in 50 μl staining mix, incubate 30 min at 4°C
- Wash cells with PBS with 0.5% FCS and analyze by FCM

1.4.4 Materials.

- Wash Medium: HBSS/ 2% FCS
- EDTA Medium: HBSS 10% FCS mix, 5 mM EDTA, 1 mM DTT
- PBS
- Percoll (GE, 17-0891-01, density 1,13 g/ml, prepare isotonic 90% Percoll by mixing with 10x or 20x PBS, dilute with PBS to 60% and 40%)
- Surface stain mix (in PBS with 0,5% FCS):

  - Anti-murine CD8α BUV395 (BD, cat # 563786, 53–6.7, 1:200)
  - Tetramer (D^b GP33 PE, R. Arens, LUMC)
  - Anti-murine CD69 PeCy7 (eBioscience, cat # 25-0691-82, H1.2F3, 1:200)
  - Anti-murine CD62L BV510 (Biolegend, cat # 104441, MEL-14, 1:400)
  - Anti-murine CD103 PerCpCy5.5 (BD, cat # 563637, M290, 1:200)
  - LIVE/DEAD^TM Fixable Near-IR Dead Cell Stain Kit (Thermo Fischer, cat # L10119, 1:1000)

1.4.5 Pitfalls and Top tricks.

- Know the cells you study: Correct selection of markers for identification and exclusion of other cell populations is key to avoid misclassification.
- Sample processing can affect detection of your markers, cell viability, and the outcomes of functional assays.

1.5 Immune senescence (aging) in murine T cells

1.5.1 Overview.
Aging leads to loss of immune functionality with a well-documented impact on adaptive immunity, and in particular the T cell lineage [756]. Such changes have shown similarities in humans and mice. Therefore, this chapter will focus on the phenotyping of T cells in models of aging in mice.

1.5.2 Introduction.
To study immune aging in mouse models, we need to consider the overlaps and the differences between the aging process in mice and humans. Such differences may be reflections of intrinsic differences between the two species (e.g., in lifespan, body mass, telomere length, or telomerase activity [757]), or of the fact that humans are observed in the context of environmental exposures of the real world, whereas mice are typically studied in controlled and sterile environments of SPF facilities. Therefore, long-term exposure of mice to ubiquitous environmental microorganisms may reflect natural aging processes better than their maintenance in sterile environments [758, 759]. When working with mice, 18 months of age or older is considered truly aged [760], as many mouse strains survive longer than 600 days in standard SPF housing [761]. While 3-month-old young mice have high frequencies of naïve T cells in blood and lymphoid tissue, the relative frequency (Fig. 92) and absolute counts of naïve T cells decline substantially with age as the thymus involutes. In contrast, the frequency (Fig. 92) and counts of memory T cell subsets, particularly more differentiated populations, increase with age as the collective history of antigenic encounters makes a mark on the aging host.

Phenotyping of naïve and memory T cell subsets by FCM relies on a combination of markers that are acquired or lost during T cell differentiation, from naïve and memory to terminally differentiated T cells [762]. Some markers that are used to identify naïve and memory T cell subsets in humans such as CD45RA [762] are not suitable for phenotyping murine T cell subsets, mainly because they do not allow reasonable separation in discrete positive and negative fractions. As a result, markers such as CD44 and CD62L or CCR7 are used in mice to identify naïve (TN), central memory (TCM), and effector memory (TEM)/effector (TEFF) subsets, as well as KLRG1 and CD127, which are used to identify memory precursor effector cells (MPEC) and the short-lived effector cells (SLEC) populations, as described previously (See Chapter VI Section 1.1 Murine CD4 and CD8 T cells, Section 1.4 Murine tissue resident memory T cells).

In addition to these classical T cell subsets, we can assess senescence markers in T cells. Some surface markers used in humans such as CD57, the lack of CD28 and the re-emergence of CD45RA expression, do not translate into mice. Telomere length is also commonly assessed in humans as an indicator of cellular age and replicative senescence, sometimes by flow cytometric methods, but this approach is limited in mice as telomeres are relatively long, meaning that telomere erosion may not be a major driver of immune ageing [757]. However, senescent T cells in mice do exhibit increased expression of NK cell related markers, such as KLRG1, and the loss of CD27, allowing us to robustly separate memory subsets and more terminally differentiated populations in mice (Fig. 93). Senescent T cells in mice and humans both exhibit an increase in phosphorylated γH2Ax subunits in the cytosol as an indicator of increased ATM kinase activity, increased DNA damage, and a DNA-damage senescence phenotype [739, 763].

Accordingly, for analysis of ageing phenotypes in mice, one should profile the differentiation status of the overall T cell population and assess senescence markers in these subsets, but the exact method of T cell phenotyping may differ depending on the experimental context and infection history of the mice.

1.5.3 Step-by-step sample preparation.

1.5.3.1 Sample collection and RBC lysis.

1. Collect a defined volume of blood (up to 75 μL) using a heparinized hematocrit capillary and dispense it into an Eppendorf tube containing 300 μL of HBSS-EDTA buffer.
2. Remove 75 μL for absolute blood cell counting and process as indicated in Section 12.1.3.2.
   Proceed with the remaining blood in HBSS as indicated below.
3. Centrifuge for 5 min at 700 × g at 4°C.
4. Aspirate supernatant and resuspend pellet in 600 μL of distilled water. Immediately thereafter (max 5–10 s), add 200 μL of 4× PBS and briefly mix by pulse vortexing.
5. Centrifuge for 5 min at 700 × g at 4°C.
6. Aspirate most of the supernatant (leave approximately 100 μL), resuspend cells in the remaining volume and transfer into a 96-well plate.
7. Centrifuge for 3 min at 700 × g at 4°C.
8. Flick off the supernatant and resuspend pellet in 150 μL of distilled water using a multichannel pipette. Immediately thereafter (max 5–10 s), add 50 μL of 4× PBS with a multichannel pipette and mix thoroughly by pipetting. Discard tips between rows to avoid carryover cell contaminations.
9. Centrifuge for 3 min at 700 × g at 4°C
10. Flick off supernatant and proceed with antibody staining as described in previous chapters (see Chapter IV Section 2.5. Erythrocyte lysis).
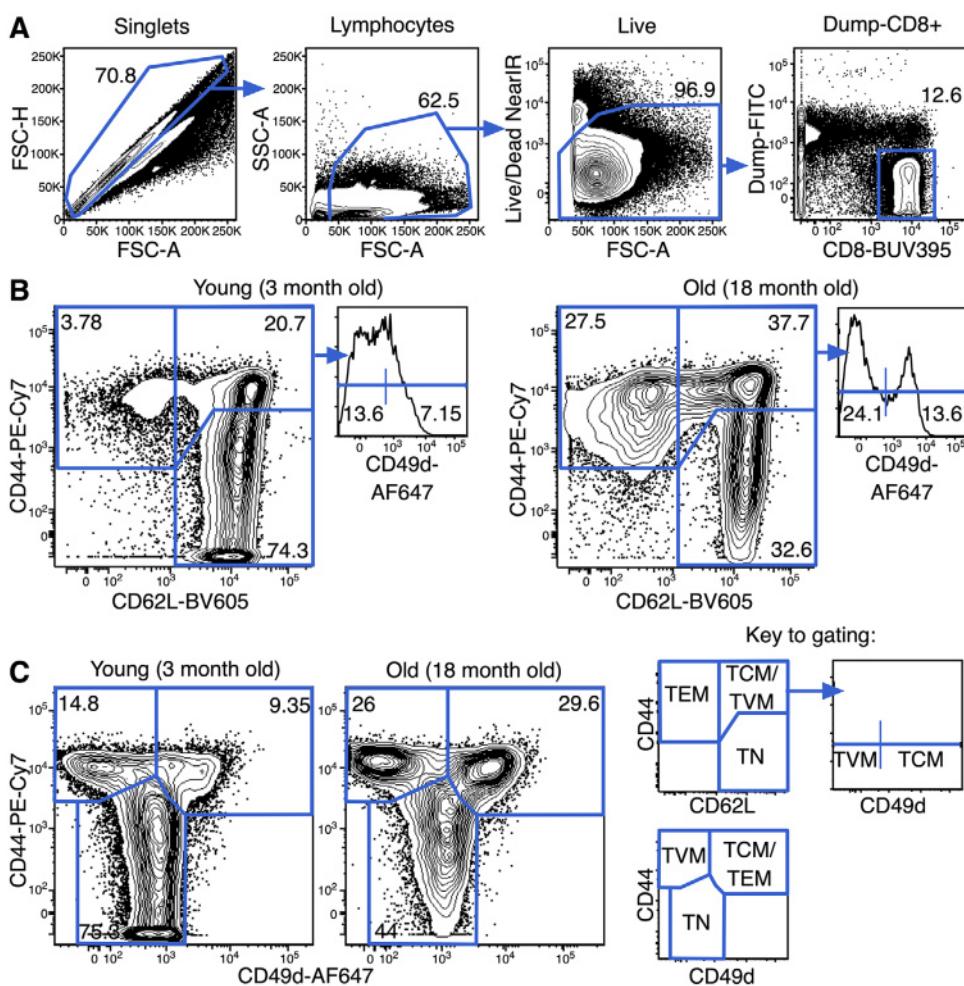
Figure 92. Gating strategy used to define TN, TVM, TCM, and TEM CD8 T cell subsets in naïve mice, using splenocytes from naïve SPF 3 month old and 18 month old C57BL/6J mice. (A) Gating strategy, where cells are gated on singlets, lymphocytes, live, dump-, CD8$^+$ T cells, and then (B) CD44 versus CD62L then CD49d or (C) CD44 versus CD49d to define the populations indicated in the key. Frequencies indicate the frequency of indicated subsets within the CD8 T cell population.

1.5.3.2 Absolute cell counts. Lymphocyte counts per volume of blood can be obtained using automated hematology analyzers according to manufacturer's guidelines. For measurements using VETSCAN HM5 (Abaxis), a minimum of 75 μL of HBSS-EDTA diluted blood (see 12.1.2.1) is transferred to an Eppendorf tube and acquired. Absolute values are calculated in relation to the volume of blood and HBSS-EDTA:

$$C_r = C_o \left(V_T / V_B \right),$$

where C_r is the real count of blood cells, C_o is the count observed in the analyzer, V_B is the volume of the blood in the acquired sample, and V_T is the total volume of the blood with HBSS-EDTA at the time of acquisition. Alternatively, absolute number of cells in a stained sample can be determined using FCM counting beads (e.g., Precision Count Beads, BioLegend) according to manufacturer's protocol.

1.5.4 Materials. Media and buffers: HBSS-EDTA: HBSS 5mM EDTA; Staining buffer: Phosphate buffered saline (PBS) 2% (v/v) FBS;

Antibodies for uninfected mice: Dump-FITC (anti-B220 (clone RA3-6B2), CD11c mAb (clone HL3), CD11b mAb (clone M1/70), anti-F4/80 (clone BM8), anti-NK1.1 (clone PK136)), Brilliant Ultraviolet 395 CD8a mAb (clone 53–6.7), Alexa Fluor 647 CD49d mAb (clone R1-2), PE-Cy7 CD44 mAb (clone IM7), Brilliant Violet 605 CD62L mAb (clone MEL-14); *Cell Viability Stain*: LIVE/DEAD Fixable Near-IR Dead Cell Stain (Molecular Probes)

Antibodies for infected mice: FITC CD11a mAb (clone M17/4), PE CD122 mAb (clone TM-β1), APC CD27 mAb (clone LG.3A10), APC-eFluor 780 CD3e mAb (clone 17A2), Pacific Blue CD62L mAb (clone MEL-14), anti-KLRG1-Brilliant Violet 510 (clone 2F1/KLRG1), Brilliant Violet 650 CD4mAb (clone GK1.5), Brilliant Violet 785 mAb CD44 mAb (clone IM7), Brilliant Ultraviolet 395 CD8a mAb (clone 53–6.7); *Cell Viability Stain*: 7-AAD
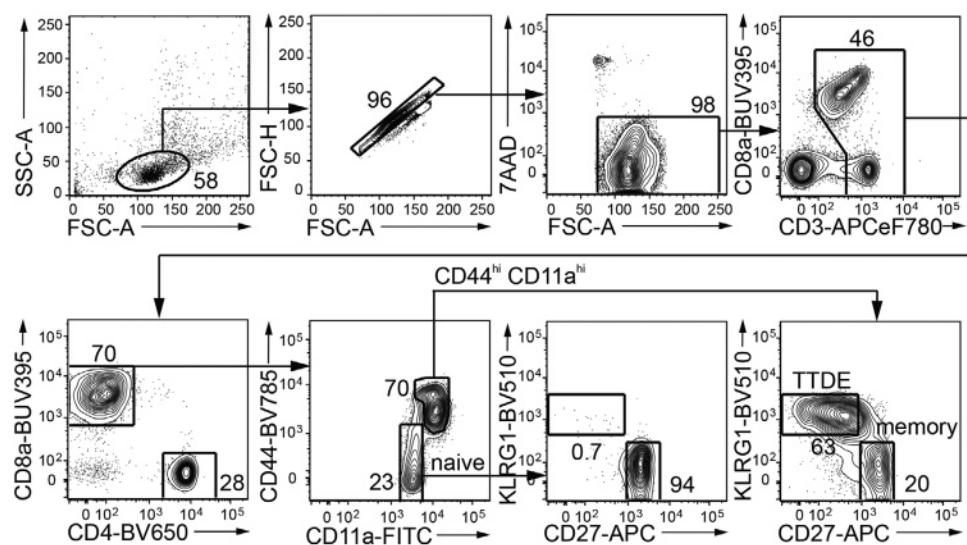
Figure 93. Gating strategy used to define naïve, memory and TTDE CD8 T cell subsets in aged chronically infected mice (applies also to Figs. 95 and 94). FCM analysis of the peripheral blood of 8-month-old C57BL/6J mouse experimentally infected for 6 months with 10^6 PFU of a chronically persistent β-herpesvirus, murine cytomegalovirus (MCMV).

Flow cytometer: Experiments were performed on an LSR Fortessa (BD Bioscience) equipped with laser excitation lines of 360, 405, 488, 561, and 640 nm and the following filter configuration: 386/23(365) for BUV395; 450/50(405) for Pacific Blue; 525/50(405) for BV510, 655/40(405) for BV650; 785/60(405) for BV785; 525/50(488) for FITC; 685/35(488) for 7-AAD; 585/15(561) for PE; 780/60(561) for PE-Cy7; 670/14(640) for APC; 710/40(640) for Alexa700; and 780/60(640) for APC-eF780.

1.5.5 Data analysis.

1.5.5.1 Identification of T cell subsets in aged, uninfected mice. Naïve aged mice that are held in a Specific Pathogen Free (SPF) facility will have had limited antigenic exposure. Using the classical markers, CD44 and CD62L, for defining naïve and memory subsets in peripheral blood and lymphoid tissue, naïve mice exhibit a clear shift with age in T cell subset frequencies, with a decrease in the naïve subset and an increase in memory subsets. Of note, this shift in frequency with age is driven by a marked decrease in naïve T cell numbers, particularly CD8 T cells, while memory cell numbers increase more modestly, consistent with their limited antigenic exposure.

As described previously (See Chapter VI Section 1.1 Murine T cells), TN cells are CD44⁻CD62L⁺ and TEM (and TEFF) cells are CD44hiCD62L⁻ cells but, for CD8 T cells, the CD44hiCD62L⁺ population contains both TCM and virtual memory (TVM) cells (Fig. 92 and Table 19). Cells must be stained with CD49d to differentiate between TCM and TVM cells, with CD49dhi denoting antigen-experienced TCM cells and CD49dlo denoting antigen-inexperienced but cytokine-exposed TVM cells. This distinction becomes important in ageing research as the proportion of CD8 T cells that are TVM cells increases markedly with age (Table 19) and these cells have been misclassified in the past as TCM cells [738]. In addition, TVM cells express high levels of CD122 and NK cell markers, both of which increase with age and would otherwise be misattributed to TCM cells [739, 764]. An additional feature of aging in mice is that the expression level of CD44 on TN cells increases, not to become CD44hi, but TN cells become predominantly CD44int (Fig. 92). This may indicate that the average post-thymic age of aged TN cells is increased or that aged TN cells are exposed to the inflamed aged environment, which is driving modest activation and increased CD44 expression.

1.5.5.2 Identification of T cell subsets in aged chronically infected mice. Upon infection, particularly infection with persistent pathogens, T cell populations progress more rapidly toward an aged phenotype, with more terminally differentiated subsets and increased expression of senescence markers (Fig. 95 and reference [758]). Therefore, a shorthand for the progression of immune aging phenotypes is given by the frequency and absolute counts of KLRG1⁺CD27⁻ Terminally Differentiated Effector T cells (TTDE). A common strategy to define naïve cells is to combine CD44 and CD62L staining, where CD44⁻ CD62L⁺ cells are considered naïve. Some commonly used mouse strains (e.g., BALB/c) show a poor separation of naïve from memory cells based on the CD44 marker so an improved separation of naïve CD8 T cells may be achieved by combining CD44 and CD11a labeling, where CD44⁻CD11alo correspond to naïve cells, although neither of these markers alone robustly separates naïve from primed cells (Fig. 93). In addition, CD122, which is expressed on TVM and TCM cells, but not on TN
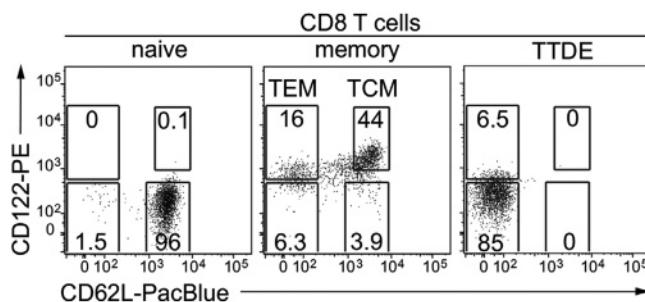
Figure 94. FCM analysis of CD122 and CD62L expression in naïve, memory, and TTDE CD8 T cell subsets (pre-gated according to the gating strategy shown in Fig. 93) in the peripheral blood of 8 month old C57BL/6J mouse experimentally infected for 6 months with 10^6 PFU of MCMV.

cells, can be used in combination with CD62L to more efficiently separate naïve cells from other subsets (Fig. 94).

is quite different to humans, where pathogen exposure accumulates over the lifespan.

Aged mice can accumulate age-related abnormalities, such as tumors, or they can overgroom, which can lead to skin abrasions and infections. This can lead to immune activation in aged mice, so many researchers exclude mice with overt abnormalities from analyses.

TVM cells are selectively retained with increasing age and are often misidentified as TCM cells. Including CD49d in staining panels enables identification of TCM cells as distinct from TVM cells.

Aged leukocytes can be more sensitive to physical manipulation, especially RBC lysis, so make sure to time this reaction carefully.

1.5.7 Summary tables.

Table 19. Summary table of aged CD8 T cell subpopulations in naïve mice

Subset of CD8 T cells	Phenotype	Percentage of CD8 T cells	
		In young mice	In aged mice
Naive	CD44^{lo} CD62L$^+$ (CD49d$^{lo/int}$)	70–85%	30–40%
Virtual memory, TVM	CD44^{hi} CD62L$^+$ CD49d^{lo}	10–15%	20–40%
Central memory, TCM	CD44^{hi} CD62L$^+$ CD49d^{hi}	5–10%	10–15%
Effector memory, TEM (and effector, TEFF)	CD44^{hi} CD62L^{lo} (CD49d^{hi})	2–5%	20–30%

Table 20. Summary table of aged CD8 T cell subpopulations in chronically infected mice

Subset of CD8 T cells	Phenotype
Naive	CD11a^{lo} CD44^{lo} CD27$^+$ KLRG1- CD62L$^+$ CD122-
Central memory, TCM, and virtual memory, TVM	CD11a^{hi} CD44^{hi} CD27$^+$ KLRG1- CD62L$^+$ CD122$^+$
Effector memory, TEM	CD11a^{hi} CD44^{hi} CD27$^+$ KLRG1- CD62L- CD122$^{-/lo}$
Terminally Differentiated Effector, TTDE	CD11a^{hi} CD44^{hi} CD27- KLRG1$^+$ CD62L- CD122-

It is important to emphasize that phenotyping for immune aging will necessarily require concurrent measurements of absolute lymphocyte counts per milliliter of blood. Namely, lowered percentages, but not absolute counts of naïve cells may also be observed due to expansions of TTDE population in persistent herpes viral infections [758], but this does not impair immune protection against infections [765]. In conclusion, a combination of six markers (CD11a, CD44, CD27, KLRG1, CD62L, and CD122) allows the distinction between TN, TCM/TVM, TEM, and TTDE T cell populations in chronically infected mice (Table 20), with a robust identification of age-related losses of naïve cell populations and increases in terminally differentiated CD8 T cells, matching functional changes in aging humans.

1.5.6 Pitfalls and Top Tricks. When working with aged mouse models, consider that mice will be housed in SPF conditions, which

1.6 Murine Foxp3$^+$ regulatory T cells

1.6.1 Overview. Tregs are a subset of CD4$^+$ T cells that have fundamental functions in the maintenance of immune homeostasis and peripheral tolerance, among others. Treg cells can be found in almost any tissue including primary lymphoid organs (thymus, bone marrow), secondary lymphoid organs (spleen, lymph nodes, Peyer's patches) as well as various non-lymphoid tissues (e.g. intestine, skin, lung, liver, fat). Importantly, the Treg cell population is extremely heterogeneous and consists of numerous, highly specialized subsets that vary tremendously between the different organs and tissues. In this section, guidelines for widely accepted FCM-based phenotyping strategies for murine Treg cells in both lymphoid organs and selected non-lymphoid tissues will be provided, and particular emphasis will be laid on markers for the identification of Treg cell subsets.
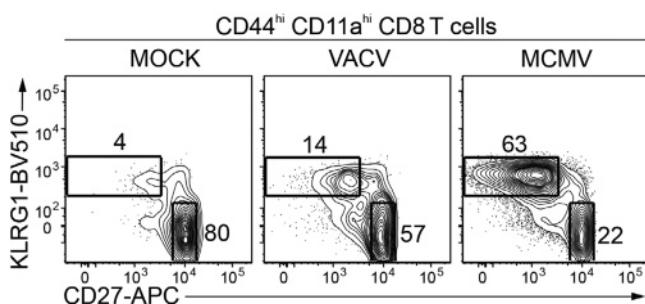
Figure 95. FCM analysis of KLRG1 and CD27 expression on total CD44hiCD11ahi CD8 T cells (pregated according to the gating strategy shown in Fig. 93) in the peripheral blood of 15-month-old (BALB/c × DBA/2) F1 mice experimentally infected for 9 months with 10^6 PFU of a nonpersistent virus, Western Reserve vaccinia virus (VACV), or 10^5 PFU of a chronically persistent β-herpesvirus, murine cytomegalovirus (MCMV) compared to uninfected littermate mice (MOCK).

1.6.2 Introduction. Treg cells were originally described as CD4+ suppressor T cells constitutively expressing CD25, the α-chain of the IL-2 receptor complex [766]. Yet, precise identification of Treg cells by CD25 expression turned out to be difficult as CD25 is also induced on many effector T cell subsets upon activation. Thus, the discovery of the transcription factor Forkhead box protein 3 (Foxp3) as the lineage-defining factor for Treg cells was a breakthrough in Treg cell-based research [767, 768]. Importantly, Foxp3 does not only serve as a marker for the more precise identification of Treg cells, but it was also shown to support Treg cell function [767, 768] through the maintenance of Treg-cell-specific gene expression signatures [769]. The physiological importance of Foxp3 can be further emphasized by mutations in the *Foxp3* gene, resulting in the development of fatal autoimmune diseases like the lymphoproliferative scurfy phenotype in mice or the IPEX-syndrome (immune dysregulation, polyendocrinopathy, enteropathy, and X-linked inheritance) in humans [770–772].

The Foxp3+ Treg cell population can be roughly categorized into two subpopulations based on the site of their development: Some Foxp3+ Treg cells are already generated within the thymus and thus named thymus-derived Treg cells (tTreg cells) [773]. These tTreg cells are complemented by peripherally induced Treg cells (pTreg cells), which convert from naive Foxp3− CD4+ T cells preferentially at mucosal sites [774]. A number of proteins like Helios, Neuropilin-1 (Nrp-1), or RAR-related orphan receptor gamma (RORγt) were suggested to distinguish between tTreg and pTreg cells [775–778], yet their usability particularly under inflammatory conditions has been questioned [779–781]. Importantly, accumulating evidence suggests that the Foxp3+ Treg cell population is not homogeneous and that co-expression of additional transcription factors, such as T-box transcription factor TBX21 (T-bet), GATA binding protein 3 (Gata-3), RORγt, or IFN regulatory factor 4 (Irf4), is required for the acquisition of unique functional properties within highly specialized Treg cell subsets [782]. The frequency of murine Foxp3+ Treg cells in both lymphoid organs and non-lymphoid tissues fluctuates considerably between individual mice and is influenced by multiple factors including genetic background, age,

gender, microbiota composition, nutrition, inflammation, and infection.

1.6.3 Treg cells in murine lymphoid organs.

1.6.3.1 Treg cells in the murine thymus. After CD4 lineage decision, some CD4 single-positive (SP) thymocytes, upon TCR stimulation, can develop into CD25+Foxp3+ tTreg cells through two distinct developmental programs involving CD25+Foxp3− and CD25-Foxp3+ Treg cell precursors (Fig. 96) [773]. Recent data suggest that the two distinct developmental programs are both required for the generation of a comprehensive Treg cell repertoire [783]. CD25+Foxp3+ tTreg cells can be further subdivided into subsets with different maturity based on CD69 and also CD24 expression (Fig. 96), which is known to correlate inversely to the maturity of CD4SP and CD8SP thymocytes [784].

Step-by-step sample preparation of Treg cells from the thymus
Protocol: Isolation and analysis

- Sacrifice 6–10 weeks old animals.
- Expose thorax.
- Remove thymus completely with forceps.
- Place thymus on a 100 μm strainer.
- Use a syringe plunger to dissociate thymus in the presence of FCM buffer.
- Centrifuge cell suspension for 5 min with $300 \times g$ at 4°C.
- Aspirate supernatant and resuspend cellular pellet with FCM buffer.
- Filter cell suspension with a 30 μm strainer and count cell number.

Surface and intracellular staining

- Transfer 2×10^6 cells to a 5 mL FCM tube.
- Centrifuge cell suspension for 5 min with $300 \times g$ at 4°C.
- Aspirate supernatant and resuspend cellular pellet with 100 μL Live/Dead fixable buffer (1:1000 diluted), keep cell suspension in the dark at 4°C for 30 min.
- Add 500 μL FCM buffer and centrifuge cell suspension for 5 min with $300 \times g$ at 4°C.
- Aspirate supernatant and resuspend cellular pellet with 100 μL FCM buffer with diluted surface Abs, anti-mouse CD16/CD32, and rat IgG, keep cell suspension in the dark at 4°C for 30 min.
- Add 500 μL FCM buffer and centrifuge cell suspension for 5 min with $300 \times g$ at 4°C.
- Aspirate supernatant and resuspend cellular pellet with 100 μL Fixation/Permeabilization working solution, keep cell suspension in the dark at 4°C for 30 min.
- Add 500 μL $1\times$ Permeabilization buffer and centrifuge cell suspension for 5 min with $300 \times g$ at 4°C.
- Aspirate supernatant and repeat the above step.
- Aspirate supernatant and resuspend cellular pellet with 100 μL $1\times$ Permeabilization buffer with intracellular Abs, anti-mouse
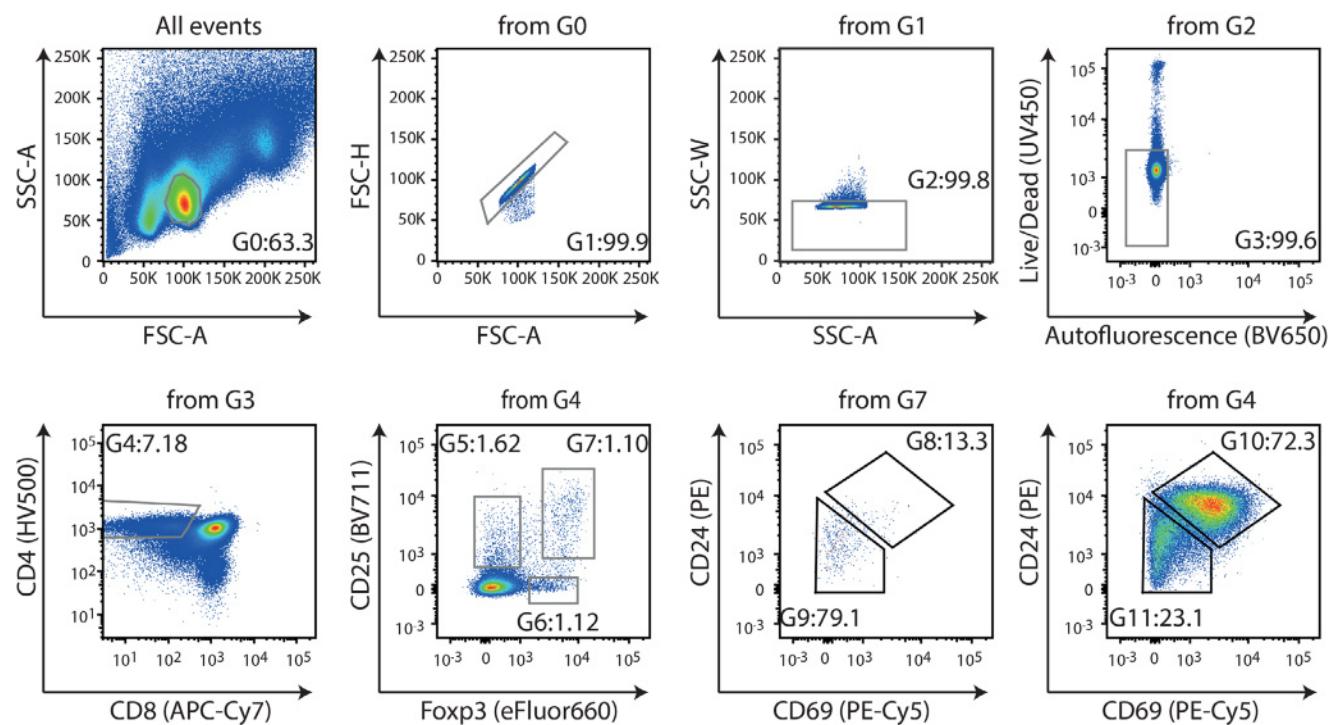
Figure 96. Phenotyping of Treg cells from the murine thymus. Gating strategy to identify Treg cells in the thymus. From all events, lymphocytes can be distinguished by their FSC/SSC properties (gate G0). After lymphocyte gating, doublets are excluded twice (gates G1 and G2), followed by exclusion of dead or autofluorescent cells (gate G3). From G3, CD4SP thymocytes (gate G4) are gated, from which two Treg cell precursors (G5 and G6) and thymic Treg cells (G7) can be identified. Thymic Treg cells (G7) and CD4SP thymocytes (G4) can be subdivided into two subsets of CD24^{high}CD69$^+$ immature (G8 and G10) and CD24$^{dim/low}$CD69$^-$ (G9 and G11) mature cells. Figures are based on thymocyte isolations from Foxp3^{EGFPCreERT2}ROSA26^{YFP} mice.

CD16/CD32 and rat IgG, keep cell suspension in the dark at 4°C for 30 min.

- Add 500 μL 1× Permeabilization Buffer and centrifuge cell suspension for 5 min with $300 \times g$ at 4°C.
- Aspirate supernatant and repeat the above step.
- Resuspend cellular pellet with 200 μL 1× Permeabilization Buffer, and cell suspension can be used for immediate analysis.

Materials: See 1.6.3.3: Isolation and analysis of Treg cells from murine lymphoid organs

Pitfalls: Isolation and analysis of Treg cells from thymus

- The CD4SP gating is critical. On the one hand, CD4SP gating needs to be strict; otherwise, contamination from CD4$^-$CD8$^-$ double-negative (DN) cells could substantially increase the frequency of CD25$^+$Foxp3$^-$ Treg cell precursors. Yet, the CD25 expression level within DN thymocytes is much higher than within CD25$^+$Foxp3$^-$ Treg precursors. On the other hand, Treg cells have lower CD4 expression compared to their CD4$^+$Foxp3$^-$ Tcon counterpart. Thus, too strict gating can negatively influence the frequency of Treg cells among CD4SP cells (Figure 96).

- Mediastinal lymph nodes are located in proximity to the thymus and can swell under inflammatory conditions. When removing thymi from mice with local inflammation, particular caution has to be paid to avoid "contamination" of the thymus material with mediastinal lymph nodes.

Top tricks: Isolation and analysis of Treg cells from thymus

- A substantial portion of Treg cells found within the thymus are Treg cells recirculating from the periphery [785]. These recirculating cells can be identified as CCR6$^+$CCR7$^-$ cells [786], or more easily when using RAG^{GFP} reporter mice. Only recently developed tTreg cells are RAG^{GFP} positive, while recirculating Treg cells are RAG^{GFP} negative.
- Not only αβ$^+$ T cells but also γδ$^+$ T cells and NKT cells develop within the thymus. An extra dump panel for NK1.1$^+$ and TCRγ/δ$^+$ cells results in higher specificity.
- Thymi will shrink upon aging. 6–10 weeks mice are most commonly used to study thymocytes. Younger or older mice may result in lower numbers of Treg cells for analysis or sorting.
- Sacrificing mice with cervical dislocation can result in bleeding into the thoracic cavity. Washing the blood-stained thymus with PBS containing 30 μM EDTA removes the "contaminating" blood.

Summary Table

Treg cells in the murine thymus

T cell population	Phenotype/subphenotype
G4: CD4SP thymocytes	CD4$^+$CD8$^-$
G5: CD25$^+$Foxp3$^-$ Treg cell precursors	CD4$^+$CD8$^-$CD25$^+$Foxp3$^-$
G6: CD25$^-$Foxp3$^+$ Treg cell precursors	CD4$^+$CD8$^-$CD25$^-$Foxp3$^+$
G7: Thymic Treg cells	CD4$^+$CD8$^-$CD25$^+$Foxp3$^+$
G8: Immature thymic Treg cells	CD4$^+$CD8$^-$CD25$^+$Foxp3$^+$ CD69$^+$CD24^{high}
G9: Mature thymic Treg cells	CD4$^+$CD8$^-$CD25$^+$Foxp3$^+$ CD69$^-$CD24$^{dim/low}$
G10: Immature thymic CD4$^+$ T cells	CD4$^+$CD8$^-$CD69$^+$CD24^{high}
G11: Mature thymic CD4$^+$ T cells	CD4$^+$CD8$^-$CD69$^-$CD24$^{dim/low}$

1.6.3.2 Treg cells in murine spleen and lymph nodes. The frequency of murine Foxp3$^+$ Treg cells among CD4$^+$ T cells usually ranges from 10% to 20% in secondary lymphoid organs such as spleen, skin-draining lymph nodes, and mesenteric lymph nodes (Fig. 97). The Treg cell population in any secondary lymphoid organ is a mixture of tTreg and pTreg cells, and Helios staining is most frequently used to discriminate tTreg (Foxp3$^+$Helios$^+$) and pTreg (Foxp3$^+$Helios$^-$) cells (Fig. 97). On a functional basis, murine Treg cells in secondary lymphoid organs can be subdivided into CD62L$^+$CD44$^-$ naive-like and CD62L$^-$CD44$^+$ effector/memory-like Treg cells. In comparison to Foxp3$^-$ conventional CD4$^+$ T cells (Tcon cells), Treg cells in secondary lymphoid organs display a higher frequency of cells with a CD62L$^-$CD44$^+$ effector/memory phenotype (Fig. 97).

Step-by-step sample preparation of Treg cells from spleen and lymph nodes

- Sacrifice animals.
- Expose abdominal cavity.
- Remove spleen, skin-draining lymph nodes (axillary, brachial, and inguinal lymph nodes), and mesenteric lymph nodes with forceps.
- Place spleen, skin-draining lymph nodes, and mesenteric lymph nodes on a 100 μm strainer separately.
- Use a syringe plunger to dissociate spleen and lymph nodes in the presence of FCM buffer.
- Centrifuge cell suspension for 5 min with 300 × g at 4°C.
- Step for spleen only: Aspirate supernatant and resuspend splenocytes pellet with 1 mL 37°C prewarmed erythrocyte lysis buffer and incubate for 3 min at room temperature (RT). Add 9 mL FCM buffer and centrifuge cell suspension for 5 min with 300 × g at 4°C.
- Aspirate supernatant and resuspend cellular pellet with FCM buffer.

- Filter cell suspension with a 30 μm strainer and count cell numbers.

Protocol: Surface and intracellular staining

- Same as described in Treg cells in thymus section.

Materials: See 1.6.3.3: Isolation and analysis of Treg cells from murine lymphoid organs

Pitfalls: Isolation and analysis of Treg cells from spleen and lymph nodes

- Properly collecting lymph nodes requires practice. Taking out fat instead of lymph nodes is one common mistake. Thus, for practicing it is easier to use young mice with lower body fat content.
- Erythrocyte lysis of spleen samples before staining is mandatory to avoid high background staining or clogging of the cytometer.

Top tricks: Isolation and analysis of Treg cells from spleen and lymph nodes

- Inspect collected lymph nodes in FCM buffer before dissociating them. Lymph nodes should sink, while fat pads float.
- Besides Helios, Nrp-1 is a commonly used maker to distinguish tTreg and pTreg cells. As Helios$^-$Nrp-1$^-$ Treg cells in mesenteric lymph nodes are mainly RORγt$^+$, this marker was also claimed as a good tool to identify pTreg cells within the intestinal system.
- For the sorting of intact Foxp3$^+$ Treg cells for the collection of RNA, various Foxp3 reporter mouse lines can be used to avoid the fixation and permeabilization during the intracellular staining.
- Stimulation of CD4$^+$ T cells before staining will result in downregulation of CD3ε and CD4, which could complicate the gating (Fig. 97). Alternatively, CD90 instead of CD3ε can be used.

Summary Table:

T cells in spleen and lymph nodes

T cell population	Phenotype/subphenotype
G4: CD4$^+$ T cells	CD4$^+$CD3ε$^+$
G5: Tcon cells	CD4$^+$CD3ε$^+$Foxp3$^-$
G6: Treg cells	CD4$^+$CD3ε$^+$Foxp3$^+$
G7: tTreg cells	CD4$^+$CD3ε$^+$Foxp3$^+$Helios$^+$
G8: pTreg cells	CD4$^+$CD3ε$^+$Foxp3$^+$Helios$^-$
G9: effector/memory Treg cells	CD4$^+$CD3ε$^+$Foxp3$^+$CD44$^+$CD62L$^-$
G9: effector/memory Tcon cells	CD4$^+$CD3ε$^+$Foxp3$^-$CD44$^+$CD62L$^-$
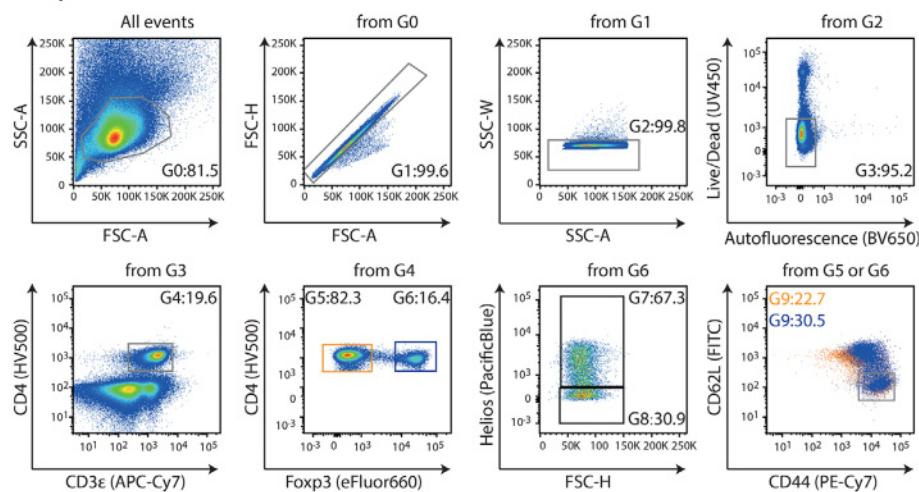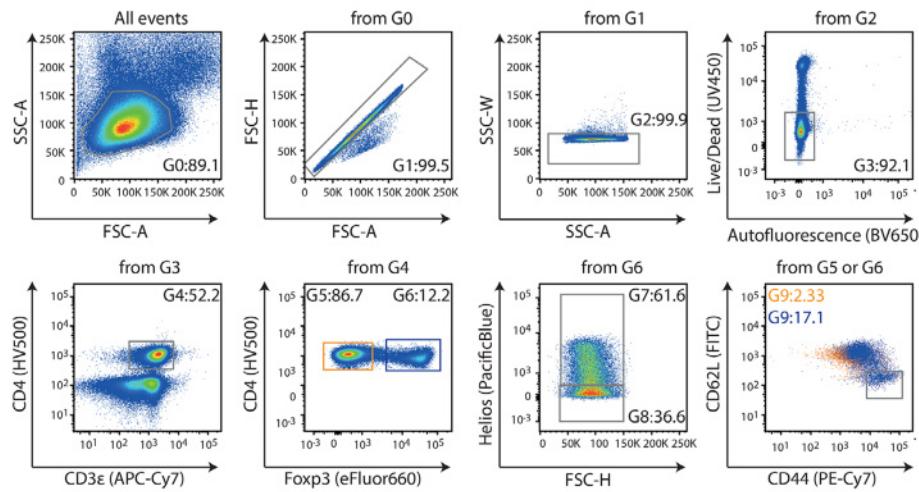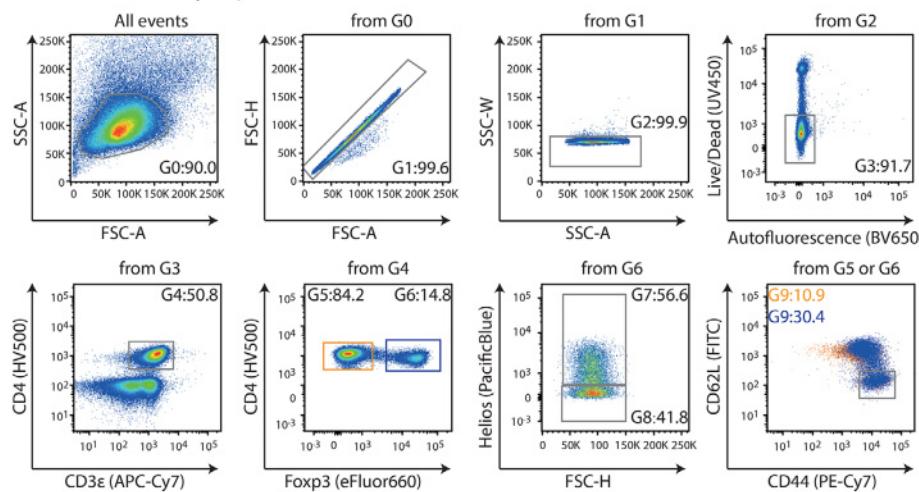
Figure 97. Phenotyping of Treg cells from murine spleen and lymph nodes. (A) Gating strategy to identify Treg cells in the spleen. From all events, lymphocytes can be distinguished by their FSC/SSC properties (gate G0). Based on G0, doublets are excluded twice (gates G1 and G2) followed by exclusion of dead or autofluorescent cells (gate G3). From G3, $CD4^+CD3\varepsilon^+$ T cells (gate G4) are gated, from which $Foxp3^+$ Treg cells (gate G6) and $Foxp3^-$ Tcon cells (gate G5) can be further identified. From G6, $Helios^+$ tTreg (gate G7) and $Helios^-$ pTreg cells (gate G8) are gated. Finally, a staining for CD62L and CD44 on Treg cells (gate G6, blue) and Tcon cells (gate G5, orange) are shown together, with $CD62L^-CD44^+$ effector/memory cells being gated (gate G9). (B and C) Gating strategy to identify Treg cells in skin-draining lymph nodes (B) and mesenteric lymph nodes (C). Gates as described in panel A. Figures are based on spleen and lymph node isolations from wild type mice.

1.6.3.3 Materials. Isolation and analysis of Treg cells from murine lymphoid organs

FCM buffer:

- 1× PBS (Gibco, #10010-056)
- 0.2% Albumin from bovine serum (Sigma–Aldrich, #SI A3912-100G)

Erythrocyte lysis buffer:

- 0.01 M KHCO₃, 0.155 M NH₄Cl, 0.1 mM EDTA

LIVE/DEAD™ Fixable Blue Dead Cell Stain Kit, for UV excitation (Thermo Fisher, #L23105)

Foxp3 Fix/Perm Buffer Set (Thermo Fisher eBiosciences, #00-5523-00)

100 µm strainer (Greiner Bio, #542070)

30 µm strainer (Partec, #04-0042-2316)

Antibodies

Dilution	Antibody	Manufacturer
1:100	CD3ε APC-Cy7 (145-2C11)	BioLegend
1:1000	CD4 HV500 (RM4-5)	BD
1:1000	CD8α APC-Cy7 (53-6.7)	BioLegend
1:200	CD25 BV711 (PC61.5)	BioLegend
1:1000	CD44 PE-Cy7 (IM7)	BioLegend
1:1000	CD62L FITC (MEL-14)	eBioscience
1:1000	CD69 PE-Cy5 (H1.2F3)	BioLegend
1:400	Foxp3 eFluor660 (FJK-16S)	eBioscience
1:100	Helios PacificBlue (22F6)	BioLegend
1:400	Rat IgG (11.5 mg/ml)	JacksonImmuno Research
1:400	Anti-mouse CD16/CD32(1mg/ml)	Bioxcell

Mice

Foxp3^EGFPCreERT2^ROSA26^YFP^ mice (C57BL/6 background) and wild-type (WT) mice (BALB/c background) were bred under SPF conditions in isolated, ventilated cages (Helmholtz Centre for Infection Research, Braunschweig, Germany).

Cytometer

BD LSR Fortessa™ 5-laser cytometer (UV, Violet, Blue, Yellow-Green, Red)

Analysis

FlowJo Version 10.5.3 (Windows 10)

1.6.4 Treg cells in murine non-lymphoid tissues. Apart from their fundamental immune regulatory function, Treg cells perform highly specialized functions in non-lymphoid tissues [787]. They have been shown to support tissue homeostasis and regeneration, ranging from regulating metabolic parameters in the adipose tissue [788–790] to potentiating tissue repair, e.g. in skeletal muscles [791] or lung tissue [792]. In addition, Treg cells in non-lymphoid tissues can manipulate tissue precursor cells to maintain tissue homeostasis. For example, Treg cells can promote oligo-dendrocyte progenitor cell differentiation and, thereby, myelin regeneration in the central nervous system [793]. In the skin, Treg cells promote hair follicle regeneration by augmenting hair follicle stem cell proliferation and differentiation [794]. Several publications identified the epidermal growth factor receptor lig-and amphiregulin as a key factor of tissue Treg cells to maintain homeostasis or induce tissue regeneration in a diverse set of tissues, including lung, muscle, and brain [791, 792]. All data show that these noncanonical Treg cell functions to directly or indirectly promote organ homeostasis and tissue repair warrant a new definition of Treg cells: Treg cells are not only regulatory as their historic name implies, but subpopulations of Treg cells residing in non-lymphoid tissues are tissue-supporting and have ability to promote tissue regeneration. Recently, Treg cells residing in non-lymphoid tissues were studied on an epigenetic and transcriptional level, and a subset of Treg cells expressing the marker KLRG1 and the IL-33 receptor ST2 was identified [795]. This subset of tissue-resident Treg cells expressing ST2 was termed tisTregST2. This population can be found in every organ and tissue analyzed so far, vigorously increases in number upon IL-33 treatment in vivo, and is dependent on the transcription factor Batf [795, 796]. TisTregST2 cells are strongly Th2-like biased (among others, high expression of Gata-3) compared to other Treg cell populations or Tcon cells found in the same tissue, and express the epidermal growth factor receptor ligand amphiregulin in high amounts [795].

In the following, we describe the isolation and characterization of these tisTregST2 cells from different murine organs, including liver, skin, adipose tissue, lung, and colon.

1.6.4.1 Treg cells in murine liver. Step-by-step sample preparation: Isolation and analysis of Treg cells from liver

- Sacrifice animals.
- Expose thorax as well as abdominal cavity.
- Open inferior vena cava and inject PBS-filled syringe into left ventricle of heart and flush with >10 mL PBS to clear body circulation; liver should change from red color to pale.
- Remove whole organ including right, left, caudate, and quadrate lobes.
- Place pieces on metal strainers, add 5 mL liver digestion buffer and cut liver lobes into small pieces as shown in Fig. 98A. A syringe plunger is used to mash liver, and the metal strainer and Petri dish can be flushed with additional 5 mL of liver digestion buffer to collect all remaining cells and fragments.
- Digest sample for 25–40 min on a rotating shaker in incubator (37°C) or in horizontal-shaking water bath preheated to 37°C.
- Add 50 mM EDTA-PBS to a final concentration of 2 mmol/L and incubate for 2 min.
- Centrifuge for 5 min with 300 × g at RT.

- Remove supernatant and resuspend cellular pellet in 10 ml of 40% Percoll-PBS solution; use a 5 mL pipette to dissociate pellet completely.
- Use pipetting aids to slowly and carefully place 10 mL of 80% Percoll-PBS beneath cell suspension to establish a two-phase system as shown in Fig. 98B. It is helpful to turn off the electric force in the pipet aid to slowly release the 80% Percoll-PBS.
- Centrifuge for 20 min with $2000 \times g$ at 4°C, acceleration off, deceleration off. If successful, hepatocytes will float on top of gradient and can be removed via aspiration. The middle phase contains immune cells and should be collected in a separate tube, while the pellet contains RBCs and other cell types and can be discarded (Fig. 98B).
- Dilute middle phase with PBS to a volume of 50 mL.
- Centrifuge for 5 min with $300 \times g$ at 4°C. Cellular pellet contains lymphocyte fraction and, following RBC lysis, can be used for immediate analysis or sorting.

Materials: See 1.6.5: Isolation and analysis of Treg cells from murine non-lymphoid organs

Pitfalls: Isolation and analysis of Treg cells from liver

- Incomplete perfusion of the animal will result in RBC contamination. Fast experimental protocols and fast animal handling are required. Do not forget to open the vena cava prior to flushing the circulation with PBS.
- Poor recovery after mashing step with large livers: add more digestion buffer to completely wash filter mesh. Do not use medium or PBS to wash filter mash since collagenase levels will be diluted.
- Gradient setup fails and poor lymphocyte recovery after gradient centrifugation: Slowly add 80% Percoll to solution and use a pipetting aid without acceleration/deceleration to avoid mixing 40% and 80% solutions. Handle tubes carefully to avoid mixing both phases. Carefully balance the centrifuge to avoid imbalance or rotor damage.
- Low CD4$^+$ T cell content (<0.5%) in final preparation: Avoid collecting cellular pellet after gradient centrifugation since it contains unwanted cells. Completely remove top layer containing hepatocytes.

Top tricks: Isolation and analysis of Treg cells from liver

- If you analyze animals <12 days of age, the liver can be measured without the need of gradient centrifugation.
- Even after complete perfusion, an RBC contamination can occur. Perform RBC lysis to deplete red blood cells.
- If you are unsure about the phases after gradient centrifugation (top: hepatocytes; middle phase: lymphocytes and other cells; pellet: other cells), harvest each phase and perform a T-cell staining to calculate your yield.
- Stain for CD45 to discriminate bone marrow-derived cells such as T or B cells from other cell types.

Summary Table

Treg cells in murine liver and murine spleen

T cell population	Phenotype/subphenotype
G5: Liver Tcon cells	CD8$^-$CD19$^-$MHCII$^-$CD4$^+$CD3ε$^+$ CD25$^-$Foxp3$^-$
G6: Liver Treg cells	CD8$^-$CD19$^-$MHCII$^-$CD4$^+$CD3ε$^+$ CD25$^+$Foxp3$^+$
G7: Liver tisTregST2 cells	CD8$^-$CD19$^-$MHCII$^-$CD4$^+$CD3ε$^+$ CD25$^+$Foxp3$^+$Klrg1$^+$ST2$^+$ Gata-3$^+$
G5: Spleen Tcon cells	CD8$^-$CD19$^-$MHCII$^-$CD4$^+$TCRβ$^+$ CD25$^-$Foxp3$^-$
G6: Spleen Treg cells	CD8$^-$CD19$^-$MHCII$^-$CD4$^+$TCRβ$^+$ CD25$^+$Foxp3$^+$
G7: Spleen tisTregST2 cells	CD8$^-$CD19$^-$MHCII$^-$CD4$^+$TCRβ$^+$ CD25$^+$Foxp3$^+$Klrg1$^+$ST2$^+$ Gata-3$^+$

1.6.4.2 Treg cells in murine skin. Step-by-step sample preparation: Isolation of Treg cells from skin with or without GentleMACS®

- Sacrifice animals.
- Animals older than 10 days require hair removal via a small animal electric shaver.
- Treat shaved skin with commercially available hair removal creme and incubate for 3 min at RT.
- Wash off hair removal creme with tap water and try to remove any remaining patches of hair.
- Separate hair-free skin from dorsal surface tissue and place in 10 mL skin digestion buffer.
- Cut into small pieces either in a 50 mL tube or directly in the GentleMACS® C tube as shown in Figure 99A.
- When using the GentleMACS®, the sample can be incubated using the program "37_C_Multi_H" for 90 min.
- When digesting manually, the sample is digested for 60 min on a rotating shaker in the incubator (37°C) or in a shaking water bath preheated to 37°C.
- Place sample on a metal strainer located in a petri dish and use a syringe plunger to dissociate remaining tissue pieces (see Fig. 99B).
- Filter sample via a 100 μm filter unit (Fig. 99C).
- Centrifuge for 5 min with $300 \times g$ at RT.
- Filter sample via a 70 μm filter unit.
- Centrifuge for 5 min with $300 \times g$ at RT.
- Filter sample via a 40 μm filter unit.
- Centrifuge for 5 min with $300 \times g$ at RT.
- Stain sample for analysis or cell sorting.

Materials: See 1.6.5: Isolation and analysis of Treg cells from murine non-lymphoid organs

Pitfalls: Isolation and analysis of Treg cells from skin

- Filter clogged during filtration: Remove hair completely, either by shaving or hair removal cream. Repeat hair removal if patches of hair remain.
- Filter clogged during filtration: Filter samples sequentially as listed in Fig. 99C.
- In case of abnormally high lymphocyte content/low Treg cell percentage (<15%): Possible lymph node contamination. Avoid collecting inguinal lymph nodes during separation of skin tissue from dorsal surface tissue. A typically-sized patch of skin from the back of a >100 day old animal contains not more than 5000–10 000 Foxp3$^+$ Treg cells when applying the proposed method, and Foxp3$^+$ Treg cell frequency of CD4$^+$ T cells is usually above 40%.
- GentleMACS$^®$ mechanical failure or tube squeaking sounds: Cut skin into very small pieces using sharp scissors. When using thick skin patches or large (>2 g) amounts of skin, recut skin tissues during incubation on the GentleMACS$^®$ machine. Use more skin digestion buffer or distribute skin among more C tubes if required.
- Being unable to find lymphocytes: It is sometimes tricky to identify lymphocytes during flow cytometric analysis of skin. Use gating strategy provided in Fig. 99D to identify T cells. If in doubt, use additional T-cell markers (other than CD4) to clearly identify the T-cell population, such as TCR-β, CD45, or CD90. Be aware that CD4 staining is weak if you use the protocol described above. It is helpful to use an autofluorescence-free channel with high staining index (such as PE or APC) for CD4 staining.
- Poor sort purity or contamination with skin keratinocytes after sorting: Use a double-sort approach (yield and four-way-purity) to avoid contaminating sample with skin-resident cells. See top tricks for more details.
- Machine clogging or no events: Wash machine and filter sample again and re-acquire. Keep sample cool at 4°C and continuous rotation (300 rpm).

Top tricks: Isolation and analysis of Treg cells from skin

- We were unable to perform pre-enrichment using magnetic beads for murine skin-based samples. Still, because of the very low frequency of Foxp3$^+$ Treg cells as well as the high viscosity of the resulting cell mixture in murine skin samples, enrichment would be beneficial to decrease sorting and measurement time.
- Sorting bulk skin Treg cells can lead to poor recovery of cells (low "sort efficiency") and, based on the parameters of the sorting instrument, also to contamination with skin keratinocytes (aggregates with immune cells). Therefore, we propose a two-step sorting protocol: first, a pre-enrich sort (sort strategy: "yield") where target cells are sorted into FCM buffer. Second, the sample is re-acquired and sorted again with high purity (sort strategy: "purity" or "4-way-purity"). Using this strategy, skin samples can be sorted at high speed without losing many target cells.
- For flow cytometric analysis, samples should be filtered again immediately before acquisition. If acquisition takes more than

5 min, the sample should be filtered again to avoid a clogging of the instrument. Samples should be cooled at 4°C to avoid clogging.
- Fixing samples will generally increase the sample flow through cytometers. Be careful when setting your FCS/SSC voltages to include your target cells. Include a positive staining control (e.g., splenocytes) to validate the panel and antibody staining before acquiring skin cells.

Summary Table: T cells in murine skin

T cell population	Phenotype/subphenotype
G5: Skin Tcon cells	CD8$^-$CD19$^-$MHCII$^-$CD4^{low}TCRβ$^+$ CD25$^-$Foxp3$^-$
G7: Skin tisTregST2 cells	CD8$^-$CD19$^-$MHCII$^-$CD4^{low}TCRβ$^+$ CD25$^+$Foxp3$^+$Klrg1$^+$ST2$^+$Gata-3$^+$

1.6.4.3 Treg cells in murine fat tissue. Step-by-step sample preparation: Isolation of Treg cells from fat

- Sacrifice animals.
- Excise abdominal/epididymal fat pads (male mice) and move into 10 ml fat digestion buffer in a 50 ml tube. Avoid collecting the gonads.
- Cut fat pads into small pieces with scissors and digest for 40–45 min on a rotating shaker in the incubator (37°C) or in a shaking water bath preheated to 37°C.
- Add EDTA-PBS to a final concentration of 2 mmol/L and incubate for 2 min.
- Centrifuge for 5 min with 300 × g at RT.
- Remove supernatant containing fat cells and lipids and perform erythrocyte lysis as described in spleen section.
- Stain sample for FCM or cell sorting (Fig. 100A).

Materials: See 1.6.5: Isolation and analysis of Treg cells from murine non-lymphoid organs

Pitfalls: Isolation and analysis of Treg cells from fat

- Little abdominal/epididymal fat depots in abdominal cavity: Animals might be too young (<10–12 weeks), sick, or fasting. Gonadal fat depots increase with age, and so does the lymphocyte recovery. Gender also influences fat, with male mice having larger depots.
- Abnormally low Treg cell frequency: Animals might be too young. Frequency and total number change with age and/or disease. In general, older animals have more Treg cells in their abdominal/epididymal fat depots.
- Filter clogged and abnormal big pellet after digestion: Be careful not to include gonads in your digestion. When using old animals with large gonadal fat depots, use 20 mL of fat digestion buffer per animal.

Top tricks: Isolation and analysis of Treg cells from fat

- Older animals harbor bigger fat depot, and, in general, a higher frequency and total number of Treg cells can be expected. Use retired breeding animals for fat isolation.
- Treg cells from gonadal fat express Gata-3, while Tcon cells express T-bet. This can serve as a quality control to detect contaminations.

Summary Table

T cells in fat

T cell population	Phenotype/subphenotype
G5: Fat Tcon cells	CD8⁻CD19⁻MHCII⁻CD4⁺TCRβ⁺CD25⁻ Foxp3⁻
G6: Fat Treg cells	CD8⁻CD19⁻MHCII⁻CD4⁺TCRβ⁺CD25⁺ Foxp3⁺
G7: Fat tisTregST2 cells	CD8⁻CD19⁻MHCII⁻CD4⁺TCRβ⁺CD25⁺ Foxp3⁺Klrg1⁺ST2⁺Gata-3⁺

1.6.4.4 Treg cells in murine lung tissue. Step-by-step sample preparation: Isolation and analysis of Treg cells from lung

- Sacrifice animals.
- Expose thorax as well as abdominal cavity.
- Open inferior vena cava and inject PBS-filled syringe into right ventricle of heart and flush with >10 mL PBS to clear the lung circulation; lung should change from reddish to colorless.
- Excise lungs and move into 10 mL lung digestion buffer using a 50 ml tube.
- Cut lungs into small pieces with scissors and digest for 30–45 min on a rotating shaker in the incubator (37°C) or in a shaking water bath preheated to 37°C.
- Filter lungs via a 100 μm filter unit into a new 50 mL tube. Add PBS or DMEM to wash filter and use a syringe plunger to dissociate all tissue pieces.
- Centrifuge for 5 min with 300 × *g* at RT.
- The cellular pellet contains lymphocyte fraction and can be resuspended buffer in 500 μL MACS® buffer following filtration.
- Add 20 μL Fc-blocking reagent (e.g., Miltenyi #130-092-575) and incubate for 5 min at 4°C
- Add 5 μL CD25 mAb (e.g., Biolegend clone PC61) or CD4 mAb (e.g., Biolegend clone RM4-5) and incubate for 10 min at 4°C.
- Add 500 μL MACS® buffer (when using 1.5 mL tube) or 10 mL MACS® buffer (when using 15 mL tube).
- Centrifuge for 4 min with 800 × *g* at 4°C.
- Add 50 μL of magnetic-labeled beads in 500 μL MACS® buffer and incubate for 10 min at 4°C.
- Add 500 μL MACS® buffer (when using 1.5 mL tube) or 10 mL MACS® buffer (when using 1 mL tube).
- Centrifuge for 4 min with 800 × *g* at 4°C.
- Filter sample and load onto primed magnetic column.
- Collect eluted cells and stain for sorting or analysis (Fig. 100B).

Materials: See 1.6.5: Isolation and analysis of Treg cells from murine non-lymphoid organs

Pitfalls: Isolation and analysis of Treg cells from lungs

- Incomplete perfusion of the animal will result in RBC contamination. Fast experimental protocols and fast animal handling are required. Do not forget to open the vena cava prior to flushing the circulation with PBS.
- Blood in the thoracic cavity: Do not use cervical dislocation to avoid bleeding into the thoracic cavity. Rupture of the thoracic vessels will make the perfusion more difficult.
- High CD25 or CD4-negative fraction following column-based enrichment: Use Fc-blocking reagents and perform the procedure at 4°C to avoid unspecific binding to beads and columns.

Top tricks: Isolation and analysis of Treg cells from lungs

- Be aware of the thymus. The thymus is located in the apex of the heart and in relatively close proximity to the lung tissue; avoid rupturing the thymus to avoid thymocyte contamination. If in doubt, use CD4 and CD8 staining in separate channels to identify CD4⁺CD8⁺ thymocytes. There are almost no CD4⁺CD8⁺ cells in lung tissue, but they are the majority of cells in the thymus.
- Be aware of the mediastinal lymph nodes. Lymph node contamination can be identified by a strong decrease in the proportion of lung tisTregST2 cells (lymph node: <1 %; lung: >10 %) and a general increase in total T and B cell numbers.

Summary Table: T cells in the murine lung

T cell population	Phenotype/subphenotype
G5: Lung Tcon cells	CD8⁻CD19⁻MHCII⁻CD4⁺TCRβ⁺CD25⁻ Foxp3⁻
G6: Lung Treg cells	CD8⁻CD19⁻MHCII⁻CD4⁺TCRβ⁺CD25⁺ Foxp3⁺
G7: Lung tisTregST2 cells	CD8⁻CD19⁻MHCII⁻CD4⁺TCRβ⁺CD25⁺ Foxp3⁺Klrg1⁺ST2⁺Gata-3⁺

1.6.4.5 Treg cells in the murine colon tissue. Step-by-step sample preparation: Isolation and analysis of Treg cells from colon with lamina propria dissociation kit and GentleMACS®

- Sacrifice animals.
- Expose abdominal cavity and excise colon from appendix to rectum; it is usually filled with feces (Fig. 101A).
- Remove feces and open colon longitudinally (Fig. 101B).
- Cut colon into 1 cm pieces (Fig. 101B) and wash three times with predigestion buffer as described in the methods section of the Miltenyi lamina propria dissociation kit (Miltenyi #130-097-410).
- Digest samples in a GentleMACS® C tube with respective collagenase mixture for 25 min.
- Filter sample on a 100 μm filtration unit and mash using a syringe plumber.

- Use more PBS to flush the filter and the C tube.
- Centrifuge for 5 min with 300 × g at RT.
- Filter and transfer cells to 1.5 mL tube and in 500 μL MACS® buffer.
- Add 20 μL Fc-blocking reagent (e.g., Miltenyi #130-092-575) and incubate for 5 min at 4°C
- Add 5 μL CD4 mAb (e.g., Biolegend clone RM4-5) and incubate for 10 min at 4°C.
- Add 500 μL MACS® buffer (when using 1.5 mL tube) or 10 mL MACS® buffer (when using 15 mL tube)
- Centrifuge for 4 min with 800 × g at 4°C.
- Add 50 μL of magnetic-labeled beads in 500 μL MACS® buffer and incubate for 10 min at 4°C.
- Add 500 μL MACS® buffer (when using 1.5 mL tube) or 10 mL MACS® buffer (when using 15 mL tube).
- Centrifuge for 4 min with 800 × g at 4°C.
- Filter sample and load onto primed magnetic column.
- Collect eluted cells and stain for sorting or analysis

Materials: See 1.6.5: Isolation and analysis of Treg cells from murine non-lymphoid organs

Pitfalls: Isolation and analysis of Treg cells from colon

- Few T cells in colon of young animals: T cell seeding starts from day 10–15 after birth. Younger animals have no detectable Foxp3+ Treg cell population in the colon.
- Column is clogged: use a large column (LS) for positive selection of T cells from colon.
- Poor CD25 staining: Use a tested clone for this protocol (e.g., Miltenyi clone REA568) or stain for Foxp3 intracellularly to identify Treg cells.

Top tricks: Isolation and analysis of Treg cells from colon

- Feces can be removed from the intact colon by carefully squeezing the colon with forceps.
- After each 20-min-digestion step in the incubator, the sample is vortexed. Filters can be reused until they are fully clogged.

Summary Table

T cells in colon

T cell population	Phenotype/subphenotype
G5: Colon Tcon cells	CD8⁻CD19⁻MHCII⁻CD4⁺TCRβ⁺CD25⁻Foxp3⁻
G6: Colon Treg cells	CD8⁻CD19⁻MHCII⁻CD4⁺TCRβ⁺CD25⁺Foxp3⁺
G7: Colon tisTregST2 cells	CD8⁻CD19⁻MHCII⁻CD4⁺TCRβ⁺CD25⁺Foxp3⁺Klrg1⁺ST2⁺Gata-3⁺

As a reference, the tissue staining panels (Figs. 98–101) were applied also on a spleen sample (Fig. 98D) from the same animal. The population in gate G7 (tisTregST2: CD8⁻CD19⁻MHCII⁻CD4⁺TCRβ⁺CD25⁺Foxp3⁺Klrg1⁺ST2⁺Gata-

3⁺) comprises less than 2% of all Treg cells found in lymphatic organs. Non-lymphoid tissues showed a clear enrichment for the tisTregST2 population, with organ to organ variation (liver: 26.4%, skin: 95.3%, abdominal/epididymal fat: 48.4%, lung: 11.5%, colon: 17.2% of all Foxp3⁺ Treg cells isolated from the individual tissues) (Figs. 98–101). The frequency and number of tisTregST2 cells is dependent on the age of the analyzed animals. For example, the frequency of tisTregST2 cells in abdominal/epididymal fat tissue can vary depending on the age of the animals, with older animals showing higher frequencies. In 20–30 weeks old male mice, the frequency of tisTregST2 cells among all Treg cells isolated from the abdominal/epididymal fat depot can be up to 95%.

1.6.5 Materials: Isolation and analysis of Treg cells from murine non-lymphoid tissues.

FCM staining buffer

- Base medium 1× PBS
- 1% FBS

MACS® isolation buffer

- Base medium 1X PBS
- 1% w/v BSA (Sigma–Aldrich #A4503)
- 1 mM EDTA (Roth #X986.2)

EDTA-PBS 50 mM

- Base medium 1× PBS
- 50 mM EDTA (Roth #X986.2)

Liver digestion buffer (10 mL per digestion)

- Base medium DMEM (Gibco #41965)
- 1 mg/mL collagenase type IV (Sigma–Aldrich #C5138)
- 20 μg/mL DNAse I (Roche #11284932001)
- 5 mg/mL BSA (Sigma–Aldrich #A4503)

40% Percoll solution

- Base medium DI water
- 40% Percoll (GE Healthcare #17-0891-01)
- 1% PBS (from 10× PBS Gibco #14200-067)

80% Percoll solution

- Base medium DI water
- 80% Percoll (GE Healthcare #17-0891-01)
- 1% PBS (from 10X PBS Gibco #14200-067)

Skin digestion buffer (10 mL per digestion)

- Base medium DMEM (Gibco #41965)
- 4 mg/mL collagenase type IV (Sigma–Aldrich #C5138)
- 10 μg/mL DNAse I (Roche #11284932001)
- 2% FBS
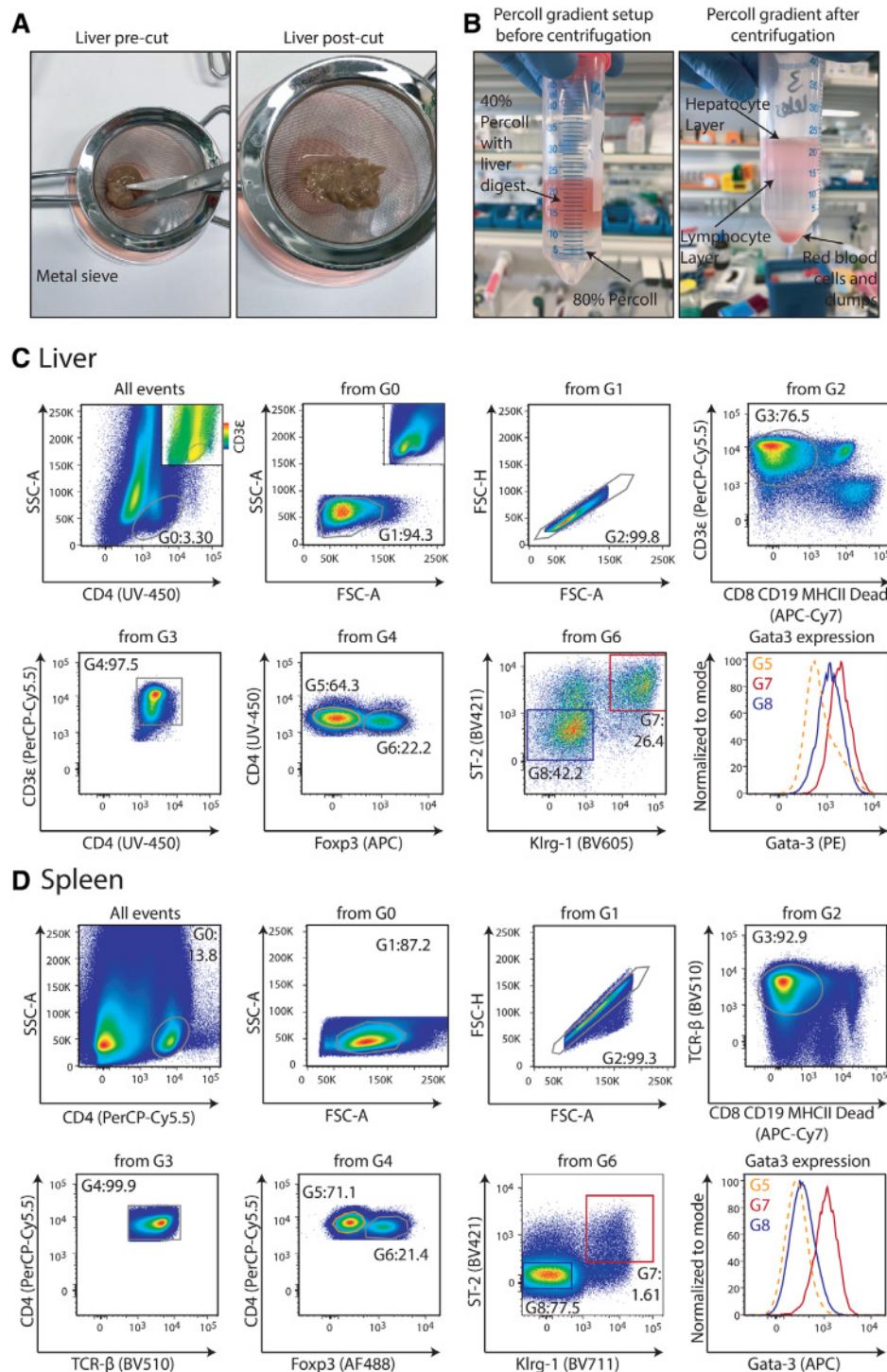
Figure 98. Isolation and analysis of Treg cells from murine liver and spleen. (A) Image of liver tissue pre-cut (left) and after cutting (right) in a metal sieve. After cutting, a syringe plunger can be used to disseminate the tissue. (B) Image of the preparation of a liver suspension in the Percoll gradient (left). The bottom phase consists of 80 % Percoll-PBS, the top phase of 40 % Percoll-PBS and the digested liver cells. On the right, a representative image of a sample after centrifugation is shown. Three layers can be discriminated: a top layer consisting mainly of hepatocytes, the middle layer with target cells, and a bottom layer with unwanted cells. (C) Gating strategy to identify tisTregST2 cells in liver. From all events, a CD4-gate to identify T cells can be drawn (gate G0). In the plot, the smaller color-coded plots indicate expression of CD3ε in the same SSC-A vs CD4 plot. Presence of CD3ε+ cells in the G0 gate can be appreciated. Based on G0, lymphocytes can be identified by their FSC/SSC properties (gate G1). Next, doublets are excluded (gate G2) as well as unwanted, dead or autofluorescent cells (gate G3). From G3, CD4+CD3ε+ T cells (gate G4) are gated, from which Treg cells (gate G6) and Tcon cells (gate G5) can be identified. Finally, Klrg1+ST2+ tisTregST2 (gate G7) are gated from Treg cells (gate G6). A staining of Gata-3, shown in the histogram, exemplifies the expression of this marker in liver Tcon cells (gate G5, orange, dotted line), liver Klrg1+ST2+ tisTregST2 cells (gate G7, red), and liver Klrg1−ST2− Treg cells (gate G8, blue). In (D), the same gating strategy as described for liver is applied to a spleen sample. In both tissues, CD4+Foxp3+Klrg1+ST2+Gata-3high tisTregST2 cells can be identified with the proposed gating strategy. CD3ε or TCRβ antibodies can be used. Figures are based on liver digestions and spleen isolations from Foxp3DTR, GFP animals.

Fat digestion buffer (10 mL per digestion)

- Base medium DMEM (Gibco #41965)
- 1 mg/mL collagenase type II (Sigma-Aldrich #C6885)
- 20 µg/mL DNAse I (Roche #11284932001)
- 20 mg/mL BSA (e.g., Sigma A4503)

Lung digestion buffer (10 mL per digestion)

- Base medium DMEM (Gibco #41965)
- 1 mg/mL collagenase type IV (Sigma-Aldrich #C5138)
- 20 µg/mL DNAse I (Roche #11284932001)
- 5 mg/mL BSA (e.g., Sigma A4503)
- GentleMACS® C tube (Miltenyi #130-096-334)
- Lamina Propria Dissociation Kit (Miltenyi #130-097-410)
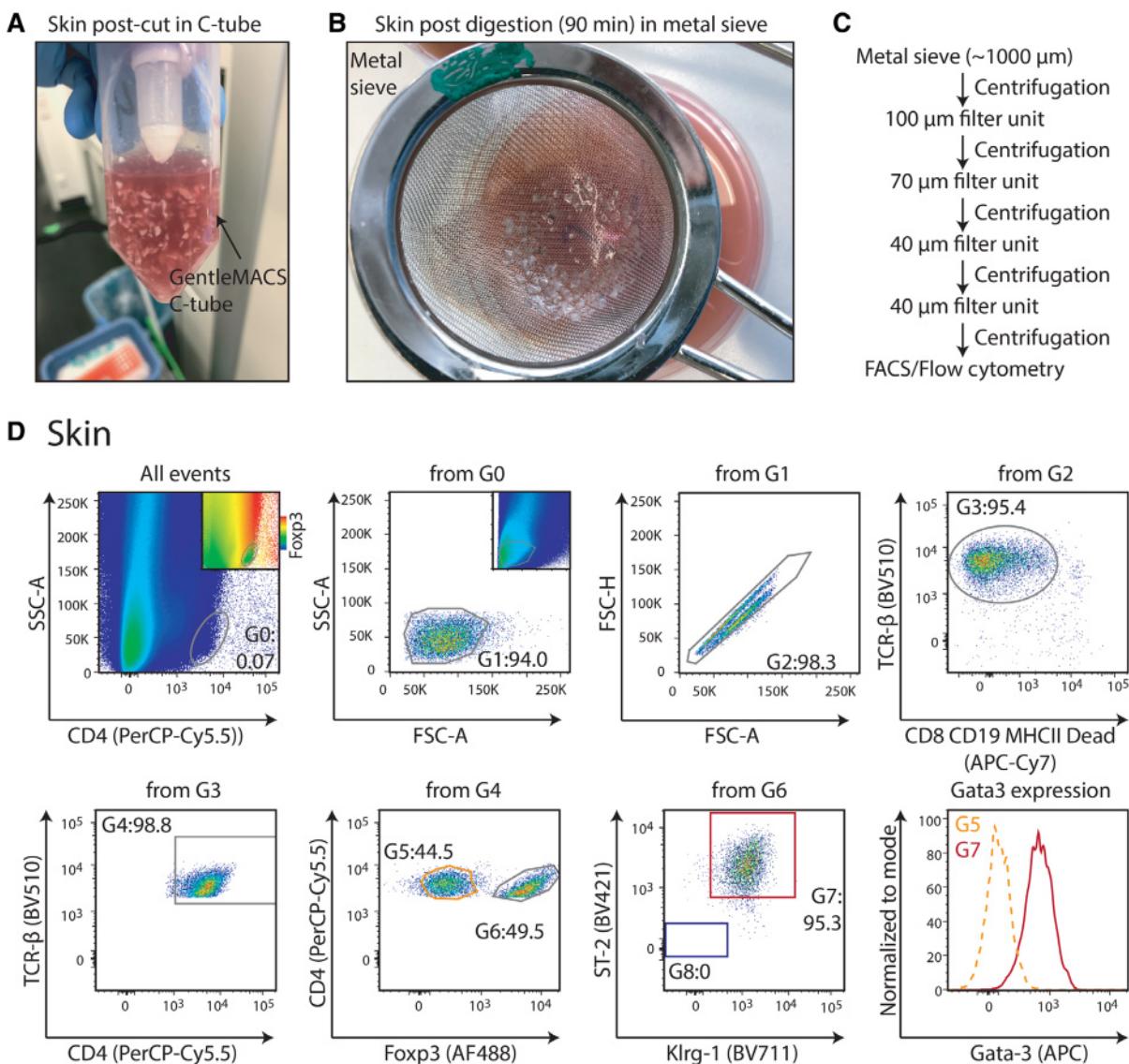
Figure 99. Isolation and analysis of Treg cells from murine skin. (A) Representative image of skin tissue in digestion buffer after cutting with scissors. Cutting can be performed directly in the GentleMACS® C tube. (B) Image of the skin tissue after digestion. The sample is poured onto a metal mesh and can be dissociated manually using a syringe plunger. (C) Sequential filtration workflow for skin samples. (D) Gating strategy to identify tisTregST2 cells in skin tissue. From all events, a CD4-gate to identify T cells can be drawn (gate G0). In the plot, the smaller color-coded plots indicate expression of Foxp3 in the same SSC-A vs CD4 plot. Presence of Foxp3+ cells in the G0 gate can be appreciated. Based on G0, lymphocytes can be identified by their FSC/SSC properties (gate G1). Smaller plot shows FCS/SSC of all events without CD4 pre-gating. Next, doublets are excluded (gate G2) as well as unwanted, dead or autofluorescent cells (gate G3). From G3, CD4+TCRβ+ T cells (gate G4) are gated, from which Treg cells (gate G6) and Tcon cells (gate G5) can be identified. Finally, Klrg1+ST2+ tisTregST2 (gate G7) are gated from Treg cells (gate G6). A staining of Gata-3, shown in the histogram, exemplifies the expression of this marker in skin Tcon cells (gate G5, orange, dotted line) and skin Klrg1+ST2+ tisTregST2 cells (gate G7, red). Figures are based on skin digestions from Foxp3DTR, GFP animals.

- MACS® separation columns, size L (Miltenyi #130-042-401)
- Anti-biotin ultrapure magnetic beads (Miltenyi #130-105-637)
- Anti-PE ultrapure magnetic beads (Miltenyi #130-105-639)
- Anti-APC magnetic beads (Miltenyi #130-090-855)

Antibodies

- 1:100 CD8 APC-Cy7 (53-6.7)
- 1:100 CD19 APC-Cy7 (6D5)
- 1:200 MHCII APC-Cy7 (M5/114.15.2)

- 1:500 Life/dead e780 (Thermo Fisher eBiosciences #65-0866-14)
- 1:100 CD4-PerCP-Cy5.5 or BUV-395 (RM4-5)
- 1:100 TCRβ-BV 510 (H57-597)
- 1:100 CD25 APC (PC61 for all tissues except colon)
- 1:20 CD25 APC (REA568 for colon samples)
- 1:100 IL-33R/ST2 BV 421 (DIH9)
- 1:100 Klrg1 BV 711 (2F1)
- 1:100 Foxp3 AF488 (FJK-16S)
- 1:100 Gata-3 PE (16E10A23)
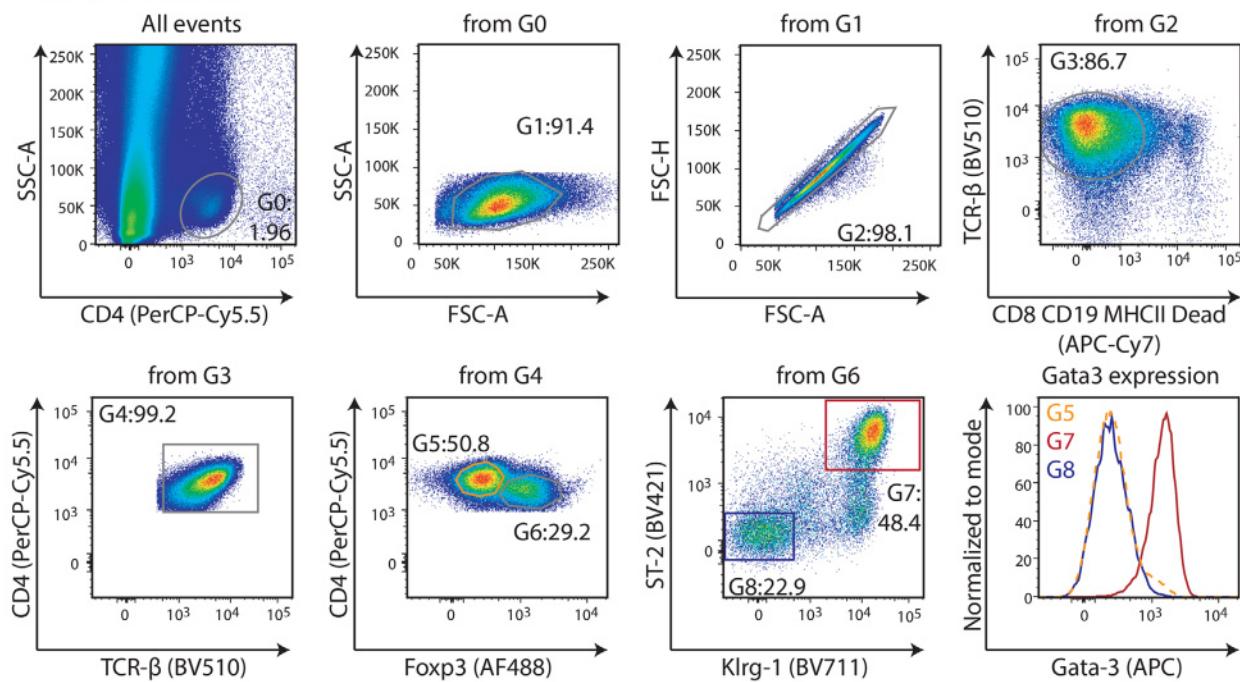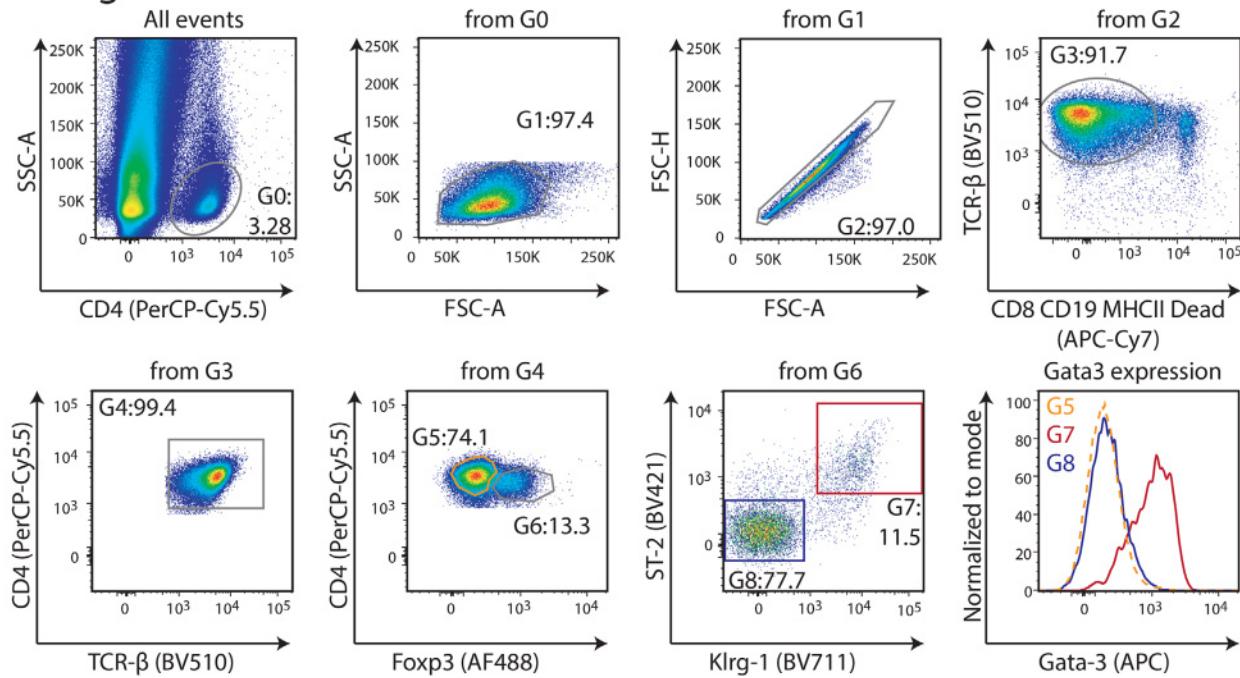
Figure 100. Isolation and analysis of T cells from the murine fat and lung tissue. Gating strategy to identify Treg cells in fat (A) and lung (B) tissue. From all events, a CD4-gate to identify T cells can be drawn (gate G0). Based on G0, lymphocytes can be identified by their FSC/SSC properties (gate G1). Next, doublets are excluded (gate G2) as well as unwanted, dead or autofluorescent cells (gate G3). From G3, CD4$^+$TCRβ$^+$ T cells (gate G4) are gated, from which Treg cells (gate G6) and Tcon cells (gate G5) can be identified. Finally, Klrg1$^+$ST2$^+$ tisTregST2 (gate G7) are gated from Treg cells (gate G6). A staining of Gata-3, shown in the histogram, exemplifies the expression of this marker in Tcon cells (gate G5, orange, dotted line), Klrg1$^+$ST2$^+$ tisTregST2 cells (gate G7, red), and Klrg1$^-$ST2$^-$ Treg cells (gate G8, blue). Figures are based on lung and fat digestions from Foxp3$^{DTR, GFP}$ animals.
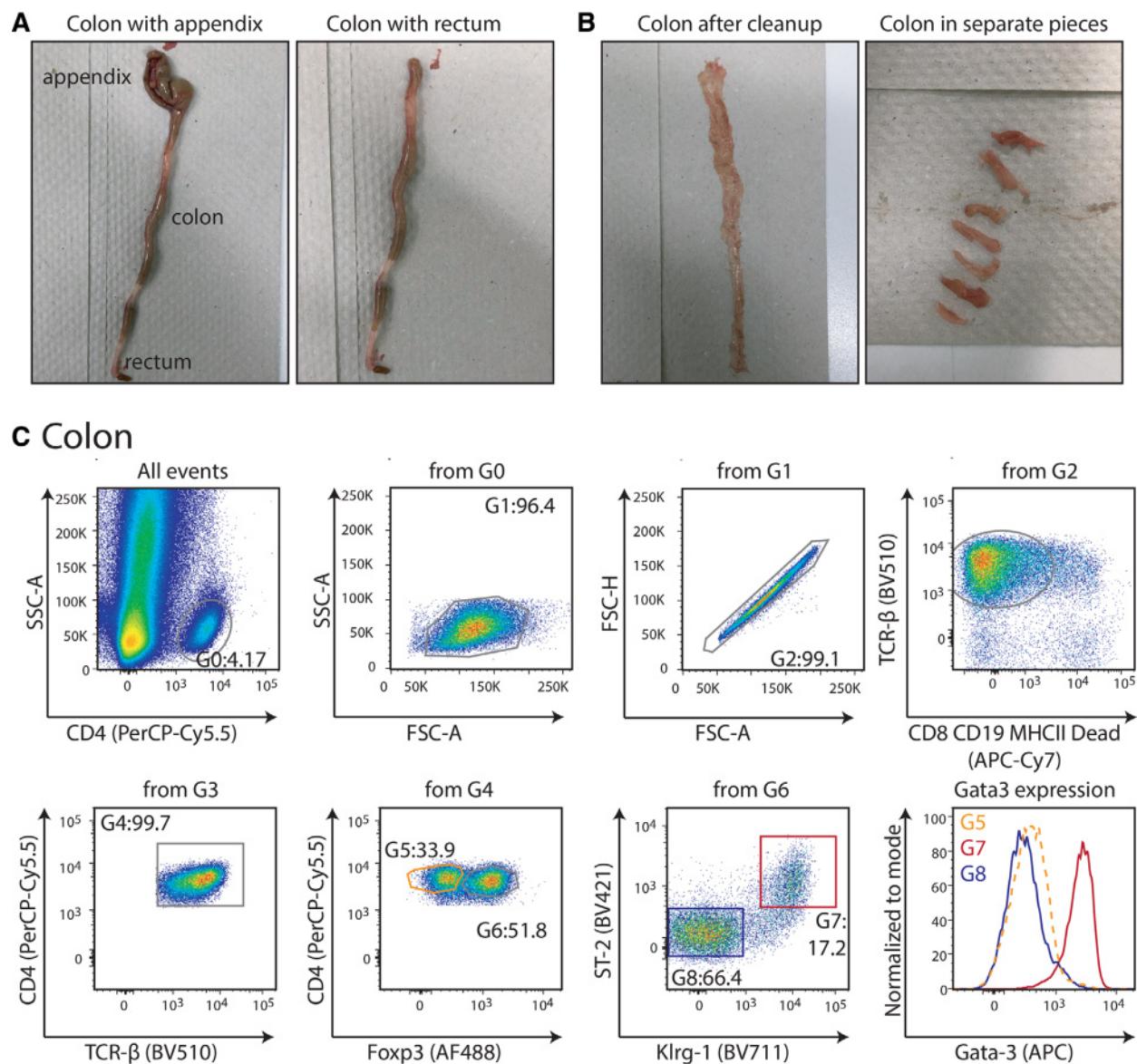
Figure 101. Isolation and analysis of Treg cells from the murine colon tissue. (A) Image of colon tissue after excision. The appendix is still attached (left image) and should be removed (right image). (B) Image of the colon tissue after cleanup (left). Feces have been removed and the colon has been cut longitudinally. The colon is then cut into 1 cm pieces (right) and can be washed. (C) Gating strategy to identify Treg cells in colon tissue. From all events, a CD4-gate to identify T cells can be drawn (gate G0). Based on G0, lymphocytes can be identified by their FSC/SSC properties (gate G1). Next, doublets are excluded (gate G2) as well as unwanted, dead or autofluorescent cells (gate G3). From G3, CD4$^+$TCRβ$^+$ T cells (gate G4) are gated, from which Treg cells (gate G6) and Tcon cells (gate G5) can be identified. Finally, Klrg1$^+$ST2$^+$ tisTregST2 (gate G7) are gated from Treg cells (gate G6). A staining of Gata-3, shown in the histogram, exemplifies the expression of this marker in Tcon cells (gate G5, orange, dotted line), Klrg1$^+$ST2$^+$ tisTregST2 cells (gate G7, red), and Klrg1$^-$ST2$^-$ Treg cells (gate G8, blue). Figures are based on colon digestions from Foxp3$^{DTR, GFP}$ animals.

Foxp3 Fix/Perm Buffer Set (Thermo Fisher eBiosciences #00-5523-00)

Mice
Foxp3^{GFP,DTR} mice (C57BL/6 background) were bred in the animal facility of the Regensburg University Hospital.

Cytometer
BD LSR Fortessa™ 5-laser cytometer (UV, Violet, Blue, Yellow-Green, Red)
BD LSRII™ 3-laser cytometer (blue-red-violet)

Analysis
BD Flowjo™ Version X (10.5.3 Mac OS)

1.7 Murine γδ T cells

1.7.1 Overview. In this section, we discuss the specific requirements to analyze γδ T cells by FCM. This includes general recommendations, an overview of the specific tools available to study γδ T cells by FCM, a detailed protocol to stain for a specific subset of

γδ T cells, and a point-by-point protocol to isolate and analyze γδ T cells from mouse ear skin. Protocols to isolate γδ T cells (and αβ T cells) from the mouse intestine are given in a subsequent related section.

1.7.2 Introduction. γδ T cells develop in the thymus together with αβ T cells but rearrange a different T-cell receptor (TCR) consisting of a TCR-γ and TCR-δ chain (see also Chapter VI Section 1.15 Human γδ T cells). These TCRγδ are not MHC restricted, thus their antigen recognition does not rely on CD4 or CD8 co-receptors, although the majority of mouse intestinal intraepithelial γδ T lymphocytes (γδ iIELs) express the CD8αα dimer. Mouse γδ T-cells comprise significantly different populations, and these γδ T-cell subsets are typically grouped by the variable γ-chain (Vγ) segments employed by their TCRγδ [797]. Alternatively, γδ T-cell subsets may also be grouped according to γδ T-cell tissue location or with respect to γδ T-cell function [798, 799].

1.7.3 γδ T cells in peripheral lymph nodes. FCM of γδ T cells is technically not different to FCM of αβ T cells. However, γδ T cells are up to 100-fold less frequent than αβ T cells in blood and secondary lymphoid organs and therefore their detection faces the usual challenges connected to identifying rare cell types, i.e., make sure to include all real γδ T cells but avoid false positive events due to autofluorescence and unspecific staining. On the other hand, γδ T cells can make up the majority of lymphocytes in tissues such as the skin and the small intestinal epithelium.

1.7.3.1 Step-by-step sample preparation. A dedicated step-by-step sample preparation protocol to obtain single cell suspensions from peripheral lymphoid organs is described in the murine Treg section (Chapter VI Section 1.6 Murine Foxp3+ regulatory T cells). Briefly, lymph nodes are collected and mashed through a cell strainer or similar and filtered through or a piece of gaze (pore size 70–100 μm) before adding FcBlock and staining with specific mAbs.

1.7.3.2 Materials/ Specific tools for FCM of γδ T cells. There are a number of mAb clones available for detection of γδ TCR using specific Vγ and Vδ segments. Below is a list of commercially available mAb clones (Table 21). However, be aware that several conflicting nomenclatures exist for mouse (and human) Vγ and Vδ segments, which can be misleading even for insiders to the field. Please check online resources such as the IMGT website (http://www.imgt.org) for further explanation. Here, we use the so-called Heilig/Tonegawa nomenclature [800], while suppliers like BD Bioscience or BioLegend utilize the Garman nomenclature [801].

Two additional important, but not currently commercially available mAb clones are F2.67 directed against Vγ7 by Pablo Pereira (Institute Pasteur, Paris, France) [802], and the clone 17D1 directed against Vγ5 from Bob Tigelaar (Yale University,

New Haven, USA) [803]. Later, Christina Roark and colleagues found that 17D1 was cross-reactive to Vγ6 under certain conditions, see below [804].

1.7.3.3 Data analysis. Practically, faithful detection of γδ T cells is warranted by gating on the lymphocyte area in the FSA versus SSA plot, gating out doublets, exclusion of dead and auto-fluorescent cells, followed by a positive gate according to the **two parameters** expression of γδ TCR, best clone is GL3 [805] and CD3ε in the same plot (Fig. 102A). If the experimental design and equipment allow further parameters, it is advisable to gate out αβ T cells (clone H-57) and eventually B cells (CD19 mAb) prior to the GL3 versus CD3ε gate (Fig. 102B).

1.7.3.4 Pitfalls/top tricks. Furthermore, the *Tcrd*-H2BeGFP reporter mouse [806], JAX Stock No. 016941, can serve to detect γδ T cells independent of TCR expression on the cell surface (e.g., after TCR downregulation following strong TCR activation in vitro). Note that for visualizing γδ T cells in secondary lymphoid organs or other tissues containing a large excess of αβ T cells over γδ T cells in microscopy applications, the use of F1 heterozygotes from *Tcrd*-H2BEGFP mice and *Tcra*$^{-/-}$ (B6.129S2-Tcratm1Mom/J, JAX Stock No. 002116) will genetically exclude highly fluorescent false-positive cells. In FCM applications it is sufficient to counter-stain for TCRβ (Figure 103).

Notably, these *Tcrd*-H2BeGFP reporter mice were used to demonstrate that in vivo application of the mAb clones GL3 and UC7-13D5 does not lead to a depletion of γδ T cells, but rather renders them invisible for flow cytometric detection due to TCR downregulation [807]. However, a new genetic knock-in model for diphtheria toxin-mediated conditional γδ T cell depletion will circumvent these problems [808].

1.7.4 Intracellular cytokine staining for IL-17-versus IFN-γ-producing γδ T cells.

1.7.4.1 Introduction. Recent studies suggested that discrete subsets of γδ T cells; namely IFN-γ- and IL-17-producing γδ T cells, develop and act as pre-activated effector cells. In particular, a combination of the the surface markers CD27, CD44, and Ly6C can be used to indirectly discriminate between those subsets without intracellular cytokine staining [809–811].

1.7.4.2 Step-by-step sample preparation. For Intracellular cytokine staining, isolated cells are first stimulated ex vivo with PMA (50 ng/mL, Calbiochem) and Iono (2 μg/mL, Invitrogen) together with Brefeldin A (1 μg/mL, Sigma) for 3 h at 37°C., Next, stimulated cells are stained against extracellular surface molecules. After fixation with BD Cytofix/Cytoperm solution for 20 min on ice and permeabilization with BD Perm/Wash buffer for 10 min on ice according to the manufacturer's protocol (BD Fixation/Permeabilization Solution Kit), cells are stained for intra-

Table 21. List of commercially available mAb clones directed against mouse Vγ and Vδ segments

Target			
Garman nomenclature (used by BD/Biolegend)	Heilig/Tonegawa nomenclature	Clone	Non-exclusicve list of Supplierer(s)
pan γδ TCR		GL3	many sources
pan γδ TCR		UC7-13D5	BD Biosciences, Biolegend
pan γδ TCR		REA633 (recombinant GL3)	Miltenyi
Vγ3	Vγ5	536	Biolegend and BD Biosciences
Vγ1.1/Cr4	Vγ1	2.11	Biolegend, BD Biosciences
Vγ1.1/Vγ1.2	Vγ1/ Vγ2	4B2.9	Biolegend
Vγ2	Vγ4	UC3-10A6	Biolegend, BD Biosciences
Vδ1		TS8.2	Abcam
Vδ6.3		C504.17C	Biolegend
Vδ6.3/2		8F4H7B7	BD biosciences
Vδ4		GL2	Biolegend and BD Biosciences
Vδ4		REA372 (recombinant GL2?)	Miltenyi

cellular cytokines for 45 min on ice, washed once with PBS, and analyzed.

1.7.4.3 Data analysis. Surface staining against CD27, CD44, and Ly6C serves to discriminate activated γδ T cells with an IL-17-producing effector phenotype (CD44^{high+}CD27$^-$) or with an IFN-γ-producing effector phenotype (CD44$^{high/int}$CD27$^+$) (Fig. 104).

1.7.5 Isolation of lymphocytes from mouse ear skin.

1.7.5.1 Introduction. The skin as well as several mucosal tissues such as the intestine harbor strong and thick walls on their surface, which are composed of different layers. Hence, isolation of lymphocytes from these tissues warrants elaborated protocols. The skin consists of two primary layers, the keratinized epidermis on the surface and the beneath dermis. In mice, lymphocytes of both, epidermal and dermal layers, can be preferably isolated from ear skin according to the following protocol (Figure 105).

1.7.5.2 Step-by-step sample preparation and Materials.

- Separate dorsal and ventral sites of the ears
- Remove the cartilage from the ventral sites
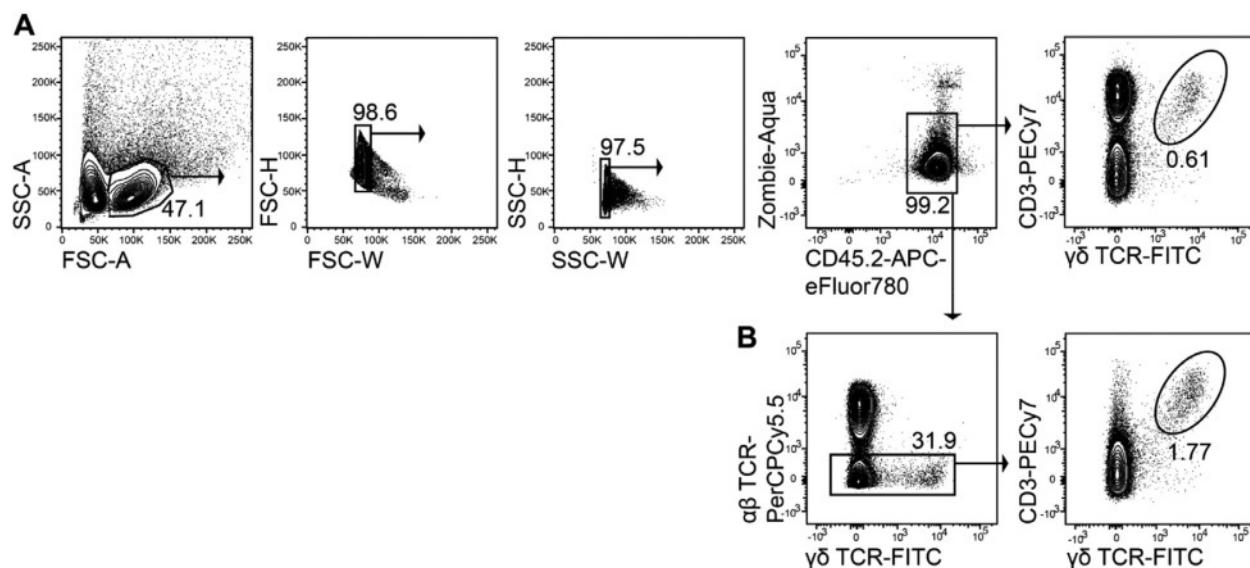
Figure 102. Representative gating strategy for γδ T cells among live peripheral lymph node cells. (A) Representative contour plot for direct gating of γδ T cells. (B) Representative contour plots for exclusion of αβ T cells before gating γδ T cells.
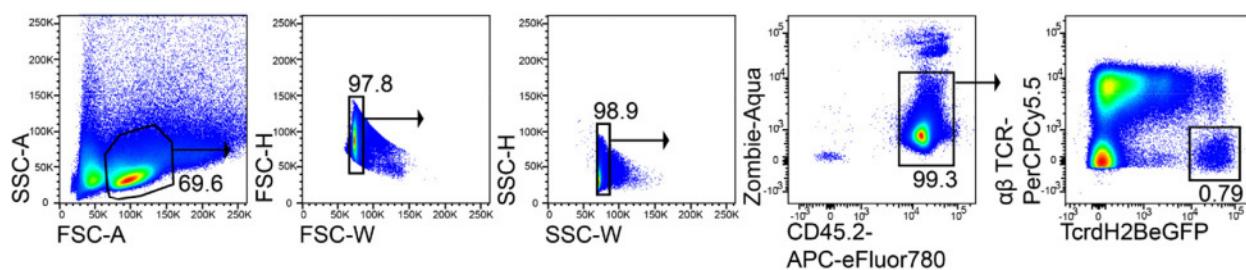
Figure 103. Representative gating strategy for the identification of genuine γδ T cells in pLN based on the H2BeGFP fluorescence in *Tcrd*-H2BeGFP mice and counterstaining with anti-TCRβ.

- Place the tissue (4 separated halves) in one 2 mL Eppendorf tube containing 1900 µL digestion medium and cut it into small pieces
- Digest medium: RPMI (1810 µL)+ 2 mg/mL Col IV (Worthington) (40 µL of 100 mg/mL) + 187.5 µg/mL DNAseI (Roche)(150 µL of 2.5 mg/ml)
- Incubate at 37°C, 1400 rpm, 75 min in an Eppendorf ThermoMixer
- Add EDTA, final concentration approx. 37.5 mM (+150 µL 0.5 M EDTA)
- Incubate for additional 15 min at 37°C, 1400 rpm (ThermoMixer)

- Dissociate the remaining tissue by sucking up and down the sample through an approximately 1–2 cm long 19G syringe needle
- Filter the sample through a Cellstainer (70 µm) and separate lymphocytes by density gradient centrifugation using Percoll-gradients (40% and 70% Percoll solutions)

1.7.5.3 Data analysis. The skin harbors a high amount of lymphocytes. While αβ T cells are barely present in the mouse skin, the vast majority of lymphocytes are γδ T cells. γδ T cells localized in the epidermis (dendritic epidermal T cells (DETC)) can be easily distinguished from γδ T cells present in the dermis
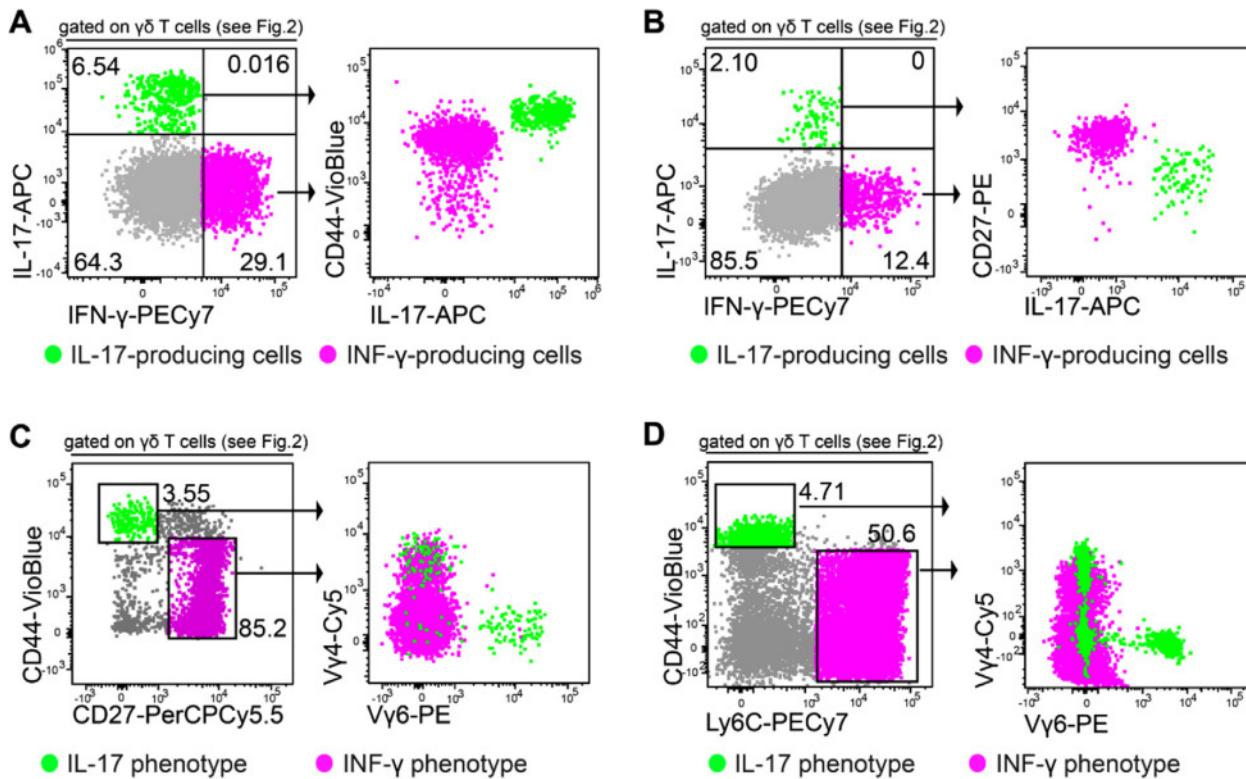
Figure 104. Dot plots show strategies to identify IL-17- versus IFN-γ-producing γδ T cells. γδ T cells from pLN of *Tcrd*-H2BeGFP mice were gated as in Fig. 103 above. (A and B) Intracellular cytokine staining in correlation to CD44 (A) and CD27 (B) surface marker expression. (C and D) Representative analyses of γδ T cells from pLN of *Tcrd*-H2BeGFP mice correlate CD27, CD44, and Ly6C surface staining to expression of Vγ4 and Vγ6.
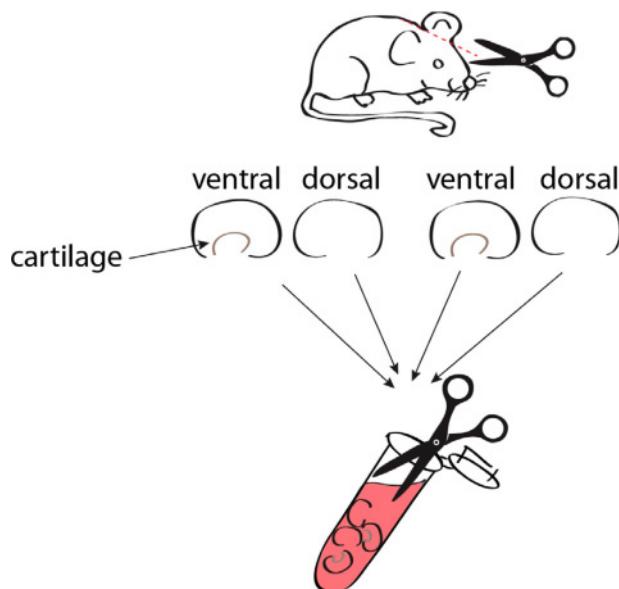
Figure 105. Preparation of ear skin. Schematic illustration of preparing ear skin for subsequent isolation of lymphocytes after enzymatic digestion of the tissue.

due to their high TCR expression levels as detected by GL3 and CD3 staining in (Figure 106).

1.7.6 The auxiliary Ab-assisted direct staining of Vγ6$^+$ γδ T cells.

1.7.6.1 Introduction. Vγ6$^+$ γδ T cells solely develop in embryonic thymus before birth, and later persist as long-lived self-renewing lymphocytes in the skin dermis and in many mucosal tissues such as the uterus or the tongue [812]. Vγ6$^+$ γδ T cells recently sparked a lot of interest because they rapidly produce IL-17 and thus contribute to bacterial homeostasis and clearance, but also enhance autoimmunity and inflammatory diseases [813, 814]. The detection of Vγ6$^+$ γδ T cells requires a combined staining of GL3 together with the unconjugated rabbit 17D1 IgM Ab followed by a secondary staining with labeled anti-rabbit IgM. A validated staining protocol for the identification of Vγ6$^+$ γδ T cells works as follows.

1.7.6.2 Step-by-step sample preparation and Materials.

Prepare single cell suspension	
Block cells with 5% Fc receptor block	5 min on ice
Stain cells in antibody mix with extracellular surface markers and GL3 diluted in PBS containing 3% FCS and 4mM EDTA, hre called FCM buffer	15 min on ice
Add unconjugated 17D1 (final dilution 1:25) and mix thoroughly (for example: add 4μl of 17D1 to 100μl cell suspension)	30 min on ice
Wash cells with flow cytometry buffer	
Stain cells with labeled secondary anti-IgM Antibody	
diluted in FCM buffer	30 min on ice
Wash cells with flow cytometry buffer	

1.7.6.3 Data analysis. Importantly, in skin, clone17D1 not only stains Vγ6$^+$ γδ T cells in combination with GL3, but also
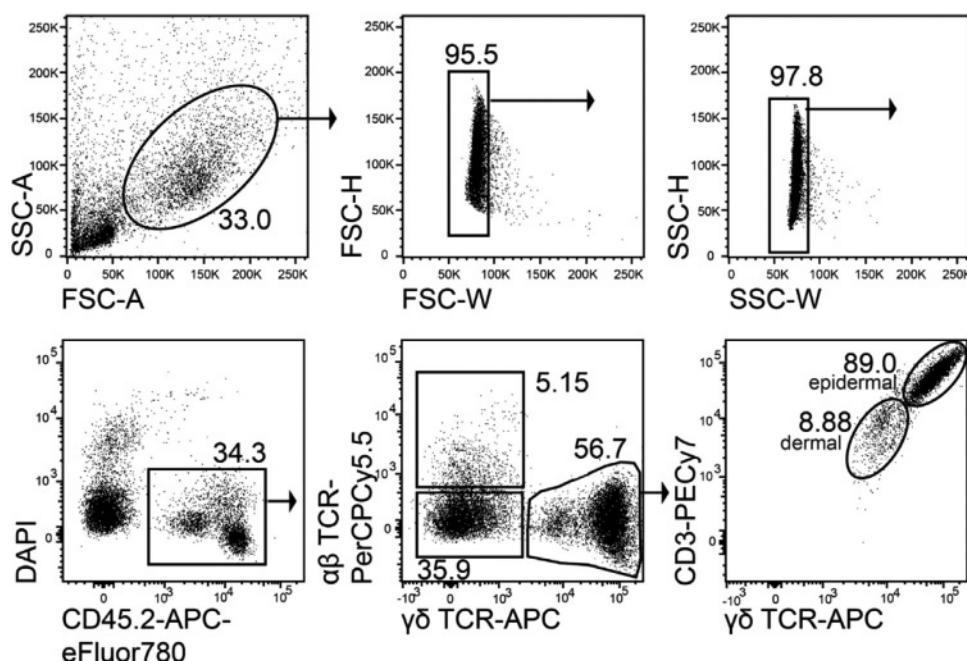
Figure 106. Representative gating strategy of murine ear skin lymphocytes stained with DAPI, anti- CD45, TCRαβ (H57), γδ TCR (GL3), and CD3 to detect dermal γδ T cells (CD3$^+$ and GL3$^+$) and epidermal γδ T cells (DETC, CD3^{hi}, and GL3^{hi}).
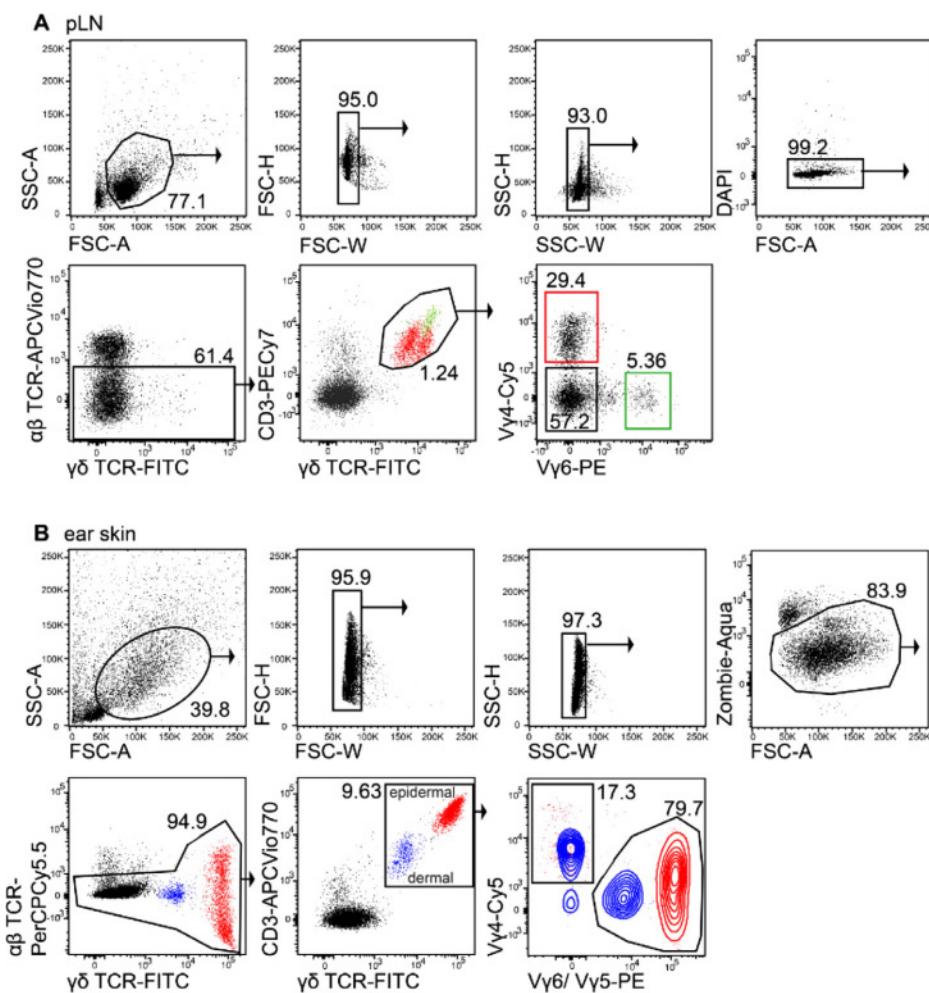
Figure 107. Representative gating strategies of Vγ4+ (red) and Vγ6+ (green) γδ T cells in peripheral lymph nodes (pLN) (A) as well as epidermal Vγ5+ γδ T cells (red) and dermal Vγ4+ and Vγ6+ γδ T cells (blue) in ear skin (B) GL3+CD3+ γδ T cells among TCRß− cells were separated into different γδ subsets by staining with anti-Vγ4 as well as 17D1 followed by conjugated anti-IgM to detect Vγ6+/Vγ5+ γδ T cells.

recognizes the Vγ5 gene segment expressed in dendritic epidermal T cells (DETC). However, dermal Vγ6+ γδ T cells and epidermal Vγ5+ γδ T cells can be easily distinguished because of the very high TCR levels levels in Vγ5+ γδ T cells leading to bright GL3 and CD3 staining. The epidermis solely contains Vγ5+ γδ T cells, while the dermal compartment comprises high frequencies of Vγ4+ and Vγ6+ γδ T cells (Fig. 107).

It follows that an additional counterstaining of 17D1+ skin T cells with a specific anti-Vγ5 mAb clone 536, see Table 21, would further help to discriminate between dermal and and TCRhigh epidermal T cells (Fig. 107B and not shown). In contrast, peripheral lymph nodes lack Vγ5+ γδ T cells. While Vγ6+ γδ T cells only represent a small population in peripheral lymph nodes, a large proportion of γδ T cells are Vγ4+ γδ T cells and Vγ6−Vγ4− γδ T cells (mainly Vγ1+ T cells).

1.8 Murine NKT cells

1.8.1 Overview. Murine natural killer T (NKT) cells were originally defined by their co-expression of surface markers charac-

teristic for T cells (i.e., the TCR) and NK cells (e.g., NK1.1 in C57BL/6 mice) [815, 816]. This chapter focuses on the phenotypic characterization of so-called murine invariant iNKT cells, which express an invariant Vα14Jα18 TCRα chain and a limited set of TCRβ chains with a preference for Vβ8, Vβ7, and Vβ2 [817, 818]. iNKT cells recognize lipids, such as α-galactosyl ceramide (αGalCer), in the context of the nonclassical MHC molecule CD1d [819]. As a consequence, iNKT cells can be unambiguously identified by surface staining using CD1d tetramers loaded with αGalCer or its derivatives, such as PBS-57 [820, 821] (Fig. 108). Subphenotyping of developmental stages in the thymus and effector subsets based on surrogate surface markers and key transcription factors is described.

1.8.2 Introduction. Development of iNKT cells diverges at the CD4+CD8+ double-positive stage of T-cell development. Selection of iNKT cells is mediated by cortical thymocytes rather than epithelial cells. Similar to other unconventional T cells, iNKT cells are selected by strong TCR signals in a process referred to as agonist selection [822]. iNKT cells, with the notable exception of some
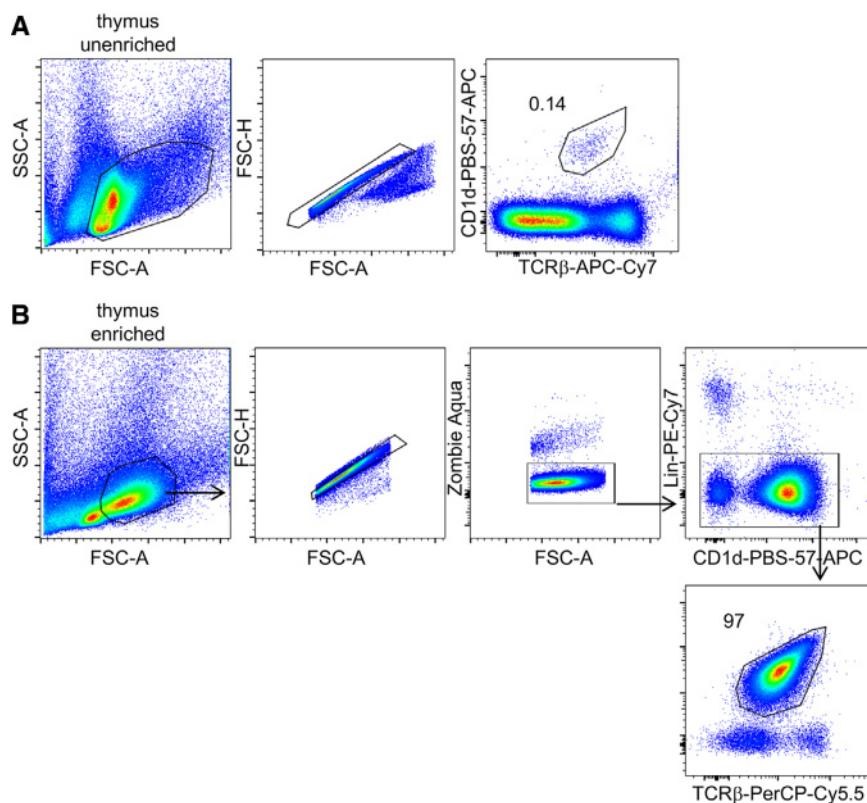
Figure 108. (A) Basic gating strategy for murine thymic iNKT cells. (B) Basic gating strategy for thymic iNKT cells following magnetic-bead enrichment. Sample was additionally stained with Zombie Aqua viability dye and Abs against lineage markers. Numbers adjacent to gates indicate frequency of parent population.

tissue-resident subsets, express and are dependent on the prototypical transcription factor for innate-like T cells, PLZF (encoded by *Zbtb16*) [823, 824]. Intrathymic development of iNKT cells has originally been described to progress through four phenotypically distinct stages (stage 0–3), characterized by differential expression of the surface markers CD24, CD44, and NK1.1 (in C57BL/6 mice) as well as cell size [825–827] (Fig. 109A). More recent studies showed that stage 3 iNKT cells represent

long-term resident cells in the thymus [828, 829]. The thymus of young adult C57BL/6 mice contains around $3–6 \times 10^5$ iNKT cells, corresponding to an overall frequency of 0.3–0.5% of all thymocytes.

More recently, iNKT cells have been categorized into functional subsets based on expression of type 1, 2, or 17 cytokines [830] (Fig. 109B). Like their conventional T-cell counterparts, NKT1 cells are characterized by expression of the transcription factor
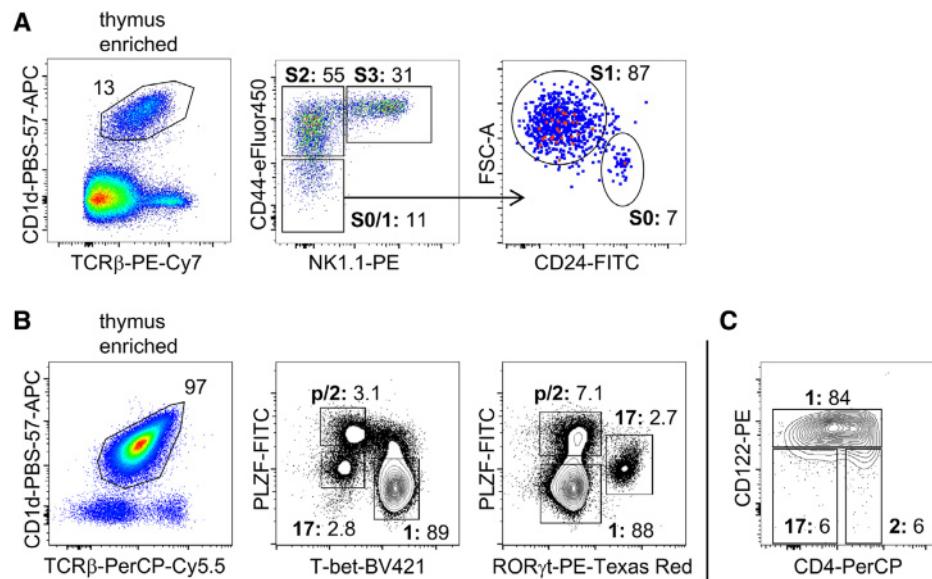
Figure 109. Murine thymic iNKT cell populations. (A) Magnetic-bead enriched iNKT cells from C57BL/6 mice were additionally stained with antibodies against CD44, NK1.1, and CD24. The upstream gating strategy is shown in Fig. 108. (B) Magnetic-bead enriched iNKT cells from C57BL/6 mice were additionally stained intracellulary with Abs against PLZF, T-bet, and RORγt. The upstream gating strategy is shown in Fig. 108. (C) Magnetic-bead enriched iNKT cells from C57BL/6 mice were additionally stained with antibodies against CD122 and CD4. Numbers adjacent to gates indicate frequency of parent population. The upstream gating strategy is shown in Fig. 108. Boldface S0, S1, S0/1, S2, S3 adjacent to gates indicate developmental stages. Boldface p, 1, 2, and 17 adjacent to gates indicate NKTp, NKT1, NKT2, and NKT17 subsets, respectively.
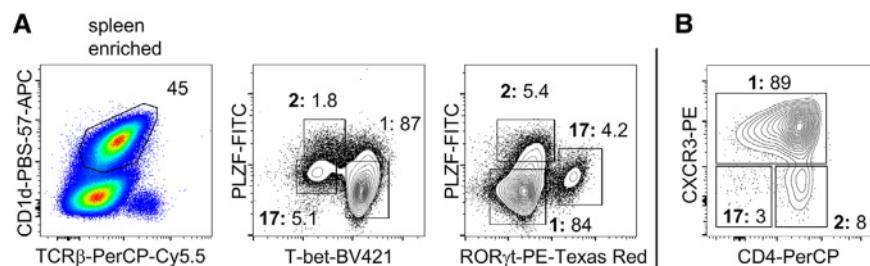
Figure 110. Murine peripheral iNKT cell populations. (A) Magnetic-bead enriched iNKT cells from C57BL/6 mice were additionally stained intracellulary with Abs against PLZF, T-bet, and RORγt. The upstream gating strategy is analogous to that shown in Fig. 108. (B) Magnetic-bead enriched iNKT cells from C57BL/6 mice were additionally stained with Abs against CXCR3 and CD4. Numbers adjacent to gates indicate frequency of parent population. The upstream gating strategy is analogous to that shown in Fig. 108. Boldface 1, 2, and 17 adjacent to gates indicate NKT1, NKT2, and NKT17 subsets, respectively.

T-bet, NKT17 cells express RORγt, whereas NKT2 cells are most frequently characterized by absence of expression of both transcription factors while simultaneously expressing very high levels of PLZF (See Chapter VI Section 1.1 Murine T cells). The prototypic type 2 transcription factor GATA-3 is variably expressed in all iNKT cells and cannot be employed for discrimination of NKT2 cells. As a consequence, in the thymus PLZF^{hi} NKT cells contain both, precursors (NKTp) and NKT2 cells. These cells can be further distinguished by differential expression of CCR7 (NKTp) and PD-1 (NKT2) [828]. Notably, relative proportions of the three NKT subsets vary widely between mouse strains with BALB/c mice showing a strong bias towards NKT2 cells in the thymus, whereas thymi in C57BL/6 mice predominantly contain NKT1 cells [830]. To circumvent intracellular staining for transcription factors, discrimination of NKT-cell subsets can also be achieved by analysis of surface expression of CD4 and CD122 (thymus) (Fig. 109C) or CXCR3 (periphery) (Fig. 110C).

Outside the thymus, iNKT cells can be found in lymphoid and as tissue-resident cells in non-lymphoid organs with distinct subset composition for each organ (for review [831, 832]). In mice (but not humans) up to 40% of all mononuclear cells in liver constitute iNKT cells [815, 821]. The vast majority of these cells are of the NKT1 type. Upon stimulation iNKT cells rapidly produce large amounts of cytokines essentially according to their transcription factor profile with the notable exception of IL-4, which can be produced by NKT1 and NKT2 cells. Similar to other unconventional T cells, iNKT cells are considered innate-like, because they can be stimulated both by cognate ligand via the TCR and in a non-cognate manner through LPS or cytokines like IL-12 and IL-18 [833, 834]. Whereas stimulation through the TCR results in rapid release of multiple cytokines, non-cognate stimulation results mostly in production of IFN-γ.

NKT cells serve a vast variety of functions shaped by their distinct tissue distribution (reviewed in ref. [831, 835]. Thus, NKT cells may protect from infection in lung and liver, but may exacerbate inflammatory conditions and asthma. Although being comparatively rare in intestinal tissues, NKT cells contribute to tissue homeostasis and to shaping the intestinal microbiota. Other roles in tissue homeostasis comprise regulation of T-cell development and egress from the thymus through IL-4 as well as protective functions in type 1 diabetes and graft-versus-host disease [836].

1.8.3 Step-by-step sample preparation. Cell isolation: Single-cell suspensions of whole lymphoid organs (thymus, spleen, lymph nodes) are generated by crushing organs through a 70 μm filter. RBCs are lysed (spleen only) using Qiagen RBC Lysis Solution according to the manufacturer's instructions. For lymphocyte isolation from the lung and liver, mice are euthanized and liver/lungs are immediately perfused with PBS. Lymphocytes are then isolated using standard procedures for solid organs or using commercially available kits, for instance as described in ref. [837].

Surface staining: Following incubation with Fc block (anti mouse CD16/32, clone 2.4G2) cells are stained using APC-conjugated CD1d-PBS-57 or CD1d-unloaded (background control) tetramers for 30 min at room temperature in FCM buffer [838]. Cells are washed once in FCM buffer followed by Ab staining for surface markers for 10 min at 4°C. In order to minimize background, it is pivotal to perform lineage exclusion by staining for the following markers: B220, CD19, CD11b, CD11c. Dead cells are excluded using the Zombie Aqua Fixable Viability kit as per manufacturer's instructions (Biolegend).

Magnetic-bead enrichment: Following CD1d-PBS57-APC tetramer staining, iNKT cells may be enriched using anti-APC magnetic microbeads following the manufacturer's instructions (Miltenyi Biotec). See also Chapter IV Section 1.4 Magnetic pre-enrichment for high-resolution detection and analysis of rare cell populations.

Intracellular staining: To analyze transcription factor expression, magnetic-bead-enriched CD1d-PBS-57 tetramer$^+$ cells from lymphoid organs are stained for surface markers and viability as described above. Samples are then fixed and permeabilized using the Foxp3/Transcription Factor Staining Buffer Set (eBioscience) as per the manufacturer's instructions, following which, cells are stained for intracellular transcription factors for 30 min or overnight.

1.8.4 Materials.

FCM buffer: PBS, 3% FCS
RBC lysis buffer (Qiagen)
Zombie Aqua Fixable Viability kit (Biolegend)
anti-APC magnetic microbeads (Miltenyi Biotec)
Foxp3/Transcription Factor Staining Buffer Set (eBioscience)
Tetramers: Mouse CD1d-PBS-57-APC (NIH tetramer core facility, Atlanta, USA)
              Unloaded mouse CD1d-APC (NIH tetramer core facility, Atlanta, USA)
Antibodies: CD16/32 mAb (clone 2.4G2)
              CD19 mAb (clone 6D5)
              Anti-B220 (clone RA3-6B2)
              CD11b mAb (clone M1/70)
              CD11c mAb (clone N418)
              Anti-TCRβ (clone H57-597)
              CD4 mAb (clone GK1.5)
              Anti-NK1.1 (clone PK136)
              CD44 mAb (clone IM7)
              CD24 mAb (clone M1/69)
              Anti-PLZF (clone Mags.21F7)
              Anti-T-bet (clone O4-46)
              Anti-RORγt (clone Q31-378)
              Anti-CXCR3 (CD183, clone CXCR3-173)
              CD122 mAb (clone TM-b1)

1.8.5 Pitfalls.   Simultaneous staining of cells with tetramer and anti-TCRβ is possible. However, due to distinct staining conditions, it may result in different staining intensities. CD24 Ab staining is sensitive to EDTA. Distribution of iNKT cell subsets varies between organs and also between mouse strains. For instance, in liver iNKT1 cells constitute the predominant iNKT cell subset, whereas mesenteric lymph nodes predominantly contain iNKT2 cells [839]. Furthermore, BALB/c mice display a strong bias towards iNKT2 cells when compared to C57BL/6 mice [830].

1.8.6 Top tricks.   iNKT cells are a rare population of T cells. Therefore, for some downstream analyses it is advisable to perform enrichment using magnetic beads (see also Chapter IV Section 1.4 Magnetic pre-enrichment for high-resolution detection and analysis of rare cell populations). We and others have found that differences in frequencies of iNKT cells in mouse strains with iNKT cell deficiency, such as miR-181a/b-1-deficient mice, compared to wild-type mice are essentially retained upon enrichment via tetramers [840]. The underlying reason remains elusive but may be attributed to lower affinity of tetramers when compared to Ab–antigen interaction. We and others have employed Rag-GFP reporter mice to delineate developmental progression of iNKT cells in the thymus. Such a mouse model may help to further resolve NKT cell precursors and mature NKT cell populations in the thymus [828, 841].

1.8.7 Summary table.

Murine NKT cell population (TCRβ⁺CD1d⁻PBS-57/αGalCer tetramer⁺)	Phenotype/subphenotype
Thymus	
Stage 0	CD44$^-$NK1.1$^-$CD24^{hi}FSC^{hi}
Stage 1	CD44$^-$NK1.1$^-$CD24^{lo}FSC^{lo}
Stage 2	CD44$^+$ NK1.1$^-$
Stage 3	CD44$^+$NK1.1$^+$
NKT1	CD122$^+$PLZF^{lo}T-bet$^+$RORγt$^-$
NKT2	CD122$^-$CD4$^+$PLZF^{hi}T-bet$^-$RORγt$^-$PD-1$^+$CCR7$^-$
NKT17	CD122$^-$CD4$^-$PLZF^{int}T-bet$^-$RORγt$^+$
Periphery	
NKT1	CXCR3$^+$PLZF^{lo}T-bet$^+$RORγt$^-$
NKT2	CXCR3$^-$CD4$^+$PLZF^{hi}T-bet$^-$RORγt$^-$
NKT17	CXCR3$^-$CD4$^-$PLZF^{int}T-bet$^-$RORγt$^+$

1.9 *Murine mucosal-associated invariant T (MAIT) cells*

1.9.1 Overview.   Murine mucosal-associated invariant T cells (MAIT) share many features with iNKT cells. They express a semi-invariant TCR comprised of an invariant Vα19Jα33 TCRα chain, preferentially paired with Vβ6 and Vβ8. MAIT cells recognize vitamin B metabolites, such as 5-(2-oxopropylideneamino)-6-D-ribityl-aminouracil (5-OP-RU), in the context of the nonclassical MHC molecule MHC class I-related protein 1 (MR1) [842]. Despite their virtually simultaneous discovery with NKT cells, understanding of MAIT cell biology is substantially more limited for two main reasons [843, 844]: (i) MAIT cells are rare in mice and (ii) MR1-tetramer reagents have only recently been developed [845, 846] (Fig. 111). This section describes the characterization of MAIT cell subsets based on MR1-tetramers, surface markers, and key transcription factors. In addition, magnetic-bead based enrichment of MAIT cells is described.

1.9.2 Introduction.   The study of MAIT cells in mice is of profound interest, mostly because MAIT cells constitute a very abundant population in various human tissues, comprising almost 10% of all blood T cells and 20–40% of all liver T cells (See also Chapter VI Section 1.17 Human mucosal-associated invariant T (MAIT) cells). In contrast, in C57BL/6 mice, thymus contains only around 5000 MAIT cells, corresponding to 0.002% of all thymocytes. Comparably low frequencies are also found in peripheral lymphoid organs.

Intrathymic development of MAIT cells shares some similarities with that of NKT cells: MAIT cells are selected on cortical CD4$^+$CD8$^+$ double-positive thymocytes. They progress through phenotypically distinct precursor stages (stages 1–3) characterized
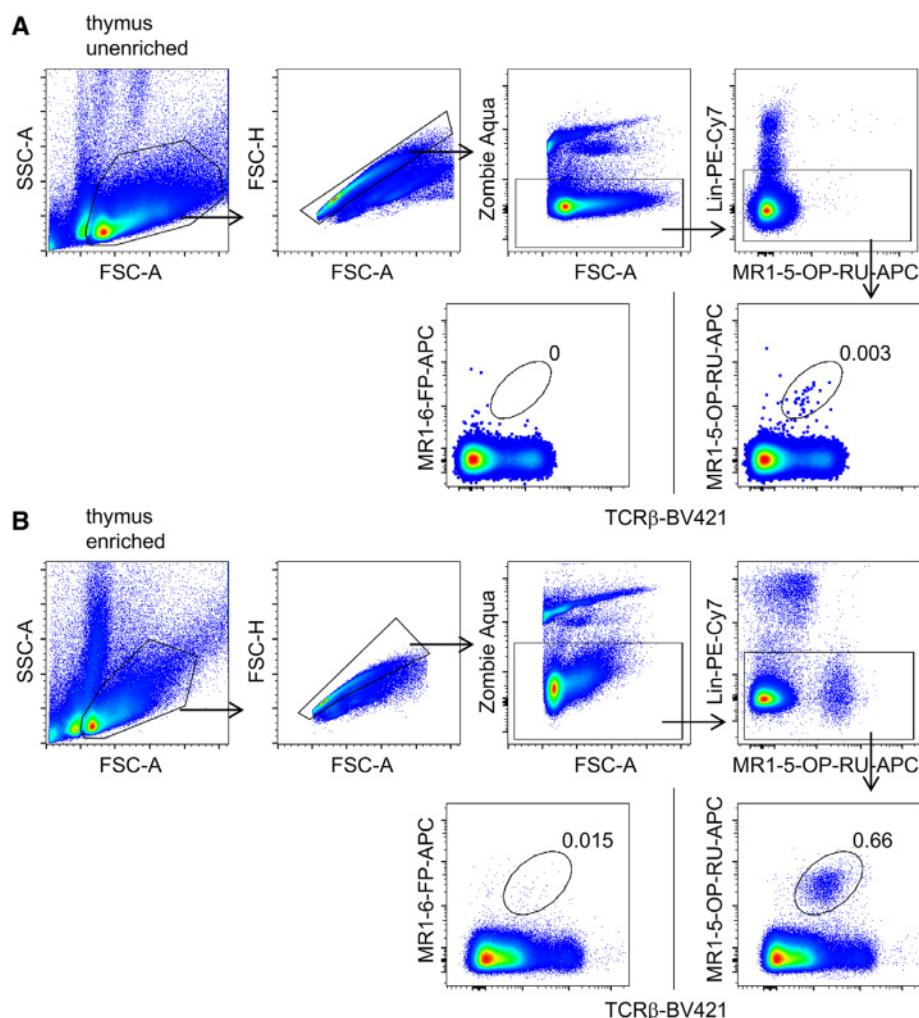
Figure 111. A) Basic gating strategy for thymic MAIT cells. B) Basic gating strategy for thymic MAIT cells following magnetic-bead enrichment. Numbers adjacent to gates indicate frequency of parent population. Stainings with control tetramer MR1-6-FP-APC are displayed as well.

by differential expression of CD24 and CD44 [847] (Fig. 112A). Development of MAIT cells depends on the transcription factor PLZF and miRNA, in particular miR-181a/b-1 [840, 841, 847]. These similarities are further underscored by characterization of T-bet+RORγt^{lo} MAIT1 and T-bet−RORγt^{hi} MAIT17 cell transcriptomes, which within matching tissues are virtually identical to those of NKT1 and NKT17 cells, respectively [832]. MAIT cells also display a large degree of tissue residency in non-lymphoid organs [832] (Fig. 112B). In addition to these similarities between MAIT cells and iNKT cells, there are a number of critical differences. MAIT cell development is characterized by a later onset of PLZF expression at developmental stage 3 only, whereas at
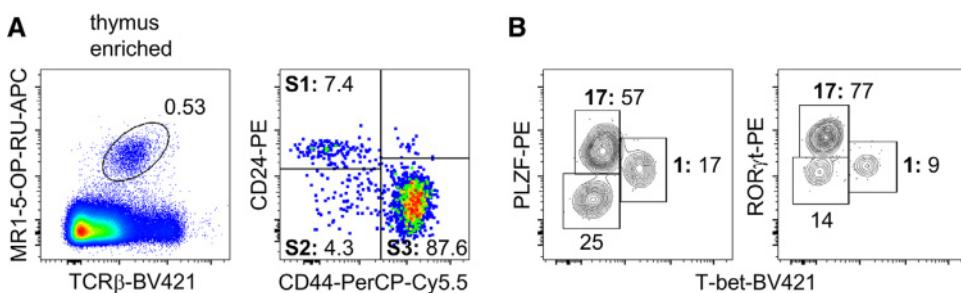
Figure 112. Thymic MAIT cell populations. A) Magnetic-bead enriched MAIT cells from C57BL/6 mice were additionally stained with antibodies against CD44 and CD24. Upstream gating was performed as shown in Fig. 111. B) Magnetic-bead enriched MAIT cells from C57BL/6 mice were additionally stained intracellulary with antibodies against PLZF, T-bet and RORγt. Numbers adjacent to gates indicate frequency of parent population. Upstream gating was performed as shown in Fig. 111. Boldface S1, S2, S3 adjacent to gates indicate developmental stages. Boldface 1 and 17 adjacent to gates indicate MAIT1 and MAIT17 subsets, respectively.

least some NKTp already express high levels of PLZF [828, 847]. Furthermore, no MAIT2 cells have been described and the ratio between MAIT1 and MAIT17 cells is geared toward the latter, whereas NKT1 cells are more abundant than NKT17 cells. It remains an open question whether MAIT cells undergo agonist selection in a similar manner as NKT cells.

Analysis of in vivo function of MAIT cells in immunity is compromised by their scarcity in mice. In addition, many Vα19Jα33 TCRα$^+$ T cells in Vα19Jα33 TCR transgenic mice lack expression of PLZF, indicating that they do not represent true MAIT cells [846]. These obstacles may be overcome by employing B6-MAIT^{CAST} congenic mice that contain high frequencies of MAIT cells due to increased usage of Vα19 in TCR gene rearrangements [848]. This mouse model revealed that MAIT cells alleviated urinary tract infections. MR1-deficient mice are more susceptible to a broad range of bacterial infections (for review see ref. [849]). Given that MAIT cells have also been implicated in clearance of viral infections suggests that antigen-independent stimulation via cytokines, such as IL-12 and IL-18, is also possible, in keeping with their innate-like nature and overall similarity to iNKT cells.

1.9.3 Step-by-step sample preparation.

1.9.3.1 Cell isolation.
Single-cell suspensions of whole lymphoid organs (thymus, spleen, lymph nodes) are generated by crushing organs through a 70-μm filter. RBCs are lysed (spleen only) using Qiagen RBC Lysis Solution according to manufacturer's instructions. For lymphocyte isolation from the lung and liver, mice are euthanized and liver/lungs are immediately perfused with PBS. Lymphocytes are then isolated using standard procedures for solid organs or using commercially available kits for instance as described in ref. [837]. It is advisable to pool cell suspensions from at least three animals to obtain sufficient cell numbers for analysis.

1.9.3.2 Surface staining.
Following incubation with Fc block (anti-mouse CD16/32, clone 2.4G2) cells are first stained using APC- or PE-conjugated MR1-5-OP-RU or MR1-6-FP (background control) tetramers for 40 min at room temperature in FCM buffer [850]. Cells are washed once in FCM buffer followed by Ab staining for surface markers for 10 min at 4°C. In order to minimize background, it is pivotal to perform lineage exclusion by staining for the following markers: B220, CD19, CD11b, and CD11c. Dead cells are excluded using the Zombie Aqua Fixable Viability kit as per manufacturer's instructions (Biolegend).

1.9.3.3 Magnetic-bead enrichment.
Due to the scarcity of murine MAIT cells in typical laboratory strains it is strongly advised to bead-enrich MAIT cells prior to downstream analysis. Bead enrichment should be performed in between tetramer staining and staining for additional surface markers. Single-cell suspensions are stained with biotinylated CD19 mAb and anti-

B220 Abs. B cells are then depleted using streptavidin microbeads as per the manufacturer's instructions (Miltenyi Biotec). Following MR1-5-OP-RU-APC tetramer staining, MAIT cells are enriched using anti-APC magnetic microbeads following the manufacturer's instructions (Miltenyi Biotec). See also Chapter IV Section 1.4 Magnetic preenrichment for high-resolution detection and analysis of rare cell populations.

1.9.3.4 Intracellular staining.
To analyze transcription factor expression, magnetic-bead-enriched MR1-5-OP-RU tetramer$^+$ cells from lymphoid organs are stained for surface markers and viability as described above. Samples are then fixed and permeabilized using the Foxp3/Transcription Factor Staining Buffer Set (eBioscience) as per the manufacturer's instructions, followed by antibody staining for 30 min or overnight.

1.9.4 Materials.

FCM buffer:	PBS, 3% FCS
RBC lysis buffer (Qiagen)	
Zombie Aqua Fixable Viability kit (Biolegend)	
streptavidin microbeads (Miltenyi Biotec)	
anti-APC magnetic microbeads (Miltenyi Biotec)	
Foxp3/Transcription Factor Staining Buffer Set (eBioscience)	
Tetramers:	Mouse MR1-5-OP-RU-APC/-PE (NIH tetramer core facility, Atlanta, USA)
	Mouse MR1-6-FP-APC (NIH tetramer core facility, Atlanta, USA)
Antibodies:	CD16/32 mAb (clone 2.4G2)
	CD19 mAb (clone 6D5)
	Anti-B220 (clone RA3-6B2)
	CD11b mAb (clone M1/70)
	CD11c mAb (clone N418)
	Anti-TCRβ (clone H57-597)
	Anti-NK1.1 (clone PK136)
	CD44 mAb (clone IM7)
	CD24 mAb (clone M1/69)
	Anti-PLZF (clone Mags.21F7)
	Anti-T-bet (clone O4-46)
	Anti-RORγt (clone Q31-378 or B2D)

1.9.5 Pitfalls. MAIT cells constitute an extremely rare cell population, rendering subset analysis prone to errors based on background staining (see Chapter V Section 1 Rare cells—General rules). This difficulty is exacerbated in the analysis of genetically modified mice with developmental defects in the MAIT cell lineage. To minimize background, it is pivotal to include lineage markers in a dump channel and/or enrich prior to downstream analysis. B cells in particular show a high degree of nonspecific binding of the MR1 tetramer (both 5-OP-RU and 6-FP loaded). Simultaneous staining of cells with tetramer and anti-TCRβ is possible. However, due to distinct staining conditions it may result in different staining intensities. CD24 antibody staining is sensitive to EDTA.

1.9.6 Top tricks. In order to overcome problems associated with low frequencies of MAIT cells, it is generally recommended to enrich for MR1-5-OP-RU-tet$^+$ cells for subset analysis whenever possible; see also Chapter IV Section 1.4 Magnetic pre-enrichment for high-resolution detection and analysis of rare cell populations. Notably, it has been demonstrated that magnetic-bead-based enrichment via tetramers essentially retains differences between wild-type frequencies and reduced MAIT-cell frequencies observed in genetically modified mice [841, 847]. The underlying mechanism remains unclear, but may be related to the relative inefficiency of tetramer-based enrichment, which in turn may be due to lower affinity of tetramer when compared to antibody-mediated binding. Furthermore, it is absolutely essential to exclude non-T lineage cells, most notably B cells, during gating to limit background staining. It is also advisable to include nonbinding MR1-6-FP tetramers as background controls. Finally, for exact quantitation of MAIT cells, dual tetramer staining using a combination of MR1-5-OP-RU-APC and PE labeled tetramers may help to reduce background [841]. We and others have employed Rag-GFP reporter mice to delineate developmental progression of MAIT cells in the thymus. Such a mouse model may help to further resolve MAIT cell precursors and mature MAIT cell populations in the thymus [828, 841].

1.9.7 Summary table.

Murine MAIT cell population (Lin$^-$TCRβ$^+$MR1-5-OP-RU tetramer$^+$)	Phenotype/subphenotype
Thymus	
stage 1	CD24$^+$CD44$^-$CCR7$^-$PLZF$^-$
stage 2	CD24$^-$CD44$^-$CCR7$^+$PLZF$^-$
stage 3	CD24$^-$CD44$^+$CCR7$^-$PLZF^{hi}
MAIT1	T-bet$^+$RORγt^{lo}
MAIT17	T-bet$^-$RORγt^{hi}
Periphery	
MAIT1	T-bet$^+$RORγt^{lo}
MAIT17	T-bet$^-$RORγt^{hi}

1.10 *Murine intestinal intraepithelial T cells*

1.10.1 Overview. In this section, we describe protocols to isolate and analyze murine intestinal intra-epithelial lymphocytes (iIELs) and lamina propria lymphocytes (LPLs) by FCM. In particular, the protocol iIEL isolation and most of the subsequent flow cytometric analysis applies similarly to αβ and γδ iIELs, which are very similar cell types.

1.10.2 Introduction. The intestinal epithelium constitutes one of the greatest surface barriers in mammals and is in continuous contact with the (gut luminal) environment. Composed by a mucosa, the intestine wall is made up of primary two layers,

namely a one cell layer epithelium and the underlying lamina propria [851, 852]. In addition, the mouse small intestine contains five to seven Peyer's patches in anti-mesenteric position, which are excised and removed during the protocol below, and numerous smaller aggregates of immune cells called cryptopatches and isolated lymphoid follicles, which will be largely included within the fraction of lamina propria lymphocytes. Continuously exposed to environmental cues and highly susceptible for pathogen assault, the intestine bears sophisticated and complex immune cell networks specific to each of the compartments [853]. In order to study the immune cells resident in both compartments of the murine intestine, a refined isolation of intra-epithelial lymphocytes (IELs) and lamina propria lymphocytes (LPLs) is advised according to the following protocols.

1.10.3 Step-by-step sample preparation of lymphocytes from the mouse small intestine.

1.10.3.1 Isolation of IELs.

1. Preheat the IEL isolation medium at 37°C at the water bath
   (a) IEL isolation medium: 1 mM DTT + 10 μM KN-62 (stock at 50 mM) [854] + complete T cell medium (35 mL/sample)
   (b) Complete T cell medium—RPMI 1640 + 10% FBS +1% Penny-strep + 1% NEAMM +0.1% β- mercapto-ethanol + 1%HEPES 1M +1% Sodium Pyruvate
2. Harvest SI into ice cold PBS
3. Flush the intestine with ice cold PBS with a syringe and a gavage needle until it's clean.
4. Carefully remove fat and the Peyer's patches
5. Open longitudinally and clean it again in a petri dish in ice cold PBS. Transfer it to a 50 mL falcon tube (n1) in ice with PBS
6. Vortex the tubes to further clean the intestine
7. Transfer the tissue to a new clean 50 mL falcon (n2) containing 10mL of the pre-warmed IEL isolation medium. Note that some protocols recommend to cut the small intestine into smaller pieces (sized 0.5–2 cm), which may help to avoid the formation of knots or clews.
8. Shake the tube in the vortex for 30seconds
9. Incubate the 50 mL falcon tubes at 37°C and 220 rpm for 15 min. (inside plastic beakers—4–5 tubes–or in a falcon tube support fixed to the shaker plate)
10. After incubation vortex each tube for 10 s
11. Transfer the solution to a new 50 mL tube (n3) containing ≈15–20 mL of ice cold complete T cell medium. If you prefer to cut the small intestine into pieces (see point 6), than you should use a cell strainer here to retain the tissue.
12. Repeat steps 5–9 for two more times (using the same tube - n2).
13. Wash the intestine one last time with 10 mL of cold complete T cell medium and a kick vortex. Transfer the wash to the respective tubes (n3). *For the LPL isolation keep the*
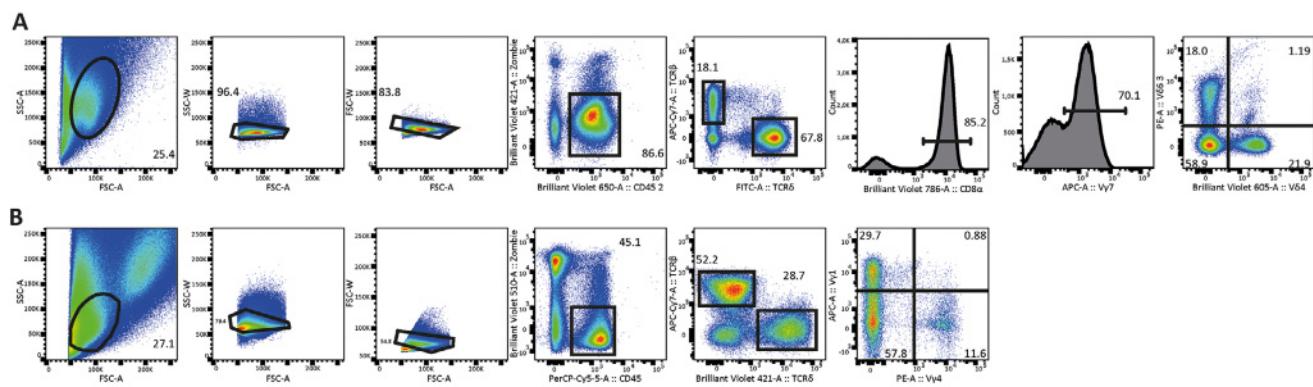
Figure 113. Representative gating strategy for TCRγδ$^+$ population analysis of (A) murine small intestine intraepithelial lymphocytes (IEL) and (B) lamina propria (LPL). After isolation, lymphocytes were stained with Zombie (Live/Dead-Biolegend), CD45 (104 -Biolegend), Tcrß (REA318 - Miltenyi), TCRγ/δ (GL3 -Biolegend), CD8α (53-6.7 -Biolegend), Vγ7 (F2.67 - provided by P. Pereira: Institut Pasteur, Paris, France), Vδ6.3 (C504.17C -eBioscience), Vδ4 (GL2 -Biolegend) for the IEL cell suspension A and Vγ1 (2.11 -Biolegend) and Vγ4 (UC3-10A6 -Biolegend) for the LPL cell suspension.

intestines in a falcon tube on ice and proceed with the LPL protocol.

14. Centrifuge the tubes (n3) at 1250 rpm for 10 min at 4°C
15. Aspirate the supernatant
16. Resuspend the pellet in 4mL of the 40% Percoll in complete T cell medium (5 mL per sample) and transfer to a 15 mL tube
17. Wash the 50 mL tube with 1 mL of the 40% Percoll solution and transfer to the same 15 mL tube
18. Under lay the 80% Percoll in complete T cell medium (3 ml per sample) and centrifuge the tubes at 2400 rpm for 30min at RT (1 up and 1 down)
19. Remove the waste on top and recover the pinkish/white ring in-between the two phases. Place it in another falcon containing 3–5 mL of the complete T cell medium or MACS® Buffer and top it up to 5mL

20. Centrifuge the samples for 10 min at 1250 rpm 4°C
21. Proceed to staining

1.10.3.2 Isolation of LPLs.

1. Prewarm the Digestion Medium in the water bath at 37°C
   (a) Digestion medium: DNAse I 125 μg/mL (stock 10 mg/mL) + Collagenase D 250 μg/mL (stock 50 mg/mL) + Complete T cell Medium (32 mL/ sample)
2. After line 12. on IEL isolation protocol transfer the intestines into a petri dish and cut the tissue into smaller pieces with curved scissors (≈0.1cm).
3. Transfer the intestine to a 50 mL tube (n4) containing the 10mL digestion medium (at 37°C).
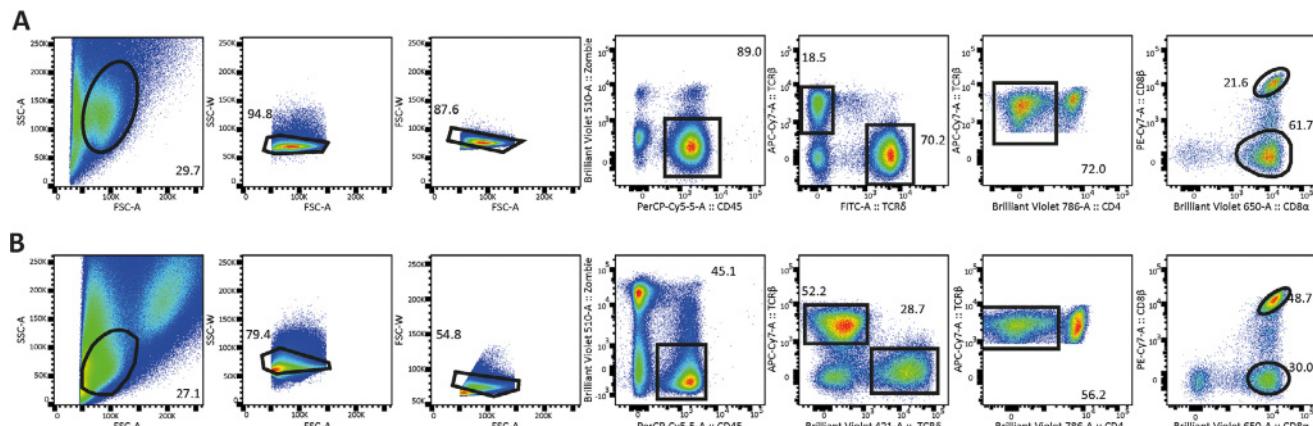
Figure 114. Representative gating strategy and analysis of A TCRαβ$^+$ murine small intestine intraepithelial lymphocytes (IEL) and B lamina propria (LPL). After isolation, lymphocytes were stained with Zombie (Live/Dead - Biolegend), CD45 (104- Biolegend), Tcrß (REA318 - Miltenyi), TCRγ/δ (GL3 - Biolegend), CD8α (53-6.7- Biolegend), CD8β (YTS156.7.7 - Biolegend) and CD4 (GK1.5 - Biolegend).

4. Just like for the IEL isolation protocol: Incubate the 50mL falcon tubes at 37°C and 220 rpm for 15 min. (inside plastic beakers—4–5 tubes or in a falcon tube support fixed to the shaker plate)

5. After incubation, with a plastic transfer-pipet pipet up and down the solution containing the intestine.

6. With the same transfer-pipet transfer the solution and filter it through a 70μm cell strainer placed on new 50mL tube (n5) containing ice cold complete T cell Medium + 100μL of 4mM EDTA.

7. Collect the tissue in the cell strainer and repeat the procedure in steps 2–5, two more times (using the same tube n4).

8. After filtering the last time, with a syringe lid (green) smash the pieces of tissue left behind in the strainer adding some more 4°C complete T cell medium.

9. Centrifuge the tubes (n5) at 1250 rpm for 10 min at 4°C

10. Aspirate the supernatant

11. Resuspend the pellet in 4 mL of the 40% Percoll solution in complete T cell medium (5 mL per sample) and transfer to a 15 mL tube

12. Wash the 50 mL tube with 1 mL of the 40% Percoll solution and transfer to the same 15 mL tube

13. Under lay the 80% Percoll solution in complete T cell medium (3 mL per sample) and centrifuge the tubes at 2400 rpm for 30 min at RT (1 up and 1 down)

14. Remove the waste on top and recover the pinkish/white ring in-between the two phases. Place it in another falcon containing 3–5 mL of the complete T cell medium or MACS® Buffer and top it up to 5 mL

15. Centrifuge the samples for 10 min at 1250 rpm 4°C

16. Proceed to staining

1.10.4 Materials.

1.10.4.1 Reagents.

- Dithiothreitol (DTT) (Sigma–Aldrich, cat # 43816)
- KN-62 – Selleckchem, cat. number: S7422
- RPMI 1640 (Gibco, cat # 11875093)
- FBS (Sigma, cat # F7524)
- Penny-strep (Gibco, cat #: 1514-122)
- MEM Non-Essential Amino Acids solution (MEM NEAA) 100X (Gibco, cat # 11140050)
- βmercapto-ethanol (Sigma, cat # M3148)
- HEPES (Sigma, cat # H0887)
- Sodium Pyruvate (Gibco, cat # 11360-039)
- Percoll (GE Healthcare, cat # 17-0891-01)
- PBS 1× (Gibco, cat # 1419-09)
- DNAse (Roche, cat # 11284932001)
- Collagenase D (Roche, cat # 1108886601)
- EDTA (Roth, cat # 8043.4)
- MACS® Buffer – PBS 1X, 3% FBS, 5mM EDTA

1.10.4.2 Antibodies.

Antigen	Company	Clone	Catalog number
CD45.2	Biolegend/ Miltenyi	104/104-2	109836/ 130-103-787
CD4	Biolegend	GK1.5	100453
CD8α	Biolegend	53-6.7	100742
CD8ß	Biolegend	YTS156.7.7	126615
TCRß	Miltenyi	REA318	130-104-811
TCRδ	Biolegend	GL3	118120
Vδ4	BD Bioscience	GL2	745116
Vδ6.3	eBioscience	C504.17C	555321
Vγ1	Biolegend	2.11	141108
Vγ4	Biolegend	UC3-10A6	137706
Vγ7	provided by P. Pereira: Institut Pasteur, Paris, France	F2.67	-
Viability dye (Zombie)	Biolegend	-	423102

1.10.5 Data analyses of mouse iIELs and LPLs. The intestinal mucosa harbors lymphocytes, which are responsible not only for its protection but also to maintain integrity. Scattered along the intestinal epithelia IELs are a heterogeneous population of T cells. Distinguished by their development and origin, IELs can be divided in two populations: the "natural" and the "induced" IELs. Derived from conventional αß T cells expressing CD4 (TCRαß$^+$CD4$^+$) and classical CD8αβ molecules (TCRαß$^+$CD8αß$^+$), "induced" IELs relocate in the intestine mucosal tissue after cognate antigen engagement in the periphery and accumulate over time [853]. On the other hand, "natural" IELs differentiate in the thymus and characterized by their TCRs ability to recognize self-antigens. Composed of both γδ T cells and αβ T cells the large majority of "natural" IELs express the homodimer CD8αα but neither CD4 or CD8αβ [855] (Figs. 113A and 114A). Moreover, acquisition of surface markers during development such as CD103 (αE integrin), α$_4$β$_7$ and CCR9 ensure homing and tissue residency of IELs [856]. In addition, "natural" CD8αα$^+$ IELs display a chronically activated phenotype which can be translated by the expression of some activation markers such as CD69, CD122, and CD44 [857].

Interestingly, γδ T cells homing in the small intestine display a biased expression of TCRγ chains according to their localization. While γδ IELs are mostly Vγ7$^+$, γδ T cells that home in the γδ LPLs express a broader variety of TCRγ chains (Figure 113) [797, 802].

Whereas the small intestine epithelium is enriched in "unconventional" CD8αα$^+$ γδ T cells, approximately 60% of all lymphocytes (Figure 114A), the lamina propria is mostly composed of conventional αß T cells expressing CD8αß and CD4 (Figure 114B) [855]. Thereby, frequencies of CD4$^+$ αß T cells within the iIEL preparation, and CD8αα$^+$ αß T cells within the LPL preparation serve as reliable indicators of the level of unavoidable cross contamination during the isolation process.

1.10.6 Pitfalls.

Be cautious to not exceed the incubation times point 8 (IEL) and point 3 (LPL) as this would decrease viability and yield of the protocols.

1.10.7 Top tricks.

Adding the KN-62 reagent is helpful to support the viability of the cells once isolated, but does not increase the yield.

Do not omit the DTT or try to replace it with beta-mercaptoethanol.

Some IEL isolation protocols suggest to use HBSS medium, which we did not find helpful as compared to RPMI-based complete T cell medium.

Follow advises to pre-warm the isolation and digestion media and to use chilled PBS for cleaning the intestine.

1.11 Human CD4 and CD8 T cells

1.11.1 Overview. The use of FCM allows for high resolution delineation of T cell heterogeneity. Different features of the remarkable heterogeneity of memory, but also seemingly naïve, T cells can be addressed depending on the questions raised. T cell heterogeneity can be delineated by addressing surface markers or intranuclear transcription factors indicative for differentiation stages, chemokine receptors to address homing capacities, and production of cytokines to assess functional stages. Depending on the resolution required for monitoring T cell heterogeneity best is to combine multiple of these aspects.

1.11.2 Introduction. The body is under constant threat of pathogen attack. Microbes and viruses lurk in the environment and are evolutionary adapted to seize every opportunity to invade the system. The network of cells that make up the immune system works tightly together to protect against novel but also persistent pathogens. If pathogens manage to get through the body's physical barriers the first line of immunological defense is made up of innate immune cells. Innate cells are rapidly activated by pathogen-associated molecules in a nonantigen specific way. As a consequence, innate cells can react equally well to a variety of pathogens. Simultaneously, innate cell activation also paves the way for the second line of immunological defense by presenting antigen processed peptides, which primes the adaptive phase of the T-cell response. After priming in the secondary organs, T cells migrate to the affected tissue where they execute cytotoxicity and other effector functions. In addition, antigen-specific T-cell memory is formed. T-cell immunity is complex and there are an increasing number of subsets defined by differentiation stage, function, and cellular location. In the last decades, FCM proved itself to be the key technology to study heterogeneity among human T-cell subsets. However, as the options for multicolor FCM panel design emerged due to technical innovation, this went hand-in-hand with the increasing complexity to define T-cell subsets. As new T cell

Table 22. A four-dimensional model to address T-cell differentiation stages

Subset		Expression			
Number	Name	CD27	CD45RA	CCR7	CD28
1	TN	+	+	+	+
2	TCM	+	−	+	+
3	Early	+	−	−	+
4	Intermediately	+	−	−	−
5	Early-like	−	−	−	+
6	TE RA-	−	−	−	−
7	TE RA+	−	+	−	−

subsets are defined at increasing rates, it is virtually impossible to be complete. Hence, in this section we will review the best-established cellular markers that can be measured to shed light on these complexities.

Conventional human T cells are a subpopulation of lymphocytes that can be characterized by the expression of a T-cell receptor (TCR), through which they can recognize peptides presented in the context of HLA-molecules. The conventional TCR is composed of a transmembrane alpha- and beta-chain heterodimer that is embedded in the cell membrane in combination with the CD3 protein complex. In the thymus, T cells mature and develop into two main cell lineages of CD4$^+$ and CD8$^+$ single positive T cells that are released as naive cells, bearing either an αβ-TCR or γδ-TCR, into the circulation (Fig. 115). The lack of expression of any of these markers identifies a third fraction of T cells in the periphery. These so called double-negative T cells (DN) are a legitimate component of the immune system but remain poorly understood [858]. In the periphery, large numbers of naïve T cells (**TN**) survey the secondary lymphoid tissues and blood for cognate antigen. In response to antigen exposure, **TN** start to proliferate and differentiate rapidly into large numbers of effector and memory precursor T cells. Following pathogen clearance, the majority of effector cells die while the memory precursor cells develop into long-lived memory T cells [696, 859]. Although the precise model of T-cell differentiation has not been fully deciphered, two models, progressive versus asymmetric differentiation, are currently discussed that explain how T cells diversify into effector and memory subsets. Despite this discussion a consensus was reached about markers that define naive and memory T-cell subsets [860]. Markers that can be used to phenotypically differentiate both CD4$^+$ and CD8$^+$ **TN**, effector, and memory cells are two of the four isoforms of the CD45 family. While **TN** and effector T cell (**TE RA+**) express the CD45RA molecule, both the central memory (**TCM**) and the effector type RA- (**TE RA-**) cells preferentially express CD45R0 and lack CD45RA, CD45RB, and CD45RC. To identify **TN** the CD45RA marker should be combined with minimally one additional marker. Markers that can be used include the L-selectin CD62L, which guides T cells to the lymph nodes. Expression of this marker can only be honestly assessed using freshly isolated cells, as cryopreservation results in a profound decrease of CD62L
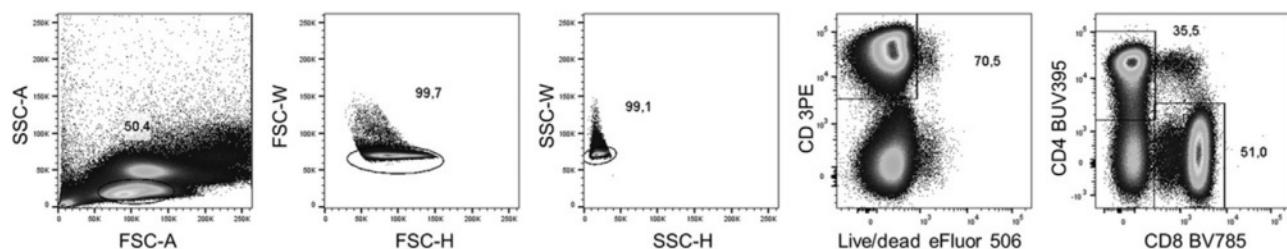
Figure 115. Gating of CD4+ and CD8+ T cells in peripheral blood. Lymphocytes are identified on based of the FSC and SSC. Single cells are discriminated from doublets by plotting the pulse width and height against each other for both the SSC and FSC. CD3+ T cells are gated and excluded from apoptotic cells by viability dye. Including dead cells can result in large errors because of their property to bind nonspecifically to antibody conjugates. Although not applied here, in the same channel other cell types may be excluded by using a DUMP channel, meaning a channel that contains all cellular markers in one color that should be excluded e.g. Abs against CD14 (monocytes), CD19, and CD21 (B cells). Peripheral blood ratios of CD4+ and CD8+ T cells vary from donor to donor. A normal CD4:CD8 ratio is between 1 and 2. Low frequencies of double negative CD3+CD4−CD8− cells are common and contain populations of NKT cells.

expression [861]. In addition the homing marker CCR7, costimulatory molecules CD27 and CD28 and adhesion molecule CD31 are used to define **TN**. Although the preferred marker to identify **TN** appears redundant it is important to realize that little differences may be observed by using different markers. Furthermore, there will be small populations of naïve-like but differentiated T cells not accounted for that require the use of specific additional markers to be identified among naïve T cells. These include regulatory CD4+ T cells (**Treg**), stem cell memory T cells (**Tscm**), and virtual memory T cells (**TVM**) [862].
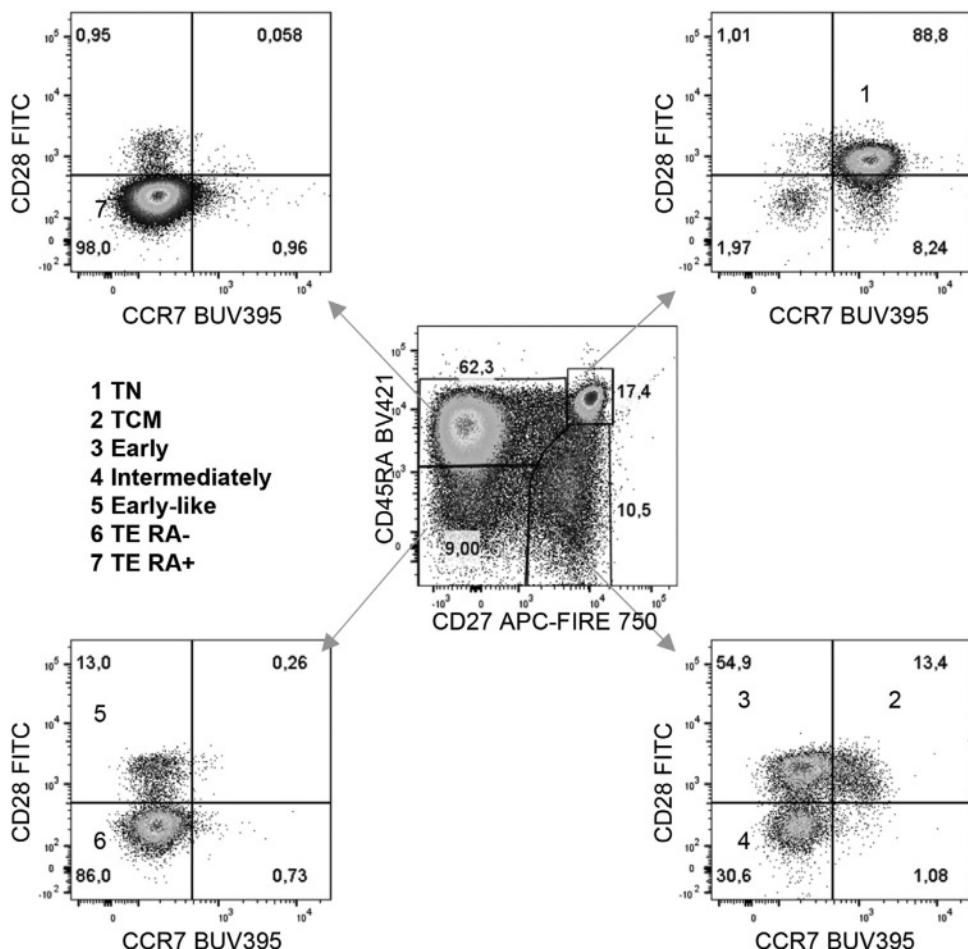
Figure 116. A 4D model to address T-cell differentiation stages. At least seven stages of T-cell differentiation can be distinguished for peripheral blood derived CD8+ T cells by using the markers; CD45RA, CD27, CD28, and CCR7. Phenotyping and gating of T cells in peripheral blood according to backbone described in Figure 115.
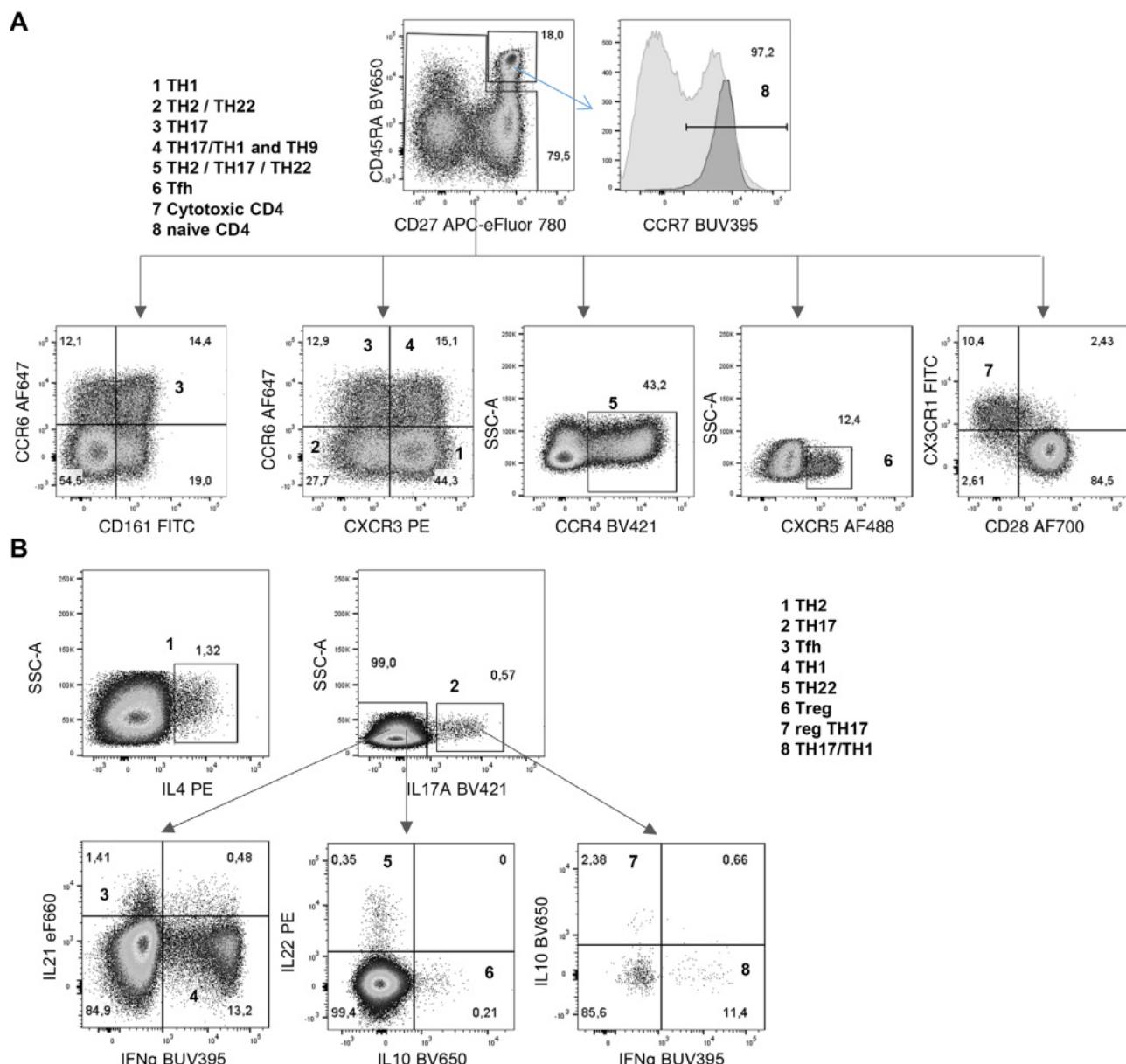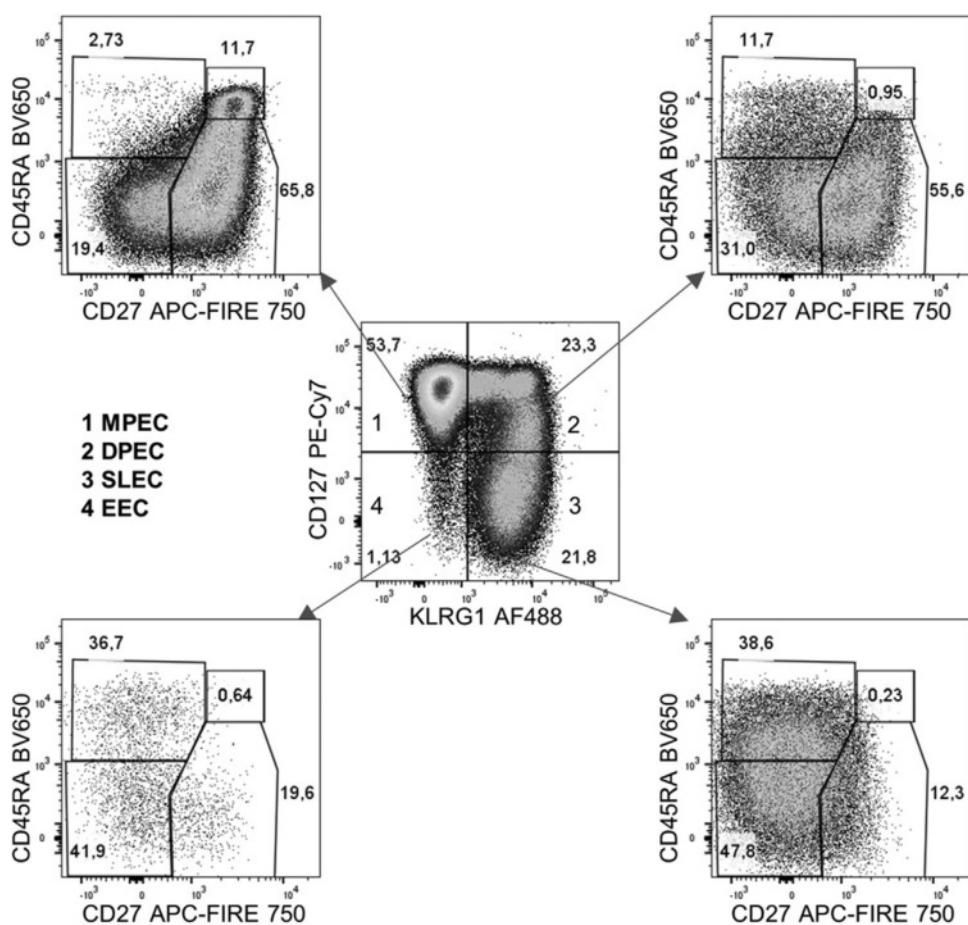
Figure 117. Adhesion, chemokine and cytokine receptor expression identify up to eight functional subsets within the human CD4$^+$ memory pool. Peripheral blood derived CD4$^+$ T cells can be divided between naïve, cytotoxic, and eight different T-helper subsets based on the surface expression of (A) CCR4, CCR6, CXCR3, CXCR5, CX3CR1, CD28, and CD161 and (B) production of IFN-γ, IL-4, IL-10, IL-17, IL-21, and IL-22. For detection cells were stimulated with Ionomycin and PMA in the presence of BFA and MN. Phenotyping and gating of T cells in peripheral blood according to backbone described in Fig. 115.

Table 23. Gating on naive T cells

Subset		Expression			
Number	Name	CD27	CD45RA	CCR7	CD28
8	Naive CD4	+	+	+	+

1.11.3 CD4 T-cell differentiation. To date, the most appreciated model to define CD4$^+$ T-cell differentiation stages relies on the differential expression of adhesion and chemokine recep-

tors (Fig. 117A, Tables 23 and 24). Naive CD4$^+$ TN can be recognized by the mutual expression of CD45RA and CD27 combined with a bright CCR7 staining. Below we describe a model by which eight different antigen-experienced CD4$^+$ T cell subsets can be distinguished. Type 1 helper (**TH1**) cells are critical for cell-mediated immunity as they produce vast amounts of the anti-viral IFN-γ (Fig. 117B, Table 25). **TH1** cells can be identified by the expression of CXCR3, which guides these cells to the infected tissues. Other chemokine receptors expressed by **TH1** are CCR5 and CXCR6 [863]. While **TH1** cells are critical for cell-mediated immunity, CD4$^+$ **TH2** cells are traditionally considered

Figure 118. Effector CD8$^+$ T-cell differentiation during acute infection using KLRG1 and CD127. In humans four different effector populations can be identified during acute infection based on the expression of KLRG1, CD127, CD45RA, and CD27. Phenotyping and gating of T cells in peripheral blood according to backbone described in Fig. 115.

to support activation of other leucocytes such as B cells and are associated with the production of the cytokines IL-4, IL-5, and IL-13 (Fig. 117B, Table 25). However, latest insights suggest that TH2 are not the principal B helper cells but are crucial for IL-5 mediated activation of eosinophils. **TH2** cells are enriched in the CCR4 positive fraction and some express the surface marker CRTH2 [864]. TH2 can be further distinguished by the variable co-expression of other chemokine receptors including CCR3, CCR6, CCR8, and CCR10 [865]. Caution is required when using CCR4 as expression is shared by TH17 and TH22 cells. Differentiation of T cells into **TH1** and **TH2** subsets is controlled in a bipha-sic model by the transcription factors T-bet and *GATA binding*

Table 24. Identification of CD4$^+$ T cell subsets by surface marker expression

Subset		Expression								
Number	Name	CCR6	CD161	CXCR3	CCR4	CCR10	CCR3	CD28	CX3CR1	CXCR5
1	TH1	–		+	–					
2+5	TH2	–		–	+					
4	TH9	+		+	–		+			
3+5	TH17	+	+	–	+					
4	TH17/TH1	+	+	+	–					
2+5	TH22	+		–	+	+				
6	Cytotoxic CD4							–	+	
5	Tfh									+
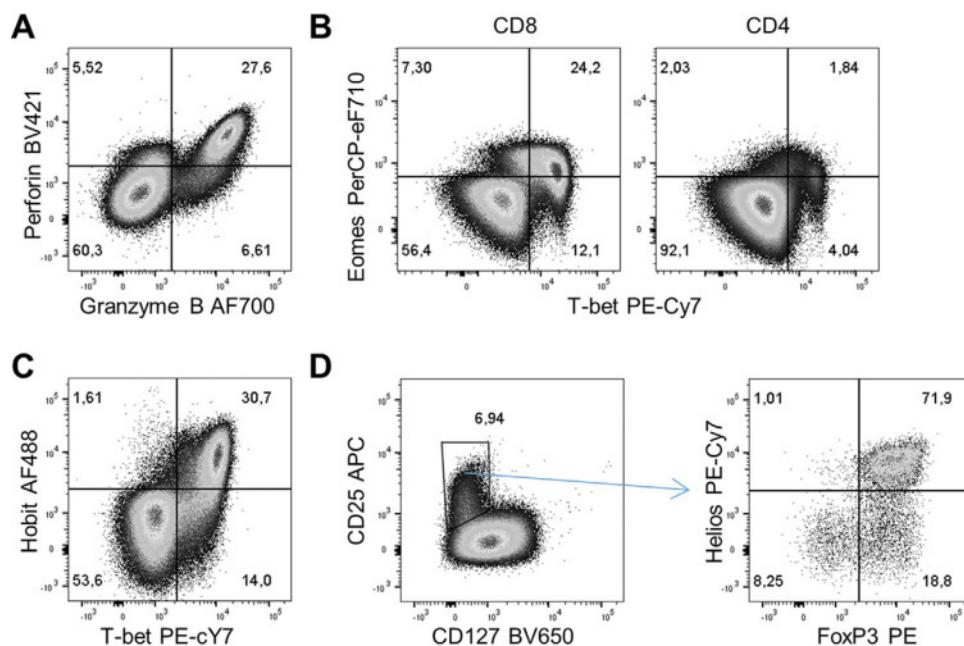
Figure 119. T-cell subsets as identified by intracellular staining of transcription factors and cytolytic molecules. Peripheral blood derived CD3$^+$ T cells are divided between CTL and T_H cells. (A) CTL can be identified by the mutual expression of GZMB and Perforin. (B) CTL but also T_H1 cells can be identified within the CD8 and CD4 lineage by the expression of T-bet and further divided by the expression of Eomes. (C) Hobit expression strongly correlates with T-bet expression in CD8$^+$ T cells. (D) Treg cells can be identified among the CD25$^+$CD4$^+$ T cells by the expression of FoxP3 and Helios. Phenotyping and gating of T cells in peripheral blood according to backbone described in Figure 115.

protein 3 (GATA3) [720, 866]. T-bet has been shown to antagonize GATA-3, the master regulator differentiation and maintenance of **TH2** cells [867]. In recent years, **TH** subsets have been identified that differ from the traditional **TH1** and **TH2** subsets by the preferential production of IL-9 (**TH9**), IL-17 (**TH17**), and IL-22 (**TH22**) (Fig. 117B, Table 25); multiple functions have been attributed to the IFN regulatory factor 4 (IRF4) driven **TH9** cells of which a significant fraction expresses CCR3, CCR6, and CXCR3 [868], and the pro-inflammatory **TH17** cells play an important role in pathogen clearance of extracellular pathogens at barrier sites. In
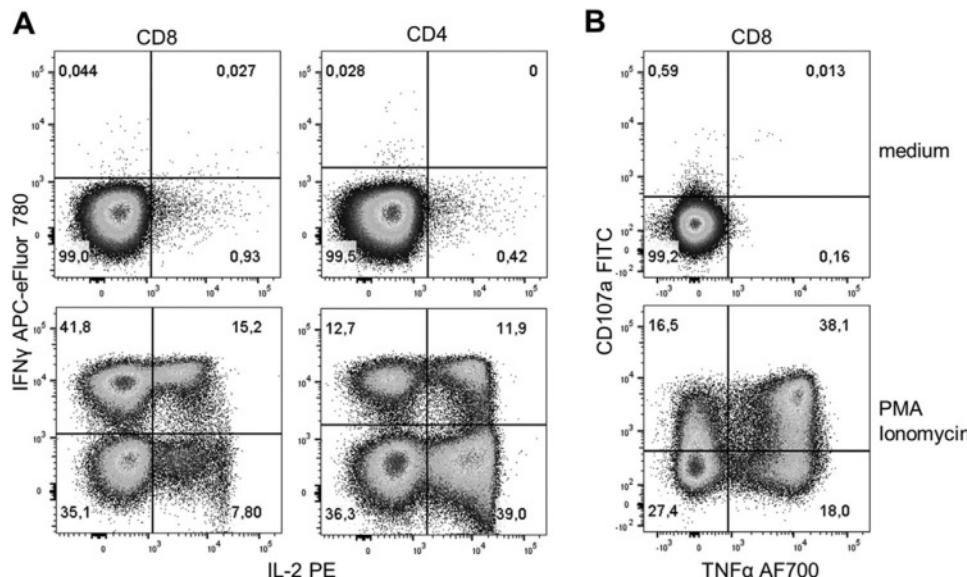
Figure 120. Detection of cytokine production and degranulation after stimulation of T cells. Peripheral blood T cells were stimulated for 4 h with Iono and PMA or medium control in the presence of BFA and MN. (A) Stimulated CD8$^+$ and CD4$^+$ T cells were stained for expression of IFN-γ and IL-2. (B) TNF-α production was captured in combination with degranulation of stimulated CD8$^+$ T cells as detected by capture of CD107. Phenotyping and gating of T cells in peripheral blood according to backbone described in Fig. 115.

Table 25. Identification of CD4+ T cell subsets by cytokine production

Subset		Expression					
Number	Name	IL17A	IL21	IFNγ	IL22	IL10	IL4
4	Th1	–	–	+			
1	Th2	–					+
2	Th17	+					
7	reg Th17	+		–		+	
8	TH17/TH1	+		+			–
5	Th22	–			+		–
3	Tfh	–	+	–			
6	Treg	–			–	+	

humans, **TH17** cells can be identified by the mutual expression of CCR6, and CD161 [869]. The TH17 lineage can be further divided into more or less cytotoxic subsets based on the selective expression of CXCR3 (TH17/TH1) and CCR4, respectively [870]. Several studies have demonstrated that a fraction of **TH17** can also secrete IFN-γ besides IL-17 [870–872] (Fig. 117B, Table 25). These cells are generally referred to as **TH17/TH1** cells. More recently a third subset of **TH17** was characterized that harbored regulatory T cell features. These cells can be identified by the production of IL-10, which can be also produced by subsets of **TREG,** referred to as Type 1 regulatory (TR1) cells, and rare effector CD4 T cells (Fig. 117B) [873–876]. Differentiation of **TH17** cells is driven by the expression of RAR-related orphan receptor γ t (RORγt) which controls IL-17 transcription [721]. In addition, the skin-homing **TH22** cells appeared to be regulated by the aryl hydrocarbon receptor (AHR) transcription factor and can be identified by the mutual expression of CCR6, CCR4, and CCR10 [877, 878]. Finally, a decade ago a specific subset of **TH** cells was discovered that resided in B-cell areas of follicular regions in secondary lymphoid tissues. Consequently, these cells were named follicular helper cells (**TFH**) and are identified by the constitutive expression of the chemokine receptor CXCR5. Since their discovery multiple **TFH** and **TFH-like** circulating cells have been characterized based on the expression of *programmed cell death protein 1* (PD-1), CXCR3, CCR6, and the secretion of IL-21 (Fig. 117B, Table 25) [879]. **TFH** differentiation is orchestrated by the transcription factor *B-cell lymphoma 6* (BCL6) and is elementary for the activation of B cells in germinal centers and are therefore crucial for the induction of humoral immune responses [880]. The relationship between follicular BCL6+ **TFH** and circulating **TFH-like** cells is still largely unclear. Finally, CD4+ T cells can also directly mediate viral clearance and suppress tumor growth through cytotoxic function. Loaded with cytotytic molecules such as Granzyme B and perforin these cells can be identified by the surface expression of the Fractalkine receptor CX3CR1 and the lack of CD28 (Fig. 117A, Table 24) [881].

1.11.4 CD8+ T-cell differentiation. Several markers are proposed in combination with CD45RA/R0 to precisely define phenotypi-

cally different CD8+ T-cell subsets. Among these markers is CD27, a member of the TNF receptor family that promotes survival of T cells, CCR7, a chemokine receptor that mediates LN homing, and the co-stimulatory molecule CD28, which is required for T-cell activation and survival (Fig. 116, Table 22) [882–885]. mAbs directed against these markers are widely available and conjugated to plenty of different fluorescent dyes that enables broad application in various multicolor phenotyping panels. The 4D model to address T-cell differentiation stages starts with **TN** (CD27+CD28+CCR7+CD45RA+). After priming **TN** differentiate through early-differentiated (CD27+CD28+CCR7−CD45RA−), early-like (CD27−CD28+CCR7−CD45RA−), and intermediately differentiated (CD27+CD28−CCR7−CD45RA−) T cells to give rise to **TE RA+** (CD27−CD28−CCR7−CD45RA+), **TE RA-** (CD27−CD28−CCR7−CD45RA−) and **TCM** (CD27+CD28+CCR7+CD45RA−) cells. **TE RA-** are memory cells that in contrast to **TCM** lack constitutive expression of CCR7. In healthy individuals without any clinical signs of viral infection, from now on referred to as steady state, naive and early differentiated type form the most abundant circulating CD8+ T-cell subsets. In humans that are chronically infected with Cytomegalovirus (CMV) or HIV the effector type RA+ also contributes substantially to the CD8+ T cell compartment composition. Similar phenotypic heterogeneity exists in the CD4+ T cell compartment although subdivisions of differentiation stage based on the expression of CD28 and CCR7 are not generally recognized. However, although effector type CD4+ T cells are virtually absent during steady state, increasing evidence suggests that cytolytic CD4+ T cells play an important role during infections and these cells are appreciated to lack CD28 expression [881, 886].

In multiple well established models of CD8+ T cell differentiation during acute infection, expression of the IL-7 receptor α-chain (CD127) is used to discriminate between the short-lived effector cells (SLEC) and the memory-precursor effector cells (MPEC) [887]. Although mice and human differ significantly in life span and pathogen encounter, immune cell gene expression demonstrated high similarities [888, 889]. In humans, the combined use of these markers is less established and combinations of different markers have been used to define T-cell differentiation during acute infections. In combination with the cell-surface markers CD45RA and CD27, the human equivalent of MPEC cells can be identified by an increased expression of CD127 that goes hand-in-hand with a decreased expression of the killer cell lectin-like receptor G1 (KLRG1) (Fig. 118). In addition, the human equivalent of SLEC can be identified by the selective expression of KLRG1. In contrast to the bi-phasic model in mice, the majority of the human effector CD8+ T-cell compartment consists of *double positive effector cells* (DPEC). In addition, low number of early effector cells (EEC) can be identified that lack both CD127 and KLRG1 expression. Although these markers can be used to define distinct subsets in the circulation and lymph nodes during the acute phase and in "steady state" in humans [890], it remains to be elucidated to what degree these populations are functionally comparable between both species.

1.11.5 Transcriptional regulation of human T-cell differentiation.
The relationship between phenotype and function has been subject of much investigation. Although the association between the above mentioned surface markers and T-cell function are mostly well established, ultimately not all phenotypically similar T cells share the same cell fate and effector response. The emerging complexity among T-cell subsets and their potential to elicit a plethora of effector functions require a more thorough characterization of each subset that would reflect its function. The actual regulator of T-cell development and function is the circuitry of transcription factor expression. Complex interactions of transcription factors drive expression of target genes that ultimately determine T cell functionality and many use opposing mechanisms to counter-regulate each other [741]. Multicolor FCM is the preferred method of choice to detect low frequent T-cell subsets with differential transcription factor expression within heterogeneous T-cell populations. As these factors bind to DNA, they are concentrated in the nucleus. To allow Abs to reach their nuclear epitopes T cells need to be fixated and permeabilized. There is a variety of commercial kits and procedures available to accommodate these stainings. Permeabilization may induce cell shrinkage and loss of surface marker staining intensity and protocols should therefore be validated and optimized. Generally the FSC and SSC voltage are amplified for intracellular protein staining. The CD8$^+$ T-cell lineage is enriched for cytolytic cells (**CTL**) that are very effective in direct lysis of infected target cells. During chronic infections CTL-like cells can also be detected among the CD4$^+$ lineage. These cells can be recognized by the expression of *Granzyme B* (GZMB) and *Perforin* that are stored in acidic lysosomes (Fig. 119A). Differentiation of **CTL**, but also **TH1** differentiation was demonstrated to be regulated by expression of the T-box transcription factor *Tbx21* (T-bet) [732]. While T-bet drives terminal differentiation of effector T cells, expression of a second T-box transcription factor, *Eomesodermin* (Eomes), enables **TH1** cells to generate memory with a certain degree of redundancy (Fig. 119B) [885, 891]. In addition, Eomes expression can also be used to define a subset of **Treg** cells, referred to as TR1 cells that lacks FoxP3 expression and produces IL-10 [875, 876]. Recently, the zinc finger protein *ZNF683* (Hobit) was identified as a transcriptional regulator of CD8$^+$ and CD4$^+$ effector type T cells in humans and the lack of CD28 (Fig. 117A) [892, 893]. Expression of Hobit strongly correlates with T-bet and regulates production of IFN-γ (Fig. 119C). To prevent immune-mediated pathology by ongoing effector function and unrestricted expansion of **CTL** and **TH1** cells, the stimulatory activities of these subsets are counterbalanced by natural and induced **Tregs**. These suppressor cells are CD4$^+$ T cells, exert their modulatory function by direct interaction with target cells, by the secretion of immunosuppressive cytokines such as TGF-β and IL-10 and by increasing the consumption of IL-2. Two lineages of **Treg** cells can be distinguished in humans. Both express the *IL-2 receptor alpha chain* (CD25) and the transcription factor *forkhead box 3* (FoxP3) and can be distinguished by the expression of the transcription factor Helios [767, 768, 894] (Fig. 119D). Although in mice the expression of Helios is used to identify natural and peripheral induced **Treg** cells, that developed in the thymus

or periphery, respectively [775], this model is controversial in humans.

1.11.6 Human T-cell effector function. To define specific T-cell subsets on basis of cytokine production usually in vitro stimulation is required. Since cytokines are not preformed, their levels are typically low in resting cells. Accumulation of cytokines within the ER is achieved by adding an inhibitor of protein transport to stimulated cells. The two most frequently used inhibitors are Monensin (MN) and Brefeldin A (BFA). The choice of protein transport inhibitor is very important as they can have differential effects on surface and intracellular protein expression after stimulation. For example, BFA will help to maximize the capture of TNF-α, IFN-γ, and IL-17 but blocks the surface expression of the T-cell activation marker CD69 (Fig. 120A). In addition, MN maximizes the detection of the T-cell degranulation marker CD107 (Fig. 120B). After polyclonal stimulation of T cells cytokines are produced with different kinetics. For most cytokines a stimulation and accumulation period of 4–6 h is optimal. However, for several cytokines such as IL-10 and IL-12 the production kinetics are relatively slow and up to 24 h stimulation may be required for optimal detection. As both MN and BFA are toxic, exposure of stimulated cells should be limited. Consequently, for the longer stimulations (>6 h) MN and BFA may be added during the last 4–6 h. MN was demonstrated to be less toxic and can be added for periods up to 24 h. When there is no prior knowledge regarding the specific cytokines that will be produced by the stimulated T cells, expression of activation induced markers can be considered. Both CD4$^+$ and CD8$^+$ T cells depict CD69 and HLA-DR expression as early as 4 h after stimulation. Other markers like the CD8$^+$ biased 4-1BB (CD137) and the CD4$^+$ T-cell biased *CD40L* (CD154) peak at 24 h after stimulation. One problem with defining T-cell phenotypes after stimulation is the internalization of TCR and the CD4 and CD8 coreceptors. This will result in a decreased staining intensity for CD4, CD8, and especially CD3, which makes it more difficult to define T cells. By either staining the cells before stimulation or by intracellular staining of these markers, this problem can be circumvented.

1.11.7 Step-by-step sample preparation.

1. Freezing PBMC

1. Isolate PBMC from heparinized blood or buffy coat by using Ficoll or lymphoprep according to manufacturer's protocol.
2. Collect the PBMC in 50 mL tubes.
3. Add washing medium up to 50 mL and centrifuge for 10 min at 500 × *g* at room temperature.
4. Aspirate supernatant, resuspend pellet in 50 mL washing medium and centrifuge for 10 min at 250 × *g* at room temperature.
5. Aspirate supernatant, resuspend pellet in 35 mL washing medium and centrifuge for 10 min at 250 × *g* at room temperature.
6. Resuspend in 1–2 mL of thawing medium and put on ice.

7. Count cells and adjust concentration to 10—25 × 106 cells/mL.

8. Prepare a similar amount of freezing medium and put on ice.

9. Make sure your cells, cryovials, and freezing medium are cold before freezing.

10. Add drop by drop, while gently shaking, 1 mL of freezing medium for every mL of cell suspension.

11. Transfer 2 mL of the cell suspension to each vial.

12. Freeze the cryovials by using a Mr. Frosty (Nalgene), Cool-Cell (Corning), or a freezing apparatus at −80°C for a period of four to 24 h.

13. Store the vials until further use in liquid nitrogen.

2. Thawing PBMC

1. Thaw the vials by gently shaking in a 37°C water bath, until little ice remains.

2. Transfer the contents of the vial to a 50 mL tube.

3. Add drop by drop, while gently shaking, 18 mL of cold thawing medium.

4. Let the cell suspension rest for 20 min and centrifuge for 10 min at 500 × *g*.

5. Aspirate supernatant, resuspend pellet in 50 mL washing medium and centrifuge for 10 min at 250 × *g* at 4°C.

6. Aspirate supernatant, resuspend pellet in desired volume of FCM buffer (for surface and intracellular stainings) or culture medium (for stimulations) and count cells.

3. Surface staining

1. Transfer up to 2 × 106 PBMC to a 96-well round buttom plate (Greiner BioOne).

2. Centrifuge the plate at 390 × *g* at 4°C for 3 min.

3. Aspirate supernatant and resuspend cells by gently vortexing the plate.

4. Add 30 μL FCM *buffer* containing a pretitrated appropriate amount of tetramer for each well (prepare 1× extra).

5. Incubate for 30 min at 4°C, shaking, protected from light.

6. Meanwhile prepare surface staining (including the live/dead exclusion dye) in a total volume of 30 μL FCM-buffer for each well (prepare 1 × extra).

7. Add 30 μL surface staining mix, without washing the cells, directly into the well and incubate for a further 30 min at 4°C, shaking, protected from light.

8. Add 150 μL FCM buffer and centrifuge at 390 × *g* at 4°C for 3 min.

9. Resuspend cells by gently vortexing the plate.

10. Add 100 μL FCM buffer, and analyze by FCM cell sorting in the desired format, or continue with the intracellular staining protocol.

Note: Always use appropriately titrated Abs and tetramers, which is usually "not" the concentration suggested by the supplier. The ins and outs of titrating Abs can be found in the ref. [608].

4. Intracellular stainings of transcription factors and cytolytic molecules

1. After surface staining add 200 μL *Fixation/Permeabilization* buffer.

2. Gently resuspend the cells by pipetting up and down three times.

3. Incubate for 20 min at 4°C, shaking, protected from light.

4. Centrifuge for 5 min at 700 × *g* at 4°C.

5. Aspirate supernatant and resuspend cells in 200 μL FCM buffer *and c*entrifuge for 5 min at 700 × *g* at 4°C.

6. Aspirate supernatant and resuspend cells by pipetting up and down 3 times in 50 μL of the intracellular staining mix prepared in Permeabilization Buffer.

7. Incubate 30 min at 4°C, shaking, protected from light.

8. Add 150 μL Permeabilization Buffer to each well and centrifuge for 5 min at 700 × *g* at 4°C.

9. Aspirate supernatant and resuspend cells in 200 μL Permeabilization Buffer *and c*entrifuge for 5 min at 700 × *g* at 4°C.

10. Aspirate supernatant and resuspend cells in 100 μL FCM buffer and analyze by FCM cell sorting in the desired format.

5. Cytokine staining

1. Transfer PBMC into suspension culture flasks (690 190, Greiner) at 1 × 106 cells/mL in culture medium (flask standing upright, or 45° tilted depending on volume) and rest them overnight in a 37°C 5% CO_2 incubator.

2. Transfer cells to a 15 mL tube and centrifuge for 10 min at 500 × *g* at room temperature.

3. Aspirate supernatant, resuspend cells and add 1 mL of culture medium.

4. Count the cells and adjust concentration to 10–20 × 106 cells/mL.

5. Add 100 μL control mix to the correct wells of a non-tissue culture treated 96-well round bottom plate (3788, Corning).

6. Add 100 μL stimulation mix to the correct wells of the 96-well plate.

7. Then add 100 μL cell *suspension*.

8. Incubate for 4 h in a 37°C 5% CO_2 incubator.

9. Put plate on ice for 15 min after incubation.

10. Centrifuge plate for 5 min at 700 × *g* at 4°C.

11. Aspirate supernatant, resuspend cells in 200 μL FCM buffer and centrifuge plate again for 5 min at 700 × *g* at 4°C.

12. Aspirate supernatant, resuspend cells in 50 μL FCM buffer containing a pretitrated appropriate amount of surface staining mix.

13. Incubate for 30 min at 4°C, shaking, protected from light.

14. Add 150 μL FCM buffer and centrifuge at 700 × *g* at 4°C for 3 min.

15. Aspirate supernatant and add 100 uL of Cytofix/Cytoperm reagent (554722, BD Biosciences) to each well and resuspend by pipetting three times up and down.

16. Incubate for 20 min at room temperature protected from light.

17. Add 100 μL FCM buffer and centrifuge at 700 × g at 4°C for 3 min.

18. Aspirate supernatant and add 50 μL intracellular staining mix prepared in 1× perm/wash and resuspend by pipetting three times up and down.

19. Incubate for 30 min at 4°C, shaking, protected from light.

20. Add 150 μL 1 × perm/wash to each well and centrifuge for 5 min at 700 × g at 4°C.

21. Aspirate supernatant, add 200 μL 1× perm/wash to each well and centrifuge for 5 min at 700 × g at 4°C.

22. Aspirate supernatant and resuspend cells in 100 μL FCM buffer and analyze by FCM cell sorting in the desired format.

Note: Protocol adapted from Lamoreaux et al. [608].

1.11.8 Materials.

6. Monoclonal antibodies

1. Surface staining:

   BD Biosciences: CD4 BUV 395 (SK3), CD45RA BV421 (HI100), CCR7 BUV395 (150503), CD45RA BV650 (HI100), CXCR5 Alexa Fluor R ₋ 488 (clone RF8B2), CD25 APC (clone 2A3) CD161 FITC (DX12).

   eBioscience: CD3 PE (UCHT1), KLRG1 AF488 (clone 13F12F2), CD4 PerCP-eFluor 710 (clone SK3), CD127 PE-Cy7 (clone eBioRDR5), CD27 APC-eFluor 780 (clone O323), CD107a FITC (clone H4A3)

   Biolegend: CD27 APC-Fire 750 (O323), CCR6 Alexa Fluor R ₋ 647 (clone G034E3), CCR7 BV421 (clone G043H7), CX3CR1 FITC (clone 2A9-1), CCR4 BV421 (L291H4), CD28 Alexa Fluor 700 (CD28.2), CD127 BV650 (A019D5). R&D Systems: CXCR3 PE (clone 49801)

   Sanquin: CD28 FITC (15E8)

2. Live/dead exclusion dyes: Live/dead fixable dyes (Thermofisher) or Fixable viability dye (eBioscience); we here use Fixable viability dye eFluor 506 (eBioscience).

3. Intracellular stainings:

   BD Biosciences: IL-4 PE (3010.211), IFNγ BUV395 (B27), granzyme B Alexa Fluor R ₋ 700 (clone GB11), IL-2 PE (clone 5344.111), IL-10 BV650 (JES3-9D7), TNF-α Alexa Fluor R ₋ 700 (clone MAb11), Perforin BV421 (clone B-D48), Hobit (clone 5A);

   eBioscience: IL-21 eFluor 660 (eBio3A3-N2), Eomes PerCPeFluor 710 (WD1928), Helios PE-Cy7 (22F6), IFN-γ APCeFluor 780 (clone 4S.B3), FoxP3 PE (clone PCH101), T-bet PE-Cy7 (clone 4B10)

   Biolegend: IL-17A BV421 (BL168), IL22 PE (BG/IL22), Anti-IgM PE (clone ma-69)

7 Flow cytometer

All experiments were performed on a LSR Fortessa flow cytometer with a 365 nm, 405 nm, 488 nm, 561 nm and 640 nm configuration (BD Bioscience). Filters: 379/34(365) for BUV395; 530/30(488) for FITC or AF488; 665LP(488) for PerCP-eFluor 710; 450/50(405) for BV421; 525/50(405) for BV510, V500 and Fixable viability dye eFluor 506; 660/20(405) for BV650; 710/40(405) for BV711; 800/50(405) for BV785; 585/15(561) for PE; 780/60(561) for PE-Cy7; 675/20(640) for APC or AF647; 730/45(640) for AF700; 780/60(640) for APC-eF780 and APC-FIRE 750.

8 Media and buffers:

Thawing medium:

- IMDM
- 20% (v/v) FCS
- 0.00036% (v/v) 2-ME

Freezing medium (after addition of DMSO use within 1 h):

- IMDM
- 20% (v/v) FCS
- 20% (v/v) DMSO
- 0.00036% (v/v) 2-ME

Washing medium:

- HBSS
- 5% (v/v) FCS
- 10% (v/v) TRIS-HCL pH 7.0 (as extra buffering)

Culture medium:

- RPMI
- 10% (v/v) FCS

FCM buffer:

- Phosphate buffered saline (PBS)
- 0.5% (w/v) BSA
- 0.01% (w/v) sodium azide
- 2mM EDTA pH 8.0 (to prevent clots)
- Fixation/Permeabilization buffer (FOX-P3 kit eBioscience)
- 75% Fixation/Permeabilization Diluent (cat. 00–5223)
- 25% Fixation/Permeabilization Concentrate (cat. 00–5123)
- Permeabilization Buffer (FOX-P3 kit eBioscience)
- 90% Fixation/Permeabilization Diluent (cat. 00–5223)
- 10% Permeabilization Buffer (10 ×) (cat. 00–8333)

Stimulation mix:

- Culture medium
- 2 μg/mL Ionomycin
- 20 ng/mL PMA
- 20 μg/mL BFA
- 2.8 μLl/mL GolgiStop (BD Bioscience)

Control mix:

- Culture medium
- 20 µg/mL BFA
- 2.8 µL/mL GolgiStop (BD Bioscience)

1 × perm/wash:

- 10% 10 × perm/wash (554723 BD Biosciences)
- 90% ddH2O

1.12 Human tissue resident memory T cells

1.12.1 Overview. Resident memory T cells (T_{RM}) reside in human tissues, ranging from peripheral organs such as skin to internal organs such as the liver. These T_{RM} are specifically programmed to remain within these tissue compartments there within providing protection. Techniques to isolate and identify human T_{RM} by FCM were developed and verified by multiple research groups and are described below.

1.12.2 Introduction. In the last decade a subset of memory T cells has been identified that is specifically adapted for survival and function within tissues. These so-called tissue resident memory T cells (T_{RM}) are important for rapid local protection within tissues and can be identified by a variety of markers, including adhesion molecules and chemokine receptors. The vast majority of human T cell knowledge has been based on T cells isolated from peripheral blood due to the lack of tissue accessibility until recent years. Both CD8$^+$ and CD4$^+$ T_{RM} have been identified in human skin, lung, intestines, salivary glands, bone marrow, brain, spleen, tonsils, and lymph nodes [895–903]. In mice, the existence of T_{RM} was proven by parabiosis experiments (see Section 1.4 Murine resident memory T cells). In humans, the possibilities of validating T_{RM} are far fewer, but recently the maintenance of T_{RM} in the lung was shown by transplantation [904].

T_{RM} lack the expression of lymph node homing molecule CCR7 and tissue egress molecule S1PR1. Human T_{RM} have a memory phenotype CD45RA$^-$CD45RO$^+$ and CCR7$^-$CD27$^{+/-}$CD28$^{+/-}$. The most widely/classical used marker of T_{RM} is CD69. CD69 that inhibits the function of S1PR1 so T_{RM} are not attracted to the high SIP gradient in the blood and lymph and therefore retains T cells within tissues [905]. It should be noted that in mice it was shown that CD69 is an imperfect marker of T_{RM} as T_{RM} lacking CD69 also exist [906]. However, markers categorizing T_{RM} within CD69$^-$ T cells in human tissues are yet to be confirmed. Furthermore, CD69 is a classical activation markers, which should be kept in mind especially when performing functional assays. T_{RM} do not express other classical activation markers, such as CD25, CD38, or HLA-DR [895, 897, 902, 907]. An identifier of T_{RM} at mucosal sites is CD103 (α subunit of αEβ7 integrin), which helps T_{RM} dock to E-cadherin expressing epithelial cells [908]. These T_{RM} co-express CD69 and CD103 and are found mainly in the skin, lung, salivary glands, brain, and intestines [899–902]. T_{RM} reside in other tissues, such as the liver and bone marrow, and in these tissues T_{RM} express CD69 but not CD103. T_{RM} also express chemokine

receptors CXCR6, CXCR3, CCR5, and integrin CD49a (α subunit of α1β1 integrin) throughout the different tissues. CD69$^+$ T_{RM} lack the expression of CX3CR1, mainly expressed by effector T cells.

T_{RM} are polyfunctional and rapidly produce cytokines upon stimulation [900, 901], which can be quantified with in vitro stimulation in the presence of brefeldin A and staining for cytokines intracellularly. In the skin CD49a identifies CD8$^+$ T_{RM} poised for cytotoxic function [909]. This rapid effector function needs to be tightly controlled in order to protect the tissues where T_{RM} reside. Inhibitory receptors PD-1, CTLA-4, and 2B4 are expressed by T_{RM} [899–901], which may control the effector function of these T_{RM}.

In the recent years, T_{RM} have also taken the spotlight in cancer immunotherapy. The use of tumor infiltrating lymphocytes (TILs) and Ab immunotherapy were one of the big breakthroughs of cancer immunotherapy. Further research revealed that the presence of CD103$^+$CD8$^+$ TILs are a positive prognostic marker in several cancers [910–913]. A subset of TILs in tumors of NSCLC share the phenotype of T_{RM} in adjacent lung tissue (expression of CD103, CD69, CXCR6, CD49a) [913, 914]. A proportion of PD-1^{++} TILs with a T_{RM} phenotype also express CXCL13, the ligand of CXCR5 [914–916]. Furthermore, tumors consist of tumor-specific TILs as well as tumor nonspecific T cells so-called bystander T cells. While tumor-specific TILs express high levels of CD39, the bystander T cells lack CD39 expression [917].

In order to further unravel the heterogeneity of human T_{RM} Single cell RNA-sequencing platforms should be utilized and the results obtained from these experiments should be validated by multicolor FCM and functional assay.

1.12.3 Step-by-step sample preparation.

1.12.3.1 Isolation of human T_{RM}. The following protocol was designed for isolating mononuclear cells from various tissues, including intestines, lung, and tumor tissue, described previously [895, 918].

1. Cut tissue into small pieces and incubated for 1–2 h at 37°C in digestion medium while shaking/rolling
2. Dissociate the tissue using gentleMACS® Tissue Dissociator (Miltenyi)
3. Pass the digested tissue through a flow-through chamber to achieve a single cell suspension
4. After centrifugation, incubate the samples with 50 µg/mL DNase for 15 min in a 37°C water bath
5. To isolate mononuclear cells from the cell suspension, use standard Percoll density gradient technique
6. Isolated mononuclear cells can be used directly for experimentation or cryopreserved in liquid nitrogen until further analysis
7. For cryopreservation, resuspend cells in cold FCM buffer and add the same volume of 2× freeze medium dropwise and take directly to cryo.
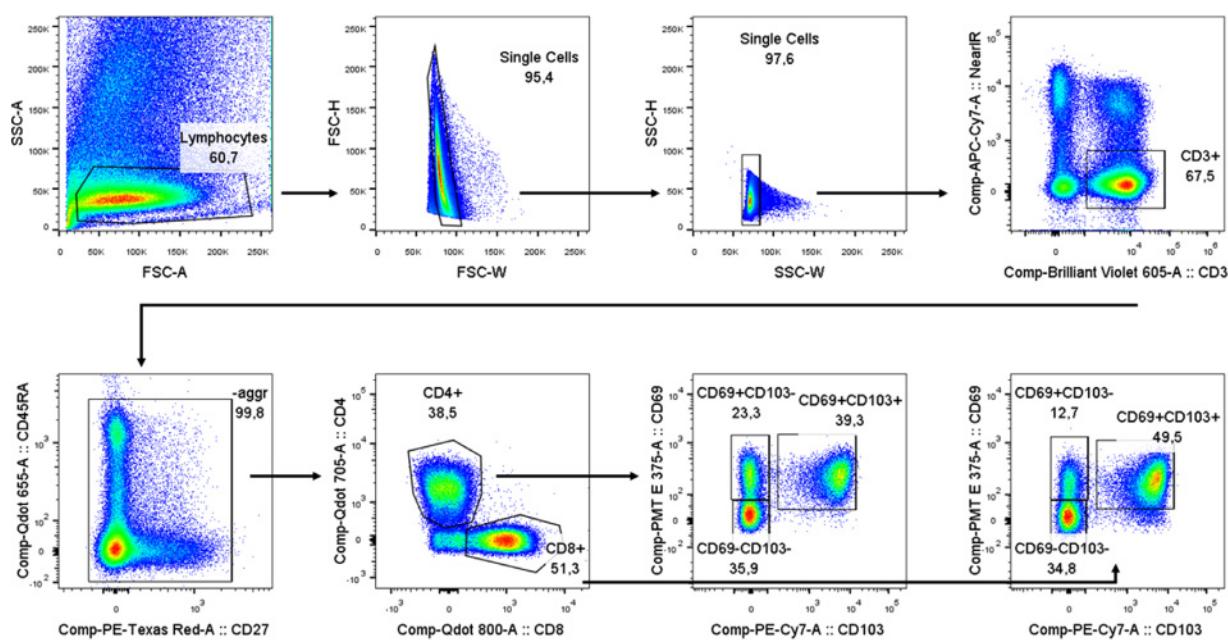
Figure 121. Gating strategy for human T_{RM}. The above gating strategy is shown for human lung tissue T_{RM}, but similar gating strategies apply for other tissues. Side (SSC) and forward (FSC) scatter are used to gate on lymphocytes, followed by gating out doublets also using SSC and FSC. Live/dead marker Near-IR is used to gate out dead cells and CD3 eVolve605 to gate on T cells. To gate out aggregates, CD45RA QDot655 and CD27 PE-CF594 are used. Whether or not this aggregate gating is necessary depends on your antibodies and cells used. To distinguish between CD4+ and CD8+ T cells, CD4 BUV737 and CD8 BUV805 are used. The most widely used markers of TRM are CD69 and CD103, which can be stained for on both CD4+ and CD8+ T cells

1.12.3.2 FCM staining of human T_{RM}.

1. Prepare surface staining mix in FCM buffer
2. For staining use 1×10^5–2×10^6 cells
3. Add cells to 96-well V-bottom plate and centrifuge ($350 \times g$, 5 min, 4°C)
4. Remove the supernatant
5. Resuspend cells in 25–50 µL staining mix per well (amount depends on number of cells)
6. Incubate for 15–20 min on ice
7. Wash cells by adding 150 µL FCM buffer and centrifuge ($350 \times g$, 5 min, 4°C)
8. Remove supernatant
9. For only surface staining, resuspend in 80–120 µL FCM buffer (depending on amount of cells) and measure
10. Cells can also be fixed with a mild fixative (0.5% PFA)
11. For intracellular stainings, fix cells by resuspending the cells in 50 µL of fixation solution
12. Incubate for 30 min on ice
13. In the meantime, prepare intracellular staining mix in 1× permeabilization buffer
14. Wash cells by adding 150 µL FCM buffer and centrifuge ($550 \times g$, 5 min, 4°C)
15. Resuspend cells in 25–50 µL intracellular staining mix per well (amount depends on number of cells)
16. Incubate for 30 min on ice
17. Wash by adding 150 uL 1× permeabilization buffer and centrifuge ($550 \times g$, 5 min, 4°C)
18. Remove supernatant and resuspend cells in 80–120 uL of FCM buffer (depending on amount of cells) and measure

1.12.4 Materials.

- Medium: RPMI with 20 mM Hepes, 10% fFCS, 1% pen/strep, 1% L-glutamine
- Digestion mix: medium, 50 U/mL DNase type I (Sigma–Aldrich), 300 U/mL collagenase D (Worthington)
- DNase (Sigma–Aldrich) (dilute in medium)
- Percoll (GE Healthcare)
- FCM buffer: 0.5% FCS PBS
- PFA: paraformaldehyde
- 2× Freeze medium: 20% DMSO, 30% PBS, 50% FCS
- Fixation solution from Foxp3 Transcription Factor Staining kit (Thermofisher)
- 1× Permeabilization buffer from Foxp3 Transcription Factor Staining kit (Thermofisher)
- Flow cytometer: LSR II, LSRFortessa or FACSymphony (BD)
- In Table 26 is a list of Abs that can be used to identify human T_{RM}, this list is not complete.
- Live/dead fixable dead cell dyes (Thermofisher)/Zombie fixable viability kits (Biolegend) should be used in the surface staining mix to distinguish live cells

1.12.5 Data analysis and gating. For analysis of FCM data FACS Diva (BD) or FlowJo (Tree Star) software should be used. First, lymphocytes and single cells should be gated, after which the compensations should be checked. Single stainings should be used for compensation controls. After the compensations are adjusted the analysis can continue. General gating includes exclusion of dead cells using a live/dead fixable dye (in this case Near-IR from Thermofisher) and gating on CD3+ cells to distinguish T cells.

Table 26. List of useful antibodies for identifying human T_{RM}

Species	Epitope	Clone	Company	Fluorochrome
Human	CD3	UCHT1	BD	BUV661, BUV395
Human	CD4	SK3	BD	BUV737
Human	CD8	SK1	BD	BUV805
Human	CD69	FN50	BD	BUV395, BV421
Human	CD28	CD28.2	BD	BV605
Human	CD103	Ber-ACT8	BD	FITC
Human	CD49a	SR84	BD	PE
Human	TNFα	Mab11	BD	FITC, PeCy7
Human	CD45RA	HI100	BD	BUV563
Human	CD25	2A3	BD	PE, BV605
Human	GZMB	GB11	BD	AF700, AF647
Human	CD137	4B4-1	Thermofisher	AF647, PeCy7
Human	CD4	S3.5	Invitrogen	QD705
Human	CD3	UCHT1	Invitrogen	QD605
Human	CD45RA	MEM-56	Invitrogen	QD655
Human	CD3	OKT3	ThermoFisher	eVolve605, SuperBright600
Human	CD103	B-Ly7	ThermoFisher	PE, PeCy7, FITC
Human	Eomes	WD1928	ThermoFisher	eFluor660
Human	HLA-DR	LN3	ThermoFisher	FITC
Human	2B4	eBioDM244	ThermoFisher	APC
Human	CXCR6	K041E5	Biolegend	APC
Human	CCR5	J418F1	Biolegend	BV421
Human	CD27	O323	Biolegend	BV510, BV650
Human	CD103	Ber-ACT8	Biolegend	AF647, BV711, BV605, BV421
Human	CD69	FN50	Biolegend	PeDazzle594, AF647
Human	Tbet	4B10	Biolegend	BV421
Human	IFNγ	4S.B3	Biolegend	eF450, BV785, Pe
Human	PD-1	EH12.2H7	Biolegend	BV421, PeCy7
Human	CTLA4	L3D10	Biolegend	PE
Human	TNFα	Mab11	Biolegend	PeDazzle594, BV421

CD3$^+$ T cells should then be separated into CD4$^+$ and CD8$^+$ T cells. The common markers of T_{RM} are CD69 and CD103 (as shown in Fig. 121), but many more markers have been identified up to now (described above and listed in Tables 27 and 28).

1.12.6 Pitfalls. Isolation of T cells from human tissues often requires enzymatic digestion with collagenases, which can affect the expression of certain proteins, particularly chemokine receptors, such as CCR6 [920], due to their large structure and multiple transmembrane domains. This should be kept under consideration when staining tissues that have undergone enzymatic digestion. The preferred collagenase used by multiple research groups is collagenase D [895, 899, 901]. Furthermore, cryopreservation can also affect expression of proteins, such as L-selectin/CD62L. Various markers of T_{RM} are shared between tissues, but it should be kept in mind that some markers and ratios of certain populations can vary per tissue compartment. The amount of unconventional T cells, such as TCR-γδ, MAIT cells and NK T cells, should also be determined, which varies per tissue. If there are significant amounts of these unconventional T cells, a dump channel should be applied.

1.12.7 Tips/tricks.

1. Careful panel design is important with more than 10 color flow
   (a) The major problem is the scatter caused by compensation of some fluorochromes, not per se the amount needed to compensate
2. Some examples of compensation issues
   (a) To use BUV805, BV737, and BV785 in the same panel, BD FACSymphony is required
   (b) BUV661 spills into APC so BUV661 signal should not be too bright and APC signal should be relatively bright
   (c) BUV737 spills into BUV805 so using markers that are clearly distinct from each other such as CD4 and CD8 is advisable
   (d) A lot of compensation is required between BV605 and BV650
   (e) Properly titrating antibodies and not using antibodies at too high concentrations can significantly help
3. Some tissues suffer from autofluorescence
   (a) It can help to keep a Brilliant violet channel empty or sometimes the autofluorescence can be gated out when

Table 27. Markers used to identify human T$_{RM}$

Marker	Expression	Functional implication	Reference
CD69	+	Tissue retention	[895–903]
CD103	+ (mucosa/skin)	Tissue retention	[895–897, 899–902]
CD45RA	−	Memory defining	[895–897, 899–902]
CD45RO	+	Memory defining	[895–897, 899–902]
CD27	+/−	Co-stimulation	[899, 901]
CD28	+/−	Co-stimulation	[896, 901]
CCR7	−	Lymph node homing	[895–902]
CD49a	+	Retention	[900–902]
CXCR6	+	Recruitment/retention	[900–903]
CCR5	+	Recruitment/retention	[901–903]
CXCR3	+	Recruitment/retention	[901, 902]
CX3CR1	−	Cytotoxic function/endothelial adhesion	[900, 903]
IL-7Ra	+	Homeostasis	[896, 900]
PD-1	+	Inhibitory	[899, 901, 902, 907]
CTLA-4	+	Inhibitory	[901, 902]
2B4	+	Inhibitory	[901]
CD101	+ (CD8 T$_{RM}$)	Inhibitory	[907]
NKG2A	+ (CD8 T$_{RM}$)	Inhibitory NK receptor	[919]
CD94	+ (CD8 T$_{RM}$)	Forms inhibitory receptor complex with NKG2A	[919]
Eomes	−	Effector function/effector differentiation	[899, 901, 902]
T-bet	-/+	Effector function/differentiation/lineage defining	[899, 901, 902]
HLA-DR	−	Activation	[907]
CD25	−	Activation	[895, 897, 902, 907]
CD38	−	Activation	[907]
Ki67	−	Proliferation	[897, 902, 907]

two fluorochromes, where no double positive signal is expected, are plotted against each other

4. Isotype controls or FMOs (fluorescence minus one) should be used if there is only a shift in a population instead of a clear staining/bimodal populations
5. To avoid aggregates caused by some fluorochromes, the antibody mixes can be centrifuged at 1400 rpm for 10 min. Afterwards the aggregates should be pelleted and the antibody mix should not be pipetted from the bottom of the tube or resuspended again.
6. A dump channel may be necessary for unconventional T cells such as TCR-γδ, MAIT cells, and NK T cells and these can be for example put in the same channel as the live/dead marker to exclude them

1.13 Immune senescence (aging) of human T cells

In human aging, the functionality of the adaptive immune system diminishes, known as immunosenescence. Immunosenescence leads among others to increased susceptibility to infectious diseases through diminished responses to pathogens [921]. In addition, a continual low-grade pro-inflammatory milieu is associated with aging (inflammaging), which is linked to several aging-associated diseases with an inflammatory pathophysiology such as various neurodegenerative [922] and metabolic diseases [923], leading to increased mortality. There is great interest in the physiology of aging to better understand the aging process and techniques to monitor them. Within the T-cell repertoire, aging is known to lead to a loss of naïve T-cells, with a reciprocal increase in effector memory T-cells [921]. This process is fueled among others due to involution of the thymus from adolescence onward.

Table 28. Effector molecule expression/production by human T$_{RM}$

Marker	Expression	Function	Reference
IFN-γ	+ (upon stimulation)	Kill or recruit cells	[899–901]
TNF-α	+ (upon stimulation)	Kill or recruit cells	[901]
IL-2	+ (upon stimulation)	Survival/proliferation	[900, 901]
IL-17a	+ (upon stimulation)	Extracellular pathogen protection	[900]

Table 29. Examples of flow cytometry markers used to identify aged T-cells in humans

Marker	Expression	Functional implication	References
Loss of naïve cells			
CD28	−	Co-stimulation	[430, 921, 924, 926, 927, 929, 931–933]
CD27	−	Co-stimulation	[924, 927, 928, 931]
CD45RA	−	Memory	[925, 928, 930, 931, 933]
CCR7	−	Homing to secondary lymphoid organs	[924, 931, 933]
CD62L	−	Homing to secondary lymphoid organs	[932]
Decrease in recent thymic emigrants			
PTK7	−	Tyrosine-kinase	[933]
CD103	−	Integrin	[933]
Increase in senescent cells			
CD57	+	Terminal differentiation	[430, 924, 926, 927, 930, 933]
KLRG1	+	Immune checkpoint	[924, 927, 931]
HLA-DR	+	T-cell activation	[926]
Loss of mitochondrial function			
MitoSOX	+	Mitochondrial reactive oxidative species	[928]
MTG	+/−	Mitochondrial mass	[928]
TMRM	+	Mitochondrial membrane potential	[928]
Impaired autophagy			
LC3	−	Autophagosomes	[427, 430, 928]
LysoID	−	Lysosomes	[430]

This naïve T-cells fraction is conventionally studied by FCM using Abs against a panel of (co-stimulatory) surface antigens such as CD28 [924]. See Table 29 for examples of commonly used FCM markers for the identification of aged human T cells. The decrease of the naïve T-cell population is accompanied by an increase of oligoclonal effector memory populations [925]. This process is driven by latent viral infections, such as cytomegalovirus (CMV). Especially in the oldest-old individuals, large proportions of the T-cell repertoire seems to be occupied by CMV-specific effector memory T-cells [926]. Therefore, when studying human aging in T-cells, the CMV seropositivity status of the subject must be taken into account. Age-associated T-cell dysfunction include replicative senescence that is characterized by the expression of CD57 and KLRG1, which were found to be increased in both CD4 and $CD8^+$ T-cells in the elderly [927]. Other age related processes include perturbations in T-cell homeostasis and mitochondrial dysfunction, which can both be assessed using FCM. For example, a recent study found that while mitochondrial mass increased in $CD8^+$ T-cells with age, they exhibited a diminished membrane potential, indicating a loss of mitochondrial function which was accompanied by an increase of mitochondrial reactive oxygen species [928]. Another process, which is known to be vital to T-cell homeostasis during aging, is autophagy. Lysosomal degradation of defective proteins and recycling thereof is critical for the homeostasis of the metabolically active T-cell. Indeed, in T-cells of older individuals a decreased (basal) autophagy level was found [430], with lower levels in effector memory T-cells [929]. Most methods to quantify changes in autophagy (see Chapter V Section 9: Autophagy) use immunoblotting (requires a protein quantity that is not always available in human aging studies) or immunofluorescence imaging (laborious and not high-throughput), however

recently several flow-cytometric assays for quantifying autophagy were developed. These assays require transfection with reporter constructs which could potentially alter the characteristics of the cells of interest [427]. To better understand healthy aging, one approach is to study the offspring of long-lived individuals compared to their partners. Interestingly, the T-cells of offspring possess higher proportions of naïve T-cells [930], lower levels of senescent T-cells [927], better responses after stimulation with viral antigens [931] and improved activation-induced autophagic activity [932]. Finally, markers of T-cell immunosenescence can be used as biomarkers to monitor lifestyle interventions in the context of human aging. For example, a recent study demonstrated that high level of physical activity maintains higher levels of naïve T-cells and T-cells with phenotypes of recent thymic emigrants in the elderly, as compared to inactive elderly [933].

1.14 Human FOXP3⁺ regulatory T cells

1.14.1 Overview. Regulatory T cells (Tregs) are necessary to protect against autoimmune disease and maintain immune homeostasis. Human Tregs are usually defined by high co-expression of the FOXP3 transcription factor and CD25, as well as low expression of CD127. Other aspects of their phenotype can vary widely depending on their state of activation and location throughout the body. In order to identify human Tregs on the basis of FOXP3 expression, flow cytometric staining protocols need to ensure effective permeabilisation of both cellular and nuclear membranes. Another consideration is how to differentiate between Tregs and activated conventional T cells (Tconvs) that transiently express FOXP3 and CD25. In this section, we will discuss

protocols and key considerations for staining human Tregs in whole blood, peripheral blood mononuclear cells (PBMCs) and intestinal biopsies.

1.14.2 Introduction.

1.14.2.1 Human Treg frequencies and distribution.   Tregs are present throughout the human body and their abundance in circulation and tissues is age dependent [907, 934]. For example, in early life (i.e., under two years), Tregs (defined as CD25^{high}CD127^{low}FOXP3$^+$ cells) make up 30–40% of CD4$^+$ T cells in the lung and gut but these proportions decline to 1–10% in adults [935]. In peripheral blood, Tregs decrease from ~20% of total CD4$^+$ T cells in infants (i.e., under two years) to ~5% in healthy adults [935]. However, once adult proportions of Tregs are reached, their frequencies in blood do not appear to change with age (from 20 to 75 years; Tregs defined as CD25^{high}CD127^{low} cells in this study) and they maintain suppressive capacity [936, 937].

1.14.2.2 Human Treg subsets.   As in mice, it is generally accepted that human Tregs can be thymically derived or induced from Tconvs in the periphery under specific conditions [938]. In mice, high expression of Helios and low expression of Neuropillin-1 (Nrp-1) has been proposed to discriminate between thymus Treg and peripherally-induced Tregs [775, 776]. See also Chapter VI Section 1.6 Murine Foxp3$^+$ regulatory T cells. In humans, however, the validity of these markers is less clear because not all naive/thymus-derived Tregs express Helios [939] and it has been reported that this protein can also be expressed by activated T cells [779]. On the other hand, human Tregs that express high levels of Helios have a potent suppressive phenotype and are more stable [940], so it is still useful to monitor its expression. Nrp-1 is almost undetectable in human peripheral Tregs [941].

Of particular interest is that Tregs subsets can be readily identified in healthy adults with phenotypes similar to the well-described CD4$^+$ T helper (Th) cell subsets (see also Chapter VI Section Human CD4 and CD8 T cells). Specifically, Th1, Th2, Th17, and Th17.1-cell-like Tregs can be detected in peripheral blood and identified on the basis of expression of Th-cell-associated chemokine receptors and/or transcription factors [942]. In contrast to Th cell subsets, however, in healthy individuals, Treg subsets typically do not make high amounts of lineage-associated cytokines (e.g., IFN-γ, IL-2, IL-4, IL-13) [943], likely because of the transcriptional repressor function of FOXP3. An exception is IL-17: Th17 Tregs co-express FOXP3 and IL-17 yet remain functionally suppressive [944, 945]. Although the relevance of Th-like Tregs in human disease and homeostasis is an area of intense investigation, it currently appears that they are tailored to regulate immune responses driven by their corresponding Th cell subset. Mechanistically, this could occur by differential homing receptor expression, thus ensuring that Th-like Tregs co-localize with their Th cell subset counterparts [946].

1.14.2.3 Measuring human Tregs by FCM.   Identifying human Tregs using FCM is complicated by the facts that FOXP3 is an intranuclear marker with a relatively low intensity of expression, and there is currently no known single marker that is unique to human Tregs. Moreover, even within Tregs the intensity of FOXP3 expression can change, with naive or resting populations of Tregs expressing lower levels of FOXP3 than activated Tregs [675, 947]. Hence, accurate separation between Tconvs, resting Tregs, and activated Tregs can only be done if there is a relatively high dynamic range of FOXP3 staining and often requires addition of other makers such as CD45RA. Currently the only way to confidently quantify human Tregs is to use a panel of different markers and then carry out parallel functional [672], gene expression [948], and/or epigenetic analyses [949, 950].

In terms of surface phenotype, the best accepted combination of markers is high expression of the IL-2 receptor α chain (CD25) and low expression of the IL-7R α chain (CD127) [936, 951]. Importantly this CD25^{high}CD127^{low} Treg definition can be used to isolate relatively pure populations of viable peripheral Tregs in both the memory (CD45RO$^+$) and naïve (CD45RA$^+$) compartments. As described above FOXP3, CD25 and CD127 are both expressed as a continuum, so in order to be confident in gating strategies, it is essential that there is good separation between low, medium, and high expressing populations.

An outstanding question is should human Tregs be defined as CD4$^+$ cells that are CD25^{high}CD127^{low}, CD25^{high}FOXP3$^+$, FOXP3$^+$, or CD25^{high}CD127^{low}FOXP3$^+$. Currently the literature reports "Tregs" as cells defined by any one of these different variations. It is therefore critical to consider how studies define "Tregs" and whether or not the gating strategies used are sufficiently stringent. On the basis of current knowledge, the most rigorous way to define Tregs is as CD25^{high}CD127^{low}FOXP3$^+$ cells. However, use of FOXP3 is not possible when viable cells are being sorted and sometimes it may not be feasible to include all three markers due to instrument limitations. If all three markers are not possible then at a minimum two should be used, either CD25^{high}FOXP3$^+$ or CD25^{high}CD127^{low}. Measuring only CD25 or only FOXP3 does not provide sufficient resolution on a dot plot to set an accurate gate. Since Tconvs can also upregulate CD25 and FOXP3, and downregulate CD127 [947, 952], it is critical to set gates for all of these markers on resting populations of T cells, typically using blood cells from healthy individuals. This is particularly helpful when analyzing Tregs and Tconvs in tissues where there can be a significant proportion of activated Tconvs and it thus become important to differentiate between these cells on the basis of the intensity of CD25 and FOXP3 expression. Addition of other human Treg-associated markers can help increase confidence in Treg identification in these settings.

Here, we detail optimized protocols for detecting human Tregs in whole blood, PBMCs, and intestinal biopsies. We also provide some tips in Table 30 for staining additional human Treg markers that are not specifically included in the protocols outlined and highlight some key differences between mouse and peripheral human Tregs. The reader is also referred to our previously

Table 30. Summary of key functional and phenotypic human Treg markers

Marker	Technical notes*	References
Functional and/or phenotypic makers of human Tregs		
IL-10	Difficult to detect in peripheral Tregs. PMA/Ionomycin stimulation for at least 6 hours is required; staining with the IL-10 capture assay (Miltenyi Biotech) or other stimuli may give better results. Recommended clone is JES3-9D7.	[959–961]
LAP and GARP	Expression is optimal after 24 h of TCR stimulation.	[962, 963]
LAG-3	Low expression on non-activated Tregs. Recommended clone for activated cells is REA351. Also described as a marker of type 1 regulatory T cells.	[961, 964, 965]
PD-1	Levels are increased after activation or with intracellular staining.	[966]
AREG	Expression is optimal after PMA/Ionomycin stimulation for 4 hours. Works with FOXP3 buffers. Recommended Ab clone is BAF262 (RnD systems).	[967]
CD39	A common single nucleotide polymorphism (SNP) in humans results in low CD39 expression. Individuals who are homozygous for this SNP have <10% CD39$^+$ Tregs compared to ~50% CD39$^+$ in heterozygotes or noncarriers. Clone A1 does not block CD39 enzymatic function.	[968–970]
HLA-DR	Not expressed on murine Tregs; defines a memory and highly suppressive population.	[971]
CTLA-4; CD152	Due to rapid receptor internalization, staining is improved with intracellular staining or inclusion of the mAb for a period of time in culture.	[972, 973]
Blimp-1	Expression is increased after activation and in the presence of IL-2. Recommended clone is 6D3.	[974]
CD49d	In combination with CD127, low level expression of CD49d can be used to differentiate between activated Tconv and Treg.	[975]
Ki67	Marker of cell proliferation. Although anergic in vitro, when tested directly ex vivo, Tregs show a high proportion of cells expressing Ki67.	[976]
Not known to be detectable on human peripheral blood Tregs		
CD73	Despite being expressed on murine Tregs, low/no expression of these markers	[977, 978]
CD103	(CD73, CD103, ST2, neuropilin-1 and OX40) has been observed on	[935, 979]
ST2 (IL33R)	non-activated, peripheral human Tregs in healthy individuals. More	[953, 967]
Neuropilin-1	research is needed to asses if these proteins may be expressed on	[941, 980]
OX40	tissue-infiltrating Tregs, and/or in various disease/cell activation states	[981, 982]

* Technical notes are from our experience and largely unpublished.

published methods for staining human Tregs within omental adipose tissue [953], thymus tissue [954] and using a mass cytometry platform [955, 956], as well as a review describing a comprehensive comparison of mouse and human Treg markers [957]. The methods described here are focused on studying Tregs in healthy subjects. The markers of choice may vary in different disease contexts. For example, tumor infiltrating Tregs often have a distinctive phenotype associated with T cell exhaustion and the addition of markers such as PD-1 may be beneficial in a FCM panel [958].

The following points are key for analysing human Treg by FCM:

1. In order to accurately define Tregs, at least two markers must be used—either CD25 and CD127 or CD25 and FOXP3; use of all three is optimal. If FOXP3 cannot be used then CD25 must be used in combination with CD127.
2. To set an accurate FOXP3 gate, a biologically negative population (e.g., CD4$^+$ Tconvs or CD8$^+$ T cells) is required.
3. The selected CD25 mAb and anti-FOXP3 mAbs must be conjugated to a bright fluorochrome so that there is good separation

between mid and high expressing cells (e.g., BB515, PE-Cy7 or PE).
4. Separation of cells expressing mid and high levels of CD25 and FOXP3 can be enhanced by the use of two monoclonal Ab clones recognising independent binding epitopes, conjugated to the same fluorochome.

1.14.3 Staining Tregs from unmanipulated whole blood.

1.14.3.1 Step-by-step sample preparation. In a clinical context, it is desirable to quantify Tregs in unmanipulated whole blood. In contrast to the more widely used approach of phenotyping cryopreserved PBMCs, this method allows quantification of absolute Treg numbers and avoids variability introduced by cryopreservation [983]. Several studies have compared different anti-human FOXP3 Ab clones, and although there is some debate, there is a general consensus that the 236A/E7 and 259D clones are optimal [984–988]. The following protocols and associated Ab panels should be used as a guide; substitution of Ab clones/conjugations
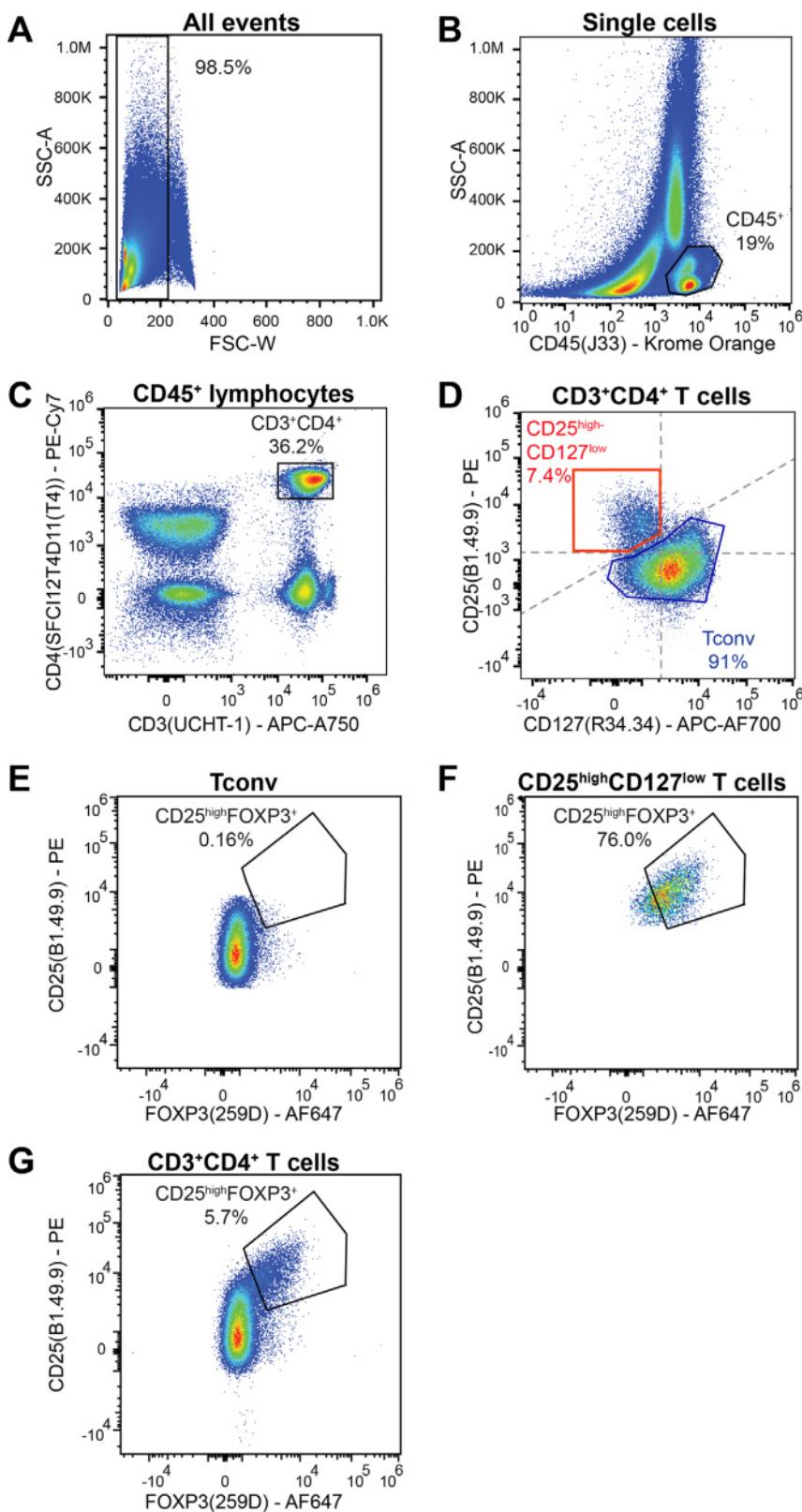
Figure 122. Gating strategy to quantify $CD25^{high}CD127^{low}FOXP3^+$ Tregs using whole blood and DuraClone tubes. (A–C) From total events, single cells were selected and $CD45^+$ lymphocytes were gated based on SSC properties and CD45 expression. (D) From $CD4^+CD3^+$ T cells the $CD25^{high}CD127^{low}$ gate was identified. If the CD25 resolution is adequate then typically there is a clear separation of this population on a diagonal axis indicated by the grey dashed line. (E and F) show the expression of $FOXP3^+$ within the indicated $CD25^{high}CD127^{low}$ or Tconv cells gates. (G) Identification of $CD25^{high}FOXP3^+$ Tregs from total $CD3^+CD4^+$ T cells (panel C).

Table 31. DuraClone Treg panel (Beckman Coulter #B53346)

Marker	Fluorochrome	Clone
CD3	APC-A750	UCHT-1
CD4	PE-Cy7	SFCI12T4D11(T4)
CD25	PE	B1.49.9
FOXP3	AF647	259D
Helios	PacBlue	22F6
CD39	PC5.5	BA54
CD45RA	FITC	2H4LDH11LDB9(2H4)
CD45	KromeOrange	J33
CD127**	APC-AF700	R34.34

** An additional Ab added in liquid form in step 1. Beckman Coulter, #A71116

requires titration and testing in combination with the selected buffer system. Below we present two protocols using reagents from different manufacturers to quantify Tregs in whole blood.

1.14.3.2 Whole Blood Protocol 1A. Staining CD25^{high}CD127^{low}FOXP3+ Tregs from whole blood using pre-formatted DuraClone tubes from Beckman Coulter (Figure 122).

Beckman Coulter DuraClone tubes are precoated with dried down Ab cocktails (Table 31), thus reducing pipetting time, and increasing reproducibility because there is no variation introduced by day-to-day mixing of wet Ab cocktails. The use of these reagents is an ideal way to standardize the FCM of longitudinally samples collected in multi-site clinical trials [983]. Many Beckman-Coulter Abs are designed for clinical use so they have low lot-to-lot variation and are thus ideal for use as drop-in Abs with DuraClone tubes (providing fluorochrome brightness, clone affinity, etc., is acceptable). For optimal results with these tubes cytometers must be calibrated with standardized beads to maintain target voltages over time.

1.14.3.3 Surface and intracellular staining.

1. Add 100 μL of whole blood to the DuraClone Treg tube (Table 31) and vortex immediately. Add any extracellular drop in Abs at this step (e.g., we drop in 5 μL of CD127 APC-AF700, Beckman Coulter, #A71116).
2. Incubate for 15 mins at room temperature in the dark.
3. Wash with 3 mL of PBS.
4. Remove the supernatant with a 1 mL pipette followed by a 200 μL pipette.
5. Adjust volume to exactly 100 μL with FBS.
6. Add 10 μL of PerFix-nc reagent buffer 1 (Fixing buffer— Beckman Coulter, #B31164).
7. Incubate for 15 min in the dark.
8. Add 800 μL of PerFix-nc Buffer 2 (Permeabilization buffer – Beckman Coulter, #B31165).
9. Incubate for 15 min at RT in the dark.

10. Centrifuge for 3 min 500 × g and remove only the top 400 μL of buffer with a 1 mL pipette.
11. Transfer contents from original to Treg Tube 2 and vortex at high speed for 2 × 4 s.
12. Incubate at room temperature for 60 min in the dark.
13. Wash with 3 mL of PBS, vortex, and incubate at room temperature for 5 mins.
14. Centrifuge at 500 × g for 5 min at room temperature.
15. Decant in one smooth motion and gently blot tube.
16. Vortex for 8 s.
17. Re-suspend the cell pellet in 3 mL of 1× perFix nc buffer 3 (Beckman Coulter, #B31166) and vortex.
18. Centrifuge at 500 × g for 5 min at room temperature
19. Decant supernatant in one smooth motion and gently blot tube.
20. Vortex the cell pellet for 8 s.
21. Add 350 μL of 1× Perfix-nc Buffer 3 (final volume should be 400 μL as residual volume will be around 50 μL) for data acquisition.

1.14.3.4 Data analysis. From total events, doublets were excluded and CD45+ lymphocytes were gated based on SSC properties and CD45 expression (Fig. 122A and B). CD4+CD3+ T cells were then gated and followed by CD25^{high}CD127^{low} cells (Fig. 122C and D). If the CD25 resolution is adequate then typically there is a clear separation of this population on a diagonal axis indicated by the grey dashed line (Fig. 122D). The remainder of the cells in the CD3+CD4+ gate were classified as Tconvs (Fig. 122D). The FOXP3 gate is made on the basis of FOXP3 and CD25 expression in Tconvs (gated as CD25$^-$ cell); i.e., the gate should be set such that there are very few FOXP3+ cells in the Tconv population (Fig. 122E). This FOXP3 gate is then applied to the CD25^{high}CD127^{low} cells (Fig. 122F). If CD127 is not used, then Tregs can be identified as CD25^{high}FOXP3+ cells (Fig. 122G), but this population is harder to clearly discriminate.

1.14.3.5 Pitfalls.

1. Ensure that the volume is exactly 100 μL before the fix-perm buffers are added for optimal transcription factor staining. The Beckman SOP suggests using 50 μL of whole blood but the reagents also work well with 100 μL of blood. Use of more blood allows collection of more cells and thus better quantification of rare populations.

1.14.3.6 Top tricks.

1. In step 1, other markers of interest can be dropped in as wet Abs (e.g., CD127$^-$APC-AF700).
2. Dropping in CD25 mAb M-A251 PE improves CD25 resolution.

1.14.3.7 Whole Blood Protocol 1B. Staining CD25^{high}CD127^{low}FOXP3+ Tregs using Ab cocktails (Figure 123).
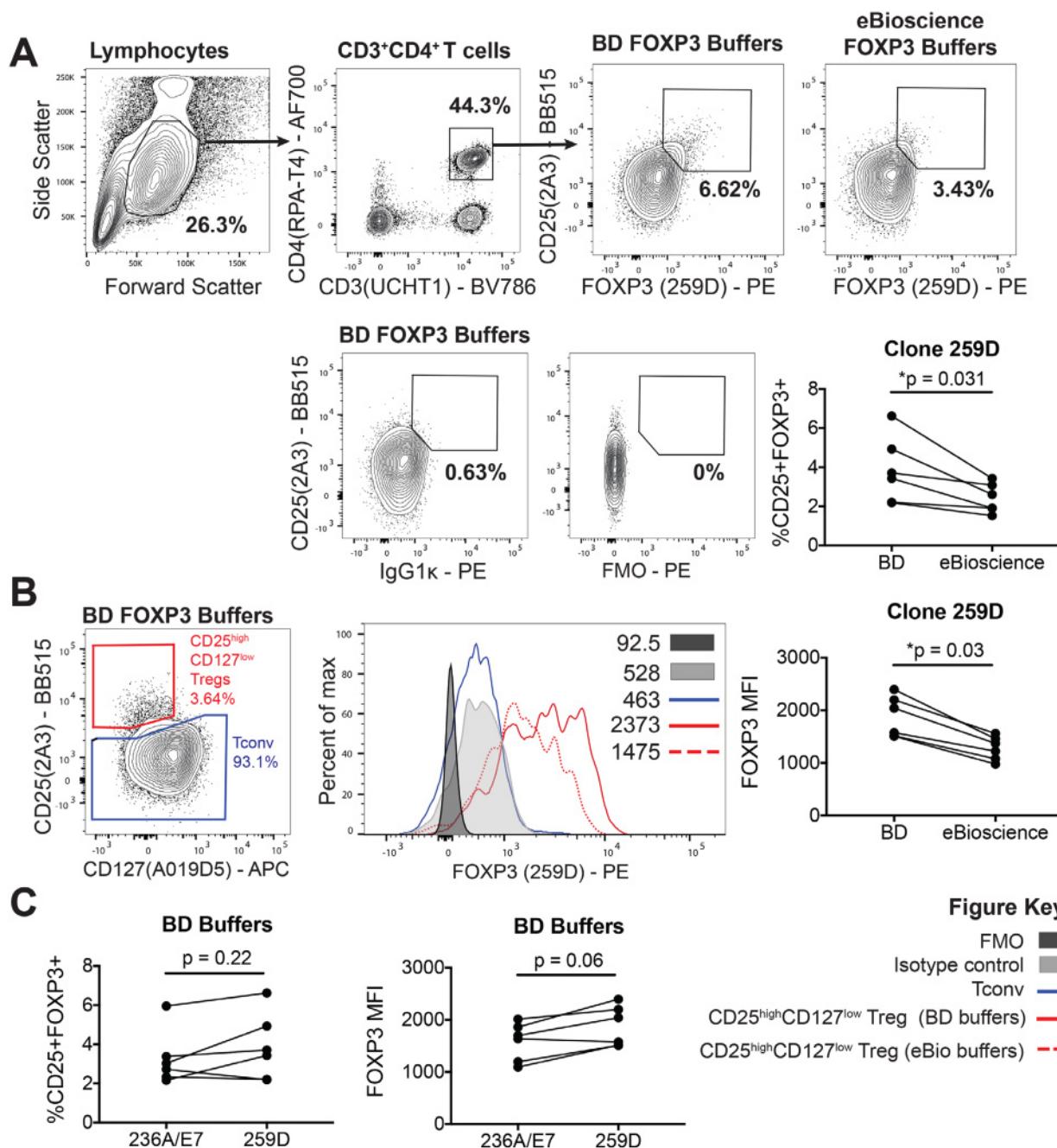
Figure 123. Phenotyping CD25^{high}CD127^{low}FOXP3$^+$ Tregs in whole blood. Representative staining of healthy adult peripheral whole blood with the Ab panel listed in Table 32. (A) Gating strategy and representative data for CD25^{high}FOXP3$^+$ staining following fixation and permeabilisation with either BD or eBioscience FOXP3 buffer sets. Gates were set on the basis of an isotype control (for comparison the lack of utility of an FMO control for setting the FOXP3 gate is shown). (B) Representative data for CD25^{high}CD127^{low} staining and FOXP3 MFI with the indicated gated populations of CD25^{high}CD127^{low} or Tconv cells. Right graph shows the FOXP3 MFI if samples are processed with BD or eBioscience buffers. (C) CD25^{high}FOXP3$^+$ frequencies and FOXP3 MFI in CD25^{high}CD127^{low} cells if staining is performed with the 236A/E7 or 259D anti-FOXP3 mAbs. All graphs show data from 6 healthy adults. Wilcoxon signed-rank tests were performed on paired samples.

This protocol was optimized by carrying out comparisons between the BD FOXP3 Buffer Set (#560098) and Thermo Fisher eBiosciences FOXP3 Fix/Perm Buffer Set (#00-5523-00), as well as the anti-FOXP3 259D and 236A/E7 mAb clones, as per Table 32.

1. Aliquot whole blood (up to 500 μL) into 5 mL round bottom tubes.
2. Add extracellular Abs and stain for 15 min at room temperature.
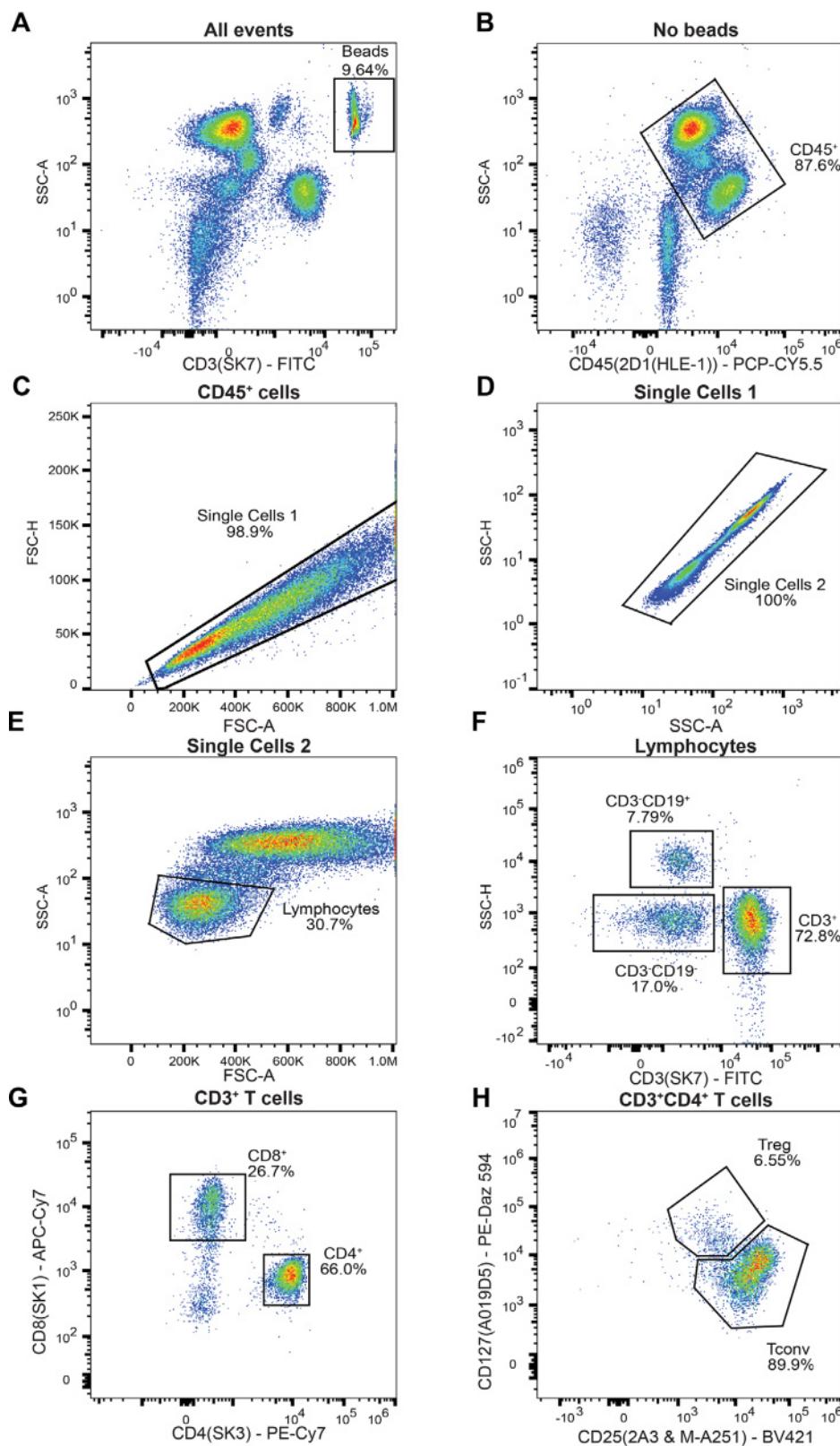
Figure 124. Quantification of CD25^{high}CD127^{low} Tregs using whole blood. (A) Count beads were gated based on SSC properties and CD3 expression. (B-E) After the exclusion of the beads, CD45$^+$ whole blood cells were selected, doublet cells were excluded, and total lymphocytes were gated based on SSC and FSC properties. (F–H) From CD3$^+$ T cells, CD4$^+$CD8$^-$ T cells were selected. Within the latter gate, CD25^{high}CD127^{low} Tregs and T conventional cells were identified. The Trucount tubes contain a number of beads that is used to calculate the absolute counts of the Tregs per μL based on the equation: (Number of positive Treg events/Number of bead events) × (Number of beads per tube/Test blood volume).

Table 32. Panel for liquid Ab cocktail-based staining of CD25^{high}CD127^{low}FOXP3$^+$ Tregs in whole blood

Marker	Dilution	Fluorochrome	Clone	Company	Catalog
CD3	1/100	BV786	UCHT1	BD	565491
CD4	1/100	AF700	RPA-T4	BD	557922
CD25	1/25	BB515	2A3	BD	564467
CD127	1/50	APC	A019D5	BioLegend	351315
FOXP3*	1/25	PE	259D	BioLegend	320207
FOXP3*	1/25	PE	236A/E7	Invitrogen	12-4777-42

* These FOXP3 clones are equivalent and either can be used in this panel.

3. Lyse red blood cells by adding 2 mL of BD FACSLyse solution (10× concentrate diluted to 1× stock in distilled water). Vortex to mix and incubate for 10–15 min at room temperature.
4. Add 2 mL staining buffer to wash and centrifuge at 500 × *g* for 5 min.
5. Transfer cell pellet (usually up to 10^6 cells per condition) into a V-bottom 96-well plate.**
6. Add 200 µL of Buffer A solution from BD Human FOXP3 buffer set (10× buffer A concentrate diluted to 1× stock in distilled water) and incubate for 10 min at room temperature.
7. Centrifuge plate at 1000 × *g* for 3 min, flick off supernatant, and blot to dry. It is important that the cell pellet is as dry as possible.
8. Add 100 µL of Buffer C solution from the BD Human FOXP3 buffer set (50× buffer B concentrate diluted to 1× stock in Buffer A) for at least 45 min in the dark at room temperature.
9. Add 100 µL of PBS and spin at 1000 × *g* for 3 min, flick off supernatant.
10. Repeat step 9 as residual Buffer C can interfere with Ab staining.
11. Add intracellular Abs to cells and incubate for 30 min in the dark at room temperature.
12. Wash cells in 100 µL of staining buffer, spin at 1000 x *g* for 3 min, flick off supernatant.
13. Resuspend in at least 150 µL of staining buffer for data acquisition.

**From step 6 onwards comparisons with eBiosciences FOXP3 staining kit used method in section 1.14.4.2

1.14.3.8 Data analysis. Optimal staining of FOXP3 requires efficient fixation and permeabilisation. Here, two commercially available FOXP3 staining buffer kits were compared. Cells in whole blood were stained as described above using either BD or eBioscience FOXP3 staining buffers. FOXP3 and CD25 staining in total CD3$^+$CD4$^+$ T cells was analyzed and the percent of cells that were CD25^{high}FOXP3$^+$ was determined using a gate set on cells stained with an isotype control (Figure 123A). The data show that in this case there is better resolution of FOXP3 when cells are prepared with BD buffers compared to eBioscience buffers (Figure 123B). No difference in FOXP3 staining was observed between the 236A/E7 or 259D anti-human FOXP3 Ab clones (Figure 123C).

1.14.3.9 Pitfalls.

- Insufficient removal of residual buffer A will result in less effective permeabilization in buffer B. If staining in a 96-well V bottom plate is not possible, then use a tube with a conical (not round) bottom to aid in removing all residual buffer after centrifugation steps.
- Buffer B deteriorates with exposure to light so always make fresh (i.e., on the same day) working stocks of FOXP3 buffers.

1.14.3.10 Top tricks.

- Human FOXP3 buffer set (BD, #560098) is superior to FOXP3 Fix/Perm Buffer Set (Thermo Fisher eBiosciences, #00-5523-00) for FOXP3 staining when whole blood is used.
- An alternate to step 2 is to add all extracellular and intracellular Abs together in step 11 (provided extracellular Ab epitopes are not affected by FOXP3 buffers; this must be determined empirically).

1.14.3.11 Whole Blood Protocol 1C. Determination of CD25^{high}CD127^{low} Treg absolute counts using BD Truecount tubes, supplemented with drop in Abs (Figure 124)

As cells can be lost during wash and centrifugation steps involved in routine FCM protocols, the use of a lyse-no-wash procedure (LNW) is optimal to accurately determine the absolute count of leucocyte populations [989]. However, as LNW procedures preclude fixing and permeabilization, in this protocol, Tregs can only be identified using CD25 and CD127. The protocol is based on combining of BD Trucount tubes and a 6 colour TBNK Ab cocktail (commonly used for leucocyte enumeration in clinical immunology laboratories) with drop in Abs to identify Tregs as listed in Table 33. This procedure can be used to enumerate both Tregs and other leucocyte populations (CD3, CD4, CD8, B cells, and NK cells).

1.14.3.12 Staining Procedure.

1. Add the Abs listed in Table 33 to a Trucount tube (Cat number 340334).
2. Invert tube containing whole blood several times to ensure homogeneity

Table 33. Panel enumeration of Tregs (defined as CD25^{high}CD127^{low}) in whole blood

Marker	Volume	Fluorochrome	Clone	Company	Catalog
CD3	20 µL BD 6 color TBNK cocktail	FITC	SK7	BD	644611 or 337166 (with 50 Trucount Tubes)
CD16/56	″	PE	B73.1/NCAM16.2	″	″
CD45	″	PerCP-Cy5.5	2D1	″	″
CD4	″	PE-Cy7	SK3	″	″
CD19	″	APC	SJ25	″	″
CD8	″	APC-Cy7	SK1	″	″
CD25	1 µL	BV421	2A3	BD	564033
CD25	1 µL	BV421	M-A251	BD	356114
CD127	1 µL	PE-Dazzle 594	A019D5	Biolegend	351336

3. Aliquot exactly 100 µL whole blood into the bottom of a Trucount tube and vortex. Adopting a sound pipetting technique (e.g., a low immersion depth of the pipette tip) and possibly reverse pipetting in this step is advisable to ensure accuracy.

4. Incubate for 15 min at room temperature in the dark.

5. Prepare 1× lysing solution by adding 900 µL distilled water to 100 µL BD 10× Lysing solution (Cat number 349202).

6. Once 15 min incubation is complete, add 900 µL of diluted 1× lysing Buffer and vortex immediately.

7. Incubate at room temperature for 15 min in the dark, vortex* half way through incubation.

8. Vortex again and leave on ice until acquisition.

9. Vortex thoroughly immediately before acquisition.

Data analysis

Count beads were gated based on SSC properties and CD3 expression (Fig. 124A). After the exclusion of the beads, CD45^{+} whole blood cells were selected, doublet cells were excluded, and total lymphocytes were gated based on SSC and FSC properties (Figure 124B-E). From CD3^{+} T cells, CD4^{+}CD8^{-} T cells were selected. Within the latter gate, CD25^{high}CD127^{low} Tregs and Tconvs were identified. The Trucount tubes contain a number of beads that is used to calculate the absolute counts of the Tregs per µL based on the equation: (Number of positive Treg events/Number of bead events) × (Number of beads per tube/Test blood volume).

Top tricks

1. Efficient lysis of red blood cells is vital for optimal assay performance. Ensure tubes are vortexed vigorously at each step indicated.

2. Enumeration of Tregs is stable for up to 44 h post staining.

1.14.4 Staining Th-cell like Treg subsets in PBMCs.

1.14.4.1 Step-by-step sample preparation. The following protocol details how to stain Th-cell like Treg subsets in PBMCs (isolated as previously described [983]). The gating strategy is in Fig. 125 and the panel is detailed in Table 34. This gating strategy is based on the current literature [863, 942, 990–992]. Additional markers such as CD161 [869], CRTH2 [864] and CCR10 [878]

can also be added to further subcategorize the Th-cell like Treg subsets (Table 35).

1.14.4.2 Staining of Th Treg subsets within PBMCs (Figure 125).

1. Transfer up to 10^5 cells per condition into a V-bottom 96-well plate and wash in PBS.

2. Resuspend cells in PBS and add extracellular Abs and fixable viability dye (FVD) (Table 34).

3. Incubate for 30 min in the dark at 4°C.

4. Top up with staining buffer, spin at 350 x g for 5 min at room temperature, flick off supernatant and blot dry.

5. Wash cells with Fix/Permeabilization solution (1:4 dilution of eBioscience fix/perm concentrate (#00-5123) in fix/perm diluent (#00-5223)).

6. Add 100 µL Fix/Permeabilization solution and incubate either for 1 h at room temperature, or for optimal results, at 4°C overnight (NOTE: this is contrary to the manufacturer's protocol).

7. Wash cells with 1× eBioscience permeabilization buffer (#00-8333; diluted with distilled water) and centrifuge at 1000 × g for 7 min at room temperature.

8. Flick off supernatant and blot dry. It is critical that the cell pellet is dry so that the subsequent step is optimal, see below.

9. Resuspend cells in 1× permeabilization buffer and add intracellular Abs.

10. Incubate for 40 min in the dark at 4°C.

11. Wash cells in 100 µL of permeabilisation buffer.

12. Wash cells in 100 µL of staining buffer.

13. Resuspend in at least 150 µL of staining buffer for data acquisition.

Note: This protocol can be modified to only carry out extracellular staining so that viable Th-cell like Tregs can be isolated. In this case, it is highly recommended to first perform a CD25 pre-enrichment step, for example using Miltenyi Biotech's human CD25 microbeads II (#130-092-983). Note that this product blocks the epitope for the CD25 2A3 mAb, so alternate mAb clones such as M-A251 or 4E3 are required for staining.
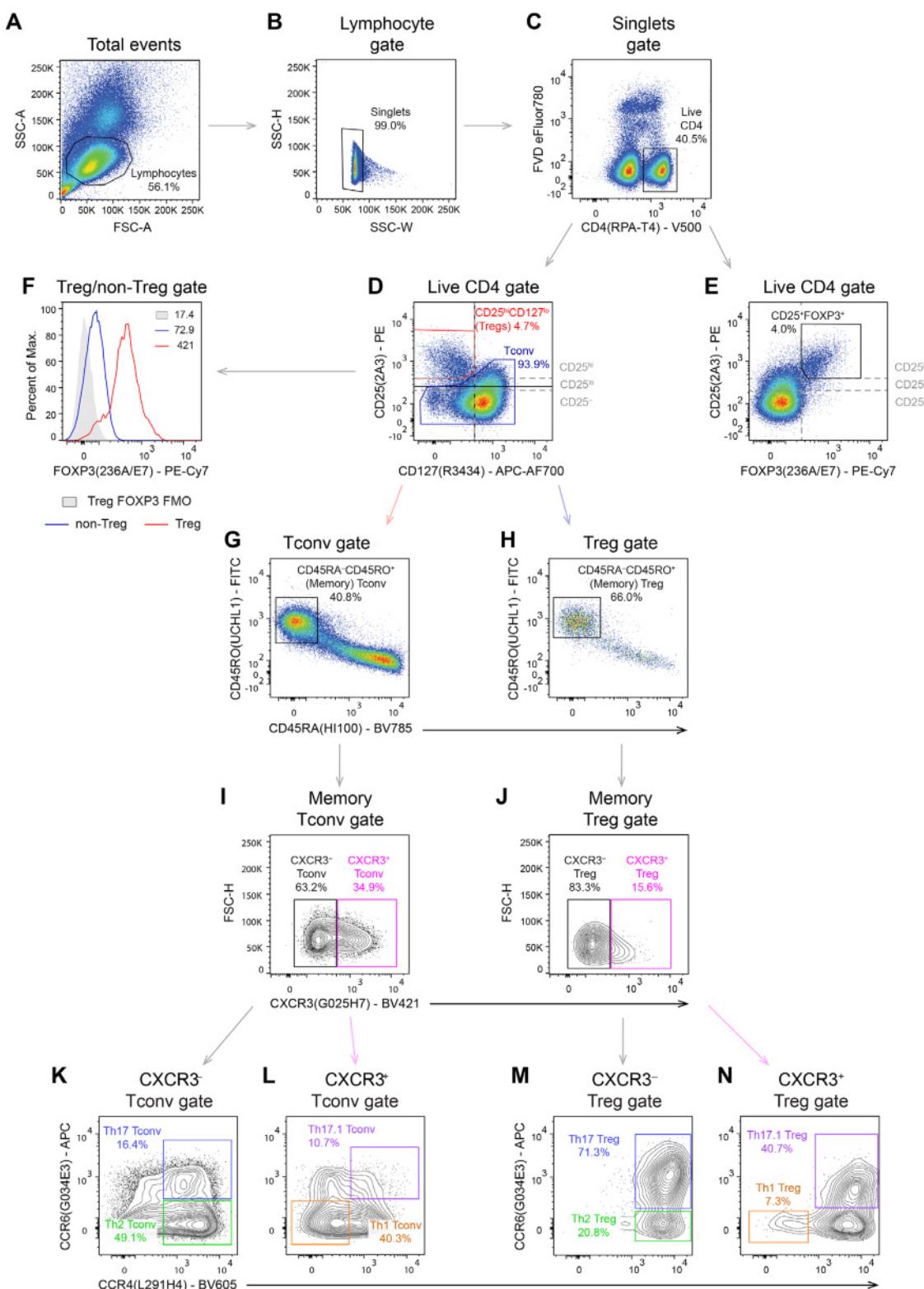
Figure 125. Identification of human Treg subsets in PBMCs. (A–C) Lymphocytes were gated according to their size and granularity, doublets excluded and live CD4$^+$ T cells gated. (D) Regulatory T cells (Treg) were identified as CD4$^+$CD25^{high}CD127^{low} (red gate) and the remaining cells were identified as "non-Treg" Tconvs (blue gate). (E & F) If the cells are fixed and permeabilized, FOXP3 staining can be performed. In (E), Dashed lines show how CD25 negative, low and high expression are defined. In (F), FOXP3 expression in the CD4$^+$CD25^{high}CD127^{low} Tregs (red line) and non-Tregs (blue line) is shown, relative to a Treg FOXP3 FMO control (solid grey). Mean fluorescence intensity (MFI) values are provided. (G and H) Memory Tregs and non-Tregs were selected as CD45RA$^-$ CD45RO$^+$. (I–N) Treg and non-Treg Th subsets were defined according to their expression of CXCR3, CCR4, and CCR6 as follows: Th17 (CXCR3$^-$CCR4$^+$CCR6$^+$), Th1 (CXCR3$^+$CCR4$^-$ CCR6$^-$), Th17.1 (CXCR3$^+$CCR4$^+$CCR6$^+$), and Th2 (CXCR3$^-$CCR4$^+$CCR6$^-$).
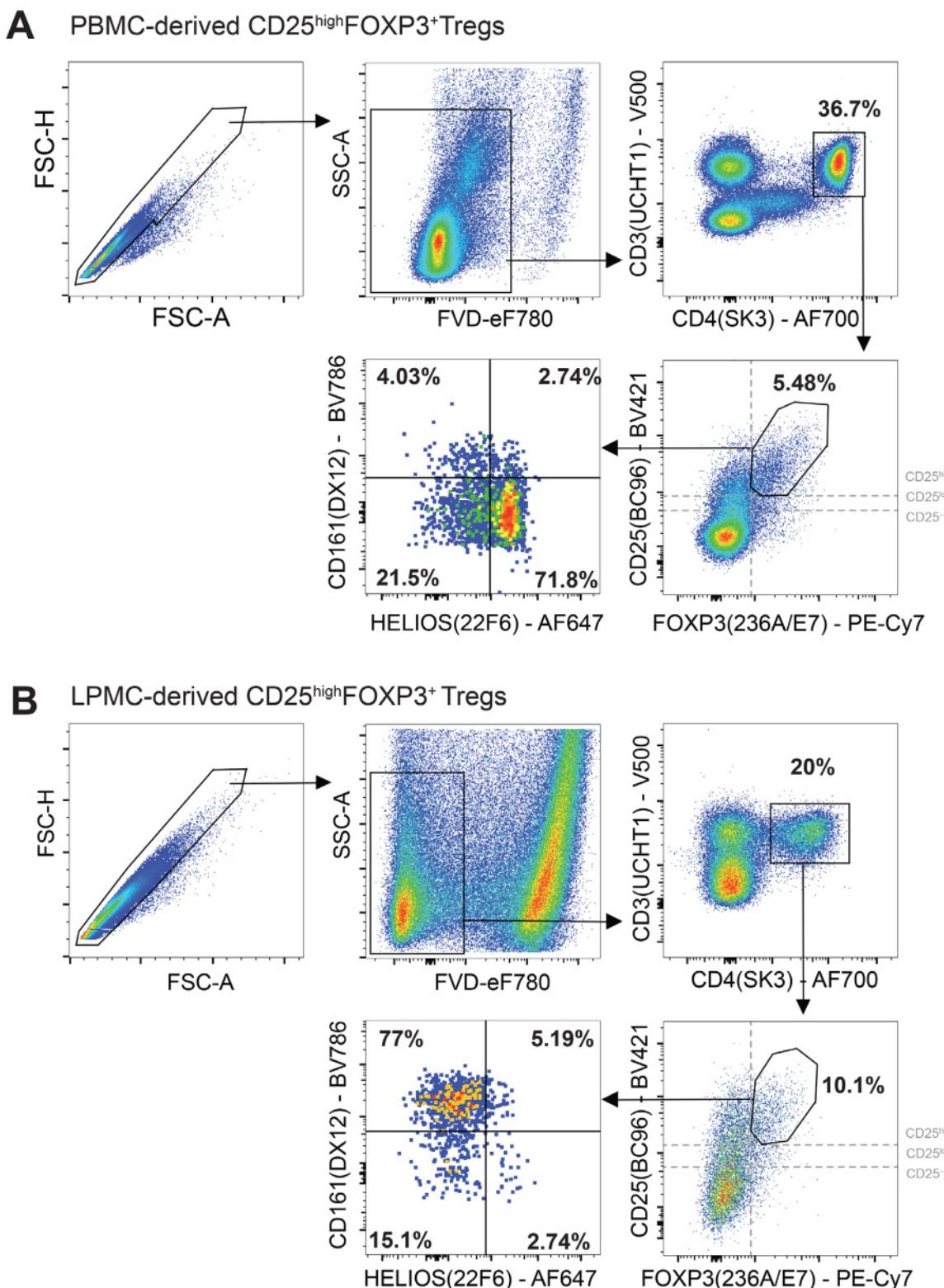
Figure 126. Gating strategy to identify CD25^{high}FOXP3$^+$ Tregs in human intestinal biopsies. (A) Representative Tregs staining from PBMCs and (B) LPMCs. From total events, doublets were excluded based on FSC-H and FSC-A. Live cells were selected based on negative expression of FVD and CD4$^+$ T cells were gated based on CD3 and CD4 expression. From CD4$^+$ T cells, Tregs were gated as CD25^{high}FOXP3$^+$ cells. From the Treg gate, the expression of CD161 and Helios are shown. Dashed lines show how CD25 negative, low, and high expressions are defined.

Table 34. List of Abs used for staining Tregs subsets from PBMCs

Marker	Dilution**	Fluorochrome	Clone	Company	Catalog
Fixable viability dye	1/1000	eFluor780		eBioscience	65-0865-18
CD4	1/100	V500	RPA-T4	BD	560768
CD25	1/50	PE	2A3	STEMCELL Technologies	60153PE
CD127	1/50	APC-AF700	R3434	Beckman Coulter	A71116
CCR4	1/50	BV605	L291H4	BioLegend	359418
CCR6	1/50	APC	G034E3	BioLegend	353416
CXCR3	1/50	BV421	G025H7	BioLegend	353716
FOXP3	1/50	PE-CY7	236A/E7	Invitrogen	25-4777-42
CD45RA	1/50	BV785	HI100	BioLegend	304140
CD45RO	1/50	FITC	UCHL1	BD	561887

** These dilutions have been optimised for our specific Ab lots. Each new mAb lot should be re-titrated.

Table 35. Treg populations in the blood

T cell population	Phenotype	Relative frequency
Total Tregs	$CD4^+CD25^{high}CD127^{low}$	~5% of $CD4^+$ T cells
Th1 Tregs	$CCR6^-CCR4^-CXCR3^+$	~5% of $CD25^{high}CD127^{low}$
Th17 Tregs	$CCR6^+CCR4^+CXCR3^-$	~30% of $CD25^{high}CD127^{low}$
Th17.1 Tregs	$CCR6^+CCR4^+CXCR3^+$	~20% of $CD25^{high}CD127^{low}$
Th2 Tregs	$CCR6^-CCR4^+CXCR3^-$	~5% of $CD25^{high}CD127^{low}$

1.14.4.3 Data analysis. Total lymphocytes were gated according to their forward and side scatter properties (Fig. 125A), doublet events were excluded (Fig. 125B) and live $CD4^+$ T cells were gated (Fig. 125C). Tregs can be identified from the total live $CD4^+$ T cells according to their expression of CD25, CD127, and/or FOXP3 (Fig. 125D and E). As previously mentioned, at least two of these markers should be used to defined human Tregs and where possible, the use of all three markers is ideal. In this analysis, Tregs were defined as $CD4^+CD25^{high}CD127^{low}$ (Fig. 125D) or $CD4^+CD25^{high}FOXP3^+$ (Fig. 125E). As shown in Fig. 125F, the majority of $CD4^+CD25^{high}CD127^{low}$ cells are $FOXP3^+$ but $FOXP3^-$ cells still exist in this population, emphasising the importance of using a combination of different markers to identify human Tregs. CD4 helper T cell and Treg subpopulations can be delineated from $CD45RA^-CD45RO^+$ memory cells (Fig. 125G and H) by analysing the expression of various homing receptors. Here, Th cell subsets were defined according to their expression of CXCR3, CCR4 and CCR6. Memory cells were separated according to their expression of CXCR3 (Fig. 125I and J), after which CCR4 and CCR6 expression was used to subgate Th cell subsets (Figure 125K–N). Th cell subsets were defined as follows: Th17 ($CXCR3^-CCR4^+CCR6^+$), Th17.1 ($CXCR3^+CCR4^+CCR6^+$), Th1 ($CXCR3^+CCR4^-CCR6^-$), and Th2 ($CXCR3^-CCR4^+CCR6^-$).

1.14.4.4 Pitfalls.

1. If the cell pellet isn't effectively dried before the fixation or permeabilization steps, then fixation and intracellular staining are not optimal. Use a V-bottom plate to stain and blot plate dry after flicking off supernatant for best results. (Steps 5 and 8)

1.14.4.5 Top tricks.

1. Ensure Fixable Viability Dye is stained in PBS as the presence of FCS will inhibit staining.
2. If the panel contains more than one Brilliant Violet conjugated Ab, then staining should be performed in Brilliant Stain Buffer (BD, #566385).
3. Make up FOXP3 buffers on the same day for each experiment.
4. Wash with fix/perm before step 5 and wash with perm buffer before step 8.

1.14.5 Staining $CD25^{high}FOXP3^+$ Tregs from human intestinal biopsies.

1.14.5.1 Step-by-step sample preparation. There is increasing interest in the role of tissue-resident Tregs [787]. As discussed above, it is significantly more difficult to confidently identify Tregs in tissues versus blood because of the high proportion of activated Tconv cells. In addition, tissues must often be treated with collagenase which can lead to removal of Treg-associated cell surface proteins. Below we detail a protocol to stain Tregs in intestinal biopsies and illustrate how the resulting data compare to that obtained with PBMCs.

1.14.5.2 Isolation and analysis of lymphocytes from intestinal biopsies (Figure 126).

- Intestinal biopsies (usually 4–6 punches ~4 mm in diameter) are collected in complete media at room temperature and lamina propria mononuclear cells (LPMCs) are isolated within

Table 36. List of Abs used for staining CD25^{high}FOXP3$^+$Tregs from intestinal biopsies

Marker	Dilution**	Fluorochrome	Clone	Company	Catalog
Fixable viability dye	1/1000	eFluor780		eBioscience	65-0865-18
CD3	1/50	V500	UCHT1	BD Biosciences	561416
CD4	1/50	AF700	SK3	BioLegend	344622
CD25	1/25	BV421	BC96	BioLegend	302630
FoxP3	1/25	PECy7	236A/E7	eBioscience	25-4777-42
Helios	1/25	AF647	22F6	BioLegend	137218
CD161	1/25	BV875	DX12	BD Biosciences	744096

** These dilutions have been optimised for our specific Ab lots. Each new mAb lot should be re-titrated.

2—4 h of collection following the protocol described in ref. [993].

- Briefly, biopsy specimens are transferred to a 10 mL solution of Collagenase VIII and DNAse and incubated for 1 h at 37°C, shaking vigorously every 20 min. After incubation, cells are passed through a 100 μm cell strainer, washed and LPMCs are isolated by centrifugation over a Percoll gradient (resuspended in 40% Percoll, underlayed by an equal volume of 80% Percoll).
- After washing, cells are incubated in complete medium overnight at a concentration of 2×10^6 cells/mL before staining. Expected average yields are 2×10^6 LPMCs per sample (if —four to six biopsies are pooled together).
- Staining of LPMCs is then performed using the PBMC staining protocol (Protocol 2) using the panel outlined in Table 36.

1.14.5.3 Data analysis. From total events, doublets were excluded based on FSC-H and FSC-A and live CD4$^+$ T cells were selected based on negative expression of FVD and positive expression of CD3 and CD4 From CD4$^+$ T cells, Tregs were gated as CD25^{high}FOXP3$^+$ cells. From the Treg gate, the expression of CD161 and Helios are shown. Dashed lines show how CD25 negative, low, and high expression are defined. This strategy was used to gate Tregs based on CD25^{high} and CD127^{low} expression from PBMCs and LPMCs.

1.14.5.4 Pitfalls.

- Many surface markers are affected by collagenase digestion so it is imperative to systematically test all Ab clones before finalizing the staining panel (Summary table of validated clones is shown in Table 37).

1.14.5.5 Top tricks.

- Ensure that the collagenase incubation is done in a 50 mL, rather than a 14 mL, falcon tube even if only using 10 mL of solution. The added room allows more vigorous shaking, which is key to getting a good yield.

Subjects and samples. Human peripheral blood and human colon biopsies were obtained following protocols approved by

Table 37. Collagenase VIII compatible Abs for human Treg staining. Note that this compatibility may be affected by different tissue digestion protocols

Marker	Validated Clone
CD127	A019D2
LAG3	3D5223H
CD25	BC96
ICOS	C398.4a
CD3	UCHT1
CD4	SK3
CD45	HI30
CD45RA	HI100
CD45RO	UCHL1
CD69	FNSO
CTLA-4	BN13

Clinical Research Ethics Boards of the University of British Columbia (H18- 02553 and H15-01034).

1.14.5.6 Materials. Common Reagents:

- Staining buffer: 1× Dulbecco's PBS (ThermoFisher Scientific, #14190-144) supplemented with 2% FBS (VWR, #97068-085).
- Complete media: RPMI 1640 (ThermoFisher Scientific, #11879020) supplemented with 10% FBS, 1% Penicillin/Streptomycin (ThermoFisher Scientific, #15140122), and 1% GlutaMAX (ThermoFisher Scientific, #35050061).
- Lymphoprep (Stemcell Technologies, #07861).
- Ammonium Chloride (StemCell, #07850).
- FOXP3 Fix/Perm Buffer Set (Thermo Fisher eBiosciences, #00-5523-00).
- Human FOXP3 buffer set (BD, #560098).
- BD FACS^{TM} Lysing Solution (BD, #349202).
- Collagenase VIII (Sigma-Aldrich, #C2139).
- DNAse (STEMCELL Technologies, #7900).
- Percoll (GE Healthcare, #17-0891-02).

Cytometer and analysis

BD Fortessa X20, configuration as per Table 38. Analysis performed using Flowjo^{TM} Version X (Treestar Inc, v10.5.3).

Table 38. Fortessa X20 cytometer configuration

	Filters	Mirrors
488 nm Blue Laser	488/10	
	530/30	505 LP
	695/40	685 LP
640 nm Red Laser	670/30	
	730/45	710 LP
	780/60	750 LP
561 nm Yellow-Green Laser	585/51	
	610/20	600 LP
	670/30	635 LP
	710/50	685 LP
	780/60	750 LP
405 nm Violet Laser	450/50	
	525/50	505 LP
	560/40	545 LP
	585/52	570 LP
	610/20	600 LP
	670/30	630 LP
	710/50	685 LP
	780/60	750 LP

1.15 Human $\gamma\delta$ T cells

1.15.1 Overview. Recently there has been a surge of interest in $\gamma\delta$ T cells, as this cell type is increasingly being recognized to play important roles in multiple disease settings, such as in cancer, autoimmune disorders, and microbial infections. A relatively easy and quick method to analyze these cells is by FCM. Recently, new markers and Ab combinations have been deployed that identify the major $\gamma\delta$ T cell subsets. However, phenotyping of $\gamma\delta$ T cells using FCM remains challenging and thus here we provide an optimized protocol and mAb combinations to detect these human $\gamma\delta$ T cell subsets.

1.15.2 Introduction. $\gamma\delta$ T cells represent an unconventional T cell subset that express a T cell receptor (TCR) constructed of a $\gamma-$ and $\delta-$chain. These immune cells play important roles in the responses against microbes [994] and tumors [995]. In contrast to classical $\alpha\beta$ T cells, $\gamma\delta$ cells have been described to respond to an array of non-peptide antigens (Ags) [996] independent of MHC proteins [997]; see also Chapter VI Section 1.7 Murine $\gamma\delta$ T cells. In humans, $\gamma\delta$ T cells are typically divided into Vδ2$^+$ and Vδ2$^-$ subsets [998]. Most $\gamma\delta$ T cells in the peripheral blood are Vγ9$^+$/Vδ2$^+$ and respond to phosphoAgs (pAgs) such as prenyl pyrophosphate metabolites that are commonly produced by microbes and host derived pAgs are upregulated in some tumor cells [999–1001]. Conversely, Vδ2$^-$ subsets are positioned across multiple tissues and are a minor subset in the peripheral blood [798, 1002]. A current overview of human $\gamma\delta$ T cell subsets is provided in Fig. 127.

1.15.2.1 Human Vδ2$^+$/Vγ9$^+$ T cells (innate-like). Vδ2$^+$/Vγ9$^+$ T cells (also referred to as Vγ2$^+$/Vδ2$^+$ T cells in some publications) expand extra-thymically and microbial-derived pAgs potentially trigger polyclonal expansion of these cells in the periphery following birth [1003, 1004]. Enriched Vδ2$^+$/Vγ9$^+$ T cell numbers are already present in fetal peripheral blood and these cells show restricted complementarity determining region 3 (CDR3) γ9 usage [1005]. In addition, similar Vγ9 TCR sequences are detected in multiple donors (i.e., "public" sequences) and are shared in samples from cord and adult blood [1000, 1006]. Vδ2$^+$/Vγ9$^+$ T cells are generally enriched in the circulation and respond to pAgs such as isopentenyl pyrophosphate (IPP), which are elevated in tumor cells and (E)-4-Hydroxy-3-methyl-but-2-enyl pyrophosphate (HMB-PP), which is produced by bacteria and parasites [999]. Together, this evidence hints at the innate-like functions of these $\gamma\delta$ T cells.

1.15.2.2 Human Vδ2$^-$ and Vδ2$^+$/Vγ9$^-$ T cells. The functions of Vδ2$^-$ $\gamma\delta$ T cells are currently unclear, but these cells have been demonstrated to expand in response to tumor cells, bacteria, parasites, and viruses. The majority of Vδ2$^-$ $\gamma\delta$ T cells express a Vδ1 TCR chain pairing, while a minority express other Vδ TCR chains, notably Vδ3, Vδ4, Vδ5, and Vδ8. Studies investigating Vδ1 and Vδ3 have been aided by critical commercial Ab reagents, although Vδ3 Abs are currently only available upon request (from Beckman Coulter; clone P11.5B). The identification of Vδ4, Vδ5, and Vδ8 has been restricted to sequencing based approaches as commercial FCM reagents are not available. Studies that have focused on Vδ1 and Vδ3 have now shed light on the receptor diversity and physiology of these subsets in the tissues and in infection, such as cytomegalovirus [1000, 1007]. Vδ1$^+$ T cells display a CD27$^{lo/-}$CD45RA$^+$ phenotype when clonally expanded [1000, 1007] and display heterogeneous γ chain usage [1000, 1007]. Moreover, uniformly in cord and, at mixed levels, in adult blood, Vδ1$^+$ T cells exhibit a diverse and polyclonal population, expressing markers of a naïve T cell population—this is reviewed in ref. [1008]. This subset of $\gamma\delta$ T cells is suggested to play a role in the adaptive immune response, as clonal expansions of these cells can be found in peripheral blood and liver tissue of adults whereas this is not evident in cord blood [1000, 1009]. These clones are likely generated in response to cellular stress or microbial infection, as observed in acute cytomegalovirus infection [1000, 1010]. Additionally, a sub-population of Vδ2$^+$ T cells has been identified that generally do not express the Vγ9 chain pairing (termed Vδ2$^+$/Vγ9$^-$ T cells). This population of $\gamma\delta$ T cells undergoes dramatic clonal expansion in cytomegalovirus infection and can be identified using FCM markers similar to Vδ1$^+$, i.e., CD27$^{lo/-}$CD45RA$^+$ CX$_3$CR1$^+$ cells (effector) and a naïve polyclonal compartment characterized as CD27^{hi}CD45RA$^{+/-}$ CX$_3$CR1$^-$ [1000]. Together, these recent findings surrounding Vδ2$^-$ and Vδ2$^+$/Vγ9$^-$ $\gamma\delta$ T cells indicated that these cells follow an adaptive biology.
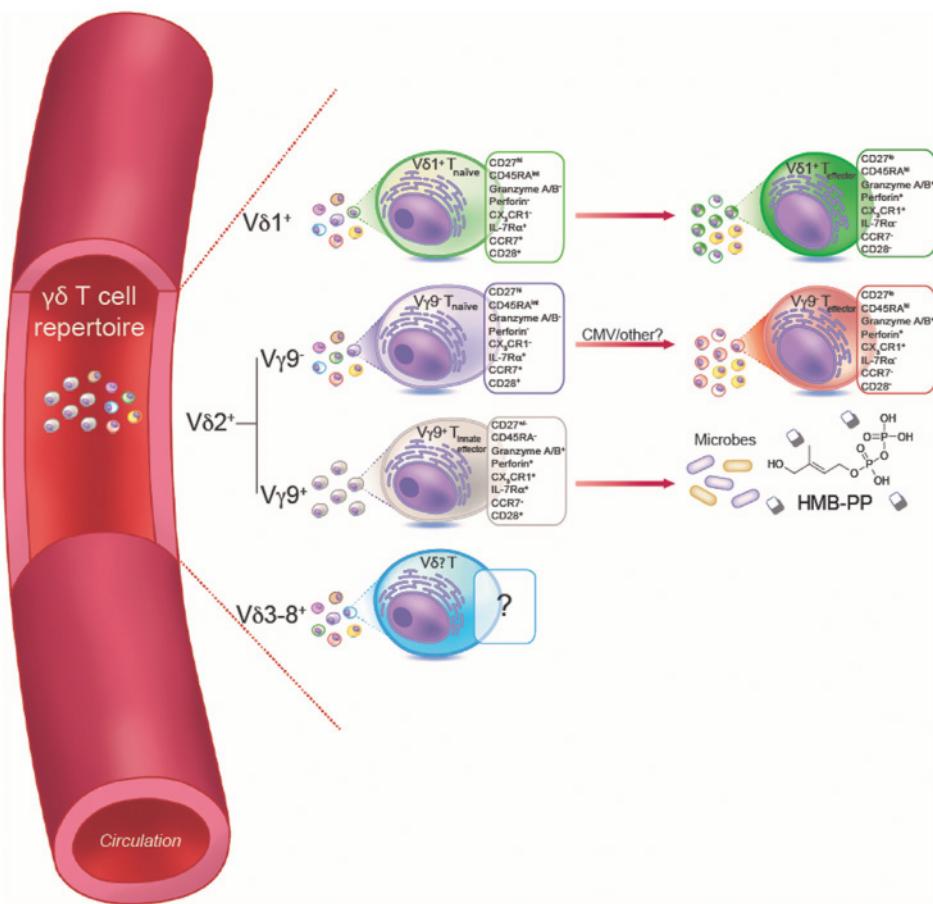
Figure 127. Human γδ T cells found in the peripheral blood. Each population is divided based on their Vδ chain usage, primarily due to the availability of TCR Vδ1 and TCR Vδ2 mAbs. Each subset is displayed alongside a set of cell surface markers that accurately define them in the steady state. Vγ9⁻/Vδ2⁺ and Vδ2⁻ γδ T cells seem to undergo postnatal selection in the periphery from a naïve γδ T cell pool. Vδ2⁺/Vγ9⁺ T cells are established in the perinatal period and are rapidly matured after birth, resulting in a uniform responsiveness to pAgs. Non-Vδ1 or -Vδ2 T cells express a Vδ3-8 TCR chain pairing and are rare in the peripheral blood but enriched in the tissues, such as the liver. The markers that define them and if they form further subsets is unclear.

1.15.2.3 Human γδ T cells in cancer immunotherapy. γδ T cells are now considered a major target for the development of novel cellular immunotherapies. This is in part due to their ability to recognize tumor cells through the γδTCR or natural killer cell receptors (NKRs), such as NKG2D, NKp30, NKp44, and NKp46 that decorate their cell surface [1011]. The endogenous host pAg, isopentenyl pyrophosphate, and the ligands for NKRs are often overexpressed in transformed cells. As such, Vδ2⁺/Vγ9⁺ T cells have been a principal candidate for immunotherapy as they exert strong lytic activity toward tumor cell lines [1012], which can be mediated via the production pro-inflammatory cytokines and apoptosis-inducing molecules [1013]. More recently, Vδ1⁺ T cells have rapidly become a major avenue for the creation of a cellular immunotherapy and display potent cytolytic capacity toward a range of tumor cell lines [1014]. The main avenue of delivery is via adoptive transfer of in vitro expanded γδ T cells into cancer patients and some clinical trials have shown that these cells may be effective at limiting tumor progression.

1.15.2.4 FCM for human γδ T cells. A uniform staining and gating strategy is needed to identify γδ T cells and their subsets. The need for a well-optimized protocol has recently been highlighted, as it was shown that Vδ2⁺/Vγ9⁻ T cells could only be identified with FCM when using the anti-Vδ2 Ab clone 123R3 (Miltenyi), while this population could not be identified when the anti-Vδ2 Ab clone B6 (BD and BioLegend) was used [1000]. Moreover, the combination of some commercial pan γδ TCR mAb (Biolegend (B1), BD (11F2) and Beckman Coulter (IMMU510) can interact with Vγ9, Vδ1, and Vδ2 (example in Fig. 128), causing disruption to γδ TCR staining. Thus, here, we describe the materials and a well-optimized protocol to identify subsets of human γδ T cells.

1.15.3 Step-by-step sample preparation.

1.15.3.1 PBMC Isolation. PBMCs can be isolated from heparinized venous blood or a buffy coat. First, the buffy
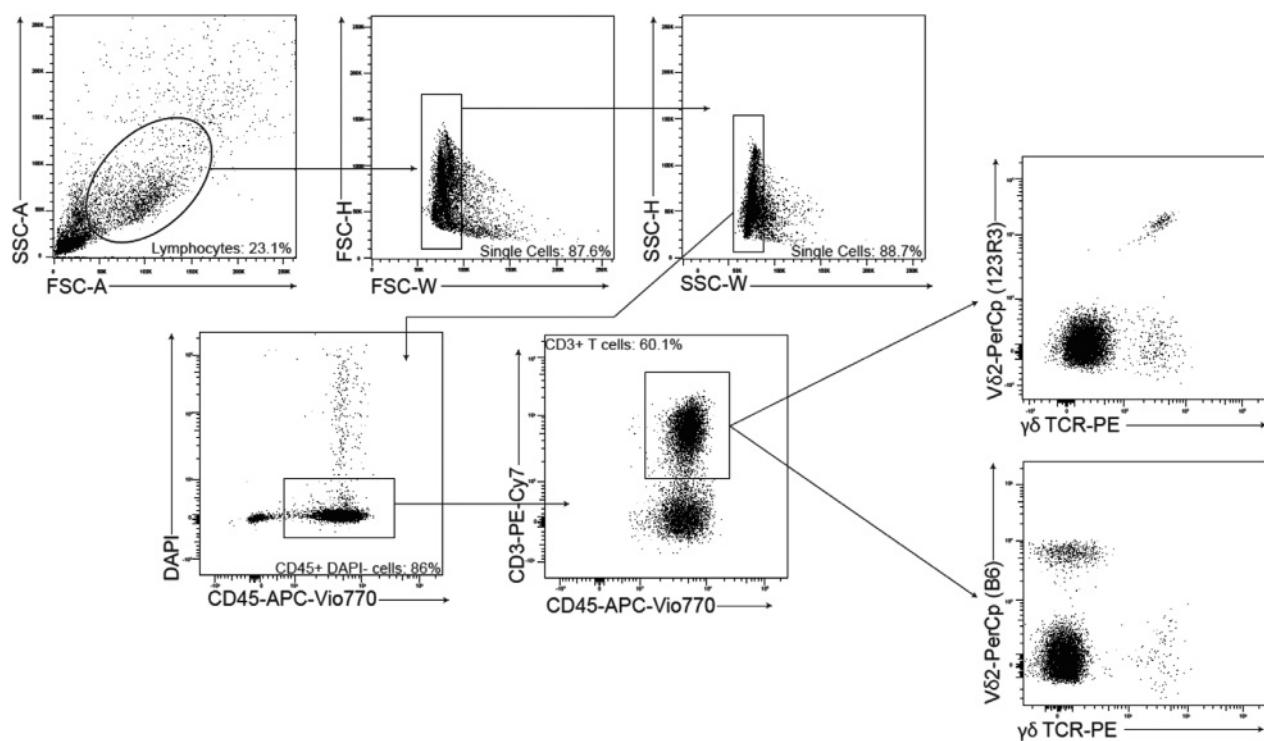
Figure 128. Representative dot plots of Vδ2⁺ γδ T cells in human peripheral blood mononuclear cells (hPBMCs). This gating strategy involves gating of Lymphocytes > Single cells (FSC-W/FSC-H) > Single cells (SSC-W/SSC-H) > CD45+DAPI- cells > CD3⁺ T cells. CD3⁺ cells were stained with Vδ2 clone 123R3 (top) or Vδ2 clone B6 (bottom) and anti-γδ TCR (clone 11F2). (Figure kindly contributed by Inga Sandrock [Hannover Medical School, Germany]).

coat/peripheral blood has to be diluted 1× in PBS, followed by transfer of the cell suspension on Lymphoprep™, which is density gradient centrifuged according to the manufacturers' instructions. PBMCs are frozen in 90% FCS and 10% DMSO. See Table 39 for details on buffers and reagents.

1.15.3.2 FCM: Surface marker staining. After mononuclear cells have been obtained from either tissue or peripheral blood, the following protocol should be followed for the staining of surface markers on γδ T cells (subsets):

1. Thaw the PBMCs, centrifuge for 2 min at 400 × *g* at 4°C. Add 500 000 PBMCs to a U-bottomed 96-well plate.
2. Wash PBMCs in 200 μL PBS per well for 2 min at 400 × *g* at 4°C. Discard the supernatant.
3. Add 50 μL Zombie Aqua™ diluted in PBS (to stain dead cells; Table 39) per well and incubate for 10 min at room temperature in the dark.
4. Add 150 μL FACS buffer per well, consisting of sterile PBS + 20% FCS + 0.04% Sodium Azide, and centrifuge the plate for 2 min at 400 × *g* at 4°C. Discard the supernatant.
5. Block Fc receptors to prevent nonspecific binding of mAbs by adding 50 μL TruStain FcX (diluted 1:100 in FACS buffer). Incubate for 10 min on ice in the dark.

6. Prepare a cocktail of the mAbs according to Table 39. Dilute the mAbs in FACS buffer. Stain the cells with 50 μL Ab cocktail per well on ice in the dark for 15 min.
7. Add 150 μL FACS buffer per well and centrifuge the plate for 2 min at 400 × *g* at 4°C. Discard the supernatant.
8. Resuspend cells in 200 μL FACS buffer per well, transfer the cell suspension to FACS tubes, and keep on ice until acquisition at the BD LSRFortessa™ X-20 (BD Biosciences, San Jose, CA).

1.15.3.3 FCM: Intracellular marker staining. The protocol can be extended by staining for intracellular targets, such as for example, Granzyme A and B and perforin. The following steps should be followed after step 6 of the surface marker staining protocol:

1. Add 50 μL IC Fixation buffer (eBioscience; Table 39) per well and incubate for 30 min at 4°C in the dark. Centrifuge the plate for 2 min at 400 × *g* at 4°C. Discard the supernatant.
2. Add 50 μL Permeabilization buffer (Perm buffer; eBioscience; Table 39) per well and centrifuge the plate for 2 min at 400 × *g* at 4°C. Discard the supernatant.
3. Add 50 μL Fc block, diluted 1:100 in Perm buffer to block aspecific binding of mAbs to Fc receptors. Incubate for 10 min at room temperature in the dark.
4. Prepare a cocktail of the mAbs (example for intracellular targets in Table 40). The mAbs should be diluted in Perm buffer.
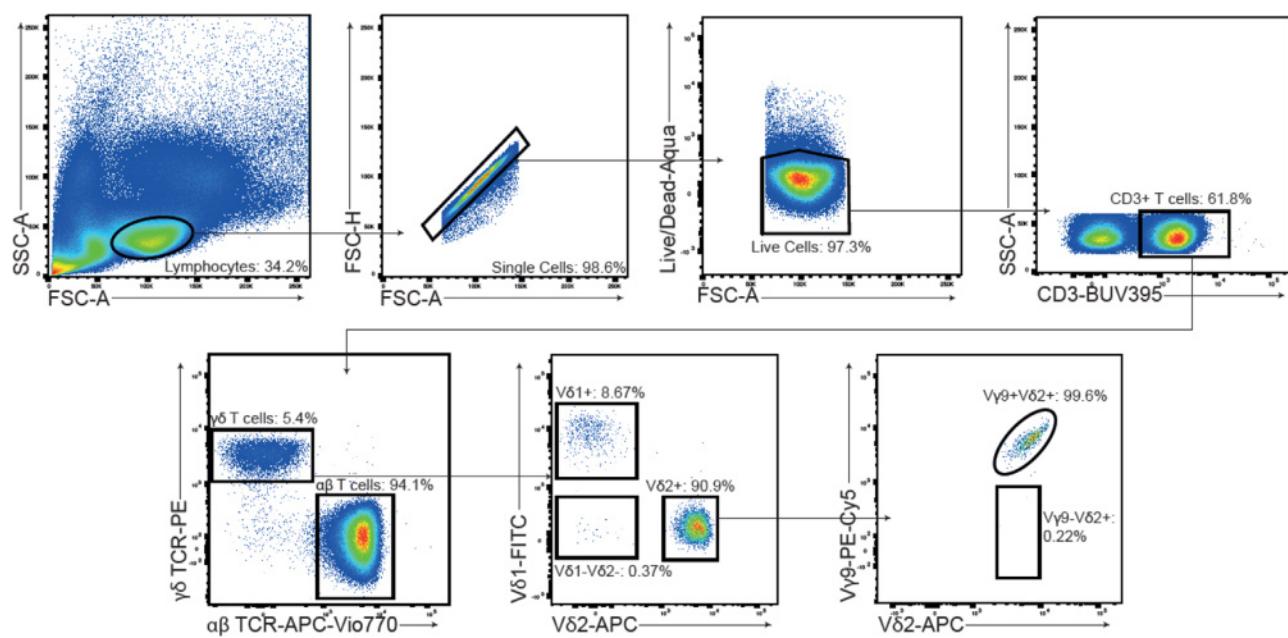
Figure 129. Gating strategy to define human γδ T cells in the peripheral blood. The gating strategy used to define human γδ T cells involves manual gating of Lymphocytes > Single Cells > Live cells > CD3$^+$ cells > TCRγδ$^+$ T cells. The use of TCRγδ vs TCRαβ mAbs provides the consistent ability to accurately discriminate γδ T cells even in the most challenging samples i.e. where γδ T cells numbers are very low or viability is poor. γδ T cell subsets are then defined based on expression of TCRγδ$^+$ T cells > Vδ1$^+$, Vδ2$^+$, Vδ1/2$^-$. Vδ2$^+$ T cells can then be sub-divided in those that express Vγ9$^+$ or not Vγ9$^-$ (rare in peripheral blood).

Per well, add 50 μL Ab cocktail and incubate for 30 min at room temperature in the dark. Centrifuge the plate for 2 min at 400 × g at 4°C. Discard the supernatant.

5. Resuspend cells in 200 μL FACS buffer per well, transfer to FACS tubes, and keep on ice until acquisition at the BD LSRFortessa^{TM} X-20.

Table 39. Characteristics of mAbs to identify γδ T cell subsets in peripheral blood

Buffers/Reagents for FCM

Buffer/Reagent	Provider	City	Country	Catalogue Number	Dilution
Lymphoprep	Axis-Shield PoC	Oslo	Denmark	NA	NA
Zombie Aqua	BioLegend	San Diego, CA	USA	423101	1:500
TruStain FcX	Biolegend	San Diego, CA	USA	422302	1:100
IC Fixation Buffer	eBioscience	San Diego, CA	USA	NA	1:4
Perm Buffer	eBioscience	San Diego, CA	USA	NA	1:10

Abs for FCM

mAb	Fluorochrome	Clone	Provider	Catalog number	Dilution
anti-CD3	BUV395	UCHT1	BD Biosciences	563546	1:150
anti-CD8	BUV496	RPA-T8	BD Biosciences	564804	1:200
anti-Vγ9	PE-Cy5	IMMU 360	Beckman Coulter	A63663	1:400
anti-CD27	PE-Dazzle 594	M-T271	BioLegend	356422	1:150
anti-CD45RA	BV711	HI100	BioLegend	304138	1:200
anti-CX$_3$CR1	PE-Cy7	2A9-1	BioLegend	341612	1:150
anti-IL-7Rα	BV605	A019D5	BioLegend	351333	1:100
anti-γδ TCR	PE	REA591	Miltenyi	130-114-038	1:200
anti-Vδ1	FITC	REA173	Miltenyi	130-100-532	1:100
anti-Vδ2	APC	123R3	Miltenyi	130-095-803	1:200
anti-αβ TCR	APC-Vio770	REA652	Miltenyi	130-114-062	1:100

Table 40. Characteristics of mAbs to identify intracellular targets in γδ T cell subsets in peripheral blood

mAb	Clone	Provider	Catalogue Number	Dilution
anti-Granzyme A	CBO9	BioLegend	507221	1:100
anti-Granzyme B	GB11	BioLegend	372209	1:100
anti-Perforin	B-D48	BioLegend	353303	1:80
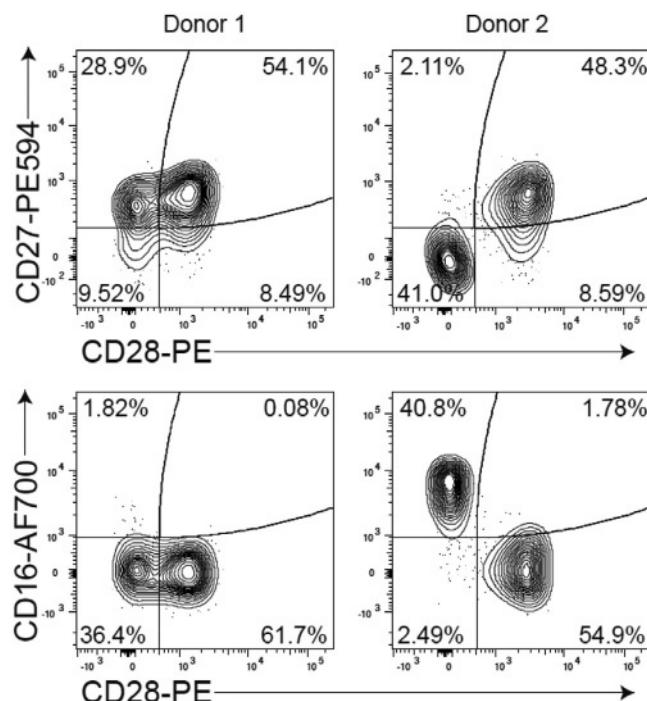
Figure 130. Functional sub-populations of human Vδ2⁺/Vγ9⁺ T cells. After using the gating strategy to define human γδ T cells described in Fig. 129, human Vδ2⁺/Vγ9⁺ T cells can be further split into effector subsets based on CD27, CD28, and CD16 expression. These populations are highly variable between individuals and it is unclear how these populations are derived.

1.15.4 Data analysis/gating strategy. We analyzed our data using the FlowJo software (version 10.5.3, Tree Star). In Fig. 129, we show the gating strategy that we used. First, the lymphocytes are gated in the FSC-A/SSC-A plot. After exclusion of doublets in the FSC-A/FSC-H plot, we gated on live CD3⁺ T cells in the CD3/Live/dead (L/D) plot. In the αβ TCR/γδ TCR plot, γδ TCR⁺ T cells and αβ TCR⁺ T cells were gated. The γδ TCR⁺ T cell population can be further divided into Vδ1⁺ and Vδ2⁺ T cells using the Vδ2/Vδ1 plot. Lastly, within the Vδ2⁺ T cells we gated on Vδ2⁺/Vγ9⁺ T cells. Within the αβ TCR⁺ T cell population, we gated on CD8⁺ T cells in the CD8/SSC-A plot (plot not shown).

Vδ2⁺/Vγ9⁺ γδ T cells can be further delineated into functional subsets based on the expression of CD27, CD28, and the acquisition of CD16 (Fig. 130). Definitions of these subsets are detailed in ref. [1015]. These subsets may play a role in the
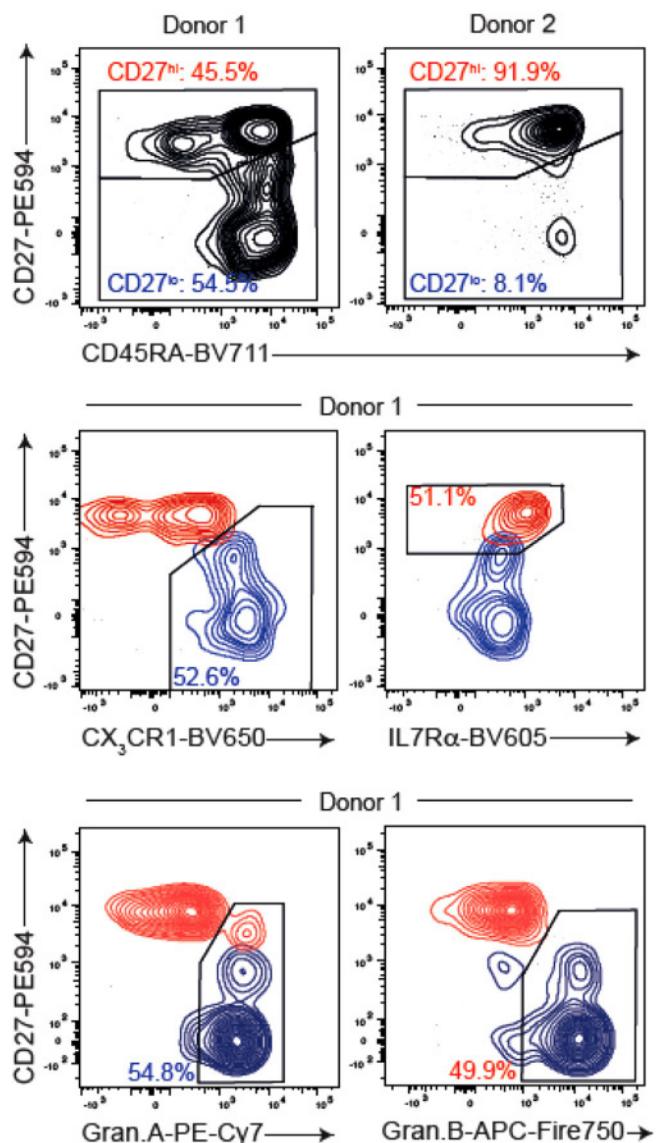
Figure 131. Identifying naïve and effector sub-groups of adaptive Vδ2⁺/Vγ9⁻ and Vδ2⁻ γδ T cells. After application of the gating strategy described in Fig. 129, the distribution of clonally diverse naïve γδ T cells can be identified by the expression of CD27 and CD45RA (CD27^hi; marked in red) and clonally expanded effector γδ T cells (CD27^lo; marked in blue), see Davey et al. 2017 [1009]. These naïve and effector subsets display very distinct phenotypes and can be further defined by the expression of CX₃CR1, Granzyme A/B, or IL7Rα. The data shown here is an example of the expression of these markers in human Vδ1⁺ γδ T cells.

potent antimicrobial activity in bacterial infections producing HMB-PP.

Vδ2⁺/Vγ9⁻ and Vδ2⁻ γδ T cell subsets can be further divided into naïve (CD27^hi) and effector (CD27^lo) cells (Fig. 131) [1000]. CD8⁺ T cells were included as a control subset. Within each subset, CD27^hi γδ T cells are characterized by the absence of CX₃CR1 and presence of IL-7Rα expression (Fig. 128). On the other hand, CD27^lo γδ T cells do express CX₃CR1, whereas these cells do not express IL-7Rα (Figure 128).

1.15.5 Pitfalls and top tricks. When analyzing γδ T cells by FCM, several pitfalls should be kept in mind. First, with this 12-color staining panel it is very important to have a well setup compensation. Second, the mAbs should be tested and titrated so that correct dilutions can be determined. This not only saves valuable mAbs but also ensures that the dilution is matched to the expression level of the target and fluorochrome intensity. Third, γδ T cells represent only a small proportion within T cells in the peripheral blood and in a scatter plot it might be harder to set gates. In this case a contour or pseudocolor plot might be used to be better able to detect different populations. Lastly, flow cytometric analysis of in vitro stimulated human γδ T cells expanded with mitogenic CD3 mAb (OKT-3 or UCHT-1 clones), anti-Vδ1 (TS8.2), or anti-TCRγδ (B1) mAbs, can be particularly challenging. The internalization of the γδTCR complex upon stimulation with these mAbs usually occurs within minutes, causing a decreased surface expression of the γδTCR. Additionally, these mitogenic Abs remain bound to their epitopes and can block the staining of γδTCR and CD3 molecules in later Ab staining protocols, hampering the discrimination of CD3+TCRγδ+ and CD3+TCRαβ+ cells. This problem can be circumvented by sub-culturing cells for 2 to 3 days in the absence of CD3 mAb and/or -TCRγδ mAbs, thereby restoring the availability of the γδTCR complex. Of note that TCR internalization does not occur when γδ T cells are cultured in the presence of pAgs (IPP or HMB-PP).

Top tricks for the staining protocol are to work cold and quick when following this staining protocol. When analyzing intracellular targets, the FoxP3 intranuclear staining buffer set should be used as it gives the best staining results.

1.16 Human NKT cells

1.16.1 Overview. Natural Killer T cells (NKT cells) are a subset of lipid-reactive T cells restricted to the MHC I-like molecule CD1d. Like other "unconventional" T cell subsets (such as MAIT and γδ T cells), NKT cells display a memory-like phenotype and rapidly release a broad array of cytokines following activation [997]. Indeed, the functional diversity displayed by NKT cells underpins their appreciated immunomodulatory role in various diseases, including infection, autoimmunity, and cancer [1016–1018]. The NKT cell family can be subdivided into Type I and Type II NKT cells based on TCR gene usage and/or CD1d-lipid antigen reactivity [1019]. As methods to definitively identify Type II NKT cells are still developing, this section provides guidelines for the identification of the more extensively described Type I, or invariant (iNKT) NKT cell subsets using FCM, with an emphasis upon the different reagents and techniques required to study these evolutionarily conserved cells.

1.16.2 Introduction. Initially, NKT cells were described in mice as a lymphocyte population displaying restricted αβ TCR usage and the co-expression of the NK cell-associated receptor NK1.1, which resulted in the moniker "Natural Killer T cells"

being adopted [1020] (see also Chapter VI Section 1.8 Murine NKT cells). However, expression of NK1.1 in mice, and the ortholog CD161 in humans have since been shown to be inefficient markers for this T cell subset, which are now more definitely categorized by their T cell receptor (TCR) composition, and their recognition of particular CD1d-ligands. The canonical human NKT cell TCR is composed of an invariant α-chain comprising Vα24 and Jα18 (TRAV10 and TRAJ18) gene segments, paired with a Vβ11+ (TRBV25-1) β-chain. This represents a TCR heterodimer that is highly conserved throughout the human population, with orthologous sequences also being common to other mammalian species [1021–1024]. Accordingly, this T cell subset is often referred to as "invariant," or iNKT cells from primates to rodents [1020]. One of the hallmarks of iNKT cell TCRs is their recognition of the prototypic CD1d-ligand α-galactosylceramide (α-GalCer) [1025]. While this interaction is also used to demarcate Type I (α-GalCer-reactive) NKT cells from the more TCR-diverse (α-GalCer-non-reactive) Type II NKT cell subset, not all T cells capable of recognizing the CD1d-α-GalCer complex necessarily express the Vα24-Jα18/Vβ11 iNKT cell TCR. For example, human CD1d-α-GalCer reactive αβ T cells that lack Vα24 and/or Vβ11 expression have been widely described [1026–1030] and γδ T cells that interact with CD1d-α-GalCer have also been reported [1031]. Thus, an appreciation of the complexities that exist within the NKT/CD1d-restricted T cell pool is crucial for those designing experiments to study these cells. Although it is common for the terms "NKT cells," "iNKT cells," and "Type I NKT cells" to be used synonymously, there are significant differences between these classifications, and differences in the approaches used to identify the cells. The best choice for individual researchers will depend on the specific question(s) they are aiming to address. Herein, we discuss the various ways that NKT cells can be identified using FCM, and the potential advantages and disadvantages of these alternate methodologies.

1.16.3 Identifying human NKT cells via their antigenic-recognition. The prototypic NKT cell antigen KRN7000 was developed by the Kirin brewing company in the 1990's [1025, 1032, 1033]. This α-linked galactosylceramide compound was modeled on glycolipids isolated from extracts of marine sponge displaying antitumor activity in murine disease models. This reagent (KRN7000) has since been widely used to study the functional properties of both mouse and human NKT cells [1034]. Despite the curious origins of this T cell antigen, structurally similar glycolipids have since been identified from numerous bacterial species [1035], supporting the physiological relevance of NKT cell-specificity for such compounds. In addition to KRN7000, various α-GalCer analogues have also been synthesized, which elicit distinct functional responses [1036–1038] and display varied affinities for NKT cell TCRs [1039, 1040]. While the potency of KRN7000 has made it the most widely used antigen for investigating NKT cell functionality, its saturated lipid-component renders it a relatively insoluble reagent. Thus, for the purpose of identifying NKT cells using CD1d-tetramers, it can prove suboptimal, due to its inefficient
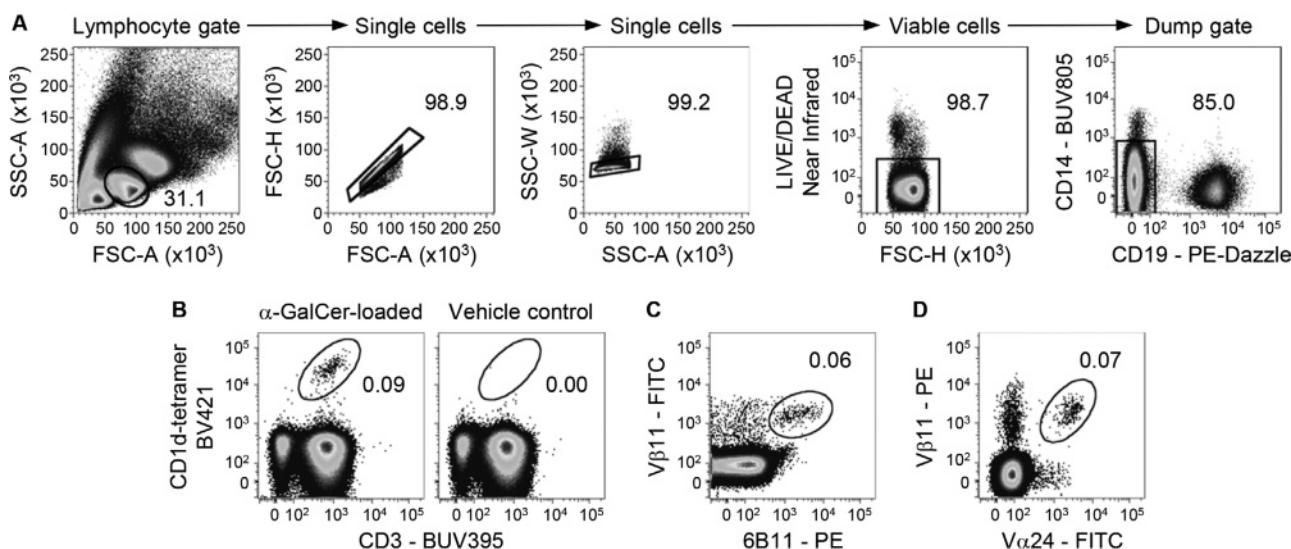
Figure 132. Gating on human blood NKT cells. (A) Lymphocytes are distinguished amongst PBMCs based on their relative FSC-A and SSC-A intensities. Single cells are then isolated by their relationship between FSC-H versus FSC-A, and SSC-W versus SSC-A. To remove any non-specific or TCR-independent CD1d-tetramer staining, dead cells are removed from analysis based on their uptake of LIVE/DEAD™ Fixable Near-IR viability dye. Monocytes and B cells are also excluded based on their CD14 and CD19 expression respectively. (B) The frequency of circulating Type I NKT cells, as determined by co-staining for CD3ε and α-GalCer (PBS-44)-loaded CD1d-tetramer (left) in relation to a vehicle control CD1d-tetramer (right). (C) The frequency of iNKT cells assessed by co-staining with 6B11 and anti-Vβ11. (D) Co-staining with anti-Vα24 and anti-Vβ11, which nonexclusively enriches for iNKT cells.

loading into CD1d in a cell-free, in vitro setting. Due to this, more soluble α-GalCer analogues (with unsaturated lipid fractions), such as PBS-44 [1041] and PBS-57 [838] have become preferred alternatives. For researchers wanting to investigate Type I or iNKT cells, PBS-57-loaded CD1d tetramers are currently available from the NIH tetramer core facility [1042], conjugated to a number of fluorochromes. Alternatively, the manufacture of soluble CD1d for tetramer manufacture is a viable option, described elsewhere within the literature [821, 1043, 1044]. For those wishing to explore the differential antigenic-recognition characteristics within the larger CD1d-restricted T cell pool [1019], the "in-house" production of CD1d tetramers loaded with antigen of choice, will provide scope to interrogate interactions with the diverse range of established, and putative CD1d-ligands.

1.16.4 Identifying human NKT cells via their TCR usage. The highly conserved TCR usage displayed by Type I or iNKT cells is a factor that can be exploited to identify these cells via FCM, and there are two approaches commonly used to achieve this. First, co-staining with anti-Vα24 and anti-Vβ11, which enriches for T cells expressing the canonical iNKT cell TCR αβ heterodimer. However, there is no assurance that all cells isolated by this means will be α-GalCer-reactive, or CD1d-restricted. The second, and arguably more convincing, approach is using the mAb 6B11, which displays specificity toward the CDR3α loop of the Vα24-Jα18 iNKT cell TCR [1045, 1046]. This approach, in conjuncture with anti-Vβ11 staining, will further ensure isolation of cells that express the canonical iNKT cell TCR.

1.16.5 Step-by-step sample preparation. The following methodologies specifically relate to the experiment depicted in Fig. 132. However, adherence to these general principles will enable the specifics to be adjusted to suit other experimental requirements.

1.16.5.1 Protocol: Generating α-GalCer-loaded CD1d-tetramer. Human CD1d was generated in modified human embryonic kidney 293S cells (HEK293S cells) and enzymatically biotinylated as previously described [1047, 1048].

- Biotinylated monomeric CD1d was loaded with α-GalCer (0.5% [v/v] tyloxapol in TBS) by incubation overnight at 37°C at a 6:1 molar ratio (α-GalCer:CD1d). Vehicle control included the tyloxapol in TBS, but not did not contain α-GalCer.
- CD1d tetramers were generated in house using 10 µg of biotinylated CD1d monomer, mixed with a total 2 µg of streptavidin BV421 added in eight sequential steps (in order to optimize CD1d tetramerization) at 10 min intervals at 4°C.

1.16.5.2 Protocol: Isolation and analysis of NKT cells in cryopreserved PBMCs.

- Add thawed PBMCs (5 × 10^7 cells) to a 50 mL conical tube containing 40 mL of RF-10 (Gibco) media.
- Centrifuge cell suspension for 4 min with 400 × *g* at 4°C.
- Aspirate supernatant and resuspend cellular pellet with 20 mL RF-10 (Gibco) containing 100 µg DNAse I (Sigma–Aldrich) then keep cell suspension at 4°C for 30 min.

1.16.5.3 Protocol: Surface staining.

- Centrifuge cell suspension for 4 min with 400 × *g* at 4°C.
- Aspirate supernatant and resuspend cellular pellet with 500 μL of (1:10 diluted) human FcR-blocking reagent (Miltenyi Biotec) in FCM buffer and incubate at 4°C for 20 min.
- Aspirate supernatant and resuspend cellular pellet with 500 μL of LIVE/DEAD™ Fixable Near-IR (ThermoFisher) diluted in PBS, keep cell suspension in the dark at 4°C for 30 min (The concentration of this reagent should be titrated to ensure optimal staining).
- Add 20 mL of FCM buffer and centrifuge cell suspension for 4 min with 400 × *g* at 4°C.
- Aspirate supernatant and resuspend cellular pellet with 200 μL FCM buffer with diluted CD3ε mAb, CD14 mAb, and CD19 mAb (see FCM Ab table). Keep cell suspension in the dark at 4°C for 30 min.
- Add 20 mL of FCM buffer and centrifuge cell suspension for 4 min with 400 × *g* at 4°C.
- Aspirate supernatant and resuspend cellular pellet in 20 mL of FCM buffer, then split sample evenly into four 10 mL conical tubes.
- Centrifuge cell suspensions for 4 min with 400 × *g* at 4°C.
- Aspirate supernatant and resuspend cellular pellet with 100 μL FCM buffer containing CD1d tetramers (1 μg/mL), or a combination of anti-Vβ11 and anti-Vα24, or anti-Vβ11 and 6B11 (FCM Ab table). Keep cell suspension in the dark at 4°C for 30 min.
- Add 5 mL of FCM buffer and centrifuge cell suspension for 4 min with 400 × *g* at 4°C. Aspirate supernatant and repeat this step.
- Aspirate supernatant and resuspend cellular pellet with 400 μL FCM buffer.
- Analyze samples on the flow cytometer.

1.16.6 Materials: Isolation and analysis of NKT cells in human blood.

RF-10 media

- Base Medium RPMI media 1640, no glutamine (Gibco)
- 10% Heat-inactivated fetal calf serum (Gibco)
- 2 mM L-Glutamine (Gibco)
- 0.1 mM Nonessential amino acids (Gibco)
- 15 mM HEPES (Gibco)
- 100 U/mL of Penicillin/Streptomycin (Gibco)
- 1 mM Sodium pyruvate (Gibco)
- 50 mM 2-Mercaptoethanol (Sigma-Aldrich)

Flow cytometry (FCM) buffer

- Base Medium 1× PBS (made in-house)
- 2% heat-inactivated FBS (Gibco)

DNAse I (Sigma–Aldrich)

Human FcR-blocking reagent (Miltenyi Biotec)

LIVE/DEAD™ Fixable Near-IR Dead Cell Stain Kit, for 633 or 635 nm excitation (ThermoFisher)

Tyloxapol (Sigma–Aldrich)

Streptavidin BV421 (BioLegend)

α-GalCer (PBS-44) was supplied by Prof. P. Savage, Brigham Young University

- α-GalCer (KRN7000) is commercially available from several suppliers [1049, 1050]
- α-GalCer (PBS-57)-loaded CD1d tetramer is available from the NIH tetramer core facility [1042]

Flow cytometry antibodies table: Isolation and analysis of NKT cells in human blood

Antibody	Manufacturer
BUV395 CD3ε mAb (UCHT1)	BD Biosciences
BUV805 CD14 mAb (M5E2)	BD Biosciences
PE/Dazzle™ CD19 BUV805 (HIB19)	BioLegend
anti-Vβ11 FITC or PE (C21)	Beckman Coulter
anti-Vα24 FITC (C15)	Beckman Coulter
6B11 PE	BD Biosciences

*Antibodies should be individually titrated to ensure optimal staining

Flow Cytometer

BD LSR Fortessa™ 5-laser configuration (UV, Violet, Blue, Yellow-Green, Red) was used in the experiments depicted here. However, similar results can be achieved using other multi-parameter flow cytometers.

Analysis

FlowJo (TreeStar)

1.16.7 Data analysis.

The following descriptions and figures specifically relate to the identification of NKT cells from human blood samples. However, these general principles can also be applied to the detection of NKT cells from other tissues. Standard procedures for the isolation of PBMCs can be used for the study of human NKT cells, including density gradient centrifugation with Ficoll-Paque at a density of 1.077 g/mL [1051]. A typical gating strategy for detecting human blood NKT cells is depicted in Fig. 132. This first involves gating on lymphocytes based on a combination of their size and granularity, assessed by their FSC area (FSC-A) and SSC area (SSC-A) intensities, respectively (Fig. 132A). The exclusion of doublets should also be included, as the failure to do so may lead to false-positive staining being incorporated during analysis. There are several techniques to exclude doublets, Fig. 132A depicts an example of single cells being identified based on their relative FSC-A and FSC height (FSC-H). As these two parameters both provide readouts of cell-size, single cells exhibit a linear relationship between these

two parameters, enabling doublets to be excluded. While a secondary doublet exclusion gate is not essential, their elimination can be further assured based on assessing relative SSC intensities. For example, the relationship between SSC-A and SSC-H is used to further exclude doublets within Fig. 132A. Although it is not uncommon for researchers to rely solely on FSC and SSC to differentiate between live and dead cells, this technique is not 100% effective, as seen in Fig. 132A. In this example, LIVE/DEAD fixable Near-IR cell viability dye has been used, which shows that some dead cells have been incorporated within the previous gates. Thus, the inclusion of a viability dye is highly recommended to exclude nonspecific Ab, or CD1d-tetramer staining of dead cells, or cellular debris – a consideration that is particularly important when investigating rare populations, such as NKT cells. In order to further discount any TCR-independent CD1d-tetramer binding that may occur, B cell (CD19$^+$) and monocyte (CD14$^+$) markers are typically included within Ab cocktails to facilitate their exclusion (Fig. 132A). From this point, Type I, or iNKT cells can be identified, enumerated, or sort-purified by the methods described below.

1.16.7.1 α-GalCer-loaded CD1d-tetramer. Type I NKT cells can be identified based on their double positive staining for α-GalCer-loaded CD1d-tetramer and CD3ε mAb. This is depicted within Fig. 132B in relation to a CD1d-tetramer control, which has been exposed to the vehicle reagent (0.5% tyloxapol/TBS) used to solubilize α-GalCer (PBS-44). As this technique relies on CD1d-antigen recognition rather than TCR usage, it has the potential to isolate cells that do not express the canonical iNKT cell TCR [1026–1031]. As such, cells isolated by this manner are more accurately described as Type I NKT cells, rather than iNKT cells. However, iNKT cell TCR usage among α-GalCer-loaded CD1d-tetramer positive cells can be addressed by co-staining with anti-Vα24 [1052].

1.16.7.2 6B11 and Anti-Vβ11 co-staining. The 6B11 Ab clone recognizes the canonical iNKT cells TCR α-chain [1045, 1046]. Hence, the vast majority of 6B11-reactive T cells from individual donors will also co-stain with anti-Vβ11, as seen within Fig. 132C. However, a point worth mentioning is that the proportion of 6B11$^+$, Vβ11$^+$ cells detected within any given sample may differ from that of α-GalCer-loaded CD1d-tetramer$^+$ CD3$^+$ cells (Fig. 132B), as the recognition of this complex can be achieved by T cells with atypical sequences [1026–1031]. While in the majority of cases these differences may appear negligible [1053], variations can occur based on the technique being employed (Fig. 132B and C).

1.16.7.3 Anti-Vα24 and anti-Vβ11 co-staining. T cells expressing the canonical iNKT αβ TCR heterodimer can be enriched for by co-staining with Abs against both Vα24 and Vβ11, as depicted within Fig. 132D. While this technique may identify a population of cells that largely overlap with that of Type I (Fig. 132B), or iNKT cells (Fig. 132C), there is no assurance that cells isolated by this approach will contain the iNKT cell TCR, or even be CD1d-restricted. Hence, despite this method providing a useful means of enriching for, or approximating "NKT cell" numbers, this technique is considered the less stringent of those exemplified here.

1.16.8 Pitfalls: Isolation and analysis of NKT cells in human blood.

- Adherence to the strategies described above should prevent autofluorescent cells from being falsely incorporated within NKT cell (α-GalCer-loaded CD1d-tetramer vs. CD3ε) gates during the analysis of human PBMC samples. However, the presence of autofluorescent cells can be more pronounced with other tissue samples. Therefore, an appreciation of the potential for autofluorescence to adversely impact flow cytometric data [406], and the knowledge of techniques that can prevent such complications are crucial for all FCM users, particularly those wishing to study rare populations such as NKT cells. When designing Ab cocktails it is advisable to leave a channel open for autofluorescence detection, such as 530/30-blue (FITC), 450/40-violet (BV421), or 525/50-violet (BV510). If spectral overlap has been correctly compensated for, positive signaling within this parameter can be used to exclude autofluorescence.

1.16.9 Top tricks: Isolation and analysis of NKT cells in human blood.

- While not typically required when working with fresh PBMCs, it can be beneficial to treat cryopreserved PBMCs with DNAse after thawing. This will digest "sticky" DNA released by cells lysed during this process, preventing cellular-pellets from irreversibly clumping following centrifugation steps.
- The efficiency of glycolipid-loading into CD1d in an in vitro-setting is typically antigen-dependent. Therefore, various conditions such as molar loading ratio, loading temperature and the pH condition all need to be considered when assessing NKT cell-recognition of CD1d-ligands via the use of lipid-loaded CD1d-tetramers.
- Despite CD1d-ligands such as α-GalCer typically being solubilized in Tween 20-based (0.5% [v/v] Tween 20, sucrose [56 mg/mL] and L-histidine [7.5 mg/mL] in PBS) vehicle reagent or DMSO for in vitro studies, the use of a tyloxapol-based (0.5% [v/v] tyloxapol in TBS) vehicle may enhance loading efficiencies of some glycolipid-antigens for CD1d-tetramer studies [1054].
- Although the strength of the interaction between the iNKT cell TCR and α-GalCer-loaded CD1d-tetramer is sufficient to enable clear detection of iNKT cells with CD1d-tetramers generated with streptavidin conjugated to a number of different fluorochromes [1042], the study of lower avidity interactions may require the use of streptavidin conjugated to fluorochromes displaying optimal SNRs, such as PE.

- Due to the rarity of NKT cells within human blood (typically ranging from 0.01 to 0.1% of lymphocytes) [1052, 1053], it can be useful to enrich for these cells prior to cell-sorting, or general FCM analysis using techniques such as anti-PE-magnetic microbead enrichment [1055]. These procedures can be employed to enrich for α-GalCer-loaded CD1d-tetramer, Vα24, Vβ11, or 6B11 positive cells. The choice depending on the individual needs of the researcher, and the availability of reagents conjugated to a suitable fluorochrome.

1.17 Human mucosal-associated invariant T (MAIT) cells

1.17.1 Overview. Mucosal-associated invariant T (MAIT) cells are a population of unconventional T cell with potent antimicrobial function. In humans, these cells are highly abundant and have been implicated in wide-ranging disease settings including infectious disease, autoimmunity, allergy, and cancer [997]. Accordingly, the high abundance and unique biology of MAIT cells has garnered the attention of researchers and clinicians alike, and there is great interest in studying the biology of these cells and understanding how they may contribute to disease clearance or pathology or be manipulated for novel immunotherapies. Key to studying MAIT cells is the efficient use of tools for isolating them from biological samples. This was a major challenge for the field for many years, however, the advent of MR1-Ag tetramers to detect and isolate MAIT cells has facilitated a rapid progression in our understanding of these cells. In this section, we provide recommended guidelines for FCM-based identification strategies for human peripheral blood MAIT cells, with particular emphasis on comparing tetramer and Ab-based identification techniques, and analysis of MAIT cell phenotypic diversity.

1.17.2 Introduction. In contrast to conventional CD8+ and CD4+ TCRαβ T cells that express diverse T cell receptors to recognize polymorphic MHC class I and II molecules, respectively [1056], MAIT cells are defined by expression of a semi-invariant TCR that recognizes microbial-derived vitamin-B2 (riboflavin) derivatives, presented by the monomorphic MHC-related protein 1 (MR1) [850, 1057, 1058] (see also Chapter VI Section 1.9 Murine MAIT cells). This unique antigen-restriction drives a divergent thymic developmental pathway relative to conventional αβ T cells, resulting in a unique, transcriptional landscape characterized by expression of the innate transcription factor promyelocytic leukemia zinc finger (PLZF) [823, 847, 1059] that drives an innate-like, antimicrobial functional capacity. In humans, mature MAIT cells comprise ~3% of total T cells within adult peripheral blood, although this can range from 0.1 to 10% depending on the individual [1060, 1061]. MAIT cells are also highly enriched in liver where they can comprise up to 40% of T cells [1062, 1063], and are abundant in certain mucosal sites, such as the gut [842, 846]. Moreover, upon activation, MAIT cells rapidly produce large quantities of proinflammatory cytokines and chemokines [1063, 1064] and lyse infected cells [1065].

Accordingly, MAIT cells are emerging as key players in antimicrobial immunity [1066–1068]. More recently, MAIT cells have been shown to respond to inflammatory queues independent of TCR-mediated signaling [1069], providing a mechanism for MAIT cells to play a role during the many viral [1070–1072] and nonmicrobial diseases in which MAIT cells have been implicated, including autoimmune disease [1073] and cancer [1018]. In humans, there is evidence of distinct functionality in peripheral tissues [1074]. MAIT cells are largely CD8+, expressing either CD8αα homodimers or CD8αβ heterodimers, or are CD4-CD8- double negative (DN) [846, 1060, 1063]. Rare populations of CD4+ and CD4+CD8+ DP MAIT cells also exist [1060, 1075]. Whether these populations represent functionally distinct subsets remains unclear, although some reports suggest the CD8+ population may have enhanced cytotoxic capacity [1076], while CD8αα+ cells only emerge post-thymic development of mature MAIT cells [847]. Likewise, CD4+ MAIT cells may have distinct tissue localization [1077] and cytokine profiles [1060]. Further studies on this axis are needed, but nonetheless, inclusion of CD4 and CD8 mAbs in FCM experiments analyzing MAIT cells may prove informative. Indeed, several studies have noted modulation of these markers during progression of diverse diseases [1078].

Central to MAIT cell biology is their expression of a "semi-invariant" αβTCR that binds MR1-Ag complexes. The MAIT TCR-α chain is composed of the TRAV1-2 gene segment, which is joined with TRAJ33, or less commonly TRAJ12 or TRAJ20. These TRAV1-2+ TCR α-chains display heavily biased pairing with TCR-β gene segments including TRBV6 family members and TRBV20-1 [1079]. The development of an mAb against the TRAV1-2 TCR-α chain segment of the MAIT TCR provided the first means to isolate these cells from human samples [1080]. This was then further refined to include surface-markers highly expressed by MAIT cells, such as the C-type-lectin CD161, the IL-18Rα CD218, and the ectopeptidase CD26. Co-staining of samples with anti-TRAV1-2 and either CD161 mAb, CD218, or CD26 mAbs was the gold standard to identify MAIT cells for many years. MAIT cells were thus identified as TRAV1-2+ and either CD161HI [1080], IL-18RαHI [1061], or CD26HI [1081]. To date, four clones of anti-TRAV1-2 have been produced (3C10 [1080], D5 [1057], OF5A12 [1082], and REA179 (Miltenyi), however the original clone, 3C10, produced by Lantz and colleagues [1080] is by far the most widely used. A major drawback to the use of this surrogate identification technique, however, is that is has been unclear as to whether all MAIT cells express high levels of the surrogate markers, and likewise, whether all TRAV1-2+ cells that express high levels of the surrogate markers are MAIT cells, particularly in tissues. Indeed, clinical studies analyzing MAIT cells in HIV [1083] and rheumatoid arthritis [1084] have suggested that MAIT cells may downregulate CD161 during disease progression, raising concerns about the use of surrogate markers to identify MAIT cells in disease settings.

The discovery that the MAIT TCR specifically recognizes the antigen (Ag) 5-(2-oxopropylideneamino)-6-D-ribitylaminouracil (5-OP-RU), derived from an intermediate in the microbial riboflavin biosynthesis pathway, facilitated the development of

tetramerised soluble MR1 molecules, loaded with 5-OP-RU (MR1-5-OP-RU tetramers) [846, 850]. These fluorescently tagged tetramers bind all cells expressing TCRs that confer reactivity to MR1-5-OP-RU and provide a highly specific method for the detection and isolation of MAIT cells from human blood and other tissues. As a control, MR1 tetramers loaded with non-stimulatory antigen 6-FP (MR1-6-FP) [846] or synthetic analog Acetyl (Ac)-6-FP [1085] (MR1-Ac-6-FP) are used to validate the specificity of MR1-5-OP-RU tetramers, similar to a conventional isotype control.

A recent direct comparison of MR1 tetramers and surrogate mAb-based identification techniques revealed that while the surrogate markers generally highly enriched for CD8+ and CD4−CD8− DN MAIT cells, they were poor at identifying CD4+ MAIT cells, as many TRAV1-2+ CD4+ T cells expressing high levels of CD161, IL-18Rα, or CD26 were not labeled with MR1-5-OP-RU tetramer [1060, 1075, 1086]. Similarly, the existence of many CD161+ TRAV1-2+ T cells in thymus and neonatal blood samples that do not stain with MR1 tetramer (and are not MAIT cells) [847, 1060, 1087] also limits the use of these surrogate marker combinations in developmental studies. Moreover, across a large cohort of healthy blood donors, there were outliers in which a substantial proportion of MAIT cells lacked expression of surrogate markers, and immature MAIT cells in thymus are defined by a lack of CD161 expression [847]. More recently, MR1 tetramers have been used to identify a population of nonclassical MAIT cells that are phenotypically equivalent to TRAV1-2+ MAIT cells, but utilize a TRAV36+ TCR and thus do not stain with anti-TRAV1-2 mAbs [1088]. Accordingly, where possible, MR1 tetramers should be used for the highly specific isolation of MAIT cells, particularly when studying CD4+ MAIT cells, or when analyzing samples from patient cohorts where the modulation of MAIT cell surface marker expression is unknown, or in developmental studies where thymus or neonatal blood is being assessed. MR1 tetramers are available from the NIH tetramer core-facility upon request conjugated to a variety of fluorochromes or in the form of biotinylated monomers [1089].

1.17.3 Isolation and staining of MAIT cells from single cell suspensions using MR1-tetramers.

1.17.3.1 Step-by-step sample preparation.

1. If using biotinylated MR1 monomers, tetramerize with Streptavidin conjugated to fluorochrome of choice at a 4:1 to 8:1 ratio of monomers to streptavidin, adding Streptavidin sequentially (one-fourth of the required volume) at a series of 10-min incubations at 4°C. This sequential addition facilitates the formation of tetramers and prevents a final mixture of lower degree monomers/dimers/trimers [1090]. A titration of monomer to streptavidin ratio assessed by optimal staining is recommended as monomer and streptavidin conjugate stock concentration can differ between batches or companies.

2. The simplest staining protocol when using fluorochrome-conjugated-MR1-tetramers (hereafter referred to as MR1-

tetramers) is to include them within an appropriate Ab cocktail (see Table 41 for a list of Abs), as the interaction between MR1-5-OP-RU tetramers and MAIT cells is of sufficient avidity to achieve clear staining during a standard 30 min incubation at room temperature or 4°C.

1.17.3.2 Data analysis.
When identifying any T cell population using tetramer staining, a negative control tetramer is recommended, particularly when the target population is rare, of low intensity staining, or there is possible non-TCR-specific background staining. Thus, MR1-5-OP-RU tetramers that bind MAIT cells are used in parallel with MR1-6-FP or MR1-Ac-6-FP that do not stain the majority of MAIT cells [846, 1091]. As such, MR1-6-FP or MR1-Ac-6-FP tetramers provide a valuable negative control for the vast majority of donors, as shown in a representative example of MAIT cell staining of human blood (Figure 133). The following descriptions and figures specifically relate to the identification of MAIT cells from human PBMCs, however, these general principles can also be applied to the detection of MAIT cells in single cell suspensions prepared from other human tissue samples. As these cells can be relatively rare, it is important to carefully apply gates to focus on viable lymphoid cells. A typical gating strategy for detecting human blood MAIT cells by FCM is depicted in (Fig. 134A).

The most commonly utilized surrogate identification method prior to the advent of MR1-tetramers was co-expression of the TRAV1-2 TCR-α chain and high levels of CD161 (CD161++ or CD161HI), often including a gate on CD8α+ T cells. By comparing these markers to MR1-5-OP-RU tetramer stained cells, it has been shown that these surrogate markers are generally quite effective for detecting human CD8+ MAIT cells in the absence of MR1-tetramer [1060, 1086, 1092], however, this efficiency can vary somewhat between individuals and is less stringent when studying CD8− and CD4+ MAIT cells [1060] (Figure 134B and Table 42).

1.17.3.3 Top Tricks: Isolation and staining of MAIT cells using MR1-tetramers.

- Like standard Abs, MR1-tetramers should be titrated prior to use in formal experiments to ensure optimal signal-to-noise separation of staining. MR1-tetramers provided from the NIH facility are used within a staining concentration range of 1:500 to 1:1000 [1089] depending on the fluorochrome conjugated. MR1 tetramer staining conditions (time and temperature) should also be initially tested to ensure best signal-to-noise results. MR1 tetramers work at 4°C, room temperature, and 37°C, with staining intensity proportional to temperature.

- The protein-kinase inhibitor dasatinib can greatly enhance the detection of lower affinity TCR interactions that may otherwise go undetected via tetramer staining [1093]. While unnecessary for the identification of MR1-5-OP-RU tetramer-reactive, TRAV1-2+ MAIT cells, pretreating cells with dasatinib (working concentration 50 nM) may prove advantageous for detecting
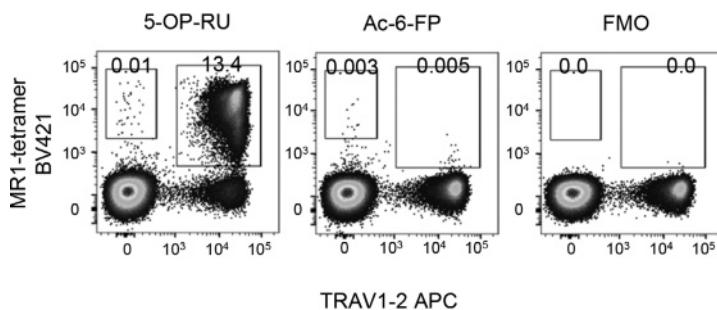
Figure 133. MR1-tetramer staining controls. Representative plots depict MR1-5-OP-RU tetramer staining among CD19$^-$ lymphocytes from human PBMCs in comparison to a MR1-Ac-6-FP tetramer control and a fluorescence minus one (FMO) control. Refer to Fig. 134A for gating strategy.

other populations of MR1-reactive T cells with lower affinity for the MR1 ligands being assessed [1091].

- If staining includes more than one tetramer (such as MR1-5-OP-RU tetramer on one color with MR1-6-FP tetramer on another color), it is highly recommended that tetramer incubations are sequentially applied, with an intervening avidin and biotin blocking step [1094], such as with the Dako Biotin blocking system (see Materials). This will prevent any potential excess streptavidin-conjugated fluorochrome from one tetramer binding available biotin sites that may be present on the other tetramer, which may falsely lead to double-positive tetramer staining.

- In order to exclude any TCR-independent MR1-5-OP-RU tetramer binding and maximize the potential scope of MAIT cell phenotyping that can be achieved within a single antibody cocktail, the detection of B cells, monocytes and dead cells can be restricted to one fluorescence parameter or 'dump channel' akin to a lineage marker dump. For example, a combination

that can be used to achieve this is: APC-Cy7 CD14 mAb, APC-Cy7 CD19 mAb, and Live/Dead fixable Near-IR (ThermoFisher) (Fig. 134A). Gating on CD3/TCR$^+$ cells can also be helpful to exclude TCR-independent MR1 tetramer binding (Fig. 134A).

1.17.3.4 Pitfalls: Isolation and staining of MAIT cells using MR1-tetramers.

- It should be noted that in most individuals, minor populations of TRAV1-2$^+$ MAIT cells can be isolated that display reactivity to both 5-OP-RU and 6-FP. Further, populations of cells that lack the classical MAIT cell TRAV1-2$^+$ TCR α-chain have been identified that preferentially bind MR1-6-FP in comparison to MR1-5-OP-RU [1091]. Therefore, while these atypical MAIT cell subsets may be rare in comparison to classical MAIT cells, caution needs to be taken when using MR1-6-FP tetramers as a negative
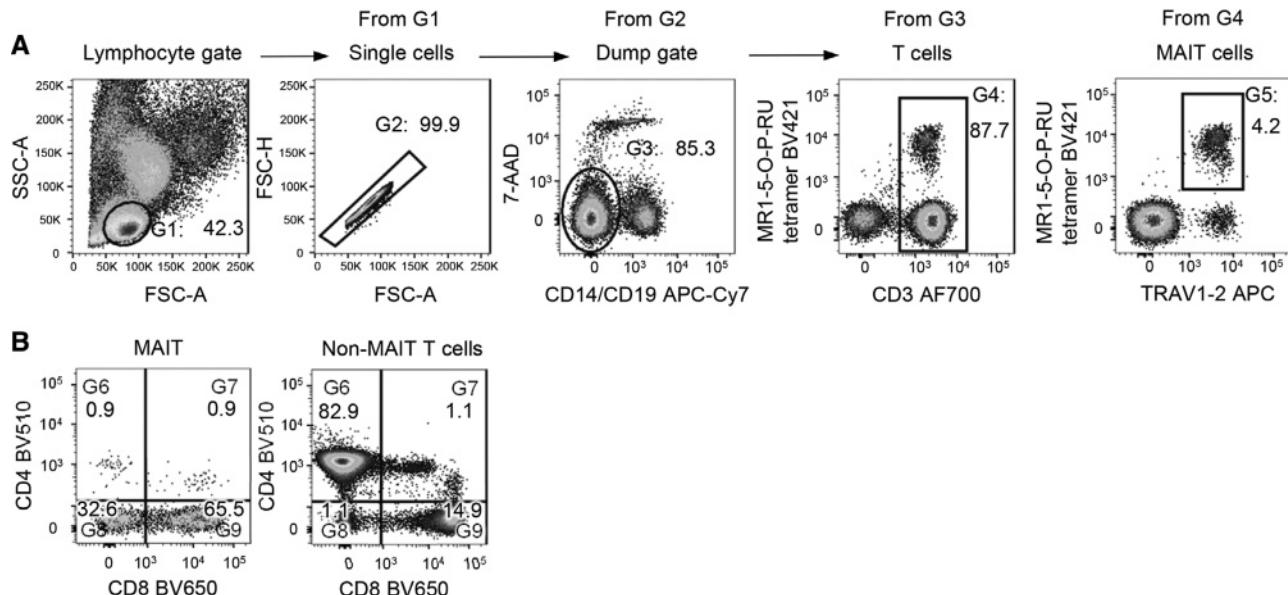
Figure 134. (A) Gating on human peripheral blood MAIT cells. Lymphocytes are distinguished from PBMC preparations based on their FSC-A and SSC-A. Single cells are identified by their linear relationship between FSC-H versus FSC-A, enabling doublets to be excluded. To remove any nonspecific or TCR-independent MR1-5-OP-RU tetramer staining, dead cells are excluded with the use of a viability dye (7-AAD), and monocytes and B cells are excluded based on the expression of CD14 and CD19, respectively. MAIT cell frequencies can be presented as a percentage of CD19$^-$ lymphocytes, or as a percentage of T cells. (B) MAIT cells can be divided into subsets based on expression of CD4 and CD8 co-receptors and, relative to non-MAIT T cells, are typically enriched for CD8$^+$ and CD4$^-$CD8$^-$ double negative (DN) subsets, with only minor populations of CD4$^+$ or CD4$^+$CD8$^+$ double positive (DP) cells.
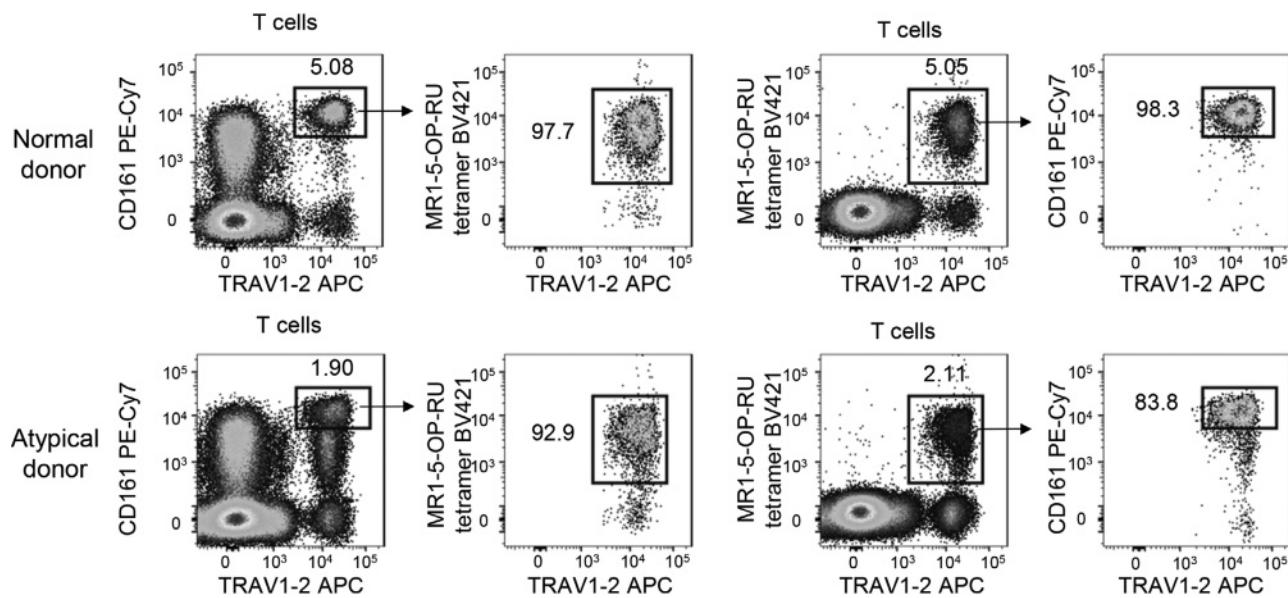
Figure 135. Identifying MAIT cells using surrogate markers. Gating strategy utilized similar to Fig. 134A. Plots depict the identification of human MAIT cells among CD19⁻, CD3⁺ lymphocytes via their expression of TRAV1-2 and CD161 and how this relates to MR1-5-OP-RU tetramer staining from a normal donor (top) and an abnormal donor (bottom).

control, as positive staining cannot automatically be ascribed as non-specific or background.

- Surrogate markers are slightly less reliable for CD4⁻CD8⁻ MAIT cells, and they do not work well for CD4⁺ MAIT cells [1060, 1086, 1092]. Therefore, when using surrogate markers to study these populations, it is important to consider that not all TRAV1-2⁺, CD161⁺⁺ cells will necessarily be MAIT cells

and not all MAIT cells will necessarily be TRAV1-2⁺, CD161⁺⁺, and that CD4⁺ MAIT cells cannot be reliably detected using this approach. The inclusion of other cell-surface receptors typically expressed at high levels by MAIT cells such as the IL-18 receptor alpha chain CD218a (IL-18αR), the ectopeptidase CD26 and the chemokine receptor CD195 (CCR5) may be useful to improve the stringency of their identification [1061, 1063, 1081, 1092].
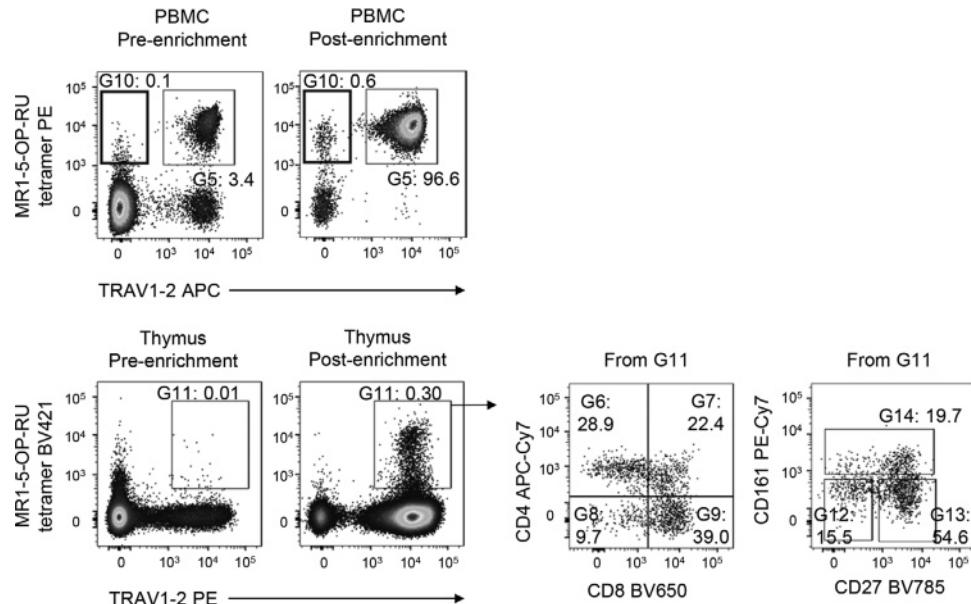
Figure 136. MAIT cell enrichment. Gating strategy utilized similar to Fig. 134A. Top panel depict plots with the percentages of MAIT cells among CD19⁻, CD3⁺ lymphocytes from PBMCs either prior to (first panel) or following MR1-5-OP-RU tetramer enrichment (second panel). Bottom panel depict plots with the percentages of MAIT cells among CD19⁻, CD3⁺ thymocytes either prior to (first panel) or following TRAV1-2 Ab enrichment (second panel). Further phenotypic analysis of MAIT cells reveal heterogeneous subpopulations based on CD4, CD8, CD27, and CD161 (third and fourth panel).

Table 41. Table of Abs used

Dilution	Antigen	Clone	Stock Concentration	Fluorophore	Manufacturer
1:50	CD3	UCHT1	100 tests	BUV395	BD Pharmingen
1:50	CD3	UCHT1	100 tests	PE	BD Pharmingen
1:50	CD3	UCHT1	100 tests	AF700	BD Pharmingen
1:100	CD4	SK3	100 tests	BV510	BD Pharmingen
1:100	CD4	SK3	100 tests	APC-Cy7	BD Pharmingen
1:100	CD8	SK1	100 tests	BUV805	BD Pharmingen
1:200	CD8	SK1	100 tests	BV650	BD Pharmingen
1:50	CD14	MφP9	100 tests	APC-Cy7	BD Pharmingen
1:50	CD19	SJ25C1	100 tests	APC-Cy7	BD Pharmingen
1:50	CD27	O323	100 μg/ml	BV785	Biolegend
1:50	CD161	HP-3G8	100 μg/ml	BV650	Biolegend
1:100	CD161	HP-3G8	100 μg/ml	PE-Cy7	Biolegend
1:50	TRAV1-2	3C10	100 μg/ml	BV711	Biolegend
1:50	TRAV1-2	3C10	100 μg/ml	APC	Biolegend
1:50	TRAV1-2	3C10	200 μg/ml	FITC	Biolegend

Table 42. Summary of subpopulations as part of this section and figures

T cell population	Phenotype/sub-phenotype
G4: CD3 cells	CD14− CD19− CD3ε+
G5: MR1-5-OP-RU+ MAIT	CD3+ TRAV1-2+ MR1-5-OP-RU+
G6: CD4+ MAIT	CD3+ TRAV1-2+ MR1-5-OP-RU+ CD4+ CD8−
G7: CD4+ CD8+ MAIT	CD3+ TRAV1-2+ MR1-5-OP-RU+ CD4+ CD8+
G8: CD4−CD8− MAIT	CD3+ TRAV1-2+ MR1-5-OP-RU+ CD4− CD8−
G9: CD8+ MAIT	CD3+ TRAV1-2+ MR1-5-OP-RU+ CD4− CD8+
G10: Non TRAV1-2 MR1-5-OP-RU+	CD3+ TRAV1-2− MR1-5-OP-RU+
G11: Thymic MR1-5-OP-RU+ TRAV1-2 MAIT	CD3+ TRAV1-2+ MR1-5-OP-RU+
G12: Immature Stage 1 Thymic MAIT	CD3+ TRAV1-2+ MR1-5-OP-RU+ CD27− CD161−
G13: Immature Stage 2 Thymic MAIT	CD3+ TRAV1-2+ MR1-5-OP-RU+ CD27+ CD161−
G14: Mature Stage 3 Thymic MAIT	CD3+ TRAV1-2+ MR1-5-OP-RU+ CD27+/− CD161+

Of note, these markers are validated to be associated with MAIT cells in the blood, but not as extensively in tissues, where some of them can be expressed by conventional T cells both at steady state and during disease.

- There are potential problems in using these surrogate markers to detect MAIT cells in settings other than healthy adult human blood. For example, there is growing evidence that the normal CD161++ phenotype of MAIT cells may be perturbed among donors (Figure 135), under certain disease settings [1083, 1084], and the proportion of CD161++ cells that are MAIT cells as defined by MR1 tetramer also alters with age [847, 1087]. Furthermore, it is also worth considering that a reliance on TRAV1-2 expression to detect MAIT cells will fail to detect those with atypical TCR α-chain usages [847, 1079, 1095, 1096].

- It should be noted particularly for functional studies that the use of either TRAV1-2 mAb or MR1-tetramer poses the possibility of positive selection or activation of MAIT cells. Furthermore, antigen (such as 5-OP-RU) originally on the tetramers may be recycled for presentation causing subsequent cell-mediated MAIT cell activation. In cases like this, it is worth considering a mAb cocktail that enriches for MAIT cells but does not include tetramers for labeling or isolating. Alternatively, cells isolated by tetramer can be rested 37°C overnight prior to performing downstream functional assays.

1.17.4 MAIT cell enrichment.

1.17.4.1 Step-by-step sample preparation.

1. Resuspend cells in 10^7 cells/mL of FCM buffer, stain with PE-conjugated MR1-tetramer OR PE-conjugated anti-TRAV1-2.
2. Wash cells twice with FCM buffer after staining and resuspend cells in 80 μL of MACS® buffer/10^7 total cells.
3. Mix in 20 μL of Anti-PE MACS® MicroBeads/10^7 total cells and incubate for 30 min at 4°C.
4. Wash cells twice with MACS® buffer and resuspend up to 10^8 cells in 5 mL MACS® buffer.
5. Prepare LS column on LS separator by rinsing with 5 mL MACS® buffer, and discard flow-through.
6. Prepare a flow-through collection tube under the column.
7. Apply 5 mL cell suspension onto the column reservoir.
8. After column reservoir is empty, wash column with 3 mL of MACS® buffer as the unlabeled cells pass into the flow-through.
9. Wash column with 3 mL of MACS® buffer three times.

10. Remove LS column and place away from magnet separator, on top of a new 10 mL collection tube.
11. Elute magnetically labeled cells by adding 5 mL MACS® buffer in column reservoir, and firmly pushing the LS plunger into the LS column.
12. Centrifuge to pellet the cells and to use for FCM without further staining with PE-conjugated Abs or tetramers.

1.17.4.2 Data analysis. MAIT cell numbers vary widely among individuals, and the factors influencing that remain poorly understood. Therefore, while it is possible to analyze or sort-purify MAIT cells via FCM directly from PBMC preparations, this is not always sufficient to get enough cells for downstream experiments. Thus, a useful approach is to first enrich for either MR1-5-OP-RU tetramer+ or TRAV1-2+ cells using magnetic-activated cell sorting (MACS®). Figure 136 depicts the enrichment of MAIT cells following PE-microbead enrichment of PBMCs that have been labeled with PE-conjugated MR1-5-OP-RU tetramer. This technique may also prove useful for investigating minor population of MAIT cells, such as the TRAV1-2− cells that can become evident following the enrichment of MR1-tetramer+ cells (Fig. 136). Furthermore, MAIT cell numbers can be extremely rare in organs such as the thymus, but become clearly detectable following enrichment based on TRAV1-2 expression (Fig. 136 and Table 42).

1.17.4.3 Top tricks: MAIT cell enrichment. This protocol describes the use of PE-conjugated MR1-5-OP-RU tetramer or PE-conjugated anti-TRAV1-2 enrichment using anti-PE microbeads, but can be adapted to use with the other fluorochrome options available via MACS® technology or from other manufacturers offering similar magnetic strategies. It is highly recommended that researchers familiarize themselves with detailed tools, resources, and manufacturers' datasheets to determine the most suitable enrichment strategy.

1.17.4.4 Pitfalls: MAIT cell enrichment. The choice of either TRAV1-2 or MR1-tetramer to enrich for MAIT cells will depend on the particular aims of the experiment. While both approaches are highly effective, the enrichment of TRAV1-2+ cells will not enrich for MAIT cells with atypical TCR usages [1091]. This technique may also prove advantageous when aiming to isolate MAIT cells from tissues where they are consistently present at low frequencies, such as the thymus (Figure 136) [847].

1.17.4.5 Materials. Ligand loaded MR1-monomers or tetramers [1089]
FCM buffer

1× PBS
2% FCS

Ficoll-Paque density 1.077 g/mL (Sigma, #GE17-1440-02)
Dako Biotin blocking system (Agilent Dako, #X059030)

Dasatinib (Sigma–Aldrich, #CDS023389)
Magnetic-activated cell sorting (MACS®) buffer

1× PBS
0.5% FCS and 2 mM EDTA.

Anti-PE MACS® MicroBeads for magnetic labelling of cells (Miltenyi Biotec, Order no: 130-048-801)
MACS® LS Columns (Miltenyi Biotec, Order no: 130-042-401)
MACS® Separator with LS column adaptor (Miltenyi Biotec, Order no: 130-091-051)
Flow Cytometer: example: BD LSR Fortessa equipped with yellow-green laser or similar.
Analysis: Flowjo Version 10 (macOS)

2 B cells and their subsets

2.1 Murine B cells and their subsets, including Bregs

2.1.1 Overview. Several murine B cell subsets are known that differ with respect to differentiation stage, B cell receptor repertoire, contribution to the production of natural and adoptive Abs, pro-, and anti-inflammatory capacity, tissue localization, and distribution within tissues. In addition to various B cell subsets, the bone marrow (BM) also contains B cell precursors, which express the prominent "B cell markers" CD19 and B220 (CD45R). Here, we describe strategies to identify the most prominent murine B cell precursors and mature B cell subsets in the BM, as well as secondary lymphoid organs. Plasma cells are not included but are described separately in Section 3 of this chapter.

2.1.2 Introduction. Human and murine B cells exhibit many similarities in terms of their subpopulations, development, and function. Therefore, results obtained in studies investigating B cell compartments in murine models have significantly contributed to our current understanding of immunity. Three murine B lymphocyte lineages B-1a, B-1b, and B-2 cells have been described to exhibit different ontogenies [1097], and can be further subdivided into several subsets and developmental stages, including immature and mature, follicular, marginal zone (MZ), germinal center (GC) B cells, among others. While all B cell lineages are capable of giving rise to Ab-secreting plasma cells, they exhibit different B cell receptor repertoires (BCR), recognize different antigens (protein-, lipid-, or carbohydrate antigen), express different Toll-like receptors and contribute preferentially either to T-independent (B-1a, B-1b; MZ) or to T-dependent (follicular B cells) Ab responses [1098–1101].

B-1 cells are the major B cell subset in the body cavities, e.g., the peritoneum. These cells represent an important source of innate Abs that are produced independently of foreign antigen and T cells, and resemble an important first line of defense against infection [1102]. Stall et al. were the first that described the existence of two distinct subsets of B-1 B cells, termed B-1a and B-
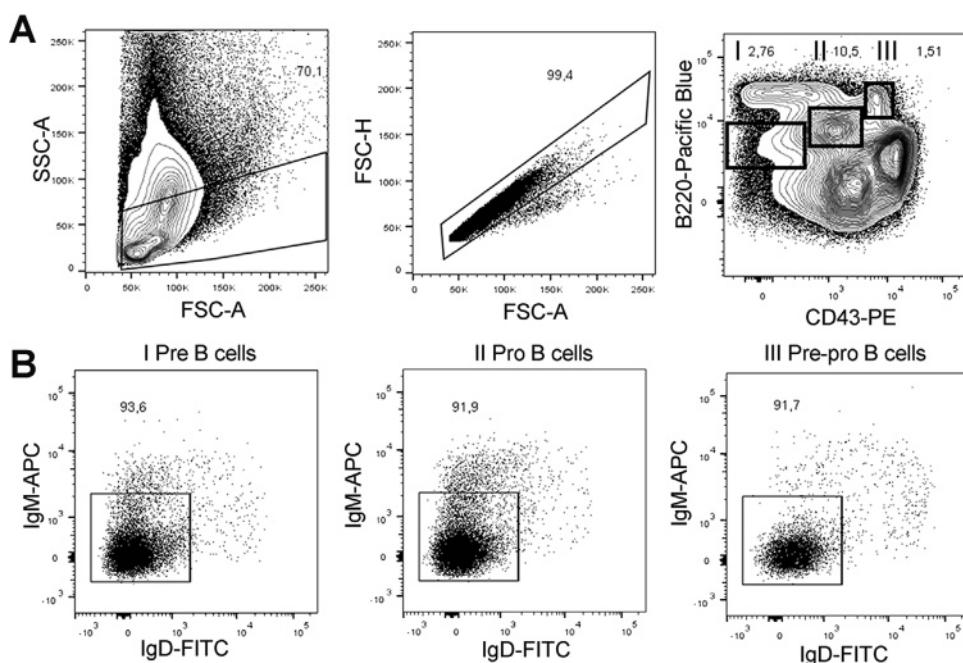
Figure 137. Discrimination of B cell progenitors in BM. Single cell suspensions from BM were stained for B220, CD43, IgM, and IgD. (A) Left plot: Gating strategy to exclude debris. Middle plot: Gating strategy to exclude doublets. Right plot: Pre-B cells (gate I), pro-B cells (gate II) and pre-pro-B cells (gate III) are identified by their distinct B220/CD43 phenotypes. (B) Cells were gated through the gates I, II or III as indicated. Exclusion of IgD^{pos} and IgM^{pos} cells eliminates contaminating immature and mature B cells.

1b [1103]. Self-renewing populations of CD5^{pos} B-1a and CD5^{neg} B-1b cells are found in the peritoneal cavity of adult mice, a small population of B-1a cells is also present in spleen [1104, 1105]. B-2 cells are continuously generated from progenitors found in the adult BM [1097]. This tissue contains various B cell progenitors, including a small population of CD19^{pos}/B220[low/neg] B-1 B cell progenitors, CD19^{neg}/B220^{pos} B-2 progenitors, immature B cells, but also a significant population of re-circulating mature B cells, representing successive developmental stages defined according to surface marker expression and Ig gene rearrangement status [1106, 1107]. The complex rearrangements that produce complete Ig heavy and light chains occur during B cell development. This process of somatic mutation is described in detail elsewhere [1106, 1108–1111]. The principal B cell progenitor populations in the BM are pre-pro B cells, pro-B cells, and pre-B cells, which can still be further subdivided into various developmental stages such as early pro-, late pro-, large pre-, small pre-B cells, among others [1112, 1113]. Of note, these distinct B cell developmental stages are associated with particular Ig-gene rearrangement patterns [1113–1115].

Immature B cells leave the bone marrow and migrate to the spleen to eventually become mature B cells. This process involves the three transitional stages T1, T2, and T3 that are subjected to negative selection of autoreactive cells, while only non-self-reactive cells become fully mature and functional [1116]. The main mature B cell populations in the spleen are follicular B cells and MZ B cells, while B-1 cells represent only a minor population [1117, 1118].

Controlled by autocrine expression of low levels of IFN-γ, immature B cells selectively migrate to the spleen neglecting other secondary lymphoid organs [1119]. An MZ is not existing in these tissues. Therefore, lymph nodes and Peyer's patches contain mainly follicular B cells of the B-2 lineage. Here, we provide strategies for the analysis of the main B cell and B cell progenitor stages, with a focus on the analysis of BM and secondary lymphoid tissues, each containing several different B cell subpopulations.

2.1.3 Step-by-step sample preparation. Single cell suspension of murine spleens, bone marrow (femurs and tibia) and the peritoneal cavity were prepared and filtered through a 70 μm cell strainer (BD Falcon). The primary cells were resuspended (10^7 cells/ml) in PBS containing 0.5% BSA. Fc receptors were blocked with CD16/CD32 mAb for 10 min at 4^0C (5μg/ml in PBS/BSA, clone 2.4G2, in house production). Subsequently, cells were washed with ice-cold PBS/0.5%BSA, and incubated with fluorescent labeled Abs for 15 min at 4^0C. After washing twice, cells were resuspended in PBS/0.5% BSA/ supplemented with 100 μg/ml DNase I, and analyzed by FCM.

2.1.4 Materials.

2.1.4.1 Abs and buffers. PBS (8 g/l NaCl, 0.2 g/l KCl, 1.44 g/l Na2HPO4) containing 0.5% BSA was used for washing and as staining solution. Anti-mouse Abs used in FCM staining
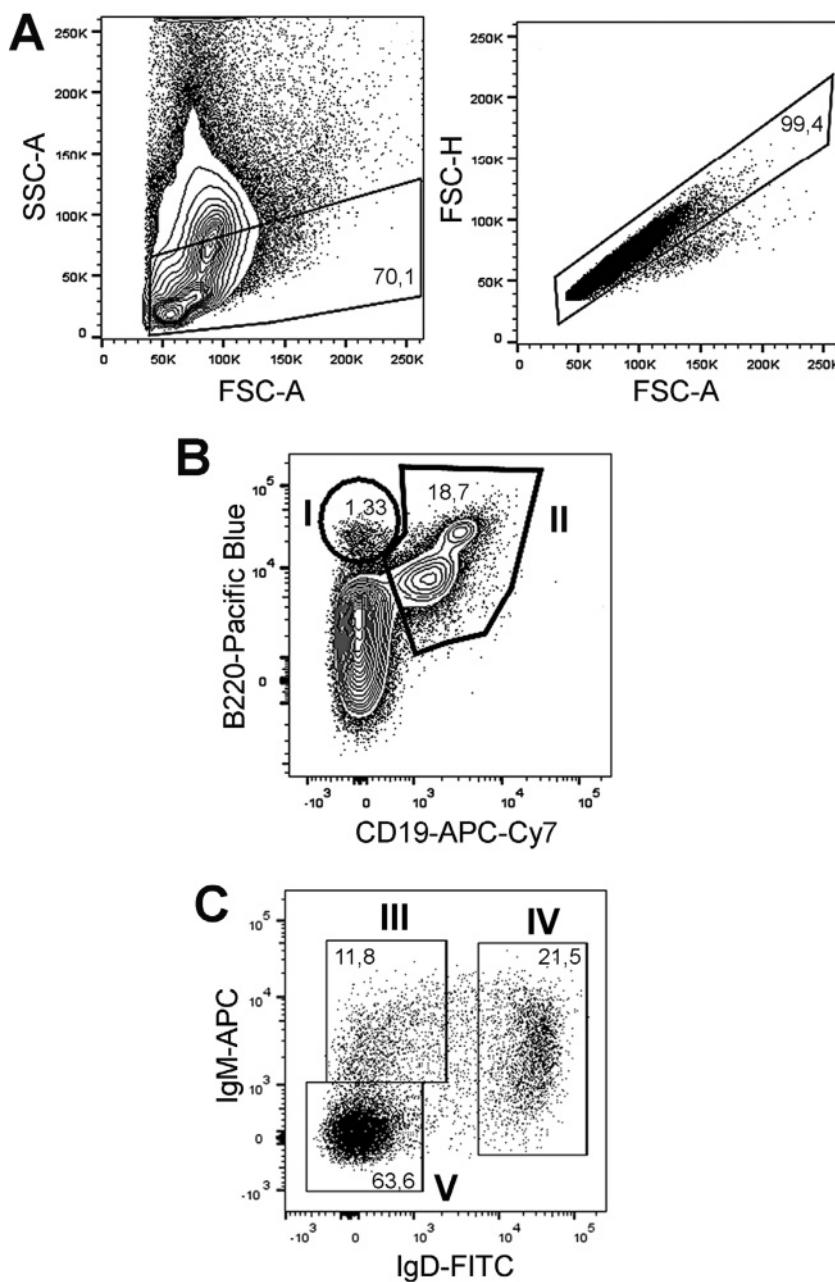
Figure 138. Discrimination of immature and mature B cells in BM. Single cell suspensions from BM were stained for CD19, B220, IgM, and IgD. (A) Gating strategy to exclude doublets and debris. (B) B220^{high}/CD19^{neg} cells (gate I) include pre-pro B cells, while all other B cell subtypes (except plasma cells) are included in the B220 [high]/CD19^{pos} population (gate II). (C) Cells were gated through gate II. Immature (gate III) and mature B cells (gate IV) were identified according to their IgM/IgD phenotypes. Gate V includes a mixture of pre- and pro B cells.

analysis: CD11b mAb (clone M1/70.15.11, in house production); CD19 mAb (clone 1D3, BioLegend, Fell, Germany); anti-B220 (clone RA3.B2, in house production); anti-IgM (clone M41, in house production), anti-IgD (clone 11–26c.2a, BioLegend), CD21/CD35 mAb (clone 7E9, BioLegend), CD23 mAb (clone B3B4, BioLegend), CD43 (clone S11, BioLegend), CD5 mAb (clone 53–7.3, BioLegend), CD3 mAb (clone 90/CD38, BD Pharmingen), anti-GL7 (clone GL7, BioLegend), Fixable Viability Dye (eBioscience).

2.1.4.2 Flow cytometer and analyzing software.   Samples were measured in an LSRII flow cytometer (BD Biosciences) and the

resulting data were analyzed using the FlowJo software (TreeStar, Ashland, OR).

2.1.5 Data analysis: Murine B lineage cells in BM.   After isolation and generation of single cell suspensions, typically from femurs and/or tibia, BM lymphocytes should be gated according to their scatter properties, and doublets should be excluded from the analysis (Fig. 137A). Several B lineage developmental stages within this tissue include proliferating blasts, therefore the FSC gate should be not too restrictive. Removal of dead cells by using either DNA stains such as PI, DAPI or 7AAD, or alternative stains that bind to amines of proteins can be used to further improve the
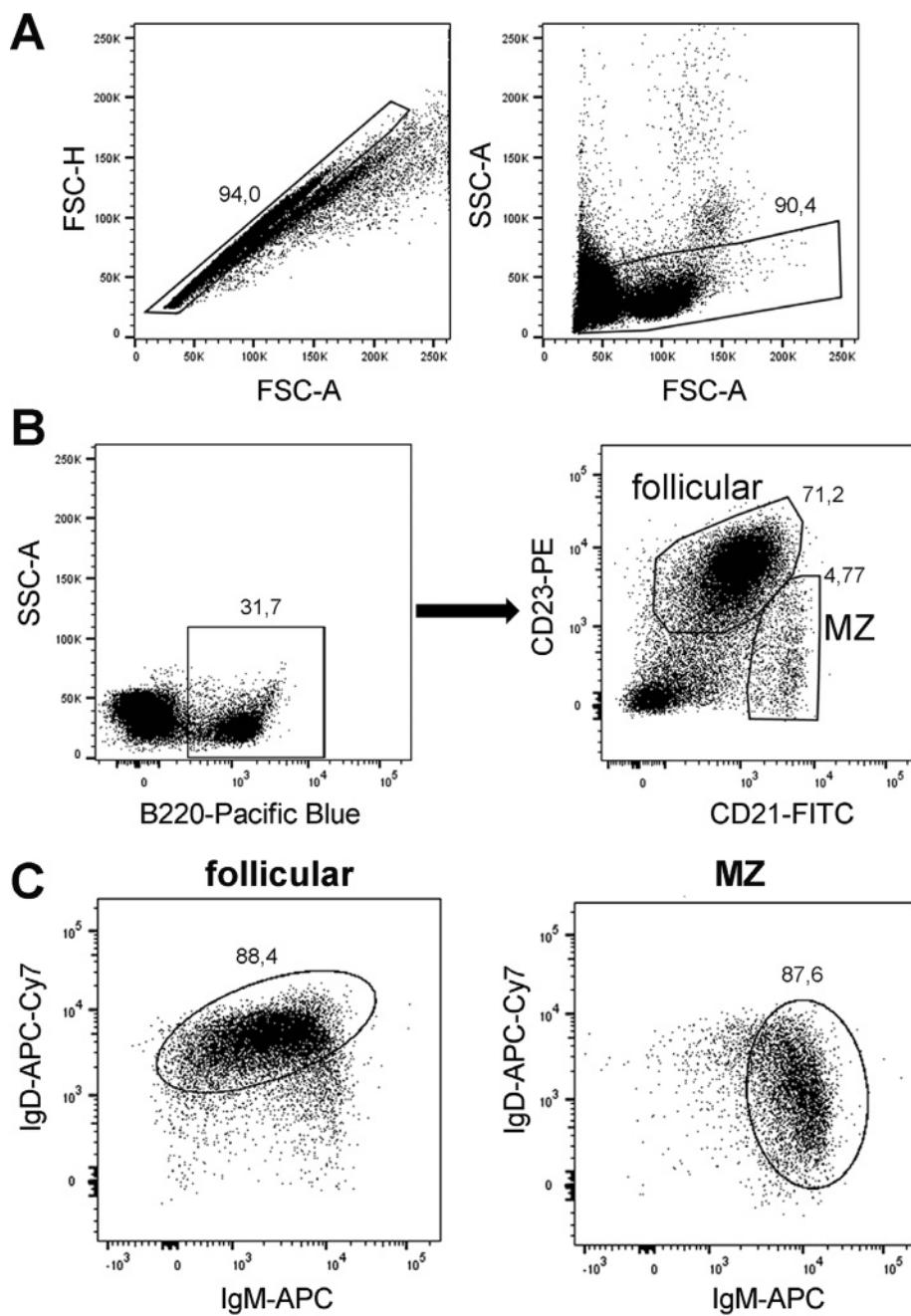
Figure 139. Analysis of follicular and MZ B cells. Single cell suspensions from spleen were stained for B220, CD21, CD23, IgM, and IgD. (A) Gating strategy to exclude doublets and debris. (B) B cells are gated according to B220 expression and follicular and MZ B cells were further discriminated by their CD21^{intmed}/CD23^{high} and CD21^{high}/CD23$^{low/neg}$ phenotype, respectively. (C) Gated follicular and MZ B cells exhibit distinct IgD/IgM expression characteristics.

quality of the data. The choice of the most suitable live/dead discrimination reagent depends on the individual project, e.g., if the samples need to be fixed [1].

In order to cover the major B lineage developmental stages in BM from very early progenitors to the mature B cell stage using only a minimum number of different markers, we suggest to stain with a combination of CD19, B220, CD43, IgM, and IgD mAb. Depending on the specific purpose of the study and the availability of more fluorescent channels, these markers could be complemented by additional ones.

CD19 and B220 serve as specific surface markers for the identification of B lineage cells. CD19 is a co-receptor of the B-cell receptor that is expressed under the control of the PAX5 encoded "B-cell lineage specific activator protein" [1120]. B220 and CD19 are found on the surface of all later B lineage cells except for a subpopulation of terminally differentiated plasma cells [547].

As originally described by Hardy and colleagues, pre-pro B cells, pro-B cells, and pre-B cells are defined according to their distinct expression pattern of B220 and CD43 [1121], Pre-pro B cells resemble very early precursors showing a B220^{pos}/CD43^{pos} phenotype. Pro-B cells and pre-B cells are B220$^{pos/int}$/CD43^{pos} and B220^{low}/CD43^{neg}, respectively (Fig. 137A). All three progenitor populations are distinguishable from the later immature and mature stages by the absence of IgM and IgD expression. Hence,
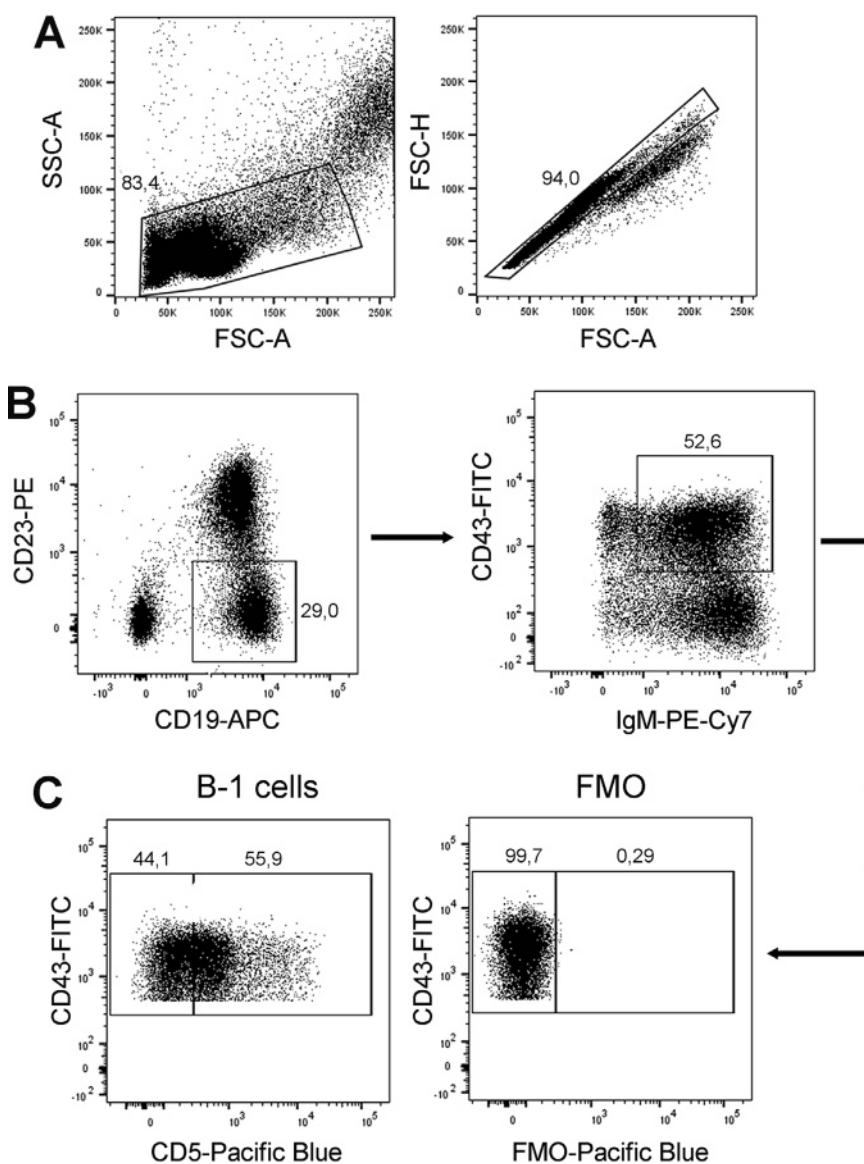
Figure 140. Analysis of B-1 cells. Single cell suspensions from the peritoneal cavity were stained for CD19, CD5, CD23, CD43 and IgM. (A) Gating strategy to exclude doublets and debris. (B) B-1 cells were identified by CD19, CD43 and IgM expression. (C) B-1a and B-1b cells are distinguished according to CD5 expression.

exclusion of IgM^{pos} and IgD^{pos} cells could help to test for the accuracy of the gating (Fig. 137B).

Immature and mature B cells exhibit a CD19^{pos}/B220^{pos}/CD43^{neg}/IgM^{pos}/IgD^{neg} and CD19^{pos}/B220^{pos}/CD43^{neg}/IgM^{pos}/IgD^{pos} phenotype, respectively [1122, 1123]. Following staining with CD19, B220, CD43, IgD, and IgM, all B lineage cells except plasma cells and pre-pro B cells are included within the CD19^{pos}/B220^{pos} population (Fig. 138A and B). Pre-pro B cells are found within the B220^{high}/CD19^{neg} fraction. However, this population does also contain non-B lineage cells [1124]. Pro-B cells, pre-B cells, immature, and mature B cells are included within the CD19^{pos}/B220^{pos} populations. Immature and mature B cells can be further discriminated by the expression of surface IgM and IgD (Fig. 138C).

According to the complexity of the B cell development and heterogeneity of B lineage cells, other marker combinations are useful to study B lineage cells in bone marrow as well. The Basel nomenclature of B cell development classifies B cell progenitors differently from the Hardy system described above [1125]. B cell progenitor phenotypes defined by the surface markers CD25 and CD117 (c-kit) correlate with the stepwise rearrangements of the genes coding for the Ig heavy and light chains [1126, 1127]. The Ig gene loci are rearranged in an ordered fashion, with the D-heavy (D$_H$) segments being first rearranged to -J-heavy (J$_H$) segments, followed by V heavy (V$_H$) to D$_H$ J$_H$. The gene loci coding for the Ig light chains are rearranged later, after successful rearrangement of the Ig heavy gene segments [1128]. B220^{pos}/CD117^{pos}/CD25^{neg} cells typically exhibit rearrangements of the D$_H$–J$_H$ Ig-gene segments, with light chain loci in germline configuration. This population resemble early pre-B cells (pre-B I cells) that are the precursors of large B220^{pos}/ CD25^{pos} cells that, in turn, are the precursors of small B220^{pos}/CD25^{pos} cells [1129]. Since all these progenitor stages do not have completed their Ig gene rearrangements yet, they are surface IgM^{neg}/IgD^{neg}. The

Table 43. Identification of B lineage cells in bone marrow

Subpopulation	Marker combination	Ig gene status	References
Pre-pro	$B220^{high}$ / $CD19^{neg}$ / IgM^{neg} / $CD43^{pos}$	germline configuration	[1108, 1123, 1126, 1129, 1132]
	$B220^{pos}$ / $CD19^{neg}$ / $CD43^{pos}$ / $AA4.1^{pos}$ / HSA^{neg}		[1113, 1121, 1130]
*Pro	$CD19^{pos}$ / $B220^{pos}$ / $CD43^{pos}$ / IgM^{neg} / IgD^{neg}		[1123]
	$CD19^{pos}$ / $B220^{pos}$ / $CD43^{pos}$ / $AA4.1^{pos}$ / HSA^{pos}		[1113, 1121, 1130]
Early pro	$CD19^{pos}$ / $B220^{pos}$ / $CD43^{pos}$ / IgM^{neg} / HSA^{pos} / $BP-1^{neg}$	$**D_H$ - J_H	[1108, 1126, 1129]
Late pro	$CD19^{pos}$ / $B220^{pos}$ / $CD43^{pos}$ / IgM^{neg} / HSA^{pos} / $BP-1^{pos}$	V_H - DJ_H	[1106, 1108, 1126, 1129]
*Pre	$CD19^{pos}$ / $B220^{pos}$ / $CD43^{neg}$ / IgM^{neg} / IgD^{neg}		[1108, 1123]
	$CD19^{pos}$ / $CD43^{neg}$ / IgM^{neg} / $AA4.1^{pos}$ / HSA^{pos}		[1113, 1121]
***Early pre (pre B I)	$B220^{pos}$ / $CD117^{pos}$ / $CD25^{neg}$	D_H - J_H	[1126, 1129]
***Late pre (pre B II)	$B220^{pos}$ / $CD25^{pos}$	$V_H D_H J_H$	[1126, 1129]
Large pre	$CD19^{pos}$ / $B220^{low}$ / $CD43^{neg}$ / HSA^{pos} / $AA4.1^{neg}$ / $preBcR^{pos}$ ($VpreB^{pos}$ / $\lambda5^{pos}$)	$V_H D_H J_H$	[1113, 1114, 1121, 1129]
Small pre	$CD19^{pos}$ / $B220^{pos}$ / HSA^{pos} / IgM^{neg}	rearrangement of the V_L-J_L starts **	[1113, 1121, 1129]
Immature	$CD19^{pos}$ / $B220^{pos}$ / $CD43^{neg}$ / IgM^{pos} / IgD^{neg}	Ig rearrangement complete	[1116, 1117]
	$CD19^{pos}$ / $B220^{pos}$ / HSA^{pos} / IgM^{pos} / IgD^{neg}		[1113, 1121, 1131]
Mature	$CD19^{pos}$ / $B220^{pos}$ / $CD43^{neg}$ / IgM^{pos} / IgD^{pos}		[1123]

* Refers to the Hardy nomenclature. **D_H, J_H, V_H, are the respective gene segments of the Ig heavy chain. **V_L and J_L are the respective gene segments of the Ig light chain. ***Refers to the Basel nomenclature.

great majority of large $B220^{pos}$/$CD25^{pos}$/IgM^{neg}/IgD^{neg} cells have at least one heavy chain locus $V_H D_H J_H$ rearranged. These cells are called large pre-B cells (pre-B II cells). Staining for additional markers such as AA.4.1, heat-stable antigen (HSA), surrogate light (SL) chains VpreB and lambda5 can be used to perform a more detailed analysis of B lineage subpopulations in BM [1113, 1114, 1121–1123, 1130, 1131] (Table 43).

2.1.6 Data analysis: Murine B cells in secondary lymphoid organs.

For identification of B cells in the spleen and other secondary lymphoid organs, single cells should be gated according to their scatter properties, and doublets should be excluded from the analysis (Figure 139A). In order to avoid exclusion of activated/proliferating B cells, the FSC gate should be not too restrictive. Exclusion of dead cells through application of live/dead discrimination reagents is strongly recommended [1], this measure is of crucial importance particularly when smaller subpopulations are included in the analyses.

The spleen contains MZ B cells that are unique to this organ. The immature B cells stages T1, T2 and T3 are also selectively found in the spleen. In contrast, lymph nodes and Peyer's patches contain neither MZ nor immature B cells, but harbor mainly follicular B cells.

In spleen and other secondary lymphoid tissues, all B cells are $CD19^{pos}$ and $B220^{pos}$ (of note, not all plasma cells express

these two markers, see Chapter VI Section 3.1 Murine Ab-secreting plasmablasts and plasma cells). Therefore, CD19 or B220 can be used as alternative markers for the identification of B lineage cells in these tissues. In spleen, staining for B220 (or CD19), CD21, CD23 and IgM allows identification of follicular B cells and MZ B cells [1132, 1133]. We also recommend to stain additionally for IgD. Using this marker combination, follicular B cells are identified by their $B220^{pos}$/$CD21^{intmed}$/$CD23^{high}$ phenotype, MZ B cells are $B220^{pos}$/$CD21^{high}$/$CD23^{low/neg}$ (Fig. 139B). While their characteristic B220/CD21/CD23 expression profile is sufficient to identify follicular and MZ B cells, their identity can be further proofed by their distinct IgD^{pos}/IgM^{intmed} and $IgD^{low/neg}$/IgM^{high} phenotype, respectively (Fig. 139C). After further gating $B220^{pos}$ cells on IgM vs CD21 and CD23, this marker combination also allows to identify T1 and T2 cells [1134].

All secondary lymphoid organs can contain GCs where B cells can develop Abs of increased affinity, after proper stimulation in the context of a T-dependent immunization. GCs are transient structures present after immunization with T-dependent (protein) antigens which are absent in steady state. Flow cytometric analysis of GC B cells is described in section Chapter VI Section 2.2 Murine Germinal Center B cells. Eventually, the GC reaction gives rise to plasma cells and memory B cells. Plasma cells are described in detail in Section 3 of this chapter (Murine Ab-secreting plasmablasts and plasma cells. Memory B cells are found in spleen and in the peripheral blood. The murine B cell memory

compartment appears in several subsets and exhibits a very heterogeneous phenotype [1135].

Memory B cells specific for one particular antigen can be identified by staining with fluorescent-labeled antigen. However, due to the low frequencies of these cells and unspecific binding to other B cells, this method is challenging and needs careful controls [1136, 1137]. Usage of adoptive transfer of B cells from BCR transgenic mice allows to increase the frequencies of monospecific B cells. In the recipients, these cells could be identified by staining with a fluorescent-labelled antigen or by an idiotype specific marker. Staining for CD35, CD73, CD80, and CD273 (PD-L2) defines functionally distinct subsets of murine memory B cells, including IgM[pos] and IgG^{pos} cells [1138–1143]. The spleen also contains a small population of B-1 cells. An overview of marker combinations suitable to identify B lineage cells in spleen is provided in Table 44.

2.1.7 Data analysis: B-1 cells in peritoneum.   B-1 cells mainly reside in the peritoneum, the pleura and other body cavities [1154]. Compared to other B cells, they express lower levels of B220, but normal or high levels of CD19. Therefore, we recommend usage of CD19 mAb to identify B cells in body cavities.

B-1 cells come in two flavors, B-1a and B-1b which are distinguishable by differential expression of CD5.

After isolation, peritoneal lymphocytes should be gated according to their scatter properties, and doublets should be excluded from the analysis (Figure 140A). To some extent, B-1 cells recognize self-antigens and may often exhibit an activated blast phenotype even in the absence of an external stimulus [1146]. Therefore we recommend to set the FSC gate not too restrictive. Removal of dead cells is recommended in case the peritoneal immune cells were activated, e.g. by infectious agents, thioglycollate, or other stimuli. B-1 cells could be identified according to their CD19^{pos}/CD23^{neg}/CD43^{pos}/IgM^{pos}phenotye (Figure 140B). B-1a and B-1b are discriminated by their CD5^{pos} and CD5^{neg} phenotype, respectively (Figure 140D).

2.1.8 Data analysis: Regulatory B cells.   B cells can modulate immune responses and induce or suppress inflammation through the production of Abs, but also by contact-dependent interactions and through the secretion of various pro-and anti-inflammatory cytokines such as IFN-gamma, GM-CSF, IL-10, IL-17, and IL-35 [1155–1160].

B cells with a suppressive function are generally termed "regulatory B cells" (Bregs) [1161]. Breg subtypes typically express immunosuppressive IL-10 but otherwise exhibit a very heterogeneous phenotype [1162]. Several protocols are in use to identify Breg subtypes by distinct combinations of markers such as IL-10, IgM, IgD, CD1d, CD5, CD21, CD23, CD24, CD43, and CD93, among others [1146, 1156, 1162–1175] (Table 45).

At least one of the IL-10 producing Breg subtypes termed B10 cells, which exhibits a CD1d^{hi}/CD5^{pos}/CD19^{pos} phenotype, represents a direct precursor stage of Ab-secreting cells [1163].

Interestingly, production of immunosuppressive IL-10 is common among Ab-secreting plasmablasts and plasma cells [1164–1166]. Recently, the inhibitory receptor LAG-3 was identified as a marker for a population of natural regulatory plasma cells [1167].

2.1.9 Pitfalls and tricks.   B lineage cells exhibit a broadly heterogeneous phenotype. This includes proliferating and/or activated cells that are larger than resting lymphocytes and might be excluded by the usually lymphocyte scatter gate. Moreover, B cell subsets can express markers typical for other lineages, i.e., the "myeloid marker" CD11b that is found on B-1 cells in the body cavities. Therefore, we recommend to start the analysis of the cytometric data with an unbiased approach, avoiding exclusion of cells potentially belonging to the B lineage. This could be achieved by analyzing all CD19 or B220 positive cells among the total, ungated population. In a second step, non B lineage cells could be excluded by appropriate gating.

2.2 Murine germinal center B cells

2.2.1 Overview.   Germinal centers (GCs) are the sites of antigen-dependent clonal expansion and affinity maturation of B lymphocytes, thereby generating high-affinity B cell clones that can develop into memory B cells and long-lived plasma cells secreting high amounts of Abs. Here, we describe a staining protocol to unambiguously identify murine GC B cells, as well as B cell subpopulations within the GC.

2.2.2 Introduction.   Upon the encounter with antigen, antigen-activated T cells interact with B cells at the T-B cell border. Antigen-specific B cells that present antigen on MHC class II molecules to activated T cells in turn secrete cytokines to induce survival and proliferation of B cells (see also Chapter VI Sections 2.3 Human B cells and their subsets and 2.4 Human B cells recognizing defined (auto)antigens), which can then enter the B cell follicles [1176, 1177]. Germinal centers (GCs) arise in B cell follicles in secondary lymphoid organs like the spleen or lymph nodes [1178]. These GCs are the site of antigen-dependent clonal expansion and affinity maturation and lead to the development of high-affinity Abs [1179].

GCs can be divided into anatomically defined zones, namely the dark zone (DZ) and the light zone (LZ) that were historically classified based on their appearance under a light microscope [1180].

In a Darwinian evolution process, B cells with low affinity undergo apoptosis whereas B cell clones with higher affinity for their cognate antigen are positively selected to survive.

Within the DZ, a massive proliferation of B cells takes place. Additionally, the enzyme activation-induced cytidine deaminase (AID) generates mostly point mutations within the variable region of the heavy chain (HC) and the light chain (LC) of the BCR, which is known as somatic hypermutation [1181]. These mutations alter

Table 44. Identification of B lineage cells in spleen

Subpopulation	Marker combination	References
T1	$B220^{pos}$ / $CD21^{low}$ / $CD23^{low/neg}$ / $IgD^{low/neg}$ / IgM^{high}	[1134, 1144, 1145]
	$B220^{pos}$ / $CD23^{neg}$ / IgM^{high} / $AA4.1^{pos}$	[1116]
T2	$B220^{pos}$ / $CD21^{high}$ / $CD23^{pos}$ / $IgD^{low/neg}$ / IgM^{high}	[1134]
	$B220^{pos}$ / $CD23^{pos}$ / IgM^{high} / $AA4.1^{pos}$	[1116]
	$B220^{pos}$ / $CD21^{high}$ / $CD23^{pos}$ / IgD^{high} / IgM^{high}	[1144]
T3	$B220^{pos}$ / $CD23^{pos}$ / IgM^{low} / $AA4.1^{pos}$	[1116]
FO	$B220^{pos}$ / $CD21^{intmed}$ / $CD23^{high}$ / IgD^{pos} / IgM^{intmed}	[1133, 1134]
	$B220^{high}$ / $CD23^{pos}$ / IgM^{low} / $AA4.1^{neg}$	[1132]
	$CD19^{intmed}$ / $CD1d^{intmed}$ / $CD23^{pos}$ / $CD43^{neg}$ / IgM^{low} / IgD^{high} / $CD5^{neg}$	[1146]
MZ	$B220^{pos}$ / $CD21^{high}$ / $CD23^{low/neg}$ / $IgD^{low/neg}$ / IgM^{high}	[1133, 1134, 1144]
	$CD9^{pos}$ / $CD21^{pos}$ / $CD23^{neg}$ / IgD^{low} / IgM^{high}	[1132]
	$CD19^{intmed}$ / $CD1d^{high}$ / $CD21^{high}$ / $CD23^{neg}$ / $CD43^{neg}$ / IgM^{high} / IgD^{low} / $CD5^{neg}$	[1146, 1147]
B-1	IgM^{high} / $CD43^{pos}$ / $IgD^{low/neg}$ / $CD23^{low/neg}$	[1132]
	$CD19^{pos}$ / $B220^{low}$ / $CD43^{pos}$ / $CD23^{neg}$ / $AA4.1^{neg}$	[1118, 1148]
B-1a	$CD19^{pos}$ / IgM^{pos} / $CD43^{pos}$ / $CD5^{pos}$	[1149, 1150]
	$CD19^{high}$ / $CD1d^{intmed}$ / $CD23^{neg}$ / $CD43^{pos}$ / IgM^{high} / IgD^{low} / $CD5^{pos}$	[1146]
B-1b	$CD19^{pos}$ / IgM^{pos} / $CD43^{pos}$ / $CD5^{neg}$	[1149]
	$CD19^{high}$ / $CD1d^{intmed}$ / $CD23^{neg}$ / $CD43^{pos}$ / IgM^{high} / IgD^{low} / $CD5^{neg}$	[1146]
Memory	$antigen^{pos}$, $CD73^{low}$ / $CD80^{low}$ / $CD273^{low}$	[1138–1143]
	$antigen^{pos}$, $CD73^{hi}$ / $CD80^{hi}$ / $CD273^{hi}$	
	$antigen^{pos}$, $CD73^{hi}$ / $CD80^{low}$ / $CD273^{low}$	
	$antigen^{pos}$, $CD73^{low}$ / $CD80^{hi}$ / $CD273^{hi}$	
	*$antigen^{pos}$, $CD73^{hi}$ / $CD80^{low}$	
GC	$CD19^{pos}$ / $B220^{pos}$ / $CD38^{neg}$ / $GL7^{pos}$	[1151, 1152]
	$B220^{pos}$ / $GL7^{pos}$ / Fas^{pos}	[1134]
	$B220^{pos}$ / $GL7^{pos}$ / PNA^{pos}	[1153]

*$Antigen^{pos}$ = cells are specific for the immunizing (memory) antigen

the binding of the BCR to its cognate antigen, allowing the B cells to acquire higher affinity. The process of class switch recombination (CSR), also known as isotype switching, is mediated by the same enzyme and leads to the replacement of the $C\mu$ heavy chain by either $C\gamma$, $C\varepsilon$, or $C\alpha$, resulting in the expression of IgG, IgE, or IgA, respectively [1182].

The selection of B cell clones with enhanced affinity to their cognate antigen occurs in the LZ of the GC and is mediated

Table 45. Identification of regulatory B cell subsets[a]

Subpopulation	Marker combination	References
Breg	$CD5^{pos}$ / $CD19^{high}$ / $CD1d^{high}$ / $CD21^{high/intmed}$ / $CD23^{pos/neg}$ / $CD43^{neg}$ / IgM^{high} / $IgD^{low/intmed}$	[1146]
T2-MZP	$CD19^{pos}$ / $CD21^{high}$ / $CD23^{high}$ / IgM^{high} / HSA^{high} / $CD1d^{high}$ / $IL-10^{pos}$	[1162, 1168, 1169]
MZ	$CD19^{pos}$ / $CD21^{high}$ / $CD23^{neg}$ / $IL-10^{pos}$	[1170, 1171]
B10	$CD5^{pos}$ / $CD1d^{high}$ / $CD19^{pos}$ / $IL-10^{pos}$	[1156, 1163, 1172]
Tim-1^{+} cells	$Tim-1^{pos}$ / $CD19^{pos}$ / $IL-10^{pos}$	[1173, 1174]
Plasma cells	$CD138^{pos}$ / $B220^{pos}$ / $MHC-II^{low}$ / $IL-10^{pos}$	[1164, 1166]
Plasmablasts	$CD138^{pos}$ / $CD44^{high}$ / $IL-10^{pos}$	[1165]
Natural regulatory PCs	$CD19^{pos/neg}$ / $B220^{neg}$ / $LAG-3^{pos}$ / $CD138^{high}$ / $IL-10^{pos}$	[1167, 1175]

[a] including "regulatory plasma cells"
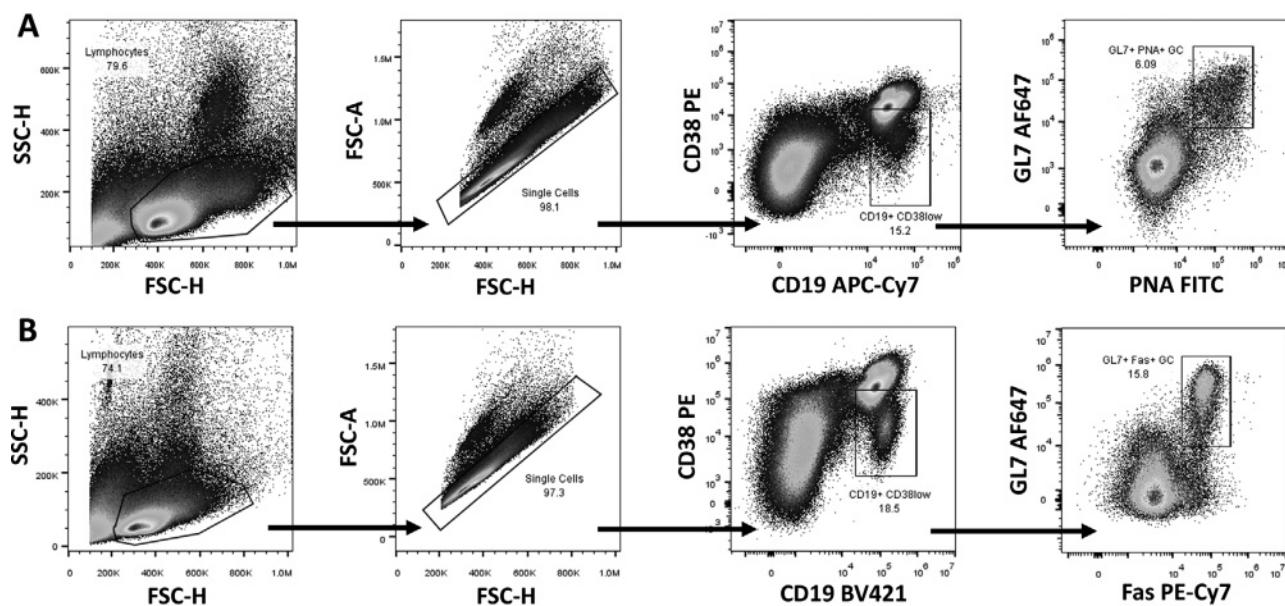
Figure 141. Two gating strategies for the identification of murine splenic GC B cells from single cell suspensions by flow cytometry. C57BL/6 mice were immunized with sheep red blood cells (SRBC) and analyzed on d10 post-immunization. In (A) GC B cells were stained as being CD19$^+$ CD38^{low} and GL7$^+$ PNA$^+$. In (B) GC B cells were stained as being CD19$^+$ CD38^{low} and GL7$^+$ Fas$^+$. Both variants unambiguously help to identify GC B cells.

by two cell types: follicular dendritic cells (FDCs) capture antigen in the form of immune complexes that is presented to B cells [1183]. Antigen-specific B cells internalize antigen and load it onto MHCII peptides for the presentation to T follicular helper (T$_{fh}$) cells. Besides FDCs, these are the other class of cells that mediate selection of high-affinity B cell clones. It has been proposed that peptide-MHCII density on GC B cells

is the limiting factor that leads to positive survival signals by T$_{fh}$ cells [1179]—that means the higher the affinity of the BCR of the B cell, the more antigen it will capture, internalize and finally present to T$_{fh}$ cells. However, Yeh et al. have shown that halving peptide-MHCII density on B cells does not alter selection of high-affinity B cell clones but rather their initial entry into early GCs [1184] and therefore the precise mechanism for
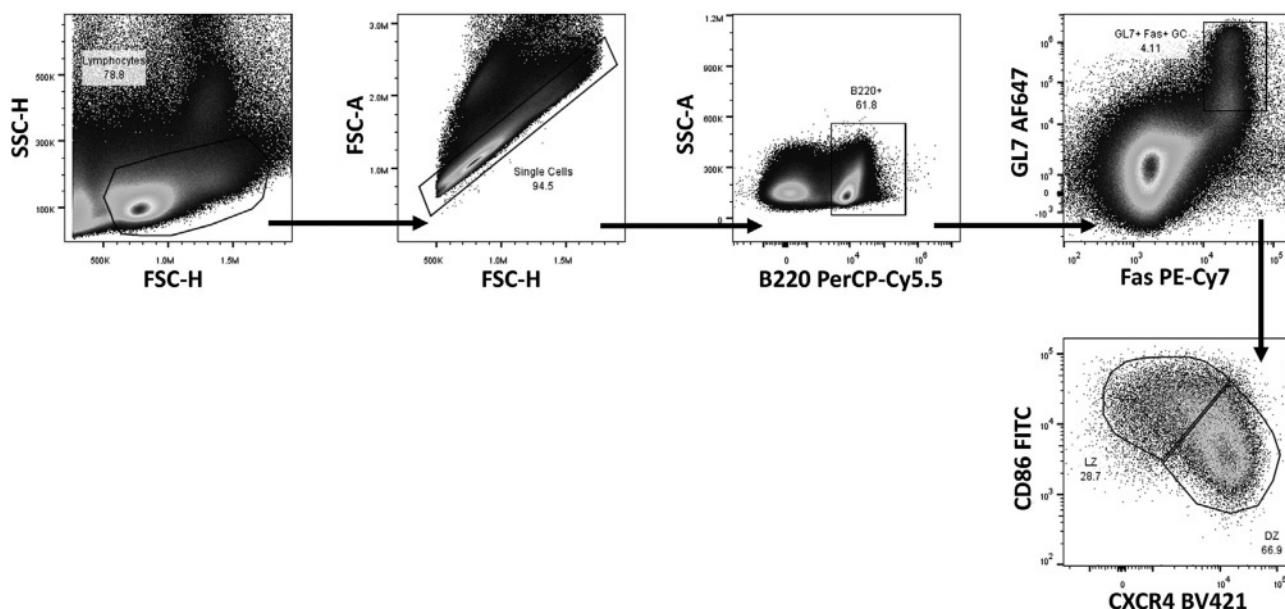
Figure 142. Staining of murine splenic GC B cells from single cell suspensions to identify GC subpopulations by flow cytometry. C57BL/6 mice were immunized with sheep red blood cells (SRBC) and analyzed on d10 post-immunization. The GC can be divided into the dark zone (DZ, CXCR4^{hi} CD86^{low}) and the light zone (LZ, CXCR4^{low} CD86^{hi}) and can be distinguished by their respective surface makers.

positive selection of high-affinity B cells within the LZ still remains unclear.

B cells can then either leave the GCs to become memory B cells [1185, 1186] or plasma cells [1187, 1188] or cycle back to the dark zone to undergo further rounds of division and somatic hypermutation to increase affinity even more [1189, 1190]. See also Chapter VI Sections 2.1 Murine B cells and their subsets, incl Breg cells and 3.1 Murine Ab-secreting plasmablasts and plasma cells.

2.2.3 Step-by-step sample preparation.   For the generation of single cell splenocytes, spleens of mice were harvested and crushed through a 100 μM nylon mesh filter and finally resuspended in FCM buffer (PBS, 2% FCS, 2 mM EDTA). Lysis of erythrocytes was performed at room temperature for 5 min, cells were washed two times and Fc-blocking solution was added (20 min at 4°C). Finally, cells were incubated with FCM buffer containing respective directly conjugated Abs (20 min at 4°C) and resuspended in FCM buffer for analysis. All centrifugation steps were performed at $400 \times g$ and 4°C for 8 min.

2.2.4 Materials.   FCM buffer: PBS (137 mM NaCl + 2.7 mM KCl + 4.3 mM Na$_2$HPO$_4$ + 1.4 mM KH$_2$PO$_4$, pH 7.3), 2% FCS (PAN Biotech), 2 mM EDTA (Lonza).

Erythrocyte lysis buffer: 0.15 M NH$_4$Cl, 0.02 M HEPES, 0.1 mM EDTA.

Fc-blocking solution: CD16/32 mAb (clone 2.4G2, Hölzel Diagnostika) in FCM buffer.

Antibodies: Anti-mouse Abs that were used for FCM analysis: CD19 APC-Cy7 (clone 1D3, BioLegend), CD19 BV421 (clone 6D5, BioLegend), B220 PerCP-Cy5.5 (clone RA3-6B2, BioLegend), CD38 PE (clone 90, BioLegend), PNA FITC (Vector Laboratories), GL7 AF647 (clone GL7, BioLegend), Fas PE-Cy7 (clone Jo2, BD Biosciences), CD86 FITC (clone GL1, eBioscience), and CXCR4 BV421 (clone, L276F12, BioLegend). FCM analysis was performed on a Cytoflex instrument (Beckman Coulter) and FlowJo v10.5.3 analysis software (FlowJo, LLC).

2.2.5 Data analysis: Germinal Center B cells.   Although the sample preparation leads to a single cell suspension, doublets can occur through cell–cell interactions (which can be reduced by adding EDTA to the FCM buffer) and can be easily excluded from the analysis by a plot that shows FSC Height versus Area (Fig. 141A). The lymphocytes gate should not be too stringent, as GC B cells tend to be larger in size. In order to stain for murine GC B cells, we suggest to use the markers CD19 or B220, CD38, GL7, and either PNA (Fig. 141A) or Fas (Fig. 141B). (See also Chapter VI Section 2.1, why to use CD19 or B220). In contrast to human GC B cells, murine GC B cells show reduced expression of the surface marker CD38 and can be gated accordingly [1191]. Here, it is important to set a larger gate for CD38 to not exclude any GC B cells, since these cells tend to have varying CD38 expression levels. Further, the rat mAb GL7 that reacts with a sialic acid glycan moiety called Neu5Ac [1152], previously reported as

a marker for polyclonally activated B and T cells [1192], can be used in the staining protocol. In addition, the plant lectin peanut agglutinin (PNA) from *Arachis hypogaea* with specificity for terminal galactosyl residues on cell surface oligosaccharides [1193] has been shown to bind GC B cells and can be used to specifically identify these cells [1194–1196]. Instead of using PNA (see "pitfalls"), the Fas receptor (CD95, Apo-1) can be used to identify GC B cells (Fig. 141B), which is highly upregulated in these cells [1197].

With the mentioned four colors, CD19 or B220, CD38, GL7, and either PNA (Fig. 141A) or Fas (Fig. 141B), GC B cells can unambiguously be identified. Since GC B cells also downregulate IgD [1194, 1198, 1199], this is an additional marker that can be added to the staining protocol.

Pitfalls

One pitfall of the staining in Fig. 141A is that the PNA signal is downregulated quite fast if the time between staining and measurement of the samples is long (own observation). Constantly keeping samples on ice however helps to counteract this downregulation.

2.2.6 Data analysis: Germinal Center B cell subpopulations.   The GC has a certain microanatomic structure that can be divided into the DZ, where B cell proliferation and somatic hypermutation take place, and a LZ, where selection of high-affine B cell clones occurs. In order to stain for these two zones, GC B cells are first stained as described in the section "Murine Germinal Center B cells" above (Fig. 141).

CD86 (also known as B7-2) is a surface protein that is expressed on activated B cells [1200, 1201] and has a costimulatory function for T cell proliferation [1202]. Together with the chemokine receptor CXCR4, that has been shown to be important for GC organization [1203], Victora et al. used the combination of CD86 and CXCR4 to differentiate DZ cells (CXCR4^{hi} CD86^{low}) from LZ cells (CXCR4^{low} CD86^{hi}) [1204]. The staining for DZ/LZ cells is shown in Fig. 142.

Pitfalls

A pitfall of this staining is the difficulty to set an accurate gate for the DZ/LZ, since these two populations are not clearly separable from each other by FCM. Especially if fluorochromes for CXCR4 and CD86 are used that are known for fluorescence spillover, proper compensation is very important to not distort DZ/LZ ratios. See also Chapter II Section 1 Compensation.

2.3 Human B cells and their subsets

2.3.1 Overview.   B cells represent the Ab-producing cells developing from naïve B cells to Ab-secreting PC. One feature of B cells is their capacity to differentiate upon antigen dependent and independent stimulation to Ab secreting cells, also called plasma cells. The stages of B cell differentiation share several common features between the human and the rodent immune system. In this section, we focus on human B cells.
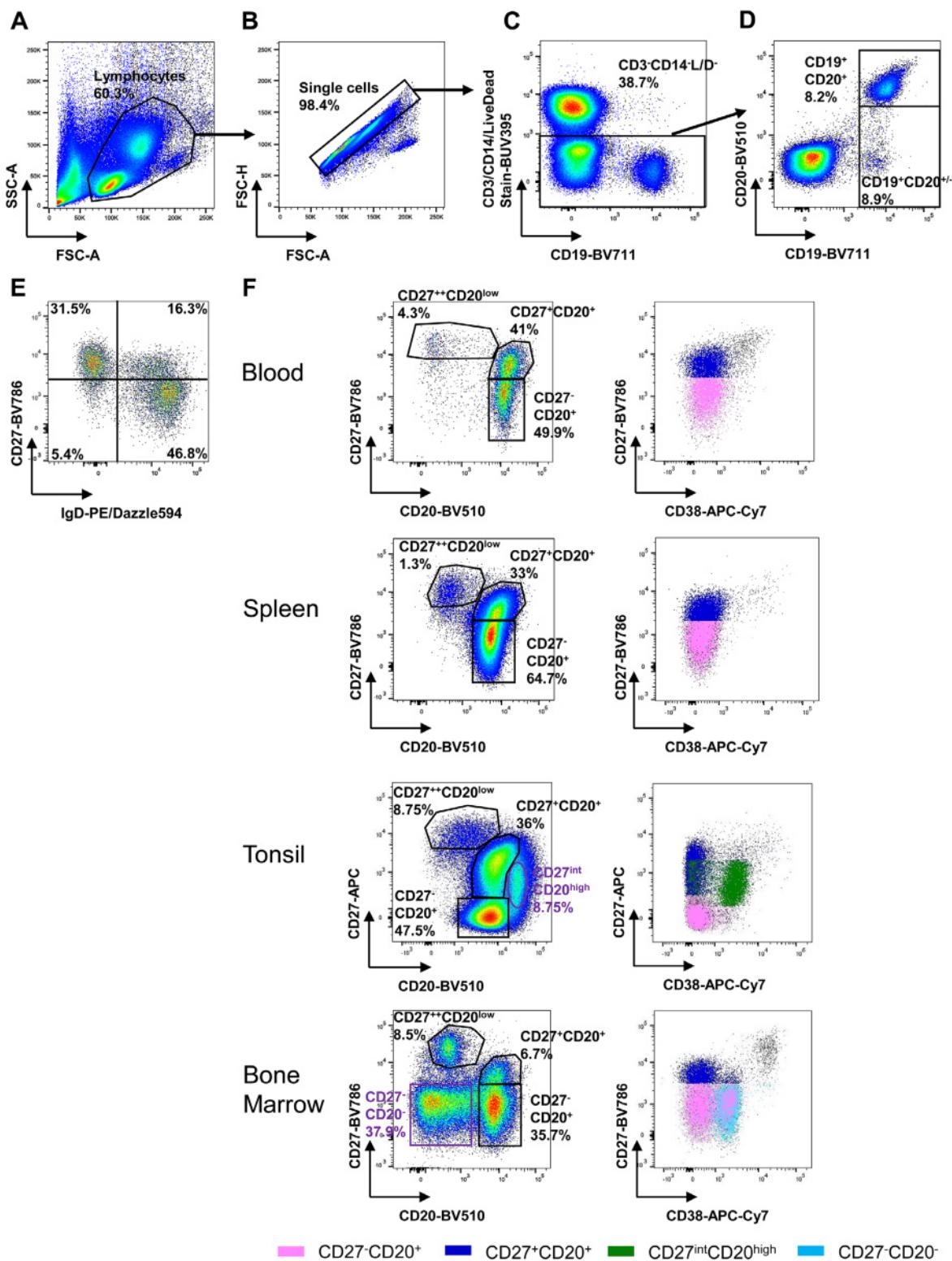
Figure 143. Gating strategy for the identification of human B cells. (A–E) Gating example for peripheral blood: (A) Lymphocytes are identified by their light scattering properties. (B) Exclusion of doublets. (C) Cells positive for CD3 and CD14 and DAPI stained dead cells are excluded. (D) B cells are identified by their expression of CD19 and CD20 including CD20^{low} plasmablasts. (E) B cell subsets are discriminated by CD27 and IgD: CD27$^-$IgD$^+$ naïve B cells, CD27$^+$IgD$^+$ pre-switch memory B cells, CD27$^+$IgD$^-$ switched memory B cells, CD27$^-$IgD$^-$ B cells containing switched memory B cells. (F) B cell subsets discriminated by CD27 and CD20 in peripheral blood, spleen, tonsil, and bone marrow: conventional naive B cells are CD27$^-$ CD20$^+$ (containing CD27$^-$ memory B cells) memory B cells CD27$^+$ CD20$^+$ and plasmablasts CD27^{++} CD20^{low}. Cell subsets defined by CD27 and CD20 expression were color-coded and depicted in a CD27 versus CD38 plot (pink: CD27$^-$CD20$^+$ B cells, dark blue: CD27$^+$CD20$^+$ B cells, green (only in tonsil): CD27^{int}CD20^{high}, turquois (only in bone marrow): CD27$^-$CD20$^-$).
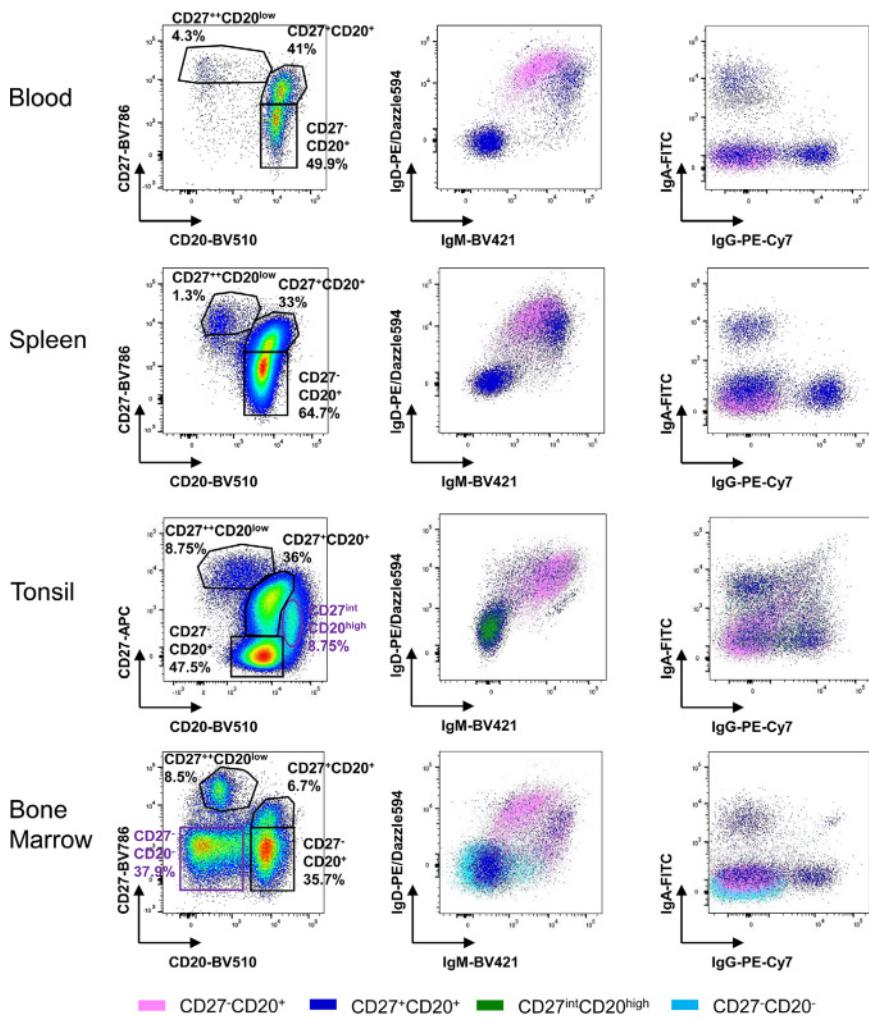
Figure 144. Ig isotype expression of B cell subsets in different human tissues. Gating strategy is the same as depicted in Figure 143A–D. B cell subsets discriminated by CD27 and CD20 in peripheral blood, spleen, tonsil and bone marrow: conventional naive B cells are CD27⁻ CD20⁺ (containing CD27⁻ memory B cells) memory B cells CD27⁺ CD20⁺ and plasmablasts CD27⁺⁺ and CD20ˡᵒʷ. Cell subsets defined by CD27 and CD20 expression were color-coded and depicted in a IgD versus IgM and IgA versus IgG plot to show Ig surface expression of each subset (pink: CD27⁻CD20⁺ B cells, dark blue: CD27⁺CD20⁺ B cells, green (only in tonsil): CD27ⁱⁿᵗCD20ʰⁱᵍʰ, turquois (only in bone marrow): CD27⁻CD20⁻).

2.3.2 Introduction. To identify B cells, the B cell specific molecules CD19 and/or CD20 serve as specific surface markers (Fig. 143). CD19 is a B cell surface molecule expressed at the time of immunoglobulin heavy chain rearrangement [1205], CD20 is expressed by all mature B cells beyond the pro B cell stage in the bone marrow and disappears on the surface of mature plasma cells [1206, 1207]. For further discrimination of B cell developmental stages, combinations of additional markers such as CD27, CD38, CD23, CD77, and expression of surface Igs are used. Immature CD19⁺ B cells in the bone marrow express high levels of CD38 and variable levels of CD20 and IgM, which increase with their further differentiation (Figs. 143F and 144) [1208]. CD38⁺⁺ CD20⁺⁺ immature B cells express IgM and IgD, leave the bone marrow and become CD38⁺⁺ CD24⁺⁺ CD10⁺ transitional B cells [1208]. Naïve B cells express IgM and IgD and are CD27⁻ and CD38⁻, they comprise about 60% of B cells in the peripheral blood (Figs. 143F and 144) [1209, 1210]. After antigen encounter and T cell help, memory B cells and Ab-secreting plasma cells are generated in the germinal center reaction. Human memory B cells (mBCs) can be identified by the expression of CD27 and carrying of mutated Ig VDJ gene rearrangements [1209, 1211]. In the peripheral blood, between 30 and 40% of circulating B cells express CD27 (Fig. 143F, Fig. 144) [1209, 1212]. PC carry distinct FSC and SSC characteristics, express high levels of CD27 and lack the expression of CD20 but are also highly positive for CD38 and partially CD138⁺⁺ [1213]. A CD19⁻ PC population is uniquely enriched in the bone marrow [1214].

An alternative staining protocol of CD20⁺/CD19⁺ B cells has applied co-staining of CD38 and IgD together with CD77 and CD23 to mark differentiation stages of B cells in human tonsils [1215]. CD23 is a low-affinity Fcε receptor and associated with the activation of B cells. It was found to be co-expressed with IgM and IgD in the tonsil and in peripheral blood but not with IgA and IgG and hence is lost during isotype class-switching [1216]. CD77 is strongly expressed by germinal center B cells and can be used to differentiate centroblasts from centrocytes [1215, 1217]. In this protocol, naive IgD⁺ CD38⁻ B cells are separated by CD23 into Bm1 (CD23⁻) and Bm2 (CD23⁺) B cells. IgD⁻ CD38⁺ germinal center B cells can be further discriminated into CD77⁺ centroblasts (Bm3) and CD77⁻ centrocytes (Bm4). IgD⁻ CD38⁻ B cells comprise the memory compartment (Bm5).

The expression of IgD can be used as a marker to further discriminate certain naïve and memory B cell populations. CD19$^+$ CD20$^+$ B cells can be separated in a CD27 versus IgD dot plot (Fig. 143E). In this regard, naïve B cells express IgD and are CD27$^-$. Further quadrants represent different subsets of memory B cells: in detail, CD27$^+$ IgD$^+$ are memory B cells that mostly express high levels of IgM and carry somatic mutations of their V(D)J rearrangements, whereas CD27$^+$ IgD$^-$ memory B cells are class-switched and also carry somatic mutations [1209]. Interestingly, the CD27$^-$ IgD$^-$ B cell subset appears to be very heterogeneous and contains IgA- and IgG-expressing cells [1218, 1219]. It has been shown that this phenotypic population contains a memory B cell subset expressing CD95 with an activated phenotype, which is especially enhanced in patients with systemic lupus erythematosus (SLE) and correlated with disease activity and serologic abnormalities, whereas healthy donors only show minor frequencies of CD95$^+$ cells [1220]. Among other disturbances, B cells lacking expression of the complement receptor CD21, which is part of a signaling complex, together with CD19 have been reported to be expanded in patients with SLE [1221, 1222]. An overview of markers expressed on different B cell subsets can be found in Table 47.

2.3.3 Step-by-step sample preparation. Depending on the starting material, different methods for cell isolation can be applied. A common start is to isolate mononuclear cells (MNCs) by density gradient centrifugation (see also Chapter IV Section 1.2 Pre-enrichment by physical properties). When starting with tissue, a lysate of the minced material can be layered over the Ficoll (e.g., GE Healthcare) solution, when starting with blood, this is carried out with a mixture of blood and PBS according to the manufacturer's instructions. After collecting the MNC layer and subsequent washing steps, the number of isolated cells can be assessed and one can start with the staining procedure or further experiments. The washing buffer should be chosen according to the following experiments, for example PBS containing a carrier protein like BSA (e.g., 0.1–0.5%) for staining or medium for subsequent stimulation experiments. One should be aware that using EDTA in wash buffers might have an effect on following stimulation experiments by chelating calcium ions. For basic staining of B cells, 1–2 × 10^6 MNCs should suffice as input. For analysis of antigen-specific cells, a higher input number might be useful.

For further applications, enrichment of B cells, e.g., by MACS$^®$ technology (Miltenyi) might be necessary (see Chapter IV Section 1.3 Pre-enrichment by immunological properties). Depending on the experiment planned after enrichment, an approach with untouched cells of interest (negative selection) can be applied (e.g., B cell isolation kit II). If specific subpopulations are desired, a positive selection might be required. MACS$^®$ sorting gives high purities, nonetheless the purity check of the desired fraction by FCM staining should be performed.

A different approach for staining starting with peripheral blood is a lysis protocol of red blood cells (see also Chapter IV Section 2.5 Erythrocyte lysis, e.g., with BD PharmLyse, Qiagen EL buffer).

After erythrocyte lysis and washing, the obtained cell suspension can be stained.

Depending on the application, blocking of Fc receptors can be useful prior to staining. One should be aware that Ig staining might not work after adding Fc blocking reagents to cell suspensions. Most manufacturers recommend surface staining at 4°C for 15–30 min but some molecules might require different staining conditions.

For intracellular staining, isolated MNCs can be lysed and permeabilized directly or after stimulation experiments to assess for example phosphorylation of intracellular proteins (see Chapter III Section 5: Cell fixation and permeabilization for flow cytometric analyses). There are different protocols and reagents available depending on the intracellular location of the antigen to be stained (e.g., BD, Biolegend, eBioscience and others). For antigens in the cytoplasm, a less harsh permeabilization buffer can be used than for example for antigens located in the nucleus. Blood or tissue lysates can also be prepared for intracellular staining directly (whole blood staining) by lysis and permeabilization and stained after washing steps. Twenty to 60 minutes at room temperature are frequently used for intracellular staining. One should be aware that some epitopes might be destroyed after lysis and permeabilization and thus may not be identified. This should be validated for each application.

2.3.4 Materials.

1. Ficoll Paque (GE Healthcare)
2. PBS (Biochrom)
3. Staining buffer (PBS/0,5% BSA/EDTA (Miltenyi autoMACS$^®$ Rinsing Solution/MACS$^®$ BSA Stock Solution))
4. Buffers for cell permeabilization (e.g., Phosflow Lyse/Fix Buffer (BD Biosciences), Phosflow Perm Buffer II (BD Biosciences))
5. Buffers for erythrocyte lysis (e.g., Lysing Buffer (BD PharmLyse ^{TM} BD Biosciences, Buffer EL (Qiagen)),
6. Anti-Mouse Ig, κ/Negative Control Compensation Particles Set (BD Biosciences)
7. Live/Dead stain (e.g., DAPI (Molecular Probes) or LIVE/DEAD Fixable Dead Cell Stain Kit, (Invitrogen))
8. Instrument: LSR Fortessa X-20 (BD Biosciences)
9. Fluorescently labeled mAbs (Table 46):

2.3.5 Gating for human B cells subsets. After MNC preparation or lysing whole blood, lymphocytes should be gated according to their scatter properties and by the exclusion of doublets and dead cells from the analysis (Fig. 143A–C). In order to detect plasma cells simultaneously, the initial FSC/SSC gating should be larger and not limited to a conventional lymphocyte gate [1213].

When gating on CD19$^+$ B cells, CD3$^+$ T cells and CD14$^+$ monocytes need to be excluded. If these cells are not of further interest, they can be assigned to a so called "dump channel" with CD3 mAb and CD14 mAb together with other markers for cells that should be excluded from subsequent analyses, e.g., CD16/CD56

Table 46. Fluorescently labeled monoclonal antibodies used for the stainings in Figs. 143 and 144

Fluorophore	Marker	Manufacturer	Clone	Isotype
BUV395	CD3	BD	UCHT1	mouse IgG1κ
BUV395	CD14	BD	M5E2	mouse IgG2aκ
BV711	CD19	BD	SJ25C1	mouse IgG1κ
BV510	CD20	Biolegend	2H7	mouse IgG2bκ
BV786	CD27	BD	L128	mouse IgG1κ
APC-Cy7	CD38	Biolegend	HIT2	mouse IgG1κ
BV421	IgM	BD	G20-127	mouse IgG1κ
PE-Dazzle594	IgD	Biolegend	IA6-2	mouse IgG2aκ
PE-Cy7	IgG	BD	G18-145	mouse IgG1κ
FITC	IgA	Chemicon	M24A	mouse IgG1

mAb for NK cells. One approach frequently applied is to gate on $CD3^- CD14^- DAPI^-$ cells (Fig. 143C) and, in a subsequent step, identification of $CD19^+$ and $CD20^{+/-}$ cells (Fig. 143D). This gating permits reliable identification of $CD20^+$ B cells and additionally of $CD20^{low}$ plasmablasts. For the analysis of B cell subsets, a classical combination using CD27 and CD20 of $CD19^+$ B cells has been established. Using CD27, a number of B cell subsets can be identified independent of the expressed Ig subclasses. As a result, conventional $CD27^- CD20^+$ naïve B cells, $CD27^+ CD20^+$ mBCs, including both preswitched and class-switched memory B cells, as well as $CD27^{++} CD20^{low}$ PBs can be identified (Fig. 143F). While the distribution of these subsets can vary between different diseases with slight variations [1223], it has been demonstrated that CD27 can serve as a reliable marker for human healthy controls memory B cells, since CD27-expressing B cells differentiate timely into Ab-secreting cells after stimulation and carry somatic mutations in their immunoglobulin V regions [1209, 1211]. Of note, this gating strategy will not allow to identify class-switched B cells that lack the expression of CD27 [1218, 1219] and occur at higher frequencies among patients with systemic autoimmune diseases

When comparing the CD27 versus CD20 plot in the different tissues (Fig. 143F), an additional population has been found in the tonsil and another population in the bone marrow compared to peripheral blood and spleen. In the tonsil, a subset expressing high levels of CD20, intermediate levels of CD27 and CD38 expression appears in this plot and represent germinal center B cells that lack IgD expression [1224]. In the bone marrow, an additional population positive for CD19 but lacking the expression of CD20 and CD27 can be found. These B cells express CD38, do not show surface IgD expression and low to no IgM surface expression (Fig. 144) and represent immature B cells [1225].

2.3.6 Pitfalls.

1. Blocking Fc receptor prior to staining might interfere with staining of immunoglobulins on B cells
2. Choose an appropriate buffer for cell isolation: Buffers containing EDTA can decrease effects of stimulation by chelating calcium ions

2.3.7 Summary Table.

Table 47. Phenotypic differentiation of human B-lineage cell subsets based on their characteristic expression of surface markers

B cell population ($CD19^+$)	Phenotype/Subphenotype
Transitional	
T1+T2	$CD24^{++}CD38^{++}CD10^+CD27^-IgM^{++}$
Naive	
Resting	$CD24^{+/-}CD38^{+/-}CD27^-IgM^{++/+}$ $IgD^{++}CD21^+CD95^-$
Activated	$CD24^-CD38^-CD27^-IgM^{++}IgD^{++}$ $CD21^-CD95^+MTG^+$
Memory (Ki$^-$67$^-$)	
Preswitched	$IgM^+IgD^{+/-}CD27^+CD1c^+$
Switched	$IgG/IgA^+CD27^+CD21^+$
Atypical memory	
a) Double negative	IgD^-CD27^-
b) activated double negative	$IgD^-CD27^-CD95^+$
c) Syk^{++}	$IgD^{+/-}CD27^-CD95^{+/-}CD21^{+/-}$ $CD38^-MTO^-Syk^{++}$
d) tissue-resident	$IgM/IgG/IgA^+CD27^-FcRL4^+$
Marginal Zone	
Spleen	$IgD^+IgM^+CD27^{++}CD21^{++}CD1c^+$
Circulating	$IgD^+IgM^+CD27^+CD1c^+$
Ab secreting cells	
Circulating	
PB	$CD38^{++}CD27^{++}CD138^-Ki^-67^+$
PC	$CD38^{++}CD27^{++}CD138^{+/-}Ki^-67^{+/-}$
Bone marrow	
a) $CD19^+$ PC	$CD19^+CD38^{++}CD27^{++}CD138^+$ Ki^-67^-
b) $CD19^-$ PC	$CD19^-CD38^{++}CD27^{++}CD138^+$ Ki^-67^-

2.4 Human B cells recognizing defined (auto)antigens

2.4.1 Overview.
Detection of human antigen-specific B cells has been challenging mainly due to their low frequency and the potential biases introduced by their ex vivo expansion. Naive B cells present with a diverse BCR repertoire that is usually of low avidity to the antigen. Upon antigen challenge, naive B cells undergo processes of somatic hypermutation, class switch recombination, and selection giving rise to memory B cells with high-avidity BCRs and PCs secreting highly specific Abs. Memory B cells and long-lived plasma cells are responsible for generation and maintenance of serologic memory. In some conditions, serum Ab titers correlate with the frequency of antigen-specific memory B cells in the circulation [1226, 1227]. Here, we present two recently established methodologies to identify human antigen-specific B cells by FCM.

2.4.2 Introduction.
The identification of human antigen-specific B cell populations by FCM has become an extremely valuable
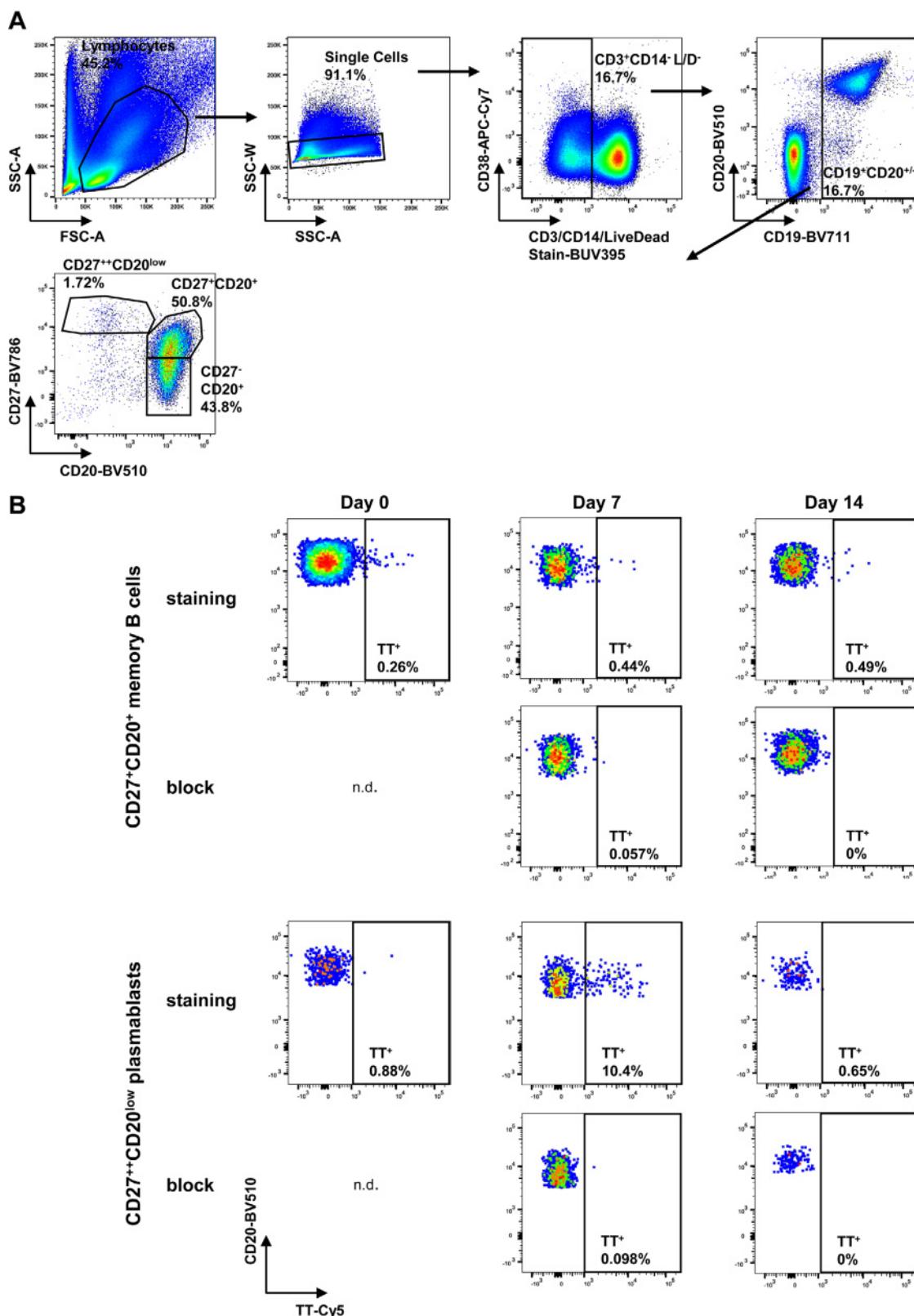
Figure 145. (A) After gating on lymphocytes, doublets, and in the subsequent gating step, CD3^{+} T cells, CD14^{+} monocytes, and dead cells are excluded. B cells including CD20^{low} plasmablasts are gated by their CD19 and CD20 expression. Conventional naïve and memory B cells and plasmablasts are identified by using CD20 and CD27. (B) Identification of TT-specific memory B cells and plasmablasts before (day 0) and after TT vaccination (day 7 and day 14) in peripheral blood. Staining and block with unlabeled TT are shown.
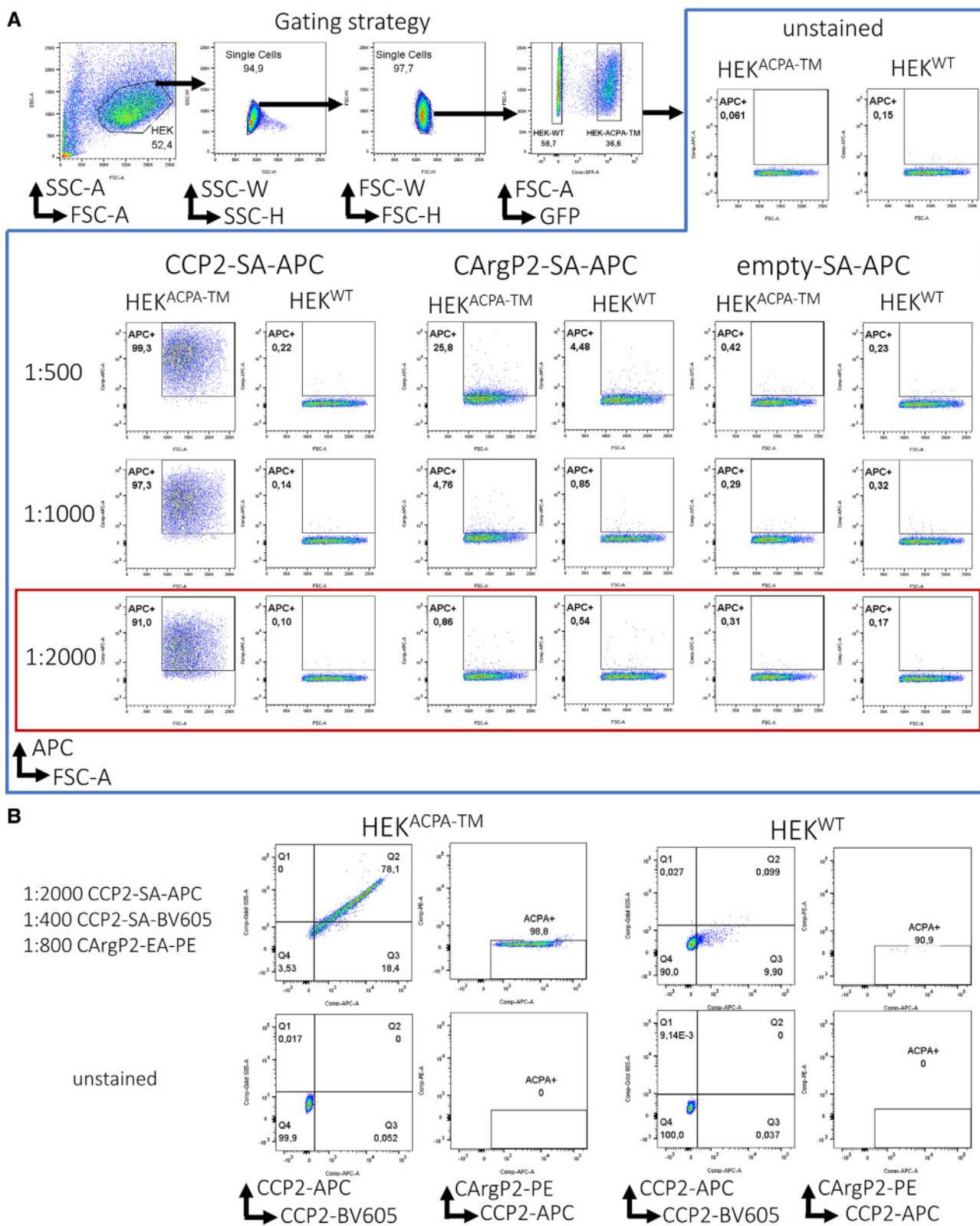
Figure 146. Determining optimal concentrations of multimerized antigen-tetramers for staining. (A) titration of CCP2-SA-APC, CArgP2-SA-APC, and of "empty" streptavidin APC tetramers on ACPA-expressing HEK 293T (HEK-ACPA[TM]) and wild-type HEK 293T (HEK[WT]) cells. Gates are based on unstained controls. The red square marks the optimal concentration of CCP2-SA-APC. (B) Staining of HEK-ACPA[TM] and HEK[WT] cells with combinatorial CCP2 and CArgP2 tetramers.
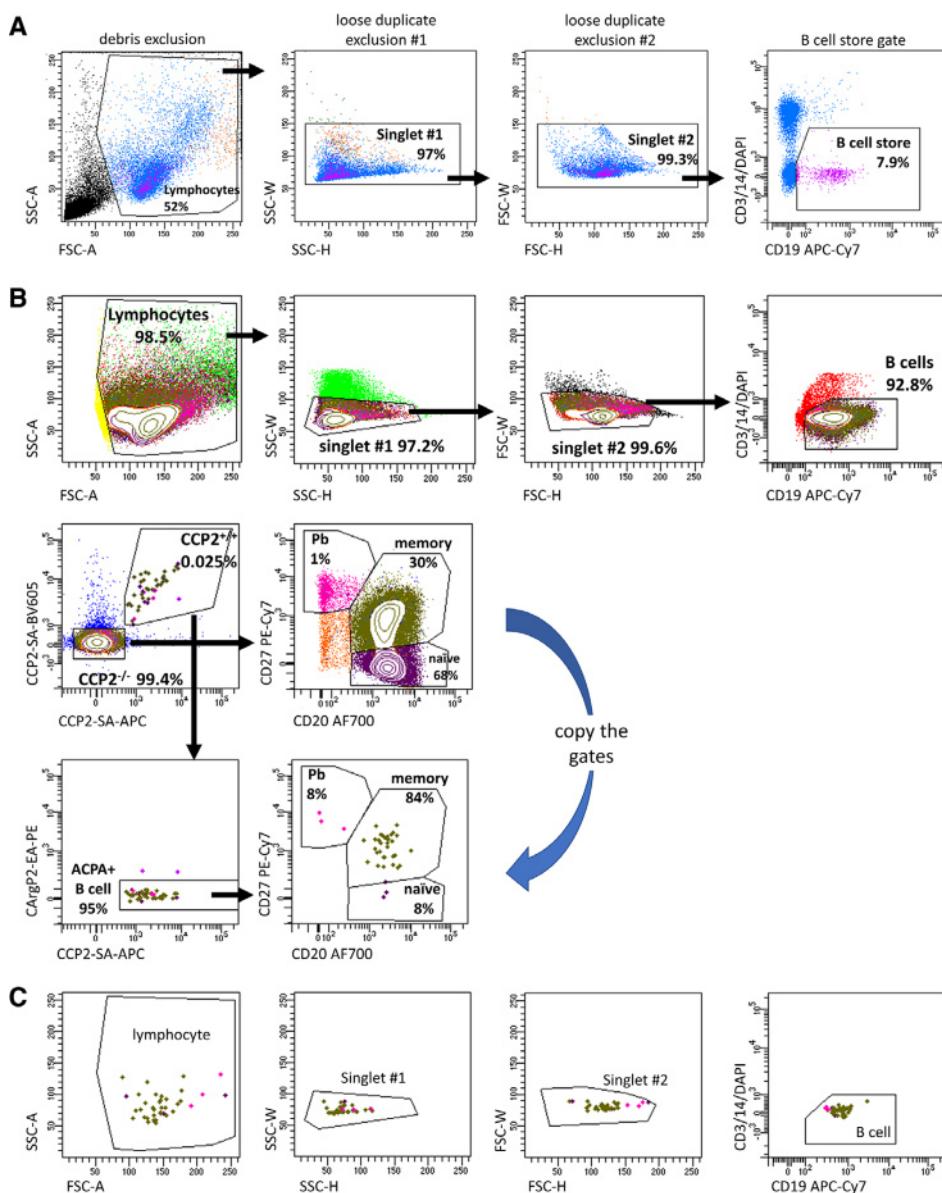
Figure 147. Gating strategy to identify ACPA-expressing B cells. (A) Setting up a "B cell store gate" that will be used during sample measurement to store data in order to obtain a manageable size of data to be analyzed. (B) Gating strategy to identify ACPA-expressing B cell subsets. The CD20 versus CD27 gates for ACPA-expressing B cells are copies of the same gates from the CCP2$^{-/-}$ population. (C) Back-gating of ACPA-expressing B cells as an additional measure of control to verify cell size and granularity within the large pool of PBMC-derived B cells.

tool for a detailed understanding of both protective and autoreactive human immune responses. Depending on the research questions, antigen-specific B cell responses can be analyzed and monitored upon vaccination, during "steady state," in different diseases including different disease stages, phases of treatment, and in different compartments of the human body [1228–1231]. It allows for the phenotypic analysis of antigen-induced B cells by assessing various markers on the cell surface and inside the cell. In combination with cell sorting, it also allows subsequent analysis, such as transcriptomic profiling by single cell-based ("next generation") sequencing techniques. Furthermore, it is possible to analyze antigen-specific B cell receptor (BCR) repertoires, to obtain full-length BCR sequences for mAb generation, and to perform functional studies of isolated single B cells or B cell populations, which includes the generation of immortalized, antigen-specific B cell clones [1232, 1233]. This wealth of possibilities permits

unprecedented insights into human B cell biology; it requires, however, particular care and adherence to relevant and tedious control steps to ensure that the antigen-specific B cell populations identified by FCM, which are frequently very rare, indeed represent the antigen-specific B cell population of interest. Here, we provide a detailed description of the necessary considerations prior to starting out, the technological possibilities, approaches and necessary tools, and the relevant steps for performing experiments. We do so by using two examples of human antigen-specific B cell responses: (i) a vaccine-induced, high-avidity immune response identified by direct labeling of antigen with a fluorescent dye; and (ii) an autoreactive, low-avidity B cell response identified in an autoimmune disease setting using biotinylated self-antigens tetramerized with fluorescently labeled streptavidin molecules. In general, the examples described aim at identifying antigen-specific B cells within a polyclonal B cell repertoire to the highest validity. This implies

that strong emphasis is placed on the exclusion of nonspecific background signals and on several steps aimed at the verification of antigen-specificity. Notably, certain research questions might not require this strive for purity but can be answered by mere enrichment of the antigen-specific cell population. In other cases, such as single-cell transcriptomics, purity is crucial. In both cases, it is important to consider a number of general aspects before choosing the most suitable technical approach.

2.4.3 General considerations before starting out.

2.4.3.1 Estimated frequency of the antigen-specific B cell population of interest.
In contrast to murine studies, in which the spleen and other lymphoid organs are readily accessible, most attempts to identify antigen-specific human B cells will need to rely on peripheral blood. In this compartment, CD19$^+$ B cells comprise around 4% of total PBMCs in adult healthy individuals (See also ChVI Section 2.3 Human B cells and their subsets). Frequencies of antigen-specific B cell populations, however, can be very low (<0.01% of total B cells). In an ideal setting, this requires, for example, 1×10^6 B cells to identify 100 antigen-specific B cells, and hence, a starting population of 25×10^6 PBMCs. In other compartments such as bone marrow, tonsils, or spleen, CD19$^+$ B cells are more frequent (mean of 19% in BM, 33% in the spleen, 43% in tonsils [1234]), as might be the frequency of antigen-specific subsets. Depending on the compartment studied, it can be important to estimate the expected frequency of the antigen-specific B cell population in order to determine the amount of starting material required for the identification of a minimum number of antigen-specific cells. This can be achieved by culturing ex vivo isolated PBMC or pre-enriched B cells in limiting dilution, followed by the assessment of antigen-specific B cell presence by either ELISA or ELISPOT [1235, 1236]. These approaches will likely underestimate the number of antigen-specific B cells in the circulation, but will provide a minimum estimate of the cell numbers that can be expected. In addition, this initial estimate can provide information on isotype usage of the antigen-specific B cell response to be studied, and allow determining whether the frequency of circulating, antigen-specific B cells correlates with serum titers of the corresponding Abs. This, in turn, will help in selecting donors and, hence, increase the yield of antigen-specific B cells for the eventual assessment.

2.4.3.2 Expected phenotype of the cell population of interest.
Next, to determining compartmental frequencies, it can be relevant to use additional phenotypic markers in the eventual panel that allow to more specifically select the B cell subpopulation in which the antigen-specific cells are expected. For example, markers could identify the isotype or the Ig subclass that appears to be most prominent for the Ig produced by PC measured by ELISA. Also, if IgM-expressing B cells are to be identified, low-affinity antigen binding can be expected, which in turn indicates that multimerization of antigens can be helpful to increase the fluorescent signal. Other antigen-specific responses, for example, might be enriched in IgG4 expressing B cells, which allows to significantly narrow the cell numbers that need to be studied (see also Chapter VI Section 2.3 Human B cells and their subsets). The identification of plasma cells that lack surface Ig expression, on the other hand, might require an intracellular staining approach. If the expression of such phenotypic characteristics is known, these should be incorporated in the staining panel and included in the frequency estimation described above.

2.4.3.3 Source of cells.
In general, any single cell suspension that contains B cells, whether derived from peripheral blood, bone marrow, spleen, tonsils, or solid tissues, can be assessed for the presence of antigen-specific B cells. Limitations are caused by the frequency of the antigen-specific population of interest, and by the viability of cells (including pre-analytical treatment, i.e., shipment). Freezing cells, for example, is likely to compromise the plasmablast compartment, while naïve and memory B cells are less sensitive (See also Chapter III Section 4.6 Freezing cell samples). Pre-enrichment of B cells from larger populations by positive or negative selection can increase the percentage of antigen-specific B cells and shortens the time required on the flow-cytometer; it can, however, also compromise B cell subsets, depending on the isolation technique used. Therefore, due to the usually very low frequency of antigen-specific B cell populations, we recommend—whenever possible—using fresh, directly ex-vivo isolated B cells or B-cell containing suspensions such as PBMC as a starting point. This will minimize the loss of antigen-specific cells during work-up. For certain B cell populations and research questions, however, the use of frozen cells can be acceptable [1237].

2.4.3.4 Choice of antigen.
In most cases, the antigen used for flow-cytometric assessment will be the antigen for which reactivity has been demonstrated in serum ELISA measurements or epitope mapping studies, or which has been used for inducing the immune response in, for example, vaccination studies. Both peptide and protein antigens are possible candidates. Protein antigens might be preferred in case of conformational epitopes; in addition, proteins are more likely to carry multiple epitopes, which increases the chance for higher avidity interactions with the BCRs. However, protein synthesis usually requires cells or expression systems and purification steps after which impurities (such as LPS) can remain that can influence and confound binding properties and introduce nonspecific background signals. Peptides are easier to synthesize to high purity and contain one or more, sometimes synthetic, defined epitopes. Small sequence modifications can easily be introduced to generate nonbinding control peptides. However, peptides are usually too short to build appropriate 3D epitopes or structures that crosslink BCRs and, hence, monomeric peptides are usually insufficient for B cell identification. Therefore, peptide antigens are multimerized by generating either biotin–streptavidin tetramer complexes, or by coupling peptides to dextran backbones or other scaffolds using click-chemistry.

2.4.3.5 Choice of fluorescent labels. In general, and in particular for low-avidity B cell immune responses, it is strongly recommended to reserve at least two fluorescent channels in a given staining panel for the identification of ultra-low frequency antigen-specific B cells. For reasons described below, identification of antigen-specific B cells by double-positivity for two identical yet differentially labeled antigens significantly reduces nonspecific background signals and, hence, the risk for misinterpretation of fluorescent signals as antigen-specific cells. This concept of a dual labeling approach has been described in detail elsewhere, an example is provided bellow [1230, 1238, 1239]. We recommend using fluorescent dyes with emission spectra that show no or very little spectral overlap in order to reduce the need for extensive compensation. Use of single label antigens might suffice for certain, high avidity B cell responses in combination with blocking studies (see below), but additional measures should then be taken to demonstrate staining specificity, in particular in cases in which blocking with access, unlabeled antigen is incomplete.

2.4.3.6 Establishing positive and negative controls. To ensure the highest reliability, we strongly recommend the use of both positive and negative controls in the establishment of antigen-specific staining approaches. In the specific setting described here, controls need to be established at two levels:

1. Control cells that do or do not express the BCR of choice. Such cells allow determining the specificity of antigen binding, the use of optimal concentrations of labeled antigen or antigen-multimers, and the degree of nonspecific background binding. Furthermore, they allow controlling for variations between batches of labeled antigens and can be used to determine the sensitivity of the approach to detect antigen-specific cells within a larger pool of cells. Such control cells are particularly useful during the experimental setup phase of antigen-specific staining approaches aimed at identifying very low-frequency B cells. However, they maintain their relevance also once protocols have been established. Examples for control cells include B cell hybridomas that have maintained cell surface Ig expression [1240], immortalized human B cell clones of known specificity [1232, 1233], or cell lines transfected with mAb sequences with or without the transmembrane domain of IgG [1230]. An example of the latter option using HEK293T cells is provided below. Non-transfected cells or cells with known specificity to an unrelated antigen can serve as negative controls.
2. Control populations of donors that do or do not harbor the antigen-specific B cell population of interest. In disease settings, these should include matched healthy donors but also disease controls [1230]. In this context, a particular point for careful consideration lies in the possibility that control donors might harbor naïve B cells in their unmutated repertoire that specifically recognize the antigen of interest. Such recognition patterns have been described for nuclear autoantigens and studies suggest that healthy individuals harbor a consid-

erable proportion of mature naïve B cells capable of recognizing autoantigens. For protective antigens, vaccinated donors can be analyzed as a control. Secondary vaccinations, e.g., with Tetanus Toxoid (TT), give rise to antigen-specific plasmablasts and memory B cells, which can be analyzed 1 and 2 weeks after vaccination, respectively [1241]. FCM is limited in the possibility to discern whether such staining signals reflect true antigen-specific B cells or nonspecific interaction between labeled antigens and cell surfaces by, for example, hydrophobic interaction or charge. If positive signals are observed in control donors in FCM, we highly recommend that additional measures be taken to determine/verify antigen specificity. Possible steps to do so are described below.

2.4.3.7 Verification of antigen-specificity. Different direct and indirect measures are available to determine whether fluorescent signals detected by FCM indeed identify B cells that specifically bind the antigen of interest via the BCR. Given that detection of ultra-low frequency B cells requires the assessment of large cell numbers of a given total B cell pool, it is almost inevitable that also nonspecific background signals are detected. Using a dual staining approach as described above significantly reduces such non-specific signals but does not suffice as a single argument to claim antigen-specificity. Additional options include:

1. Blocking (also called competition) experiments in which the binding of fluorescently labeled antigens to the BCR is blocked by an excess of unlabeled antigen. Note that an excess of unlabeled antigen should completely block the fluorescent signal. If this is not the case, nonspecific interaction between the labeled antigen and the cell cannot be excluded and additional verification steps (see below) should be taken. This method can also be applied in a stepwise approach with increasing amounts of unlabeled antigen where the increase of competing for binding sites results in a gradual decrease of labeled antigen occupying the BCR.
2. Single cell isolation by FCM followed by immediate cell lysis, mRNA isolation, and BCR sequencing using published protocols; alternatively, single cells can be cultured with relevant stimuli followed by the assessment of supernatants for the production of total and antigen-specific Ig by ELISA [1242]. Cells obtained from supernatants containing antigen-specific Ig can subsequently be lysed followed by mRNA isolation and BCR sequencing. In both cases, full-length BCR sequences can be obtained by primer-binding bias-free PCR protocols, which can subsequently be used for mAb expression [1243]. Note that it can be extremely useful during experimental setup to use the "index sort" function for single cell isolation protocols as this option allows to identify the localization of antigen-specific cells in the FCM dot plot.

Together, verification of antigen specificity is crucial as this step is, in the end, the only way to determine whether cells identified by FCM indeed represent the cell population of interest. Next to blocking experiments, the ultimate golden standard relies on

single cell isolation followed by BCR cloning and monoclonal Ab expression.

2.4.4 Step-by-step sample preparation.

1. Identification of a vaccine-induced, high-avidity immune response identified by direct labeling of antigen with a fluorescent dye

In order to detect B cells specific for a certain antigen, we here make use of the ability of B cells to bind the proteins they recognize through the BCR in a 3D manner. To illustrate this approach, we provide an example of the detection of TT-specific human memory B cells and plasmablasts in the circulation at several time points before and after TT vaccination (Fig. 145). Vaccination can be a highly useful tool in the initial setup of the staining procedure, but will not be available to aid the detection of autoreactive B cells described below. Nonetheless, the technological approach presented in this example has also successfully been used for the detection of autoreactive B cells [1244]. Therefore, the example provided can be seen as a template, which can be adapted to the identification of other antigen-specific B cell responses with similar characteristics.

In order to assure specificity of the staining, we show how the fluorescent signal in the same sample can be blocked with unconjugated protein used in excess. This methodology has been used successfully to analyze B cells specific for TT [1241, 1245]; cholera toxin B (CTB) [1246]; Keyhole Limpet Hemocyanin (KLH) [1227]; and Pentraxin-3 (PTX-3) [1244]. The possibility to down-titrate binding of antigen-specific cells (competitive assay principle) has long been recognized to ensure specificity.

Notes:

1. As discussed above, antigen-specific B cells are found at very low frequencies in the circulation; therefore, it is crucial to start with more input cells/blood that one would usually do to stain B cell subsets. The input depends on the estimated frequency of the antigen-specific B cells in the population of interest.
2. For sample preparation and staining of naive, memory B cells, and plasmablasts (see section 2 - B cells and their subsets).
3. For intracellular staining, permeabilize and fix the cells (see Section III.5: Cell fixation and permeabilization for flow cytometric analyses).

Steps:

1. Preparation of fluorescently labeled antigens. The fluorescently labeled antigens should be titrated (see ChIII Sect Titration: Determining optimal reagent concentration) independently for surface and intracellular detection. (Note: for intracellular staining usually a smaller quantity of labeled antigen is sufficient).
2. Upon sample preparation, wash cells twice with PBS before incubation with fluorescently labeled antigen.
3. Divide the sample in two: incubate half of the cells with fluorescently labeled antigen and the second half with unconjugated antigen. Incubate both at 4°C for 15–30 min.

4. Wash with PBS and prepare for acquisition on a flow cytometer of choice.

2. Identification of an auto-reactive, low-avidity B cell response identified in an autoimmune disease setting using biotinylated peptide self-antigens tetramerized with fluorescently labeled streptavidin molecules.

The example provided demonstrates the identification of B cells directed against citrullinated protein antigens in patients with rheumatoid arthritis (RA). Citrullination represents the posttranslational modification of arginine residues in a given protein to the amino acid citrulline. The citrulline-directed, auto-reactive B cell response is a hallmark of this disease and can be detected in >70% of patients by serum measurement of anti-citrullinated antigen Ig reactivity in ELISA. The humoral immune response uses all Ig isotypes and is, on the polyclonal level, of remarkably low avidity [1247]. Circulating, antigen-specific B cells in peripheral blood are expected at a frequency of ~1:10 000 total B cells and can comprise naïve and memory B cells as well as plasmablasts and plasma cells [1230, 1235, 1236]. Specific antigen recognition is determined by BCR binding to citrullinated antigens but not to the arginine-containing peptide control variants. A biotinylated, cyclic citrullinated peptide (CCP2) and its arginine control variant (CArgP2) are used for specific detection. HEK293T cells that express, in membrane-bound form, a mAb that specifically recognizes the citrullinated peptide antigen of choice (HEK[ACPA-TM]), serve as controls during experimental setup [1230]. Note that this example can be seen as a template, which can be adapted to the identification of other antigen-specific B cell responses with similar characteristics.

1. Generating biotinylated peptide-avidin tetramers.

1. Incubate biotinylated peptides in excess with fluorescently labeled streptavidin or extravidin overnight at 4°C. The molar ratio between peptide and streptavidin should exceed 4:1.
Note: In the example provided, six different peptide tetramers have been generated.
- CCP2-biotin coupled to APC-labeled streptavidin (CCP2-SA-APC)
- CArgP2-biotin coupled to APC-labeled streptavidin (CArgP2-SA-APC)
- CCP2-biotin coupled to BV605-labeled streptavidin (CCP2-SA-BV605)
- CArgP2-biotin coupled to BV605-labeled streptavidin (CArgP2-SA-BV605)
- CCP2-biotin coupled to PE-labeled extravidin (CCP2-EA-PE)
- CArgP2-biotin coupled to PE-labeled extravidin (CArgP2-EA-PE)
2. Remove unlabeled peptide with Bio-Spin® Columns with Bio-Gel® P-30. This will trap the free peptide in the gel and release peptide–streptavidin tetramers in the flow through. The removal of unlabeled peptides is crucial to avoid binding competition between unlabeled and labeled antigen during staining.

3. Store the labeled antigen tetramers at 4°C. In case of longer storage times (weeks to months), perform regular testing of the stability of the tetramers and fluorescent signal by using the positive/negative control cells (see below).

2. Determining optimal concentrations of multimerized antigen-tetramers for staining.
Notes:

- The optimal concentration of labeled peptide tetramers to be used for staining needs to be determined by titrating the labeled antigens on a fixed number of positive and negative control cells. Here, HEK$^{ACPA-TM}$ cells are used as positive control; non-transfected HEK293T wild-type cells (HEK^{WT}) serve as negative controls.
- For each tetramer, use the concentration at which the positive control stains highly positive and the negative control is negative.
- Combine the differentially labeled peptide tetramers at their optimal concentration to stain the positive (HEK$^{ACPA-TM}$) and negative (HEK^{WT}) control cells and determine whether a double positive population emerges in the diagonal of a FCM dot plot (Fig. 146). Should the double positive population deviate from the diagonal, adjust the concentrations of differentially labeled peptide tetramers accordingly until the double positive population falls into the diagonal. No signals should fall into this diagonal upon staining of the negative control cells.
- Upon determination of the optimal concentrations of labeled peptide tetramers to use, it can be helpful to spike positive control cells (HEK$^{ACPA-TM}$) in different numbers into healthy donor PBMC and to determine by subsequent antigen-specific staining whether the predetermined optimal concentrations remain optimal in a mixed population of cells.

Steps:

1. Prepare serial dilutions of peptide tetramers and of "empty"-labeled avidin molecules.
2. Stain a fixed number (here: 2×10^5) of positive and negative control cells with labeled peptide tetramers diluted in FCM buffer to 20 μL staining volume. Incubate for 30 minutes at 4°C.
3. Wash cells twice with FCM buffer and suspend in 100 μL FCM buffer for analysis on a flow cytometer.
4. In the example, CCP2-SA-APC tetramers at a dilution of 1:2000 stain >90% of HEK$^{ACPA-TM}$ cells, and less than 1% of HEK^{WT} cells (Fig. 146A). At the same concentration, CArgP2-SA-APC control tetramers show minimal background staining. Also, the empty labeled streptavidin molecules give minimal background at all concentrations. Therefore, a dilution of 1:2000 for this particular batch of CCP2-SA-APC tetramers is chosen for the subsequent combinatorial staining.
5. Perform similar titrations for BV605 and PE-labeled tetramers to obtain optimal dilutions for the subsequent combinatorial staining. To decide which concentration of CArgP2-EA-PE tetramers to use, choose the concentration at which CCP2-

EA-PE tetramers give the highest signal and CArgP2-EA-PE tetramers minimal background HEK$^{ACPA-TM}$ cells.

6. In the example, dilutions of 1:2000 are optimal for CCP2-SA-APC, 1:400 for CCP2-SA-BV605, and 1:800 for CArgP2-EA-PE tetramers for the combinatorial staining. This combination identifies HEK$^{ACPA-TM}$ cells positive for CCP2-SA-APC and CCP2-SA-BV605 in the upper-right quadrant of the CCP2-APC versus CCP2-BV605 dot plot, while the CCP2 double positive population remains negative in the PE control channel (Fig. 146B). Also, no APC/BV605 double positive signal is observed for HEK^{WT} cells.

3. Staining of a sample containing human antigen-specific B cells.
Notes:

- Given the very low frequency of antigen-specific, ACPA-expressing B cells in the circulation, we here used 50 mL of freshly drawn peripheral blood as starting material.
- Here, we deliberately chose to stain whole PBMC and not to enrich B cells by subsequent isolation techniques in order not to compromise B cell subpopulations such as plasmablasts.
- In the example provided, DAPI is used to identify and exclude dead cells.
- We assume in this example that all labeled mAbs and their respective isotype control Abs have been titrated and tested in appropriate FMO-stainings to determine optimal concentrations. These steps are necessary but not mentioned in the description below.

Steps:

Identification of ACPA-expressing B cells in a peripheral blood sample of an ACPA-positive rheumatoid arthritis patient.

1. Isolate PBMC from a peripheral blood sample using Ficoll-Paque gradient centrifugation following standard protocols. Count the isolated PBMCs.
2. Suspend the PBMCs at 8×10^6 cells per 100 μL in FCM buffer in a 15 mL tube and stain with the fluorescently labeled Abs/streptavidin tetramers for 30 min on ice protected from light. In the example, we used: CD3 Pacific Blue (PB), CD14 Pacific Blue (PB), CD19 APC-Cy7, CD20 AF700, CD27 PE-Cy7, CCP2-SA-BV605, CCP2-SA-APC, and arginine peptide control CArgP2-Extravidin-PE at the appropriate concentrations.
   The emission wavelength of Pacific Blue is used in this example as a "dump channel" in which markers are combined that identify cells that are to be excluded from further analysis.
3. Add 1ml FCM buffer and centrifuge the cells for 5 min at 1500 rpm on ice.
4. Repeat the washing step at least two times.
5. Resuspend the cell pellet with 100 μL FCM buffer and transfer to an FCM tube (we use Micronic tube MP32022). Keep the sample on ice and in the dark at all times.
6. To compensate for spectral overlap between fluorescent dyes, we employ compensation beads (BD Biosciences) that bind to mouse IgG (provided that all of the fluorescently labeled

Abs used are of a murine IgG isotype). The beads are used to compensate for CD3 PB, CD19 APC-Cy, CD20 AF700, and CD27 PE-Cy7 spectral overlaps. For the tetramers, however, surrogate murine IgG that is conjugated with BV605, APC, and PE are used to allow fluorescence compensation using beads.

7. Set up a flow cytometer of choice (here: BD LSRFortessa) that allows simultaneously detecting and discriminating fluorescent signals from PB, APC-Cy7, AF700, PE-Cy7, BV605, APC, and PE dyes. For the analysis, we here used BD FACS-DIVA software (version 8.0.2).

8. Perform fluorescence compensation using single-stained compensation beads and apply the compensation setup to the whole experiment.

9. Add 100 μL of 200 nM DAPI to the cell suspension (leading to a final concentration of 400 nM).

10. Place the sample into the cytometer and record 50 000 events. Put the sample back on ice and keep protected from light.

11. Place gates in a Global Worksheet of the DIVA program on the cell populations as follows (Fig. 147a):
    (a) In the FSC-A versus SSC-A plot, make an inclusive gate containing lymphocytes and monocytes to include plasmablasts that are larger in size and more granular than other subsets of B cells.
    (b) Subsequently, exclude duplicates using SSC-H versus SSC-W and FSC-H and FSC-W plots. The gates for duplicate exclusion should not be strict at this moment.
    (c) Lastly, in a PB versus CD19-APC-Cy7 plot, gate loosely on CD19 positive cells that are PB-negative. This gate is referred to as "B cell Store" (Fig. 147A).

12. Click "Next Tube" on the Acquisition Dashboard of the BD FACSDIVA workspace.

13. In the Acquisition Dashboard, choose "B cell Store" for both Stopping and Storage Gates. Set 10 000 000 events for both "Events to Record" and "Maximum Events to Display." This step is necessary to obtain a manageable size of data to analyze the antigen-specific cell population of interest (here: ACPA-expressing B cells).

14. Place the sample back into the flow cytometer. Record the "B cell store" and adjust the threshold rate to a maximum of 20 000 events/s. Measure the sample until it is finished.

15. Store the data appropriately.

2.4.5 Materials. Purified or Biotinylated peptide or protein antigens of choice depending on the protective/auto-reactive B cell response(s) to be studied.

- Fluorescently labeled streptavidin and/or extravidin molecules, e.g., BV605-streptavidin (Biolegend, catalog nr.: 405229), APC-labeled streptavidin (Invitrogen, catalog nr.: S32362), and PE-labeled extravidin (Sigma–Aldrich, catalog nr.: E4011-1ml).
- Fluorochrome for labeling of respective antigen, e.g. Cy5
- Bio-Spin® Columns with Bio-Gel® P-30 (BIO-RAD, catalog nr.: 732–6006)

Table 48. Fluorescently labeled monoclonal antibodies used in the example provided

No.	Marker	Clone	Fluorophore	Supplier	Catalog number
1	CD3	UCHT1	PB	BD	558117
2	CD14	M5E2	PB	BD	558121
3	CD19	Sj25C1	APC-Cy7	BD	557791
4	CD20	2H7	AF700	Biolegend	302322
5	CD27	M-T271	PE-Cy7	BD	560609

Table 49. Abs used as "surrogate" Abs for the compensation of avidin-tetramer derived fluorescent signals

No.	Marker	Clone	Fluorophore	Supplier	Catalog number
1	CD56	HCD56	BV605	Biolegend	318333
2	CD4	SK3	APC	BD	345771
3	CD8	RPA-T8	PE	BD	555367

- PBS
- BSA (Sigma–Aldrich, catalog nr.: A7906-1KG).
- FCM buffer (PBS, 0.5% BSA and 0.02% Azide)
- DAPI (Invitrogen, catalog-nr.: D1306)
- Fluorescently labeled mAbs (all Abs used in the present example are of mouse origin, expressed as IgG isotypes and directed against the respective human proteins, Table 48):
- Fluorescently labeled Abs to be used as "surrogate" Abs for the compensation of avidin-tetramer derived fluorescent signals (all Abs used in the example provided are murine Abs expressing the IgG$_1$ isotype directed against the respective human proteins indicated, Table 49):
- BD^{TM} CompBeads anti-mouse Ig, κ (BD Biosciences, Catalog nr.: 51-90-9001229)
- BD^{TM} CompBeads negative control (BD Biosciences, Catalog nr.: 51-90-9001291)
- Instrument: BD LSRFortessa (BD Biosciences)
- Software: BD FACSDIVA version 8.0.2 (BD Biosciences),
- Appropriate positive and negative control cells (here: HEK$^{ACPA-TM}$ and HEK^{WT}).

2.4.6 Data analysis/gating.

1. Identification of a vaccine-induced, high-avidity immune response identified by direct labeling of antigen with a fluorescent dye

Analysis and gating for the example provided are straightforward. B cell subsets can be gated as described in Section 2 B cells and their subsets. Following this step, fluorochrome specific plasmablasts, memory B cells, and naive B cells can be determined as shown for plasmablasts and memory B cells in Fig. 145.

2. Identification of an auto-reactive, low-avidity B cell response identified in an autoimmune disease setting using biotinylated peptide self-antigens tetramerized with fluorescently labeled streptavidin molecules

1. Open the experiment file using BD FACSDIVA version 8.0.2 (BD Biosciences)
2. Check and adjust the compensation of spectral overlap according to standard procedures.
3. Create a new "Normal Worksheet" in the file that stored only the "B cell store" gate, gate lymphocytes, single cells, and live B cells strictly (Fig. 147B)
4. Starting from the "live single B cell gate," create a CCP2-SA-BV605 versus CCP2-SA-APC plot to identify CCP2$^{+/+}$ and CCP2$^{-/-}$ populations. Place a gate around those CCP2$^{+/+}$ cells that strictly fall into the diagonal.
5. Display the cells identified in this gate (the CCP2$^{+/+}$ population) in a CCP2-SA-APC versus CArgP2-Extravidin-PE plot and place a gate on the CArgP2-PE negative population. These cells represent the antigen-specific B cell population of interest (i.e., ACPA-expressing B cells).
6. In the CCP2-SA-BV605 versus CCP2-SA-APC plot, place a gate on the CCP2$^{-/-}$ population, create a CD20-AF700 versus CD27-PE-Cy7 plot and gate on naïve (CD20$^+$CD27$^-$), memory (CD20$^+$CD27$^+$) and plasmablast (CD20$^-$CD27^{high}) subsets of these avidin-tetramer negative B cells.
7. From the gate identifying the ACPA-expressing B cell population (the CCP2$^{+/+}$ CArgP2$^-$ population), create a CD20-AF700 versus CD27-PE-Cy7 plot. Copy the gates identifying naïve (CD20$^+$CD27$^-$), memory (CD20$^+$CD27$^+$) and plasmablast (CD20$^-$CD27^{high}) subsets from the avidin-tetramer negative B cell population to the plot displaying the ACPA-expressing B cell population. This step is taken as it can be difficult to define the gates for these B cell subsets on the basis of very few cells. Therefore, copying the gates from a larger population (the avidin-tetramer negative B cells) to the antigen-specific B cell population (the ACPA-expressing B cells) is necessary for further analysis.
8. In the given example, the majority of ACPA-expressing B cells displays a memory (CD20$^+$CD27$^+$) phenotype, while avidin-tetramer-negative B cells mostly fall in the naïve B cell gate (CD20$^+$CD27$^-$) (Fig. 147B).
9. As an additional step of control, perform "back-gating" of the ACPA-expressing B cell population. Should some cells fall at the edge of the gates identifying lymphocytes, single cells, and live B cells, adjustment of these gates might be necessary to minimize the possibility that doublets or otherwise nonspecifically stained cells are misinterpreted (Fig. 147C).

2.4.7 Pitfalls.

- Be aware that the quality of the fluorescent signal of the labeled avidin-tetramers decreases overtime. Take along a staining control using the positive and negative control cells with each sam-

ple to control for such signal decay and/or an increase of non-specific background staining.
- The fluorochrome itself can be recognized by B cells giving rise to false positive signals; this can be overcome by using the same antigen labeled with a second fluorochrome, as described.

2.4.8 Top tricks.

- During setup and once a cell population has been identified that meets the criteria of antigen-specific cells delineated above, subsequent verification of antigen-specificity is indispensable. Please refer to the section "Verification of antigen-specificity" in the introduction for details on how antigen-specificity can be determined, and refer to [1230], supplementary data section, for examples.
- For differential labeling of antigens, we recommend using fluorescent dyes with emission spectra that show no or very little spectral overlap in order to reduce the need for extensive compensation.

2.4.9 Summary Table.   See Summary Table 47 of Chapter VI Section 2.3 Human B cells and their subsets.

2.5 *Human regulatory B cells*

2.5.1 Overview.   B cells play a key role in immune responses through the production of Abs, antigen presentation to other immune cells, and production of cytokines. Suppressive cytokines, such as IL-10, play a pivotal role in controlling inflammation and immune tolerance. Importance of regulatory B cells (Bregs) producing suppressive cytokines was described in murine models and in several human diseases. Depending on the disease studied or on the in vitro stimulation, different functional Breg subsets were described. Detailed characterization of individual Breg subsets, therefore, can improve our understanding of regulation of immune responses. This section describes a method for detection of individual Breg subsets in human PBMC samples. This panel can be considered a basis in which additional markers can be included to interrogate their expression among the different Breg subsets.

2.5.2 Introduction.   The existence of B cells with regulatory function (Breg) was first proposed in studies using B cell-depleted rodents, which showed reduced suppressive capacity of the lymphocyte fraction and were unable to recover from experimental autoimmune encephalitis [1248–1250]. Later, Mizoguchi et al. [1251] and Fillatreau et al. [1252] demonstrated that B cells can suppress immunity through production of immunosuppressive cytokines.

Bregs is an umbrella term used for immunosuppressive B cells [1253]. Bregs were often described in the context of chronic inflammatory diseases and in human they are mostly characterized
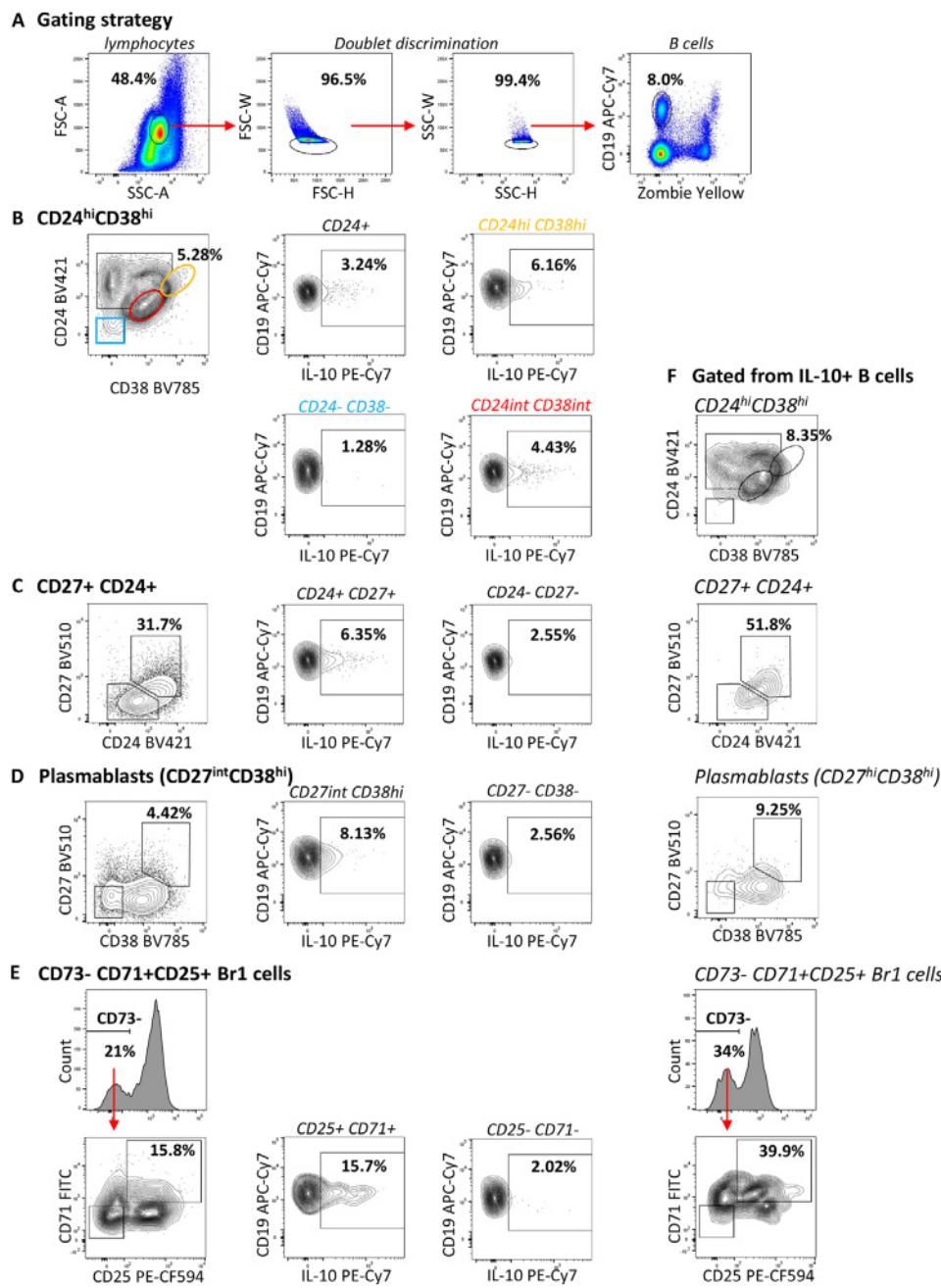
Figure 148. Identification of regulatory B cell subsets from CpG-stimulated PBMC. PBMC from healthy female adult subject cultured for 72 h with media alone or media containing 1μM CpG-ODN 2006. Before staining, cells stimulated for 5 h with 25 ng/mL PMA and 1 μg/mL Iono and for the last 2 h with 10 μg/mL Brefeldin A. Cells harvested and surface and intracellular antibody stainings performed. Total viable B cells gated from lymphocytes after doublet discrimination (A). Breg subsets gated from viable single $CD19^+$ B cells (B–E). IL-10$^+$ B cells gated from (B) $CD19^+$ $CD24^{high}$ $CD38^{high}$ B cells, (C) B10/pro-B10 cells ($CD19^+$ $CD24^{high}$ $CD27^+$), (D) suppressive plasmablasts ($CD19^+$ $CD27^{int}$ $CD38^+$), and (E) $CD19^+$ $CD73^-$ $CD25^+$ $CD71^+$ B cells. Breg subsets gated from IL-10$^+$ $CD19^+$ B cells based on surface markers showing enrichment of IL-10$^+$ B cells (F).

by production of the suppressive cytokine IL-10 [1162, 1253]. Generally, expression of IL-10 has been a very useful marker for B cells with suppressive phenotype [1162, 1253]. However, several Breg-related surface markers can be either down- or upregulated upon stimulation, making it difficult when Breg subsets are compared among different stimulatory environments [1162]. For example, CD25 and CD71 are often upregulated in activated B cells [1254, 1255] and they are widely used also as activation markers. Another activation marker, CD38, is expressed in naïve B cells and plasmablasts (the main IL-10 producing subsets) but is downregulated when naïve B cells develop into memory B cells [1256]. Furthermore, CD1d can be downregulated upon

stimulation [1254]. In contrast to regulatory T cells, no Breg-specific transcription factor could be identified so far [1162]. Furthermore, the high diversity of B cell subsets with suppressive capacity strongly suggests that there is not one single lineage of B cells giving rise to Bregs but that there are precursors from various stages of B cell ontogeny that gain suppressive phenotype in response to stimulation.

In mice, Bregs were reported to act mainly via production of suppressive cytokines IL-10, IL-35, and TGF-β [1162] and inhibitory receptors such as LAG-3 [1167]. IL-10 can suppress production of pro-inflammatory cytokines by antigen presenting cells and induce T regulatory cells [1165, 1257]. IL-35 was reported

Table 50. Human B cell subsets

Name	Marker	Suppressor molecules	Induction	Associated disease
Immature B cells	CD19$^+$ CD24^{high} CD38^{high} CD1d$^+$	IL-10	CD40 ligation	Suppressive role in RA, SLE and CHB virus infection [1277–1279]
B10/pro-B10 cells	CD19$^+$ CD24^{high} CD27$^+$ CD48^{high} CD148^{high}	IL-10	CpG-ODN, LPS (+ CD40 ligation)	Various autoimmune diseases [1280].
Br1 cells	CD19$^+$ CD73$^-$ CD25$^+$ CD71$^+$ B cells	IL-10, IgG4, PD-L1	CpG-ODN	Allergen tolerance [1255]
Suppressive plasmablasts	CD19$^+$ CD27^{int} CD38$^+$	IL-10, immunoglobulins	CpG-ODN + IL-2, IL-6, and IFN-α/γ	Healthy subjects [1165]
Suppressive plasma cells	CD138$^+$	IL-10	n/a	Multiple sclerosis lesions [1281]

to inhibit T helper 1 (Th1) cell responses [1159], while TGF-β can inhibit APCs and induce apoptosis in Th1 cells as well as bring on anergy in CD8$^+$ T cell [1258, 1259]. In murine spleen, CD19$^+$, CD21^{hi} CD23^{hi} CD24hi B cells (T2-MZP cells) [1168, 1169, 1260, 1261] and CD19$^+$, CD21^{hi} CD23$^-$ B cells (MZ B cells) [1170, 1262, 1263] were found suppressing CD4$^+$ and CD8$^+$ T cells while inducing Tregs. Similarly, IL-10-producing CD1d^{high} CD5$^+$ B cells (B10) were found in the spleen, suppressing CD4$^+$ T cells, dendritic cells (DC), as well as monocytes thereby playing a protective role in a plethora of mouse models including EAE [1264, 1265], lupus [1266], myasthenia-gravis [1267], collagen-induced arthritis [1268], colitis [1269], allergic inflammation [1270, 1271], and contact hypersensitivity [1272]. In spleen, also CD19$^+$ TIM-1$^+$ B cells were identified, suppressing CD4$^+$ T cells [1173, 1273]. Interestingly, suppressive phenotype was also found among B cells of later differentiation stages, such as CD138$^+$ CD44^{hi} plasmablasts [1165], CD138$^+$ MHC-11^{lo} B220$^+$ plasma cells [1159, 1274] and LAG-3$^+$ plasma cells [1167]. Suppressive plasmablasts were found in LN, suppressing CD4$^+$ T cells and DCs [1165] while IL-10 and IL-35 secreting plasma cells were found in spleen, suppressing effector CD4$^+$ T cells as well as neutrophils and NK cells [1159, 1274]. LAG-3$^+$ plasma cells, in addition to LAG-3 also expressed additional inhibitory receptors, including CD200, PD-L1, and PD-L2 [1167]. A common characteristic among all the above-mentioned murine Breg subsets is their capability to produce of IL-10 [1162].

In this section, we focus on human Breg cell subsets (see Table 50 for a summary of human B cell subsets). The first data that indicated a potential role for regulatory B cells in humans came from the reports of new onset of colitis and psoriasis after CD20 mAb treatment with rituximab [1275, 1276]. In human Bregs, regulatory function is mainly conferred via secretion of IL-10. IL-10 can be produced by naïve B cells [1255, 1277–1280], plasmablasts [1165] from the blood and plasma cells from tissue [1281] while it is unclear which subset is the most potent producer. IL-10 can be induced from peripheral human B cells by ligation of TLR9 (using CpG-ODN) [1165, 1255, 1280] or CD40 [1277, 1280] in vitro. Bregs originating from immature CD19$^+$

CD24^{high} CD38^{high} B cells were found in blood and in inflamed tissue having a suppressive role in rheumatoid arthritis (RA), systemic lupus erythematosus (SLE), and chronic hepatitis B (CHB) virus infection [1277–1279]. These cells suppress Th1, TH17 cells, and virus-specific CD8$^+$ T cells while inducing Tregs [1277–1279]. Suppressive B10/pro-B10 cells (CD19$^+$ CD24^{high} CD27$^+$ CD48^{high} CD148^{high}) were found in blood suppressing CD4$^+$ T cells, monocytes, and DCs [1280]. B10/pro-B10 cells regulate innate immunity and are upregulated in patients with various autoimmune diseases [1280]. IL-10-producing CD19$^+$ CD73$^-$ CD25$^+$ CD71$^+$ Bregs play an important role in developing tolerance to allergens. This subset was shown to mature at increased frequency into plasma cells that secrete the suppressive Ab isotype IgG4 [1255]. In addition, CD27^{int} CD38$^+$ plasmablasts derived either from naïve immature B cells or naïve mature B cells suppress effector CD4$^+$ T cells and DCs by expressing IL-10 [1165]. Recently, it was shown that in multiple sclerosis lesions, plasma cells (but not B cells) produced large amounts of suppressive IL-10 [1281]. An FCM panel was described combining several Breg-associated markers, including CD19, CD1d, CD5, CD24, CD25, CD38, CD71, CD73, and IL-10 [1254]. This allows to identify CD24^{hi} CD38^{hi} IL-10$^+$ Bregs (Fig. 148B), CD73$^-$ CD25$^+$ CD71$^+$ IL-10$^+$ Bregs (Fig. 148E), and a CD5$^+$ CD1d^{high} IL-10$^+$ Breg subset, which was mainly described in mice. In humans, CD1d was also reported to more expressed in regulatory B cell subsets [1280, 1282]. Here, we included CD27, a marker for memory B cells, which allows additional distinction of CD19$^+$ CD24^{high} CD27$^+$ B10/pro-B10 cells (Fig. 148C) and CD19$^+$ CD27^{int} CD38$^+$ suppressive plasmablasts (Fig. 148D). These Breg subsets show enrichment for IL-10-producing B cells compared to total IL-10 producing B cells (Figure 149).

2.5.3 Step-by-step sample preparation. This staining protocol is optimized for human peripheral B cells. PBMCs were isolated from heparinized blood of healthy individuals by density gradient centrifugation (Biochrom, Berlin, Germany). Isolated PBMC were directly plated and stimulated for 72 h with CpG-ODN. Before staining, cells were incubated with PMA and Iono (5 h) and Brefeldin A (2 h), followed by viability staining with zombie
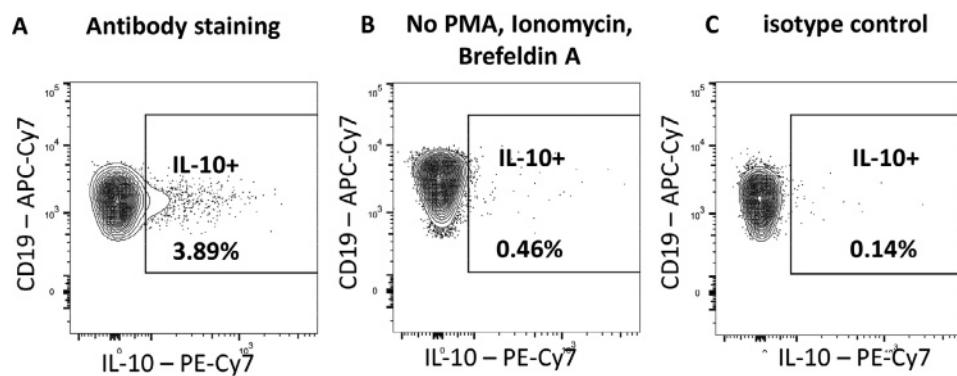
Figure 149. IL-10 staining and control stainings. PBMC cultured for 72 h with media alone or media containing 1 μM CpG-ODN 2006. The last 5 h before staining, PBMC additionally stimulated with 25 ng/mL PMA and 1 μg/mL ionomycin and for the last 2 h with 10 μg/mL Brefeldin A (A and C) or medium control (B). IL-10$^+$ B cells gated from single viable CD19$^+$ B cells. Upstream gating was performed as in Fig. 148. Anti-IL-10 antibody staining (A) after stimulation with PMA, Iono, and Brefeldin-A or (B) without stimulation and (C) isotype control staining.

yellow viability dye (Biolegend, San Diego, CA) and staining for surface markers with the Abs listed in Table 51 in staining buffer. Cells were washed, permeabilized, and Ab staining for intracellular IL-10 was performed. Then, samples were washed and measured on a BD LSR Fortessa with BD FACSDiva Software Version 8.0.1 and analyzed using Flowjo version 10.4.

Detailed protocol:

1. Collect fresh blood in heparinized containers (BD vacutainer 170 I.U. of lithium heparin)
2. Isolate PBMC:
   (a) Dilute blood samples at a 1:1 ratio with PBS supplemented with 2 mM EDTA.
   (b) For each 30 mL of diluted blood prepare a tube of Biocoll. Add 15 ml of Biocoll separating solution (room temperature) to a 50 mL blood-sep-filter tube. Spin down 1 min at 1100 × g to collect the Biocoll at the bottom of the tube below the filter.
   (c) Slowly add 30 mL of diluted blood to each filter tube and centrifuge the tubes at 800 × g for 20 min at 18°C and no break at end of program.
   (d) Collect the interphases and pool up to two interphases and transfer them to a new 50 mL centrifugation tube. Fill up tube with PBS supplemented with 2 mM EDTA. Centrifuge tubes at 780 × g for 10 min at 18°C.
   (e) Remove supernatant and resuspend cell pellet in 2 mL PBS supplemented with 2 mM EDTA. Pass cells through a 70 μM cell strainer into a new 50 mL centrifugation tube. Fill up tube with PBS supplemented with 2 mM EDTA. Centrifuge tubes at 220 × g for 10 min at 4°C.
   (f) Discard supernatant and resuspend PBMC in 5 mL of complete RPMI (cRPMI; RPMI 1640 medium supplemented with MEM Vitamin Solution, penicillin, streptomycin, kanamycin, MEM Non-essential Amino Acid Solution, Sodium pyruvate solution (Sigma-Aldrich Chemie GmbH), and 10% heat-inactivated FCS (Sigma–Aldrich Chemie GmbH).
3. Count PBMC and plate two million PBMC at concentration of 1 million/mL in cRPMI in 12-well tissue culture plate.

Table 51. Antibodies

Marker	Label	Clone	Manufacturer	Product number	Dilution
CD38	BV785	HIT2	Biolegend, San Diego, CA, USA	303530	1:50
CD27	Brilliant Violet 510	L128	BD Biosciences, Pharmingen, San Diego, CA, USA	563092	1:33
CD24	Brilliant Violet 421	ML5	Biolegend, San Diego, CA, USA	311122	1:40
CD71	FITC	CY1G4	Biolegend, San Diego, CA, USA	334104	1:20
CD25	PE-CF594	M-A251	BD Biosciences, Pharmingen, San Diego, CA, USA	562403	1:40
CD1d	PE	51.1	eBioscience, Affymetrix Inc., San Diego, CA, USA	12-0016-42	1:40
CD19	APC-Cy7	HIB19	Biolegend, San Diego, CA, USA	302218	1:100
CD73	APC	AD2	Biolegend, San Diego, CA, USA	344006	1:40
IL-10	PE-Cy7	JES3-9D7	Biolegend, San Diego, CA, USA	501420	1:200
Isotype ctrl	PE-Cy7	RTK2071	Biolegend, San Diego, CA, USA	400416	1:200

4. Stimulate PBMC with 1 µM CpG ODN 2006 or medium (control) for 72 h.

2.5.4 Materials.

Reagent	Product number	Manufacturer
BD vacutainer 170 I.U. of lithium heparin	367526	BD, Plymouth, UK
Blood separation filter tube	03-7100SI	Dacos, Esbjerg N, Denmark
Biocoll	L 6115	Biochrom, Berlin, Germany
BD Falcon 70 µM cell strainer	431751	BD Biosciences, Franklin Lakes, NJ, USA
Cell culture medium:		
RPMI-1640 Medium, with sodium bicarbonate and L-glutamine	R8758-500ML	Sigma–Aldrich Chemie GmbH
Fetal calf serum (FCS)	F7524	Sigma–Aldrich Chemie GmbH
MEM Vitamin Solution (100×)	M6895-100ML	Sigma–Aldrich Chemie GmbH
Penicillin-Streptomycin (100×)	P4333-100ML	Sigma–Aldrich Chemie GmbH
Kanamycin (100×)	15160-047	GIBCO, Paisley, UK
MEM Nonessential Amino Acid Solution (100×)	M7145-100ML	Sigma–Aldrich Chemie GmbH
Sodium pyruvate solution	S8636-100ML	Sigma–Aldrich Chemie GmbH
TPP® tissue culture plates, 12-well plate, polystyrene	Z707775-126EA	Sigma–Aldrich Chemie GmbH
CpG ODN 2006		MicroSynth, Balgach, Switzerland
PMA	P-8139	Sigma–Aldrich Chemie GmbH
Ionomycin	I9657-1MG	Sigma–Aldrich Chemie GmbH
Brefeldin A	B7651	Sigma–Aldrich Chemie GmbH
FCM staining buffer:		
PBS		GIBCO, Paisley, UK
2 mM EDTA		
BSA	A3294-500G	Sigma–Aldrich Chemie GmbH, Buchs, Switzerland
Zombie Yellow™ Fixable Viability Kit	423104	Biolegend, San Diego, CA, USA
Fixation/Permeabilization Solution Kit	554714	BD Biosciences, Pharmingen, San Diego, CA, USA

5. Harvest PBMC and spin down (300 × *g*, 10 min).
6. Staining for FCM:
   (a) Briefly vortex cell pellet and stain cells with 100 µL of Zombie yellow viability dye diluted 1:100 in staining buffer. Incubate 20 min at room temperature in dark. Wash once with 1 mL of staining buffer.
   (b) Stain cells with Abs specific for surface markers listed in Table 51 in a total staining volume of 100 µL. Incubate 15 min at 4°C in dark. Wash once with 1 mL of staining buffer.
   (c) Briefly vortex the cell pellet and resuspend with 250 µL of Fixation/Permeabilization solution (BD Biosciences, 554714) for 20 min at 4°C.
   (d) Wash the cell pellet two times with 1 mL BD Perm/Wash™ buffer (BD Biosciences, 554714).
   (e) For intracellular staining of IL-10, dilute Ab in 50 µL BD Perm/Wash™ buffer. As isotype staining control for IL-10, use isotype control Ab in equal concentration. Incubate 30 min in the dark at 4°C.
   (f) Wash the cells two times with 1 mL BD Perm/Wash™ buffer (BD Biosciences, 554714).
7. Resuspend cell pellet in 200 µL staining buffer and measure sample.

2.5.5 Data analysis. We first gate on lymphocytes in FSC versus SSC, followed by doubled discrimination (Fig. 148A). From single cells we gate on viable (Zombie Yellow negative) CD19$^+$ B cells. Total IL-10$^+$ cells are gated from viable B cells (Fig. 149A). B cells can be sub-gated into CD24$^+$ CD38$^+$ IL-10$^+$ Bregs (Fig. 148B), CD19$^+$ CD24$^+$ CD27$^+$ B10/pro-B10 cells (Fig. 148C), CD19$^+$ CD27^{int} CD38$^+$ suppressive plasmablasts (Fig. 148D), and CD73$^-$ CD25$^+$ CD71$^+$ IL-10$^+$ Bregs (Fig. 148E). These four Breg subsets contain increased percentage of IL-10$^+$ B cells compared to total IL-10 producing B cells (Figs. 148B–E and 149A). Alternatively, when we gate Breg subsets based on their surface marker expression from total IL-10$^+$ B cells, we find that these Breg subsets are enriched among total IL-10$^+$ B cells (Fig 148F). However, even though IL-10$^+$ B cell are enriched among gated Breg subsets, there are also other IL-10-producing B cells, which are not falling into a described Breg gate. Also, Breg subsets are overlaping to some extent.

2.5.6 Pitfalls. Some of the surface expressed proteins used as markers for Bregs are also known as general activation markers. Depending on the stimulation used, surface markers of Bregs therefore might be up- or downregulated. For example, upon

stimulation with CpG or BCR ligation+CD40L for 72 h, it was seen that while number of CD19$^+$ CD73$^-$ CD25$^+$ CD71$^+$ B cells (Br1 cells) showed a tendency to be increased among total IL-10 producing B cells, CD19$^+$ CD24$^+$ CD38$^+$ B cells and CD19$^+$ CD1d$^+$ CD5$^+$ B cells were decreased [1254]. Therefore, it is important to carefully consider the length of the stimulation period when performing in vitro stimulation of regulatory B cells.

2.5.7 Top tricks.   Depending the exact research question and on the flow cytometer available, several other Abs can be included to the panel. Since B cells sometimes produce inflammatory cytokines (e.g., TNF) together with IL-10 [1283], it can be useful to include Abs for exclusion of inflammatory cytokine-producing cells.

2.6 *Human immunoglobulin heavy chain isotypes*

2.6.1 Overview.   B cells play a key role in immune responses through the production of Abs. Detailed characterization of individual subsets of B cells that have switched to distinct Ig heavy chain isotypes can improve our understanding of the development of humoral immune responses. This section describes a method for detection of individual Ig heavy chain expressing B cells in human PBMC samples. This panel can be considered a basis in which additional markers can be included to interrogate their expression among the different B cell subsets.

2.6.2 Introduction.   B cells develop in the bone marrow and are released into the circulation, after which they mature predominantly in the spleen to become mature naive B cells. Mature B cells can be roughly divided into two subsets: conventional follicular B cells (frequently referred to as B-2 cells) and non-conventional extrafollicular B cells (including B-1 cells, which have been mainly characterized in the mouse, and marginal zone (MZ) B cells) [1284, 1285].

Extrafollicular B cells mount thymus-independent (TI) humoral responses, which are rapidly induced in response to conserved microbial carbohydrate or glycolipid structures. These responses often result in the production of polyspecific low-affinity IgM Abs, and typically do not involve somatic hypermutation or class switch recombination (CSR) [1286]. T-independent CSR and somatic hypermutation have been reported [1287]. Follicular B cells participate in thymus-dependent (TD) responses. These cells interact with follicular helper T (Tfh) cells in germinal centers, which are mainly found in secondary lymphoid organs [1288]. Follicular B cells that receive T cell help (through CD40L and cytokines) will become germinal center B cells and upregulate BCL6 and activation-induced deaminase expression, and will undergo CSR and somatic hypermutation [1286, 1289]. The B cells that emerge from such a germinal center reaction will either become circulating memory B cells or plasma cells. Some plasma cells will home to the bone marrow where they can survive for many years as long-living immunoglobulin-secreting plasma cells [1290].

B cell activation to T-cell dependent antigens requires BCR stimulation and CD40 ligation. Antigens can be captured directly by B cells or can be presented by follicular DCs in the lymphoid follicles. BCR stimulation is typically mediated through binding of a specific antigen to the BCR leading to internalization, processing and presentation of antigenic peptides in MHC class II molecules. Antigens are presented to CD4$^+$ T cells, which are activated in this manner. Activated CD4$^+$ T cells upregulate CD40L and secrete cytokines. The type of cytokines that are produced by these T cells depends on how these cells were primed as naïve T cells. CD40-CD40L interaction and the local cytokine milieu provide the second signal that is required for efficient B cell activation including proliferation, CSR, and plasma cell differentiation.

Abs are identical to the BCR of the B cell from which they originate, with the exception of a C-terminal sequence that anchors the molecule to the cell membrane. As a result, Abs are secreted and do not form surface-bound receptors. Abs have a functionally polarized structure, with on one side the Fab region harboring a hypervariable region, which is responsible for antigen binding, and on the other side a constant Fc region. The structure of the constant region determines the effector function of the Ig. Abs are typically classified according to the isotype of their heavy chain. Humans have nine major Ig heavy chain isotypes: IgM, IgD, IgG1, IgG2, IgG3, IgG4, IgA1, IgA2, and IgE [1291] while there are eight murine Ig isotypes: IgM, IgD, IgG1, IgG2a, IgG2b, IgG3, IgA and IgE [1291]. Each of these Ab isotypes mediates distinct functions through interaction with specific receptors on effector cells and serum factors.

Each Ig molecule consists of two heavy (IgH) and two light chains, both of which contain variable (V) and constant (C) regions. The region of the heavy chain that determines antigen-specificity is made up by the variable (V$_H$), diversity (D), and joining (J$_H$) segments that are rearranged during early B cell development to form a VDJ cassette or V-region. The V-region is located upstream of the CH exons. The C region of the IgH chain determines the isotype of the Ig. In mature naïve B cells, the V-region is linked to the constant region of the μ chain (Cμ) [1292]. Consequently, mature naïve B cells express surface IgM and, as a result of alternative splicing, IgD as their BCR. A population of IgM$^-$IgD$^+$ class switched B cell has been reported. These cells are primarily found in secondary lymphoid organs and are not readily detected in peripheral blood [1293].

Upon activation, naïve IgM$^+$IgD$^+$ B cells can undergo CSR, resulting in a change of the heavy chain isotype of the produced immunoglobulin, while its antigen-specificity is retained. Nonswitched B cells are CD19$^+$ and express IgM and IgD on their cell surface (Fig. 150A and B). The nonswitched IgM$^+$IgD$^+$ B cell population contains transitional B cells, Naïve mature B cells, and IgM$^+$CD27$^+$ memory B cells. The staining procedure outlined below is designed for detection of human immunoglobulin heavy chain isotypes expressed as BCRs on B cells.

2.6.3 Step-by-step sample preparation.   This staining procedure is designed for human peripheral B cells. PBMCs were isolated
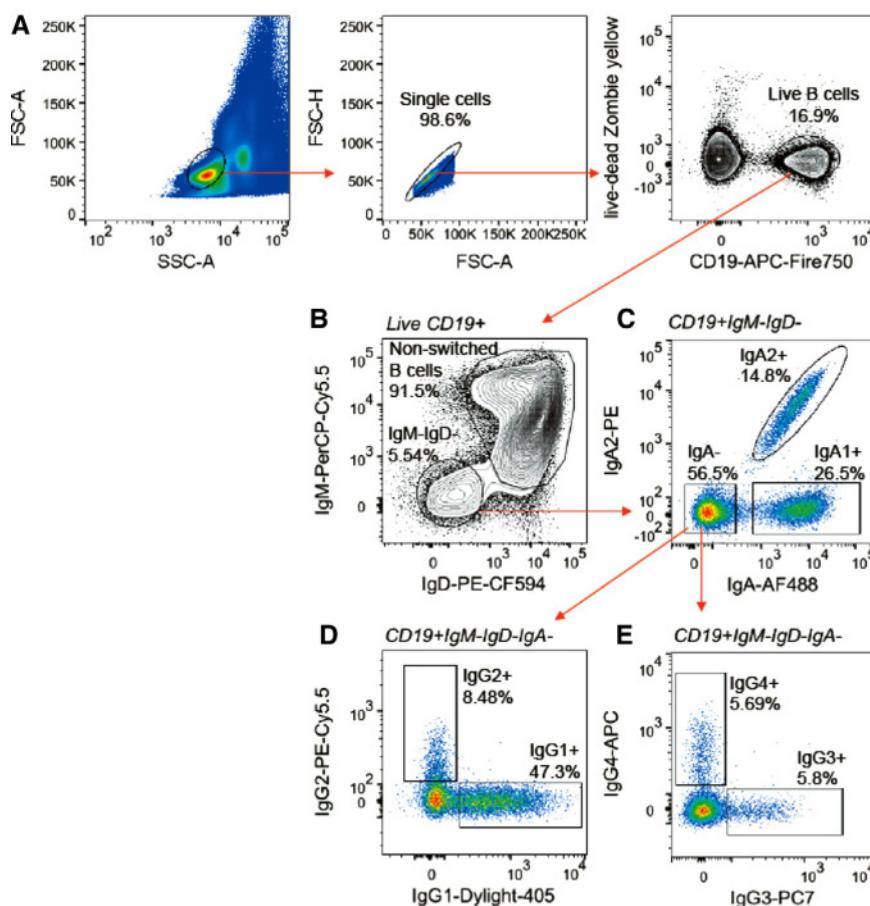
Figure 150. Identification of B cells expressing different Immunoglobulin heavy chain isotypes in a human PBMC sample (healthy individual age 47, male). (A) Lymphocytes were identified based on their FSC and SSC, Doublet exclusion was performed on FSC-H vs FSC-A, and B cells were gated as CD19^{+} and zombie yellow (viability dye) negative. (B) Nonswitched B cells (IgD^{+}) and class-switched (IgM^{−}IgD^{−}) were gated. (C) Within the IgM^{−}IgD[−] population, IgA^{+} B cells, IgA2^{+}, and IgA^{−} cells can be distinguished. IgA1^{+} B cells were defined as IgA[+]IgA2^{−}. (D and E) IgA[−] B cell were further differentiated based on expression of IgG1, IgG2 (D), IgG3, and IgG4 (E).

from heparinized blood of healthy individuals by density gradient centrifugation (Biochrom, Berlin, Germany). PBMC were counted and stained in PBS with zombie yellow viability dye (Biolegend, San Diego, CA). Samples were washed and incubated with antibodies listed in Table 52 and measured on a BD LSR Fortessa with BD FACSDiva Software Version 8.0.1 and analyzed using Flowjo version 10.4.

Detailed protocol:

1. Collect fresh blood in heparinized containers (BD vacutainer 170 I.U. of lithium heparin)
2. Isolate PBMC:
   (a) Dilute blood samples at a 1:1 ratio with PBS supplemented with 2 mM EDTA.
   (b) For each 30 mL of diluted blood prepare a tube of Biocoll. Add 15 mL of Biocoll separating solution to a 50 mL blood-sep-filter tube. The Biocoll should be at room temperature. Spin down 1 min 1100 × g to collect the Biocoll at the bottom of the tube.
   (c) Slowly add 30 mL of diluted blood to each filter tube and centrifuge the tubes at 800 × g for 20 min at 18°C and no break at end of program.
   (d) Collect the interphases and pool up to two interphases and transfer them to a new 50 ml centrifugation tube. Fill up tube with PBS supplemented with 2 mM EDTA. Centrifuge tubes at 780 × g for 10 min at 4°C.
   (e) Remove supernatant and resuspend cell pellet in 2 mL PBS supplemented with 2 mM EDTA. Pass cells through a 70 µM cell strainer into a new 50 mL centrifugation tube. Fill up tube with PBS supplemented with 2 mM EDTA. Centrifuge tubes at 220 × g for 10 min at 4°C.
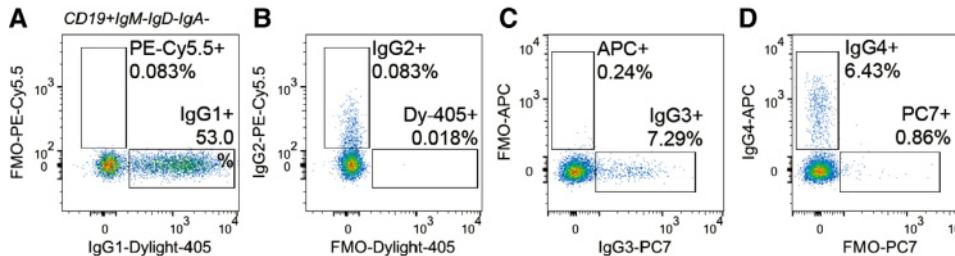
Figure 151. FMO controls for IgG subclasses. (A) FMO for IgG1-Dylight-405. (B) FMO for IgG2-PE-Cy5.5. (C) FMO for IgG4-APC. (D) FMO for IgG3-PC7. Upstream gating was performed as in Fig. 150.

(f) Discard supernatant and resuspend PBMC in 5 ml PBS supplemented with 2 mM EDTA.

3. Count PBMC and use between one and five million PBMC per staining.

4. Stain cells with Zombie yellow viability dye. Incubate 20 min at 4°C in dark. Wash 1x with staining buffer

5. Stain cells with Abs listed in Table 53 in a total staining volume of 100 μL. Incubate 15 min at 4°C in dark. Wash 1x with staining buffer

6. Stain cells with Streptavidin-PC7, incubate 15 min at 4°C in dark. Wash 1x with staining buffer.

7. Resuspend cells in 200 μL staining buffer and measure sample.

2.6.4 Materials.

Table 52.

Reagent	Manufacturer
Biocoll	Biochrom, Berlin, Germany
Blood separation filter tube	Dacos, Esbjerg N, Denmark
BD Falcon 70 μM cell strainer	BD Biosciences, Franklin Lakes, NJ, USA
Staining buffer: PBS + 2 mM EDTA + 2% BSA	Sigma, St Louis, MO, USA

B cell population (CD19$^+$)	Phenotype (all CD19$^+$)	Expected frequency range within total CD19+ B cells	Expected frequency range within parent population
Non-switched	IgM$^+$IgD$^+$	40-95%	40-95%
IgA1-switched	IgM$^-$IgD$^-$IgA$^+$IgA2$^-$	2-10%	10-40%
IgA2-switched	IgM$^-$IgD$^-$IgA$^+$IgA2$^+$	1-5%	5-20%
IgG1-switched	IgM$^-$IgD$^-$IgA$^-$IgG1$^+$	5-10%	40-70%
IgG2-switched	IgM$^-$IgD$^-$IgA$^-$IgG2$^+$	0.5-6%	5-30%
IgG3-switched	IgM$^-$IgD$^-$IgA$^-$IgG3$^+$	0.2-1%	3-15%
IgG4-switched	IgM$^-$IgD$^-$IgA$^-$IgG4$^+$	0.01-1%	0.1-8%

2.6.5 Data analysis.   B cells that undergo CSR will lose expression of IgM and IgD and can be gated as CD19$^+$IgM$^-$IgD$^-$ (Fig. 150B). A major fraction of the switched B cell compartment consists of IgA$^+$ B cells, which can be subdivided into IgA1$^+$ and IgA2$^+$ B cells. Here, we used an Ab against total IgA to identify all IgA$^+$ B cells combined with an anti-IgA2 Ab to separate IgA2$^+$ and IgA2$^-$ (i.e., IgA1$^+$) B cells (Fig. 150C). The IgA$^-$ B cells can be further separated into IgG1$^+$, IgG2$^+$, IgG3$^+$, and IgG4$^+$ B cells (Fig. 150D and E), of which the IgG1$^+$ population is the most abundant (Fig. 150D). IgE$^+$ B cells are hardly detectable in healthy individuals and this population is not shown in this analysis. Expression of most Ig heavy chain isotypes, with the exception of IgM and IgD on non-switched B cells, is mutually exclusive. Thus a class-switched (IgM$^-$IgD$^-$) B cell will only express a BCR with one immunoglobulin heavy chain isotype. FMO controls for IgG subclasses are shown in Fig. 151.

2.6.6 Pitfalls.   This protocol has been established for staining of PBMC samples. It may be applicable to other material such as tonsil, or other tissue-derived single cell suspensions. Cell suspensions from B cell rich tissues such as tonsils may require optimization of the antibody dilutions. Also when staining more than five million PBMCs, the amount of antibodies and/or the staining volume may need to be adjusted.

To the best of our knowledge, the heavy chain isotype-specific Abs that were used in this staining panel have do not cross-react with other isotypes. We did not observe significant populations of cells that were double positive for more than one Ig heavy chain isotype (other than IgM and IgD double positive non-switched cells). This can be easily confirmed by plotting every heavy chain isotype against every other.

2.6.7 Top tricks.   This panel can be extended by adding selected surface markers of interest to study, in detail, the different heavy stain isotype-switched B cell subsets. The addition of fluorescently labeled antigens to the panel allows the measurement of the distribution of antigen-specific B cells among different heavy chain isotypes as we have demonstrated before [1294].

2.6.8 Summary table.

3 Ab-secreting cells (plasmablasts and plasma cells)

3.1 *Murine Ab-secreting plasmablasts and plasma cells*

3.1.1 Overview.   Plasma cells are terminally differentiated B lineage cells that secrete large amounts of Abs, a key step in establishing effective adaptive humoral immunity against pathogens and other toxic substances. After being activated in either a T cell-dependent or T cell-independent manner, B cells proliferate and initiate a transcriptional program (controlled by e.g., Irf4 and Blimp1) to adapt to the challenge of secreting enormous quantities of Abs. The induction of the plasma cell program begins with the transition of activated B cells to the proliferating plasmablast stage, where Ab secretion starts. Ab-secreting cells enter the blood stream, migrate to effector sites or survival niches, e.g., in the bone marrow, spleen, gut, or sites of inflammation and develop into mature, nondividing plasma cells. Some of these cells may
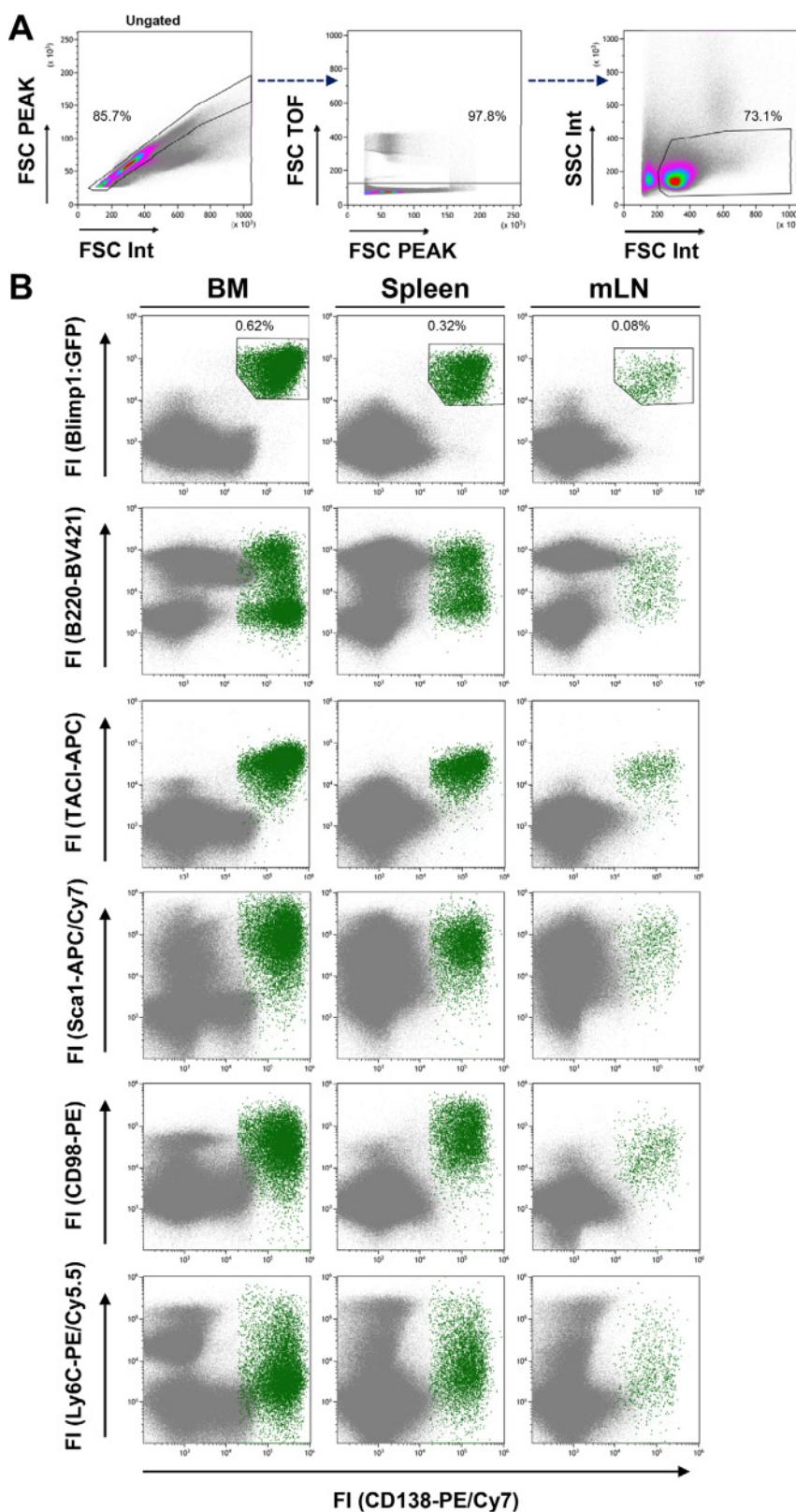
Figure 152. Comparison of common two-color flow cytometric analyses of plasma cell populations. (A) Exemplary gating strategy for single extended lymphocytes in spleen. (B) Single cell suspensions from bone marrow (BM), spleen and mesenteric lymph nodes (mLN) of Blimp1:GFP-reporter mice were isolated and stained as described with Abs against CD138 and one additional surface marker indicated on the y-axis. The Blimp1:GFP^{hi}/CD138^{hi} gate was used as the reference gate for the plasmablast/plasma cell populations and events in this gate are highlighted in green in the following plots.

Table 53. Antibodies and other reagents used for staining

Antibody	Clone	Species reactivity	isotype	Company	Dilution
IgA-AF488	Polyclonal	Human	polyclonal goat IgG	Jackson Immunoresearch, West Grove PA, USA	1:1500
IgA2-PE	REA995	Human	human IgG1	Miltenyi biotec, Bergisch Gladbach, DE	1:100
IgG1-Dylight405*	HP6188	Human	mouse IgG2b,k	Sanquin, Amsterdam, NL	1:1000
IgG2-PE/Cy5.5*	HP6014	Human	mouse IgG1,k	Sanquin, Amsterdam, NL	1:1000
IgG3-biotin* (followed by Streptavidin-PC7)	HP6095	Human	mouse IgG1,k	Sanquin, Amsterdam, NL	1:1000
IgG4-APC	SAG4	Human	mouse IgG1,k	Cytognos, Salamanca, Spain	1:400
IgM-PerCP/Cy5.5	MHM-88	Human	mouse IgG1,k	Biolegend, San Diego, CA, USA	1:100
IgD-PE-CF594	IA6-2	Human	mouse IgG2a,k	BD Biosciences, Franklin Lakes, NJ, USA	1:35
CD19-APC/FIRE750	HIB19	Human	mouse IgG1,k	Biolegend, San Diego, CA, USA	1:100
CD27-BV510#	L128	Human	mIgG1,k	BD Biosciences, Franklin Lakes, NJ, USA	1:100
CD38-BV786#	HIT2	Human	mIgG1,k	Biolegend, San Diego, CA, USA	1:100
Zombie yellow viability dye	–	–	–	Biolegend, San Diego, CA, USA	1:100
Streptavidin-PC7	–	–	–	Biolegend, San Diego, CA, USA	1:2000

*These antibodies were labeled using lightning link labeling kits from Novus Biologicals, Centennial, CO, USA.
#These antibodies were included in the staining panel but are not applied in the gating strategy shown in Fig. 150.

persist for weeks up to years and continuously provide protective as well as pathogenic Abs. The following chapter will provide an overview of surface markers and detailed protocols to identify proliferating plasmablasts and nondividing plasma cells in various murine lymphatic tissues by FCM.

3.1.2 Introduction. Ab-secreting cells are a heterogeneous population ranging from very early proliferating (i.e., plasmablasts) to late nondividing and long-lived Ab-secreting cells (i.e., plasma cells); see also Chapter VI Section 3.2 Human Ab-secreting cells. Utilizing the Blimp1:GFP-reporter mouse line, which is frequently used to detect Ab-secreting cells [1295], we tested the efficiency of different surface marker combinations and gating strategies to distinguish plasmablasts from early and late plasma cells with a single staining panel.

Maturation of proliferating early Ab-secreting plasmablasts into resting long-lived plasma cells is accompanied by an increased abundance of immunoglobulins (Ig), Blimp1, CD138 (Syndecan-1), Transmembrane activator, and CAML interactor (TACI) and B cell maturation antigen (BCMA), while B cell-specific surface proteins such as CD19, CD20, MHCII, and B220 are downregulated [1296]. Combinations of these markers can be used to track the various subsets of Ab-secreting cells. In addition, Blimp1-reporter mouse lines (e.g., Blimp1:GFP) represent a handy tool to identify Ab-secreting cells by FCM or fluorescence microscopy. However, there are several limitations to consider when using the Blimp1:GFP reporter mouse. Most importantly, the GFP reporter signal alone is not sufficient for a reliable analysis of plasmablasts/plasma cells because Blimp1 is also produced by other immune cells, e.g., effector T cell subsets in the spleen and other lymphatic and nonlymphatic tissues [1297]. In addition, the knock-in of the GFP reporter cassette into the *Prdm1* gene (encodes Blimp1) results in an inactive *Prdm1* allele [1295]. Furthermore, in contrast to formaldehyde fixation the fluorescence of the GFP molecule is abolished by methanol/ethanol-based fixation protocols. Finally, the Blimp1:GFP reporter mouse might either be not available, or it might be too time consuming to cross the *Prdm1* reporter allele into other transgenic lines or disease mouse models. Therefore, alternative surface staining protocols to detect Ab-secreting cells on a single-cell basis by FCM have been developed.

As plasma cells produce large amounts of Igs, surface CD138 staining together with staining of intracellular Ig-kappa and Ig-lambda light chains was considered the gold standard for identifying Ab-secreting cells by FCM for many years [1298, 1299]. However, this protocol does not allow sorting of live cells. This can be accomplished by using a combination of a variety of other surface markers. Among the available markers, CD138 is most commonly used to analyze plasma cells, albeit its expression is not restricted to Ab-secreting cells. Therefore, CD138 staining with the detection of Blimp1-reporter expression, e.g., in the Blimp1:GFP mouse [1295], is frequently used as a reference staining to detect murine plasma cells. However, to allow the detection of Ab-secreting cells in mice that do not carry a Blimp1 reporter allele, CD138 staining together with a surface markers, e.g., TACI [1300], Sca-1 [1301], CD98 [1302], Ly6-C [1303], and B220 [1304], have been described in recent years. A caveat is that most of these double-stainings do not differentiate between early dividing plasmablasts and late nondividing plasma cells.
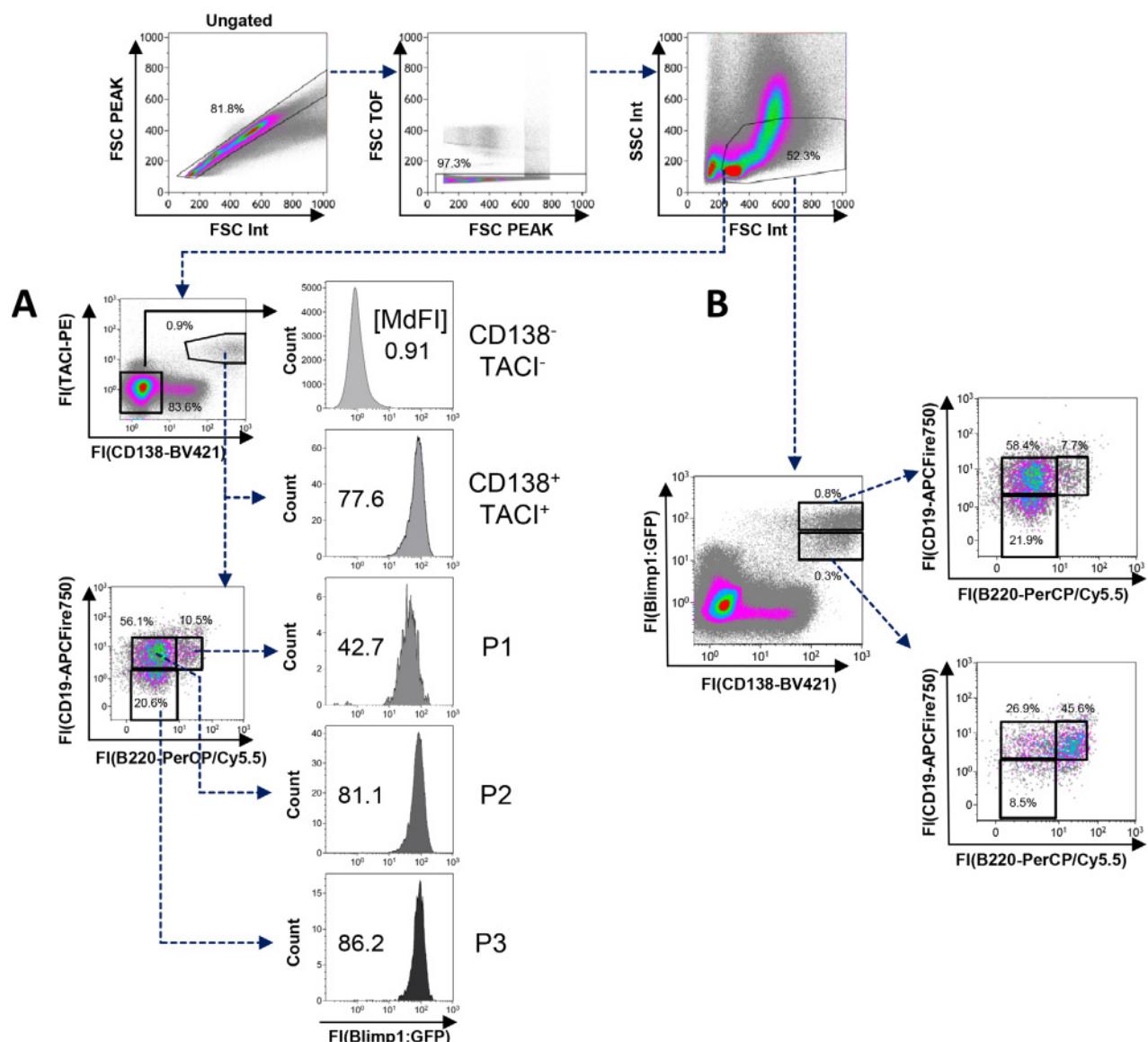
Figure 153. Flow cytometric distinction between plasmablasts, early- and late mature plasma cells. Single cell suspensions from the bone marrow (femur and tibia) of Blimp1:GFP-reporter mice were analyzed for their surface expression of CD138, TACI, CD19, and B220. Viable cells were defined using FSc/SSc characteristics. (A) CD138$^+$/TACI$^+$ cells and subpopulations defined on their B220 and CD19 abundance were analyzed for their Blimp1:GFP-expression (MdFI: Median fluorescence intensity); MdFI values are indicated in the depicted histograms. CD19 and B220 surface expression was used to further subdivide the CD138$^+$TACI$^+$ population (P1: CD19$^+$/B220$^+$; P2: CD19$^+$/B220^{low}; P3: CD19^{low}/B220^{low}). CD138$^-$/$^-$TACI$^-$ cells were used as a negative control for Blimp1:GFP-expression. (B) Blimp1:GFP$^+$/CD138$^+$ cells were divided based on their fluorescence intensities in high-expressing population (CD138^{high}/Blimp1:GFP^{high}) and low- expressing population (CD138$^+$/Blimp1:GFP$^+$). These two subpopulations are further subdivided based on heterogeneous CD19/B220 expression.

To distinguish dividing plasmablasts from nondividing plasma cells, analysis of the proliferation marker Ki-67 can be useful. However, for staining of Ki-67, cells have to be fixed and permeabilized, which is incompatible with cell viability [547, 1214]. Another frequently used method to analyze Ab-secreting cells in mice is the treatment with the nucleotide analog BrdU (bromodeoxyuridine) or EdU (5-Ethynyl-2'-deoxyuridine) via the drinking water [1305, 1306]. In combination with additional surface markers such as CD138, this allows to (i) distinguish between BrdU/EdU-positive proliferating plasmablasts or freshly differentiated plasma cells and previously generated BrdU/EdU-negative mature plasma cells, as well as (ii) the tracking of BrdU/EdU-positive mature resting plasma cells over time.

Although the combined analysis of B220 and CD138 has also been used to identify plasmablasts and plasma cells for many years, the recently published four-color staining including CD138, TACI, B220, and CD19 is superior in separating proliferating plasmablasts from early and late plasma cell subsets because it (1) does not require intracellular Ki67-staining or a plasma cell reporter-mouse line, (2) it clearly excludes CD138-positive B cell

progenitors in the bone marrow (Fig. 153A), and (3) it allows the sorting of viable plasma cell subsets [547].

3.1.3 Step-by-step sample preparation.

3.1.3.1 Bone marrow. Bones (e.g., femurs, tibiae, humeri, vertebrae) were isolated, cleaned from surrounding tissue, and crushed with mortar and pestle in PBS + 2% FCS or RPMI 1640 medium supplemented with 10% FCS (R10). Residual bone fragments were removed by using a 70 μm cell strainer or decapped and flushed with 27G cannula and PBS + 2%FCS or R10. The bone marrow suspension was subsequently centrifuged at $300 \times g$ for 5 min at 4°C. The pellet was resuspended in RBC-lysis buffer and incubated for 5 min at room temperature. Lysis was stopped by addition of PBS + 2% FCS or R10 medium, and the cell suspension was filtered through a 30 μm mesh filter.

3.1.3.2 Spleen. The spleen was isolated, cleaned from surrounding tissue, and gently disrupted in PBS + 2% FCS or R10 through a 70 μm cell strainer using the plunger of a 2 mL syringe.

and blocked for 15 min on ice (or 5 min at room temperature). Cells were washed again in PBS + 2% FCS + 0.05% NaN_3 and centrifuged at $300 \times g$ for 5 min at 4°C. The pellet was then resuspended in 50 μL PBS + 2% FCS + 0.05% NaN_3 containing the respective fluorochrome-coupled Abs and incubated for 20 min on ice in the dark. After staining, the cells were washed twice with PBS + 2% FCS + 0.05% NaN_3 and centrifuged at $300 \times g$ for 5 min at 4°C. The pellet was resuspended in PBS + 2% FCS + 0.05% NaN_3 for flow cytometric analysis.

3.1.4 Materials.

- Dulbecco's PBS
- FCS, heat-inactivated (56°C, 1 h)
- Sodium azide (NaN_3)
- Falcon® 70 μm cell strainer (Becton Dickinson)
- CellTrics® 30 μm filter (Sysmex)
- Red blood cell (RBC) lysis buffer (BioLegend, product number 420301)
- Gallios flow cytometer (Beckman Coulter)

Antigen	Fluorochrome	Supplier	Clone	Identifier
B220 (CD45R)	BV421	BioLegend	Ra3-6b2	103251
B220 (CD45R)	PerCP/Cy5.5	ThermoFisher	Ra3-6b2	103236
CD16/32	unlabeled	eBioscience	93	14-0161-86
CD19	APC/Fire750	BioLegend	6D5	115558
CD98	PE	BioLegend	RL388	128207
CD138 (Sdc1)	PE/Cy7	BioLegend	281-2	142514
CD138 (Sdc1)	BV421	BioLegend	281-2	142507
Ly6-C	PerCP/Cy5.5	ThermoFisher	HK1.4	45-5932-82
Sca-1 (Ly6-A/E)	APC/Cy7	BioLegend	D7	108125
TACI (Tnfrsf13b)	APC	ThermoFisher	eBio8F10-3	17-5942
TACI (Tnfrsf13b)	PE	ThermoFisher	eBio8F10-3	12-5942

The cells were pelleted by centrifugation at $300 \times g$ for 5 min at 4°C, resuspended in RBC-Lysis buffer and incubated for 5 min at room temperature. The lysis was stopped by addition of PBS + 2% FCS or R10 medium, and the cell suspension was filtered through a 3 0μm mesh filter.

3.1.3.3 Mesenteric lymph node. Mesenteric lymph nodes (typically about 4) were isolated and cleaned from surrounding fatty tissue. The lymph nodes were then gently disrupted in PBS + 2% FCS or R10 medium through a 70 μm cell strainer using the plunger of a 2 mL syringe.

3.1.3.4 Staining protocol. Cells from organ suspensions were pelleted by centrifugation at $300 \times g$ for 5 min at 4°C, resuspended in PBS + 2% FCS and adjusted to a density of 2×10^7 cells/mL. A total of 4×10^6 cells from each tissue were washed in PBS + 2% FCS + 0.05% NaN_3 and pelleted at $300 \times g$ for 5 min at 4°C. To avoid unspecific binding, cell pellets were resuspended in 50 μL of unlabeled CD16/32 mAb (1:100 in PBS + 2% FCS + 0.05% NaN_3)

3.1.5 Gating and analysis. In Fig. 152, we compared the presence or absence of one additional commonly used surface markers on CD138+ cells to the CD138+/Blimp1:GFP+ reference population in bone marrow, spleen, and mesenteric lymph node. CD138 together with a B cell marker, e.g., B220 [1304], is the most commonly used staining protocol to distinguish between early dividing plasmablasts (CD138+/B220+) and mature CD138+/B220− plasma cells (Fig. 152B, first row). However, without the addition of a Blimp1:GFP reporter (Fig. 152B, second row), it is difficult to clearly separate bone marrow B220+/CD138+ plasmablasts from B220+ pro-B/pre-B cells with a moderate staining for CD138 [1097, 1307]. The detection of the survival receptor TACI on CD138+ cells prevents these problems because almost all Blimp1:GFP-positive cells are included within a clearly separated TACI+/CD138+ population (Fig. 152B, compare row 1 with row 3 and [547]). CD98 and Sca-1 can also be used in conjunction with CD138 staining to detect Ab-secreting cells in bone marrow and spleen, but these populations are more

diffuse, and especially in the lymph node, are interspersed by cells outside of the CD138$^+$/Blimp1:GFP$^+$ reference gate (Fig. 152B rows 4 and 5). These protocols might be improved by the use of "dump" markers, e.g., F4/80 and CD4/CD8 as suggested by Wilmore et al. [1301]. Despite being described as a plasma cell marker, in our hands Ly6C is not suitable for the detection of all Ab-secreting cells, as it is not ubiquitously expressed in the Blimp1$^+$/CD138$^+$ plasmablast/plasma cell population (compare row 1 with row 6 in Fig. 152B). Therefore, the combination of CD138 and TACI staining is a robust protocol to detect a clearly separated plasmablast/plasma cell population in very high concordance with the CD138$^+$/Blimp1:GFP$^+$ reference across all analyzed lymphatic organs.

The double staining strategies described in Fig. 152 do not discriminate plasmablasts and plasma cells. Therefore, it is necessary to add additional surface markers. For example, the inclusion of the B cell markers CD19 and B220 into the TACI/CD138 staining protocol resulted in three sub-populations. All three subsets (P1–P3) were Blimp1:GFP-positive with a stepwise increase in the abundance of Blimp1:GFP fluorescence from P1 to P3 (Fig. 153A), indicating an increase in maturity from the P1 (dividing plasmablasts) to the P2 (early predominantly nondividing plasma cell) and the P3 (late nondividing plasma cells) subpopulation. While the B220$^+$/CD19$^+$ P1 population contains a high frequency of proliferating (Ki-67$^+$) cells, most of the cells in the subpopulations P2 and P3 are mature Ki-67-negative resting plasma cells [547]. In the spleen of non-immunized mice, the P1- and P2- subpopulations are dominant, while in the bone marrow the CD19$^-$/B220$^-$ P3 population is most prevalent.

In humans, CD19-negative plasma cell subpopulations have been described [1214]. However the biological origin and functional differences between the CD19$^+$ and CD19$^-$ plasma cell subpopulations remain largely unclear [1308].

3.1.6 Pitfalls and top tricks. To guarantee a reliable flow cytometric analysis of plasma cells in mice, some points should be considered. As mentioned before, other cells express markers used for detecting plasmablast/plasma cells such as Blimp1 (T cells) or CD138 (pro-B /pre-B cells). Therefore, strategies to identify plasma cells based on only one marker should be avoided. In addition, plasma cells express markers usually associated with other cell types (e.g., Ly6C [1303], CD11c [1309], CD56 [1310]). Therefore, care has to be taken when using "dump" gate markers. Furthermore, methanol/ethanol-based fixation methods will often result in a loss of the GFP-reporter signal. A prefixation step can prevent the leakage of cytosolic GFP and enable the retention of GFP fluorescence in a co-staining for cytosolic/nuclear antigens [522].

TACI/CD138 staining is also sensitive to different fixation strategies, e.g., formaldehyde fixation. In addition, TACI harbors protease cleavage sites (shedding) [1311] and can, therefore, be degraded when enzymes, e.g., collagenases are used to dissociate tissues. Plasma cells are also quite sensitive to mechanical stress due to their enlarged cytoplasm; therefore, vortexing of the

samples should be avoided and cell pellets should rather be resuspended by finger tipping the reaction tube or careful pipetting.

Higher abundance of Blimp1 and CD138 is associated with a more mature stage of plasma cell differentiation [1295, 1296]. As demonstrated in Fig. 153B, the CD138$^+$/Blimp1:GFP$^+$-population in the bone marrow of mice contains two clearly separated subpopulations, CD138$^+$/Blimp1:GFP$^+$cells and CD138^{high}/Blimp1:GFP^{high} cells. Analysis of CD138 and B220 abundances revealed that the CD138$^+$/Blimp1:GFP$^+$population still expresses surface B220, while the majority of the CD138^{high}/Blimp1:GFP^{high} cells is negative for surface B220. Therefore, cells gated on Blimp1:GFP and CD138 contain early and late plasma cells.

In the bone marrow of unimmunized mice, frequencies of plasma cells range between 0.4 and 0.6% of viable cells, while frequencies in spleen and lymph nodes vary between 0.3 and 0.5% and 0.1 and 0.2%, respectively. Therefore, at least 1×10^6 events (optimally $3–4 \times 10^6$ events) should be acquired during the flow analysis in order to collect a sufficient number of events in the plasma cell gate for valid conclusions. As plasma cells have a larger cell size compared to other lymphocytes, the regularly used "lymphocyte gate" in the FSC/SSC plot has to be extended.

The paradigm of plasma cell differentiation includes the termination of membrane-bound IgH chain and a switch toward the production of only the soluble form of the B cell receptor. However, Pinto and colleagues found that human plasma cells still express functional IgM and IgA receptors on the cell surface, overturning the dogma of complete membrane-BCR loss upon plasma cell differentiation [1312]. We and others confirmed this finding in mice, i.e., almost all IgM- and IgA-producing CD138$^+$/TACI$^+$-plasmablasts and mature plasma cells present these IgH-isotypes as BCRs on their cell surface [547, 1166]. In contrast, IgG-producing mature plasma cells have lost the expression of surface IgG. Therefore, one could determine the frequency of IgH-isotype-expressing plasmablasts/plasma cells by including the detection of surface IgM and IgA in the previously described four-color staining (see Fig. 153).

3.2 Human antibody-secreting cells

3.2.1 Overview. Plasma cells (PC) are terminally differentiated B lymphocytes specialized on large-scale Ab production and secretion. PC are implicated in both protective and pathogenic humoral immunity, and, as long-lived cells, in humoral memory. Thus, they are being studied as therapeutic targets for the treatment of Ab-mediated diseases and as biomarkers for B cell activation in various clinical settings such as infection, inflammation, and vaccination.

In this chapter, we describe human ASC analyses by FCM. The vast majority of PC and their immediate precursors, the plasmablasts (PB), are characterized by high expression of CD27 and CD38, low or no expression of CD20, and variable expression of CD19, HLA-DR, and CD138. PB/PC represent approximately 0.01–1% of leukocytes in different tissues, and phenotypical
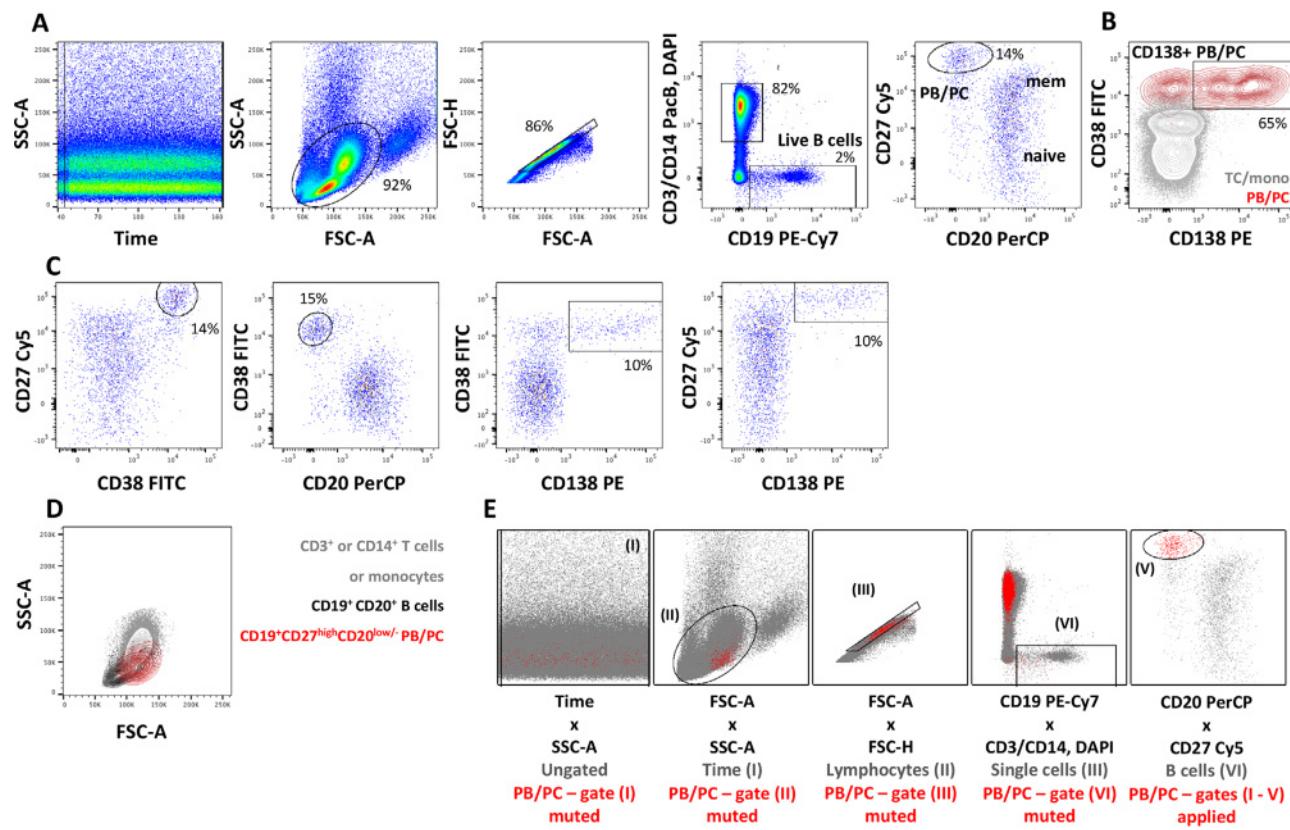
Figure 154. Representative gating strategy and analysis of human peripheral blood PB/PC. Whole blood from a patient with systemic lupus erythematosus (SLE) was diluted with PBS at room temperature, and subjected to density gradient centrifugation over Ficoll (GE Healthcare, Uppsala, Sweden) to isolate PBMC. Active SLE patients exhibit significant B lymphopenia, with increased frequencies and absolute numbers of PB/PC in peripheral blood [1246, 1315]. PBMC were washed with PBS/0.2% BSA, and stained at 4°C for 15 min with a cocktail of the following mAbs: CD19 (clone SJ25C1, BD), CD27 (clone 2E4; Sanquine), CD20 (L27, BD), CD14 (M5E2, BD), CD3 (UCHT1, BD), CD38 (HIT2, BD), CD138 (B-B4, Miltenyi Biotec). Cells were washed with PBS/0.2% BSA. DAPI was added prior to acquisition of the sample on a BD FacsCANTO II instrument for dead cell labeling. In total, 300 000 events were collected. (A) Gating strategy. Data were analyzed for changes of scatter or fluorescence parameters over the time of data acquisition, and optionally gated to remove parts of the acquisition that show irregular or discontinuous cytometric patterns. Then, a large light scatter parameter gate was used to identify lymphocytes and monocytes. FSC^{high} cells represent doublets and were excluded. SSC^{high} cells correspond to remaining granulocytes, likely low density granulocytes described before in SLE [1332] that were co-enriched along with PBMC. Next, cell aggregates were removed by gating on cells showing closely correlating area and height values of the FSC signal. Most cell doublets are characterized by a relatively increased FSC-area vs. FSC-height ratio. Live B cells were detected by staining for CD19, and exclusion of T cells, monocytes and dead cells according to CD3, CD14, and DAPI staining. Note that the B cell gate captures CD19^{dim} cells, which can be strongly enriched for PB/PC. CD19 expression itself is subject to regulation in, e.g., autoimmune conditions [1328, 1333], so that boundaries of the CD19 B cell gate should be carefully validated. CD19$^+$CD3$^-$CD14$^-$DAPI$^-$ B cells were then analyzed for CD20 and CD27 expression, revealing CD20$^+$ subsets of naive and memory B cells besides PB/PC with a CD27^{high}CD20$^{low/-}$ phenotype. In this (SLE) sample, PB/PC are detectable at increased frequencies; normal donors show commonly less than 2% PB/PC among CD19$^+$ B cells. (B) PB/PC were then analyzed for expression of CD38 and CD138. Virtually all CD27^{high}CD20$^{low/-}$ gated PB/PC (red) expressed high levels of CD38, and two thirds expressed CD138. CD3$^+$ T cells and CD14$^+$ monocytes not expressing CD138 and containing very few CD38^{high} cells are shown for comparison (grey). (C) As an alternative to the PB/PC gating shown in (A-B), total PB/PC, or CD138$^+$ PB/PC can be gated in various combinations of the markers CD20, CD38, CD27 and CD138, with consistent results. (D) PB/PC show a unique FSC and SSC profile distinct from that of total lymphocytes, B lymphocytes, and monocytes. (E) Backgating confirms the validity of the gating strategy. In particular, it shows that the entire PB/PC subsets was included during light scatter gating, some PB/PC events were excluded as doublets, and that significant amounts of T cells and/or monocytes share the CD27^{high}CD20$^{-/low}$ phenotype of PB/PC and may contaminate this population unless careful CD19 gating and DUMP channel exclusion is employed. An example for the detection of blood PB/PC by icIg staining is published in ref. [1322].

characteristics of PB/PC are associated with tissue origin, maturity level, and clinical context. Their low frequency, variable phenotype, and their uncommon light scatter properties should be considered when analyzing PB and PC by FCM.

3.2.2 Introduction. Plasma cells are terminally differentiated B cells capable of continuous production of Ab [1313]. Next to their immediate precursors, the PB, they are the only cells of the body that secrete Ab and contribute the vast majority of Ig detectable in serum and mucosal secretions. Thus, PC (also termed plasmacytes, plasmocytes, or named according to detection assays other than FCM: spot-forming cells (SFC), Ab-secreting cells (ASC), Ab-forming cells (AFC), plaque-forming cells (PFC), or Ig-secreting cells (ISC)) are the foundation and the cellular correlates of humoral immunity by secreting specific, commonly adaptively shaped Abs that neutralize or opsonize pathogens.
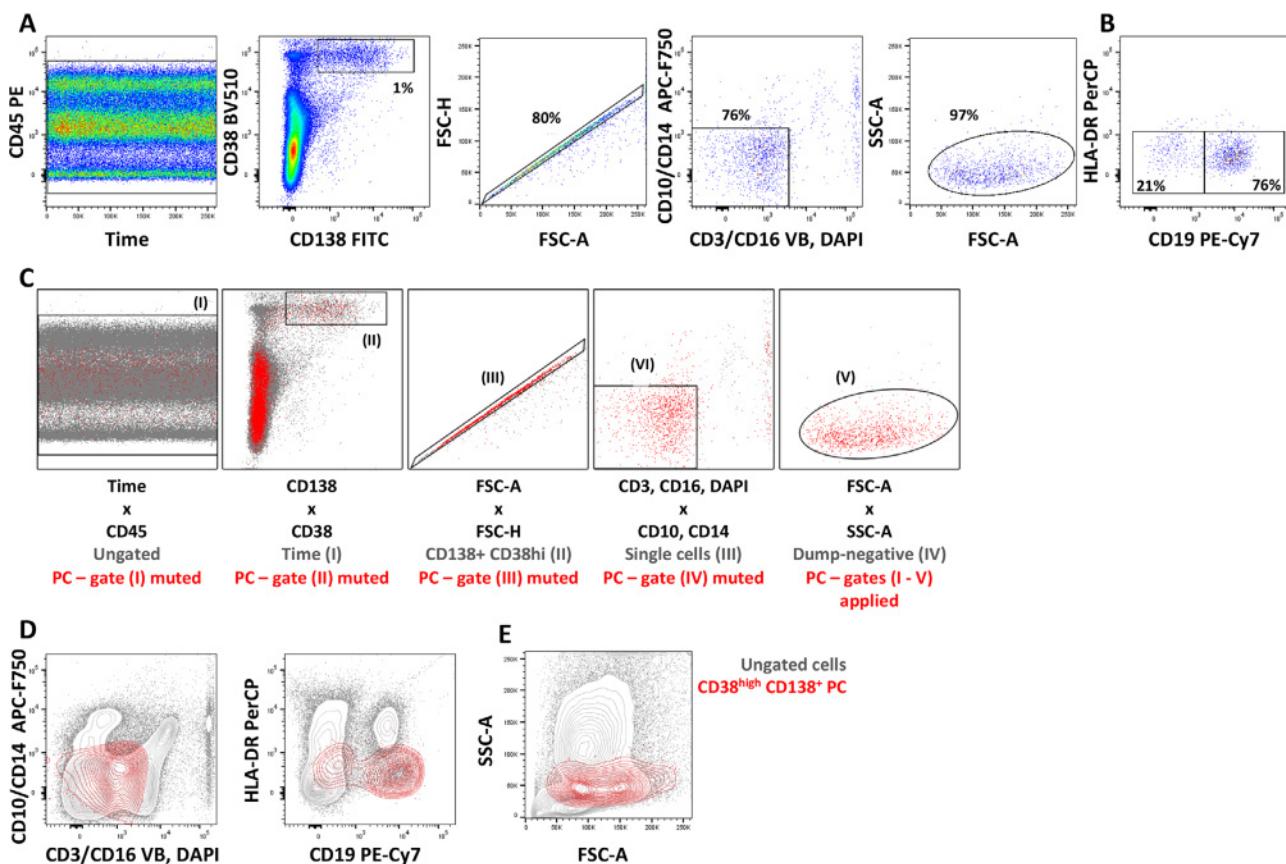
Figure 155. Representative gating strategy and analysis of human bone marrow PC. Bone marrow (BM) cells were flushed from a femoral head piece of a healthy donor using PBS/0.2% BSA/5 mM EDTA buffer and mononuclear cells were isolated via density gradient centrifugation over Ficoll. BM cells were washed with PBS/0.2% BSA/5 mM EDTA and stained at 4°C for 15 min with a cocktail of the following Abs:CD3-VioBlue (BW264/56, Miltenyi), CD16-VioBlue (REA423, Miltenyi), CD38-BV 510 (HIT2, BioLegend), CD138-FITC (44F9, Miltenyi), CD45-PE (HI30, BioLegend), HLA-DR-PerCP (L243, BioLegend), CD19-PE-Cy7 (HIB19, BioLegend), CD10-APC-Fire 750 (HI10a, BioLegend), CD14-APC-Fire 750 (M5E2, BioLegend). Cells were then washed with PBS/0.2% BSA/5 mM EDTA and stained with DAPI for later dead cells exclusion prior to acquisition of the sample on a MACS® Quant Analyzer. (A) Analytical gating strategy. Time/CD45 visualization confirms the stability of the cytometric measurement over time. Time frames showing discontinuous data should be excluded. As PC exhibit particular light scatter and background fluorescence properties, the CD138$^+$CD38^{high} PC population was gated first, followed by cell aggregate exclusion and gating on CD3$^-$, CD16$^-$, CD10$^-$, CD14$^-$, and DAPI$^-$ cells, for exclusion of dead cells and cell types potentially contaminating the gated PC population. Then, the FSC-A/SSC-A plot reveals that PC show a broader light scatter value distribution than typical lymphocytes, which is in agreement with their increased size and ellipsoid shape. Should the FSC-A/SSC-A plot reveal remaining FSC^{low} and/or SSC^{low} cell debris or electronic artifacts, these should be excluded by gating at this step. (B) Human BM PC consistently display distinct populations with either high or low to no expression of CD19 [1214, 1324]. The absence of HLA-DR expression confirms at large the absence of PB [1245, 1322], and remaining HLA-DR$^+$ PB are excluded. (C) Backgating analyses of the procedure shown in (A). (D) Comparison of antibody staining and light scatter properties of total CD138$^+$CD38$^+$ BM PC vs total, ungated BM mononuclear cells. PC exhibit increased background fluorescence signals compared to other cells (possibly integrating cell size effects, autofluorescence, and nonspecific binding of labelled antibodies) stressing that subset gating should be adjusted at the level of PC rather than at global levels. Consistent with their increased size, nonspherical shape, and high organelle content, BM PC show a FSC/SSC pattern distinct from that of other BM cells.

So-called long-lived or memory PC can gain longevity and directly contribute to immune memory by long-term secretion of specific Ab [1305, 1314], a phenomenon termed humoral (or serological) memory.

Plasma cells are of interest to medical and biological research in various regards. Vaccines are tailored to induce long-lasting and specific Ab titres that result from the generation and persistence of vaccine-specific PC. On the other hand, PC are also the source of pathogenic Abs in autoimmune diseases and humoral transplant rejection, and constitute a potential therapeutic target in these conditions. Furthermore, the abundance of PB and PC in the peripheral blood serves as a biomarker for acute B cell responses in

systemic autoimmune disease such as SLE [1315, 1316]. Upon vaccination and infection, especially antigen-specific PB are expanded in the blood [1214, 1246, 1317–1319]. The diagnosis, treatment, monitoring, and research in lymphoid tumors recapitulating PC features and biology, such as multiple myeloma, monoclonal gammopathy of undetermined significance (MGUS), reactive plasmacytoma, or Morbus Waldenstrom, are commonly associated with PC analyses by FCM.

Technically, antigen-specific PC can serve as a template for cloning Abs for new biomedical assays, diagnostics or therapeutic purposes. Furthermore, PC are investigated in a number of interrelated biological contexts such as apoptosis and survival

mechanism(s), large-scale protein production, and balancing the consequential cellular stress, transcriptional reprogramming, cell adhesion, and homing.

3.2.3 Activated B cells become plasma cells.

Upon activation of B cells by B cell antigen receptor (BCR) stimulation by antigen, by cytokines, TLR ligands, cognate T cells, or combinations thereof, they start proliferating and differentiating into PB, or memory B cells. In vivo, this activation can target naïve, or antigen-experienced memory B cells, and leads to B cell differentiation within germinal centers (including somatic hypermutation and class-switching of Ig gene rearrangements, or in follicular or extrafollicular processes. In line with the observation that the differentiation of PB is fairly easy to mimic in vitro by different stimuli [1320, 1321], PB differentiation appears as the default differentiation pathway upon B cell activation.

Once formed, PB may either reside at the site of their generation (such as spleen or lymph nodes), or emigrate and transit via the blood to PC deposits in the gut lamina propria (LP) or the bone marrow (BM), or die. Immunization studies have been particularly useful for determining PB dynamics and biology in man [1214, 1245, 1246, 1313, 1319, 1322]. While PB and PC types are common in lymphoid tissues such as spleen and BM [1214, 1313], and are present at very low frequencies in peripheral blood at all times [1322], additional PB specific for the vaccination antigen appear in the blood as a sharp peak approximately 1 week after intramuscular or subcutaneous immunizations [1241, 1245]. Their presence in blood lasted longer when the immunization was applied via mucosal routes [1323]. At the PB stage circulating in peripheral blood, the cells have already started to secrete antibody that is detectable by Elispot assays [1245], express the proliferation marker Ki-67 [1214, 1322], and migrate along gradients of the chemokines CXCL12 and/or CCL28 (using CXCR4 and CCR10, respectively), navigating them into their BM or mucosal niches.

Besides primary and secondary lymphoid tissues including mucosa-associated lymphoid tissues, PB/PC can also be found at different sites under pathological conditions, such as inflammation (brain, cerebrospinal fluid, kidney, joints, and synovial fluid [1214], or in the form of multiple myeloma metastases.

3.2.4 Detection of PB and PC according to unique cell-surface receptor expression profiles.

In the blood, PB and PC express the unique phenotype $CD19^+CD27^{high}CD38^{high}$ and show low or no expression of CD20 [1213, 1322, 1324]. CD138, often referred to as a PC marker, is expressed to only variable extents in the blood [1324, 1325] (Figure 154). Besides $CD38^{high}$ PB/PC, a minor $CD38^{low}$ subset has been defined in tonsils [1326], and CD27-negative differentiation stages have been described in in vitro studies [1327]. Blood PB/PC can show downregulated, yet still present levels of the B cell marker CD19 [1328]. During steady-state, PB/PC make up about 1% of peripheral blood B cells. One week after immunization, antigen-specific PB circulating in blood

express high levels of HLA-DR, distinguishing them from HLA-DR^{low} cells sharing the typical $CD19^+CD27^{high}$ phenotype, but being non-migratory and non-proliferating, thus resembling BM PC [1313, 1322]. Taken together, blood PB and PC can be well distinguished from other B cells and other leukocytes according to their unique cell-surface marker expression profile. However, as all mentioned markers alone are also expressed by other cell types or B cell differentiation stages, multiple markers need to be co-stained to obtain a PB/PC population (i) that covers most of the PB/PC present in the sample under normal conditions and (ii) is sufficiently pure to permit their reliable quantification and phenotypical characterization. PC in deposit tissue such as the bone marrow (BM) express intermediate to high levels of CD138, usually very high levels of CD38 (a molecule that candidates as a therapy target for depletion of malignant PC in patients with MM [1329], lack CD20 expression, and show low or no expression of HLA-DR. Notably, CD19 is differentially expressed among mature BM and LP PC, and $CD19^-$ PC show consistent features of PC that have reached an exceptionally mature state [1214, 1330, 1331]. A representative analysis of human BM PC is shown in Fig. 155.

3.2.5 Detection of PB/PC according to high expression of intracellular Ig and by cellular affinity matrix assay.

Apart from cell-surface staining, PB and PC can be detected by staining intracellular Ig (icIG) [1322]. Consistent with large-scale Ab production by PB and PC, they accumulate large amounts of it in their cytoplasm, and intracellular flow cytometric staining without prior in vitro stimulation and/or secretion inhibition yields high signal intensities that are suitable to distinguish $icIg^{high}$ PB/PC from Ig^+ B cells, which do not express extraordinarily high levels of icIg and to which anti-Ig Abs bind mainly via their cell-surface Ig (BCR). Fixation with 1.5% formaldehyde solution and mild permeabilization with 0.1–0.5% saponin solution is sufficient to permit detection of icIg in PB/PC.

The above cell-surface markers, IgD, and intracellular (ic)IgM, icIgA, and icIgG, were combined in an optimized multicolor panel (OMIP) for the detection of PB/PC [1334].

Furthermore, affinity matrix technology has been developed to cytometrically capture PB and PC according to their ability to secrete Ab, thus providing access to live and functional PB/PC [621, 1326]. Abs capturing the Ig of interest are immobilized on the cell surface, and the cell suspension is short-term cultured to permit antibody secretion by PB/PC. The secreted antibody is bound by the cell-bound capture antibody and detected by a second, fluorochrome-labeled anti-Ig antibody, which specifically stains the cells that have secreted Ig during the culture phase.

Activated B cells undergoing PC differentiation gradually downregulate the expression of the membrane B cell receptor, and start to secrete the soluble form of Ab. At the PB stage in the blood, cell-surface IgM^+, and IgA^+ PB are detectable, and cell-surface IgG is also expressed at least after recent vaccination, as evidenced by specific cell-surface binding of fluorescently labeled antigen) [1241] Notably, cell-surface BCR is not detectable

anymore in mature IgG$^+$ PC, while IgM$^+$, and IgA$^+$ PC in deposit tissues can maintain expression of cell-surface Ig [1312, 1335].

3.2.6 Receptors expressed by plasma cells. Besides Ig of different classes and subclasses, PB and PC, or their subsets express receptors and transcription factors that are implicated in their survival, maturity, and homing, such as, for example, the cytokine receptors IL-6R (CD126), BCMA, and TACI, selectins, integrins, and chemokine receptors such as CD62L, α4β1, and α4β7 integrins, CXCR4, CXCR3, CCR9, and CCR10, transcription factors BLIMP-1, IRF4, and the anti-apoptotic protein Bcl-2 [1214, 1245, 1313, 1324, 1330, 1336, 1337]. Notably, highly mature PC lose expression of PAX5, leading to the expression of a number of receptors that are typically absent from B lineage cells such as CD56, CD28, and CCR2 [1214, 1338].

3.2.7 Light scatter properties of plasma cells. PB and PC exhibit a unique morphology reflecting their role as protein factories. They show an enlarged cytoplasm with expanded Golgi apparatus and endoplasmatic reticulum content, and an eccentrically located nucleus. Coherently, PB/PC show increased FSC/SSC light scatter signals, and a broader distribution, compared to small lymphocytes (Figs. 154 and 155). This entails an important caveat when analyzing PB/PC in routine immune profiling studies in which gating strategies start off from a small lymphocyte gate. Any gating performed "upstream" of the PB/PC gate should be carefully checked for unwanted selection against PB/PC fractions. The increased cell size may also lead to increased fluorescent background signal of PB/PC compared to smaller lymphocytes (Figs. 154 and 155), thus, control staining (such as isotope controls if helpful, or FMO controls) should always be evaluated on the same PB/PC fraction that is subject to analysis.

3.2.8 Sample preparation. Flow cytometric assessment of PB/PC is commonly performed from single-cell suspensions obtained by either red blood cell lysis of whole blood, density gradient centrifugation to obtain mononuclear cells (such as PBMC), or tissue cell suspensions obtained by protocols tailored for individual tissue types. Since collagenase treatment has been shown to liberate additional fractions of PC from tonsillar tissue compared to mechanical processing alone [1339], digestion protocols can be considered to retrieve PC or certain fractions of PC. It should be noted that different enzymes used for this purpose may differently impact on the detectability of different cell-surface receptors, including the above mentioned used to detect human PC. PB/PC tend to die rapidly during longer preparation protocols and when cultured in the absence of survival promoting cytokines. Thus, keeping cells cool and working quickly is key. Protocols should be kept short to avoid excessive death of PB/PC after preparation, and dead cell detection and exclusion should be performed.

When analyzing rare fractions of PB/PC such as antigen-specific cells, PB/PC may be pre-enriched for FCM analyses by magnetic cell sorting, e.g., by depleting large, unwanted sample

fractions such as granulocytes, T cells, and monocytes, etc., or by direct enrichment of CD138$^+$ cells. One should carefully choose depletion markers (and DUMP channel markers) as mature PC subsets (and especially malignant PC) can express markers like CD28, CCR2, and CD56 commonly associated with T cells, monocytes, or NK cells, respectively.

Live-cell cryopreservation using standard procedures and media such as FCS/DMSO impacts on detection of PB/PC. Usually, after freezing and thawing, frequencies of PB/PC are much lower compared to fresh cell preparations, and the detection of some receptors including CD138 have been described to be impaired after cryopreservation [1340].

Since PB/PC are commonly found at low to very low frequency in cell suspensions, the separation of PB/PC from cells that share elements of the PC phenotype is key, and the use of carefully designed DUMP channels is advised. For example, PBMC contain high frequencies of CD27^{high} expressing T cells that may contaminate the CD19^{dim}/CD27^{high} PB/PC gate unless T cells are excluded from the analysis. Since PB/PC are infrequent in many cell suspensions from primary tissue, care must be taken to acquire suitable total cell numbers, which ensure that sufficient PB/PC are recorded for the desired statistical analysis.

Generally, it must be stressed that, to deliver accurate results, PB/PC analyses require careful experimental and cytometric setup and validation that can be very specific to a certain project (considering what readout parameters are to be measured), tissue specific phenotypes and sample logistics.

4 Innate lymphoid cells

4.1 *Overview*

This section will give an overview on the flow cytometric strategy to gate on different subsets of tissue-derived innate lymphoid cells (ILCs) in humans and mice. While only murine small intestine and human tonsils are representatively shown, the use of master transcription factors in combination with established surface markers can be generally used across different tissues to identify ILC subsets.

4.2 *Introduction*

During the past years, an emerging family of CD45$^+$ innate lymphoid cells (ILCs) has been described in both mouse and man. CD45$^+$ ILCs lack rearranged antigen receptors as well as lineage (Lin) markers typically expressed on T cells, B cells, or dendritic cells (DCs) [1341]. ILCs can be classified into distinct groups according to the expression of surface markers, transcription factors and effector cytokines (reviewed in ref. [1342]). ILC1 express T-box transcription factor T-bet (T-bet) and produce IFN-γ in response to IL-12 and IL-18 or activating receptor engagement, thus contributing to the response against viruses and intracellular pathogens [1343–1346]. ILC2 express GATA binding protein-3 (GATA3), produce IL-13 and IL-5 in response
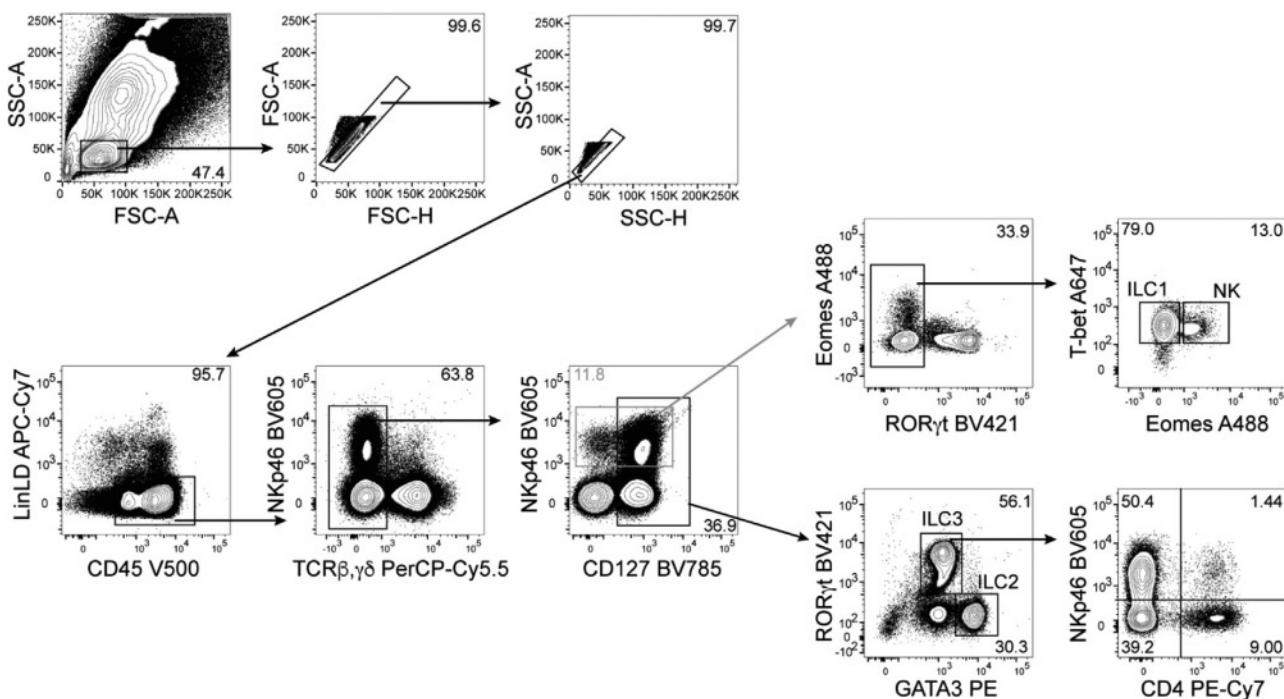
Figure 156. Identification of murine SI LP ILCs. Representative gating strategy of ILCs derived from the small intestinal (SI) lamina propria LP of 6-week-old C57BL/6 mice. Mononuclear cells (MCs) were prepared as previously described [1350]. Cells were gated as viable (LD$^-$), B220$^-$ CD11c$^-$ Gr-1$^-$ F4/80$^-$ FcεR1α^- (Lin$^-$) CD45$^+$ TCRβ^- TCR$\gamma\delta^-$ and either as NKp46$^+$ (grey gate) T-bet$^+$ Eomes$^-$ ILC1, Eomes$^+$ T-bet$^+$ NK cells or as CD127$^+$ (black gate) GATA3$^+$ RORγt$^-$ ILC2 and RORγt$^+$ GATA3^{lo} ILC3 which can be further separated according to NKp46 and CD4 expression.
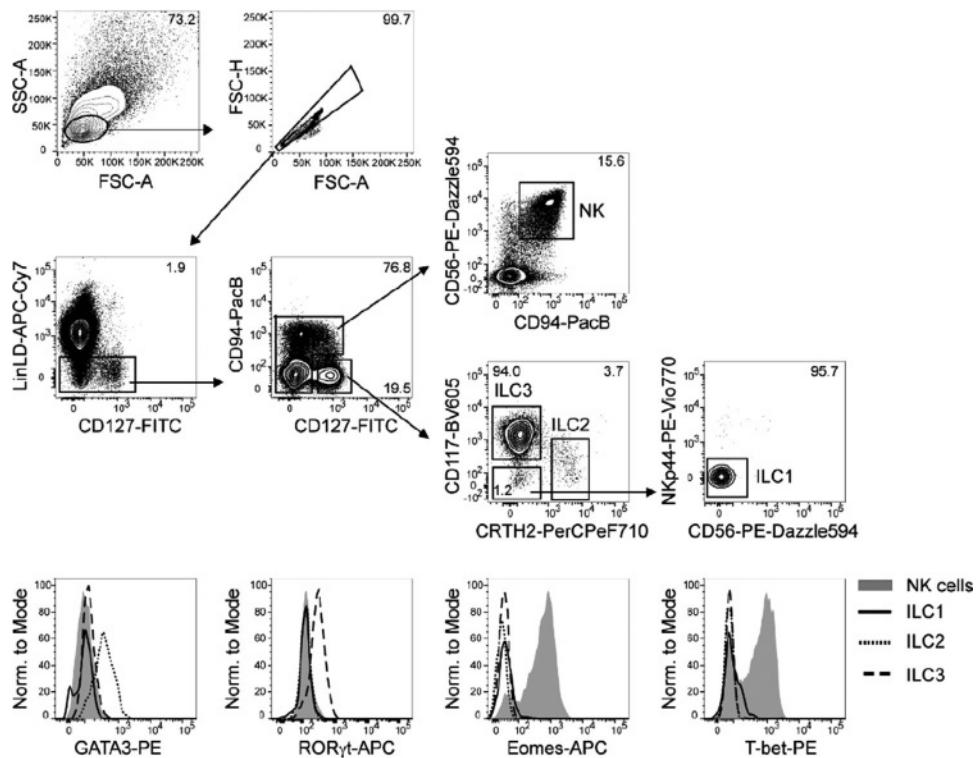
Figure 157. Identification of human tonsil ILCs. Representative gating strategy (upper panel) and expression of transcription factors (lower panel) of human tonsil ILCs. After magnetic depletion of CD3$^+$ cells, cells were gated as viable (LD$^-$), CD3$^-$ CD14$^-$ CD19$^-$ FcεR1α^- CD123$^-$ CD11c$^-$ BDCA3$^-$ (Lin$^-$) and either CD94$^+$ CD127$^{-/lo}$ CD56$^+$ NK cells; CD94$^-$ CD127^{hi} CD117$^+$ CRTH2$^-$ ILC3; CD94$^-$ CD127^{hi} CD117$^{+/lo}$ CRTH2$^+$ ILC2; or CD94$^-$ CD127^{hi} CD117$^-$ CRTH2$^-$ NKp44$^-$ CD56$^-$ ILC1.

to IL-25, IL-33, and Thymic stromal lymphopoietin (TSLP) and contribute to the defense against helminthic infections as well as to the pathogenesis of allergic inflammation [1347]. ILC3 express retinoic acid receptor (RAR)-related orphan receptor RORγt, and produce IL-17 and/or IL-22 in response to IL-1β and IL-23 or activating receptor engagement. ILC3 include both fetal-derived lymphoid tissue-inducer (LTi) cells (considered as a distinct subset [1342]) and post-natal ILC3; LTi are required for the embryonic development of lymph nodes and Peyer's patches, while ILC3 contribute after birth to defense against extracellular pathogens, containment of commensals, epithelial tissue home-ostasis, and regulation of inflammatory disorders, such as IBD and psoriasis [1348]. As such, ILC1, ILC2, and ILC3 show similarities with CD4$^+$ T helper (Th) subsets Th1, Th2, and Th17 and mirror the functional analogies between natural killer (NK) cells and adaptive CD8$^+$ cytotoxic T lymphocytes (CTL) [1341, 1349]. Accordingly, the International Union of Immunological Societies (IUIS) now recognizes five related innate lymphoid subsets: NK cells, ILC1, ILC2, ILC3, and LTi cells [1342].

4.3 Step-by-step sample preparation

For isolation of murine SI LP MCs a previously described protocol was used [1350]: residual fat tissue, Peyer's Patches and feces were removed, and the intestine was cut open longitudinal and washed with PBS. After clearing, tissue was cut into pieces of 1 cm length and digested with a lamina propria dissociation kit (Miltenyi), according to the manufacturer's instructions. Lymphocytes were further enriched on a 40%/80% Percoll gradient.

Written informed consent was obtained from all patients prior to sample acquisition and experiments have been approved by the Ethics Committee of the Charité Medical University, Berlin (EA2-078-16, EA1/149/1). Mononuclear cells (MCs) from human tonsils were isolated from patients undergoing tonsillectomy as previously described [1351]. After mashing and density gradient centrifugation using Ficoll-Paque PLUS, ILCs were enriched by using magnetic cell depletion of CD3$^+$ T cells with CD3 mAb microbeads and LD columns (Miltenyi) according to the manufacturer's instructions.

4.4 Materials

Flow cytometry:

Phenotypic analysis of murine lymphocytes was performed using the following Abs reactive to murine surface or intracellular antigens: eFluor780 Fixable Viability Dye, APC-eFluor780 anti-FcεRIα (MAR-1), PerCP-Cy5.5 anti-TCRβ (H57-597), PerCP-eFluor710 anti-TCRγδ (GL-3), eFluor660 anti-T-bet (4B10), Alexa488 anti-Eomes (Dan11mag) (eBioscience); APC-Vio770 anti-B220 (RA3-6B2), PE anti-GATA3 (REA174) (Miltenyi); APC-Cy7 CD11b mAb (M1/70), CD11c mAb (N418), anti-Gr-1 (RB6-8C5), anti-F4/80 (BM8), BV785 CD127 mAb (A7R34), BV605 anti-KLRG1 (2F1/KLRG1), BV711 CD4 mAb (RM4-5), PE-Cy7

anti-NKp46 (29A1.4) (BioLegend); V500 CD45 mAb (30F11), and BV421 anti-RORγt (Q31-378) (BD).

Staining for transcription factors was performed using the Foxp3 Transcription factor staining buffer set (eBioscience) according to manufacturer's instructions and cells were immediately analyzed. Flow cytometric analysis was performed by using BD LSRII or Fortessa employing FACSDiva Software (BD Biosciences), and data were analyzed by using FlowJo software (Tree Star).

Phenotypic analysis of human lymphocytes was performed using the following Abs reactive to human surface or intracellular antigens: eFluor780 Fixable Viability Dye, APC-eFluor780 CD14 mAb (61D3), CD19 mAb (HIB19), CD3 mAb (SK7), CD123 mAb (6H6), eFluor660 anti-Eomes (WD1928), PE anti-T-bet (eBio4B10), or anti-GATA-3 (TWAJ), PE-Cy7 anti-T-bet (eBio4B10), APC anti-RORγt (AFKJS-9) (eBioscience); APC-Vio770 CD141 mAb (AD5-14H12), anti-FcεRIα (CRA1), and CD11c mAb (MJ4-27G12), Fitc CD127 mAb (MB15-18C9), PE-Dazzle594 CD56 mAb (HCD56), PE-Vio770 NKp44 (2.29) (Miltenyi Biotec); BV605 CD117 mAb (104D2), PerCP-Cy 5.5 anti-CRTH2 (BM16), Pacific Blue CD94 mAb (XA185) (conjugated in house).

4.5 Data analysis

How can we identify these different NK cell and ILC subsets in different tissues from different species? The analysis of NK cells is described in the NK chapter by Moretta et al., where readers can find more details (See also Chapter VI Section 5 Natural Killer cells). ILCs are present in diverse organs as tissue-resident cells but are also detected in the circulation [1346, 1352]. In mouse small intestinal (SI) lamina propria (LP), all ILCs, namely NK cells, ILC1, ILC2, and ILC3 could be described [1345, 1353]. In Fig. 156 a gating strategy for murine ILCs derived from SI LP is shown; however, it should be stressed that ILC populations are not equally distributed in all organs and display some tissue-specific phenotypic differences. Combination of intranuclear staining of master transcription factors, namely T-bet (expressed on ILC1, NK cells and a subset of murine ILC3), Eomes (NK cells), RORγt (ILC3), and GATA3 (ILC2) together with NKp46 and CD127 (IL-7Rα) (Figure 156) or CD90 (not shown) enables identification of ILC subsets in all organs analyzed. Among SI LP CD45$^+$ Lin$^-$ cells, NKp46 (or NK1.1) can be expressed not only on NK cells but also on ILC1 and a subset of ILC3. Thus, staining of transcription factors is helpful to dissect their identity (see also Chapter V Section 13 Transcription factors). It has been proposed that SI LP NK cells can be defined as NKp46$^+$ RORγt$^-$ T-bet$^+$ Eomes$^+$ cells, while ILC1 are NKp46$^+$RORγt$^-$ T-bet$^+$ Eomes$^-$ cells [1345] (Figure 156). However, a population of cytotoxic NKp46$^+$ RORγt$^-$ T-bet$^+$ Eomes$^+$ intraepithelial ILC1 has been also described [1354]. Moreover, the analysis of NK/ILC1 in different mouse compartments revealed a high degree of phenotypic and functional complexity [1346, 1355], suggesting that distinction between NK and ILC1 cells might be more challenging.

ILC2 and ILC3 are enriched among SI LP CD45$^+$ Lin$^-$ CD127$^+$ lymphocytes and can be identified after intranuclear staining of GATA3 and RORγt as GATA3^{hi} RORγt$^-$ ILC2 and of GATA3^{lo} RORγt$^+$ ILC3 (Figure 156) [1353, 1356]. Surface markers such as ST2 (IL-33R), CD25, ICOS, or KLRG1 have also been commonly used to identify ILC2 [1353, 1357, 1358]. As previously mentioned, expression of these markers slightly varies in different compartments.

SI LP RORγt$^+$ ILC3 can be dissected into three major subsets according to NKp46 and CD4 expression (Figure 156), namely CD4$^+$ ILC3, which functionally and phenotypically resemble fetal LTi and preferentially produce IL-17 and IL-22; NKp46$^+$ ILC3, which expand postnatally, co-express RORγt and T-bet and pro-

duce IL-22 and IFN-γ; and CD4$^-$ NKp46$^-$ ILC3, which actually represent a heterogeneous population of CCR6$^+$ cells (related to LTi) and CCR6$^-$ ILC3, co-expressing RORγt and T-bet, similar to NKp46$^+$ ILC3 [1359–1361]. As it has been shown that ILC3 can be plastic in vivo, and downregulate RORγt expression while acquiring NK/ILC1-cell features such as T-bet expression and IFN-γ production, the use of RORγt fate mapping (RORγt^{fm}) can be helpful to distinguish ex-ILC3 (RORγt^{fm+} RORγt$^-$ T-bet$^+$) from ILC1 [1361, 1362]. Although this distinction is conceptually important, ex-ILC3 behave functionally similar to NK/ILC1 cells.

In humans, ILCs have been documented in several tissues and in the circulation, although a larger characterization has been performed in tonsils, where all ILC subsets have been described

Table 54. Selection of important markers for flow cytometry analysis of mouse and human ILC

	Mouse					Human				
	NK cells	CD127$^+$ ILC1	ILC2	NCR$^-$ ILC3	NCR$^+$ ILC3	NK cells	CD127$^+$ ILC1	ILC2	NCR$^-$ ILC3	NCR$^+$ ILC3
Marker										
CD127	−	+	+	+	+	lo/-	+	+	+	+
CD117	lo/-	−	+	−	lo	lo/-	−	+/−	+	+
CD25	−	lo	+	+	ND	+/−	lo	+	+/−	lo
IL-23R	−	lo/-	ND	+	+	lo	+/−	lo	+	+
IL-17RB	−	−	+	−	−	−	lo/-	+	ND	−
ST2	−	−	+	−	−	−	ND	+	ND	−
IL-1R1	−	lo	ND	+	+	+/−	lo/-	lo	+	+
CCR6	−	−	−	+/−	−	−	+	+	+	+
RANKL	lo/-	ND	ND	+	+	−	ND	ND	+	+
CRTH2	ND	ND	ND	ND	ND	−	−	+	−	−
ICOS	−	ND	+	ND	+	−	−	+	ND	+
NK1.1/CD161	+	+	−	−	lo/-	+/lo	+	+	+	+
CD56	NA	NA	NA	NA	NA	+	−	−	+/−	+/−
CD94	+/−	ND	+/−	−	+/−	+/−	−	−	−	−
CD16	+/−	ND	−	−	−	+/−	−	−	−	−
NKp30	NA	NA	NA	NA	NA	+	ND	+/lo	+/−	+
NKp44	NA	NA	NA	NA	NA	+^{a}	−	−	−	+
NKp46	+	+	−	−	+	+	−	−	+/−	+
Ly49/KIR	+/−	lo	−	−	−	+/−	−	−	−	−
CD57	NA	NA	NA	NA	NA	+/−	ND	ND	ND	ND
CD27	+/−	+	−	−	−	+/−	+	−	−	−
CD11b	+/−	−	−	ND	ND	+/−	ND	ND	ND	ND
Perforin	+	lo	−	−	−	+	−	−	−	−
Transcription factors										
T-bet	+	+	−	+/−	+	+	+	−	−	−
Eomes	+	−	−	−	+	+	−	−	−	−
RORγt	−	−	−	+	+	−	−	−	+	+
GATA3	−	lo	+	lo	lo	lo/-	lo/-	+	lo/-	lo/-
Cytokines										
IFNγ	+	+	-/lo	-/lo	-/lo	+	+	−	−	−
IL-22	−	−	+	+	+	−	−	lo	lo/-	+
IL-17	−	−	−	+/−	−	−	−	−	+	−
IL-13	−	−	+	−	−	lo	−	+	−	lo
IL-5	−	−	+	−	−	−	−	+	−	−

+ Indicates high expression, - indicates no expression, +/− indicates bimodal expression, lo indicates low expression, a indicates expression on activated cells, ND indicates not determined, and NA indicates not applicable according to published reports [1344–1347, 1350, 1353, 1354, 1356–1365, 1367, 1374–1384]

[1354, 1363–1365]. In tonsils, magnetic depletion of CD3$^+$ T cells and of CD19$^+$ B cells is recommended for better detection of ILCs, due to their low frequency. After pre-enrichment and further gating on Lineage negative cells, staining of CD94 and CD127 enables the identification of NK cells, as CD94$^{+/lo}$ CD127$^{neg/lo}$ CD56$^+$ cells, which express high levels of T-bet and Eomes, and of other ILCs enriched among Lin$^-$ CD127^{hi} CD94$^-$ cells (Fig. 157).

It has been proposed that staining of CD117 (the receptor for stem cell factor, c-kit) and CRTH2 (prostaglandin D2 receptor chemoattractant receptor-homologous molecule expressed on T helper type 2 cells) facilitates identification of ILC3 and ILC2 in tonsils [1366]. ILC3 are enriched among CD117$^+$ CRTH2$^-$ cells and express NKp44 and RORγt, while lacking T-bet and Eomes [1365, 1367]. ILC2 are enriched among CD117$^{-/lo}$ CRTH2$^+$ cells and express GATA-3, while lacking T-bet and Eomes (Figure 157) [1364, 1365]. Among Lin$^-$ CD127^{hi} CD94$^-$ CD117$^-$ CRTH2$^-$ cells, a population of ILC1 has been described that lacks NKp44 and CD56 and is enriched in the SI LP of patients affected with inflammatory bowel diseases [1365]. This population displays only low amount of T-bet protein expression (Figure 157). In line with mouse data, additional populations of NK cells/ILC1 subsets with different phenotypic characteristics have been described in human tissues, including tonsils [1354, 1368–1371], making the selection of markers for the identification of NK/ILC1 quite challenging.

Recently, a human CD117$^+$ NKp44$^-$ ILC subset was identified in peripheral blood and in tissues that represents a "naïve" ILC precursor [1372]. This population was able to give rise to all ILC subsets in vitro and in vivo and did not express signature transcription factors associated with mature ILCs (T-bet, Eomes, GATA-3, RORγt). Accordingly, CD117 staining on human ILCs should not be equated with ILC3 identification but should additionally include markers such as NKp44.

Notably, the resolution of transcription factor staining in humans is not as good as in murine tissues and, therefore, combined staining of the above-mentioned surface markers is highly recommended in order to reliably gate on different human ILC subsets. However, as for their murine ILC counterparts, tissue-specific differences of surface markers should be taken into account as it has been shown for expression of CRTH2 for lung ILC2 [1373]. A selection of markers shown to be expressed by human and/or mouse ILC subsets is depicted in Table 54 (see also ref. [1342]).

5 Natural killer cells

5.1 *Overview*

NK cells represent a first fundamental line of defense against tumors and virus infected cells. In this section, we describe for both humans and mice, the most important strategies used to isolate and identify their subpopulations in an unequivocal manner.
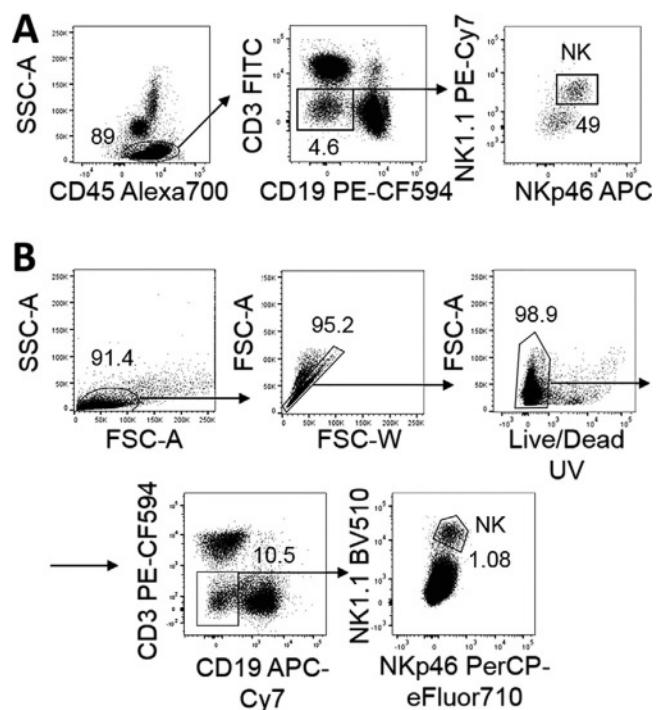
Figure 158. Identification of NK cells in the blood and spleen of C57BL/6 mice. Whole blood (A) was stained in BD Trucount tubes and analyzed after red blood cell lysis. Lymphocytes were gated among CD45$^+$ leucocytes based on their morphology and, after exclusion of CD3$^+$ T cells and CD19$^+$ B cells, NK cells were gated as NK1.1$^+$NKp46$^+$ cells. For the analysis of spleen NK cells (B), due to extraction techniques, doublets and dead cells need to be gated out. CD3$^+$ T cells and CD19$^+$ B cells were excluded and NK cells were gated as NK1.1$^+$NKp46$^+$ splenocytes.

5.2 *Murine NK cells*

5.2.1 Introduction. Mouse NK cells are commonly identified by FCM by the expression of the surface markers NK1.1, NKp46, and CD49b. The lack of expression of the T cell marker CD3 is used to exclude from the NK cell gate contaminating T cell subsets, such as NKT cells and NK-like T cells, that express NK1.1 and NKp46 respectively [1385]. In blood and spleen NK cells represent the most abundant innate lymphoid cell (ILC) subset, and the expression of NKp46 and NK1.1 is sufficient to identify them (Fig. 158). However, these NK markers vary depending on the mouse strain. NK cells from C57B/6 and SJL mice can be identified by NK1.1 expression, while in other mouse strains, such as BALB/c, NK cells display no reaction to the widely used anti-NK1.1 Ab PK136, because of allelic variations in Nkrp1b and Nkrp1c [1386]. In this case, NK cells can be identified only with CD49b and NKp46.

Even if mouse NK cells share many characteristics with human NK cells, it is not easy to identify functionally comparable NK cell subpopulations in the two species. Indeed, mouse NK cells lack the expression of human NK cell surface markers, including CD56 and some activating and inhibitory receptors. Murine NK cells lack KIRs, but express structurally divergent lectin-like Ly49 receptors that are functionally equivalent to the human KIRs and recognize MHC class I molecules. Most mouse Ly49 receptors recognize the

Table 55. Human- and mouse-specific and shared NK cell receptors

Receptor	Ligand	Human	Mouse
KIR2DL1 (CD158a)	Group 2 HLA-C	X	
KIR2DL2, KIR2DL3 (CD158b1, -b2)	Group 1 HLA-C, some group 2 HLA-C and some HLA-B	X	
KIR3DL1 (CD158e1)	HLA-Bw4	X	
KIR2DS1 (CD158h)	HLA-C2	X	
KIR2DS4 (CD158i)	Some HLA-C1 and HLA-C2, HLA-A11	X	
KIR2DL4 (CD158d)	HLA-G	X	
Ly49A (Klra1)	H2-Dd, H2-Dk, H2-Ld, H2-Db, H2-Kb, H2-Dp, H2-M3		X
Ly49C (Klra3)	H2-Db, H2-Kb, H2-Dd, H2-Kd, H2-Dk		X
Ly49E (Klra5)	Urokinase plasminogen		X
Ly49G (Klra7)	H2-Dd, H2-Kd, H2-Ld, H2-Db, H2-Dk, H2-Dr		X
Ly49I (Klra9)	H2-Kb, H2-Kd, H2-Dk, H2-Kk, m157 (MCMV)		X
Ly49D (Klra4)	H2-Dd, H2-Dr, Dsp2		X
Ly49H (Klra8)	m157 (MCMV)		X
Ly49P (Klra16)	H2-Dd, H2-Dk, m04 (MCMV)		X
NKG2A (CD159A)/CD94	HLA-E (human), Qa-1b (mouse)	X	X
NKG2C (CD159C)/CD94,	HLA-E (human), Qa-1b (mouse)	X	X
NKG2D (CD314)	Human: MICA/B, ULBP1, ULBP2, ULBP3, ULBP4, ULBP5, ULBP6 Mouse: RAE-1a, RAE-1b, RAE-1d, RAE-1e, RAE-1g, H60a, H60b, H60c, MULT1	X	X
KLRG1	E-, N-, and R-cadherin	X	X
NKp46 (NCR1; CD335)	CFP (properdin), hemagglutinin, PfEMP1	X	X
NKp30 (NCR3; CD337)	B7-H6, BAT3	X	
NKp44 (NCR2; CD336)	21spe-MLL5	X	
NKp80 (KLRF1)	AICL (activation-induced C-type lectin)	X	
DNAM-1 (CD226)	Nectin-2, PVR	X	X
2B4 (CD244)	CD48	X	X

classical MHC class I molecules H2-K and –D/L, while Ly49H and Ly49I recognize the MHC class I-related m157 molecule encoded by cytomegalovirus (CMV). The CD94/NKG2 heterodimer is conserved between mouse and human and, in mice, it recognizes the non-polymorphic Qa-1. The activating receptor NKG2D is also conserved between the species, and it is triggered by stress-induced MHC class I-related ligands retinoic acid early inducible (RAE)-1 and, in mice, the minor histocompatibility complex H60. Among the natural cytotoxicity receptors (NCRs), NKp30, and NKp44 are not expressed in mice, while NKp46 is considered to be the most specific NK cell marker, as it is expressed by all NK cells in mammals (Table 55) [1385].

Analogously to human NK cells for which the levels of CD56 and CD16 expression are used to define the maturation from immature CD56^{bright} CD16$^-$ NK cells to mature CD56^{dim} CD16$^+$ cells [1387], CD27 and CD11b expressions are used to identify several murine NK cell maturation steps. Immature NK cells are CD11b^{low} CD27^{high}, then they mature into double-positive CD27$^+$CD11b$^+$ cells and, finally, into fully mature CD27^{low} CD11b^{high} NK cells (Table 56). This developmental program is associated with the acquisition of NK cell effector functions [1376]. Both CD27$^+$ and CD27$^-$ subsets express equivalent levels of activating Ly49 receptors and CD94/NKG2 receptors, but CD27$^-$ NK cells contain higher levels of inhibitory Ly49s.

Recently, using high-throughput single-cell-RNA-seq, the gene expression of human and murine NK cells from spleen and blood was analyzed at the single cell level. In this study, two major NK cell subsets transcriptionally similar across organ and species were identified: it was shown a correspondence between the CD27$^-$CD11b$^+$ and the CD27$^+$CD11b$^-$ mouse NK cell subsets and the CD56^{dim} and CD56^{bright} human NK cell subsets, respectively [1388]. Moreover, this study revealed spleen- and blood-specific NK cell signatures common in both species, highlighting the importance of the organ of origin in the definition of a cell population.

While in blood and spleen NK cells represent the most abundant ILC subset, in tissues, there are high proportions of the other ILCs subsets, which are largely tissue-resident. CD127 is classically used to identify ILCs and distinguish them from NK cells, as it is not expressed by NK cells of liver, intestine, skin, uterus, salivary gland, bone marrow, or lymph nodes. However, CD127 is expressed by NK cells in the thymus and in some spleen populations, and it is not expressed by liver and intraepithelial gut ILC1s. Thus, the phenotypic characterization of tissue-resident NK cells is more complicated and requires the analysis of additional markers. In particular, NK cells share many features with ILC1s, they both produce IFN-γ as the main cytokine and require Tbet for this function. However, while NK cells require Eomes for their
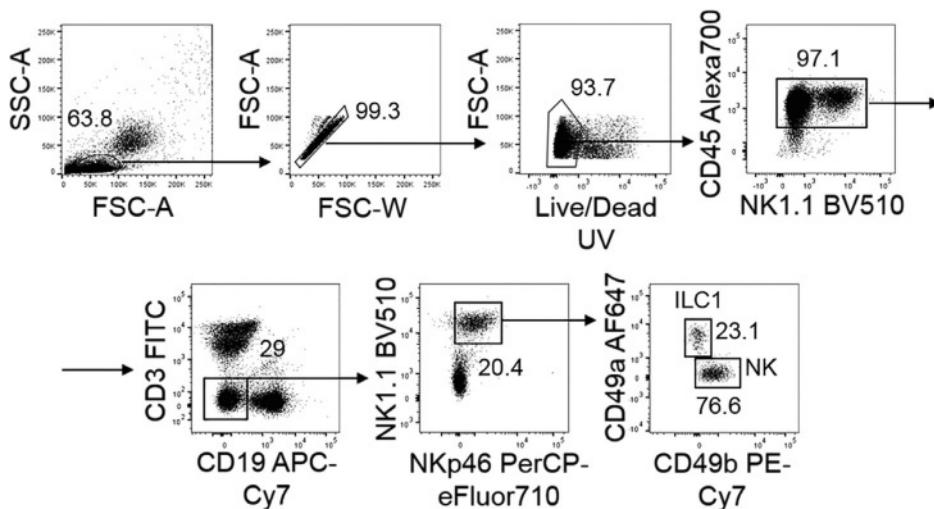
Figure 159. Identification of liver NK cells in C57BL/6 mice. After Percoll density gradient centrifugation of single cell suspension obtained scratching the liver, lymphocytes were analyzed. Doublets, dead cells, CD45− cells, CD3+ T cells, and CD19+ B cells were sequentially excluded. Among NK1.1+NKp46+ cells NK cells were gated as CD49b+CD49a− cells, and distinguished from CD49b−CD49a+ ILC1s.

development process, ILC1s develop in the absence of this transcription factor. Moreover, ILC1s are generally noncytotoxic and express lower levels of perforin compared to NK cells [1342]. Regardless these developmental and functional differences, ILC1s have some phenotypic markers in common with NK cells (see Chapter VI Section 4 Innate lymphoid cells), including NK1.1 in mice and NKp46 in both humans and mice. In the liver, for example, to distinguish these two populations, it is useful to include additional markers such as CD49b, exclusively expressed by NK cells in mice, and CD49a and TRAIL, preferentially expressed by ILC1s in both humans and mice (Fig. 159). Recently, CD200R has been shown to be an additional marker to distinguish ILC1s from NK cells in mice (Table 56) [1389].

In addition to ILC1s, NK cells share the expression of some markers with ILC3s. In mice ILC3s are dependent on RORγt for their development and function [1381] and two subsets can be distinguished on the basis of NKp46 expression: NCR+ and NCR− ILC3s. As NK cells and NCR+ ILC3s both express NKp46, the analysis of the expression of the transcription factors RORγt and Eomes can be useful to distinguish them (Figure 160, See also Chapter VI Section 4 Innate lymphoid cells).

Unlike NK cells, ILC2s are characterized by the capacity to produce type 2 cytokines. They contain larger amounts of the transcription factor GATA3 compared to the other ILC subsets but upon activation can express high levels of KLRG1, an inhibitory receptor also expressed by mature NK cells [1390].

For the identification and distinction of NK cells from other ILCs by FCM, it must be considered that, like T helper cell subsets, ILC subsets also display a certain degree of plasticity. For example, fate mapping and adoptive transfer studies in mice have shown that gut CCR6−NKp46− ILC3s can convert into IFN-γ producing NK1.1+NKp46+ ILC1s via a CCR6−NKp46+ intermediate through a decrease in RORγt expression and parallel increase in Tbet [1362, 1391].

5.2.2 Step-by step sample preparation. <u>Cell isolation:</u> Spleens and livers were scratched through 70 and 100 μm cell strainers,

respectively. Liver lymphocytes were isolated on a 37.5–67.5% Percoll gradient. For isolation of small intestine lamina propria cells, intestines were cut longitudinally, then transversally in 2–3 cm pieces, thoroughly rinsed with PBS, and shaken for 30 min in PBS containing 10% FBS, 15 mM Hepes and 5 mM EDTA to remove intraepithelial and epithelial cells. Intestines were then digested with collagenase VIII (300 UI/mL) in complete RPMI for 45 min at 37°C under agitation, and lamina propria lymphocytes were isolated on a 40–100% Percoll gradient. Whole blood was analyzed using BD Trucount tubes according to the manufacturer's instructions (BD Biosciences) [1392].

5.2.3 Materials. The following Abs were used and/or are suggested for the surface and intracellular staining of mouse NK cells:

BD Biosciences: CD45.2 AlexaFluor700 (1:200, clone 104), CD3 PE CF594 (1:100, clone 145-2C11), CD19 PE CF594 (1:200, clone 1D3), NK1.1 BV510 (1:50, clone PK136), CD49a AlexaFluor647 (1:400, clone Ha31/8), CD11b BV510 (1:400, clone M1/70), NKp46 BV421 (1:50, clone 29A1.4), TCRb FITC (1:400, clone H57-597), granzyme B PE (1:50, clone GB11), Rorγt PE (1:100, clone Q31-378), CD107a FITC (1:60, clone 1D4B), Fc block CD16/CD32 (1:200, clone 24G2);

eBiosciences: NKp46 PerCP-eFluor710 (1:50, clone 29A1.4), CD49b PE-Cy7 (1:200, clone DX5), Eomes APC (1:100, Dan11mag);

Biolegend: IFN-g BV421 (1:100, clone XMG1.2), CD19 APC-Cy7 (1:200, clone 6D5), NKp46 APC (1:50, clone 29A1.4), NK1.1 PE-Cy7 (1:50, clone PK136), CD3 FITC (1:100, clone 145-2C11), CD19 FITC (1:100, clone 6D5).

Dead cells were identified using the fixable blue dead cell stain kit (Invitrogen). For surface staining cells, Abs were diluted in PBS 5 mM EDTA (Euroclone). For intracellular staining, cells were fixed and permeabilized with an intracellular staining kit (eBioscience). Flow cytometric data were acquired with a BD LSR II flow cytometer equipped with FACS DIVA software (BD Biosciences), and analyzed by using FlowJo software (FlowKo, LLC).
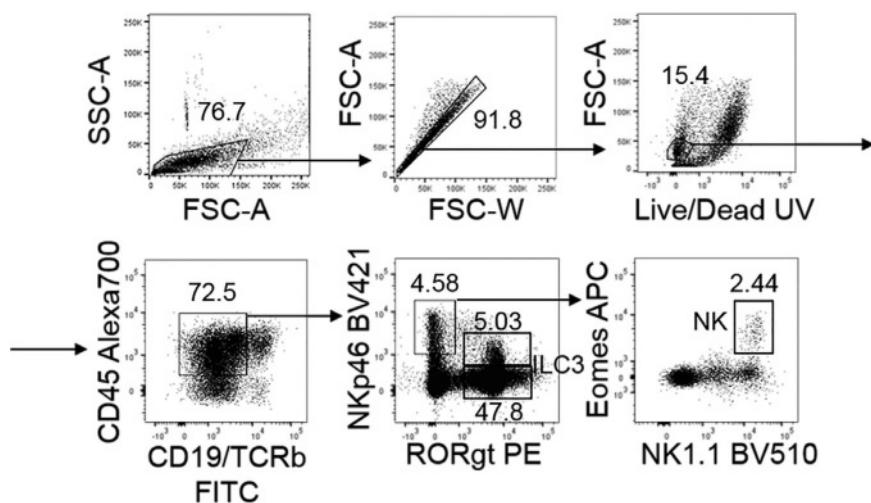
Figure 160. Identification of small intestine lamina propria NK cells in C57BL/6 mice. After enzymatic digestion and Percoll density gradient centifugation, single cell suspension obtained from the small intestine was analysed. As in figure 159, doublets, dead cells, CD45⁻ and CD19⁺ B cells were sequentially excluded. T cells were gated out based on their expression of TCRβ. RORγt⁺ cells represent ILC3s, which can be further distinguished in NCR⁺ and NCR⁻ ILC3s. Among RORγt⁻ NKp46⁺ cells, NK cells are gated as NK1.1⁺Eomes⁺ cells.

Table 56. Key markers for murine NK cell identification and characterization

Marker	Expression
NK lineage	
NK1.1 (CD161)	Surface
NKp46 (NCR1; CD335)	surface
CD49b	Surface
T-bet	Nucleus
Distintion from other ILCs	
IL7Rα (CD127)	Surface, ILC1, ILC2, ILC3
CD49a	Surface, ILC1
CD200R	Surface, ILC1
TRAIL	Surface, ILC1
Eomes	Nucleus, NK cells
Rorγt	Nucleus, ILC3
Development/ maturation stages	
CD27	Surface, immature NK cells
CD11b (Mac-1/CD18)	Surface, mature NK cells
KLRG1	Surface, mature NK cells
CD43	Surface, mature NK cells
CXCR6	Surface, "memory" NK cells in the liver

5.2.4 Pitfalls. When including CD11b in cytometry panels to exclude myeloid cells from the analysis, it must be taken into account that mature murine NK cells express this marker too. Therefore, one must check carefully that NK1.1⁺ and/or NKp46⁺ CD11b⁺ cells do not get excluded in the associated gating strategy.

5.3 Human NK cells

5.3.1 Introduction. Natural killer (NK) cells were described over 40 years ago as cells capable of killing tumor cells without prior sensitization. They are lymphoid cells derived from hemopoietic stem cells (HSCs) [1393, 1394] and belong to the innate immunity cell family. In contrast to T and B cells, NK cells do not express receptors encoded by rearranging genes and they play a major role in innate immunity as both effector and regulatory

cells, participating in the first line of defense against pathogens and tumors. Notably, NK-cell-susceptible tumors are primarily those lacking or expressing insufficient amounts of MHC class I molecules (missing-self hypothesis) [1395]. Another requirement for NK-cell-mediated tumor cell killing is the surface expression of a series of different stress-induced structures [1396]. The NK cell function appears to complement the cytolytic T cell–mediated MHC-I-dependent activity [1397].

The recognition of MHC class-I is mediated by a family of receptors termed Killer Ig-like receptors (KIRs), by the NKG2A/CD94 heterodimer and by LIR-1 (CD85j). In particular, NKG2A/CD94, expressed early during the process of NK cell maturation, recognizes the nonclassical HLA-E molecule [1398, 1399] while KIRs, expressed at later stages of NK cell maturation, recognize allelic determinants of HLA-A -B or -C [1400, 1401]. Other non-HLA-related inhibitory receptors including Siglec7 (CD328), PD1 (CD279), and IRP60 (CD300a) may be expressed at the surface of NK cells (see Tables 57 and 58). In most instances, the NK receptors that mediate their activation upon binding to target cells are non-HLA-specific and recognize cell stress-induced molecules. These receptors include NKp30, NKp44, and NKp46 (which constitute the natural cytotoxicity [NCR] family), NKp80, 2B4 (CD244), and NKG2D [1402–1404]. Of note, activating isoforms of KIRs also exist [1405]. While inhibitory KIRs are characterized by immune-receptor tyrosine-based inhibition motif (ITIM) domains in their long intracytoplasmic tail, the various activating receptors bear a short intracytoplasmic tail and are associated with signaling polypeptides containing immune-receptor tyrosine-based activating motifs (ITAM) domains [1406]. A fundamental activating receptor is also CD16, the low affinity Fcγ receptor, which binding to IgG complexes mediates the Ab-dependent cell-cytotoxicity (ADCC). In resting conditions, the bright expression of CD16 is restricted to mature NK cells.

Among peripheral NK cells, two major subsets have been identified on the basis of the cell surface density of CD56 molecules (neural cell adhesion molecule, N-CAM). CD56ᵇʳⁱᵍʰᵗ (CD3⁻CD56⁺⁺CD16⁻ᐟ⁺) represent approximately 10% of the
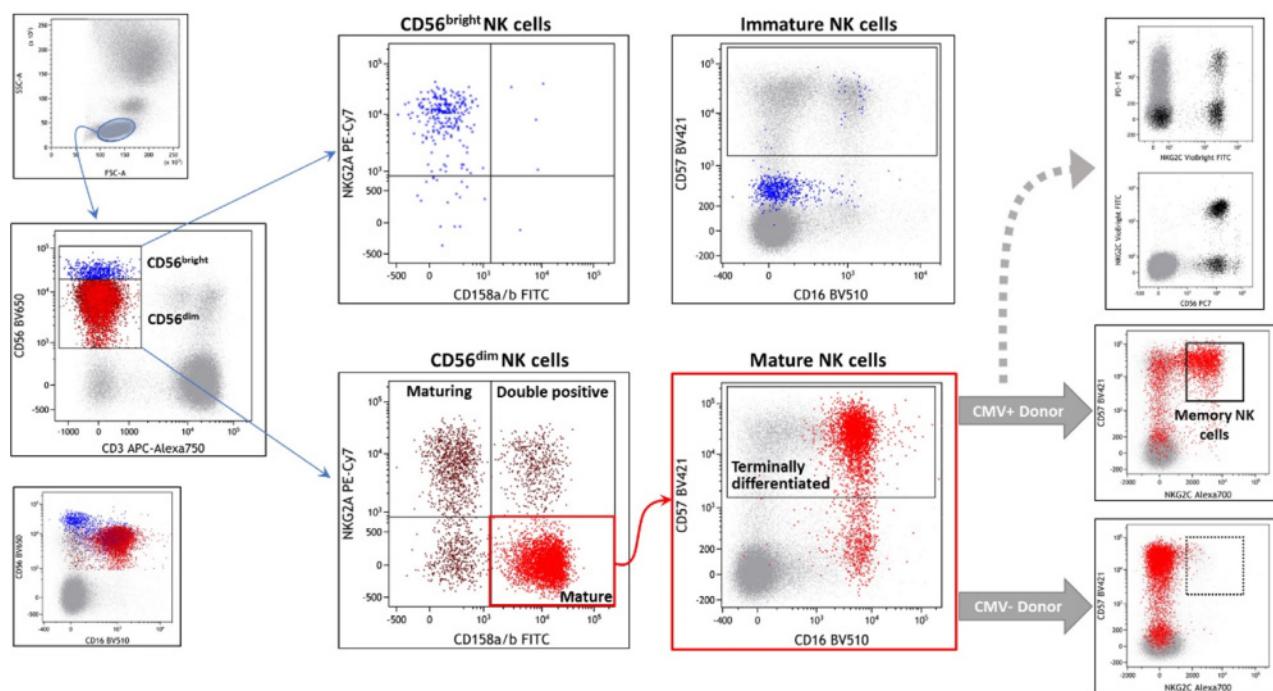
Figure 161. In this PB samples, lymphocytes are first gated based on their physical parameters (upper left grey dot plot) then human NK cells can be identified for their CD56 surface expression and lack of CD3. The CD56^{bright} NK subpopulation (in blue) is positive for NKG2A, negative for KIRs and CD57 while CD16 can be either negative or dimly expressed (as shown). NKG2A and KIR surface expression allows three subpopulations of CD56^{dim} NK cells (in red), namely "maturing" (NKG2A$^+$KIR$^-$ in dark red), "double positive" (NKG2A$^+$KIR$^+$ in dark red) and "mature" (NKG2A$^-$KIR$^+$ in light red), to be identified. To discriminate among these CD56^{dim} maturation steps, we used a cocktail of anti-KIR (clones: EB6B, GL183, Z27) that did not include anti-LIR1, for this reason in the dot plot also a double negative population is present. Among the mature population (in light red), CD57 molecule is expressed on the, so called, "terminally differentiated" NK cells. In CMV positive donors, a percentage of this latter population could also express NKG2C representing the so called "memory NK cells." Recently it has been demonstrated that in some CMV positive individuals a fraction of the NKG2C subset can also express PD1. Percentage of subpopulation are not specified because they are extremely diverse among different individuals and do not give additional information to the gate strategy.

circulating PB NK cells while they prevail in secondary lymphoid organs (liver, synovial fluid and decidua). CD56^{dim} (CD3$^-$CD56$^{+/-}$ CD16^{++}) cells are largely predominant (∼90%) in PB NK cells. They derive from CD56^{bright} NK cells, as revealed by different studies in vitro (differentiation from HSC) and in vivo after HSC transplantation [1407, 1408]. Moreover, the existence of a third NK cell population totally lacking CD56 has been widely demonstrated both on virus infected patients and, more rarely, on healthy donors. This population is characterized by a reduced expression of NCRs and, in in vitro studies, by a poor cytotoxic activity [1409–1412].

5.3.2 CD56^{bright} NK cells.　In resting conditions all CD56^{bright}, in contrast to CD56^{dim}, NK cells are poorly cytolytic but secrete cytokines, primarily IFN-γ and TNF-α and express both high (CD25) and intermediate (CD122/CD132) affinity IL-2 receptors and c-Kit (CD117), rendering them highly susceptible to IL-2–induced cell proliferation [1413, 1414]. Moreover, CD56^{bright} NK cells express high levels of both CD62L [1415] and CXCR3 which, together with the surface expression of CCR7, dictates their preferential homing into secondary lymphoid organs [1416–1418] Notably, although poorly cytotoxic under resting conditions,

CD56^{bright} NK cells may acquire cytolytic activity comparable to that of CD56^{dim} cells upon stimulation with cytokines, such as IL-2, IL-12, IL-15. While CD56^{bright} NK cells express CD94/NKG2A (i.e., the receptor for HLA-E) they lack KIRs. Regarding activating NK receptors, CD56^{bright} cells express higher levels of NKp46 and NKp30 than CD56^{dim} cells, while CD56^{bright} cells lack or express low amounts of CD16.

5.3.3 CD56^{dim} NK cells.　CD56^{dim} NK cells under resting conditions express granules containing perforin and granzymes, and display cytolytic activity. Until recently, CD56^{dim} NK cells were mainly associated with cytotoxicity while cytokine production was thought to be confined to the CD56^{bright} subset. However, more recently, it has been shown that, upon stimulation via activating receptors, CD56^{dim} NK cells rapidly release cytokines such as IFN-γ- and TNF-α (even more efficiently than CD56^{bright} cells) and chemokines such as MIP-1β and MIP-1α [1419, 1420]. In contrast to CD56^{bright} NK cells, the CD56^{dim} population is phenotypically heterogeneous. Thus, as shown in Fig. 161, NKG2A versus KIR expression allows identification of three distinct subset of human NK cells that recapitulate the consecutive steps of PB NK cell maturation to be distinguished.

Table 57. Human NK cell inhibitory and activating receptors

Receptor	Ligand	CD56^{bright}	CD56^{dim}
Activation			
NKG2C (CD159a)	HLA-E	−	Subsets
NKG2D (CD314)	MIC-A - MIC-B - ULPBs	All PB NK cells	
KIR2DS1 (CD158h)	HLA-C2	−	Subsets
KIR2DS2/3 (CD158j)	???	−	Subsets
KIR2DL4 (CD158d)	HLA-G	−	Subsets
KIR2DS4 (CD158i)	HLA-A*11 and some HLA-C	−	Subsets
KIR2DS5 (CD158f)	???	−	Subsets
KIR3DS1 (CD158e1)	HLA-Bw4, HLA-F	−	Subsets
NKp30 (CD337)	B7-H6 - BAG6/BAT3	++	+
NKp44 (CD336)	21spe-MLL5, Nidogen 1	On activated NK cells	
NKp46 (CD335)	CFP (properdin), haemagglutinin, PfEMP1	++	+
NKp80	AICL	+	+
DNAM1 (CD226)	Nectin-2 (CD112), PVR (CD155)	+	+
2B4 (CD244)	CD48	All PB NK cells	
NTB-A (CD352)	NTB-A (CD352)	All PB NK cells	
CRACC/CS1 (CD319)	CRACC/CS1 (CD319)	All PB NK cells	
Tactile (CD96)	PVR (CD155)	All PB NK cells	
FcγRIII (CD16)	IgG	−/+	+/++
Inhibition			
NKG2A/KLRD1 (CD159a/CD94)	HLA-E	+	Subsets
KIR2DL1 (CD158a)	HLA-C2	−	Subsets
KIR2DL2/3 (CD158b)	HLA-C1, few HLA-C2	−	Subsets
KIR2DL4 (CD158d)	HLA-G	−	Subsets
KIR2DL5 (CD158f)	???	−	Subsets
KIR3DL1 (CD158e1)	HLA-A-Bw4 and HLA-B-Bw4	−	Subsets
KIR3DL2 (CD158k)	HLA-A*03 and *11	−	Subsets
ILT2/LIR-1 (CD85J)	Different MHC-I alles	−	Subsets
PD-1 (CD279)	PDL1 (CD274) and PDL2 (CD273)	−	Subsets
Siglec-7 (CD328)	Ganglioside DSGb5	Most of PB NK cells	
IRP60 (CD300a)	α-herpes virus Pseudorabide virus Phosphatidylserine Phosphatidylethnolamine	+	+
TIGIT	PVR (CD155)	PB NK cells	

The "maturing" population (NKG2A$^+$KIR$^-$) is characterized by the NKG2A$^+$/KIR$^-$ phenotype, similar to that of CD56^{bright} cells, while the "mature" population expresses the NKG2A$^-$KIR$^+$ phenotype. An intermediate step of maturation is identified by the "double positive" NKG2A$^+$KIR$^+$ cells [1377, 1387]. The unidirectional nature of NK cell differentiation is further supported by the presence of CD57 on the surface of the "terminally differentiated" NK subset. When compared with the CD57-negative counterpart, the NKG2A$^-$KIR$^+$CD57$^+$ population shows a decreased surface expression of NKp30 and NKp46, and a reduced proliferative potential, possibly as the result of downmodulation of IL-2Rβ (CD122) and IL-18Rα (CD218a) [1377, 1379].

In CMV-positive healthy donors, it is possible to identify an additional subset of mature cells that expresses CD57 and the activating HLA-E-specific receptor NKG2C dimerizing with CD94 [1421]. This subset appears to contain cells endowed with an adaptive/memory-like capability (i.e., clonal expansion, prompt response to restimulation, and epigenetic modification including that of the intracytoplasmic FcεRγ chain) [1411, 1422, 1423]. Recent data have shown that, in CMV positive individuals, a fraction of CD57 positive cells may also express PD-1 [1412].

The recruitment of CD56^{dim} NK cells to inflamed peripheral tissues is driven by several chemokines and homing receptors including, for example, CXCR1, CX3CR1, and in certain subsets CD62L and CXCR3^{low} also [1416].

5.3.4 NK cells present in decidua. During the first trimester of pregnancy, NK cells represent the main lymphoid population (50–70%) in human decidua where they bear a unique phenotypic and functional profile. Their phenotypic features resemble to an extent those of CD56^{bright} PB NK cells; however, in addition to

Table 58. Other human NK cell receptors

Receptor	Ligand	CD56^{bright}	CD56^{dim}
Adhesion			
LFA-1 (CD11a/CD18)	ICAM-1, ICAM-2, ICAM-3	−/+	++
LFA-2 (CD2)	CD15, CD58, CD59	Most of mature NK cells	
LFA-3 (CD58)	CD2, CD48, CD58	Most of mature NK cells	
MAC-1 (CD11b/CD18)	iC3b, C4b, ICAM-1, fibrinogen	Most of circulating NK, up-regulated upon activation	
ICAM-1 (CD54)	LFA-1, MAC-1	++	+/−
N-CAM (CD56)	???, FGFR	++	+
HNK-1 (CD57)	???	−	Subsets
L-Selectin (CD62L)	GLyCAM-1 MadCAM-1	++	Subsets
Cytokine /Chemokine receptors			
IL-2Rα (CD25)	IL-2	+	−
IL-2Rβ/IL-2Rγ (CD122/CD132)	IL-2 AND IL.15	Almost all PB NK cells	
c-Kit (CD117)	SCF (KL)	+	−
IL7Rα (CD127)	IL-7	+	−
CXCR1 (CD181)	CXCL8 (IL-8)	−	+
CXCR2	IL8-RB	−	+
CXCR3 (CD183)	CXCL9, CXCL10, CXCL11	++	Subsets
CXCR4 (CD184)	CXCL2	Subsets of PB NK cells	
CCR5 (CD195)	RANTES, CCL3 (MIP1α) and CCL4 (MIP1β)	Subsets of PB NK cells	
CCR7 (CD197)	CCL19, CCL21	+	−
IL-18R (CD218a)	IL-18	++	+
ChemR23	Chemerin	−	+
CX3CR1	Fraktaline	−	+
Death Receptors			
Fas/APO-1 (CD95)	Fas ligand (CD95L)	Activated NK cells They induce target apoptosis	
Fas ligand (CD95L)	Fas/APO-1 (CD95)		
CD40L (CD154)	CD40		
TRAIL (CD253)	DR4 (TRAIL-R1), DR5 (TRAIL-R2)		
Other surface molecules			
LAMP1 (CD107a)	—	Briefly expressed on NK cell surface after degranulation	
LAMP2 (CD107b)	—		
LAMP3 (CD63)	—		
TNFRSF7 (CD27)	CD70	+	−

the NKG2A^{high}NKp30^{high}NKp46^{high} surface phenotype, they also display characteristics of CD56^{dim} NK cells including high expression of KIR and lytic granules. Of note, in contrast to PB NK cells, the 2B4 (CD244) receptor on decidual NK cells displays a strong inhibitory (and not activating) activity, similar to that seen in NK cell precursors [1424], that renders this population poorly cytolytic [1425, 1426] [Moreover, in contrast to PB NK cells, decidual NK cells release a unique set of cytokines, including IL-8 (CXCL8), VEGF, CXCL12 (stromal-derived factor–1 [SDF-1α]), and IFN-γ–inducing protein 10 (IP-10, CXCL10), that play a pivotal role in tissue remodeling (i.e., placenta development processes) and neo-angiogenesis [1427].

5.3.5 NK cells present in lymph nodes. In normal conditions, NK cells are present in lymph nodes where they occupy the T-cell

areas [1428]. They are consistently CD56^{bright}CD16^{neg}KIR^{neg} and lack perforin and granzymes. In contrast to PB CD56^{bright} NK cells, lymph node NK cells do not express CCR7 or CD62L. Concerning the NCR family, lymph node NK cells express low levels of NKp46 and may lack NKp30. Remarkably, however, upon IL-2 activation, lymph node NK cells may express KIRs and CD16, and upregulate NCR [1428, 1429].

5.3.6 Step-by-step sample preparation. PB NK cell surface staining:

1. Put 100 μL of heparinized whole blood in a sample tube
2. Add 50 μL of Brilliant Stain Buffer to each tube
3. (a) To study PB subpopulations, add the following antibodies: CD158a FITC (10 μL) CD158b FITC (10 μL), CD158e FITC
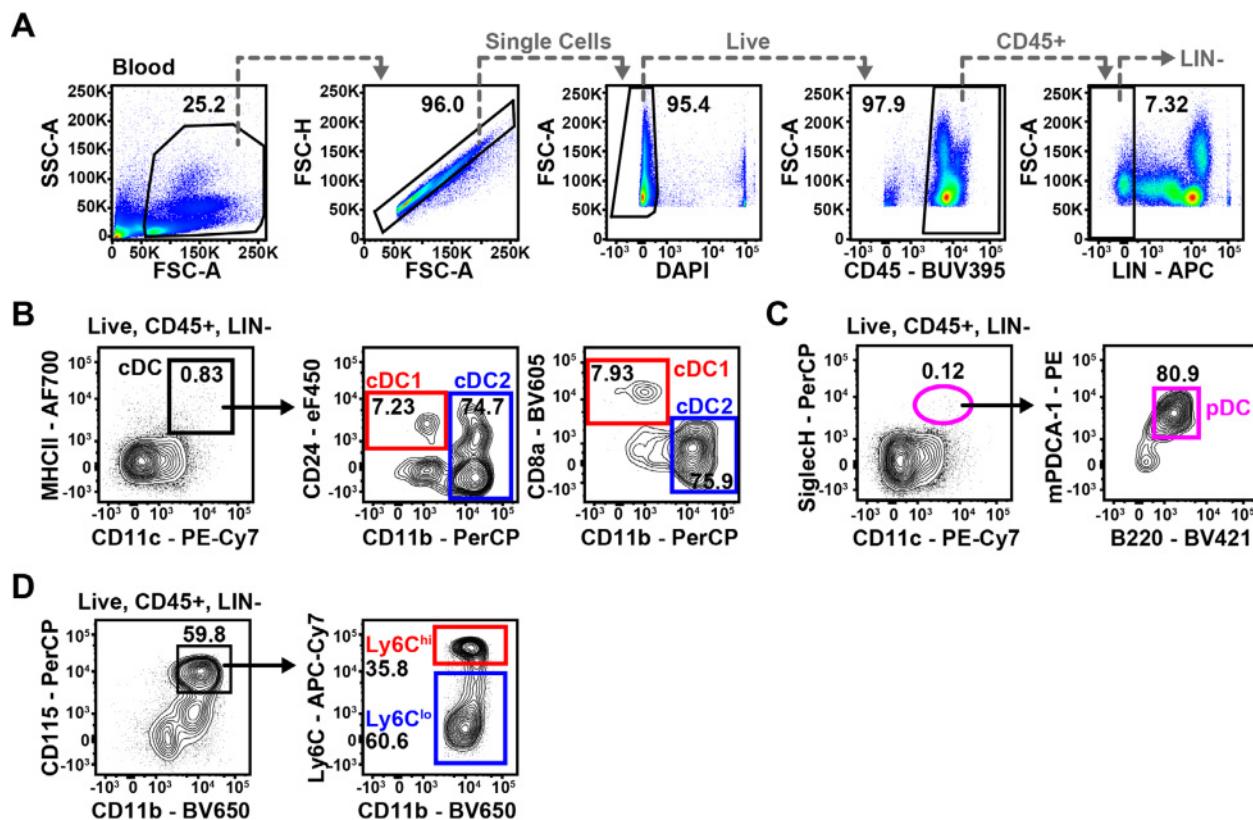
Figure 162. Flow cytometric analysis of mouse blood DCs and monocytes. Example for basic gating strategy from FSC-A/SSC-A, over doublet exclusion and gating on Live, CD45$^+$ LIN$^-$ cells (defined as CD3/CD19/CD49b/Ly6G$^-$) on a blood sample (A), as used for all tissues. Conventional DCs are identified as CD11c^{hi}MHCII$^+$ cells and can be divided into cDC1 (CD8/CD24$^+$CD11b$^-$, red gates) and cDC2 (CD8$^-$CD11b$^+$, blue gates) (B). Plasmacytoid DCs are identified as CD11c^{int}SiglecH$^+$ and can be further purified by gating on B220$^+$mPDCA-1$^+$ cells (pink gates; C). Monocytes are identified as CD115$^+$CD11b$^+$ cells and can be further divided into Ly6C^{lo} and Ly6C^{hi} monocytes (blue and red gates, respectivley; D).

(5 μL), CD279 PE (10 μL), CD159a PE-Cy7 (3 μL), NKG2C A700 (3 μL), CD3 APC-A750 (3 μL), CD57 BV421 (3 μL), CD16 BV510 (3 μL), CD56 BV650 (3 μL).

(b) To study only NKG2C/PD1 co-expression this simpler cocktail can be used: NKG2C VioBright FITC, CD279 PE (10 μL), CD56 PC7 (3 μL) CD3 APC-A750 (3 μL).

4. Incubate 20 min at 4°C.
5. After incubation, lyse sample in 2 mL of Pharm Lyse^{TM}, for 5–8 min
6. Centrifuge 5 min at 1300 rpm
7. Discard supernatant
8. Resuspended in 300 μL of PBS for acquisition.

5.3.7 Materials. Pharm Lyse^{TM} and Brilliant Stain buffer are from Becton Dickinson (San Josè, CA), PBS is from (Sigma–Aldrich).

Beckman Coulter: CD3 APC or APC-Alexa Fluor 750 (UCHT1, IgG1), CD56 PC7 (N901), CD158a PE (EB6B, IgG1), CD158b PE (GL183, IgG1), CD158e FITC or PE (Z27, IgG2a), CD159a PE-Cy7 (Z199 IgG2b), NKp30 (Z25, IgG1), NKp44 (Z231, IgG1) NKp46 (BAB281, IgG1), NKp80 (MA152, IgG1) NKG2D (ON72, IgG1).

Becton Dickinson: CD16 BV510 (3G8, IgG1), CD56 BV650 (NCAM16.2, IgG2b), CD57 BV421 (NK-1, IgM), CD158b (CH-L, IgG2b).

Miltenyi: PD1 PE (PD1.3.1.3, IgG1), NKG2C VioBright FITC (REA205, Ig1).

R&D System: NKG2C Alexa Fluor 700 (134591, IgG2a).

Flow cytometric data were acquired with a BD LSR II flow cytometer equipped with FACS DIVA software (BD Biosciences), and analyzed by using Kaluza software (Beckman Coulter).

5.3.8 Top Tricks. When using many different Brilliant Violet fluorochromes in the same sample, in order to avoid aspecific interactions between these polymer dyes, it is better to add always Brilliant Stain Buffer to the sample before adding the conjugated mAbs.

While for PD1 detection in human T cells most of commercial mAb clones are equally good, when working with human NK cells the situation is totally different. In our experience, the best clone to discriminate PD1 positive NK cells is PD1.3.1.3 conjugated with PE.

6 Mononuclear phagocytes: Monocytes, macrophages, and dendritic cells

6.1 Overview

This chapter aims to provide basic guidelines for researchers interested in analyzing mononuclear phagocytes that include monocytes, macrophages, and dendritic cells. We describe here processing and FCM-staining techniques for various murine and human tissues such as blood, bone marrow, spleen, lung, skin, intestine, or lymph nodes. Furthermore, this chapter provides basic gating strategies as well as tips and tricks and background information for each tissue in order to easily identify the various subpopulations of monocytes, macrophages, and dendritic cells.

6.2 Introduction

Both mouse and human lymphoid and non-lymphoid tissues contain a high number of mononuclear phagocytes, innate myeloid cells that play crucial roles in homeostasis as well as host–pathogen interactions. This pool is composed of monocytes, macrophages, and dendritic cells (DCs). Ontogeny, heterogeneity and specific functions of these cells have been extensively described in various recent reviews (e.g., [1430–1435]).

Briefly, the murine DC compartment is currently divided into classical DCs (cDCs) and plasmacytoid DCs (pDCs), with cDCs being further subdivided into cDC1 (CD11b$^-$ CD8$^+$ in lymphoid tissues or CD11b$^-$ CD103$^+$ in non-lymphoid tissues) or cDC2 (CD8/CD103$^-$ CD11b$^+$SIRPα^+ cells) [1433, 1436, 1437] (Table 60). While all cDCs express high levels of CD11c and MHCII across tissues, pDCs are rather CD11c^{int} cells that are characterized by the expression of markers such as SiglecH, B220, and mPDCA-1, while lacking expression of CD11b. Note that the dendritic cell nature of pDCs is currently being challenged as recent studies have reported that pDCs arise rather from a lymphoid lineage [1438–1440]. Langerhans cells (LCs) are epidermal-specific antigen presenting cells that were originally classified as members of the DC family as they express CD11c, CD11b, and MHCII and shown to migrate to lymphoid organs. However, LCs were shown to be more of fetal macrophage origin, hence, these cells are now rather classified as the resident macrophages of the epidermis [1441–1443]. Monocytes are also heterogeneous and have been categorized into two subsets: inflammatory CXCR1^{hi}CCR2$^-$CD62L$^-$CD43^{hi}Ly6C^{lo} and patrolling CX3CR1^{int}CCR2$^+$CD62L$^+$CD43^{lo}Ly6C^{hi} monocytes [1444, 1445]. Ly6C^{hi}MHCII^{lo} monocytes recruited in tissues in steady state continually differentiate into Ly6C^{lo}MHCII^{hi} macrophages, a phenomon referred to as the monocyte to macrophage "waterfall," mostly described in the gut and skin [1446, 1447].

Human mononuclear phagocytes also include cDCs, namely CD1c$^+$ cDC2 and CLEC9A$^+$XCR1$^+$CADM1$^+$CD141$^+$ cDC1; CD123$^+$ pDCs; monocyte-derived cells (termed CD14$^+$ cells here) and tissue-resident macrophages [1431, 1448, 1449]. We have recently described cDC progenitors in the blood, namely pre-

DC [1450], that were previously included into the classic HLA-DR$^+$CD123$^+$ pDC gate. Similar to mouse, in humans, monocytes can be distinguished into CD14^{hi}CD16$^-$ classical versus CD14^{lo}CD16$^+$ non-classical monocytes [1451], that are the equivalent of the inflammatory CXCR1^{hi}CCR2$^-$CD62L$^-$CD43^{hi}Ly6C^{lo} and patroling CX3CR1^{int}CCR2$^+$CD62L$^+$CD43^{lo}Ly6C^{hi} monocytes, respectively, with an additional minor population of CD14$^+$CD16$^+$ intermediate monocytes.

The efficient processing of both mouse and human tissues is highly valuable to properly characterize tissue-associated mononuclear phagocytes in steady state or inflammation. Here, we explain techniques for the enrichment and FCM-based identification of all mononuclear phagocyte populations across a number of mouse and human tissues.

6.3 Materials

6.3.1 Mouse tissue processing materials.

6.3.1.1 General reagents and materials.

Reagent	Manufacturer	Catalog number
Bovine Serum Albumin, lyophilized powder (BSA)	Sigma–Aldrich	A2058
Collagenase IV	Sigma	C5138
DAPI	Life Technologies	D1306
Dispase	Gibco	17105041
DNase I	Roche	10104159001
Dulbecco's Phosphate Buffered Saline (PBS)		
Dithiothreitol (DTT)	Gold Biotechnology	DTT50
Foetal Bovine Serum (FBS)	Serana	S-FBS-SA-015
n-mouse serum	Sigma-Aldrich	M5905-10ML
n-rat serum	Sigma-Aldrich	R9759-10ML
1× RBC Lysis Buffer	eBioscience	00-4333-57
RPMI 1640	HyClone	SH30255.01

Prepare:

- RPMI 1640 containing 10% FBS (or FCS)
- FCM buffer: 0.5% w/v BSA + 2 mM EDTA in 1X PBS
- FCM staining buffer (as used for indicated tissues): 1% n-mouse serum + 1% n-rat serum in FCM buffer
- Digestion buffer (solution 1): 0.2 mg/ml collagenase IV + 0.03 mg/ml DNase I in RPMI + 10% FBS/FCS
- Fine scissors and forceps/tweezers
- 5 mL FCM tubes, round bottom, polystyrene
- Six-well/12-well plates for harvesting tissues/digestion of tissues
- 15 mL/50 mL conical tubes
- 70 µm cell strainer

6.3.1.2 Additional materials for mouse bone marrow processing.

- 25 G needles and 20 mL syringes to flush bone marrow

6.3.1.3 Additional materials for mouse lung processing.

- 70 μm nylon mesh sheet—cut into approximately 1 × 1 cm squares
- 18 G blunt needles and 3 mL syringes for dissociation

6.3.1.4 Additional reagents and materials for mouse intestine processing.

- Six-well plates: one well per mouse for harvesting; one well per mouse for digestion of small intestine and one well per mouse for digestion of large intestine
- Beaker of cold PBS (keep on ice)
- Metal trays or petri dishes for various washing steps
- Three 50 mL centrifuge tubes for each small intestine and colon sample (four if the epithelial compartment is to be isolated for analysis as well)
- Epithelium dissociation solution (50 mM EDTA + 100 μL 20 mM DTT in PBS)
- Digestion solution **1** (0.2 mg/mL collagenase IV, 0.03 mg/mL DNase in RPMI + 10% FCS)
- Digestion solution **2** (0.4 mg/mL collagenase IV, 0.03 mg/mL DNase in RPMI + 10% FCS)
- 70 μm cell strainers
- Percoll* (see * in chapter)

6.3.1.5 Additional reagents and materials for mouse skin (ears) processing.

- Dispase solution (4 U/mL in RPMI 1640)
- Six-well plate for Dispase incubation
- 12-well plate for digestion incubation
- Digestion solution **1** (0.2 mg/mL collagenase IV, 0.03 mg/mL DNase in RPMI + 10% FCS)
- Flat clean surface for separating dorsal and ventral halves, and epidermis from dermis
- 70 μm nylon mesh sheet—cut into approximately 6 × 6 cm squares

6.3.1.6 Additional reagents for mouse lymph node (LN) processing.

- Digestion solution **3**: 0.4 mg/mL collagenase IV + 0.06 mg/mL DNase I in RPMI + 10% FBS/FCS (2× concentrated digestion buffer/solution **1**)
- 25 G needles and 1 mL syringes for dissociation of LNs for digestion
- 70 μm nylon mesh sheet—cut into approximately 6 × 6 cm squares

6.3.2 Abs for murine mononuclear phagocyte identification.

Antibody	Fluorochrome	Clone	Provider	Cat #
CD3ε	APC	145-2C11	BioLegend	100312
CD8α	BV605	53-6.7	BioLegend	100744
CD11b	BV650	M1/70	BioLegend	101259
CD11c	PE-Cy7	N418	BioLegend	117318
CD11c	BV605	N418	BioLegend	117334
CD16/32	Pure	2.4G2	BD	553142
CD19	APC	eBio1D3	eBioscience	17-0193-82
CD24	eFluor 450	M1/69	eBioscience	48-0242-82
CD45	BUV395	30-F11	BD	564279
CD49b	APC	DX5	BioLegend	108909
CD64 / FcγRI	PE	X54-5/7.1	BD	558455
CD64 / FcγRI	BV711	X54-5/7.1	BioLegend	139311
CD103	APC	2E7	eBioscience	17-1031-82
CD115	PerCP	AFS98	eBioscience	46-1152-82
CD172α	Biotin	P84	BioLegend	144006
CD317/m-PDCA-1	PE	eBio97	eBioscience	13-1721-82
B220/CD45R	BV421	RA3-6B2	BioLegend	103240
CCR2	FITC	FAB5538F	R&D	475301
CX3CR1	PE	SA011F11	BioLegend	149006
EpCAM	BV605	G8.8	BioLegend	118227
F4/80	Biotin	BM8	BioLegend	123106
F4/80	PE-CF594	T45-2342	BD Horizon	565613
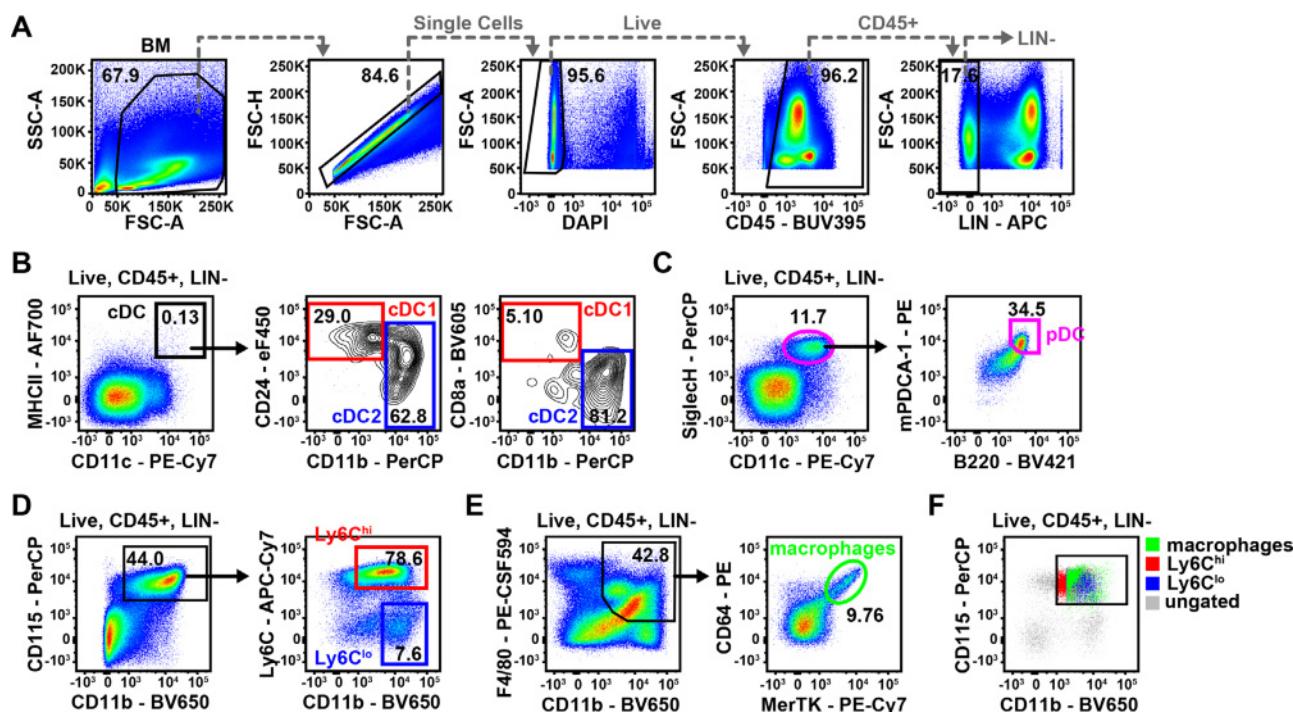
Figure 163. Flow cytometric analysis of mouse bone marrow DCs, macrophages, and monocytes. Example for basic gating strategy from FSC-A/SSC-A, over doublet exclusion and gating on Live, CD45$^+$ LIN$^-$ cells (defined as CD3/CD19/CD49b/Ly6G$^-$) on a BM sample (A). Conventional DCs are identified as CD11c^{hi}MHCII$^+$ cells and can be divided into cDC1 (CD8/CD24$^+$CD11b$^-$, red gates) and cDC2 (CD8$^-$CD11b$^+$, blue gates) (B). Plasmacytoid DCs are identified as CD11c^{int}SiglecH$^+$B220$^+$mPDCA-1$^+$ cells (pink gates; C). Monocytes are identified as CD115$^+$CD11b$^+$ cells and can be further divided into Ly6C^{lo} and Ly6C^{hi} monocytes (blue and red gates, respectivley; D), while macrophages can be gated as CD11b$^+$F4/80$^+$ (green gate; E). Backgating of monocyte and macrophage populations, that were gated independently of CD115 expression, onto CD115 versus CD11b expression confirms CD115 as a valid marker for these populations (F).
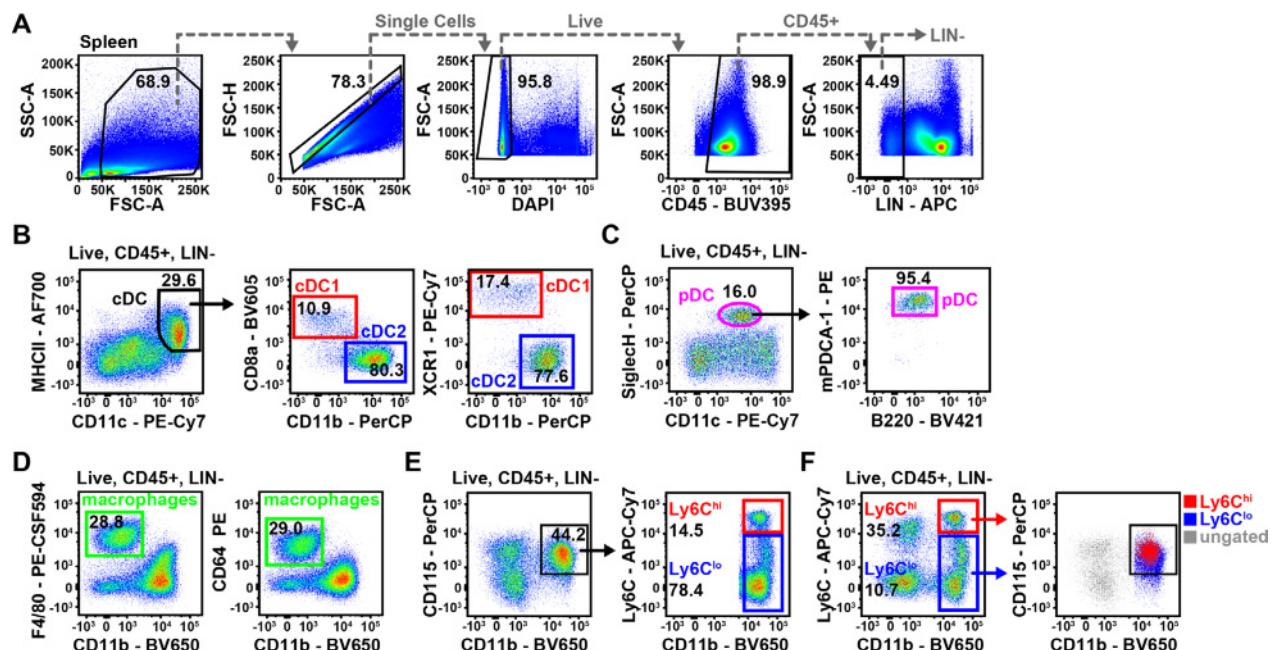
Figure 164. Flow cytometric analysis of mouse spleen DCs, macrophages, and monocytes. Example for basic gating strategy from FSC-A/SSC-A, over doublet exclusion and gating on Live, CD45$^+$ LIN$^-$ cells (defined as CD3/CD19/CD49b/Ly6G$^-$) on a spleen sample (A). Conventional DCs are identified as CD11c^{hi}MHCII$^+$ cells and can be divided into cDC1 (CD8$^+$/XCR1$^+$CD11b$^-$, red gate) and cDC2 (CD8$^-$CD11b$^+$, blue gate) (B). Plasmacytoid DCs are identified as CD11c^{int}SiglecH$^+$ but can also be identified by using B220 or mPDCA-1 (pink gates; C). Red pulp macrophages are identified as CD11b^{lo}F4/80$^+$ or CD11b^{lo}CD64$^+$ (green gate; D). Monocytes are identified as CD115$^+$CD11b$^+$ cells and can be further divided into Ly6C^{lo} and Ly6C^{hi} monocytes (blue and red gates, respectivley; E). Backgating of Ly6C^{lo} and Ly6C^{hi} monocytes that were gated independently of CD115 expression confirms CD115 as a valid marker for both populations (F).

Antibody	Fluorochrome	Clone	Provider	Cat #
MerTK	PE-Cy7	DS5MMER	Invitrogen	25-5751-82
MHCII	Alexa Fluor 700	M5-114.15.2	BioLegend	107622
Ly6C	APC-Cy7	HK1.4	BioLegend	128026
Ly6G	APC	1A8	BioLegend	127614
SiglecF	BV421	E50-2440	BD	562681
SiglecH	PerCP-Cy5.5	551	BioLegend	129614
XCR1	PE	ZET	BioLegend	148204
Streptavidin	PE-Cy7		BioLegend	405206
Streptavidin	PE-CF594		BD	562284
Streptavidin	PerCP-Cy5.5		BioLegend	405214
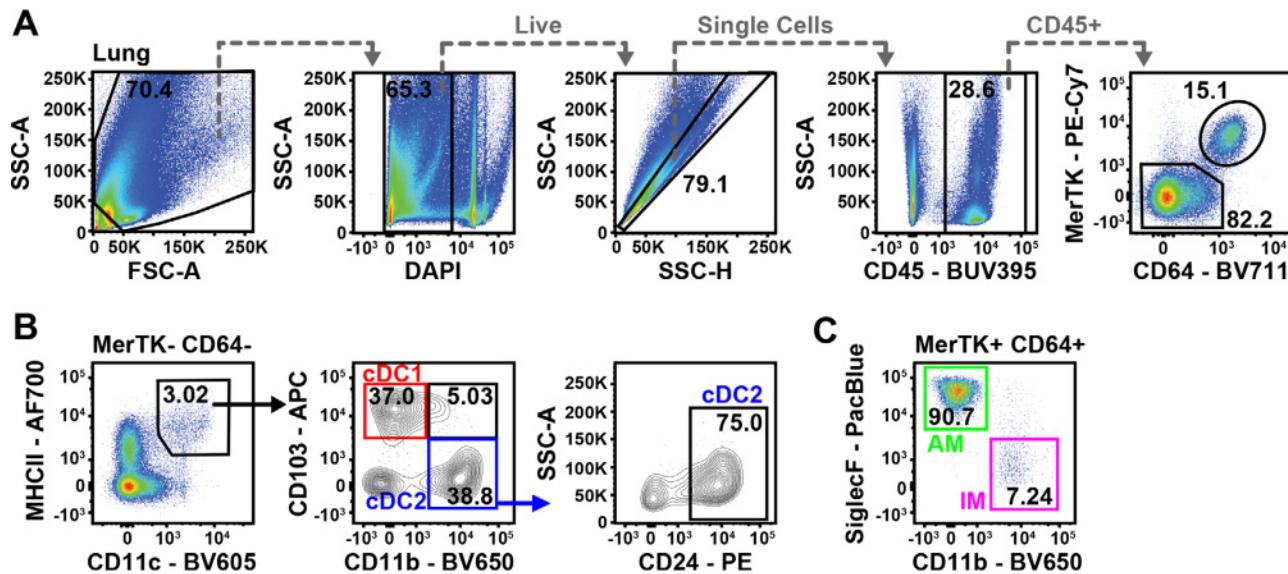
Figure 165. Flow cytometric analysis of mouse lung macrophages and DCs. Example for basic gating strategy from FSC-A/SSC-A, over doublet exclusion and gating on Live, CD45+ cells on a lung sample (A). Conventional DCs are gated as MerTK− CD64− MHCII+ CD11c+ before being identified for cDC1 (red) and cDC2 (blue) (A and B). Macrophages are first gated as MerTK+ CD64+ cells, before being separated into SiglecF+ CD11b− Alveolar Macrophages (AM, green) and SiglecF− CD11b+ Interstitial Macrophages (IM, pink) (A and C).
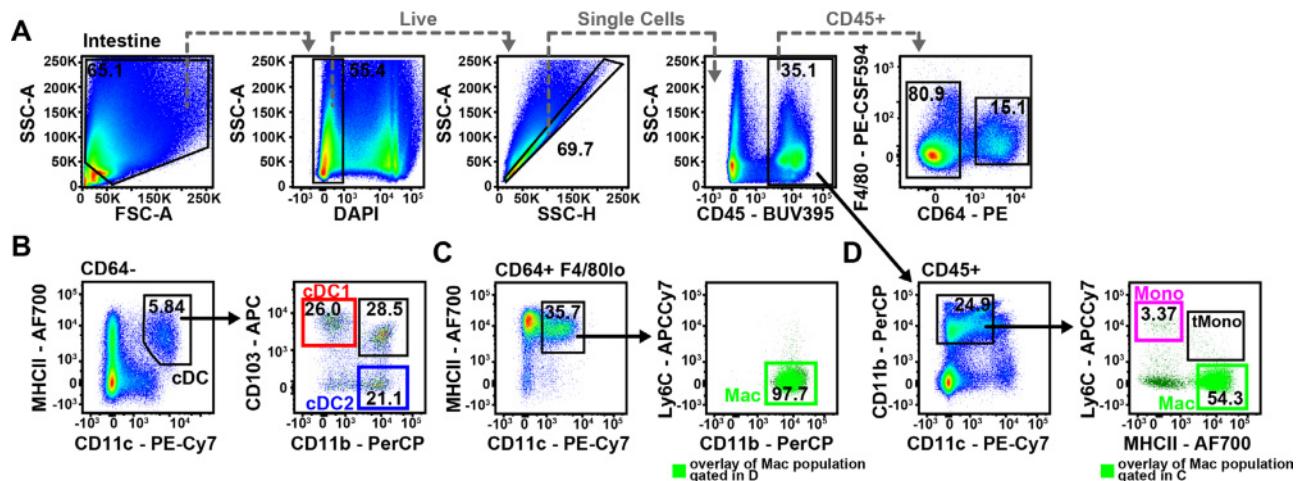
Figure 166. Flow cytometric analysis of mouse small intestine macrophages and DCs. Example for basic gating strategy from FSC-A/SSC-A, over doublet exclusion and gating on Live, CD45+ cells on a small intestine sample (A). Conventional DCs are gated as CD64− MHCII+ CD11c+ before being identified as CD103+ CD11b− cDC1 (red), CD103− CD11b+ cDC2 (blue), and CD103+ CD11b+ "double positive" cDC2 (black) (B). Macrophages can be identified as CD64+ F4/80lo MHCII+ CD11c+ CD11b+ (green) (C) or alternatively can be gated from the CD11b+ CD11clo population. From this gate cells can be split into Ly6Chi MHCII− monocytes (pink), Ly6C+ MHCII+ transitional monocytes (tMono, black) and Ly6C+ MHCII+ macrophages (green; D).
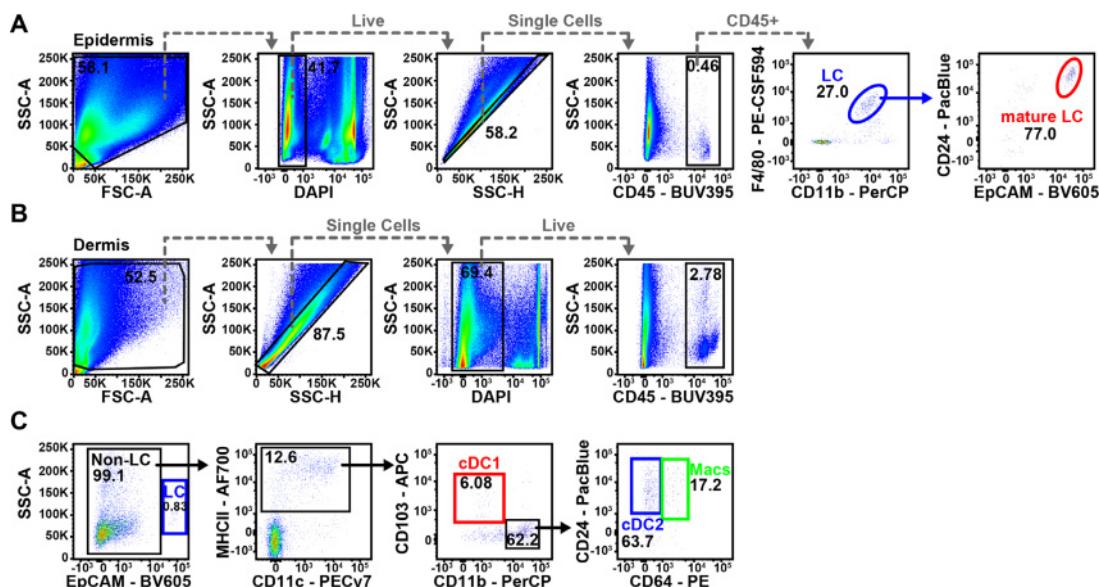
Figure 167. Flow cytometric analysis of mouse skin macrophages and DCs. Example for basic gating strategy from FSC-A/SSC-A, over doublet exclusion and gating on Live, CD45$^+$ cells on an epidermis sample (A). Langerhans cells (LC) are mainly found in the epidermis and are gated as F4/80$^+$ CD11b$^+$ (blue), while mature LC can be further identified by being CD24$^+$ EpCAM$^+$ (red; A). Example for basic gating strategy from FSC-A/SSC-A, over doublet exclusion and gating on Live, CD45$^+$ cells on a dermis sample (B). Conventional DCs are gated as EpCAM$^-$ MHCII$^+$ CD11c$^+$ before being identified as CD103$^+$ CD11b$^-$ cDC1 (red) or CD24$^+$ CD11b$^+$ cDC2 (blue; C) Within this last gate macrophages can be identified as CD64$^+$ cells (green; C).

6.3.3 Human tissue processing materials.

6.3.3.1 General reagents and materials.

Reagent	Manufacturer	Catalog number
Collagenase IV	Sigma	C5138
Worthington's Collagenase, Type IV	Worthington Biochemical	LS004188
DNase I	Roche	10104159001
Dulbecco's Phosphate Buffered Saline (PBS)		
Ficoll-Paque	GE Healthcare	17-1440-02
FCS	Sigma–Aldrich	F2442
L-Glutamine	Sigma–Aldrich	G7513-100ML
LIVE/DEAD^{TM} Fixable Blue Dead Cell Stain Kit	Life Technologies	L23105
Penicillin-Streptomycin	Sigma–Aldrich	F4333
1× RBC Lysis Buffer	eBioscience	00-4333-57
RPMI 1640	HyClone	SH30255.01

Prepare:

- FCM buffer: 2% FCS + 2 mM EDTA in PBS + 0.05% Azide in 1× PBS
- Digestion solution: 0.2 mg/mL collagenase + 0.05 mg/mL of DNase I in RPMI1640 + 10% FCS.

6.3.4 Antibodies for human mononuclear phagocyte identification. see Table 59.

6.3.5 General Remarks.

- All staining procedures in this chapter are described for staining in 5 mL FCM polystyrene tubes (in "lab slang": FACS tubes) but alternatively one may choose to do the staining in 96-well round or V-bottom plates. **Note**: This is very convenient when handling larger numbers of samples (or for in vitro assays where cells where cultured in these plates) but will increase the risk of cross-contamination during staining/washing steps!
- In general, we recommend aspirating any supernatant after centrifugation steps, as this will yield consistent staining results. An alternative method is to discard the supernatant by simply pouring it out. This usually results in a higher loss of cells (as compared to aspirating) and may leave an unknown volume of residual supernatant in the tube that might affect staining efficiency and therefore results! **Fun Fact**: We calculated the time it takes to aspirate larger numbers of FCM tubes containing ~2 mL of buffer. Result: 5 min for 100 tubes ($n = 3$ experiments with 70 to 130 tubes each, SEM ±1 min).
- It is highly recommended to count cell numbers wherever possible (ideally after RBC lysis), so one can calculate absolute numbers of individual cell populations per tissue, once the data are obtained. Depending on your lab
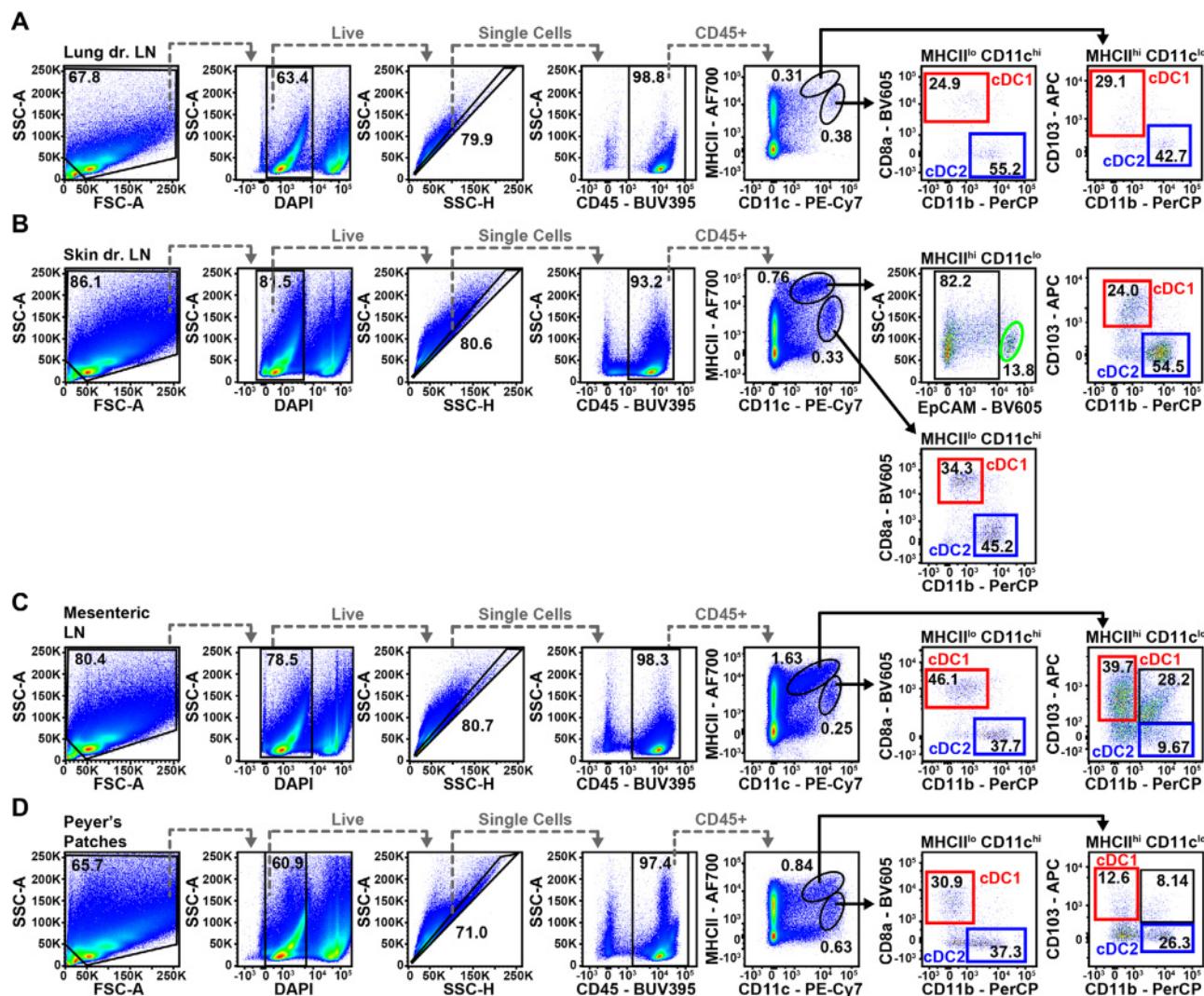
Figure 168. Flow cytometric analysis of mouse lymph node macrophages and DCs in steady-state. Example for basic gating strategy from FSC-A/SSC-A, over doublet exclusion and gating on Live, CD45+ cells on lung draining (dr.) LN sample (A), skin draining LN sample (B), mesenteric LN sample (C) and for Peyer's Patches (D). Generally, migratory cDCs express higher levels of MHCII but lower levels of CD11c on their surfaces as compared to lymphoid resident cDCs (MHCII^{lo} CD11c^{hi}). Lymphoid-resident cDC1 are further gated as CD8+ CD11b− (red), cDC2 as CD8− CD11b+ (blue) (A–D). Migratory cDC1s (MHCII^{hi} CD11c^{lo}) can be identified by their subsequent expression of CD103 (red) while migratory cDC2s are identified as CD103− CD11b+ (blue; A–D). The skin dr. LN migratory fraction further consists of EpCAM+ Langerhans cells (green; B). In the mesenteric LNs and Peyer's Patches the migratory cDC2 population can be divided into CD103− CD11b+ cDC2 (blue) and CD103+ CD11b+ "double positive" cDC2 (black; C and D).

or institute you might have access to, e.g., Neubauer chambers for manual counting, to automatic cell counters or be able to include cell counting beads to your sample (e.g., Count-Bright Absolute Counting Beads, Invitrogen, catalog number C36950). All methods are equally fine and should be chosen by the researcher fitting to their experimental setup/question. We simply recommend to use the same method for all related experiments to gain comparable and consistent results.

- Ab concentrations/dilutions stated in the protocols are meant as a guideline for first-time users and can be used as a starting point. Alternatively, check the manufacturer's recommendations when trying a new Ab. Ideally, the exact concentration needed should be determined by titration.

- Be aware that EDTA may interfere with the staining quality specifically for lectin receptors and you may opt to use an EDTA-free staining buffer.
- In the protocols, 1350 rpm equals roughly 400 × g.

6.4 Step-by-step sample preparation for mouse tissues

6.4.1 Step-by-step sample preparation for mouse blood DCs and monocytes.

1. Collect blood (e.g., from the heart, retro-orbital plexus, facial vein, etc.) and immediately transfer into a sample tube containing either PBS + 10 mM EDTA or heparin (e.g., from Sigma–Aldrich, catalog number H3393). This will prevent

Table 59. Primary and secondary antibodies for staining of human DCs and monocytes/macrophages in different tissues

Target Molecule	Fluoro chrome	Isotype	Clone	Dilution	Provider	Cat#	Target Cell	Target Tissue
Primary ab								
CADM1	Purified	chicken IgY	3E1	1/400	MBL	CM004-3	cDC1	Bl, Sp, Lu, Sk*
CD1a	AF700	mouse IgG2a	NA1/34-HLK	1/20	Novus Bio	NB100-64852AF700	LCs	Sk
CD1c	PE/Cy7	mouse IgG1	L161	1/200	Biolegend	331516	cDC2	Bl, Sp, Lu
CD1c	BV421	mouse IgG1	L161	1/20	Biolegend	331526	cDC1, cDC2	Sk
CD3	BV650	Mouse IgG2a	OKT3	1/20	Biolegend	317324	T cell	Bl, Sp, Lu, Sk
CD5	BV711	mouse IgG1	UCHT2	1/20	BD Biosciences	563170	Early pre-DC	Bl
CD11c	BV605	mouse IgG1	3.9	1/20	Biolegend	301636	cDC2	Sk, Bl, Sp, Lu
CD14	BV711	mouse IgG2a	M5E2	1/20	Biolegend	301838	DCs, Mac	Sk
CD14	ECD	mouse IgG2a	RMO52	1/10	Beckman Coulter	IM2707U	DCs, Mo	Bl, Sp, Lu
CD16	APC/Cy7	mouse IgG1	3G8	1/40	Biolegend	302018	Mo/Mac, NK cell	Bl, Sp, Lu, Sk
CD19	BV650	mouse IgG1	HIB19	1/20	Biolegend	302238	B cell	Bl, Sp, Lu, Sk
CD20	BV650	mouse IgG2b	2H7	1/20	Biolegend	302336	B cell	Bl, Sp, Lu, Sk
CD26	PE/Cy7	mouse IgG2a	BA5b	1/20	Biolegend	302714	cDC1, cDC2	Sk
CD26	PE	mouse IgG2a	BA5b	1/20	Biolegend	302706	cDC1, cDC2	Bl, Sp, Lu
CD45	V500	mouse IgG1	HI30	1/20	BD Biosciences	560777	DCs, Mo/Mac	Bl, Sp, Lu, Sk
CD123	BUV395	mouse IgG2a	7G3	1/40	BD Biosciences	564195	pDC, early pr-DC	Bl, Sp, Lu
CD169 (Siglec-1)	PE/eFluor610	mouse IgG1	7-239	1/20	eBioscience	61-1699-42	Early pre-DC	Bl
HLADR	BV786	mouse IgG2a	L243	1/20	Biolegend	307642	DCs, Mo/Mac	Bl, Sp, Lu, Sk
SIRPa (CD172a)	Purified	mouse IgG1	DH59B	1/400	King Fischer Biotech Inc	WS0567B-100	LCs	Sk
Secondary ab								
anti-Chicken IgY	Alexa Fluor 647	Donkey Fab'2	N/A	1/200	Jackson Immunoresearch	703-606-155	cDC1	Bl, Sp, Lu, Sk

* Bl, blood; Sp, spleen; Lu, lungs; and SK, skin.

blood from coagulating. Place tubes on ice till further processing.

2. Centrifuge at 1350 rpm, 4°C for 4 min.
3. Carefully aspirate supernatant. Try to avoid aspirating the blood and containing cells, as the pellet will be rather fluid.
4. Resuspend pellet in 2 mL of RBC lysis buffer, incubate for 5 min at room temperature.
5. After 5 min stop reaction by adding 10 mL of FCM buffer.
6. Centrifuge at 1350 rpm, 4°C for 4 min.
7. Carefully aspirate supernatant. **Tip**: If the pellet still contains a lot of red blood cells, you might want to repeat RBC lysis step a second time for 3 min. Try avoiding further RBC lysis rounds, as the lysis buffer is very harsh on your immune cells.
8. Resuspend pellet in FCM buffer and transfer $1–10 \times 10^6$ cells to FCM tube for cell surface staining.
9. Centrifuge at 1350 rpm, 4°C for 4 min, aspirate supernatant.
10. Prepare blocking buffer (FCM buffer + 1:50 rat/mouse serum or purified CD16/32 (FC-block)) and cocktail containing all Abs required (dilution as recommended by manufacturer, or 1:100) for primary staining, store in the dark on ice or at 4°C.
11. Add 25 μL of blocking buffer to the pellet, vortex, incubate for 10–15 min in the dark, at 4°C. This will help prevent unspecific binding of subsequently used antibodies.
12. Add 25 μl of Ab cocktail* to the cell suspension, vortex, incubate for 15–30 min in the dark, at 4°C.
13. Add 2–3 mL of FCM buffer to the cell suspension to wash off Ab cocktail.
14. Centrifuge at 1350 rpm, 4°C for 4 min, aspirate supernatant.

15. Optional: If required, add secondary Ab, e.g., fluorochrome-conjugated Streptavidin (dilution 1:300 usually is sufficient), vortex, incubate for 15 min in the dark, at 4°C. Wash off with 2–3 mL of FCM buffer, centrifuge at 1350 rpm, 4°C for 4 min, aspirate supernatant.
16. Resuspend pellet in ~200 μL of FCM buffer containing DAPI (1:200).
17. Proceed to analyze sample on flow cytometer. **Note**: Filter sample using a 70 μm nylon mesh/cell strainer prior acquisition to avoid clogging of the analyzer.

*Staining Abs: CD45 (30-F11), F4/80 (BM8), CD64/FcγRI (X54-5/7.1), MHC Class II IA/IE (M5/114.15.2), CD11c (N418), CD11b (M1/70), Ly6C (HK1.4), CD115 (AFS98), CD24 (M1/69), CD3 (145-2C11), CD19 (eBio1D3), CD49b (DX5), Ly6G (1A8), mPDCA-1 (eBio97), SiglecH (551), B220 (RA3-6B2). Lineage (LIN) consists of CD3, CD19, CD49b (alternatively NK1.1), and Ly6G.

6.4.1.1 Gating for mouse blood DCs and monocytes (Fig. 162). Gating from single, live, $CD45^+$ LIN^- cells:

- Dendritic cells: $CD64^-$, $F4/80^-$, $MHCII^+$, $CD11c^+$

cDC1: $CD8\alpha^+/CD24^+$ $CD11b^-$
cDC2: $CD8\alpha^-$ $CD11b^+$

- pDCs: $CD11c^{int}$ $CD11b^-$ $SiglecH^+$ $mPDCA-1^+$ $B220^+$
- Monocytes: $CD115^+$ $CD11b^+$ $Ly6C^{lo/hi}$

Table 60. Phenotypic characterization of DC subsets in mouse and human tissues

Marker	Peripheral or Migratory cDC1		Lymphoid-resident cDC1		cDC2		Plasmacytoid DCs		Early pre-DC
	Mouse	Human	Mouse	Human	Mouse	Human	Mouse	Human	Human
CD4	−	+	−	+	+	+	+/−	+	+
CD8a	−	−	+	−	−	−	+/−	+/− *2	−
CD9		+		+		+	+/−	+	+
CD11b	−	−	−	−	+	(gut +)	0	−	−
CD11c	+	lo/-	++	lo/-	+	+	int	−	+/−
CD24	+	−	+	−	+	−	−	−	−
CD26	+	+	+	+	+	+ (bl −/+)	+	+	+
CD45	+	+	+	+	+	+	+	+	+
CD64	−	−	−	(spl +)	−	+/−	−	−	−
CD80	+/− *2	−		−	+/− *2	(mat +)	+/− *2	−	−
CD86	+/− *2	+		lo/+	+/− *2	+	+/− *2	lo/+	+
CD103	+	- (gut+)	−	+	−/+ *1	- (gut +)	−	−	−
CD115	−	−	−	−	−	−	−	−	−
CD117	−	+	−	+	−	−	−	−	−
CD169		−		−		−		−	+
CD172a	−	−	−	−	+	+	+	+	int
B220	−	−	−	−	−	−	+	n/a	n/a
CADM1	+	+	+	+	−	−	−	−	−
CCR7	+/− *2	+/− *2	+/− *2	+/− *2	+/− *2	+/− *2	lo/+ *2	+	−
CCR9							+/−		
Clec9a	+	+	+	+	−	−	+/−	−	−
EpCAM	−	−	−	−	−	−	−		
F4/80	−	−		n/a	−/+	n/a	−	n/a	n/a
mPDCA-1	−	−	−	−	−	−	+	n/a	n/a
MHCII *3	+	+	+	+	+	+	+/− *2	+	+
Langerin	- (der +)	−	−	−	−	−	−	−	−
Ly6C	−	−	−	−	−	−	+/−	n/a	n/a
Ly49Q							+/−	n/a	n/a
XCR1	+	−	+	−	−	−	−	−	−
IRF4	−	−	−	−	+	+	+	+	+
IRF8	+	+	+	+	−	−	+	+	+
CD1a	n/a	- (der +)	n/a	−	n/a	- (der +)	n/a	−	−
CD1c	n/a	- (der +)	n/a	−	n/a	+	n/a	−	−
CD14	n/a	−	n/a	−	n/a	−/+	n/a	−	−
CD16	n/a	−	n/a	−	n/a	−	n/a	−	−
CD123	n/a	−	n/a	−	n/a	−	n/a	+	+
CD141	n/a	+	n/a	+	n/a	−	n/a	−	int
CD303	n/a	−	n/a	−	n/a	−	n/a	+	+
CD304	n/a	−	n/a	−	n/a	−	n/a	+	+

bl, blood; der, dermis; int, intermediate; sple, spleen; mat, mature.
n/a: gene coding this protein absent in this species
Not defined
*1: CD103+ CD11b+ DP cDC2 population of gut, mesenteric LN, and Peyer's patches
*2: + upon activation
*3: HLA-DR in humans

Table 61. Phenotypic characterization of monocytes/macrophages in mouse and human tissues

Marker	Classical Monocyte		Intermediate Monocyte		Non-classical Monocyte		Macrophages	
	Mouse	Human	Mouse	Human	Mouse	Human	Mouse	Human
CD11b	+	hi		+	+	lo	+/−	+ (skin)
CD14	(+)	hi		+	(+)	lo		+ (skin
CD16	lo	−		+	+	+		lo/- (skin)
CD43	lo	+		+	hi	+		+
CD45	+	+		+	+	+	+	+
CD62L	+	lo		lo/-	−	−	−	
CD64	−	+		+	−	lo/-	+	+
CD115	+	lo		hi	+	int	+	+
CD169	+/−	+/−			+/−	+/−	+	+
CCR2	+	hi		int	−	−	+/−	−
CX3CR1	int	lo		int	hi	hi	+	
F4/80	−	n/a		n/a	−	n/a	+	n/a
HLA-DR		+		hi		lo		+ (skin)
MerTK	+/−				+/−		+	+
Ly6C	hi	n/a		n/a	lo	n/a	−	n/a
Lyve-1	−				−		+/−	

n/a: gene coding this protein absent in this species
Not defined

6.4.1.2 Top tricks and pitfalls.

- Additionally to CD11b and Ly6C other monocyte marker may be included for further/more detailed separation of Ly6C^{hi} and Ly6C^{lo} monocytes, such as, e.g., CX3CR1, CCR2, or TremL4 (see Table 61; [1452]).

6.4.2 Step-by-step sample preparation for mouse bone marrow DCs, monocytes, and macrophages.

1. Remove femur and tibia from euthanized mouse and, using scissors, free bones from surrounding muscle tissue and tendons. **Tip**: Use a paper towel to gently remove tissue that is stuck to the bones. This will also make it easier to detach the knee to separate femur and tibia, and to detach the foot from the tibia—use a turning/rotating motion to gently remove the foot/knee without breaking the bone.
2. Place clean bones in ice-cold PBS in a six-well plate, on ice, till all tissues have been harvested.
3. To flush out the bone marrow: take bones out of PBS, e.g., place on the inside of the lid of your six-well plate and carefully cut off a tiny bit at both ends of the bone.
4. Fill a 20 ml syringe with ice-cold FCM buffer. Use a 23 G needle to flush out the bone marrow, directly into a 15 mL or 50 mL conical tube. **Note**: This needle size should fit into most mouse bones, allowing to sufficiently flush out all the bone marrow but other G sizes will work just as well. **Tip**: For best results flush bone from both sides, moving the needle up and down within the bone while flushing.
5. Centrifuge at 1350 rpm, 4°C for 4 min.
6. Aspirate supernatant.

7. Thoroughly suspend pellet in about 1 mL of RBC lysis buffer, incubate for 3 min at room temperature. **Note**: You want to reach a single cell suspension at this step to ensure proper RBC lysis. Make sure you have no BM "pieces" left.
8. After 3 min stop reaction by adding 10 mL of FCM buffer. **Note**: You may want to filter the single cell suspension using a 70 μm nylon mesh/cell strainer to remove lose bone particles and clumps.
9. Centrifuge at 1350 rpm, 4°C for 4 min.
10. Resuspend pellet in ice-cold FCM buffer and transfer 1–10 × 10^6 cells to FCM tube for cell surface staining.
11. Centrifuge at 1350 rpm, 4°C for 4 min, aspirate supernatant.
12. Prepare blocking buffer (FCM buffer + 1:50 rat/mouse serum or purified CD16/32 (FC-block)) and cocktail containing all Abs required (dilution as recommended by manufacturer, or 1:100) for primary staining, store in the dark on ice or at 4°C.
13. Add 25 μL of blocking buffer to the pellet, vortex, incubate for 10–15 min in the dark, at 4°C. This will help prevent unspecific binding of subsequently used Abs.
14. Add 25 μl of Ab cocktail* to the cell suspension, vortex, incubate for 15–30 min in the dark, at 4°C.
15. Add 2–3 mL of FCM buffer to the cell suspension to wash off Ab cocktail.
16. Centrifuge at 1350 rpm, 4°C for 4 min, aspirate supernatant.
17. Optional: If required, add secondary Ab, e.g., fluorochrome-conjugated Streptavidin (dilution 1:300 usually is sufficient), vortex, incubate for 15 min in the dark, at 4°C. Wash off with 2–3 mL of FCM buffer, centrifuge at 1350 rpm, 4°C for 4 min, aspirate supernatant.
18. Resuspend pellet in ~200 μL of FCM buffer containing DAPI (1:200).

19. Proceed to analyze sample on flow cytometer. **Note**: Filter sample using a 70 μm nylon mesh/cell strainer prior acquisition to avoid clogging of the analyzer.

*Staining Abs: CD45 (30-F11), F4/80 (BM8), CD64/FcγRI (X54-5/7.1), MHC Class II IA/IE (M5/114.15.2), CD11c (N418), CD11b (M1/70), Ly6C (HK1.4), CD115 (AFS98), MerTK (DS5MMER), CD24 (M1/69), CD3 (145-2C11), CD19 (eBio1D3), CD49b (DX5), Ly6G (1A8), mPDCA-1 (eBio97), SiglecH (551), B220 (RA3-6B2). LIN consists of CD3, CD19, CD49b (alternatively NK1.1), and Ly6G.

6.4.2.1 Gating for mouse bone marrow DCs/monocytes/macrophages (Fig. 163). Gating from single, live, CD45$^+$ LIN$^-$ cells:

- Dendritic cells: CD64$^-$, F4/80$^-$, MHCII$^+$, CD11c$^+$

cDC1: CD8α$^+$/CD24$^+$ CD11b$^-$
cDC2: CD8α$^-$ CD11b$^+$

- pDCs: CD11c^{int} CD11b$^-$ SiglecH$^+$ mPDCA-1$^+$ B220$^+$
- Macrophages: F4/80$^+$ CD11b$^+$ MerTK$^+$ CD64$^+$
- Monocytes: CD115$^+$ CD11b$^+$ Ly6C$^{lo/hi}$

6.4.2.2 Top tricks and pitfalls.

- Cytokine receptors such as CSF-1R (CD115) are often shed off if samples are treated too harsh or processed over long periods or even internalized. Avoid receptor shedding/internalization by working quickly and keeping samples chilled.
- If working with frozen/thawed bone marrow samples one may incubate the freshly thawed samples in RPMI1640 for 6 h at 37°C to allow for proper expression of cell surface receptors. This will improve staining results.
- When gating on pDCs in the bone marrow, it is advisable to include SiglecH, mPDCA-1 and B220, as SiglecH also labels pDC progenitors, which either do not or only express low levels of B220 and mPDCA-1 yet.
- Inclusion of CD117 into the panel, followed by gating on CD117$^-$ LIN$^-$ cells prior the monocyte gating can lead to a better resolution of these populations.

6.4.3 Step-by-step sample preparation for mouse spleen DCs, monocytes, and macrophages.

- Harvest spleen from euthanized mouse and place in ice-cold PBS in a six-well plate, on ice, till all tissues have been harvested.
- Prepare digestion buffer (as described in reagents list), keep at room temperature.
- Aliquot 2 mL of digestion buffer into a fresh well in a six-well plate.

- Take spleen out of PBS, quickly dry off on clean paper towel, if necessary remove fat and place spleen in digestion buffer.
- Use fine tweezers (or scissors) to tear spleen into very fine pieces.
- Incubate in digestion buffer at 37°C for 30 min.
- Stop digestion by adding 3 mL of PBS + 10 mM EDTA.
- Carefully, but thoroughly, pipette spleen suspension up and down using either a 5 mL pipette or a 18 G needle with a 5 mL syringe, up to 20 times to gain a single cell suspension.
- Transfer spleen cell suspension over a 70 μm nylon mesh/cell strainer into a 50 mL conical tube.
- Centrifuge at 1350 rpm, 4°C for 4 min.
- Aspirate supernatant.
- Thoroughly suspend pellet in about 1 mL of RBC lysis buffer, incubate for 3 min at room temperature.
- After 3 min stop reaction by adding 10 ml of FCM buffer.
- Centrifuge at 1350 rpm, 4°C for 4 min.
- Resuspend pellet in ice-cold FCM buffer and transfer 1–10 × 10^6 cells to FCM tube for cell surface staining.
- Centrifuge at 1350 rpm, 4°C for 4 min, aspirate supernatant.
- Prepare blocking buffer (FCM buffer + 1:50 rat/mouse serum or purified CD16/32 (FC-block)) and cocktail containing all Abs required (dilution as recommended by manufacturer, or 1:100) for primary staining, store in the dark on ice or at 4°C.
- Add 25 μL of blocking buffer to the pellet, vortex, incubate for 10–15 min in the dark, at 4°C. This will help prevent unspecific binding of subsequently used antibodies.
- Add 25 μL of Ab cocktail* to the cell suspension, vortex, incubate for 15–30 min in the dark, at 4°C.
- Add 2–3 mL of FCM buffer to the cell suspension to wash off Ab cocktail.
- Centrifuge at 1350 rpm, 4°C for 4 min, aspirate supernatant.
- Optional: If required, add secondary Ab, e.g., fluorochrome-conjugated Streptavidin (dilution 1:300 usually is sufficient), vortex, incubate for 15 min in the dark, at 4°C. Wash off with 2–3 mL of FCM buffer, centrifuge at 1350 rpm, 4°C for 4 min, aspirate supernatant.
- Resuspend pellet in approximately 200 μL of FCM buffer containing DAPI (1:200).
- Proceed to analyze sample on flow cytometer. **Note**: Filter sample using a 70 μm nylon mesh/cell strainer prior acquisition to avoid clogging of the analyzer.

*Staining Abs: CD45 (30-F11), F4/80 (BM8), CD64/FcγRI (X54-5/7.1), MHC Class II IA/IE (M5/114.15.2), CD11c (N418), CD11b (M1/70), Ly6C (HK1.4), CD115 (AFS98), CD8α (53-6.7), XCR1 (ZET), CD3 (145-2C11), CD19 (eBio1D3), CD49b (DX5), Ly6G (1A8), mPDCA-1 (eBio97), SiglecH (551), B220 (RA3-6B2). LIN consists of CD3, CD19, CD49b (alternatively NK1.1), and Ly6G.

6.4.3.1 Gating for mouse spleen DCs/monocytes/macrophages. Gating from single, live, CD45$^+$ LIN$^-$ cells:

- Dendritic cells: CD64$^-$, F4/80$^-$, MHCII$^+$, CD11c$^+$

cDC1: CD8α$^+$ CD11b$^-$ or XCR1$^+$ CD11b$^-$
cDC2: CD8α$^-$ CD11b$^+$

- pDCs: CD11c^{int} CD11b$^-$ SiglecH$^+$ mPDCA-1$^+$ B220$^+$
- Macrophages: F4/80$^+$ CD11b$^+$
- Monocytes: CD115$^+$ CD11b$^+$ Ly6C$^{lo/hi}$

6.4.3.2 Top tricks and pitfalls.

- Note that this protocol will yield mainly red pulp macrophages, while other splenic macrophages subsets such as marginal zone macrophages are more difficult to isolate. These can be better identified by inclusion of a Tim4 Ab into the panel [1453].
- cDC1 traditionally were identified using CD8α but we highly recommend the use of XCR1 instead, as this marker is more specific than CD8α and yields a better discrimination of cDC1 from cDC2 (as can be seen in **Figure** 164) [1437, 1454, 1455].

6.4.4 Step-by step sample preparation of mouse lung macrophages/DCs.

1. Thoroughly perfuse freshly euthanized mouse intracardially with cold PBS, and harvest lungs into a 12-well plate containing cold PBS, on ice.
2. Place individual lung samples into 1.5 mL microcentrifuge tube containing 500 μL of digestion solution **1**.
3. Mince lung into small pieces using fine scissors (in the tube).
4. Transfer to 12-well plate containing additional 1–1.5 mL digestion solution (final volume 1.5–2 mL of digestion solution **1**).
5. Incubate at 37°C for 30 min.
6. Homogenize minced and digested sample using a 18 G syringe needle and 3 mL syringe and filter through 70 μm cell strainer (you may use the syringe plunger to push tissue through the strainer) into 50 mL conical tube.
7. Wash remaining cells from strainer with 20 mL FCM buffer.
8. Centrifuge at 400 × *g* for 5 min, at 4°C
9. Lyse any remaining erythrocytes by resuspending cell pellet in 500 μL of RBC lysis buffer for 3 min, at room temperature. Then stop reaction by topping up with FCM buffer.
10. Centrifuge at 400 × *g* for 5 min, at 4°C
11. Resuspend pellet in FCM buffer.
12. Filter cell suspension again through a 70 μm cell strainer to remove any clumps that may have formed after erythrocyte lysis and transfer cells to FCM tube.
13. Resuspend the appropriate number of cells (e.g., 1–10 × 10^6 cells) in FCM staining buffer (see 6.2.2.1) containing the required Abs* and incubate in the dark at 4°C.
14. Wash with FCM buffer.
15. Centrifuge at 400 × *g* for 5 min, at 4°C
16. Resuspend cells in an appropriate amount of FCM buffer.
17. Filter with 70 μm nylon mesh into a new (clean) FCM tube and analyze sample in FCM cell sorting machine.

*Staining Abs: CD45 mAb (30-F11), CD64/FcγRI mAb (X54-5/7.1), SiglecF (E50-2440), MerTK (DS5MMER), MHC Class II IA/IE mAb (M5/114.15.2), CD24 (M1/69), CD11c mAb (N418), XCR1 mAb (ZET) or CD103 mAb (2E7), SIRPα/CD172a mAb (P84) or CD11b mAb (M1/70), and Ly6C mAb (HK1.4).

6.4.4.1 Gating for mouse lung macrophages/DCs.   Gating from single, live, CD45$^+$ cells:

- Alveolar macrophages (AMs): CD64$^+$, MerTK$^+$, SiglecF$^+$, CD11b$^-$
- Interstitial macrophages (IMs): CD64$^+$, MerTK$^+$, SiglecF$^-$, CD11b$^+$
- Dendritic cells: CD64$^-$, MerTK$^-$, MHCII$^+$, CD11c^{hi}

cDC1: XCR1/CD103$^+$, SIRPα/CD11b$^-$
cDC2: XCR1/CD103$^-$, SIRPα/CD11b$^+$, CD24$^+$

6.4.4.2 Top tricks and pitfalls.

- The two major macrophage populations in the mouse steady-state lung are the AMs and IMs. They express MerTK$^+$ CD64$^+$, but can also be differentiated from each other according to differences in SiglecF, MHCII, CD11c, and CD11b expression. Further markers like Lyve-1 and others (not included in the example FCM plots) have been shown to be very useful for AM versus IM discrimination [1456, 1457].
- In addition, if the configuration of the used flow cytometer allows for it, a "blank" channel (e.g., the FITC channel) is useful for discriminating "auto-fluorescent" AMs from non-autofluorescent IMs.
- Note that "aggressive" perfusion can lead to loss of alveolar resident cells.
- Two major conventional DC subsets in the lung are cDC1 and cDC2. cDC1s express XCR1 and CD103, while cDC2s express CD172α/SIRPα or CD11b, and CD24 [1437, 1456, 1458]. A minor fraction of CD103/CD11b-double-positive cDC2 can be found as well (Figure 165).

6.4.5 Step-by-step sample preparation of mouse intestinal macrophages/DCs.

1. From a freshly euthanized mouse, open up the abdominal cavity by dissecting through the skin and peritoneal membrane in a line along the ventral midline.
2. Remove the intestinal tract by dissecting the small intestine just after the pyloric sphincter, dissecting the colon by sectioning it as caudally as possible, and then carefully lift the intestines out while severing any places of attachment to the abdominal cavity and other organs.
3. Place the dissected intestine into six-well plate with cold PBS on ice. **Note**: At this point you may retrieve the mesenteric LNs from the mesenteric fat for analysis, if desired.

4. Remove as much attached mesenteric fat from intestines as possible, pulling the fat from one end and following through to the other end until the intestines have been linearized.

5. Follow the following steps for cleaning the fecal content of small intestine and colon, respectively:

   (a) For the small intestine: Dissect just above the caecum, retrieve the Peyer's Patches that lie along the length of the intestine by either cutting or plucking them (they can be analyzed separately or discarded), open the lumen lengthwise with scissors, and wash away fecal content from the opened small intestine in a beaker containing cold PBS before sectioning washed small intestine into 0.5–1 cm long pieces and placing into 50 m conical tube.

   (b) For the colon: Separate away from the cecum (discard the cecum), use two pairs of forceps to squeeze solid fecal content out of the lumen, open the lumen lengthwise wish scissors, and wash away remaining fecal content from the opened colon in beaker containing cold PBS before placing washed colon into a 50 mL conical tube.

6. Add 25 mL of cold PBS into the 50 mL conical tube with the washed intestinal sections and place on ice while completing previous steps for other samples.

7. Vigorously shake the intestinal sections in 50 mL conical tube with cold PBS to get rid of the mucus for around 10 s each round (four rounds with fresh cold PBS each round for small intestine, only once for colon).

8. Put the washed pieces into a new 50 mL conical tube and keep on ice while completing the wash step(s) for other samples.

9. When all samples are ready, add 10–12.5 mL of epithelial dissociation buffer to each sample and incubate for 20 min at 37°C in an orbital shaker set to 250 rpm.

   (a) During this incubation prepare two Petri dishes, one clean and the other filled with cold PBS, and 1.5 mL microcentrifuge tubes with 300–500 μL of digestion buffer **1** (for small intestine) or digestion buffer **2** (for colon).

   (b) If the epithelial compartment is to be retained, prepare the additional 50 mL conical tubes and cell strainers for collection.

10. Dilute epithelium dissociation buffer with 25 mL of cold PBS and shake vigorously for 10 s in the 50 mL conical tube.

11. Pour out the tube contents into the first clean Petri dish (or through a cell strainer into an additional 50 mL conical tube if the epithelium compartment is to be retained for further analysis).

12. Transfer the pieces to the second Petri dish with cold PBS and move them around to wash away traces of DTT/EDTA and epithelium cells.

13. Dry briefly on a piece of tissue before transferring the tissue pieces to the 1.5 mL microcentrifuge tube with the appropriate digestion buffer.

14. Mince tissue into small pieces with fine scissors, and then pour into six-well plate, washing out the remaining tissue from the microcentrifuge tube with digestion solution **1** (to a final volume of 2.5–3 mL in the well).

15. Incubate for 45 min at 37°C. **Note**: Some protocols state that agitation at this step will enhance the digestion process but usually this does not have any effect on digestion efficiency.

16. Homogenize minced digested sample with 18 G syringe needle and 3 mL syringe and filter through a 70 μm cell strainer (you may use the syringe plunger to push tissue through the strainer) into the final 50 mL conical tube.

17. Centrifuge at $400 \times g$ for 5 min, at 4°C.

18. If cell pellet is still loose after centrifugation, repeat step 17.

19. Resuspend pellet in FCM buffer* (see Top Tricks and Pitfalls below)

20. Resuspend the appropriate number of cells in FCM staining buffer (see 6.2.2.1) containing the Abs[1], incubate in the dark at 4°C.

21. Wash with FCM buffer.

22. Centrifuge at $400 \times g$ for 5 min, at 4°C.

23. Resuspend cells in an appropriate amount of FCM buffer.

24. Filter with 70 μm nylon mesh into a new, clean FCM tube and analyze sample using a FCM cell sorting machine.

[1]Staining Abs: CD45 mAb (30-F11), F4/80 mAb (BM8), CD64/FcγRI mAb (X54-5/7.1), MHC Class II IA/IE mAb (M5/114.15.2), CD11c mAb (N418), CD103 mAb (2E7), CD11b mAb (M1/70), Ly6C mAb (HK1.4).

6.4.5.1 Gating for intestinal macrophages/DCs. Gating from single, live, CD45$^+$ cells:

- Macrophages (Mac): CD64$^+$, F4/80^{lo}, CD11b$^+$, CD11c^{lo}, Ly6C$^-$, MHCII$^+$
- Monocytes (Mono): CD11b$^+$, CD11c^{lo}, MHCII$^-$, Ly6C$^+$
- Transitional Monocytes (tMono): CD11b$^+$, CD11c^{lo}, MHCII$^+$, Ly6C$^+$ [1459]
- Dendritic cells: CD64$^-$, MHCII$^+$, CD11c$^+$

cDC1: CD103$^+$, CD11b$^-$
cDC2: CD103$^-$, CD11b$^+$
DPs: CD103$^+$, CD11b$^+$

6.4.5.2 Top tricks and pitfalls.

- *At this point, some protocols opt to perform a 45/65% [1460] or 45/70% [1461] Percoll separation to further enrich for macrophages and DCs while removing debris. However, in our experience (and previously reported by [1462], cell yield is greatly reduced when this step is performed.
- The processing of both small intestine and large intestine for the purpose of analyzing macrophages/DCs in the lamina propria (LP) is detailed here. There are little to no macrophages/DCs in the gut epithelium compartment at steady state, hence in this protocol the dissociated epithelium is normally discarded. However, if desired, simple modifications that are mentioned here can be made to the protocol to retain the dissociated epithelium for separate analysis

- The intestinal LP contains a substantial population of eosinophils; exclusion of these can be achieved by inclusion of SiglecF (an eosinophil-specific marker) and CD64 (LP macrophage specific) into the panel. Monocyte-derived macrophages can be further gated using Ly6C [1463].
- Tim4 can be a useful marker to be added, for further delineation of macrophage populations [1453].
- There are three main subsets of lamina propria DCs: cDC1, cDC2, and an intestine-specific subset of "double positive" CD103$^+$ CD11b$^+$ DP cDC2 (Fig. 166). While in some publications intestinal cDC1 are delineated from cDC2 using XCR1 and SIRPα [1437], these markers alone are not sufficient to delineate the DP cDC2 fraction from the CD103$^-$ CD11b$^+$ cDC2.
- In general, inclusion of a lineage channel containing B, T, or neutrophil markers (e.g., CD19, CD3, Ly6G, respecitively) and gating on LIN$^-$ cells prior gating on mononuclear phagocytes might lead to a cleaner separation of these populations and will lower the risk of contamination with other cell types.

6.4.6 Step-by-step sample preparation of mouse skin (ears).

1. Harvest ears from euthanized mouse by dissection with a fine scissors.
2. The following steps depend if total skin is analyzed, or if the epidermis and dermis are analyzed separately:
   (a) If processing total skin, proceed to place ears directly into digestion solution 1 and mince into small pieces using a pair of fine scissors, and then proceed on with step 7.
   (b) If analyzing the epidermis and dermis separately proceed on to step 3.
3. Using two pairs of fine forceps, split each ear into dorsal and ventral halves to expose the inner dermal layer.
4. Float the ear halves dermis side down in 3 mL of Dispase solution/well in 6-well plate, ensuring that they are sufficiently spread out on the solution surface.
5. Incubate for 1 h at 37°C.
6. Place each ear half on a suitable clean flat surface (polystyrene dish or lid, stainless steel tray, or a dark ceramic tile are all suitable) dermis side down.
7. In order to separate epidermis and dermis, carefully scrape the epidermis from the dermis using forceps and wash the dermis thoroughly in PBS or medium to remove any remaining epidermis.
8. Using forceps, place tissues into microcentrifuge tubes containing 500 μL digestion solution **1**, and mince into small pieces with fine scissors.
9. Pour out the cut up tissue into a 12-well plate and wash remaining minced tissue into same well using an additional 1 mL of digestion solution **1** (final volume 2 mL)
10. Incubate for 1 h at 37°C.
11. Homogenize with 3 mL syringe and 18 G needle and siphon it through 70 μm nylon mesh into FCM tube, using a 1 mL pipette tip as a funnel.
12. Centrifuge at 400 × *g* for 5 min, at 4°C.

13. Resuspend the cell pellet in FCM staining buffer (see 6.2.2.1) containing the Abs*, incubate in the dark at 4°C.
14. Wash with FCM buffer.
15. Centrifuge at 400 × *g* for 5 min, at 4°C.
16. Resuspend cells in an appropriate amount of FCM buffer.
17. Filter with 70 μm nylon mesh into a new, clean FCM tube, and analyze sample using a FCM cell sorting machine.

*Staining Abs: CD45 mAb (30-F11), F4/80 mAb (BM8), CD64 mAb (X54-5/7.1), MHC Class II IA/IE mAb (M5/114.15.2), CD11c mAb (N418), XCR1 mAb (ZET) or CD103 mAb (2E7), SIRPα/CD172a mAb (P84) or CD11b mAb (M1/70), EpCAM mAb (G8.8).

6.4.6.1 Gating for mouse skin macrophages/DCs.   Gating from single, live, CD45$^+$ cells:

- LCs: F4/80$^+$, CD11b$^+$, EpCAM$^+$
- Dendritic cells: MHCII$^+$, CD11c$^+$

cDC1 – CD103$^+$, CD11b$^-$
cDC2 – CD103$^-$, CD11b$^+$, CD24$^+$, CD64$^-$

- Macrophages (Mac): CD64$^+$, CD11c^{lo}, MHCII$^+$

6.4.6.2 Top tricks and pitfalls.

- This protocol can be used for analysis for total skin, or the epidermis and dermis separately. However, each method comes with its own drawbacks. Total skin preparations tend to have significantly less Langerhans cells (LCs) but better yield of DCs. Separation of the epidermis and dermis has good yield of LCs in the epidermal compartment, but results in a decreased yield of dermal DCs in the dermal compartment.
- Various methods whereby different enzymes are used for processing mouse skin have been reported [1464–1466]. The effect certain enzymes can have on the surface expression of some markers should be considered.
- LCs are the main macrophage population in the epidermis. LCs express numerous markers including F4/80, CD11b, EpCAM, Langerin, and CD24 [1467, 1468]. However, EpCAM alone is sufficient to distinguish them from other CD45$^+$ cells in the skin if there are limitations to machine configuration.
- Do note that some populations of mouse DCs express Langerin as well [1467]. The dermis may contain some migratory LCs and these can be identified using EpCAM [1469] before gating for dermal cDC1 and cDC2 (Fig. 167).

6.4.7 Sample preparation of mouse LNs.

1. Harvest lymph nodes of interest from euthanized mouse into 12-well plate with 1 mL of RPMI + 10% FCS in each well.

2. Add 1 mL of 2× concentrated digestion solution **1** (=digestion solution **3**; hence, the final digestion solution will be 1× working concentration).

3. Tear apart lymph nodes in the well and digestion solution using two 25 G needles mounted on 1 mL syringes.

4. Incubate for 30 min at 37°C.

5. Homogenize with 3 mL syringe and 18 G needle and siphon it through 70 μm nylon mesh into FCM tube, using a 1 mL pipette tip as a funnel.

6. Centrifuge at 400 × *g* for 5 min, at 4°C.

7. Resuspend the cell pellet in FCM staining buffer (see Section 6.3.1.1) containing the Abs*, incubate in the dark at 4°C.

8. Wash with FCM buffer

9. Centrifuge at 400 × *g* for 5 min, at 4°C.

10. Resuspend cells in an appropriate amount of FCM buffer

11. Filter with 70 μm nylon mesh into a new, clean FCM tube and analyze sample using a FCM cell sorting machine

*Staining antibodies: CD45 mAb (30-F11), MHC Class II IA/IE mAb (M5/114.15.2), CD11c mAb (N418), XCR1 mAb (ZET), or CD103 mAb (2E7) and CD8α mAb (53-6.7), SIRPα/CD172a mAb (P84) or CD11 mAb (M1/70).

Additional staining Abs: EpCAM mAb (G8.8) for skin draining LNs.

6.4.7.1 Gating for mouse LN DCs. Gating from single, live cells:

- Migratory DCs: CD45$^+$, MHCII$^+$, CD11c$^+$
- Migratory cDC1: XCR1/CD103$^+$, SIRPα/CD11b$^-$
- Migratory cDC2: XCR1/CD103$^-$, SIRPα/CD11b$^+$
- Migratory LCs: EpCAM$^+$
- Migratory intestinal DP cDC2: CD103$^+$, SIRPα/CD11b$^+$
- Lymphoid resident DCs: CD45$^+$, MHCII$^+$, CD11c$^+$
  Lymphoid resident cDC1: XCR1/CD8a$^+$, SIRPα/CD11b$^-$
- Lymphoid resident cDC2: XCR1/CD8a$^-$, SIRPα/CD11b$^+$

6.4.7.2 Top tricks and pitfalls.

- This protocol is used to digest all LNs including Peyer's patches.
- As LNs are small pieces of tissue, we opted to do digest the LNs in the same well they are harvested into, to avoid the need to transfer LNs into a separate plate for digestion.
- Also, as LNs are highly concentrated in lymphocytes, it is recommended not to stain too many cells (especially in the case of mesenteric LNs and Peyer's patches) to avoid saturating the Ab staining mix.
- Further, inclusion of a lineage channel containing, e.g., B, T, NK cell, or neutrophil markers (e.g., CD19, CD3, CD49b/NK1.1, or Ly6G, respecitively) and gating on LIN$^-$ cells prior gating on mononuclear phagocytes might lead to a cleaner separation of these populations and will lower the risk of contamination with other cell types.

- Mouse lymph nodes at steady-state contain two fractions of conventional DCs. The first fraction are migratory DCs that come from the peripheral tissues and express high levels of MCHII and lower levels of CD11c, and can be further split into cDC1 and cDC2 subsets using similar markers used for gating peripheral tissue DCs [1430]. The second fraction are lymph node resident conventional DCs, which express high levels of CD11c and lower levels MHCII, are also comprised of cDC1 and cDC2, and are gated using either XCR1 or CD8a, and SIRPα or CD11b for cDC1 and cDC2, respectively [1430] (Figure 168).

6.5 Step-by-step sample preparation for human tissues

6.5.1 Step-by-step sample preparation for human blood DCs, monocytes, and macrophages. Critical: This protocol is designed for 10 ml of human blood. If working with lower blood volumes ensure to keep the appropriate ratio for blood versus PBS versus Ficoll-paque.

1. Aliquot 10 mL of Ficoll-paque (pre-warmed to RT) into a 50 mL conical tube.

2. Dilute 10 mL of blood with PBS to a final volume of 40 mL.

3. Carefully layer the 40 mL of diluted blood on top of the Ficoll-Paque layer.

4. Centrifuge at 1800 × *g* for 25 min, at room temperature. Critical: set centrifuge to acceleration = 0 - 1 and brake = 0 - 1.

5. Collect the PBMC layer, which is found at the Plasma (PBS)–Ficoll interface, and transfer it into a 50 mL conical tube. Top up with PBS to a final volume of 50 mL.

6. Centrifuge at 365 × *g* for 5 min, at 4°C. Critical: set centrifuge to maximum acceleration and maximum brake.

7. Aspirate the supernatant.

8. Re-suspend the pellet in 1 mL of RBC lysis buffer, incubate for 5 min, at room tempertaure in the dark.

9. Top up with PBS to a final volume of 50 mL

10. Centrifuge at 365 × *g* for 5 min, at 4°C.

11. Aspirate the supernatant and re-suspend the pellet (which contains the immune cells) in 1 mL of PBS.

12. Transfer cells into a 1.5 mL microcentrifuge tube, perform cell count, and proceed with staining protocol as described in **6.4.5**.

6.5.2 Step-by-step sample preparation for human spleen DCs, monocytes, and macrophages.

1. Prepare 20 mL of digestion buffer (see Section 6.3.3.1).

2. Transfer spleen sample into 2 mL microcentrifuge tube containing 0.5 mL of the digestion solution. Using a small sterile pair of scissors mince spleen tissue into small pieces.

3. Transfer the tissue suspension into one well of a six-well plate and add on 4 mL (per well) of the digestion solution.

4. Incubate for 1 h at 37 °C.

5. Pipette up and down –six to eight times with a 10 mL disposable transfer pipette in order to disrupt the remaining tissue/gain a single cell suspension, and transfer suspension over a 70 μm cell strainer into a 50 mL conical tube. Rinse the well with PBS and add to cell suspension in the 50 mL conical tube (via filter; to ensure minimum cell loss). Adjust the volume of the suspension with PBS to a total of 50 mL.

6. Centrifuge at 365 × g for 5 min, at 25°C.

7. Aspirate supernatant and re-suspend the pellet in 40 mL of PBS, to achieve a proper dilution of the spleen cell suspension.

8. Aliquot 10 mL of pre-warmed (room temperature) Ficoll-paque into a new (clean) 50 mL conical tube.

9. Carefully transfer the 40 mL of the diluted spleen cell suspension as a top layer onto the 10 mL of pre-warmed (room temperature) Ficoll-paque.

10. Follow steps 4–12 from Chapter 6.5.1 (Sample preparation for human blood DCs, monocytes and macrophages).

6.5.3 Step-by-step sample preparation for human lung DCs, monocytes, and macrophages.

1. Follow Steps 1–7 from Chapter 6.5.2 (Sample preparation for human spleen DCs, monocytes, and macrophages).

2. Then, follow Steps 4–12 from Chapter 6.5.1 (Sample preparation for human blood DCs, monocytes and macrophages).

6.5.4 Step-by-step sample preparation for human skin (epidermis) DCs, monocytes, and macrophages. Critical: Skin should be immediately immersed in RPMI1640 upon collection and incubated on ice until further processing.

1. Cut skin into strips (1 × 5–10 cm) using disposable scalpels, in a large petri dish.

2. Cover circular Styrofoam with a rubber mat and place a sterile silicon mat on top.

3. Pin down the skin longitudinally at one end with 2 × 25 G needles, keeping it stretched while pulling down from the other end.

4. Shave skin using a Goulian knife by applying a side-to-side slow motion, to make it thinner. Critical: Blades should not be re-used (to avoid contamination).

5. Spread shaved strips in a 15 cm Petri dish containing 50 mL of RPMI1640 supplemented with: 10% FCS, 1% L-glutamine, 1% Pen/Strep, 0.8 mg/mL Worthington's collagenase (1×), and 0.05 mg/mL DNase.

6. Cut the skin strips into pieces of 1 cm² and incubate them for a minimum of 18 h, at 4°C.

7. Pipette up and down for about –eight to ten times using a 10 mL disposable transfer pipette, in order to disrupt the epidermis and dermis layers. Filter through a 70 μm cell strainer into a 50 mL conical tube. Rinse the Petri dish with PBS and add through filter to cell suspension to ensure minimum loss of cells.

8. Adjust volume of the skin cell suspension with PBS, to a total of 50 mL.

9. Follow steps 6–12 from Chapter 6.5.1 (Sample preparation for human blood DCs, monocytes, and macrophages).

6.5.5 Staining for human DCs and monocytes/macrophages from different tissues. Notes:

- The following protocol is used for staining DCs and monocytes/macrophages (optimal 1–5 × 10^6 cells/tube for staining) isolated from human blood (see Section 6.5.1), spleen (see Section 6.5.2), lungs (see Section 6.5.3), and skin (see Section 6.5.4).
- For Abs and reagents, see Table 59
- Staining can be performed either in a 1.5 mL microcentrifuge tube or a V-shaped 96-well plate (non-culture-treated).

1. Aliquot required number of cells, and centrifuge at 650 × g for 2 min, at 4°C.

2. Aspirate/discard the supernatant and re-suspend the cell pellet in 1 mL of PBS containing Live/Dead blue dye (1:1000), incubate for 20 min, at 4°C in the dark.

3. Add human AB serum or FCS, at a final dilution of 5%, and incubate for 15 min, at 4°C in the dark, in order to block FC receptors on the immune cells and to neutralize free Live/Dead molecules that bind protein N-terminal amines. **Tip**: During the incubation time for steps 2 and 3 prepare the Ab pre-mix at final dilutions as described in Table 59.

4. Add 200 μL of FCM buffer and centrifuge at 650 × g for 2 min, at 4°C.

5. Aspirate/discard the supernatant and re-suspend the cell pellet in 50 μL of Ab pre-mix. Incubate for 30 min, at 4°C in the dark.

6. Add 200 μL of FCM buffer, and centrifuge at 650 × g for 2 min, at 4°C.

7. Aspirate/discard the supernatant, then:
   (a) For staining monocytes/macrophages: proceed to step 9.
   (b) For staining DCs: since a purified Ab is used to stain CADM1 you will need to perform an additional staining step, as described in step 8 before proceeding to step 9.

8. Re-suspend the cell pellet in 50 μL of FCM buffer containing anti-Chicken-IgY-Alexa-Fluor 647. Incubate for 15 min, at 4°C. Then add 200 μL of FCM buffer and centrifuge at 650 × g for 2 min, at 4°C. Aspirate/discard the supernatant.

9. Re-suspend the cell pellet in 200–400 μL of FCM buffer, filter through a 70 μm cell strainer into a new (clean) FCM tube and analyze using a suitable flow cytometer.

6.5.6 Gating strategies for identification of human DCs and monocytes/macrophages in tissues. As depicted in Figs. 169 and 170, a similar gating strategy is adopted for human blood, spleen, and lung samples to characterize their cDC1, cDC2, as well as classical monocytes (cMo), intermediate monocytes (iMo) and non-classical monocytes (ncMo) subsets. We also recently described
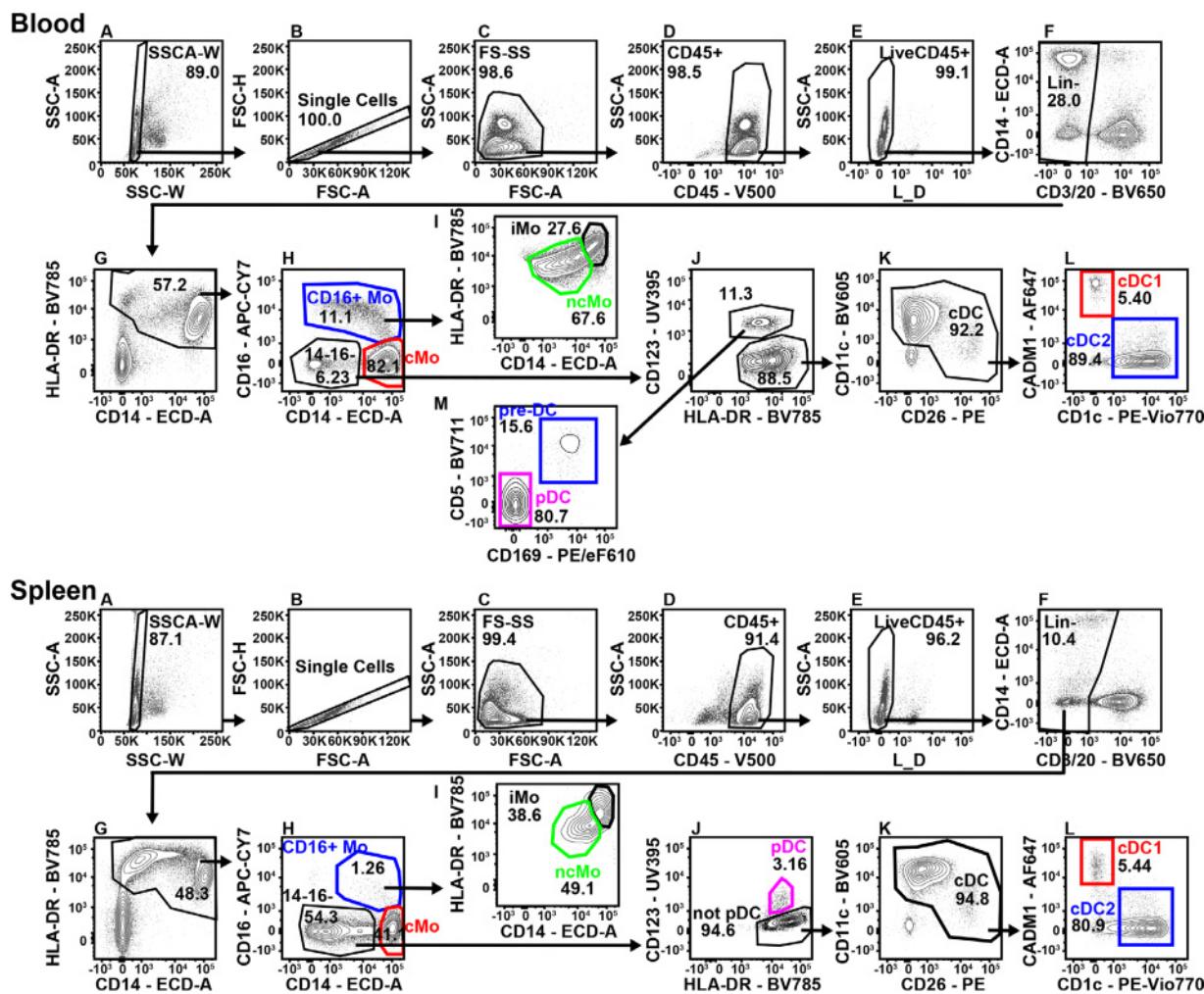
Figure 169. Gating strategies for flow cytometric analysis of human DCs and monocytes in blood and spleen. *For blood and spleen*: (A) Exclusion of doublets, (B) exclusion of doublets, (C) identification of cells based on their Forward and Side Scatter profile, (D) gating on CD45+ cells, (E) exclusion of Live/Dead+ dead cells, (F) gating on Lin(CD3/CD19/CD20)− cells, and (G) gating on HLA-DR+ cells. (H) Gating on CD14−/lo CD16− DCs, CD14−/+ CD16+ monocytes and identification of CD14hi CD16− classical monocytes (cMo). (I) Identification of HLA-DRlo/+ CD14lo/+ nonclassical monocytes (ncMo) and HLA-DRhiCD14hi intermediate monocytes (iMo). *For Blood*: (J) Gating on HLA-DR+ CD123+ cells for identification of early pre-DCs and pDCs as well as HLA-DR+ CD123− cDCs. (K) Gating on classical DCs (cDC) based on expression of CD11c and CD26 (exclusion of CD11c− CD26− non-cDCs). (L) Identification of CD1c− CADM1+ cDC1 and CD1c+ CADM1− cDC2 (M) Identification of CD123+ CD5+ CD169+ pre-DCs and CD123+ CD5− CD169− pDCs. *For spleen*: (J) Identification of HLA-DR+ CD123+ pDCs. (K) Gating on classical DCs (cDC) based on expression of CD11c and CD26 (exclusion of CD11c− CD26− non-cDCs). (L) Identification of CD1c− CADM1+ cDC1 and CD1c+ CADM1− cDC2.

cDC progenitors in the blood, namely early pre-DC [1450], that fall into the pDC gate and their respective gating is thus described for human blood. A distinct gating strategy is also used to define Langerhans cells (LCs) and macrophages in addition to cDC1, cDC2, and pDC in the skin.

In the blood, spleen and lungs, DCs are identified by gating on CD45+Lin− (CD3−CD20−) HLADR+CD14−/loCD16− cells, among which cDC1 is identified as CD1c−/loCD11c−CD123−CADM1+ and cDC2 as CD1c+CD11c+CD123−CADM1−. In addition, for blood, a unique gate is added to define CD123+CD5−CD169− pDC and the recently described human cDC progenitors, that is CD123+CD5+CD169+ early pre-DC [1450], while the spleen and lungs' pDCs are defined as HLADR+CD123+. Moreover,

cMo in the blood, spleen, and lungs are initially identified by gating on CD45+Lin−HLADR+CD14hiCD16− cells, while CD45+Lin−HLADRlo-hiCD14lo-hiCD16+ cells are further classified into two subsets of HLA-DRlo/+CD14lo/+ ncMo and HLA-DRhiCD14hi iMo.

In the skin, DCs are identified by gating on CD45+Lin− (CD3−CD19−CD20−)HLADR+CD14−CD16− cells, among which LCs are defined as CD1ahiCD11c−/lo cells, while CD1a−/+CD11c−/+ non-LCs are classified as two subsets of CD1c+CD11c−SIRPα−CADM1+ cDC1 and CD1c+CD11c+SIRPα+CADM1− cDC2. In addition, skin macrophages are identified by gating on CD45+Lin−HLADR+CD14+CD16−/lo cells.
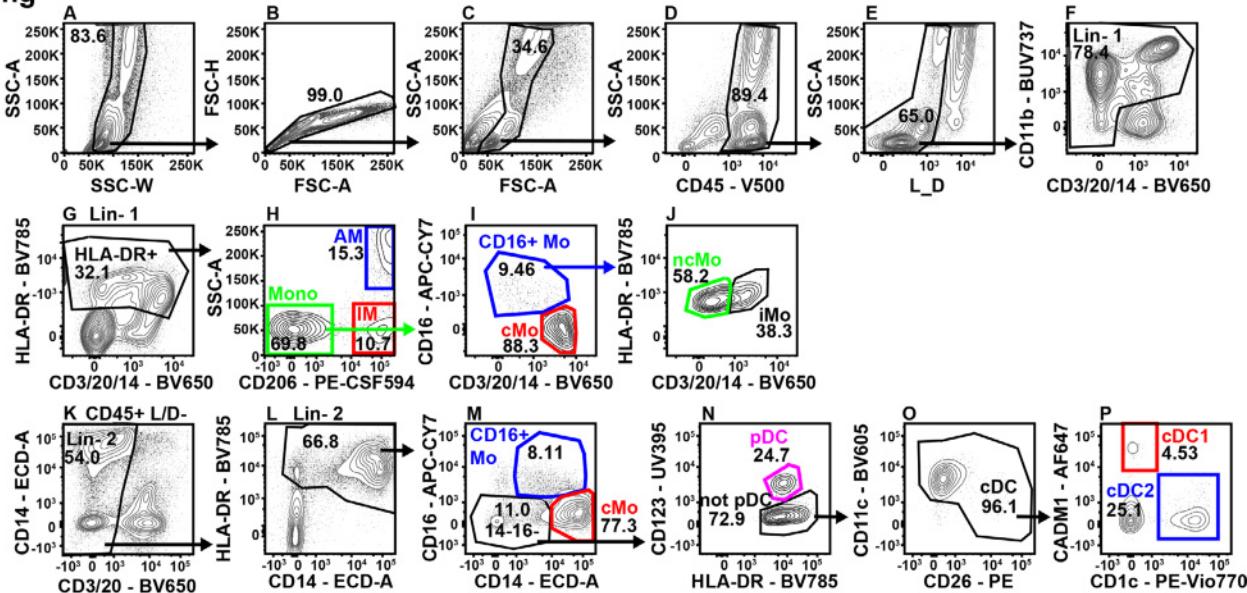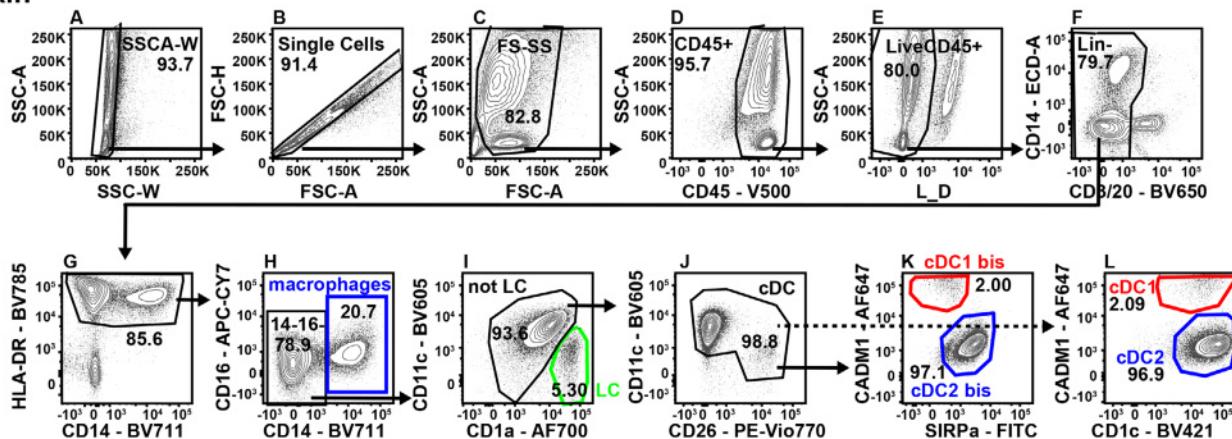
Figure 170. Gating strategies for flow cytometric analysis of human DCs and monocytes in lung and skin. *For lung and skin*: (A) Exclusion of doublets, (B) exclusion of doublets, (C) identification of cells based on their Forward and Side Scatter profile, (D) gating on CD45+ cells, (E) exclusion of Live/Dead+ dead cells, (F) gating on Lin(CD3/CD19/CD20)− cells, and (G) gating on HLA-DR+ cells. *For lung*: (H) Gating on SSC-Ahi CD206hi alveolar macrophages (AM) (blue), SSC-Alo CD206hi interstitial macrophages (IM) (red) and SSC-Ahi CD206− monocytes. (I) Monocytes are divided into CD14+ CD16− classical monocytes (cMo) (red) and CD16+ monocytes (blue), and from there (J) into HLA-DRlo CD14lo non-classical monocytes (ncMo) and HLA-DRlo CD14+ intermediate monocytes (iMo). (K) Gating on LIN- cells and (L) HLA-DR+ cells. (M) Gating on CD14−/lo CD16− DCs (and also CD14−/+ CD16+ monocytes (blue) and identification of CD14hi CD16− classical monocytes (cMo; red)). (N) Identification of CD123+ pDCs. (O, P) Gating on classical DCs (cDC) based on expression of CD11c and CD26 (exclusion of CD11c− CD26− non-cDCs) and identification of CD1c− CADM1+ cDC1 and CD1c+ CADM1− cDC2. *For Skin*: (H) Identification of CD14+ CD16−/lo macrophages, (I) Identification of CD1ahi CD11c−/lo Langerhans cells (LCs), (J) Gating on cDC based on expression of CD11c and CD26, (K) Identification of SIRPα− CADM1+ cDC1 and SIRPα+ CADM1− cDC2, (L) Alternative way to identify CD1c−/+ CADM1+ cDC1 and CD1c+ CADM1− cDC2 if using the same strategy as the other organs.

6.6 Pitfalls

First, generating qualitative FCM data requires proper combinations of fluorochromes/markers. It should be avoided to use Abs binding co-expressed markers conjugated with fluorochromes that have a lot of fluorescence spill-over into channels in which they are detected. Second, analyzing DC and monocyte/macrophages by FCM requires using more than ten Abs and thus complexifies the definition of a correct compensation matrix. Third, when analyzing FCM data using manual gating, a major challenge is to avoid dropping out cells of interest along the gates. To facilitate these two latter critical aspects of FCM data analysis, an initial manual gating should be done to define major DC and monocyte subsets.

Then, using a compatible software (Diva, Kaluza, and eventually Flow Jo), n dot plot (for an n color FCM panel) should be defined (fluorochrome A on the *x*-axis vs. all the other fluorochromes on the *y*-axis) all displaying CD45+ cells with all

the DC and monocyte subsets overlayed (each having a defined color). This will allow the proper setting of "all fluorochromes-the A fluorochrome" compensations. When all "fluorochrome X-fluorochrome A" compensations are properly set, the next fluorochrome must be displayed on the x-axis, and so on, until all fluorochromes have been properly compensated.

Once compensations are properly set, two methods can be used for analysis, manual gating or unsupervised dimensionality reduction, latter being the most reliable method.

For manual gating, the different cell subsets must be displayed in all gates defined to reach them by "back gating" to ensure that each of them are present at all steps of the gating strategy. To ensure that all populations can be properly visualized in all gates, back gated cell subsets should be ordered by count, with the rarest populations displayed above all the other cell subsets.

A major drawback of manual gating is that gates are defined based on one (histogram) or two markers' (dot plot) expression, which in some cases does not allow the proper separation of cell populations that share overlapping phenotypes. Thus, unsupervised dimensionality reduction is now becoming the gold standard method to avoid this, since it reduces all dimensions (one marker = one dimension) into a 2D or 3D space. Machine learning-based algorithms such as t-SNE [144], or UMAP [1470]; [1470, 1471] combined with clustering algorithms [1450, 1472, 1473] allow the proper identification and separation of cell subsets by integrating all markers analyzed. When performing dimensionality reduction on a very heterogeneous population, such as total CD45$^+$ leukocytes, minor cell subsets will not be finely resolved, such as DC subsets. Thus, dimensionality reduction can be first done on total CD45$^+$ cells using a dimensionality reduction method such as UMAP that contrary to tSNE, allows the analysis of millions of cells (events). As an illustration, total Live CD45$^+$ cells from the same FCM data of human blood, spleen, and lung from Fig. 169 and 170 were analyzed using the UMAP algorithm (Fig. 171A–C). The same manual gating strategy was applied and for each step, the corresponding populations were overlayed on the UMAP space, demonstrating that manual gating leads to minor contaminations as illustrated by cells falling into the dashed black delimited regions (Fig. 171A). We next plotted major cell subsets defining markers expression as meaning plots to guide the unsupervised delineation of all major mononuclear cell subsets (Fig. 171B–C). In the UMAP bidimensional space obtained, Lin$^-$HLA-DR$^+$ cells (DC and monocyte/macrophages) were not clearly resolved and thus, were gated and reanalyzed with both the UMAP and t-SNE dimensionality reduction algorithm together with the Phenograph clustering algorithm to obtain a higher resolution of the cells comprised in this gate (Fig. 171D–F). Analysis of the expression of DC and monocyte/macrophage markers allowed the delineation of Phenograph clusters corresponding to DC and monocyte/macrophage subsets (Fig. 171D,E), and to compare the relative phenotype and distribution of cell subsets in the blood, spleen, and lung (Fig. 171E–F). This subgating can be done again in a particular subpopulation of the second dimensionality reduced space obtained to further increase the resolution of discrete cell populations.

7 Granulocytes

7.1 Neutrophils, eosinophils, and basophils

7.1.1 Overview. This chapter aims to provide guidelines for researchers interested in analyzing polymorphonuclear leucocytes. We describe a gating strategy to distinguish different subsets of PMNs via FCM staining for human and murine blood samples. Furthermore, we provide a simple method to examine phagocytosis via FCM staining as well as basic tips and tricks for handling neutrophils appropriately to prevent activation.

7.1.2 Introduction. Granulocytes are highly granular cells with a distinct lobed nuclear morphology. They can further be divided in basophils (0.5–1% of WBC), eosinophils (1–3% of WBC) and neutrophils (50–70% of WBC). Neutrophils exert potent antibacterial functions and are involved in inflammatory diseases (see also Chapter VI Section 7.2 Bone marrow and umbilical cord blood neutrophils), whereas basophils and eosinophils help to control parasitic infections and contribute to allergic reactions. Granulocytes are rapidly recruited to sites of infection, providing robust early microbial control. This feature is essential for the survival of the host, however, comes with the need for special arrangements when working with isolated granulocytes: All instrumentation and buffers/media need to free of LPS and other pathogen-associated molecular patterns (PAMPS) to prevent undesired activation. Further, granulocyte exhibit a relatively short life span of only a few hours to a few days and are sensitive to inappropriate treatment, for example, harsh physical handling or high concentrations of calcium. It is advisable to work rapidly, reduce manipulation steps that could mechanically activate the cells and use the cells immediately upon isolation. Therefore, it is necessary to use optimized protocols for the dissociation of different tissues to prepare single cell suspensions for FCM. The easiest way to obtain granulocytes for analysis is to use whole blood (human or mouse) and perform lysis of erythrocytes.

7.1.3 Step-by-step sample preparation. Successful FCM analysis requires high quality single cell suspensions. Minimal manipulation of the cells is essential for the quality of both Ab and cell death staining. Human granulocytes are abundantly present in peripheral blood and can be isolated via density centrifugation or analyzed as a subpopulation of total leukocytes. Note that some inflammatory disorders are characterized by low density granulocytes that colocalize with PBMCs during density centrifugation. In mice, granulocytes can be obtained from peritoneal lavage, i.e., after intraperitoneal injection of thioglycolate, whole blood, or bone marrow (see Isolation Chapter VI: Section 8 Murine bone marrow stromal cells). In some cases, enrichment for granulocytes might be necessary and this can be achieved via density gradient centrifugation (see Chapter IV Section 1.2 Pre-enrichment by physical properties) or negative selection via magnetic beads (see Chapter IV Section 1.3 Pre-enrichment by immunological
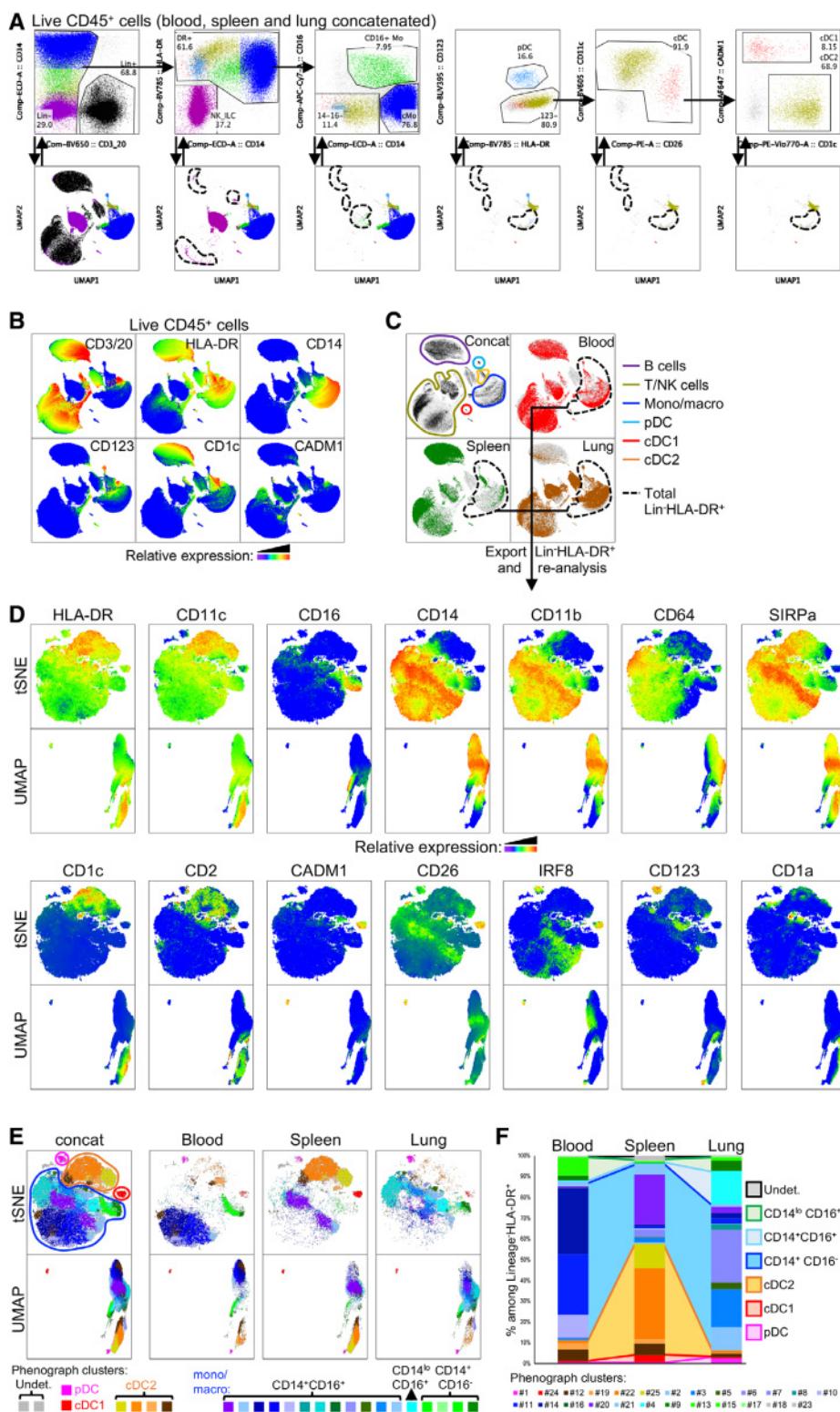
Figure 171. Unsupervised analysis of human DCs and monocyte/macrophages in different tissues. Lin⁻HLA-DR⁺ cells from Blood, Spleen and Lung data from Figures 169 and 170 were analysed using two dimensionality reduction methods, Uniform Manifold Approximation and Projection (UMAP) and t-Distributed Stochastic Neighbor Embedding (t-SNE) combined with the Phenograph automated clustering method. (A) Manual gating strategy of the concatenated data obtained from blood, spleen and lung starting from Live CD45⁺ cells. The upper panels show the different steps of the manual gating strategy and the lower panels show the projection of each step of the gating strategy into a UMAP space. (B) Meaning pots of lineage-defining markers overlayed on the UMAP plot. (C) UMAP plot showing the concatenated data obtained in the three organs (upper left panel), in the blood (red, upper left panel), in the spleen (green, lower left panel) and in the lung (brown, lower right panel) where Lin⁻HLA-DR⁺ cells are defined. (D) Meaning pots of the relative expression of all parameters overlayed on the tSNE and UMAP plots of the concatenated data (blood, spleen and Lung) from Lin⁻HLA-DR⁺ cells exportes as shown in (C). (E) Visualisation of phenograph clusters overlayed on the tSNE and UMAP plots of the concatenated data (left panel), or of each individual sample. Clusters corresponding to pDC (pink), cDC1 (red), cDC2 (yellow = enriched in DC2 to brown -= enriched in DC3 [1474, 1475], CD14⁺CD16⁻ (blue to purple), CD14⁺CD16⁺ (cyan), CD14^lo CD16⁺ (green) monocyte/macrophages, and three minor undetermined clusters are shown. (F) Frequencies of Phenograph clusters defined in (B) regrouped by cell subsets defined in (B).

properties). For FCM analysis, the initial cell suspension should be depleted of erythrocytes (e.g., short hypotonic lysis with water, ammonium chloride treatment, or use of commercially available RBC lysis buffers).

7.1.3.1 Flow cytometric characterization of human and murine granulocytes. Staining can either be performed before or after lysis of RBC. In the protocol described below, lysis of erythrocytes was performed prior to Ab staining. Due to the abundant expres-

sion of Fc receptors on granulocytes, use of an Fc block is strongly advised.

1. A total of 100 μL of human or murine whole blood is pelleted via centrifugation at 300 × g for 5 min. The cell pellet is resuspended in a small volume and subjected to lysis with hypotonic water (900 μL) for 20 s to lyse erythrocytes. Physiological osmolality is re-obtained by addition of 100 μL of 10× PBS.
2. Cells are pelleted via centrifugation at 300 × g for 5 min and resuspended in 100 μL HBSS (with 2% heat inactivated FCS and Fc block). The samples are incubated for 15 min on ice.
3. Cells are pelleted via centrifugation at 300 × g for 5 min and resuspended in 100 μL HBSS (with 2% heat inactivated FCS and Abs). The samples are incubated for 30 min on ice in the absence of light.
4. One milliliter of HBSS (with 2% heat inactivated FCS) is added to the suspension and cells are pelleted via centrifugation at 300 × g for 5 min, resuspended in an appropriate volume of HBSS (with 2% heat inactivated FCS) and subjected to FCM analysis.

7.1.3.2 Flow cytometric detection of cell death in human granulocytes. Human granulocytes can easily be obtained via density gradient centrifugation of human blood. Several different protocols have been published, with some involving dextran sedimentation of RBCs. The protocol we describe here omits the lengthy dextran sedimentation step without affecting the purity of the granulocyte fraction.

1. A total of 20 mL of anti-coagulated blood is diluted with 15 mL PBS and gently layered on top of 15 mL Lymphoflot. Cells are separated via centrifugation at 300 × g for 30 min without break. The granulocytes layer directly on top of the RBCs (whitish veil) and are collected and washed once in PBS. Note that this fraction contains mainly neutrophils and eosinophils, whereas basophils sediment in the PBMC fraction.
2. The cell pellet is resuspended in 200 μL of PBS. Hypotonic lysis of erythrocytes is performed by addition of 36 mL of ice-cold water for 20 s. Physiological osmolality is re-obtained by addition of 4 mL of 10× PBS.
3. The granulocytes are resuspended in RPMI-1640 supplemented with 100 U/mL penicillin/streptomycin, 2 mM glutamine, and 10% heat-inactivated FCS and 25 mM HEPES at a concentration of 2×10^6 cells/mL and cultivated at 37°C/5% CO$_2$. Due to the short life span of granulocytes, detectable cell death will occur in less than 12 h.
4. Cell death is assessed by harvesting of cells via centrifugation at 300 × g for 5 min and resuspension at a concentration of 1×10^6 cells/mL in HBSS supplemented with 2% heat inactivated FCS, 100 ng/mL PI, and 1 μg/mL ANX-V. Staining is performed on ice for 30 min.
5. Without an additional washing step, samples are directly subjected to FCM analysis. Note that washing is not recommended

as this can result in the loss of subcellular particles and compromise integrity of apoptotic cells.

7.1.3.3 Flow cytometric detection of particle uptake in human granulocytes.

1. A total of 20 mL of anti-coagulated blood is diluted with 15 mL PBS and gently layered on top of 15 mL Lymphoflot. Cells are separated via centrifugation at 300 × g for 30 min without break. The granulocytes layer directly on top of the RBCs (whitish veil) and are collected and washed once in PBS. Note that this fraction contains mainly neutrophils and eosinophils, whereas basophils sediment in the PBMC fraction.
2. The cell pellet is re-suspended in 200 μL of PBS. Hypotonic lysis of erythrocytes is performed by addition of 36 mL of ice-cold water for 20 s. Physiological osmolality is re-obtained by addition of 4 mL of 10× PBS.
3. The granulocytes are re-suspended in in HBSS supplemented with 2% heat inactivated FCS. A total of 20 μg/mL micro monosodium urate crystals and 250 μg/mL Lucifer Yellow are added and cells are incubated at 37°C/5% CO$_2$ for various time points.
4. Cells are collected and without additional washing directly subjected to FCM analysis.

7.1.4 Materials.

7.1.4.1 Reagents. HBSS, calcium, magnesium, no phenol red (ThermoFisher Scientific, 14025050)
Lymphoflot (Bio-Rad, #824012)
Lucifer Yellow CH (ThermoFisher Scientific, L453)
RPMI 1640 Medium (ThermoFisher Scientific, 21875034)
L-Glutamine (ThermoFisher Scientific, 25030081)
Penicillin–Streptomycin (ThermoFisher Scientific, 15140122)
HEPES (ThermoFisher Scientific, 15630056)
Fetal Calf Serum (Biochrom, S 0115)
Propidium iodide (Sigma, P4170)
Anx-V-FITC (Immunotools, 31490013)
Human TruStain FcX™ (Biolegend, 422301)
TruStain FcX™ PLUS (anti-mouse CD16/32) (Biolegend, 156603)

7.1.4.2 Instruments/Software.

GALLIOS flow cytometer (Beckman-Coulter)
Kaluza Analysis Software (Beckman-Coulter)
Prism 7 (Graphpad)

7.1.5 Data Analysis. Differential light scattering of cells depending on the size and morphology is useful to discriminate subsets of cells. The SSC is considered to be an indicator for the internal structure of the cell (e.g., nuclear morphology) and the FSC
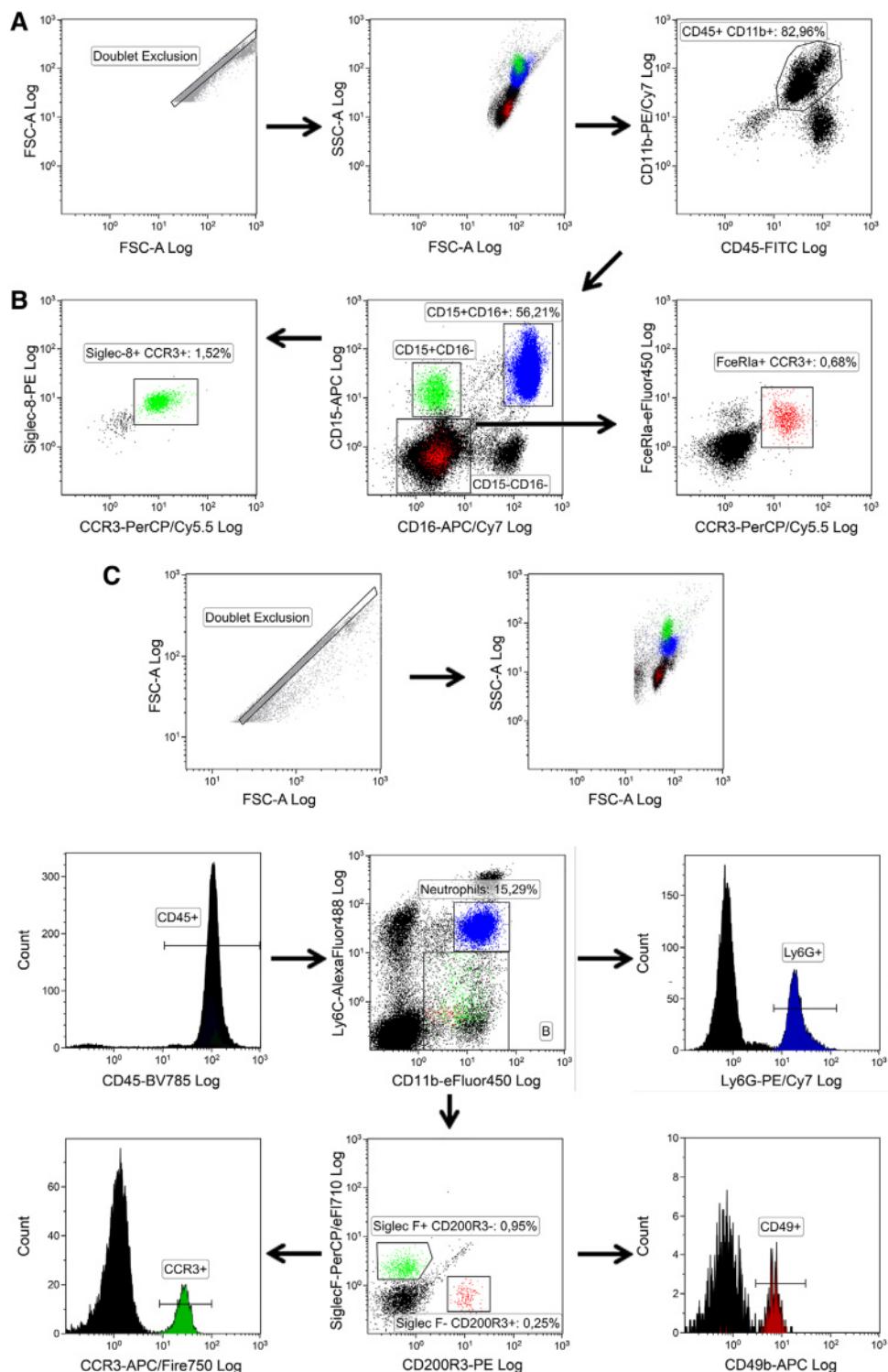
Figure 172. Discrimination of granulocyte subpopulations. (A) Human cells were displayed in a SSC versus FSC dot plot to show the location of eosinophils (green, high SSC), neutrophils (blue, high SSC), and basophils (red, low SSC). (B) Human cells were stained with Abs against CD45, CD11b, CD15, CD16, CCR3, Siglec-F, and FcεRIα. CD45$^+$/CD11b$^+$ cells were gated on CD15 versus CD16 to distinguish granulocyte subpopulations. CD15$^+$/CD16$^+$ cells were determined as neutrophils, CD15$^+$CD16$^-$ were further designated as eosinophils by their expression of Siglec-8 and CCR3, and the CD15$^-$/CD16$^-$ population was depicted in a FcεRIα versus CCR3 plot to identify the double positive basophil fraction. (C) CD45$^+$ murine cells were gated on CD11b/Ly6C to display the CD11b$^+$/Ly6^{int} population that was further analyzed using Ly6G to identify neutrophils (blue). CD11b$^+$/Ly6C$^{neg-low}$ cells were gated on Siglec-F versus CD200R3 and were subsequently analyzed for expression of additional cell subset markers. CD200R3-cells expressing Siglec-F and CCR3 were designated as eosinophils (green) and Siglec-F-cells were marked as basophils (red) supported by their expression of CD200R3 and CD49b.

Table 62. List of Abs used for characterization of human granulocyte populations

Target	Fluorophore	Supplier	Cat#	Clone	Host	Isotype	Cross-Reactivity
CCR3	PerCp/Cy5.5	BioLegend	310717	5E8	Mouse	IgG2b, κ	None
CD11b	PE/Cy7	BioLegend	301321	ICRF44	Mouse	IgG1, κ	Yes
CD15	APC	BioLegend	301907	HI98	Mouse	IgM, κ	Yes
CD16	APC/Cy7	BioLegend	302017	3G8	Mouse	IgG1, κ	Yes
CD45	FITC	BioLegend	304005	HI30	Mouse	IgG1, κ	Yes
FcRε1	eFluor450	eBioscience	14-5899-82	AER-37	Mouse	IgG2b, κ	None
Siglec-8	PE	BioLegend	347103	7C9	Mouse	IgG1, κ	None

reflects cellular size. Since both human and murine neutrophils and eosinophils have a multi-lobulated nucleus, they exhibit a high SSC signal, with eosinophils showing a slightly higher signal in this parameter. The nuclear morphology of basophils is less complex and therefore they are found among the lymphocyte population and cannot be distinguished in such manner (Fig. 172A). Furthermore, changes in SSC and FSC may also represent other morphological features of various cellular processes (e.g., phagocytosis, cell death). These changes can also be detected in this manner as described below in this section. It is recommended to start your analysis with excluding doublets by gating on FS PEAK Log versus FS INT Log to prevent an impact of doublets on, e.g., population frequencies. Then, to detect either human or murine granulocytes, it is useful to start with a staining for CD45 to define WBCs accompanied by the simultaneous staining for CD11b. These two markers together with FSC and SSC features are enough to roughly narrow down granulocytes from whole blood preparations (Fig. 172A and C). Human neutrophils are the most abundant cell type within the granulocyte family. They can be further distinguished from other granulocytes by their positivity for both CD15 and CD16. Eosinophils are positive for CD15, but do not express CD16. Additional staining for CCR3 and Siglec-8 allows a specific detection of eosinophils. Basophils neither express CD15 nor CD16; therefore staining with anti-FcεRIα identifies them in the CD15^{neg}/CD16^{neg} population (Fig. 172B).

Murine neutrophils and eosinophils are CD11b positive and exhibit an intermediate to low expression of Ly6C. Neutrophils are detected as Ly6G positive cells, whereas eosinophils are identified by their expression of CCR3 and Siglec-F. Basophils also show positivity for CD11b, but have only a low expression of Ly6C.

They can be further identified by the expression of CD200R3 and CD49b (Fig. 172C).

Especially in the context of inflammatory infiltrates it is sometimes necessary to further determine neutrophil viability. During the resolution of inflammation, neutrophils undergo apoptosis, mediate anti-inflammatory and immunosuppressive effects, and secrete factors that prevent the additional influx of neutrophils. Apoptosis and necrosis can be detected by a combination of PI and fluorophore-conjugated ANX-V. PI is a DNA-intercalating substance that only enters cells that have lost their membrane integrity (necrotic cells and NETotic cells). ANX-V binds to phosphatidylserine exposed by cells undergoing apoptosis (Fig. 173A). If granulocytes have been purified prior to the L/D analysis, no Ab staining is needed. However, if more than one cell type is present, the cell death staining should be supplemented with an Ab combination allowing the identification of granulocytes as mentioned above. FCM allow the simultaneous use of multiple fluorophores. If such an instrument is available, the classical apoptosis staining deploying ANX-V-conjugates and PI can be supplemented with two additional dyes (e.g. Hoechst33342 and 1,1′,3,3,3′,3′-hexamethylindodicarbo-cyanine iodide (DilC1(5)) that allow a more detailed characterization of cell death. This staining takes into account the condition of the nucleus and the mitochondrial membrane potential, respectively, and can also be deployed for live-cell imaging [2256, 2257].

Further, neutrophils show a strong capacity to take up particulate matter. If confronted with nanoparticles or small-sized monosodium urate crystals, neutrophils engulf these particles and respond in an appropriate manner. Since such material cannot be easily conjugated with fluorophores, one has to rely on other methods to monitor their uptake. Soluble dyes, such as Lucifer

Table 63. List of Abs used for characterization of murine granulocyte populations

Target	Fluorophore	Supplier	Cat#	Clone	Host	Isotype	Cross-Reactivity
CCR3	APC/Fire750	BioLegend	144521	J073E5	Rat	IgG2a, κ	None
CD11b	eFluor450	eBioscience	48-0112-82	M1/70	Rat	IgG2b, κ	Yes
CD45	BV785	BioLegend	103149	30-F11	Rat	IgG2b, κ	None
CD49b	APC	BioLegend	108909	DX5	Rat	IgM	None
CD200R3	PE	BioLegend	142205	Ba13	Rat	IgG2a, κ	None
Ly6C	AlexaFluor 488	BioLegend	128021	HK1.4	Rat	IgG2c, κ	None
Ly6G	PE/Cy7	BioLegend	127617	1A8	Rat	IgG2a, κ	None
Siglec-F	PerCP-eFluor710	eBioscience	46-1702-82	1RNM44N	Rat	IgG2a, κ	None
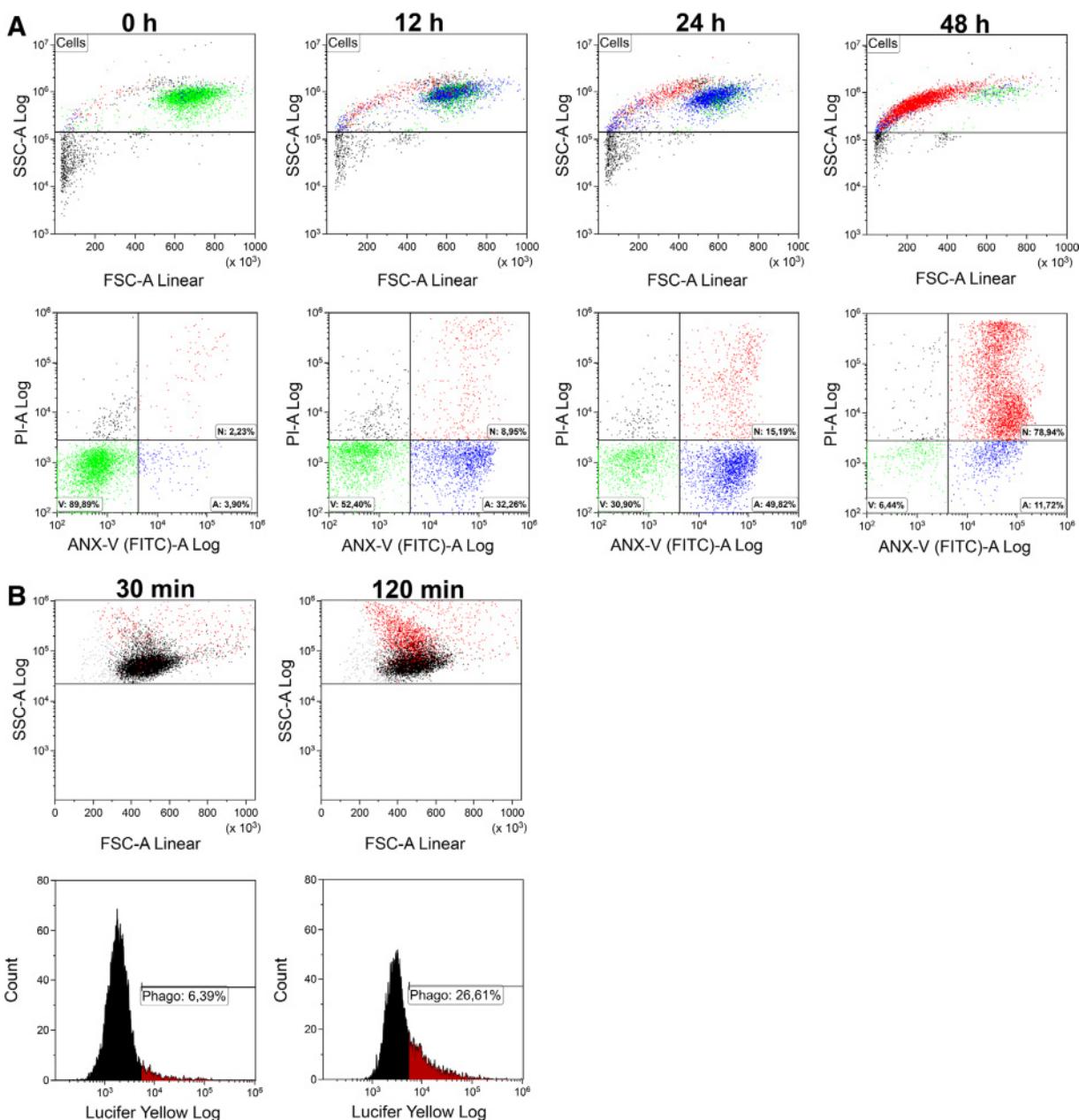
Figure 173. Apoptosis detection and uptake of nanoparticles in purified human granulocytes. (A) Granulocytes were cultivated at 37°C/5% CO_2 for indicated time points and stained according to the cell death protocol. Subsequently, they were subjected to FCM analysis. During apoptosis, granulocytes shrink and increase in granularity, as indicated by a decrease in FSC and an increase in SSC. Viable cells (V) first start to expose ANX-V-FITC and become apoptotic (A), before they lose their plasma membrane integrity and become necrotic as indicated by PI-positivity (N). Note that in the N-gate the population high in PI reflects cells without the loss of nuclear content. In contrast, the population low in PI reflects cells with a subG1 DNA content, which is considered a hallmark of apoptosis. (B) A total of 20 µg/mL micro monosodium urate crystals and 250 µg/mL Lucifer Yellow were added to the granulocytes and the suspension was incubated at 37°C/5% CO_2 for the time points indicated. Subsequently, FCM analysis was performed. The increase in Lucifer Yellow (in red) is restricted to the population of cells that increase in granularity. Therefore, the simultaneous increase in Lucifer Yellow and SSC can be used to monitor the uptake of nanoparticles by granulocytes.

Yellow, can be added together with the prey that will subsequently be co-ingested during phagocytosis. In addition, the uptake of particulate matter tends to increase the complexity of the phagocyte. As shown in Fig. 173B, the increase in SSC and in Lucifer Yellow strongly correlates. Combined observation of both represents a feasible method for addressing such questions.

7.1.6 Pitfalls and top tricks.

- Neutrophil released from the BM are following a circadian rhythm [1476]. To ensure the highest comparability, neutrophils from different donors (murine and human) should be isolated roughly at the same time of the day.
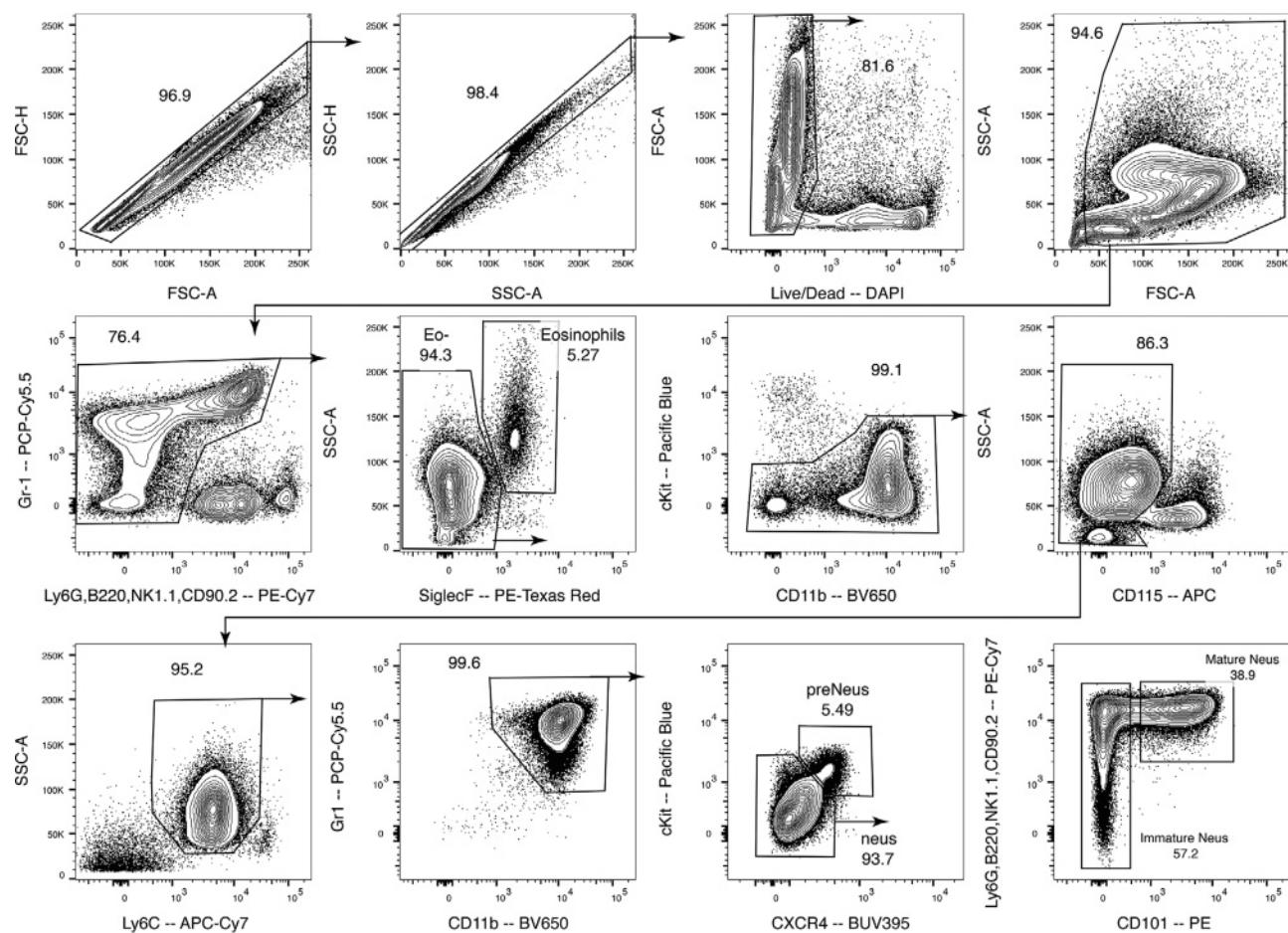
Figure 174. Flow cytometric analysis of murine bone marrow neutrophil subsets. Samples are first gated to exclude doublets and dead cells. Debris are also excluded based on FSC and SSC information. Lineage positive cells (T, B, and NK cells) are then excluded followed by the exclusion of eosinophils and monocytes. Ly6C is then used to further remove any Ly6C^{hi} and Ly6C^{lo} monocyte contamination. Gr-1 and CD11b gates for total bone marrow neutrophils. cKit and CXCR4 is used to gate proliferative pre-neutrophils and CD101 distinguishes mature neutrophils from immature neutrophils.

- When FCM analysis is performed, proper arrangements are necessary to prevent neutrophil adhesion. Neutrophils show a tendency to adhere under serum free conditions, to glass or adhesive plastic surfaces and especially fast in response to stimulation.
- Neutrophils are susceptible to changes in pH and readily form NETs even under mildly alkaline conditions. Buffers should be checked for pH prior to use. RPMI and HBSS can be supplemented with HEPES to stabilize the pH [1477].
- Neutrophils have a very limited life time. They undergo full blown apoptosis in less than 24 h. In addition, several stimuli induce the formation of neutrophil extracellular traps. Although it is possible to detect NETs as material with very high SSC, FCM is not robust enough to quantify NETs. Furthermore, NETs tend to aggregate and form material that cannot be collected by standard needles.
- Phagocytic uptake of particles alters the morphology of a variety of cell types. It is therefore not advisable to identify granulocyte populations only by SSC.

- Activation of leucocytes is usually accompanied by shedding or membrane renewal consequently changing their phenotype (e.g., CD16 downregulation).
- L/D stainings deploying ANX-V must be performed in the presence of at least 2 mM calcium, since binding of ANX-V to phosphatidylserine is calcium-dependent. Avoid washing to prevent loss of subcellular particles and impairment of apoptotic cell integrity.
- Granulocytes express a variety of Fc receptors. To prevent false-positive staining's and to reduce the background fluorescence, we advise to always block unspecific bindings with 2% FCS and to prevent Fc-mediated Ab binding via the use of an Fc blocking agent.

7.2 Bone marrow and umbilical cord blood neutrophils

7.2.1 Overview. The developmental pathway of neutrophils has been recently investigated with great interest [1478–1480]. However, there is still no universally accepted characterization of
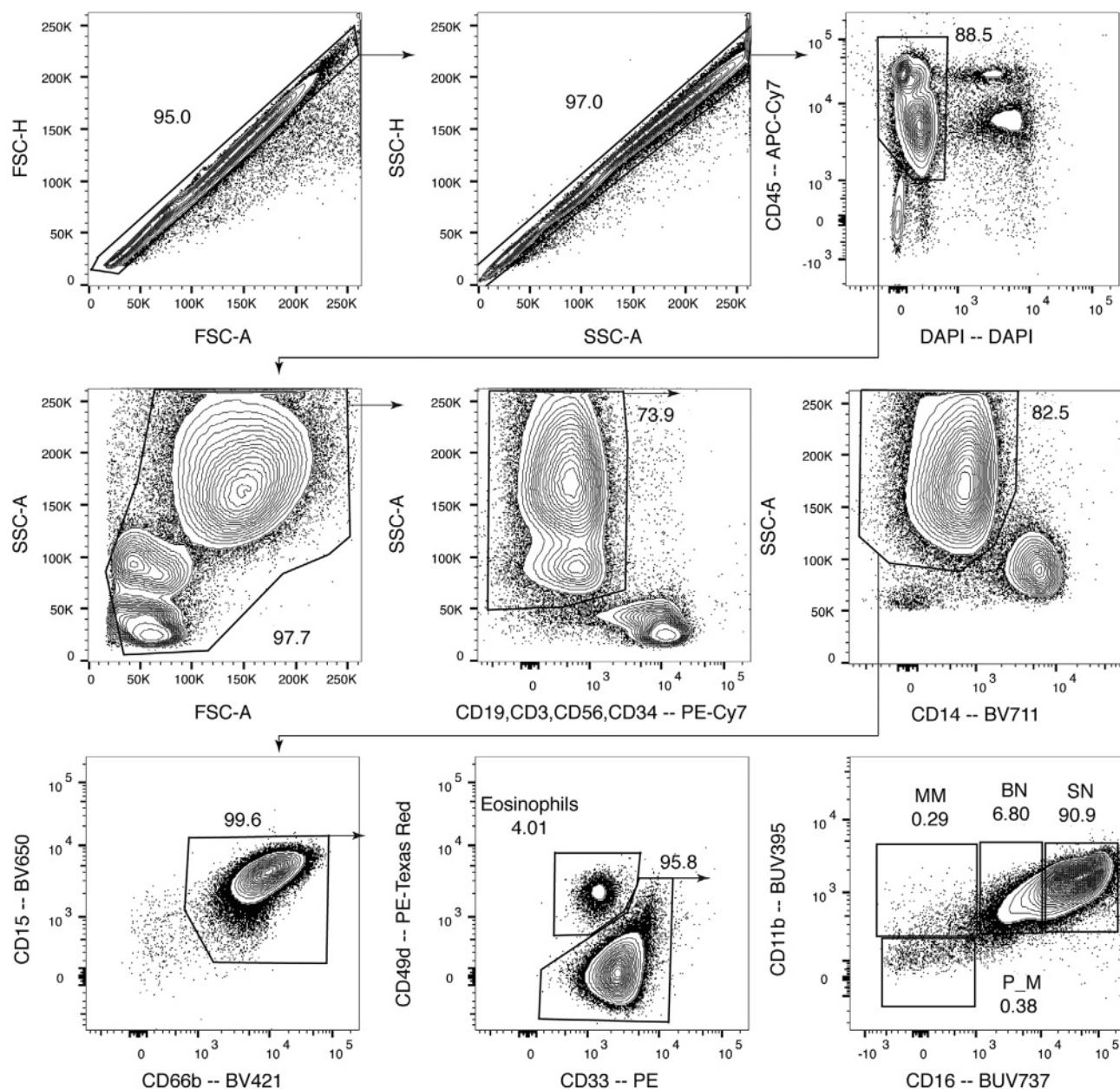
Figure 175. Flow cytometric analysis of human umbilical cord blood neutrophil subsets. Similarly, to the mouse neutrophil subsets, doublets, and dead cells are first excluded, followed by the exclusion of CD45⁻ cells and debris. Lineage cells and CD14⁺ conventional monocytes are excluded before total granulocytes are gated with CD15 and CD66b. From there, eosinophils are excluded before gating on the classical nomenclature of neutrophil subsets using CD11b and CD16. P_M = Promyelocytes and Myelocytes, MM = Meta-myelocytes, BN = Band cells, SN = Segmented neutrophils. Gating is adapted from ref. [1487, 1494].

neutrophils by FCM. Moreover, tissues such as bone marrow and spleen contain multiple cell types, which may share overlapping surface markers that can lead to contamination and improper identification. Here, we propose an FCM framework to identify and isolate pure populations of neutrophil subsets, which can be generally applied to most tissues in mice and human. We provide the necessary surface markers, reagents, and tips for successful characterization of neutrophil subsets.

7.2.2 Introduction. Granulocytes are the granule-producing branch of the myeloid cell lineage that includes neutrophils, eosinophils, and basophils [1481]. Neutrophils represent the large majority of granulocytes and are involved in a myriad of immune functions and diseases [1482–1484]. Flow cytometric analysis and characterization of neutrophils has been performed over 20 years ago [1485]. The stages of granulopoiesis—myeloblasts, promyelocytes, myelocytes, metamyelocytes, band cells, and hyper-segmented neutrophil—have been characterized
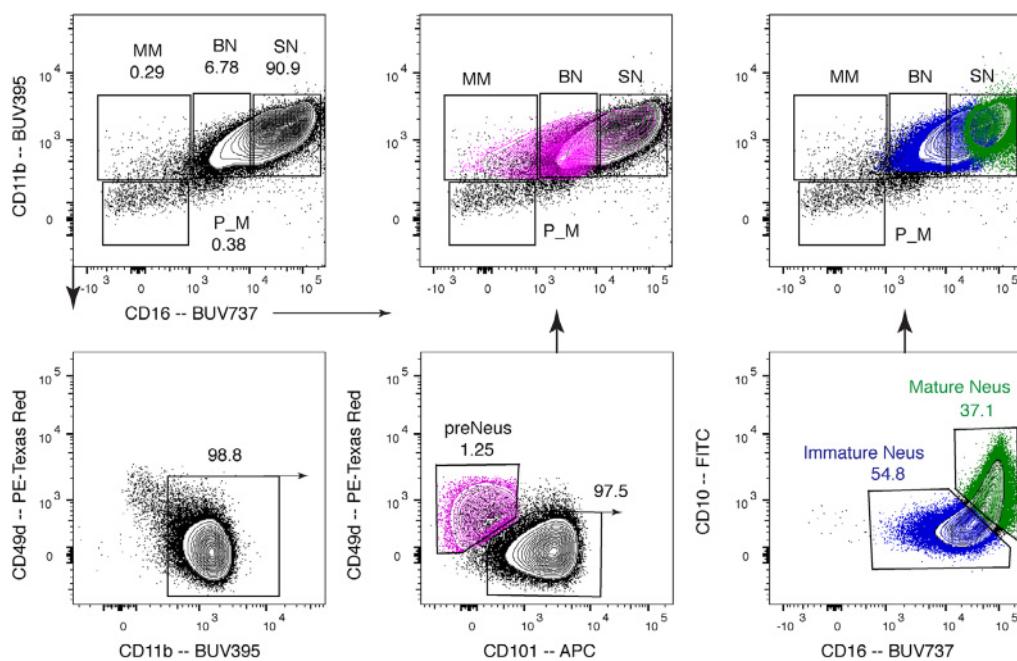
Figure 176. Potential improvements to classical nomenclature and gating. Using proliferation as a marker, total neutrophils can be first gated (according to Figure 175) before gating on proliferative CD11b$^+$ preNeus using CD101 and CD49d as shown previously [1478]. The remaining non-proliferative pool of neutrophils can be separated with CD10 as described recently [1489].

by the use of markers such as CD11b, CD15, and CD16. Traditionally, these analyses were performed by correlating surface marker expression levels with the morphological characteristics of the different stages of terminal granulopoiesis [1486, 1487].

Recently, neutrophil heterogeneity in disease has been of a growing interest with the introduction of neutrophil subsets with the underappreciated roles previously [1484, 1488, 1489]. Many of these reports suggest an immature phenotype of granulocytes [1480, 1490–1492], suggesting the importance of investigating neutrophil function in relation to the various developmental stages.

Therefore, understanding the stages of neutrophil maturation provides a firm foundation to study these novel functions of neutrophils. Indeed, recent evidence shows how clearly defined subsets of neutrophils can specifically perform distinct functions that influence the disease progression of arteriosclerosis [1493]. In this section, we provide guidelines in analyzing neutrophil subsets characterized by their distinct functions and the roles they play during inflammatory states [1478].

7.2.3 Step-by-step sample preparation.

7.2.3.1 Step-by-step sample preparation of murine bone marrow neutrophils.

1. Isolate femur bone with a scalpel by dislocating ball–socket joint at the hip. Detach kneecap joint connecting the tibia.

Table 64. Most important markers for FCM analysis of human and murine granulocytes. All cell types were first gated on CD45 and CD11b positivity

Cell type	Human	Mouse
Neutrophil	CD15^{pos}, CD16^{pos}, CD66b^{pos}	Ly6C^{int}, Ly6G^{pos}
Eosinophil	CD15^{pos}, CD16^{neg}, Siglec-8^{pos}, CCR3^{pos}	Ly6C$^{low/int}$, Siglec-F^{pos}, CCR3^{pos}
Basophil	CD15^{neg}, CD16^{neg}, CD117^{neg}, *FcεRIα^{pos}, CCR3^{pos}, *CD203c^{pos}	Ly6C^{low}, CD200R3^{pos}, CD49b^{pos}, *FcεRIα^{pos}

* These markers were not used in our analysis, but are valid markers for the given cell types.

Clean off muscle tissue and cut off the ball of the femur to create an opening.

2. Using a 1mL syringe with a 19-gauge needle containing 1 mL wash buffer (PBS + 2% FCS + 2 mM EDTA), flush marrow out through the opening into a 15 mL falcon tube containing 1 mL of buffer. Aspirate and repeat twice. Flush marrow from the opposite end. Aspirate and repeat twice.

3. Filter suspension through a 70 μM strainer to remove clumps and bone chips. Wash strainer with 4 mL of buffer. Centrifuge cells at 4°C, 400 × g for 5 min.

4. Discard supernatant and re-suspend pellet with 1 mL of buffer. Aliquot a fraction out for staining purposes. One-fifth is typically adequate.

5. Wash and centrifuge sample aliquot with buffer. Discard supernatant and re-suspend cells in 50 μL blocking buffer. Add 50 μL

of staining buffer with the Abs (See Tables 63 and 64). Incubate at 4°C for 30 min.

6. Add 2 mL of wash buffer and centrifuge. Discard supernatant.
7. Lyse erythrocytes with 200 μL 1× RBC lysis buffer for 3 min. Wash.
8. Re-suspend in wash buffer, add DAPI, and filter sample before acquisition.

#Gating: pre-Neutrophils are defined as Lin$^-$ Gr-1$^+$ CD11b$^+$ cKit^{hi} CXCR4^{hi} cells. Immature Neutrophils are defined as Lin$^-$ Gr-1$^+$ CD11b$^+$ cKit$^-$ CXCR4^{lo} CD101$^-$ cells. Mature Neutrophils are defined as Gr-1$^+$ CD11b$^+$ Ly6G$^+$ CD101$^+$ cells (See Fig. 174).

7.2.3.2 Step-by-step sample preparation of human bone marrow neutrophils.

1. Collect donor bone marrow aspirate in heparin saline containing ACD-A (acid-citrate-dextrose formula A).
2. Wash sample aliquot with 2 mL of 1× PBS. Centrifuge at 4°C, 400 × *g* for 5 min. Discard supernatant. Perform cell count.
3. Using 5 million cells, block Fc-receptors using purified anti-human CD16/32 Ab for 30 min at 4°C. Add staining buffer containing Abs (see Tables 62 and 64). Incubate at 4°C for 30 min.
4. Wash sample with PBS and centrifuge at 4°C, 400 × *g* for 5 min. Discard supernatant.
5. Lyse erythrocytes with 500 μL 1× RBC lysis buffer for 3 min. Wash.
6. Add DAPI and acquire cells.

7.2.3.3 Step-by-step sample preparation of human cord blood neutrophils.

1. Lyse erythrocytes with 1 mL of 1× RBC buffer for every 100 μL of cord blood. Incubate at room temperature for 6 min or until sample becomes translucent.
2. Neutralize with 1× PBS. Centrifuge at 4°C, 400 × *g* for 5 min.
3. Using 5 million cells, block Fc-receptors using purified anti-human CD16/32 Ab for 30 min at 4°C (See Table 64). Add staining buffer containing Abs. Incubate at 4°C for 30 min.
4. Wash sample with PBS and centrifuge at 4°C, 400 × *g* for 5 min. Discard supernatant. Add DAPI and acquire cells (See Figs. 175 and 176 for gating strategies).

7.2.3.4 Materials.

General reagents.

- Dulbecco's PBS with calcium and magnesium
- Wash buffer: PBS with 2% heat-inactivated FCS and 2 mM EDTA.
- 70 μM Cell-strainer mesh
- 1× RBC lysis buffer (eBiosciences)

Staining reagents for murine neutrophils

Table 64. List of antibodies used for characterisation of neutrophil subsets

Marker	Fluorophore	Supplier	Catalog number	Clone	Host	Isotype
CD101	PE	eBioscience	12-1011	Moushi101	Rat	IgG2a, κ
Siglec-F	PE-Texas Red	BD Biosciences	562757	E50-2440	Rat	IgG2a, κ
Ly6G	PE-Cy7	Biolegend	127618	1A8	Rat	IgG2a, κ
B220	PE-Cy7	eBioscience	25-0452	53-6.7	Rat	IgG2a, κ
NK1.1	PE-Cy7	eBioscience	25-5941	PK136	Mouse	IgG2a, κ
CD90.2	PE-Cy7	eBioscience	25-0902-82	53-2.1	Rat	IgG2a, κ
Gr-1	PerCP-Cy5.5	eBioscience	45-5931-80	RB6-8C5	Rat	IgG2b, κ
cKit	SB436	eBioscience	62-1171	2B8	Rat	IgG2b, κ
CD11b	BV655	Biolegend	101259	M1/70	Rat	IgG2b, κ
CD115	APC	eBioscience	61-1152	AFS98	Rat	IgG2a, κ
Ly6C	APC/Cy7	eBioscience	47-5932	HK1.4	Rat	IgG2a, κ
CXCR4	Biotin	eBioscience	13-9991-80	2B11	Rat	IgG2b, κ
Streptavidin	BUV395	BD Biosciences	564176	—	—	—

Staining reagents for human neutrophils

Marker	Fluorophore	Supplier	Catalogue Number	Clone	Host	Isotype
CD10	FITC	Biolegend	312208	HI10a	Mouse	IgG1, κ
CD33	PE	Biolegend	303404	WM53	Mouse	IgG1, κ
CD49d	PE-Texas Red	BD Biosciences	563645	9F10	Mouse	IgG1, κ
CD3	PE-Cy7	Biolegend	300420	UCHT1	Mouse	IgG1, κ
CD19	PE-Cy7	eBioscience	25-0199	HIB19	Mouse	IgG1, κ
CD56	PE-Cy7	Biolegend	318318	HCD56	Mouse	IgG1, κ
CD34	PE-Cy7	Biolegend	343516	581	Mouse	IgG1, κ
CD66b	BV421	BD Biosciences	562940	G10F5	Mouse	IgM, κ
CD15	BV655	BD Biosciences	564232	HI98	Mouse	Ig2M, κ
CD14	BV711	Biolegend	301838	M5E2	Mouse	IgG2a, κ
CD101	APC	Biolegend	331010	BB27	Mouse	IgG1, κ
CD45	APC-Cy7	Biolegend	304014	HI30	Mouse	IgG1, κ
CD16	BUV737	BD Biosciences	564434	3G8	Mouse	IgG1, κ
CD16/32	Purified	BD Biosciences	564219	2.4G2	Mouse	IgG2b, κ
CD11b	BUV395	BD Biosciences	563839	ICRF44	Mouse	IgG1, κ

Flow Cytometer. All experiments were performed on a LSRII flow cytometer with a 365, 405, 488 nm, 561, and 640 nm configuration (BD Bioscience). Filters: 379/34(365) for BUV395; 740/35(365) for BUV737; 450/50(365) for DAPI; 530/30(488) for FITC or AF488; 685/35(488) for PerCP-Cy5.5; 450/50(405) for BV421 or SB436; 525/50(405) for BV510 or V500; 660/20(405) for BV650; 710/40(405) for BV711; 800/50(405) for BV785; 585/15(561) for PE; 610/20(561) for PE-Texas Red; 780/60(561) for PE-Cy7; 675/20(640) for APC or AF647; 730/45(640) for AF700; 780/60(640) for APC-eF780 and APC-Cy7.

7.2.3.5 Pitfalls.

- Human neutrophils are sensitive to Ficoll, and will change the expression of certain markers. For example, Ficoll will down-regulate CD49d expression that prevents the isolation of proliferative preNeus from immature Neus.

7.2.3.6 Top tricks.

- In certain inflammatory conditions, such as a bacterial challenge, neutrophils may lose Ly6G expression. Make use of SSC information and Ly6C expression level to gate for neutrophils.
- Perform titration of Abs for optimal staining index. Typically, 0.25 μL is used for mouse Abs for one-fifth of femur marrow and 2 μL per 5 million cells is used for human Abs.
- Bone marrow composition in tibias, humeri, pelvis, and sternum are similar to the femur. Therefore, use these bones if large numbers of neutrophils are required for sorting purposes.
- Gr-1 labels both Ly6G and Ly6C. When staining, use twice the amount of Ly-6G to prevent competitive binding by Gr-1.

7.2.3.7 Table summary of neutrophil subset phenotypes in mouse and human.

Neutrophil Subset	Mouse	Human
Pre-Neutrophils	CD115$^-$SiglecF$^-$Gr-1^{hi}CD11b$^+$CXCR4^{hi}cKit^{hi}Ly6G^{lo}CD101$^-$	CD66b$^+$CD15$^+$CD49d^{lo}CD101$^-$CD16$^+$CD10$^-$
Immature Neutrophils	CD115$^-$SiglecF$^-$Gr-1^{hi}CD11b$^+$CXCR4^{lo}cKit^{lo}Ly6G$^{-/+}$CD101$^-$	CD66b$^+$CD15$^+$CD49d$^-$CD101$^+$CD16^{++}CD10$^-$
Mature Neutrophils	CD115$^-$SiglecF$^-$Gr-1^{hi}CD11b$^+$CXCR4^{lo}cKit^{lo}Ly6G$^+$CD101$^+$	CD66b$^+$CD15$^+$CD49d$^-$CD101$^+$CD16^{++}CD10$^+$

- Besides Ficoll, temperature can affect marker expression. Therefore, keep cells on ice throughout sample preparation as markers like CD115 will down-regulate.

Eosinophils can be a big source of contamination as they share many markers like CD15 and CD11b with neutrophil subsets. They are CD101$^+$CD49d$^+$CD16$^-$ and express Siglec-8. Gating them out is essential, especially in eosinophilic patient samples.

Classical Human Nomenclature	Markers
Promyelocyte/Myelocyte	CD66b+CD15+CD11b$^-$ CD16$^-$
Metamyelocyte	CD66b+CD15+CD11b$^+$ CD16$^-$
Band Cells	CD66b+CD15+CD11b$^+$ CD16$^+$
Segmented Neutrophil	CD66b+CD15+CD11b$^+$ CD16^{++}

8 Murine bone marrow stromal cells

8.1 *Overview*

The bone marrow (BM) stroma plays a critical role in the maintenance of hematopoietic homeostasis. The ability to isolate BM stromal cells at high efficiency is critical to maximize cell recovery and reproducibility of the isolation procedure. In this section, we describe the processing of BM samples through sequential enzymatic digestion and the gating strategy used to identify stromal and mesenchymal stem cells (MSCs).

8.2 *Introduction*

The bone marrow stroma is composed of non-hematopoietic cells responsible for the structural organization of the marrow cavity where they support blood cell development. Early work by Friedenstein et al. has shown that stromal cells could be distinguished from hematopoietic cells by their adherence to plastic culture dish and their ability to form fibroblastic colonies (called CFU fibroblasts or CFU-F) when plated at clonal density [1495]. Subsequently, a single CFU-F was shown to generate heterotopic ossicles when transplanted in vivo [1496]. These studies paved the way to our understanding of how BM stromal cells regulate developmental and steady-state hematopoiesis. MSCs located at the top of the stromal hierarchy can self-renew and differentiate into bone, fat, and cartilage [1497]. MSC populations are found in distinct perivascular niches where they regulate hematopoietic stem and progenitor functions through the action of cell-bound or secreted cytokines [1498]. In the developing mouse marrow, $CD45^- Tie2^-$ $Thy1.1^- CD105^+ CD51^+$ progenitors undergo endochondral ossification and contribute to the formation of the BM cavity by promoting vascularization and the formation of an hematopoietic stem cell (HSC) niche [1499]. In the adult mice BM, MSCs can be labeled by GFP in Nestin-GFP transgenic mice, wherein Nestin-GFP^+ cells contain all CFU-F activity or mesensphere formation capacity of the BM [1500]. Nestin-GFP^{bright} cells mark periarteriolar stromal cells that are significantly associated with quiescent HSCs and secrete niche factors such as Cxcl12 and Stem Cell Factor (SCF) that contributes to HSC localization and maintenance [1501]. Nestin-GFP^+ cells also highly overlap with stromal cells expressing the Leptin receptor [1502], Cxcl12-abundant reticular (CAR) cells [1503] or Prx-1-cre cells [1504] that have also been described as regulators of hematopoietic stem and progenitors functions. Lineage tracing has also revealed the osteogenic and stromal contribution of MSCs during development [1505]. Furthermore, skeletal stem cells found in the periosteum of long bones have been shown to contribute to bone formation at steady state or after injury [1506–1508].

To study murine BM stromal cells populations, cell surface markers have been proposed to facilitate their identification, but many of these markers are expressed on cultured cells and may differ from freshly isolated stromal cells [1509]. In addition, dis-

tinct stromal cell populations can be extracted depending on the isolation methods. Sequential digestion of BM plugs results in efficient extraction of stromal cells with MSC activity [1510]. $CD51^+$ $PDGFRa^+ CD45^- Ter119^- CD31^-$ cells comprise most of detectable BM MSC activity isolated from flushed BM plugs and can reconstitute an ectopic HSC niche when transplanted under the kidney capsule [1511]. Crushed bone can result in an enrichment of $PDGFRa^+ Sca-1^+ CD45^- Ter119^- CD31^-$ MSCs [1512, 1513] or skeletal stem cells expressing Gremlin1 [1514] and CD200 [1506]. While a hierarchal organization for skeletal stem cells and downstream progenitors responsible for cartilage, bone, and stromal cell generation has been proposed [1506], it remains unclear how the bone-associated skeletal stem cells and BM-associated MSCs relate to each other. Therefore, the isolation method (enzymatic treatments, bone crushing, or flushing) will influence the content and heterogeneity found within the stromal cell fraction.

8.3 *Step-by-step sample preparation*

The stromal fraction of the BM is classically defined by the absence of CD45 (hematopoietic), Ter119 (erythroid) and CD31 (endothelial) marker expression. $CD45^- Ter119^- CD31^-$ or triple-negative cells (TNCs) are known to contain stromal cells as well as hematopoietic cells [1515]. In order to isolate BM stromal cells, femurs or tibias from mice can be cut below the metaphysis toward the epiphysis and the BM is flushed out as an intact plug using syringe with 21G (femur) or 25 ½ G (tibia) needle containing digestion buffer (collagenase type IV 2 mg/mL and dispase 1 mg/mL in HBSS). While CD45, CD31, Ter119, and CD51 epitopes have been shown to be resistant to cell digestion [1515], it is important to compare the sensitivity of each marker to be tested on digested cells and undigested or flushed cells. BM plugs are sequentially digested three times for 10 min at 37°C. The supernatant, which contains cells released by the digestion process, is collected after each digestion and pooled into a 50 mL tube containing ice-cold FCM buffer (PBS, EDTA 2 mM, BSA 0.1%) to prevent any loss of cell surface markers or cell viability. Following the digestion process, enzymatically dissociated cells can be centrifuged and the pellet can be subjected to RBC lysis. Cells are then filtered through a 100 μm cell strainer to remove any clumps prior to staining for FCM analysis. For cell sorting, it is recommended to perform $CD45^+$ cells depletion using microbeads directly conjugated with CD45 mAb (Miltenyi Biotec) that will enrich for TNCs. After incubation with CD45 microbeads the cell suspension is washed, pelleted and resuspended in 500 μL FCM buffer. Cells are applied to a column (Miltenyi Biotec) coupled with a magnet which will retain $CD45^+$ hematopoietic cells. Cells are eluted by washing the column with $2 \times 1mL$ of FCM buffer and can be used for antibody staining (Table 65) for 15 min at 4°C. Stained cells are washed and resuspended in FCM buffer containing a viability dye such as DAPI or 7-AAD.
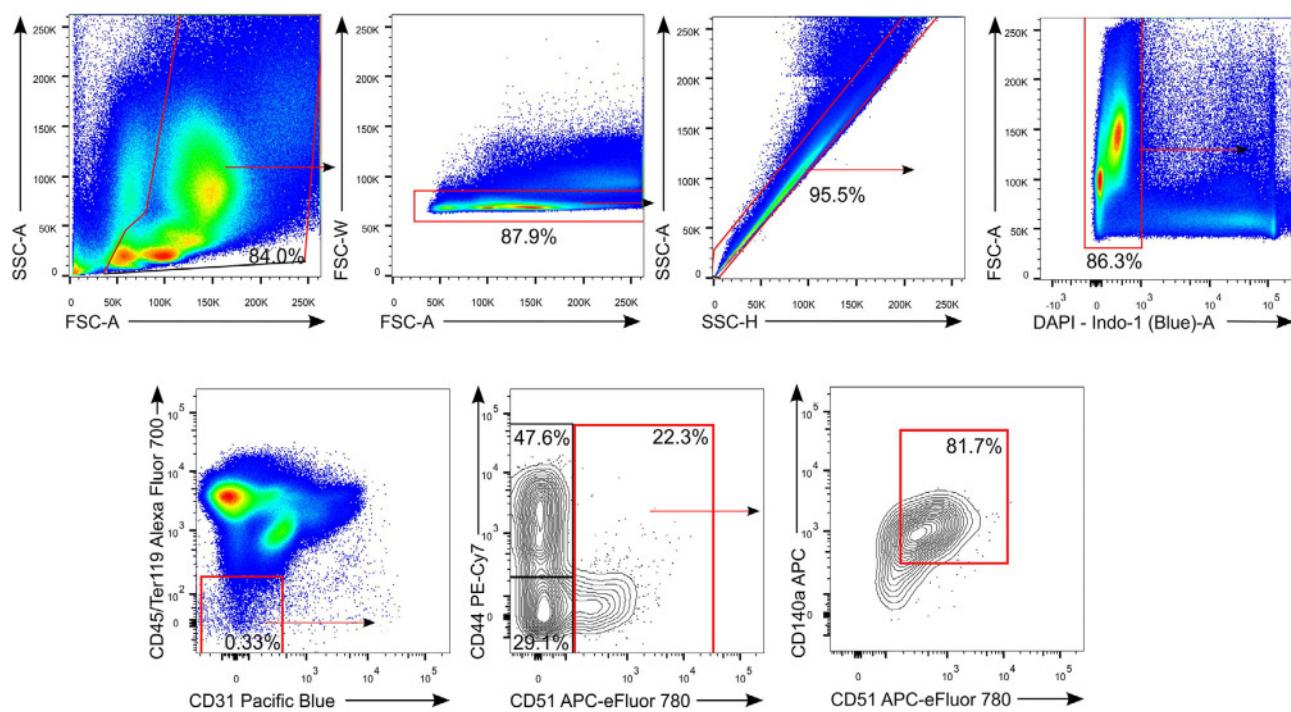
Figure 177. Gating strategy for murine BM stroma. Live single cells are separated using CD45, Ter119, and CD31 markers (left panel). Gated TNCs are then analyzed for their expression of stromal marker CD51 and for excluding hematopoietic cells by using CD44 (middle panel). MSC populations can be found within CD51$^+$ TNCs where PDGFRα expression can be detected (right panel).

Table 65. Antibodies to analyze mouse bone marrow stromal cells

Antibody	Fluorochrome	Clone	Company
CD45	Alexa Fluor 700	30-F11	BioLegend
Ter119	Alexa Fluor 700	Ter-119	BioLegend
CD31	Pacific Blue	390	BioLegend
CD51	Biotin	RMV-7	eBioscience
CD44	PE-Cy7	IM7	eBioscience
PDGFRα	APC	APA5	eBioscience
Streptavidin	APC-eFluor 780	–	eBioscience

8.4 Materials

8.4.1 Animals. Adult mice such as C57BL/6 (8–12 weeks old).

8.4.2 Reagents.

1. Collagenase type IV (Gibco, Cat #17104019)
2. Dispase (Gibco, Cat #17105-041)
3. Ammonium chloride (Sigma, Cat #A4514)
4. DAPI (Sigma, Cat #D9542)

8.4.3 Solutions.

1. HBSS (Corning, Cat #21-023-CV)
2. FCM buffer (PBS 1×, EDTA 2 mM, BSA 0.1%)
3. RBC lysis buffer (NH$_4$Cl 0.17 M, KHCO$_3$ 0.01 M, EDTA 0.1 mM)

4. Digestion buffer (Collagenase IV 2 mg/mL, Dipase II 1 mg/mL in HBSS)
5. DAPI (0.05 µg/mL in FCM buffer)

8.4.4 Equipment.

1. 1 mL syringe with 21G × 1 needle (for femurs) or 25 G × 5/8 needle (for tibias)
2. 100 µM cell strainer (Falcon, Cat #08-771-19)
3. CD45 microbeads, mouse (Miltenyi Biotec, Cat #130-052-301)
4. MACSR® LS column (Miltenyi Biotec, Cat #130-042-401)
5. QuadroMACSR® separator (Miltenyi Biotec, Cat #130-090-976)
6. FCM cell sorter (at least five colors and equipped with UV laser)

8.5 Data analysis

When using adult mice, TNCs represent approximately 0.5% of total single live BM cells (Figure 177). The TNC fraction contains mostly hematopoietic cells (~85%), which are found in the CD44$^+$ CD51$^-$ and CD44$^-$ CD51$^-$ TNCs. Gating on CD51$^+$ cells allows the separation of bona fide stromal cells from hematopoietic TNCs, while MSCs can be further selected by gating on CD51$^+$ PDGFRa$^+$ TNCs (Fig. 177). Cell surface markers such as CD200, Thy-1, and 6C3 can be used to distinguish among cartilage, bone, and stromal cells when samples are made from crushed bones [1499, 1506, 1513]. Consistency in the processing of BM plugs should limit the variation in the frequency of isolated TNCs or MSCs.

8.6 Pitfalls

In the event that additional markers are to be included in the gating strategy, their sensitivity to the enzymatic digestion should be addressed. Samples should be analyzed as soon as possible after processing and staining since digested BM cells have a higher tendency of clumping together than undigested samples.

8.7 Top tricks

To ensure equal digestion throughout all samples, first harvest all bones and place on ice, in PBS. Then, flush the first sample with digestion buffer and directly put at 37°C. Start timer for the first 10 min of incubation and proceed with the second sample and so on. A constant digestion incubation time is critical in order to avoid overdigestion which could result in a loss of cell surface markers, and to reduce variation among samples.

9 Hematopoietic Stem Cells

9.1 Overview

This chapter deals with the characterization, isolation, and preparation of murine and human hematopoietic stem cells (HSCs).

9.2 Introduction

Throughout life of mice and humans the major site of HSCs is bone marrow [1516–1518]. HSCs are thought to reside in cellular niches [1519–1521], generated by environmental non-hematopoietic stromal cells of mesenchymal and endothelial origin (See Chapter VI Section 8 Murine bone marrow stromal cells) and of other, hematopoietic cells, which ensure their quiescence and longevity and their capacity to proliferate and/or differentiate to more lineage restricted progenies. This proliferation and differentiation continuously regenerates, and thereby maintains the differentiated compartments of erythroid, myeloid, and lymphoid cell lineages. Differentiation can occur in a hierarchical order from LT-HSC to ST-HSC, to erythroid and megakaryocytic progenitors and to lymphoid–myeloid progenitors (LMPP, MPP) and from them to common lymphoid progenitors (CLP) and common myeloid progenitors (CMP). These progenies give rise to erythrocytes, megakaryocytes, and platelets, monocytes, macrophages, and granulocytes, and to lymphoid cells (T- and B-, dendritic, innate, and natural killers and innate lymphoid cells). A part of the generation of myeloid and erythroid cells can be initiated directly from a special subpopulation of HSCs. Under stress, such as a bacterial or viral infection, this direct differentiation to granulopoiesis, erythropoiesis, and the development of megakaryocytes and platelets is increased and accelerated directly from HSC [1522–1524].

Transplantation of HSC into suitably recipient hosts populates all HSC and progenitor compartments in bone marrow of the host and regenerates erythroid, myeloid, and lymphoid compartments with donor-derived cells to normal sizes.

9.3 Murine hematopoietic stem cells

The first part of this chapter describes the methods for adult murine hematopoietic stem cells.

In mice, HSCs are generated during embryonic development, first extra-embryonically from cells in yolk sac, then from cells in the embryonic aorta-gonad-mesonephros area via hemangioblasts, which are common progenitors of vascular endothelium and hematopoietic cells [1525, 1526]. These early progenitors seed into fetal liver and fetal thymus to generate first, transient waves of hematopoiesis. Shortly before birth, the developing marrow of bone becomes the site, where HSC find an environment for their life-long residence, hematopoietic renewal and differentiation capacities [1527].

HSCs are identified by FCM, based on surface-marker expression. One set of fluorescent mAb combinations, and the FCM profiles of the stained bone marrow cells is given in Fig. 178. HSCs are found in the 0.1% of all $CD45^+$ bone marrow cells, which do not yet express the markers of differentiated hematopoietic cells, i.e., of $F4/80^+/Mac1^+$ monocytes and macrophages, $Gr1^+$ granulocytes, $CD11c^+$ dendritic cells, $CD4^+/CD8^+/CD3^+$ T cells, $CD5^+CD19^+B220^+$ B cells, $NK1.1^+$ NK cells, and $Ter119^+$ erythrocytes. Thus, they are "lineage-negative" (Lin-. L). The absence of these antigens and expression of CD45 is necessary to identify the hematopoietic population within the lineage-negative (Lin^-) cells of the bone marrow. On the other hand, HSC express Sca-1 (S) and c-Kit (K), thus are called LSK-cells.

Furthermore, differences in surface expression of the CD150 and CD48 "SLAM" markers allow to distinguish long-term self-renewing HSCs and transiently reconstituting multipotent progenitors [1531–1533]. Thus, a $Lin^-c\text{-}Kit^+Sca\text{-}1^{+-}CD150^+CD48^-$ population contains mainly long-term self-renewing HSCs, a $Lin^-c\text{-}Kit^+Sca\text{-}1^+ CD150^+CD48^+$ population mainly transiently self-renewing multipotent progenitors, and a $Lin^-c\text{-}Kit^+Sca\text{-}1^+CD150^-CD48^+$ population mainly non-self-renewing multipotent progenitors [1531–1533]. Their functions have been determined by transplantation analyses. These three distinct populations vary with each stage in the progression toward lineage commitment in their frequency, engraftment-kinetics, self-renewal potential, cell-cycle status, gene expression, and lineage distribution of the mature cells they can generate in vivo.

In the bone marrow of 2–3 month-old mice between 1 and 3 × 10^3 LSK, $CD150^+CD48^-$ cells remain in a non-proliferating, cell cycle Go-resting state for life [1534, 1535].

Barcoding of these early progenitors shows that most of them have clone sizes of less than ten cells, and most of them retain these small clone sizes, because they divide at best once a year in the life of a mouse [1534, 1535]. A part of this HSC population can be transplanted, remarkably even as single (e.g. $CD45.1^+$) HSC with carrier ($CD45.2^+$) bone marrow cells into lethally irradiated (ideally histocompatible CD45.1xCD45.2) recipients. They home
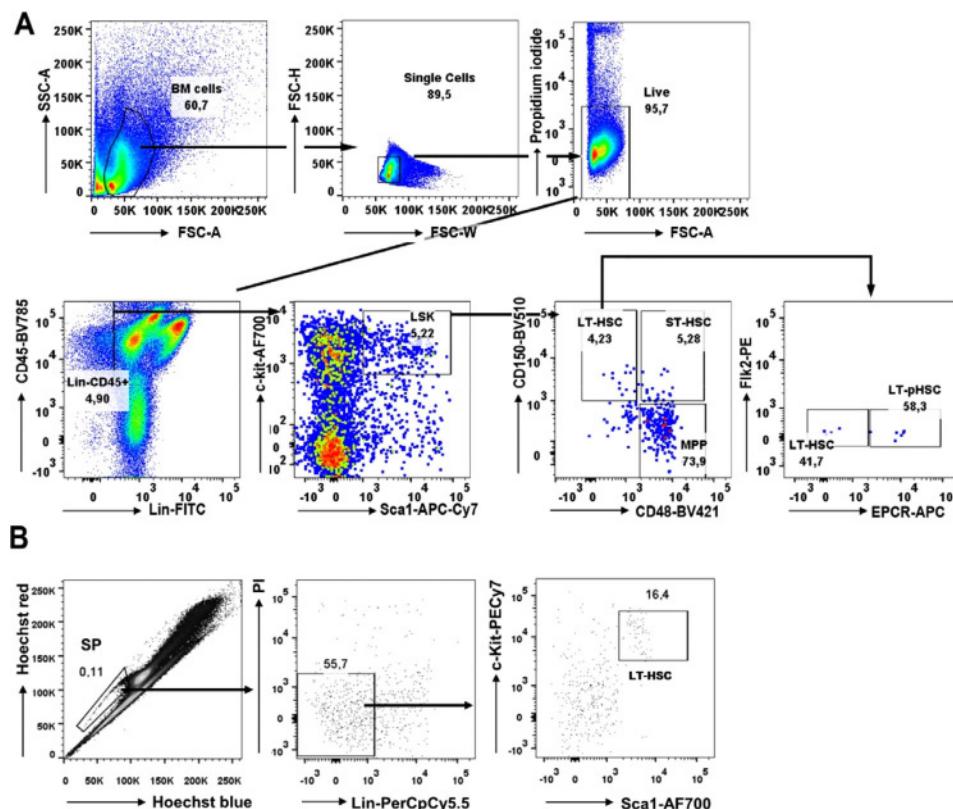
Figure 178. Gating strategy of mouse hematopoietic stem cells. Phenotypic characterization of mouse bone marrow derived HSCs. LSK cells were identified as c-kit$^+$ Sca1$^+$ cells within the CD45$^+$ Lin- compartment. LT-HSCs were further identified as CD150$^+$ CD48$^-$, ST-HSCs as CD150$^+$ CD48$^+$, and MPPs as CD150$^-$ CD48$^+$ cells. LT-pHSCs can be further characterized as Flk2$^-$EPCR$^+$ (CD201) population within the CD150$^+$ CD48$^-$ gate. Gating for all colors were set according to the isotype control staining (not shown). Forward and side scatter voltages can be increased to dissect bone marrow cell populations into more differentiated subpopulations, differing in size and density (see general introduction).

to bone marrow and then repopulate all HSC compartments, all hematopoietic progenitors and all mature cell lineages, except of the long-lived resident myeloid cells generated from fetal liver progenitors during embryonic development [1536]. These HSC are called long-term repopulating (LT-HSC). Upon transplantation LT-HSC can home back to bone marrow into special niches near hypoxic areas of arteriolar vascular endothelium and barcoding reveals a smaller number of these LT-HSC with much larger clone sizes [1522].

Between 4 and 8×10^3 HSC are lin-sca1$^+$c-kit$^+$CD150$^+$CD48$^+$ HSC, which are in active G1-S-G2-M cell cycle, renewing their HSC state by symmetric or asymmetric cell divisions. In asymmetric cell divisions a fraction of them can enter differentiation to more mature states of hematopoietic developments. When transplanted, these HSC repopulate all different lymphoid and myeloid cell lineages in subsiding waves, again without populating the embryonically derived resident myeloid cell lineages. They do not repopulate the LT-HSC. Since they repopulate the transplanted host only for a short time, they are short-term active HSC (ST-HSC). ST-HSCs have also been described to be lin-sca1+c-kit+CD150$^-$CD48$^-$ cells [1534]. The relationship of these "SLAM"-negative HSC to the double "SLAM"-positive ST-HSC remains to be investigated.

HSC can be mobilized to enter blood circulation. They might differentiate in the periphery or pick up intracellular infections, such as *Mycobacterium tuberculosis*, and then use their exceptionally efficient capacity to return to bone marrow and become again resident in their niches [1537].

9.3.1 Isolation of murine HSCs. The first step in the preparative isolation of adult mouse HSCs from BM is the erythrolysis with hypothonic ACK (ammonium-chloride-potassium) solution. The next step usually consists of removing mature cells that express "lineage" (Lin) antigens specific to terminally differentiated blood cells, including F4/80$^+$/Mac1$^+$ monocytes and macrophages, Gr1$^+$ granulocytes, CD11c$^+$ dendritic cells, CD4$^+$/CD8$^+$/CD3$^+$ T cells, CD5$^+$CD19$^+$B220$^+$ B cells, NK1.1$^+$ NK cells, and Ter119$^+$ erythrocytes. HSC are then enriched from the remaining cells as Lin$^-$ CD45$^+$ cells that express combinations of cell surface markers, c-Kit and Sca1. Multipotent hematopoietic progenitors, purified as LSK (Lin$^-$ c-Kit$^+$Sca-1$^+$) make up <0.1% of nucleated BM cells. They contain all multipotent progenitors in mice [1538–1541]. However, they are still heterogeneous, containing transiently reconstituting multipotent progenitors in addition to long-term reconstituting HSCs.

The differences in "SLAM"-marker expression between long-term self-renewing HSCs and transiently reconstituting multipotent progenitors permit the separation and independent isolation of these different progenitor populations [1531–1533] as Lin$^-$c-Kit$^+$Sca-1$^+$ CD150$^+$CD48$^-$, mainly long-term self-renewing (LT-)HSCs, Lin$^-$c-Kit$^+$Sca-1$^+$ CD150$^+$CD48$^+$, mainly transiently renewing HSC (ST-HSC), and Lin$^-$c-Kit$^+$Sca-1$^+$ CD150$^-$CD48$^+$, mainly non-renewing multipotent progenitors (MPP), as characterized by transplantation analyses. These three distinct populations vary with each stage in the progression toward lineage commitment in their frequency, engraftment-kinetics, self-renewal

potential, cell-cycle status, gene expression, and lineage distribution of the mature cells they can generate in vivo.

However, "SLAM"-defined cells themselves are still heterogeneous populations in which HSCs represent, at most, 20% of all cells. Further enrichment of LT-HSCs can be achieved by the purification of SLAM-defined cells that express high levels of EPCR (CD201) [1542]. The expression of CD34 and Flk2 further defines the ST-HSC and MPP sub-populations, respectively [1543, 1544] (Fig. 178A). Although transiently reconstituting multipotent progenitors are enriched in the CD34$^+$ fraction, they usually are not purified based on CD34 expression. Rather, the current purification protocols are based on the LSK, SLAM, and endothelial protein C receptor (EPCR) expression patterns of these HSCs and progenitors.

Alternatively, HSCs can be isolated due to their hypoxia-induced high expression of the multidrug transporter proteins MDR1 and ABCG2, thus, cells that retain only low levels of DNA dyes, such as Rhodamine-123 (Rho123) and Hoechst 33342. Rho123^{lo} or Hoechst^{lo} cells ("side population," SP cells), and that are Lin$^-$c-Kit$^+$Sca-1$^+$ are nearly pure populations of long-term reconstituting HSCs [1545, 1546] (Fig. 178B).

It should be kept in mind, that all these purified HSC populations are still a heterogeneous collection of cells, when their functions are considered. Thus, it is believed that myeloid-biased HSCs express higher levels of CD150 and efflux Hoechst 33342 more efficiently than lymphoid-biased HSCs. They also exhibit higher self-renewal ability as demonstrated by serial transplantation of BM cells from primary recipients into secondary hosts. Quantitative analyses of the frequencies of single HSC/progenitors for a given function "in vitro" or "in vivo" (e.g., as done with single cells) should be attempted to define their potencies [1547] or [1522] or [1548] or [1549–1551].

9.3.2 Materials.

1. Adult mice such as C57BL/6, typically, 6- to 10-week-old mice are used for the isolation of HSCs.
2. Staining medium: PBS Solution (1xPBS) with 0.5% BSA fraction V, 2 mM EDTA, without azide.
3. Nylon screen (40 μm nylon mesh) to filter the cells after isolation.
4. 10-mL syringes with 25-gauge needles to flush marrow out of femurs and tibias.
5. Use 15-mL tubes to stain BM cells. Abs described in this protocol are available from eBioscience and BioLegend.
6. Lineage-marker Abs: anti-Mac1/CD11b (M1/70), anti-Gr1 (RB6-8C5), anti-Ter119 (TER-119), CD19 mAb (6D5), anti-B220 (RA3-6B2), CD5 mAb (53-7.3), CD3ε mAb (145-2C11), CD11c mAb (N418), CD4 mAb (GK1.5), CD8 mAb (53-6.7), and anti-NK1.1 (PK136). Note that all Abs should be titrated before use, and used at dilutions that brightly stain antigen positive cells without nonspecific staining.
7. Anti-CD45 (30-F11), anti-Flk2 (A2F10), anti-EPCR/CD201 mAb (RCR-16), anti-Sca-1 (D7), anti-c-kit (ACK2), CD150 mAb

(TC15-12F12.2), CD34 mAb (RAM34), and CD48 mAb (HM48-1).
8. SP buffer (PBS, 2% FCS, 2 mM HEPES buffer; GIBCO, Life Technologies), Hoechst 33342 (5 μg/mL, Molecular Probes, Life Technologies).
9. A viability dye such as PI or 7-AAD.

9.4 Human hematopoietic stem cells

In this chapter we provide an overview on the identification and isolation of human hematopoietic stem cells (HSCs) from different sources (see Fig. 179 for identification of HSCs from BM).

9.4.1 Isolation of human HSCs. Primary sources of human HSCs are human bone marrow, G-CSF-mobilized blood, umbilical cord blood, and fetal liver. Human HSCs can also be isolated from immune-deficient mouse models engrafted with primary human HSCs.

Isolation from human sources: Mononuclear cells are prepared from human bone marrow, peripheral blood, or umbilical cord blood using Ficoll-Paque density gradient centrifugation (e.g., 3–5 mL bone marrow for $1–10 \times 10^7$ MNCs or 15–20 mL cord blood for $1–15 \times 10^7$ MNCs). After collection of the MNCs, cells are washed three times in PBS/2% FCS. If the cell pellet is very red after two washes of the MNCs, a RBC lysis may be performed (5 minutes in ACK lysing buffer).

Isolation from mouse recipients: Bone marrow cell suspensions are prepared as outlined above (See Chapter V Section 9.3.1 Isolation of murine HSCs).

Perform Ab staining in PBS/2% FCS (100 μL Ab mix for $1–2 \times 10^7$ MNCs) for 40 min at 4°C. Refer to Table 66 for a list of the antibodies. Wash cells once in PBS/2% FCS and resuspend in appropriate volume of PBS/ 2% FCS containing a viability dye such as DAPI, PI, or Sytox Green.

Filter cells prior to analysis through a 40 μm filter.

Analyze cells on a flow cytometer or cell sorter with at least eight-color capability.

Gatings to determine positivity are performed using FMO. Isotype controls are used to show that no unspecific binding is observed in the chosen gates.

HSCs from all sources display a similar pattern of surface marker expression and can therefore be isolated using the same panel of antibodies (See Table 66). Like murine HSCs, human HSCs do not express antigens of mature blood cell lineages (Lin$^-$). Further, the glycoprotein Thy-1 (CD90) has been shown to be expressed on human HSCs [1552, 1553]. But other than this, there is not much correspondence of cell surface markers identifying HSCs in mice and humans.

The most important surface marker used to enrich human hematopoietic progenitor cells (HPCs) is the glycoprotein CD34, which is expressed on HSCs and committed progenitors but not mature blood cells [1554]. In mice, LT-HSCs do not express CD34 whereas ST-HSCs and progenitors are CD34$^+$ [1543, 1555].
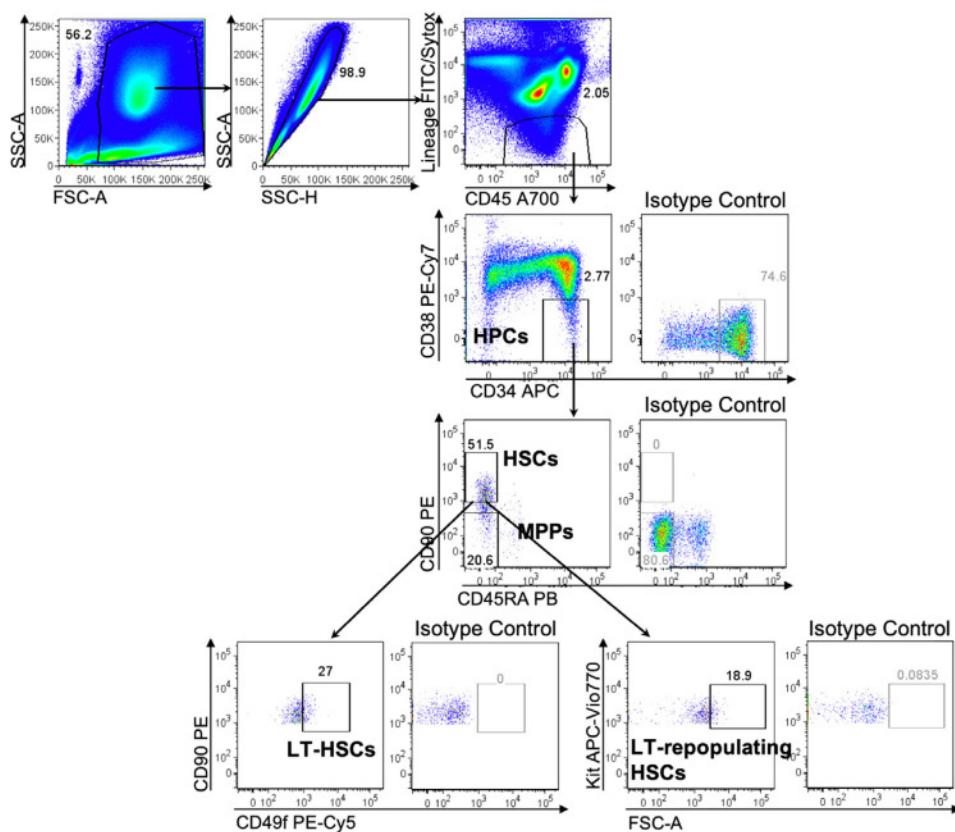
Figure 179. Phenotypic characterization of HSCs from human BM. HSPCs were identified as CD34+ CD38− cells within the CD45+ Lin− compartment. HSCs were identified as CD34+ CD38− CD90+ CD45RA− cells and MPPs as CD34+ CD38− CD90− CD45RA− cells [1528, 1529]. LT-HSCs can be identified using CD49f [1529] or Kit (CD117) (Cosgun et al., [1530]). Gatings for CD38, CD90, CD49f, and Kit were performed according to isotype controls, which are depicted in the right side of each plot.

CD34-enriched cells from human bone marrow or mobilized peripheral blood are frequently used in clinical stem cell transplantation [1556]. However, HSC activity has also been reported in the CD34− population of human cord blood and bone marrow, even though those cells are extremely rare [1557–1559].

However, CD34 expression alone does not provide an accurate measure of HSCs because also hematopoietic progenitor cells are positive for CD34, and additional markers are required to identify and isolate the most primitive HSCs [1560]. Multilineage reconstitution in vivo models in combination with FCM allowed to further separate the Lin- CD34+ population using markers that are differentially expressed on immature and more differentiated cells. Bhatia et al. showed that the CD38− fraction of CD34+ human bone marrow and cord blood cells was highly enriched for cells with the ability to repopulate immune-deficient mice [1561]. Limiting dilution analysis showed that one in 617 purified CD34+ CD38− cells was able to engraft in a NOD/SCID mouse for at least 8 weeks. Ten years later, Majeti et al. showed that Lin− CD34+ CD38− human bone marrow and cord blood cells could be further subdivided using the cell surface markers CD90 and CD45RA [1528]. They identified Lin− CD34+ CD38− CD90+ CD45RA− cells as HSCs with long-term repopulation capacity for up to 30 weeks with as few as ten transplanted cells being able to engraft NOG newborn mice. Purified Lin− CD34+ CD38− **CD90−** CD45RA− cells were also capable of long-term multilineage engraftment in immunodeficient mice, but more cells were required to achieve engraftment and the cellular output per transplanted stem cell was lower. Sec-

ondary transplantations showed that CD90+ HSCs generated secondary transplants at a significantly higher frequency than CD90− cells. Thus, Majeti and colleagues postulated that human HSCs with long-term repopulation and self-renewal capacity are contained within the Lin− CD34+ CD38− CD90+ CD45RA− population of human cord blood and bone marrow cells whereas Lin− CD34+ CD38− **CD90−** CD45RA− cells mainly contain the less primitive multipotent progenitors [1528].

The group of John Dick identified CD49f (VLA-6) as an additional marker for human long-term HSCs using limiting dilution assays and single-cell transplantation into NSG mice [1562]. They showed that one of ten Lin− CD34+ CD38− CD90+ CD45RA− CD49f+ cells had long-term repopulation activity and could be serially transplanted, representing the most purified population of human HSCs to date. Recently, the laboratory of Claudia Waskow showed that human HSCs with increased long-term repopulating activity could be further enriched by high expression of the Kit receptor on the cell surface of CD34+ CD38− CD90+ CD45RA− human HSCs [1530]. Transplanted Lin− CD34+ CD38− CD90+ CD45RA− Kit^hi cord blood cells led to a human chimerism of around 60% in peripheral blood for up to 30 weeks and an increased frequency of human HPCs in bone marrow of recipient mice compared to Lin− CD34+ CD38− CD90+ CD45RA− Kit^lo cells (22% blood chimerism). Whether HSCs with long-term repopulation potential within the CD49f+ and the Kit^hi HSC populations are overlapping remains to be shown in future studies. The

Table 66. Abs used for the identification of human cell types

Antibody	Clone	Conjugate	Supplier	
CD2	RPA-2.10	FITC	eBioscience	Lineage mix
CD3	HIT3a	FITC	eBioscience	
CD10	SN5c L4-1A1	FITC	eBioscience	
CD11b	CBRM1/5	FITC	eBioscience	
CD14	61D3	FITC	eBioscience	
CD15	HI98	FITC	eBioscience	
CD16	CB16	FITC	eBioscience	
CD19	HIB19	FITC	eBioscience	
CD56	MEM188	FITC	eBioscience	
CD235a	HIR2	FITC	eBioscience	
CD34	581	APC	BioLegend	
CD38	HIT2	PE-Cy7	eBioscience	
CD45	HI30	Alexa Fluor® 700	BioLegend	
CD45RA	HI100	eFluor® 450	eBioscience	
CD49f	GoH3	PE-Cy5	BD Biosciences	
CD90	5E10	PE	BD Biosciences	
CD117	A3C6E2	APC Vio770	Miltenyi	
Isotype Controls				
Mouse IgG1 κ	MOPC-21	PE	BioLegend	
Mouse IgG1 κ	P3.6.2.8.1	PE-Cy7	eBioscience	
Rat IgG2a κ	eBR2a	PE-Cy5	eBioscience	
Mouse IgG1 κ		APC Vio770	Miltenyi	

Table 67. Cell surface phenotype for the identification of human HSPC populations

HPC population (CD45+ Lin−)	Phenotype/ subphenotype	Reference
HPCs	CD34+ CD38−	[1561]
HSCs	CD34+ CD38− CD90+ CD45RA−	[1528]
MPPs	CD34+ CD38− CD90− CD45RA−	[1528, 1529] add PMID 26541609
LT-HSCs	CD34+ CD38− CD90+ CD45RA− CD49f+	[1562]
LT-HSCs	CD34+ CD38− CD90+ CD45RA− CD117hi	[1530]

different cell surface phenotypes of human HSPC populations are summarized in Table 67.

Another marker, which was only lately proposed to identify a subset of human HSCs in cord blood, is the EPCR [1563]. The group of Guy Sauvageau showed that only EPCR+ CD34+ but not EPCR− CD34+ cord blood cells were able to engraft secondary NSG recipients. Interestingly, EPCR can also be used to identify murine bone marrow and fetal liver HSCs [1542, 1564]. However, it remains unknown whether EPCR is also expressed on human bone marrow and mobilized blood HSCs.

To discriminate human from murine HSCs in a humanized mouse model, Abs specific for murine and human CD45 need to be used. The high amount of RBCs in samples of any source may result in background dots. To avoid that, a gate can be set on Ter119 and CD235 negative cells to exclude mouse or human erythrocytes, respectively.

9.4.2 Materials.

1. Source of adult human HSCs such as bone marrow, G-CSF mobilized peripheral blood or umbilical cord blood, or humanized mice.
2. Ficoll-Paque solution (d = 1.077) (e.g., Biocoll separating solution, Biochrom)
3. PBS containing 2% FCS
4. Optional: ACK lysing buffer
5. Flow cytometer able to measure FITC, PE, PE-Cy7, PE-Cy5, APC, Alexa Fluor700, Alexa Flour780, and Pacific Blue (eFluor 450)

9.4.3 Pitfalls.

1. The quality of primary samples may differ depending on the donor, the way of extraction, and the used anti-coagulant. Thus, frequencies of HSCs might not always be comparable between specimens.
2. If there is no clear cell fraction after Ficoll-Paque density gradient centrifugation, check whether the centrifuge break was set to 0 or 1.

9.4.4 Top tricks.

1. Try to use samples as fresh as possible to obtain a high HSC yield.
2. Dilute bone marrow or blood with PBS (1:1 to 1:2) prior to Ficoll-Paque density gradient centrifugation.
3. To avoid surplus hours at the sorting machine, you can enrich human CD34$^+$ cells with magnetic beads prior to staining and sorting.

10 Tumor cells

10.1 *Overview*

The FCM-based characterization of tumors is instrumental for the improvement of existing, and the development of novel, therapeutic strategies against all types of cancers [1565]. The various alterations involved in malignant transformation are elegantly summarized in "Hallmarks of cancer—the next generation" by Hanahan and Weinberg 2011 [1566].

Many of the proteins involved in transformation mechanisms can be detected using FCM. The most relevant examples are summarized in this section, detailing the surface expression of hematopoietic, epithelial, endothelial, and neuroectodermal markers for the classification of tumor cells according to their cellular origin. Importantly, flow cytometric analysis of surface receptors associated with the tissue of origin is helpful for a detailed characterization of solid and hematopoietic tumor types with respect to their surface expression of growth factor receptors, as well as molecules important for the interaction with immune effectors cells, such as MHC molecules as ligands for T cells, as well as adhesion molecules. The most common strategies for the definition and characterization of human and murine tumor cells are presented, along with several practical examples.

10.2 *Introduction*

Tumor cells are derived from nontransformed cells of either hematopoietic, epithelial, endothelial, neuroectdermal, or mesenchymal origin, resulting from a sophisticated process of malignant transformation. Therefore, the origin of a tumor cell indicates which markers are suitable for its flow cytometric characterization. Since hematopoietic tumor cells, i.e., leukemias and lymphomas, are derived from their non-malignant counterparts, they retain expression of the pan-leukocyte marker CD45, originally defined as the leukocyte common antigen (LCA). In this section, the definition of subsets of leukemias and lymphomas will be briefly mentioned in the context of EuroFlow (http://euroflow.org/usr/pub/pub.php), a consortium developing novel flow cytometric diagnostic tests. Solid tumor cells, on the other hand, do not express hematopoietic markers and therefore the absence of CD45 can be used to discriminate solid tumor cells from all hematopoietic cells, including progenitor cells (HCS,

see Chapter VI Section 9: Hematopoietic stem cells [1567]). In the case of tumor tissue preparations, this basic discrimination of solid tumor cells from hematopoietic cells is especially helpful because it represents the first step for a detailed characterization of solid tumor cells.

10.2.1 Hematological malignancies. The classification of leukemias and lymphomas can be guided by FCM and the procedure has been harmonized, standardized and successfully integrated into the clinical immunophenotying routine [1568]. Of note, the EuroFlow (www.euroflow.org) consortium, represented and headed by Jacques M. van Dongen, has designed panels for n-dimensional flow cytometric immunophenotyping of leukemias and lymphomas. Beyond the staining and gating protocols, the group has developed novel computerized evaluation procedures for the characterization and quantification of human hematopoietic malignancies. The EuroFlow guidelines represent the gold standard of hematopoietic malignancy immunophenotyping (http://euroflow.org/usr/pub/pub.php). For research laboratories working on hematopoietic malignancies in patients, it is important to mention that virtually all hematopoietic malignancies are accompanied by a disturbed distribution of the lymphocyte subsets in peripheral blood. Therefore, a detailed knowledge of the "normal" distribution of leukocytes in healthy individuals is instrumental for the analysis of the influence of malignant cells on hematopoiesis and immune function. To this end, "The ONE Study" group guided by Birgit Sawitzki and Edward Geissler has established an advanced FCM panel for human immune-cell phenotyping in order to define the distribution of the most important T-cell, B-cell, NK-cell and monocyte, dendritic cell subsets in healthy individuals [1569]. In addition, the International Society for Advancement of Cytometry (ISAC, https://isac-net.org/), the CIP consortium (CIMT immunoguiding program, https://www.cimt.eu/about-cip-1) of the Cancer Immunotherapy Consortium (CIMT, http://www.cimt.eu), the International Clinical Cytometry Society (ICCS, http://www.cytometry.org/web/index.php), the Federation of Clinical Immunology Societies (FOCIS, http://www.focisnet.org/) represent other initiatives that aim to harmonize and standardize protocols for immunophenotyping, primarily of human peripheral blood. The tremendous efforts of these consortia to establish guidelines, protocols and tools for the quantification of leukocytes, tumor cells, and immune responses will be instrumental not only for research projects but also for future clinical studies, in particular those with immunological endpoints.

10.2.2 Solid tumors. Due to their origin from a given tissue, solid tumor cells are not, or only at very low frequencies, present as circulating tumor cells in the blood, rather being located in the primary or metastatic tumor tissue. Since tumor tissue comprises a peculiar "contexture" of tumor cells, stroma, endothelial, and other parenchymal cells, as well as infiltrating immune cells, it
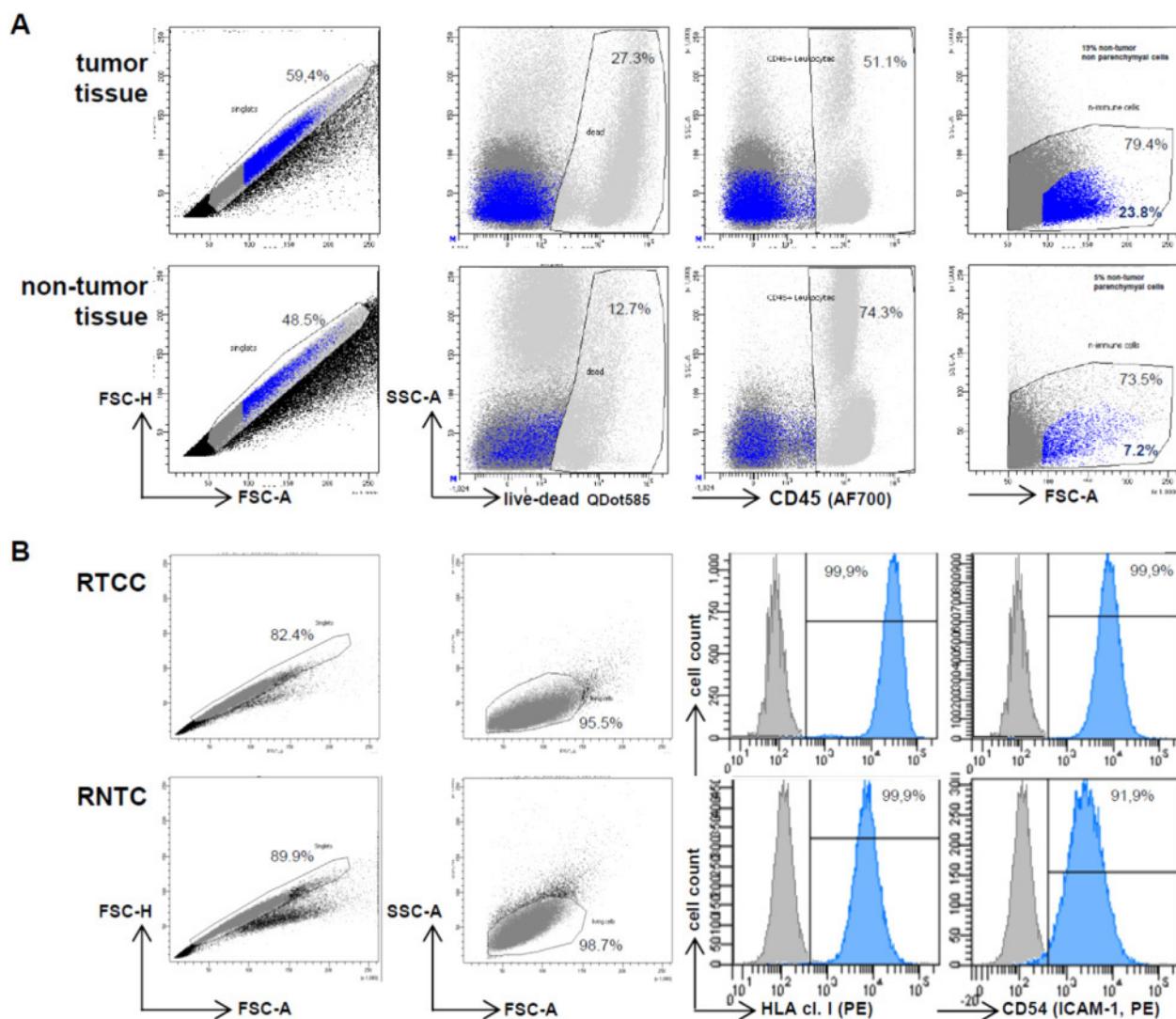
Figure 180. Single cell preparations from human tumor versus nontumor tissues and characterization of human tumor versus nontumor epithelial cells. (A) Human tumor (upper row) and adjacent nontumor tissue (lower row) was obtained as surplus tissue in the course of a pulmonary tumor resection with informed consent (MHH number 1747). After tissue digestion, single cells were stained with a live/dead dye (QDot585) and anti-human CD45 (Alexa-Fluor700) mAb. The hierarchical gating strategy starts with exclusion of doubles and aggregates in the FSC-A/FSC-H plot, followed by exclusion of dead cells in the QDot585/SSC-A plot and leukocytes, i.e., CD45-positive cells in the CD45/SSC-A plot. The remaining living CD45-negative single cells are shown in the FSC-A/SSC-A plot and in the blue gate, epithelial cells including tumor cells in the tumor tissue, can be identified according to their relative size and granularity. (B) A renal tubular cancer cell (RTCC) and the corresponding nontumor tubular cell line (RNTC) derived from tumor and adjacent non-tumor tissue of the same patient are compared with respect to surface expression of the following markers: HLA class I (mAb W6/32) and the adhesion molecule ICAM-1 (CD54, mAb gp89). All primary mAb are mouse IgG2a and were stained with a goat-anti-mouse PE-labeled secondary Ab.

is important to discriminate the tumor cells from all the non-malignant cells by tailored FCM panels.

This chapter will give an overview on suitable surface markers to use for the characterization of human and murine tumor cells.

10.3 *Procedure for the staining of surface markers for the characterization of solid tumor cells*

For the establishment of FCM panels for hematopoietic and solid tumors, it is helpful to start with tumor cell lines that available

from research groups, several vendors, and the ATCC (American Type Tissue Collection, https://www.lgcstandards-atcc.org/). Recommended surface antigens for FCM staining of human solid tumor cells are listed in Table 68 and for murine tumor cells in Table 69. The procedures for cell staining, fixation, sample acquisition, data analysis, and visualization are identical to the general recommendations for direct and indirect surface marker staining and the intracellular staining protocols, which are presented in Chapters I: Cytometry equipment, Chapter II: Setup – Instrument setup and quality control and Chapter III: Before you start: Reagent and sample preparation, experimental design.

Table 68. Collection of surface molecules for staining of human solid tumor cells

Antigen	Molecules/synonyms	Antibodies/clones (selection)
HLA class I	all HLA-A, -B, -C, -G, -E alleles	W6/32, HC10
	beta$_2$-microglobuline, β_2m	HB28, B2M-01, 2M2
HLA class II	HLA-DR	L243
	HLA-DQ	TÜ169, SK10
	HLA-DP	B7/21
NKG2D ligands	MICA	clone #159227
	MICB	clone #236511
	ULBP1	clone #170818
	ULBP2	clone #165903
	ULBP3	clone #166510
ICAM-1	CD54	9H21L19, LB-2, gp98
VCAM	CD106	51-10C9
Ep-CAM	CD326	EBA-1, 9C4, 22HCLC
VE-cadherin	CD144	BV13, 55–7H1, BV9
E-cadherin	CD234	36/E-cadherin, 5HCLC, 67A4
EGFR	HER1	EGFR.1, H11, 199.12
PDGFR	CD140a (alpha chain)	AlphaR1, 16A1
	CD140b (beta chain)	28D4, 18A2, Y92
c-Met	HGF-receptor	3D6, ebioclone97
Pan-cytokeratin	pan-cytokeratin	C-11, PAN-CK
Cytokeratin 18	CK18	CK2, C-04, DC10, AE1, E431-1
Cytokeratin 8	CK8	K8.8, 5D3, C-43, M20
CD99	MIC2; single-chain type-1 glycoprotein	TÜ12, 3B2/TA8, EPR3096

Table 69. Collection of surface molecules for staining of murine solid tumor cells

Antigen	Molecules/synonyms	Antibody/clone (selection)
MHC class I	MHC class I, all H-2 molecules	M1/42
	H-2K H-2D H-2L	K^d+D^d (ab131404); D^d (ab25590) K^b (ab93364)
	beta$_2$-microglobuline, β_2m	S19.8
MHC class II	I-A, I-E	M5/114.15.2
NKG2D ligands	Rae-1γ	CX1
	H60	MAB1155
	MULT1	MULT1 (5D0)
ICAM-1	CD54	YN1/1.7.4
VCAM	CD106	429
Ep-CAM	CD326	G8.8
VE-cadherin	CD144	ab33168, MC13.3
E-cadherin	CD234	DECMA-1, M168
EGFR	HER1	EP38Y
PDGFR	CD140a (alpha chain) CD140b (beta chain)	APA-5 APB-5
c-Met	HGFR	ebioclone7, EP1454Y
Pan-cytokeratin	pan-cytokeratin	C-11, ab9377, AE1/AE3
Cytokeratin 18	CK18	6-19
Cytokeratin 8	CK8+CK18	EP1628Y
CD24		J11d, M1/69, 30-F1
CD34		RAM34, MEC14.7, MAB6518
CD44		IM7
CD133		13A4, 315-2C11

10.3.1 Preparation of tissue, staining of samples, and gating strategy. The staining protocols for human or murine tumor cell lines, or tumor cells derived from fresh tumor tissue after enzymatic digestion, follow the general recommendations summarized in Chapters I to III. With respect to mechanical dissociation for instance, by Gentle-MACS® procedures, and enzymatic digestion, the protocols do not differ between human or murine tumor tissue. The experimental protocols presented Chapter III Section 3 "Preparation of Single Cell Suspensions" are recommended using enzymatic digestion with DNAse, collagenase, and/or hyaluronidase, which are known not to affect surface expression of the molecules listed in Tables 68 and 69. In brief, after enzymatic digestion of tumor tissue, Ficoll or Percoll density centrifugation and optional lysis of erythrocytes, the resulting single cell suspensions should be comprised of tumor cells, endothelial cells, fibroblasts, and infiltrating immune cells. Ideally, these cells should be immediately applied to flow cytometric analyses using the FCM staining protocols provided in Chapters I to III for single cell suspensions but they can also be cryopreserved in liquid nitrogen as living cells for later analyses but the potential instability of some surface markers should be taken into account. Below

some examples of staining protocols are provided in more detail (10.3.2 to 10.3.4).

10.3.2 Direct and indirect staining of surface molecules expressed by solid tumor cells isolated from tissue or in vitro culture. Single cell suspensions from tumor tissue:

After preparation of single cell suspensions (see Chapters I to III) from tumor tissue, solid tumor cells, for instance carcinoma cells of epithelial origin, can be detected by a FCM panel, using the CD45 marker to exclude hematopoietic cells, in combination with epithelial markers for the identification of carcinoma cells. In the following protocol, steps a or b should be followed depending on the indicated circumstances. Steps indicated by a number only are common for all circumstances.

1a. Staining strategy for single cell suspensions derived from tumor tissue:

Single cell suspensions of tumor tissue should be stained first with the unlabeled mAb that is specific for the surface molecule of interest on the tumor cells, followed by the respective sec-

ondary mAb and finally a directly labeled CD45 Ab to exclude hematopoietic cells. Figure 180A, 10.3.2 shows single cell preparations from human tumor tissue and the nontumor tissue counterpart, stained with CD45 to discriminate between leukocytes and parenchymal cells. Details of the gating strategy are given in section 10.3.4.

1b. Staining strategy for cultured tumor cells:

Cultured adherent tumor cells are detached and singularized by washing with 5 mL PBS followed by treatment with 0.05% trypsin/0.02% EDTA solution (1 mL per T25 culture flask) for 2–5 min, gentle shaking, and detachment by adding 5 mL medium (RPMI1640 + 5% heat-inactivated FBS).

2. The cell count of the single cell suspension is determined using trypan blue solution for discrimination of dead cells.

3. A total of 1×10^5 cells of the tumor suspension or 1×10^5 cultured tumor cells for each tube are pelleted by centrifugation ($800 \times g$, 5 min) in FCM tubes and resuspended (15 s vortex) in PBS or FCM buffer (PBS, 1% FBS, 0.1% Na-azide).

4a. For indirect staining, unlabeled mAb or isotype control mAb solutions (previously titrated for each antigen to determine the optimum concentration to use) are added in a volume of 50 µL to the single cell suspensions for 30 min at 4°C. After washing twice with 500 µL PBS or FCM buffer, and vortexing, goat-antimouse Ab solutions labeled with FITC, PE, APC, pacific blue, or other fluorochromes (100 µL of dilutions between 1:100 and 1:200) are added for 30 min at 4°C in the dark. Many reagents (e.g., fixable live/dead dyes such as the frequently used Zombie-series) cannot be used with FCM buffer but require PBS instead.

4b. For direct staining, cells are resuspended in 50 µL FCM buffer and directly labeled titrated mAb (usually 1–5 µL) are added for 30 min at 4°C in the dark.

5. After two washing steps with 500 µL PBS or FCM buffer, cell suspensions are stained with a titrated directly labeled CD45 Ab for 30 min at 4°C in the dark for the exclusion of hematopoietic cells.

6. After three washing steps, cells are resuspended in 150 µL FCM buffer if measured immediately or in FCM fixation buffer (PBS, 1% FCS, 1% paraformaldehyde) and stored at 4°C until measurement.

7. Exclusion of dead cells without cell fixation is highly recommended, for instance by live/dead staining with 2 µL PI stock solution (20 µg/mL PI, PE channel) that requires immediate acquisition of the cells. Other live/dead staining protocols for instance using 7AAD or other live/dead fluorochromes are available in different colors. Most protocols recommend staining for 10 to 15 min and washing steps are according to the manufacturer's instructions.

An example of the comparison between human renal tubular cancer cells (RTCC) and renal nontumor tubular cells (RNTC) from the same individuum is shown in Fig. 180B (10.3.2). Surface expression of HLA class I, CD155, CD166, and CD54 was compared between tumor (RTCC) and renal nontumor tubular epithelial cells (RNTC) showing indeed some differences in the density of these molecules.

10.3.3 Detection of circulating tumor cells in the peripheral blood and bone marrow.   The detection of circulating tumor cells in the peripheral blood and bone marrow has clinical relevance for several forms of carcinomas and sarcomas in terms of disease staging and treatment response [1570]. Although molecular methods such as real-time PCR of tumor-specific mRNA expressed by carcinoma, sarcoma, or melanoma tumor cells, and so on, recently called "real time liquid biopsy," have a higher sensitivity compared to FCM, FCM is still valid for the quantification and characterization of circulating cancer cells [1571]. Under nonmalignant conditions, cells of epithelial, mesenchymal, or neuroectodermal origin cannot be detected in blood or bone marrow aspirates. However, the process of metastasis formation is associated with dissemination of malignant cells through the blood stream and bone marrow. Therefore, disseminating cancer cells are detectable in these compartments but at very low frequencies that are close to the detection limit of <0.01% cells within the gate for living cells. Hence, enrichment techniques such as Ab -based magnetic positive or negative selection are used to increase the sensitivity of detection. For the quantification of tumor cells, the direct or indirect staining protocol outlined in 10.3.2 can be combined with the CD45 marker for the exclusion of all leukocytes. The epithelial markers Ep-CAM (CD326) or cytokeratin 18 (CK18) are suitable markers for the detection of carcinoma cells. For sarcomas, the mesenchymal marker (CD99) is recommended and for the detection of melanoma cells, growth factor receptors like c-Met or PDGF-R are appropriate markers, and although not tumor-specific are characteristic for the tissues of origin.

10.3.4 Gating strategy for the identification of tumor cells.   The hierarchical gating strategy should follow the recommendations shown in Fig. 180A 10.3.2. starting with FSC-A/FAC-H to exclude doublets and cell aggregates but taking into account the different sizes for leukocytes and the non-immune cell fractions containing tumor cells as well as other cell types. In this FSC-A/FSC-H gate, dead cells should be excluded by live/dead staining (in this case with a QDot585 dye). In the case of staining tumor cells in single cell suspensions derived from tumor tissue, leukocytes should be excluded by gating only on single cells negative for CD45 in the plot showing CD45 versus SSC-A. Then, the non-immune (CD45-negative) cells are displayed in a FSC-A/SSC-A plot to allow detection of the postulated tumor cell proportion, which can be further identified by surface markers of interest, for example, EGFR for carcinoma cells using histogram or dot plot images depending on the marker combinations. In Fig. 180B, renal tubular cancer cells (RTCC) are compared to renal nontumor tubular epithelial cells (RNTC) with respect to expression of HLA class I, CD155 (poliovirus receptor), CD166 (ALCAM), ICAM-1 (CD54) molecules (Figure 180B). Although pairs of tumor vs.

non-tumor cells from one individuum are rare, they allow a comparison of the expression density of several surface markers involved in immune recognition like HLA class I or adhesion molecules (CD54).

10.4 Specific recommendations for human and murine solid tumors

Details of suitable antigens and the respective mAbs are given in Table 68 for human tumor cells and Table 69 for murine tumor cells.

In contrast to leukemias and lymphomas, solid tumor cells are classified according to their originating cell type, i.e., tumor cells derived from (i) epithelial cells are defined as carcinoma cells, (ii) mesenchymal cells as sarcoma cells, (iii) neuroendocrine tumors are defined as originating from endocrine glands, and (iv) neuroectodermal tumors are defined as originating from neuroectodermal cells of the skin or brain. This classification is identical for all species, such as humans, nonhuman primates, dogs, cats, and rodents. Although many solid tumor cells can express a variety of tumor-associated antigens (TAA), including cancer-testis (CT), carcinoembryonal (CEA), and neo-antigens, most of these antigens are not suitable for flow cytometric characterization of tumor cells due to either their poor expression, intracellular localization or simply the lack of specific Abs [1572, 1573]. Therefore, the characterization of solid tumor cells relies on surface markers associated with their tissue origin, in combination with exclusion markers for hematopoietic cells such as CD45.

The induction of tumor-specific immune responses can result in immune escape mechanisms through which the tumor cells aim to evade their recognition and elimination by effector cells, in particular T cells and NK cells. One frequent mechanism of immune evasion is mediated by loss or downregulation of major histocompatibility complex (MHC) or human leukocyte antigen (HLA) class I molecules because, in the absence of MHC class I molecules, recognition of tumor cells by T cells is prevented. Mutation or deletion of beta-2-microglobulin (β_2m), leading to MHC class I-deficiency, represents a major tumor escape strategy occurring in vivo in cancer patients, as well as in murine tumor models. Thus, MHC class I (mouse H-2) or HLA class I (human) surface staining by FCM is highly recommended for all immunological experiments with solid tumor cells [1574]

In addition to T cells, NK cells can also recognize tumor cells but via other receptor/ligand interactions. Expression of ligands for NK-cell receptors, for instance NKG2D ligands (NKG2DL), are important for recognition by the activating NKG2D receptor and for the sensitivity of tumor cells to NK cell-mediated recognition and tumor-cell elimination [1575]. NKG2D (CD314) belongs to the group of activating receptors that are conserved between humans, nonhuman primates, and rodents and are expressed by NK and CD8^{+} T cells. In contrast to NKG2D, MHC class I molecules, human HLA-C in particular, serve as inhibitory ligands for NK cells by specific binding to inhibitory receptors of the

killer-immunoglobulin–like (KIR) or C-type lectin (CD94/NKG2A) families. Thus, NK-cell recognition of tumor cells is regulated by a balance between activating and inhibitory signals derived from interactions with the respective ligands on the surface of tumor cells. In order to investigate the immunogenicity of tumor cells, it is therefore, recommended to determine the surface expression of NKG2D ligands on human or mouse tumor cells (Tables 68 and 69). Moreover, these ligands for T-cell and NK-cell receptors can be modulated during tumorigenesis, for instance MHC class I and NKG2D are targeted by oncogenic signaling via mutated MAP kinase signaling [1576].

In addition, surface expression of adhesion molecules such as ICAM-1, and VCAM should also be included in the flow cytometric characterization of solid tumor cells due to their increased expression upon development of metastases in human tumors and mouse models and, thus, their relevance for T-cell and NK-cell activation, as well as for the formation of metastases. Besides these surface molecules, which are commonly expressed by non-malignant as well as malignant cells of both hematopoietic and parenchymal origin, solid tumor cells can be also characterized by cell fate markers. For instance, splice variants of CD44, especially CD44v6, have a long-standing and controversial history as potential "tumor stem cell" markers, together with the hematopoietic stem cell markers CD34, CD133 with a recent revival of CD24 as potential prognostic marker for some carcinomas [1577, 1578]. A selection of the most relevant human cancers, grouped into carcinomas, sarcomas, neuroectodermal tumors, and their tumor biology, "the hallmarks of cancer," is given below with the respective recommendation for their flow cytometric characterization.

10.4.1 Human carcinomas.　Carcinomas, i.e., epithelial tumors, represent the most frequent human cancers [1579] and their malignant transformation is often based on "driver mutations" in growth factor receptors, receptor tyrosine kinases in particular, as well as their downstream signaling pathways. For the identification of carcinoma cells, epithelial markers such as CK18 and CK8 are useful, although they have to be detected by intracellular staining procedures [1580]. In addition, epithelial cells selectively express growth factors such as epidermal growth factor receptor (EGFR), platelet-derived growth factor receptor (PDGFR), fibroblast growth factor receptor (FGFR), Her-2, c-Met, and others [1581]. These surface receptors often directly contribute to tumorigenesis by carrying "tumor-driving mutations" in their signaling domains; providing constitutive proliferative signals independently of the availability of growth factors. Therefore, these receptors can be useful for the identification and characterization of tumor cells in terms of their growth factor receptor repertoire. Importantly, the intracellular protein vimentin serves as a specific marker for the discrimination of tumor cells from fibroblasts.

Some of the most frequent human carcinomas are listed in Table 70 together with their originating epithelial cell type [1579, 1582–1587].

Table 70. Overview of the most frequent human carcinomas

Carcinoma tissue	Most frequent form of carcinoma	Originating cell	Reference
Lung cancer	Non-small cell lung cancer (NSCLC)	Type I / II alveolar epithelial cells	[1579]
Breast cancer	Mammary carcinoma	Epithelial cells of the milk duct	[1582]
Colon cancer	Colorectal carcinoma (CRC)	Epithelial cells of inner mucosal layer	[1579]
Prostate cancer	Prostate carcinoma	Epithelial basal cells of the prostate	[1583]
Liver cancer	Hepatocellular carcinoma (HCC)	Hepatocytes	[1579]
Stomach cancer	Stomach carcinoma	Epithelial cells transformed by H. pylori	[1579]
Cervical cancer	Cervical carcinoma	Cervical epithelial cells after HPV infection	[1584]
Esophagus cancer	Esophagus carcinoma	Epithelial cells lining the oesophagus	[1585]
Bladder cancer	Bladder carcinoma	Transitional epithelium of the bladder wall	[1586]
Pancreatic cancer	Pancreatic carcinoma	Endocrine ductal epithelial cells	[1587]
Kidney cancer	Renal cell carcinoma (RCC)	Proximal tubular epithelial cells	[1579]
Ovarian cancer	Ovarian carcinoma	Ovarian tubal-type epithelium	[1579]
Squamous cancer	Squamous cell carcinoma	Epithelial cells of skin or glands	[1579]

10.4.2 Human sarcomas. Mesenchymal tumors, i.e., sarcomas [2254], develop from tissue cells originating from mesenchymal progenitors and manifest primarily in soft tissue like fat, muscle, tendons, nerve or connective tissue cells, blood and lymph vessels, or fibroblasts (Table 71). The family of osteosarcomas, including Ewing osteosarcomas, comprises a severe form of juvenile sarcoma with manifestations preferentially in the bone, bone marrow, and organs like the lung or, in rare occasions, the kidney. For the flow cytometric detection of Ewing sarcoma cells in the peripheral blood of patients, CD99, the MIC2 gene product, which is normally expressed by osteoclasts and leukocytes, has been proposed in conjunction with the absence of CD45 [1588]. Kaposi's sarcoma represents a virally induced form of sarcoma mediated by the human herpesvirus 8 (HHV8), also called Kaposi's sarcoma-associated herpesvirus (KSHV). The viral HHV8 genome contributes to dysregulation and tumorigenesis by its manipulation of mechanisms regulating viral latency and lytic replication [1589]. For bone and soft tissue sarcomas, dysregulation of the Hippo signaling pathway has been shown to affect several surface receptors including EGFR,

E-cadherin, CD44, and tight junctions indicating that oncogenic signaling can impinge on the stability of these surface receptors as markers for sarcoma cells [1590].

10.4.3 Human neuroectodermal tumors. Neuroectodermal tumors, i.e., malignant cells derived from neuroectodermal cells, belong to less prevalent but life-threatening cancers such as melanoma (black skin cancer) and several forms of brain cancer (Table 72). In malignant melanoma, melanocytes originating from neuroectodermal cells acquire "driver" mutations in components of the MAK kinase signaling, most frequently in the BRaf kinase (with the highest prevalence being the BRaf^{V600E} mutation) or in the upstream NRas GTPase [1591]. Although these mutations cannot directly be utilized for the FCM of melanoma cells, their mutation status may have an impact on the recognition by T-cells and NK-cells [1592, 1593]. Since melanoma cells do not express unique tumor-associated surface molecules, there are no specific FCM panels available for the discrimination of malignant

Table 71. Overview of the most frequent human sarcomas

Sarcoma tissue	Mesenchymal tumor	Originating cell	Reference
Ewing sarcoma	Ewing's sarcomas (bone, bone marrow, lung, kidney)	Soft tissue cell of the respective organ	[1587, 1588]
Kaposi's sarcoma	Soft tissue sarcoma	Induced after infection with HHV-8	[2254]

Table 72. Overview of the most frequent human neuroectodermal tumors

Tumor tissue	Neuroectodermal tumor	Originating cell	Reference
Black skin cancer	Malignant melanoma	Melanocytes of the skin	[1589–1591]
Brain cancer	Gioblastoma, glioma	Glial cells of the brain	[1592, 1593]
Brain cancer	Astrocytoma	Astrocytes of the brain	[1594]

melanoma cells from melanocytes. However, melanoma cells can be detected in single cell suspensions of tumor tissue, by combinations of ICAM-1, MUC18/MCAM (CD146) and the exclusion of CD45.

Several forms of brain cancers are derived from neuroectodermal cells including some of the most aggressive brain tumors like glioblastoma with the malignant cells being derived from glial cells [1594]. Besides their poor MHC expression, glioblastoma cells utilize a broad selection of immune evasion strategies that are in part responsible for their aggressive nature and the resulting poor survival of glioma patients [1595]. Other forms of brain tumors are represented by astrocytomas, a group of differentially graded variants, i.e., diffuse, polycystic, and anaplastic astrocytoma with different degrees of aggressiveness. For gliobastoma, the GD2 and CD90 antigens are accepted as tumor-associated surface molecules for FCM and also as targets for chimeric antigen-specific T cell (CAR-T cell) therapeutic strategies. Due to the lack of additional, reliable and tumor-specific surface markers for FCM, molecular characterization, i.e., expression profiling, is currently used for a more detailed classification at the level of gene profiles, signaling pathways, and regulatory networks. Despite these molecular analyses, the cellular origin is still controversial ranging from stem cell-like precursors to neuronal stem cells [1596].

10.5 Characterization of murine tumor cells

For the flow cytometric characterization of murine tumor cells, both hematopoietic tumors like mouse leukemias and lymphomas, and solid tumors like carcinomas of the mouse breast, liver, or colon, melanomas, or sarcomas, the same recommendations can be applied as outlined above for human tumor cells. Since the numerous mouse tumor models cannot be discussed here comprehensively, only general remarks are provided regarding FCM of murine tumor cells. Mouse solid tumor cells are also classified into carcinomas, sarcomas, and neuroectodermal tumors according to their originating tissue. Therefore, the same surface molecules can be utilized for their characterization by FCM as are listed in Table 69 showing a selection of known mAbs for mouse antigens. In addition, the protocols do not differ from the general protocols of direct, indirect surface and intracellular staining (Chapters I to III). Furthermore, the protocol in section 10.3.2 can also be used for staining of murine tumor cells. In the case of unlabeled mAbs, the secondary mAb needs to be adapted to the species of the mAb, rat or goat for instance, and then, fluorochrome-labeled goat-anti-rat or rabbit-anti-goat secondary antibodies have to be utilized for indirect FCM.

Final remarks: The recent clinical advances in immunotherapy of human solid tumors could only be achieved using sophisticated preclinical mouse models. Since the early days of transplanted tumor cells into immunodeficient mice, numerous elegant mouse models with spontaneously developing tumors based on germline or inducible mutations have been developed over the past decade [1597]. More recently, humanized mouse models utilizing severely immunodeficient mice reconstituted with human peripheral or even hematopoietic stem cells have gained tremendous insight into immune recognition of human tumor cells, escape mechanisms and opened the door for new therapeutic approaches that finally made their way into clinical application [1598].

10.6 Pitfalls

The major pitfalls in the characterization of tumor cells are the selection of surface antigens suitable for either the discrimination between tumor and nonmalignant cell or the definition of their antigenicity, respectively. Since many tumor cells maintain their overall surface expression profile and rather modulate the density of certain surface receptors or ligands, it is highly recommended to perform a rather broad analysis of their receptor and ligand profile with standardized protocols that allow a quantitative assessment for each surface molecule. In Fig. 180B, the quantitative differences between a tumor and nontumor renal epithelial cell line as shown with respect to HLA class I and ICAM-1 (CD54) expression. In the case of single cell preparations derived from fresh tissue, it is important to include live/dead staining in combination with an exclusion of leukocytes in order to identify tumor cells that may represent a minor cell type within the entire complex tumor tissue. Therefore, a stepwise hierarchical gating strategy is instrumental for the identification of tumor cells.

10.7 Top tricks

In the context of tumor cell analyses, one of the top tricks is the direct comparison of tumor versus nontumor samples, i.e., tissue or cell lines because the genetic alterations in the course of malignant transformation result in a gradient of changes rather than in an on/off situation for most surface markers. Therefore, a side by side analysis of tumor and nontumor samples allows a direct comparison of the expression levels of the marker of interest and, hence, this facilitates the interpretation of general or even individual changes associated with tumor development or progression, respectively. Addition of genetic analyses can of course further

improve tumor cell and tissue characterization at the molecular level.

11 Human plasma cells in multiple myeloma

11.1 *Overview*

Multiple myeloma is defined by the accumulation of monoclonal plasma cells in the bone marrow and usually preceded by non-malignant monoclonal gammopathy of undetermined significance. FCM can accurately identify multiple myeloma cells, associated immune phenotypes, and confirm clonal expansion by detection of immunoglobulin light chain restriction. The technology can critically contribute to initial diagnostics, definition of disease heterogeneity, risk stratification, selection of targeted therapeutics, decisions in clinical trials, and detection of minimal residual disease among others.

11.2 *Introduction*

Plasma cells are terminally differentiated B cells and the major source of circulating soluble Abs. Plasma cell differentiation is thought to be driven by B cell receptor–target antigen affinity [689, 1599]. Upon stimulation, B cells can proliferate and increase in size, a process referred to as becoming a B cell blast. B cell blasts that secrete Ab are termed plasmablasts. Plasma cells are plasmablasts without proliferation [1600] and circulate in the peripheral blood of healthy individuals at very low frequencies (<0.1% of PBMCs).

More than 90% of plasma cells are so-called long-lived plasma cells, which are assumed to arise from germinal centers. In contrast, short-lived plasma cells can develop independent from germinal centers and consequently mostly lack somatic hypermutations [689, 1214, 1599, 1601].

Multiple myeloma is defined by the accumulation of monoclonal plasma cells in the bone marrow. In contrast to plasma cells from healthy individuals, in multiple myeloma, (epi-)genetic aberrations are assumed to restore proliferative capacity in variable proportions of plasma cells, enabling malignant clonal expansion [1602]. Their substantial number of somatic hypermutations and completed class switch recombination suggest that malignant transformation of plasma cells occurs at the (post) germinal center stage of B cell development [1603–1605]. Consequently, immunoglobulin gene sequences can act as unique molecular barcodes for disease tracking at the single cell level [1606]. In the clinical setting, immunoglobulin light chain restriction can indicate clonal plasma cell expansion.

Multiple myeloma uniquely programs its microenvironment to support tumor growth [1607], and to protect from T cell responses [1608] and chemotherapeutics [1609–1611]. Microenvironmental features in combination with (epi-)genetic aberrations [1612–1616] result in intra- and interclonal diversity of the malignant plasma cells including their expression of aberrant (surface) molecules.

FCM can accurately identify multiple myeloma cells, associated immune phenotypes, and confirm clonal expansion by detection of Ig light chain restriction. The technology can critically contribute to initial diagnostics, definition of disease heterogeneity, risk stratification, selection of targeted therapeutics, decisions in clinical trials, and detection of minimal residual disease among others. In this section, we present a basic FCM panel and give technical advice for the reliable identification of plasma- and multiple myeloma cells in human bone marrow. The experimental setup can serve as a possible foundation for individual design of detailed immunological studies of the plasma cell compartment.

11.3 *Step-by-step sample preparation*

1. Collect bone marrow samples, use EDTA as in vitro anticoagulant (1.2–2.0 mg EDTA/mL bone marrow sample).
2. Filter the bone marrow sample through cell strainer with 100 μm pore size (Falcon).
3. Pipette 100 μL of bone marrow blood into a FCM tube.
4. Add 2 mL lysing solution and incubate for 10 min.
5. Wash three times: add 2 mL wash medium, re-suspend, centrifuge for 3 min at 420 × *g*, and aspirate supernatant.
6. Vortex to fully re-suspend the cell pellet.
7. Add mAbs for surface staining: 3 μL CD138 (V500C, MI15, BD Biosciences), 3 μL CD19 (PECy7, HIB19, BD Biosciences), 3 μL CD45 (V450, 2D1, BD Biosciences), 5 μL CD38 (PE, HB-7, BD Biosciences), and 5 μL CD56 (FITC, NCM16.2, BD Biosciences).
8. Incubate for 15 min in the dark at room temperature.
9. Add 100 μL of Reagent A (FIX&PERM Cell Fixation and Permeabilization Kit, Nordic-MUbio) and incubate for 15 min in the dark at room temperature.
10. Wash once: add 2 mL wash medium, re-suspend, centrifuge for 3 min at 420 × *g*, aspirate supernatant.
11. Add 100 μL of Reagent B (FIX&PERM Cell Fixation and Permeabilization Kit, Nordic-MUbio).
12. Add mAbs for intracellular staining: 3 μL kappa light chain (APC, TB28-2, BD Biosciences) and 3 μL lambda light chain (APC-H7, 1-155-2, BD Biosciences).
13. Incubate for 15 min in the dark at room temperature.
14. Wash once: add 2 mL wash medium, re-suspend, centrifuge for 3 min at 420 × *g*, and aspirate supernatant.
15. Resuspend cells in sheath fluid for immediate analysis.

11.4 *Materials*

11.4.1 *Media and buffers.*

Wash medium: 100 mL 10× PBS (Gibco) + 900 mL Aqua dest (Braun)

FIX&PERM Cell Fixation and Permeabilization Kit, Nordic-MUbio

Lysing solution: Lysing Solution 10x Concentrate (BD FACS™)
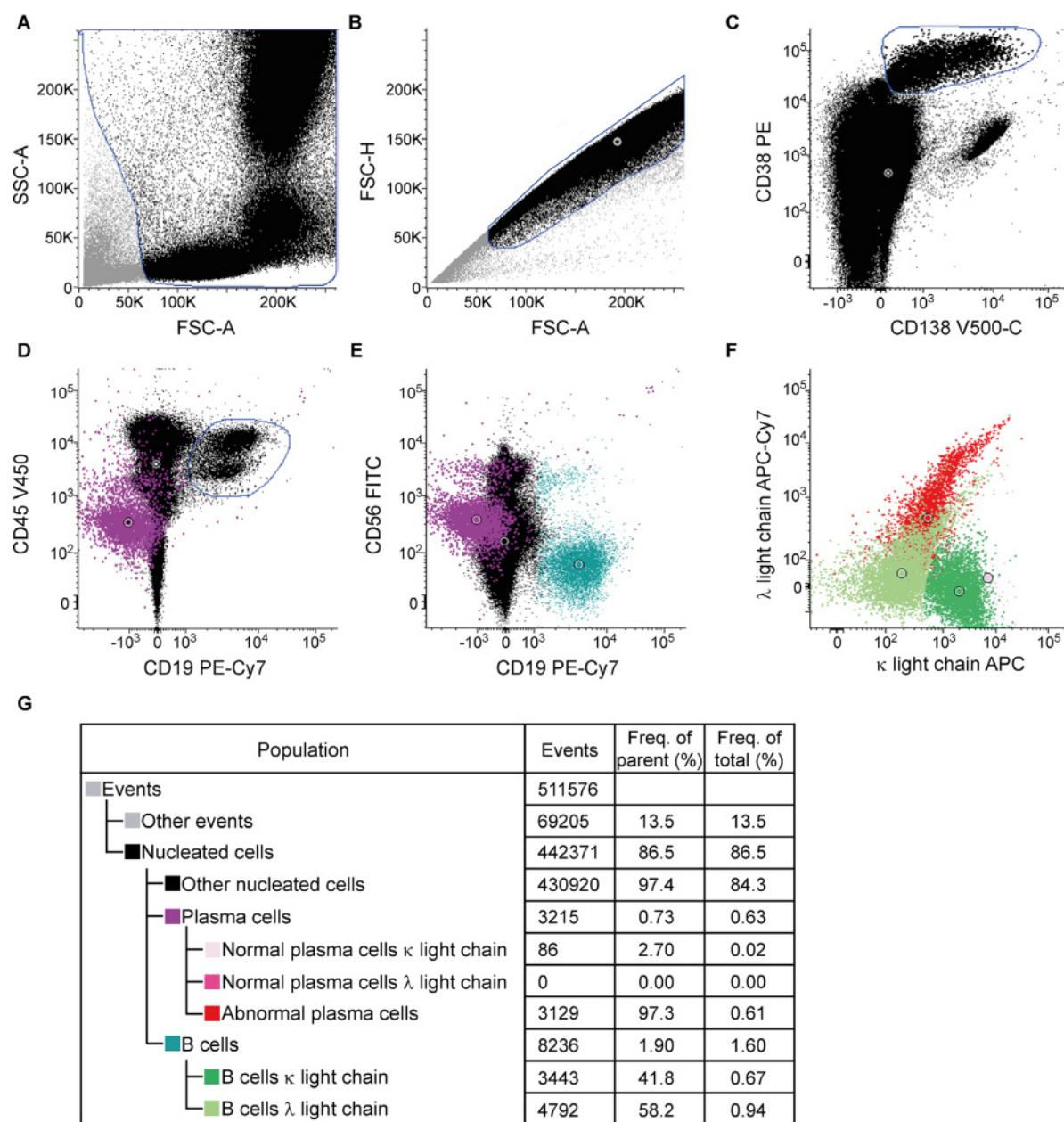
Figure 181. Identification of aberrant plasma cells in human multiple myeloma bone marrow. Plasma cells are defined as the CD38- and CD138-positive population (gate shown in C, purple in D and E) among leukocytes (black) after exclusion of debris (A) and doublets (B). No live/dead staining is performed. Aberrant plasma cells in this sample are partially CD56-positive, homogeneously negative for CD19 and CD45-low (D and E). Moreover, aberrant plasma cells do show immunoglobulin light chain restriction (in this case lambda, indicated in red, F), which ultimately characterizes them as abnormal plasma cells. As an internal comparison, B cells (gate shown in D) present characteristic CD19 and heterogeneous kappa/lambda expression (F). The hierarchy of defined populations as well as absolute and relative numbers of events are shown in (G). Open circles indicate population centers. Gating was performed with Infinicyt™ Flow Cytometry Software. SSC-A, side scatter area; FSC-A, forward scatter area; FSC-H, forward scatter height.

11.4.2 Monoclonal antibodies.

11.4.2.1 Surface staining.

CD138 (V500C, MI15, BD Biosciences)
CD19 (PECy7, HIB19, BD Biosciences)
CD45 (V450, 2D1, BD Biosciences)

CD38 (PE, HB-7, BD Biosciences)
CD56 (FITC, NCM16.2, BD Biosciences)

11.4.2.2 Intracellular staining.

kappa light chain (APC, TB28-2, BD Biosciences)
lambda light chain (APC-H7, 1-155-2, BD Biosciences)
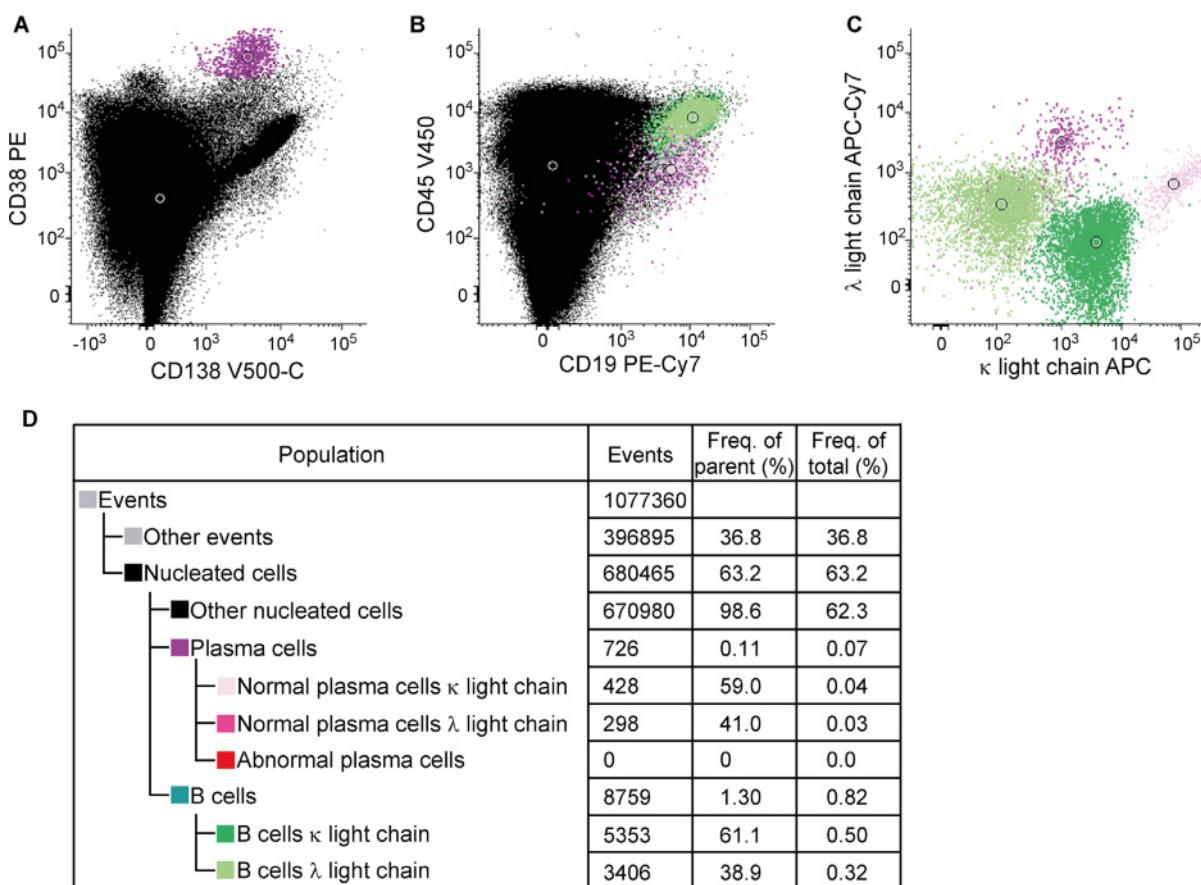
Figure 182. Identification of non-malignant plasma cells in human bone marrow. An example of a normal plasma cell population is shown. The gating strategy for identification of single nucleated cells, plasma cells, and B cells as well as color coding are identical to Fig. 181. Plasma cells are defined as the CD38- and CD138-positive population (purple, A) among leukocytes (black). Normal plasma cells usually express CD19 and CD45 (B) in combination with heterogeneous kappa/lambda light chain expression (C). The hierarchy of defined populations as well as absolute and relative numbers of events are shown in (D). Open circles indicate population centers. Gating was performed with Infinicyt™ Flow Cytometry Software. SSC-A, side scatter area; FSC-A, forward scatter area; FSC-H, forward scatter height.

11.4.3 Flow cytometer. All experiments were performed on a BD FACSLyric (BD Biosciences).

11.5 Data analysis/gating

FCM can identify plasma and multiple myeloma cells by forward/side scatter characteristics in combination with uniquely high expression of CD38 and CD138 (Fig. 181A–C) [1617–1619]. While CD45 and heterogeneous CD19 expression indicate different maturation states of normal plasma cells [1618, 1620], the identification of malignant plasma cells can be complicated by considerable variation in marker expression between and within individual patients. For example, phenotypes frequently associated with multiple myeloma cells (absence of CD19 and expression of CD56, example in Fig. 181D and E) can also be part of nonmalignant differentiation [1214, 1330, 1331, 1621]. The detection of Ig light chain restriction (Fig. 181F) can help identifying clonal expansion in most cases [1622] but may be technically challenging (intracellular staining, low target cell numbers, absence of light chain expression). In comparison to normal plasma cells that do

not show light chain restriction (Fig. 182) the light chain restriction on aberrant plasma cells is particularly convincing.

11.6 Pitfalls

11.6.1 FCM underestimates the number of plasma cells in bone marrow aspirates. Although, providing key information on plasma cell clonality and aberrant phenotype, FCM consistently underestimates the number of plasma cells in bone marrow samples compared to morphological assessment [1623]. This might result from an increased fragility of plasma cells compared to other leukocytes, loss of plasma cells during sample preparation, hemodilution, and a discrepancy in content of plasma cells in different samples (first versus subsequent pulls during bone marrow aspirate collection). As an accurate plasma cell quantification is crucial for diagnosis of plasma cell disorders, a morphologic assessment of bone marrow smears and/or histopathological evaluation of bone marrow biopsies should be performed. However, providing an immediately available lower limit estimate and differentiating between

normal and aberrant plasma cells, FCM is a powerful method in first diagnosis and determination of minimal residual disease.

11.6.2 mAbs used in multiple myeloma treatment can interfere with flow cytometric analysis. As CD38 is frequently expressed on a high percentage of normal and aberrant plasma cells, immunotherapeutical approaches in multiple myeloma target CD38 with mAbs, such as daratumumab, isatuximab (SAR650984), MOR03087 (MOR202) and Ab79 [1623–1625]. Recent studies have shown that CD38 mAb treatment, in particular daratumumab, can interfere with diagnostic plasma cell detection caused by a long-term CD38 saturation leading to an absence of CD38-positive events [1626, 1627]. As plasma cells are identified as CD38 and CD138-positive cells, CD38 mAb treatment might lead to false negative results in plasma cell detection. It can be assumed that also further therapeutically used mAbs directed against plasma cell surface antigens that are crucial for detection of plasma cells (e.g., CD138) may also interfere with flow cytometric analysis. Therefore, bone marrow samples from patients treated with mAbs should also be evaluated by morphologic techniques as aspirate smears and immunohistopathology. Moreover, alternative plasma cell-specific antigens, as SLAMF7, or intracellular transcription factors, as BLIMP1 and IRF4, might be used for plasma cell identification in FCM [1621, 1628, 1629]. Furthermore, CD27 and CD81 expression indicates different maturation stages of normal plasma cells and might be helpful in detection of an aberrant phenotype (Table 73) [1618, 1620].

11.7 *Top tricks: Focus on minimal residual disease detection*

Minimal residual disease (MRD) is defined as a small number of malignant plasma cells that persist after treatment. MRD represents the treatment efficacy, is highly predictive for outcome and is considered as the major cause of relapse in multiple myeloma [1631, 1632]. Multicolor FCM is one of the available MRD detection methods that can reach a sensitivity of up to 10^{-5}–10^{-6}. The simultaneous detection of multiple sets of surface and intracellular markers enables reliable and fast identification of multiple myeloma cells making FCM an indispensable tool in basic research and clinical diagnostics alike. The high-throughput characterization of millions of cells in a reasonable amount of time allows minimal residual disease detection with high sensitivity comparable to next generation sequencing [1633]. Similarly to the detection of aberrant plasma cells at first diagnosis the antigen panel for MRD detection includes CD38, CD138, CD45, CD19, kappa, and lambda light chains. However, assessment of >10^6 nucleated cells is crucial to reach adequate MRD sensitivity levels. Moreover, high level of standardization with regard to used Abs, sample preparation and measurement and data analysis is crucial. The Multiple Myeloma MRD Kit, a EuroFlow™ approach to monitor MRD by FCM, offers a ready-to-use solution for sensitive and accurate MRD detection [1633]. Automatic software tools lead to an automated identification of cell populations and aberrant plasma cells offering high levels of standardization. These approaches are expected

to overcome heterogeneity of MRD detection protocols [1634] across different FCM laboratories and provide reliable MRD data particularly within clinical trials.

11.8 *Summary table*

Table 73. Frequent immunophenotypes of normal and aberrant plasma cell populations

Plasma cell population	Frequent phenotype
Normal	Positive: CD38, CD138, CD319 (SLAMF7) Usually positive: CD19, CD45, CD27, CD81 Usually negative: CD56 Immunoglobulin light chain restriction: none
Aberrant	Positive: CD38, CD138, CD319 (SLAMF7) Usually positive: CD56 Usually negative: CD19, CD45, CD27, CD81 Immunoglobulin light chain restriction: yes

References: [1621, 1630].

12 Brain/neural cells

12.1 *Overview*

In contrast to peripheral immune cells, the application of FCM for cells from the central nervous system (CNS) is most often not the method of choice. It is limited mainly due to the lack of CNS cell-specific markers, high lipid content (through myelin), and the high integration of cells within the parenchyma. Preparing brain homogenates without severely damaging cells and their processes has proven technically challenging and special caution has to be taken toward keeping the integrity of the antigens during tissue digestion. For any of the non-hematopoietic cells of the CNS, FCM sorting and subsequent culturing therefore requires specific protocols and is facilitated by the use of reporter mouse lines. Yet FCM can also be a useful tool if the expression of genes or proteins directly after isolation are of interest [1635] but also in the analysis of resident microglia or infiltrating and nonparenchymal myeloid cells. Another complication of FCM analysis of CNS-resident cells, however, is the identification of pan-neuronal, astrocyte, microglia, and oligodendrocyte markers due to the common origin of many CNS cells as well as the regional and intracellular heterogeneity of the CNS [1636]. Different cell types, species, and even regions and age of the brain will need different dissociation protocols. We here provide three exemplary approaches for tissue preparation and subsequent FCM of brain cells. Two protocols describe the isolation of murine CNS cells and one outlines the isolation of nuclei, yet we advise to establish individual tissue dissociation procedures to account for cell-, region-, age-, and species-specific requirements.
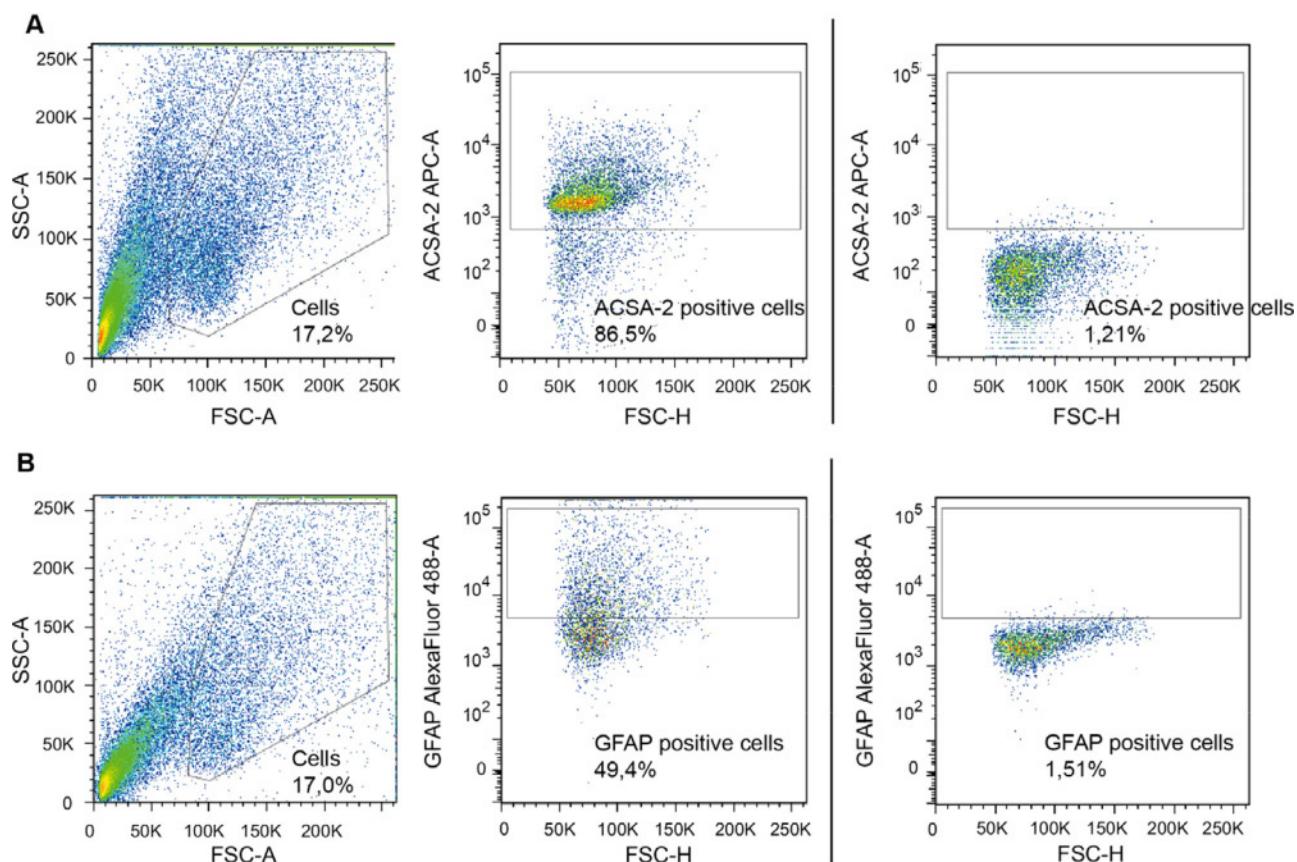
Figure 183. FCM analysis of murine neonatal astrocytes. (A) Neonatal astrocytes were harvested and stained with the cell surface marker ACSA-2 (recombinant human anti-mouse, APC-conjugated, 1:10 dilution, Miltenyi Biotec). (B) Neonatal astrocytes were harvested, fixed in 2% PFA and permeabilized in 0.5% saponin. Cells were stained with the intracellular marker GFAP (mouse monoclonal, Alexa Fluor-488-conjugated, 1:20 dilution, BD Biosciences). Ab gates were based on unstained controls for each Ab as shown on the far right. A total of 10 000 cells of the SSC-A/FSC-A gate were set as a stopping point during FCM. FSC and SSC axes are linear, fluorochrome axes are log.

12.2 Introduction

The human and rodent CNS, which include the brain and spinal cord, are composed of many various cell types that together orchestrate brain metabolism, neuronal signal transduction, and all bodily functions. The primary difference between the human brain and that of other species is the enormous expansion of the neocortex (with its neurons) relative to total brain volume [1637].

Neurons are the primary components of the CNS and transfer chemical and electrical signals throughout the central and peripheral nervous systems. Depending on region and function, several neuronal subtypes exist [1638]. Next to the subsets of neuronal cells, the CNS is also composed of glia cell populations. The cells belonging to the glial compartment are oligodendrocytes, astrocytes and microglia. Oligodendrocytes are cells that form myelin sheaths around neurons, insulating the neuronal processes to enable fast electric signal transduction (reviewed in ref. [1639]). Astrocytes are the most numerous cells in the CNS that have essential roles in its development, homeostasis, and disease contexts. Astrocytes are linked via vast intercellular networks, yet despite this global connectivity, astrocytic microenvironments are formed within specific brain regions or within astrocytic sub-

populations (reviewed in ref. [1640]). Neurons, astrocytes, and oligodendrocytes all originate from neural stem cells (NSCs) with patterned migration and maturation phases during development (reviewed in ref. [1641]). Microglia as well as perivascular and subdural meningeal macrophages, on the other hand, originate from hematopoietic stem cells in the yolk sac that migrate to the brain throughout development [1642, 1643]. Microglia are the innate immune cells of the brain and constantly surveil the CNS parenchyma for pathogens and cellular changes.

12.2.1 Astrocytes. FCM sorting can be used to obtain astrocytes from neonatal to adult tissue. Depending on the downstream application of the sorted astrocytes (culturing, freezing, etc.), some considerations need to be kept in mind. Most cell surface Abs found on astrocytes are not cell-specific and often also found on NSCs, oligodendrocytes, and/or neurons. Additionally, only few fluorochrome-conjugated FCM Abs are commercially available (see summary table at the end of the chapter). A suitable Ab for FCM sorting both neonatal and adult murine astrocyte is ATP1B2/ACSA-2 [1644, 1645]. Labeling of intracellular markers such as GFAP requires cell permeabilization and is therefore not
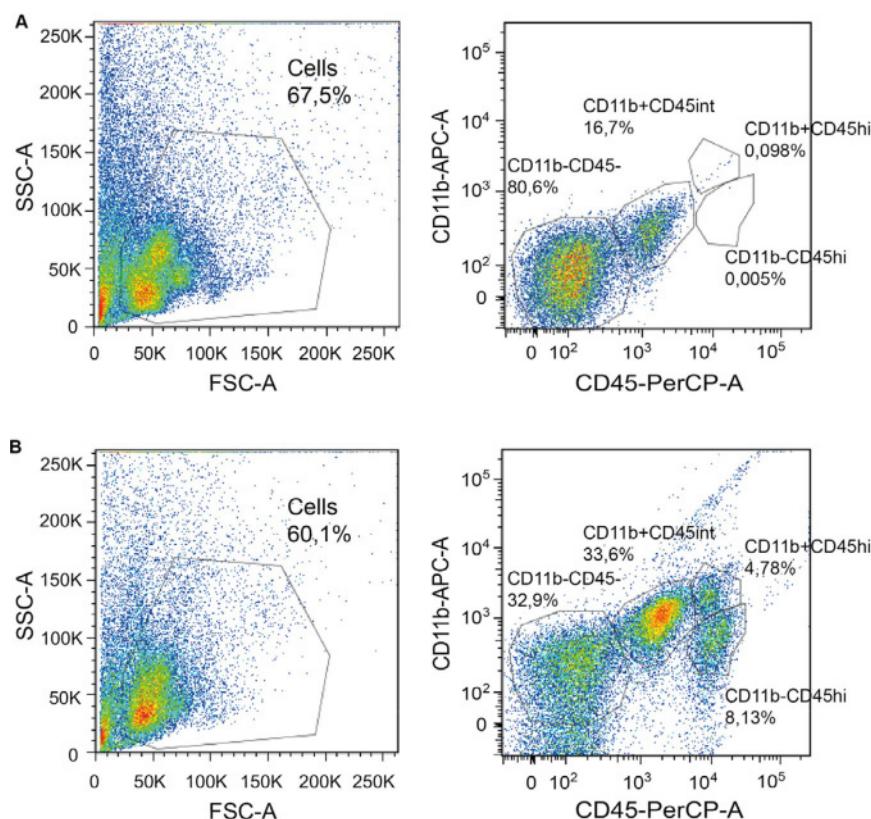
Figure 184. FCM strategy for the classification of brain-resident microglia and infiltrating macrophages and lymphocytes. (A) Analysis of brain cell suspension from a non-immunized wild-type mouse via CD45 and CD11b marker expression. (B) Analysis of monocyte-derived macrophages, infiltrating lymphocytes, and microglia in a mouse immunized with MOG35-55 at chronic phase. Cell populations were distinguished by CD45 and CD11b expression levels with macrophages showing CD11b positive, CD45 high expression (CD11b$^+$CD45^{hi}), microglia showing CD11b positive, CD45 intermediate expression (CD11b$^+$,CD45^{int}), infiltrating lymphocytes showing CD11b negative, CD45 high expression (CD11b$^-$CD45^{hi}) and non-leukocytes being CD11b and CD45 negative (CD11b-CD45-). Abs used: rat anti-mouse CD45, PerCP-conjugated, 1:200 clone 30-F11, Biolegend; rat anti-mouse CD11b, APC-conjugated, 1:400 clone M1/70, Biolegend. A total of 100 000 cells of the SSC-A/FSC-A gate were set as a stopping point during FCM. FSC and SSC axes are linear, fluorochrome axes are log.

suitable for subsequent culture. Combining different Abs can also assist in generating pure astrocyte populations and even distinguish between astrocytic subpopulations. For example, [1646]) identified astrocyte populations based on Aldh1l1 expression combined with CD51, CD71, and/or CD63 cell surface expression, which showed clear regional specificities. Mouse lines containing fluorescent labeling of astrocytes also provide a useful tool for FCM (Table 74). Currently, the Aldh1l1-EGFP reporter line [1647] is the only line labeling solely mature astrocytes in the mouse brain. All other lines are therefore only useful in astrocyte enrichment

and contamination by other neural cell types needs to be considered.

12.2.2 Neurons. Neurons are cells that are very sensitive to isolation methods. Traditionally, neurons have been isolated from late-embryonal or early-postnatal murine brain tissue with culture conditions removing contaminating glial cells. This method provides a large number of cells; however, still faces the risk of contamination by other cell types. To obtain purer cultures, FCM sorting of neuron-labeled reported mice can be used [1666–1668].
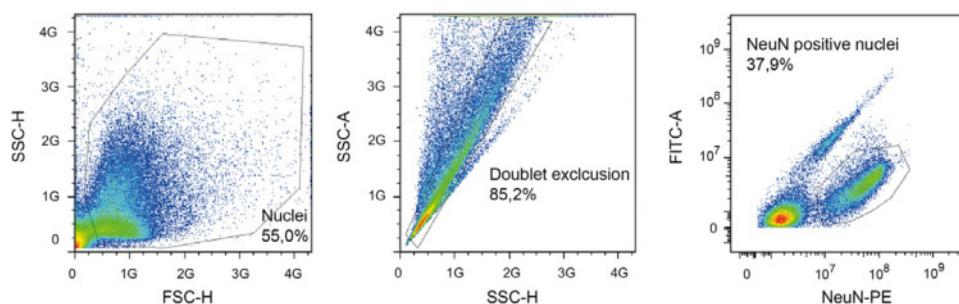
Figure 185. Fluorescence-activated nuclear sorted analysis of nuclei prepared from human surgical brain tissue. Nuclei were prepared from frozen adult brain tissue (>100 mg), stained with nuclear marker NeuN (monoclonal mouse anti-NeuN, clone A60, 1:1000 and PE-conjugated goat anti-mouse IgG 1:1000) and submitted to sorting. Gating for identification of NeuN-PE positive neuronal and non-neuronal cell populations or respective nuclei was based on the first 20 000 events. FITC fluorescence was included to identify and exclude autofluorescent nuclei. FSC and SSC axes are linear, fluorochrome axes are log.

Table 74. List of all astrocyte- and microglia- targeted fluorescent reporter lines. Modified from ref. [1648] with permission

Reporter gene	CNS cells targeted	Reference
Aldh1l1	Astrocytes	[1635, 1647]
GFAP	Astrocytes + NSCs But not expressed in all astrocytes/different expression levels	[1649–1652]
SLC1A3 (GLAST/EAAT1)	Astrocytes + NSCs	[1653, 1654]
SLC1A2 (GLT1/EAAT2)	Astrocytes + ependymal cells	[1653–1655]
Vimentin	Astrocytes + NSCs	[1656]
CX3CR1	Microglia, NK cells, monocytes, dendritic cells and some macrophages	[1657, 1658]
Sall1	Microglia	[1659]
Iba1/Aif1	Microglia, macrophages, other leukocytes	[1660]
CSF1R	Microglia, macrophages, other leukocytes	[1661]
CD11b	Microglia, macrophages, other leukocytes	[1662]
TMEM119	Mature microglia	The Jackson Laboratory #031823
CD45	Microglia, macrophages, other leukocytes	[1663]
CD68	Phagocytic microglia, macrophages	[1664, 1665]

Again, this is only possible with neonatal tissue and thus only certain aspects of neuronal development and physiology can be analyzed using this technique.

Limited neuronal cell surface markers and their respective Abs exist. CD24 labeling has been used for neuronal cell sorting, however sorting procedures dramatically decrease cell integrity and viability of neurons. Thus, FCM sorting of neurons for cell culture from both adult murine and human tissue is not possible. Reports exist that describe tissue fixation for subsequent analysis of cytoplasmic or nuclear neuronal proteins or genes [1669]. Another method to analyze neurons is via nuclei sorting that has proven successful for many applications including genetic [1670, 1671], epigenetic [1672], transcription factor, or gene expression profiling [1638]. The Akbarian method of neuronal nuclei isolation provides a useful alternative to analyzing neurons [1673].

12.2.3 Oligodendrocytes. The study of oligodendrocytes has provided valuable insights into neuronal signal transduction and its changes in disease settings. Especially in demyelinating diseases such as multiple sclerosis (MS) the relationship between myelin sheath integrity and neuronal health has become apparent. As with other brain cells, oligodendrocytes have traditionally been analyzed in vitro and a plethora of culture protocols exist [1674–1677]. Based on varying medium supplements and other culture conditions, it is thus possible to grow each of the oligodendrocyte subsets and maturation stages ranging from oligodendrocyte precursors cells (OPCs) to pre-myelinating and mature oligodendrocytes. Again, these cultures are derived from neonatal brain and contain multiple cell types. FCM is mainly used to enrich oligodendrocytes from these cultures and only very few studies are published using FCM [1678] or immunopanning [1679] to isolate oligodendrocyte lineage cells

from the CNS directly and reduced yield and viability need to be considered. An overview of oligodendrocyte markers available for FCM can be found at the end of the chapter. Additionally, oligodendrocyte reporter mice are also available such as EGFP-labeled CNP mice [1680], Olig2 mice [1656], and NG2 mice [1681].

12.2.4 Microglia. Microglia are CNS-resident phagocytes that are distinct from macrophages originating in the periphery. To date, microglia have been distinguished from other CNS or myeloid cells by FCM sorting mainly based on CD45 expression levels. Non-myeloid CNS cells are CD45-negative, while perivascular macrophages or infiltrating myeloid cells and leukocytes show CD45 high expression. Microglia on the other hand can be sorted by selecting for intermediate CD45 expression (CD45 int) in the combination with CD11b [1682]. However, it needs to be considered that CD45 expression may change due to activation of the cells. Similar to other CNS cells, the same limitations regarding the need of tissue dissociation and myelin removal hold true for microglia, yet the overlap with antigens shared with other glial/neuronal cell types is not very extensive. The main challenge therefore is not to separate microglia from other CNS cells but from macrophages originating in the periphery. Microglial expression of the fractalkine receptor, CX3CR1 and CCR2, overcame some of these limitations. CX3CR1, however, is also highly expressed by circulating monocytes (Ly6C^{lo}) and other tissue resident macrophages [1657, 1658]. Only recently, new microglia-specific markers such as Tmem119 were identified, enabling robust selection of mature microglia independent of activation status in humans and in mice [1683]. Reporter lines for microglia/myeloid cells also exist for facilitating FCM sorting (Table 74). Mass cytometry, or CyTOF, has also proven a very successful tool in characterizing heterogeneity of human and murine CNS-specific myeloid

and microglial cell populations in both health and disease based on expression profiles of up to 50 cell and functional markers [1684–1688].

12.3 Step-by-step brain preparation

12.3.1 From integrated cells to a single cell suspension (example for glial cells).

Obtaining single cell suspensions from adult brain tissue can be challenging due to the vast extension of cellular processes within the brain parenchyma that upon disruption can influence cell viability and morphology. The commercially available Neural Tissue Dissociation Kit (NTDK, Miltenyi Biotec) or Adult Brain Dissociation Kit (ABDK, Miltenyi Biotec) provide gentle methods to homogenize rodent brain tissue for downstream applications such as cell enrichment and/or culture. The NTDK is recommended for dissociation of neonatal mouse tissue and adult mouse tissue with subsequent microglia isolation. Use of the ABDK is recommended for dissociation of adult mouse tissue with subsequent astrocyte, neuron, or oligodendrocyte isolation. A list of Abs available can be found at the end of this chapter.

Detailed protocol:

1. Obtain fresh mouse brain tissue and store in HBSS without Ca^{2+} and Mg^{2+} (for NTDK) or D-PBS supplemented with glucose, sodium pyruvate, CaCl, and MgCl (D-PBS (w), for ABDK). For microglia isolation from adult tissue, perfuse mouse brain with PBS before dissociation.
2. Transfer 400–1000 mg neural tissue into C tube (Miltenyi Biotec) and add NTDK or ABDK enzyme mixes according to manufacturer's protocol.
   (a) For neonatal murine tissue and murine adult microglia use NTDK
   (b) For murine adult astrocytes, neurons, and oligodendrocytes use ABDK
3. Run the samples on the gentleMACS® with heaters (Miltenyi Biotec):
   (a) Neonatal murine cells: 37C_NTDK_1.
   (b) Murine adult cells: Program 37C_ABDK_01
4. Resuspend cell suspensions and pass through a 70 μM cell strainer placed on a 50 mL tube.
5. Wash cell strainer with 10 mL HBSS with Ca^{2+} and Mg^{2+} (for NTDK) and 10 mL D-PBS (w) (for ABDK).
6. Centrifuge samples at $300 \times g$ for 10 min, 4°C and remove the supernatant.
7. Resuspend pellet according to kit used:
   (a) NTDK: Resuspend in buffer and volume required for further applications.
   (b) ABDK: Resuspend in D-PBS (w) according to input material and transfer to 15 mL tube
      i) 400–500 mg tissue: 3100 μL D-PBS (w)
      ii) 800–1000 mg tissue: 6200 μL D-PBS (w)

8. (ABDK only) Add cold Debris Removal Solution depending on input material, mix well, and overlay very gently with 4 mL of D-PBS (w). Centrifuge at $3000 \times g$ for 10 min, 4°C with full acceleration and brake.
   (a) 400–500 mg tissue: 900 μL
   (b) 800–1000 mg tissue: 1800 μL
9. (ABDK only) Aspirate the top two phases and fill up with D-PBS to a final volume of 15 mL. Invert tube three times.
10. (ABDK only) Centrifuge samples at $1000 \times g$ for 10 min, 4°C with full acceleration and brake.
11. (ABDK only) Discard supernatant and resuspend cell pellet in 1 mL 1× Red Blood Cell Removal Solution (diluted in ddH2O). Incubate for 10 min at 4°C.
12. (ABDK only) Add 10 ml cold PBS + 0.5% BSA and centrifuge samples at 300 x g for 10 min, 4°C.
13. (ABDK only) Remove the supernatant and resuspend pellet in buffer and volume required for further applications.

12.3.2 From integrated cells to a single cell suspension 2 (example for immune cells).

Depending on the immune cell subtype of interest different Percoll-based protocols are available that can additionally be combined with enzymatic digestion, whilst the resistance of antigens to digestion enzymes needs to be considered and protocols optimized accordingly. We present here a rapid, easy and cheap protocol not requiring enzymatic digestion that is suitable for the isolation of the majority of peripheral immune cells as well as microglia.

Detailed protocol:

1. Mechanically dissociate neural tissue using a 70 μm nylon cell strainer and the plunger of a 5 mL syringe into 15 mL tubes containing complete RPMI medium or HBSS.
2. Centrifuge at $400 \times g$ for 10 min at 4°C.
3. Aspirate supernatant and vortex pellet.
4. Add 6 mL 37% Percoll (dissolved in Percoll mix, recipe in table with materials) to each tube at room temperature.
5. Resuspend pellet thoroughly by repeated pipetting.
6. Spin in swinging bucket centrifuge at $2800 \times g$, 20 min, no brake, at room temperature. It is important to use a centrifuge in which the buckets swing out a full 90° to ensure good separation of the myelin layer.
7. Aspirate myelin, take care to clean the sides of the tube.
8. Aspirate Percoll solution, down to ~500 μL and do not break up the pellet, as you are trying to dilute the residual Percoll.
9. Add 6 mL complete medium (or HBSS) (1st wash).
10. Centrifuge at $400 \times g$ for 10 min at 4°C.
11. Completely aspirate medium, vortex pellet, add 10 mL complete medium (2nd wash).
12. Centrifuge at $400 \times g$ for 10 min at 4°C.
13. Resuspend in FCM Fc-block (see materials table) for 15 min and count a diluted fraction of cells (e.g., for a mouse brain, resuspend in 1 mL FCM Fc-block, for a single murine spinal cord, use 0.5 mL).

14. Wash the cells in medium and subsequently stain with Abs as desired.
15. Following antibody stain, cells may be fixed in 4% paraformaldehyde (Electron Microscopy Science) for 10 min at room temperature. Following a wash step the cells can be resuspended and stored at 4°C until measurement.

12.3.3 From integrated cells to nuclei (example for neurons). This method can be used to extract nuclei from >100 mg of fresh or frozen human cortical tissue. Immunotagging with an anti-NeuN Ab robustly stains human cortical neuron nuclei for subsequent FCM sorting. Other cell populations beyond neurons can be captured the same way (e.g., astrocytes, oligodendrocytes) if specific nuclear antigens are known and respective Abs available. Other methods to study single neurons in the adult human brain include the use of microfluidic devices as the Fluigdime C1 and ultra-high-throughput droplet-based technologies [1689].

Detailed protocol:

1. Chill a clean B-type 7 mL pestle on ice and add 5 mL of lysis buffer (see materials section). Note: Lysis buffer can be prepared on day prior to sorting, but DTT should be added fresh on the day of use.
2. Cut 100—500 mg fresh-frozen human surgical or postmortem brain tissue and transfer to lysis buffer in homogenizer. Homogenize tissue on ice using pestle.
3. Put 8 mL sucrose cushion buffer in a Beckman Ultra-clear 14 $\times$ 95 mm centrifuge tube.
4. Note: Tube size and type have to fit with the ultracentrifuge and rotor system used (here, e.g., Beckmann OPTIMA XE – 90 ultracentrifuge and SW-40Ti rotor).
5. Carefully overlay homogenized sample on top of sucrose cushion without mixing the two solutions.
6. Centrifuge for 2 h in pre-chilled swing-out rotor at 4°C, 30 000 $\times$ g.
7. After centrifugation, put tube on ice and carefully remove supernatant. Add 500 μL of 3 mM $MgCl_2$ in PBS and let stand on ice. After 10 min very gently re-disperse pellet. Note: Do not vortex nuclei. Always keep nuclei on ice.
8. Pass nuclei suspension through a 40 μM cell strainer into a clean 1.5 mL tube and dilute with 3 mM $MgCl_2$ in PBS. Keep a fraction for manual counting.
9. Add mouse anti-NeuN Ab (1:1000), Goat anti-Mouse IgG (H+L) Secondary Ab, PE-conjugated (1:1000), and incubate for at least 30 min at 4°C on a rotator.
10. Manual counting of a fraction of nuclei and quality control with bright field microscopy.
11. Proceed to sorting.

12.4 Materials

12.4.1 Cell suspension (glial protocol).

Reagent	Manufacturer
OctoMACS® with Heaters	Miltenyi Biotec
Adult Brain Dissociation Kit	Miltenyi Biotec
Neural Tissue Dissociation Kit (P)	Miltenyi Biotec
C tubes	Miltenyi Biotec
HBSS with Ca^{2+} and Mg^{2+} (NTDK only)	Life technologies
HBSS without Ca^{2+} and Mg^{2+} (NTDK only)	Life technologies
D-PBS with 0.55 mM glucose, 0.033 mM sodium pyruvate, 0.9 mM CaCl, 0.49 mM MgCl (pH 7.2, keep cold) (ABDK only)	–
PBS + 0.5% BSA (pH 7.2, keep cold)	–

12.4.2 Cell suspension (immune cell protocol).

Reagent	Manufacturer
Cell Strainer size 70 μm Nylon	BD Falcon
5 mL syringe	BD Falcon
15 mL tubes	BD Falcon
Complete RPMI medium (5% FCS, Penicillin/Strepdavidine, b-Mercapto) or HBSS	Sigma
37% Percoll (100% Percoll mixed with respective amount of mastermix of 45 mL 10$\times$ PBS, 3 mL 0.6 N HCl, 132 mL H_2O, pH 7–7.2 filter sterilized)	Sigma
FCM Fc-block (to a given volume of FCM buffer add 50 μg/mL rat IgG and 1 μg/mL CD16/CD32 mAb	eBioscience

12.4.3 Nuclei preparation (neurons).

Reagent	Specifications
7 mL Dounce tissue grinder	Wheaton #357542
Lysis buffer	0.32M Sucrose, 5 mM $CaCl_2$, 3 mM $MgAc_2$, 0.1 mM EDTA, 10 mM Tris-HCL pH 8, 1 mM fresh DTT, 0.1% Triton X100
Sucrose cushion buffer	1.8 M Sucrose, 3 mM $MgAc_2$, 10 mM Tris-HCL pH 8, 1 mM fresh DTT
Beckman ultra-clear 14 $\times$ 95mm centrifuge tube	Beckman Coulter #344060
3 mM MgCl2 in PBS	–
40 μM nylon cell strainer	BD Falcon
Mouse anti-NeuN Ab, Clone A60 (1:1000)	Millipore
Goat anti-Mouse IgG (H+L) Secondary Ab, PE (1:1000)	

12.5 Data analysis/gating

Fig. 183 provides representative FCM blots of neonatal murine astrocytes labeled with the cell surface marker ACSA-2 (Fig. 183A) and the intracellular marker GFAP (Fig. 183B). For the intracellular GFAP stain, cells were fixed in 2% PFA and permeabilized with 0.5% saponin.

12.6 Microglia (human/mouse)

To analyze microglia and macrophages, brain tissue from a mouse immunized with MOG35-55 peptide in the chronic phase of experimental autoimmune encephalomyelitis (EAE) and tissue from non-immunized mice was mechanically dissected and myelin removed via Percoll layering as described in the step-by-step preparation. Fig. 184 provides representative FCM blots of gating strategies for macrophages (CD11b positive, CD45 high expression), microglia (CD11b positive, CD45 intermediate (int) expression), infiltrating lymphocytes (CD11b negative, CD45 high expression), and non-leukocytes (CD11b negative, CD45 negative expression). In contrast to non-immunized mice, where only brain-resident microglia and some perivascular macrophages are present (Fig. 184A), infiltrating macrophages and lymphocytes are present in MOG35-55 immunized mice (Figure 184B).

12.7 Neurons

Figure 185 shows a representative blot of fluorescence-activated nuclear sorted nuclei prepared from human surgical brain tissue. Nuclei were prepared from frozen adult brain tissue and stained with the neuronal nuclear marker NeuN. FITC fluorescence was included in order to select for autofluorescence.

12.8 Pitfalls

As already mentioned in the introduction, the low yield and reduced cell viability are challenging when wanting to FCM sort CNS cells. Cell purity is also an issue in the CNS as cell markers are often expressed by more than one cell type and are region specific. Since neurons, astrocytes and oligodendrocytes share the same precursor, many cell markers are shared between them. Microglia and peripheral myeloid cells also share many of the same cell surface markers, that change during activation state and/or pathology and which need to be carefully selected for.

Special attention should be also paid during analysis of antigens on the surface of microglia/macrophages and astrocytes as unspecific binding via Fc receptors or membrane absorption can create false positive results. These cells do express different Ig Fc receptors. By incubating cells in the presence of blocking reagents, Fc receptor-mediated binding of Igs can be suppressed. Blocking can be performed by purified Igs, serum, or purified CD16/32, but also different commercial special blocking solutions are available or included in kit protocols. When Fc receptors itself are of interest as antigen it has to be checked whether the used block-

ing approach enables a detection after blocking. Besides binding to Fc receptors membrane adsorption can generate false positive results. Fast processing, repeated washing steps as well as addition of EDTA and BSA to the buffer solutions are helping to reduce unwanted membrane adsorption (see Chapter V Section 5: Surface Parameters).

In some experiments, microglia and/or macrophages can affect the analysis/sorting of other cells from the CNS. In setups where the focus is, e.g., on astrocytes, nonspecific Ab binding can be reduced by an additional microglia/macrophage depletion step.

Additionally, myelin debris can lead to essential problems during data acquisition and labeling of cells with Abs and protocols need to be adapted accordingly [1690, 1691]. This is especially important for the analysis of adult white matter regions. Through high myelin content, clogging of the instruments may occur and cells of interest might not be detectable in the sample. Therefore, we highly recommend including an effective but gentle myelin removal step when analyzing CNS tissue with FCM.

When wanting to analyze human tissue, it needs to be taken into account that it can only be obtained from very limited fresh biopsies or from postmortem autopsies. Fresh healthy controls are therefore not available and in the case of autopsy material, a high postmortem interval can dramatically reduce tissue quality.

12.9 Top tricks

In the past, the study of CNS resident cells has largely relied on ex vivo slice cultures, histological means or the in vitro culture of neonatal cells. FCM analysis was traditionally used only on microglial cells that show similar expression of cell surface markers to peripheral myeloid cells. Advances in brain dissociation techniques and the vast array of reporter mice have made the analysis of other brain cells amenable to methods such as FCM, MACS®, immunopanning, and single cell or nuclear sequencing. Each of these methods has limitations with regards to cell viability, purity, yield, and Ab availability. It is thus essential to choose the most appropriate method depending on the scientific question.

For studies using neonatal murine CNS tissue, obtaining enriched cell suspensions from mixed cultures or by FCM/MACS®, offers a high yield of cells, however cultures may be contaminated by other CNS cells. Additionally, some cells only reach maturity at late postnatal stages and these cultures thus contain many precursor cells. Here, selecting the appropriate cell culture medium before FCM sorting may help in selecting for a specific cell type [1692]. Obtaining adult cells from murine brain or cells from human tissue is best achieved using gentle dissociation techniques. Enriched cell populations can then be generated by FCM or MACS®, yet reduced cell viability, yield, and Ab availability need to be considered. CyTOF also offers a high-throughput technique for analyzing cells of myeloid origin including microglia on a single-cell level. For mouse tissue, reporter lines are a valuable tool for FCM sorting of specific cell populations. When interested in isolating more than one cell type, immunopanning is a suitable method since all cells are sequentially purified from whole brain suspensions [1693]. Neuron isolation of both adult murine

and human tissue remains challenging to this day. A suitable alternative when interested in gene expression or nuclear proteins/transcription factors is nuclei sorting via FCM, which also is applicable to immunolabeled neurons and methods such as single-nuclei RNA sequencing.

12.10 *Summary table (Table 75)*

Table 75. Selection of molecules that discriminate subpopulations of brain cells

Antigen	Cells targeted	Species reactivity	Cellular compartment	Company
ACSA-2	Astrocytes	Mouse	Cell surface	Miltenyi Biotec
SLC1A3 (GLAST/EAAT1)	Astrocytes + NSCs	Human, Mouse, Rat	Cell surface	Miltenyi Biotec
SLC1A2 (GLT-1/EAAT2)	Astrocytes + ependymal cells	Human, Mouse, Rat	Cell surface	Biorbyt
ITGAV (CD51)	Specific astrocyte populations	Mouse/Human	Cell surface	BD Biosciences/ Biolegend
CD63	Specific astrocyte populations	Mouse/Human	Cell surface	eBioscience/BD Biosciences
CD71	Specific astrocyte populations	Mouse, Human	Cell surface	BD Biosciences
GFAP	Astrocytes + NPCs	Human, Mouse, Rat	Intracellular	BD Biosciences
AQP4	Astrocytes + ependymal cells	Human, Mouse, Rat	Cell surface	Biorbyt
CD45	Microglia, macrophages, other leukocytes	Mouse, human	Cell surface	eBioscience
CD11b	Microglia, macrophages, other leukocytes	Mouse, human	Cell surface	eBioscience
CD68	Phagocytic microglia, macrophages	Mouse, human	Intracellular	eBioscience
CX3CR1	Microglia, NK cells, monocytes, dendritic cells and some macrophages	Mouse, human	Cell surface	Biolegend
Tmem119	Mature microglia	Mouse, human	Cell surface	Abcam
Iba-1 (AIF-1)	Microglia, macrophages, other leukocytes	Mouse, human	Intracellular	Abcam
NG2/AN2	OPCs	Human, Mouse	Cell surface	Miltenyi Biotec
CD140a (PDGFRα)	OPCs	Human, Mouse	Cell surface	Miltenyi Biotec
GalC/O1	Pre-myelinating and mature oligodendrocyte	Human, Mouse, Rat	Cell surface	Merck
O4	Pre-myelinating and mature oligodendrocytes	Human, Mouse, Rat	Cell surface	Miltenyi Biotec
MOG	Mature oligodendrocytes	Mouse, Rat	Cell surface	Merck
CNPase	Mature oligodendrocytes	Human	Cell surface	Merck
Nestin	NSCs	Human, Mouse, Rat	Intracellular	R&D systems
NeuN	Neurons	Human, Mouse, Rat	Nuclear	Merck
CD24	Neurons and peripheral cells	Human, Mouse, Rat	Cell surface	Biolegend
Thy-1	Neurons	Human	Intracellular	Biolegend
Tuj-1 (beta III tubulin)	Neurons	Human, Mouse, Rat	Intracellular	R&D systems

13 Cells from liver

13.1 *Overview*

The section gives a short introduction into the unique immunological milieu of the liver and the different hepatic immune cells of the innate and adaptive immune system. Moreover, this section provides detailed protocols for isolation and subsequent staining of hepatic immune cells from murine and human liver tissue.

13.2 *Introduction*

The liver is an organ that exerts both metabolic and immunological functions. Due to a dual blood supply, the liver receives blood from the hepatic artery as well as from the portal vein containing gut-derived food and microbial antigens. There are unique hepatic immune regulatory mechanisms, which induce tolerance against innocuous antigens including nutrients and microbiome-derived degradation products like LPS. The liver is a site of primary T-cell activation mediated by local conventional and unconventional antigen-presenting cells, such as liver sinusoidal endothelial cells, which promote tolerance by induction of T-cell anergy and apoptosis as well as generation and expansion of Tregs. The tolerogenic properties of the liver ensure the maintenance of local
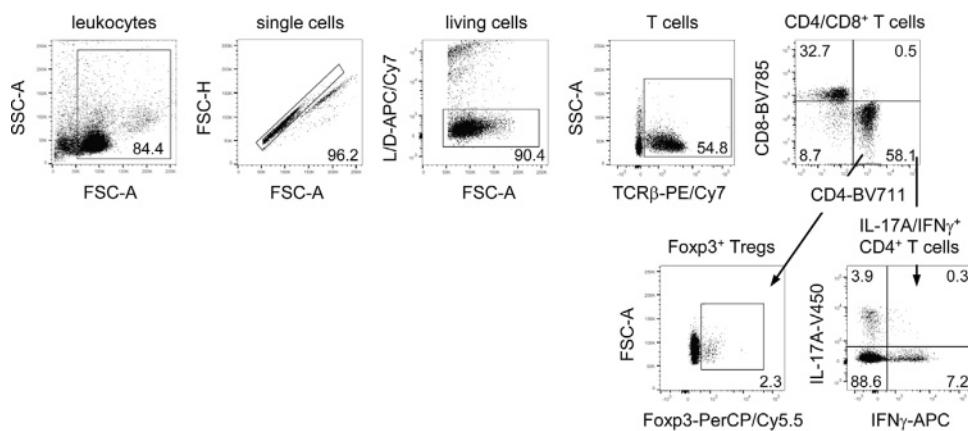
Figure 186. Gating strategy for T-cell populations in the murine liver. Hepatic leukocytes from $TNFR1^{-/-}$ x $Mdr2^{-/-}$ mice, which develop chronic liver inflammation, were used for analysis. Single cells were discriminated from doublets by plotting FSC-A against FSC-H. To exclude dead cells, a fixable dead cell staining was performed. Hepatic leukocytes were stained with anti-TCRβ-PE/Cy7 (H57-597; BioLegend), BV711 CD4 mAb (RM4-5; BioLegend), BV785 CD8 mAb (53-6.7; BioLegend), anti-Foxp3-PerCP/Cy5.5 (FJK-16s; ThermoFisher Scientific), anti-IL-17A-V450 (TC11-18H10; BD Pharmingen), and anti-IFNγ-APC (XMG1.2; ThermoFisher Scientific) Abs to distinguish between TCRαβ+ CD4+ T cells, TCRαβ+ CD8+ T cells, CD4+ Foxp3+ Tregs, and CD4+ T cells expressing IFN-γ and/or IL-17A.

and systemic immune tolerance, but they also contribute to the persistence of hepatic viral infections and tumor metastasis. However, the liver is also able to mount effective immune responses against pathogens. The liver consists of parenchymal cells (hepatocytes and cholangiocytes) and non-parenchymal cells comprising liver sinusoidal endothelial cells, hepatic stellate cells, and various immune cell populations belonging to the innate and adaptive immune system. The quantitative and qualitative composition of hepatic immune cells markedly differs from secondary lymphoid organs. The majority of hepatic DCs display an inactive phenotype. Moreover, the liver contains the largest population of resident macrophages, termed Kupffer cells, and there is an increased proportion of hepatic NK cells, NKT cells, and γδ T cells compared to secondary lymphoid organs [1694–1698].

To study the complex network of hepatic immune cell populations in healthy and diseased liver, flow cytometric analysis is the best validated method. In this section, we provide detailed protocols for the isolation of leukocytes from murine and human liver as well as for surface and intracellular/intranuclear hepatic leukocyte staining. In the murine section, we further provide Ab panels for the analysis of T cells, Tregs (Fig. 186), NK cells, NKT cells, γδ T cells (Fig. 187), and macrophage subsets (Fig. 188). In the human section, we provide Ab panels for the analysis of NK cells (Fig. 189), T cells (Fig. 190), and myeloid cells (Fig. 191). The phenotypic markers in T-cell and NK-cell subsets, and monocytes and macrophages are summarised in Tables 75 and 76 respectively.
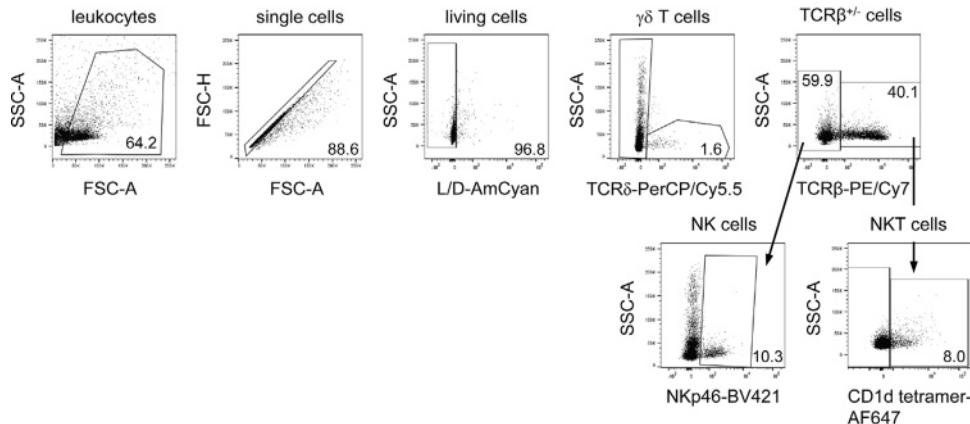
Figure 187. Gating strategy for NK cells, NKT cells, and γδ T cells in the murine liver. Hepatic leukocytes from $Mdr2^{-/-}$ mice, which develop chronic liver inflammation, were used for analysis. Single cells were discriminated from doublets by plotting FSC-A against FSC-H. To exclude dead cells, a fixable dead cell staining was performed. Hepatic leukocytes were stained with anti-TCRβ-PE/Cy7 (H57-597; BioLegend), anti-TCRδ-PerCP/Cy5.5 (GL3; BioLegend), anti-NKp46-BV421 (29A1.4; BioLegend), and CD1d tetramer-AF647 (NIH Tetramer Core Facility) Abs to distinguish between TCRαβ− TCRγδ+ T cells, TCRαβ+ CD1d tetramer+ NKT cells, and TCRαβ− NKp46+ NK cells.
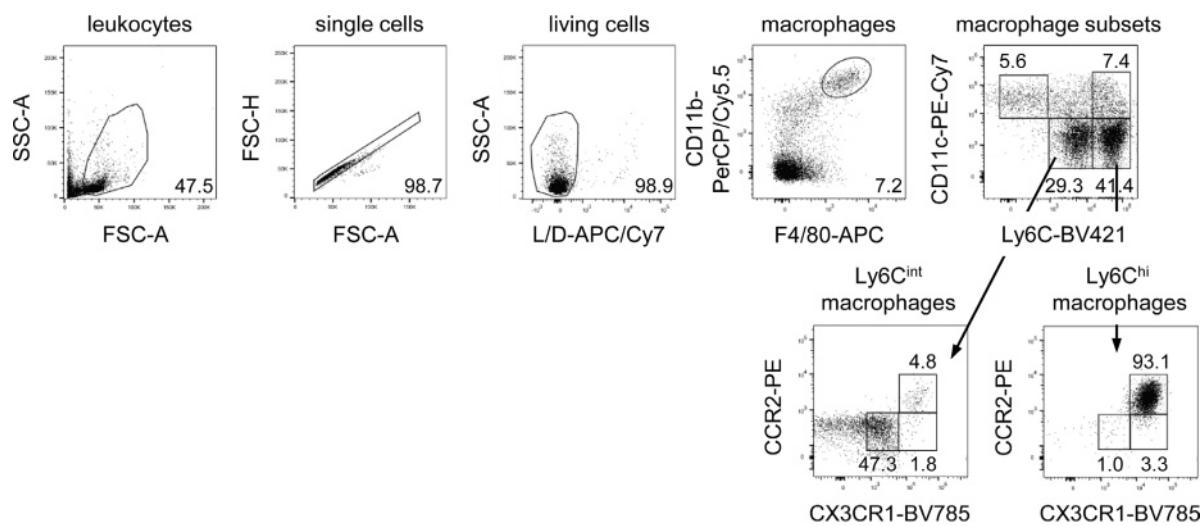
Figure 188. Gating strategy for macrophage subsets in the murine liver. Hepatic leukocytes from naive C57Bl/6 mice were used for analysis. Single cells were discriminated from doublets by plotting FSC-A against FSC-H. To exclude dead cells, a fixable dead cell staining was performed. Hepatic leukocytes were stained with PerCP/Cy5.5 CD11b mAb (M1/70; BioLegend), anti-F4/80-APC (BM8; BioLegend), PE/Cy7 CD11c mAb (N418; BioLegend), anti-Ly6C-BV421 (AL-2l; BD Pharmingen), anti-CCR2-PE (475301; R&D Systems), and anti-CX3CR1-BV785 (SA011F11; BioLegend) Abs. CD11b$^+$ F4/80$^+$ macrophages can be further divided into CD11c$^-$ Ly6C^{int}, CD11c$^-$ Ly6C^{hi}, CD11c$^+$ Ly6C$^-$, CD11c$^+$ Ly6C^{int}, and CD11C$^+$ Ly6C^{hi} subsets, which differ from each other by distinct expression of the chemokine receptors CCR2 and CX3CR1.

13.3 *Murine*

13.3.1 Protocol for liver tissue harvest and leukocyte isolation. Reagents

- 1× HBSS (for 1 L): 403 mg KCl, 53 mg Na_2HPO_4 × 2 H_2O, 54 mg KH_2PO_4, 353 mg $NaHCO_3$, 191 mg $CaCl_2$ × $2H_2O$, 102 mg $MgCl_2$ × 6 H_2O, 148 mg $MgSO_4$ × 7 H_2O, 8.006 g NaCl, 1.11 g D-glucose-monohydrate
  Add ddH_2O and adjust to pH 7.2–7.4; filtrate solution through 0.22 μm filter
- Liver Digest Medium (ThermoFisher Scientific)
- Liver Perfusion Medium (ThermoFisher Scientific)
- ACK-lysis buffer (for 1 L): 8.25 g NH_4Cl, 1 g $KHCO_3$, 29.2 mg EDTA
  Add ddH_2O and adjust to pH: 7.2-7.4
- Percoll^{TM}, density 1.130 g/mol (GE Healthcare)
- 10× PBS (for 1 L): 80 g NaCl, 11.6 g Na_2HPO_4 × $2H_2O$, 2 g KH_2PO_4, 2 g KCl

- add ddH_2O and adjust to pH7.2–7.4; autoclave
- 7.5% $NaHCO_3$ in ddH_2O
- Heparin 5000 I: E/mL (Ratiopharm)
- ddH_2O
- Percoll solution A: 3.70 mL Percoll, 0.29 mL 10× PBS, 0.05 mL 7.5% $NaHCO_3$
- Percoll working solution (10 mL; for one liver): Add 6 mL HBSS and 0.2 mL Heparin to Percoll solution A and store it at room temperature
- 4% PFA

  Equipment

- CO_2/O_2 vaporizer
- Styrofoam pad
- 70% EtOH v/v
- Half-curved blunt microsurgery scissors
- Curved forceps
- Falcon^{TM} Cell Strainer, 100 μm (Fisher Scientific)
- Petri dishes with scratched bottom
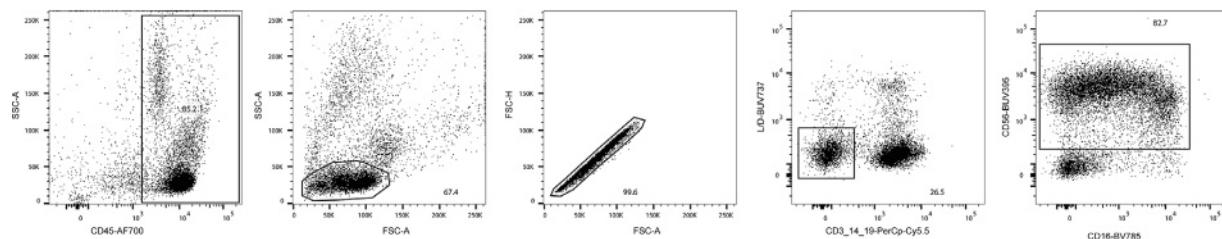
Figure 189. Gating strategy to identify NK cells in cells derived from the human liver. Hepatic leukocytes from individuals undergoing liver resection due to liver tumor metastases were used after leukocyte purification (see 16.3.1). Gating on CD45$^+$ cells (anti-human CD45; 2D1; AF700; Biolegend) was performed followed by standard leukocyte size gating and doublet exclusion. T cells, B cells, monocytes, and dead cells were excluded by employing a fixable dead cell staining (LIVE/DEAD Blue; Invitrogen) as well as Abs against CD3 (anti-human CD3; UCHT1; PerCP-Cy5.5; Biolegend), CD14 (anti-human CD14; HCD14; PerCP-Cy5.5; Biolegend), and CD19 (anti-human CD19; HIB19; PerCP-Cy5.5 Biolegend). CD56 (anti-human CD56; HCD56; BUV395, BD Biosciences) and CD16 (anti-human CD16; EG8; BV785; Biolegend) were used to identify NK cells.
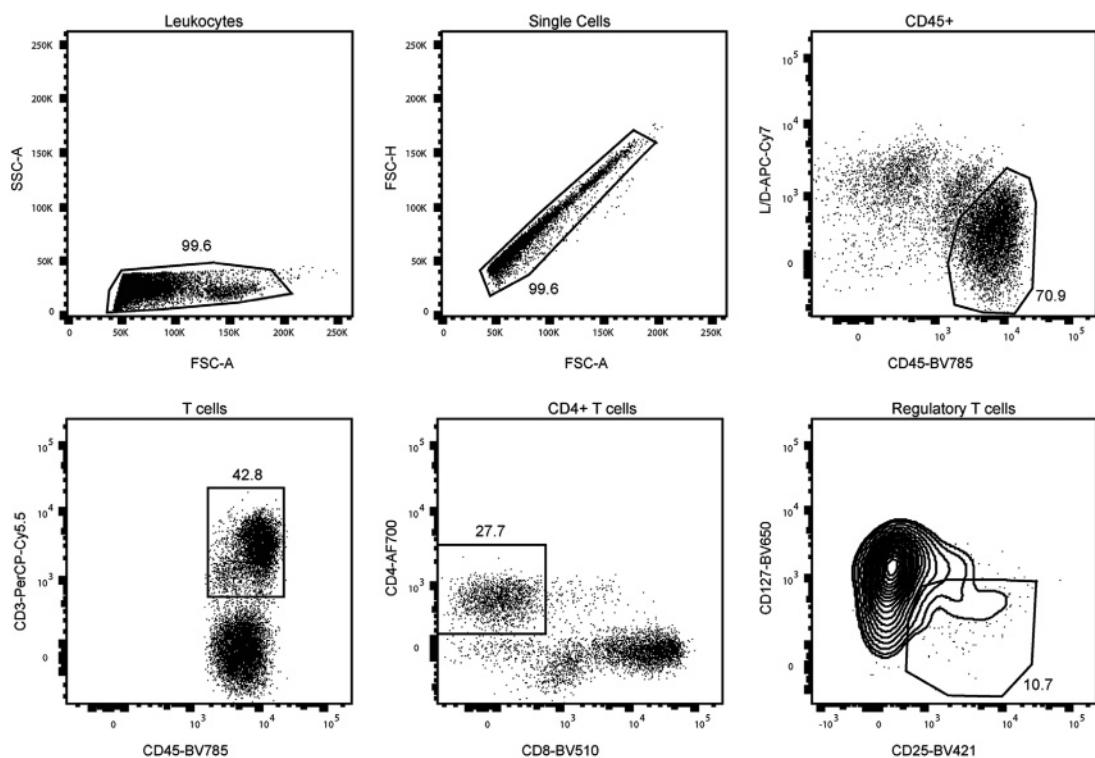
Figure 190. Gating strategy to identify T cells in cells derived from the human liver. Hepatic leukocytes from individuals undergoing liver resection due to liver tumor metastases were used without leukocyte purification (see 16.3.1). Leukocytes were exported in and subsequently analyzed. Gating on standard leukocyte sized cells, followed by doublet exclusion and gating on CD45$^+$ cells (anti-human CD45; HI30; BV785; Biolegend). CD3$^+$ T cells (antihuman CD3; OKT3; PerCP-Cy5.5; Biolegend) and subsequently CD4$^+$ and CD8$^+$ (anti-human BV510; RPA-T8; BV510; Biolegend) T cells were identified. Finally, regulator T cells were identified through CD127 (antihuman CD127; A019D5; BV650; Biolegend) and CD25 (antihuman CD25; BC96; BV421; Biolegend). We would like to thank Tobias Poch and Gloria Martrus for providing the T cell and myeloid cell flow plots.

- 50 mL centrifugation tube
- 15 mL centrifugation tube
- 2 mL syringes
- Centrifuge (Eppendorf 5810R)
- Optional:
  - Histology cassettes
  - 1.5 mL centrifugation tubes with safe lock
  - Liquid nitrogen

  Procedure

- Place the mice into the CO_2/O_2 vaporizer and anesthetize by gently flowing the chamber*
- Once the mice are anesthetized, euthanize the animal by cervical dislocation, and confirm death
- Place the mouse on a styrofoam pad with the ventral side upward and fix the animal
- Spread the abdomen with 70% EtOH and open the abdomen by making an incision in the cranial direction
- Flap the skin to the side and fix with a needle
- Take blood by cardiac puncture (~1 mL) to prevent contamination with peripheral blood cells Alternatively, the liver can be perfused in situ as described in Blom et al. [1699]
- Push the intestine sideward by using the blunt end of a forceps to get access to the liver
- Optional: if no blood sampling is required, in situ perfusion of the liver is recommended, using liver perfusion media or PBS

  - Perfuse the liver by gently injecting Liver Perfusion Media or PBS into the vena cava
  - The liver becomes blanched and swollen
  - Cut the portal vein, once the liver is swollen. Blood and media should visibly flow from the vein
  - Continue perfusion with a total volume of 10 mL

- Remove the gall bladder**
- Remove the liver and transfer it into 5 mL HBSS; store at room temperature
- Discard the HBSS and transfer the liver on a scribed petri dish
- Homogenize the liver by rubbing over the scribed surface using the pistil of a 2 ml syringe
- Fill ~5 mL of HBSS (room temperature) into the petri dish and transfer the homogenate into a 100 μm cell strainer placed on a 50 mL centrifugation tube. Alternatively, digestion of smashed liver tissue might improve cellular recovery, especially from fibrotic or cirrhotic livers as this procedure degrades extracellular matrix components, to which immune cells might adhere.

  - If choosing liver digestion, take up the smashed homogenate in 10 mL Liver Digest Medium and transfer it into a fresh 50 mL centrifugation tube
  - Incubate the cells for 30 min at 37°C

- Mince the homogenate through the cell strainer and wash with HBSS (room temperature) thereby removing fatty debris
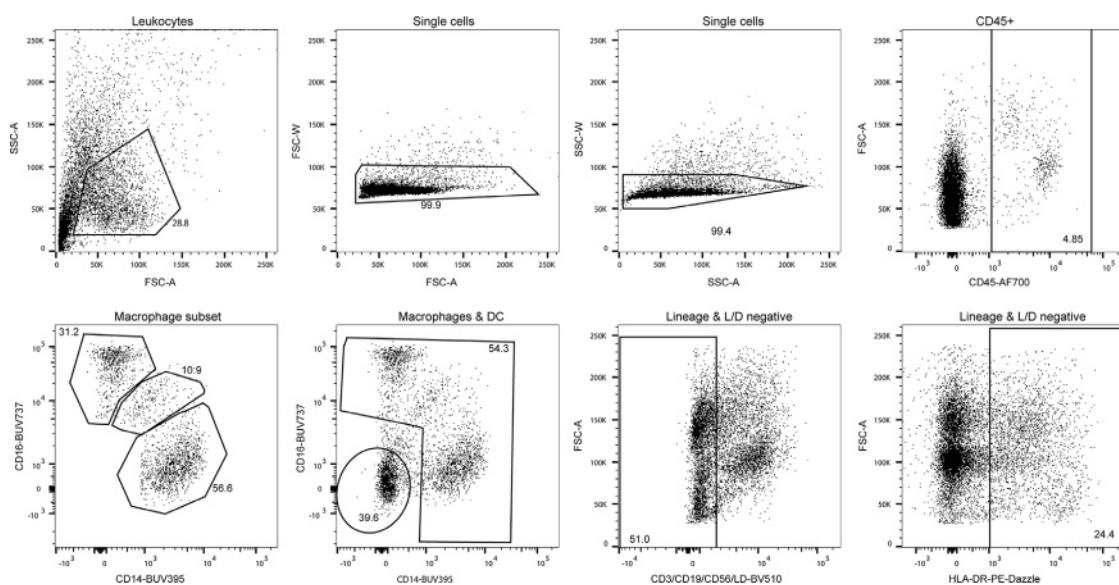
Figure 191. Gating strategy to identify myeloid cells in cells derived from human liver. Hepatic leukocytes from individuals undergoing liver resection due to liver tumor metastases were used without leukocyte purification (see 16.3.1). Gating on standard leukocyte sized cells, followed by doublet exclusion and gating on CD45$^+$ cells (antihuman CD45; HI30; AF700; Biolegend). Gating on HLA-DR$^+$ cells (antihuman HLA-DR; L243; PE-Dazzle; Biolegend) followed by lineage (antihuman CD3; UCHT1; BV510/antihuman CD19; HIB19; BV510/antihuman CD56; HCD56; BV510; all Biolegend) and L/D negative gating. Finally macrophages, dendritic cells and macrophage subsets were identified using CD14 (antihuman CD14; MΦP9; BUV395; BD Biosciences) and CD16 (antihuman CD16; 3G8; BUV737; BD Biosciences). We would like to thank Tobias Poch and Gloria Martrus for providing the T cell and myeloid cell flow plots.

- Fill up with HBSS to ∼20–25 mL and centrifuge for 5 min at 500 × g, room temperature
- Carefully discard the supernatant and re-suspend the pellet in 10 mL 37% Percoll working solution
- Transfer the Percoll suspension into a 15 mL centrifugation tube and centrifuge for 20 min at 800 × g, room temperature Caution: Switch off the brake to assure proper assembly of the different phases
- Leukocytes and erythrocytes are pelleted on the bottom of the tube. Remove the upper, light brown layer, which contains hepatocyte debris and carefully discard the supernatant
- For erythrocyte lysis, re-suspend the pellet in 3 mL ACK-lysis buffer and transfer the suspension into a fresh 50 mL centrifugation tube
- Incubate the cells for 3 to 5 min at room temperature and stop the reaction by adding 12 mL cold HBSS
- Centrifuge for 5 min at 500 × g, 4°C
- Discard the supernatant and re-suspend the pellet in 1 mL cold HBSS
- Determine the cell number
- Centrifuge for 5 min at 500 × g, 4°C
- Discard the supernatant and re-suspend the pellet in an appropriate volume of HBSS, depending on the amount of FCM-panels, which are designated for analysis***

*If whole blood is required for analysis of hepatic enzyme activity, euthanize the animals by intravenous injection of a mixture of ketamine (120 mg/kg), xylazine (16 mg/kg), and heparin (8333 I: E/kg). Harvest blood by cardiac puncture as this allows a high yield and does not interfere with subsequent procedures such as liver perfusion. Caution: This treatment requires a specific approval according to national laws and institutional regulations.

**If liver tissue is used for histology (i) or RNA isolation (ii), take little pieces for each procedure prior to removal of the liver.

(i) Cut a piece of 1–2 cm^2 and transfer into a histology cassette; fix tissue in 4% PFA
(ii) Cut 2 to 3 small pieces of liver tissue and transfer into a 1.5 mL centrifugation tube with safe lock; immediately shock freeze tissue in liquid nitrogen and subsequently store the samples at -20°C***200 μL HBSS per FCM panel is recommended. Caution: For analysis of cell populations with rare frequency, such as ILCs, a maximum of three different FCM panels per liver is recommended.

13.3.2 Protocol for hepatic leukocyte staining.   Reagents

- 1× PBS, optional 1× PBS/1% FCS (v/v)
- RPMI 1640 media (ThermoFisher Scientific)
- PMA, ionomycin, brefeldin A (all Sigma Aldrich), monensin (BioLegend)
- TruStain FcX™ (anti-mouse CD16/32) Antibody (Fc-receptor blocking solution; BioLegend)
- LIVE/DEAD™ Fixable Red Dead Cell Stain Kit or LIVE/DEAD™ Fixable Aqua Dead Cell Stain Kit (both ThermoFisher Scientific)
- Antibodies (see staining panels)
- Foxp3/Transcription Factor Staining Buffer Set (ThermoFisher Scientific)
- ddH$_2$O

Equipment

- 96-well microtiter plate, v-bottom (Nunc^{TM})
- Centrifuge (Eppendorf 5810R)
- FCM tubes
- Flow cytometer BD LSR Fortessa^{TM}

  o Laser: violet (405 nm), blue (488 nm), green (561 nm), red (640 nm)
  o Filter: 530/30(488) for FITC and AF488, 695/40(488) for PerCP/Cy5.5, 780/60(561) for PE/Cy7, 582/15(561) for PE, 780/60(640) for APC/Cy7, 670/14(640) for APC and AF647, 450/50(405) for BV421 and V450, 525/50(405) for AmCyan, 710/50(405) for BV711, 785/60(405) for BV785

Procedure

Note: the following protocol is described in the absence of protein carrier such as FCS. However, the addition of protein carrier (i.e., 1% FCS (v/v)) to the blocking and extracellular staining solutions might improve cellular vitality and reduce unspecific binding of the respective Abs.

- Transfer the cells into a 96-well microtiter plate
- Centrifuge for 5 min at 500 × g, 4°C; discard supernatant
- Prepare a working solution of 5 μg/mL Fc-receptor block in 1× PBS and store it at 4°C*
- To block unspecific Ab binding, incubate the cells in 50 μL Fc-receptor blocking solution/well for 10 min at 4°C
- Fill 150 μl 1× PBS to each well and centrifuge for 5 min at 500 x g, 4°C; discard supernatant
- For detection of death cells, prepare a live/dead staining solution in 1× PBS*
- Add 50 μL live/dead staining solution/well and re-suspend the cells
- Incubate for 30 min at 4°C in the dark**
- Fill 150 μL 1× PBS/well and centrifuge for 5 min at 500 × g, 4°C; discard supernatant
- For detection of surface molecules, prepare an Ab solution in 1× PBS* and re-suspend the cells in 50 μL Ab solution/well
- Incubate for 30 min at 4°C in the dark
- Fill 150 μL 1× PBS/well and centrifuge for 5 min at 500 × g, 4°C; discard supernatant
- Repeat the washing step
- If no intracellular staining is required, take up the cells in 150 μL PBS/well and proceed to flow cytometric analysis
- Note: For detection of cytokines and transcription factors, an intracellular and intranuclear Ab staining is required. For cytokine expression analysis, a re-stimulation of cells is recommended prior to cell staining. Incubate the cells in RPMI 1640 medium supplemented with 10% FCS, PMA (20 ng/mL) and Iono (1 μg/mL) for 5 h. After 30 min, add brefeldin A (1 μg/mL) and/or monensin (2 μM) to the cell culture medium. Monensin impairs protein secretion by blocking the Na^{++}/H^{+} transport from the Golgi apparatus while brefeldin A causes a re-shuttling of proteins from the Golgi apparatus to the endo-

plasmic reticulum. Overall, this results in intracellular aggregation of proteins and thus, cellular stress, which might impact cellular viability. Although both methods allow subsequent analysis of produced cytokines, it is recommended to do previous literature search in order to select the respective transport inhibitor for the specific cytokine.

- Prepare a Fixation/Permeabilization working solution by mixing 1 volume Fixation/Permeabilization concentrate with three volumes Fixation/Permeabilization diluent (Foxp3/Transcription Factor Staining Buffer Set)
- Add 100 μL Fixation/Permeabilization working solution/well, immediately re-suspend the cells and incubate for 30 min at 4°C in the dark***
- Prepare 1× Permeabilization Buffer by mixing one volume 10× Permeabilization buffer (Foxp3/ Transcription Factor Staining Buffer Set) with nine volumes ddH$_2$O
- Fill 150 μL 1× Permeabilization Buffer/well and centrifuge for 5 min at 500 × g, 4°C***; discard supernatant
- Repeat the washing step
- Prepare an antibody solution in 1x Permeabilization Buffer and re-suspend the cells in 50 μl Ab solution/well
- Incubate for 30 min at 4°C in the dark***
- Add 150 μl 1× Permeabilization Buffer/well and centrifuge for 5 min at 500 × g, 4°C; discard supernatant
- Repeat the washing step
- Take up the cells in 150 μL 1× PBS and proceed to flow cytometric analysis or store at 4°C in the dark. The staining is stable for at least three days.
- Prior to acquisition, re-suspend the cells in the 96-well microtiter plate and transfer them into flow cytometry-tubes supplemented with 150 μl 1x PBS

*Solution can be prepared on the day before and stored at 4°C in the dark

**To our experience, LIVE/DEAD^{TM} Fixable Red Dead Cell Stain Solution can be directly added to the antibody cocktail without an additional incubation step. However, we cannot recommend this for the LIVE/DEAD^{TM} Fixable Aqua Dead Cell Stain Solution.

***Incubation at 4°C is approved for detection of Foxp3 and cytokines. If staining of other transcription factors, such as T-Bet, Eomes, GATA3, or RORγt is required, all incubation and washing steps should be performed at room temperature.

13.4 Human

13.4.1 Protocol for hepatic leukocyte isolation.   Reagents

- OptiPrep Density Gradient Medium (e.g., Sigma–Aldrich)
- R10 (RPMI+10% FBS+1% Pen/Strep)
- PBS or HBSS
- ACK Lysing Buffer (e.g., Biozym)
- Freezing solution (90% FBS+10% DMSO)

  Equipment

- Petri dish

- Tweezers
- Scalpel
- gentleMACS®
- gentleMACS® tubes
- Cell strainers (300/200/100/70/40 μm)
- 15/50 mL conical tubes
- 1.5 mL Eppendorf tubes
- Cryo tubes
- 10 mL syringes

  Procedure
  Sample preparation

- Obtain fresh liver tissue and transport on 4°C to the lab for further downstream processing immediately[a]
- Weigh liver piece in petri dish
- Cut Liver into pieces of ~5 × 5 × 5 mm
- Split up into —four to six C-Tubes[b] (in general 5 g per C-Tube works best)
- Add 1–2 mL of R10

  Mechanical dissociation

- Put tubes onto gentleMACS® (should go in easy) and hash for 36 s[c]
- Remove tubes from machine (do not twist!)
- Remove pieces stuck in hashing blades with a pipette tip
- Repeat procedure five times

  Serial Filtering

- Pour contents through 300 μm strainers into a 50 mL conical and push hashed liver through filter carefully with the plunger of a syringe
- Pour the 300 μm filtered content through a 200 μm cell strainer into a new 50 mL conical
- Pour the 200 μm filtered content through a 100 μm cell strainer into a new 50 mL conical
- Pour the 100 μm filtered content through a 70 μm cell strainer into a new 50 mL conical
- Pour the 70 μm filtered content through a 40 μm cell strainer into a new 50 mL conical
- Fill up to 50 mL with PBS or Hank's

  Sample assessment

- Centrifuge 10 min/500 × *g*/room temperature, discard supernatant
- Resuspend pellet in 10 mL of R10
- Count cells[d,g]
- Move on to lymphocyte purification

  Lymphocyte purification

- Distribute the (remaining, see [d]) cells into 50 mL conicals (1 tube per ~10^9 cells)
- Fill up to 50 mL with PBS/Hank's

- Centrifuge 4 min/40 × *g*/room temperature
- Transfer supernatant carefully with 25 mL Pipette to 50 mL conical, discard pellet
- Fill up to 50 mL with PBS/Hank's
- Centrifuge 4 min/40 × *g*/room temperature
- Transfer supernatant carefully with 25 mL Pipette to 50 mL conical, discard pellet
- Fill up to 50 mL with PBS/Hank's
- Centrifuge 4 min/500 × *g*/room temperature
- Discard supernatant
- Fill up to 50 mL with PBS/Hank's
- Centrifuge 4 min/500 × *g*/room temperature
- Discard supernatant
- Resuspend each pellets in PBS at a final volume of 4.5 mL
- Pipette 25 mL of OptiPrep™* (2.5 mL each) into 15 mL conicals (1 tube per ~10^9 cells)
- Add the 4.5 mL of cell suspension per tube and mix it by carefully pipetting up and down (avoid any bubbles)
- Layer 1 mL of PBS above the OptiPrep suspension
- Centrifuge 20 min/400 × *g*/room temperature **without brake**[e]
- Carefully take erythrocyte/leukocyte containing interphases and pool them
- Fill up to 50 mL with PBS/Hank's
- Centrifuge 4 min/500 × *g*/room temperature → discard supernatant
- Resuspend pellet (redish) in 3 mL ACK lysis buffer and incubate for 3 min/room temperature
- Fill up to 50 mL with PBS/Hank's
- Centrifuge 5 min/500 × *g*/room temperature discard supernatant
- Resuspend pellet (should be white) in 10 mL R10
- Count cells

  Move forward to perform either direct staining's of the isolated leukocytes or cyro preserve[f,g] them for later use

  [a]If liver tissue is used for histology (i) or RNA isolation (ii), take little pieces for each procedure prior to weighting the tissue depending on the size we would recommend storing tissue pieces in

(i) In 4% PFA as well as Tissue-Tek™ (depending on the planned procedures)

(ii) In cyro-tubes and freeze immediately at –80°C

  [b]For the mechanical dissociation of the tissue, we use a gentleMACS™ Octo Dissociator, other means of mechanical dissociation could also be viable, but have not been tested with this procedure.

  [c]We refrain from using any enzymes during the mechanical dissociation as in our experience this leads to alterations in or loss of expression of surface proteins (e.g., CD56) without leading to improvements in cell yield or higher viability

  [d]Depending on cell yield storing 10 aliquots of 1.5 × 10^7 cell in 1 mL of freezing medium can be performed. The following procedure has been tested:

- Centrifuge 1.5 × 10^8 cells at 5 min/500 × *g*/room temperature, discard supernatant

- Resuspend pellet in freezing medium for a final concentration of 1.5×10^7 cells/mL
- Pipette cells into 10 cryo tubes
- Put tubes into precooled stratacooler (4°C) and store at –80°C for 24 h before transferring into liquid nitrogen

[e]Adhering to basic density centrifugation protocol is relevant for this step. Use minimum acceleration and no brakes on the centrifuge.

[f]Cyro preservation of isolate leukocytes can be performed at this step (see also [d]):

- Centrifuge 5 min/500 $\times$ g/room temperature discard supernatant
- Resuspend pellet in freezing medium for a final concentration of 1×10^7 cells/mL
- Pipette cells into cryo tubes (1 mL each)
- Put tubes into precooled stratacooler and store at –80°C for 24 h before transferring into liquid nitrogen

[g]Cells stored at these points have been successfully used for both phenotypical as well as functional analysis. When using cells stored without leukocyte purification step[d], we advise using a method of depleting dead cells (e.g., EasySep[TM] Dead Cell Removal (Annexin V) Kit) as well as resting the cells before functional assessment.

13.4.2 Protocol for hepatic leukocyte staining.   Reagents

- 1$\times$ PBS
- LIVE/DEAD[TM] Fixable Dead Cell Stain Kit
- Antibodies (see staining panels)
- Foxp3/Transcription Factor Staining Buffer Set (or comparable)
- ddH$_2$O

Equipment

- 96-well microtiter plate, u- or v-bottom
- Centrifuge
- FCM tubes
- Flow cytometer BD LSR Fortessa[TM]

  - Laser: ultraviolet (355), violet (405 nm), blue (488 nm), green (561 nm), red (633 nm)
  - Filter: 740/35, 380/14 for 355; 780/60, 710/40, 675/50, 610/20, 586/15, 525/50, 450/50 for 405; 710/40, 530/30, 488/10 for 488; 780/60, 670/30, 610/20, 586/15 for 561; 780/60. 730/45, 670/14 for 633

Procedure

Continued from 16.3.1 or after thawing of cryo-preserved samples

Surface staining

- Transfer the cells into a 96-well microtiter (preferably u- or v-bottom) plate

- Centrifuge for 5 min/500 $\times$ g/room temperature, discard supernatant
- Fill add 150–200 μL 1$\times$ PBS to each well and centrifuge for 5 min at 500 $\times$ g, discard supernatant
- For detection of surface molecules, prepare an Ab master mix in PBS and re-suspend the cells in 100 μL Ab solution/well[a,b]
- Incubate for 30 min/4°C in the dark
- Fill 150–200 μL PBS/well and centrifuge for 5 min/500 $\times$ g/room temperature, discard supernatant
- Repeat the washing step
- Resuspend the cells in 150 μL PBS/well and proceed to flow cytometric analysis[c]

Intracellular staining[d]

- Add 100 μL of Fixation/Perneabilization working solution per well, resuspend the cells, and incubate for 30 min at 4°C in the dark[e]
- Add 150 μL 1$\times$ Permeabilization Buffer/well and centrifuge for 5 min/500 $\times$ g/4°C; discard supernatant
- Repeat the washing step
- Prepare the Ab solution for intracellular staining in Permeabilization Buffer and re-suspend the cells in 100 μL Ab solution/well
- Incubate for 30 min at 4°C in the dark
- Add 150 μL Permeabilization Buffer/well and centrifuge for 5 min/500 $\times$ g/4°C; discard supernatant
- Repeat the washing step
- Resuspend the cells in 150 μL PBS/well and proceed to flow cytometric analysis, alternatively stained cells can be keep at 4°C in the dark

[a]The use of Ab master mixes is recommend, these can be prepared either fresh before the experiments or prepared beforehand and stored at 4°C in the dark. Preparation beforehand should be tested and validated against freshly prepared master mixes for each panel. The volume of the antibody master mix added might be modified based on panel size or cell numbers.

[b]In our experience, LIVE/DEAD Fixable Viability Dye's can be added directly to the Ab master mix and stained simultaneously. Alternatively, an additional staining and washing step can be included beforehand:

- For detection of death cells, prepare a live/dead staining solution in PBS
- Add 50 μL live/dead staining solution/well and re-suspend the cells
- Incubate for 30 min at 4°C in the dark
- Fill 150 μL PBS/well and centrifuge for 5 min/500 $\times$ g/4°C; discard supernatant

[c]Alternatively and depending on time-to-flow, we can recommend fixing the cells with 100 μL 4%PFA for 20 min at 4°C (or similar fixation reagents, e.g., BD CellFIX[TM]) before washing once

and resuspending in 150 µL PBS. Keep stained cells at 4°C in the dark until proceeding to flow cytometric analysis

[d]For dection of cytotoxic properties, cytokines and transcription factors, an intracellular and intranuclear Ab staining is required. Some functional properties of immune cells might only be detectable after stimulation with the appropriate stimulus (e.g., target cells, cytokines). In general we add protein transport inhibitors containing Monensin and Brefeldin A (e.g., GolgiStop[TM] & GolgiPlug[TM], BD Bioscience) after 1 h of stimulation for the rest of the stimulation period.

[e]We have tested and successful used a number of different fixation and permeabilization reagents, e.g., BD Fixation/Permeabilization Solution Kit, eBioscience Intracellular Fixation & Permeabilization Buffer Set, FIX & PERM[TM] Cell Permeabilization Kit or Foxp3/Transcription Factor Staining Buffer Set (ThermoFisher Scientific). Following the provided protocols, all of those yield satisfying results. Depending on the panel and staining used testing of different reagents is recommend.

13.5 Summary of immune cell subsets in murine and human liver

Table 76. Phenotypic marker molecules of murine and human T-cell and NK-cell subsets according to references [1342, 1700–1703]

Mouse							Human						
Cell surface	CTL	T_h	T_{reg}	$\gamma\delta$	NK	NKT	Cell surface	CTL	T_h	T_{reg}	$\gamma\delta$	NK	NKT
CD45	+	+	+	+	+	+	CD45	+	+	+	+	+	+
CD3	+	+	+	+	−	+	CD3	+	+	+	+	−	+
CD4	−	+	+	+/−	−	+/−	CD4	−	+	+	+/−	−	−
CD8	+	−	−	+/−	−	−	CD8	+	−	−	+/−	−	−
CD25	+/−[i]	+/−[i]	+[i]	+	+/−[i]	−	CD25	+/−[i]	+/−[i]	+	+	+/−[i]	−
CD107a	+	−	−	−			CD107a	+	−	−	−	+/−[i]	−
CD127	+/−	+/−	+	+	−	+	CD127	+/−	+/−	+	+	−	+
CD1 specific	−	−	−	+	−	+	CD1 specific	−	−	−	+	−	+
FasL	+	−	−	−	+/−	−	FasL	+	−	−	−	−	−
NK1.1	−	−	−	+	+	+	CD56	−	−	−	+	+	+
NKp46	−	−	−	−	+	+	CD335	−	−	−	−	+	+
NKG2D	−	−	−	+	+	+	CD314	−	−	−	+	+	+
TCRαβ	+	+	+	−	−	+	TCRαβ	+	+	+	−	−	+
TCRγδ	−	−	−	+	−	−	TCRγδ	−	−	−	+	−	−
TRAIL	+	−	−	+	+	−	TRAIL	+	−	−	−	+	−
Surface activation/exhaustion markers													
CD44[ii]	+	+	+	+	−	+	CD45RO[ii]	+	+	+	+	−	+
CD69[iii]	+/−	+/−	+/−	+/−	−	−	CD69	+/−	+/−	+/−	+/−	+/−	−
CD62L[iv]	+/−	+	+/−	−	−	−	CD62L	+/−	+	+/−	−	−	−
PD-1[v]	+/−	+/−	+	+/−	+/−	+/−	PD-1	+/−	+/−	+	+/−	+/−	+/−
Secreted cytokines													
GZMB	+	−	−	+	+	+	GZMB	+	−	−	+	+	+
IFNγ	+	+	−	+	−	+	IFNγ	+	+	−	+	−	+
IL-5	−	+	−	−	−	−	IL-5	−	+	−	−	−	−
IL-10	−	−	+	+	−	+	IL-10	−	−	+	+	−	+
IL-13	−	+	−	−	−	+	IL-13	−	+	−	−	−	+
IL-17A	−	+	−	+	−	−	IL-17A	−	+	−	+	−	−
Perforin	+	−	−	+	+	−	Perforin	+	−	−	+	+	−
TNFα	+	+	−		−	+	TNFα	+	+	−		+/−[i]	+
Transcription factors													
Eomes	+	−	−	−	+	+	Eomes	+	−	−	−	+	+
Foxp3	−	−	+	−	−	−	Foxp3	−	−	+	−	−	−
GATA3	−	+[vi]	−	−	−	−	GATA3	−	+[vi]	−	−	−	−
RORγt	−	+[vi]	−	+	−	−	RORγt	−	+[vi]	−	+	−	−
T-bet	+	+[vi]	−	+	+	+	T-bet	+	+[vi]	−	+	+/−	+

[i]Expressed following activation; downregulated on effector Tregs
[ii]Low expression by naive T cells
[iii]Early activation marker
[iv]Expressed on naive and central memory T cells; downregulated on effector T cells
[v]Expressed by activated and/or exhausted T cells
[vi]Depending on Th subset

Table 77. Phenotypic marker molecules of murine and human monocyte and macrophage subsets according to references [1444, 1704–1707]

Mouse						Human					
Cell surface	Mo	M1	M2	KC	DC	Cell surface	Mo	M1	M2	KC	DC
CD45	+	+	+	+	+	CD45	+	+	+	+	+
CD11b	+	+	+	+	+/−	CD11b	+	+	+	+	+/−
CD11c	−	−	−	−	+	CD11c	+	+	−	−	+
CD80	−	+	+	low	+	CD80	−	+	+	low	+
CD86	+	+	+	−	+	CD86	+	+	+	−	+
CD206	+	−	+	+	+/−	CD206	+	−	+	+	+/−
F4/80	+	+	+	+	low	CD14	+	high	+	+	+/−
IL-4Rα	+	−	+	ND	ND	IL-4Rα	+	−	+	ND	−
Ly6c	+	high	low	low	+/−	CD16	+/−	−	high	+	−
MHC-II	+	+	+	+	+	HLA-DR	+	+	+	+	+
PDL-1	−	−	+	+	−	PDL-1	−	−	+	+	−
Chemokine receptors											
CCR2	+/−	+	+/−	−	−	CCR2	+/−	high	low	−	−
CCR5	+	+	+	ND	ND	CCR5	+	+	+	ND	−
CX$_3$CR$_1$	+/−	+/−	+	−	+/−	CX$_3$CR$_1$	−	low	high	−	+/−
Secreted cytokines											
IL-6	−	+	−	−	+	IL-6	−	+	−	−	+
IL-10	−	−	+	+	+/−	IL-10	−	−	+	+	+/−
IL-12	−	+	−	−	+	IL-12	−	+	−	−	+
TNF-α	−	+	−	−	+	TNF-α	−	+	−	−	+

Mo, monocytes; M1, inflammatory Mo-derived macrophages; M2, alternatively activated Mo-derived macrophages; KC, Kupffer cells; ND, not detected

13.6 Pitfalls

Albeit sampling of whole blood by cardiac puncture minimizes the risk of contamination, this can further be reduced by in situ perfusion of liver tissue prior to organ isolation. Additionally, incubation of liver homogenate in Liver Digest Medium may reduce intercellular junctions and thus, increase the total recovery of immune cells within the tissue. If choosing additional incubation in digestion medium, the incubation time should not be prolonged as this might impact cell viability and shed surface molecules from the cells of interest and thus, might cause false results during analysis.

13.7 Top tricks

If performing cellular stimulation for subsequent analysis of intracellular effector cytokines, the choice of the respective transport inhibitor should be considered. For instance, brefeldin A is recommended to block intracellular transport of murine IL-6, IL-12, or TNF-α, while monensin is recommended to impair secretion of IL-10, IL-5, or GM-CSF. Please compare the recommendations of pharmaceutical companies for the right choice of transport inhibitors.

14 Porcine cells

14.1 Overview. This chapter will introduce FCM for immune cells of the pig (*Sus scrofa*) with a strong focus on T-cell phenotypes and myeloid cells. Best practice staining examples and step-by-step sample preparations are provided, mainly for blood-derived cells. Protocols describe the isolation of porcine immune cells from blood and spleen, however, we advise to establish individual tissue dissociation protocols to account for age-, cell-, and organ-specific differences. Phenotypes of immune cells present in lymphatic and nonlymphatic organs are briefly described and referenced.

14.2 Introduction. Pigs represent an excellent model for various human diseases, in particular infectious diseases [1708]. Exploitation of the pig as human-relevant model but also the study of pig diseases requires a detailed knowledge of the pig's immune system and adequate detection tools. In contrast to SPF mice, but comparable to human individuals, conventionally raised pigs are exposed to persistent and non-persistent pathogens, diverse food and environmental antigens and are routinely vaccinated. Therefore, the pig's immune system undergoes similar priming processes as observed in humans.

For flow cytometric assessment of porcine immune cells, recent updates summarize available reagents reacting with porcine CD markers including pig-specific mAbs and polyclonal Abs, but also cross-reactive mAbs from different species [1709, 1710]. In addition, a website listing Abs specific
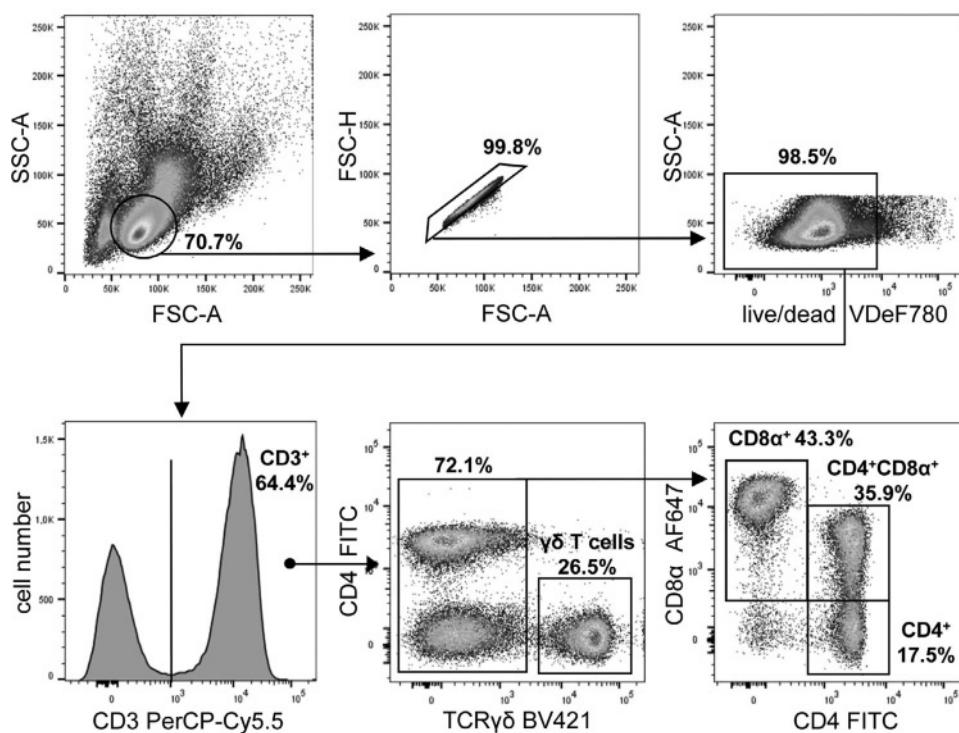
Figure 192. Identification of CD4$^+$, CD4CD8α double-positive, conventional CD8$^+$, and $\gamma\delta$ T cells in porcine peripheral blood. Lymphocytes are identified based on the forward (FSC) and side (SSC) scatter. Single cells are discriminated from doublets by plotting FSC area against height. Dead cells are excluded by a viability dye and total CD3$^+$ T cells (mAb clone BB23-8E6-8C8) are gated further. $\gamma\delta$ T cells are identified by mAb PPT16. Remaining T cells can be considered as $\alpha\beta$ T cells (currently no TCR-$\alpha\beta$-specific mAb available). Within this subpopulation, cells can be distinguished on their expression of CD4 (mAb clone 74-12-4) with CD4$^+$ T cells separating into a CD8α^+ population (mAb clone 11/295/33) and CD8α^- population. CD3$^+$TCR-$\gamma\delta^-$CD4$^-$CD8α^{high} cells represent conventional CD8$^+$ T cells. Data are generated from defrosted PBMC from an animal of approximately 6 months of age.

for porcine immune-related molecules (but also for cattle, sheep, goat, horse and chicken) has been launched in 2019 (https://www.immunologicaltoolbox.co.uk/). According to the human CD nomenclature, currently listing 419 human CD markers, 359 corresponding orthologous swine CD proteins have been identified [1710]. However, many CD orthologs have been iden-

tified based on genomic data, but still lack species-specific functional description or specific Abs and imply an urgent need for developing pig specific immune reagents. As a major remark, anti-human CD mAb cross-reactivity to porcine immune cell molecules should be experimentally defined (see Chapter VI Section 15 Cross-reactive Ab clones).
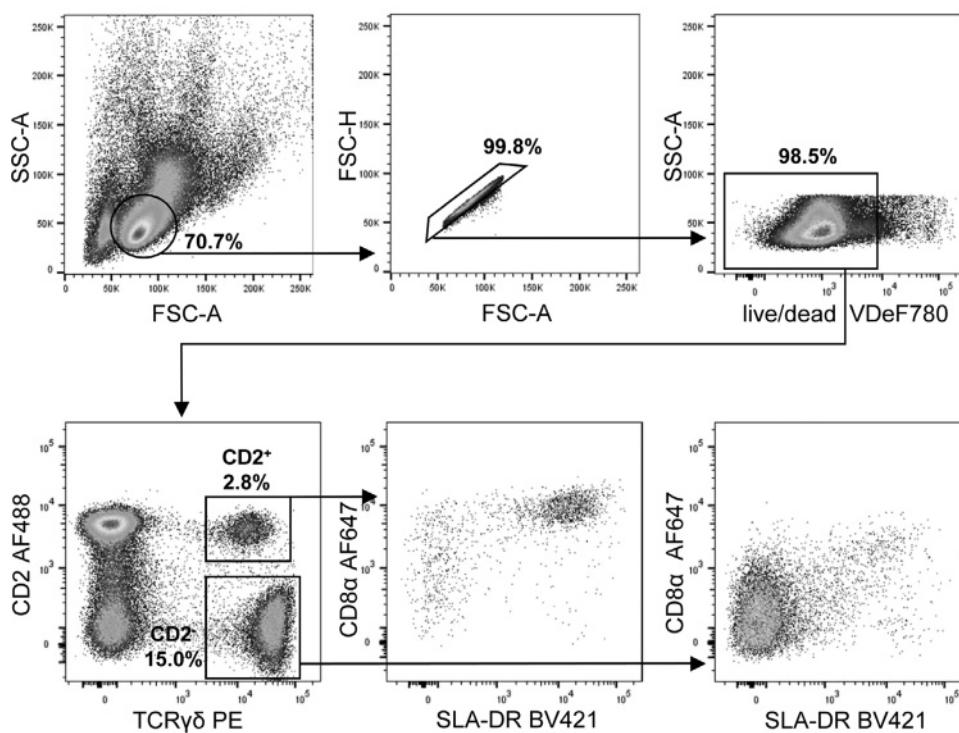
Figure 193. Identification of porcine $\gamma\delta$ T-cell subpopulations in peripheral blood. Lymphocytes are identified based on the forward and side scatter. Single cells are discriminated from doublets by plotting FSC area against height. Dead cells are excluded by a viability dye. Two subsets of $\gamma\delta$ T cells (mAb clone PGBL22A) can be distinguished in the pig by their CD2 expression (mAb clone MSA4). The majority of CD2$^+$ $\gamma\delta$ T cells express CD8α (mAb clone 11/295/33) and SLA-DR (mAb clone MSA3). In contrast, the majority of CD2$^-$ $\gamma\delta$ T cells have a CD8α/SLA-DR double-negative phenotype. Data is generated from defrosted PBMC from an animal of approximately 6 months of age.
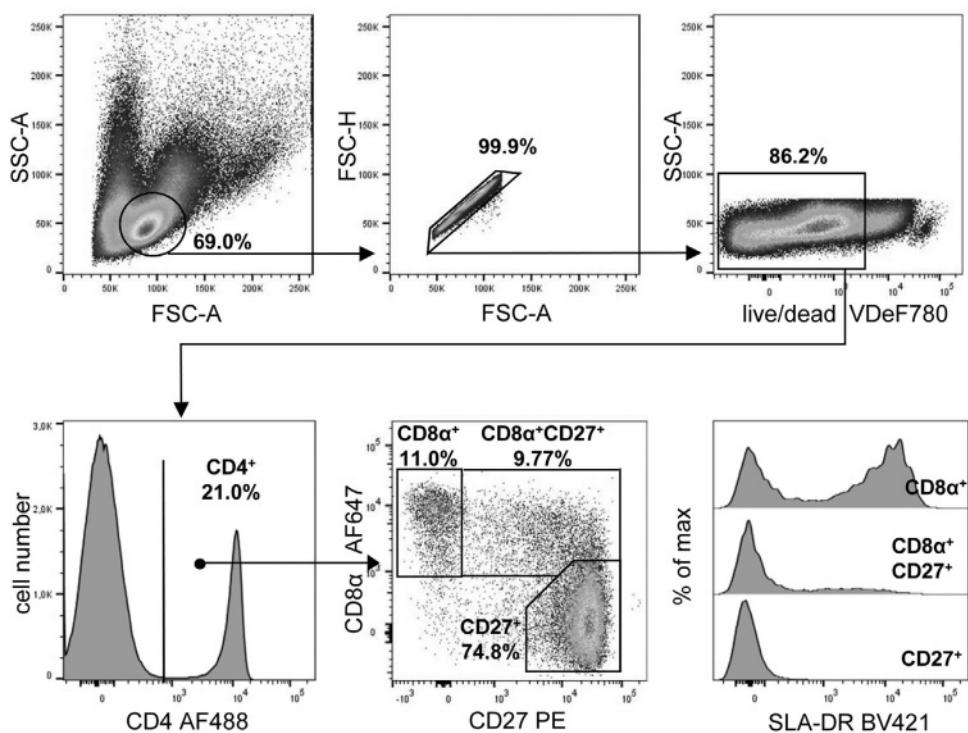
Figure 194. Identification of porcine CD4$^+$ T-cell subpopulations in peripheral blood. Lymphocytes are identified based on the forward and side scatter. Single cells are discriminated from doublets by plotting FSC area against height. Dead cells are excluded by a viability dye and cells were gated on CD4$^+$ cells (mAb clone 74-12-4) for further analysis. Naïve CD4$^+$ T cells are defined as CD8α$^-$ CD27$^+$ (mAb clone CD8α 11/295/33; mAb clone CD27 b30c7), while CD8α$^+$CD27$^+$ cells represent central memory cells and CD8α$^+$CD27$^-$ effector memory cells in the pig. Different SLA-DR expression patterns (mAb clone MSA3) of the three subsets are shown in the histograms. Data is generated from freshly isolated PBMC from an animal of approximately 2.5 months of age.

Porcine CD marker expression as compared to humans and mice include several peculiarities such as

(i) The expression of CD8αα homodimers and MHC-II (swine leukocyte antigen-DR) molecules on activated or memory CD4 T cells [1711–1713],
(ii) Major subsets of NK cells that lack CD335 (NKp46) [1714],
(iii) Expression of CD33 on neutrophils and monocytes [1715],
(iv) Varying levels of CD45RA expression on plasmacytoid DCs (pDCs) [1716]
(v) Siglec-10 expression on B cells [1717].
(vi) The high abundance of peripheral γδ T cells, ranging from ~8 to 57% within total peripheral blood lymphocytes (PBL) [1718].

14.3 Porcine T cells.   Porcine T cells from peripheral blood can be identified by gating on lymphocytes according to scatter, excluding doublets and dead cells and gating on CD3$^+$ cells. Compared to humans, pigs have a high proportion of circulating γδ T cells identified by mAbs recognizing the constant region of porcine TCR-δ chain or TCRγδ-associated CD3 molecules (Fig. 192). Pig γδ T-cell numbers are highest in young animals and decrease with age [1719]. The different porcine γδ T-cell subsets currently known are phenotypically divided based on CD2 expression into TCRγδ$^+$CD4$^-$CD8α$^-$CD2$^-$ γδ T cells and

TCRγδ$^+$CD4$^-$CD8α$^{-/+}$CD2$^+$ γδ T cells [1720, 1721] (Fig. 193). Current studies suggest that similar to human γδ T cells, CD2$^+$ γδ T cells can be activated either in direct response to PAMPs via TLRs or upon APC interaction [1722, 1723], secrete various cytokines involved in pathogen defense analogous to porcine αβ T cells and partially express MHC-II molecules on their surface [1724] (Fig. 193). In addition, cytotoxic activity, antigen- and MHC-independent, is reported for TCRγδ$^+$CD4$^-$CD8α^{low}CD2$^+$ γδ T cells (H. [1725, 1726]). The role of TCRγδ$^+$CD4$^-$CD8α$^-$CD2$^-$ γδ T cells is less clear since those cells remain unresponsive for antigenic stimuli tested so far. More recently, it was shown that these cells express high levels of GATA-3, but the functional relevance of this phenotype is not clear yet [1727].

Porcine CD4$^+$CD8α$^+$ T cells recall antigens in a MHC-II dependent manner and increase strongly in number over life time [1728, 1729]. CD8α expression on porcine Th cells is therefore perceived as marker for activated and memory T helper cells. While naïve, porcine Th cells are defined as CD4$^+$CD8α$^-$CD27$^+$, differential expression of CD27 on CD4$^+$CD8α$^+$ defines terminally differentiated effector memory cells (CD4$^+$CD8α$^+$CD27$^-$) and central memory cells (CD4$^+$CD8α$^+$CD27$^+$) (Fig. 194) [1713]. Additional markers that have been investigated to characterize differentiation of activated/memory Th cells are CD45RC and SLA-DR (MHC-II) but there is currently no unifying differentiation model based on all four molecules (i.e., CD8α, CD27, CD45RC,
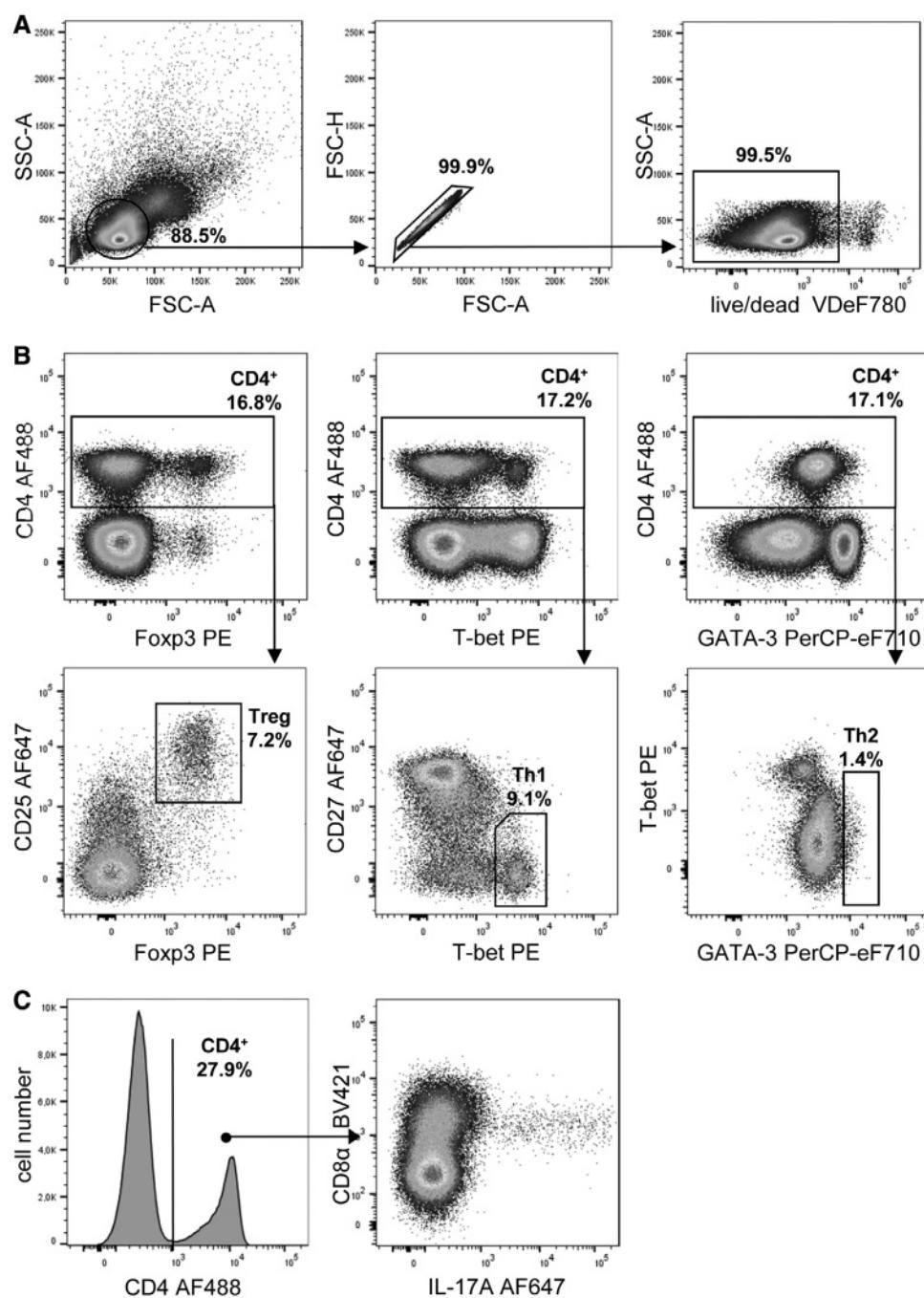
Figure 195. Functional subsets of porcine CD4$^+$ T cells can be identified based on expression of master transcription factors using cross-reactive mAbs developed against mouse and human. (A) Lymphocytes are identified based on the FSC and SSC. Single cells are discriminated from doublets by plotting FSC area against height. Dead cells are excluded by a viability dye. (B) Following surface staining of CD4 (mAb clone 74-12-4), cells were fixed and permeabilized to perform intranuclear transcription factor staining. Master transcription factors are used to identify distinct CD4$^+$ subsets: Tregs – Foxp3$^+$ (cross-reactive mAb clone FJK-16s) with CD25^{high} expression (mAb clone 3B2), Th1 – T-bet$^+$ (cross-reactive mAb clone 4B10) that are mainly negative for CD27 (mAb clone b30c7), Th2 –GATA- 3$^+$T-bet$^-$ (cross-reactive mAb clone TWAJ). (C) CD4$^+$ Th17 cells can be identified by their IL-17A expression (cross-reactive mAb clone SCPL1362) after PMA/ Ionomycin stimulation for 4 h. Data was generated from defrosted PBMC of healthy, uninfected pigs of approximately 6 months of age.

and SLA-DR) (Fig. 194). While all CD4$^+$ T cells have a CD27$^+$ phenotype in newborn piglets, a distinct subpopulation of CD45RC$^-$ cells could already be detected in neonates [1730].

Porcine CD4$^+$ T-cell subsets can be further discriminated using cross-reactive mAbs against master transcription factors. Treg cells are identified by Foxp3/CD25 co-expression [1731] (Fig. 195). T-bet expression correlates with the capacity for IFN-γ production and appears to be suitable to identify Th1 cells [1729]. GATA-3 expression is inducible in a subset of porcine CD4$^+$ T cells in vitro by ConA + IL-4 stimulation and in vivo after helminth
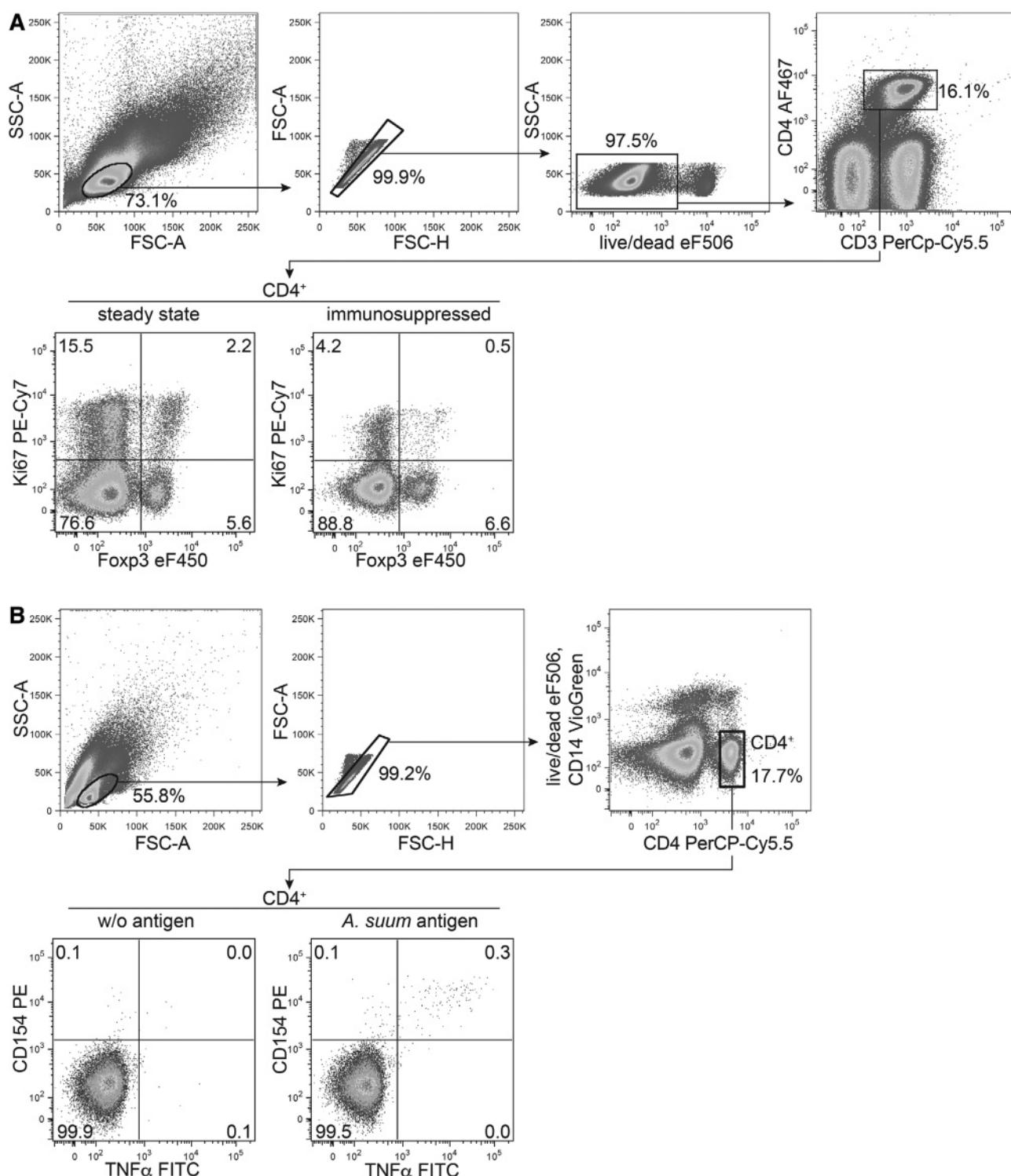
Figure 196. Proliferation- and activation-associated markers of porcine CD4^{+} T cells. Porcine CD4^{+} T cells are identified according to the gating strategies shown. (A) Nuclear staining of Ki-67 and Foxp3 using cross-reactive mAbs (mAb clone Ki-67 SolA15, mAb clone Foxp3 FJK-16s) before (left) and after (right) cyclophosphamide and methylprednisolone induced immunosuppression of a piglet aged 8 weeks. (B) PBL from an *Ascaris suum* infected pig (9 days post-infection) were subjected to short-term stimulation (7h) with *Ascaris suum* larval worm antigen (40 μg/mL) (right), or left untreated (left), followed by intracellular staining of CD154 (CD40L) using a cross-reactive mAb (mAb clone 5C8). Data is generated from fresh PBMC from an animal of approximately 3 month of age.
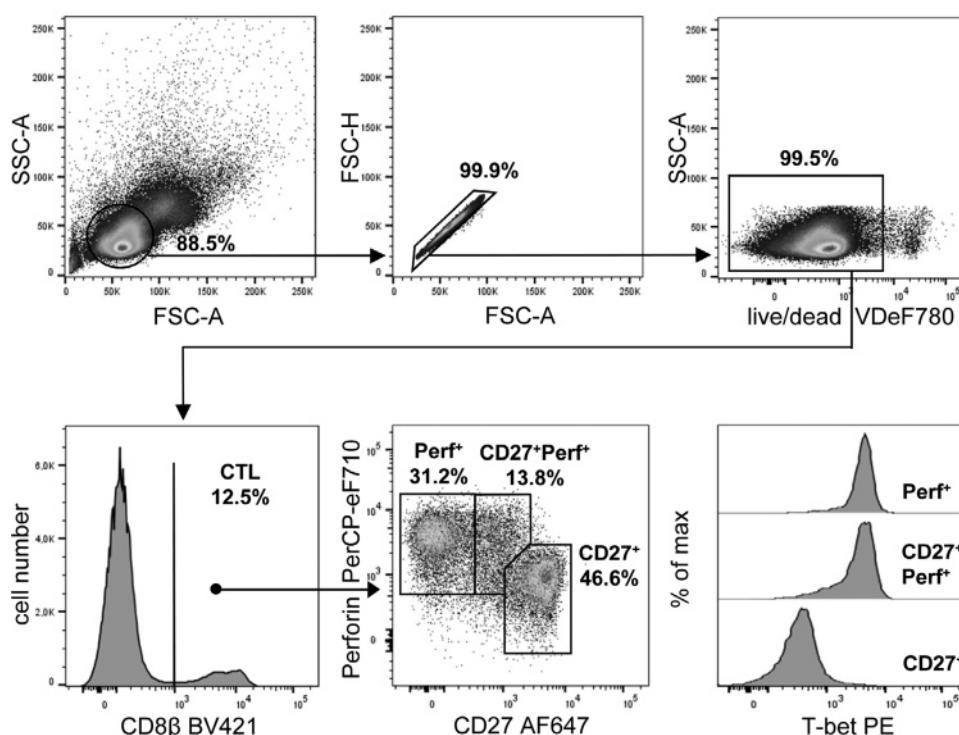
Figure 197. Identification of porcine CD8$^+$ T cells in peripheral blood. Lymphocytes are identified based on the forward and side scatter. Single cells are discriminated from doublets by plotting FSC area against height. Dead cells are excluded by a viability dye and porcine CD8$^+$ T cells are gated as CD8β^+ cells (mAb clone PPT23). Three subsets can further be identified on the basis of CD27 (mAb clone b30c7) and perforin expression (cross-reactive mAb clone δG9). Both, perforin$^+$CD27^{dim} and perforin$^+$CD27$^-$ CD8$^+$ T cells express T-bet. Data is generated from defrosted PBMC from an animal of approximately 6 months of age.

infection [1732]. However, in pigs kept under conventional housing conditions, the frequency of GATA-3$^+$ CD4$^+$ T cells is quite low. Instead, the majority of naïve CD4$^+$ T cells express low levels of GATA-3 (Fig. 195) [1729]. Th17 cells can be identified by intracellular cytokine staining with various cross-reactive anti-human IL-17A mAbs (Fig. 195 and Chapter VI 15). Nuclear staining using cross-reactive anti-mouse Ki-67 mAb identifies proliferating porcine cells [1733] (Fig. 196).

The CD4 T-cell activation marker CD154 (CD40L) is upregulated shortly (5–16 h) after TCR-dependent antigen encounter and is, also in porcine CD4$^+$ T cells, found to be co-expressed with cytokines [1734]. An anti-human cross-reactive mAb reactive to CD154 can be used to identify antigen-reactive porcine CD4$^+$ T cells by intracellular staining (Fig. 196) [1734].

In contrast to the abundant expression of CD8αα homodimers on subsets of CD4$^+$ and γδ T cells, porcine CD8$^+$ T cells with the capacity to differentiate into CTLs express CD8αβ heterodimers and hence can be identified by using mAbs against CD8β. Alternatively, they can be identified by a CD3$^+$TCR-γδ$^-$CD4$^-$ CD8α^{high} phenotype (Fig. 192). Perforin expression can be identified by cross-reactive anti-human mAbs and perforin expression has been suggested to identify antigen-experienced CD8$^+$ T cells. T-bet shows a clear positive correlation with perforin expression and ex vivo time course studies with aging pigs suggest that a lack of CD27 expression identifies terminally differentiated CTLs [1730] (Fig. 197).

Porcine T-cell development in the thymus follows the phenotypic pattern described in other vertebrates, with CD4$^-$CD8α$^-$ thymocytes representing the most immature stage, followed by a CD4$^+$CD8α$^+$ phenotype and further development into CD4$^+$CD8α$^-$ and CD4$^+$CD8α$^+$ thymocytes [1711, 1719]. The more immature phenotypes express high levels of GATA-3 [1729]. TCR-γδ T cells separate already in the thymus into a CD2$^+$ and CD2$^-$ subset [1735]. In lymph nodes, T cells with a naïve phenotype dominate, whereas in non-lymphatic organs effector (memory) phenotypes are enriched [1736]. Recently, tissue-resident memory T cells were described in porcine lung tissue and bronchoalveolar lavage [1737]. Abs for porcine CD103 are currently not available and pig-specific mAbs for CD69 were described just recently [1738] but are not yet commercialized. All reagents and Abs for porcine T-cell stainings shown in Figs. 192 to 197 are listed in Table 78.

14.4 Porcine NK cells and B cells. In contrast to NK cells in humans and mice, porcine NK cells are small dense lymphocytes [1739, 1740]. Porcine NK cells can be found within the CD3$^-$CD16$^+$ subset of lymphocytes, representing non-T and non-B cells. Up to date, no pan-NK cell marker exists in swine as the activating receptor NKp46 (CD335, NCR1) that is proposed as marker for NK cells across mammalian species [1741], is differentially expressed in pigs. Three distinct NK-cell subsets can be identified on the basis of their NKp46 expression: NKp46$^-$, NKp46$^+$, and NKp46^{high} [1714, 1742] (Fig. 198). NKp46^{high} NK cells are more abundant in spleen and non-lymphatic organs compared to blood and show a reduced or lacking expression of CD8α (dim/-) compared to the NKp46- and NKp46$^+$ CD8α$^+$ subsets [1714, 1742, 1743]. All porcine NK-cell subsets express perforin, CD2, and CD27. For the latter, a positive correlation to
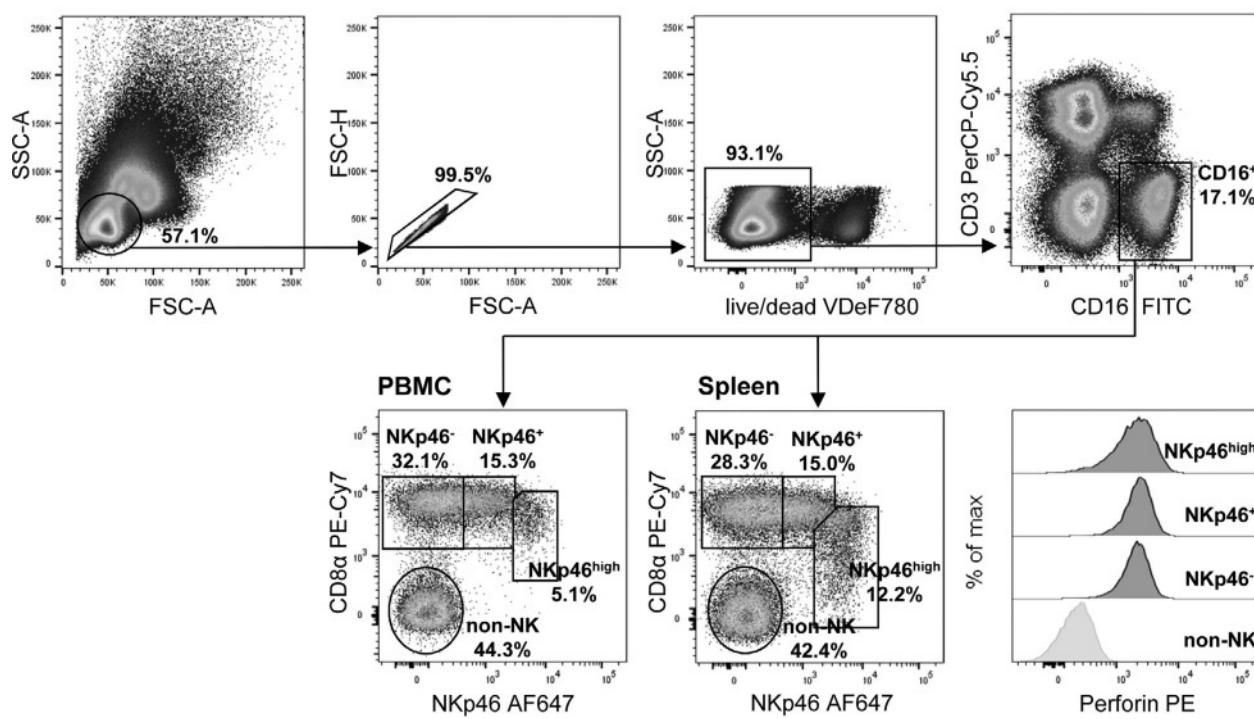
Figure 198. Identification of porcine NK cells in cells isolated from peripheral blood and spleen. Lymphocytes are identified based on the forward and side scatter. Single cells are discriminated from doublets by plotting FSC area against height and dead cells are excluded by a viability dye. CD3$^-$CD16$^+$ non-T and non-B cells (mAb clone CD3 B23-8E6-8C8; mAb clone CD16 G7) are further gated on three NK-cell subsets on the basis of their different CD8α (mAb clone 11/295/33) and NKp46 (mAb clone VIV-KM1) expression in blood as well as spleen. Perforin expression (cross-reactive mAb clone δG9) can be detected in all three NK-cell subsets in contrast to CD8α^-NKp46$^-$ non-NK cells. Data is generated from defrosted PBMC and lymphocytes isolated from spleen of an animal of approximately 6 months of age.

NKp46 expression is described [1742]. In contrast to human NK cells that show a functional dichotomy of the CD16^{bright}CD56^{dim} (higher cytotoxicity) and CD16$^{dim/-}$CD56^{bright} (higher potential to produce cytokines) subsets, porcine NKp46^{high}CD8$\alpha^{dim/-}$ NK cells have the highest capacity for both functions [1742].

Up to date, a detailed phenotypic and functional analysis on porcine B cells is hampered due to the lack of a pan-B cell marker like CD19 as used in humans and mice. For the detection of total porcine B cells a cross-reactive mAb against CD79α can be used [1744] (Fig. 199). As the mAb recognizes a cytoplasmic epitope, fixation and permeabilization of the cells is required prior to CD79α staining with this mAb, excluding subsequent functional analyses with sorted B cells. Furthermore, no species-specific or cross-reactive mAbs for the identification of distinct functional B-cell subsets like transitional B cells and plasma cells/plasmablasts (e.g., CD38 and CD138) are available. In humans, CD27 is used to distinguish memory from naïve B cells, whereas in the pig, no CD27 expression was detected on B cells [1745]. Cross-reactive mAbs against CD21 have been used to distinguish more mature (CD21$^-$) from less mature B cells (CD21$^+$) in the pig [1746]. Monoclonal Abs against IgM, IgG, and IgA [1747] can also be used in FCM and recently IgM$^+$CD21$^-$ B cells have been proposed to represent B1-like B cells [1748]. Interestingly, this cell population also express high levels of CD11R1 and CD11c, markers that are also found in high levels on myeloid cells [1748]. Intracellular

staining for Ig-molecules, to identify plasma cells and memory B cells, has not been thoroughly applied yet in the phenotyping of porcine B cells. All reagents and Abs for porcine NK- and B-cell staining shown in Figs. 198 and 199 are listed in Table 79 and 80.

14.5 Porcine myeloid cells. Although common features are found between mononuclear phagocytes of mice, humans, and pigs, each species has its own features in terms of marker expression and subset function [1749]. Only recently, cross-species similarities were addressed by, e.g., cross-species transcriptome comparison [1750] and phenotypic differences were investigated at the protein and transcriptome level to identify different dendritic cell (DC) and macrophage subsets in swine [1751–1753].

The porcine equivalents of conventional DCs (cDC) cDC1, cDC2, and plasmacytoid DCs (pDCs) in the peripheral blood can be discriminated from monocytes by the absence of CD14 expression as follows: cDC1 are CD14$^-$CD172a^{low}CADM1$^+$ cells, cDC2 are CD14$^-$CD172a^{high}CADM1$^+$ cells, and pDCs are CD14$^-$CD172a$^+$CADM1$^-$CD4$^+$cells (Fig. 200) (based on the results and gating described in ref. [1752]). The phenotypic characterization of porcine blood cDC1 revealed species-conserved features such as high surface expression of CD135, CADM1, CD205, low levels of CD172a, and a lack of CD115 [1752]. Opposing to murine DC, where CD11b is used as a cDC2-specific marker,
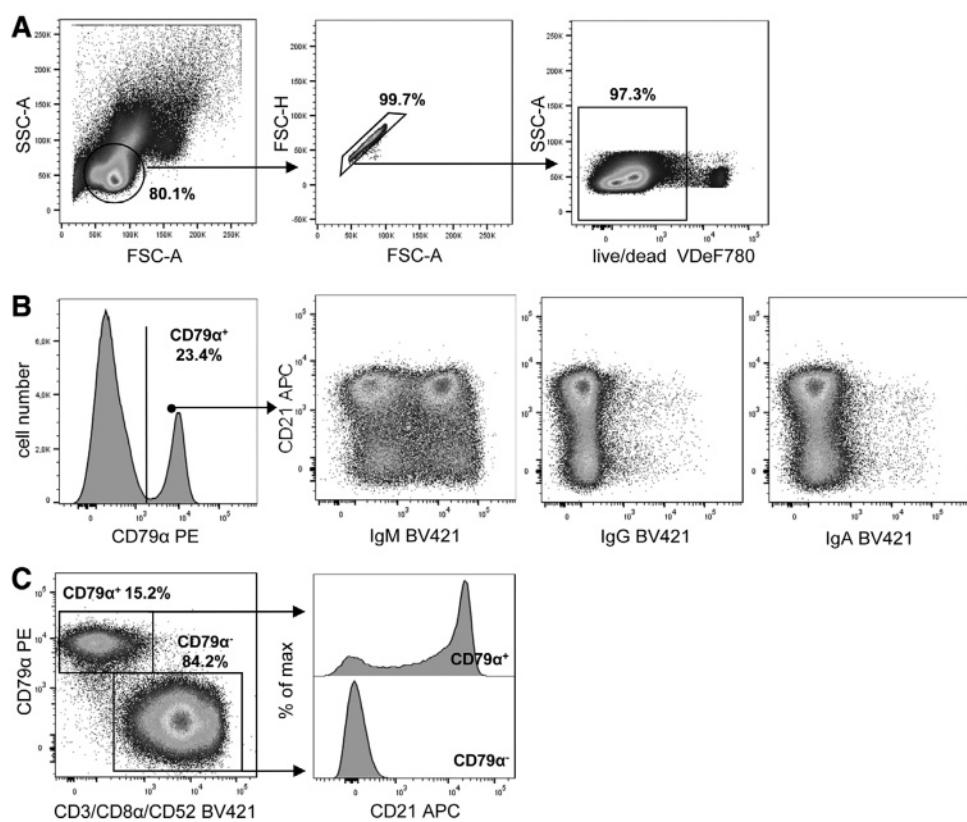
Figure 199. Identification of porcine B cells in peripheral blood. (A) Lymphocytes are identified based on the forward and side scatter. Single cells are discriminated from doublets by plotting FSC area against height and dead cells are excluded by a viability dye. (B) CD79α⁺ B cells (cross-reactive mAb clone HM57) within live PBL can be further analyzed for expression of CD21 (cross-reactive mAb clone B-ly4), IgM (mAb clone K52 1C3), IgG (mAb clone 23.7.1b) and IgA (mAb clone K61 1B4). A comprehensive functional characterization of the various porcine B-cell subsets has not been performed so far. (C) Bulk staining for CD3 (mAb clone PPT3), CD8α (mAb clone 11/295/33), and CD52 (mAb clone 11/305/44) in combination with a co-staining for CD79α and CD21 shows that CD79α⁺ B cells are CD3⁻CD8α⁻CD52⁻ but contain CD21⁻ and CD21⁺ cells. Non-B cells (CD3⁺CD8α⁺CD52⁺) are CD21⁻. Data is generated from freshly isolated PBMC from an animal of approximately 6 months of age.

porcine CD11R1 (equivalent to murine and human CD11b) is highly expressed on circulating cDC1 and cDC2 [1752]. The phenotypic characterization of the porcine blood cDC2 subset is difficult as different markers (e.g., CD163, CSF1R) are expressed also on porcine monocytes, but the lack of the porcine monocyte-specific marker CD14 and high FLT3 expression approved these as DCs [1752]. Species-specific characteristics of porcine cDC2 are reflected by the high surface expression of CD1.1 (equivalent to CD1a [1754]), which is restricted to dermal cDC2 in humans [1755], and CADM1, which is a feature of other mammalian cDC1 subsets [1756]. Like in other species, the porcine pDC subset (typically CD4⁺SLA-DR^low^CD80/86^low^), produces high amounts of type I IFNs after virus stimulation [1716] and produces high amounts of cytokines following TLR ligand stimulation (e.g., IL-12p35 after CpG stimulation) compared to the porcine cDC subsets. Similar to human pDC, porcine pDC express CD303 (BDCA-2), and CD304 (BDCA-4) [1752].

In contrast to human monocyte classification based on CD14 and CD16, and mouse monocyte classification based on Ly6C⁺/⁻, porcine monocytes can be identified as CD14⁺CD172a⁺ mononu-

clear leukocytes that can be further divided into different subpopulations based on the expression levels of CD163, SLA-DR, and CD14 (Fig. 201) [1757, 1758]. Two major subpopulations of blood monocytes have been described in pigs (CD14^high^CD163⁻ SLA-DR⁻ and CD14^low^CD163⁺SLA-DR⁺) that show differences in CD11a, wCD11R1 (α-integrins), CD29 (integrin β1), CD49d (integrin α4), CD61 (integrin β3), CD80/86, and CD1a expression [1757, 1759, 1760] and also differ in chemokine receptor expression of CX3CR1 and CCR2 [1761]. So far state of the art is that these cells divide into distinct subsets in the bone marrow, thereafter circulating monocyte subpopulations represent different maturation stages and comprise distinct functional capacities [1758, 1762, 1763]. Compared to mouse, gene expression profiles suggest that porcine blood-derived monocyte subsets are close to human monocytes as certain genes (e.g., CD36, CLEC4E, TREM-1 expressed in human monocytes) were selectively expressed in pig monocyte subsets [1759]. The same profiles revealed also that the pig CD14^low^CD163⁺ cells are actually equivalent to intermediate human monocytes (CD14^high^CD16⁺), and that there is no CD14⁺CD16⁺ "nonclassical" population [1759]. Porcine
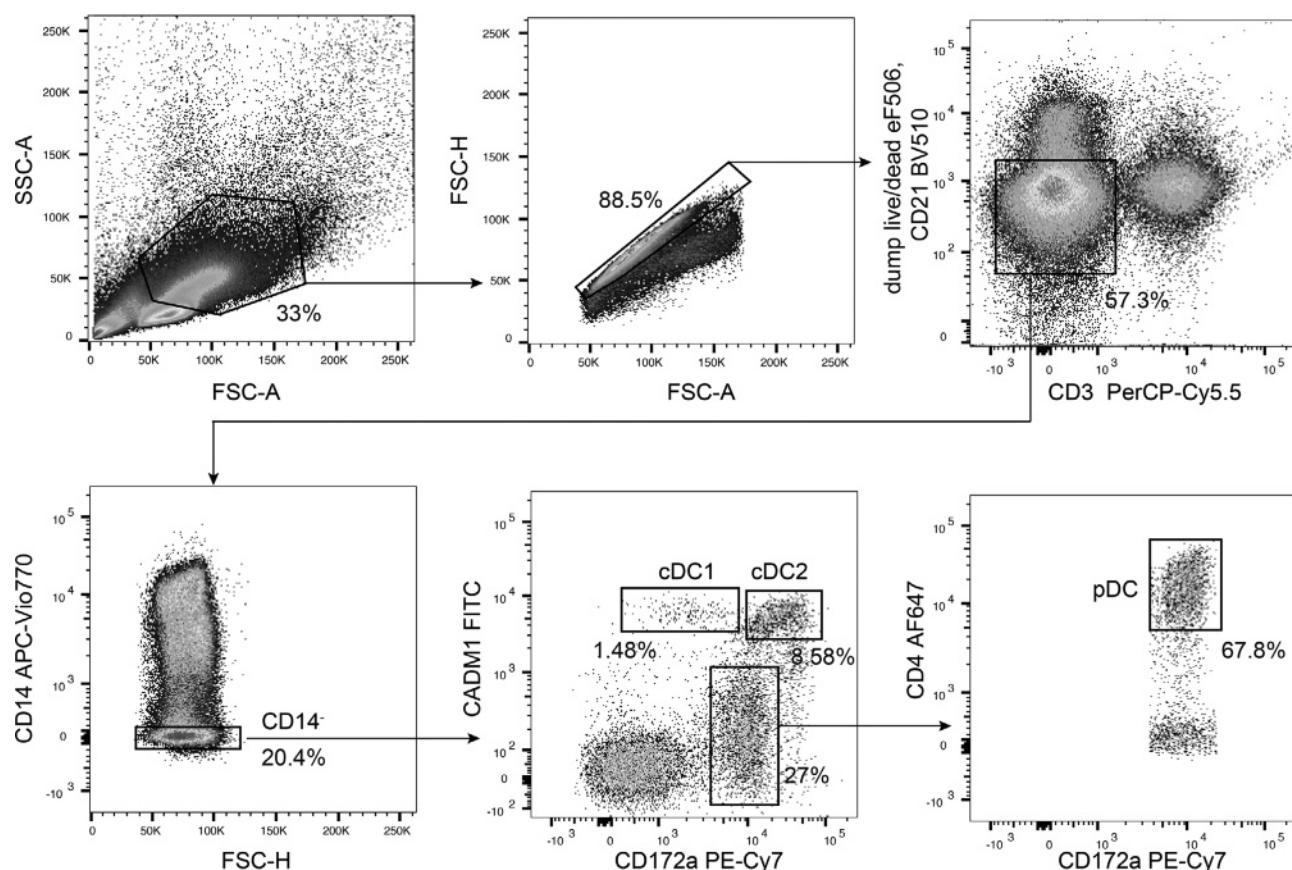
Figure 200. Identification of porcine conventional dendritic cells (cDC) and plasmacytoid dendritic cells (pDC) in peripheral blood. Large mononuclear cells are identified based on FSC and SSC. Single cells are discriminated from doublets by plotting FSC area against height. Dead cells are excluded by a viability dye combined with a dump channel for exclusion of porcine CD21$^+$ B cells (mAb clone B-ly4). Viable CD3$^-$ non-T cells (mAb clone BB23-8E6-8C8) can be further discriminated from porcine monocytes by the absence of CD14 expression (mAb clone TÜK4). Subsequently, three different DC subsets can be identified based on the expression of CD172a (mAb clone 74-22-15), CADM1 (mAb clone 3E1) and CD4α (mAb clone 74-12-4) as follows: cDC1 are CD14$^-$ CD172a^{low}CADM1$^+$ cells, cDC2 are CD14$^-$CD172a^{high}CADM1$^+$ cells and pDC are CD14$^-$ CD172a$^+$CADM1$^-$CD4$^+$cells. Data are generated from fresh PBMC of a sow of approximately 2 years of age.

CD14^{high}CD163$^-$ monocytes likely correspond to classical monocytes (CD14^{high}CD16$^-$) in humans [1762]. However, cross-species subset comparison of blood monocytes among human, bovine, murine, and pig cells using transcriptomics indicated that CD163-based discrimination of porcine monocytes into classical and non-classical monocytes might need to be reevaluated [1750, 1764]. CD14 expression can also be found at lower levels on granulocytes in the pig [1762]. Of note, porcine granulocytes are also positive for CD172a and some mature B cells can be induced to express low levels of CD172a after antigen stimulation [1762, 1765].

Quite recently, the phenotypic characterization of lung tissue resident DC and macrophage network segregated porcine mononuclear phagocytes as follows: conventional cDC1 (MHCII^{++}CD172a$^-$CD163$^-$CD1$^-$CADM1$^+$CD14$^-$) and cDC2 (MHCII^{++}CD172a$^+$CD163$^-$CD1^{low}CADM1^{low}CD14$^-$), inflammatory monocyte-derived DCs (MHCII^{++}CD172a$^+$CD163^{low}CD1$^-$CADM1$^+$CD14$^-$), monocyte-derived macrophages (MHCII^{++}CD172a$^+$CD163^{int}CD1$^-$CADM1^{low}CD14$^+$), and alveolar macrophage-like cells/interstitial macrophages (MHCII^{++}CD172a$^+$CD163^{++}CD1$^-$CADM1$^-$CD14$^-$) and alveolar macrophages (MHCII^{++}CD172a$^+$CD163^{++}CD1$^-$CADM1$^{-/low}$CD14$^-$) [1753, 1766, 1767]. This nomenclature is based on the origin and the function of the myeloid cells [1768], and offers the advantage to assign one single name per DC/Macrophage subpopulation for all the species facilitating trans-species comparisons [1753, 1766]. The FLT3-dependent cDC being Sirpα (CD172a) negative or low are named cDC1 in the pig lung and correspond to the BDCA3$^+$ cDC and CD103$^+$ cDC in human and mouse, respectively [1753, 1766]. Referring to the BDCA1$^+$ and CD11b$^+$ DC subset in human and mouse, the CD172a^{++}/CD11b$^+$ cDC in the porcine respiratory tract are named cDC2 [1753]. Porcine alveolar macrophages express high levels of CD172a, CD163, CD169, CD16, and SLA-II molecules, whereas CD14 and CD11R1 expression is minimal or negative on alveolar macrophages [1762]. Moreover, CD203a (originally clustered as SWC9) is expressed widely in porcine macrophage populations with notably high levels on alveolar macrophages, but is not expressed on monocyte populations [1762]. Like in other
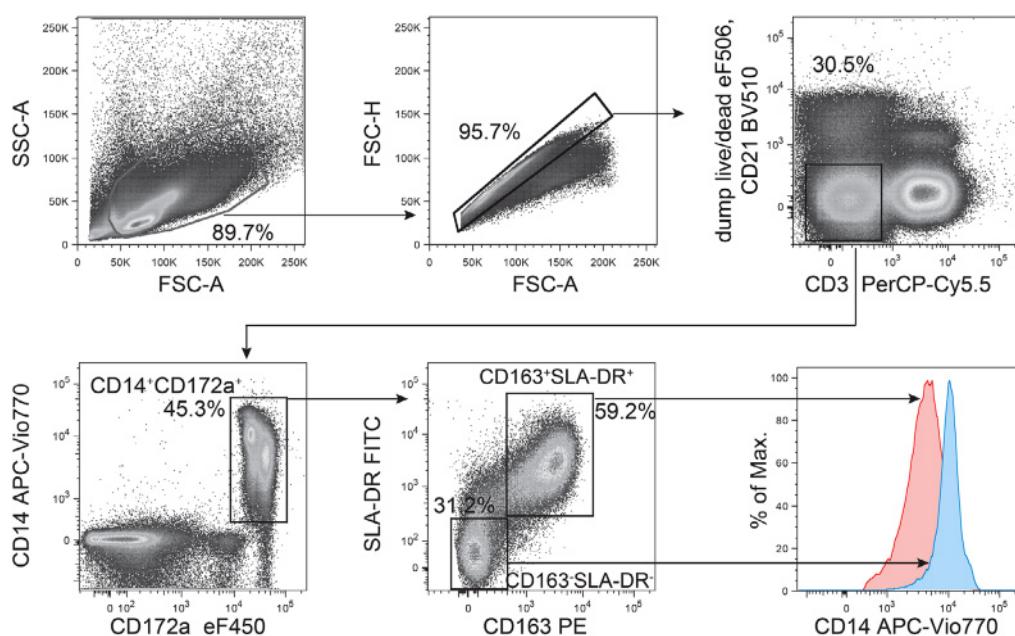
Figure 201. Identification of porcine monocyte subsets in peripheral blood. Mononuclear cells are identified based on the forward and side scatter. Single cells are discriminated from doublets by plotting FSC area against height. Dead cells are excluded by a viability dye combined with a dump channel for exclusion of porcine CD21$^+$ B cells (cross-reactive mAb clone B-ly4). Monocytes can be further discriminated from viable CD3$^-$ non-T cells (mAb clone BB23-8E6-8C8) as CD14$^+$CD172a$^+$ cells (mAb clone CD14 TÜK4; mAb clone CD172a 74-22-15). Different monocyte subsets can be identified based on the expression of CD163 (mAb clone 2A10/11) and SLA-DR (mAb clone 2E9/13). The histogram shows CD14 expression (mAb clone TÜK4) of the two monocyte subsets representing the major "steady-state" subsets (CD14^{high}CD163$^-$SLA-DR$^-$ and CD14^{low}CD163$^+$SLA-DR$^+$) in porcine peripheral blood. Data is generated from fresh PBMC of a sow of approximately 2 years of age.

species, alveolar macrophages of the pig are also highly autofluorescent [1753]. Contrary to porcine alveolar macrophages those in mice do not express MHC-II and are all negative for CD11b [1456], whereas human alveolar macrophages widely express CD11b and MHC-II [1769]. Porcine alveolar macrophage-like cells are pulmonary intravascular macrophages that have not been observed yet at steady-state in mice or non-human primates, and have nearly the same phenotype like porcine alveolar macrophages [1767, 1770]. Interstitial CD169$^-$ macrophages are a prominent cell type in human lung tissue, whereas CD169$^+$ macrophages are located in the alveolar space/airway, defining them as alveolar macrophages [1771]. Whether this CD169$^-$ negative macrophage population in the human lung refers to the porcine alveolar macrophage-like cells is not resolved yet.

In the skin of pigs, similar to humans, the classical DC subsets of epidermal Langerhans cells (LC) and dermal DC are found [1772]. Dermal DC can be divided into three main subsets according to their CD163 and CD172a expression: CD163$^-$CD172a$^-$, CD163$^+$CD172a$^+$, and CD163^{low}CD172a$^+$ that differ in the expression of CD16, CD206, CD207, CD209, and CADM1 [1772]. Based on comparative transcriptomics, phenotypic analysis, and functional studies, Marquet and colleagues proposed the allocation of porcine dermal DC to those of the human system as follows: the porcine CD163$^-$CD172a$^-$ subset corresponds to the human CD141$^+$ dermal DC subset, the porcine

CD163^{low}CD172a$^+$ subset to the human CD1c$^+$ dermal DC, and the porcine CD163$^+$CD172a$^+$ subset to the monocyte-derived human CD14$^+$ dermal DC subset.

In porcine tonsils, plasmacytoid DC (CD172a^{low}CD4$^+$MHCII^{low}) and conventional DC (cDC1, CD172a$^{-/low}$CADM1^{++}MHCII^{++} and cDC2, CD172a^{++}CD14$^-$CD163$^-$MHCII^{++}CADM1^{low}) but also monocyte-derived cells (CD172a^{++}CD163$^-$CD14$^+$MHCII^{++}) and macrophage-like cells (CD172a^{++}, CD163$^+$CD14$^-$MHCII^{++}) have been identified [1751]. Compared to blood, not all tonsil-resident cDC1 and cDC2 cells express the C-type lectin receptor DEC205 [1773]. All reagents and Abs for porcine myeloid cell staining shown in Figs. 200 and 201 are listed in Table 81.

For analyzing neutrophils, eosinophils and basophils in porcine whole blood, granulocytes are identified based on their high SSC and FSC properties and expression of CD172a. To separate between them, SWC8, a marker defined by the International Workshop on Swine Leukocyte Differentiation Antigen (A. [1774]), SWC1 (now identified being porcine CD52 [1775]) and the antigens 2B2 and 6D10 [1776] can be used. Mature neutrophils in blood express CD172a$^+$SWC8^{++}CD52$^+$6D10$^+$2B2$^+$CD14$^+$, whereas mature eosinophils are CD172a$^+$SWC8^{++}CD52$^-$6D10$^-$2B2$^+$CD14$^-$ and mature basophils will identify as CD172a$^+$SWC8$^-$CD52$^+$6D10$^-$2B2$^+$CD14$^-$ [1762].

Table 78. Reagents and Abs for T-cell staining

Reagent/antibody	Clone	Manufacturer
Mouse anti-pig CD2 - Alexa Fluor® 488	MSA4	In house[1]
Mouse anti-pig CD3 - PerCP-Cy™5.5	BB23-8E6-8C8	BD Biosciences
Mouse anti-pig CD4	74-12-4	In house[2]
Mouse anti-pig CD4 - FITC	74-12-4	BD Biosciences
Mouse anti-pig CD4 - Alexa Fluor® 647	74-12-4	BD Biosciences
Mouse anti-pig CD8α - Alexa Fluor® 647	11/295/33	In house[3]
Mouse anti-pig CD8α - Biotin	11/295/33	In house[4,5]
Mouse anti-pig CD8β - Biotin	PPT23	In house[4,6]
Mouse anti-human CD14 - VioGreen	TÜK4	Miltenyi Biotec
Mouse anti-pig CD25	3B2	In house[7]
Mouse anti-pig CD27	b30c7	BioRad
Mouse anti-pig CD27 - Alexa Fluor® 647	b30c7	In house[8]
Mouse anti-pig TCRγδ	PGBL22A	Kingfisher Biotech
Mouse anti-pig TCRγδ - Biotin	PPT16	In house[4,9]
Mouse anti-pig SLA-DR - Biotin	MSA3	In house[4,10]
Mouse anti-human Perforin - PerCP-eFluor710	δG9	ThermoFisher Scientific
Rat anti-mouse Foxp3 - PE	FJK-16s	ThermoFisher Scientific
Rat anti-mouse Foxp3 - eFluor™ 450	FJK-16s	ThermoFisher Scientific
Mouse anti-human T-bet - PE	4B10	ThermoFisher Scientific
Rat anti-human/ mouse GATA-3 - PerCP-eFluor710	TWAJ	ThermoFisher Scientific
Mouse anti-human IL-17A - Alexa Fluor® 647	SCPL1362	BD Biosciences
Mouse anti-human TNFα - FITC	MAb11	BD Biosciences
Rat anti-mouse Ki-67 - PE-Cy7	SolA15	ThermoFisher Scientific
Mouse anti-human CD154 - PE	5C8	Miltenyi Biotec
Goat anti-mouse IgG1 - PE	−	SouthernBiotech
Goat anti-mouse IgG2b - Alexa Fluor® 488	−	ThermoFisher Scientific
Streptavidin - Brilliant Violet 421™	−	BioLegend
Fixable Viability Dye eFluor™ 780	−	ThermoFisher Scientific
Fixable Viability Dye eFluor™ 506	−	ThermoFisher Scientific

[1]Conjugation with Alexa Fluor® 488 Protein Labeling Kit (ThermoFisher Scientific); non-conjugated mAb available from Kingfisher Biotech
[2]Commercially available from BD Biosciences
[3]Conjugation with Alexa Fluor® 647 Protein Labeling Kit (ThermoFisher Scientific); mAb commercially available from BD Biosciences
[4]Biotinylation with EZ-Link™ Sulfo-NHS-LC-Biotin (ThermoFisher Scientific)
[5]Alternative mAb clone 76-2-11 available from BD Biosciences and ThermoFisher Scientific
[6]Non-biotinylated mAb commercially available from Bio-Rad
[7]mAb commercially available from Bio-Rad (clone name K231.3B2)
[8]Conjugation with Alexa Fluor® 647 Protein Labeling Kit (ThermoFisher Scientific); mAb commercially available from Bio-Rad
[9]mAb currently not commercially available, alternative clone: PGBL22A, available from Kingfisher Biotech
[10]mAb commercially available from Kingfisher Biotech

14.6 Step-by step-sample preparation.

14.6.1 General comments.   Blood samples from pigs are most commonly taken by venipuncture from the external jugular vein and require fixation but no sedation. Terminal blood samples are obtained intracardially under deep anesthesia and Lithium–Heparin or Sodium–Heparin as anticoagulants are recommended with respect to the duration of large animal dissections.

14.6.2 Step-by-step sample preparation of porcine PBMC.

1. Draw blood and transfer to an anti-coagulant containing tube.
2. Dilute blood 1:2 in 0.9% sodium chloride solution or PBS.
3. Carefully overlay Pancoll (e.g. Pancoll human, Cat# P04-601000 by PAN-Biotech, density 1.077 g/mL) with diluted blood in a ratio of 1:3.

4. Centrifuge at room temperature at 800 × g without brake for 20 min.
5. Collect interphase, transfer to new tube and wash with 0.9% sodium chloride solution or PBS.
6. [optional] Perform erythrocyte lysis (for example using 3 mL ACK lysis buffer at RT for 3 min).
7. Wash with staining buffer.
8. Pellet cells (300 × g, 4°C, 6 min) and discard supernatant.

14.6.3 Step-by-step sample preparation of porcine lymphocytes from spleen.

1. Cut dissected spleen into small pieces.
2. Mechanically dissociate tissue pieces by forcing through a sieve and rinse with PBS.

3. Centrifuge at 4°C at 350 × g and discard supernatant.
4. Resuspend cells in 20 mL PBS and force through a cell strainer (70 μm).
5. Carefully overlay Pancoll (for example Pancoll human, Cat# P04-601000 by PAN-Biotech) with cell suspension in a ratio of 1:3.
6. Centrifuge at room temperature at 800 × g without brake for 20 min.
7. Collect interphase, transfer to new tube and wash twice with PBS at 300 × g, 4°C, 6 min and discard supernatant.

14.6.4 FCM staining of porcine leukocytes from blood and spleen.

1. Transfer up to 2×10^6 cells into a 96-well conical or U-bottom shaped plate.
2. Centrifuge the plate at 300 × g at 4°C for 3 min.
3. Aspirate or decant supernatant.
4. [optional] For blocking of Fc receptors add 1:200 to 1:500 diluted mouse serum (in staining buffer) for 5 min at 4°C or use 10% porcine plasma in PBS staining buffer.
5. [optional] Add True-Stain Monocyte Blocker™ according to the manufacturer's instruction.
6. Add a max of 30 μL surface staining mix per well and incubate for 15 min at 4°C.
7. Two washing steps: add up to 200 μL staining buffer and centrifuge the plate at 300 × g at 4°C for 3 min and aspirate or decant supernatant.
8. [optional] Add secondary reagents as described above including the two washing steps.
9. [optional] Add Fix/ Perm reagent for 20 min at 4°C, following two washing steps in permeabilization buffer as described above.
10. [optional] Add mAbs specific for intracellular or intranuclear antigens for 20 min at 4°C, following two washing steps in permeabilization buffer as described above.

N.B. If unlabeled and directly-conjugated Abs with identical isotypes are used in the same sample, a sequential staining should be performed: After labeling with unconjugated primary mAb and isotype-specific dye-conjugated secondary Abs, free binding sites should be blocked by whole mouse IgG molecules (typically 2 μg per sample, vendor: Jackson ImmunoResearch).

14.7 Materials.   Flow cytometer:

- FACSCanto II flow cytometer
- FACSAria III sorter (both BD Biosciences)

　Media and buffers:

- RPMI+AB: RPMI 1640 (PAN-Biotech) supplemented with 100 U/mL Penicillin, and 100 μg/mL Streptomycin (PAN-Biotech)

Table 79. Reagents and Abs for NK-cell staining

Reagent/antibody	Clone	Manufacturer
Mouse anti-pig CD3 - PerCP-Cy™5.5	BB23-8E6-8C8	BD Biosciences
Mouse anti-pig CD8α - Biotin	11/295/33	In house[1]
Mouse anti-pig CD16 - FITC	G7	BioRad
Mouse anti-pig NKp46 - Alexa Fluor® 647	VIV-KM1	In house[2]
Mouse anti-human Perforin - PE	δG9	ThermoFisher Scientific
Streptavidin - PE-Cy7	–	ThermoFisher Scientific
Fixable Viability Dye eFluor™ 780	–	ThermoFisher Scientific

[1]Biotinylation with EZ-Link™ Sulfo-NHS-LC-Biotin (ThermoFisher Scientific), alternative mAb clone 76-2-11 available from BD Biosciences and ThermoFisher Scientific
[2]Conjugation with Alexa Fluor® 647 Protein Labeling Kit (ThermoFisher Scientific), mAb commercially available from Bio-Rad

Table 80. Reagents and Abs for B-cell staining

Reagent/Antibody	Clone	Manufacturer
Mouse anti-pig CD3	PPT3	In house
Mouse anti-pig CD8α	11/295/33	In house
Mouse anti-human CD21 - APC	B-ly4	BD Biosciences
Mouse anti-pig CD52	11/305/44	In house[1]
Mouse anti-human CD79α - PE	HM57	Dako
Mouse anti-pig IgM	K52 1C3	Bio-Rad
Mouse anti-pig IgA	K61 1B4	Bio-Rad
Mouse anti-pig IgG	23.7.1b	ThermoFisher Scientific
Rat anti-mouse-IgG1 - Brilliant Violet 421™	RMG1-1	BioLegend
Goat anti-mouse-IgG2a - Brilliant Violet 421™	–	Jackson Immuno Research
Goat anti-mouse-IgG2b - Brilliant Violet 421™	–	Jackson Immuno Research
Fixable Viability Dye eFluorTM 780	–	ThermoFisher Scientific

[1]mAb commercially available from Bio-Rad

- cRPMI: Complete RPMI 1640 (PAN-Biotech) supplemented with 10% FCS (PAN-Biotech), 100 U/mL Penicillin, and 100 μg/mL Streptomycin (PAN-Biotech)
- cIMDM: Complete IMDM (PAN-Biotech) supplemented with 10% FCS (PAN-Biotech), 100 U/mL Penicillin, and 100 μg/mL Streptomycin (PAN-Biotech)
- ACK lysis buffer: 150 mM NH4Cl, 10 mM KHCO$_3$, and 0.1 mM Na$_2$EDTA
- Fixation and Permeabilization reagents: for detection of intracellular cytokines: Fixation/Permeabilization solution kit (BD Biosciences); For detection of intranuclear molecules and per-

Table 81. Reagents and Abs for the staining of mononuclear phagocytes

Reagent/antibody	Clone	Manufacturer
Mouse anti-pig CD163 – PE	2A10/11	BioRad
Chicken anti-human CADM1 - FITC	3E1	MBL
Mouse anti-human CD21 - BV510	B-ly4	BD Biosciences
Mouse anti-pig CD3 - PerCP-Cy^{TM}5.5	BB23-8E6-8C8	BD Biosciences
Mouse anti-pig CD4 - Alexa Fluor® 647	74-12-4	BD Biosciences
Mouse anti-human CD14 - APC-Vio770	TÜK4	Miltenyi Biotec
Mouse anti-pig CD172a - Biotin	74-22-15	SouthernBiotech
Mouse anti-pig SLA-DR - FITC	2E9/13	BioRad
Streptavidin - PE-Cy®7	–	ThermoFisher Scientific
Streptavidin - eFluor^{TM} 450	–	ThermoFisher Scientific
eBioscience^{TM} Fixable Viability Dye eFluor^{TM} 506	–	ThermoFisher Scientific
True-Stain Monocyte Blocker^{TM}	–	BioLegend®

forin: Foxp3/Transcription factor staining buffer set (ThermoFisher Scientific)

- Staining buffer: PBS (PAN-Biotech) supplemented with 2 mM EDTA and 0.5% BSA (AppliChem) or PBS (PAN-Biotech) supplemented with 10% porcine plasma

　In vitro stimulation

- PMA (50 ng/mL) and Ionomycin (500 ng/mL, both Sigma–Aldrich) for 4 h in combination with Brefeldin A (GolgiPlug, BD Biosciences, 1 µg/mL)
- Antigen preparation of selected pathogens for antigen induced T-cell responses (in total 6–8 h, in titrated concentrations (e.g., 25–80 µg/mL) and for 4 h in combination with Brefeldin A (Brefeldin A solution, 1000×, ThermoFisher Scientific)

14.8 Data Analysis. Flow cytometric analysis was performed by using FACSCanto II flow cytometer and FACSAria III sorter employing FACSDiva Software v6.1.3 (BD Biosciences), and data were analyzed by using FlowJo software v9.9.4 and v10.5 (FlowJo, LLC).

14.9 Pitfalls.

- Be aware that CD8α does not identify conventional CD8$^+$ T cells per se, but is also expressed on CD4 T cells, NK cells, and subsets of γδ T cells.

- Keep in mind the strong age-dependency of the expression of several porcine markers (e.g., CD8α, MHC-II).
- Porcine monocytes do not separate from peripheral blood lymphocytes by FSC/SSC properties as clearly as human monocytes.
- Carefully test cross-reactivity of anti-human or anti-murine Abs before use (see also section 15.6).

14.10 Top tricks.

- If working with frozen/thawed samples we advise to incubate freshly thawed samples in cRPMI overnight at 37°C to improve cytokine responses after subsequent stimulation.

Summary of major porcine immune cell subpopulations

γδ T-cell populations	Phenotype/sub-phenotype
	TCRγδ$^+$CD4$^-$CD8$^-$CD2$^-$
	TCRγδ$^+$CD4$^-$CD8$^{-/+}$CD2$^+$

CD4$^+$ T-cell populations	Phenotype/sub-phenotype
Naïve	CD4$^+$CD8α$^-$CD27$^+$
Effector-memory	CD4$^+$CD8α$^+$CD27$^-$
Central-memory	CD4$^+$CD8α$^+$CD27$^+$
Treg	CD25^{high}Foxp3$^+$
Th1	Tbet$^+$
Th2	GATA3^{high}

CD8$^+$ T-cell populations	Phenotype/sub-phenotype
Naïve	CD3$^+$TCR-γδ$^-$CD4$^-$CD8α^{high}CD8β$^+$CD27$^+$perforin$^-$
Effector-(memory)	CD3$^+$TCR-γδ$^-$CD4$^-$CD8α^{high}CD8β$^+$CD27$^{-/dim}$perforin$^+$

NK-cell populations	Phenotype/sub-phenotype
highly activated	CD3$^-$CD8α^{dim}CD16$^+$NKp46^{high}
less activated	CD3$^-$CD8α$^+$CD16$^+$NKp46$^{-/+}$

B-cell populations	Phenotype/sub-phenotype
Naïve	CD79α$^+$CD21$^+$IgM$^+$
B-1	CD79α$^+$CD21$^-$IgM^{++}
Class-switched memory	CD79α$^+$CD21$^{-/+}$IgG$^+$/IgA$^+$

Myeloid populations in blood	Phenotype/sub-phenotype
Monocytes	CD14$^+$CD16$^+$CD163$^{+/-}$CD135$^-$
Steady state	CD14^{++}CD163$^{-/low}$
	CD14^{low}CD163$^{+/++}$
Inflammatory	CD14^{low}CD163$^+$SLA-DR$^-$
cDC1	CD14$^-$CD172a^{low}CADM1$^+$CD4$^-$wCD11R1$^+$CD135$^+$
cDC2	CD14$^-$CD172a$^+$CADM1$^+$CD4$^-$CD115$^+$wCD11R1$^+$CD135$^+$CD1$^+$
pDC	CD14$^-$CD172a$^+$CADM1$^-$CD4$^+$CD135$^+$CD123$^+$CD303$^+$

Myeloid populations in lung	Phenotype/sub-phenotype
Alveolar macrophages	SLA-DR^{++}CD172a$^+$CD163^{++}CD1$^-$CADM1$^{-/low}$CD14$^-$
Pulmonary intravascular macrophages	SLA-DR^{++}CD172a$^+$CD163^{++}CD1$^-$CADM1$^-$CD14$^-$
Monocyte-derived macrophages	SLA-DR^{++}CD172a$^+$CD163^{int}CD1$^-$CADM1^{low}CD14$^+$
Monocyte-derived DC	SLR-DR^{++}CD172a$^+$CD163^{low}CD1$^-$CADM1$^+$CD14$^-$
cDC1	SLA-DR^{++}CD172a$^-$CD163$^-$CD1$^-$CADM1$^+$CD14$^-$
cDC2	CD14$^-$CD172a$^+$CADM1$^+$CD4$^-$CD115$^+$wCD11R1$^+$CD135$^+$CD1$^-$
pDC	CD14$^-$CD172a$^+$CADM1$^-$CD4$^+$CD135$^+$CD123$^+$CD303$^+$

Myeloid populations in tonsils	Phenotype/sub-phenotype
Macrophages	CD172a^{++}CD163$^+$CD14$^-$MHCII$^+$
Monocyte-derived DC	CD172a^{++}CD163$^-$CD14$^+$MHCII^{++}
cDC1	SLA-DR^{++}CD172a$^{low/-}$CD4$^-$CADM1^{++}CD14$^-$CD163$^-$
cDC2	SLA-DR^{++}CD172a^{++}CD4$^-$CADM1^{low}CD14$^-$CD163$^-$
pDC	SLA-DR^{low}CD172a$^{low/-}$CD4$^+$CADM1$^-$CD14$^-$CD163$^-$

Myeloid populations in skin	Phenotype/sub-phenotype
Langerhans cells	CD172a$^+$CD1$^+$CD16$^-$CD163$^-$CADM1$^+$CD207$^+$MHCII$^+$
Dermal DC	CD163$^-$CD172a$^-$CD16$^-$CD206$^-$CADM1$^+$
	CD163$^+$CD172a$^+$CD1$^+$CD14$^+$CD16$^+$CD209^{low}CD206^{low}
	CD163^{low}CD172a$^+$CD1$^+$CD14^{low}CD16^{low}

Granulocyte populations in blood	Phenotype/sub-phenotype
Neutrophils	CD172a$^+$SWC8^{++}CD52$^+$6D10$^+$2B2$^+$CD14$^+$
Eosinophils	CD172a$^+$SWC8^{++}CD52$^-$6D10$^-$2B2$^+$CD14$^-$
Basophils	CD172a$^+$SWC8$^-$CD52$^+$6D10$^-$2B2$^+$CD14$^-$

15 Cross-reactive Ab clones

15.1 Overview.   The testing of existing mAbs for reactivity with orthologous molecules in species different from the one the Ab was originally raised for is a frequent task to overcome limitations in the toolbox of available mAbs. This section provides an outline how experiments for cross-reactivity testing should be performed and what pitfalls might be encountered.

15.2 Introduction.   For immunophenotyping studies in mice and humans researchers can choose from a large variety of mAbs specific for cluster of differentiation (CD) molecules, but also cytokines, transcription factors, and molecules involved in signal transduction. However, when it comes to other animal species this collection is severely diminished. One possibility to overcome this limited availability of mAbs is to test already existing mAbs for cross-reactivity with the orthologous molecule of the species under investigation. Although this might sound like a simple and straightforward task, like with any other immunophenotyping experiment, certain problems and pitfalls might be encountered. Hence, this chapter will give an outline for solid and successful cross-reactivity testing.

In the framework of the 8th Human Leukocyte Differentiation Antigen Workshop (HLDA8) a community-based effort was undertaken to identify commercially available mAbs for cross- reactivity with 17 different animal species, ranging from more frequently studied ones like swine, dog, or cattle up to more "exotic" species like mink and carp. This study revealed that for the typical cell membrane-located CD-molecule, the likelihood of cross-reactivity even within mammalian species is relatively low. A few exceptions applied to this observation, including mAbs against CD18, CD29, or CD49d, all forming either α or β-chains of integrins, or the cartilage link protein CD44 [1777, 1778].

15.3 General considerations on cross-reactivity testing.   This study was far from being comprehensive and hence new tests for cross-reactivity are a frequent task if species different from mice and humans are studied. Work from our team and others on the cross-reactivity of mAbs with various porcine immune-related molecules revealed certain approaches that can be used not only to identify cross-reactive mAbs but also to scrutinize specific binding to the molecule of interest (see Fig. 202 for a general overview). In a first step commercially available Abs for the molecule of interest need to be identified. Online search tools like "biocompare" (https://www.biocompare.com/Antibodies/) or "antibodypedia" (https://www.antibodypedia.com/) might be helpful for this task, but the online catalogs of established producers for FCM-approved Abs are also a good source. Numerous Ab data sheets from the respective companies do provide information on cross-reactivity but such statements should be treated with caution as the claim of cross-reactivity is frequently based on sequence alignments and lacking solid experimental testing (see also Fig. 205 for an example). Under ideal circumstances, references are provided that demonstrate the claimed cross-reactivity, allowing a further scrutiny of the Ab.

If no information on cross-reactivity is provided, sequence alignments comparing the amino acid sequence of the target antigen in the species under investigation with the sequence of the species the Ab is specific for give a first indication of the likelihood of cross-reactivity. Our empirical observations show that homology rates below 75% usually indicate a low probability for cross- reactivity. However, for some Abs the sequence of the immunogen is provided in the data sheet, allowing a more focused
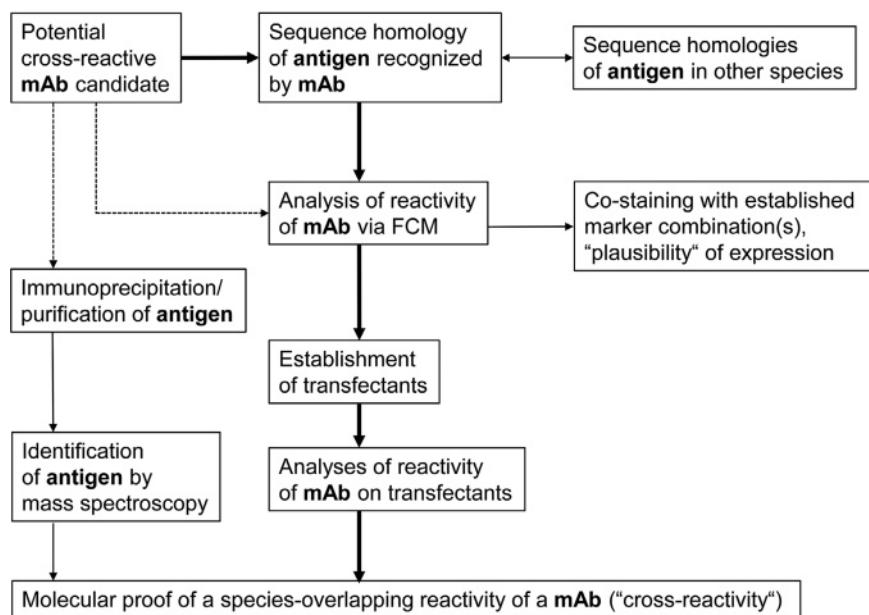
Figure 202. Strategies on cross-reactivity testing for mAbs for FCM. After identification of mAb candidates for cross-reativity testing, sequence homology analyses, ideally for the immunogen used to generate the Ab, will provide a first prognosis of the likelihood of cross-reactivity testing. Homologies higher than 90% indicate a good chance for cross-reactivity. High homology of target antigens across several species increases the likelihood of cross-reactivity further (typical examples: transcription factors or molecules involved in signal transduction). FCM staining experiments with the Ab under investigation in combination with an established marker or larger marker panels helps to evaluate cross-reactivity. As a final proof for cross-reactivity, cells transfected for expression of the target antigen should be generated and tested. Alternatively, the mAb candidate might be tested for its suitability in immunoprecipitation and precipitates can be subjected to mass spectroscopy for the identification of the target antigen.

homology total protein: **98.2 %**
homology in immunogen sequence: **96.9%**
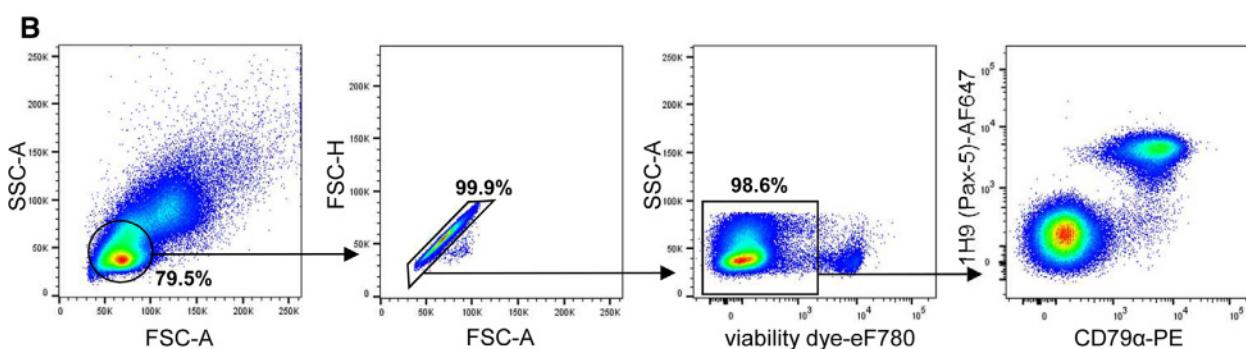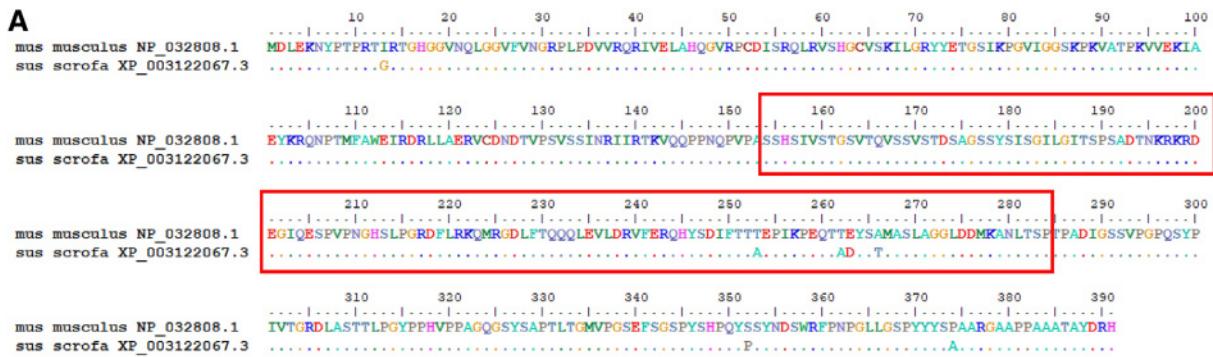
Figure 203. Test of anti-mouse Pax-5 mAb for cross-reactivity with the porcine orthologue. (A) Protein sequence alignment of murine (NCBI accession no. NP_032808.1) and porcine (NCBI accession no. XP_003122067.3) Pax-5 sequence. The homology of Pax-5 between the two species is 98.2%. The anti-mouse Pax-5 mAb clone 1H9 (BD Biosciences, catalogue no. 562814) is derived from an immunization of mice with recombinant mouse Pax-5 protein spanning amino acid residues 154–284. The alignment of the region of the immunogen is framed in red and has a homology of 96.9% between the two species. (B) Test of anti-mouse Pax-5 mAb on porcine PBMC. Lymphocytes were gated according to their light scatter properties and single cells are discriminated from doublets by plotting FSC area against height. Dead cells are excluded by a viability dye. The anti-Pax-5 mAb was tested in combination with a CD79α-specific mAb for the staining of porcine B cells, as Pax-5 is expressed from the pro-B to the mature B cell stage and only repressed during terminal plasma cell differentiation [1779]. A distinct co-staining of both mAbs is observed, indicating cross-reactivity of the 1H9 mAb clone with porcine Pax-5. The final proof of cross-reactivity still needs to be obtained by testing the mAb on cells transfected with recombinant porcine Pax-5.
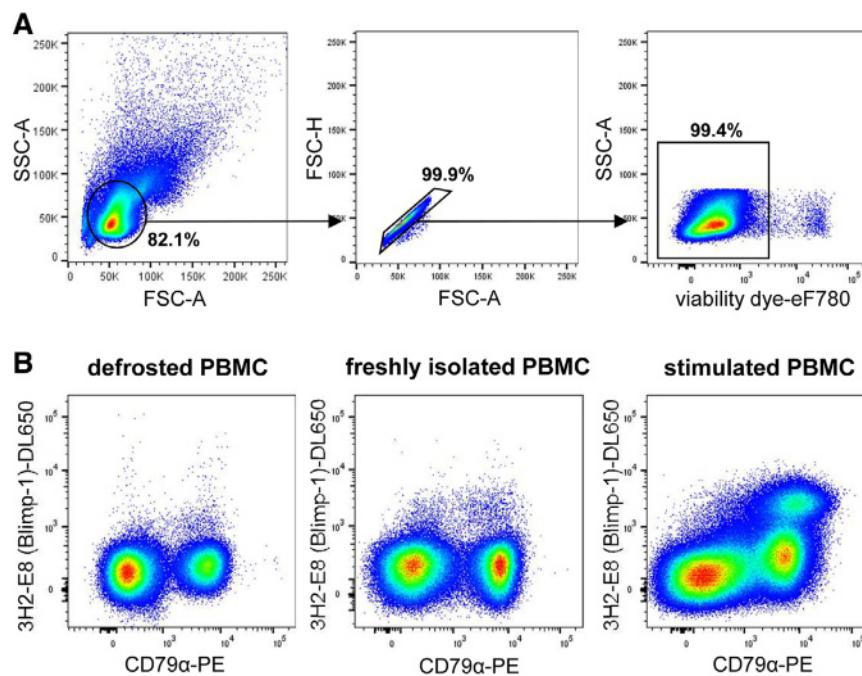
Figure 204. Test of anti-mouse Blimp-1 mAb for cross-reactivity with the porcine ortholog. For the anti-mouse Blimp-1 mAb clone 3H2-E8 (ThermoFisher Scientific, catalogue no. 13207588) cross-reactivity to the porcine protein is indicated on the data sheet. Flow cytometric analyses of the mAb on porcine PBMC were performed. (A) Lymphocytes were gated according to their light scatter properties and single cells are discriminated from doublets by plotting FSC area against height. Dead cells are excluded by a viability dye. The gating strategy is shown for freshly isolated PBMC and is representative for all experiments shown. (B) The anti-Blimp-1 mAb was tested in combination with a CD79α-specific mAb for staining of porcine B cells, as the transcription factor Blimp-1 is known to be essential for the generation of plasma cells [1781]. Only obscure staining patterns were observed when analyses were performed on defrosted cells. A more distinct population of porcine Blimp-1+CD79α+ B cells was detected with freshly isolated cells. For further analyses on the cross-reactivity of clone 3H2-E8, PBMC were stimulated with the TLR7/8 agonist resiquimod (R848, 2.5 mg/ml) as TLR-mediated activation is described to promote expression of Blimp-1 [1782, 1783]. After three days of in vitro stimulation, a clear increase in Blimp-1+CD79α+ B cells was detected. The final proof of cross-reactivity still needs to be obtained by testing the mAb on cells transfected with recombinant porcine Blimp-1.
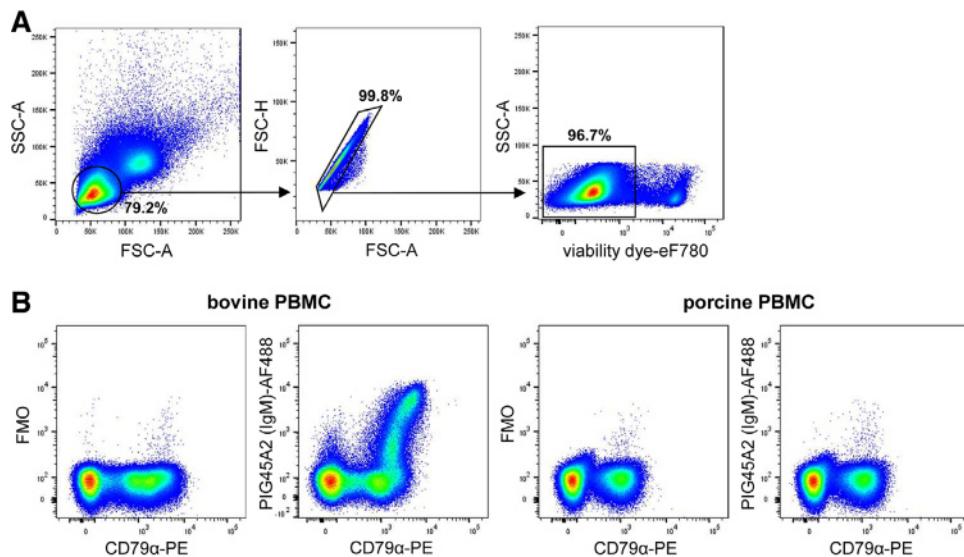
Figure 205. Test of anti-bovine IgM mAb for cross-reactivity with the porcine orthologue. For the anti-bovine IgM mAb clone PIG45A2 (Kingfisher Biotech, catalogue no. WS0620B-100) cross- reactivity to the porcine protein is indicated on the Kingfisher Biotech data sheet. (A) Porcine and bovine lymphocytes were gated according to their light scatter properties and single cells are discriminated from doublets by plotting FSC area against height. Dead cells are excluded by a viability dye. A representative gating strategy for bovine PBMC is shown. (B) The anti-IgM mAb was tested in combination with a CD79α-specific mAb for staining of either bovine or porcine B cells. A clear IgM-specific staining was obtained with the mAb on bovine B cells in contrast to a FMO control by using only secondary antibodies. No clear difference in the staining of the anti-IgM mAb on porcine B cells in comparison to the FMO control could be observed. The same staining patterns were obtained by different concentrations of the anti-IgM mAb (data not shown).

sequence alignment. High homology rates here (> 90%) are usually a strong indicator of Ab cross-reactivity. An example on this given in Fig. 203A. According to the data sheet for the anti-mouse paired box protein-5 (Pax-5) mAb clone 1H9, distributed by BD Biosciences, the immunogen used for its generation spanned the amino acid residues 154 to 284 of the murine Pax-5 sequence. This part of the murine sequence has a homology of 96.9% with the corresponding porcine Pax-5 sequence. Of note, also the entire murine Pax-5 sequence has 98.2% homology with porcine Pax-5, suggesting in general a high likelihood that anti-murine Pax-5 Abs will cross-react with porcine Pax-5. Indeed, this Ab showed a clear co-staining with CD79α+ porcine B cells (see further details below and Fig. 203B).

Sequence alignments are also helpful to get a first impression on the likelihood of Ab cross-reactivity between closely related species e.g. within the families of Bovidae or Suidae. However, this requires that sequence data is available at all. If sequence data is lacking or the sequence alignments reveal a number of amino acid changes in the region of interest (for example the binding site of the mAb) carefully performed experiments for cross-reactivity testing become inevitable, as described in the following.

15.4 Practical guidelines for cross-reactivity testing. In any case, once one or several Ab candidates have been identified for cross-reactivity testing, first FCM experiments become inevitable. Prudent planning is required, since negative results will be frequently encountered. This leads to the question whether the Ab under investigation is indeed not cross-reactive or whether other conditions may have caused a failure of the experiment. Hence, one important aspect is to make sure that cells used in the experiment have a high likelihood to express the molecule of interest. For example, if Abs specific for homing markers from the gut tissue are investigated, leukocytes isolated from the intestine should be used. Similarly, chemokine receptor expression might be affected by freezing/ thawing procedures or the staining temperature [1780]. Additionally, particular cell subsets can be more affected by freezing/ thawing procedures than others, e.g. plasma cells. Therefore, here likewise testing on freshly isolated cells is highly recommendable. If the subset to be stained with the putative cross-reactive mAb is very small or likely to be expected on activated cells, *in vitro* stimulation of cells prior to staining can also increase the likelihood of a positive result. An example on these phenomena is shown in Fig. 204. The anti-mouse B lymphocyte–induced maturation protein-1 (Blimp-1) mAb clone 3H2-E8 was tested for cross-reactivity with its orthologous molecule in swine. With thawed porcine PBMC only a small and somewhat obscure positively stained subset was found (Fig. 204B, left plot). With freshly isolated PBMC, a more distinct subset of CD79α+ that co-stained with the anti-Blimp-1 mAb became visible. Finally, in porcine PBMC, which were *in vitro* stimulated with the Toll-like receptor (TLR) 7/8 agonist resiquimod, a clear CD79α+ putatively Blimp-1 double-positive subset was observed.

To ensure that the tested Ab is of sufficient quality, especially when encountering negative results, we frequently test it in paral-lel on cells from the species the Ab has been raised for. In this way, potential doubts on the quality of the mAb or the overall performance of the staining procedure can be ruled out. An example on this is shown in Fig. 205. The anti-bovine IgM mAb clone PIG45A2, distributed by Kingfisher Biotech, is claimed to be cross-reactive with porcine IgM in the Ab data sheet. Hence, we tested the Ab on bovine and porcine PBMC in parallel. Whereas in bovine PBMC a clear IgM/CD79α double-positive population was observed, with porcine PBMC putatively IgM+ cells were on the level of an FMO-control, which was only stained with the isotype-specific secondary Ab (Fig. 205B). Hence, anti-bovine IgM mAb clone PIG45A2 does not seem to cross-react with its porcine orthologue.

In a comparable way, also positive findings for a newly tested mAb should be thoroughly questioned. One first approach is to test putatively cross-reactive mAbs from the very beginning (i.e. already during the initial titration) in combination with other established mAbs that allow the identification of phenotypes on which expression of the target antigen is expected. For example, for a target antigen that is expected to be expressed only by B cells, a co-staining with pan-B cell-specific mAbs allows a first assessment whether the cells stained by the putatively cross-reactive mAb are indeed labeled in a specific manner. As shown in Fig. 203B, the anti-mouse Pax-5 mAb clone 1H9 was tested in combination with CD79α, an anti-human mAb that cross-reacts with CD79α in multiple mammalian species [1744]. As expected from the high sequence homology between murine and porcine Pax-5 (Fig. 203A), a clear CD79α+ putatively Pax-5 double-positive subset was observed. In the same manner, also in Figures 204 and 205 a co-staining against CD79α was performed in order to test Abs against Blimp-1 and IgM for their reactivity with porcine B cells (see also above for further details).

Once the optimal quantity or dilution of the mAb under investigation has been established, more complex phenotyping experiments should be performed to ensure that the stained cell populations match with phenotypes identified in more thoroughly studied species like human or mouse. Like for any other experiment, investigations with cells from several animals of the new species and different lymphatic and non-lymphatic organs should be performed to further scrutinize the obtained results. Nevertheless, it should be noted that expression patterns for particular immune-related molecules might not be completely conserved between different species. Examples for this would be the abundant expression of CD8αα homodimers on porcine NK cells as well as substantial subsets of CD4 and γδ T cells [1784], a phenomenon not seen in the corresponding human or mouse lymphocyte subsets. Likewise, differently from human or mouse T cells, MHC-II molecules are frequently expressed on activated and memory T-cell subsets in pigs [1712, 1785].

From a pedantic view, the aforementioned experimental strategies do not provide the final proof of cross-reactivity. This proof can be achieved by cloning and recombinant expression of the species-specific protein in a cell line with the subsequent analysis in immunofluorescence staining as performed to demonstrate the cross-reactivity of mAbs against porcine and ovine Foxp3 [1786, 1787] as well as porcine Helios [1788]. Also, Abs against

Table 82. Abs cross-reacting with porcine immune-related non-CD molecules in FCM[1]

Molecule	Species Ab was raised for	Clone name	Vendor(s)	References
Transcription factors				
Eomes	human	WD1928	ThermoFisher Scientific	[1729]
Foxp 3	mouse/ rat	FJK-16s	ThermoFisher Scientific	[1786]
GATA-3	human/ mouse	TWAJ	ThermoFisher Scientific	[1732]
Helios	human/ mouse	22F6	BioLegend	[1788]
T-bet	human	eBio4B10	ThermoFisher Scientific	[1732]
Cytokines				
IFN-γ	cattle	CC302	Bio-Rad	[1791]
IL-17A	human	SCPL1362	BD Biosciences	[1724]
TNF-α	human	MAb11	BioLegend	[1792]
Miscellaneous				
Ki-67	human	B56	BD Biosciences	[1793]
Perforin	human	δG9	BD Biosciences, ThermoFisher Scientific	[1740]

[1] Table is not claimed to be complete

ovine TNF-α [1789] and bovine and ovine IL-17A [1790] have been tested in this way. Similar experiments are currently under way in our laboratory to confirm the cross-reactivity of the anti-mouse Pax-5 mAb 1H5 and anti-mouse Blimp-1 mAb 3H2 2E8 with the respective porcine orthologs. However, it is important to state that numerous cross-reactive Abs, which are in use in the pig (and in other species), have not been tested in this way. Indeed, in those cases where the amino acid sequence of the immunogen used to raise the Ab is known and has a 100% identity to the orthologous sequence of the species under investigation, the testing on a recombinant protein is irrelevant. For all other cases, the authors of this chapter strongly recommend a testing on recombinant proteins in order to achieve the highest possible quality standards. Finally, an alternative approach to prove cross-reactivity is an immunoprecipitation of the target antigen by the putatively cross-reactive mAb and subsequent analysis of the precipitate by mass spectroscopy.

15.5 Examples on cross-reactive mAbs in pigs.   Pigs have received increasing interest as a large animal model in recent years [1708], which has also resulted in publications on the knowledge of CD-molecule expression in porcine leukocytes, including listings of available mAbs to study their expression [1709, 1710]. Moreover, very recently a website was launched that lists currently available mAbs not only for the pig but also cattle, sheep, goat, chicken, horse, cat, and some fish species: https://www.immunologicaltoolbox.co.uk/. Cross-reactive mAbs are also interspersed in these sources of information, but should be treated with caution since several of these mAbs have not been scrutinized according to the guidelines above. In addition, these publications do not cover intracellular molecules, which are also of high relevance in immunophenotyping. Hence, Table 82 provides a list of miscellaneous molecules that are not CD-molecules and for which mAbs that cross-react with the porcine orthologue have been identified.

Table 83. Reagents and Abs used for cross-reactivity testing

Reagent/ Antibody	Clone	Manufacturer
Mouse anti-human CD79α - PE	HM57	Dako
Rat anti-human/ mouse Pax-5 - AlexaFluor® 647	1H9	BD Biosciences
Mouse anti-human/ mouse Blimp-1 - DyLight650	3H2-E8	ThermoFisher Scientific
Mouse anti-bovine sIgM	PIG45A2	Kingfisher Biotech
Goat anti-mouse IgG2b - AlexaFluor® 488	–	ThermoFisher Scientific
Fixable Viability Dye eFluor™ 780	–	ThermoFisher Scientific

15.6 Step-by-step sample preparation.
Step-by-step sample preparation of porcine PBMC

1. Draw blood and transfer to an anti-coagulant containing tube.
2. Dilute blood 1:2 in PBS (PAN-Biotech)
3. Carefully overlay Pancoll (for example Pancoll human, Cat# P04-601000 by PAN-Biotech) with diluted blood in a ratio of 1:3.
4. Centrifuge at room temperature at $800 \times g$ without brake for 20 min.
5. Collect interphase, transfer to new tube and wash twice with PBS at $300 \times g$, 4°C, 6 min and discard supernatant.
6. Wash with staining buffer
7. Pellet cells ($300 \times g$, 4°C, 6 min) and discard supernatant.

Step-by-step FCM staining of porcine leukocytes from blood and spleen

1. Transfer up to 2×10^6 cells into a 96-well conical or U-bottom shaped plate.

2. Centrifuge the plate at $300 \times g$ at 4°C for 3 min. Aspirate or decant supernatant.

3. Add a max of 30 μL surface staining mix per well and incubate for 15 min at 4°C.

4. Two washing steps: add up to 200 μL staining buffer and centrifuge the plate at $300 \times g$ at 4°C for 3 min and aspirate or decant supernatant.

5. Add secondary reagents as described above including the two washing steps.

6. Add Fix/ Perm reagent for 20 min at 4°C, following two washing steps in permeabilization buffer as described above.

7. Add mAbs specific for intracellular or intranuclear antigens (Table 83) for 20 min at 4°C, following two washing steps in permeabilization buffer as described above.

Materials
Flow cytometer:

- FACSCanto II (BD Biosciences)

  Media and buffers:

- cRPMI: complete RPMI 1640 (PAN-Biotech) supplemented with 10% FCS (Sigma-Aldrich), 100 U/mL Penicillin, and 100 μg/mL Streptomycin (PAN-Biotech)
- Fixation and Permeabilization reagents for detection of intranuclear molecules: Foxp3/ Transcription factor staining buffer set (ThermoFisher Scientific)
- Staining buffer: PBS (PAN-Biotech) supplemented with 10% porcine plasma (in house preparation) for freshly isolated or thawed cells and PBS (PAN-Biotech) supplemented with 3% FCS (Sigma–Aldrich) for cells that were cultivated in vitro

  In vitro stimulation

- TLR7/8 agonist resiquimod (R848, 2.5 mg/mL, InvivoGen) for 3 days

VII Data handling, evaluation, storage and repositories

1 Data analysis

1.1 *Introduction*

During the last decade, the field of FCM has gone through a number of revolutionary, technological advances that have resulted in a wide array of novel single-cell platforms. These include classical, multiparameter FCM, mass cytometry, spectral FCM, imaging FCM, and imaging mass cytometry, to name only a few (See Chapter VIII: Advanced techniques in, and management of, FCM). Many of these novel technologies generate large and/or high-dimensional data sets, which cannot be analyzed adequately anymore using the classical, manual analysis techniques. For example, current flow and mass cytometers can measure tens of parameters,

while techniques such as imaging FCM are producing several hundreds of parameters at the single cell level. In addition, manual analysis techniques, such as manual gating to identify cell populations, have a number of important limitations [1794]. These include the fact that they are hard to reproduce, are subjective and biased, and are inefficient when exploring high-dimensional parameter spaces [599]. In addition, manual analysis is very time consuming when analyzing large cohorts of samples.

To mitigate these limitations of manual analysis, computational techniques can be used to take full advantage of the power of high-dimensional cytometry data analysis [1795]. However, this does not mean computational techniques completely replace the manual analysis. Rather, they should be considered as complementary tools that offer new insights, and performing an additional, manual inspection is still good practice as a quality control check. Computational methods can be used at several stages of the data analysis pipeline, including storage of the well-annotated data in repositories, during data cleaning and pre-processing, and for different types of analyses such as data visualization, population identification, and biomarker detection. Figure 206 presents an overview of the different stages of the data analysis pipeline where computational techniques can be used. Crucial to all these data analysis techniques is the fact that data should be of the best quality, and thus care should be taken to correctly design the experiment, take into account all the appropriate controls, and generate the data in such a way that is suited for all the computational analyses to be performed afterward.

A wide variety of methods from the fields of statistics, data mining, and machine learning is used to extract knowledge from cytometry data [1796]. These techniques can be broadly categorized into two groups: unsupervised learning and supervised learning strategies. Unsupervised learning techniques are descriptive models that aim at better characterizing the data, and are typically used to explore the structure of the data. These include techniques such as dimensionality reduction, clustering, and trajectory inference. Briefly, dimensionality reduction techniques aim at transforming the original, high-dimensional data set to a lower-dimensional space, often two or three dimensions, where it is easy to visually appreciate the structure in the data. This would, for example, allow detecting population structures, outliers, batch effects, or other trends present in the data. Clustering and trajectory inference methods aim to look for specific structures present in the data. Clustering techniques typically look for groups of cells (clusters) that are similar within a group, but different between groups, and mostly assume groups are well separated. Trajectory inference methods on the other hand rather look for structures that behave more like gradients, e.g., cells smoothly transitioning between different stages of a developmental process. These gradients should not necessarily be linear gradients, but can include branching processes and cycles as well.

Supervised methods take another approach to data analysis, and are typically used to construct predictive models. In this case, one wants to relate the cellular data to an outcome variable of interest, for example, the disease status of a patient, or the cell type of a particular cell of interest. Different types of supervised

methods exist, the most important of which are classification techniques, regression techniques, and techniques for survival analysis. The typical use of these methods is to construct a model based on data for which the outcome variable is already known, which is referred to as training the model. Such a trained model can later be used to predict the outcome variable for new data, not seen before.

1.2 Cell-population analysis: Data preprocessing, manual and automated gating, and quality control

1.2.1 Overview. Manual analysis is still an important component of FCM experiments in many labs, however, automated methods for identifying cell subpopulations in FCM data have proliferated rapidly [1797]. As manual gating is inherently subjective, it is important to follow defined protocols to improve analysis reproducibility. Preprocessing of data is necessary to remove errors and establish the appropriate data transformation parameters. Gating decisions should carefully consider different types of controls, and populations represented as a shoulder of a larger population should be analyzed with caution. Back-gating is critical for determining whether the initial gates are appropriate for the final subpopulation being analyzed, instead of being appropriate for the majority populations.

1.2.2 Complementary manual and automated analysis methods. FCM data analysis presents a complex problem because of recent rapid increases in the number of parameters measured, and because of some peculiarities of flow data. Current datasets include 20 or more parameters even by conventional fluorescence cytometry, and other methods yield 35 or more channels. Traditional bivariate gating (manually drawing boundaries on sequential two-parameter plots) can still be performed on high-dimensional data sets, but this becomes progressively more time

consuming and less thorough as the parameter number increases. The current generation of flow cytometers is capable of simultaneously measuring 50 characteristics per single cell. These can be combined in 3^{50} possible ways using traditional bivariate gating, resulting in a massive data space to be explored [1798]. There has been rapid development of unsupervised clustering algorithms, which are ideally suited to biomarker discovery and exploration of high-dimension datasets [599, 1795, 1796, 1799–1804], and these strategies are described in more detail in Chapter VI, Section 1.2. However, the directed identification of specific cell populations of interest is still critically important in flow analysis for providing "reality checks" for the results returned by different algorithmic strategies, and for the generation of reportable data for clinical trials and investigations. This is the approach used by investigators who prefer to continue manual gating for consistency with previous results, now complemented by the availability of supervised cell population identification methods. This section will describe common issues in this type of analysis, in three stages: preprocessing, gating, and postprocessing (Fig. 207).

1.2.3 Principles of analysis.

1. **Preprocessing flow data in preparation for subpopulation identification**:

Batch effects: FCM data are difficult to standardize between batches analyzed days or months apart, because cytometer settings can change with time, or reagents may fade. Imperfect protocol adherence may also lead to changes in staining intensity or machine settings. Such variations need to be identified, and where possible corrected. In addition to batch variation, individual outlier samples can occur, e.g., due to temporary fluidics blockage during sample acquisition. Identification of these changes can be performed by detailed manual examination of all samples. However, this involves evaluating the MFI between samples after gating
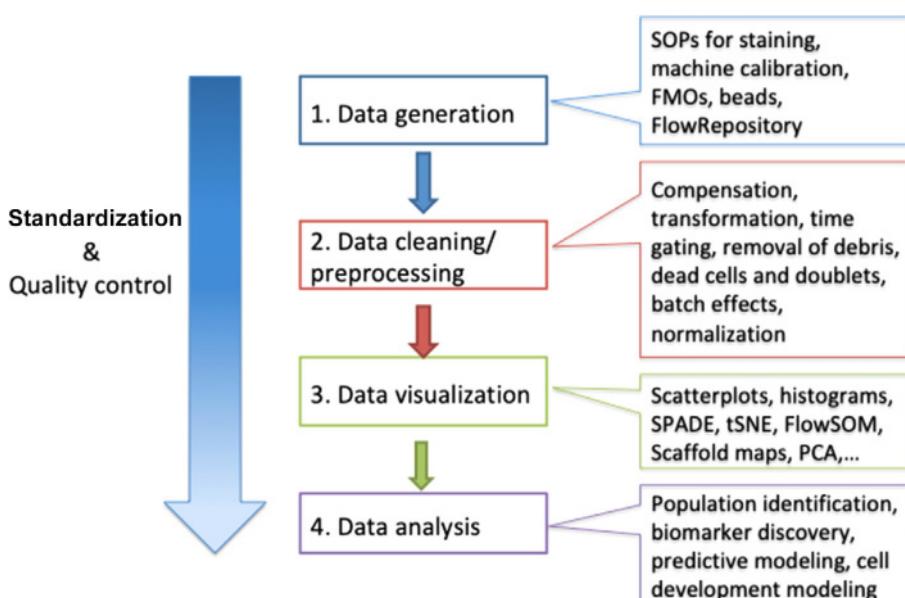
Figure 206. Computational methods offer great potential to automate many stages in the analysis of cytometry data. For every stage, computational pipelines can greatly contribute to standardization and quality control, leading to better standards in the FCM field.
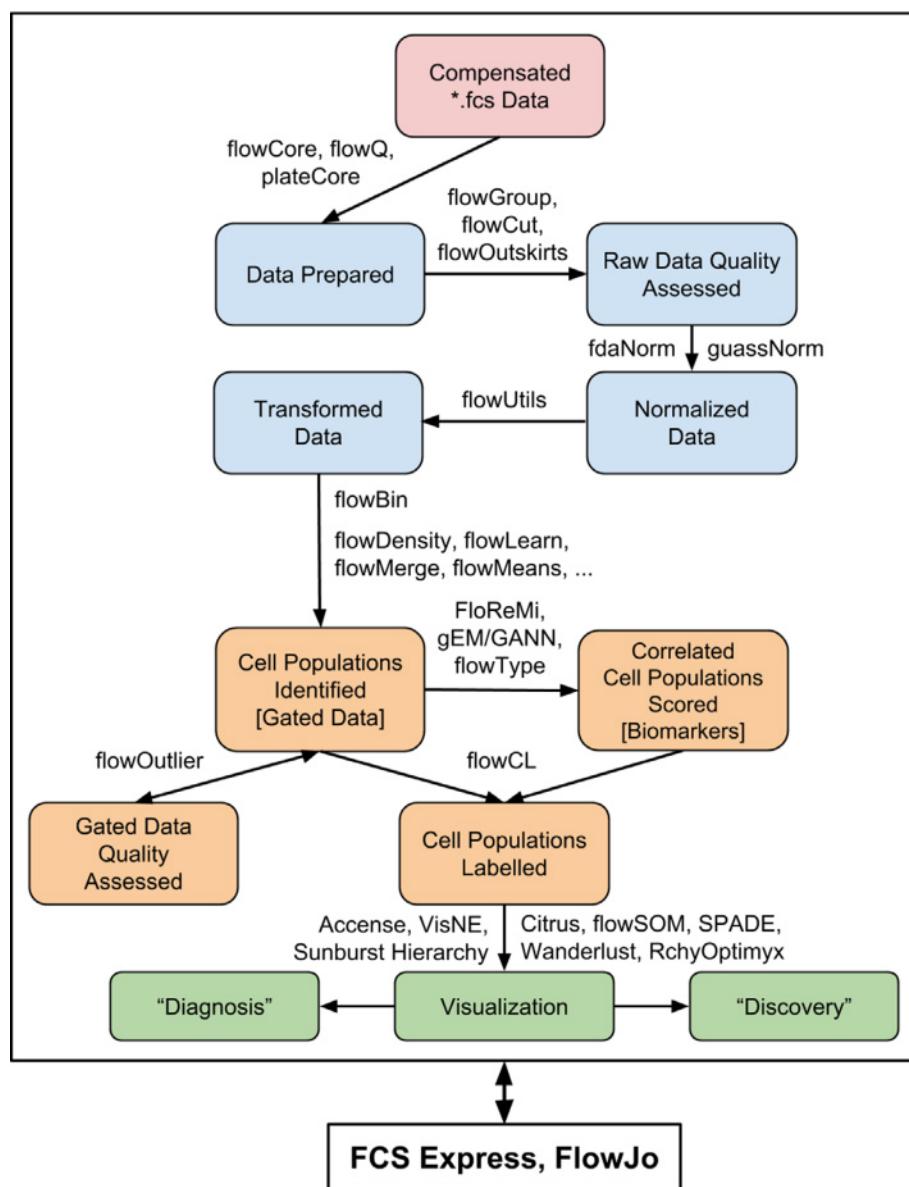
Figure 207. Typical analysis workflows in FCM for the identification of specific cell populations of interest by either manual or automated analysis. Analysis usually starts with several preprocessing steps on compensated data, including quality assessment, data normalization, and data transformation (blue boxes). Preprocessing is followed by identifying cell populations of interest (orange boxes), and finally visualization and interpretation (green boxes).

down to meaningful subpopulations. For high-dimensional data, this is difficult to perform exhaustively by manual analysis, and is more easily achieved by automated methods. As an example, samples from a study performed in two batches, on two cytometers, were analyzed by the clustering algorithm SWIFT [1801, 1805], and the resulting cluster sizes were compared by correlation coefficients between all pairs of samples in the study (Fig. 208). The most consistent results (yellow squares) were seen within samples from one subject, analyzed on 1 day and one cytometer. Samples analyzed on the same day and cytometer, but from different subjects, showed the next smallest diversity (compare subjects 1 vs. 2, and 4 vs. 5). Weaker correlations (blue shades) occurred between samples analyzed on different days, or different cytometers. Similar batch effects are seen in data sets from many labs. These effects should be addressed at two levels: experimental and computational. At the experimental level, day-to-day variation can be minimized by stringent adherence to good protocols for sam-

ple handling, staining, and cytometer settings (see Chapter III, Sections 1 and 2). For multisite studies, cross-center proficiency training can help to improve compliance with standard protocols. If shipping samples is possible, a central laboratory can reduce variability in the staining and flow cytometer settings. Clearly, performing a study in a single batch is ideal, but in many cases this is not possible.

Ameliorating batch effects during analysis: At the analysis level, some batch effects can be reduced during further analysis. In experiments in which batch effects occur due to variability in staining or cytometer settings, algorithms for reducing this variation by channel-specific normalization have been developed (below). Batch effects due to other causes may be more difficult to correct. For example, increased cell death is another potential batch problem that is not completely solved by just gating out dead cells, because marker levels on other subpopulations can also be altered before the cells die.
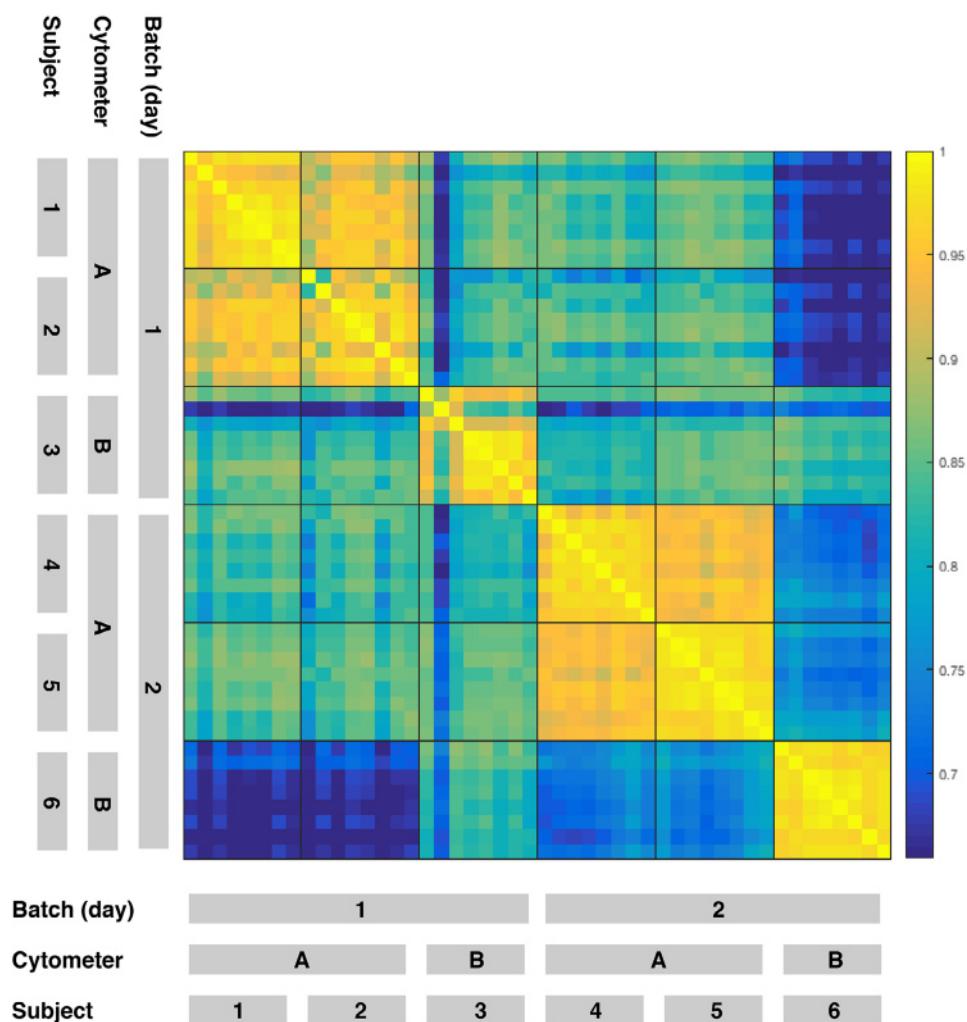
Figure 208. Quality control analysis to detect batch effects. Eight sequential blood samples each from six subjects were analyzed by FCM, clustered using the SWIFT algorithm, and Pearson correlation coefficients in the number of cells per cluster were calculated between all pairs of subjects. Samples were analyzed for 2 days, and on two identically configured LSR-II cytometers. Data files can be found here: https://flowrepository.org/id/FR-FCM-ZZ8W

Curation of datasets: In some datasets, curating names and metadata may be necessary, especially when following the MIFlowCyt Standard (See Chapter VIII Section 3 Analysis presentation and publication (MIFlowCyt)). The manual entry error rate can be greatly reduced by using an automated Laboratory Information Management System (e.g., FlowLIMS, http://sourceforge.net/projects/flowlims) and automated sample data entry. As manual keyboard input is a major source of error, an LIMS system can achieve a lower error rate by minimizing operator input through automated data input (e.g., by scanning 2D barcodes) or pre-assigned label choices on pull-down menus. Although compensation is conveniently performed by automated "wizards" in popular FCM analysis programs, this does not always provide the best values, and should be checked by, e.g., $N{\times}N$ displays showing all possible two-parameter plots. Further information on compensation can be found in [60]. CyTOF mass spectrometry data needs much less compensation, but some cross-channel adjustment may be necessary in case of isotope impurities, or the possibility of M+16 peaks due to metal oxidation [1806].

In some data sets, further data curation is necessary. Defects at specific times during data collection, e.g., bubbles or changes

in flow rate, can be detected and the suspect events removed by programs such as flowClean [1807]. Furthermore, compensation cannot be performed correctly on boundary events (i.e., events with at least one uncompensated channel value outside the upper or lower limits of its detector) because at least one channel value is unknown. The upper and lower detection limits can be determined experimentally by manual inspection or by programs such as SWIFT [1801]. The investigator then must decide whether to exclude such events from further analysis, or to keep the saturated events but note how this may affect downstream analysis.

Transformation of raw flow data. Fluorescence intensity and scatter data tend to be log-normally distributed, often exhibiting highly skewed distributions. Flow data also typically contain some negative values, mainly due to compensation spreading but also partly because of subtractions in the initial collection of data. Data transformations (e.g., inverse hyperbolic sine, or logicle) should be used to facilitate visualization and interpretation by reducing fluorescence intensity variability of individual events within similar subpopulations across samples [1808]. Several transformation methods are available in the package flowTrans [1809], and should be evaluated experimentally to determine their effects on

the data with regard to the automated methods used and further downstream analysis.

Registration/normalization of fluorescence intensity values: Normalization between data sets with regard to fluorescence intensities can be accomplished either by adjusting gates (i.e., manually specified filters or probabilistic models designed to enumerate events within defined regions of the data) between samples, or by moving sample data closer to the gates via fluorescence intensity registration. Auto-positioning "magnetic" gates can reconcile slight differences between samples in programs like FlowJo (Tree Star) and WinList (Verity Software House), but large shifts in subpopulation locations are difficult to accommodate. Several semi-automated methods of fluorescence intensity registration are available (e.g., fdaNorm and gaussNorm [1810, 1811]). These attempt to move the actual data-points across samples to similar regions, thus allowing gates to be applied to all samples without adjustment. Both fdaNorm and gaussNorm register one channel at a time, and do not address multidimensional linkages between biological sub-populations. The methods further require pregating to expose subpopulation "landmarks" (peaks or valleys in 1D histograms) to register effectively. However, this "global" approach does not adequately capture the semantics of biologically interesting rare subpopulations that are often obscured by high-density data regions. A recent extension [1811] of the fdaNorm method attempts to address this shortcoming by tightly integrating "local" (subpopulation specific) registration with the manual gating process, thus preserving the multidimensional linkages of rare sub-populations, but still requiring a hierarchy of manual gates derived from a reference sample. Fully automated fluorescence intensity registration methods are in development.

2 Identification of subpopulation sizes and properties by gating

Sequential bivariate gating: Once data preprocessing steps are complete, users can identify cell populations using manual analysis or one or more of more than 50+ automated gating algorithms currently available [599, 1812]. Sequential gating in 2D plots is the standard method for manual analysis. Rectangular gates are convenient for well-separated sub-populations, but more subtle gates are often required, e.g., elliptical gates to define subpopulations in close proximity, or "spider" gates (available in FlowJo) to allow for fluorescence spreading due to compensation. The sequence of gates can be important because the desired subpopulation may be visualized more effectively by particular marker combinations.

Back-gating: A critically important step for gating high-dimensional data is to **optimize the gates using back-gating,** which involves examining the cell subpopulations that satisfy all but one of the final gates. This procedure is performed for each gate in turn, and is critically important because small cell subpopulations may be defined by boundaries that are different from the boundaries of bulk subpopulations, e.g., stimulated cytokine-producing T cells display less CD3 and CD4 than unstimulated T cells, so setting the CD3$^+$ and CD4$^+$ gates on the bulk T-cell sub-

population will give suboptimal gates for the stimulated T cells (Fig. 209). Back-gating partly compensates for the inability of manual gating to use all dimensions simultaneously, as can be achieved in algorithmic clustering.
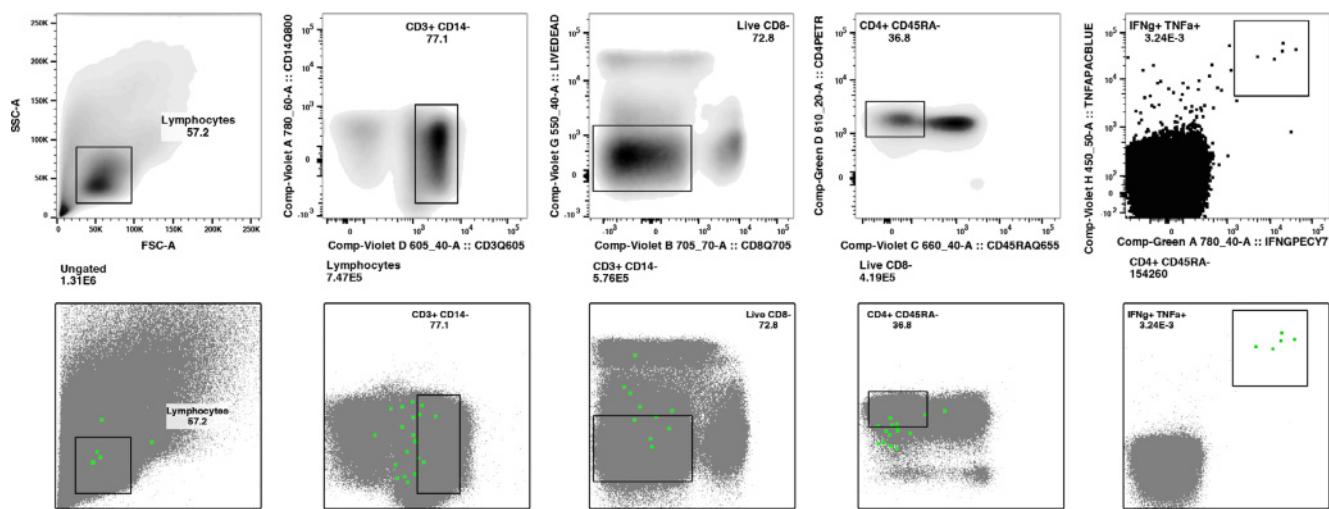
Validation of gated or clustered sub-populations: Another critical issue is to **examine the final gated sub-populations** carefully, using prior knowledge and expectations from the biology. Figure 210 illustrates the importance of detailed examination using three artificial samples—a negative control that has no positive cells in either dimension (left); a positive sample that has small subpopulations of A+B– and A–B+ cells (middle); and a sample that has no obvious positive subpopulations, but has a slightly increased fluorescence intensity resulting in cells appearing in the A+B– and A–B+ gates (right). If the results of gating are accepted blindly, then samples 2 and 3 will be evaluated as having similar A+B– and A–B+ responses, whereas examination of the plots suggests a very different interpretation. Biological insight is also very useful—if a large subpopulation appears to be positive for a marker that is usually expressed only on a minor subpopulation, it should be suspected that there is an unusually high background for that marker on some cells and further experiments should be done to confirm the specificity of binding.

A limitation of manual gating in sequential two-dimensional plots is that two sub-populations may not be fully resolved in any combination of two dimensions, even though the sub-populations are fully resolved if all dimensions are considered simultaneously (which is only possible by algorithmic analysis). Thus in manual gating, it is sometimes necessary to make choices based either on recovering the largest number of the target cells (wider gates, at the expense of increased contamination), or identifying cells with the most certainty (narrower gates, at the expense of some loss of positive cells).

Another limitation of manual gating in sequential 2D plots is that human subjectivity has been identified as a primary source of variation within analyzed results [609, 1804]. Automated analysis methods have reached a state where they can now provide a solution to the challenge of analyzing big sets of FCM data. If chosen and used with care, many of these automated tools show as good, or even better, as well as more consistent analytic results compared with those performed by "human" users [1795, 1802, 1813, 1814].

Automated gating algorithms can be categorized as supervised or unsupervised. Supervised approaches to cell population identification incorporate user knowledge into the algorithm at various points. As such, supervised approaches are especially beneficial when users have project-specific expectations (e.g., target cell populations of interest, based on an existing gating strategy the user is trying to replicate). The most general type of supervised learning is where the method takes as input one or few training sample(s) in which all cells are manually gated and assigned to a cell population. This sample(s) trains a classification model that then classifies the cells of similar ungated samples. Examples of models tested in this category include the neural network [1815], support vector machine [1816], and hierarchical agglomerative hierarchy construction [1817]. On the other hand, OpenCyto [1818] and flowDensity [1819] approach the problem

Gated on bulk CD4 T cell populations

Gated on cytokine-producing CD4 T cell populations
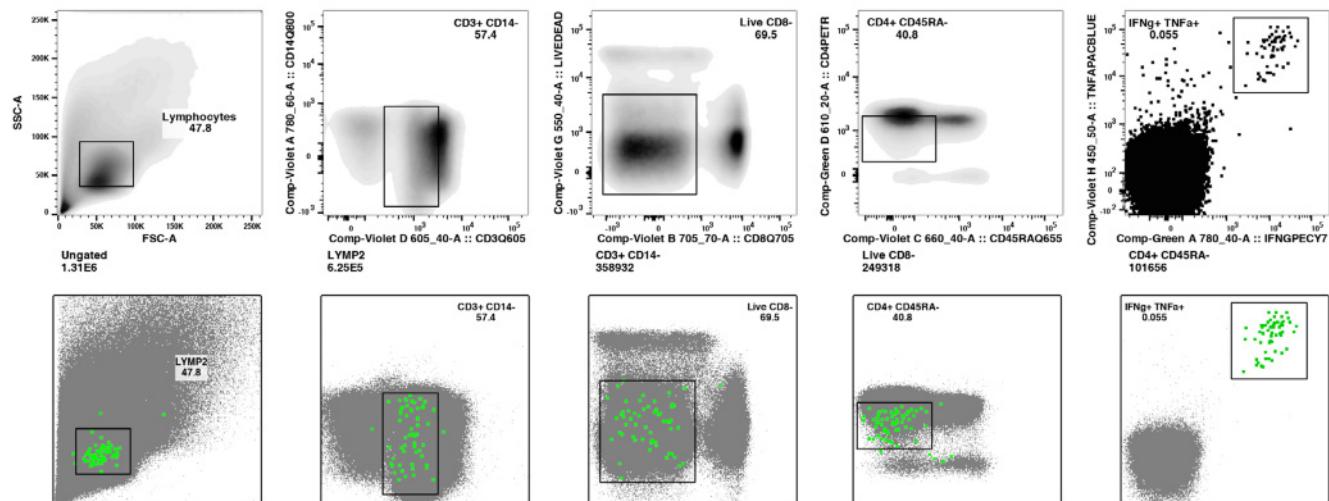
Figure 209. Importance of back-gating for minor subpopulations. A sample from the study described in Fig. 207 was stimulated in vitro with influenza peptides, and cytokine-producing cells were then identified by Intracellular Cytokine Staining and FCM. The top row shows the sequential gating of memory CD4 T cells (CD3$^+$CD4$^+$CD8$^-$CD14$^-$ Live CD45RA$^-$), using gates appropriate for the bulk memory population. However, backgating in FlowJo (row 2) shows that these gates do not capture many of the CD4 T cells secreting cytokines in response to the influenza peptides. Adjusting the gates by back gating results in much better identification of the stimulated, cytokine-expressing T cells that have slightly different values for several parameters (rows 3 and 4). The negative control sample contained zero cells in the final TNFα^+ IFNγ^+ gate. Data files can be found here: https://flowrepository.org/id/FR-FCM-ZZ8H

by mimicking the manual gating process. Machine learning methods such as flowLearn aim to automate the parameterization of supervised methods [1820]. Users can specify everything from desired gate characteristics to the dimensions on which the algorithm should gate. Users can even provide a single or few gated samples for the algorithm to learn gate characteristics from ref. [1820]. When using machine-learning methods, these samples must have similar fluorescent value and shape distributions as their ungated counterparts for the methods to work [1815, 1820]. The development of machine learning approaches for supervised

gating is still in its infancy, but holds great potential to ease the burden of automating the identification of specific cell populations of interest based on a prescribed gating hierarchy. The resulting gates can then be extracted, plotted, and adjusted until they are satisfactory. Since the plots produced can be specified to match a gating strategy, they can easily be used to communicate with those who are not familiar with the computational aspects of analysis. Moreover, comprehensive analysis of state-of-the-art supervised algorithms through the FlowCAP effort has shown that these approaches produce unbiased results and can reduce
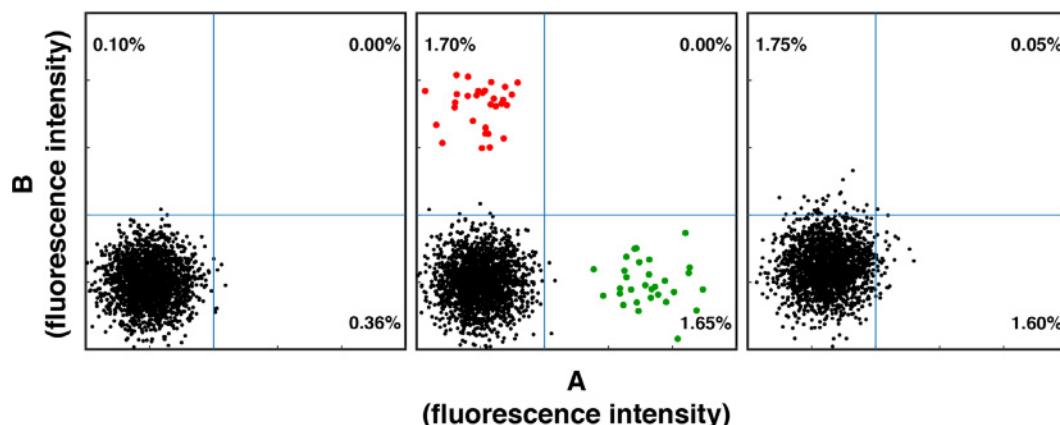
Figure 210. Model data illustrating the very different interpretations of two samples with similar proportions of cells in a positive gate. Left: A double-negative (A–B–) population with a random normal distribution is modeled. Middle: Two extra small sub-populations with random normal distributions are added to the A–B– sub-population. The red and green subpopulations contain few cells, but are well-separated from the A–B– population. Right: The "negative" subpopulation has been shifted slightly, but no distinct smaller subpopulations are present.

analysis variability by up to 94% compared with that occurring with manual analysis [1802]. Given the inputs required, it is ideal to have a well-made or established gating strategy in hand when operating these methods, as indicated in refs. [1802, 1821].

While supervised algorithms take into account user specified cell populations, unsupervised algorithms, such as flowMerge [1800] and flowMeans [1822], "cluster" or group cells with similar fluorescent intensities for similar groups of markers directly in high-dimensional space. In contrast with supervised methods, unsupervised methods often do not require user input. However, many methods do allow users to tweak results by changing few global parameter(s), such as the number of cell populations expected. Clustering procedures are great for discovering new natural cell populations which can then be manually validated and gated for using optimized gating strategies generated by tools such as GateFinder [1823] (convex hull gates) and Hyper-Gate [147] (rectangular gates)—note that these are also good for finding optimized gates that may differ for sorting and gating purposes. These approaches are described more fully in the Clustering section (Chapter VII section 1.5).

Regardless of whether manual or automated gating is used to identify cell populations, careful examination of the results on test data sets through examination of familiar bivariate scatter plots is necessary to validate the results. Dimensional reduction tools such as *t*-distributed stochastic neighbor embedding [144, 1824] can be helpful in this regard. Tools for examining the output of automated methods are built in to programs such as FLOCK and SWIFT, and available as plugins in FlowJo, Cytobank, and FCS Express.

For scientists interested in adopting automated methods, collaboration with bioinformaticians is perhaps the quickest path to explore. Learning how to use the algorithms is another option. The most comprehensive library of FCM analysis tools built to date can be found on R/Bioconductor [599]. Although not the most user-friendly choice, R uses a command-line interface to provide a powerful foundation for many data mining and statisti-

cal computational tools. A subset of Bioconductor tools are available and can be integrated with more user friendly graphical user interfaces [1825] such as FlowJo, CytoBank [1826], FCSExpress, SPICE [1827], and GenePattern [1828].

With the growing amount of data becoming available, automated analysis is becoming an essential part of the analysis procedure [1829]. Only by taking advantage of cutting-edge computational abilities will we be able to realize the full potential of data sets now being generated.

Description of final sub-populations: The final subpopulations identified by analysis are identified mainly by their fluorescence intensities for each marker. For some markers, e.g., CD4 on T cells, the positive cells comprise a log-symmetrical, clearly separated peak, and the center of this peak can be described by the geometric mean, the mode, or the median with very similar results. However, if a positive peak is incompletely separated from negative cells, the fluorescence values obtained by these methods can vary substantially, and are also highly dependent on the exact positioning of a manual gate. If a subpopulation is present as a shoulder of a larger, negative peak, there may not be a mode, and the geomean and median may have substantially different values.

3 **Post-processing of subpopulation data: Comparison of experimental groups and identification of significantly altered subpopulations.**

Regardless of the primary analysis method, the output of most FCM analyses consists of the sizes (cell numbers) and MdFIs of many cell subpopulations. Differences between samples (e.g., in different groups of a clinical study) can be performed by standard statistical analysis, using methods appropriate for each particular study. It is very important to address the problem of multiple outcomes, and this is even more critical in high-dimensional datasets because the potential number of subpopulations is very large, and so there is a large potential multiple outcome error. By automated

analysis, hundreds or even thousands of subpopulations can be identified [1801, 1805], and manual analysis also addresses similar complexity even if each subpopulation is not explicitly identified. As in the analysis of microarray and deep sequencing data, it is important to consider the false discovery rate, using a strong multiple outcomes correction such as the Benjamini–Hochberg strategy [1830] or alternative strategies [1831]. Applying corrections to data from automated analysis is relatively easy because the total number N of subpopulations is known [1832], but it is very difficult to identify N for manual bivariate gating, because a skilled operator exploring a dataset will consider many subpopulations before intuitively focusing on a smaller number of "populations of interest." To avoid errors in evaluating significance due to multiple outcomes in manual gating, strategies include: performing the exploratory gating analysis on half of the data, and calculating the statistics on the other half; or performing a confirmatory study with one or a few predictions; or specifying the target subpopulation before starting to analyze the study.

Comprehensible visualizations are essential for the communication, validation, exploration, and discovery of possibly significant cell populations. In conjunction with cell population identification algorithms, visualization is an often overlooked but essential part of the discovery and diagnosis process (see green box in Fig. 207).

Visualization can be a challenge for unsupervised clustering algorithms, as it is difficult for users to comprehend the cell populations identified in high-dimensional space. Therefore, dimension reduction is increasingly being applied to map multidimensional (i.e., samples using more than two markers) results onto a 2D plane for viewing. For instance, the SPADE algorithm colors and connects significant, structurally similar immunophenotypes together in the form of a minimum spanning tree, or a tree-like form [1804]. Dimensionality reduction techniques such as those based on *t*-distributed stochastic neighbor embedding arrange cell populations in a way that conserves the spatial structure of the cell populations in high-dimensional space (See Chapter VII Section 1.4 Dimensionality reduction). This way, users get a more representative view of cluster distributions [1833]. However, these and some other dimensionality reduction methods do not explicitly identify and partition cells into subpopulations. Other methods, such as PhenoGraph [2252] and Cytometree [2250], opt to combine all the analysis processes—segmenting cells into their phenotypically similar subpopulations, which are then labeled and visualized—without loss in performance and accuracy [1814].

Conversely, RchyOptimyx [1834, 1835], gEM/GANN [1836], and FloReMi [1837] use already-labeled samples (e.g., subject has or does not have a certain disease) to extract and display only the cell populations that most significantly discriminate between the differently labeled samples. These cell populations can then be used as indicators, and thus one can target these cell populations, when determining the label of future samples [1813]. Such visualizations aim to focus in on only the most important data structures present to facilitate human interpretation of the data. A comprehensive review of the available visualization algorithms is covered in ref. [1838].

1.3 Artificial intelligence in FCM

Since the advent of the first computing devices, scientists have been fascinated by the possibility to use these machines to mimic the remarkable capacities of the human brain. The broad field of artificial intelligence (AI) spans a wide variety of different techniques to represent knowledge and infer new knowledge from it. For FCM data analysis, the machine learning field, a subfield of AI that focuses on learning models from data, can be considered the most relevant. These techniques include the various types of supervised and unsupervised learning that we have discussed earlier. However, some novel types of machine learning approaches are making their way into the single cell field, most notably the novel types of deep learning approaches.

Deep neural networks are a recent development in the AI field [1839], building further on the classical techniques of neural networks that have already been proposed in the 1950's [1840]. Deep neural networks further build on classical neural networks, but include a much larger number of feature transformations that allow them to make high-level abstractions that are useful for model learning. These networks have been shown particularly suited to work on image types of representations [1841]. Therefore, deep learning methods are suitable models for different types of cytometry where image data is produced [1842], such as imaging FCM [1843] and imaging mass cytometry [1844].

However, deep learning models are generally applicable, and recent work in the field has shown promising results, such as the CellCNN network [1845], an adaptation of convolutional neural networks (CNNs) for cytometry data, or DeepCyTof [1846], a deep learning framework for automated gating. As the number of deep learning papers on single-cell data has recently exploded in the literature, it can be expected that also many of these new techniques will be applicable for FCM data, including novel methods for batch effect correction, data visualization, and automated cell type identification.

1.4 Dimensionality reduction

Visual data exploration is a powerful tool for hypothesis generation. Traditionally, FCM data are being visualized by a set of 2D scatter plots, where in each plot two of the available markers are selected and plotted against each other on the two axes of the plot. With the increasing number of markers provided by novel acquisition techniques [31, 1847] pairwise analysis becomes infeasible. Instead, so-called dimensionality reduction techniques aim to visualize the data by finding a low-dimensional representation that preserves as much structure as possible from a high-dimensional input. In the context of FCM, the original high-dimensional space is formed by treating each marker as a dimension.

However, unless the original data is of low-dimensional nature, embedded in the high-dimensional space, the dimensionality-reduced representation cannot preserve all existing structure. A number of approaches with different goals with regard to the preserved structure have been employed in single-cell analy-

sis. The most common ones are Principal Component Analysis (PCA) [1848], t-distributed stochastic neighbor embedding (t-SNE) [144], and very recently Uniform Manifold Approximation and Projection (UMAP) [1471].

1.4.1 PCA. PCA is a well-known technique that has been used early on for cytometry analysis [1849, 1850]. In short, PCA uses a set of linear transformations, on the original high-dimensional space, such that the axes of main variation (the principal components) in the data are mapped to the axes of the resulting space in order of the amount of variation. For visualization in a 2D scatter-plot, the two principal components with the highest variation are then chosen as the axes of the plot and the other components are simply projected onto the given 2D plane. The resulting mapping preserves relative distances, however, due to its rigid transformations, it cannot faithfully represent nonlinear structure, typically present in single-cell cytometry data [1824].

1.4.2 t-Distributed stochastic neighbor embedding. Recently, t-SNE was established as the gold standard for dimensionality reduction of cytometry data. Introduced into the field under the name viSNE [1824], it is implemented in a plethora of widely used cytometry analysis platforms such as Cytobank [1851], Cytosplore [1852], or cytofkit [1853]. t-SNE is a nonlinear dimensionality reduction technique and as such has largely different goals than the above described PCA. Instead of using only transformations that conserve relative distances, t-SNE aims at preserving local neighborhoods. For a detailed description of the mathematical background of t-SNE, we refer to the original publication [144]. In short, t-SNE first computes local neighborhoods in the high-dimensional space. Such neighborhoods are described by low pairwise distances between data points, for example in Euclidean space. Intuitively, the size of these neighborhoods is defined by the perplexity parameter. In a second step, t-SNE iteratively optimizes the point placement in the low-dimensional space, such that the resulting mapping groups neighbors of the high-dimensional space into neighborhoods in the low dimensional space. In practice, cells with a similar expression over all markers will group into "islands" or visual clusters of similar density in the resulting plot while separate islands indicate different cell types (Fig. 211). When interpreting the resulting t-SNE maps, it is important to understand that the optimization only preserves relative distances within these islands, while the distances between islands are largely meaningless. While this effect can be softened, by using large perplexity values [1854], this hampers the ability to resolve fine-grained structure and comes at large computational cost.

The perplexity is only one of several parameters that can have major impact on the quality of a final t-SNE embedding. Wattenberg et al. provide an interactive tool to get a general intuition for the impact of the different parameters [1855]. In the context of FCM rigorous parameter exploration and optimization, particularly for large data, has been carried out recently by Belkina et al. [1856].

While t-SNE has gained wide traction due to its ability to effectively separate and visualize different cell type in a single plot, it is limited by its computational performance. The exact t-SNE implementation becomes computationally infeasible with a few thousand points [1857]. Barnes Hut SNE [1858] improves on this by optimizing the pairwise distances in the low dimensional space only close data points exactly and grouping large distance data points. A-tSNE [1859] only approximates neighborhoods in the high-dimensional space. FIt-SNE [1860] also uses approximated neighborhood computation and optimizes the low dimensional placement on a grid in the Fourier domain. All these techniques can also be combined with automated optimal parameter estimation [1856].

1.4.3 Uniform Manifold Approximation and Projection. As a result of these optimizations, t-SNE embeddings for millions of data-points are feasible. A similar technique called UMAP [1471] has recently been evaluated for the analysis of cytometry data [1470]. UMAP has similar goals as t-SNE, however, also models global distances and, compared to the exact calculation, provides a significant performances improvement.

While UMAP as well as optimized t-SNE methods provide the possibility to show millions of points in a single plot, such a plot will often lack detail for fine-grained structures, simply due to the limited visual space. Hierarchical SNE [1861] builds a hierarchy on the data, respecting the nonlinear structure, and allows interactive exploration through a divide and conquer approach. It has been adapted and tested with cytometry data in Cytosplore [1862].

Generally, dimensionality reduction provides means to visualize the structure of high-dimensional data in a 2D or 3D plot, however it does not provide automated cell classification or clustering. For biological interpretation or quantification, the dimensionality reduced data needs to be augmented with additional information and tools. viSNE [1824] allows to overlay a single marker as color on each of the plotted cells. Multiple plots with different markers overlayed can then be used to interpret the biological meaning of each cell and manually gate. It has been shown that t-SNE relates to spectral clustering [1863], meaning that visual clusters in the t-SNE embedding can be extracted using automatic clustering techniques as is being done with tools like ACCENSE [1864], or mean shift clustering implemented in Cytosplore [1852] where the resulting clusters can also directly be inspected in standard visualizations such as heatmaps.

1.5 Clustering

To identify subpopulations of cells with similar marker expressions, most researchers apply hierarchical gating, an iterative procedure of selecting subpopulations based on scatter plots showing two markers at a time. To automate the detection of cell populations, clustering algorithms are well suited. These algorithms do not make any assumptions about expected populations and take all markers for all cells into account when grouping cells with
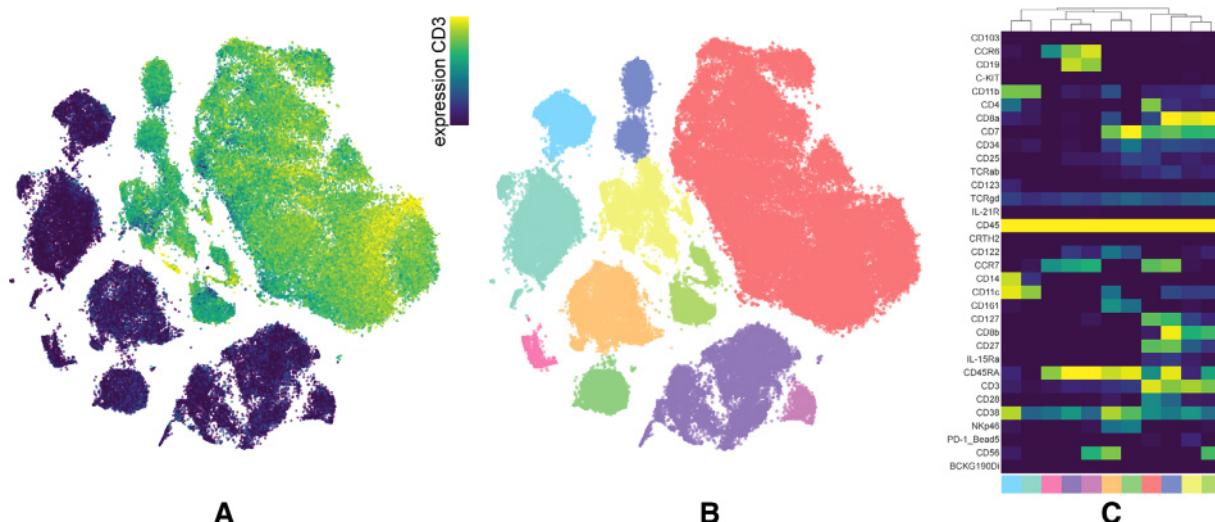
Figure 211. A t-SNE embedding of a mass cytometry dataset consisting of 100.000 cells. Each dot represents a cell. The typical islands of similar cells can be seen. Color overlay in (A) represents expression of one marker, in (B) identified islands of similar cells and the median expression for all markers/islands as a heatmap in (C).

similar marker expressions. The results correspond with cell populations, like typically obtained by manual gating, but without any assumptions about the optimal order in which markers should be evaluated or which markers are most relevant for which subpopulations, allowing the detection of unexpected populations. This is especially valuable for bigger panels, as the possible amount of 2D scatter plots to explore increases quadratically.

The first time a clustering approach was proposed for cytometry data was in 1985, by Robert F. Murphy [1865]. Since then, many clustering algorithms have been proposed for cytometry data and benchmark studies have shown that in many cases they obtain solutions very similar to manual gating results [1795, 1814].

From the many clustering algorithms proposed, several types can be distinguished. Model-based tools try to identify clusters by fitting specific models to the distribution of the data (e.g., flowClust, flowMerge, FLAME, immunoclust, Aspire, SWIFT, BayesFlow, flowGM), while others rather try to fit an optimal representative per cluster (e.g., kMeans, flowMeans, FlowSOM). Some use hierarchical clustering approaches (Rclusterpp, SPADE, Citrus), while others use an underlying graph-structure to model the data (e.g., SamSPECTRAL, PhenoGraph). Finally, several algorithms use the data density (e.g., FLOCK, flowPeaks, X-shift, Flow-Grid) or the density of a reduced data space (ACCENSE, DensVM, ClusterX). Overall, these algorithms make different assumptions, and it is important to understand their main ideas to have a correct interpretation of their results.

All these clustering algorithms belong to the group of unsupervised machine learning algorithms, meaning that there are no example labels or groupings given for any of the cells. Only the measurements of the flow cytometer and a few parameter settings (e.g., the expected number of clusters) are given as input to the algorithm. It should be noted that most clustering algorithms thus only identify groups of cells with similar marker expressions,

and do not yet label the subpopulations found. The researcher still needs to look at the descriptive marker patterns to identify which known cell populations the clusters correspond with. Some tools have been developed which can help with this, such as GateFinder [146] or MEM [1866]. Alternatively, if the user is mainly interested in replicating a well-known gating strategy, it would be more relevant to apply a supervised strategy instead of a clustering approach (e.g., making use of OpenCyto [1818] or flowLearn [1820]).

One important aspect of an automated cell population clustering is choosing the number of clusters. Several clustering tools take the number of clusters explicitly as input. Others have other parameters that are directly correlated with the number of clusters (e.g., neighborhood size in density based clustering algorithms). Finally, there also exist approaches that will try several parameter settings and evaluate which clustering was most successful. In this case, it is important that the evaluation criterion corresponds well with the biological interpretation of the data. In those cases where the number of clusters is not automatically optimized, it is important that the end user does several quality checks on the clusters to ensure they are cohesive and not over- or under-clustered.

1.6 Integration of cytometric data into multiomics analysis

While FCM enables detailed analysis of cellular systems, complete biological profiling in clinical settings can only be achieved using a coordinated set of omics assays targeting various levels of biology. Such assays include, transcriptomics [1867–1869], proteomics [1870–1872], metabolomics analysis of plasma [1873–1875], serum [1876–1878] and urine [1879, 1880], microbiome analysis of various sources [1881], imaging assays [1882, 1883],

data from wearable devices [1884], and electronic health record data [1885]. The large amount of data produced by each of these sources often requires specialized machine learning tools. Integration of such datasets in a "multiomics" setting requires a more complex machine learning pipeline that would remain robust in the face of inconsistent intrinsic properties of these high throughput assays and cohort specific variations. Such efforts often require close collaborations between biorepositories, laboratories specializing in modern assays, and machine learning consortiums [1795, 1813, 1886, 1887].

Several factors play a key role in integration of FCM and mass cytometry data with other high-throughput biological factors. First, much of the existing data integration pipelines are focused on measurements of the same entities at various biological levels (e.g., genomics [1867, 1888] profiled with transcriptomics [1869] and epigenetics [1889] analysis of the same samples). FCM, being a cellular assay with unique characteristics, lacks the biological basis that is shared among other popular datasets. This makes horizontal data integration across a shared concept (e.g., genes) challenging and has inspired the bioinformatics subfield of "multiomics" data fusion and integration [1890–1893]. In order to facilitate meaningful sample subgroup discovery and to uncover between-modality correlations, recently developed methodologies apply a variety of existing machine learning techniques, such as, matrix factorization and latent space modeling [1894, 1895], graph-based analysis [1896, 1897], consensus clustering [1898], and canonical correlation analysis [1899]. The implementation of principled multiomics analysis techniques therefore help to reveal the joint biological system and crosstalk between all measured biological datasets.

A second consideration for integration of FCM data with other omics modalities is the targeted nature of FCM. While FCM typically produces fewer measurements compared to genomics, transcriptomics, and proteomics datasets, the panel of markers measured is often carefully curated to target key cell types and signaling pathways. Therefore, if FCM data are simply combined with other high-throughput and high-content data modalities, the predictions will be primarily driven by the larger datasets [1900]. This is further complicated by the facts that large untargeted datasets often include highly correlated measurements (e.g., a large number of gene expressions measured from the same biological pathway). Therefore, an FCM data set, despite its smaller size, may have a higher information context than traditional untargeted assay. An example of this is demonstrated in a recent study of normal pregnancy in which a mass cytometry data set, despite its relatively small number of cell types and signaling pathways measured, required a higher number of principal components to account for 90% variance than large microbiome and transcriptomics datasets with tens of thousands of measurements [1901]. Therefore, computationally accounting for not only the number of measurements but also the redundancy of the measurements is of critical importance when integrating FCM data with other omics platforms [1901–1903].

1.7 Modeling cell dynamics using trajectory inference

While automated population identification techniques, such as the ones based on clustering, often make the assumption that cell populations are well separated in the space defined by all markers, trajectory inference methods intent to model dynamic biological processes. In this case, the assumption is made that differences between populations might not be well separated, but rather can be modeled as a continuum. This continuum then represents different stages, e.g., of a cell developmental process, and when sufficient cells are present in the different stages of the continuum, a model can be learned to represent this gradient. The first method to describe this novel class of techniques, Wanderlust [1904], was applied to mass cytometry, but since the advent of single-cell sequencing techniques the field of trajectory inference methods has exploded and currently more than 70 techniques are available [1905]. Many of these techniques have been developed for single-cell transcriptomics data, but often they can be applied equally well to cytometry data.

An example of the result of a trajectory inference method applied to a dataset of reprogramming fibroblasts is presented in Fig. 212. Here the black, bifurcating curve represents the model, where MEF cells either develop further to neurons or to myocytes [1906]. As cell developmental processes can be quite complex, e.g., resulting in very complex tree structures, accurately reconstructing the underlying topology of the trajectory is a very complex and challenging computational problem.

Conceptually, trajectory inference methods (sometimes also referred to as pseudo-temporal ordering methods) typically consist of two steps: a dimensionality reduction step, and a trajectory modeling step [1907]. Since many methods exist to perform either of those steps, a wide variety of combinations is available, and the current next challenge in the field is to compare these methods and find out which ones work best for which situation, providing a biological user with guidelines on good practices in the field [1905], along with novel ways of extracting dynamics of the system under investigation [1908].

2 Statistics for flow cytometry

2.1 Background

One of the attributes of cytometric systems is that a large number of cells can be analyzed. However, the data sets produced are just a series of numbers that need to be converted to information. Measuring large numbers of cells enables meaningful statistical analysis, which "transforms" a list of numbers to information.

At the most basic level, the objective of cytometric measurements is to determine if there is more than one population in a sample. In the case that two or more populations are completely separated, e.g., the subsets studied can be gated by virtue of phenotypic markers or easily separated by cluster analysis (for more
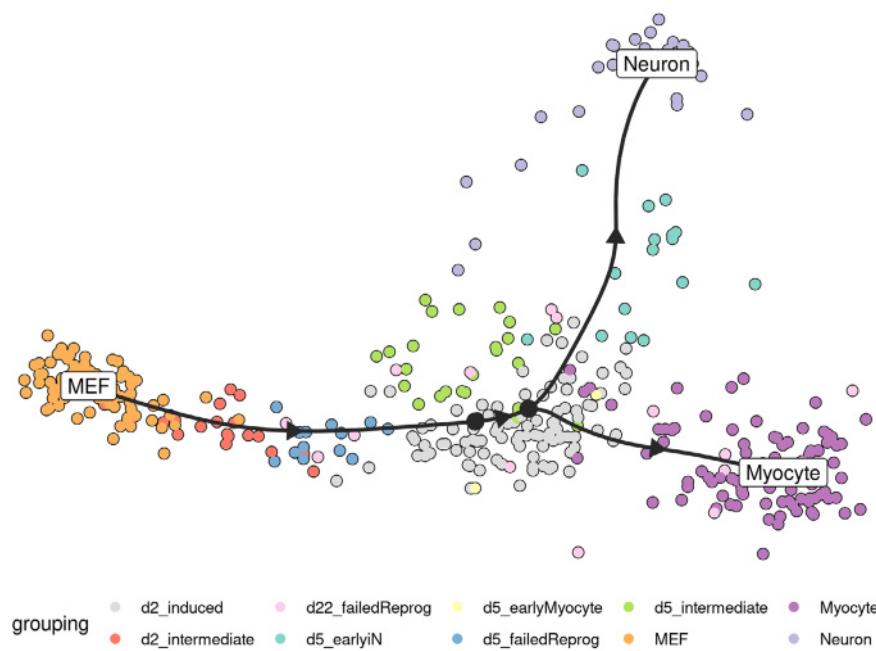
Figure 212. Example of a bifurcating trajectory, automatically constructed for a data set of reprogramming fibroblasts from ref. [1906].

detail please see Chapter VI Section 2: Automated data analysis: Automated FCM cell population identification and visualization), then the proportions of cells within each subset and additional measurement parameters for each subset can easily be calculated, and the analysis would be problem-free. However, problems arise when there is overlap between subsets, based on the parameters of the specific measurement, e.g., fluorescence or light scatter intensity.

Those performing DNA histogram cell-cycle cytometric analysis are accustomed to resolving the problem of overlap as this occurs at the G1:S and the S:G2+M interfaces of the histogram. G0, G1, S, and G2+M are phases during cell division and obviously have different DNA contents, which can be measured with DNA reactive fluorescent dyes by flow or image cytometry. A considerable body of analytical work has addressed this problem [1909–1912]. In contrast, relatively little such work has been carried out in immunocytochemical studies, where the time-honored method of resolving histogram data has been to place a delimiter at the upper end of the control and then score any cells above this point as (positively) labeled. This approach can lead to large errors and is best overcome by improvements in reagent quality to increase the separation between labeled and unlabeled populations in a cytometric data set, or by the addition of extra independent measurements like additional fluorescence parameters [1795]. But, this may not always be possible and any subset overlap needs to be resolved. See Chapter VII Section 1.2 that discusses data analysis and display. The tools available to resolve any subset overlap in mixed populations require an understanding of (i) probability, (ii) the type of distribution, (iii) the parameters of that distribution, and (iv) significance testing. An overlapping immunofluorescence example is shown below in subsection 3.6-Immunofluorescence example Table 91. Additionally the use of statistical methods for drawing conclusions at the level of data, derived from cytometric measurements, is essential, but not covered here specifically.

2.2 Probability

Qualitative statements on probability are not very useful for quantitative analysis of cytometric data, which are affected by variability of sample collection, sample preparation, sampling, measurement imprecision, and variability in manual or automated data analysis. Statistics allows us to derive quantitative probabilities from cytometric data, especially as many data points are generally measured in FCM. Probability designated with a p-value has a measurement range of zero, or absolutely impossible, to unity, or absolute certainty. Very few events, if any, occur with a p-value at these extremes. "The sun will rise tomorrow," is a statement with a p-value very close to unity. In contrast, "Man, one day, will run the 100 meters in 1 second," has a p-value of zero.

2.3 Types of distributions

There are many distributions but those most commonly encountered in the biological sciences are the Gaussian, binomial, and Poisson distributions.

2.3.1 The Gaussian distribution. The Gaussian distribution (error function, "normal" distribution) is a bell-shaped curve symmetrical about a mean value with the following formula

$$Y = \frac{1}{\sigma\sqrt{2\pi}}e^{-(X-\bar{X})^2/2\sigma^2} \tag{1}$$

where σ is the SD and $\bar{X}$ is the mean of the distribution. Algorithms, based on the Gaussian distribution, have been used extensively for cell cycle analysis by FCM [1912].

2.3.2 The binomial distribution. The binomial distribution is concerned with occurrences of mutually exclusive events and is given by the formula

$$(p + q)^n = 1 \qquad (2)$$

where p is the chance of something happening and q is the chance of that same something not happening. If we throw two regular six-faced dice, n in the binomial equation is 2 and this expands the equation to $p^2 + 2pq + q^2 = 1$. The chance of getting 2 threes on a single paired throw is $p^2 = (1/6)^2$, the chance of getting one three and any other number is $2\ pq = 2 \times 1/6 \times 5/6$ and the chance that neither die will be a three is $(5/6)^2$. Hence, the total probability is given by $((1/6) \times (1/6)) + (2 \times 1/6 \times 5/6) + ((5/6) \times 5/6))$, which sums to unity. Rosenblatt et al. describe the use of a binomial distribution based algorithm to optimize flow cytometric cell sorting [1913].

2.3.3 The Poisson distribution. The Poisson distribution is used to describe the distribution of isolated events occurring in a continuum, originally formulated by Poisson [1914]. A good example is the number of cells passing the analysis point in the cytometer per second. Clearly you cannot ask the question of how many cells did not pass the analysis point per second, so neither the Gaussian nor the binomial distributions can handle this type of problem. In order to use the Poisson distribution all we need is z, the average number of times the event occurs within the continuum, where the probability of observing the event n times, $p(n)$, is given by

$$p(n) = 2^n \mathrm{e}^{-z}/n! \qquad (3)$$

where $n!$ is factorial n. The notation for the whole distribution that sums to unity is

$$P = \sum_{n-0}^{n-\infty} Z^n \mathrm{e}^{-s}/n! \qquad (4)$$

The Poisson distribution is important in cytometric cell sorting purity for investigating coincidence in which there could be a possibility of two or more cells being in the analysis point simultaneously. Poisson statistics also applies to the measurement of low intensity signals, where just a few photons contribute to the measurement, and to the counting of rare subpopulations, discussed in some more detail below.

2.4 Distribution parameters

These include measurement of (i) central tendency namely, the mean, percentiles, median, and mode, and (ii) dispersion parameters namely, the mean deviation, variance, SD, and CV, wherein the last of these, the CV of limited statistical significance, is the SD divided by the mean.
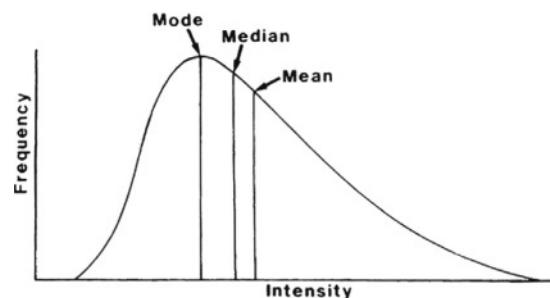
Figure 213. Measurements of central tendencies for cytometric intensity histograms. The curve is an ideal distribution, showing key measurements. Cytometric intensity histograms span a finite intensity range with a noisy curve and frequently with off-scale events at the lower and/or upper end(s) of the scale. Generally the median is the most robust measure, because the mean is heavily influenced by off-scale events and the mode by noise.

2.4.1 Central tendency. The goal of many cytometry measurements is the determination of the expression level of a given marker in a cell and its distribution in a cell population. The mean of a distribution is the sum of all the data points divided by the number of the values in the distribution. The *median* is the point in the distribution where half the data lie on either side; it is also known as the 50th percentile, the point, where 50% of the data has been accumulated. Twenty-fifth percentiles and 75th percentiles are also determined for distributions. The *mode* is the maximum frequency. But, this is an unreliable measurement of central tendency in cytometry for two reasons. First, the mode is meaningless if this is located in the first or last channel of the histogram. In some cases cytometry histograms have many off-scale events, which makes the fist or last channel in the histogram the highest point. Second, even though a large number of cells will have been sampled, the distribution is not continuous, due to the analog-to-digital conversion (ADC) step, i.e., intensity values are used as indices for incrementing histogram channels (e.g., 0 to 1023), and counting statistics as the SD of a count in a discrete "channel" is equal to the square root of the count (more below in Chapter VII Section 2.7: Rare cell analysis). Therefore, typical unsmoothed cytometry histograms are often very noisy. Any "noise" around the mode will give an erroneous result. The relationship between these parameters is shown in Fig. 213.

2.4.2 Dispersion parameters. Just as central tendency gives a measure of the overall "average" difference between Gaussian distributions, the dispersion parameters give a measure of the different spreads within and between those distributions.

The mean deviation is given by $\Sigma(X - \bar{X})$.
The variance, mean squared deviation, is given by $\Sigma(X - \bar{X})^2$.
The SD is given by $\sqrt{[\Sigma(X - \bar{X})^2]}$.

2.5 *Significance testing*

The central axiom in statistical theory is that the variance of the sum or difference of two independent and noncorrelated random variables is equal to the sum of their variances. These tests are designed to give a measure of how different two or more distributed populations might be.

The most commonly asked questions in cytometry are (i) is there more than one subset? and (ii) if there is more than one, how many cells are in each? This is far too naive a perspective, and with the statistical tools available we should be asking the following:

1. Is there more than one subset?
2. If there is more than one, how far "separated" are they?
3. What is the significance of that separation?
4. If the subsets are significantly separated, then what are the estimates of the relative proportions of cells in each ?
5. What significance can be assigned to the estimated proportions?

The statistical tests can be divided into two groups. (i) Parametric tests include the *SE of difference*, *Student's t-test*, and *variance analysis*. (ii) Non-parametric tests include the *Mann-Whitney U-test*, *Kolmogorov–Smirnov test*, and *rank correlation*.

2.5.1 *Parametric tests.*
These may best be described as functions that have an analytic and mathematical basis where the distribution is known.

2.5.1.1 *Standard error of difference.*
Every cytometric analysis is a sampling procedure as the total population cannot be analyzed. And, the SD of a sample, *s*, is inversely proportional to the square root of the sample size, $\sqrt{N}$, hence the SEM, $SE_m = s/\sqrt{N}$. Squaring this gives the variance, V_m, where

$$V_m = s^2/N \qquad (5)$$

We can now extend this notation to two distributions with $\bar{X}_1$, s_1, N_1, and $\bar{X}_2$, s_2, N_2 representing, respectively, the mean, SD, and number of items in the two samples. The combined variance of the two distributions, V_c, can now be obtained as

$$V_c = (s_1^2/N_1) + (s_2^2/N_2) \qquad (6)$$

Taking the square root of Equation (6), we get the SE of difference between means of the two samples. The difference between means is $(\bar{X}_1 - \bar{X}_2)$ and dividing this by $\sqrt{V_c}$ (the SE of difference) gives the number of "standardized" SE difference units between the means; this standardized SE is associated with a probability derived from the cumulative frequency of the normal distribution.

2.5.1.2 *Student's t-test.*
The approach outlined in the previous section is perfectly satisfactory if the number of items in the two samples is "large," as the variances of the two samples will approximate closely to the true population variance from which the samples were drawn. However, this is not entirely satisfactory if the sample numbers are "small." This is overcome with the *t*-test, invented by W.S. Gosset, a research chemist who very modestly published under the pseudonym "Student" [1915]. Student's *t* was later consolidated by Fisher [1916]. It is similar to the SE of difference but, it takes into account the dependence of variance on numbers in the samples and includes Bessel's correction for small sample size. Student's *t* is defined formally as the absolute difference between means divided by the SE of difference:

$$\text{Student's } t = \frac{|\bar{X}_1 - \bar{X}_2|\sqrt{N}}{\sigma} \qquad (7)$$

When using Student's *t*, we assume the null hypothesis, meaning we believe there is no difference between the two populations and as a consequence, the two samples can be combined to calculate a pooled variance. The derivation of Student's *t* is discussed in greater detail in ref. [1917].

2.5.1.3 *Variance analysis.*
A tacit assumption in using the null hypothesis for Student's *t* is that there is no difference between the means. But, when calculating the pooled variance, it is also assumed that no difference in the variances exists, and this should be shown to be true when using Student's *t*. This can first be addressed with the standard-error-of-difference method similar to Section 2.5.1.1 Standard Error of Difference, where Var_s, the sample variance after Bessel's correction, is given by

$$Var_s = \left\{ \frac{(n_1 \times s_1^2) + (n_2 \times s_2^2)}{n_1 + n_2 - 2} \right\} \times \left\{ \frac{1}{2n_1} + \frac{1}{2n_2} \right\} \qquad (8)$$

The SE of the SD, SE_s, is obtained as the square root of this best estimate of the sample variance (equation (8)). This is now divided into the difference between the two sample deviations.

The second method of addressing the variance analysis is to use the variance ratio [1918], designated the *F*-test by Snedcore [1919]. *F* is calculated as the ratio of the greater variance estimate of sample variance to the lesser estimate of sample variance. After Bessel's correction, we get the best estimate of the variances, σ^2, as,

$$\sigma^2 = Var_s \times \left\{ \frac{N}{N-1} \right\} \qquad (9)$$

2.5.2 *Nonparametric tests.*
These rely on ranking methods when there is no known, or suspected, distribution that can be assigned to samples being analyzed.

2.5.2.1 *Mann–Whitney U.*
This problem was originally addressed by Wilcoxon [1920] and was later refined by Mann and Whitney [1921]. Consider two sets of data, the X-group and Y-group, containing 5 and 4 values respectively; these are illustrated in Table 84. These values have been ordered according to

Table 84. Comparison of two data sets X and Y in a rank analysis[a]

Y-group			y_1			y_2		y_3	y_4
X-group	x_1	x_2		x_3	x_4		x_5		
Values	3	7	9	15	23	31	36	44	51
Rank	1	2	3	4	5	6	7	8	9

[a]The values have been ordered according to magnitude in the third row with their rank position in the last row. The populations from which the data were drawn are shown in rows 1 and 2, the Y-group and X-group, respectively. It is clear that the Y-group is tending to be more to the right (greater magnitude) than the X-group, and the question is whether this arrangement could have occurred purely on a random basis. Reproduced with permission from ref. [1917].

magnitude in the third row with their rank position in the last row. The populations from which the data were drawn are shown in rows 1 and 2, the Y-group and X-group, respectively. It is clear that the Y-group is tending to be more to the right (greater magnitude) than the X-group, and the question is whether this arrangement could have occurred purely on a random basis. To do this, we determine how many x-values lie to the right of every y-value and sum the result to get U_y for the Y-group. There are three x-values (x_3, x_4, and x_5) to the right of y_1 and one x-value to the right of y_2, thus Uy sums to four. The same process is now carried out for the x-group to give U_x equal to 16. For small sample numbers, this procedure is satisfactory but it can be prohibitively time consuming for large samples for which the following expressions are used.

$$U_y = NxNy + \frac{Ny(Ny-1)}{2} - T_y$$

$$U_x = NxNy + \frac{Nx(Nx-1)}{2} - T_x \quad (10)$$

Nx and Ny are the number of values in the X- and Y-groups, respectively, and T_y and T_x are the sums of the rank positions for the Y- and X-groups, respectively.

If the X- and Y-values are randomly distributed in the rank, the sum of the rank position T has a mean value of T and a variance of σ_T^2 given by the following expressions:

$$\bar{T}_x = \frac{Nx(Nx+Ny+1)}{2} \quad \text{and} \quad \bar{T}_y = \frac{Ny(Nx+Ny+1)}{2} \quad (11)$$

These values of $\bar{T}_x$ and $\bar{T}_y$ will be identical if Nx and Ny are equal, but the variance, σ_T^2, will be the same irrespective of the numbers in each group and is given as

$$\sigma_{T^a} = \frac{NxNy(Nx+Ny+1)}{12} \quad (12)$$

If both samples are large, >20, we take the values of T and $\bar{T}$ associated with the smaller of the pair of U-values, in this example the Y-group, to calculate the Z-statistic as follows:

$$Z = \frac{|T_y - \bar{T}_y|}{\sqrt{((NxNy(Nx+Ny+1))/12)}} \quad (13)$$

The numerator in equation (13) represents the difference between the values of T for the Y-group and the mean, $\bar{T}$, that

Table 85. Part of the Mann–Whitney probability table example for the X-group size of Table 84 ($N_2 = 5$)[a]

U	$N_1 = 1$	$N_1 = 2$	$N_1 = 3$	$N_1 = 4$	$N_1 = 5$
0	.167	.047	.018	.008	.004
1	.323	.095	.036	.016	.008
2	.500	.190	.071	.032	.016
3	.667	.286	.125	.056	.023
4		.429	.196	**.095**	.048
5		.571	.286	.143	.075
6			.393	.206	.111
7			.500	.278	.155
8			.607	.365	.210
9				.452	.271

[a]Reproduced with permission from ref. [1917].

would be expected if the numbers were randomly distributed within the rank structure and the denominator is the square root of the variance. Hence, Z represents the observed deviation from the mean in SD units and the associated probability can be read off from the cumulative frequency of the normal curve because, for large samples, the Z-distribution approximates very closely to the Gaussian distribution.

With small sample sizes, e.g., with less than 30 values, the Z-distribution does not approximate to a Gaussian curve, and Mann–Whitney computed the probabilities associated with U-values for different-sized samples. These data are arranged in tables for N_2 = 3, 4, 5, 6, and so on and within each table there are sample sizes for N_1 = 1, 2, 3, 4, 5 and so on versus the U-values and associated probabilities for the N_2 and N_1 sample sizes. The example for N_2 = 5 is shown in Table 85. The sample size of the X-group (N_2 in Table 85) is 5, and the associated U-value is 4. The number of data points in the Y-group is also 4, and hence, the probability that this distribution of data points in Table 84 is different can be read off as 0.095 in Table 85 and does not reach "significance" at the 1:20 level (0.05).

2.5.2.2 Kolmogorov–Smirnov statistic. In the Kolmogorov–Smirnov (K–S) statistic, D is a measure of the maximum vertical displacement between two cumulative frequency distributions. The one-tailed test compares an experimentally derived distribution with a theoretical cumulative frequency distribution and, the two-tailed test compares two experimentally derived distributions (for more detail, see Chapter 6 in ref. [1922]). In any biological system, a test sample should always be compared with a control, i.e., the two-tailed test, and this was first used in FCM by Young [1923].

The cumulative frequency distributions containing n_1 and n_2 cells in the control and test samples respectively can be calculated as follows for $i = 1 \leq 256$,

$$F_{n1}(i) = \sum_{j=1}^{j=i} f\,n1(j) \quad \text{and} \quad F_{n2}(i) = \sum_{j=1}^{j=i} f\,n2(j) \quad (14)$$

Table 86. Kolmogorov–Smirnov (K–S) statistic critical values, D_c, with their associated p-values (probabilities)[a]

D_c	1.0727	1.2238	1.3581	1.5174	1.6276	1.7317	1.8585	1.9525
p	0.200	0.100	0.050	0.020	0.010	0.005	0.002	0.001

[a]Reproduced with permission from ref. [1917].

Table 87. Hypothetical results of the same determinations from two different laboratories[a]

Sample	1	2	3	4	5	6	7	8	9	10
Lab A	.61	.23	.31	.11	.41	.19	.10	.03	.07	.17
Lab B	.54	.38	.42	.20	.36	.27	.21	.11	.14	.12

[a]Reproduced with permission from ref. [1917].

These cumulative frequencies are now normalized to unity and the null hypothesis is assumed (i.e., both distributions are samples derived from the same population) where the probability functions $P_1(j)$ and $P_2(j)$ that underlie the respective frequency density functions (the histograms) $f_{n1}(j)$ and $f_{n2}(j)$ are samples assumed to be drawn from the same populations so that

$$P_1(j) = P_2(i), \quad -\infty \leq j \leq +\infty \quad (15)$$

The D-statistic is computed as the maximum absolute difference between the two normalized cumulative frequency distributions over the whole of the two distributions, where

$$D = \max_j |f_{n1}(j) - f_{n2}(j)| \quad (16)$$

As with the Mann–Whitney U, there is a variance, Var, associated with the assumed common population from which the two samples, containing n_1 and n_2 items, respectively, are drawn. This is given by

$$Var = \frac{(n_1 + n_2)}{n_1 \times n_2} \quad (17)$$

The SD s can now be found by taking the square root of this relationship, then dividing D by s gives D_{crit}, where

$$D_{crit} = \frac{\max |F_{n1} - F_{n2}|}{\sqrt{((n_1 + n_2)/(n_1 \times n_2))}} \quad (18)$$

This type of relationship, in which we divide a difference by a measure of dispersion, has been seen in all the other statistical tests described previously. Two-tailed critical D_c for large samples, along with their probabilities, are shown in Table 86.

2.5.2.3 Rank correlation. Correlation between two or more sets of measurements can be determined with Spearman's rank correlation coefficient [1924]. This enables an objective assessment to be made regarding the consistency between paired laboratory results as in the purely hypothetical data shown in Table 87.

When we look through these data, we find that both laboratories score sample 8 with the lowest results and in both cases these

Table 88. Ranking of the data from Table 87 with rank differences (d, and d^2)[a]

Sample	1	2	3	4	5	6	7	8	9	10
Lab A	10	7	8	4	9	6	3	1	2	5
Lab B	10	8	9	4	7	6	5	1	3	2
Rank difference, d	0	−1	−1	0	2	0	−2	0	−1	3
d^2	0	1	1	0	4	0	4	0	1	9

[a]Reproduced with permission from ref. [1917].

are ranked 1. Sample 9 from lab A has the next lowest value (0.07) and is ranked 2 but, it is sample 10 (0.12) that is ranked 2 in the lab B series, and these ranking positions are shown in Table 88.

In terms of ranking alone, the two laboratories agree exactly for only four of the ten samples, namely 1, 4, 6, and 8. Spearman's rank correlation coefficient R is given by the expression:

$$R = 1 - \left\{ \frac{6\Sigma d^2}{n^3 - n} \right\} \quad (19)$$

Σd^2 is the sum of the squared rank differences and n is the number of samples; in our particular example, these values are 20 and 10, which gives $R = 0.8787$. This coefficient was designed to have a value of $+1$ if there is perfect ranking agreement and -1 where there is total ranking disagreement.

This value of 0.8787 for R would suggest that there is fairly close agreement between laboratories and where there are ten or more samples being compared we can use Student's t to assess the significance of comparison:

$$\text{Student's } t = R \times \sqrt{((n - 2)/(1 - R^2))} \quad (20)$$

which gives $t = 5.2$ with eight degrees of freedom associated with $P < 0.01$, which is highly significant and suggests there is close agreement between laboratories. However, this does not tell us anything about the quality of the "intersample" agreement from the two laboratories. This can be addressed by analysis of the differences in results from the laboratories as shown in Table 89.

The mean difference $\bar{X}$ is calculated by summing the data in the difference row and dividing by n, the number of samples, which gives -0.052. If there are no differences between laboratories, this mean value should not differ significantly from zero since any random differences should cancel out.

The variance, s^2, is calculated from the convenient relationship as

$$s^2 = (\Sigma X^2 / n) - \bar{X}^2 \quad (21)$$

where ΣX^2 is equivalent to $\Sigma d^2 = 0.0824$ yielding $s^2 = 0.0055$. After Bessel's correction and using equation (6), we get Student's $t = 2.1$. This value of t, with nine degrees of freedom, does not quite reach the 5% probability level and we can conclude that the inter-laboratory differences are not significant. However, in a quality control exercise such as this, we would be justified in setting more stringent statistical criteria. If we now take a probability level of 0.1 for magnitude discrepancies between laboratories,

Table 89. Differences between values from Table 87 by subtracting Lab B results from those of Lab A

Sample	1	2	3	4	5	6	7	8	9	10
Lab A	0.61	0.23	0.31	0.11	0.41	0.19	0.10	0.03	0.07	0.17
Lab B	0.54	0.38	0.42	0.20	0.36	0.27	0.21	0.11	0.14	0.12
Sample difference, d	0.07	−0.15	−0.11	-0.09	0.05	−0.08	−0.11	−0.08	−0.07	0.05
d^2	0.0049	0.0225	0.0121	0.0081	0.0025	0.0064	0.0121	0.0064	0.0029	0.0025

which would be reasonable as we know they should be getting the same results, we must conclude there is something suspicious occurring in the generation of the results, which would require further investigation.

2.6 An example of immunofluorescent staining in cytometry

Figure 214 shows a histogram representation of weak staining of a small population. Statistical analysis of this datum must ask a number of questions.

First, is there any difference between these two datasets? This is addressed with a K–S analysis, which reveals that there is a maximum normalized vertical displacement of 0.0655 at channel 37 with 8976, N_1, and 8570, N_2, cells in the control and test sample, respectively (Fig. 215). K–S statistic gave $P < 0.05$, suggesting there is a statistical difference between the two datasets at the 1:20 probability level. The remaining data shown in this figure will become apparent later.

Second, can we establish the "meaning" of the discernible shoulder in the lower histogram of Fig. 214? This is addressed analytically using a concept derived from mechanics; namely, taking moments about a point. Imagine a weightless beam with two different weights hanging from the beam that will balance according to equation (22)

$$W_1(B - \bar{X}_1) = W_2(\bar{X}_2 - B) \qquad (22)$$

where W_1 and W_2 are the "weights" hung from the beam, B is the balance point, and $\bar{X}_1$ and $\bar{X}_2$ are the distances of the respective weights from the balance point, B. On rearranging equation (22), we get

$$B = ((W_1\bar{X}_1) + (W_2\bar{X}_2))/(W_1 + W_2) \qquad (23)$$

Let us suppose that the distances $\bar{X}_1$, $\bar{X}_2$, and B are known for a normalized total mass of unity, where $W_1 + W_2 = 1$. We can now calculate the relative proportion of W_2 by replacing W_1 with $(1.0 - W_2)$ in equation (23) and simplifying to give

$$W_2 = (B - \bar{X}_1)/(\bar{X}_2 - \bar{X}_1) \qquad (24)$$

The "weight" in equation (24) that will now be referred to as "labeled cells," is defined by three distances namely, $\bar{X}_1$, $\bar{X}_2$, and B. $\bar{X}_1$ is the mean of the control unlabeled fraction, B is the mean of the test sample containing labeled and unlabeled cells,
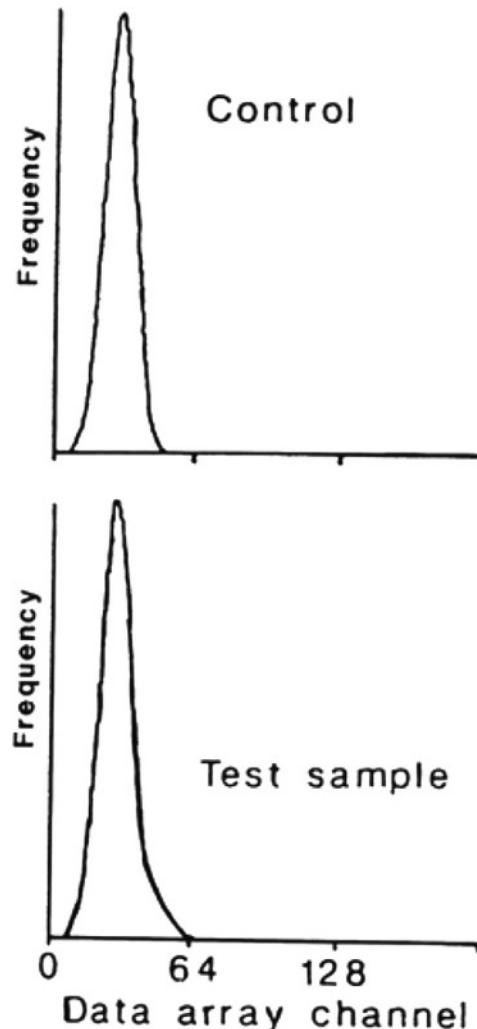
Figure 214. The histogram representation of fluorescence from a weak staining of a small (rare) population. The upper histogram shows an unstained control. A small shoulder from the staining of the rare population is visible in the lower histogram. Reproduced with permission from ref. [1925].

and both of these can be obtained directly from the experimental data. We now need to obtain $\bar{X}_2$, the mean of the labeled fraction, as follows:

It has been shown in ref. [1925] that the mean of the distribution obtained by subtracting the N_2 cumulative frequency from the cumulative frequency of N_1, is independent of the number of cells in N_1, and the mean of the subtracted distribution D_m, depicted in
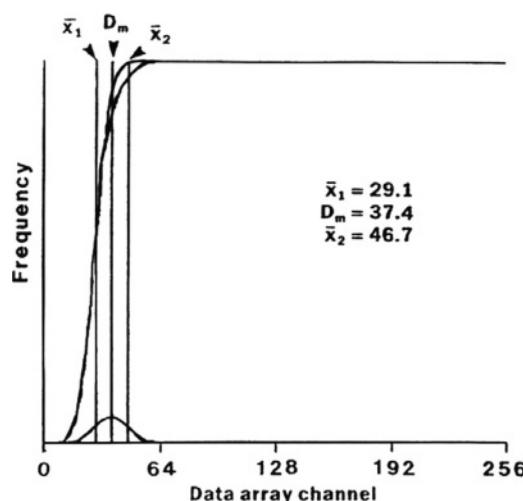
Figure 215. Cumulative frequencies from the two histograms in Fig. 214 and difference. Details on the calculation of $\bar{X1}$, $\bar{X2}$, and D_m are described in the text. Reproduced with permission from ref. [1925].

Fig. 215, is exactly halfway between the means of N_1 and N_2. However, this applies to a continuous distribution and all cytometric distributions are not continuous due to the ADC conversion and a half channel correction must be applied to give the mean of the N_2 distribution as

$$\bar{X}_2 = (2.0 \times (D_m + 0.5)) - \bar{X}_1 \tag{25}$$

All the data have now been derived to calculate the proportion of cells in the N_2 distribution as W_2 from equation (24) by substituting the $\bar{X}_2$ of equation (25) and simplifying to give

$$W_2 = (B - \bar{X}_1)/(2.0 \times (D_m + 0.5 - \bar{X}_1)) \tag{26}$$

The data depicted in Fig. 214 were analyzed according to this ratio analysis of means to give $X_1 = 29.1$, $D_m = 37.4$ and $\bar{X}_2 = 46.7$ as shown in the figure and the predicted proportion in N_2 was 0.08. These data are shown in Fig. 216 where the control, test sample, and the predicted labeled fraction are labeled in the figure. The test sample results are shown Table 90. We now have to ask if this result is reasonable and what significance can be placed on the result.

2.6.1 K–S analysis.   The cumulative frequency distributions of the control and test sample were re-analyzed over a range of ±3 SD about the mean of the predicted labeled distribution, X_2. With the number of cells involved, the K–S analysis showed that the two cumulative frequency distributions over this ±3 SD range had
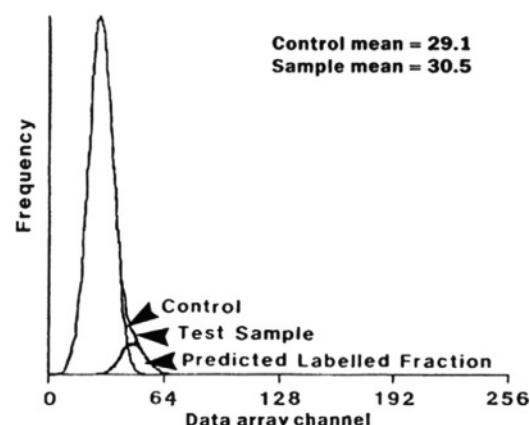
Figure 216. Result of the histogram analysis. The two original histograms and the calculated stained population are shown with population means. Reproduced with permission from ref. [1925].

a probability of being different at the 99% confidence interval, $P < 0.01$.

2.6.2 Student's t.   The results from the analysis of the test sample shown in Table 90 were also submitted to Student's t analysis (Chapter 7 in ref. [1917]). This gave $t = 65.58$ with 8568 degrees of freedom, $P < 0.001$.

Hence, we can present the results in probabilistic terms by saying the analysis was compatible with two subsets with means separated by 17.6 channels containing 92% and 8% of the population at the 99% confidence interval.

This analysis should only be used for symmetrical data sets with constant, or near constant, variance, and these data were chosen for illustration as they conformed to this condition. However, there are a number of other factors that should be considered, including positive skew that tends to be minimized with log-amplification as discussed elsewhere [1925]. Nevertheless, this analysis goes some way to producing a more statistically convincing method of presenting results of immunofluorescence data.

2.7 Rare cell analysis

Flow cytometric analysis of cell samples is often applied to characterize subsets of very low frequency, ranging from 1% to less than 1 ppm. In those cases, it is very important to understand the inherent variation when randomly sampling a small number of events. As mentioned above, the SD of a count is the square root of the number, e.g., when sampling from a cell/particle

Table 90. Results of the immunofluorescence analysis example, data from Watson [1925]

Test sample	Number of cells	proportion	Mean	Standard deviation
Unlabeled	7889, N_1	0.92	29.1,′X_1	6.69, s_1
Labeled	681, N_2	0.08	46.7,′X_2	7.13, s_2

Table 91. Illustration of potential interpretation problems, when counting extremely rare cells

Run	1	2	3	4
	11	11	9	9
	15	13	9	10
	15	13	11	7
	10	7	9	8
	5	8	9	7
Mean	11.2	10.4	9.4	8.2
St.Dev	4.1	2.8	0.9	1.3
Overall mean:	9.8			
Overall St.Dev:	2.7			

[a]The table shows integers from four different runs with five measurements each from a random number generator. This could reflect a study with four conditions with five replicates each. The table indicates a trend from run 1 to 4; however, all of the data is from the same distribution, and there is no change from runs 1 to 4 (generated with ROUND(NORMINV(RAND(),9,3),0) with a mean of 9.0 and an SD of 3.0 in MS Excel. The cumulative mean and SD from the 20 values approximate the real population numbers well.)

suspension several times a volume, which should contain four cells per particles the SD will be 2, the CV 50%.

If enough cells in the full sample are available, cytometric data acquisition should be continued until a number of cells is reached in the rare subset that assures the desired measurement precision—a feature available in most commercial data acquisition software. If not enough cells are available, care must be taken to not come to conclusions, which are not supported by the limited precision associated with limited acquisition.

Table 91 shows an example, where four consecutive determinations indicated a progressive change of a property; but all of the data are from the same distribution, and there is no change from series 1 to series 4 (the data is from a simulation with a Gaussian random number generator with a mean of 9.0 and a SD of 3.0). This issue is discussed in more detail in a paper by [196].

In certain cases the limitation of the imprecision of counting small numbers of cells can be overcome. For example, one can evaluate a bulk cell separation technology by dispensing a known number of cells into a sample, subjecting the sample to a separation process, and analyzing the total volumes of the resulting fractions.

2.8 Measurements of central tendency. Arithmetic mean, geometric mean, median, and mode

In order to accurately measure the average of a population, measurements of central tendency such as the arithmetic mean, geometric mean, median, and mode can be used. The arithmetic mean, often referred to as just mean, is the sum of all events divided by the total number of events. The geometric mean is the nth root of the product of events. The median is the middle point in a number series, while the mode is simply the most common number. These measures of central tendency are applied to fluorescence intensity, generated by a flow cytometer to give the MFI,

geometric MFI (gMFI), or MdFI. The mode is rarely appropriate as a single measure of central tendency and is not commonly used in this context.

2.9 MFI, gMFI, MdFI which to use?

Which of these measurements is appropriate is dependent on the distribution of the data itself. The MFI is appropriate where data has a normal (Gaussian) distribution. The gMFI is appropriate where data has a log-normal distribution, i.e., the logs of the raw data are normally distributed, but is influenced by outliers and cannot account for any values below zero that may be created during compensation. The median, on the other hand, is robust, i.e., it is not affected by the data distribution and is not strongly influenced by outliers. In practice, most fluorescence data collected on modern flow cytometers, is skewed and conforms to an approximately log-normal distribution, indicating that the gMFI and MdFI may be better choices than the MFI. For example, in the logarithmic number series 1, 10, 100, 1000, 10 000; the arithmetic mean is 1700, the geometric mean is 100, and the median is 100, indicating that the arithmetic mean is not appropriate for estimating the average of log-normally distributed data. While no one measurement may be suitable for all purposes, generally speaking, the MdFI is the most reliable and, as a result, is the basis for many machine calibration methods (BD Cytometer Setup and Tracking Application Guide V3.0 [41, 48]). However, while the MdFI is advantageous due to its insensitivity to extreme outlier events and skewness, this loss of sensitivity may also prove a disadvantage where outliers are of interest, in which case the gMFI is also a valid option. Use of MFI, despite its enduring popularity, is likely to be inappropriate unless the raw data is confirmed to have a normal distribution.

2.10 Pitfalls

Measurements of central tendency are useful to estimate the average of a unimodal population. However, when data is bimodal or multimodal (has two or more distinct populations), measurements of central tendency may be misleading. For example, if the data has two equally numbered populations centered at 0 and 1000, the average would be 500 despite there being no events in this area. In these situations, it is more effective to use gating to enumerate the percentage of cells in the different peaks rather than relying on measurements of average fluorescence.

3 Analysis presentation and publication (MIFlowCyt)

3.1 Overview

Basic research is often criticized to be non-reproducible. To ensure reproducibility of cytometry data, it is the aim of journals to express standards that data should be minimally provided to
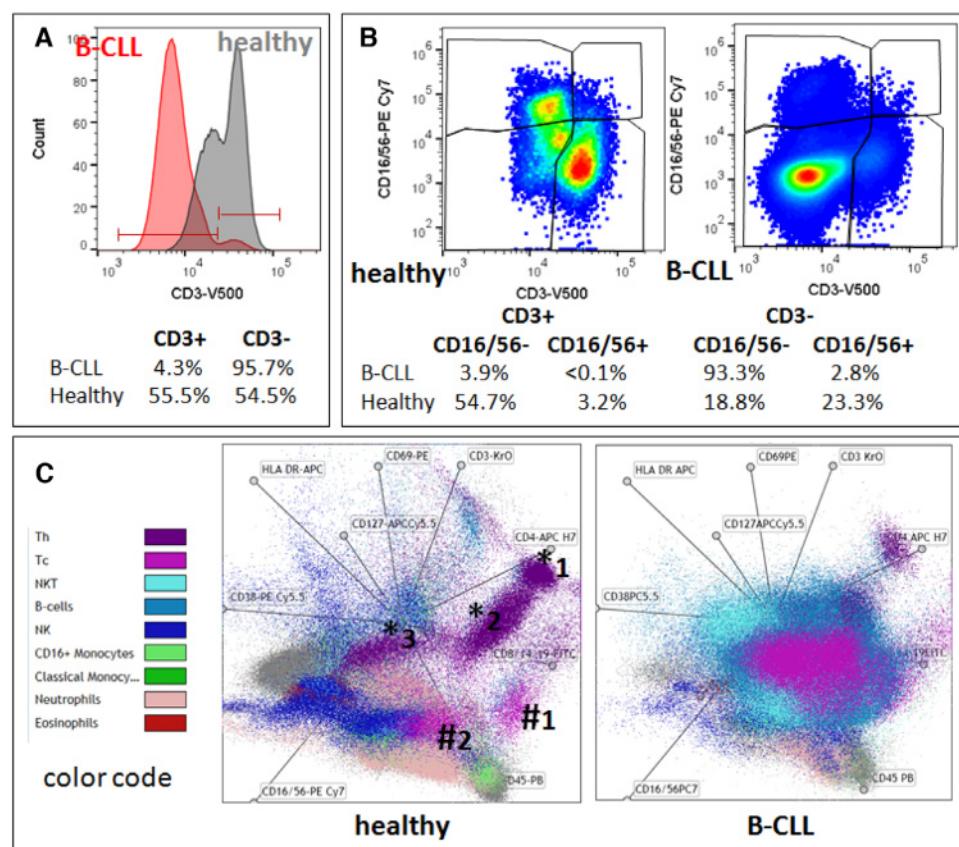
Figure 217. Uni-, bi-, and multi-parameter presentation of flow data. Comparison of two gender and age matched patients: a healthy one (67 years) and a patient with B-CLL (64 years). (A) 1D-Histogram presentation of CD3 expression on lymphocytes (red, B-CLL; grey, healthy), (B) 2D-Dot-plot presentation of CD3 expression on *x*-axis versus CD16/56 expression on *y*-axis, (C) multivariate presentation of expression of 13 different antibodies on ten colors (OMIP-023 [1926]) for nine different leukocyte subsets in a radar-plot. Abbreviations: B-CLL, B-cell chronic lymphocytic leukemia; Th, CD4+ T-helper cell; Tc, CD8+ cytotoxic T-cell; NK, natural killer cell. Data analysis: (A and B) FlowJo, V10.2; (C) Kaluza, Beckman-Coulter, V 1.1.

understand the paper and in the best case to reproduce these data. This section describes the MIFlowCyt standard, gives examples for good and current data visualization, and highlights the necessity of providing example data for the readers.

3.2 Introduction

The complexity of cytometric data requires careful consideration of how to display results in scientific presentations and publications in order to make them understandable "at a glance." To easily reproduce published cytometric experiments, the used methods and results need to be described and presented comprehensively.

By FCM, thousands of cells are acquired within seconds by gaining information of their scatter properties and expression of multiple markers. Manual analysis of these multidimensional and complex data requires special software skills, gating knowledge, time, and can be quite laborious. Manual gating is still considered by most cytometrists to be the "standard," although semi-automated algorithms exist (see Chapter VII, Sections 1 and 2). Some basic rules for data visualization allow presenting these data in a directly comprehensible format.

3.3 Principles of the technique

What data should be minimally displayed to fully understand research papers? First of all, the full gating strategy should be displayed so that data analysis strategy used is obvious to the reader. This display should also include the position of positive and negative controls and essential statistical information, such as the percentage of cells in the region or gate or event count. Axis legends should include the marker (e.g., antigen) and the dye used, and show the scaling (log/lin; Fig. 217). Simple experiments with one or two colors can be presented in 1D histograms; this allows easy comparison of the expression level of the marker of interest for different samples (positive, negative controls, and samples) in overlay histograms (Fig. 217A). Within these histograms, positive and negative populations can be easily distinguished from one another. For better comparison, the histograms should be normalized, i.e., the maximum values set to 100%.

More common is a display using 2D pseudocolor density plots (Fig. 217B). Plotting the expression of two markers against each other allows a more precise distinction of double negative, single positive, and double positive, as well as weakly or strongly labeled subsets. The 2D-plot presentation also helps to identify errors of

automated compensation for manual correction, as needed. Multicolor experiments are normally analyzed by a sequential gating strategy. A full gating strategy is performed in a step-by-step procedure (examples can be found in ref. [1926, 1927]). To analyze discrete populations such as T-cell subsets within blood samples in a first step CD45 negative red blood cells (CD45 expression vs. scatter) are excluded. Furthermore, only lymphocytes are gated based on their scattering (FSClow, SSClow). By exclusion of CD3 negative B cells (CD16/56$^-$) and NK cells (CD16/56$^+$) only CD3 positive cells will be analyzed in the next step. By the expression of CD16/56, NKT-cells (CD3 vs. CD16/56) can be excluded from T-cells. In a final step, CD4$^+$ T-helper cells and CD8$^+$ cytotoxic T cells (CD4 vs. CD8) can be analyzed. This process is strongly driven by a priori expectation and knowledge of the scientist analyzing the data. That means the scientists will expect, for example, to analyze within the T-cells at least four subsets: CD4$^+$ CD8$^-$ T-helper cells, CD8$^+$ CD4$^-$ cytotoxic T-cells, CD4$^+$ CD8$^+$ immature T-cells and CD4$^-$ CD8$^-$ mature T-cells. But within these subsets additional T-cell subsets might be neglected that will be taken into count by automated approached. Keep in mind that by using small (conservative) gates instead of overlapping gates, disease-specific cells might be excluded already in the first step of the analysis, or novel subsets might not be recognized. Analyzing data by the conventional step by step method in sequential 2D-plots has several drawbacks: for example, loss of information by the loss of rare cell subsets by pregating, and some marker combinations that might help to further subdivide a subset might not be analyzed. With the constant increase of the complexity of cytometric measurements and data (in the last year several standardized OMIP protocols with 28 colors became available; [1928]), there is also a need to develop new algorithms to analyze and visualize these complex data (see Chapter VII, Section 1.3.–1.6).

One example for a user-friendly visualization of multidimensional data at one glance is the radar plot (e.g., provided as a visualization tool in the Kaluza® software by Beckman–Coulter), which plots pregated subpopulations in a multiparameter way (Fig. 217C); this allows analysis of the heterogeneity of the pregated populations and to identify new subpopulations (For further details see Cossarizza et al. Eur J Immunol 2017, 47:1584-1797).

Besides manual analysis and their visualization, several methods exist to perform software-assisted, unsupervised, or supervised analysis [1838]. For example, using several open source R packages and R source codes often requires manual pregating, so that they finally work just as a semi-automated computational method. For identification of cell populations, for example, *FLAME* (suitable for rare cell detection based on clustering techniques), *flowKoh* (self-organizing map networks are produced), or *NMFcurvHDR* (density-based clustering algorithm) are available [1795]. Histograms (*2DhistSVM, DREAM–A, fivebyfive*), multidimensional cluster maps (*flowBin*), spanning trees (*SPADE*), and tSNE (stochastic neighbor embedding) maps are suitable visualization tools for sample classification [1795, 1838, 1929]. To find and identify new cellular subsets of the immune system in the context of inflammation or other diseases analysis in an
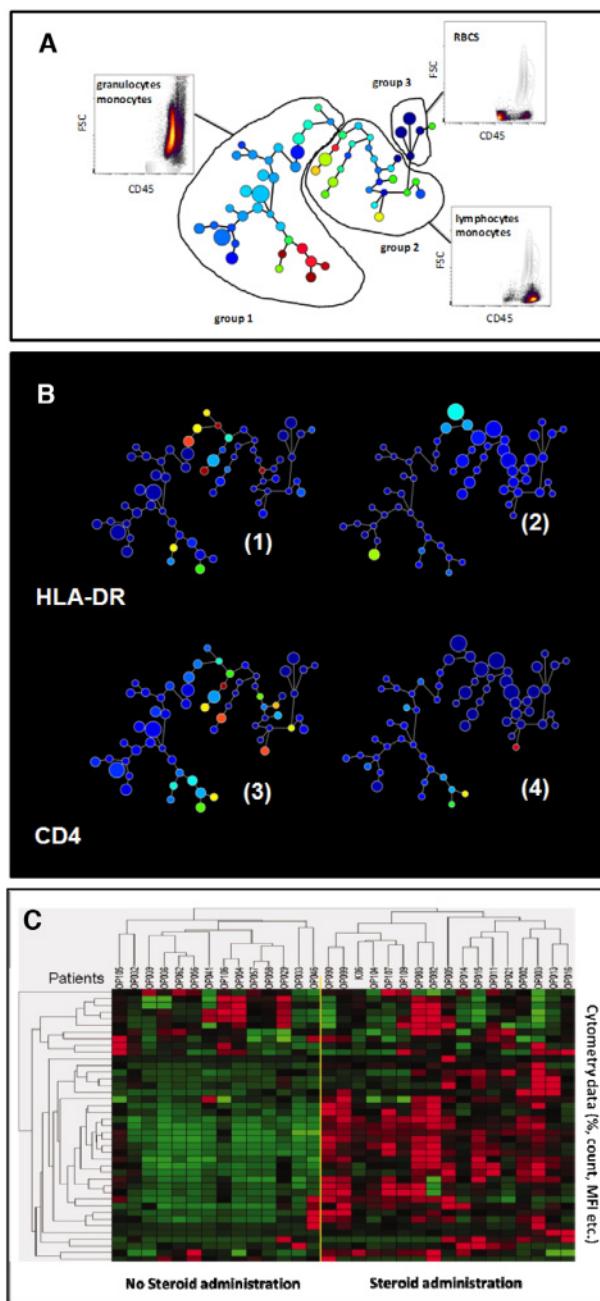
Figure 218. Semi-automated clustering and analysis of flow cytometric data by SPADE (Qui et al., 2011) and hierarchical clustering. (A) SPADE tree display and CD3 expression on blood cells from two male patients. Dot-plot analysis reveals groups of cluster (circles) belonging to the same cell type. (B) Color codes correlate with expression level from low (blue) to high (red) and size of the nodes correlate with cell frequencies. Data of (A) and (B) are from a healthy (B1 and 3; 67 years) and a B-CLL patient (B.2 and 4; 64 years). (C) Hierarchical clustering of flow-cytometry data to visualize and distinguish immune response of pediatric patients (columns) who underwent elective cardiovascular surgery with (left of the yellow line) or without synthetic steroid administration (right) before surgery. PBL were immunophenotyped at day 1 after surgery. FCM parameters (MFI and cell counts) are displayed horizontally. Red indicates relative upregulation and green relative downregulation of the respective parameter. Reproduced with permission from ref. [1931]. (SPADE analysis by Cytoscape, V 3.4.0, Nolan Lab; hierarchical clustering by free software Genes@Work).
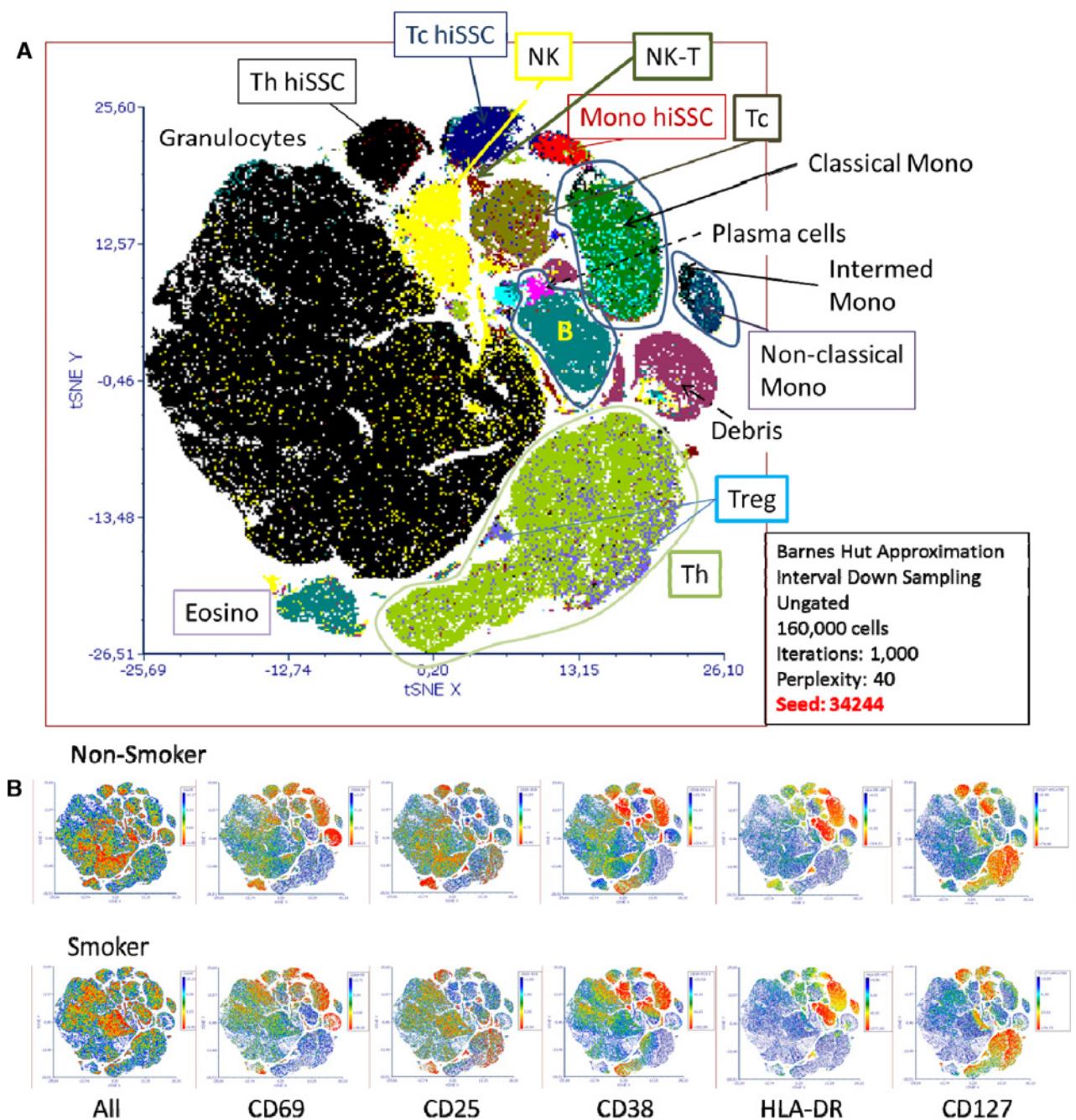
Figure 219. Semi-automated analysis of flow cytometry data by tSNE. (A) 16-Part differential of ten individuals (five smokers, five nonsmokers) by OMIP-23 (ten colors, 13 antibodies; [1926]) showing the location of regular T-helper (Th) and cytotoxic T-cells (Tc) with high side scatter (Th hiSSC, Tc hiSSC), T-regulatory cells (Treg), natural killer (NK), and NK-T cells on the tSNE map. Bottom left box contains information for calculating the tSNE plot. (B) Heat map display of expression level of 5 activation markers in nonsmokers and smokers and distribution of cell count (All). Scale bars right of each tSNE plot show color coding of fluorescence intensity or cell count levels. (Data of individuals from the LIFE study [1934]; data analysis by FCS Express V.6, De Novo Software.)

unsupervised manner, such as by SPADE (spanning-tree progression analysis of density-normalized data [1804]) can be a better approach.

SPADE is a density normalization, agglomerative clustering, and minimum-spanning tree algorithm that reduces multidimensional single cell data down to a number of user-defined clusters of abundant but also of rare populations in a color-coded tree plot. In near vicinity, nodes with cells of similar phenotype are arranged. Therefore, related nodes can be summarized in immunological populations determined by their expression pattern. SPADE trees are in general interpreted as a map of phenotypic relationships between different cell populations and not as a developmen-

tal hierarchical map. But finally SPADE tree maps help to (1) reduce multiparameter cytometry data in a simple graphical format with cell types of different surface expression, to (2) overcome the bias of subjective, manual gating, to (3) resolve unexpected, new cell populations, and to (4) identify disease-specific changes (Fig. 218A,B). Other ways for comprehensive analysis and display of complex data by unsupervised approaches can be found in ref. [1930] and include Heatmap Clustering (Fig. 218C, for details, see captions and ref. [1931]), viSNE/tSNE (Fig. 219 new) and Phenograph, and FlowSOM [1932] (Chapter VII, section 2, 3). Fig. 219 shows an example of tSNE display of immunophenotyping data (10 colors, 13 antibodies) from 10 individuals (five smokers, five nonsmokers). The position of the various leukocyte types in the tSNA map can be color coded based on their antigen expression from 2D dot-plots (Fig. 219A). As displayed in the Fig. 219A, sufficient information should be provided to reproduce the calculations. Then (Fig. 219B) for example antigen expression levels for the different patient groups can be visualized (for more detail see captions).

Data reduction and display aids also improved visualization of between group differences and generally different tools are used in combination to achieve this aim. A useful tool is hierarchical clustering cytometry data indicating by color differences [1931]; Fig. 218 and/or color intensity differences [1933] highly discriminative parameters. These can then be further visualized using SPADE or tSNE display. There are several new tools such as Phenograph, FlowSOM and others for patient or experiment group discrimination that are explained in detail elsewhere (Chapter VII, Section 1).

Finally, irrespective of which dimensionality approaches are used, it is essential that all preprocessing information is provided (pregating procedures, data normalization; see Chapter VII, Section 1.2) either with the graphs or as supplementary material. Also, authors should provide information of the calculation of the SPADE. tSNE, etc. graphs (e.g., n iterations, perplexity, n nodes, Fig. 218, Fig. 219). Also software tools used have to be named and in case of own development also made available for the readership.

Next to the appropriate illustration of flow cytometry data it is crucial that the essential details of flow experiments are displayed in order to allow others to accurately reproduce the experiments. Lack of reproducibility is of great concern in biomedical research and rough estimates say that up to 50% of the results published are not reproducible, meaning billions or trillions US$ of funding money lost [1935]. To reduce this problem, the MIBBI (Minimum Information for Biological and Biomedical Investigations) project was launched in 2008 [1936]. Its goal is to provide comprehensive checklists for different types of experiments so that all essential information for repeating the experiment is provided. Relevant for flow cytometry is MIFlowCyt (Minimum Information about a Flow Cytometry Experiment) [39]. These standards were defined by an international group of cytometry experts from bioinformatics, computational statistics, software development, and instrument manufacturers, from clinical and basic research. With this information, cross-experiment comparisons are possible. Several scientific journals, first of all *Cytometry Part A*, have adopted these regulations, but also journals from the Nature Publishing Group have accepted these standards. MIFlowCyt-compliant manuscripts should have a checklist table containing information on reagents, instrumentation, and experimental setup, including information on controls, gating strategies, among others (for details see ref. [39], Table 92). Importantly, it is required that original primary list-mode data are made publicly available in an open access data base such as the FlowRepository (See Chapter VII Section 4 Data repositories: Sharing your data). This allows others to analyze published data by alternative methods and better understand the published material. In the following manuscripts, you can find examples for MIFlowCyt checklists with different MIFlowCyt score values and original FCS data in the FlowRepository for Flow [1937, 1938] and mass cytometry [1939]. Since October 2018 MIFlowCyt compliance and reposition of original data are mandatory for *Cytometry Part A* publications [1940].

Although several *MIFlowCyt*-compliant manuscripts for flow data have been published in *Cytometry Part A*, comparable guidelines for image cytometry (e.g. *MIImaCyt*) have not been adapted so far [1941, 1942]. In order to improve the quality of polychromatic flow cytometry, a special publication type for multicolor flow cytometry protocols, Optimized Multicolor Immunofluorescence Panels (*OMIP*), was developed in *Cytometry Part A* [1943]. The central issue in multicolor flow cytometry is to demonstrate that the developed multiplexed panel has been optimized by testing different reagents and reagent combinations. Until now, over 50 different OMIPs have been published with the aims of (1) reducing the time to develop similar panels and (2) providing a starting point for the development of new panels, or (3) for optimizing existing ones. OMIPs present unique reagent combinations, document the developing progress, explain the final choice

Table 92. Important provided data for cytometric publications. (*part of MiFlowCyt)

Data set	Details
Sample/specimen	*Type*, source*, source treatment*, taxonomy, age*, gender*, phenotype*, genotype*, location**
Sample treatment	*Analytes*, Ab clone*, names/numbers*, manufacturer*, catalogue numbers**
Reagents	*Concentration, purity*
Controls	*Quality Control Measures*, FMOs*, Positive/negative control**
Instrument	*Manufacturer*, model*, configuration*, settings*, detector voltages*, optical filters**
Data analysis	*List-mode data file*, compensation*, gating*, flow repository data access code**

and should be useful to a wide range of readers. OMIPs are by nature MIFlowCyt compliant.

To avoid biases by manual analysis of high complex flow, data software tools are available that work partly operator independent. This stresses also the importance of the reproducibility in complex, (semi)-automated data analysis [1944]. O'Neill and Brinkman have suggested that certain data besides compensation, gating details and mathematical algorithms, should be shared for reproducible FCM bioinformatics [1945]. One major aim is to make FCM data easily accessible to the users by open-access databases for flow data (e.g., *FlowRepository*), as well as the code sources. A series of data sets have already been provided by the *FlowCAP* (Critical Assessment of Population Identification Methods) project, comparing different mathematical models and automated methods for analysis. The cytometry community has already made great steps toward reproducible research by standardizing instrumentation, measurement, and data analysis, but still looks forward to optimize the reproducibility in different cytometry fields.

3.4 *Advantages*

The major advantage of the MIFlowCyt concept is that each reader of MIFlowCyt-compliant manuscripts can access all necessary data so that experiments can be reproduced step by step as easily as cooking recipes, because the focus is on the transparency of scientific data.

Advanced data analysis tools offer the advantage of objective data evaluation that works completely user-independently. To be able to reproduce these analyzes, essential data such as the seeding cell must be provided.

3.5 *Pitfalls*

In order to be able to evaluate data by means of automated methods, it is necessary to pre-purify the data beforehand; this includes, for example, normalization or downsampling of data. On the one hand, these processes are time consuming and on the other hand, they can also be sources of error (data loss, data distortion), since a minimum of expert knowledge is necessary for the correct execution. The output of the visualized data subsequently requires a high manual effort to e.g. identify the populations. If high data sets are to be evaluated, the user is often limited to the computing power of the used device. And since not every user has a supercomputer with high computing power available, long times for the calculation can be expected or even multiple crashes of the software might be obtained before the optimal result is achieved. Since automated data visualization methods (SPADE, SNE, etc.) are stochastics, small changes in the initial algorithm setting will results in (sometimes totally) different maps or trees. For reproducibility, it is therefore important to document the exact setup of the algorithm (example see Fig. 219A).

Also, it is not always easy to meet the MIFlowCyt requirements. For example, the provision of original data is required.

This can sometimes face a privacy problem. First, it is necessary to anonymize patient data, which in turn may require the presence of special software tools, which are however in the most cases open access. Sometimes the studies may be designed in such a way that it is not allowed to share data with third parties or to make it publicly available, so that the MIFlowCyt/Flowrepository requirements cannot be sufficiently met in all cases of manuscript submission.

4 Data repositories: Sharing your data

Scientific research is more data intensive and collaborative than ever before. Transparency and public availability of well annotated data is crucial for independent validation, verification, and extending research from prior results [1946]. The availability of primary data is therefore increasingly required by national policies, international regulatory bodies, scientific journals as well as research funding agencies [1947–1951].

In both, fluorescence-based and mass-based FCM, primary data is generally represented by FCS files that contain a matrix (table) of expression values of all measured "channels" (characteristics) of all particles (cells) analyzed by the instrument. These files should be properly annotated as per applicable domain-specific guidelines. In FCM, such guidelines are represented by the Minimum Information about a Flow Cytometry Experiment (MIFlowCyt) [39]. The MIFlowCyt standard includes recommendations about descriptions of the specimens and reagents included in the FCM experiment, the configuration of the instrument used to perform the assays, and the data processing approaches used to interpret the primary output data. In additional, the biosharing.org portal (Minimum Information for Biological and Biomedical Investigations (MIBBI) project) [1936] should be checked for extra requirements that may be applicable. MIBBI is a common portal to a group of nearly 40 checklists of Minimum Information for various biological disciplines.

Depositing data in a public repository is generally the recommended, and increasingly the required way of sharing FCM data. Below, we introduce four public repositories suitable for FCM data: Cytobank [1826, 1851] (http://www.cytobank.org/), FlowRepository [1941, 1952] (https://flowrepository.org/), ImmPort [1953, 1954] (https://immport.niaid.nih.gov), and ImmuneSpace [1955] (https://www.immunespace.org/). An overview with technical notes and highlighted features is provided in Table 93.

Cytobank is an online data analysis and management platform developed and hosted by Cytobank Incorporated. A community (basic) version of Cytobank provides free functionality including web access, data storage, experiment sharing, and basic online analysis. The Community version of Cytobank contains close to 300 public experiments (data sets). In addition, Cytobank offers paid Premium and Enterprise versions with advanced data analysis options (including SPADE [1804], t-SNE [144, 1824], and FlowSOM [1932]), better customer support, and dedicated computing resources. If your lab is using Cytobank already, then choosing its Community version presents a straightforward option of sharing

Table 93. Public repository sites: technical notes and highlighted features

Name	URLs and references	Technical notes and highlighted features
Cytobank	• http://www.cytobank.org/ • PMID: 24590675 • PMID: 20578106	• Free community version, requires registration • Web access • Advanced online data analysis options in paid versions
FlowRepository	• https://flowrepository.org/ • PMID: 22887982 • PMID: 22752950	• Free and open source, no registration required to download data • Web access, R library, FlowJo plugin • Full MIFlowCyt support • Basic online data analysis options • Integrated FCS de-identification (optional) • Recommended by Nature, Cytometry Part A and PLOS journals
ImmPort	• https://immport.niaid.nih.gov/ • PMID: 24791905	• Free, requires registration and approval • Web access • Data from dozens of assay types including cytometry • Online data analysis tools • Templates for data deposition, management and dissemination • Used mainly for NIAID/DAIT funded studies
ImmuneSpace	• https://www.immunespace.org/ • PMID: 24441472	• Free, requires registration • Web access, R library • Database and analysis engine that leverages ImmPort infrastructure • Exploring, integration and analyses of data across assays • Ontology support through standards-aware data templates • Used mainly for HIPC data

your data publicly. In addition, all versions of Cytobank give you the option of sharing data privately with your collaborators. A potential drawback of Cytobank is that public datasets can be set back to private—and thus "disappear."

FlowRepository is a public repository allowing researchers to deposit, annotate, analyze, share, and publish FCM data, mainly those associated with peer-reviewed manuscripts. The repository is provided free of charge by the International Society for Advancement of Cytometry. While FlowRepository was developed by extending Cytobank's code base, the two platforms drifted apart significantly over the past 8 years. However, there are still some common aspects allowing users of one system to adapt to the other easily. While Cytobank's platform offers more advanced data analysis options, FlowRepository focuses on data sharing and annotations, including a full support of MIFlowCyt. In addition, FlowRepository works closely with several scientific journals and allows for linking data with related publications. Unlike with most other repositories, users do not need to register in order to download public data from FlowRepository. They can do so anonymously by using a web-based interface, or from within the R statistical language using the FlowRepositoryR BioConductor library, or from within FlowJo using the FlowRepositoryServer plugin. At this point, FlowRepository contains over 1500 data sets from 1700

scientists and links to papers in 40 different journals. Half of the data sets are currently public and most of the remaining data are related to ongoing studies where underlying data will be released along with publication of the study results. Depositing data to FlowRepository is recommended by *Nature*, *Cytometry Part A*, and *PLoS* journals.

The Immunology Database and Analysis Portal (ImmPort) system provides an archive of immunology research data generated by investigators mainly funded through the National Institutes of Health (NIH), National Institute of Allergy and Infectious Diseases (NIAID), and Division of Allergy, Immunology, and Transplantation (DAIT). It is an extensive data warehouse containing an integration of experimental and clinical trial data generated by dozens of assay types, including 131 FCM and 24 CyTOF data sets. In addition, the ImmPort system also provides data analysis tools and it contains implicit knowledge and "best practices" for clinical and genomic studies in the form of ~50 templates for data deposition, management, and dissemination. ImmPort has been developed under the Bioinformatics Integration Support Contract (BISC) by the Northrop Grumman Information Technology Health Solutions team for the NIH NIAID/DAIT. If your research funding comes from this source and you are generating immunology data, you should deposit it in ImmPort. Immport's support for different

data types can be another reason to choose it if you are generating FCM data as well as data from different types of assays. A (free) registration and approval by DAIT is required in order to deposit and access data from ImmPort. A potential drawback of using this resource is that there can be a long delay in publication of deposited datasets.

ImmuneSpace is a database and analysis engine built by customizing the LabKey server for the Human Immunology Project Consortium (HIPC). ImmuneSpace can be used to find and explore studies, integrate, and analyze data across assays, and perform custom analysis directly from within R. ImmuneSpace takes advantage of the infrastructure already developed for ImmPort, and in many cases, ImmuneSpace provides a new interface and new complimentary tools to data that are also available in ImmPort. Currently, ImmuneSpace can be used to access several large HIPC studies with FCM and CYTOF data. The typical data submission work flow consists of data submission to ImmPort using a set of standardized data templates. If you are a HIPC participant, then your data should be deposited to ImmuneSpace; otherwise, you can still use ImmuneSpace as a valuable resource of HIPC data and analysis tools.

If you are in a clinical setting, there is one important thing to consider before you start sharing your FCM data by depositing it in any of the repositories. Besides the expression matrix, FCS data files contain a segment with keyword/value pairs. Most of the keyword values keep basic information essential for the interpretation of the raw data matrix and acquisition settings related values. These include the number of acquired parameters, their names, acquisition voltage settings, the total number of events (particles), and many other keywords as specified in the FCS data file standard. In clinical settings, some of the keywords may include information that could be used to identify the subject that was the source to generate the data in the file. Such information has to be removed prior to sharing the data file in order to comply with patient privacy requirements as specified by the Health Insurance Portability and Accountability Act (HIPAA) [1956] in the United States and similar rules enforced by regulatory agencies in most other countries. Patient data must be properly protected and cannot be publicly shared; however, those rules generally do not apply as long as the data is properly de-identified. De-identification is the process of removing identifiers that could be used to identify an individual. Identifiers include items such as patient name, social security number, other public ID numbers, date of birth, and so on as specified by HIPAA and other applicable regulations. There are several standalone tools available for the de-identification of FCS files as listed, for example, in the FlowRepository Quick Start Guide (http://flowrepository.org/quick_start_guide).

There is widespread agreement in the biomedical research community that data sharing is a primary ingredient for ensuring that science is more transparent and reproducible [1957]. While FCM has lagged behind other technologies in this area, the recent availability of public repositories provides the means to satisfy this necessary component for data sharing and its long-term stewardship.

VIII Advanced techniques in, and management of, flow cytometry

1 Imaging flow cytometry

1.1 *Overview*

Imaging FCM (IFC) adds to the power of conventional FCM by also providing spatial and morphological information within the cell. IFC combines the statistical power and phenotyping capabilities of FCM with the image analysis of microscopy. The following section is an overview to the principles of the technology, the wide range of areas of research where it is utilized, detail into the experimental workflow and analysis, and finally any pitfalls to look out for and tips that may assist researchers based on experience with the platforms.

1.2 *Introduction*

IFC was first introduced in the late 1970's with a slit-scan cytometer [1958] and since then improvements to the original concept came slowly until the development of the ImageStream (Amnis Corp; now part of Luminex Corp) [1959]. Imaging cytometry also includes technologies such as laser scanning cytometry and high-throughput microscopy where cells are interrogated in situ on a slide [1960]. This is useful in circumstances where placing cells in laminar flow would disrupt their phenotype or where spatial context within tissue is important. The slit-scan cytometry technology has also been developed into a microfluidic imaging assay [1961] and, most recently, into a microfluidic chip capable of sorting cells [1962]. This section will focus on the ImageStream IFC.

1.3 *Principles of IFC*

In IFC, the cells enter the flow cell in much the same way as conventional FCM, where they are placed in a hydrodynamically focused flow cell. Cells are then illuminated by both LEDs, for bright-field images, and lasers, for fluorescent images, and this light is collected by the objective lens. The light then intersects with a spectral decomposition element, a stack of angled wide BP filters that separate the light based on wavelength into six individual channels (Fig. 220). On the ImageStream Mk-II, these filters are 457/45, 528/65, 577/35, 610/30, 702/85, and 762/35. The major difference in IFC is the use of charge-coupled device (CCD) detectors instead of PMTs. The six separated images are collected using time delay integration (TDI) technology. The CCD converts photons from images into photocharges on a pixel array containing 256 rows. With TDI, as the cell moves through the flow cell the information collected from the pixels from the first row are integrated into subsequent rows until the light leaves the detector. The collective images' pixel content is then formed from the pixels on the last row. For this technology to be successful, the
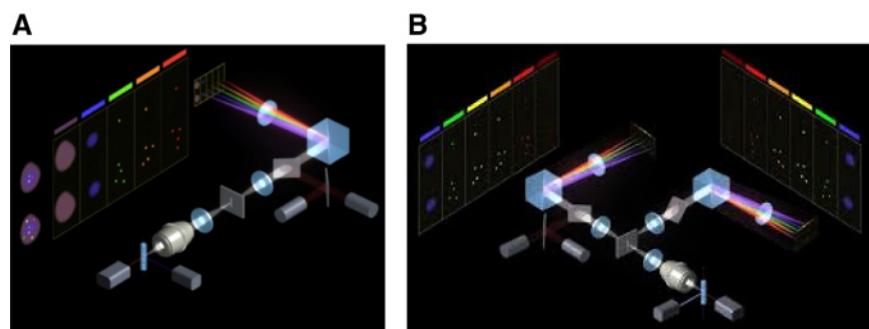
Figure 220. The optical layout of the ImageStreamX Mk-II one camera, six channel (A), and two camera, 12 channel (B) systems. Figure modified with permission from ref. [1959] and reproduced with permission from Luminex.

CCD camera must maintain synchrony with the flow cell speed. This is achieved by tracking the speed of 1 μ polystyrene beads (speedbeads) that continually run through the flow cell during operation. An advantage of using CCD detection with TDI is that cells can be running through the flow cell at high speed and will still produce a focused image thus allowing for image analysis of large numbers of cells per sample. In order to achieve 12 channels from which to image, the ImageStream Mk-II can be equipped with two CCD cameras (Fig. 220) and two spectral decomposition elements to which different lasers are directed toward, e.g., the 375, 488, and 561 nm lasers would be directed toward camera 1, while 405, 592, 642, and 730 nm lasers would be directed toward the second camera. The cameras capture sequential images from the cells allowing for fluorochromes emitting at the same wavelength but excited by different lasers to be interrogated sequentially. A bright-field image is taken on both cameras so that images can be accurately spatially correlated in analysis. To eliminate scatter from each of the lasers, narrow BP notch filters are placed in front of the cameras.

1.4 Applications

The applications of IFC are wide and varied. Not intended to be an exhaustive list, this section describes some of the most common applications to date. It is useful to remember that any research question that would be answered by microscopy or FCM could potentially be answered by IFC. The IDEAS software used to analyze ImageStream data contains a large number of possible image analysis parameter or "features" that may be applied based on the question.

IFC is particularly useful in cell signaling. Expression of proteins, such as transcription factors, that are part of signaling cascades are typically unchanged during activation. Instead, activation is determined by relocation of the transcription factor into the nucleus to initiate transcription of downstream targets. Staining the transcription factor of interest alongside the nucleus can determine activation based on "Similarity" of the two images. This information alongside the ability to simultaneously phenotype cells enables detection of heterogeneity of activation in subpopulations. Examples of cell signaling pathways studied in this way include NF-κB, NFAT, JNK, IRF, and STAT [1963–1969].

Phagocytosis has been extensively studied using this technology with phagocytes or macrophages stained for a particular marker, and the cell to be taken up stained with another [1970, 1971]. The level of "Internalization" can then be quantified. As the name suggests, internalization is performed by measuring the uptake of a protein/cell or other material into a specific cell. More recently, this feature has been utilized to determine exosome uptake into a cell [1972, 1973].

In addition to internalization, the protein/marker of interest can also be tracked to where in the cell it traffics to or whether it interacts with a specific marker in the cell. For example, dyes can be used to stain mitochondria, endosomes, and/or lysosomes and their 'Co-localization' with certain markers can be assessed. Co-localization uses a feature known as Bright Detail Similarity. This takes the brightest pixels (with a choice of radius of 3 or 7 pixels) of both markers and determines their similarity in spatial distribution, if they overlap, the value will be higher indicating co-localization [1974].

Since a bright-field image is collected by the ImageStream, changes in morphology can be studied. Chemotaxis is a good example when change in cell shape can be measured using its "Circularity." A normal monocyte would be circular, whereas one undergoing chemotaxis would have an irregular shape. The bright-field is also a useful parameter in the measurement of apoptosis. Those cells undergoing apoptosis will have a relatively higher contrast in their bright-field images than healthy cells. This can be combined with a DNA stain such as PI, DRAQ5, or DAPI where the area of the nucleus can also be measured, showing cells undergoing apoptosis with a lower nuclear area. Stains such as for caspases or Annexin-V can also be added to obtain information regarding the specific stage of the apoptotic process [1975, 1976].

Antigen presentation is central to the immune response and this event can be quantified using IFC. The antigen presenting cells and T cells are stained alongside actin. Those doublets that contain one of each cell and have a high actin expression concentrated at the "Interface" between the two are involved in the immune synapse [1977, 1978].

IFC can also be used to characterize cytotoxic immune synapses for multiparametric analysis of molecular mechanism involved in the cytotoxicity of human CD8 T-cells [668].

The extended depth of field (EDF) component of the ImageStream, where the focal plane can be expanded to 16 microns, makes analysis of small areas of fluorescence within

the cell possible. Fluorescent in site hybridization has been successfully adapted to cells in suspension, and recently with phenotyping, thus allowing measurement of numerical chromosomal aberrations in large number of cells, increasing the sensitivity of the assay [928, 1979].

A major advantage of IFC is the high volume of information available from the data acquired. Recently, researchers have begun to expand how this may be analyzed. An open source machine learning model has been developed (Cell Profiler Analyst), which can process hundreds of different features and morphological information in the thousands of data rich images [1980].

1.5 Equipment

The original ImageStream platform began with the IS-100 in 2004, followed by the ImageStream^X and most recently the third generation instrument; the ImageStream^X Mk-II. The ImageStream^X Mk-II can be configured for up to seven lasers (the standard 488, 375, 405, 561, 592, 642, and 730 nm) as well as the dedicated 785 nm laser for darkfield (side) scatter, and a dedicated 830 nm laser for autofocus. Most common configurations contain four or five of the seven lasers offered. There are 12 channels with up to ten fluorescent channels available. The Mk-II has a 40× magnification that has resolution of 0.5 μ/pixel. With the optional 60× magnification, this resolution increases to 0.3 μ/pixel making the Mk-II a potentially useful instrument in the emerging field of microvesicle research [1972, 1973]. The 60× magnification combined with the EDF function is useful when measuring small organelles such as mitochrondria, or small chromosomal spots by fluorescent in site hybridization -IS [928, 1979]. EDF extends the focal depth from 4 to 16 μ to allow for the entire cell (in most circumstances) or nucleus to be in focus [1981]. The EDF image is automatically deconvoluted in the analysis software resulting in a focused image. The Mk-II may also have the 20× magnification for larger cells/aggregates. The FlowSight (Amnis) is a more compact IFC with a 20× magnification only, with a resolution of 1 μ/pixel. It also has 12 channels but with a maximum of four lasers (the standard 488, 405, 561, and 642 nm). The lower resolution indicates that it is limited in its image analysis when compared to the Mk-II. A third cytometer from Amnis, part of Luminex Corp. is the CellStream. While not strictly an imaging flow cytometer since images cannot be saved, this instrument can save morphology data from the brightfield image during acquisition. The remaining sections will apply to the two camera Mk-II unless otherwise specified.

1.6 Experimental workflow and acquisition

For the daily start up, the ImageStream has a fluidics initialization routine and a quality control software suite (ASSIST) that checks that the instrument performance is within the factory-set margins. Any test that falls outside of these margins will be flagged and may require adjustments. Depending on the comfort level of the user, these adjustments can be made by the operator themselves or may

require intervention by the manufacturer. For the latter, in many cases, troubleshooting and making adjustments can be performed remotely by establishing an internet screen sharing connection.

For the daily shutdown, the ImageStream has an instrument shutdown routine that soaks the fluidics with bleach and rinses it with water. The shutdown procedure ends by turning the electronics of the ImageStream off and optionally, the instrument can be instructed to shut down the computer workstation as well. Both the startup and shutdown procedures, once initiated, proceed automatically without the need of operator interaction.

The same rules for panel design that are applicable to conventional FCM apply to ImageStream cytometry. The proper balance between epitope density and fluorochrome intensity needs to be observed. The use of too many tandem conjugate dyes simultaneously should be avoided to reduce cross-excitation problems by multiple lasers. Single color controls need to be prepared for multicolor panels. Note that the volume of sample loaded can be as low as 20 up to 200 μL. Rule of thumb is to prepare the same cell number as would be prepared for conventional FCM; commonly between 0.5 and 1 x 10^6 cells per sample if possible. Since the standard sample acquisition rate is 1.2 μL/min, which is 20 nL/s, a concentration of 10^6 cells/mL would therefore only yield 20 total events/s. Therefore, following the staining procedure samples should be resuspended in 50 μL instead of 500 μL as is common in conventional FCM to achieve a much higher cell density; the higher the cell density, the faster the event rate. However, be careful not to exceed a cell density above ∼30 × 10^6 cells/mL since this may lead to cavitation/bubble formation and loss of laminar flow (see Pitfalls section). When a sample is loaded, the INSPIRE acquisition software displays a volume gauge that shows how much acquisition time is left.

The single color controls are acquired with the bright-field LEDs and scatter laser off but with the full complement of lasers that are used for the experimental samples on and set at the laser outputs that will be used for the experimental samples. The number of events needed to be acquired for single color controls is low, commonly between 500 and 1000 positive events.

When desired, compensation can be applied during acquisition but this would only be necessary, for example, if acquisition gates are used based on a fluorescence intensity signal that may suffer highly from spectral overlap from a neighboring fluorochrome. For most applications, post-acquisition compensation is recommended.

During acquisition, acquisition gates can be set with the options to collect the desired number of events to include only events within the gate or include all events with the acquisition time determined by the number of events defined within the set acquisition gate. When setting the laser intensities saturation of the intensity signal should be avoided. This can be monitored with the "raw max pixel" parameter, which reaches saturation above the value of 4096.

If the detection channels of the designed panel are spread over both cameras (camera 1: channels 1–6 and camera 2: channels 7–12), and spatial correlative analysis is desired, the acquisition of two bright-fields (one in each camera) is required. The two

bright-field images are used by the software to spatially align the acquired images by each camera. The bright-field pairs can be selected not to interfere with the optimal detection wavelengths of the fluorochromes in the panel.

If SSC measurements are desired, the ImageStream uses a dedicated 785 nm laser for SSC. The SSC signal can be collected either in channel 6 (camera 1) or camera 12 (camera 2), the preferred choice of which is dependent on the fluorochromes used in the panel.

1.7 *Data analysis*

The acquisition of data with the ImageStream platform produces proprietary raw image files with a .rif extension. The data analysis is performed with the IDEAS software package. For multicolor experiments, a compensation matrix (.ctm file) is first calculated using appropriately acquired single color controls [1982]. IDEAS can then open a .rif file with a corresponding .ctm to produce a compensated image file (.cif) and a data analysis file (.daf). The IDEAS software has a separate work space area for the image gallery and one for data analysis in which single and dual parameter plots can be created using default or custom-made features and regions can be drawn on and applied to plots for which statistical information can be derived. The image gallery and the data analysis workspaces are interactively correlated in that images of interest can be clicked and their position in the data analysis plots be identified by a cursor and vice versa, that the image galley can display individual events or regional events of interest identified from the data analysis plots.

The most challenging part of introducing imaging FCM data analysis to someone who is familiar with conventional FCM is the concept of "masks"—defining the region of interest of an image (e.g., the nucleus, the cytoplasm, the immunological synapse region)—and "features"—what parameter is measured in that mask (e.g., intensity, co-localization, area). Although the software calculates numerous features related to size, location, shape, texture, and signal strength by default, these features are calculated for the default masks only. Commonly, a custom feature would be created depending on the specific experimental setup and analysis question. The software also by default will create several default masks (regions of interest), which in turn can be modified to suit the specific experimental setup and analysis question. The software has a guided analysis function (wizard) in which the user is guided through the sequential data analysis steps of creating masks and features for many of the most commonly used applications such as nuclear translocation, internalization, co-localization, immune synapse formation, and so on. A data analysis commonly follows a hierarchical gating strategy that starts with the identification of single cells that are in focus from which then various subpopulation can be derived and features can be calculated. Once the analysis strategy has been completed, this can be saved as an analysis template (.ist file) that can be applied to subsequent data files through batch processing.

Following data analysis, images can be exported as .TIFF files and data files of the parameters of interest as .fcs files, which then can be read in any FCM analysis software package. Of note, FCSExpress has the ability to directly read .daf files for use in its analysis package. It is important to be aware that any image analysis such as designing masks and features will still have to be done in the IDEAS software package before exporting as .fcs files or reading in the .daf files in FCSExpress.

1.8 *Advantages*

The obvious major advantage of imaging FCM is the added spatial information that is provided with the intensity parameters. That spatial information enables the study of co-localization, cellular redistribution, cell morphology beyond what is possible based in FSC and SSC only (e.g., shape), and verification that obtained signals are not artificial (e.g., a nuclear parameter should not be detected in the cytoplasm or cell membrane). Even with the study of events that are not dependent on spatial parameters, such as the study of exosomes, the inherent differences between sensitivity of the CCD cameras with detectors used in conventional FCM (PMTs) are advantageous.

1.9 *Pitfalls*

Not all panel designs that work well for FCM will work for imaging FCM (See Fig. 221). Among the main reasons for this are the vastly larger bandwidths for the collection filters used making spectral overlap correction more challenging; the use of so-called notch filters to block the scatter of the excitation lasers from reaching the detector that will also block the corresponding emission wavelengths of any fluorochrome; the fact that instead of the sensitivity of the detector, the output of the excitation laser is adjustable thus any intensity adjustment will affect all fluorochromes excited by the same laser; the colinear arrangement of the lasers that are directed to the same camera that prevents the application of laser-delays to discriminate between excitation sources.

Air bubbles should be eliminated from sample before loading. Bubbles can create a break in the sample volume loaded in the fluidics that the equipment will sense as a small volume (the volume detected is the first contiguous volume until a bubble is detected).

The acquisition is limited by the sample acquisition rate that in turn is dependent on the cell density of the sample. As a general rule of thumb, do not exceed a cell density of 30×10^6 cells/mL since too high of a cell concentration (dependent on size and stickiness of cells) will lead to cavitation/bubble formation and loss of laminar flow, leading to reduced sample recovery. Depending on the desired number of events to be acquired, long acquisition times may be necessary that requires one to take into consideration how long acquisition times at room temperature may affect the biological sample analyzed since no temperature control is applied once sample is taken up into injection syringe.
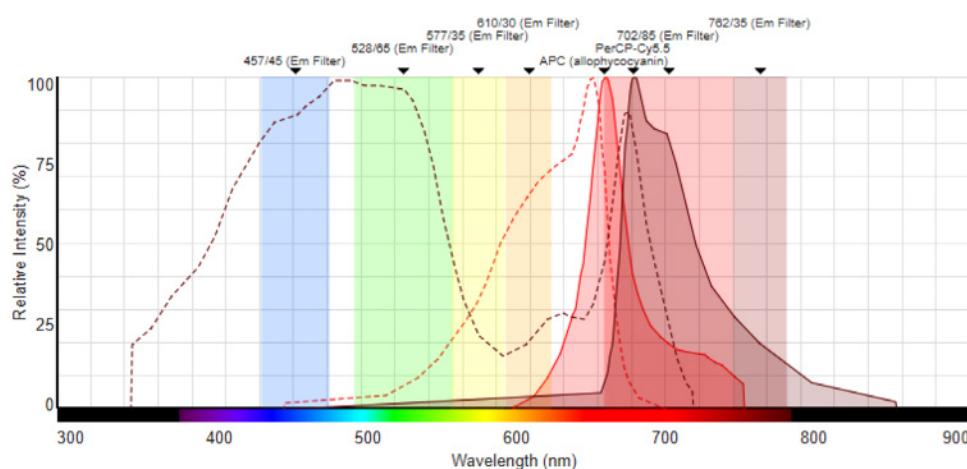
Figure 221. Excitation (broken lines) and emission spectra (solid lines) of APC and PerCP-Cy5.5 and BP emission filters used on the ImagestreamX MkII demonstrate that APC is suboptimally detected and therefore may appear less bright in a panel compared to the same panel acquired on a conventional flow cytometer that would typically be configured with a 660/20 BP. The problem is that by attempting to make the APC signal brighter by increasing the 642 laser output the cross-excitation of PerCP-Cy5.5 by the 642 laser is also increased making the compensation challenging. In this case, the use of AlexaFluor 647 instead of APC would be a suitable alternative.

1.10 Top tricks

- Data file sizes (and subsequent computer processing time) can be reduced by acquiring only images for the acquisition channels of interest to the experiment. Each omission of a channel will reduce the file size by ~10%. For example, a three-color experiment only requires the three fluorescence channels of interest, the scatter channel if desired, and two bright-field channels.

- When large numbers of cells are required for analysis, it is more efficient to acquire and analyze ten 10 000 event files than one 100 000 event file since for analysis all the information of the events within one file are stored in memory. Once the analysis is finished, the files can be merged into one if desired.

- When analysis of co-localization is required (for example, by calculating a similarity score), it is advisable to choose the fluorescent markers associated with the analysis to be on the acquisition channels within the same camera (within channels 1–6 or 7–12) for the most accurate assessment. For any other multicolor experiment, spread out the choice of fluorochromes evenly between the two camera systems.

- When studying signal transduction events (e.g., nuclear translocation of transcription factors), it is important to be aware that cell enrichment procedures that are very common to flow cytometric immunophenotyping (e.g., Ficoll density gradient separation or RBC lysis) can affect the activity of the signaling pathway especially those involved with stress response such as NF-κB.

- Displaying a graph of the raw max pixel intensity during the setup is helpful to determine that the laser powers are not set too high to a level where pixel saturation will occur (>4096).

- For accurate measurement of punctate images (e.g., spot counting), the optional EDF optics are necessary.

- The system should be flushed with 10% bleach after the use of dyes that stick to the fluidics tubing such as DAPI and PI. This is especially important when collecting the single color controls required to construct the compensation matrix.

- The algorithm used to calculate the compensation matrix for multicolor experiments requires information on all available channels. When the number of acquisition channels has been reduced during acquisition make sure that when acquiring the single color controls that all channels are being collected.

- For day-to-day consistency between ImageStream measurements, a standardized fluorescence intensity bead set should be acquired and laser settings adjusted so that the intensities are consistent between runs.

- In the experimental setup, include biological positive and negative controls, not just single-color and FMO compensation controls. This would be stimulated or unstimulated cells, i.e., in which you see populations positive or negative for the feature of interest (nuclear translocation, internalization, colocalization, immune synapse formation, etc.).

2 Barcoding in cytometric assays

2.1 Overview

Sample barcoding denotes a procedure in which distinct cell samples are stained with unique labels, pooled, and then further processed and acquired as a mixture of samples, often referred to as a "sample convolute." After acquisition of the convolute, data of the original samples are recovered by resolving the label signature used for sample tagging (Fig. 222). Barcoding allows for multiplexed analyses in FCM and mass cytometry. Importantly,
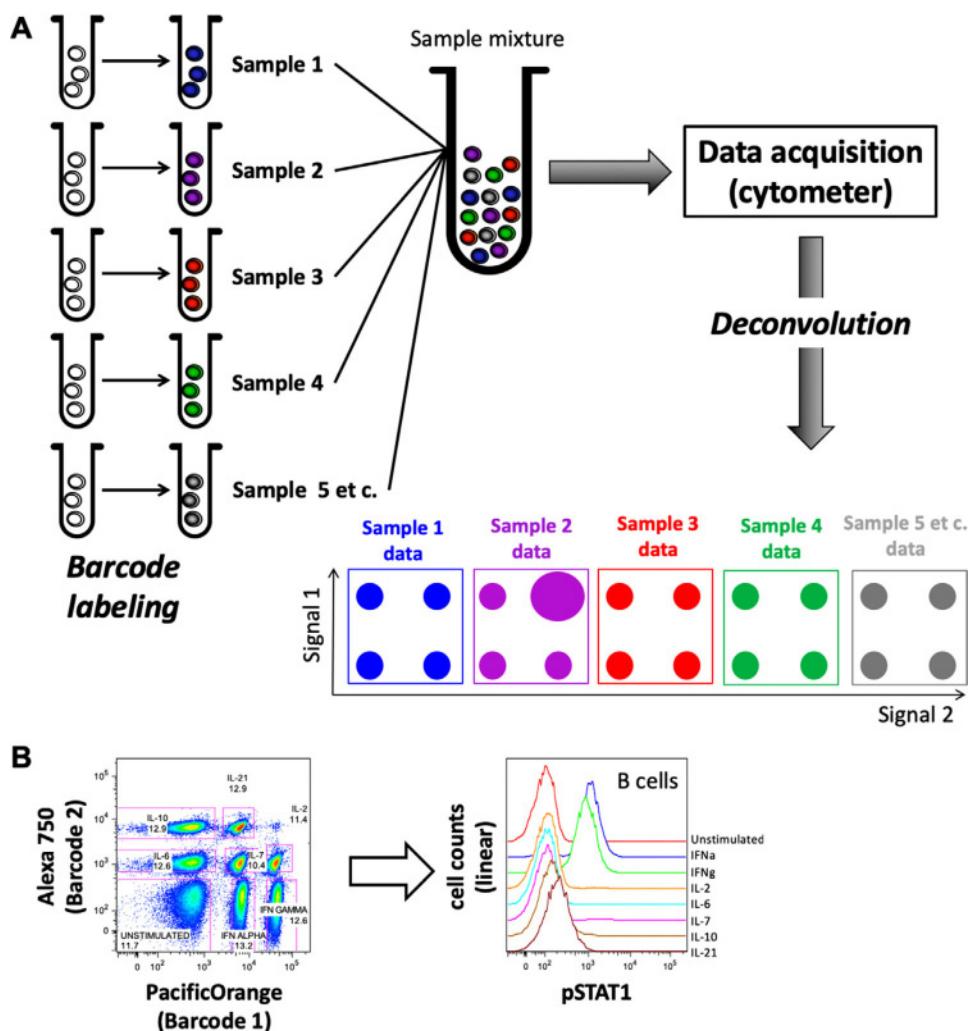
Figure 222. Workflow of cell sample barcoding for FCM and mass cytometry. (A) Schematic overview of sample barcoding. Individual reagents and reagent combinations are indicated by different color; schematic 2D plots are shown in the same corresponding colors. Individual sample properties are illustrated by staining patterns, the sample 2 plot depicting a pattern clearly deviating from the others. (B) Example of fluorescent sample barcoding for a Phospho-Flow experiment. PBMC were stimulated in vitro with eight different stimuli or controls, fixed with formaldehyde, and permeabilized with ice-cold methanol. Cells from each condition were barcoded using different concentrations and combinations of Alexa Fluor 750 and/or PacificOrange succinimidyl esters (eBioscience). Following the barcoding reaction, single samples were washed, pooled, and further stained for major lymphocyte lineage antigens and phosphorylated STAT3 in the pooled sample. After selecting CD33$^+$ monocytes by gating, the barcode was deconvoluted by gating in the two barcode dimensions. The left plot depicts the barcode labeling of all cells in that pool. Eight major populations corresponding to different stimulation conditions can be discriminated (indicated by gating). Cells of a given single sample group together as a "population" with homogeneous Alexa Fluor 750 and PacificOrange labeling, respectively. Annotations indicate stimulation conditions applied prior to barcoding, as well as the frequencies of gated populations. The similarity of these frequency values confirms that the pool contains similar amounts of cells from each barcoded condition. On the right side, the histogram overlay representation depicts pSTAT1 expression in the different stimulation conditions. pSTAT1 signal was induced in B cells treated with IFN-α and IFN-γ, but not or only minimally in the other conditions, which are visually indifferent in pSTAT1 signal from the "unstimulated" control. Data were generated by Patty Lovelace, HIMC, Stanford.

this contributes to harmonization of assay conditions, and reductions in the amount of wet work, technical errors resulting from pipetting and staining variability, and reagent consumption, as compared to preparing and acquiring multiple single samples. For example, minimizing the number of total pipetting steps means an overall reduction of pipetting error along the entire sample preparation, and since all individual samples are stained, washed, and optionally fixed and permeabilized in the very same sample tube, no sample-specific artifacts can arise from these procedures.

This results in increased data consistency and robustness. After samples have been pooled, the assay is performed in a single vial, which reduces the complexity of sample preparation work and allows for sample acquisition with only a minimal need for manual interference. Compared to running multiple single samples, no instrument cleaning cycles are necessary when acquiring one barcoded convolute, thereby reducing instrument run-time. Similarly, barcoding practically excludes sample-to-sample carry-over, which can occur during one-by-one sample acquisition by the

cytometer. Barcoding of samples is particularly useful when high data consistency is required, e.g., when shifts in median signal are used as the assay readout, such as in the case of cell signaling studies. The reduction of unwanted noise in cytometric data by sample barcoding/pooling benefits the quality of results achieved with algorithmic data analyses, which require a high degree of technical data consistency [1794, 1983].

2.2 Introduction—Benefits and caveats of cell sample barcoding

Cytometric sample barcoding was first developed as intracellular barcoding for phospho-flow applications [1984]. Barcoding was later similarly applied to mass cytometry [1985] with two barcode staining intensity levels (present/absent) for each channel (see also Chapter VIII Section 3 Mass Cytometry). More recent efforts moved barcoding to earlier steps in the sample preparation protocol to extend the number of protocol steps that benefit from sample barcoding. Behbehani et al. [1986] introduced intracellular barcoding with only minimal permeabilization using 0.02% saponin buffer. Mei and colleagues and Lai et al. [1987–1989] used differently labeled CD45 Abs to achieve cell surface barcoding of PBMCs in mass cytometry. The concept has also been transferred to FCM [1990] using Abs against murine CD4 and B220.

While barcoding of samples has many benefits, it represents an additional step in the protocol, needs to be optimized on its own, and usually occupies cytometric channels that would be otherwise available to the measurement of target analytes. Preparation of larger barcoding reagent mixtures can be time consuming and require a high degree of precision. For larger studies, and to avoid errors and variability in barcoding from experiment to experiment, one should consider automating the generation of barcode reagent mixtures [1991], and/or to prepare them in batches that can be stored frozen or lyophilized. A drawback of using sample barcoding is that any error associated with only one or a few samples in the convolute will not be discovered until deconvolution, such as the lack of cells in a sample, unexpectedly low cell number, high frequency of dead cells, excess presence of debris, or contamination events such as erythrocytes in PBMCs. Additionally, errors in barcoding can result in issues during deconvolution, which can lead to the loss of some or all data of the barcoded sample convolute. When using unrestricted combinatorial barcoding schemes (Fig. 223), mishaps during barcode preparation result in miscoding of the sample(s), while with restricted schemes, only the miscoded sample will be lost in most of the cases.

2.3 Barcoding schemes

Principally, any number of samples can be processed as a barcoded sample convolute. The capacity of a barcoding scheme is determined by the number of cytometric channels reserved for barcode markers and the number of different signal intensity levels per channel. The simplest approach is to label each sample by one unique marker (Fig. 223A). By leveraging the capacity of some barcoding reagents to stain at different signal intensities when used at different dilutions in the assay [1984], more samples can be barcoded using the same number of channels, multiplying the capacity by the number of intensity levels used (Fig. 223B). This strategy is frequently used in FCM, while barcode labeling for mass cytometry assays typically makes use of two intensity levels (stained and unstained) to achieve robust barcode labeling. This is mainly due to the fact that (i) more channels are available in mass cytometry, and that resolution-limiting, lower sensitivity channels or reagents, e.g., in the palladium range are used for barcoding to keep higher sensitivity ones for analytical readouts. In combinatorial barcoding, samples are labeled by unique combinations of multiple markers rather than by a single marker (Fig. 223C). In a scheme with two intensities per channel (i.e., "positive" and "negative"), the capacity of such a scheme is 2^n. However, using the full combinatorial capacity entails certain limitations. Different barcode labels often compete for identical binding sites, leading to different barcode marker signal intensities. For example, a sample marked by one label usually exhibits higher signal than another sample where that label is one of four different labels. In addition, nonhomogeneous barcode labeling of a sample may limit or even entirely preclude the retrieval of the original sample cells from the barcoded convolute. Doublet events, containing differently barcoded cells (intersample doublets), can mimic cells of a third sample that carries the marker combination of the other two cells combined. This is especially relevant in mass cytometry, which lacks the light scatter parameters available in FCM, which are applicable for cell doublet removal. When occupying the full capacity of a combinatorial barcoding scheme, such issues can neither be reliably detected nor corrected. Mislabeled cells will be lost for analysis, and will contaminate another barcoded sample of the convolute.

As a consequence, a restricted combinatorial scheme has been developed, in which only unique combinations, with equal numbers of barcode labels per sample are used. This strategy allows for the detection of samples erroneously labeled by more or fewer of the fixed number of labels, thereby permitting exclusion of wrongly labeled cells, as well as virtually all intersample doublets [1988, 1992]. With identical numbers of barcoding channels, the capacity of restricted schemes is significantly lower, but this is justified by the removal of doublets, especially in mass cytometry. Technically, intrasample doublets are not removed by barcoding. However, with increasing numbers of samples barcoded and pooled, the likelihood of cell doublets being intersample (removed in restricted barcoding schemes) increases relative to intrasample doublets, and leads to indirect but significant reduction of intrasample doublets [1988]. The sample accommodation capacity of restricted barcoding schemes equals $n!/(k!(n − k)!)$, with n being the number of barcode channels and k being the number of labels per sample [1992]. Pascal's triangle provides quick visual access to the sample capac-
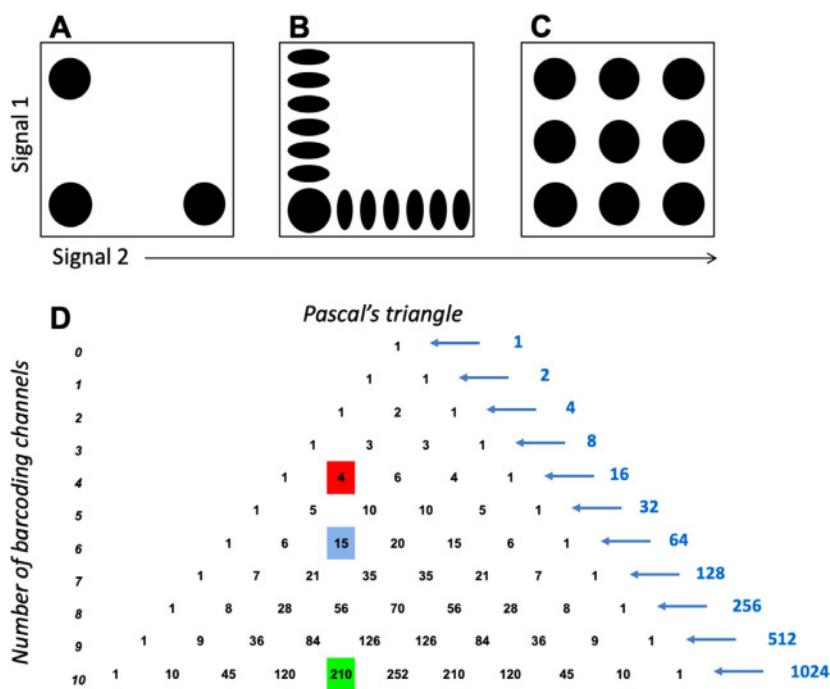
Figure 223. Barcoding schemes. (A–C) Schematic 2D dot plot representations of (A) three samples, each barcoded by presence or absence of one of two barcode labeling reagents, (B) 13 samples barcoded by gradually increasing label signals (six levels each) in two channels, or by the absence of a label, or (C) nine barcoded samples using a combinatorial barcoding scheme based on three intensity levels per channel. Circles/ellipses indicate different barcode-labeled samples. Note that the samples characterized by the absence of barcode labels (lower left populations), tend to accumulate insufficiently labeled cells of other samples and debris, and is therefore recommended not to be used for barcoding. (D) Pascal's triangle can be used as a tool for the construction of barcoding schemes. The line numbering indicates the number of barcode channels, and the ordering of numbers in each line reflects the number of labels per sample, not counting the "1." Different scenarios are indicated by the numbers highlighted. Four samples labeled by one marker each consumes four barcoding channels (red), dual barcode marker labeling in six channels (blue) can be used to barcode and pool 15 unique samples, and, in theory, 210 samples could be barcoded by quadruple combinations in ten cytometric channels (green). Blue numbers denote sums of each line that equal the capacity of unrestricted combinatorial barcoding schemes consuming the indicated number of barcoding channels.

ity of restricted and exhaustive combinatorial barcoding schemes (Fig. 223D).

2.4 Establishing and validating barcoding schemes

The effort required to establish sample barcoding for FCM or mass cytometry depends on the complexity of the desired scheme, and includes its development and validation. Development steps include the selection of the barcode scheme fitting the study's needs, the barcoding reagent type (depending on sample type, aspired protocol coverage, and the available mass/flow cytometer in combination with available dyes or mass-tags), the titration of barcoding reagents and the optimization of labeling conditions, which is especially key when more than two signal intensity levels per cytometric channel are desired. Optimal reagent concentrations and labeling conditions need to be experimentally determined, using the type and number of target cells the barcoding is finally intended for. This is specifically important when using intracellular, protein-reactive barcoding reagents, as these bind to proteins in a stoichiometric fashion, under commonly nonsaturating conditions, so that fluctuations in cell numbers (or protein content and composition), buffer composition, incubation time, and

temperature can lead to differing barcode label staining intensities, which can complicate deconvolution of data. It is important to use protein-free media for covalent barcode labeling to avoid reaction of barcode reagents with buffer proteins instead of cellular proteins. CD45 or other cell surface Ab-based barcoding operates at ideally saturating conditions, which make the barcode stainings more robust to small assay fluctuations, but leads to competition between Ab conjugates for target epitopes in the case of combinatorial barcoding, causing a decrease in barcode staining intensity depending on how many different Ab conjugates are combined on the same cell sample. It is therefore essential to incubate cells with premixed cocktails of barcoding Abs rather than adding barcoding reagents one by one to the cell suspension. Finally, cell washing conditions following the barcode labeling reaction prior to sample pooling have to be established. Careful washing of cells is required to minimize the carryover of barcode reagents into the sample pool. Remaining reagents can cause unwanted low-level labeling of all cells in the pool, which negatively impacts on cytometric resolution of barcode signals, thereby complicating deconvolution. More washing steps usually mean a better separation of barcode/labeled cells from unlabeled background but also cause greater cell loss due to removal of supernatant. In our hands, three to five washing cycles are usually sufficient to achieve a clean bar-

code staining pattern. As for covalent barcoding reagents, washing buffer should contain protein such as BSA or FCS, which serves to catch unbound barcode reagents. The barcoding reaction typically lasts 10–15 min.

Experiments such as the checkerboard test or the retrieval of sample-specific traits should be conducted, which address the reproducibility of results achieved by measuring the samples separately (without barcoding) [1985, 1987, 1992, 1993] to establish and validate sample barcoding protocols. Analyses of unique sample characteristics, such as the known lack of a certain cell population within PBMCs in individual samples, which are either run barcoded or separately must provide matching results. The checkerboard test is an extension of the above strategy that takes into account that many experiments involving sample barcoding are prepared in microtiter plates. When plotting data (e.g., cell frequencies or signal intensities) of samples with and without a known characteristic that have been plated in different orders, heatmap representations generate a characteristic checkerboard or similar pattern. It should also be confirmed that barcoding does not introduce systematic error, e.g., by interfering with the binding of specific probes post-barcoding, or due to spill-over between barcode marker and analyte-specific signals.

Barcoded sample convolutes typically contain unusually large amounts of cells that mandates titration of the post-barcoding Ab staining cocktail on the same amount of cells. Nevertheless, this generally still results in a several-fold reduction of Ab use per sample, especially if the staining volume of the convolute is kept to a minimum. Careful control of the staining volume is of course an important aspect of consistent staining results.

2.5 De-multiplexing of barcoded data

Original sample data can be extracted from barcoded, pooled samples by deconvolution through consecutive manual gating in standard FCM software, by Boolean gating for combinatorically barcoded samples [1988], or using scripts developed for that purpose [1992, 1994, 1995]. Debarcoding software can be developed in-house or retrieved from https://github.com/nolanlab/single-cell-debarcoder (accessed August 15, 2016) [1992], Premessa (https://github.com/ParkerICI/premessa), and has been implemented in the regular CyTOF software (Fluidigm). The better the cytometric separation of the barcoded samples from each other, the better the recovery of original sample cells in the deconvolution. When different cell types in a given sample show heterogeneous barcoding marker staining intensity, resulting in suboptimal cytometric separation in the barcode channels, one should consider separating those first (e.g., by gating for lineage markers), and then deconvoluting the data of different cell types separately.

2.6 Barcoding reagents

Different barcoding reagents have been explored. Usually, sample barcoding is achieved by covalently labeling cellular proteins with dyes or mass tags via reactive thiols or primary amines [1984–1986, 1992, 1996], or by Abs [1987–1990, 1997–1999]. In mass cytometry, lipid-reactive RuO_4 and OsO_4 have also been demonstrated as applicable for barcoding [1993]. Covalent labeling is usually used for barcoding of fixed and permeabilized cells, giving the reagent access to the cell interior with many more binding sites than present on the cell surface. In principle, dead cell labeling reagents that function by binding to the cellular protein content ("fixable" viability reagents) should work well as intracellular sample barcode labels. In flow cytometry, succinimidyl derivatives of fluorescent dyes such as PacificBlue[TM], PacificOrange[TM], or Alexa Fluor dyes [2000, 2001] are frequently applied [1984, 2002–2007]. In mass cytometry, thiol-reactive mDOTA loaded with lanthanide isotopes [1985, 1996], thiol-reactive BABE, or amine-reactive isothiocyanobenzyl-EDTA loaded with palladium isotopes [1986, 1992, 2008] have been used for intracellular barcoding. DNA intercalators (containing rhodium or iridium) are also candidates for intracellular barcode labels, as are cisplatins that are available in different formats holding isotopically enriched platinums [2009]. A commercial kit suitable for intracellular barcoding of up to 20 samples is available from Fluidigm. For intracellular barcoding, cells require fixation and at least "partial" permeabilization [1986] prior to barcode labeling, which limits the benefits of barcoding to subsequent steps in the protocol. Sample barcoding by Abs [1987–1989, 1998] is implemented earlier in sample preparation protocols. Because of this, more protocol steps—including surface staining of live cells—are performed on the barcoded sample convolute, facilitating the staining of fixation-sensitive markers in barcoded samples [1988]. When using Ab-based sample barcoding, choosing the right target is key. The selected Ab target should be stably and abundantly expressed by the cells of interest and should not be modified by the clinical or experimental conditions applied in the assay prior to sample barcoding. Since CD45 is expressed by all mature leukocytes circulating in blood, and particularly by lymphocytes and PBMCs at high levels, combinations of CD45-Ab conjugates have been used to barcode PBMCs in immune phenotyping experiments [1988]. For other cell types or conditions, such as immature leukocytes in thymus and BM, or malignant progenitors, using CD45 must be treated with caution, and different Ab targets might be more suitable, such as β2 microglobulin to capture leukocytes including CD45^{low} neutrophils [2010], or by combined targeting of CD298 and β2 microglobulin to additionally capture tumor and stem cells [1997]. The use of multiple noncompeting Ab targets also increased the overall barcode signal intensity. It should be kept in mind that antibody labeling of live cells can induce biologically functional responses to Ab-based sample barcoding. Barcode labeling can be applied to fixed cells, if target epitopes are fixation-insensitive, which is the case for, e.g., CD45 (Mei et al., unpublished observation). Recently, barcoding of live and fixed cells by a tellurium compound was described [2011], expanding the available options for live-cell barcoding to situations in which cell-surface markers suitable for barcoding are not known or available. Another variation is ratiometric barcoding, in which signal

intensities relative to each other rather than discrete absence or presence of signals are used as barcode labels, and for deconvolution, removing the strict requirement for cytometric separation in each individual barcoding channel. While this has been demonstrated using lanthanide-coordinated polymer dots [2012, 2013], similar scenarios can be envisioned using different reagents. Ratiometric barcoding increases the barcoding capacity, but complicates the depletion of cell doublets through the application of barcoding.

2.7 Application of cytometric barcoding to different cell types

The decision regarding using cell-surface versus intracellular barcoding is usually determined by the overall study outline and protocol. For complex immune phenotyping of live cells, cell-surface barcoding prior to fixation will be more suitable. Intracellular barcoding is often used in signaling studies in which cell activation is stopped by fixation, and therefore all cytometric stainings are performed post-fixation. Sample barcoding has been frequently applied not only to human and mouse primary leukocytes, PBMCs, and cell lines, but also to platelets [2006], and erythrocytes [2007]. The technique is often used in cell signaling analysis using FCM and mass cytometry. Since the induction of phosphorylated states of intracellular signaling mediators is usually characterized by shifts in staining intensity/signal, which can be small and can therefore be affected by technical tube-to-tube variations, barcoding of sample aliquots that underwent different stimulation conditions and their pooling for joint acquisition and analysis is often employed to protect against such error and resulting misinterpretation. Fluorescent and/or mass-tag barcoding has been employed in B cell signaling studies [2014] and various other cell signaling studies [2001, 2004], in the characterization of the effects of pharmacological inhibitors on primary mouse and human immune cell subsets [1985, 2003], in the mapping of myeloid cells in mice [2008], in stem cell research [1992], and also in clinical immune monitoring [2015].

3 Mass cytometry

3.1 Overview

Mass cytometry takes advantage of metal-conjugated Abs and other metal-containing probes for cell characterization that are detected by time-of-flight mass spectrometry, providing a cytometric platform that is able to assess up to 135 parameters, ∼50 of which are being used. It facilitates high-dimensional single-cell cytometry, especially in experimental setups where fluorescent spillover and autofluorescence are limiting in conventional FCM. This chapter outlines the principles, specifics, applications, advantages, and bottlenecks and of mass cytometry, and outlines workflow details promoting its successful implementation.

3.2 Introduction

Since its introduction in 2009 [2016], mass cytometry (or Cytometry by Time-Of-Flight technology, CyTOF) has pioneered a new era of high-dimensional single-cell analysis, surpassing the limits set by the availability of spectrally resolvable fluorochromes in conventional FCM [1849, 2017]. The innovative concept of mass cytometry is the use of stable rare earth metal isotopes of very high isotopic purity coupled to Abs or other target-specific probes for labeling of single-cell suspensions. These probes are characterized by and detected based on the metals' mass/charge ratios by inductively-coupled plasma time of flight mass spectrometry [2018]. Thereby, it is comparatively easy to perform single-cell cytometric experiments with currently more than 50 parameters in a single measurement in which typical obstacles inherent to fluorescence-based cytometry, such as spectral overlap/compensation and autofluorescence are absent or have only minimal, and manageable, impact.

3.3 Mass cytometry in biomedical research

Mass cytometry is ideally applied to research requiring high parametrization at single-cell resolution, e.g. for resolving cellular heterogeneity in complex mixtures of cells (such as blood or tissue cells); complex phenotypes of isolated cell types (such as T-cell subsets according to intracellular cytokine expression and chemokine receptor expression) [561, 1850, 2019]; or when a maximum of information is to be extracted from a given, limited sample, such as from certain cell cultures, fluids, tissue biopsies, children's or certain patients' blood samples [1688, 2015, 2020–2023]. While mass cytometry is able to assess many parameters from a single cell sample, the information gained by high parametrization needs to be balanced against the limited sample transmission efficacy of mass cytometry.

Metal-labeled Abs used in mass cytometry largely resist the methanol treatment that is used for permeabilization of cells in order to detect phosphorylated states of intracellular signaling mediators. Therefore, mass cytometry is a sought-after tool in cell signaling studies [1849, 1985, 2015]. Mass cytometry also facilitates large-scale immune monitoring and drug effect screening in clinical/translational research and systems immunology [1849, 1985, 2024]. To date, mass cytometry has been performed not only on leukocytes from different species including mouse, man, and nonhuman primates [2025], but also on cell lines and bacteria [2026, 2027], and has been used to track metal nanoparticles [2027, 2028]. Metal-containing polystyrene or Ab capture beads [1994, 2029] are used as internal standards in mass cytometry measurements and could potentially be modified to work as capture beads for serological analysis using the CyTOF platform, similar to fluorescence-based Luminex technology.
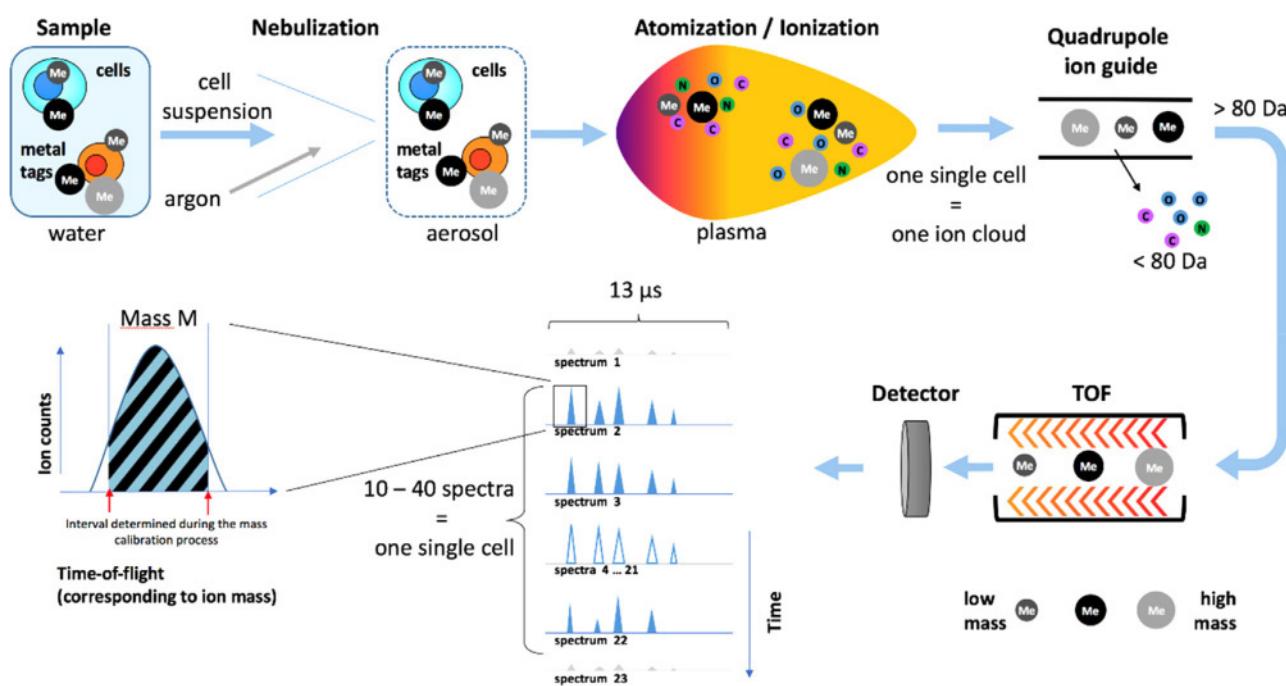
Figure 224. Schematic overview of a mass cytometric measurement. A suspension of cells stained with different rare-earth-metal-conjugated Abs (metal, Me, different sizes reflect different isotopically enriched metals) is injected into the CyTOF instrument. First, an aerosol of single-cell-carrying water droplets is generated by spray nebulization, which is then dried on the fly and introduced into the inductively-coupled argon plasma. In the hot plasma, cellular matter is completely atomized and ionized, resulting in the formation of a single ion cloud from each individual cell. Next, uncharged material and low weight ions (<80 Da), such as carbon (C), nitrogen (N), or oxygen (O) are removed from the ion cloud by quadrupole ion guides. The remaining heavier ions, including the rare earth metal ions are then separated by time-of-flight (TOF) analysis according to their mass-to-charge ratio, and analyzed for their abundance. An entire TOF spectrum is recorded every 13 µs, so that a single ion cloud is represented by a series of about 10–40 consecutive TOF spectra. The abundance of each atomic mass (defined by TOF windows) in each spectrum belonging to one cell is then integrated to yield a data format in which each cell event is assigned an ion count (similar to a "signal intensity") reflecting the amount of the respective metal-conjugated antibody that was bound to the cell.

3.4 *The mass cytometer: Cell introduction and signal detection*

The mass cytometer combines a cell introduction system with a mass spectrometer consisting of three basic components: the ion source, the ion analyzer, and the ion detector. Essential parts and steps of the measurement are summarized in Fig. 224. During a CyTOF measurement, single cells labeled with metal-tagged probes typically suspended in water are injected at a flow rate of 30 µL/min into a nebulizer. Using argon as a carrier gas, the nebulizer creates an aerosol that is guided into the mass cytometer. The nebulizer orifice of about 80–150 µm diameter limits in theory the size of cells or particles measurable by mass cytometry, while in practice, a large variety of primary cells and cell lines have been successfully analyzed. The CyTOF instrument utilizes an inductively-coupled argon plasma. At a plasma temperature of ~8000 K, injected cells traveling through the plasma are vaporized, and entirely disintegrate into their atomic, ionized constituents. Thus, each cell generates an ion cloud that expands by diffusion and charge repulsion and enters the vacuum of the mass cytometer. Afterward, the vast majority of matter is removed from these ion clouds: uncharged material is depleted by an electrostatic deflector, and low-weight ions, including those of elements abundant in organic material such as C, O, H, N, and Ar (serving as carrier gas), as well as ions carrying multiple charges, filtered out by a quadrupole ion guide. Only heavy-weight single-charged ions pass on to the time-of-flight (TOF) analyzer. There, ions are separated and identified by their flight time difference after acceleration in an electric field of a defined strength, in which all ions receive the same energy. Since the TOF of a given ion depends on its mass and on its charge, the charge has to be the same (+1) for all ions to correctly determine the mass an ion by its TOF. The velocity of lighter ions is higher and they reach the detector first, followed by heavier (and slower) ions, in the sequence of increasing ion mass.

The ion cloud of a given cell is measured in small portions, termed pushes. The CyTOF instrument performs 76 800 measurements (pushes) per second, which means that one mass spectrum is captured every 13 microseconds. Since the CyTOF technology is currently limited to detection of metal isotopes with high atomic mass, only the segment of the spectrum corresponding to atomic masses higher than 75 Da is taken in consideration. Typically, a single ion cloud is captured by ~10–40 spectra. An electron multiplier is used for ion detection and consists of a series of dynodes maintained at increasing potentials, resulting in serial amplification of the original signal. The output signal

of the detector is further amplified and subsequently digitized by an analog-to-digital converter. The spectra are then analyzed by two successive integration steps, to obtain information about the amount of metal associated with each ion cloud corresponding to a single cell event. The first integration is an area under curve calculated over an around 19–26 ns interval according to the region of a given mass spectrum and represents the intensity of the peak for a given isotope. The region used for the first integration is determined during the instrument setup procedure termed mass calibration, using a tuning solution. The second integration summarizes consecutive positive peaks corresponding to a single (cell) event. The signal with the maximum number of consecutive spectra is taken as reference to identify the spectra contributing to an ion cloud representing a single-cell event. Finally, the integrated signal intensities obtained for one cell in the different mass channels are converted into FCM standard (FCS) 3.0 format files. Thus, mass cytometric data can be viewed and analyzed manually using standard FCM software packages. However, considering the high complexity of mass cytometric data, manual data analysis is time consuming, subjective, and may miss much information contained in complex mass cytometric data. It is advisable to employ automated cell clustering, population identification, and dimensionality reduction techniques such as PCA or t-stochastic neighbor embedding (t-SNE)-based, UMAP, or similar methods [1470, 1794, 1983, 2030, 2031] for the analysis of high-content mass cytometry data (see also Section VI.1: Data analysis: An overview; and Section VI.5: Data repositories: Sharing your data). An important point to consider is that data analyses of a given study increasingly employ several algorithms organized in an analysis pipeline, very similar to an experimental procedure that needs to be described and annotated in appropriate detail [2032]. Finally, the technical identity of cell populations defined by mass cytometry in combination with, e.g., data clustering approaches can be validated by algorithms that break down high dimensionality into a lower dimensionality that can be handled by routine FCM analyzers, so that cell populations can be gated by conventional human-defined analysis [146, 147]. The same tools help to further characterize identified cell populations by providing a lead that markers to use for isolating them for further functional or molecular analyses.

3.5 Equipment

At present, Fluidigm Corp. is the only commercial provider of mass cytometry instruments and of almost all mass cytometry-tailored reagents. Mass cytometers can be run in a high-throughput manner by employing either an autosampler suitable for consecutive measurements of larger number of samples of limited sample size (from a 96-well plate), or an add-on device that permits acquisition of larger samples of any volume (Supersampler, Victorian Airship LLC), which is ideally used in combination with sample barcoding approaches (for more details, see Section VIII.2 Barcoding in cytometric assays). The latest mass cytometer version ("Helios") can sample volumes of up to 5 mL. A tube is placed in a

chamber where an applied pressure drives the intermittently agitated sample from the tube to the injection line. More recent mass cytometer versions (CyTOF version 2 and Helios) do not necessarily require in-depth technical knowledge of mass spectrometry, as the daily tuning and instrument alignment is largely performed automatically. However, it is advisable to have the instrument maintained and managed by an expert operator. The installation of a mass cytometry platform usually requires the additional setup of air conditioning, an exhaust system, argon gas supply and an IT infrastructure suitable to store and manage mass cytometry data.

Mass cytometry has also been used for imaging of tissue sections stained with metal-conjugated Abs, similar to those used in immunofluorescence microscopy [1883, 2033, 2034] (see also Sections IMC and microscopy). The stained section is dissected into a series of vaporized samples corresponding to µm-sized tissue section spots by high-resolution laser ablation; these tissue section spots are then consecutively analyzed on a CyTOF instrument [1883]. The data of each spot reveal the amount of metal isotopes that was bound to the spot when the tissue section was stained with metal-tagged Abs. By plotting the single-spot data next to each other in the order they were ablated from the entire tissue section, highly multiplexed images are reconstructed. Similar data can be generated using an alternative approach, i.e., multiplexed ion beam imaging (MIBI) that, does not rely on the mass cytometry equipment discussed here [2035, 2214].

3.6 Coping with bottlenecks in mass cytometry

While the advantages of mass cytometry are striking for various applications, it should be noted that due to the destruction of the cells in the argon plasma, CyTOF instruments cannot recover the original cell sample for subsequent experiments. Instrument sensitivity, cell throughput, and overall recovery should be taken in consideration when planning a study involving mass cytometry. Cells labeled with metal-conjugated Abs usually deliver signal intensities sufficient for gating and quantitative analyses. Current mass cytometers have a manufacturer-specified dynamic range of 4.5 orders of magnitude, which is comparable to fluorescence-based FCM. The variability in sensitivity for the detection of different reporters is lower in mass cytometry compared with that in FCM [2017]. However, mass cytometry currently lacks reporters that provide a specifically "bright" signal such as PE in conventional FCM [2017], due to an upper limit of metal ions that can currently be loaded onto a probe (~140 lanthanide ions per Ab using MAXPAR labeling kits [1987]). In addition, of any 10 000 heavy metal ions of the CyTOF detection mass range injected, only about 3–10 are counted by the instrument [2036]. These limitations are in part compensated for by the lack of inherent biological background signal (no "autofluorescence") and minimal signal spillover, which both can negatively impact fluorescent FCM data (see also Chapter II Section 1.2 Principle of spillover and compensation for a complete discussion about spillover). However,

this principally does not protect from background signals due to nonspecific binding of metal-labeled probes to cells. Significant background binding of MAXPAR-labeled Abs has been reported for fixed eosinophils, which could be eliminated by pre-incubation of cells with heparin [2037]. The sensitivity could be improved by probes that carry more metal per specific probe, such as heavy metal nanoparticles [2038–2040].

The volume of a single-cell derived ion cloud expands by diffusion to ~2 mm in size, restricting the instrument's throughput to ~1000 cells per second. A lower throughput (<500 events per second) usually delivers data comprising fewer doublet events. Thus, in contrast to most fluorescence-based flow cytometers with event acquisition rates of usually up to 10 000 events/s, acquisition times in mass cytometry are significantly longer and might necessitate pre-enrichment of target cells prior to mass cytometric analysis [2041]. In addition, a CyTOF measurement recovers data for about 30–50% of the injected cells, while the remaining sample is lost, e.g., by accumulating on the walls of the spray chamber and injector. Mass cytometers need to be set up and tuned daily (procedure detailed in ref. [1806], and instrument manuals) to confer stable instrument performance during day-to-day operations, while only very minor variations, e.g., due to slightly differing oxide ratios may remain.

Generally, the implementation of standardized tuning, sample barcoding (described in greater detail in Chapter VIII Section 2 Barcoding in cytometric assays) [1985, 1988, 1992], signal normalization according to bead standards [2042], and spillover compensation [1994], and Ab cocktail cryopreservation [2043] secure the generation of high quality data in mass cytometry.

All above approaches however do not account for experimental variability at the time of sample biobanking. To further improve data consistency, sample banking and assay automation are actively pursued in the mass cytometry field (covered in Chapter VIII section 11 Sample banking and Section 12 High throughput screening). Concerns for potential batch effects introduced at the time of sample banking and their long-term storage are particularly relevant to mass cytometry, as algorithmic analyses are particular sensitive to batch effects, complicating and limiting the discovery of biological features. Since different cell types behave differently during, e.g., cryostorage procedures [2044], proper sample banking must be confirmed for individual target cell populations.

In addition, the inclusion of a reference sample, that is, an aliquot of cells isolated from a single batch of sample material similar in nature to the study material, spiked into a series of batches of jointly processed samples that belong to a given study [2045], inform about remaining staining, and measurement variability across batches and may serve for normalization of batch effects in the future.

Ring trials have been adopted as a means to analyze the comparability of mass cytometry data generated by on different instruments and locations, showing that sample and reagent distribution rather than individual instrument performance were determinants of variability [2046].

3.7 Experimental workflow, reagents, and controls

The experimental workflow for preparing mass cytometry assays is typically very similar to that for conventional FCM, except for the strict requirement of cell fixation and their resuspension in water or cell acquisition solution prior to acquisition on the CyTOF instrument. Briefly, cells are subjected to cell surface staining and optional dead cell label incubation, fixed (usually using formaldehyde), permeabilized, stained for intracellular antigens and DNA content, finally resuspended in water or commercially available cell acquisition solution, and optionally supplemented with normalization beads for injection into the mass cytometer. Cryostorage of stained cell samples has been explored to improve the logistics of assay preparation and acquisition [2047]. Cell-surface and intracellular sample barcoding solutions are available and can be applied prior to surface staining or after permeabilization, respectively. Protocols are available for in-depth surface marker-based immune phenotyping [2024, 2048, 2049], intracellular cytokine staining [1850], tetramer-based detection of antigen-specific T cells [561, 1850], cell signaling analyses based on the detection of phosphorylated signaling mediators [1849, 1985, 2015], in vitro proliferation assays [2050] and the detection of RNA in single cells [2051, 2052]. In addition, recent developments in mass cytometry reagents allow the single-cell assessment of global epigenetic modifications [2053]. As such, the EpiTOF (Epigenetic landscape-profiling using cytometry by time-of-flight) Ab panel allows the assessment of different classes of histone modifications and variants. Functional probes available for mass cytometry include 5-iodo-2-deoxyuridine for assessing cell proliferation [2050], enzymatic activity [2054], and a tellurium-based hypoxia probe [2055]. Wheat germ agglutinin (WGA) and osmium tetroxide staining were proposed as a proxy for cell size in mass cytometry [2056], besides ASCQ-Ru for cell volume respectively, which, in conjunction with the Celltracer software has been used to correct for confounding cell size effects in signaling studies [2057]. Further, osmium tetroxide has been used to stain functionalized polystyrene beads, making beads manufactured for conventional FCM readily detectable by mass cytometry (Budzinski et al., 2019). Ab-binding quantum simply cellular beads modified by this method have been used to determine antibody binding capacities of immune cells [2058], and to study receptor occupancy after mAb therapy [2059] by mass cytometry.

Mass cytometers do not measure the light scatter parameters usually employed in FCM for detection of cell events and separation of cell aggregates; cells (or any other particles) are solely detected by the metal associated with them. Nucleated cells are typically revealed by rhodium- or iridium-based DNA intercalators [2060], and probes specific to characteristic cell antigens can be envisaged to reveal non-nucleated cells such as erythrocytes or platelets [2061]. Doublet events can be minimized by (i) filtering cells prior to injection, (ii) avoiding high cell densities in the injected sample, (iii) excluding cell events with high DNA signal and/or high cell/event length parameter values by gating, or (iv) sample barcoding using a restricted barcoding scheme efficiently filtering out doublet events formed between cells of differently bar-
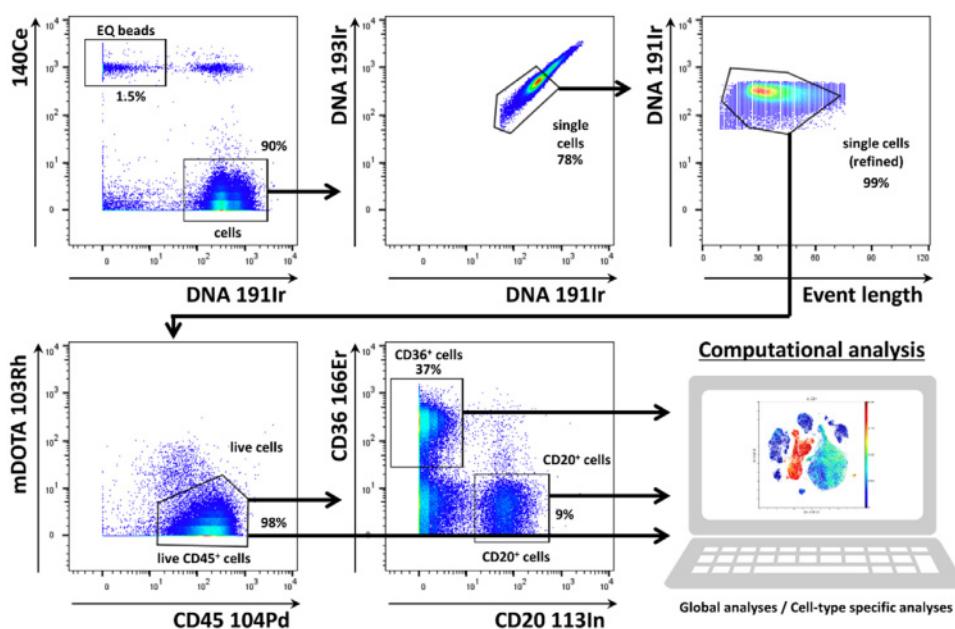
Figure 225. Typical gating strategy for PBMC analyzed by mass cytometry. Intact cells are identified by staining of DNA. Normalization beads elicit high signals in defined channels such as ^{140}Ce in the present example. Cells (unless stained with ^{140}Ce conjugated Abs) do not elicit high ^{140}Ce signals, and beads do not elicit high DNA/iridium signals. Events that appear in the upper right are cell-bead doublets, which could be either physical aggregates, or due to timely overlapping acquisition of two ion clouds with one cloud representing a cell, and the other one a bead event. Events not stained in either channel (lower left) are usually debris associated with metal amounts sufficient to be detected by the CyTOF instrument (first dotplot). Cell events are further restricted to events showing strongly correlating DNA signals according to their ^{193}Ir and ^{191}Ir staining. Both Ir isotopes almost equally contribute to the natural abundance iridium used in the DNA intercalator. Thus, signals are expected to correlate. Events with high iridium staining intensity are excluded since the DNA^{high} fraction is enriched for cell doublets. This procedure does not fully eliminate doublets but reliably reduces their presence when barcoding was not used to filter out doublets. However, back gating should be used to confirm that target cells are not excluded in this step (second dotplot). Gating according to "cell length" or "event length" is often employed in order to minimize the presence of doublets. The "length" parameter corresponds to the number of spectra that belong to a given event. Events labeled with large amounts of metal (and doublets) tend to show higher, and those with little metal tend to show lower "length" values. Upper and lower cell length boundaries are defined in the acquisition software. The length parameter is not indicative of cell size. Again, backgating should be employed to ensure that target cells are not excluded (third dotplot). Next, dead cells are excluded by gating on ^{103}Rh $^{low/-}$ cell events. High ^{103}Rh signals result from stronger labeling of dead cells by ^{103}Rh-mDOTA compared to live cells. PBMC identity is confirmed by CD45 staining (in-house ^{104}Pd conjugate, fourth dotplot), and CD36 and CD20 staining differentiate between monocytes/dendritic cells and B cells, respectively (in-house conjugates, fifth dotplot). Total cell events and/or select subsets are typically subjected to further computational analysis.

coded samples [1988, 1992]. Gaussian discrimination parameters have also been suggested for doublet identification and exclusion [2062]. Finally, DNA intercalators, cisplatin [2063], DCED-Pd [1997], or metal-loaded DOTA-maleimide [2048, 2064], are used for cell viability staining. A typical initial gating strategy is provided in Fig. 225.

The CyTOF instrument ("Helios" version) quantifies ions with atomic masses between 75 and 209, providing 135 channels. More than 50 of these can be used for detection metal-conjugated Abs, and additional channels accommodate DNA intercalators or dead cell detection. A central part of any mass cytometry experiment is Ab panel design, for which various mass tagged-Abs and pre-designed panels are commercially available. Abs can be labeled in-house using commercial kits for lanthanides and indium isotopes, or according to published protocols with isotopes of palladium, yttrium, bismuth, and platinum [1987, 1988, 2047, 2065, 2066]. Moreover, metal-containing nanoparticles such as Qdots containing cadmium [1850, 2067] and silver nanoparticles [2038] have been successfully employed as mass tags for reporting binding of specific probes to cells. The design of mass cytometry panels is generally easier as compared to fluorescent flow cytometric panels of similar marker capacity, since signal spillover and sensitivity differences are comparably minor issues [2017]. However, the mere number of parameters and the implementation of quality control for Abs, as well as choosing appropriate Ab clones [2049] make panel design a significant effort. Panel design includes optimizing the pairing of specific probes with unique heavy metal isotopes considering instrument sensitivity for that particular isotope mass, target antigen abundance, and additionally potential signal spillover (see ref. [2068] for details). Signal spillover in mass cytometry can arise from (i) isotopic and elemental impurities of mass tags, (ii) between adjacent mass channels at high signal abundance (usually Mass (M) +1 spillover, but M-1 spillover is also possible), and (iii) because of metal oxide formation (M+16 spillover) [2049, 2068]. A careful panel design, an optimally tuned instrument and highly pure reagents, however, can minimize these spillovers to very low levels that are orders of magnitude lower than fluorescent spectral overlaps. In addition, residual spillover effects in mass cytometry and imaging mass cytometry data can be compensated [1994] using a nonnegative least square (NNLS)

approach [37] that applies correction at the single cell level and constrains data to signals higher than zero after compensation.

Isotype and FMO controls are typically used in conventional FCM experiments to distinguish between specific and background signal (for further detail see Section III.1 Controls: Determining positivity by eliminating false positives). In theory, isotype and FMO controls (termed in mass cytometry as Signal-minus-one or Metal-minus-one controls, SMO and MMO, respectively) are easily applicable to mass cytometry. However, the sole fact that, in mass cytometry, typical panels include approximately 40 Abs renders the routine and consistent realization of these controls laborious and complicated, and often unfeasible. Isotope controls require the use of an antibody with a matching isotype and the same amount of metal per antibody as the reagent that is to be controlled, and are presently not commercially available. As a result of these practical limitations, the SMO/MMO controls are either performed exemplarily or combined in a metal-minus-many (MMM) strategy, in which several rather than individual Ab conjugates are omitted during the staining procedure, e.g., a group of markers specific to a certain panel on the backbone lineage marker panel. In addition to these, biological controls are particularly adapted to mass cytometry, since they take advantage of the high dimensional level of the data. Counterstaining for multiple cell lineage markers in Ab conjugate evaluation experiments enables the identification of reference cell populations in the sample serving as positive and negative controls for a given Ab conjugate in the multitude of populations commonly identifiable by a 40-parameter panel. For example, B cells also present in the sample could be used as a negative control for a T-cell-specific marker. Ab titrations can also benefit from the high dimensional level of the data since multiple markers can be titrated concurrently across subsets defined by a backbone of lineage markers to facilitate assessment of the titration results on specifically gated populations of interest. Finally, mass cytometry data sets and their evaluation, especially by computational means, benefit from bundled, batchwise sample processing, and data acquisition (as compared to processing samples individually) to achieve a high degree of data consistency.

Generally, experimental workflows for mass cytometry are typically very specific to individual studies, and many factors should be considered during the setup of mass cytometry studies [2069].

3.8 *Conclusions*

Mass cytometry is a recent hybrid technology employing principles of FCM and mass spectrometry. The core technology is rapidly developing along with bioinformatics and reagent chemistry, thereby creating a largely universal and extendable next generation platform for high-dimensional single-cell cytometry applied in translational research, systems biology, and biomarker discovery.

4 Combinatorial cytometry

Combinatorial cytometry is the subfield of cytometry, or single-cell analysis, whereby researchers describe, study, and model complex relationships between multiple combined cytometry samples exposed to varying stimuli, environment, treatment, and so on.

Examples include various techniques of multiplexing, such as fluorescence barcoding [1984], high-throughput cytometry, and cytometry-based compound screening [2070], as well as multiple computational techniques that combine multiple data files either during the data collection [2071] or post hoc in order to create multifactorial and multidimensional datasets to allow for analytical comparisons across properties not readily available or accessible via a single experiment [1795].

Combinatorial cytometry approaches have been implemented successfully with innovative mass cytometry (CyTOF) systems (For more information on the equipment and concept, see Section VIII.3 Mass cytometry) [2072], multispectral cytometry [31], multi-angle elastic light scatter cytometry [2073], high-throughput screening FCM [2070], and computational clinical and research cytometry of the immune system [2074–2076].

There is often a significant difference in the design of a traditional FCM and a high-throughput or high-content assay. This can be visualized in Fig. 226 where both traditional tube (or even plate based) FCM assays are performed, and high-throughput assays exclusively using 96 or 384 or larger plates. Using such large arrays of data creates a fundamental difference in how the data are both collected and analyzed. What is clear is that a high degree of organization and structure, complete with significant metadata is required to establish high-throughput or high-content FCM assay systems.

One of the key advantages of the combinatorial cytometry approach is the opportunity to employ advanced statistical and machine-learning methods, such as various techniques of clustering, supervised learning/classification, Bayesian techniques, and other state-of-the-art methodologies. On the other hand, combinatorial methodologies introduce complexity to the experimental planning and design. As a result, they may increase the cost of the experiential setup and heighten the risk of failure. Ultimately, the benefits of complex, information-rich "all-in-one" assays, must be balanced against the cost of assay development which is likely to be greater than that of performing assays using regular techniques.

Compound screening is a prime example of a combinatorial cytometry approach. Multiple multicolor flow-cytometry cell-stress assays can be rapidly executed in a sequential manner using an automated robotic sampler. The cellular populations are exposed to different concentrations of the compounds tested, but they can also be measured in different environments (different media) and/or at different times after exposure to the stress. The assay can scan a dense grid of possible combinations incorporating all the stress factors in various permutations. Consequently, a huge number of individual cytometry measurements may be required to complete the screen. It is self-evident that the key requirement for successful execution of such an assay is a well-defined, repeatable,

The Operational Modality of Flow Cytometry
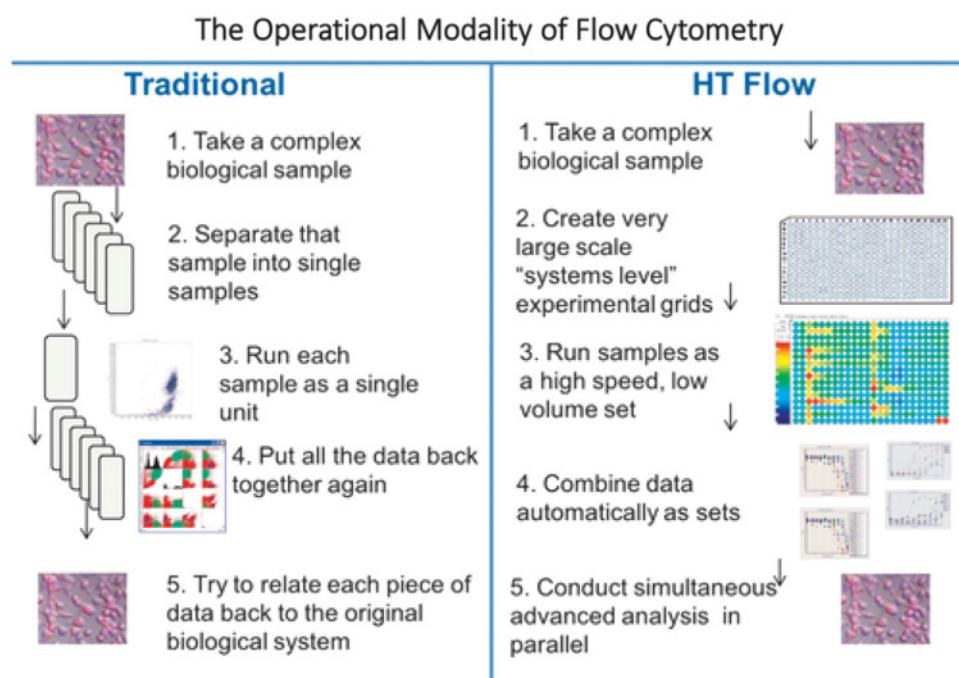
Figure 226. This is an example of how a traditional FCM assay might be designed using test tubes or even a 96-well plate assay. Because of the limitation in the number of tubes or samples that can be run by traditional instruments, it is not possible to create very large arrays. Using high-throughput cytometry, typical assays might be 384-well plates that can be processed in 10–20 min and produce a huge amount of data that can be processed using advanced statistical operations.

and reproducible assay layout (sample organization), which must be consistent throughout the entire cycle of experiments.

The assay sample organization defines the resultant data structure and organization as well, as schematically indicated in Fig. 227. A typical automated phenotypic assay executed using a cytometry screen would employ a 96- or even a 384-well layout that provides space for up to 32 drugs at 10 doses each, as well as negative and positive controls. Preparing such a layout in an automated, repeatable fashion allows glitch-free assay execution and subsequent feature extraction. Figure 228 shows a window of one example of a custom-built screening software package, *Plate-Analyzer*, which automatically outputs response curves and fits log-logistic models on the basis of the templates and gates predefined by an operator [2077]. Since such a system performs the operations involving up to 384 FCS files per plate, it is crucial that all the steps in the analytical procedure be fully automated and be executed without the need for any interactive operator input.

A screening system such as the one described above also relies on automated sample preparation and robotic liquid handling, as the probability of pipetting errors and inaccuracies is too high to allow for a manual assay setup. Automation of sample preparation not only ensures a high level of reproducibility, but also shortens the preparation time and guarantees that the minimal required amount of sample and reagents can be accommodated to make the assay more cost effective.

Opportunities for automated or semi-automated analysis of FC screens can be achieved using many available toolsets for FCM data processing. R-language for statistical computing is a com-

monly used environment for cytometrists who are interested in developing their own analysis tools and unique data processing pipelines. Combinatorial FCM incorporating dimensions of time, concentration, media, and other factors certainly expands the horizons for this field. Conversely, the availability of rapid development tools for custom design of data processing pipelines is a condition sine qua non for successful implementation of the described combinatorial and multifactorial approaches, see also Section VII.1 Data analysis an overview. When it is desirable to measure biological responses across multiple conditions (e.g., concentration, medium type, stress, temperature, time, etc.) with FCM, it is advantageous to approach the assay in an organized fashion. The technique is enabled by fast autosamplers, and informatics pathways aware of the multifactorial nature of the collected data as demonstrated in Fig. 227 where the differences in analysis of traditional flow data are compared with combinatorial analysis routines. These routines can be highly complex, but depend upon the ability to automatically extract features for all samples in the array.

Other examples of combinatorial cytometry are the well-known bead-based assays. Among those, cytokine assays are probably the most widely used and broadly accepted [2078]. In this technology, two to ten types of cytometry-compatible beads of various sizes (recognized by FCM by forward light scatter) can be dyed with increasing amounts of a tracer dye to encode their ability for capturing/measuring different analytes. For example, Fig. 228 shows 13 cytokines simultaneously recognizable by a commercially available FCM assay (any commercial plate could be entered into the

Figure 227. Combinatorial cytometry integrates the ideas of screening biological responses. Biological responses can be screened across multiple conditions (e.g., concentration, medium type, stress, temperature, time, etc.) with FCM. The technique is enabled by fast autosamplers, and informatics pathways aware of the multifactorial nature of the collected data.
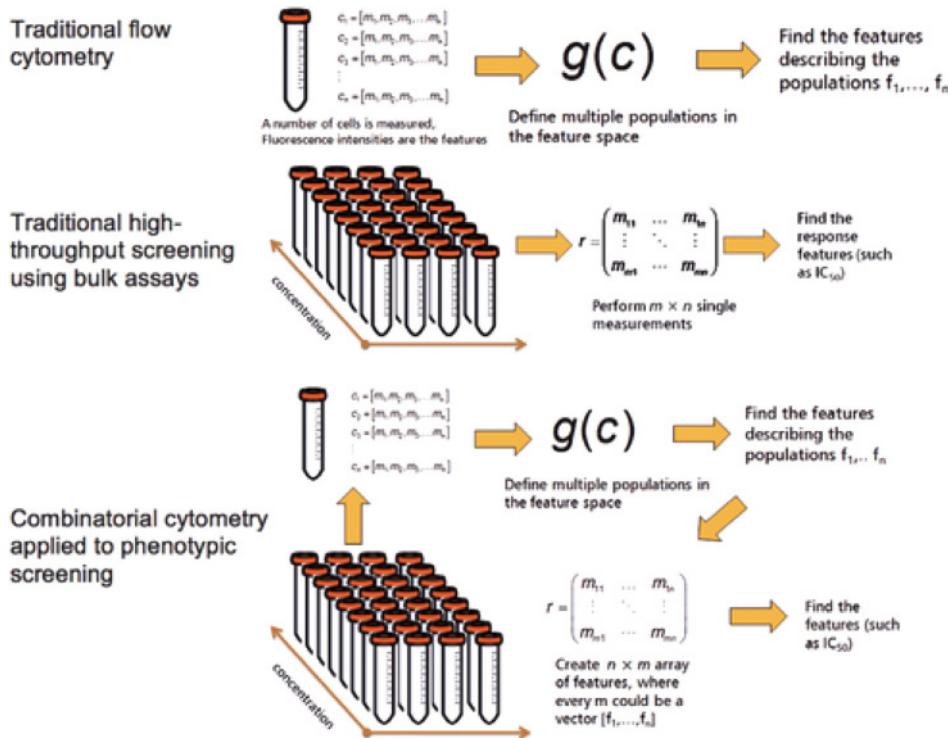
Table 94. Cytokine assay reagents. This table shows the multiplex cytokine assay with bead location and target molecule. Using beads of different sizes, with increasing amount of bead fluorescence, many assays can be performed on very small samples of plasma (<15 μL). This example demonstrates how one particular kit (which uses beads identities as A4, A5 . . . .B2, B3, etc.) where each bead is associated with one particular analyte. Each of these beads are in a small size (A) or larger size (B) group. These are shown graphically in the upper right panel of Fig. 228

Target	Bead ID
IL-10	A4
IFN-g	A5
IL-5	A6
IL-2	A7
TNF-a	A8
CM-CSF	A10
IL-4	B2
IL-17F	B3
IL-9	B4
IL-17A	B5
IL-13	B6
IL-22	B7
IL-6	B9

system). In this system there are two bead sizes, and each bead type carries a different amount of target marker, in this case APC (see Table 94). Although the discussed technique employs only a 13-plex method, frequently up to 20 or 30 different cytokine tags can easily be simultaneously quantified in a minimal volume of plasma. If the organization of samples on multiwell plates is consistent, one can execute an automated data-processing task immediately after assay completion. Gating, recognition of dif-

ferent bead types, computation of calibration curves, and other necessary tasks can be executed automatically without operator intervention or a manual setup.

As mentioned before, multiplexing offers a huge advantage in terms of assay execution time and reagent/sample cost saving. As a result, the multiplexed bead assays allow researchers to identify concentration of analytes of interest in many samples essentially simultaneously. A dedicated software package (such as the PlateAnalyzer Cytokine edition in Fig. 229) provides the means to show all the calibration and to visualize the concentration of analytes across the entire plate. Such visualization techniques are commonly used for other combinatorial approaches in biomedical research and are equally valuable for FCM data.

A third example of a combinatorial cytometry technique is multispectral single-cell analysis. In contrast to traditional multicolor cytometry, which uses a dedicated detection channel for each fluorescent label in the hope of separating signals from multiple labels, the spectral system essentially acts as a superfast spectroscope connected to a flow cytometer. An approximation of the entire spectrum using about 30–40 bands for every cell is measured, and the data can be further processed via spectral unmixing techniques or directly used for spectral classification. There are a number of advantages to the spectral approach, mainly related to the less complex hardware as traditional optical filters are not utilized and neither are individual detectors. This approach creates a new opportunity for combining fluorescent probes that may not be feasible in conventional FCM [2079]. For example, dyes such as GFP and FITC can be used together because chemometric techniques to process spectral cytometry data can be utilized to classify and/or unmix the resultant signals. There are several excellent recent examples of this approach
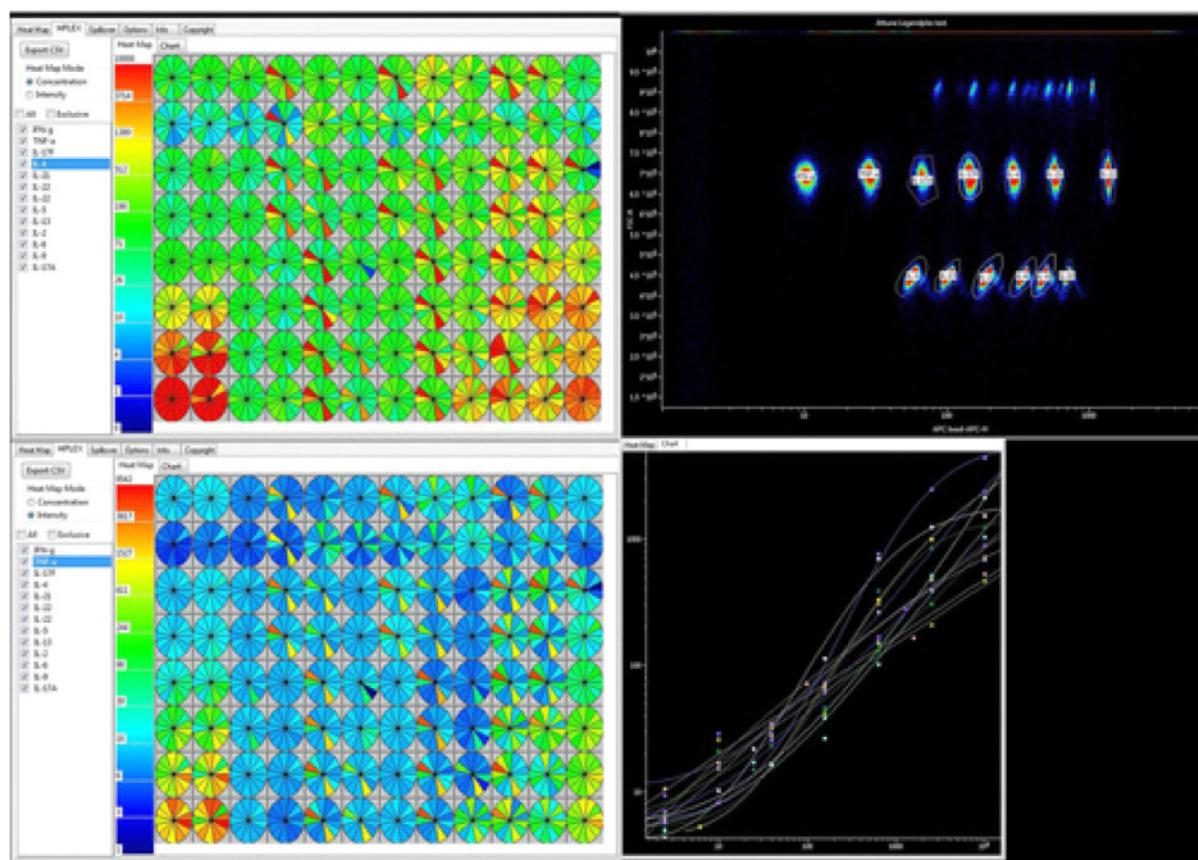
Figure 228. Automated processing of bead-based cytokine assay. Results obtained in a cytometric bead assay in graphical representation of the cytokine concentration in every well of the multi-well plate. Samples were run on an Attune NxT flow cytometer (ThermoFisher) using the instrument plate reader. On the left side of the figure is a list of the analytes used in the assay. In the center part of the figure is a 96-well plate layout showing a representation of each cytokine in a 13-piece pie chart. The colors represent the values in picograms per milliliter. The top right figure shows the bead populations used to define each cytokine. On the bottom left, the heat map describes the fluorescence intensity measurements for each well and each cytokine. The figure on the bottom right shows the standard curve derived from the standards run for this assay.

in FCM [32, 33] in which combinations of fluorescent proteins, together with a variety of fluorochromes, allowed a total of 11 markers to be used simultaneously and then separated by spectral unmixing.

A final example of combinatorial cytometry and one that demonstrates the extraordinary power of multiparameter datasets can be seen in data collected by the CyTOF technology and demonstrated in Fig. 230 (for an overview of the equipment, see Section VIII.3 Mass cytometry). This approach uses lanthanide-conjugated Abs, as opposed to the fluorescently labeled probes of a conventional FC system, and time-of-flight mass spectroscopy for analyzing single cells to produce information-rich population statistics [1849]. The final complexity of such data can be very high indeed, requiring innovative techniques for data processing and visualization. An ad hoc "what-if" analysis is possible using visual development environments allowing for interactive construction and modifications of data processing pipelines. A demonstration of such a pipeline, capable of tackling an input of 30–40 different biological parameters encoded by lanthanides, is represented in Fig. 230. The data processed in this example (courtesy of B. Boden-

miller, University of Zurich, Institute of Molecular Life Sciences) were produced by analyzing a bulk sample with seven lanthanide tags used to encode the position of individual subsamples in a 96-well plate. This experimental approach was applied to characterize human PBMC signaling dynamics and cell-to-cell communication, signaling variability between PBMCs from human donors, and the effects of various inhibitors on this biological system. For each inhibitor, 14 phosphorylation sites in 14 PBMC phenotypes were measured [1985].

The demonstrated data pipeline (or "logic map," in PlateAnalyzer terminology) can extract individual dose-response curves for the 14 phosphorylation states from each of the 14 cell phenotypes. This is a striking example of combinatorial FC analysis, which first creates relationships between different vectors of FC measurements and subsequently explores and quantifies these relationships. Where traditional cytometry is focusing on mapping individual cells in a multidimensional space of phenotypic descriptors, combinatorial cytometry looks at vectors of multidimensional measurements and explores the differences and similarities between those under various conditions.
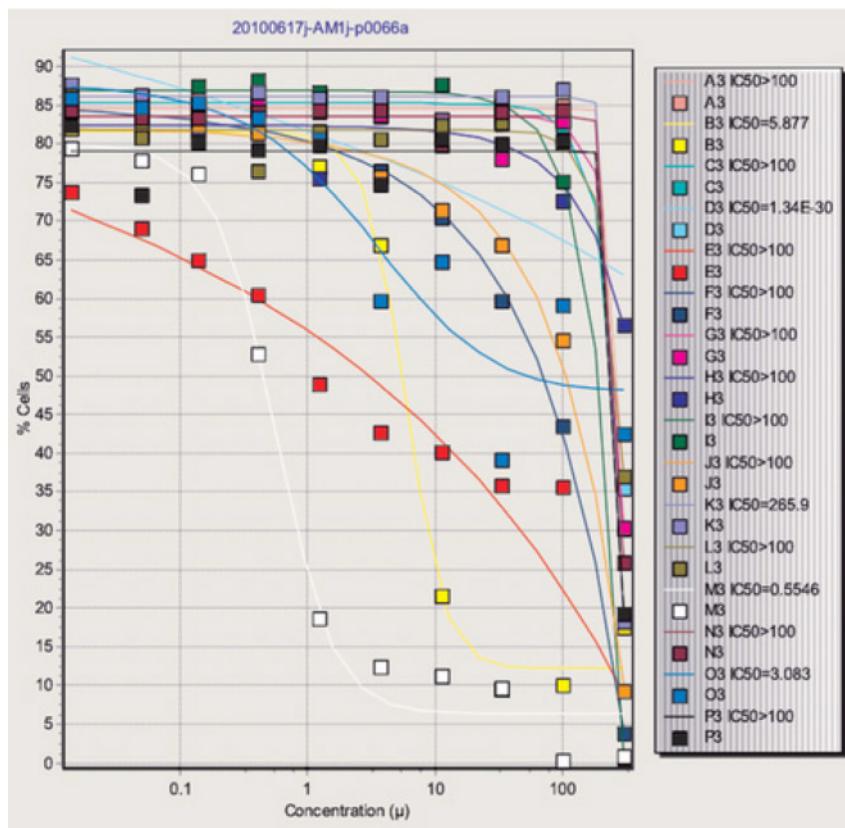
Figure 229. Response curves automatically produced from data extracted from multiple FCS files. Data across FCS files are collected using a robotic sampler connected to a flow cytometer. The PlateAnalyzer software recognizes the plate layout and creates response curves on the basis of pre-defined gates. Each curve results in an automatically calculated IC50 value as shown on the right side of the figure.

Conclusion. The key requirements for combinatorial cytometry are (i) well-defined reproducible assay layout, (ii) highly controlled, preferably automated, assay setup and preparation, (iii) data-collection method recognizing the relationships between the collected FCS files and organizing the measurements in higher-order data structures, and (iv) automated data analysis and reporting software. When this combination of tools is available, complex multiparameter and multifactorial experiment designs can be executed and the resultant data can be rapidly processed to produce
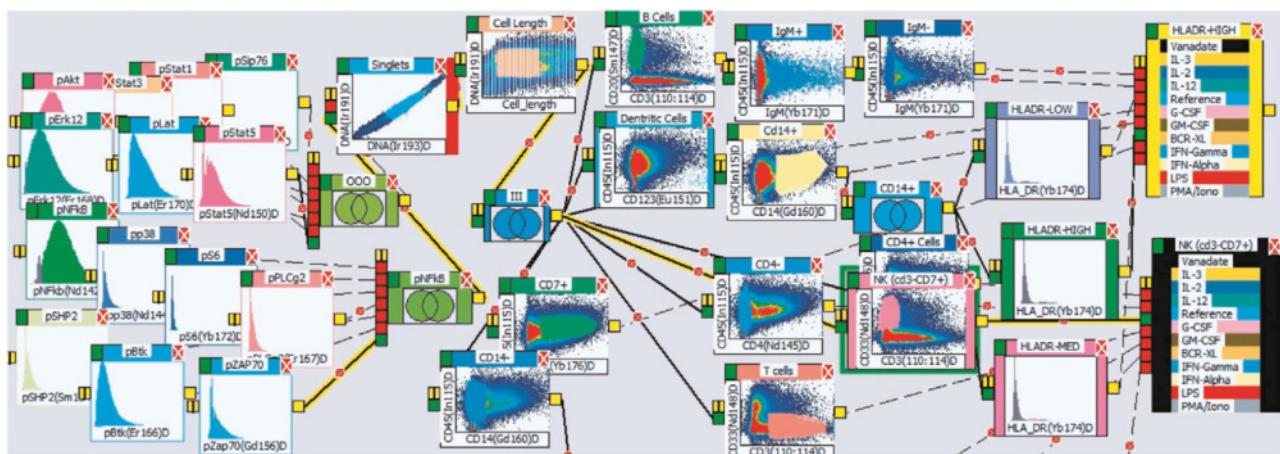
Figure 230. The pipeline design canvas of the PlateAnalyzer. This particular example of an analysis package (http://vault.cyto.purdue.edu) allows rapid development of data-processing maps for complex combinatorial cytometry experiments. In contrast to traditional FC software packages, all the operations are by definition applied to vectors or matrices of FCS files, rather than to individual datasets. On the left of the figure are shown histograms of each of the phosphorylated proteins in the assay, the central group identifies the phenotype of cells being evaluated, and the two boxes on the far right show the stimulating molecules (12 rows) each of which contains eight concentrations. Yellow lines show the active analysis connection pathway—i.e., the resulting dose response curves would be based on the phenotypic result of each component linked within this pathway. As an example in the figure, the phosphorylation state is ZAP70- and the phenotype is NK cells (CD3−, CD7+).

useful insight leading to mechanistic models of the studied biological systems.

5 High dimensional FCM

5.1 Overview

The characterization of the complex nature of immunological processes in health and disease requires multi-dimensionality as well as high resolution to detect all targets of interest. While the availability of novel technologies such as mass cytometry by time of flight (CyTOF) and single-cell RNA sequencing (sc-RNAseq) have greatly increased the number of features (protein and/or transcript) that can be measured at the single-cell level, fluorescence-based FCM remains a primary tool for immunophenotyping due to its low cost, high dynamic range, and high throughput. Furthermore, the most recent generation of instruments with five or even more spatially different laser lines allows the detection of 30 parameters, with up to 40 on the horizon (based on personal communication).

Though the general principles of experimental design have not changed (for review, see ref. [56]), reliable fluorescent panels of more than 10 parameters require not only a more thorough and systematic planning to ensure optimal resolution of all markers even at low Ag expression, but they also critically depend on validation and controls as a means to avoid misinterpretation of data. Within this section we describe a step-by-step approach for panel design based on the concept of the spillover spreading matrix (SSM), pointing out important considerations for fluorochrome–antigen combinations and address some of the most common misconceptions and caveats. In addition, we outline key steps in visual quality control of the obtained data to ensure a meaningful subsequent multidimensional data analysis.

5.2 Introduction

Most commonly, fluorescent flow cytometers dedicate one detector to the measurement of one fluorophore and use a compensation-based approach to correct for spectral overlap between the different fluorophores used. Improvements in electronics and the usage of multiple spatially separated laser lines have resulted in the latest generation of instruments that can measure up to 28 fluorescent parameters (such as the BioRad ZE5 or the BD FACSymphony) [2080]. In turn, spectral cytometry instruments have been developed that detect every single fluorochrome across all available detectors, thus measuring a complex composite spectrum for every cell, with individual signals being separated by spectral unmixing algorithms (originally developed at Purdue University and now commercialized by Sony Biotechnology as well as Cytek Biosciences) [33, 2081]. Currently, these instruments have reportedly been used for the measurement of up to 24 parameters. The availability of new dyes, dyes are presently limiting

all fluorescent-based cytometers, will advance the field and push these limits toward 40, and possibly even beyond. While this section focuses on conventional, compensation-based FCM, most of the principles discussed are applicable to spectral cytometry as well.

Systematic panel design for a high-dimensional experiment requires multiple considerations. Inevitably, the used fluorochromes will show some degree of spectral overlap into more than one detector. The detector intended to capture the major emission peak of the respective fluorochrome is usually called the primary detector, and the secondary detector(s) is (are) the one(s) collecting the spillover. The mathematical process used to correct for spectral overlap is termed compensation [2082] (See Chapter II, Section 1- Compensation), and reports a percent value describing the relative fluorescence detected in the secondary detector compared to the primary detector. This signal portion is subtracted from the total signal detected in the secondary detector. A common misconception is that the magnitude of the compensation value is used as a representation for the amount of spectral overlap between fluorophores, while in fact the compensation value is highly dependent on detector voltages [2083].

The most useful metric in this context is the so-called spreading error, which was first described by the Roederer laboratory at NIH [38]. In short, the spreading error quantifies the spreading that the fluorochrome-positive population (in the primary detector) shows in any secondary detector. This increased spread (as measured by SD of the positive population) is sometimes erroneously attributed to compensation. In fact, compensation does not generate the spreading error, but rather makes it visible at the low end of the bi-exponential or logarithmic scale (Fig. 231a, left panel). Spreading error is a consequence of the imprecise measurement of fluorescent signals at the detector (typically a PMT), which show some variance due to the Poisson error in photon counting.

In short, there are three key aspects of spreading error that need to be considered for panel design: First, spreading error is proportional to signal intensity, i.e., the brighter a signal in the primary detector, the more pronounced the spreading error in the secondary detector will be (Fig. 231A, right panel). Second, spreading error reduces the resolution in the secondary detector, i.e., the detector that is collecting spillover (Fig. 231B). Third, spreading error is additive, i.e., if a detector collects spreading error from multiple different fluorophores, the overall loss of sensitivity will be more pronounced (Table 95).

Besides considering spreading error, which will be discussed in more detail in the next section, other relevant aspects of panel design include the relative expression level of target antigens per cell, co-expression of target markers, and the relative brightness of the used fluorochromes. Importantly, the consideration of spreading error is overall more relevant than fluorochrome brightness if dealing with co-expressed markers (Fig. 231C and D). Furthermore, for any high-dimensional fluorescence experiment the quality of single-stained controls is of utmost importance, thus these have to follow the four basic rules as described in detail in Chapter II Sections 1.3 (Measuring SOVs/compensation controls) and 1.4 (Compensation controls) and in ref. [165]. Finally, the chemical
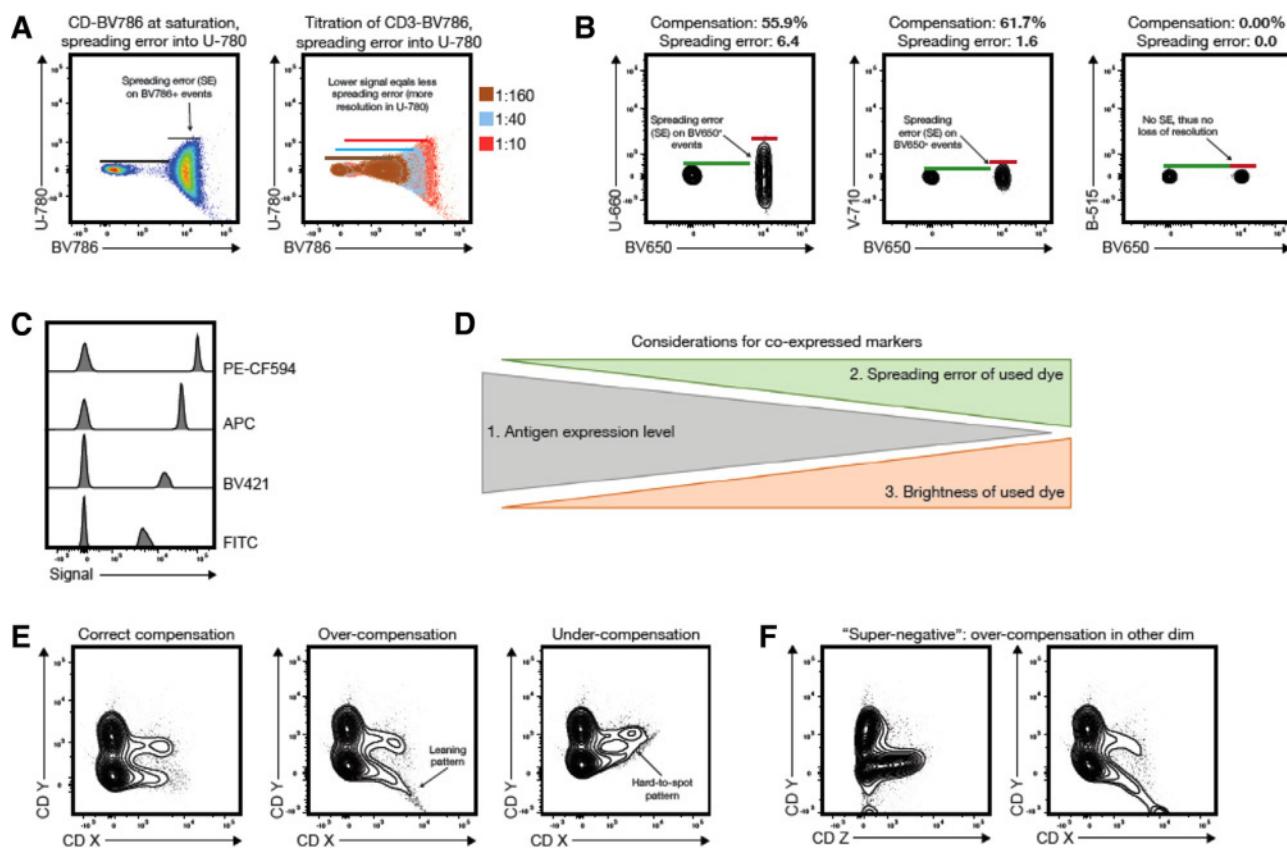
Figure 231. Spreading error and fluorochrome brightness in panel design and common compensation artifacts in quality control. (A) A typical example of spreading error is illustrated: BV786 shows significant spectral overlap in the U-780 detector (excitation by UV laser), which manifests as visible spread of the positive population. The relative loss of resolution on this population compared to the negatives is indicated by black bars on the left plot. Right plot shows how spreading error is proportional to signal intensity, and decreases with lower titers of the respective Ab. (B) The absolute compensation value and spreading error are not directly related, as exemplified for BV650+ events in different detectors (spreading error and compensation values for each combination are displayed above the plot). (C) Examples of staining intensities for different fluorochromes: FITC (dim), BV421 and APC (medium), and PE-CF594 (bright). Note that fluorochrome brightness can be instrument-specific. (D) Overview on the critical considerations for fluorochrome assignment for co-expressed markers. Highly expressed targets should preferably be paired with dim fluorochromes generating little spreading error. Dimly expressed (or unknown) targets should be paired with bright fluorochromes and utilize detectors that receive little spreading error. Numbers 1–3 indicate the relevance of the considerations. (E) and (F) show erroneous patterns that usually indicate incorrectly compensated data: (E) example of a correctly compensated plot, and respective over- and undercompensation of marker CD X into detector for CD Y. (F) Example of an incorrectly compensated population CD X (right plot) appearing as "super-negative" population if displayed against an unrelated detector measuring CD Z (left plot). The erroneous pattern is only visible if displayed against the detector measuring CD Y.

properties of the used dyes can impact complex panels, as unexpected dye–dye interactions or dye–cell/dye–buffer interactions can change the fluorescence spectrum of a given dye (also see *"Top tricks"* of this chapter). This aspect needs to be addressed by using appropriate controls, which will be discussed together with spreading error in the next section.

5.3 *Principles of the technique being described*

The SSM is a fundamental tool for successful panel design. It is specific for each instrument and provides comprehensive information on the relative contribution of any fluorochrome to spreading error in secondary detectors, and the relative loss of resolution in all the available detectors. As such, the SSM provides a way

to tackle spreading error in a systematic manner. It is important to note that the extent of spreading error cannot be predicted from the corresponding value in the compensation matrix, which is exemplified in the plots displayed in Fig. 231B.

The SSM can be calculated from single-cell stained controls in a common data analysis package, FlowJo (version 10.4 and higher), or manually using the formulas provided by Nguyen et al. [38]. The information on spreading error obtained from the SSM can be translated into panel design in two ways: First, the SSM highlights individual fluorophore-detector pairs with high spreading error, which in turn should be used for mutually exclusive markers (e.g., CD3 and CD19) as in this case spreading error will not interfere with detection of either signal. Second, the SSM can be used to assess the additive loss of resolution in a secondary detector by calculating the column sums, and to assess the additive

Table 95. Example spillover spreading matrix (SSM)

Detector / fluorochrome	B-530 (FITC)	B-710 (PerCPCy5.5)	R-670 (APC)	R-710 (AF700)	R-780 (APC-Cy7)	U-379 (BUV395)	U-570 (BUV563)	U-610 (BUV610)	U-660 (BUV661)	U-740 (BUV737)	U-800 (BUV805)	V-450 (BV421)	V-470 (BV510)	V-570 (BV570)	V-610 (BV605)	V-655 (BV650)	V-710 (BV711)	V-780 (BV785)	YG-586 (PE)	YG-610 (Pe-Tx)	YG-670 (Pe-Cy5)	YG-780 (Pe-Cy7)	Total spreading error contributed
FITC		0.599	1.07					0.356		0.729	1.76	1.72	0.396	0.449	0.455	0.386	0.24	2.4	1.37	1.06	1.57	0.296	7.406
PerCPCy5.5	0.247		2.24	4.18	1.91	0.223	0.0775		0.275	2.92	0.486	0.361	0.465	4.92E-03	0.183	0.698	1.91	0.433	0.811	1.57	3.3	3.1	28.92292
APC AF700	0.132	1.09		2.78	1.29	0.0662	0.139		0.268	0.889	0.738	0.44	0.143	1.99E-03		0.905	0.55	0.737	1.29	0.391	4.28	1.23	16.0907
APC-Cy7	0.0822	0.5	0.767	0.639	2.18	0.119	0.125	4.87E-04	0.132	1.62	2.06	0.0922	0.0922		0.0874	0.143	0.368	1.33		0.907	0.444	1.77	12.439477
BUV395	0.896	0.231	0.847	0.861		0.0796		0.0848	0.853	0.747	2.06	0.974	0.492	1.39	1.39	0.196	0.142	0.709			0.507	5.49	13.8462
BUV563	0.375	1.33	2.55	1.15	0.442	2.01		1.26	0.781	2.32	1.29	0.602	4.11E-03	2.66	1.4	0.739	0.53	0.302	22.3	11.7	3.23	1.2	5.98
BUV610	0	2.22	3	6.44	3.07	1.34		0.535		3.34	1.97	0.517	0.565	1.27	1.39	1.03	1.01	0.63	8.39	18.8	5.12	2.43	57.133
BUV661	0	1.66	12.9	1.72	1.22	0.953		0.194		7.07	3.77	0.627	0.627	1.4	0.627	1.9	0.979	1.11		1.91	5.4	2.68	54.84411
BUV737	0	0.519	0.513	5.15E-03	1.07	0.182		0.165		0.641	2.17	0.347	0.565	0.533	0.627	0.175	0.337	0.605	1.97	1.07	0.649	0.816	52.729
BUV805	0.237	4.24E-03	0.738	0.534	0.193	0.967		0.148	0.224	0.576	0.19	0.381		0.242	0.165	0.157	0.132	0.549	0.0998		7.97E-03	0.849	12.041
BV421 BV510	0	0.235	1.27	0.449	0.466	0.123	0.153	0.485	0.283	1.37	0.416	0.563	0.386	0.294	0.214	0.627	0.284	0.118	1.51	0.865	1.59	0.176	6.1058
BV570	0.207	0.749	2.23	1.38	1.86	0.13	0.223	0.81	1.18	2.04	0.971	1.48	0.396	1.39	0.952	2.03	0.695	0.313	7.75	4.02	2.42	0.794	3.51321
BV605	0.205	0.927	1.27	3.72		3.11E-03		0.584	0.638	3.71	1.28	1.35	0.914	2.61	2.76	3.22	1.27	0.761	4.74	5.48	3.28	1.36	7.97515
BV650	0	0.889	1.05	0.608	0.809	0.784	1.15	0.349	0.161	1.94	3.15	2.54	0.641	1.64	1.12	0.655	1.5	1.42		3.28	0.834	1.57	27.518
BV711	0.839	1.61	0.688	0.129	0.124	0.316		0.153	0.122	0.505	2.47	3.22	0.113	1.32	0.62	0.544	1.65	3.59	2.03	2.03	1.16	1.85	32.44511
BV785	0.144	0.389	0.552	0.455	0.695	0.0902		0.254	0.0805	0.513	0.18	0.338	0.0573	1.44	0.349	0.465	0.567			3.32	0.834	0.62	19.579
PE Pe-Tx	0	0.505	2.58	1.68	0.559	1.01E-03		0.101	0	0.885	0.259	0.249	0.0746	0.511	0.81	0.597	0.239	0.225	3.4		1.16	0.382	34.094
Pe-Cy5	0.0981	1.09	0.444	0.257	0.124	0.0638		0.254	0.122	0.513	0.409	0.305	0.0573	0.158	0.736	0.681	0.531	0.446	1.52	0.683		1.08	16.736
Pe-Cy7	0.207	2.05	2.58	1.68	0.559	0.187	0.306	0.101	0.0805	0.721	0.874	0.629	0.225	0.158	0.151	0.225	1.07	0.865	1.52	1.25	0.489	2.07	11.0472 / 12.87331 / 15.801 / 7.584
total SE collected	3.6693	16.94324	34.709	26.12615	16.749	7.63792	3.2735	5.479287	4.9975	36.306	24.443	18.627	6.74621	16.09099	12.02432	15.373	12.354	18.475	55.4148	58.336	32.99097	29.938	

Columns are to be interpreted as the detectors that are receiving spreading error. The value of the spreading error is relative and additive, i.e. a detector that is receiving spreading error from several fluorochromes is overall showing a higher loss in resolution. Examples as to how the SSM can be utilized during panel design are described in "experimental workflow".

contribution of spreading error from a single fluorochrome across all detectors by calculating the row sums. An example of a SSM and how to interpret it is shown in Table 95 and described in "*Experimental workflow*."

In many applications, researchers aim to target as many markers of interest on the same cell type as possible. Hence, for these applications, the antigen expression levels play an important role and need to be assessed beforehand—either experimentally or by utilizing published work. Useful resources in this context are optimized multicolor immunophenotyping panels (OMIPs) (See Chapter VIII, Section 3 Analysis presentation and publication (MIFlowCyt)), which usually show raw data of every Ab in their supplementary material [1943]. Using the information of antigen density, low-expression antigens should be detected in channels receiving little spreading error and fluorochromes generating large spreading error can be used for their detection, as this will decrease the relative spreading error (which is proportional to signal intensity). In turn, highly expressed antigens should be paired with fluorochromes generating little spreading error. Alternatively, one can assign highly expressed targets to detectors that receive a lot of spreading error, as a bright signal will typically still remain above the spreading error. A step-by-step approach for this process is outlined in the section *"Experimental workflow"* below.

In order to draw accurate conclusion and to avoid interpreting artifacts that result from spreading error, validation of Ab combinations and using the right controls is mandatory. In most cases, and especially for markers with unknown Ag expression levels FMO controls are required as they can help to identify gating boundaries, especially in detectors with spreading error [2084] (See Chapter III 1.2 Fluorescence spreading into the channel of interest: Fluorescence minus one controls before you start controls). However, it is important to note that FMO controls cannot account for unspecific binding of the Ab that it controlled for, which can cause a shift of the entire negative population in the fully stained sample that is absent in the FMO control. In this case, either a biological control is required, or one can use another cell type in the same experimental sample as a gating control. Isotype controls can serve the function to identify staining issues, especially when secondary Abs are used. Unstained controls have historically often been used to give information about the background autofluorescence of the measured cells, but these controls are of little use in most complex polychromatic experiments.

Finally, high-dimensional cytometry data can only partially be analyzed by traditional manual gating, but rather requires computational data analysis approaches. Prior to this, appropriate quality control and preprocessing of the data is mandatory, as specified below. For details on computational analysis techniques, we refer the reader to several recent reviews [1794, 1838, 1983] and to the corresponding section of the guidelines (see Chapter VII).

5.4 *Applications*

Multidimensional FCM with up to 30 parameters enables a deeper phenotyping and characterization of the immune system, which is required as cellular subsets require more and more mark-

ers for accurate definition [2085]. Besides basic research, clinical research can especially benefit from this analysis as a high amount of information can be extracted from limited, and thus precious, sample sources. Especially for longitudinal high-content immunomonitoring of big patient cohorts, multidimensional FCM serves a fast and highly sensitive tool to correlate responses and observe changes of treatment as the basis to predict outcome of the myriads of immunotherapeutic approaches to treat diseases. The computational approaches allow for interrogating large data sets generated in these types of studies and enable the unbiased analysis of the data, possibly leading to the detection of rare cell types and can be of predictive value for treatment outcome.

5.5 *Experimental workflow*

Here, we describe the key steps that should be taken for a systematic panel design approach.

1. Define the experimental hypothesis and the relevant cellular populations (e.g., CD8$^+$ T cells)
2. Make a list of lineage markers that are necessary for consistent identification of the populations of interest (e.g., CD3/CD8 and CD45 for CD8$^+$ T cells).
3. List all target markers of interest and categorize expected expression patterns and (if known) antigen density into low, medium, and high.
4. Generate an SSM on your instrument by running single-stained controls with all desired fluorochromes and calculating the SSM in FlowJo or another suitable analysis program.
5. Look for the three highest values in the SSM and assign the corresponding fluorochromes to mutually exclusive antigen targets, i.e., targets not expressed on the same cell (in our example SSM in Table 95 the most problematic pair would be BUV563 spread into the YG-586 PE detector).
6. Calculate the row sums in the SSM. The fluorophores with the lowest row sum overall contribute the least spreading error to your experiment—these should be assigned to your lineage markers, e.g., CD3 and CD8 for a CD8 T cell-centric analysis (in our example SSM in Table 95 this would be BV421 and BUV395).
7. Calculate the column sums in the SSM. The detectors with the lowest column sums receive the least amount of spreading error—these detectors are suitable for dim or unknown target markers (in our example SSM in Table 95 good examples would be the B-515 and V-510 detectors). Utilize bright fluorochromes for these antigens, if possible. The detectors with the highest column sums receive more spreading error—for these detectors perform preliminary experiments to assign target markers that deliver a bright enough signal to be above the spread (in our example SSM in Table 95 this would be YG-586 and YG-610 detectors). However, one has to keep in mind that there might be a single contribution that drives the total spreading error in a detector, and if not used on the target cell, this can improve the total spreading error received (e.g.,

in our example SSM in Table 95 the contribution of BUV661 and BUV563 to the YG-586 detector).
8. Run a test experiment including all relevant FMO controls. Perform data analysis and quality control as outlined in the next section.

5.6 *Data analysis*

For general concepts of computational analysis of high-dimensional single-cell data, we refer the reader to Chapter VII "Data handling, evaluation, storage and repositories" High dimensional FCM of the guidelines. Within this section, we focus primarily on quality control aspects prior to data analysis.

Most technical artifacts occur when samples are acquired over multiple days (i.e., batch effect), however, sometimes they also happen within one experiment due to the lack of appropriate controls or inconsistencies in instrument handling. In the authors experience, a common cause of artifacts in fluorescent cytometry is incorrect compensation, which in turn is mostly due to poorly prepared single-stained controls. To pinpoint such mistakes, visual inspection of N×N views of the final data should be performed, with N being the number of fluorescent parameters acquired, i.e., every marker against every marker. Within these plots, one should screen the data for typical erroneous patterns such as "leaning" triangular populations and "super-negative" events. Examples patterns are given in Fig. 231E and F.

Sometimes fluorescent signals vary across different experimental days or even within one experiment even though the same staining panel was applied. Correct data transformation can help to diminish this effect [2086]. Different transformation approaches such as the biexponential, arcsinh, and hyperlog display can be used, and the optimal transformation depends on the specific data and cannot always be computationally predicted [1808].

Dead cells, doublets or staining artifacts, e.g., by Ab aggregates, can appear as false positive data points or outliers in the analysis, potentially leading to wrong interpretation of the data. Thus, it is important to exclude these prior to unsupervised computational analysis by appropriate pregating or "data cleaning." Depending on the immunological question asked a pregating on the population of interest can be part of the preprocessing and may speed up the computational procedure of the analysis (e.g., per-gating and exporting of live singlet CD45$^+$ CD3$^+$ cells). Even though conventional manual gating may not be suitable to capture all the correlations between the up to 28 fluorescent parameters, it still serves as an important quality check before, during and after the computational data analysis.

5.7 *Advantages*

Thorough panel design, not only for multiparametric FCM panels, will award the researcher with robust and reproducible FCM data with a satisfying resolution also of dimly expressed markers. Even

though the optimization of a panel may appear time consuming and requires various controls to assure reliable interpretation, it will save time in the downstream analysis and interpretation of the generated data. Usage and correct interpretation of an SSM will improve the process tremendously. It may not be obvious at first, but cost will be reduced, as the unnecessary repetition of experiments due to non-interpretable data will be minimized.

5.8 *Pitfalls*

Pitfalls in high-dimensional fluorescent cytometry often arise from inappropriate planning of experiments and lack of controls. This can be avoided by systematic panel design and the inclusion of FMO controls as described above. Also, an inherent disadvantage is the necessity to obtain single-cell suspensions, which disrupts the natural architecture and interaction of cells in situ. Several emerging techniques allow high-dimensional cytometric measurements directly within tissues, as has been shown by Histocytometry [2087] or the recent commercial release of an imaging CyTOF system (Hyperion, Fluidigm) [1883].

5.9 *Top tricks*

1. It is important that the detector voltages of the used flow cytometer have been optimized using an appropriate technique. The most widely accepted approach for this is a voltage titration [48], which will determine the minimally acceptable voltage yielding optimal resolution for each detector. Voltages should not be adjusted solely for the purpose of lowering compensation values [2088].
2. To deal with spreading error beyond the above-mentioned approaches, one can utilize the fact that spreading error is directly proportional to the signal intensity. If assigning a fluorochrome to a lineage marker showing high and bimodal expression (e.g., CD8), one can utilize lower Ab titers (below saturating concentration) to lower the positive signal and in turn the spreading error generated. However, it is important to note that this approach requires consistent staining conditions in terms of cell numbers, staining temperature, and staining duration.
3. Many recent fluorochromes are based on organic polymers, which can under certain conditions show interaction due to their chemical properties. To alleviate this issue some manufacturers have released commercial buffers that are designed to minimize these unspecific interactions, and thus it is strongly encouraged to use these buffers whenever more than one polymer-based dye (e.g., all Brilliant Violet and Brilliant Ultra Violet dyes, SuperBright dyes, etc.) is included in a staining.
4. When performing experiments with staining and acquisition over several days, it is recommended to follow best practices for consistent setup of the used instrumentry [48] and to include a reference sample on every experimental day in order to detect irregularities in staining, compensation or transfor-

mation. These control samples can then be overlayed in histograms of all markers to visually control for the aforementioned errors. Should artifacts occur in the control samples, it might be useful to either exclude specific parameters or samples from the computational analysis.

6 Single cell genomics and cytometry

6.1 *Overview*

Cells for single-cell genomics are in almost all cases collected using FCM. FCM can be used to isolate cells of interest from more complex biological samples, to perform index sorting upstream of single-cell genomics workflows or to provide fluorescence intensity measurements from single cells, that can be merged into single-cell gene expression matrices as an additional layer of information. Here, we provide an overview on how FCM complements single-cell genomics technologies, together with a basic overview on currently available technologies.

6.2 *Introduction*

Single-cell technologies provide an unprecedented view on the complexity of biological systems, by uncovering how organisms are build up from single cells and how these cells are different. Classical bulk analysis tools analyze cell populations and consequently, a whole layer of biological processes stays invisible, like, for example, the presence of rare cell-types in tissues or gene-expression heterogeneity that can depend on highly time-resolved gene-expression bursts. Single-cell technologies depend on the separation of cells from tissues or cell culture and their sorting into separate reaction volumes, eventually containing a single cell per reaction. Then, DNA- or RNA-sequencing technologies are applied, specialized on low-input material. This allows to characterize the genome, epigenome, or transcriptome of each cell. Bioinformatic analysis, that takes into account the technical noise of sparse input material data, is used to extract biologically meaningful processes.

Although single-cell technologies can be technically challenging, advances in sample and library preparation methods have made single-cell analysis broadly available (Fig. 232):

1. **FCM-based multiwell plate methods**: Here, cells are sorted into multiwell plates and allow optional indexing of the sorted cells. Then, sequencing libraries are prepared from wells, most frequently using SMART-seq2 [2089]. Optionally, library preparation can be done using robotics, which increases throughput and at the same time, decreases batch effects [2090].
2. **Microfluidics- and nanowell-based methods** significantly increase throughput and decrease pipetting effort of single-cell transcriptomics. DropSeq [2091] and InDrop [2092] are frequently used and based on microfluidic chips that combine barcoded beads and cells within droplets. Especially
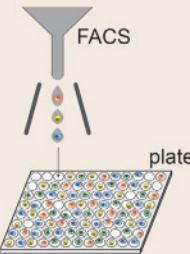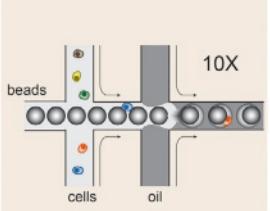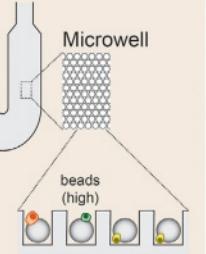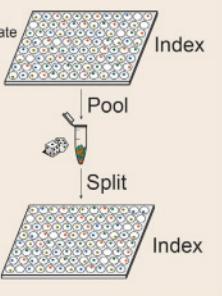
	SMART-seq	DropSeq/10X	BD Rhapsody	sci-RNA-seq
FACS-step	sc sorting into plate	bulk-sorting	bulk-sorting	sc sorting into plate
Principle	isolated cells in wells	microfluidics	microwell	split-pool indexing
Technology				

Figure 232. Examples of frequently used single-cell transcriptomics platforms. Comparison of different technologies for single-cell RNAseq, including SMART-seqs, DropSeq, 10× Chromium, BD Rhapsody and sci-RNA-seq. Basic differences are explained in the main text. Here, we only provide a collection of single-cell RNAseq methods to cover the key principles of the different technologies.

the invention of commercially available systems from 10× Genomics, Dolomite Bio, and 1Cell Bio, made these technologies broadly available. Nanowell-based systems process thousands of cells in a single step by depositing barcoded beads and cells into nanowells on a printed chip [2090, 2093]. These systems are commercially available, e. g., from BD Biosciences (Rhapsody), Fluidigm (C1), or Clontech (ICell8). Compared to microfluidics-based methods, nanowell systems have lower throughput, however, improved control over the deposition of beads and cells into wells using microscopy.

3. **FCM-based single-cell combinatorial indexing** uses a multi-step barcoding strategy to increase throughput of single-cell RNAseq without the need to set up microfluidics and nanowell systems. Cells or nuclei are sorted into wells of a multiwell plate, indexed with a primary barcode, pooled, and sorted again into wells, followed by a secondary barcoding step. Consequently, each cell receives a unique combination of barcodes, enabling RNA-molecules to be assigned to individual cells [2094].

6.3 Obtaining single cells for single-cell applications

We will focus here on the application of FCM in combination with different single-cell transcriptomics technologies. FCM upstream of single-cell RNAseq library preparation allows to enrich for singlet cells (essential for any single-cell method) and if needed, to enrich for subpopulations of interest. These subpopulations may be viable cells, non-apoptotic cells, cells in a specific cell cycle phase, or cells expressing a sortable marker to enrich for specific or rare cell types.

1. True, viable, and non-apoptotic cells can be isolated using FCM. FCM markers and dyes are available, including Caspase 3/7 or AnnexinV for apoptosis and nonpermeable nucleic acid

dyes for cell membrane permeability assessment or DNA staining. Cell separation from tissues or cell culture results in imperfect single-cell separation and enables efficient identification and isolation of singlets on an FSC/SSC plot. For such complex samples, including organ biopsies or whole embryos, it is possible to identify cells using a cell permeable DNA dye such as Hoechst 33342 or DRAQ5 [2095, 2096]. Figure 233 shows a DRAQ5 and singlet gating on *Drosophila* larvae neuronal stem cells, containing small cells that overlay with cellular debris and yolk particles.

In addition to nonviable cells, pro-apoptotic and apoptotic cells can be highly abundant in tissue preparations, but can be removed using FCM. Such stainings can be done using AnnexinV or Caspase3/7 [2097, 2098] (See Chapter V Biological assays Section 7 Measuring cell death mechanisms). Figure 234 shows example apoptosis staining in bone marrow and brain tissue preparations. The staining of pro-apoptotic cells is especially important, since these cells are difficult or impossible to distinguish from live cells computationally. Apoptosis is a biochemical process that can be initiated without prior changes in gene-expression that can be identified on transcriptome level (EMBL Genomics Core and Flow Cytometry Facility, unpublished data). There is no objection to combine the apoptosis staining with the viability stain on the same colour when the panel is tight (see Chapter V Section 7 for details). Importantly, we do not observe any influence of Hoechst, DAPI, or DRAQ5 stains on library preparation for RNAseq and single-cell transcriptome data quality.

2. Singlet gating is key to ensure that only single cells are analyzed, as multiple cells are difficult to filter out during bioinformatics analysis. The combination of sequential FSC and SSC height versus area pulse-shape analysis are reliable single cell gates [2099]. However, pulse-shape analysis-based singlet gates can become challenging when working with tissue material composed of diverse cell types (e.g., bone marrow, lung,
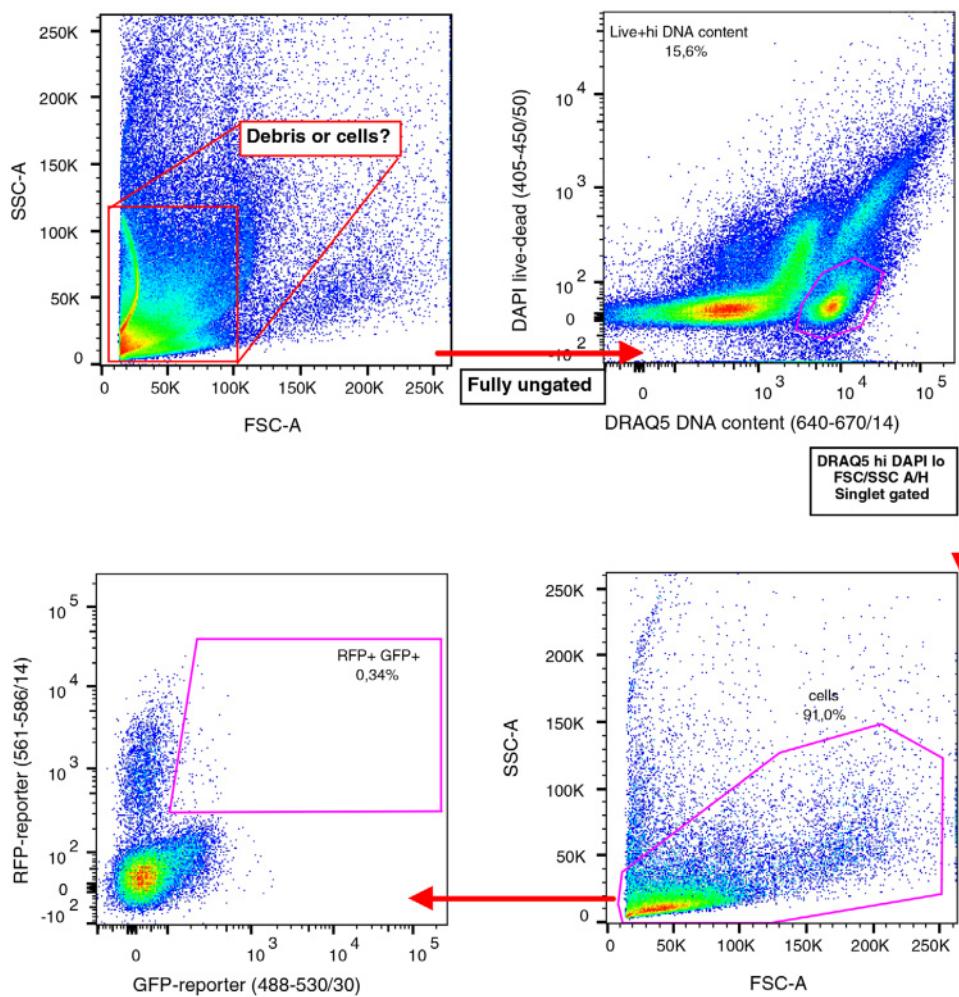
Figure 233. Cleaning up the scatter with a DNA stain resolves the masking of yolk and debris. Drosophila melanogaster larvae preparations were stained with 2μM/mL DRAQ5 to identify DNA containing particles from debris. Clear gates for fluorescence-reporter expressing cells can be drawn.

intestine, skin). In these cases, the scatter-based singlet gates (area vs. height) appear slightly spread and are often not efficient in isolating single cells. This scatter heterogeneity results from different optical densities, cell sizes, and shapes. To circumvent such limitations, the cell suspension can be stained with a cell permeable DNA dye (e.g., DRAQ5 or DAPI) and the signal is used for singlet gating (see Chapter V Biological assays Section 6 DNA synthesis, cell cycle, and proliferation). This method is independent of the scattering activity of cells, since DNA content is always the same. Implementing this strategy also allows to limit analysis to certain cell cycle phases, an often unwanted source of cellular heterogeneity important to consider during data analysis.

3. Gated cells should be of high purity and have a high chance to end up either in a microtiter-well or in the bulk sort tube for microfluidics/nanowell-based methods. Efficiency and purity of sorting depend on the sorting mode; therefore, it is important to select the best mode for the respective single-cell library preparation method. For microfluidics/nanowell-based methods, bulk sorts are done, based on sort modes ensuring purity

of the sorted cells and fast sorting. Purity modes, however, suffer of reduced probability that the gated cell is actually sorted, because the mode does not take into account the actual position of the cell within the interrogated drop: If a cell is close to the edge of the interrogated drop, it can move into the neighboring drop during its travel time between detection and the actual drop charging (Fig. 235). Generally, purity modes that are run at an optimal sampling speed have an efficiency of 80 to 90%, i.e., the number of cells within the bulk sort tube will be only 80 to 90% of the assumed cell number [2100]. It is therefore important to count cells again after sorting and if necessary, to concentrate cells again. Injection of cells at defined concentration into microfluidics/nanowell-based devices is key to prevent doublet formation (too high cell density) or an unnecessary high number of empty droplets (too low cell density).

For microtiter-plate based methods, cells are sorted directly into the wells of a plate using a single-cell sorting mode. In most instruments, such modes implement a positional limitation for the cell to be in the center third of the drop, on top of the purity mask (Fig. 235). BD Aria systems use the phase mask scanning
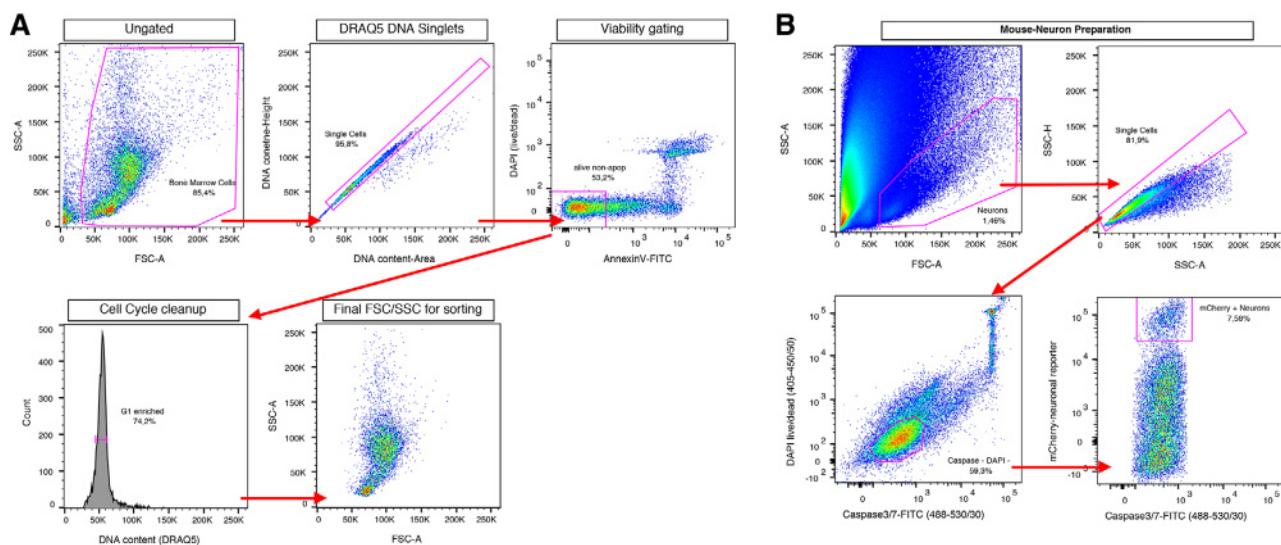
Figure 234. Advantage of combined apoptosis and viability stains upstream of single-cell RNAseq methods. (A) Scatterplots showing DRAQ5 staining (for singlet gating and cell cycle restriction) in combination with AnnexinV (apoptosis staining). Cells show a low frequency of dead cells when assessing cell death purely by staining membrane-permeability. However, adding AnnexinV or Capase3/7 probes reveals that the viability of the samples is rather mixed as many cells have started to become apoptotic. (B) High amount of pro- and late-apoptotic cells in dissected mouse brain tissue. In both cases, a significant number of non-perfectly viable cells would have been sorted for downstream sequencing if only simple live-dead staining with DNA-dyes was utilized.

the inside of the interrogated drop: If a cell falls within the phase mask, the drop will not be sorted due to a high risk of the cell moving into the leading or lagging drop (Fig. 235 and http://www.bdbiosciences.com/ds/is/others/23-6579.pdf). This results in a high probability of cells being sorted into the tube/well, but at the cost of a high number of aborted cell sorts due to phase mask violation (on average >50%) when using manufacturer's settings. Therefore, large bulk sorts are not operated using single-cell mode.

In addition to the sorting mode, the performance of sorters strongly depends on a perfect flow of the cells along the stream, which depends for example on sample properties including cell shape. One way to evaluate the machine derived drop delay for new or difficult to handle cell types is an easy to set up single-cell qPCR test, that is described in the Tips & Tricks section.

4. Both microfluidics-based (e.g., 10× Genomics) and nanowell-based (e.g., BD Rhapsody) single-cell transcriptomics solu-
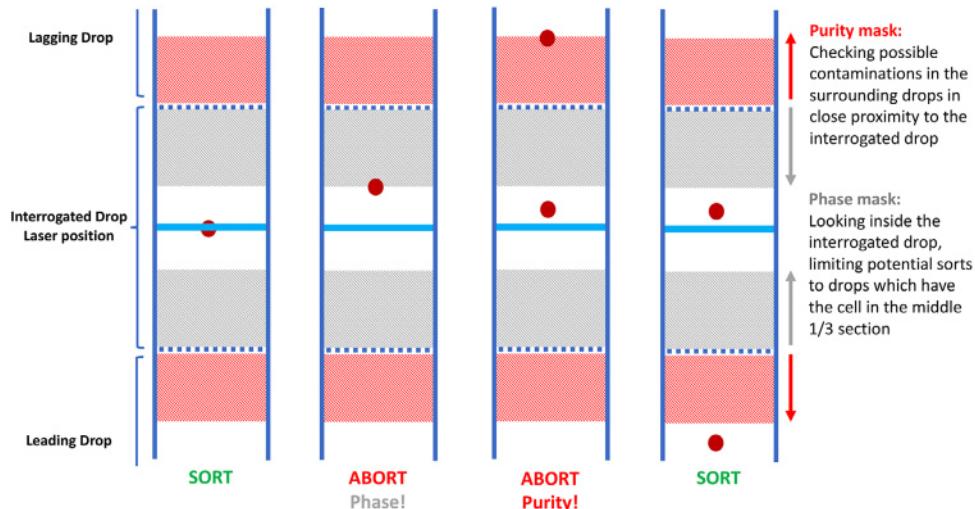
Figure 235. Technical details of different single-cell isolation modes. The single-cell mode in DiVa and FACSChorus includes a purity mask scanning the leading and lagging drop for contaminations plus a phase mask that scans the ends of the interrogated drop for the position of the cell of interest. Any violation of the purity or phase mask will lead to the termination of the drop. This results in a general loss of >50% of potential target cells—however, the mode has the highest precision for the cell to be delivered with the prospective drop while ensuring the purity and that only one cell is deposited.

tions use cell suspensions as input material that should fulfill the following requirements: (i) Cell viability must be high, ideally above 90%, as measured with a dye exclusion assay, e.g., Trypan blue (visual counting) or DAPI/Draq7 (FCM). Cell death inside the single-cell suspension and prior to droplet-generation results in ambient RNA that will be present in every droplet, reducing data quality. (ii) Only singlet cells should be present, as multiplets are packaged into droplets or wells at similar efficiency as singlet cells. (iii) Measurement of cell density should be exact and done directly before loading cells into the device. Loading too many cells results in a high multiplet rate, loading too less cells results in an unnecessary high number of empty droplets/wells and consequently, increases costs per cell. For 10× genomics, ideal cell density is between 600 and 1500 cells/μL. (iv) Cells should be suspended in a buffer like PBS or PBS + 0.04% (w/v) BSA and stored at 4°C until loading. Buffers that include residual RNase or DNase from upstream cell preparation should be replaced. Other buffers have been validated for different single-cell protocols (see respective manufacturers protocols), as for example DMEM + 10% FCS. Cell viability must be stable under these conditions, which can be tested in advance by prolonged incubation in the buffer and dye exclusion test before and after incubation. As cells settle fast, they should be mixed prior to loading. This can be done by pipetting or vortexing, depending on the cell type requirements. In case of longer runs, as often necessary when running DropSeq and other custom-built setups, cells can be constantly mixed using a magnetic mixer, preventing changes in injected cell concentration over time.

Of note, some cell types are more difficult to capture using microfluidics/microwell-based single-cell methods than others [2090, 2101]. Especially when working with complex tissues, this can result in underrepresentation of specific cell types and consequently, wrong conclusions regarding tissue biology. This is especially true using microfluidics- and nanowell-based methods, since it is not possible to see which types of cells are less efficiently packed into the reaction volumes. Here, it can make sense to do plate-based single-cell libraries using SMARTseq2.

6.4 Applications

Single-cell transcriptomics

Single cell transcriptome sequencing measures the expression level of polyadenylated transcripts within single cells. Furthermore, data contains transcript sequence information that can be used for structural variant analysis or the identification of splice-variants. Depending on the protocol and technology used, either whole transcripts or transcript 5' or 3'-ends are sequenced, with 3'-RNAseq being the most widely used technology for gene expression analysis.

Other single-cell omics technologies

Transcriptomes are highly informative, but alternative readouts reveal different views on cell-to-cell differences. These technologies include whole or targeted genome sequencing and epige-

nomics, for which both commercial and non-commercial platforms are available. Furthermore, proteomics and metabolomics are entering the single-cell field. Single-cell multiomics, i.e., the simultaneous analysis of two or more omics (e.g., genome and transcriptome) in the same cell, will become less technically challenging. Analyzing phenotypes on top of these -omics technologies, for example, by imaging-based FCM (see Chapter VIII Section 1 Imaging FCM) will become available in the future. Currently, these technologies suffer of low image quality, function at comparatively low throughput and depend on technically challenging setups that are not widely applicable.

CRISPR-screening technologies

CRISPR/Cas9 technologies can be combined with FCM and single-cell technologies, providing a powerful tool for large-scale functional genomics. CRISPR/Cas9-sgRNA libraries are applied to cells under conditions in which one cell expresses one sgRNA along with Cas9. The functional consequence of such a perturbation is then analyzed using simple or complex readouts: Simple readouts rely on FCM, e.g., by analysis of a fluorescent reporter or a proliferation dye. Then, sgRNA enrichment analysis within the binned and sorted populations is done by extracting genomic DNA and sequencing of the integrated sgRNA sequences. This allows conclusions on the influence of each sgRNA in the library on the respective phenotype. Even simpler, positive or negative selection screens analyze sgRNA enrichment after 1–3 weeks of growth with sgRNAs being either enriched or depleted depending on the function of the targeted gene. Complex readouts can be generated by coupling CRISPR/Cas9 with single-cell transcriptome readouts (CROP-Seq and similar methods). Here, the sgRNA sequence or a coupled barcode is sequenced along with the transcriptome, allowing to compute transcriptomic changes upon each perturbation in intermediate to high throughput.

6.5 Data analysis

Single-cell RNA sequencing (scRNA seq) development opened in the last couple of years new approaches to answer important questions in developmental biology [2102], cancer [2103], and neural network analysis [2104].

Detection and quantification of gene expression at single-cell level encompasses many challenges regarding data analysis. As an example, the very low starting material from a single-cell can lead to dropout genes in some cells and not in others. The stochastic nature of gene expression might imply an important cell-to-cell biological variability in single cell measurements although the specific cell is currently in a different expression cycle. These confounding factors, including variable detection sensitivity, batch effects, and transcriptional noise, complicate the analysis and interpretation of scRNA sequencing datasets.

Before using sequencing reads to extract valuable biological information, crucial considerations need to be put into the design of the experiment to lower at its minimum the impact of confounding elements and technical artifacts. These aspects have been discussed in detail in refs. [2090, 2105].

Analysis tools for bulk RNAseq have been first used and adapted to address the specific properties of scRNAseq data [1869, 2105]. Normalization is an essential first process in the global analysis workflow for scRNAseq due to high data variability and noise. The aim is to correct the biases introduced by gene expression dropouts, amplification, low library heterogeneity or batch effects (e.g., different platforms, time points, technical handling, reagent lots, etc.). External synthetic spike-in controls help to disentangle the technical noise from natural biological variability [2106]. Adaptation of formerly developed methods for bulk RNA sequencing could also be used [2107–2109]. More recent approaches are normalizing the data between sample [2110] or cell-based factors derived from the deconvolution of pool-based size factors [2111]. The popular R package Seurat integrates a comprehensive workflow from the quality assessment of each cell to analyze, exploring scRNA-seq data as well as integrating different datasets [2112].

The transcriptional landscape of a single cell can be compared based on co-expressed genes. Here, cells are grouped into clusters and marker genes, which are driving the expression signature of sub-clusters, are identified and annotated. Before the identification of cell clusters, visual exploration is usually achieved by dimensional reduction, where the dataset is projected to only a couple of dimensional spaces. Among these approaches, principal component analysis (PCA) [2113], t-SNE [2114], or UMAP [2115] are frequently used. Different clustering approaches and tools have been compared using a similarity index, i.e., the adjusted Rand index [144]. Annotation of differentially expressed (DE) genes between clusters allows biological hints on the nature of the subpopulation [145] and provides a comprehensive overview of the available DE methods. Finally, methods aiming to infer the differentiation trajectory of the clusters have been also compared in a comprehensive study [2116].We would also like to mention two interesting resources, listing software packages dedicated to the different scRNAseq applications (https://www.scrna-tools.org/ and https://github.com/seandavi/awesome-single-cell).

6.6 *Top tricks*

A simple single-cell qPCR protocol to test sorting efficiency prior to single-cell sequencing

Since single-cell sequencing can be cost-intensive and not all handling errors during sample preparation can be identified later during data analysis, We therefore provide a protocol allowing to check FCM instrument performance in advance, if using novel or difficult to sort cell types, This protocol was developed by the Stahlberg lab and is currently taught in the EMBO and EMBL single-cell trainings courses on single cell omics technologies [1905, 2117].

Testing whether the sort-stream hits the center of test tubes and microtiter plates is straight-forward. However, it is more difficult to validate if the drop-delay (as most frequently assessed with fluorescent beads) works with novel cell types or cells that show difficult behavior within the stream: Some cells, especially larger and more structured cells, have the tendency to tumble in the

stream, slowing them slightly down due to potential drag. This could lead to a reduced number of positively seeded wells or to reduced cell numbers in a bulk sort. Sorting single cells into a multiwell-plate followed by qPCR of a highly expressed gene will give a precise measurement of sorting efficacy.

Protocol

Materials required:

- Human GAPDH primers:

    GAPDHv2_Fwd CCCACTCCTCCACCTTTGAC
    GAPDHv2_Rev GCCAAATTCGTTGTCATACCAGG

- BioRAD Hard-Shell® 96-Well PCR Plates, low profile, thin wall, skirted, red/clear #hsp9611
- TATAA SYBR® GrandMaster® Mix ROX - TA01R
- TATAA GrandScript cDNA Synthesis Kit - A103c (1000 rxn) A103b (200 rxn)
- CelluLyser™ Micro lysis buffer - H104
- RNAse and nucleotide free water

Procedure:

Cell sorting into plates

In addition to standard FCM calibration, the instrument needs to be calibrated to deposit cells in the center of each collection tube. This can be tested by sorting 10–20 beads/cells on plastic film covering the plate or by checking drop formation on the bottom of a hard-skirted BioRAD PCR plate (Fig. 236). In case of non-optically tracked arms, we suggest to check the calibration every second plate, because the sorting arm may be displaced over time. A too small volume of provided buffer (here: lysis buffer) increases the risk of a cell not reaching the buffer but sticking to the tube wall, while too large volumes might not work with downstream applications. We recommend sorting two wells with each ten cells (positive control), to include at least two wells that will intentionally not receive a cell (negative control) and the rest of wells with single cells.

PCR plates (96-well) with lysis buffer should be prepared in advance: We found that 5 µL of provided Cellulyser weak lysis buffer per well works well. Immediately after sorting into the plates, place the plate on carbon ice, and store at –80°C until proceeding with reverse transcription.

Reverse transcription

We have good experience with TATAA GrandScript cDNA synthesis Kit using a mix of oligo-dT and random hexamers. We generally use the following reverse transcription protocol (added directly to the frozen cells, per well): 2 µL 5× TATAA GrandScript RT reaction mix, 0.5 µL TATAA GrandScript RT enzyme, and 2.5 µL nuclease-free water (according to the manufacturer's instructions). The total volume per well is 10 µL. Reverse transcription is done using the following temperature profile: 22°C for 5 min, 42°C for 30 min, and 85°C for 5 min.

Quatitative PCR

GAPDH is highly and ubiquitously expressed and can be used to detect the presence of a single cells using qPCR amplification irrespective of the cell type. Normal qPCR-MIQE guidelines apply
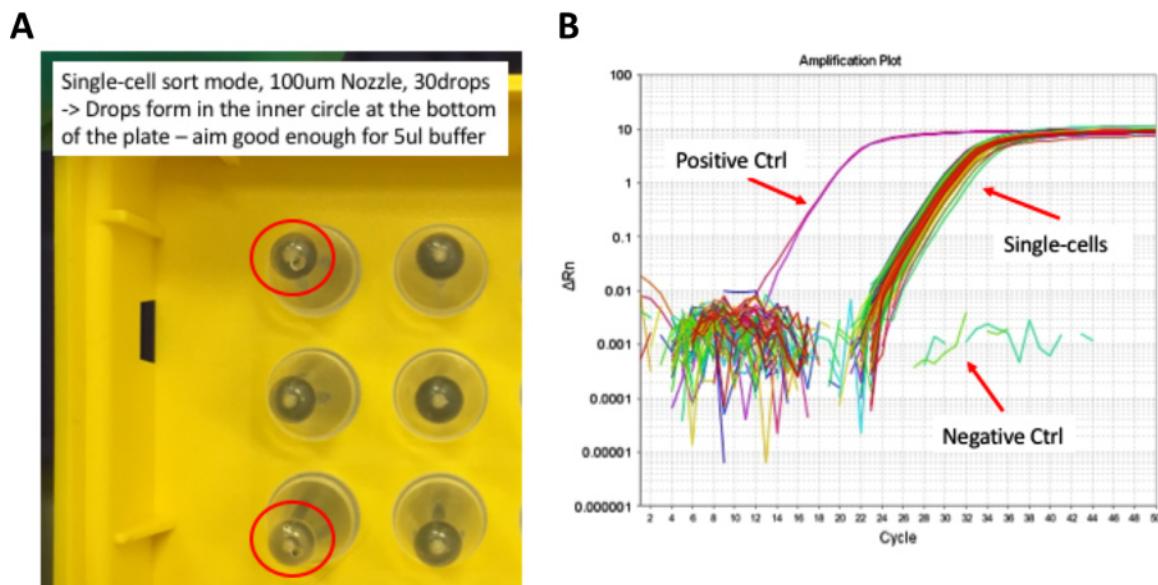
Figure 236. (A) Transparent hard-shell PCR plates can be used to check the correct deposition of sorted drops into 96-well PCR plates; controlling the aim at the bottom of the well is superior to only checking on a seal or lid above. (B) An example outcome of the single-cell qPCR protocol checking single-cell deposition of HeLa cells with GAPDH qPCR. Positive controls (ctrl) contained 10 cells per well, negative controls were empty wells. All single cells show formation of a specific PCR-product, indicating that all wells with expected single cells contained a single cell.

to the described qPCR assay For using a high number of amplification cycles due to low input material, consequently we suggest to check melt curves for byproducts and primer-dimers after PCR.

Dilute cDNA samples to a final volume of 30 μL with H_2O. Prepare qPCR reactions for a total volume of 10 μL per well: 5 μL qPCR 2×Mix, 0.4 μL 10 μM fwd/ref primer mix, 2.1 μl H_2O, 2.5 μL cDNA. A mastermix of qPCR 2×Mix, fwd/rev primer, and H_2O should be prepared. qPCR is run using SYBR Green ROX protocol for 50 cycles followed by melt curve: 30 s 95°C, 50× (5 s 95°C, 20 s 60°C, 20 sec 70°C), 65 °C to 95 °C with 0.5°C increment. Exemplary results are shown in Fig. 236.

7 Microbial cells

7.1 Overview

Recent insights into the impact of the microbiota for the environment and for human health has led to an explosion of research efforts to try to understand the role and mechanisms of bacteria, bacterial communities, and their products in regulating homeostasis and pathology. With the advent of high-throughput sequencing technologies, 16S rRNA gene amplicon sequencing and metagenomic approaches are widely applied to resolve the community structure while proteomic approaches are used to reveal functional relationships. However, these methods are still expensive, time consuming, and have high requirements for data analysis. FCM offers a fast and inexpensive alternative for the single-cell based characterization and analysis of microbial communities. Yet, flow cytometric measurement of microbial cells is still challenging and several issues that have to be considered will be discussed in

this section. If done correctly, FCM of bacteria can surpass simple applications such as counting cells or determining live/dead cell states [2118].

7.2 Introduction

Complex microbial communities occur almost everywhere, from natural environments such as fresh water systems, marine environments and soil, to managed systems such as drinking water facilities or wastewater treatment plants, to the gut or skin of humans and animals. Recent research efforts have highlighted the importance of microbial communities, not only in the environment, where they are responsible for all biogeochemical processes, but also as integral part of multicellular organisms. As bacterial microbiota, they colonize all body surfaces and have been shown to educate the immune system but also play a crucial role in inflammatory diseases such as asthma, inflammatory bowel disease (IBD), and obesity.

Bacteria can vary up to two orders of magnitude in size, but 0.8 to 3 μm are common dimensions. Unlike eukaryotic cells, bacterial cells are not compartmentalized, i.e., they do not have organelles, allowing dyes to move freely in the cytoplasm unless they bind to specific structures such as DNA. This and the small volume of the bacteria can favor interactions of fluorescent dyes leading to loss of fluorescence intensity, making the simultaneous intracellular use of more than one or two dyes challenging. Most bacteria also have a cell wall that prevents the intracellular uptake of almost all larger probes such as Abs. The major challenge but also the major advantage of bacterial cytometry is the inability to grow many bacteria as pure culture. While "culturomics" has led to a large
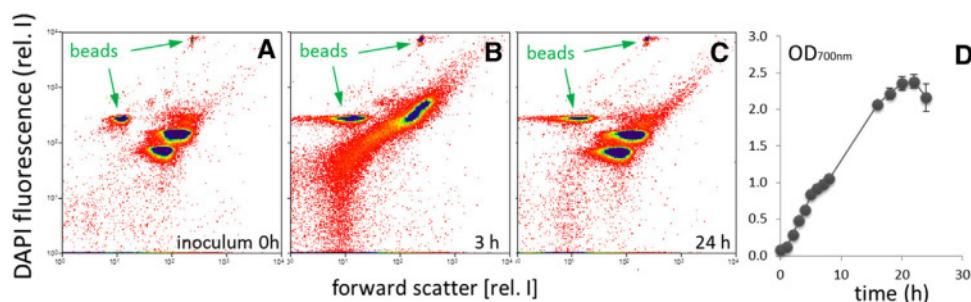
Figure 237. Flow cytometric analysis of cell states in pure cultures of *Escherichia coli* K12 grown on complex DSM 381 medium. Cells were sampled, treated with 2% PFA and fixed in 70% ice-cold ethanol. Following, cells were stained with a 0.24 μM DAPI solution and measured using a 355 nm Genesis CX laser (100 mW, both Coherent, Santa Clara, CA). Scatter was measured using a 488 nm Sapphire OPS laser (400 mW). 0.5 μm and 1 μm Fluoresbrite Microspheres (both Polysciences, 18339 and 17458, Warrington, PA, USA) were added to every sample as internal standards. A and C show nearly identical proliferation patterns during lag and stationary phases of growth. B shows the proliferation pattern (uncoupled DNA synthesis) in the log-phase. The right graph D shows the growth curve where samples were taken from 500 ml batch cultures with 200 ml medium for a time range of 24 hours. After a short lag phase the cells immediately started exponential growth which ended after about 20 hours.

increase in the number of bacteria that can be grown in culture, still many bacteria cannot. Lack of pure strains of bacteria precludes calibration and verification of specific staining. In addition, cells of the same bacterial strain change their physical and physiological properties depending on micro-environmental conditions and growth phase. Bacterial cells tend to be small in unfavorable growth conditions and increase in size during optimal growth conditions. While bacteria typically have one molecule of genomic DNA, some can have multiple copies of the same genomic DNA or have two or three genomic equivalents of different length and composition. The numbers of genomic DNA equivalents are also not evenly distributed among cells of a population as asymmetric cell division and uncoupled DNA synthesis is widespread among bacteria. The number of genomic DNA copies does not indicate the condition of the cell, as the cells often do not divide under stress conditions and retain the high copy number of genomic DNA [2119].

When considering these caveats, some of which can also be used as discriminating parameters, FCM is a well-suited method to study bacteria at the single-cell level. While the diversity of such natural communities can reach up to several thousands of different phylotypes per 1 g of sample, making cell type-specific labeling impossible [2120], approaches such as cytometric fingerprinting of natural microbial communities can be used to analyze community structures, complexity and alterations. New bioinformatics tools for quantitative and automatic evaluation of bacterial cytometric fingerprints are becoming available enabling the identification of subpopulations or sub-communities of interest for subsequent cell sorting and downstream analyses, such as NGS or proteomics approaches [2121, 2122].

7.3 Applications

A common application is the discrimination and enumeration of live bacteria using live/dead dyes. Both in biotechnology and in the environment changes in cell numbers can have major implications. Also recently, it has been shown that cell numbers are impor-

tant for the standardization and normalization of 16S rRNA gene sequencing data [2123]. Flow cytometric applications achieving high resolution of light scatter and DNA content discrimination can be used to characterize and resolve complex microbial community structures, such as environmental microbiota or intestinal microbiota by generating community patterns.

There is a wealth of methods available to analyze states of cells in pure culture [2124]. Such methods are often used to describe segregated cell states of different activity. Besides the measurement of intracellular components also the determination of energy or growth states are in the focus to understand cell behavior. Especially in medicine, the detection of pathogens and their differentiation from other bacteria is desirable. Cell type labeling and cell proliferation can give information on active cell growth. Uncoupled and fast DNA synthesis can easily be visualized by FCM (Fig. 237B) and discriminated easily from non-growing cell states (Fig. 237A and C).

7.4 Equipment

Not all flow cytometers are suitable for the measurement of bacteria but we have good experiences with the BD Influx v7 Sorter and MoFlo Legacy cell sorters [2125]. Due to the small size the amount of dyes bacterial cells bind is significantly lower resulting in the generation of low number of photons when excited compared to eukaryotic cells. Thus, high laser power starting at 50 mW and going up to 400 mW lasers, highly sensitive PMTs for signal detection and clear tubes and water streams to provide low background signals are important prerequisites for the measurement of bacteria. Forward (information related to cell size) and side (information on granularity and surface structure) scatter signals of cells are best recorded at lower laser wavelengths (i.e., 350 nm or at least 488 nm). Using machines that lack sensitive scatter detection, using fluorescence of, e.g., nucleic acid stain as trigger signal for acquisition is an option. All solutions should be filtered (0.1 μm) before use. Samples isolated from natural environments may require a sensitive shaking or even an ultrasonic treatment

to dissolve flocs (see below). Samples should be filtered before measurement through a 50 μm mesh to avoid the clogging of the nozzle.

7.5 Experimental workflow and acquisition

When measuring viable bacterial cells by FCM, one has to be aware that some bacteria have generation times of only few minutes. Although bacteria are generally easy to handle, their physiological cell states can change from one minute to the next. Therefore, techniques that include fixation tend to be more robust. Several fixation methods have been described [2126]. In short, bacterial cells are incubated for 2% PFA at for 30 min at room temperature to stabilize the cell wall and finally fixed with 70% ice-cold ethanol. As this stage, samples are stable for weeks to month at –20°C. When staining methods are sensitive to PFA pretreatment cells can be stored stably in 20% glycerol at –20°C. Alternatively, samples can be stabilized for storage and shipping at ambient temperatures by infrared supported drying [2125]. However, it is crucial to test the optimal stabilization method for the samples in questions and the downstream application.

Bacterial communities can comprise cells of different sizes and shapes. Thus, classical doublet discrimination using, e.g., width signal versus height signal is not possible. For samples, where clumping of bacteria is expected, ultrasound sonification should be considered to resolve cellular aggregates. Also here, conditions of sonification have to be established for different types of samples to maintain cellular integrity. A typical treatment is exposure to 35 kHz and 80 W effective output power for 1 min in an ultrasonic bath to disband large cell aggregates [2125].

One also has to be aware that some bacteria can be permeable to otherwise cell-impermeable dyes, such as PI, and other bacteria very efficiently shuttle out otherwise cell-permeable dyes, such as SYTO9, easily resulting in false positives and negatives when looking at complex microbial communities [2123, 2124, 2127]. Again, the non-cultivability of many bacteria precludes the validation and calibration of such staining procedures. This applies also to other viability dye approaches, such as the measurement of membrane potential. Inhibition of the respiratory chain and depolarization of the membrane potential are important controls for this method, but is not feasible for all the different cell types in complex microbial communities.

Protocols should be optimized for staining all cells to mark and visualize each cell in a community. Good dyes for this are nucleic acid dyes such as DAPI used on fixed cells together with a cell wall permeabilizing detergent to allow quantitative penetration of DAPI through the cell wall [2125]. SYBR® Green I has also been described for staining of nucleic acids of viable cells [2128], although one should be aware of the above mentioned limitations. When available, specific Abs can be used to identify specific phylotypes in communities. Further differentiation of cell types in communities can be performed by the more qualitative approaches of fluorescent in situ hybridization (FISH) and lectin probes, while

cell constituents such as lipid inclusion bodies can be stained by highly lipophilic dyes [2124].

A major limitation of microbial community cytometry as described here is the lack of any taxonomic or functional information in comparison to sequencing approaches, where cell phylotypes can be determined or genes with certain functions be detected or even metagenomics analyses be performed. To get a deeper insight, cell sorting can be used to separate interesting sub-communities [2122] or even single cells [2129] for further analyses by, e.g., NGS or proteomic technologies. Cell sorting not only provides access to bacteria that are currently not culturable, but also reduces background, as all cells outside of the sorted gates will not be included in downstream analyses increasing the resolution of the data obtained.

The positions of gates (subcommunities) to be sorted are still defined manually. Cell sorting should be done in the '1.0 Drop Pure' sort mode (BD Influx v7 Sorter). Between 500 000 and 5 000 000 cells within the selected gates should be sorted into tubes at rates from 200 up to 1000 cells/s. Sorted cells are harvested by two successive centrifugation steps (20 000 × g, 6°C, 20 min), and the cell pellets can be stored at –20°C for subsequent analyses [for proteomics: [2130]; for 16S amplicon profiling: [2122, 2131]].

7.6 Data analysis

High resolution FCM can resolve microbial community structures by generating community patterns. It is highly recommended to use a stain that labels every cell for this purpose. These communities are interpreted as pattern (see below post-processing of data) and are generally used to determine community dynamics and to allow for sort decisions.

To evaluate data as shown in Fig. 238, a master gate should be defined that contains all cell events excluding the beads (Fig. 238D). It is advisable to always measure the same number of cells. Usually 200 000 cells are sufficient for downstream analysis pipelines. For cytometric fingerprinting, a gate template has to be generated by marking all apparent sub-communities by a gate and combining all defined gates to the gate template (Fig. 238D and G). The gate template allows the determination of the cell number per gate across the different samples. The dynamic variation of community structure can then be described by quantifying the changes of events per gate [2132].

For the analysis of the cytometric microbial community fingerprint some evaluation tools are already available. FlowFP [2133, 2134] uses a geometrical grid as an alternative to cluster-based gating of FCM profiles. Alternatively, flowCHIC (cytometric histogram image comparison, http://www.bioconductor.org/packages/release/bioc/html/flowCHIC.html, [2135]), is also a grid-based algorithm that transforms 2D cytometric profiles (e.g., DAPI vs. FSC) into grey-scale images and compares the pixel density between two successive samples. FlowCybar (cytometric barcoding, http://www.bioconductor.org/packages/release/bioc/html/flow
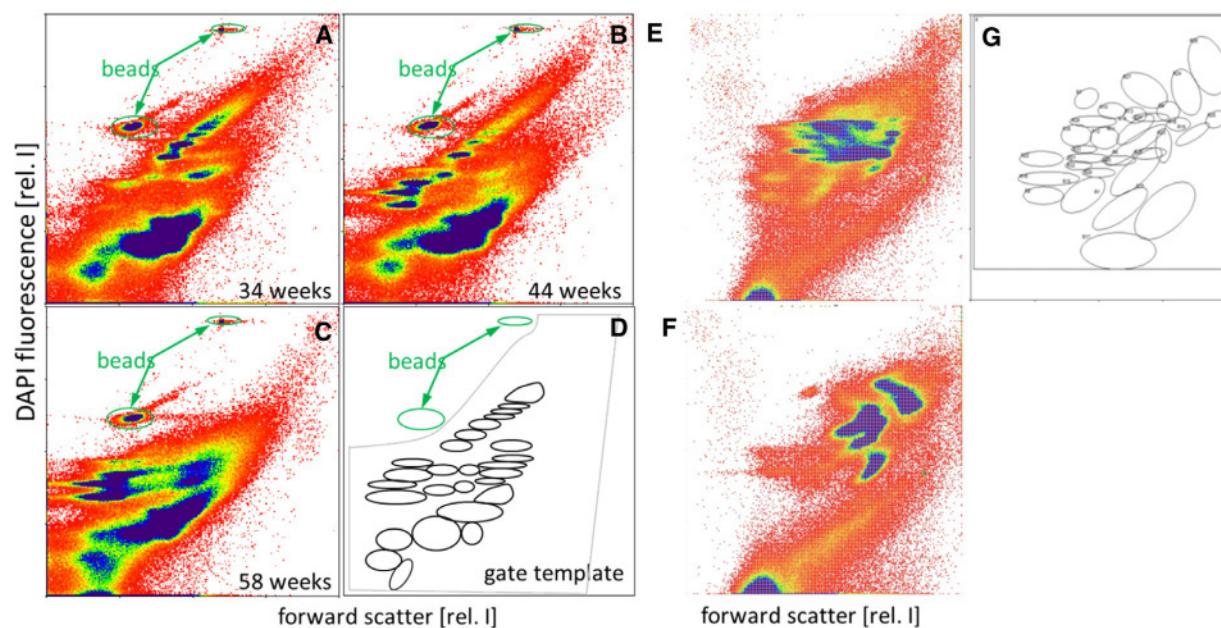
Figure 238. (A–D) A microbial community originating from a wastewater treatment plant cultivated in an aerobic and continuously operated bioreactor on a peptone medium for (A) 34, (B) 44, and (C) 58 weeks [2131], and (E–G) microbial community derived from a fecal sample of a mouse (E) before and (F) after induction of T cell-transfer colitis [2122]. Samples were taken and stained with a 0.24 μM DAPI solution and measured using a 355 nm Genesis CX laser (100 mW, Coherent, Santa Clara, CA, USA, MoFlo Legacy cell sorter, (Beckman Coulter, Brea, California, USA). Scatter was measured using a 488 nm Sapphire OPS laser (400 mW). Beads of sizes 0.5 μm and 1 μm Fluoresbrite Microspheres (both Polysciences, 18339 and 17458, Warrington, PA, USA) were amended into every sample as internal standards. A master gate (D and G: grey) was defined that comprised 200 000 cells for each measurement. Each upcoming subcommunity was marked by a gate in the three samples and a combined gate template generated (D and G: black ellipses). The three chosen samples show the highly diverse cytometric structure of the community and its evolution over time.

CyBar.html, [2132]) produces the cytometric fingerprint on the basis of the gate template as described that represents the microbial community structure by the number of clusters, the position of these clusters in the histogram, and the number of cells within each cluster. The direct comparison of cell abundance changes between gates with high and low cell numbers is facilitated by data normalization. FlowCybar can visualize variations of the cytometric fingerprint over time or in dependence on experimental/abiotic factors.

7.7 Advantages

– Relatively quick and cheap
– Absolute cell counts
– Sorting of bacteria for downstream genetic, proteomic, and functional analyses possible

7.8 Pitfalls

– Membrane-permeable DNA/viability dyes can be excluded or shuttled out by certain viable bacteria
– Taxonomic information requires FISH probes or specific antibodies
– Limited data analysis tools available

– Specific instrument requirements for high-resolution bacterial community structure measurements
– Standardization required for cross-sample comparison

7.9 Top tricks

The flow cytometer should be aligned before measurement using 1 μm or 2 μm beads that are fluorescent in the required range of light. In addition, we strongly advise to spike both 0.5 μm and 1 μm beads into each sample to guarantee comparability between samples. Creation of a gate template for these two types of beads and aligning the beads always inside the same gate template allows the comparison of data over weeks and months. It should be ensured that the beads lie outside of the cell populations to be analyzed (see Figs. 237 and 238). Beads, however, do not control for identical sample handling. When cells are stained using solutions in nanomolar concentration ranges, even small experimental variations result in handling-dependent changes of the fluorescence of the cells. To control for variations in handling, we recommend the additional use of a biological standard (with respective gate template). For this, fixed *Escherichia coli* cells that undergo the same procedure as the samples to be analyzed can be very helpful. For all published data, the cytometer setup and the applied standardizations should be specified together with the

experimental data deposited, for example, in the FlowRepository (https://flowrepository.org/).

8 Detailed and standardized methods to detect inflammasome assembly and activation in immune cells (FlowSight AMNIS)

8.1 Overview

Inflammasome is a multimeric protein platform involved in the regulation of inflammatory responses whose activity results in the production of IL-1β and IL-18.The evidences of inflammasome activation are the concentration of the inflammasome adapter protein apoptosis-associated speck like protein containing a caspase recruitment domain (ASC) into a single speck and a rapid lytic form of cell death termed pyroptosis. In this section, we will show inflammasome activation by ASC speck detection at single cell level using imaging cytometer technology by FlowSight.

8.2 Introduction

The inflammasomes are intracellular multimeric protein complexes, mainly expressed in myeloid cells, whose aggregation leads to the activation of the caspase-1 and the downstream secretion of three of its substrates, the proinflammatory cytokines IL-1β, IL-18 and gasdermin-D that in turn leads to pyroptotic cell death [2136–2138]. Nod-like receptors (NLRs), in particular, are cytoplasmic pattern recognition receptors that detect invading pathogens and initiate inflammasome-dependent innate immune responses. NLRs are activated by bacterial, fungal, or viral molecules that contain PAMPs, or by non-microbial danger signals (DAMPs) released by damaged cells [2139, 2140]. Upon activation, some NLRs oligomerize to form multiprotein inflammasome complexes that serve as platforms for the recruitment, cleavage, and activation of inflammatory caspases. At least four inflammasome complexes (NLRP1, NLRP3, IPAF, and AIM2) have been identified. These complexes contain either a specific NLR family protein or AIM2, the apoptosis-associated speck-like protein containing CARD (ASC) and/or the Cardinal adaptor proteins, and pro-caspases-1, 5 and 8 [2141, 2142]. NLRP3 is the best-characterized inflammasome; its formation requires multiple steps. In a priming step, transcriptionally active signaling receptors induce the NF-kB-dependent induction of NLRP3 itself as well as that of the caspase 1 substrates of the pro-IL-1β family [2143, 2144]. The NLRP3 is, at this stage, in a signaling incompetent conformation; this is modified upon a second signal which will result in the assembly of a multimolecular complex with ASC and caspase 1. Notably the inflammasome activation consists in the assembly of NLRP3 with ASC that in turn recruits procaspase-1 by its caspase recruitment domain (CARD) or procaspase-8 by pyrin domain (PYD) [2145] forming ASC speck [2146] and leading to caspases activation. The assembled ASC speck is the main feature of inflammasome formation and it occurs within minutes of activation, and it stabilizes, finally it is released into the intercellular space, collected by myeloid cells spreading inflammation [2147–2149]. Notably the resting myeloid cell show ASC protein diffuse in cytoplasm, after inflammasome activation the ASC shifts to form a speck.

The activated caspase-1 leads to the cleavage and release of bioactive cytokines including IL-1β and IL-18 and also of protein GSDMD causing membrane rupture and pyroptotic cell death [332]. The pyroptosis plays an important role in inflammatory response and its assessment could be of interest for therapeutic intervention (see Chapter V: Biological Applications, Section 7.4: Pyroptosis).

8.3 Applications

The assembly of a functional NLRP3 inflammasome complex results in the production of proinflammatory cytokines; although these cytokines have a beneficial role in promoting inflammation and eliminating infectious pathogens, mutations that result in constitutive inflammasome activation and overproduction of IL-1β and IL-18 were linked to inflammatory and autoimmune disorders [2150–2152]. A number of recent data strongly suggest that an excessive activation of the NLRP3 inflammasome can be observed as well in neurological diseases including multiple sclerosis as well as Parkinson's and Alzheimer's diseases, in which neuroinflammation plays a central role [2153–2157]. Indeed given that the neuroinflammation is the probable consequence of the activation of inflammasomes in immune cells that infiltrate the central nervous system, dampening of the inflammasome assembly could be beneficial in these diseases and could be envisioned as a possible therapeutic approach to these conditions. For these reasons, the quick and accurate evaluation of inflammasome assembly in peripheral immune cell could be a good methodology approach to monitoring inflammation in a number of diseases.

8.4 Principles of the technique being described and Equipment

Sester and colleagues performed an FCM method to detect ASC redistribution in myeloid cell defining speck formation by changes in fluorescence peak height and width [2156, 2157]. This protocol permits to define the true activated inflammasome by assessment ASC speck formation, because until then the detection of inflammasome, activation was made by monitor its end products, IL-1β or IL-18, or activated caspase-1 detection. Notably different pathways can secrete IL-1β and the methods to analyze caspase-1 activity are not always specific, in both cases the outcomes could be inflammasome independent. Despite to ASC speck formation microscopy analysis, used in the past, this methodology is faster, more accurate, and sensitive. Recently a better method to analyze simultaneously ASC speck and caspase-1 activity was performed by Amnis ImageStream[X] [2158]. This protocol eliminates false

positive events detected by flow-cytometry method, by specific masks to select only single cell, excluding cells with nonspecific-like aggregation of ASC and also defining ASC speck size. Finally the study analyze the presence and distribution of active caspase-1, detected by FLICA spots, and ASC speck simultaneously, evaluating inflammasome activation.

In this section we show the analysis of inflammasome activation by FlowSight, performed utilizing ASC speck formation in LPS+Nig stimulated-THP1derived macrophage.

8.5 Experimental workflow and acquisition

8.5.1 THP1 cell differentiation. THP-1 human monocytes (IZSLER, Istituto Zooprofilattico Sperimentale della Lombardia e Dell'Emilia Romagna, IT) are grown in RPMI 1640 supplemented with 10% FBS, 2mM L- glutamine, and 1% penicillin (medium)(Invitrogen Ltd, Paisley, UK). To differentiate these cells into macrophages, THP-1 human monocytes are seeded in six-well plates at a density of 1.0×10^6 cells/well in medium that contained 50 ηM of PMA (Sigma–Aldrich, St. Louis, MO) and incubated for 12 h at 37°C in 5% CO_2.

THP1-derived macrophage culture and intracellular inflammasome protein staining

THP-1-derived macrophages are cultured with medium alone (negative control) or are incubated with LPS (1 μg/mL) (Sigma-Aldrich) for 2 h and Nigericin (Nig; 5 μM; Sigma–Aldrich) for the last 1 h.

THP-1-derived macrophages (1×10^6) are harvested by 0.05% (w/v) trypsin (Seromed, Biochrom KG) in **EDTA** solution for 5 min at 37°C, washed once in RPMI supplemented with 10% FBS, seeded in polystyrene round-bottom tubes (Falcon 2052, Becton Dickinson Labware, Franklin Lakes, NJ) and centrifuged for 10 min at 1500 rcf at 4°C. Tubes containing THP-1-derived macrophages are placed on ice; cell are permeabilized with 100 μL of Saponine in PBS (0.1%; Life Science VWR, Lutterworth, Leicestershire,LE) and 5 μL (25 μg/mL) of the PE-antihuman ASC (clone HASC-71, isotype mouse IgG1,Biolegend, San Diego, CA) mAbs are added to the tubes for 1 h at 4°C. Cells are then washed with PBS and centrifuged at 1500 rcf for 10 min at 4°C. Finally, cells are fixed with 100 μL of PFA in PBS (1%) (BDH, UK) for 15 min, washed with PBS, centrifuged at 1500 rcf for 10 min at 4°C, resuspended in 50 μL of iced PBS, and immediately analyzed by FlowSight.

8.5.2 Human peripheral monocyte cell cultures. PBMC (1×10^6/mL) are cultured in RPMI 1640 supplemented with 10% human serum, 2 mM L-glutamine, and 1% penicillin (Invitrogen Ltd, Paisley, UK) and incubated at 37°C in a humidified 5% CO_2 atmosphere for 2 h in a 12-well plate. After 2 h, non-adhering PBMCs are harvested and discarded; monocytes (adhering cells) are culture in medium alone (unstimulated) or primed with 2 μg/mL LPS for 2 h (Sigma–Aldrich, St. Louis, MO) before stimulation with Nigericine (5 μM) (Sigma–Aldrich)

for 1 h at 37°C in a humidified 5% CO_2 atmosphere. Adhering cells (monocytes) are then collected by trypsin treatment and prepared for FlowSight analysis by immunofluorescence staining as THP1-derived macrophage (see above).

8.6 Data analysis

ASC-speck formation is analyzed by FlowSight (Amnis Corporation, Seattle, WA, USA) (see chapter VIII, Section 1 "Imaging flow cytometry").

8.6.1 FlowSight acquisition parameters. The FlowSight (MilliporeSigma) equipped with 488, and 642 nm lasers with two camera and twelve standard detection channels is used to acquire experimental samples using the INSPIRE software.

The flow rate is set to minimum and the objective magnification is set to 20x for all samples.

A multifluorophore-labeled sample (Flowsight Calibration Beads) is used to determine accurate laser and focus settings and avoid oversaturation.

Masks are defined region of interests that are computationally calculated by INSPIRE.

A mask defines a specific region of an image that can be used for specific feature calculations.

The saturation of an individual fluorophore in its corresponding channel is determined by plotting the Raw Max pixel feature for every channel.

Aspect ratio feature measures circularity, to distinguish between singlets, doublets, and cell clumps when used together with the area feature.

Area versus aspect ratio of the default mask on the brightfield is used during acquisition to ensure collection of single-cell events. A region is created to exclude debris and to record 2000 events for every sample.

For the compensation control, 1000 events for single-stained samples are acquired turning the Ch01 (brightfield) and Ch06 (side scatter) off.

All samples and controls are acquired as raw image files (.rif).

8.6.2 FlowSight image analysis. All sample and compensation analysis are performed using analysis software (IDEAS).

The IDEAS image analysis software allows quantification of cellular morphology and fluorescence at different cellular localizations by defining specific cellular regions (masks) and mathematical expressions that uses image pixel data or masks (feature).

Individual compensation controls of single-stained samples are loaded into the compensation wizard in IDEAS. A compensation matrix file (.ctm) is generated and applied to a positive control (nigericin-treated sample) raw data file (.rif) to generate both a compensated image file (.cif) and a corresponding data analysis file (.daf). A data analysis template (.ast) is developed by analyzing the.daf file of positive control sample. We applied the
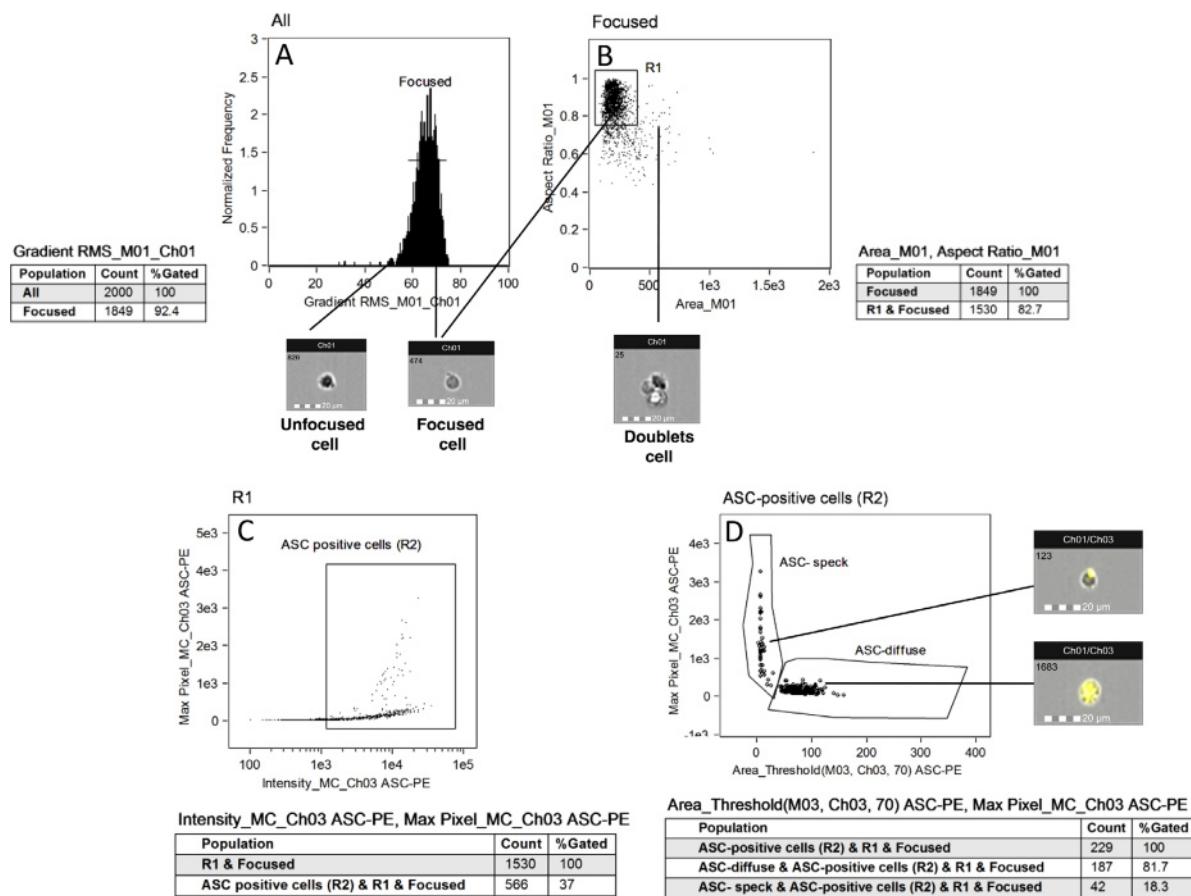
Figure 239. Representative images from unstimulated THP-1-derived macrophages (1×10^6). *Identifying focused cell* (A): The default mask (M Brightfield) used in acquisition does not discriminate between focused and unfocused cells; the object mask alows the exclusion of unfocused cell. *Identifying single cells* (B): Focused cells are plotted on AREA brightfield versus Aspect Ratio Brightfield scatterplot to exclude doublets cell. Events with an Aspect ratio of 0.6–1.0 and an area of 50–500 U representing single cell are selected (R1). *Identifying ASC positive cell* (C): Single cells (R1) are plotted on Max Pixel MC (Ch03) and intensity MC Ch03 scatterplot to indentify ASC positive cells (R2). *Identifying ASC speck* (D): ASC positive cell (R2) are plotted on Max Pixel MC (Ch03) versus Area threshold (M03,Ch03,70) scatter plot. This mask allows to discriminate between cells characterized by speck formation, in which a functional inflammasome complex is assembled, and cells with an ASC diffuse pattern.

template along with the compensation matrix to the rest of the experimental samples using the multiple file batch tool in IDEAS.

Focused cells

Unstimulated (cells kept in medium alone; Fig. 239) and LPS+Nig (Fig. 240)-stimulated THP-1-derived macrophages (1×10^6) are resuspended in 50 μL of PBS and analyzed by FlowSight.

The Gradient root mean square (RMN) of Brightfield channel is used to identify focused cells (Figs. 239A and 240A).

The focused cells are plotted on AREA bright field *vs*. Aspect Ratio Bright field scatterplot to exclude aggregates from single cells (R1) (Figs. 239B and 240B)

ASC speck mask

An intensity mask defined by Max Pixel MC (Ch03) *vs*. Intensity (Ch03) is created from the R1 gate to identify total ASC positive cells (Figs. 239C and 240C).

To define cell with ASC speck from cells with an ASC diffuse pattern a Threshold mask plotting Max Pixel MC (Ch03) *vs*. Area threshold (M03, Ch03,70) is created. This mask allows to separate within the population of ASC-fluorescent cells those with small

area and high max pixel (ASC speck) from those with large area and low max pixel (ASC diffuse) (Figs. 239D and 240D).

8.7 Advantages

This protocol allows to identify quickly and in an extremely accurate way inflammasome activation at single cell level. The gate strategy identifying the different size and brightness of ASC fluorescence differentiates between cells with speck formation, in which a functional inflammasome complex is assembled, and cells characterized by an ASC diffuse pattern.

8.8 Pitfalls/Top tricks

Inflammasome activation leads to pyroptosis and release of ASC specks into extracellular space, to avoid cellular breakdown, it is essential to keep cells on ice after detachment by trypsinization and during the staining procedure.
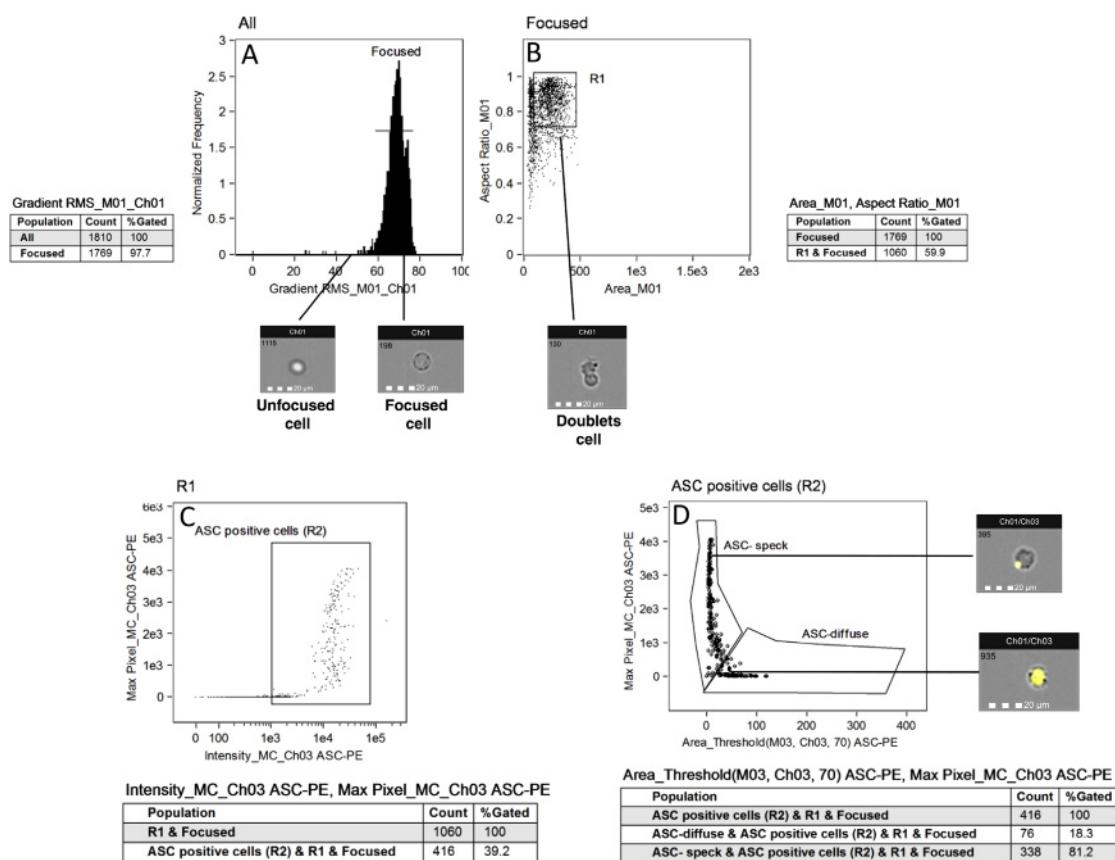
Figure 240. Representative images from LPS+Nig-stimulated THP-1-derived macrophages (1×10^6). *Identifying focused cell* (A): The default mask (M Brightfield) used in acquisition does not discriminate between focused and unfocused cells; the object mask alows the exclusion of unfocused cell. *Identifying single cells* (B): Focused cells are plotted on AREA brightfield versus Aspect Ratio Brightfield scatterplot to exclude doublets cell. Events with an Aspect ratio of 0.6–1.0 and an area of 50–500 U representing single cell are selected (R1). *Identifying ASC positive cell* (C): Single cells (R1) are plotted on Max Pixel MC (Ch03) and intensity MC Ch03 scatterplot to indentify ASC positive cells (R2). *Identifying ASC speck* (D): ASC positive cell (R2) are plotted on Max Pixel MC (Ch03) versus Area threshold (M03,Ch03,70) scatter plot. This mask allows to discriminate between cells characterized by speck formation, in which a functional inflammasome complex is assembled, and cells with an ASC diffuse pattern.

9 Multidrug resistance activity

9.1 *Overview*

Multidrug transporters, in particular MDR1, MRP1, and BCRP serve as independent biomarkers to monitor treatment efficiency and to support treatment decision in numerous clinical conditions, as the most prevalently used small molecule drugs are substrates of these efflux pumps.

Transporter activity measurement using fluorescent reporter substrates and transporter inhibitors is a simple and cost-effective assay that can be performed on primary cells or cell lines. Importantly, reagents used in transporter activity measurements are compatible with fluorescently labeled Abs, thus it is possible to perform the assay simultaneously on several cell types of interest.

9.2 *Introduction*

Multidrug resistance (MDR) transporters play an essential role in the extrusion of xenobiotics from the cell, however, small molecule drugs, like methotrexate (MTX), *Vinca* alkaloids, and other standard chemotherapeutics are also removed from target cells via these molecules. In the clinical routine, MDR1 (also known as P-gp, or ABCB1), MRP1 (also known as ABCC1), and BCRP (also known as ABCG2, or MXR) are the most important players in the development of resistance against these drugs [2159–2162].

Currently, qRT-PCR, immunohistochemistry, and Western blots are the most frequently used methods to determine the MDR transporter status in clinical samples. On the other hand, several polymorphisms affecting transporter function have been reported [2163, 2164]. Therefore, the relevance of quantitative description of these transporters is questionable. Transporter trafficking is affected by genetic variation. Therefore, FCM-based determination of cell surface expression of MDR transporters would be a significant progress [2165]. However, Abs recognizing the extracellular MDR1 and BCRP epitopes are conformation sensitive, making their accurate determination challenging [2166–2168]. Furthermore, the functional activity of these molecules still remains elusive.

Performing real-time transporter activity measurements using fluorescent reporter substrates is highly beneficial in the clini-

cal setting for personalized therapy and monitoring in certain hematologic malignancies and in autoimmune diseases, since the activities of MDR1, MRP1, and BCRP serve as biomarkers to predict the patient's response to small molecule therapy in treatment naïve conditions and during small molecule drug treatment [2169, 2170]. Furthermore, the determination of transporter activity is also relevant in cell lines in pharmaceutical research.

The following protocol provides a cost-effective method with a short turnaround time to determine MDR transporter activity. These measurements can be performed on various cell types, including cell lines, peripheral blood or bone marrow-derived cells.

9.3 Principles of the technique being described

Measuring the functional activities of MDR1, MRP1, and BCRP is based on the application of fluorescent transporter reporter substrates along with specific and pan-inhibitors of these transporters. Reporter substrates readily penetrate the cell membrane. Preferably, the non-fluorescent reporter substrate, such as calcein-AM, is cleaved by endogenous esterases to form a highly fluorescent derivative of the dye that becomes trapped in the cytoplasm due to its high hydrophilicity. However, many fluorescent substrates that are not cleaved by esterases are also used in drug discovery and in clinical practice, including mitoxantrone, Rhodamine 123, and Hoechst stains. The activity of the efflux transporters results in lower cellular accumulation of the fluorescent reporter dye. In cells expressing transporters the addition of specific inhibitors blocks dye exclusion activity of the relevant transporter and increases dye accumulation in the cells. In the absence of significant transporter activity, the net reporter substrate accumulation is faster in the cells due to a lack of transporter mediated efflux, which in turn is not influenced by the presence of an MDR transporter inhibitor [2171].

9.4 Applications

- **Basic research applications**: To characterize transporter biology and functionality, to study the pathobiology of transporter-mediated diseases, to test cell lines overexpressing multidrug transporters, to test drug–transporter interactions, and to examine drug or herb–drug interactions in the context of drug discovery and in the study of drug disposition
- **Cohort selection in Phase I trials**: Data show that up to 20% of healthy adults are characterized by high baseline transporter functions [2172]. Enrollment of these individuals in a Phase I trial may cause bias, which can be excluded by a preliminary screening of transporter function, saving cost and effort
- **Therapy tailoring to support personalized treatment**: Small molecule drugs are widely used in cancer and autoimmune diseases. As these drugs are removed from the target cell via multidrug transporters, transporter activity measurements would

be highly beneficial at the time of diagnosis and during therapy to support treatment decisions

9.5 Equipment

The flow cytometer used for measurements does not require any special features. The lasers and channels applied for the detection of the fluorescent substrate depends on the specific fluorescent substrate molecule used. For example, the 488 nm laser and the 515 nm channel is recommended for calcein-AM while the 633 nm laser and the 684 nm channel is recommended for mitoxantrone. The configuration of the instrument will determine the number of additional cell surface markers that can simultaneously be used in order to identify individual cell subsets. In conclusion, no specific flow cytometer is required for running transporter activity measurements. The following assay is not suitable for high-throughput screening format.

9.6 Experimental workflow and acquisition

9.6.1 Sample preparation. Transporter activity measurements can easily be performed on human and rodent cell lines and primary cells. Importantly, transporter activity measurements require viable cells ($2–5 \times 10^6$) in good condition, not depleted of intracellular energy stores. ATP depletion tends to decrease the activity of membrane transporters and may lead to inaccurate results.

If primary human blood or bone marrow samples are used, K_3EDTA or Na-citrate is recommended to be used as anticoagulant, since other anticoagulants, e.g., heparine may interfere with transporter activity measurements. For collecting PBMCs, Ficoll density gradient centrifugation is suggested. Primary samples should be processed within six hours after drawing, as samples stored beyond 6 h may undergo serious ATP depletion, leading to inaccurate results. If samples are stored over 6 h, PI counterstaining is recommended to exclude dead cells. Blood samples should be stored at room temperature before testing. Do not freeze samples. Cells should be diluted in HBSS buffer.

9.6.2 Assay procedure. The specific steps of the procedure may vary depending on the instructions supplied by the manufacturer of the kit used. Here, we provide general considerations for the assays.

Prepare and measure samples under same inhibitor treatment and staining conditions in triplicates. *Mix cells thoroughly by gentle pipetting rather than vortexing to avoid forming bubbles in the test tube. Always include a control sample with no inhibitors applied. The concentrations of the respective inhibitors are specified in the manufacturer's instructions of the kit used. Samples are incubated at 37°C.*

To start the staining reaction, add the transporter reporter substrate into all tubes simultaneously. After incubation, stop reaction in all tubes simultaneously by rapid centrifugation (1 min at 2000 rpm) with rapid acceleration and deceleration. Discard supernatant

and stain resuspended cells with labeled Abs *if required. Stain cells with PI solution to demonstrate viability if necessary.*

9.6.3 Staining the cells with labeled cell surface Abs. For measuring transporter activities on your cell type of interest, the use of fluorescently labeled Abs are recommended. Both immunolabeling and conjugate labeling methodologies can be followed. Please note that some Abs may interfere with transporter activity measurements. To avoid such interference, the staining of cells with Abs as per the manufacturer's instructions should be carried out following the staining with the transporter reporter substrates. Cells must not be fixed or permeabilized. The necessary isotype controls or unlabeled cell controls should be used according to the manufacturer's instructions.

9.7 Data acquisition

Mix samples thoroughly before measurement and use only the viable cell population for data analysis. In case of using commercially available kits (e.g., the SOLVO MDQ Kit^{TM}), the assay contains internal standardization, thus the results will become independent from the PMT settings, whenever the acquisition occurs within the linear range of the equipment. However, samples belonging to the same assay must be measured using the same settings for PMT amplification.

9.8 Data analysis

Apply sequential gating strategy for the analysis (an example is provided in ref. [2173]). Within the desired cell subset gate, determine the corresponding geo-MFI values of the reporter substrate applied. For this, the inclusion of at least 10 000 cells within the desired cell subset gate is recommended.

9.8.1 Calculation of multidrug resistance activity factors. Take the median geo-MFIs of triplicate parallel measurements with and without the transporter inhibitors ("F" values). We provide an example below of the equations used to calculate multidrug resistance activity factor (MAF) values for each multidrug transporter, plus the composite activity of MDR1 and MRP1 (MAF$_C$) using the SOLVO MDQ Kit^{TM}. These calculations may differ when using other kit assays.

- MAF$_C$ = $100 \times (F_{MAX} - F_0) / F_{MAX}$
- MAF$_{MRP1}$ = $100 \times (F_{MRP1} - F_0) / F_{MAX}$
- MAF$_{MDR1}$ = MAF$_C$ − MAF$_{MRP1}$
- MAF$_{BCRP}$ = $100 \times (F_{MX} - F_B) / F_{MX}$

F$_{MAX}$ and F$_{MX}$ represent reporter substrate fluorescence (calcein and mitoxantrone, respectively) with inhibitors of MRP1 and MDR1 as well as of BCRP, respectively. F$_0$ represents fluorescence without inhibitors. F$_{MRP1}$ represents reporter substrate fluorescence (calcein) with specific inhibitor of MRP1.

9.8.2 Expected results and interpretations. Theoretical MAF values can range between 0 and 100. The MAF$_C$ found in normal PBMCs are in the range of 0–20, while in drug selected cell lines exhibiting extreme high levels of MDR1/MRP1 expression, the MAF$_C$ values might be as high as 95–98. In case of hematological malignancies, the MAF$_C$ values in tumor cell populations are usually found between 0 and 50, but in extreme cases, values can be as high as 70. Reference values of MAF values in CD3$^+$ lymphocytes were determined in a healthy population of 120 individuals [2173]. Importantly, MAF values are independent from gender. MAF$_{MRP1}$ and MAF$_{BCRP}$ are also independent from age, while MAF$_C$ and MAF$_{MDR1}$ showed a negative correlation with age in healthy adults.

9.9 Advantages

- **Functional data**: In contrast with other methods detecting the presence or absence of MDR transporters at relative gene expression or protein level, transporter activity measurements by FCM assess whether efflux transporters are functionally active.
- **Clinical application**: The assay works on both primary cells and cell lines. As little as 5 mL of peripheral blood is sufficient to study transporter activity in patient samples. A CE-IVD kit (SOLVO MDQ Kit^{TM}) is available for clinical use.
- **Short turnaround time**: Functional data can be obtained within 2 h following sampling as compared with much longer turnaround times of next generation sequencing methods. Moreover, a single sample can be measured cost-effectively without the need of batching multiple samples.
- **Cost effective**: Transporter reporter substrates and inhibitors are commercially available compounds that are far cheaper than Abs and reagents required for gene expression assays.
- **Flexible**: The use of fluorescent cell surface markers allows the simultaneous detection of transporter activity in various cell subsets of interest.

9.10 Pitfalls

- It is recommended to start the assay within 6 h after obtaining the primary sample to avoid depletion of intracellular ATP stores. Detection of dead cells with PI is recommended beyond this time limit.
- As timing of the staining steps is crucial in measuring transporter activity, the addition of the fluorescent reporter substrate to the samples should be take place within 20 s. Therefore, it is not recommended to start the reaction on more than 12 test tubes at the same time. Allow 2-min intervals between starting the reactions when multiple samples are measured. It is recommended to use a repeater pipette to add substrates and inhibitors to multiple test tubes.
- Sample measurement should preferably be performed immediately (within 2 h) after staining. Keep the samples on ice and protect them from light until the measurement.

9.11 *Top tricks*

- In case of cell lines growing adherently, trypsinization is a critical step to keep cell membranes intact: for this, trypsinization time should be established for the cell line of interest.

10 Index sorting

10.1 *Overview*

Index sorting records fluorescence information and scatter characteristics indexed for each individual sorted event. This technology is especially powerful when sorting single events and allows the retrospective identification of highly accurate multidimensional phenotypes.

10.2 *Introduction*

Fluorescence-activated cell sorting is broadly available and its applications reach from large-scale sorting of millions of cells into tubes to the targeted deposition of single events into multiwell plates or onto slides. For conventional sorting, target populations have to be defined before the sorting process involving more or less sophisticated gating strategies. The advantage of index sorting is that fluorescence data for each individual sorted event can be read out retrospectively. This technology, especially when applied as single cell sorting, is invaluable for specific research questions in which sorted events of interest can only be identified with downstream technologies. Most currently commercially available sorters are capable of index sorting.

We will illustrate the technology with one example combining 12 fluorescent parameter single T cell index sorting of a T lymphoblastic lymphoma sample with downstream single cell TCRαβ sequencing (Fig. 241).

10.3 *Principles of the technique being described*

Indexed fluorescence data and scatter characteristics are recorded for each single sorted event so they can be assigned retrospectively. Index sorting itself is not different from regular cell sorting except it has to be activated in the sorter software. After sorting, scatter characteristics and fluorescence data for each single event can be exported from the sorter software—usually as a table (comma separated list). Exported data have to be individually processed and, if desired, can be combined with data from downstream assays depending on the purpose of the experiment (see example in Fig. 241).

10.4 *Applications*

Index sorting has been applied in a variety of research areas including the isolation and characterization of single circulating tumor

Table 96. Parameter panel for single cell index sorting in Fig. 241

Specificity	Clone	Fluorochrome	Vendor
CD8	RPA-T8	BV510	BioLegend
CD57	HCD574	FITC	BioLegend
PD-1	EH12.2H7	PerCP-Cy5.5	BioLegend
BTLA	J168-570	PE-CF594	BD Biosciences
TCRαβ	IP26	APC	BioLegend
CD45RA	HI100	AF700	BioLegend
CD25	CD25-4E3	PE-Cy7	Affymetrix
CTLA-4	BNI3	PE	Invitrogen
CCR7	G043H7	BV650	BioLegend
CD28	CD28.2	BV421	BioLegend
CD4	SK3	APC-Fire 750	BioLegend
live/dead		zombie yellow	BioLegend

cells [2174], the determination of cell cycle states and immune phenotypes of stem cell populations [2175–2177], the combination of genotype with phenotype data in healthy and malignant B lineage cells [1606, 2178], the definition of the phenotypic range of individual T cell clones [2179–2181], and the determination of cell size in combination with microbial single cell genomics [2129], among others.

As an example, we used index sorting to define the phenotypic range associated with clonal T cell expansion in one T lymphoblastic lymphoma lymph node (Fig. 241). The conventional approach would be to sort various T cell populations and sequence their TCR genes to detect clonal expansion. This approach is tedious and may not lead to the desired results due to shortcomings of 2D gating strategies for the definition of high-dimensional phenotypes ("Chapter VII: Data handling, evaluation, storage and repositories" and "Chapter VIII Section 5: High dimensional FCM"). Index sorting allows to stain with a multiparameter set of Abs (example in Table 96), randomly sort single T cells, sequence their TCRs, and retrospectively identify the multi-dimensional immune phenotype of each single cell belonging to the T cell clone of interest (Fig. 241).

Equipment

Most currently commercially available cell sorters are capable of index sorting. Sorting for the example in Fig. 241 was done using a FACSAria™ Fusion high-speed cell sorter equipped with a 70 μm nozzle and FACSDiva software version 8.02 (BD Biosciences). Sorter setup and preparation for index sorting does not differ from regular cell sorting with special attention on accurate drop delay ("Chapter II: Setup-Instrument setup and quality control," here). Single cells were sorted directly into 96-well plates prefilled with PCR buffer [2180].

Depending on the sorter hardware and target devices (e.g., 96-well plate), accurate and consistent mounting of the target device onto the robot can be difficult. Custom-made adapters and mounting plates onto 96-well racks can help to reduce alignment variability between plates [2176].

Experimental workflow and acquisition

Staining, preparation of single cell/particle suspensions, and the sorting process are identical to (single cell) sorting without
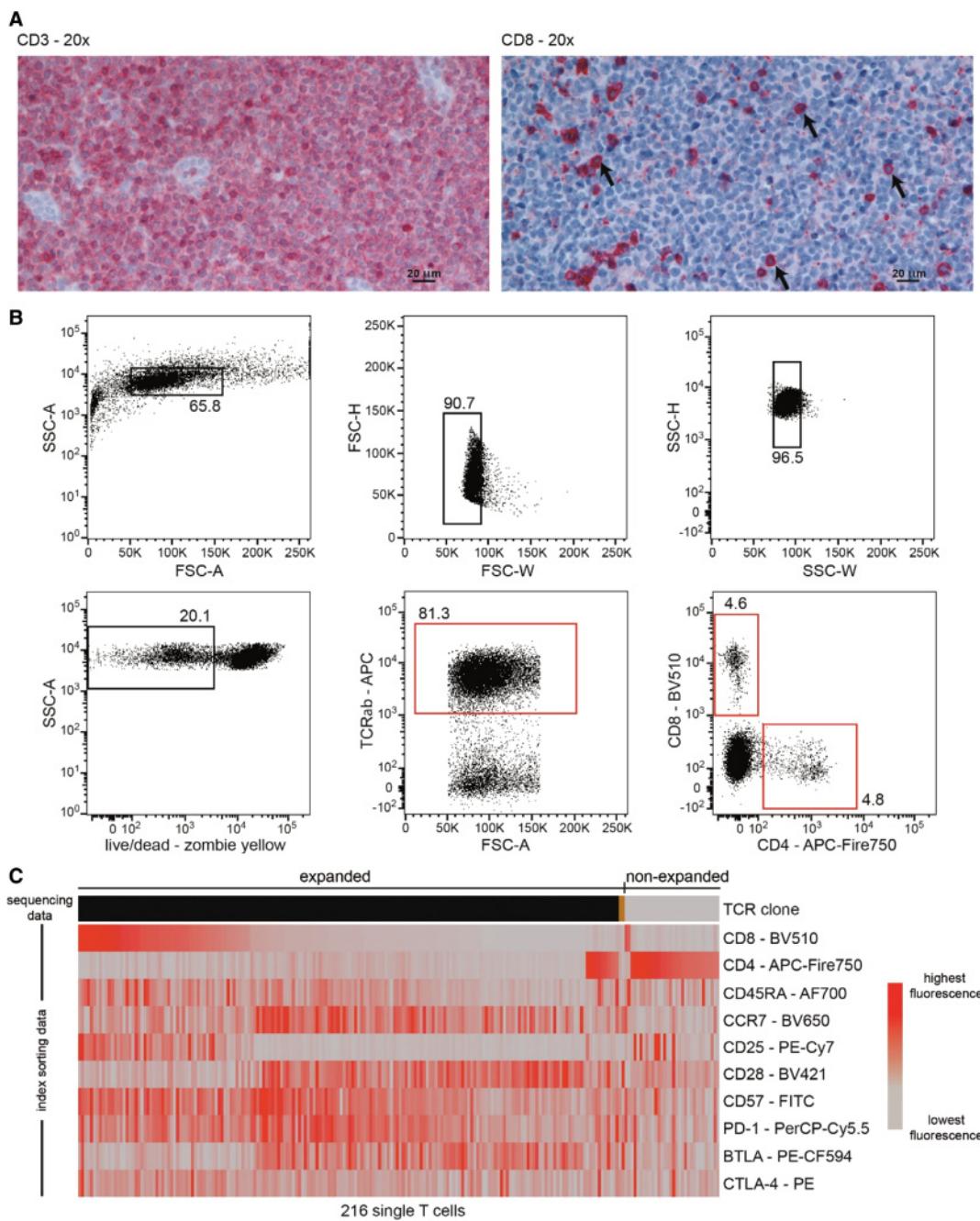
Figure 241. Determination of the phenotypic range of T lymphoblastic lymphoma cells as an application example for single cell index sorting. We combined 12 fluorescent parameter index sorting of αβ T cells with single cell TCRαβ sequencing of one single lymph node from a T lymphoblastic lymphoma patient. (A) Immunohistochemistry of a paraffin-embedded lymph node section demonstrates substantial infiltration with CD3^{+} predominantly CD8^{-} T lymphoblastic lymphoma T cells. CD3^{+} (left image) or CD8^{+} (right image) cells are stained in red. Polyclonal rabbit antihuman CD3 (A0452, Dako) and mouse antihuman CD8 (clone C8/144B, Agilent) were used for immunohistochemistry. Arrows in the right image point at single CD8^{+} cells as examples. We aimed to determine the phenotypic range of T lymphoblastic lymphoma cells and asked whether interspersed CD8^{+} T cells were polyclonal lymphoma-infiltrating T cells or part of the malignant clone. (B) Sequential gating for single cell index sorting of lymph node T cells. Upper row left: gating on lymphocytes; middle and right: gating on single cells by forward and side scatter characteristics. Lower row left: exclusion of dead cells; middle: gating on αβ T cells; right: gating on CD4^{+} or CD8^{+} T cells. Red indicates gates from which cells were ultimately sorted. (C) Combined paired TCRαβ sequencing and FCM data from cells sorted in (B). Single T cells are arranged in columns. The top bar color-codes TCRαβ CDR3 amino acid sequences; adjacent columns with the same color indicate expanded T cell clones. A clone was determined expanded if we detected at least two cells with identical TCRαβ CDR3 sequences. Grey indicates non-expanded T cells. FCM data were trimmed at the 2nd and 98th expression percentiles and scaled for each individual marker. While CD4^{+} T cells were in parts polyclonal, the dominant proportion of CD8^{+} T cells was part of the malignant clone. Data represent $n = 1$ experiment and illustrate an application example of index sorting. General findings on T lymphoblastic lymphoma biology cannot be concluded from these data. The lymph node and immunohistochemistry were provided by Martin-Leo Hansmann, Universitätsklinikum Frankfurt am Main, Dr. Senckenberg Institut für Pathologie, Germany.

index (see Chapter IV: Cell sorting). Index sorting has to be activated in the sorter software before starting the sorting process.

When sorting single events into multi-well plates or onto slides, special attention should be paid to plate targeting. Accurate plate alignment should be confirmed in regular intervals (e.g., after every fourth plate). Singlet gates should be defined stringently to reduce the chance of sorting doublets. Make sure to activate the "single cell mode" (or equivalent) in the sorter software when sorting single cells. It is recommended to run the sorter at a low flow rate (<200 events/s), which has been shown to improve the yield of rare events [2182].

Depending on the research questions and materials used, we recommend the inclusion of live/dead discriminatory dyes in the gating strategy.

For the example in Fig. 241B and C, cryopreserved cells from a lymph node sample of a T lymphoblastic lymphoma patient were stained with a 12 fluorescent parameter panel (Table 96). The panel included markers for the identification of major T cell differentiation states in combination with selected immune checkpoint molecules. Two-hundred single TCRαβ$^+$ cells were randomly index sorted into 96-well plates. Since CD4$^+$ and CD8$^+$ T cell frequencies were below 5% of all αβ T cells, we additionally sorted 88 CD4$^+$ T cells and 88 CD8$^+$ T cells. Paired TCRαβ sequences were obtained from a total of 216 T cells.

10.5 *Data analysis*

Index sort data can usually be exported from the sorter software as FCM standard (fcs) files or as tables (comma-separated values or equivalent). Detailed procedures for data export depend on the instrument manufacturer, software, and software versions. When exported as fcs files, index sort data can be visualized using commercially available software for FCM data visualization ("Chapter VII: Data handling, evaluation, storage and repositories"). If it comes to sub-setting of index sort data based on certain criteria, the combination with other data formats (e.g., single cell sequencing), data visualization as heatmaps and/or multidimensional plots, commercially available tools are rarely available. Data analysis involving programming/statistical computer languages such as R (https://www.r-project.org/) among others is the approach of choice, highly flexible and powerful but requires knowledge in (bio-) informatics.

10.6 *Advantages*

Index sorting makes exact scatter and fluorescence characteristics of each single sorted event available for downstream analyses and can help identifying multidimensional phenotypes where conventional sorting approaches are limited. With immune phenotypes being correct in >99% of sorted cells [2180], index sorting is one of the most accurate technologies for isolation and multidimensional phenotyping of single cells at the protein level.

10.7 *Pitfalls*

Currently, there are no ready-to-use software solutions that make the entire richness of index sort information available to users with limited access to advanced bioinformatics.

10.8 *Top tricks*

For single cell index sorting, accuracy of the assigned phenotypes is critical. In addition to general requirements for cell sorting ("Chapter II: Setup - Instrument setup and quality control" and "Chapter III: Before you start: Reagent and sample preparation, experimental design"), stringent gating on live single events and plate targeting are critical. Parameters that could indicate data inconsistency should be included whenever possible. For example, in healthy individuals, particular T cell clones show characteristic CD4/CD8 expression. The identification of CD4$^+$ T cells in an otherwise CD8$^+$ T cell clone could hint to data inaccuracy.

When sorting into multi-well plates, depending on the desired downstream applications and the type of sorted events, immediate centrifugation after sorting may increase yield.

11 Sample banking for FCM

11.1 *Overview*

Sample banking provides benefits for FCM, namely, that samples can be batched for a more efficient workflow and reduced sample-to-sample variability. The most common banking method involves cryopreservation of PBMC, and the principles to be followed are the same for FCM as for other downstream methods that require viable cells. Consideration should be given to optimization and standardization of the procedure, including time to processing. Alternatives to cryopreservation of PBMC include the use of transport stabilizers (Streck, Smart Tube) or methods for cryopreservation of whole blood/granulocytes. These systems can allow interrogation of cells depleted in the generation of PBMC; and the Smart Tube system captures functional readouts through stimulation of fresh whole blood prior to fixation/stabilization.

11.2 *Introduction*

With time after collection, biological samples begin to degrade with regard to their functions and phenotypic markers. Depending on the target function(s) or phenotype(s), this degradation may be on the order of hours or days. But running fresh samples immediately by FCM is often not logistically feasible. It is also not necessarily the best workflow choice for all studies, due to the inefficiency of running single samples, and the variability that can be introduced from day to day. Biobanking offers a good alternative to running fresh samples immediately after collection. By far the most common biobanking approach is cryopreservation of PBMC (or other sources of immune cells). This has the advantage

that cells can be viably stored for many years in liquid nitrogen or equivalent cryogenic storage [2183], allowing for many different types of assays to be performed downstream. An important disadvantage is the loss of granulocytes, which are generally removed by Ficoll density gradient centrifugation prior to cryopreserving the PBMC. Another limitation is the partial loss of certain labile cell-surface markers and some functional characteristics with cryopreservation, as well as differential recovery of certain subtypes of cells (discussed under "Principles" below). If these affected cells, markers, or functions are critical to the FCM assays being used, then an alternative strategy needs to be taken. This could include viable cryopreservation of whole blood/granulocytes, which may bring additional caveats in terms of cell viability and function; or activation/fix/freeze systems, which are ideal for capturing a functional and phenotypic state, but which limit the downstream applications. As such, the choice of whether and how to bank samples prior to FCM involves a set of trade-offs, in which the investigator needs to evaluate the factors of greatest importance for a particular study, as well as the logistical constraints, prior to picking a sample banking approach.

11.3 Principles

With any sample banking method, it is necessary to minimize pre-analytical variations in the collection, processing, and storage stages. The pre-analytical variations can be different depending on the type of biosample, the type of analyte, and the method of analysis. PBMC isolation methods based on density gradient centrifugation, for example, Ficoll-Paque, Lymphoprep, and cell preparation tubes (CPT, Becton Dickinson) show comparable cell counts and viability [2184], but the different handling of cells may affect their detailed phenotypes and functions. For example, compared to Ficoll-Paque density gradient centrifugation, Lymphoprep showed a higher SEB-induced cytokine response from human PBMC [2185]. CPT, on the other hand, have a potential for increased erythrocyte contamination [2185], though they provide an easier workflow than other methods. In general, the selection of a specific PBMC isolation technique, aside from the cost, should be based on the downstream analysis.

In addition to the choice of the PBMC isolation technique, key protocol factors (e.g., time to processing, buffer, DMSO mixing, cell density, freezing rate, transfer to LN2, and thawing) also play a role in good cryopreservation [2186, 2187].

The time delay between blood sampling and handling of the sample may affect the immune cell subsets, their function, and activation markers [2188]. A standardized processing time for all samples (which still preserves the desired functions and/or phenotypes) will give the most comparable results. In addition to the time interval between the collection and the processing, the time of day of blood collection may also play a role in the recovered phenotypes and functions, due to circadian effects (reviewed in ref. [2189]).

Tompa et al. [2190] compared fresh versus cryopreserved PBMC (stored for 6 or 12 months) for three different isolation techniques, analyzing the subsets of CD4$^+$, CD8$^+$, and CD25^{hi} lymphocytes. In general, there was no influence of isolation method or long-term cryopreservation. However, slightly different subsets of cryopreserved PBMC were described, e.g., naive and early-differentiated CD4$^+$ and CD8$^+$ effector memory T cells were affected by isolation and cryopreservation. Another group has reported changes in CD4$^+$CD25$^+$ T cell numbers in HIV+ individuals as a result of cryopreservation [2191], highlighting the possibility of disease-specific affects. Minor differences in B and T cell numbers with Ficoll separation versus whole blood have also been reported [2192]. Finally, resting cells post-thaw can have differential effects on T cell fine phenotyping [2193, 2194].

Some investigators have made further efforts to optimize methods and implement quality control to achieve improved cell viability [2195]. Both the centrifugation and washing conditions can be varied and a higher DMSO concentration (15%) in the freezing medium can be beneficial. A controlled cooling rate of –1°C/min can be achieved in different ways and is discussed in a previous section (see Chapter III Section 4 Dead cell exclusion, cell viability, and sample freezing).

Once banked, samples need to be kept at a constant optimal temperature. Fluctuations from liquid nitrogen to vapor phase, or frequent exposure to ambient temperatures as samples are removed will degrade their viability. Even fixed samples stored using Smart Tube proteomic stabilizer become clumped when exposed to repeated temperature fluctuations or storage above –80°C. For this reason, it may be advantageous to separate locations of samples intended for long-term storage versus those to which frequent access is needed. Additionally, when working with open sample boxes to retrieve specimens, the use of a liquid nitrogen tray is recommended, to minimize temperature fluctuation. Similarly, shipping in nitrogen dry shippers is preferable to dry ice shipments of frozen PBMC; however, a single, short-term exposure to dry ice during shipping will not result in any noticeable sample degradation [2186].

Another important consideration whenever biobanking extends to larger numbers of samples and studies is inventory management software and protocols. There are several good software packages designed specifically for freezer/biobank management (e.g., LabVantage, CentraXX, STARLIMS, SMARTLIS, Freezerworks, Biobank, Open Specimen, etc.), and they have advantages over simple solutions such as spreadsheets. These advantages may include audit controls, study–subject–sample hierarchy definition, searchability, access control, and so on, depending upon the particular software. Consideration should also be given to protocols for sample annotation. For example, a naming scheme can be used that follows the format 01-002-03, where 01=the study ID, 002=the subject ID, and 03=the visit ID. Further suffixes can designate derivative sample types, e.g., PBMC, serum, and so on. When combined with a barcode and barcode readers, such systematic naming can aid in organization and retrieval efforts. Linking relevant clinical information, de-identified to meet privacy requirements, can further make searching for desired samples much faster.

Table 97. Markers affected by cryopreservation and/or whole blood stabilization*

Affected by PBMC cryopreservation	Affected by Smart Tube stabilization
CD62L [861, 2187, 2194, 2196]	CCR6 (our unpublished data)
CCR5 [861]	CXCR5 (our unpublished data)
PD-1 [2197]	CD11b (our unpublished data)
PD-L1 [2197]	CD16 (our unpublished data)
CD20b [2198]	CD45RA (our unpublished data)
CD45RO [2187]	CD127 (our unpublished data)
CD28 [2194]	

* These lists are not exhaustive, nor do we rule out the use of the listed markers in cryopreservation or whole blood stabilization protocols. Results will depend upon the antibody clone/epitope targeted, as well as the permeabilization conditions used.

11.4 Applications

We can divide approaches for FCM sample banking into three general categories. The first is to run all samples fresh without any banking. This avoids any loss of cells, markers, or functions and thus allows for the full gamut of FCM assays to be performed. However, it also carries logistical challenges that may make it impossible for many studies; and the workflow creates more sample-to-sample variability, assuming that sample collection is staggered (i.e., not all samples are collected at once). Finally, unless combined with another method, it means no samples are available for later assays that are yet to be determined.

A second approach involves viable cryopreservation of cells for later FCM analysis. For human blood samples, this usually means cryopreservation of PBMC. While there are protocols for viable freezing of granulocytes and/or whole blood, these tend to be associated with greater loss of viability and/or staining resolution. In any case, cryopreservation allows for any number of later assays to be performed, subject only to how many cells are available. It also avoids much of the variability inherent in fresh real-time analysis of individual samples, since samples can be batched and therefore results are more comparable. However, it also means potential loss of certain cell types, markers, or functions (see Table 97). For example, CD62L is known to be variably lost upon PBMC cryopreservation [861, 2196]. Certain chemokine receptors (e.g., CCR5, [861]) can also lose some staining intensity, as can PD-1 and PD-L1 [2197]. Monocytes and their associated antigen processing functions can be preferentially lost with cryopreservation, such that functional assays that rely on protein antigen processing will be significantly compromised [638].

Both of the above approaches may be combined with initial shipping of fresh samples from a collection to an analysis or processing site. Obviously, this increases sample degradation, in ways that may be variable depending upon time and temperature in transit, and so on. NK and B cell frequencies and functional capacity may be most vulnerable to shipping [2199]. However, this may be an unavoidable sacrifice in multicenter studies. Even in cases where each individual collection site could in theory perform cryopreservation, it may be preferable to ship samples to a single processing site where there is better control of the procedure [2199].

A final approach involves using a sample preservation method (generally some type of fixation) that allows for later FCM analysis, even though the cells are no longer viable. A simple example is a blood collection tube such as Cyto-Chex (Steck, Inc.), that fixes cells upon blood draw, and confers stability of major lineage epitopes (e.g., for assays like CD4 counting) for up to 1 week. A more complex example is the Smart Tube system (Smart Tube, Inc.), which allows for stimulation of fresh blood, followed by timed release of a stabilizer solution, after which samples can be stored at –80°C for later analysis. This system has been used for signaling studies, where signals degrade quickly after sample collection (e.g., Gaudilliere et al. [2015]). Similarly, investigators have performed erythrocyte lysis followed by fixation and freezing, for later staining and analysis of leukocyte counts [2200]. Such schemes require time-dependent work at the collection site, in terms of pipetting and freezing samples. They also compromise the staining of certain cell-surface epitopes, due to fixation. Of course, these systems preserve granulocytes as well as PBMC, which may be useful in certain studies. Finally, it goes without saying that the fixed cells are no longer useful for further stimulation or functional assays not previously anticipated.

When performing an animal study, it is often possible to synchronize sampling such that fresh parallel analysis of all samples at a given time point is feasible. However, if the intent is to compare longitudinal samples from the same animals, it may be preferable to cryopreserve or stimulate/fix/freeze samples, so that all time-points from a given animal can be run in a single batch. This of course assumes that the readouts being assessed can be adequately preserved with such methods.

With clinical studies, the sample collection is almost always staggered with subject enrollment, so biobanking becomes even more attractive, to allow batching of samples for analysis. The exception, again, is if the cells, markers, and/or functions of interest can only be assessed in fresh cells. With multicenter clinical studies, the considerations become even more complex, as one needs to balance the advantages of well-controlled procedures at a single central lab with the reduced sample degradation of processing and/or assays done at multiple sample collection sites [2199]. Alternately, a central lab can provide SOPs, analysis templates, training, and so on, to collection sites that then perform the assays in parallel [2201]. Inclusion of replicate control samples into the workflow can help determine reproducibility in the context of such workflows [2202].

11.5 Equipment

The viability and concentration of isolated PBMCs are important for the planned analysis. Besides manual conventional cell counting with trypan blue (TB) and a hemacytometer, there are advanced methods for PBMC cell counting, which provide automated documentation options, e.g., Scepter™, CASY®, and

Countess™ II. However, these devices require specialized consumables that result in additional costs. Also, the accuracy of automated cell counting varies, and is still limited by factors such as cell density, erythrocyte contamination, and so on. Thus, the "Gold standard" remains the experienced laboratory professional and validation with manual cell counting using trypan blue stained cells. However, in a multicenter study with several employees working at different levels, automated counting instruments have a great advantage because the results remain consistent.

Among the aspects of PBMC processing and cell counting, the freezing conditions of PBMC on the survival of immune cells are crucial. The point should be made to avoid defrosting cysts as well as long storage at –70°C. If interim storage is necessary, a dry shipper may be an alternative, which is provided for the transport of PBMC to the final storage site. Especially in multicenter clinical studies, it is important to minimize the artifacts from freezing and intermediate storage. In addition, the long-term storage conditions are crucial. Thus, the PBMC should be stored in controlled conditions with a permanent alarm and monitoring system.

In order to keep the quality of biobanks high, excellent management of the many biosamples is required. This requires complete documentation of the work processes in real time, including the tracking of aliquots and biosamples. Other important points are logistics management and cold chain monitoring. Large biobanks use modern laboratory information management systems (LIMS) to meet these requirements [2203]. These systems are advantageous for biobanks with multiple sites or multicenter studies. There are a variety of LIMS software that includes sample acquisition and sample storage with recorded sample and related factual information [2204–2206].

Additional features such as barcodes and barcode scanners are helpful to ensure that biosamples can be easily searched in biobanks. In addition to the individually coded tubes and racks, the LIMS also visually records the storage locations, thus ensuring a genealogy of the samples with process tracking. There are many barcode-coded tubes and the corresponding SBS racks on the market. Here, there is still a great need for investigations of the shelf life and permeability of the tubes. Since the tubes with PBMC are stored in nitrogen, they have to meet appropriate conditions. The coded tubes simplify handling by eliminating the need for time-consuming labeling. However, further purchases such as barcode scanners and other software will then be required.

11.6 Experimental workflow and acquisition

From the above discussion, there are clearly many different workflows possible with regard to sample banking. These vary from exclusive analysis of fresh samples to shipping, cryopreservation, and later batch analysis. Hybrid workflows are of course possible, with some assays done fresh, or aliquots of samples stimulated and/or fixed in real time for certain assays. Figure 242 shows a small selection of options and customizations available for PBMC isolation or whole blood stabilization, detailing the studies underlying these options/customisations [2198, 2207–2213, 2215]. In addition to the time of the possible processing steps, the different handling and cryopreservation media are also important.

In any case, once a sample banking workflow has been determined, it may be useful to test it using several control or pilot samples, prior to embarking on a large study. This will not only insure that the proposed logistics are workable, but can also give an idea of the variability to be expected, if, for example, replicate samples are drawn from the same healthy subject(s).

It is also worth considering acceptance criteria for large studies. These can be applied at multiple levels. For example, one might stipulate that fresh shipped samples that are not processed within 48 h of draw should be discarded. Or, that cryopreserved PBMC that do not yield a viability of >50% should not be further analyzed. While these types of rules will not eliminate technical variability in the results, they can at least reduce it, while at the same time saving reagents and technician time. The danger, of course, is that criteria that are too strict may result in loss of data that would still have been useful.

11.7 Advantages

As already detailed above, the advantages of sample banking can include a more efficient workflow, availability of samples for later, unforeseen assays, and better comparability between samples due to batching. In some cases, logistics strongly influence certain preferred banking workflows; for example, shipping blood to a central site in multicenter studies [2199]. But, because some FCM analytes are labile to shipping and/or cryopreservation, it may be necessary to set up hybrid schemes, where some assays are done fresh onsite, or at least some sample preparation is done fresh onsite (e.g., using Smart Tube or similar systems).

11.8 Pitfalls

As also outlined above, PBMC cryopreservation can result in preferential loss of certain cell types, markers, and functions. Well-known examples include loss of CD62L, certain chemokine receptors, and PD-1/PD-L1 with cryopreservation and thawing [861, 2196, 2197]; and loss of antigen-processing capabilities for functional assays. Restimulation assays are of course still possible after cryopreservation, particularly if using preprocessed antigens, i.e., peptides [638]. More globally, cryopreservation always results in some loss of cells versus fresh blood; and of course PBMC isolation results in loss of the granulocyte fraction.

11.9 Top tricks

While also mentioned above, we collect here certain generalizations that help to create high-quality sample banking studies for FCM.
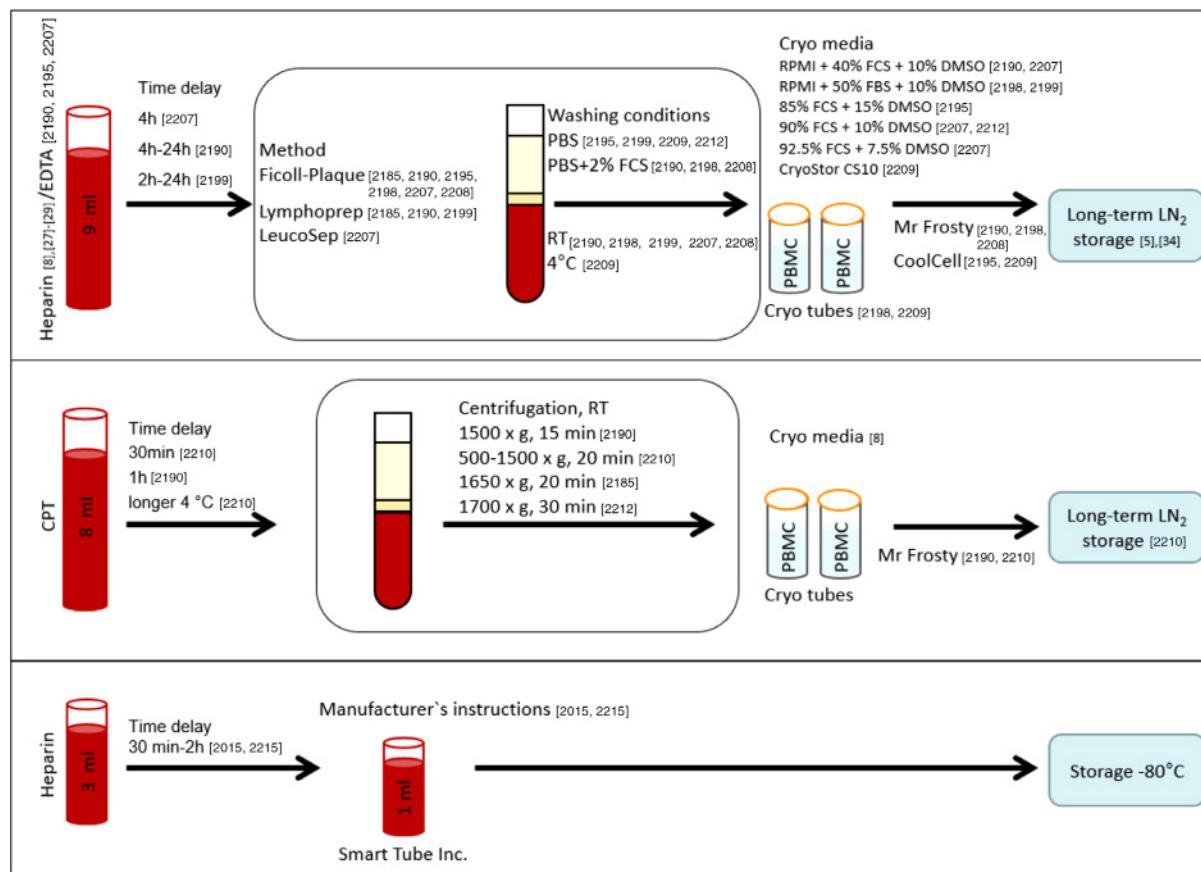
Figure 242. Brief overview of PBMC isolation or whole blood stabilization. References for each process are indicated.

1. Preanalytical variables, including time to processing, and choice of PBMC processing protocol, should be chosen accordingly to the needs of the downstream assays, and should be tightly controlled.
2. If there are highly labile cells, markers, or functions that are key analytes for a given study, some level of fresh assays and/or fresh processing may be required.
3. Consider adopting a biobanking software, and create a logical scheme for sample annotation, prior to embarking on a banking study.
4. Equipment such as automated cell counters should be validated against manual methods. Although frequently biased with regards to accuracy, they may be preferable for their reproducibility across labs and operators.
5. Keep banked samples at a constant optimal temperature. For cryopreserved PBMC, use a liquid nitrogen tray when opening boxes to select samples. As much as possible, keep long-term samples separate from those that are actively being retrieved. Consider using nitrogen dry shippers for large or long (international) shipments. Use monitors and alarms to avoid undiscovered equipment failures.
6. Implement appropriate acceptance criteria (time limit to processing, viability post-thaw, etc.). These should help to reduce technical variability as well as wasted time and reagents; but

they should not be so restrictive that samples are discarded that could still generate useful data.

12 High throughput screening

12.1 Overview

High-throughput screening is as a process by which a large number of samples are acquired in an automated fashion to identify molecules that exert biological activity on either a specific target or a cell population. Different technologies are used to detect the readout signal in a high-throughput screening assay such as automated microscopy, cell impedance measurement, time resolved fluorescence energy transfer (TR-FRET), or FCM. In this section, the use of high-throughput FCM (HTFC) will be described and examples for devices, screening assays, experimental setup, and data analysis as well as tricks and pitfalls will be shown.

12.2 Introduction

FCM has been used in almost every stage of the drug discovery process, including target identification and validation, lead and candidate selection, and safety studies for more than 30 years [2216].

This analytical technology has become very popular for drug development because of the possibility to analyze living cells out of a culture that is still available for further processing (e.g., nucleic acid extraction). However, only recently FCM has been applied also for primary high-throughput screenings. This might be due to the fact that for several years the drug screening field was dominated by target-based approaches, while cell based phenotypic assays were considered as too unspecific and risky [2217]. In addition, technical limitations of flow cytometers to process multiple samples did not make the technology very attractive for large screening campaigns. However, since microplate-based cell sampling and software capable of handling large data sets were developed the use of HTFC has become increasingly popular. In addition, affordable high quality HTFC devices were developed which also contributed to the popularity of HTFC not only in big pharma but also small companies and especially academic institutions. The possibility to use small sample and acquisition volumes and simultaneously monitor phenotypic responses of single cells in the presence of a large variety of compounds are major benefits of HTFC. The introduction of barcoding (See Chapter VIII Section 2 Barcoding) [1984] and the development of multiplex bead-based assays [2218] even allows measurement of secreted proteins or gene expression.

Recent development of laboratory automation even enable fully automated processes allowing cell culture, staining, washing, and measurement [2219]. The increasing popularity of this technology for modern drug discovery can be observed by the increasing diversity of applications in this field such as inhibition of non-homologous end joining in B cells [2220], identification of molecules inhibiting hantavirus cell entry [2221], Ab development [2222], or examination of CAR-T cell mediated cytotoxicity [2223].

12.3 *Principles of the technique being described*

HTFC is the combination of classical single cell multiparametric FCM with an autosampler delivering the sample to the FCM. The term high throughput refers to the number of samples being acquired and not to the number of cells being measured. Usually only short acquisition periods (1–3 s) are applied to ensure measurement of multiple samples in short time. Different plate formats (96, 384, or even 1536 well plates) can be handled by modern autosamplers. The preferred plate format for primary drug screenings depends on the format that the compound library is stored. Compatible plate formats are used to allow easy transfer of compounds from the storage plate to the assay plate. The most common screening format is 384-well plates, as most small molecule libraries are stored in this format. Almost all vendors of FCM offer machines capable of handling 96-well and 384-well plates. However, sampling of microvolumes (down to 1 μL) from 1536 well plates is so far only possible with the iQue screener (intellicyt). The acquisition time per sample can be individually adjusted which in turn influences the measurement time per plate. In the setup described below (Fig. 243), ten 384-well plates were

measured per day resulting in a throughput of 3840 samples per day. However, it is still possible to increase the throughput when fully automated systems like liquid handling robotics are used. Other high-throughput flow cytometers (HTFCM) on the market are based on single sample acquisition and generation of individual FCM standard (FCS) files. They also come with optional washing steps in between the samples (e.g., MACS® QuantX, Miltenyi) to prevent sample carryover. Depending on the system, there are differences in speed and sample acquisition time but usually a 384-well plate can be measured in about 30 min. Data analysis can be performed with software shaped for high-throughput data analysis, e.g., Forecyt (intellicyt) or Genedata Screener (Genedata) that displays the samples in plate format and is designed to help the user to easily identify hits on a plate, calculate thresholds, Z-factor, and even combine and overlay results from different screening campaigns. However, it is also possible to analyze the samples with software like FlowJo (FlowJo, LLC), WinList, or even free (mostly R-based) FCM software [2077].

12.4 *Applications*

High-throughput screening technologies such as automated microscopy, cell impedance measurement, or TR-FRET mostly generate only a single readout. In contrast, HTFC offers the multiparameter analysis of particles and cells. This is especially useful for phenotypic screening assays where different cellular parameters (e.g., size, viability, surface molecule expression) or even different cell populations can be simultaneously analyzed to identify the most potent and less toxic hit compounds. HTFC can be performed using living cells, fixed cells, suspension cells, or even adherent cells [2224] and bead based assays. Examples for applications are Ab development [2222, 2225], toxicology [2226, 2227] and apoptosis studies [2228], analysis of protein phosphorylation [2003], identification of stem cell expanding compounds [2229], identification of immune enhancing [2230] or immune inhibiting compounds [2231], monitoring of chemotherapy side effects [2232], and characterization and cytotoxicity monitoring of engineered T cells [2223]. In addition, secreted molecules such as chemokines or cytokines as well as gene expression can be quantified using barcoded bead based multiplex assays [2233, 2234]. Specialized HTFCM can measure up to 500 analytes per sample in high throughput (e.g., FLEXMAP 3D, Luminex). Even the simultaneous analysis of cells and beads in one sample can be performed [2235]. Thus, the variety of different HTFC applications illustrates the flexibility this method offers for assay design and high-throughput screening. The HTFC assay described in Fig. 243 was designed to identify compounds inducing the expression of Foxp3–the master transcription factor of regulatory T cells. Therefore, spleen and lymph node cells from reporter mice were incubated with 40 000 small synthetic molecules (provided by the screening unit of the FMP Berlin) and the expression of enhanced green fluorescent protein (EGFP) under the control of the Foxp3 promotor was analyzed by FCM.
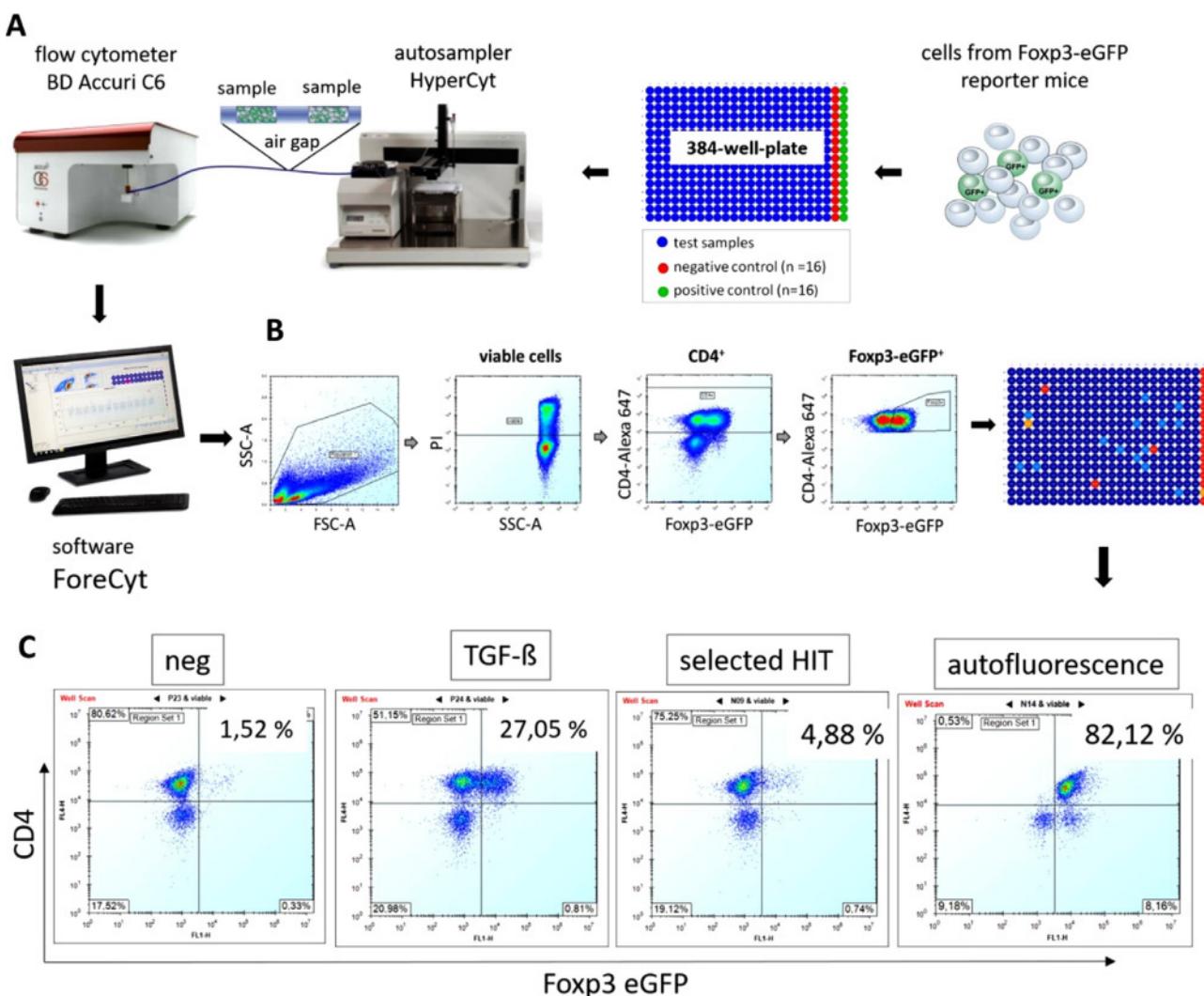
Figure 243. Experimental workflow, data deconvolution, and hit selection of an HTFC drug screen. (A) Primary immune cells from Foxp3-eGFP reporter mice are cultured in the presence of specific stimuli and compounds from a small molecule library. The autosampler is harvesting the cells from 384-plates and delivers it consecutively, without washing steps, to a connected cytometer. Air gaps in between samples created by position change of the sampling probe are necessary for sample deconvolution. (B) Data deconvolution to identify Foxp3-eGFP inducing hit compounds. Data of the entire 384-well plate is displayed. Hits and positive controls can be located on the plate heat map. (C) Single well analysis for hit verification, analysis of assay robustness, quality of controls, and exclusion of false positives (autofluorescence).

12.5 Equipment

To perform HTFC with reasonable throughput the assays should at least be set up in 96-well formats. Necessary hardware components are the autosampler, a FCM, and a computer with data analysis software. Several FCM offer already build in autosampler for 96- or even 384-well formats: iQue screener (intellicyt), MACS® Quant X (Miltenyi), ZE5 (BioRad), Cyte (ACEA Biosciences), Cytoflex (Beckman Coulter), and the spectral analyzer SA3800 (Sony). Other distributors offer compatible add-on autosampler for their devices like Attune (Thermo Fisher) or Beckton Dickinson instruments that can be easily connected. For the phenotypic assay described here, the HyperCyt® autosampler (intellicyt) [2236] connected to a FCM (Accuri) and a computer

equipped with a specialized software capable of handling and analyzing the data (ForeCyt®) (Fig. 243A) was used.

12.6 Experimental workflow and acquisition

The assay described in Fig. 243 was performed in 384-well polypropylene U-bottom plates. Compounds were diluted in RPMI medium (10% FCS, 1% Pen/Strep, 1% Pyruvat, 2.5% HEPES, 0.5% Gentamycin, 0,01% Mercaptoethanol) and spotted on the assay plate. The final concentration of the screened compounds was 1 μM. Primary immune cells of Foxp3-eGFP reporter mice (DEREGxDo11.10) [2237] were isolated from spleen and lymph nodes and depleted of CD8^{+} T cells by magnetic separation (Mil-

tenyi). Ovalbumin (1 µg/mL) and IL-2 (10 ng/mL) was added to the cell suspension for stimulation. The positive control additionally contained TGF-ß (5 ng/mL) as inducer of Foxp3 expression. The number of cells seeded per well was 3×10^5 cells. Experience showed that $CD8^+$ depleted cells from one animal are sufficient for up to four plates. The plate included 352 wells with compounds and 16 wells each for negative and positive controls (Fig. 243A). This number of controls is necessary to obtain statistical power for calculation of assay robustness (Z-factor). Incubation was performed at 37°C for 72 h and plates were subsequently centrifuged. The supernatant was discarded and staining solution containing CD4-Alexa647 mAb (GK 1.5; DRFZ) and PI (1 µg/mL) was added. The plates were shaken at 3000 rpm for 10 s on the plate shaker included in the HyperCyt autosampler and subsequently incubated for 15 min at 4°C with. Acquisition was performed right after incubation without washing. The acquisition time was set to 3 s, which results in approximately 1×10^4 recorded events per sample. Washing steps of 3 s were programmed after every 16 samples (1 column). The autosampler harvests the cells from 384-plates and delivers it consecutively, without washing steps, to a connected cytometer. When the sampling probe switches between individual wells, air gaps are created which interrupt the sample flow (Fig. 243A). As only one single FCS file is recorded for the whole plate these air gaps serve as reference point for the software to recognize individual samples and allocate them to the wells. Using these acquisition settings, the measurement time per plate was 37 min. The daily throughput was 3840 samples.

12.7 Data analysis

Following acquisition, the data are uploaded to the ForeCyt software where the data was processed and well gates were positioned automatically according to time and position of air gaps that separated the sample flow. The correct allocation of the well gates should be manually controlled to avoid misallocation and thereby misinterpretation of data. Gating of lymphocytes, live cells, $CD4^+$ T cell, and $Foxp3^+$ T cell populations was performed and percentages of $Foxp3^+$ cells are displayed in a 384-well heat map to facilitate hit identification (Fig. 243B). Frequencies of viable and $Foxp3\text{-}eGFP^+$ cells are exported to an excel sheet. Mean and SD of negative and positive controls are calculated and accordingly the Z-factor [2238] is calculated to obtain a measure of assay quality. Hit identification thresholds are set according to reporter expression ($\geq$mean of negative control $+3x\sigma$) and cell viability (mean of negative control $-3x\sigma$). Hits passing the thresholds are again reanalyzed to exclude false positives (e.g., caused by autofluorescent compounds; Fig. 243C). The final hits are selected for further validation.

12.8 Advantages

– Speedy automated acquisition of hundreds of samples

– Simultaneous multiparameter analysis of cells (cellular size, viability, surface molecule expression)
– Multifactorial analysis [2077] of different cell populations in one sample in the presence of screening compounds
– Identification of toxic compounds already at screening stage of the drug discovery process helps to identify and focus on the right drug candidates
– Autosampler capable of acquiring samples from 96-, 384-, or even 1536-well plates help to drastically reduce the sample size which in turn reduces screening material (e.g. cells, less animals if primary cells are used), costs for reagents (Abs, buffers)
– False positive results resulting, e.g., from interaction of autofluorescent compounds with cells can be easily excluded which is not possible by, e.g., automated microscopic screenings
– label-free screenings are now possible with the use of spectral analyzers (e.g., SA3800, Sony).

12.9 Pitfalls

– Cells will accumulate at the well bottom if plates (especially 384- and 1536-well) are not properly shaken.
– Clogging of the device might occur but the software does always recognize and warn.
– Make sure that samples do not evaporate during measurement especially when working with very small volumes. Plate sealing helps and autosampler probe can perforate certain seals but make sure that the glue of the seals does not clog the probe. FCM manufacturers will help identifying the right seals.
– Check for unusual high signals. False positives might result from autofluorescent compounds sticking to cells.
– Check for carry over effect of the autosampler probe.

12.10 Top tricks

– Before starting the screen perform test runs to check the following: (1) quality of the assay by comparing negative and positive controls and calculate the Z-factor to determine the quality of the assay (SNR and signal to background ratio) [2238]. A Z-factor > 0.6 is desirable, (2) check for DMSO sensitivity of the cells. DMSO concentrations should be <1%.
– The washing step after cell staining can be omitted that saves time and limits eventual loss of cells
– Determine carry over effect of autosampler probe to prevent intersample contamination. To prevent carry over include wells containing wash buffer in the assay well.
– To prevent clogging of the sampling probe or tubing QSol Buffer (intellicyt) can be used.
– Calibrate plate alignment and sampling probe depth before and if possible, also during screen to ensure proper sample uptake.
– Frequently shake the plate or mix the samples during the measurement to prevent cell accumulation at the well bottom.

– Frequently monitor data acquisition and sample flow during measurement to detect eventual problems (clogging of sampling probe, low event rate).
– Make sure to reserve enough space for positive and negative controls. On a 384-well plate it´s usually 16 positive and 16 negative controls that serve to calculate the assay robustness.
– Personalized R-based programs might help to process data as flow analysis software is often not designed to handle screening data and help with hit identification.

13 Core Facility setup and housekeeping/shared resource laboratory (SRL) management

Technologies and instrumentation are rapidly evolving and there is an increasing demand for sophisticated and high-priced technologies across the life sciences. Access to state-of-the-art infrastructure has become essential for success in scientific research. This has led to the development of Core Facilities also known as Shared Resource Laboratories (SRLs), core resources of institutions that provide highly skilled technology scientists and advanced instrumentation to enhance the scope and quality of biomedical research [2239]. The term "Shared Resource Laboratory" has been adopted to better define the role of shared instrumentation laboratories as a scientific partnership with researchers within an institution. SRLs and core facilities are called the prerequisite for breakthroughs in the life sciences, because they are collaborators who will not say "no," unless there are technical feasibility concerns [2240].

Cell sorters, high-end flow cytometers, imaging flow cytometers, and mass cytometers are usually placed in SRLs. There are two different approaches for setting up a shared resource laboratory: (i) a pool of existing instrumentation from different groups/principal investigators is put together into an SRL (bottom-up approach) or (ii) the management of an institution makes a strategic investment in central research infrastructure (top-down approach). In order to achieve the desired result—the many synergistic effects of a successful SRL—several points must be taken into consideration. Operational best practice manuals have been published recently for both FCM and advanced light microscopy SRLs, two classes of core facilities that share many challenges in common [2241, 2242]. In this section, we will give a short overview of important aspects for successful SRL management. Key topics for SRL management are staffing, education, finances, data management, quality assurance (QA)/quality control (QC), laboratory space, and safety/biosafety.

13.1 Staffing

An SRL needs a head or director to oversee and manage the facility, who consults with researchers and laboratory staff across a large range of disciplines with different level of technical expertise. The head should have a scientific background reflecting the need for scientific and research expertise in SRLs. In addition to the head,

more personnel are needed to successfully operate a larger SRL, to ensure continuous operation and cover vacations, sick leave, and business trips. Cell sorters are commonly operated by sorter operators, who need to be highly qualified, knowledgeable, and service-oriented people. In an SRL, the ability to interact with people is as important as technical skill. A recent publication describes careers in SRLs and lists skills and qualifications, because SRL positions require certain common sets of skills [2243]. Among the most important qualifications are a love of learning, the ability to keep up with new technologies, and a passion for solving problems, such as troubleshooting equipment problems. SRL staff acts in a service/customer-support-type manner, and reacts to changing tasks and priorities throughout the day. Up to hundreds of people use an SRL, therefore an ability to work with individuals with very different personalities is required [2243]. Working in an SRL is a very rewarding job if one has the right skills, interests, talents, and service-oriented attitude. Determining staffing levels is a difficult challenge for SRLs. Key factors are the number and complexity of shared instruments, and the number of users needing support and training. The best practices for FCM SRLs published by the International Society for Advancement of Cytometry (ISAC) give some advice on this topic [2241]. A certain amount of SRL staff time should be reserved for consultation with users, educational activities, and optimization and development of new techniques. Such developments may be formally published as SRL Communications within the journal *Cytometry Part A*, a new publication format created to provide a vehicle for SRL-focused subjects [2244]. SRL staff members need ongoing continuing education, for example through regular attendance of conferences or courses, in order to optimally support users.

13.2 Education

In addition to the needs of SRL staff, the users of the SRL also require education. Depending on the institution, researchers with varying and diverse expertise levels will use the SRL. The first step with a new project should always be an initial consultation in which the project is discussed between the user and SRL staff. It is crucial to offer a training program, consisting of theoretical and practical education, which includes experimental planning and data analysis. If independent usage of equipment by users is a goal, users should be made aware of all required training steps, and facilities should implement measures to ensure users' competency, for example by checking the users' skills with a practical exam at the instrument. The users must understand that training is mandatory prior to instrument usage. They should be reminded that they are operating expensive equipment that is needed for numerous scientific projects, and therefore any instrument downtime due to careless handling will affect their own projects and also those of their colleagues. Instructions are best placed next to the instruments in a written form or as standard operating procedure (SOP). Each SRL should have user guidelines in which the main topics are clarified.

13.3 *Finances*

SRLs should provide high-quality, cost-effective services. Significant costs are associated with cytometry services; depending on the institution, different financial models are in place. Usually, SRLs charge usage fees, but some institutions cover costs under a central budget. Nevertheless, the preparation and periodic review of an annual operational budget is critical. The calculation of usage fees can be based on a full economic cost calculation; in this case, institutions and facility heads must consider which costs should be covered by SRL users and which costs will be subsidized by the institution. Ferrando-May et al. published an example cost calculation; although it is for a microscopy SRL, the approach is very similar for a flow cytometry SRL [2242]. Other publications show an approach for a cost accounting method [2245], and metrics for evaluating cell sorting services [2246]. Independent of whether usage fees are charged by a facility or not, the role of the SRL should be mentioned in scientific publications in the acknowledgements section, together with any grant numbers through which instruments have been purchased. This is not just a kind way of saying 'Thank you!' for the effort SRL staff has put into a published result. It very important that SRLs and SRL staff are formally acknowledged for their contributions, because the evaluation of SRL performance is often based on numbers of published acknowledgements.

13.4 *Data management*

Data management and data analysis are critical to the experiments performed in an SRL. It is in the interest of research institutions that data obtained in their SRLs complies with the highest scientific standards. If the flow cytometers are not operated by SRL staff, the users operate the instruments independently. Therefore, the large number of users with their diverse projects does not allow for a proper quality control by SRL staff. Thus, responsibility for data, including experimental design and compliance to scientific best practices, lies in the hands of the users and their PIs. To ensure the proper description of experiments, SRLs can offer proof-reading of methods parts of scientific publications. Transferring data off instrument PCs is the first step to accessing to data. Here, users should refrain from using USB devices (flash drives, external hard drives) due to the high risk of spreading computer viruses and malware. A centrally accessible file server is an option to overcome this problem. The facility should state clearly who has the responsibility to transfer and store data and when data will be deleted from SRL computers and file servers. In clinical environment, there may be additional regulations addressing data management.

13.5 *Quality assurance and quality control*

SRLs must monitor instruments to maintain optimal performance. In a multi-user environment such as an SRL, contamination, optical misalignment, damage, or careless handling can happen on a daily basis. Regular system checks and performance tracking must be common practice, and the quality control (QC) data should be stored and made available to the SRL users, if needed. It is important to perform preventative maintenance for the instruments. Here, maintenance contracts with instrument vendors can help minimize instrument downtime. QC criteria can be rather different depending on the equipment, but Barsky et al. give some advice on this topic [2241].

13.6 *Laboratory space*

SRLs should occupy highly visible space that has the same quality as research labs. The quality of laboratory space expresses the commitment of the institution to state-of-the-art technologies [2239]. Large instrumentation, such as cell sorters, image cytometers, or mass cytometers have special room requirements, especially in regard to temperature stability. Other important physical environmental factors are square footage, humidity, presence of vibrations, electricity, and gas supplies [2241, 2242]. SRL lab space should be designed and equipped in close collaboration with SRL staff, as reconstruction after installation is expensive and will always interfere with SRL operations. High quality lab space also makes it feasible to fulfil safety and biosafety requirements.

13.7 *Safety/Biosafety*

Biosafety regulations vary depending on regional authorities; nevertheless, the main goal is always to protect people from biological hazards, such as infectious diseases caused by human pathogens. The potential of cytometers and especially cell sorters to create aerosols during cell sorting procedures places SRL staff and users at risk of laboratory-associated infections (LAI). A risk assessment must be performed, resulting in a risk management solution, encompassing personal protective equipment, safe laboratory procedures, and laboratory design for containment [143]. Placing cell sorters in biosafety cabinets for aerosol containment is one method to reduce the risk to sorter operators [2247]. The Biosafety Committee of the International Society for Advancement of Cytometry (ISAC) published cell sorter biosafety standards [143] and offers additional information on the ISAC webpage (https://isac-net.org/page/Biosafety). In an SRL, users bring a diverse range of samples to be analyzed or sorted. It is very important that the SRL keep track of the biosafety levels of all samples, including genetically modified organisms. This can be achieved by asking users to fill out questionnaires about their samples before use in the SRL. An institutional biosafety committee can help to determine the rules how to handle potentially infectious samples. SRLs may need to keep records for regional authorities. There are many additional safety topics that must be considered, including laser safety, waste management, and protection from chemical hazards, although these topics can vary due to regional regulations. Emergency and disaster planning is described elsewhere [2248].

In addition to the resources cited above, the Shared Resource Lab section of CYTO University (CYTO U) offers a seven-part series of webinars on SRL best practices, four webinars on Finance 101, and webinars on a great many other topics related to establishing and operating an SRL. CYTO U is ISAC's online portal for on-demand, peer-reviewed cytometry education, a great educational resource (http://cytou.org).

Warnatz (V.11 Intracellular Ca^{2+} mobilization by means of Indo-1 AM); Linda Schadt, Maries van den Broek, Susanne Ziegler, Glòria Martrus (V.12 mRNA); Derek Davies, Alfonso Blanco, Andrew Filby, Timothy P. Bushnell (V.13 Transcription factors); Jakob Zimmermann, Christina Stehle, Hyun-Dong Chang, Andreas Radbruch (V.14 Intracellular parameters); T. Vincent Shankey, Sue Chow, Lilly Lopez, David Hedley (V.15 Measurement of signal transduction pathways by flow cytometry); Katharina Pracht, Sophia Urbanczyk, Tobit Steinmetz, Hans-Martin Jäck, Dirk Mielenz (V.16 Assessing Lymphocyte metabolism through functional dyes); Alessio Mazzoni, Laura Maggi, Francesco Annunziato (V.17.1 Measurement of signal transduction pathways in human T cells); Steven L.C. Ketelaars, Anastasia Gangaev, Pia Kvistborg (V.17.2 Measuring antigen specific T cell responses); Matthias Schiemann, Immanuel Andrä, Kilian Schober, Dirk H. Busch (T cell assays-MHC multimers); Alexander Scheffold, Petra Bacher (Functional readouts); Alessio Mazzoni, Laura Maggi, Lorenzo Cosmi (V.17.6 Live cytokine-producing cell sorting with cytokine secretion assay™); Laura Maggi, Alessio Mazzoni, Francesco Liotta (V.17.7 Quantification of soluble cytokines with cytometric bead array); Thomas Schüler, Gerald Willimsky, Tristan Holland, Salvador Vento-Asturias, Natalio Garbi (V.17.8 Cytotoxicity); James Wing, Ilenia Cammarata, Vincenzo Barnaba, Shimon Sakaguchi (V.17.9 Treg suppression assays); Johanna E. Huber, Dirk Baumjohann (V.18 Adoptive T and B cell transfer as a read-out for antigen-specific immune responses in mice); Jessica G. Borger, Kylie M. Quinn, Mairi McGrath, Regina Stark (VI.1.1 Murine CD4 and CD8 T cells); Kylie M. Quinn, Luka Čičin-Šain, Katarzyna M. Sitnik (VI.1.5 Immune senescence (aging) in murine T cells); Michael Delacher, Juhao Yang, Markus Feuerer, Jochen Huehn (VI.1.6 Murine Foxp3+ regulatory T cells); Immo Prinz, Anneke Wilharm, Inga Sandrock (VI.1.7 Murine γδ T cells); Heike Kunze-Schumacher, Andreas Krueger (VI.1.8 Murine NKT cells); Heike Kunze-Schumacher, Andreas Krueger (VI.1.9 Murine mucosal-associated invariant T (MAIT) cells); Immo Prinz, Joana Barros-Martins (VI.1.10 Murine intestinal intraepithelial T cells); Pleun Hombrink, Ester B.M. Remmerswaal (VI.1.11 Human CD4 and CD8 T cells); Anna Oja, Pleun Hombrink (VI.1.12 Human tissue resident memory T cells); Yotam Raz (VI.1.13 Immune senescence (aging) of human T cells); Kirsten A Ward-Hartstonge, Laura Cook, Dominic A Boardman, Sabine M Ivison, Jennie H. M. Yang, Eleni Christakou, Timothy I.M. Tree, Megan K Levings (VI.1.14 Human FOXP3+ regulatory T cells); Anouk von Borstel, Martin S. Davey (VI.1.15 Human γδ T cells); Christopher M. Harpur, Dale I. Godfrey, Garth Cameron (VI.1.16 Human NKT cells); Garth Cameron, Nicholas A. Gherardin, Alexandra J. Corbett, Sidonia B. G. Eckle, James McCluskey, Dale I. Godfrey, Hui-Fern Koay (VI.1.17 Human mucosal-associated invariant T (MAIT) cells); Larissa Nogueira Almeida, Britta Frehse, Rudolf Armin Manz (VI.2.1 Murine B cells and their subsets, including Bregs); Thomas Weisenburger, Andreas Acs, Thomas H. Winkler (VI.2.2 Murine Germinal Center B cells); Annika Wiedemann, Andreia Lino, Thomas Dörner (VI.2.3 Human B cells and their subsets); Annika Wiedemann, Andreia C. Lino, H. Kristyanto, Hans U. Scherer, Thomas Dörner (VI.2.4 Human B cells recog-

nizing defined (auto)antigens); Oliver Wirz, Willem van de Veen, Mübeccel Akdis (VI.2.5 Human regulatory B cells); Willem van de Veen, Oliver Wirz, Mübeccel Akdis (VI.2.6 Human immunoglobulin heavy chain isotypes); Sebastian Schulz, Katharina Pracht, Ljiljana Cvetkovic, Dirk Mielenz, Dorothea Reimer, Wolfgang Schuh, Hans-Martin Jäck (VI.3.1 Murine antibody-secreting plasmablasts and plasma cells); Antonia Niedobitek, Henrik E. Mei (VI.3.2 Human antibody-secreting cells); Daniela C Hernández, Christina Stehle, Andreas Diefenbach, James Di Santo, Chiara Romagnani (VI.4 Innate Lymphoid cells); Lorenzo Moretta, Linda Quatrini, Genny del Zotto (VI.5 Natural Killer (NK) cells); Regine J. Dress, Alicia Wong, Ahad Khalilnezhad, Wan Ting Kong, Charles-Antoine Dutertre, Florent Ginhoux (VI.6 Mononuclear phagocytes: Monocytes, macrophages and dendritic cells); Jonas Hahn, Christian Maueröder, Jasmin Knopf, Malgorzata Justyna Podolska, Luis Enrique Muñoz, Martin Herrmann (VI.7.1 Neutrophils, eosinophils and basophils); Immanuel Kwok, Leonard Tan, Maximilien Evrard, Lai Guan Ng (VI.7.2 Bone marrow and umbilical cord blood neutrophils); Philip E. Boulais, Paul S. Frenette (VI.8 Murine bone marrow stromal cells); Peter K. Jani, Julia Tornack, Wolfgang Bauer, Fritz Melchers, Susann Rahmig, Claudia Waskow (VI.9 Hematopoietic Stem Cells); Ramon Bellmàs Sanz, Jenny Kühne, Christine S. Falk (VI.10 Tumor cells); Katharina Kriegsmann, Michael Hundemer, Leo Hansmann (VI.11 Human plasma cells in multiple myeloma); Pascale Eede, Katja Kobow, Helena Radbruch (VI.12 Brain/neural cells); Katrin Neumann, Aaron Ochel, Gevitha Ravichandran, Gisa Tiegs, Sebastian Lunemann (VI.13 Cells from liver); Friederike Ebner, Kerstin H. Mair, Josephine Schlosser, Susanne Hartmann, Armin Saalmüller, Wilhelm Gerner (VI.14.1 Porcine cells); Kerstin H. Mair, Armin Saalmüller, Wilhelm Gerner (VI.14.2 Cross-reactive Ab clones); Yvan Saeys (Introduction and Artificial intelligence in flow cytometry); Tim Mosmann, Alice Yue, Sally Quataert, Jonathan Rebhahn, Ryan R. Brinkman (Cell-population analysis: Data preprocessing, manual and automated gating, and quality control); Thomas Höllt (Dimensionality reduction); Sofie Van Gassen (VII.1 Clustering); Natalie Stanley and Nima Aghaeepour (Integration of cytometric data into multiomics analysis) James V Watson, Diether Recktenwald, James Wing (VII.2 Statistics for flow cytometry); Susanne Melzer, Attila Tarnok (VII.3 Analysis presentation and publication (MIFlowCyt)); Josef Spidlen, Ryan R. Brinkman (VII.4 Data repositories: Sharing your data); Orla Maguire, Hans Minderman (VIII.1 Imaging Flow Cytometry); Henrik E. Mei, Michael D. Leipold, Holden T. Maecker (VIII.2 Barcoding in cytometric assays); Axel Ronald Schulz, Antonio Cosma, Sabine Baumgart, Brice Gaudilliere, Helen M. McGuire, Henrik E. Mei (VIII.3 Mass cytometry); J. Paul Robinson, Bartek Rajwa (VIII.4 Combinatorial cytometry); Claudia Haftmann, Florian Mair (VIII.5 High dimensional flow cytometry); Daniel Schraivogel, Dinko Pavlinic, Bianka Baying, Diana Ordonez, Anders Stahlberg, Vladimir Benes, Malte Paulsen (VIII.6 Single cell genomics and cytometry); Hyun-Dong Chang, Jakob Zimmermann, Susann Müller (VIII.7 Microbial cells); Marina Saresella, Ivana Marventano, Federica Piancone, Francesca LaRosa, Mario Clerici (VIII.8 Detailed and standardized methods to detect inflammasome assembly and activation

in immune cells (FlowSight AMNIS); Kata Filkor, Gergely Toldi (VIII.9 Multidrug resistance activity); Leo Hansmann, Livius Penter, Hans-Peter Rahn (VIII.10 Index sorting); Chantip Dang-Heine, Holden T. Maecker (VIII.11 Sample banking for flow cytometry); Stefan Frischbutter (VIII.12 High throughput screening); Christian Kukat (VIII.13 Core Facility setup and housekeeping /Shared Resource Laboratory (SRL) management).

Conflict of interest

Some of the authors of these guidelines work for companies manufacturing FCM equipment and reagents. The mention of a particular company's equipment or reagents does not imply endorsement of these products but are included as examples. The content of these guidelines is editorially independent of any company and has been peer-reviewed.

References

1 **Cossarizza, A., Chang, H.-D., Radbruch, A., Akdis, M., Andrä, I., Annunziato, F., Bacher, P. et al.**, Guidelines for the use of flow cytometry and cell sorting in immunological studies. *Eur. J. Immunol.* 2017. **47**: 1584–1797.

2 **Mack, J.**, Fulwyler Particle Separator. US patent US 3380584 A.

3 **Kachel, V., Fellner-Feldegg, H. and Menke, E.**, Hydrodynamic properties of flow cytometry instruments. In M. R. Melamed, T. Lindmo and M. L. Mendelsohn (Eds.), *Flow cytometry and sorting*, 2nd ed., Wiley, New York, NY, 1990, pp. 27–44.

4 **Crosland-Taylor, P. J.**, A device for counting small particles suspended in a fluid through a tube. *Nature* 1953. **171**: 37–38.

5 **Gucker, F. T., Jr., O'Konski, C. T., Pickard, H. B. and Pitts, J. N., Jr.**, A photoelectronic counter for colloidal particles. *J. Am. Chem. Soc.* 1947. **69**: 2422–2431.

6 **Van den Engh, G. J.**, Flow cytometer droplet formation system. US patent US 6861265 B1.

7 **Van den Engh, G. J.**, Particle separating apparatus and method. US patent US 5819948 A.

8 **Norton, P. O., Vane, D. R. and Javadi, S.**, Fixed mounted sorting cuvette with user replaceable nozzle. US patent US 7201875 B2.

9 **Doležel, J. and Göhde, W.**, Sex determination in dioecious plants *Melandrium album* and *M. rubrum* using high-resolution flow cytometry. *Cytometry* 1995. **19**: 103–106.

10 **Steen, H. B., Lindau, T. and Sorensen, O.**, A simple, high resolution flow cytometer based on a standard fluorescence microscope. In O. D. Laerum, T. Lindmo and E. Thorud (Eds.), *Proceedings of the IVth international symposium on flow cytometry (pulse cytophotometry)*, Bergen, Norway, 1980, pp. 31–33.

11 **Pinkel, D. and Stovel, R.**, Flow chambers and sample handling. In M. A., Van Dilla, P. N. Dean, O. D. Laerum, and M. R. Melame (Eds.), *Flow cytometry: Instrumentation and data analysis*, Academic Press, London, 1985, pp. 77–128.

12 **Kaduchak, G. et al.**, Ultrasonic analyte concentration and application in flow cytometry. US patent US 7340957 B2.

13 **Kaduchak, G. et al.**, System and method for acoustic focusing hardware and implementations. US patent US 8714014 B2.

14 **Ward, M., Turner, P., DeJohn, M. and Kaduchak, G.**, Fundamentals of acoustic cytometry. *Curr. Protoc. Cytometry* 2009. **53**: 1.22.1–1.22.12.

15 **Sweet, R. G.**, Fluid droplet recorder. US patent US 3596275 A.

16 **Göttlinger, C., Mechtold, B., Meyer, K. L. and Radbruch, A.**, Setup of a flow sorter. In Radbruch, A. (Ed.), *Flow cytometry and cell sorting*. Springer Laboratory, Berlin, Germany 1992, pp. 153–158.

17 **Petersen, T. W. and Van den Engh, G.**, Stability of the breakoff point in a high-speed cell sorter. *Cytometry Part A* 2003. **56**: 63–70.

18 **Kaiser, T., Raba, K., Scheffold, A. and Radbruch, A.**, A sheath-cooling system to stabilize side-streams and drop delay during long-term sorts for FACS-Aria® cell-sorter, http://fccf.drfz.de/uploads/pdf/poster_zentrallabor_A0.pdf

19 **Lawrence, W. G., Varadi, G., Entine, G., Podniesinski, E. and Wallace, P. K.**, Enhanced red and near infrared detection in flow cytometry using avalanche photodiodes. *Cytometry A* 2008. **73**: 767–776.

20 **Kester, W.**, Understand SINAD, ENOB, SNR, THD, THD+ N, and SFDR so you don't get lost in the noise floor. MT-003 Tutorial, 2009, http://www.analog.com/media/en/training-seminars/tutorials/MT-003.pdf

21 AD9240AS by Analog Devices | Data Acquisition, Arrow.com. [Online]. Available: https://www.arrow.com/de-de/products/ad9240as/analog-devices. [Accessed: 18-Jan-2017].

22 **Snow, C.**, Flow cytometer electronics. *Cytometry Part A* 2004. **57A**: 63–69.

23 **Asbury, C. L., Uy, J. L. and van den Engh, G.**, Polarization of scatter and fluorescence signals in flow cytometry. *Cytometry* 2000. **40**: 88–101.

24 **Shapiro, H. M.**, *Practical flow cytometry*, 4th ed., John Wiley & Sons, Inc., Hoboken, NJ 2003, pp. 184–197.

25 **Watson, D. A., Brown, L. O., Gaskill, D. F., Naivar, M., Graves, S. W., Doorn, S. K. and Nolan, J. P.**, A flow cytometer for the measurement of Raman spectra. *Cytometry A* 2008. **73A**: 119–128.

26 **Nolan, J. P., Condello, D., Duggan, E., Naivar, M. and Novo, D.**, Visible and near infrared fluorescence spectral flow cytometry. *Cytometry A* 2012. **83**: 253–264.

27 **Wade, C. G., Rhyne, R. H., Woodruff, W. H., Bloch, D. P. and Bartholomew, J. C.**, Spectra of cells in flow cytometry using a vidicon detector. *J. Histochem. Cytochem.* 1979. **27**: 1049–1052.

28 **Robinson, J. P.**, Multispectral cytometry: the next generation. *Biophoton. Int.* 2004, 36–40.

29 **Robinson, J. P., Rajwa, B., Gregori, G., Jones, V and Patsekin, V**, Multispectral cytometry of single bio-particles using a 32-channel detector. In T. Tuan Vo-Dinh, W. S. Grundfest, D. A. Benaron and G. E. Cohn, (Eds.), *Advanced biomedical and clinical diagnostic systems III*, 5692 ed. Springer, Berlin/Heidelberg, 2005, Pp. 359–365.

30 **Robinson, J. P., Rajwa, B., Patsekin, V., Gregori, G. and Jones, J.** *Multispectral detector and analysis system US patent US7280204 B2*.

31 **Grégori, G., Patsekin, V., Rajwa, B., Jones, J., Ragheb, K., Holdman, C., Robinson, J. P. et al.**, Hyperspectral cytometry at the single cell level using a 32 channel photodetector. *Cytometry A* 2012. **81A**: 35–44.

32 **Goddard, G., Martin, J. C., Naivar, M., Goodwin, P. M., Graves, S. W., Habbersett, R., Nolan, J. P. et al.**, Single particle high resolution spectral analysis flow cytometry. *Cytometry* 2006. **69A**: 842–851.

33 **Futamura, K., Sekino, M., Hata, A., Ikebuchi, R., Nakanishi, Y., Egawa, G., Kabashima, K. et al.**, Novel full-spectral flow cytometry with multiple spectrally-adjacent fluorescent proteins and fluorochromes and visualization of in vivo cellular movement. *Cytometry* 2015. **87**: 830–842.

34 **Feher, K.**, **von Volkmann, K.**, **Kirsch, J.**, **Radbruch, A.**, **Popien, J. and Kaiser, T.**, Multispectral flow cytometry: The consequences of increased light collection. *Cytometry* 2016. **89**: 681–689.

35 **Roederer, M.**, Distributions of autofluorescence after compensation: Be panglossian, fret not. *Cytometry A* 2016. **89**: 398–402.

36 **Szalóki, G. and Goda, K.**, Compensation in multicolor flow cytometry. *Cytometry A* 2015. **87**: 982–985.

37 **Novo, D.**, **Grégori, G. and Rajwa, B.**, Generalized unmixing model for multispectral flow cytometry utilizing nonsquare compensation matrices. *Cytometry A* 2013. **83**: 508–520.

38 **Nguyen, R.**, **Perfetto, S.**, **Mahnke, Y. D.**, **Chattopadhyay, P. and Roederer, M.**, Quantifying spillover spreading for comparing instrument performance and aiding in multicolor panel design. *Cytometry A* 2013. **83**: 306–315.

39 **Lee, J. A.**, **Spidlen, J.**, **Boyce, K.**, **Cai, J.**, **Crosbie, N.**, **Dalphin, M.**, **Furlong, J.**, et al. MIFlowCyt: the Minimum Information about a Flow Cytometry Experiment. *Cytometry A* 2008. **73**: 926–930.

40 **Tung, J. W.**, **Parks, D. R.**, **Moore, W. A. and Herzenberg, L. A.**, New approaches to fluorescence compensation and visualization of FACS data. *Clin. Immunol.* 2004. **110**: 277–283.

41 BD Cytometer Setup and Tracking Application Guide V3.0, 2013, BD Biosciences, San Jose, CA.

42 **Wood, J. and Hoffman, R.**, Evaluating fluorescence sensitivity on flow cytometers: an overview. *Cytometry* 1998. **33**: 256–259.

43 **Wood, J.**, Fundamental flow cytometer properties governing sensitivity and resolution. *Cytometry* 1998. **33**: 260–266.

44 **Hoffman, R. A.**, Standardization, calibration, and control in flow cytometry. *Curr. Protoc. Cytom.* 2005. **79**: 1.3.1–1.3.21.

45 **Wood, J. C. S.**, 2009, Establishing and maintaining system linearity. *Curr. Protoc. Cytom.* Chapter **1**: 1.4.1–1.4.14.

46 **Jett, J. H.**, **Martin, J. C.**, **Habbersett, R. C.**, Techniques for flow cytometer alignment. *Curr. Protoc. Cytom.* 2009. **Chapter 1**: 1.10.1–1.10.7.

47 **Perfetto, S. P.**, **Chattopadhyay, P. K.**, **Wood, J.**, **Nguyen, R.**, **Ambrozak, D.**, **Hill, J. P. and Roederer, M.**, Q and B Values are Critical Measurements Required for Inter-Instrument Standardization and Development of Multicolor Flow Cytometry Staining Panels. *Cytometry* 2014. **85A**: 1037–1048.

48 **Perfetto, S. P.**, **Ambrozak, D.**, **Nguyen, R.**, **Chattopadhyay, P. K. and Roederer, M.**, Quality assurance for polychromatic flow cytometry using a suite of calibration beads. *Nat. Protoc.* 2012. **7**: 2067–2079.

49 **Steen, H. B.**, Noise, Sensitivity, and Resolution of Flow Cytometers. *Cytometry* 1992. **13**: 822–830.

50 **Friend, M.**, **Franklin, G. B. and Quinn, B.**, An LED pulser for measuring photomultiplier linearity. *Nucl. Instr. And Meth. A* 2012. **676**: 66–69.

51 **Giesecke, C.**, **Feher, K.**, **von Volkmann, K.**, **Kirsch, J.**, **Radbruch, A. and Kaiser, T.**, Determination of background, signal-to-noise, and dynamic range of a flow cytometer: a novel practical method for instrument characterization and standardization. *Cytometry* 2017. **91A**: 1104–1114.

52 Reference Manuals for discussed instruments: a) BD FACSCanto II Flow Cytometer Reference Manual, 2006, BD Biosciences, San Jose, USA; b) MACSQuant Instrument User Manual, V6, 2015, Miltenyi Biotec, Bergisch Gladbach, Germany; c) CyFlow Cube 6 Instrument Operating Manual, 2012, Partec GmbH, Germany; d) Attune NxT Acoustic Focusing Cytometer User Guide, 2015, Life Technologies, USA part of Thermo Fisher Scientific; e) Gallios Flow Cytometer Instructions for use, 2009, Beckman Coulter, USA

53 Flow Cell Care & Maintenance; Feb 2011, Precision Cells, Inc. http://ezinearticles.com/?Flow-Cytometry—Flow-Cell-Care-and-Maintenance&id=5898431

54 A Guide to Absolute Counting Using the BD Accuri C6 Flow Cytometer, Jan. 2012, BD Biosciences, Technical Bulletin.

55 BD FACSDIVA Software v 8.0 Reference Manual

56 **Maciorowski, Z.**, **Chattopadhyay, P. K. and Jain, P.**, Basic Multicolor Flow Cytometry. *Curr. Protoc. Immunol.* 2017. **117**: 5.4.1–5.4.38.

57 **Maecker, H. T. and Trotter, J.**, Flow cytometry controls, instrument setup, and the determination of positivity. *Cytometry A* 2006. **69**: 1037–1042.

58 **Chase, E. S. and Hoffman, R. A.**, Resolution of dimly fluorescent particles: a practical measure of fluorescence sensitivity. *Cytometry* 1998. **33**: 267–279.

59 **Meinelt, E.**, **Reunanen, M.**, **Edinger, M.**, **Jaimes, M.**, **Stall, A.**, **Sasaki, D. and Trotter, J.**, Standardizing Application Setup Across Multiple Flow Cytometers Using BD FACSDiva™ Version 6. Software. BD Biosciences Technical Bulletin. 2012.

60 **Roederer, M.**, Compensation in flow cytometry. *Curr. Protoc. Cytom.* 2002. **22**: 1.14.1–1.14.20.

61 **Biburger, M.**, **Trenkwald, I. and Nimmerjahn, F.**, Three blocks are not enough—blocking of the murine IgG receptor FcgammaRIV is crucial for proper characterization of cells by FACS analysis. *Eur. J. Immunol.* 2015. **45**: 2694–2697.

62 **Maecker, H. T.**, **Frey, T.**, **Nomura, L. E. and Trotter, J.**, Selecting fluorochrome conjugates for maximum sensitivity. *Cytometry A* 2004. **62**: 169–173.

63 **Nüsse, M.**, **Beisker, W.**, **Kramer, J.**, **Miller, B. M.**, **Schreiber, G. A.**, **Viaggi, S.**, **Weller, E. M**. et al., Measurement of micronuclei by flow cytometry. *Methods Cell Biol.* 1994. **42**: 149–158.

64 **Hengst, J.**, **Theorell, J.**, **Deterding, K.**, **Potthoff, A.**, **Dettmer, A.**, **Ljunggren, H. G.**, **Wedemeyer, H. and Björkström, N. K.**, High-resolution determination of human immune cell signatures from fine-needle liver aspirates. *Eur. J. Immunol.* 2015. **45**: 2154–2157.

65 **Johnson, S.**, **Nguyen, V. and Coder, D.**, Assessment of cell viability. *Curr. Protoc. Cytom.* 2013.**64**: 9.2.1–9.2.26

66 **Edward, R. and Dimmick, I.**, Compensation-free dead cell exclusion: multi-beam excitation of the far-red DNA binding viability dye-DRAQ7.(TECH2P. 873). *J. Immunol.* 2014. **192**: 135.4

67 **Pieper, I. L.**, **Radley, G.**, **Chan, C. H.**, **Friedmann, Y.**, **Foster, G. and Thornton, C. A.**, Quantification methods for human and large animal leukocytes using DNA dyes by flow cytometry. *Cytometry A* 2016. **89**: 565–574.

68 **Reardon, A. J.**, **Elliott, J. A. and McGann, L. E.**, Fluorescence as an alternative to light-scatter gating strategies to identify frozen-thawed cells with flow cytometry. *Cryobiology* 2014. **69**: 91–99.

69 **Hønge, B. L.**, **Petersen, M. S.**, **Olesen, R.**, **Møller, B. K. and Erikstrup, C.** Optimizing recovery of frozen human peripheral blood mononuclear cells for flow cytometry. *PLoS One*. 2017. **12**: e0187440

70 **Alsayed, H.**, **Owaidah, T. and Al Rawas, F.**, Validation of a modifiedcryopreservation method for leukemic blasts for flow cytometry assessment. *Hematol. Oncol. Stem Cell Ther.* 2008. **1**: 94–97.

71 **Chow, S.**, **Hedley, D.**, **Grom, P.**, **Magari, R.**, **Jacobberger, J. W. and Shankey, T. V.**, Whole blood fixation and permeabilization protocol with red blood cell lysis for flow cytometry of intracellular phosphorylated epitopes in leukocyte subpopulations. *Cytometry A*. 2005. **67**: 4–17.

72 **Woost, P. C., Solchaga, L. A., Meyerson, H. J., Shankey, T. V., Goolsby, C. L. and Jacobberger, J. W.,** High-resolution kinetics of cytokine signaling in human CD34/CD117-positive cells in unfractionated bone marrow. *Blood* 2011. **117**: e131–e141.

73 **Marvin, J., Swiminathan, S., Kraker, G., Chadburn, A., Jacobberger, J. W. and Goolsby, C.,** Normal bone marrow signal-transduction profiles: a requisite for enhanced detection of signaling dysregulations in AML. *Blood* 2011. **117**: e120–e130.

74 **Shankey, T. V., Forman, M. F., Scibelli, P., Cobb, J., Smith, C. M., Mills, R., Holdiway, K. et al.,** An optimized whole blood method for flow cytometric measurement of ZAP-70 protein expression in chronic lymphocytic leukemia. *Cytometry* 2006. **70**: 259–269.

75 **Jacobberger, J. W., Sramkowski, R. M., Frisa, P. S., Peng Ye, P., Gottlieb, M. A., Hedley, D. W., Shankey, T. V. et al.,** Immunoreactivity of STAT5 phosphorylated on tyrosine as a cell-based measure of Bcr/Abl kinase activity. *Cytometry* 2003. **54**: 75–88.

76 **Boehm, T., McCurley, N., Sutoh, Y., Schorpp, M., Kasahara, M. and Cooper, M. D.,** VLR-based adaptive immunity. *Annu. Rev. Immunol.* 2012. **30**: 203–220.

77 **Pancer, Z., Amemiya, C. T., Ehrhardt, G. R., Ceitlin, J., Gartland, G. L. and Cooper, M. D.,** Somatic diversification of variable lymphocyte receptors in the Agnathan sea lamprey. *Nature* 2004. **430**: 174–180.

78 **Velikovsky, C. A., Deng, L., Tasumi, S., Iyer, L. M., Kerzic, M. C., Aravind, L., Pancer, Z. et al.,** Structure of a lamprey variable lymphocyte receptor in complex with a protein antigen. *Nat. Struct. Mol. Biol.* 2009. **16**: 725–730.

79 **Han, B. W., Herrin, B. R., Cooper, M. D. and Wilson, I. A.,** Antigen recognition by variable lymphocyte receptors. *Science* 2008. **321**: 1834–1837.

80 **Luo, M., Velikovsky, C. A., Yang, X., Siddiqui, M. A., Hong, X., Barchi, J. J., Jr., Gildersleeve, J. C. et al.,** Recognition of the Thomsen-Friedenreich pancarcinoma carbohydrate antigen by a lamprey variable lymphocyte receptor. *J. Biol. Chem.* 2013. **288**: 23597–23606.

81 **Collins, B. C., Gunn, R. J., McKitrick, T. R., Cummings, R. D., Cooper, M. D., Herrin, B. R. and Wilson, I. A.,** Structural Insights into VLR Fine Specificity for Blood Group Carbohydrates. *Structure* 2017. **25**: 1667–1678.

82 **Chan, J. T. H., Liu, Y., Khan, S., St-Germain, J. R., Zou, C., Leung, L. Y., Yang, T. et al.,** A tyrosine sulfation-dependent HLA-I modification identifies memory B cells and plasma cells. *Sci. Adv.* 2018. **4**: eaar7653.

83 **Herrin, B. R., Alder, M. N., Roux, K. H., Sina, C., Ehrhardt, G. R., Boydston, J. A., Turnbough, C. L., Jr. et al.,** Structure and specificity of lamprey monoclonal antibodies. *Proc. Natl. Acad. Sci. USA.* 2008. **105**: 2040–2045.

84 **Haas, J., Roth, S., Arnold, K., Kiefer, F., Schmidt, T., Bordoli, L. and Schwede, T.,** The Protein Model Portal–a comprehensive resource for protein structure and model information. *Database* 2013. **2013**: bat031.

85 **Yu, C., Liu, Y., Chan, J. T., Tong, J., Li, Z., Shi, M., Davani, D. et al.,** Identification of human plasma cells with a lamprey monoclonal antibody. *JCI Insight* 2016. **1**: e84738.

86 **Alder, M. N., Rogozin, I. B., Iyer, L. M., Glazko, G. V., Cooper, M. D. and Pancer, Z.,** Diversity and function of adaptive immune receptors in a jawless vertebrate. *Science* 2005. **310**: 1970–1973.

87 **Yu, C., Ali, S., St-Germain, J., Liu, Y., Yu, X., Jaye, D. L., Moran, M. F. et al.,** Purification and identification of cell surface antigens using lamprey monoclonal antibodies. *J. Immunol. Methods* 2012. **386**: 43–49.

88 **Baker, M.,** Antibody anarchy: a call to order. *Nature* 2015. **527**: 545–551.

89 **Zhang, X., Calvert, R. A., Sutton, B. J. and Dore, K. A.,** IgY: a key isotype in antibody evolution. *Biol. Rev. Camb. Philos. Soc.* 2017. **92**: 2144–2156.

90 **Mucci, I., Legitimo, A., Compagnino, M., Consolini, R., Miglidaccio, P., Metelli, M. R. and Scatena, F.,** The methodological approach for the generation of human dendritic cells from monocytes affects the maturation state of the resultant dendritic cells. *Biologicals* 2009. **37**: 288–96.

91 **Delirezh, N. and Shojaeefar, E.,** Phenotypic and functional comparison between flask adherent and magnetic activated cell sorted monocytes derived dendritic cells. *Iran J. Immunol.* 2012. **9**: 98–108.

92 **Pribush, A., Meyerstein, D. and Meyerstein, N.,** Kinetics of erythrocyte swelling and membrane hole formation in hypotonic media. *BBABiomembrane* 2002. **1558**: 119–132.

93 **Tiirikainen, M. I.,** Evaluation of red blood cell lysing solutions for the detection of intracellular antigens by flow cytometry. *Cytometry* 1995. **20**: 341–348.

94 **Einwallner, E., Subasic, A., Strasser, A., Augustin, D., Thalhammer, R., Steiner, I. and Schwarzinger, I.,** Lysis matters: red cell lysis with FACS Lyse affects the flow cytometric enumeration of circulating leukemic blasts. *J. Immunol. Methods* 2013. **390**: 127–132.

95 **Lindahl, P. E.,** Principle of a counter-streaming centrifuge for the separation of particles of different sizes. *Nature* 1948. **161**: 648–649.

96 **McEwen, C. R., Stallard, R. W. and Juhos, E. T.,** Separation of biological particles by centrifugal elutriation. *Anal. Biochem.* 1968. **23**: 369–77.

97 **Pretlow, T. G. and Pretlow, T. P.,** Centrifugal elutriation (counter-streaming centrifugation) of cells. *Cell Biophys.* 1979. **1**: 195–210.

98 www.biologydiscussion.com/cell-biology/8-methods-involved-in-separation-of-whole-cells-with-diagram/3494

99 **Ferrone, S., Cooper, N. R., Pellegrino, M. A. and Reisfeld, R. A.,** Interaction of histocompatibility (HL-A) antibodies and complement with synchronized human lymphoid cells in continuous culture. *J. Exp. Med.* 1973. **137**: 55–68.

100 **Lustig, H. and Bianco, C.,** Antibody-mediated cell cytotoxicity in a defined system: regulation by antigen, antibody, and complement. *J. Immunol.* 1976. **116**: 253–60.

101 **Esser, C.,** Historical and useful methods of preselection and preparative scale cell sorting. In D. Recktenwald and A. Radbruch (Eds.), *Cell separation methods and applications.* Marcel Dekker Inc., New York/Basel/Hong Kong, 1998, pp. 1–14.

102 www.pluriselect.com

103 www.miltenyibiotec.com

104 **Thomas, T. E., Miller, C. L. and Eaves, C. J.,** Purification of hematopoietic stem cells for further biological study. *Methods.* 1999. **17**: 202–218.

105 **Van der Toom, E. E., Verdone, J. E., Gorin, M. A. and Pienta, K. J.,** Technical challenges in the isolation and analysis of circulating tumor cells. *Oncotarget* 2016. **7**: 62754–62766.

106 **Donnenberg, V. S. and Donnenberg, A. D.,** Identification, rare-event detection and analysis of dendritic cell subsets in bronchio-alveolar lavage fluid and peripheral blood by flow cytometry. *Front. Biosci.* 2003. **8**: s1175–s1180.

107 **Bacher, P. and Scheffold, A.,** New technologies for monitoring human antigen-specific T cells and regulatory T cells by flow-cytometry. *Curr. Opin. Pharmacol.* 2015. **23**: 17–24.

108 www.thermofisher.com/de/de/home/brands/product-brand/dynal.html

109 www.bdbiosciences.com/us/reagents/research/magnetic-cell-separation/other-species-cell-separation-reagents/cell-separation-magnet/p/552311

110 Recktenwald, D. and Radbruch, A. (Eds.), *Cell separation methods and applications.* Marcel Dekker Inc., New York/ Basel/ Hong Kong, 1998.

111 **Miltenyi, S. and Pflueger, E.**, High gradient magnetic cell sorting. In A. Radbruch (Ed.), *Flow cytometry and sorting.* Springer-Verlag, Berlin/Heidelberg, 1992, pp. 141–152.

112 **Ruffert, C.**, Magnetic bead—Magic bullet (review). *Micromachines* 2016. **7**: 21.

113 **McCloskey, K. E., Chalmers, J. J. and Zborowski, M.**, Magnetic cell separation: Characterization of magnetophoretic mobility. *Anal. Chem.* 2003. **75**: 6868–6874.

114 **Boyum, A.**, Isolation of leucocytes from human blood. Further observations. Methylcellulose, dextran, and ficoll as erythrocyteaggregating agents. *Scand. J. Clin. Lab. Invest. Suppl.* 1968. **97**: 31–50.

115 **Boyum, A.**, Isolation of lymphocytes, granulocytes and macrophages. *Scand. J. Immunol.* 1976. Suppl **5**: 9–15.

116 **Yeo, C., Saunders, N., Locca, D., Flett, A., Preston, M., Brookman, P., Davy, B. et al.**, Ficoll-Paque versus Lymphoprep: A comparative study of two density gradient media for therapeutic bone marrow mononuclear cell preparations. *Regen. Med.* 2009. **4**: 689–696.

117 **Boyum, A., Brincker, F. H., Martinsen, I., Lea, T. and Lovhaug, D.**, Separation of human lymphocytes from citrated blood by density gradient (NycoPrep) centrifugation: Monocyte depletion depending upon activation of membrane potassium channels. *Scand. J. Immunol.* 2002. **56**: 76–84.

118 **Kuhns, D. B., Priel, D. A., Chu, J. and Zarember, K. A.**, Isolation and functional analysis of human neutrophils. *Curr. Protoc. Immunol.* 2015. **111**: 7.23.1–7.23.16.

119 **Maqbool, M., Vidyadaran, S., George, E. and Ramasamy, R.**, Optimisation of laboratory procedures for isolating human peripheral blood derived neutrophils. *Med. J. Malaysia* 2011. **66**: 296–299.

120 **Bruyninckx, W. J. and Blancquaert, A. M.**, Isolation of horse mononuclear cells, especially of monocytes, on Isopaque-Ficoll neutral density gradient. *Vet. Immunol. Immunopathol.* 1983. **4**: 493–504.

121 **Pertoft, H.**, Fractionation of cells and subcellular particles with Percoll. *J. Biochem. Biophys. Methods* 2000. **44**: 1–30.

122 **Yu, L., Warner, P., Warner, B., Recktenwald, D., Yamanishi, D., Guia, A. and Ghetti, A.**, Whole blood leukocytes isolation with microfabricated filter for cell analysis, *Cytometry* 2011. **79A**: 1009–1015.

123 **Higuchi, A., Wang, C.-T., Ling, Q.-D., Lee, H. H.-C., Suresh Kumar, S., Chang, Y., Alarfaj, A. A. et al.**, A hybrid-membrane migration method to isolate high-purity adipose-derived stem cells from fat tissues. *Sci. Rep.* 2015. **5**: 10217.

124 **Huang, L. R., Cox, E. C., Austin, R. H. and Sturm, J. C.**, Continuous particle separation through deterministic lateral displacement. *Science* 2004. **304**: 987–990.

125 **Davis, J. A., Inglis, D. W., Morton, K. J., Lawrence, D. A., Huang, L. R., Chou, S. Y., Sturm, J. C. et al.**, Deterministic hydrodynamics: Taking blood apart, *Proc. Nat. Acad. Sci.* 2008. **103**: 14779–14784.

126 **Loutherback, K., D'Silva1, J., Liu, L., Wu, A., Austin, R. H. and Sturm, J. C.**, Deterministic separation of cancer cells from blood at 10 mL/min. *AIP Adv.* 2012. **2**: 042107.1–042107.7.

127 **D'Silva, J., Austin, H. and Sturm, C.**, Inhibition of clot formation in deterministic lateral displacement arrays for processing large volumes of blood for rare cell capture. *Lab Chip* 2015. **15**: 2240–2247.

128 **Civin, C. I., Ward, T., Skelley, A. M., Gandhi, K., Peilun Lee, Z., Dosier, C. R., D'Silva, J. L. et al.**, Automated leukocyte processing by microfluidic deterministic lateral displacement. *Cytometry A.* 2016. **89**: 1073–1083.

129 **Campos-González, R., Skelley, A. M., Gandhi, K., Inglis, D. W., Sturm, J. C., Civin, C. I. and Ward, T.**, Deterministic lateral displacement: the next-generation CAR T-cell processing? *SLAS Technol.* 2018. **23**: 338–351.

130 **Laurell, T., Petersson, F. and Nilsson, A.**, Chip integrated strategies for acoustic separation and manipulation of cells and particles. *Chem. Soc. Rev.* 2007. **36**: 492–506.

131 **Dykes, J., Lenshof, A., Åstrand-Grundström, I.-B., Laurell, T. and Scheding, S.**, Efficient removal of platelets from peripheral blood progenitor cell products using a novel micro-chip based acoustophoretic platform. *PLoS ONE* 2011. **6**: e23074.

132 **Urbansky, A., Ohlsson, P., Lenshof, A., Garofalo, F., Scheding, S. and Laurell, T.**, Rapid and effective enrichment of mononuclear cells from blood using acoustophoresis. *Sci. Rep.* 2017. **7**: 17161.

133 **Wysocki, L. J. and Sato, V. L.**, Panning for lymphocytes: A method for cell selection. *Proc. Natl. Acad. Sci. U S A* 1978. **75**: 2844–2848.

134 **Weiner, M. S., Bianco, C. and Nussenzweig, V.**, Enhanced binding of neuraminidase-treated sheep erythrocytes to human T lymphocytes. *Blood* 1973. **42**: 939–946.

135 **Indiviri, F., Huddlestone, J., Pellegrino, M. A. and Ferroni, S.**, Isolation of human T lymphocytes: Comparison between wool filtration and rosetting with neuraminidase (VCN) and 2-aminoethylisothiouronium (AET)-treated sheep red blood cells. *J. Immunol. Methods* 1980. **34**: 107–112.

136 **Lepe-Zuniga, J. L., Zigler, J. S. and Gery, I.**, Toxicity of light-exposed Hepes media. *J. Immunol. Methods* 1987. **103**: 145.

137 **Cowan, C. M. and Basu, S., Heng, B. C.**, Comparison of enzymatic and nonenzymatic means of dissociating adherent monolayers of mesenchymal stem cells. *Biol. Proc. Online* 2009. **11**: 161–169.

138 **Amaral, K., Rogero, M., Fock, R., Borelli, P. and Gavini, G.**, Cytotoxicity analysis of EDTA and citric acid applied on murine resident macrophages culture. *Int. Endod. J.* 2007. **40**(5): 338–343.

139 **Wiesman, U.**, Segregating cells—proteases in tissue culture. In Sterchi, E. E. and Stöcker, W. (Eds.), *Proteolytic enzymes: Tools and targets.* Springer, Berlin, Germany, 1999, pp. 298–311.

140 **Stovel, R. T.**, The influence of particles on jet breakoff. *J. Histochem. Cytochem.* 1977. **25**: 813–820.

141 **Pinkel, D. and Stovel, R.**, Flow chambers and sample handling. In Van Dilla, M. A., Dean, P. N., Laerum, O. D. and Melame, M. R. (Eds.), *Flow cytometry: Instrumentation and data analysis*, Academic Press, London, UK, 1985, pp. 77–128.

142 **Houtz, B., Trotter, J. and Sasaki, D.**, Tips on cell preparation for flow cytometric analysis and sorting. *BD FACService Technotes* 2004. **9**.

143 **Holmes, K. L., Fontes, B., Hogarth, P., Konz, R., Monard, S., Pletcher, Jr., C. H., Wadley, R. B. et al.**, International Society for the Advancement of Cytometry cell sorter biosafety standards. *Cytometry A* 2014. **85**: 434–453.

144 **van der Maaten, L. J. P. and Hinton, G. E.**, Visualizing high-dimensional data using t-SNE. *J. Mach. Learn. Res.* 2008. **9**: 2579–2605.

145 **McInnes, L., Healy, J and Melville, J.**, UMAP: uniform manifold approximation and projection for dimension reduction arXiv:1802.03426

146 **Aghaeepour, N, Simonds, E. F., Knapp, D. J. H. F., Bruggner, R. V., Sachs, K., Culos, A., Gherardini, P. F. et al.**, GateFinder: projection-based gating strategy optimization for flow and mass cytometry. *Bioinformatics* 2018. **34**(23): 4131–4133.

147 **Becht, E., Simoni, Y., Coustan-Smith, E., Maximilien, E., Cheng, Y., Ng, L. G., Campana, D. et al.**, Reverse-engineering flow-cytometry gating strategies for phenotypic labelling and high-performance cell sorting. *Bioinformatics* 2019. **35**: 301–308.

148 **Samusik, N.**, **Irvine, A.**, **Aghaeepour, A.**, **Spidlen, J. and Trotter, J.** Computational Sorting with HyperFinder, CYTO 2019, Session Parallel 06, 24 June 2019.

149 **Bøyum, A.**, **Løvhaug, D.**, **Tresland, L. and Nordlie, E. M.**, Separation of leucocytes: improved cell purity by fine adjustments of gradient medium density and osmolality. *Scand. J. Immunol.* 1991. **34**: 697–712.

150 **Loos, H.**, **Blok-Schut, B.**, **van Doorn, R.**, **Hoksbergen, R.**, **Brutel de la Rivière, A. and Meerhof, L.**, A method for the recognition and separation of human blood monocytes on density gradients. *Blood* 1976. **48**: 731–742.

151 BD FACSAria user's guide, BD Biosciences, San Jose, USA, 2006.

152 **Wixforth, A.**, Acoustically driven programmable microfluidics for biological and chemical applications. *J. Lab. Automat.* 2006. **11**: 399–405.

153 **Kaiser, T.**, **Raba, K.**, **Sickert, M.**, **Radbruch, A. and Scheffold, A.**, Integration of an ultrasonic wave device in a FACS-Aria cell sorter for continuous, noninvasive mixing of cell suspensions. Poster, Budapest, 2008 ISAC congress. https://doi.org/10.13140/RG.2.1.1760.2966

154 Radbruch, A. (Ed.), *Flow cytometry and cell sorting*, 2nd ed., Springer, Berlin/Heidelberg 2000.

155 **Freyer, J. P.**, **Fillak, D. and Jett, J. H.**, Use of xantham gum to suspend large particles during flow cytometric analysis and sorting. *Cytometry* 1989. **10**: 803–806.

156 **Fu, L.-M.**, **Yang, R.-J.**, **Lin, C.-H.**, **Pan, Y.-J. and Gwo-Bin, L.**, Electrokinetically driven micro flow cytometers with integrated fiber optics for on-line cell/particle detection. *Anal. Chim. Acta* 2004. **507**: 163–169.

157 **Telleman, P.**, **Larsen, U. D.**, **Philip, J.**, **Blankenstein, G. and Wolff, A.**, Cell Sorting in Microfluidic Systems. In Jed Harrison, D. and van den Berg, A. (Eds.). *Micro total analysis systems '98*. Springer, Amsterdam, the Netherlands, 1998, pp. 39–44.

158 **Wang, X.**, **Chen, S.**, **Kong, M.**, **Wang, Z.**, **Costa, K. D.**, **Li, R. A. and Sun, D.**, Enhanced cell sorting and manipulation with combined optical tweezer and microfluidic chip technologies. *Lab Chip* 2011. **11**: 3656–3662.

159 **Bhagat, A. A.**, **Bow, H.**, **Hou, H. W.**, **Tan, S. J.**, **Han, J. and Lim, C. T.**, Microfluidics for cell separation. *Med. Biol. Eng. Comput.* 2010. **48**: 999–1014.

160 **Chapman, G. V.**, Instrumentation for flow cytometry. *J. Immunol. Methods* 2000. **243**: 3–12.

161 **Abate, A. R.**, **Agresti, J. J. and Weitz, D. A.**, Microfluidic sorting with highspeed single-layer membrane valves. *Appl. Phys. Lett.* 2010. **96**: 203509.

162 **Shemesh, J.**, **Bransky, A.**, **Khoury, M. and Levenberg, S.**, Advanced microfluidic droplet manipulation based on piezoelectric actuation. *Biomed. Microdevices* 2010. **12**: 907–914.

163 **Chen, C. H.**, **Cho, S. H.**, **Tsai, F.**, **Erten, A. and Lo, Y. H.**, Microfluidic cell sorter with integrated piezoelectric actuator. *Biomed. Microdevices* 2009. **11**: 1223–1231.

164 **Wang, M. M.**, **Tu, E.**, **Raymond, D. E.**, **Yang, J. M.**, **Zhang, H.**, **Hagen, N.**, **Dees, B. et al.**, Microfluidic sorting of mammalian cells by optical force switching. *Nat. Biotechnol.* 2005. **23**: 83–87.

165 **Roederer, M.**, Spectral compensation for flow cytometry: visualization artifacts, limitations, and caveats. *Cytometry* 2001. **45**: 194–205.

166 Rockefeller University BD FACSAria2-3 Water-Cooled Sort Collection Integrated Tube Holder 5-15-;5-5 | NIH 3D Print Exchange. Available at: http://3dprint.nih.gov/discover/3dpx-002415. (Accessed: 20th April 2016)

167 **Sasaki, D. T.**, **Tichenor, E. H.**, **Lopez, F.**, **Combs, J.**, **Uchida, N.**, **Smith, C. R.**, **Stokdijk, W. et al.**, Development of a clinically applicable high-speed flow cytometer for the isolation of transplantable human hematopoietic stem cells. *J. Hematother.* 1995. **4**: 503–514.

168 **June, C. H.**, **O'Connor, R. S.**, **Kawalekar, O. U.**, **Ghassemi, S.**, **Milone, M. C.**, CAR T cell immunotherapy for human cancer. *Science* 2018. **359**: 1361–1365.

169 **Hoffmann, P.**, **Eder, R.**, **Boeld, T. J.**, **Doser, K.**, **Piseshka, B.**, **Andreesen, R. et al.**, Only the CD45RA+ subpopulation of CD4+CD25high T cells gives rise to homogeneous regulatory T-cell lines upon in vitro expansion. *Blood* 2006. **108**: 4260–4267.

170 GMP EudraLex Volume 4, Part I, with guidance in Annex 1 on 'Manufacture of Sterile Medicinal Products' and Annex 2 on 'Manufacture of Biological active substances and Medicinal Products for Human Use'; https://ec.europa.eu/health/documents/eudralex/vol-4_de.

171 Good Manufacturing Practice for Advanced Therapy Medicinal Products, published in Part IV of Eudralex Volume 4; https://ec.europa.eu/health/documents/eudralex/vol-4_de

172 Reflection paper on classification of advanced therapy medicinal products. EMA/CAT/600280/2010 (ed. EMA) (EMA-CAT, http://www.ema. europa.eu/docs/en_GB/document_library/Regulatory_and_procedural_ guideline/2012/04/WC500126681.pdf, 2012).

173 Commission Directive 2009/120/EC of 14 September 2009 amending Directive 2001/83/EC of the European Parliament and of the Council on the Community code relating to medicinal products for human use as regards advanced therapy medicinal product.

174 Regulation (EC) No 1394/ 2007 of the European Parliament and of the Council of 13 November 2007 on advanced therapy medicinal products and amending Directive 2001/83/EC and Regulation (EC) No 726/2004.

175 Guideline on process validation for finished products - information and data to be provided in regulatory submissions, EMA/CHMP/CVMP/QWP/BWP/70278/2012-Rev1. 27 February 2014: European Medicines Agency (EMA).

176 **USFDA**. *Guidance for industry. Process validation: General principles and practices*, U.S. Department of Health and Human Services Food and Drug Administration Washington, DC 2011.

177 ICH Q6B: Specifications: Test Procedures and Acceptance Criteria for Biotechnological / Biological Products, ICH Harmonised Tripartite Guideline. International Conference on Harmonisation of Technical Requirements for Registration of Pharmaceuticals for Human Use.

178 ICH Q2(R1): Validation of Analytical Procedures: Text and Methodology, ICH Harmonised Tripartite Guideline. International Conference on Harmonisation of Technical Requirements for Registration of Pharmaceuticals for Human Use.

179 **Leslie, D. S.**, **Johnston, W. W.**, **Daly, L.**, **Ring, D. B.**, **Shpall, E. J.**, **Peters, W. P. and Bast, R. C., Jr.**, Detection of breast carcinoma cells in human bone marrow using fluorescence-activated cell sorting and conventional cytology. *Am. J. Clin. Pathol.* 1990. **94**: 8–13.

180 **Frantz, C. N.**, **Ryan, D. H.**, **Cheung, N. V.**, **Duerst, R. E. and Wilbur, D. C.**, Sensitive detection of rare metastatic human neuroblastoma cells in bone marrow by two-color immunofluorescence and cell sorting. *Prog. Clin. Biol. Res.* 1988. **271**: 249–262.

181 **Ryan, D. H.**, **Mitchell, S. J.**, **Hennessy, L. A.**, **Bauer, K. D.**, **Horan, P. K. and Cohen, H. J.**, Improved detection of rare CALLA-positive cells in peripheral blood using multiparameter flow cytometry. *J. Immunol. Methods* 1984. **74**: 115–128.

182 **Visser, J. W. and De Vries, P.**, Identification and purification of murine hematopoietic stem cells by flow cytometry. *Methods Cell Biol.* 1990. **33**: 451–468.

183 **Cory, J. M.**, **Ohlsson-Wilhelm, B. M.**, **Brock, E. J.**, **Sheaffer, N. A.**, **Steck, M. E.**, **Eyster, M. E. and Rapp, F.**, Detection of human immunodefi-

ciency virus-infected lymphoid cells at low frequency by flow cytometry. *J. Immunol. Methods* 1987. **105**: 71–78.

184 **Jensen, R. H. and Leary, J. F.**, Mutagenesis as measured by flow cytometry and cell sorting. In M. R. Melamed, M. L. Mendelsohn and T. Lindmo (Eds.) *Flow cytometry and sorting*, 2nd ed., Wiley-LISS, New York, NY, 1990.

185 **Cossarizza, A. and Cousins, D.**, Overcoming challenges in cellular analysis: multiparameter analysis of rare cells. *Science* 2015. **347**: 443.

186 **Gross, H. J., Verwer, B., Houck, D., Hoffman, R. A. and Recktenwald, D.**, Model study detecting breast cancer cells in peripheral blood mononuclear cells at frequencies as low as 10^{-7}. *Proc. Natl. Acad. Sci. U.S.A.* 1995. **92**: 537–541.

187 **Donnenberg, A. D. and Donnenberg, V. S.**, Rare-event analysis in flow cytometry. *Clin. Lab. Med.* 2007. **27**: 627–652.

188 **De Biasi, S., Bianchini, E., Nasi, M., Digaetano, M., Gibellini, L., Carnevale, G., Borghi, V. et al.**, Th1 and Th17 pro-inflammatory profile characterizes iNKT cells in virologically suppressed HIV⁺ patients with low CD4/CD8 ratio. *AIDS* 2016. **30**: 2599–2610.

189 **Duda, D. G., Cohen, K. S., Scadden, D. T. and Jain, R. K.**, A protocol for phenotypic detection and enumeration of circulating endothelial cells and circulating progenitor cells in human blood. *Nat. Protoc.* 2007. **2**: 805–810.

190 **Mancuso, P., Antoniotti, P., Quarna, J., Calleri, A., Rabascio, C., Tacchetti, C. and Braidotti, P.**, Validation of a standardized method for enumerating circulating endothelial cells and progenitors: flow cytometry and molecular and ultrastructural analyses. *Clin. Cancer Res.* 2009. **15**: 267–273.

191 **Van Craenenbroeck, E. M., Conraads, V. M., Van Bockstaele, D. R., Haine, S. E., Vermeulen, K., Van Tendeloo, V. F. and Vrints, C. J.**, Quantification of circulating endothelial progenitor cells: A methodological comparison of six flow cytometric approaches. *J. Immunol. Methods* 2008. **332**: 31–40.

192 **Estes, M. L., Mund, J. A., Ingram, D. A. and Case, J.**, Identification of endothelial cells and progenitor cell subsets in human peripheral blood. *Curr. Protoc. Cytom.* 2010. **52**: 9.33.1–9.33.11.

193 **De Biasi, S., Cerri, S., Bianchini, E., Gibellini, L., Persiani, E., Montanari, G. and Luppi, F.**, Levels of circulating endothelial cells are low in idiopathic pulmonary fibrosis and are further reduced by anti-fibrotic treatments. *BMC Med.* 2015. **13**: 277.

194 **Cox, C., Reeder, J. E., Robinson, R. D., Suppes, S. B. and Wheeless, L. L.**, Comparison of frequency distribution in flow cytometry. *Cytometry* 1988. **9**: 291–298.

195 **Haight, F. A.**, *Handbook of the Poisson distribution.* John Wiley & Sons, New York, NY, 1967.

196 **Roederer, M.**, How many events is enough? Are you positive? *Cytometry* 2008. **73**: 384–385.

197 **Boyd, W. A., Smith, M. V. and Freedman, J. H.**, *Caenorhabditis elegans* as a model in developmental toxicology. *Methods Cell. Biol.* 2012. **889**: 15-24.

198 **Steffen, A., Ludwig, B., Krautz, C., Bornstein, S. and Solimena, M.**, Functional assessment of automatically sorted pancreatic islets using large particle flow cytometry. *Islet.* 2011. **3**: 67–270.

199 **Li, C. Y., Wood, D. K., Huang, J. H. and Bhatia, S. N.**, Flow-based pipeline for systematic modulation and analysis of 3D tumor microenvironments. *Lab. Chip.* 2013. **13**: 1969–1978.

200 **Coder, D. M.**, Assessment of cell viability. *Curr. Protoc. Cytom.* 2001. **15**: 9.2:9.2.1–9.2.14.

201 **Perfetto, S. P., Chattopadhyay, P. K., Lamoreaux, L., Nguyen, R., Ambrozak, D., Koup, R. A. and Roederer, M.** Amine reactive dyes: an effective tool to discriminate live and dead cells in polychromatic flow cytometry. *J. Immunol. Methods* 2006. **313**: 199–208.

202 **Zuba-Surman, E. K., Kucia, M. and Ratajczak, M. Z.**, Decoding the dots: the ImageStream system (ISS) as a novel and powerful tool for flow cytometric analysis. *Cent. Eur. J. Biol.* 2008. **3**: 1–10.

203 **Vindelov, L. L., Christensen, I. J. and Nissen, N. I.**, A detergent-trypsin method for the preparation of nuclei for flow cytometric DNA analysis. *Cytometry* 1983. **3**: 323–327.

204 **Hedley, D. W., Friedlander, M. L., Taylor, I. W., Rugg, C. A. and Musgrove, E. A.**, Method for analysis of cellular DNA content of paraffin-embedded pathological material using flow cytometry. *J. Histochem. Cytochem.* 1983. **31**: 1333–1335.

205 **Degtyarev, M., Reichelt, M. and Lin, K.**, Novel quantitative autophagy analysis by organelle flow cytometry after cell sonication. *PLoS One.* 2014. **9**: e87707

206 **Poot, M., Gibson, L. L. and Singer, V. L.**, Detection of apoptosis in live cells by MitoTracker CMXRos and SYTO dye flow cytometry. *Cytometry.* 1997. **27**: 358–364.

207 **Poot, M.**, Analysis of intracellular organelles by flow cytometry or microscopy. *Curr. Protoc. Cytom.* 2001. **14**: 9.4:9.4.1–9.4.24.

208 **Bailey, S. and Macardle, P. J.**, A flow cytometric comparison of Indo-1 to fluo-3 and Fura Red excited with low power lasers for detecting Ca(2+) flux. *J. Immunol. Methods* 2006. **311**: 220–225.

209 **Leverrier, S., Bergamaschi, D., Ghali, L., Ola, A., Warnes, G., Akgul, B. et al.**, Role of HPV E6 proteins in preventing UVB-induced release of pro-apoptotic factors from the mitochondria. *Apoptosis.* 2007. **12**: 549–560.

210 **Dolezel, J., Vrana, J., Safar, J., Bartos, J., Kubalakova, M. and Simkova, H.**, Chromosomes in the flow to simplify genome analysis. *Funct. Integr. Genomics.* 2012. **12**: 97–416.

211 **Davies, D. C., Monard, S. P. and Young, B. D.** Chromosome analysis and sorting by flow cytometry. In MG Ormerod (Ed.), *Flow cytometry: A practical approach*, 3rd edition, Oxford University Press, Oxford, U.K., 2000.

212 **Ng, B. L., Fu, B., Graham, J., Hall, C. and Thompson, S.**, Chromosome analysis using benchtop cell analysers and high speed cell sorters. *Cytometry A* 2018. **95**: 323–331.

213 **Rhys, H. I., Dell'Accio, F., Pitzalis, C., Moore, A., Norling, L. V. and Perretti, M.**, Neutrophil microvesicles from healthy control and rheumatoid arthritis patients prevent the inflammatory activation of macrophages. *EBioMedicine.* 2018. **29**: 60–69.

214 **Orozco, A. and Lewis, D.**, Flow cytometric analysis of circulating microparticles in plasma. *Cytometry A.* 2010. **77A**: 502–514.

215 **Zucker, R. M., Ortenzio, J. N. R., Boyes, W. K.**, Characterization, detection, and counting of metal nanoparticles using flow cytometry. *Cytometry A.* 2016. **89A**: 69–183.

216 **Morales-Kastresana, A., Telford, W., Musich, T. A., McKinnon, K., Clayborne, C., Braig, Z., Rosner, A. et al.**, Labeling extracellular vesicles for nanoscale flow cytometry. *Sci. Rep.* 2017. **7**: 1878

217 **Kastelowitz, N. and Yin, H.**, Exosomes and microvesicles: identification and targeting by particle size and lipid chemical probes. *ChemBioChem.* 2014. **15**: 923–928.

218 **Erdbrügger, U., Rudy, C. K., Etter, M. E., Dryden, K. A., Yeager, M., Kibanov, A. L. and Lannigan, J.**, Imaging flow cytometry elucidates limitations of microparticle analysis by conventional flow cytometry. *Cytometry A.* 2014. **85A**: 756–770.

219 **Marcoux, G., Duchez, A. C., Clouthier, N., Provost, P., Nigrovic, P. A. and Boilard, E.**, Revealing the diversity of extracellular vesicles using high-dimensional flow cytometry analyses. *Sci. Rep.* 2016. **6**: 35928

220 **Wallace, D. C.**, Mitochondria and cancer. *Nat. Rev. Cancer* 2012. **12**: 685–698.

221 **Wallace, D. C.**, Mitochondrial diseases in man and mouse. *Science* 1999. **283**: 1482–1488.

222 **Brand, M. D. and Nicholls, D. G.**, Assessing mitochondrial dysfunction in cells. *Biochem. J.* 2011. **435**: 297–312.

223 **Cottet-Rousselle, C., Ronot, X., Leverve, X. and Mayol, J. F.**, Cytometric assessment of mitochondria using fluorescent probes. *Cytometry A* 2011. **79**: 405–425.

224 **Lay, A. W. L. and Burton, A. C.**, Direct measurement of potential difference across the human red blood cell membrane. *Biophys. J.* 1969. **9**: 115–121.

225 **Perry, S. W., Norman, J. P., Barbieri, J., Brown, E. B. and Gelbard, H. A.**, Mitochondrial membrane potential probes and the proton gradient: A practical usage guide. *Biotechniques* 2011. **50**: 98–115.

226 **Petit, P. X., Susin, S. A., Zamzami, N., Mignotte, B. and Kroemer, G.**, Mitochondria and programmed cell death: Back to the future. *FEBS Lett.* 1996. **396**: 7–13.

227 **Rottenberg, H. and Wu, S.**, Quantitative assay by flow cytometry of the mitochondrial membrane potential in intact cells. *Biochim. Biophys. Acta* 1998. **1404**: 393–404.

228 **Johnson, L. V., Walsh, M. L. and Chen, L. B.**, Localization of mitochondria in living cells with rhodamine 123. *Proc. Natl. Acad. Sci. U.S.A.* 1980. **77**: 990–994.

229 **Troiano, L., Granata, A. R., Cossarizza, A., Kalashnikova, G., Bianchi, R., Pini, G., Tropea, F. et al.**, Mitochondrial membrane potential and DNA stainability in human sperm cells: a flow cytometry analysis with implications for male infertility. *Exp. Cell. Res.* 1998. **241**: 384–393.

230 **Ehrenberg, B., Montana, V., Wei, M. D., Wuskell, J. P. and Loew, L. M.**, Membrane potential can be determined in individual cells from the nernstian distribution of cationic dyes. *Biophys. J.* 1988. **53**: 785–794.

231 **Nicholls, D. G. and Ward, M. W.**, Mitochondrial membrane potential and neuronal glutamate excitotoxicity: Mortality and millivolts. *Trends Neurosci.* 2000. **23**: 166–174.

232 **Cossarizza, A., Baccarani-Contri, M., Kalashnikova, G. and Franceschi, C.**, A new method for the cytofluorimetric analysis of mitochondrial membrane potential using the J-aggregate forming lipophilic cation 5,5′,6,6′-tetrachloro-1,1′,3,3′;-tetraethylbenzimidazolcarbocyanine iodide (JC-1). *Biochem. Biophys. Res. Commun.* 1993. **197**: 40–45.

233 **Smiley, S. T., Reers, M., Mottola-Hartshorn, C., Lin, M., Chen, A., Smith, T. W., Steele, G. D. et al.**, Intracellular heterogeneity in mitochondrial membrane potentials revealed by a J-aggregate-forming lipophilic cation JC-1. *Proc. Natl. Acad. Sci. U.S.A.* 1991. **88**: 3671–3675.

234 **Reers, M., Smith, T. W. and Chen, L. B.**, J-aggregate formation of a carbocyanine as a quantitative fluorescent indicator of membrane potential. *Biochemistry* 1991. **30**: 4480–4486.

235 **Moudy, A. M., Handran, S. D., Goldberg, M. P., Ruffin, N., Karl, I., Kranz-Eble, P., DeVivo, D. C. et al.**, Abnormal calcium homeostasis and mitochondrial polarization in a human encephalomyopathy. *Proc. Natl. Acad. Sci. U.S.A.* 1995. **92**: 729–733.

236 **Perelman, A., Wachtel, C., Cohen, M., Haupt, S., Shapiro, H. and Tzur, A.**, JC-1: alternative excitation wavelengths facilitate mitochondrial membrane potential cytometry. *Cell Death Dis.* 2012. **3**: e430.

237 **De Biasi, S., Gibellini, L. and Cossarizza, A.**, Uncompensated polychromatic analysis of mitochondrial membrane potential using JC-1 and multilaser excitation. *Curr. Prot. Cytom.* 2015. **72**: 7.32.1–7.32.11.

238 **Troiano, L., Ferraresi, R., Lugli, E., Nemes, E., Roat, E., Nasi, M., Pinti, M. et al.**, Multiparametric analysis of cells with different mitochondrial membrane potential during apoptosis by polychromatic flow cytometry. *Nat. Protoc.* 2007. **2**: 2719–2727.

239 **Poot, M., Zhang, Y. Z., Kramer, J. A., Wells, K. S., Jones, L. J., Hanzel, D. K., Lugade, A. G. et al.**, Analysis of mitochondrial morphology and function with novel fixable fluorescent stains. *J. Histochem. Cytochem.* 1996. **44**: 1363–1372.

240 **Septinus, M., Seiffert, W. and Zimmermann, H. W.**, Hydrophobic acridine dyes for fluorescence staining of mitochondria in living cells. 1. Thermodynamic and spectroscopic properties of 10-n-alkylacridine orange chlorides. *Histochemistry* 1983. **79**: 443–456.

241 **Dickinson, B. C., Lin, V. S. and Chang, C. J.**, Preparation and use of MitoPY1 for imaging hydrogen peroxide in mitochondria of live cells. *Nat. Protoc.* 2013. **8**: 1249–1259.

242 **Mukhopadhyay, P., Rajesh, M., Hasko, G., Hawkins, B. J., Madesh, M. and Pacher, P.**, Simultaneous detection of apoptosis and mitochondrial superoxide production in live cells by flow cytometry and confocal microscopy. *Nat. Protoc.* 2007. **2**: 2295–2301.

243 **Mukhopadhyay, P., Rajesh, M., Yoshihiro, K., Hasko, G. and Pacher, P.**, Simple quantitative detection of mitochondrial superoxide production in live cells. *Biochem. Biophys. Res. Commun.* 2007. **358**: 203–208.

244 **Robinson, K. M., Janes, M. S., Pehar, M., Monette, J. S., Ross, M. F., Hagen, T. M., Murphy, M. P. et al.**, Selective fluorescent imaging of superoxide in vivo using ethidium-based probes. *Proc. Natl. Acad. Sci. U.S.A.* 2006. **103**: 15038–15043.

245 **Cossarizza, A., Ferraresi, R., Troiano, L., Roat, E., Gibellini, L., Bertoncelli, L., Nasi, M. et al.**, Simultaneous analysis of reactive oxygen species and reduced glutathione content in living cells by polychromatic flow cytometry. *Nat. Protoc.* 2009. **4**: 1790–1797.

246 **Gibellini, L., Pinti, M., Bartolomeo, R., De Biasi, S., Cormio, A., Musicco, C., Carnevale, G. et al.**, Inhibition of Lon protease by triterpenoids alters mitochondria and is associated to cell death in human cancer cells. *Oncotarget* 2015. **6**: 25466–25483.

247 **Hawkins, B. J., Madesh, M., Kirkpatrick, C. J. and Fisher, A. B.**, Superoxide flux in endothelial cells via the chloride channel-3 mediates intracellular signaling. *Mol. Biol. Cell* 2007. **18**: 2002–2012.

248 **Iuso, A., Scacco, S., Piccoli, C., Bellomo, F., Petruzzella, V., Trentadue, R., Minuto, M. et al.**, Dysfunctions of cellular oxidative metabolism in patients with mutations in the NDUFS1 and NDUFS4 genes of complex I. *Biol. Chem.* 2006. **281**: 10374–10380.

249 **Rezvani, H. R., Dedieu, S., North, S., Belloc, F., Rossignol, R., Letellier, T., de Verneuil, H. et al.**, Hypoxia-inducible factor-1alpha, a key factor in the keratinocyte response to UVB exposure. *J. Biol. Chem.* 2007. **282**: 16413–16422.

250 **van der Pol, E., Böing, A. N., Harrison, P., Sturk, A. and Nieuwland, R.**, Classification, functions, and clinical relevance of extracellular vesicles. *Pharmacol. Rev.* 2012. **64**: 676–705.

251 **van der Pol, E., Coumans, F. A. W., Grootemaat, A. E., Gardiner, C., Sargent, I. L., Harrison, P., Sturk, A. et al.**, Particle size distribution of exosomes and microvesicles determined by transmission electron microscopy, flow cytometry, nanoparticle tracking analysis, and resistive pulse sensing. *J. Thromb. Haemost.* 2014. **12**: 1182–1192.

252 **De Rond, L., Coumans, F. A. W., Nieuwland, R., Van Leeuwen, T. G. and van der Pol, E.**, Deriving extracellular vesicle size from scatter

intensities measured by flow cytometry. *Blood Coagul. Fibrinolysis* 2018. 1–14.

253 van der Pol, E., de Rond, L., Coumans, F. A. W., Gool, E. L., Böing, A. N., Sturk, A., Nieuwland, R. et al., Absolute sizing and label-free identification of extracellular vesicles by flow cytometry. *Nanomed. Nanotechnol. Biol. Med.* 2018. **14**: 801–810.

254 White, J. G., Platelet structure. In: Michelson AD, ed. *Platelets.* 2nd ed.Academic Press, San Diego, CA 2006:45–73.

255 Arraud, N., Linares, R., Tan, S., Gounou, C., Pasquet, J. M., Mornet, S. and Brisson, A. R., Extracellular vesicles from blood plasma: determination of their morphology, size, phenotype and concentration. *J. Thromb. Haemost.* 2014. **12**: 614–627.

256 Brisson, A. R., Tan, S., Linares, R., Gounou, C. and Arraud, N., Extracellular vesicles from activated platelets: a semiquantitative cryoelectron microscopy and immuno-gold labeling study. *Platelets.* 2017. **28**: 263–271.

257 Dragovic, R. A., Gardiner, C., Brooks, A. S., Tannetta, D. S., Ferguson, D. J. P., Hole, P., Carr, B. et al., Sizing and phenotyping of cellulars vesicles using nanoparticle tracking analysis. *Nanomed. Nanotechnol. Biol. Med.* 2011. **7**: 780–788.

258 van der Pol, E., Hoekstra, A. G., Sturk, A., Otto, C., van Leeuwen, T. G. and Nieuwland, R., Optical and non-optical methods for detection and characterization of microparticles and exosomes. *J. Thromb. Haemost.* 2010. **8**: 2596–2607.

259 van der Pol, E., Sturk, A., van Leeuwen, T. G., Nieuwland, R. and Coumans, F. A. W., Standardization of extracellular vesicle measurements by flow cytometry through vesicle diameter approximation. *J. Thromb. Haemost.* 2018. **16**: 1236–1245.

260 van der Pol, E., van Gemert, M. J. C., Sturk, A., Nieuwland, R. and van Leeuwen, T. G., Single vs. swarm detection of microparticles and exosomes by flow cytometry. *J. Thromb. Haemost.* 2012. **10**: 919–930.

261 Chandler, W. L., Yeung, W. and Tait, J. F., A new microparticle size calibration standard for use in measuring smaller microparticles using a new flow cytometer. *J. Thromb. Haemost.* 2011. **9**: 1216–1224.

262 Coumans, F. A. W., Brisson, A. R., Buzas, E. I., Dignat-George, F., Drees, E. E. E., El-Andaloussi, S., Emanueli, C. et al., Methodological guidelines to study extracellular vesicles. *Circ. Res.* 2017. **120**: 1632–1648.

263 Yuana, Y., Böing, A. N., Grootemaat, A. E., van der Pol, E., Hau, C. M., Cizmar, P., Buhr, E. et al., Handling and storage of human body fluids for analysis of extracellular vesicles. *J. Extracell. Vesicles.* 2015. **4**: 29260.

264 Witwer, K. W., Buzás, E. I., Bemis, L. T., Bora, A., Lässer, C., Lötvall, J., Nolte-'t Hoen, E. N. et al., Standardization of sample collection, isolation and analysis methods in extracellular vesicle research. *J. Extracell. Vesicles* 2013. **2**: 1–25.

265 Lacroix, R., Judicone, C., Mooberry, M., Boucekine, M., Key, N. S., Dignat-George, F., Ambrozic, A. et al., Standardization of pre-analytical variables in plasma microparticle determination: results of the International Society on Thrombosis and Haemostasis SSC collaborative workshop. *J. Thromb. Haemost.* 2013. **11**: 1190–1193.

266 Wachalska, M., Koppers-Lalic, D., van Eijndhoven, M., Pegtel, M., Geldof, A. A., Lipinska, A. D., van Moorselaar, R. J. et al., Protein complexes in urine interfere with extracellular vesicle biomarker studies. *J. Circ. biomarkers.* 2016. **5**: 4.

267 Berckmans, R. J., Sturk, A., Schaap, M. C. and Nieuwland, R., Cell-derived vesicles exposing coagulant tissue factor in saliva. *Blood.* 2011. **117**: 3172–3180.

268 Lippi, G., Salvagno, G. L., Montagnana, M., Franchini, M. and Guidi, G. C., Venous stasis and routine hematologic testing. *Clin. Lab. Haematol.* 2006. **28**: 332–337.

269 Jy, W., Horstman, L. L., Jimenez, J. J. and Ahn, Y. S., Measuring circulating cell-derived microparticles. *J. Thromb. Haemost.* 2004. **2**: 1842–1843.

270 Lippi, G., Salvagno, G. L., Montagnana, M., Poli, G. and Guidi, G. C., Influence of the needle bore size on platelet count and routine coagulation testing. *Blood Coagul. Fibrinolysis* 2006. **17**: 557–561.

271 Piccin, A., Murphy, W. G. and Smith, O. P., Circulating microparticles: pathophysiology and clinical implications. *Blood Rev.* 2007. **21**: 157–171.

272 Hefler, L., Grimm, C., Leodolter, S. and Tempfer, C., To butterfly or to needle: the pilot phase. *Ann. Intern. Med.* 2004. **140**: 935–936.

273 Van Ierssel, S. H., Van Craenenbroeck, E. M., Conraads, V. M., Van Tendeloo, V. F., Vrints, C. J., Jorens, P. G. and Hoymans, V. Y., Flow cytometric detection of endothelial microparticles (EMP): effects of centrifugation and storage alter with the phenotype studied. *Thromb. Res.* 2010. **125**: 332–339.

274 Rikkert, L. G., van der Pol, E., van Leeuwen, T. G., Nieuwland, R. and Coumans, F. A. W., Centrifugation affects the purity of liquid biopsy-based tumor biomarkers. *Cytometry A* 2018. **93**: 1207–1212.

275 Stoner, S. A., Duggan, E., Condello, D., Guerrero, A., Turk, J. R., Narayanan, P. K. and Nolan, J. P., High sensitivity flow cytometry of membrane vesicles. *Cytometry A* 2016. **89**: 196–206.

276 Böing, A. N., van der Pol, E., Grootemaat, A. E., Coumans, F. A. W., Sturk, A. and Nieuwland, R., Single-step isolation of extracellular vesicles by size-exclusion chromatography. *J. Extracell. Vesicles.* 2014. **3**: 23430.

277 Yuana, Y., Bertina, R. M. and Osanto, S., Pre-analytical and analytical issues in the analysis of blood microparticles. *Thromb. Haemost.* 2011. **105**: 396–408.

278 Biro, E., Sturk-Maquelin, K. N., Vogel, G. M. T., Meuleman, D. G., Smit, M. J., Hack, C. E., Sturk, A. et al., Human cell-derived microparticles promote thrombus formation in vivo in a tissue factor-dependent manner. *J. Thromb. Haemost.* 2003. **1**: 2561–2568.

279 Simak, J. and Gelderman, M. P., Cell membrane microparticles in blood and blood products: Potentially pathogenic agents and diagnostic markers. *Transfus. Med. Rev.* 2006. **20**: 1–26.

280 Trummer, A., De Rop, C., Tiede, A., Ganser, A. and Eisert, R., Recovery and composition of microparticles after snap-freezing depends on thawing temperature. *Blood Coagul. Fibrinolysis* 2009. **20**: 52–56.

281 de Rond, L., van der Pol, E., Hau, C. M., Varga, Z., Sturk, A., van Leeuwen, T. G., Nieuwland, R. et al., Comparison of generic fluorescent markers for detection of extracellular vesicles by flow cytometry. *Clin. Chem.* 2018. **64**: 680–689.

282 Baumgarth, N. and Roederer, M., A practical approach to multicolor flow cytometry for immunophenotyping. *J. Immunol. Methods.* 2000. **243**: 77–97.

283 Chattopadhyay, P. K., Gaylord, B., Palmer, A., Jiang, N., Raven, M. A., Lewis, G., Reuter, M. A. et al., Brilliant violet fluorophores: a new class of ultrabright fluorescent compounds for immunofluorescence experiments. *Cytometry A* 2012. **81**: 456–466.

284 Pieragostino, D., Lanuti, P., Cicalini, I., Cufaro, M. C., Ciccocioppo, F., Ronci, M., Simeone, P. et al., Proteomics characterization of extracellular vesicles sorted by flow cytometry reveals a disease-specific molecular cross-talk from cerebrospinal fluid and tears in multiple sclerosis. *Proteomics.* 2019. In press https://doi.org/10.1016/j.jprot.2019.103403

285 Nolan, J. P. and Stoner, S. A., A trigger channel threshold artifact in nanoparticle analysis. *Cytometry A* 2013. **83**: 301–305.

286 Arraud, N., Gounou, C., Turpin, D. and Brisson, A. R. Fluorescence triggering: a general strategy for enumerating and phenotyping extracellular vesicles by flow cytometry. *Cytometry A* 2016. **89**: 184–195.

287 **Steen, H. B.**, Noise, sensitivity, and resolution of flow cytometers. *Cytometry* 1992. **13**: 822–830.

288 **Giesecke, C., Feher, K., von Volkmann, K., Kirsch, J., Radbruch, A. and Kaiser, T.**, Determination of background, signal-to-noise, and dynamic range of a flow cytometer: A novel practical method for instrument characterization and standardization. *Cytometry A* 2017. **91**: 1104–1114.

289 **Poncelet, P., Robert, S., Bouriche, T., Bez, J., Lacroix, R. and Dignat-George, F.**, Standardized counting of circulating platelet microparticles using currently available flow cytometers and scatter-based triggering: Forward or side scatter? *Cytometry A* 2016. **89**: 148–158.

290 **Hoen, E. N. M., van der Vlist, E. J., Aalberts, M., Mertens, H. C. H., Bosch, B. J., Bartelink, W., Mastrobattista, E. et al.**, Quantitative and qualitative flow cytometric analysis of nanosized cell-derived membrane vesicles. *Nanomed. Nanotechnol. Biol. Med.* 2012. **8**: 712–720.

291 **Lanuti, P., Rotta, G., Almici, C., Avvisati, G., Budillon, A., Doretto, P., Malara, N. et al.**, Endothelial progenitor cells, defined by the simultaneous surface expression of VEGFR 2 and CD 133, are not detectable in healthy peripheral and cord blood. *Cytometry A* 2016. **89**: 259–270.

292 **van der Vlist, E. J., Nolte-'t Hoen, E. N. M., Stoorvogel, W., Arkesteijn, G. J. A. and Wauben, M. H. M.**, Fluorescent labeling of nano-sized vesicles released by cells and subsequent quantitative and qualitative analysis by high-resolution flow cytometry. *Nat. Protoc.* 2012. **7**: 1311–26.

293 **Osteikoetxea, X., Sódar, B., Németh, A., Szabó-Taylor, K., Pálóczi, K., Vukman, K. V., Tamási, V. et al.**, Differential detergent sensitivity of extracellular vesicle subpopulations. *Org. Biomol. Chem.* 2015. **13**: 9775–9782.

294 **Schwartz, A., Gaigalas, A. K., Wang, L., Marti, G. E., Vogt, R. F. and Fernandez-Repollet, E.**, Formalization of the MESF unit of fluorescence intensity. *Cytometry B Clin. Cytom.* 2004. **57**: 1–6.

295 **Wang, L., Gaigalas, A. K., Abbasi, F., Marti, G. E., Vogt, R. F. and Schwartz, A.**, Quantitating fluorescence intensity from fluorophores: practical use of MESF values. *J. Res. Natl. Inst. Stand. Technol.* 2002. **107**: 339.

296 **Wang, L. and Gaigalas, A. K.**, Development of multicolor flow cytometry calibration standards: assignment of equivalent reference fluorophores (ERF) unit. *J. Res. Natl. Inst. Stand. Technol.* 2011. **116**: 671.

297 **Welsh, J., Kepley, J., Rosner, A., Horak, P., Berzofsky, J. and Jones, J.**, Prospective use of high-refractive index materials for single molecule detection in flow cytometry. *Sensors*. 2018. **18**: 2461.

298 **Lacroix, R., Robert, S., Poncelet, P., Kasthuri, R. S., Key, N. S. and Dignat-George, F.**, Standardization of platelet-derived microparticle enumeration by flow cytometry with calibrated beads: results of the International Society on Thrombosis and Haemostasis SSC Collaborative workshop. *J. Thromb. Haemost.* 2010. **8**: 2571–2574.

299 **Lacroix, R., Robert, S., Poncelet, P. and Dignat-George, F.**, Overcoming limitations of microparticle measurement by flow cytometry. *Semin. Thromb. Hemost.* 2010. **36**: 807–818.

300 **Zhu, S., Ma, L., Wang, S., Chen, C., Zhang, W., Yang, L., Hang, W. et al.**, Light-scattering detection below the level of single fluorescent molecules for high-resolution characterization of functional nanoparticles. *ACS Nano.* 2014. **8**: 10998–11006.

301 **Welsh, J. A., Horak, P., Wilkinson, J. S., Ford, V. J., Jones, J. C., Smith, D., Holloway, J. A., and Englyst, N. A.**, FCMPASS Software Aids Extracellular Vesicle Light Scatter Standardization. *Cytometry Part A.* 2019. https://doi.org/10.1002/cyto.a.23782

302 **Scheffold, A., Radbruch, A. and Assenmacher, M.**, Phenotyping and separation of leukocyte populations based on affinity labelling. *Methods Microbiol.* 2002. **32**: 23–58.

303 **Bradbury, A. M. and Plückthun, A.**, Antibodies: validate recombinants once. *Nature*. 2015. **520**: 295.

304 **Jain, R. and Gray, D. H.**, Isolation of thymic epithelial cells and analysis by flow cytometry. *Curr. Protoc. Immunol.* 2014. **107**: 3.26.1–3.26.15.

305 **Grützkau, A., Krüger-Krasagakes, S., Baumeister, H., Schwarz, C., Kögel, H., Welker, P., Lippert, U. et al.**, Synthesis, storage, and release of vascular endothelial growth factor/vascular permeability factor (VEGF/VPF) by human mast cells: implications for the biological significance of VEGF206. *Mol. Biol. Cell.* 1998. **9**: 875–84.

306 **Santangelo, C.**, *Worthington Biochemical Corporation tissue dissociation guide*. Worthington Biochemical Corporation, Lakewood, NJ 2008.

307 **Wong, K. H. K., Sandlin, R. D., Carey, T. R., Miller, K. L., Shank, A. T., Oklu, R., Maheswaran, S. et al.**, The role of physical stabilization in whole blood preservation. *Sci. Rep.* 2016. **6**: 21023.

308 **Plate, M. M., Louzao, R., Steele, P. M., Greengrass, V., Morris, L. M., Lewis, J., Barnett, D. et al.**, Evaluation of the blood stabilizers Trans-Fix and Cyto-Chex BCT for low-cost CD4 T-cell methodologies. *Viral Immunol.* 2009. **22**: 329–32.

309 **Hayashida, K., Bartlett, A. H., Chen, Y., Park, P. W.**, Molecular and cellular mechanisms of ectodomain shedding. *Anat. Rec.* 2010. **293**: 925–37.

310 **Berhanu, D., Mortari, F., De Rosa, S. C. and Roederer, M.**, Optimized lymphocyte isolation methods for analysis of chemokine receptor expression. *J. Immunol. Methods*. 2003. **279**: 199–207.

311 **Kivisäkk, P., Liu, Z., Trebst, C., Tucky, B., Wu, L., Stine, J., Mack, M. et al.**, Flow cytometric analysis of chemokine receptor expression on cerebrospinal fluid leukocytes. *Methods* 2003. **29**: 319–325.

312 **Liu, H., Rhodes, M., Wiest, D. L., Vignali, D. A.**, On the dynamic of TCR:CD3 complex cell surface expression and downmodulation. *Immunity* 2000. **192**: 1529–1534.

313 **Mueller, A., Kelly, E. and Strange, P. G.**, Pathways for internalization and recycling of the chemokine receptor CCR5. *Blood* 2002. **99**: 785–791.

314 **Campana, S., De Pasquale, C., Carrega, P., Ferlazzo, G. and Bonaccorsi, I.**, Cross-dressing: an alternative mechanism for antigen presentation. *Immunol. Lett.* 2015. **168**: 349–354.

315 **Anselmo, A., Mazzon, C., Borroni, E. M., Bonecchi, R., Graham, G. J. and Locati, M.**, Flow cytometry applications for the analysis of chemokine receptor expression and function. *Cytometry A* 2014. **85**: 292–301.

316 **Pockley, A. G., Foulds, G. A., Oughton, J. A., Kerkvliet, N. I. and Multhoff, G.**, Immune cell phenotyping using flow cytometry. *Curr. Protoc. Toxicol.* 2015. **66**:18.8.1—18.8.34.

317 **Darzynkiewicz, Z., Halicka, H. D. and Zhao, H.**, Analysis of cellular DNA content by flow and laser scanning cytometry. *Adv. Exp. Med. Biol.* 2010. **676**: 137–147.

318 **Hamelik, R. M. and Krishan, A.**, Click-iT assay with improved DNA distribution histograms. *Cytometry A*. 2009. **75**: 862–865.

319 **Krishan, A. and Hamelik, R. M.**, Click-iT proliferation assay with improved DNA histograms. *Curr. Protoc. Cytom.* 2010. Chapter 7:Unit7 36.

320 **Lyons, A. B. and Parish, C. R.**, Determination of lymphocyte division by flow cytometry. *J. Immunol. Methods* 1994. **171**: 131–137.

321 **Wersto, R. P., Chrest, F. J., Leary, J. F., Morris, C., Stetler-Stevenson, M. A. and Gabrielson, E.**, Doublet discrimination in DNA cell-cycle analysis. *Cytometry* 2001. **46**: 296–306.

322 **van Engeland, M., Nieland, L. J., Ramaekers, F. C., Schutte, B. and Reutelingsperger, C. P.**, Annexin V-affinity assay: a review on an apoptosis detection system based on phosphatidylserine exposure. *Cytometry* 1998. **31**: 1–9.

323 **Gehrmann, M.**, Doss, B. T., **Wagner, M.**, Zettlitz, K. A., **Kontermann, R. E.**, Foulds, G. et al., A novel expression and purification system for the production of enzymatic and biologically active human granzyme B. *J. Immunol. Methods* 2011. **371**: 8–17.

324 **Gehrmann, M.**, Stangl, S., **Kirschner, A.**, Foulds, G. A., **Sievert, W.**, Doss, B. T. et al., Immunotherapeutic targeting of membrane HSP70-expressing tumors using recombinant human granzyme B. *PLoS One* 2012. **7**: e41341

325 **Abate, M**, Festa, A, **Falco, M**, Lombardi, A, **Luce, A**, Grimaldi, A, **Zappavigna, S** et al., Mitochondria as playmakers of apoptosis, autophagy and senescence. *Semin Cell Dev Biol*. 2019. S1084-9521(18)30187-3.

326 **Shalini, S.**, Dorstyn, L., **Dawar, S. and Kumar, S.**, Old, new and emerging functions of caspases. *Cell Death Differ*. 2015. **22**: 526–539.

327 **Galluzzi, L.**, Lopez-Soto, A., **Kumar, S. and Kroemer, G.**, Caspases connect cell-death signaling to organismal homeostasis. *Immunity* 2016. **44**: 221–231.

328 **Van Opdenbosch, N and Lamkanfi, M**, Caspases in cell death, inflammation, and disease. *Immunity*. 2019. **50**: 1352–1364.

329 **Galluzzi, L.**, Vitale, I., **Aaronson, S. A.**, Abrams, J. M., **Adam, D.**, Agostinis, P., **Alnemri, E. S. et al.**, Molecular mechanisms of cell death: recommendations of the Nomenclature Committee on Cell Death 2018. *Cell Death Differ*. 2018. **25**: 486–541.

330 **Galluzzi, L.**, Kepp, O., **Chan, F. K. and Kroemer, G.**, Necroptosis: mechanisms and relevance to disease. *Annu. Rev. Pathol. Mech. Dis.* 2017. **12**: 103–130.

331 **He, S. and Wang, X.**, RIP kinases as modulators of inflammation and immunity. *Nat. Immunol.* 2018. **19**: 912–922.

332 **Frank, D. and Vince, J. E.**, Pyroptosis versus necroptosis: similarities, differences, and crosstalk. *Cell Death Differ*. 2019. **26**: 99–114.

333 **Weinlich, R.**, Oberst, A., **Beere, H. M. and Green, D. R.**, Necroptosis in development, inflammation and disease. *Nat. Rev. Mol. Cell Biol.* 2017. **18**: 127–136.

334 **Fuchslocher Chico, J.**, Saggau, C. and Adam, D., Proteolytic control of regulated necrosis. *Biochim. Biophys. Acta* 2017. **1864**: 2147–2161.

335 **Newton, K. and Manning, G.**, Necroptosis and inflammation. *Annu. Rev. Biochem.* 2016. **85**: 743–763.

336 **Lin, Y.**, Devin, A., **Rodriguez, Y. and Liu, Z. G.**, Cleavage of the death domain kinase RIP by caspase-8 prompts TNF-induced apoptosis. *Genes Dev*. 1999. **13**: 2514–2526.

337 **Feng, S.**, Yang, Y., **Mei, Y.**, Ma, L., **Zhu, D. E.**, Hoti, N., **Castanares, M. et al.**, Cleavage of RIP3 inactivates its caspase-independent apoptosis pathway by removal of kinase domain. *Cell Signal*. 2007. **19**: 2056–2067.

338 **O'Donnell, M. A.**, Perez-Jimenez, E., **Oberst, A.**, Ng, A., **Massoumi, R.**, Xavier, R., **Green, D. R. et al.**, Caspase 8 inhibits programmed necrosis by processing CYLD. *Nat. Cell Biol.* 2011. **13**: 1437–1442.

339 **Vandenabeele, P.**, Galluzzi, L., **Vanden Berghe, T. and Kroemer, G.**, Molecular mechanisms of necroptosis: an ordered cellular explosion. *Nat. Rev. Mol. Cell Biol.* 2010. **11**: 700–714.

340 **Tait, S. W.**, Oberst, A., **Quarato, G.**, Milasta, S., **Haller, M.**, Wang, R., **Karvela, M. et al.**, Widespread mitochondrial depletion via mitophagy does not compromise necroptosis. *Cell Rep*. 2013. **5**: 878–885.

341 **He, S.**, Huang, S. and Shen, Z., Biomarkers for the detection of necroptosis. *Cell Mol. Life Sci.* 2016. **73**: 2177–2181.

342 **Ting, A. T. (Ed.)**, *Programmed necrosis—Methods and protocols*. Humana Press, New York, NY, 2018.

343 **Zargarian, S.**, Shlomovitz, I., **Erlich, Z.**, Hourizadeh, A., **Ofir-Birin, Y.**, Croker, B. A., **Regev-Rudzki, N. et al.**, Phosphatidylserine externalization, "necroptotic bodies" release, and phagocytosis during necroptosis. *PLoS Biol.* 2017. **15**: e2002711.

344 **Gong, Y. N.**, Guy, C., **Olauson, H.**, Becker, J. U., **Yang, M.**, Fitzgerald, P., **Linkermann, A. et al.**, Escrt-III acts downstream of MLKL to regulate necroptotic cell death and its consequences. *Cell* 2017. **169**: 286–300.

345 **Lee, H. L.**, Pike, R., **Chong, M. H. A.**, Vossenkamper, A. and Warnes, G., Simultaneous flow cytometric immunophenotyping of necroptosis, apoptosis and RIP1-dependent apoptosis. *Methods* 2018. **134-135**: 56–66.

346 **Moriwaki, K.**, Balaji, S., **Bertin, J.**, Gough, P. J. and Chan, F. K., Distinct kinase-independent role of RIPK3 in CD11c+ mononuclear phagocytes in cytokine-induced tissue repair. *Cell Rep*. 2017. **18**: 2441–2451.

347 **Pietkiewicz, S.**, Schmidt, J. H. and Lavrik, I. N., Quantification of apoptosis and necroptosis at the single cell level by a combination of Imaging Flow Cytometry with classical Annexin V/propidium iodide staining. *J. Immunol. Methods* 2015. **423**: 99–103.

348 **Giampietri, C.**, Starace, D., **Petrungaro, S.**, Filippini, A. and Ziparo, E., Necroptosis: molecular signalling and translational implications. *Int. J. Cell Biol.* 2014. **2014**: 490275.

349 **Richter, J.**, Schlesner, M., **Hoffmann, S.**, Kreuz, M., **Leich, E.**, Burkhardt, B., **Rosolowski, M. et al.**, Recurrent mutation of the ID3 gene in Burkitt lymphoma identified by integrated genome, exome and transcriptome sequencing. *Nat. Genet.* 2012. **44**: 1316–1320.

350 **Lüschen, S.**, Ussat, S., **Scherer, G.**, Kabelitz, D. and Adam-Klages, S., Sensitization to death receptor cytotoxicity by inhibition of Fas-associated death domain protein (FADD)/caspase signaling - Requirement of cell cycle progression. *J. Biol. Chem.* 2000. **275**: 24670–24678.

351 **Falk, M.**, Ussat, S., **Reiling, N.**, Wesch, D., **Kabelitz, D. and Adam-Klages, S.**, Caspase inhibition blocks human T cell proliferation by suppressing appropriate regulation of IL-2, CD25, and cell cycle-associated proteins. *J. Immunol.* 2004. **173**: 5077–5085.

352 **Philipp, S.**, Sosna, J., **Plenge, J.**, Kalthoff, H. and Adam, D., Homoharringtonine, a clinically approved anti-leukemia drug, sensitizes tumor cells for TRAIL-induced necroptosis. *Cell Commun. Signal.* 2015. **13**: 25.

353 **Aglietti, R. A. and Dueber, E. C.**, Recent insights into the molecular mechanisms underlying pyroptosis and gasdermin family functions. *Trends Immunol.* 2017. **38**: 261–271.

354 **Man, S. M.**, Karki, R. and Kanneganti, T. D., Molecular mechanisms and functions of pyroptosis, inflammatory caspases and inflammasomes in infectious diseases. *Immunol. Rev.* 2017. **277**: 61–75.

355 **Jorgensen, I.**, Rayamajhi, M. and Miao, E. A., Programmed cell death as a defence against infection. *Nat. Rev. Immunol.* 2017. **17**: 151–164.

356 **den Hartigh, A. B. and Fink, S. L.**, Pyroptosis induction and detection. *Curr. Protoc. Immunol.* 2018. e52.

357 **Zhang, Y.**, Chen, X., **Gueydan, C. and Han, J.**, Plasma membrane changes during programmed cell deaths. *Cell Res.* 2018. **28**: 9–21.

358 **Yuan, J.**, Najafov, A. and Py, B. F., Roles of caspases in necrotic cell death. *Cell* 2016. **167**: 1693–1704.

359 **Sester, D. P.**, Zamoshnikova, A., **Thygesen, S. J.**, Vajjhala, P. R., **Cridland, S. O.**, Schroder, K. and Stacey, K. J., Assessment of inflammasome formation by flow cytometry. *Curr. Protoc. Immunol.* 2016. **114**: 14.40.11–14.40.29.

360 **Cui, J.**, Zhou, Z., **Yang, H.**, Jiao, F., **Li, N.**, Gao, Y., **Wang, L. et al.**, MST1 suppresses pancreatic cancer progression via ROS-induced pyroptosis. *Mol. Cancer Res.* 2019. **17**: 1316–1325.

361 **Paddenberg, R.**, Wulf, S., **Weber, A.**, Heimann, P., **Beck, L. A. and Mannherz, H. G.**, Internucleosomal DNA fragmentation in cultured

cells under conditions reported to induce apoptosis may be caused by mycoplasma endonucleases. *Eur. J. Cell Biol.* 1996. **71**: 105–119.

362 **Zhang, D. W., Shao, J., Lin, J., Zhang, N., Lu, B. J., Lin, S. C., Dong, M. Q. et al.**, RIP3, an energy metabolism regulator that switches TNF-induced cell death from apoptosis to necrosis. *Science* 2009. **325**: 332–336.

363 **Pozarowski, P., Huang, X., Halicka, D. H., Lee, B., Johnson, G. and Darzynkiewicz, Z.**, Interactions of fluorochrome-labeled caspase inhibitors with apoptotic cells: a caution in data interpretation. *Cytometry A* 2003. **55**: 50–60.

364 **Darzynkiewicz, Z., Zhao, H., Dorota Halicka, H., Pozarowski, P. and Lee, B.**, Fluorochrome-labeled inhibitors of caspases: expedient in vitro and in vivo markers of apoptotic cells for rapid cytometric analysis. *Methods Mol. Biol.* 2017. **1644**: 61–73.

365 **Tran, T. A. T., Grievink, H. W., Lipinska, K., Kluft, C., Burggraaf, J., Moerland, M., Tasev, D. et al.**, Whole blood assay as a model for in vitro evaluation of inflammasome activation and subsequent caspase-mediated interleukin-1 beta release. *PLoS One* 2019. **14**: e0214999.

366 **Sokolovska, A., Becker, C. E., Ip, W. K., Rathinam, V. A., Brudner, M., Paquette, N., Tanne, A. et al.**, Activation of caspase-1 by the NLRP3 inflammasome regulates the NADPH oxidase NOX2 to control phagosome function. *Nat. Immunol.* 2013. **14**: 543–553.

367 **Fuchslocher Chico, J., Falk-Paulsen, M., Luzius, A., Ruder, B., Bolik, J., Schmidt-Arras, D., Linkermann, A. et al.**, The enhanced susceptibility of ADAM-17 hypomorphic mice to DSS-induced colitis is not ameliorated by loss of RIPK3, revealing an unexpected function of ADAM-17 in necroptosis. *Oncotarget* 2018. **9**: 12941–12958.

368 **Gordon, S.**, Phagocytosis: An Immunobiologic Process. *Immunity*. 2016. **44**: 463–475.

369 **Cooper, E. L., Kauschke, E. and Cossarizza, A.**, Digging for innate immunity since Darwin and Metchnikoff. *Bioessays* 2002. **24**: 319–333.

370 **Navarre, W. W. and Zychlinsky, A.**, Pathogen-induced apoptosis of macrophages: a common end for different pathogenic strategies. *Cell Microbiol.* 2000. **2**: 265–273.

371 **Savill, J.**, Recognition and phagocytosis of cells undergoing apoptosis. *Br. Med. Bull.* 1997. **53**: 491–508.

372 **Brown, G. C., Vilalta, A. and Fricker, M.**, Phagoptosis—cell death by phagocytosis plays central roles in physiology, host defense and pathology. *Curr. Mol. Med.* 2015. **15**: 842–851.

373 **Lunov, O., Syrovets, T., Loos, C., Beil, J., Delacher, M., Tron, K., Nienhaus, G. U. et al.**, Differential uptake of functionalized polystyrene nanoparticles by human macrophages and a monocytic cell line, *ACS Nano* 2011. **5**: 1657–1669.

374 **Valet, G., Jenssen, H. L., Krefft, M. and Ruhenstroth-Baued, G.**, Flow-cytometric measurements of the transmembrane potential, the surface charge density and the phagocytic activity of guinea pig macrophages after incubation with lymphokines. *Blut* 1981. **42**: 379–382.

375 **Dunn, P. A. and Tyrer, H. W.**, Quantitation of neutrophil phagocytosis, using fluorescent latex beads. Correlation of microscopy and flow cytometry. *J. Lab. Clin. Med.* 1981. **98**: 374–381.

376 **Bjerknes, R. and Bassøe, C. F.**, Human leukocyte phagocytosis of zymosan particles measured by flow cytometry. *Acta Pathol. Microbiol. Immunol. Scand. C.* 1983. **91**: 341–348.

377 **Lehmann, A. K., Sørnes, S. and Halstensen, A.**, Phagocytosis: measurement by flow cytometry. *J. Immunol. Methods* 2000. **243**: 229–242.

378 **Bassøe, C. F.**, Assessment of phagocyte functions by flow cytometry. *Curr. Prot. Cytom.* 2002. **21**: 9.19.1–9.19.22.

379 **Simons, E. R.**, Measurement of phagocytosis and of the phagosomal environment in polymorphonuclear phagocytes by flow cytometry. *Curr. Protoc. Cytom.* 2010. 9.31.1–9.31.10.

380 **Sokolovska, A., Becker, C. E. and Stuart, L. M.**, Measurement of phagocytosis, phagosome acidification, and intracellular killing of *Staphylococcus aureus*. *Curr. Protoc. Immunol.* 2012. **99**: 14.30.1–14.30.12.

381 **Elbim, C. and Lizard, G.**, Flow cytometric investigation of neutrophil oxidative burst and apoptosis physiological and pathological situation. *Cytometry Part A*. 2009. **75A**: 475–481.

382 **Thomason, J., Archer, T., Mackin, A., Stokes, J. and Pinchuk, L.**, Applications of flow cytometry in veterinary research and small animal clinical practice. *J. Vet. Med. Res.* 2014. **1**: 1004–1012.

383 **Keogh, M. J., Spoon, T., Ridgway, S. H., Jensen, E., Van Bonn, W. and Romano, T. A.**, Simultaneous measurement of phagocytosis and respiratory burst of leukocytes in whole blood from bottlenose dolphins (*Tursiops truncatus*) utilizing flow cytometry. *Vet. Immunol. Immunopathol.* 2011. **144**: 468–475.

384 **Frankenberg, T., Kirschnek, S., Häcker, H. and Häcker, G.**, Phagocytosis-induced apoptosis of macrophages is linked to uptake, killing and degradation of bacteria. *Eur. J. Immunol.* 2008. **38**: 204–215.

385 **Tartaro, K., VanVolkenburg, M., Wilkie, D., Coskran, T. M., Kreeger, J. M., Kawabata, T. T. and Casinghino, S.**, Development of a fluorescence-based in vivo phagocytosis assay to measure mononuclear phagocyte system function in the rat. *J. Immunotoxicol.* 2015. **12**: 239–246.

386 **Webb, C., McCord, K. and Dow, S.**, Neutrophil function in septic dogs. *J. Vet. Intern. Med.* 2007. **21**: 982–989.

387 **Rossi, G, Capitani, L., Ceciliani, F., Restelli, L. and Paltrinieri, S.**, Hyposialylated α1-acid glycoprotein inhibits phagocytosis of feline neutrophils. *Res. Vet. Sci.* 2013. **95**: 465–471.

388 **Moya, S. L., Gómez, M. A., Boyle, L. A., Mee, J. F., O'Brien, B. and Arkins, S.**, Effects of milking frequency on phagocytosis and oxidative burst activity of phagocytes from primiparous and multiparous dairy cows during early lactation. *J. Dairy Sci.* 2008. **91**: 587–595.

389 **Stent, G., Reece, J. C., Baylis, D. C., Ivinson, K., Paukovics, G., Thomson, M. and Cameron, P. U.**, Heterogeneity of freshly isolated human tonsil dendritic cells demonstrated by intracellular markers, phagocytosis, and membrane dye transfer. *Cytometry*. 2002. **48**: 167–176.

390 **Becker, S., Halme, J. and Haskill, S.**, Heterogeneity of human peritoneal macrophages: Cytochemical and flow cytometric studies. *J. Reticuloendothelial Soc.* 1983. **33**: 127–138.

391 **Jersmann, H. P. A., Ross, K. A., Vivers, S., Brown, S. B., Haslett, C. and Dransfield, I.**, Phagocytosis of apoptotic cells by human macrophages: analysis by multiparameter flow cytometry. *Cytometry A*. 2003. **51A**: 7–15.

392 **Linehan, E., Dombrowski, Y., Snoddy, R., Fallon, P. G., Kissenpfennig, A. and Fitzgerald, D. C.**, Aging impairs peritoneal but not bone marrow-derived macrophage phagocytosis. *Aging Cell*. 2014. **13**: 699–708.

393 **Fuller-Espie, S. L.**, Using flow cytometry to measure phagocytic uptake in earthworms. *J. Microbiol. Biol. Educ.* 2010. **11**: 144–151.

394 http://www.lgcstandards-atcc.org/

395 **Rothwell, D. J. and Doumas, B. T.**, The effect of heparin and EDTA on the NBT test. *J. Lab. Clin. Med.* 1975. **85**: 950–956.

396 **Li, W. and Chung, S. C.**, Flow cytometric evaluation of leukocyte function in rat whole blood. *In Vitro Cell Dev. Biol. Anim.* 2003. **39**(10):413–419.

397 **Ducusin, R. J., Sarashina, T., Uzuka, Y., Tanabe, S. and Ohtani, M.**, Phagocytic response of bovine polymorphonuclear leukocytes to different incubation conditions and following exposure to some effectors

of phagocytosis and different anticoagulants in vitro. *Can. J. Vet. Res.* 2001. **65**: 38–44.

398 van der Maten, E., de Jonge, M. I., de Groot, R., van der Flier, M. and Langereis, J. D., A versatile assay to determine bacterial and host factors contributing to opsonophagocytotic killing in hirudin-anticoagulated whole blood. *Sci. Rep.* 2017. **7**: 42137.

399 Sustrova, T., Ondrackova, P., Leva, L. and Sladek, Z., Isolation techniques of neutrophils and peripheral blood mononuclear cells for the comparative experiments in humans and pigs model organisms in flow cytometry. *Mendelnet* 2014. 516–521.

400 Carneiro, C., Vaz, C., Carvalho-Pereira, J., Pais, C. and Sampaio, P., A new method for yeast phagocytosis analysis by flow cytometry. *J. Microbiol. Methods* 2014. **101**: 56–62.

401 Murciano, C., Villamón, E., O'Connor, J. E., Gozalbo, D. and Gil, M. L., Killed candida albicans yeasts and hyphae inhibit gamma interferon release by murine natural killer cells. *Infect. Immun.* 2006. **74**: 1403–1406.

402 Anding, K., Rost, J. M., Jacobs, E. and Daschner, F. D., Flow cytometric measurements of neutrophil functions: the dependence on the stimulus to cell ratio. *FEMS Immunol. Med. Microbiol.* 2003. **35**: 147–152.

403 Chan, C. L., Rénia, L. and Tan, K. S. W., A simplified, sensitive phagocytic assay for malaria cultures facilitated by flow cytometry of differentially-stained cell populations. *PLoS One.* 2012. **7**: e38523.

404 Lee, C. Y., Herant, M. and Heinrich, M., Target-specific mechanics of phagocytosis: Protrusive neutrophil response to zymosan differs from the uptake of antibody-tagged pathogens. *Cell Sci.* 2011. **124**: 1106–1114.

405 Salih, H. R., Husfeld, L. and Adam, D., Simultaneous cytofluorometric measurement of phagocytosis, burst production and killing of human phagocytes using *Candida albicans* and *Staphylococcus aureus* as target organisms. *Clin. Microbiol. Infect.* 2000. **6**: 251–258.

406 Li, F., Yang, M., Wang, L., Williamson, I., Tian, F., Qin, M., Shah, P. K. et al., Autofluorescence contributes to false-positive intracellular Foxp3 staining in macrophages: a lesson learned from flow cytometry. *J. Immunol. Meth.* 2012. **386**: 101–107.

407 Yáñez, A., Flores, A., Murciano, C., O'Connor, J. E., Gozalbo, D. and Gil, M. L., Signalling through TLR2/MyD88 induces differentiation of murine bone marrow stem and progenitor cells to functional phagocytes in response to *Candida albicans*. *Cell. Microbiol.* 2010. **12**: 114–128.

408 Bicker, H., Höflich, C., Wolk, K., Vogt, K., Volk, H. D. and Sabat, R., A simple assay to measure phagocytosis of live bacteria. *Clin. Chem.* 2008. **54**: 5 911–915.

409 Schreiner, L., Huber-Lang, M., Weiss, M. E., Hohmann, H., Schmolz, M. and Schneider, E. M., Phagocytosis and digestion of pH-sensitive fluorescent dye (Eos-FP) transfected *E. coli* in whole blood assays from patients with severe sepsis and septic shock. *J. Cell. Commun. Signal.* 2011. **5**: 135–144.

410 Bajno, L. and Grinstein, S., Fluorescent proteins: powerful tools in phagocyte biology. *J. Immunol. Methods.* 1999. **232**: 67–75.

411 Zawada, A. M., Rogacev, K. S., Schirmer, S. H., Sester, M., Böhm, M., Fliser, D. and Heine, G. H., Monocyte heterogeneity in human cardiovascular disease. *Immunobiology.* 2012. **217**: 1273–1284.

412 Neaga, A., Lefor, J., Lich, K. E., Liparoto, S. F. and Xiao, Y. Q., Development and validation of a flow cytometric method to evaluate phagocytosis of pHrodo™ BioParticles® by granulocytes in multiple species. *J. Immunol. Methods.* 2013. **390**: 9–17.

413 Schrijvers, D. M, Martinet, W., De Meyer, G. R. Y, Andries, L. Herman and Kockx, M. M., Flow cytometric evaluation of a model for phagocytosis of cells undergoing apoptosis. *J. Immunol. Methods* 2004. **287**: 101–108.

414 Basiji, D. A., Ortyn, W. E., Liang, L., Venkatachalam, V. and Morrissey, P., Cellular image analysis and imaging by flow cytometry. *Clin. Lab. Med.* 2007. **27**: 653–670.

415 Kapellos, T. S., Taylor, L., Lee, H., Cowley, S. A., James, W. S., Iqbal, A. J. and Greaves, D. R., A novel real time imaging platform to quantify macrophage phagocytosis. *Biochem. Pharmacol.* 2016. **116**: 107–119.

416 Lu, S. M., Grinstein, S. and Fairn, G. D., Quantitative live-cell fluorescence microscopy during phagocytosis. *Methods Mol. Biol.* 2017. **1519**: 79–91.

417 McFarlin, B. K., Williams, R. R., Venable, A. S., Dwyer, K. C. and, Haviland, D. L., Image-based cytometry reveals three distinct subsets of activated granulocytes based on phagocytosis and oxidative burst. *Cytometry A.* 2013. **83A**: 745–751.

418 Pul, R., Morbiducci, F., Škuljec, J., Skripuletz, T., Singh, V., Diederichs, U., Garde, N. et al., Glatiramer acetate increases phagocytic activity of human monocytes in vitro and in multiple sclerosis patients. *PLoS One.* 2012. **7**: e51867.

419 Boya, P., Reggiori, F. and Codogno, P., Emerging regulation and functions of autophagy. *Nat. Cell Biol.* 2013. **15**: 713–720.

420 Cuervo, A. M. and Wong, E., Chaperone-mediated autophagy: roles in disease and aging. *Cell Res.* 2014. **24**: 92–104.

421 Li, W. W., Li, J., Bao, J. K., Microautophagy: lesser-known self-eating. *Cell Mol. Life Sci.* 2012. **69**: 1125–1136.

422 Mizushima, N., Yoshimori, T. and Ohsumi, Y., The role of Atg proteins in autophagosome formation. *Annu. Rev. Cell Dev. Biol.* 2011. **27**: 107–132.

423 Zhang, H., Puleston, D. J. and Simon, A. K., Autophagy and immune senescence. *Trends Mol. Med.* 2016. **22**: 671–686.

424 Pasquier, B., Autophagy inhibitors. *Cell Mol. Life Sci.* 2016. **73**: 985–1001.

425 Mauthe, M., Orhon, I., Rocchi, C., Zhou, X., Luhr, M., Hijlkema, K. J., Coppes, R. P. et al., Chloroquine inhibits autophagic flux by decreasing autophagosome-lysosome fusion. *Autophagy* 2018. **14**: 1435–1455.

426 Mauvezin, C., Nagy, P., Juhasz, G. and Neufeld, T. P., Autophagosome-lysosome fusion is independent of V-ATPase-mediated acidification. *Nat. Commun.* 2015. **6**: 7007.

427 Klionsky, D. J., Abdelmohsen, K., Abe, A., Abedin, M. J., Abeliovich, H., Acevedo Arozena, A., Adachi, H. et al., Guidelines for the use and interpretation of assays for monitoring autophagy (3rd edition). *Autophagy* 2016. **12**: 1–222.

428 Eng, K. E., Panas, M. D., Karlsson Hedestam, G. B. and McInerney, G. M., A novel quantitative flow cytometry-based assay for autophagy. *Autophagy* 2010. **6**: 634–641.

429 Chikte, S., Panchal, N. and Warnes, G., Use of LysoTracker dyes: a flow cytometric study of autophagy. *Cytometry A* 2014. **85**: 169–178.

430 Phadwal, K., Alegre-Abarrategui, J., Watson, A. S., Pike, L., Anbalagan, S., Hammond, E. M., Wade-Martins, R. et al., A novel method for autophagy detection in primary cells: impaired levels of macroautophagy in immunosenescent T cells. *Autophagy* 2012. **8**: 677–689.

431 Puleston, D. J., Zhang, H., Powell, T. J., Lipina, E., Sims, S., Panse, I., Watson, A. S. et al., Autophagy is a critical regulator of memory CD8(+) T cell formation. *eLife* 2014. **3**: 03706.

432 Watson, A. S., Riffelmacher, T., Stranks, A., Williams, O., De Boer, J., Cain, K., MacFarlane, M. et al., Autophagy limits proliferation and glycolytic metabolism in acute myeloid leukemia. *Cell Death Discov.* 2015. **1**: 15008.

433 Clarke, A. J. and Simon, A. K., Autophagy in the renewal, differentiation and homeostasis of immune cells. *Nat. Rev. Immunol.* 2018. **19**: 170–183.

434 **Song, Y. M., Song, S. O., Jung, Y. K., Kang, E. S., Cha, B. S., Lee, H. C. and Lee, B. W.**, Dimethyl sulfoxide reduces hepatocellular lipid accumulation through autophagy induction. *Autophagy* 2012. **8**: 1085–1097.

435 **Caro, L. H., Plomp, P. J., Wolvetang, E. J., Kerkhof, C. and Meijer, A. J.**, 3-Methyladenine, an inhibitor of autophagy, has multiple effects on metabolism. *Eur. J. Biochem.* 1988. **175**: 325–329.

436 **Klionsky, D. J., Elazar, Z., Seglen, P. O. and Rubinsztein, D. C.**, Does bafilomycin A1 block the fusion of autophagosomes with lysosomes? *Autophagy* 2008. **4**: 849–850.

437 **Spielberg, S. P., Boxer, L. A., Oliver, J. M., Allen, J. M. and Schulman, J. D.**, Oxidative damage to neutrophils in glutathione synthetase deficiency. *Br. J. Haematol.* 1979. **42**: 215–223.

438 **Min-Wen, J. C., Jun-Hao, E. T. and Shyh-Chang, N.**, Stem cell mitochondria during aging. *Semin Cell Dev. Biol.* 2016. **52**: 110–118.

439 **Watanabe, R., Fujii, H., Shirai, T., Saito, S., Ishii, T. and Harigae, H.**, Autophagy plays a protective role as an anti-oxidant system in human T cells and represents a novel strategy for induction of T-cell apoptosis. *Eur. J. Immunol.* 2014. **44**: 2508–2520.

440 **Chen, L. M., Peng, F., Li, G. D., Jie, X. M., Cai, K. R., Cai, C., Zhong, Y. et al.**, The studies on the cytotoxicity in vitro, cellular uptake, cell cycle arrest and apoptosis-inducing properties of ruthenium methylimidazole complex [Ru(MeIm)4(p-cpip)](2.). *J. Inorg. Biochem.* 2016. **156**: 64–74.

441 **Alfadda, A. A. and Sallam, R. M.**, Reactive oxygen species in health and disease. *J. Biomed. Biotechnol.* 2012. **2012**: 936486.

442 **Ilkun, O. and Boudina, S.**, Cardiac dysfunction and oxidative stress in the metabolic syndrome: an update on antioxidant therapies. *Curr. Pharm. Des.* 2013. **19**: 4806–4817.

443 **Zhou, T., Chuang, C. C. and Zuo, L.**, Molecular characterization of reactive oxygen species in myocardial ischemia-reperfusion injury. *Biomed. Res. Int.* 2015. **2015**: 864946.

444 **Gabelloni, M. L., Sabbione, F., Jancic, C., Fuxman Bass, J., Keitelman, I., Iula, L., Oleastro, M. et al.**, NADPH oxidase derived reactive oxygen species are involved in human neutrophil IL-1beta secretion but not in inflammasome activation. *Eur. J. Immunol.* 2013. **43**: 3324–3335.

445 **Vogel, D. Y., Kooij, G., Heijnen, P. D., Breur, M., Peferoen, L. A., van der Valk, P., de Vries, H. E., Amor, S. and Dijkstra, C. D.**, GM-CSF promotes migration of human monocytes across the blood brain barrier. *Eur. J. Immunol.* 2015. **45**: 1808–1819.

446 **D'Autreaux, B. and Toledano, M. B.**, ROS as signalling molecules: mechanisms that generate specificity in ROS homeostasis. *Nat. Rev. Mol. Cell Biol.* 2007. **8**: 813–824.

447 **Ray, P. D., Huang, B. W. and Tsuji, Y.**, Reactive oxygen species (ROS) homeostasis and redox regulation in cellular signaling. *Cell Signal.* 2012. **24**: 981–990.

448 **Reth, M.**, Hydrogen peroxide as second messenger in lymphocyte activation. *Nat. Immunol.* 2002. **3**: 1129–1134.

449 **Nathan, C.**, Specificity of a third kind: reactive oxygen and nitrogen intermediates in cell signaling. *J. Clin. Invest.* 2003. **111**: 769–778.

450 **Nathan, C. and Cunningham-Bussel, A**, Beyond oxidative stress: an immunologist's guide to reactive oxygen species. *Nat. Rev. Immunol.* 2013. **13**: 349–361.

451 **Solaini, G., Baracca, A., Lenaz, G. and Sgarbi, G.**, Hypoxia and mitochondrial oxidative metabolism. *Biochim. Biophys. Acta.* 2010. **1797**: 1171–1177.

452 **Wang, L., Duan, Q., Wang, T., Ahmed, M., Zhang, N., Li, Y., Li, L. et al.**, Mitochondrial respiratory chain inhibitors involved in ROS production induced by acute high concentrations of iodide and the effects of SOD as a protective factor. *Oxid. Med. Cell Longev.* 2015. **2015**: 217670.

453 **Halliwell, B. and Gutteridge, J. M.**, Oxygen toxicity, oxygen radicals, transition metals and disease. *Biochem. J.* 1984. **219**: 1–14.

454 **Diacovich, L. and Gorvel, J. P.**, Bacterial manipulation of innate immunity to promote infection. *Nat. Rev. Microbiol.* 2010. **8**: 117–128.

455 **Nauseef, W. M.**, Biological roles for the NOX family NADPH oxidases. *J. Biol. Chem.* 2008. **283**: 16961–16965.

456 **Belaaouaj, A.**, Neutrophil elastase-mediated killing of bacteria: lessons from targeted mutagenesis. *Microbes Infect.* 2002. **4**: 1259–1264.

457 **Nathan, C. and Shiloh, M. U.**, Reactive oxygen and nitrogen intermediates in the relationship between mammalian hosts and microbial pathogens. *Proc. Natl. Acad. Sci. U.S.A.* 2000. **97**(16):8841–8848.

458 **Bogdan, C., Röllinghoff, M. and Diefenbach, A.**, Reactive oxygen and reactive nitrogen intermediates in innate and specific immunity. *Curr. Opin. Immunol.* 2000. **12**(1): 64–76.

459 **Nauseef, W. M.**, Nox enzymes in immune cells. *Semin. Immunopathol.* 2008. **30**(3): 195–208.

460 **Gonzalez-Navajas, J. M., Corr, M. P. and Raz, E.**, The immediate protective response to microbial challenge. *Eur. J. Immunol.* 2014. **44**: 2536–2549.

461 **Fang, F. C.**, Antimicrobial actions of reactive oxygen species. *MBio.* 2011. **2**: e00141–11.

462 **Rahal, A., Kumar, A., Singh, V., Yadav, B., Tiwari, R., Chakraborty, S. and Dhama, K.**, Oxidative stress, prooxidants, and antioxidants: the interplay. *Biomed. Res. Int.* 2014. **2014**: 761264.

463 **Schieber, M. and Chandel, N. S.**, ROS function in redox signaling and oxidative stress. *Curr. Biol.* 2014. **24**: R453–R462.

464 **Wu, Z., Zhao, Y. and Zhao, B.**, Superoxide anion, uncoupling proteins and Alzheimer's disease. *J. Clin. Biochem. Nutr.* 2010. **46**: 187–194.

465 **Baehner, R. L., Murrmann, S. K., Davis, J. and Johnston, R. B., Jr.**, The role of superoxide anion and hydrogen peroxide in phagocytosis-associated oxidative metabolic reactions. *J. Clin. Invest.* 1975. **56**: 571–576.

466 **Kohen, R. and Nyska, A.**, Oxidation of biological systems: oxidative stress phenomena, antioxidants, redox reactions, and methods for their quantification. *Toxicol. Pathol.* 2002. **30**: 620–650.

467 **Tafazoli, S. and O'Brien, P. J.**, Amodiaquine-induced oxidative stress in a hepatocyte inflammation model. *Toxicology* 2009. **256**: 101–109.

468 **Klebanoff, S. J., Kettle, A. J., Rosen, H., Winterbourn, C. C. and Nauseef, W. M.**, Myeloperoxidase: a front-line defender against phagocytosed microorganisms. *J. Leukoc. Biol.* 2013. **93**(2): 185–198.

469 **Okado-Matsumoto, A. and Fridovich, I.**, Assay of superoxide dismutase: cautions relevant to the use of cytochrome c, a sulfonated tetrazolium, and cyanide. *Anal. Biochem.* 2001. **298**: 337–342.

470 **Trevithick, J. R. and Dzialoszynski, T.**, A new technique for enhancing luminol luminescent detection of free radicals and reactive oxygen species. *Biochem. Mol. Biol. Int.* 1994. **33**: 1179–1190.

471 **Soh, N.**, Recent advances in fluorescent probes for the detection of reactive oxygen species. *Anal. Bioanal. Chem.* 2006. **386**: 532–543.

472 **Emmendorffer, A., Hecht, M., Lohmann-Matthes, M. L. and Roesler, J.**, A fast and easy method to determine the production of reactive oxygen intermediates by human and murine phagocytes using dihydrorhodamine 123. *J. Immunol. Methods* 1990. **131**: 269–275.

473 **Amini, P., Stojkov, D., Wang, X., Wicki, S., Kaufmann, T., Wong, W. W., Simon, H. U. et al.**, NET formation can occur independently of RIPK3 and MLKL signaling. *Eur. J. Immunol.* 2016. **46**: 178–184.

474 **Sheyn, U., Rosenwasser, S., Ben-Dor, S., Porat, Z. and Vardi, A.**, Modulation of host ROS metabolism is essential for viral infection of a

bloom-forming coccolithophore in the ocean. *ISME J.* 2016. **10**: 1742–1754.

475 **van Eeden, S. F., Klut, M. E., Walker, B. A. and Hogg, J. C.**, The use of flow cytometry to measure neutrophil function. *J. Immunol. Methods* 1999. **232**: 23–43.

476 **Fornas, O., Garcia, J. and Petriz, J.**, Flow cytometry counting of CD34+ cells in whole blood. *Nat. Med.* 2000. **6**: 833–836.

477 **Fornas, O., Domingo, J. C., Marin, P. and Petriz, J.**, Flow cytometric-based isolation of nucleated erythroid cells during maturation: an approach to cell surface antigen studies. *Cytometry* 2002. **50**: 305–312.

478 **Berridge, M. J., Lipp, P. and Bootman, M. D.**, The versatility and universality of calcium signalling. *Nat. Rev. Mol. Cell Biol.* 2000. **1**: 11–21.

479 **Feske, S., Okamura, H., Hogan, P. G. and Rao, A.**, Ca2+/calcineurin signalling in cells of the immune system. *Biochem. Biophys. Res. Commun.* 2003. **311**: 1117–1132.

480 **Gwack, Y., Feske, S., Srikanth, S., Hogan, P. G. and Rao, A.**, Signalling to transcription: store-operated Ca2+ entry and NFAT activation in lymphocytes. *Cell Calcium* 2007. **42**: 145–156.

481 **Trebak, M. and Kinet, J. P.**, Calcium signalling in T cells. *Nat. Rev. Immunol.* 2019. **19**: 154–169.

482 **Varga-Szabo, D., Braun, A. and Nieswandt, B.**, Calcium signaling in platelets. *J. Thromb. Haemost.* 2009. **7**: 1057–1066.

483 **Feske, S., Skolnik, E. Y. and Prakriya, M.**, Ion channels and transporters in lymphocyte function and immunity. *Nat. Rev. Immunol.* **12**: 532–547.

484 **Putney, J. W., Jr.**, A model for receptor-regulated calcium entry. *Cell Calcium* 1986. **7**: 1–12.

485 **Armstrong, D. L., Erxleben, C. and White, J. A.**, Patch clamp methods for studying calcium channels. *Methods Cell Biol.* 2010. **99**: 183–197.

486 **Hoth, M. and Penner, R.**, Depletion of intracellular calcium stores activates a calcium current in mast cells. *Nature* 1992. **355**: 353–356.

487 **Grynkiewicz, G., Poenie, M. and Tsien, R. Y.**, A new generation of Ca2+ indicators with greatly improved fluorescence properties. *J. Biol. Chem.* 1985. **260**: 3440–3450.

488 **Greimers, R., Trebak, M., Moutschen, M., Jacobs, N. and Boniver, J.**, Improved four-color flow cytometry method using fluo-3 and triple immunofluorescence for analysis of intracellular calcium ion ([Ca2+]i) fluxes among mouse lymph node B- and T-lymphocyte subsets. *Cytometry* 1996. **23**: 205–217.

489 **Minta, A. and Tsien, R. Y.**, Fluorescent indicators for cytosolic sodium. *J. Biol. Chem.* 1989. **264**: 19449–19457.

490 **Burchiel, S. W., Edwards, B. S., Kuckuck, F. W., Lauer, F. T., Prossnitz, E. R., Ransom, J. T. and Sklar, L. A.** Analysis of free intracellular calcium by flow cytometry: multiparameter and pharmacologic applications. *Methods* 2000. **21**: 221–230.

491 **Wendt, E. R., Ferry, H., Greaves, D. R. and Keshav, S.**, Ratiometric analysis of fura red by flow cytometry: a technique for monitoring intracellular calcium flux in primary cell subsets. *PLoS One* 2015. **10**:e0119532.

492 **Foerster, C., Voelxen, N., Rakhmanov, M., Keller, B., Gutenberger, S., Goldacker, S., Thiel, J. et al.**, B cell receptor-mediated calcium signaling is impaired in B lymphocytes of type Ia patients with common variable immunodeficiency. *J. Immunol.* **184**: 7305–7313.

493 **Dolmetsch, R. E., Lewis, R. S., Goodnow, C. C. and Healy, J. I.**, Differential activation of transcription factors induced by Ca2+ response amplitude and duration. *Nature* 1997. **386**: 855–858.

494 **Griesbeck, M., Ziegler, S., Laffont, S., Smith, N., Chauveau, L., Tomezsko, P., Sharei, A. et al.**, Sex differences in plasmacytoid den-

dritic cell levels of IRF5 drive higher IFNα production in women. *J. Immunol.* 2015. **195**: 5327–5336.

495 **Martrus, G., Niehrs, A., Cornelis, R., Rechtien, A., Garc´ıa-Beltran, W., Löutgehetmann, M., Hoffmann, C. et al.**, Kinetics of HIV-1 latency reversal quantified on the single-cell level using a novel flow-based technique. *J. Virol. Sep.* 2016. **90**: 9018–9028.

496 **Baxter, A. E., Niessl, J., Fromentin, R., Richard, J., Porichis, F., Charlebois, R., Massanella, M. et al.**, Single-cell characterization of viral translation-competent reservoirs in HIV-infected individuals. *Cell Host Microbe* 2016. **20**: 368–380.

497 **Taghizadeh, R. R., Cetrulo, K. J. and Cetrulo, C. L.**, Collagenase impacts the quantity and quality of native mesenchymal stem/stromal cells derived during processing of umbilical cord tissue. *Cell Transplant.* 2018. **27**: 181–193.

498 **Martrus, G., Kautz, T., Lunemann, S., Richert, L., Glau, L., Salzberger, W., Goebels, H. et al.**, Proliferative capacity exhibited by human liver-resident CD49a+CD25+ NK cells. *PLoS One.* 2017. **12**:e0182532.

499 **Sun, H., Sun, R., Hao, M., Wang, Y., Zhang, X., Liu, Y., Cong, X.**, Effect of duration of ex vivo ischemia time and storage period on RNA quality in biobanked human renal cell carcinoma tissue. *Ann. Surg. Oncol.* 2016. **23**: 297–304.

500 **Garcia-Beltran, W. F., Hölzemer, A., Martrus, G., Chung, A. W., Pacheco, Y., Simoneau, C. R., Rucevic, M. et al.**, Open conformers of HLA-F are high-affinity ligands of the activating NK-cell receptor KIR3DS1. *Nat. Immunol. Sep.* 2016. **17**: 1067–1074.

501 **Thaler, B., Hohensinner, P. J., Krychtiuk, K. A., Matzneller, P., Koller, L., Brekalo, M., Maurer, G. et al.**, Differential in vivo activation of monocyte subsets during low-grade inflammation through experimental endotoxemia in humans. *Sci. Rep.* 2016. **6**: 30162.

502 **Krutzik, P. O. and Nolan, G. P.**, Intracellular phospho-protein staining techniques for flow cytometry: monitoring single cell signaling events. *Cytometry* 2003. **55**: 61–70.

503 **Pozarowski, P. and Darzykiewicz, Z.**, Analysis of cell cycle by flow cytometry. In A. H. Schönthal, (Ed.) *Checkpoint controls and cancer. Methods in molecular biology*, vol **281**. Humana Press, Totowa, NJ 2004, 301–311.

504 **Schmid, I. and Sakamoto, K. M.**, Analysis of DNA content and green fluorescent protein expression. *Curr. Protoc. Cytom.* 2001. **16**: 7.16.1–7.16.10.

505 **Lanier, L. L. and Warner, N. L.**, Paraformaldehyde fixation of hematopoietic cells for quantitative flow cytometry (FACS) analysis. *J. Immunol. Methods* 1981. **47**: 25–30.

506 **Filby, A., Seddon, B., Kleczkowska, J., Salmond, R., Tomlinson, P., Smida, M., Lindquist, J. A. et al.**, Fyn regulates the duration of TCR engagement needed for commitment to effector function. *The J. Immunol.* 2007. **179**: 4635–4644.

507 **Filby, A., Perucha, E., Summers, H., Rees, P., Chana, P., Heck, S., Lord, G. M. et al.**, An imaging flow cytometric method for measuring cell division history andmolecular symmetry duringmitosis. *Cytometry Part A* 2011. **79**: 496–506.

508 **Fan, J., Nishanian, P., Breen, E. C., McDonald, M. and Fahey, J. L.**, Cytokine gene expression in normal human lymphocytes in response to stimulation. *Clin. Diagn. Lab. Immunol.* 1998. **5**: 335–340.

509 **Löhning, M., Richter, A. and Stamm, T.**, Establishment of memory for IL-10 expression in developing T helper 2 cells requires repetitive IL-4 costimulation and does not impair proliferation. *Proc. Natl. Acad. Sci. U.S.A.* 2003. **100**: 12307–12312.

510 **Sanos, S. L., Vonarbourg, C., Mortha, A. and Diefenbach, A.**, Control of epithelial cell function by interleukin-22-producing RORgammat+ innate lymphoid cells. *Immunology* 2011. **132**: 453–465.

511 **Nussbaum, J. C., Dyken, S. J. and Moltke, J.**, Type 2 innate lymphoid cells control eosinophil homeostasis. *Nature* 2013. **502**: 245–248.

512 **Robinson, D., Shibuya, K., Mui, A., Zonin, F., Murphy, E., Sana, T., Hartley, S. B. et al.**, IGIF does not drive Th1 development but synergizes with IL-12 for interferon-gamma production and activates IRAK and NFκB. *Immunity* 1997. **7**: 571–581.

513 **Sattler, A., Wagner, U., Rossol, M., Sieper, J., Wu, P., Krause, A., Schmidt, W. A. et al.**, Cytokine-induced human IFN-γ-secreting effector-memory Th cells in chronic autoimmune inflammation. *Blood* 2009. **113**: 1948–1956.

514 **Zimmermann, J., Radbruch, A. and Chang, H. D.**, A Ca(2+) concentration of 1.5 mM, as present in IMDM but not in RPMI, is critical for maximal response of Th cells to PMA/ionomycin. *Eur. J. Immunol.* 2015. **45**: 1270–1273.

515 **Lohning, M., Richter, A., Stamm, T., Hu-Li, J., Assenmacher, M., Paul, W. E. and Radbruch, A.**, Establishment of memory for IL-10 expression in developing T helper 2 cells requires repetitive IL-4 costimulation and does not impair proliferation. *Proc. Natl. Acad. Sci. U. S. A.* 2003. **100**: 12307–12312.

516 **Assenmacher, M., Schmitz, J. and Radbruch, A.**, Flow cytometric determination of cytokines in activated murine T helper lymphocytes: Expression of interleukin-10 in interferon-gamma and in interleukin-4-expressing cells. *Eur. J. Immunol.* 1994. **24**: 1097–1101.

517 **Lorenz, H., Hailey, D. W., Wunder, C. and Lippincott-Schwartz, J.**, The fluorescence protease protection (FPP) assay to determine protein localization and membrane topology. *Nat. Protoc.* 2006. **1**: 276–279.

518 **Francis, G., Kerem, Z., Makkar, H. P. and Becker, K.**, The biological action of saponins in animal systems: a review. *Br. J. Nutr.* 2002. **88**: 587–605.

519 **Moller, B. K., Andresen, B. S., Christensen, E. I. and Petersen, C. M.**, Surface membrane CD4 turnover in phorbol ester stimulated T-lymphocytes. Evidence of degradation and increased synthesis. *FEBS Lett.* 1990. **276**: 59–62.

520 **Boyer, C., Auphan, N., Luton, F., Malburet, J. M., Barad, M., Bizozzero, J. P., Reggio, H. et al.**, T cell receptor/CD3 complex internalization following activation of a cytolytic T cell clone: evidence for a protein kinase C-independent staurosporine-sensitive step. *Eur. J. Immunol.* 1991. **21**: 1623–1634.

521 **Grupillo, M., Lakomy, R., Geng, X., Styche, A., Rudert, W. A., Trucco, M. and Fan, Y.**, An improved intracellular staining protocol for efficient detection of nuclear proteins in YFP-expressing cells. *Biotechniques* 2011. **51**: 417–420.

522 **Heinen, A. P., Wanke, F., Moos, S., Attig, S., Luche, H., Pal, P. P., Budisa, N. et al.**, Improved method to retain cytosolic reporter protein fluorescence while staining for nuclear proteins: transcription factor staining with retention of fluorescent proteins. *Cytometry* 2014. **85**: 621–627.

523 **Watson, M., Chow, S., Barsyte, D., Arrowsmith, C., Shankey, T. V., Minden, M. and Hedley, D.**, The study of epigenetic mechanisms based on the analysis of histone modification patterns by flow cytometry. *Cytometry* 2013. **85**: 78–87.

524 **Guha, M. and Mackman, N.**, LPS induction of gene expression in human monocytes. *Cell. Signal.* 2001. **13**: 85–94.

525 **Gantke, T., Sriskantharajah, S. and Ley, S. C.**, Regulation and function of TPL-2, an IκB kinase-regulated MAP Kinase Kinase. *Cell Res.* 2011. **21**: 131–134.

526 **Dufner, A. and Thomas, G.**, Ribosomal S6 kinase signaling and the control of translation. *Exp. Cell Res.* 1999. **253**: 100–109.

527 **Firaguay, G. F. and Nunès, J. A.**, Analysis of signaling events by dynamic phosphoflow cytometry. *Sci. Signal* 2009. **2**: pl3.

528 **West, M. A., Koons, A., Crandall, M., Skinner, R., Worley, M. and Shapiro, M. B.**, Whole blood leukocyte mitogen activated protein kinases activation differentiates intensive care unit patients with systemic inflammatory response syndrome and sepsis. *J. Trauma* 2007. **62**: 805–811.

529 **Donnelly, R. P. and Finlay, D. K.**, Glucose, glycolysis and lymphocyte responses. *Mol. Immunol.* 2015. **68**: 513–519.

530 **Caro-Maldonado, A., Wang, R., Nichols, A. G., Kuraoka, M., Milasta, S., Sun, L. D., Gavin, A. L. et al.**, Metabolic reprogramming is required for antibody production that is suppressed in anergic but exaggerated in chronically BAFF-exposed B cells. *J. Immunol.* 2014. **192**: 3626–3636.

531 **Warburg, O.** On the Origin of Cancer Cells. *Science* 1956. **123**: 309–14.

532 **Michalek, R. D., Gerriets, V. A., Jacobs, S. R., Macintyre, A. N., MacIver, N. J., Mason, E. F., Sullivan, S. A. et al.**, CD4+, cutting edge: distinct glycolytic and lipid oxidative metabolic programs are essential for effector and regulatory cell, T subsets. *J Immunol. Author.* 2012. **186**: 3299–3303.

533 **Berod, L., Friedrich, C., Nandan, A., Freitag, J., Hagemann, S., Harmrolfs, K., Sandouk, A. et al.**, De novo fatty acid synthesis controls the fate between regulatory T and T helper 17 cells. *Nat. Med.* 2014. **20**: 1327–1333.

534 **Hale, L. P., Braun, R. O. D. D., Gwinn, W. M., Greer, P. K., Dewhirst, M. W., Laura, P., Braun, R. O. D. D. et al.**, Hypoxia in the thymus: role of oxygen tension in thymocyte survival. *Am. J. Physiol. Heart Circ. Physiol.* 2002. **282**: H1467–H1477.

535 **Parmar, K., Mauch, P., Vergilio, J.-A., Sackstein, R. and Down, J. D.**, Distribution of hematopoietic stem cells in the bone marrow according to regional hypoxia. *Proc. Natl. Acad. Sci. U.S.A.* 2007. **104**: 5431–5436.

536 **Chandel, N. S., McClintock, D. S., Feliciano, C. E., Wood, T. M., Melendez, J. A., Rodriguez, A. M. and Schumacker, P. T.**, Reactive oxygen species generated at mitochondrial Complex III stabilize hypoxia-inducible factor-1alpha during hypoxia: a mechanism of O_2 sensing. *J. Biol. Chem.* 2000. **275**: 25130–25138.

537 **Bigarella, C. L., Liang, R. and Ghaffari, S.**, Stem cells and the impact of ROS signaling. *Development.* 2014. **141**: 4206–4218.

538 **Jang, K.-J., Mano, H., Aoki, K., Hayashi, T., Muto, A., Nambu, Y., Takahashi, K. et al.**, Mitochondrial function provides instructive signals for activation-induced B-cell fates. *Nat. Commun.* 2015. **6**: 6750.

539 **Barros, L. F., Bittner, C. X., Loaiza, A., Ruminot, I., Larenas, V., Moldenhauer, H., Oyarzún, C. et al.**, Kinetic validation of 6-NBDG as a probe for the glucose transporter GLUT1 in astrocytes. *J Neurochem.* 2009. **109**: 94–100.

540 **Zou, C., Wang, Y. and Shen, Z.**, 2-NBDG as a fluorescent indicator for direct glucose uptake measurement. *J. Biochem. Biophys. Methods* 2005. **64**: 207–215.

541 **Lam, W. Y., Jash, A., Yao, C. H., D'Souza, L., Wong, R., Nunley, R. M., Meares, G. P. et al.**, Metabolic and transcriptional modules independently diversify plasma cell lifespan and function. *Cell Rep.* 2018. **24**: 2479–2492.e6.

542 **Byersdorfer, C. A., Tkachev, V., Opipari, A. W., Goodell, S., Swanson, J., Sandquist, S., Glick, G. D. et al.**, Effector T cells require fatty acid metabolism during murine graft-versus-host disease. *Blood.* 2013. **122**: 3230–3237.

543 **Kolahi, K., Louey, S., Varlamov, O. and Thornburg, K.**, Real-time tracking of BODIPY-C12 long-chain fatty acid in human term placenta

reveals unique lipid dynamics in cytotrophoblast cells. *PLoS One.* 2016. **11**: e0153522.

544 **Muroski, M. E., Miska, J., Chang, A. L., Zhang, P., Rashidi, A., Moore, H., Lopez-Rosas, A. et al.**, Fatty acid uptake in T cell subsets using a quantum dot fatty acid conjugate. *Sci. Rep.* 2017. **7**: 5790.

545 **Xiao, B., Deng, X., Zhou, W. and Tan, E.-K.**, Flow cytometry-based assessment of mitophagy using MitoTracker. *Front. Cell. Neurosci.* 2016. **10**: 76.

546 **Avramidou, A., Kroczek, C., Lang, C., Schuh, W., Jäck, H.-M. and Mielenz, D.**, The novel adaptor protein Swiprosin-1 enhances BCR signals and contributes to BCR-induced apoptosis. *Cell Death Differ.* 2007. **14**: 1936–1947.

547 **Pracht, K., Meinzinger, J., Daum, P., Schulz, S. R., Reimer, D., Hauke, M., Roth, E. et al.**, A new staining protocol for detection of murine antibody-secreting plasma cell subsets by flow cytometry. *Eur. J. Immunol.* 2017. **47**: 1389–1392.

548 **Eruslanov, E. and Kusmartsev, S.** Identification of ROS using oxidized DCFDA and flow-cytometry. *Methods Mol. Biol.* 2010. **594**: 57–72.

549 **Kalyanaraman, B., Darley-Usmar, V., Davies, K. J. A., Dennery, P. A., Forman, H. J., Grisham, M. B., Mann, G. E. et al.**, Measuring reactive oxygen and nitrogen species with fluorescent probes: challenges and limitations. *Free Radic. Biol. Med.* 2012. **52**: 1–6.

550 **Hempel, S. L., Buettner, G. R., O'Malley, Y. Q., Wessels D. A. and Flaherty D. M.**, Dihydrofluorescein diacetate is superior for detecting intracellular oxidants: comparison with 2',7'-dichlorodihydrofluorescein diacetate, 5 (and 6)-caboxy-2',7'-dichlorodihydrofluorescein diacetate, and dihydrorhodamine 123. *Free Radic. Biol. Med.* 1999. **27**: 146–159.

551 Anon. Thermo Fisher. CellROX® Oxidative Stress Reagents: User manual. Available at: https://assets.thermofisher.com/TFS-Assets/LSG/manuals/mp10422.pdf

552 Anon. Thermo Fisher. MitoSOX™ Red mitochondrial superoxide indicator *for live-cell imaging* (M36008): User manual. Available at: https://assets.thermofisher.com/TFS-Assets/LSG/manuals/mp36008.pdf

553 **Tzur, A., Moore, J. K., Jorgensen, P., Shapiro, H. M. and Kirschner, M. W.**, Optimizing optical flow cytometry for cell volume-based sorting and analysis. *PLoS One.* 2011. **6**: 1–9.

554 **Stein, M., Dütting, S., Di, M., Bösl, M., Fritsch, K., Reimer, D., Urbanczyk, S. et al.**, A defined metabolic state in pre B cells governs B-cell development and is counterbalanced by Swiprosin-2/EFhd1. *Cell Death Differ.* 2017. **24**: 1239–1252.

555 **Henzi, T. and Schwaller, B.** Antagonistic regulation of parvalbumin expression and mitochondrial calcium handling capacity in renal epithelial cells. *PLoS One.* 2015. **10**: e0142005.

556 **Santarlasci, V., Maggi, L., Capone, M., Querci, V., Beltrame, L., Cavalieri, D., D'Aiuto, E. et al.**, Rarity of human T helper 17 cells is due to retinoic acid orphan receptor-dependent mechanisms that limit their expansion. *Immunity.* 2012. **36**: 201–214.

557 **Santarlasci, V, Mazzoni, A, Capone, M, Rossi, MC, Maggi, L, Montaini, G, Rossettini, B et al.**, Musculin inhibits human T-helper 17 cell response to interleukin 2 by controlling STAT5B activity. *Eur. J. Immunol.* 2017. **47**: 1427–1442.

558 **Altman, J. D., Moss, P. A., Goulder, P. J., Barouch, D. H., McHeyzer-Williams, M. G., Bell, J. I., McMichael, A. J. et al.**, Phenotypic analysis of antigen-specific T lymphocytes. *Science* 1996. **274**: 94–96.

559 **Newell, E. W., Klein, L. O., Yu, W. and Davis, M. M.**, Simultaneous detection of many T-cell specificities using combinatorial tetramer staining. *Nat. Methods* 2009. **6**: 497–499.

560 **Hadrup, S. R., Bakker, A. H., Shu, C. J., Andersen, R. S., van Veluw, J., Hombrink, P., Castermans, E. et al.**, Parallel detection of antigen-specific T-cell responses by multidimensional encoding of MHC multimers. *Nat. Methods* 2009. **6**: 520–526.

561 **Newell, E. W., Sigal, N., Nair, N., Kidd, B. A., Greenberg, H. B. and Davis, M. M.**, Combinatorial tetramer staining and mass cytometry analysis facilitate T-cell epitope mapping and characterization. *Nat. Biotechnol.* 2013. **31**: 623–629.

562 **Bentzen, A. K., Marquard, A. M., Lyngaa, R., Saini, S. K., Ramskov, S., Donia, M., Such, L. et al.**, Large-scale detection of antigen-specific T cells using peptide-MHC-I multimers labeled with DNA barcodes. *Nat. Biotechnol.* 2016. **34**: 1037–1045.

563 **Dolton, G., Zervoudi, E., Rius, C., Wall, A., Thomas, H. L., Fuller, A., Yeo, L. et al.**, Optimized peptide–MHC multimer protocols for detection and isolation of autoimmune T-cells. *Front Immunol.* 2018. **9**: 1378.

564 **Zhang, S. Q., Ma, K. Y., Schonnesen, A. A., Zhang, M., He, C., Sun, E., Williams, C. M. et al.**, High-throughput determination of the antigen specificities of T cell receptors in single cells. *Nat. Biotechnol.* 2018. **36**: 1156.

565 **Toebes, M., Coccoris, M., Bins, A., Rodenko, B., Gomez, R., Nieuwkoop, N. J., van de Kasteele, W. et al.**, Design and use of conditional MHC class I ligands. *Nat. Med.* 2006. **12**: 246–251.

566 **Luimstra, J. J., Garstka, M. A., Roex, M. C., Redeker, A., Janssen, G. M., van Veelen, P. A. and Neefjes, J.**, A flexible MHC class I multimer loading system for large-scale detection of antigen-specific T cells. *J. Exp. Med.* 2018. **215**(5): 1493–1504.

567 **Amore, A., Wals, K., Koekoek, E., Hoppes, R., Toebes, M., Schumacher, T. N., Rodenko, B. et al.**, Development of a hypersensitive periodate-cleavable amino acid that is methionine-and disulfide-compatible and its application in MHC exchange reagents for T cell characterisation. *ChemBioChem* 2013. **14**: 123–131.

568 **Choo, J. A., Thong, S. Y., Yap, J., van Esch, W. J., Raida, M., Meijers, R., Lescar, J. et al.**, Bioorthogonal cleavage and exchange of major histo-compatibility complex ligands by employing azobenzene-containing peptides. *Angew. Chem. Int. Ed.* 2014. **53**: 13390–13394.

569 **Saini, S. K., Schuster, H., Ramnarayan, V. R., Rammensee, H.-G., Stevanović, S. and Springer, S.**, Dipeptides catalyze rapid peptide exchange on MHC class I molecules. *Proc. Natl. Acad. Sci. USA* 2015. **112**: 202–207.

570 **Kuball, J., Hauptrock, B., Malina, V., Antunes, E., Voss, R. H., Wolfl, M., Strong, R. et al.**, Increasing functional avidity of TCR-redirected T cells by removing defined N-glycosylation sites in the TCR constant domain. *J. Exp. Med.* 2009. **206**: 463–475.

571 **Kvistborg, P., Philips, D., Kelderman, S., Hageman, L., Ottensmeier, C., Joseph-Pietras, D., Welters, M. J. et al.**, Anti-CTLA-4 therapy broadens the melanoma-reactive CD8+ T cell response. *Sci. Transl. Med.* 2014. **6**: 254ra128.

572 **Kvistborg, P., Shu, C. J., Heemskerk, B., Fankhauser, M., Thrue, C. A., Toebes, M., van Rooij, N. et al.**, TIL therapy broadens the tumor-reactive CD8(+) T cell compartment in melanoma patients. *Oncoimmunology* 2012. **1**: 409–418.

573 **Rizvi, N. A., Hellmann, M. D., Snyder, A., Kvistborg, P., Makarov, V., Havel, J. J., Lee, W. et al.**, Mutational landscape determines sensitivity to PD-1 blockade in non-small cell lung cancer. *Science* 2015. **348**: 124–128.

574 **van Rooij, N., van Buuren, M. M., Philips, D., Velds, A., Toebes, M., Heemskerk, B., van Dijk, L. J. et al.**, Tumor exome analysis reveals neoantigen-specific T-cell reactivity in an ipilimumab-responsive melanoma. *J. Clin. Oncol.* 2013. **31**: e439–442.

575 **Schneck, J. P.**, Monitoring antigen-specific T cells using MHC-Ig dimers. *Immunol. Invest.* 2000. **29**: 163–169.

576 **Selin, L. K., Vergilis, K., Welsh, R. M. and Nahill, S. R.**, Reduction of otherwise remarkably stable virus-specific cytotoxic T lymphocyte memory by heterologous viral infections. *J. Exp. Med.* 1996. **183**: 2489–2499.

577 **Martinez, R. J., Andargachew, R., Martinez, H. A. and Evavold, B. D.**, Low-affinity CD4+ T cells are major responders in the primary immune response. *Nat. Commun.* 2016. **7**: 13848.

578 **Xiao, Z., Mescher, M. F. and Jameson, S. C.**, Detuning CD8 T cells: down-regulation of CD8 expression, tetramer binding, and response during CTL activation. *J. Exp. Med.* 2007. **204**: 2667–2677.

579 **Bakker, A. H.**, Schumacher TNM. MHC multimer technology: current status and future prospects. *Curr. Opin. Immunol.* 2005. **17**: 428–433.

580 **McMichael, A. J. and O'Callaghan, C. A.**, A new look at T cells. *J. Exp. Med.* 1998. **187**: 1367–1371.

581 **Ogg, G. S., King, A. S., Dunbar, P. R. and McMichael, A. J.**, Isolation of HIV-1-specific cytotoxic T lymphocytes using human leukocyte antigen-coated beads. *AIDS* 1999. **13**: 1991–1993.

582 **Luxembourg, A. T., Borrow, P., Teyton, L., Brunmark, A. B., Peterson, P. A. and Jackson, M. R.**, Biomagnetic isolation of antigen-specific CD8+ T cells usable in immunotherapy. *Nat. Biotechnol.* 1998. **16**: 281–285.

583 **Xu, X. N., Purbhoo, M. A., Chen, N., Mongkolsapaya, J., Cox, J. H., Meier, U. C., Tafuro, S. et al.**, A novel approach to antigen-specific deletion of CTL with minimal cellular activation using alpha3 domain mutants of MHC class I/peptide complex. *Immunity* 2001. **14**: 591–602.

584 **Whelan, J. A., Dunbar, P. R., Price, D. A., Purbhoo, M. A., Lechner, F., Ogg, G. S., Griffiths, G. et al.**, Specificity of CTL interactions with peptide-MHC class I tetrameric complexes is temperature dependent. *J. Immunol.* 1999. **163**: 4342–4348.

585 **Daniels, M. A. and Jameson, S. C.** Critical role for CD8 in T cell receptor binding and activation by peptide/major histocompatibility complex multimers. *J. Exp. Med.* 2000. **191**: 335–346.

586 **Knabel, M., Franz, T. J., Schiemann, M., Wulf, A., Villmow, B., Schmidt, B., Bernhard, H. et al.**, Reversible MHC multimer staining for functional isolation of T-cell populations and effective adoptive transfer. *Nat. Med.* 2002. **8**: 631–637.

587 **Neuenhahn, M., Albrecht, J., Odendahl, M., Schlott, F., Dössinger, G., Schiemann, M., Lakshmipathi, S. et al.**, Transfer of minimally manipulated CMV-specific T cells from stem cell or third-party donors to treat CMV infection after allo-HSCT. *Leukemia* 2017. **31**: 2161–2171.

588 **Nauerth, M., Weißbrich, B., Knall, R., Franz, T., Dössinger, G., Bet, J., Paszkiewicz, P. J. et al.**, TCR-ligand koff rate correlates with the protective capacity of antigen-specific CD8+ T cells for adoptive transfer. *Sci. Transl. Med.* 2013. **5**: 192ra87.

589 **Nauerth, M., Stemberger, C., Mohr, F., Weißbrich, B., Schiemann, M., Germeroth, L. and Busch, D. H.**, Flow cytometry-based TCR-ligand K off -rate assay for fast avidity screening of even very small antigen-specific T cell populations ex vivo. *Cytometry A* 2016. **89**: 816–825.

590 **Stemberger, C., Dreher, S., Tschulik, C., Piossek, C., Bet, J., Yamamoto, T. N., Schiemann, M. et al.**, Novel serial positive enrichment technology enables clinical multiparameter cell sorting. *PLoS One* 2012. **7**: e35798.

591 **Davis, D. M., Reyburn, H. T., Pazmany, L., Chiu, I., Mandelboim, O. and Strominger, J. L.**, Impaired spontaneous endocytosis of HLA-G. *Eur. J. Immunol.* 1997. **27**: 2714–2719.

592 **Effenberger, M., Stengl, A., Schober, K., Gerget, M., Kampick, M., Müller, T. R., Schumacher, D. et al.**, FLEXamers: a double tag for universal generation of versatile peptide-MHC multimers. *J. Immunol.* 2019. https://doi.org/10.4049/jimmunol.1801435

593 **Lund-Johansen, F., Bjerknes, R. and Laerum, O. D.**, Flow cytometric assay for the measurement of human bone marrow phenotype, function and cell cycle. *Cytometry* 1990. **11**: 610–616.

594 **Vollers, S. S. and Stern, L. J.**, Class II major histocompatibility complex tetramer staining: progress, problems, and prospects. *Immunology* 2008. **123**: 305–313.

595 **James, E. A., LaFond, R., Durinovic-Bello, I. and Kwok, W.**, Visualizing antigen specific CD4+ T cells using MHC class II tetramers. *J. Vis. Exp.* 2009: 1–4.

596 **Scheffold, A., Busch, D. H. and Kern, F.**, Detection of antigen-specific T-cells using major histocompatibility complex multimers or functional parameters. In Sack, U. (Eds.), *Cellular diagnostics.*KARGER, Basel 2008: 476–502.

597 **Chattopadhyay, P. K., Gierahn, T. M., Roederer, M. and Love, J. C.**, Single-cell technologies for monitoring immune systems. *Nat. Immunol.* 2014. **15**: 128–135.

598 **Chattopadhyay, P. K. and Roederer, M.**, A mine is a terrible thing to waste: high content, single cell technologies for comprehensive immune analysis. *Am. J. Transplant.* 2015. **15**: 1155–1161.

599 **Kvistborg, P., Gouttefangeas, C., Aghaeepour, N., Cazaly, A., Chattopadhyay, P. K., Chan, C., Eckl, J. et al.**, Thinking outside the gate: single-cell assessments in multiple dimensions. *Immunity* 2015. **42**: 591–592.

600 **Mahnke, Y. D. and Roederer, M.**, Optimizing a multicolor immunophenotyping assay. *Clin. Lab. Med.* 2007. **27**: 469–485.

601 **Newell, E. W. and Davis, M. M.**, Beyond model antigens: high-dimensional methods for the analysis of antigen-specific T cells. *Nat. Biotechnol.* 2014. **32**: 149–157.

602 **Bacher, P. and Scheffold, A.**, Flow-cytometric analysis of rare antigen-specific T cells. *Cytometry A* 2013. **83**: 692–701.

603 **Dimitrov, S., Gouttefangeas, C., Besedovsky, L., Jensen, A. T. R., Chandran, P. A., Rusch, E., Businger, R. et al.**, Activated integrins identify functional antigen-specific CD8(+) T cells within minutes after antigen stimulation. *Proc. Natl. Acad. Sci. USA* 2018. **115**: E5536–E5545.

604 **Kutscher, S., Dembek, C. J., Deckert, S., Russo, C., Korber, N., Bogner, J. R., Geisler, F. et al.**, Overnight resting of PBMC changes functional signatures of antigen specific T- cell responses: impact for immune monitoring within clinical trials. *PLoS One* 2013. **8**: e76215.

605 **Owen, R. E., Sinclair, E., Emu, B., Heitman, J. W., Hirschkorn, D. F., Epling, C. L., Tan, Q. X. et al.**, Loss of T cell responses following long-term cryopreservation. *J. Immunol. Methods* 2007. **326**: 93–115.

606 **Romer, P. S., Berr, S., Avota, E., Na, S. Y., Battaglia, M., ten Berge, I., Einsele, H. et al.**, Preculture of PBMCs at high cell density increases sensitivity of T-cell responses, revealing cytokine release by CD28 super-agonist TGN1412. *Blood* 2011. **118**: 6772–6782.

607 **Wegner, J., Hackenberg, S., Scholz, C. J., Chuvpilo, S., Tyrsin, D., Matskevich, A. A., Grigoleit, G. U. et al.**, High-density preculture of PBMCs restores defective sensitivity of circulating CD8 T cells to virus- and tumor-derived antigens. *Blood* 2015. **126**: 185–194.

608 **Lamoreaux, L., Roederer, M. and Koup, R.**, Intracellular cytokine optimization and standard operating procedure. *Nat. Protoc.* 2006. **1**: 1507–1516.

609 **Maecker, H. T., Rinfret, A., D'Souza, P., Darden, J., Roig, E., Landry, C., Hayes, P. et al.**, Standardization of cytokine flow cytometry assays. *BMC Immunol.* 2005. **6**: 13.

610 **Reddy, M., Eirikis, E., Davis, C., Davis, H. M. and Prabhakar, U.**, Comparative analysis of lymphocyte activation marker expression and cytokine secretion profile in stimulated human peripheral blood

mononuclear cell cultures: an in vitro model to monitor cellular immune function. *J. Immunol. Methods* 2004. **293**: 127–142.

611 **Redmond, W. L., Ruby, C. E. and Weinberg, A. D.**, The role of OX40-mediated co-stimulation in T-cell activation and survival. *Crit. Rev. Immunol.* 2009. **29**: 187–201.

612 **Zaunders, J. J., Munier, M. L., Seddiki, N., Pett, S., Ip, S., Bailey, M., Xu, Y. et al.**, High levels of human antigen-specific CD4+ T cells in peripheral blood revealed by stimulated coexpression of CD25 and CD134 (OX40). *J. Immunol.* 2009. **183**: 2827–2836.

613 **Chattopadhyay, P. K., Yu, J. and Roederer, M.**, A live-cell assay to detect antigen-specific CD4+ T cells with diverse cytokine profiles. *Nat. Med.* 2005. **11**: 1113–1117.

614 **Frentsch, M., Arbach, O., Kirchhoff, D., Moewes, B., Worm, M., Rothe, M., Scheffold, A. et al.**, Direct access to CD4+ T cells specific for defined antigens according to CD154 expression. *Nat. Med.* 2005. **11**: 1118–1124.

615 **Bacher, P., Kniemeyer, O., Schonbrunn, A., Sawitzki, B., Assenmacher, M., Rietschel, E., Steinbach, A. et al.**, Antigen-specific expansion of human regulatory T cells as a major tolerance mechanism against mucosal fungi. *Mucosal. Immunol.* 2014. **7**: 916–928.

616 **Schoenbrunn, A., Frentsch, M., Kohler, S., Keye, J., Dooms, H., Moewes, B., Dong, J. et al.**, A converse 4-1BB and CD40 ligand expression pattern delineates activated regulatory T cells (Treg) and conventional T cells enabling direct isolation of alloantigen-reactive natural Foxp3+ Treg. *J. Immunol.* 2012. **189**: 5985–5994.

617 **Bacher, P., Heinrich, F., Stervbo, U., Nienen, M., Vahldieck, M., Iwert, C., Vogt, K. et al.**, Regulatory T cell specificity directs tolerance versus allergy against aeroantigens in humans. *Cell* 2016. **167**: 1067–1078.

618 **Wolfl, M., Kuball, J., Eyrich, M., Schlegel, P. G. and Greenberg, P. D.**, Use of CD137 to study the full repertoire of CD8+ T cells without the need to know epitope specificities. *Cytometry A* 2008. **73**: 1043–1049.

619 **Wolfl, M., Kuball, J., Ho, W. Y., Nguyen, H., Manley, T. J., Bleakley, M. and Greenberg, P. D.**, Activation-induced expression of CD137 permits detection, isolation, and expansion of the full repertoire of CD8+ T cells responding to antigen without requiring knowledge of epitope specificities. *Blood* 2007. **110**: 201–210.

620 **Brosterhus, H., Brings, S., Leyendeckers, H., Manz, R. A., Miltenyi, S., Radbruch, A., Assenmacher, M. et al.**, Enrichment and detection of live antigen-specific CD4(+) and CD8(+) T cells based on cytokine secretion. *Eur. J. Immunol.* 1999. **29**: 4053–4059.

621 **Manz, R., Assenmacher, M., Pfluger, E., Miltenyi, S. and Radbruch, A.**, Analysis and sorting of live cells according to secreted molecules, relocated to a cell-surface affinity matrix. *Proc. Natl. Acad. Sci. USA* 1995. **92**: 1921–1925.

622 **Jung, T., Schauer, U., Heusser, C., Neumann, C. and Rieger, C.**, Detection of intracellular cytokines by flow cytometry. *J. Immunol. Methods* 1993. **159**: 197–207.

623 **O'Neil-Andersen, N. J. and Lawrence, D. A.**, Differential modulation of surface and intracellular protein expression by T cells after stimulation in the presence of monensin or brefeldin A. *Clin. Diagn. Lab. Immunol.* 2002. **9**: 243–250.

624 **Bacher, P., Schink, C., Teutschbein, J., Kniemeyer, O., Assenmacher, M., Brakhage, A. A. and Scheffold, A.**, Antigen-reactive T cell enrichment for direct, high-resolution analysis of the human naive and memory Th cell repertoire. *J. Immunol.* 2013. **190**: 3967–3976.

625 **Bacher, P., Hohnstein, T., Beerbaum, E., Rocker, M., Blango, M. G., Kaufmann, S., Rohmel, J. et al.**, Human Anti-fungal Th17 Immunity and Pathology Rely on Cross-Reactivity against Candida albicans. *Cell* 2019. **176**: 1340–1355.e1315.

626 **Wehler, T. C., Karg, M., Distler, E., Konur, A., Nonn, M., Meyer, R. G., Huber, C. et al.**, Rapid identification and sorting of viable virus-reactive CD4(+) and CD8(+) T cells based on antigen-triggered CD137 expression. *J. Immunol. Methods* 2008. **339**: 23–37.

627 **Betts, M. R., Brenchley, J. M., Price, D. A., De Rosa, S. C., Douek, D. C., Roederer, M. and Koup, R. A.**, Sensitive and viable identification of antigen-specific CD8+ T cells by a flow cytometric assay for degranulation. *J. Immunol. Methods* 2003. **281**: 65–78.

628 **Betts, M. R. and Koup, R. A.**, Detection of T-cell degranulation: CD107a and b. *Methods Cell Biol.* 2004. **75**: 497–512.

629 **Dimitrov, S., Benedict, C., Heutling, D., Westermann, J., Born, J. and Lange, T.**, Cortisol and epinephrine control opposing circadian rhythms in T cell subsets. *Blood* 2009. **113**: 5134–5143.

630 **Dimitrov, S., Lange, T. and Born, J.**, Selective mobilization of cytotoxic leukocytes by epinephrine. *J. Immunol.* 2010. **184**: 503–511.

631 **Day, C. L., Seth, N. P., Lucas, M., Appel, H., Gauthier, L., Lauer, G. M., Robbins, G. K. et al.**, Ex vivo analysis of human memory CD4 T cells specific for hepatitis C virus using MHC class II tetramers. *J. Clin. Invest.* 2003. **112**: 831–842.

632 **Miltenyi, S., Muller, W., Weichel, W. and Radbruch, A.**, High gradient magnetic cell separation with MACS. *Cytometry* 1990. **11**: 231–238.

633 **Moon, J. J., Chu, H. H., Pepper, M., McSorley, S. J., Jameson, S. C., Kedl, R. M. and Jenkins, M. K.**, Naive CD4(+) T cell frequency varies for different epitopes and predicts repertoire diversity and response magnitude. *Immunity* 2007. **27**: 203–213.

634 **Obar, J. J., Khanna, K. M. and Lefrancois, L.**, Endogenous naive CD8+ T cell precursor frequency regulates primary and memory responses to infection. *Immunity* 2008. **28**: 859–869.

635 **Macey, M. G.**, *Flow cytometry: Principles and applications.* Humana Press, New York, NY, 2007.

636 **Krensky, A. M.**, The HLA system, antigen processing and presentation. *Kidney Int. Suppl.* 1997. **58**: S2–7.

637 **Kern, F., Faulhaber, N., Frommel, C., Khatamzas, E., Prosch, S., Schonemann, C., Kretzschmar, I. et al.**, Analysis of CD8 T cell reactivity to cytomegalovirus using protein-spanning pools of overlapping pentadecapeptides. *Eur. J. Immunol.* 2000. **30**: 1676–1682.

638 **Maecker, H. T., Dunn, H. S., Suni, M. A., Khatamzas, E., Pitcher, C. J., Bunde, T., Persaud, N. et al.**, Use of overlapping peptide mixtures as antigens for cytokine flow cytometry. *J. Immunol. Methods* 2001. **255**: 27–40.

639 **Eberl, G., Renggli, J., Men, Y., Roggero, M. A., Lopez, J. A. and Corradin, G.**, Extracellular processing and presentation of a 69-mer synthetic polypetide to MHC class I-restricted T cells. *Mol. Immunol.* 1999. **36**: 103–112.

640 **Sherman, L. A., Burke, T. A. and Biggs, J. A.**, Extracellular processing of peptide antigens that bind class I major histocompatibility molecules. *J. Exp. Med.* 1992. **175**: 1221–1226.

641 **Alanio, C., Lemaitre, F., Law, H. K., Hasan, M. and Albert, M. L.**, Enumeration of human antigen-specific naive CD8+ T cells reveals conserved precursor frequencies. *Blood* 2010. **115**: 3718–3725.

642 **Campion, S. L., Brodie, T. M., Fischer, W., Korber, B. T., Rossetti, A., Goonetilleke, N., McMichael, A. J. et al.**, Proteome-wide analysis of HIV-specific naive and memory CD4(+) T cells in unexposed blood donors. *J. Exp. Med.* 2014. **211**: 1273–1280.

643 **Geiger, R., Duhen, T., Lanzavecchia, A. and Sallusto, F.**, Human naive and memory CD4+ T cell repertoires specific for naturally processed antigens analyzed using libraries of amplified T cells. *J. Exp. Med.* 2009. **206**: 1525–1534.

644 **Su, L. F., Kidd, B. A., Han, A., Kotzin, J. J. and Davis, M. M.**, Virus-specific CD4(+) memory-phenotype T cells are abundant in unexposed adults. *Immunity* 2013. **38**: 373–383.

645 **Annunziato, F., Romagnani, C. and Romagnani, S.**, The 3 major types of innate and adaptive cell-mediated effector immunity. *J. Allergy Clin. Immunol.* 2015. **135**: 626-635.

646 **Brugnolo, F., Sampognaro, S., Liotta, F., Cosmi, L., Annunziato, F., Manuelli, C., Campi, P. et al.**, The novel synthetic immune response modifier R-848 (Resiquimod) shifts human allergen-specific CD4+ TH2 lymphocytes into IFN-gamma-producing cells. *J. Allergy Clin. Immunol.* 2003. **111**: 380–388.

647 **Annunziato, F., Cosmi, L., Santarlasci, V., Maggi, L., Liotta, F., Mazzinghi, B., Parente, E. et al.**, Phenotypic and functional features of human Th17 cells. *J. Exp. Med.* 2007. **204**: 1849–1861.

648 **Cosmi, L., Maggi, L., Santarlasci, V., Capone, M., Cardilicchia, E., Frosali, F., Querci, V. et al.**, Identification of a novel subset of human circulating memory CD4(+) T cells that produce both IL-17A and IL-4. *J. Allergy Clin. Immunol.* 2010. **125**(1): 222-230.e1-4.

649 **Becattini, S., Latorre, D., Mele, F., Foglierini, M., De Gregorio, C., Cassotta, A., Fernandez, B. et al.**, T cell immunity. Functional heterogeneity of human memory CD4+ T cell clones primed by pathogens or vaccines. *Science* 2015. **347**: 400–406.

650 **Mazzoni, A., Maggi, L., Siracusa, F., Ramazzotti, M., Rossi, M. C., Santarlasci, V., Montaini, G. et al.**, Eomes controls the development of Th17-derived (non-classic) Th1 cells during chronic inflammation. *Eur. J. Immunol.* 2019. **49**: 79–95.

651 **Mazzoni, A., Santarlasci, V., Maggi, L., Capone, M., Rossi, M. C., Querci, V., De Palma, R. et al.**, Demethylation of the RORC2 and IL17A in human CD4+ T lymphocytes defines Th17 origin of nonclassic Th1 cells. *J. Immunol.* 2015. **194**: 3116–3126.

652 **Mueller, S. N., Gebhardt, T., Carbone, F. R. and Heath, W. R.**, Memory T cell subsets, migration patterns, and tissue residence. *Annu. Rev. Immunol.* 2013. **31**: 137–161.

653 **Masopust, D. and Schenkel, J. M.**, The integration of T cell migration, differentiation and function. *Nat. Rev. Immunol.* 2013. **13**: 309–320.

654 **Murali-Krishna, K., Altman, J. D., Suresh, M., Sourdive, D. J., Zajac, A. J., Miller, J. D., Slansky, J. et al.**, *Immunity* 1998. **8**: 177–187.

655 **Masopust, D., Vezys, V., Marzo, A. L. and Lefrancois, L.**, Preferential localization of effector memory cells in nonlymphoid tissue. *Science* 2001. **291**: 2413–2417.

656 **Barber, D. L., Wherry, E. J. and Ahmed, R.**, *J. Immunol.* 2003. **171**: 27–31.

657 **Brunner, K. T., Mauel, J., Cerottini, J. C. and Chapuis, B.**, *Immunology* 1968. **14**: 181–196.

658 **Nagata, S. and Golstein, P.**, The Fas death factor. *Science* 1995. **267**: 1449–1456.

659 **Lopez, J. A., Susanto, O., Jenkins, M. R., Lukoyanova, N., Sutton, V. R., Law, R. H., Johnston, A. et al.**, *Blood* 2013. **121**: 2659–2668.

660 **Liu, L., Chahroudi, A., Silvestri, G., Wernett, M. E., Kaiser, W. J., Safrit, J. T., Komoriya, A. et al.**, Visualization and quantification of T cell-mediated cytotoxicity using cell-permeable fluorogenic caspase substrates. *Nat. Med.* 2002. **8**: 185–189.

661 **Bedner, E., Smolewski, P., Amstad, P. and Darzynkiewicz, Z.**, *Exp. Cell Res.* 2000. **259**: 308–313.

662 **Amstad, P. A., Yu, G., Johnson, G. L., Lee, B. W., Dhawan, S. and Phelps, D. J.**, *BioTechniques* 2001. **31**: 608–10, 612, 614, passim

663 **Sheehy, M. E., McDermott, A. B., Furlan, S. N., Klenerman, P. and Nixon, D. F.**, *J. Immunol. Methods* 2001. **249**: 99–110.

664 **Michonneau, D., Sagoo, P., Breart, B., Garcia, Z., Celli, S. and Bousso, P.**, *Immunity* 2016. **44**: 143–154.

665 **Aichele, P., Brduscha-Riem, K., Oehen, S., Odermatt, B., Zinkernagel, R. M., Hengartner, H. and Pircher, H.**, *Immunity* 1997. **6**: 519–529.

666 **Coles, R. M., Mueller, S. N., Heath, W. R., Carbone, F. R. and Brooks, A. G.**, Progression of armed CTL from draining lymph node to spleen shortly after localized infection with herpes simplex virus 1. *J. Immunol.* 2002. **168**: 834–838.

667 **Wabnitz, G. H., Balta, E., Schindler, S., Kirchgessner, H., Jahraus, B., Meuer, S. and Samstag, Y.**, The pro-oxidative drug WF-10 inhibits serial killing by primary human cytotoxic T-cells. *Cell Death Discov.* 2016. **2**: 16057.

668 **Wabnitz, G. H., Kirchgessner, H. and Samstag, Y.** Multiparametric analysis of molecular mechanism involved in the cytotoxicity of human CD8 T-cells. *J. Cell. Biochem.* 2017. **118**: 2528–2533.

669 **Mahnke, Y. D., Devevre, E., Baumgaertner, P., Matter, M., Rufer, N., Romero, P. and Speiser, D. E.**, Human melanoma-specific CD8(+) T-cells from metastases are capable of antigen-specific degranulation and cytolysis directly ex vivo. *Oncoimmunology* 2012. **1**: 467–530.

670 **Kurioka, A., Ussher, J. E., Cosgrove, C., Clough, C., Fergusson, J. R., Smith, K., Kang, Y. H. et al.**, MAIT cells are licensed through granzyme exchange to kill bacterially sensitized targets. *Mucosal. Immunol.* 2015. **8**: 429–440.

671 **Wing, K., Onishi, Y., Prieto-Martin, P., Yamaguchi, T., Miyara, M., Fehervari, Z., Nomura, T. et al.**, CTLA-4 control over Foxp3(+) regulatory T cell function. *Science* 2008. **322**: 271–275.

672 **McMurchy, A. N. and Levings, M. K.**, Suppression assays with human T regulatory cells: a technical guide. *Eur. J. Immunol.* 2012. **42**: 27–34.

673 **Cammarata, I., Martire, C., Citro, A., Raimondo, D., Fruci, D., Melaiu, O., D'Oria, V. et al.**, Counter-regulation of regulatory T cells by autoreactive CD8(+) T cells in rheumatoid arthritis. *J. Autoimmun.* 2019. **99**: 81–97.

674 **Walker, L. S.**, Regulatory T cells overturned: the effectors fight back. *Immunology* 2009. **126**: 466–474.

675 **Miyara, M., Yoshioka, Y., Kitoh, A., Shima, T., Wing, K., Niwa, A., Parizot, C. et al.**, Functional delineation and differentiation dynamics of human CD4+ T cells expressing the FoxP3 transcription factor. *Immunity* 2009. **30**: 899–911.

676 **Wing, J. B., Kitagawa, Y., Locci, M., Hume, H., Tay, C., Morita, T., Kidani, Y. et al.**, A distinct subpopulation of CD25(−) T-follicular regulatory cells localizes in the germinal centers. *Proc. Natl. Acad. Sci. USA* 2017. **114**: E6400–E6409.

677 **Roederer, M.**, Interpretation of cellular proliferation data: avoid the panglossian. *Cytometry A* 2011. **79**: 95–101.

678 **Grossman, W. J., Verbsky, J. W., Barchet, W., Colonna, M., Atkinson, J. P. and Ley, T. J.**, Human T regulatory cells can use the perforin pathway to cause autologous target cell death. *Immunity* 2004. **21**: 589–601.

679 **Koristka, S., Cartellieri, M., Arndt, C., Feldmann, A., Topfer, K., Michalk, I., Temme, A. et al.**, Cytotoxic response of human regulatory T cells upon T-cell receptor-mediated activation: a matter of purity. *Blood Cancer J.* 2014. **4**: e199.

680 **Pircher, H., Burki, K., Lang, R., Hengartner, H. and Zinkernagel, R. M.**, Tolerance induction in double specific T-cell receptor transgenic mice varies with antigen. *Nature* 1989. **342**: 559–561.

681 **Hogquist, K. A., Jameson, S. C., Heath, W. R., Howard, J. L., Bevan, M. J. and Carbone, F. R.**, T cell receptor antagonist peptides induce positive selection. *Cell* 1994. **76**: 17–27.

682 **Oxenius, A., Bachmann, M. F., Zinkernagel, R. M. and Hengartner, H.,** Virus-specific MHC-class II-restricted TCR-transgenic mice: effects on humoral and cellular immune responses after viral infection. *Eur. J. Immunol.* 1998. **28**: 390–400.

683 **Barnden, M. J., Allison, J., Heath, W. R. and Carbone, F. R.,** Defective TCR expression in transgenic mice constructed using cDNA-based alpha- and beta-chain genes under the control of heterologous regulatory elements. *Immunol. Cell. Biol.* 1998. **76**: 34–40.

684 **Murphy, K. M., Heimberger, A. B. and Loh, D. Y.,** Induction by antigen of intrathymic apoptosis of CD4+CD8+TCRlo thymocytes in vivo. *Science* 1990. **250**: 1720–1723.

685 **Kagi, D., Odermatt, B., Ohashi, P. S., Zinkernagel, R. M. and Hengartner, H.,** Development of insulitis without diabetes in transgenic mice lacking perforin-dependent cytotoxicity. *J. Exp. Med.* 1996. **183**: 2143–2152.

686 **Bettelli, E., Pagany, M., Weiner, H. L., Linington, C., Sobel, R. A. and Kuchroo, V. K.,** Myelin oligodendrocyte glycoprotein-specific T cell receptor transgenic mice develop spontaneous autoimmune optic neuritis. *J. Exp. Med.* 2003. **197**: 1073–1081.

687 **Mason, D. Y., Jones, M. and Goodnow, C. C.,** Development and follicular localization of tolerant B lymphocytes in lysozyme/anti-lysozyme IgM/IgD transgenic mice. *Int. Immunol.* 1992. **4**: 163–175.

688 **Phan, T. G., Amesbury, M., Gardam, S., Crosbie, J., Hasbold, J., Hodgkin, P. D., Basten, A. et al.,** B cell receptor-independent stimuli trigger immunoglobulin (Ig) class switch recombination and production of IgG autoantibodies by anergic self-reactive B cells. *J. Exp. Med.* 2003. **197**: 845–860.

689 **Allen, C. D., Okada, T., Tang, H. L. and Cyster, J. G.,** Imaging of germinal center selection events during affinity maturation. *Science* 2007. **315**: 528–531.

690 **Shih, T. A., Roederer, M. and Nussenzweig, M. C.,** Role of antigen receptor affinity in T cell-independent antibody responses in vivo. *Nat. Immunol.* 2002. **3**: 399–406.

691 **Garside, P., Ingulli, E., Merica, R. R., Johnson, J. G., Noelle, R. J. and Jenkins, M. K.,** Visualization of specific B and T lymphocyte interactions in the lymph node. *Science* 1998. **281**: 96–99.

692 **Litzenburger, T., Fassler, R., Bauer, J., Lassmann, H., Linington, C., Wekerle, H. and Iglesias, A.,** B lymphocytes producing demyelinating autoantibodies: development and function in gene-targeted transgenic mice. *J. Exp. Med.* 1998. **188**: 169–180.

693 **Bettelli, E., Baeten, D., Jager, A., Sobel, R. A. and Kuchroo, V. K.,** Myelin oligodendrocyte glycoprotein-specific T and B cells cooperate to induce a Devic-like disease in mice. *J. Clin. Invest.* 2006. **116**: 2393–2402.

694 **Jenkins, M. K. and Moon, J. J.,** The role of naive T cell precursor frequency and recruitment in dictating immune response magnitude. *J. Immunol.* 2012. **188**: 4135–4140.

695 **Buchholz, V. R., Schumacher, T. N. and Busch, D. H.,** T cell fate at the single-cell level. *Annu. Rev. Immunol.* 2016. **34**: 65–92.

696 **Stemberger, C., Huster, K. M., Koffler, M., Anderl, F., Schiemann, M., Wagner, H. and Busch, D. H.,** A single naive CD8+ T cell precursor can develop into diverse effector and memory subsets. *Immunity* 2007. **27**: 985–997.

697 **Baumjohann, D. and Ansel, K. M.,** Tracking early T follicular helper cell differentiation in vivo. *Methods Mol. Biol.* 2015. **1291**: 27–38.

698 **Paus, D., Phan, T. G., Chan, T. D., Gardam, S., Basten, A. and Brink, R.,** Antigen recognition strength regulates the choice between extrafollicular plasma cell and germinal center B cell differentiation. *J. Exp. Med.* 2006. **203**: 1081–1091.

699 **Boesch, M., Cosma, A. and Sopper, S.,** Flow cytometry: to dump or not to dump. *J. Immunol.* 2018. **201**: 1813.

700 **Beura, L. K., Hamilton, S. E., Bi, K., Schenkel, J. M., Odumade, O. A., Casey, K. A., Thompson, E. A. et al.,** Normalizing the environment recapitulates adult human immune traits in laboratory mice. *Nature* 2016. **532**: 512–516.

701 **Akondy, R. S., Monson, N. D., Miller, J. D., Edupuganti, S., Teuwen, D., Wu, H., Quyyumi, F. et al.,** The yellow fever virus vaccine induces a broad and polyfunctional human memory CD8+ T cell response. *J. Immunol.* 2009. **183**: 7919–7930.

702 **Schulz, A. R., Malzer, J. N., Domingo, C., Jurchott, K., Grutzkau, A., Babel, N., Nienen, M. et al.,** Low thymic activity and dendritic cell numbers are associated with the immune response to primary viral infection in elderly humans. *J. Immunol.* 2015. **195**: 4699–4711.

703 **van Leeuwen, E. M., de Bree, G. J., Remmerswaal, E. B., Yong, S. L., Tesselaar, K., ten Berge, I. J. and van Lier, R. A.,** IL-7 receptor alpha chain expression distinguishes functional subsets of virus-specific human CD8+ T cells. *Blood* 2005. **106**: 2091–2098.

704 **Zhou, L., Chong, M. M. and Littman, D. R.,** Plasticity of CD4+ T cell lineage differentiation. *Immunity* 2009. **30**: 646–655.

705 **Luckheeram, R. V., Zhou, R., Verma, A. D. and Xia, B.,** CD4(+)T cells: differentiation and functions. *Clin. Dev. Immunol.* 2012. **2012**: 925135.

706 **Zhu, J., Yamane, H. and Paul, W. E.,** Differentiation of effector CD4 T cell populations (*). *Annu. Rev. Immunol.* 2010. **28**: 445–489.

707 **Cua, D. J., Sherlock, J., Chen, Y., Murphy, C. A., Joyce, B., Seymour, B., Lucian, L. et al.,** Interleukin-23 rather than interleukin-12 is the critical cytokine for autoimmune inflammation of the brain. *Nature* 2003. **421**: 744–748.

708 **Murphy, C. A., Langrish, C. L., Chen, Y., Blumenschein, W., McClanahan, T., Kastelein, R. A., Sedgwick, J. D. et al.,** Divergent pro- and anti-inflammatory roles for IL-23 and IL-12 in joint autoimmune inflammation. *J. Exp. Med.* 2003. **198**: 1951–1957.

709 **Iwakura, Y., Ishigame, H., Saijo, S. and Nakae, S.,** Functional specialization of interleukin-17 family members. *Immunity* 2011. **34**: 149–162.

710 **Brown, D. M., Dilzer, A. M., Meents, D. L. and Swain, S. L.,** CD4 T cell-mediated protection from lethal influenza: perforin and antibody-mediated mechanisms give a one-two punch. *J. Immunol.* 2006. **177**: 2888–2898.

711 **Lord, G. M., Rao, R. M., Choe, H., Sullivan, B. M., Lichtman, A. H., Luscinskas, F. W. and Glimcher, L. H.,** T-bet is required for optimal proinflammatory CD4+ T-cell trafficking. *Blood* 2005. **106**: 3432–3439.

712 **Sundrud, M. S., Grill, S. M., Ni, D., Nagata, K., Alkan, S. S., Subramaniam, A. and Unutmaz, D.,** Genetic reprogramming of primary human T cells reveals functional plasticity in Th cell differentiation. *J. Immunol.* 2003. **171**: 3542–3549.

713 **Hirota, K., Yoshitomi, H., Hashimoto, M., Maeda, S., Teradaira, S., Sugimoto, N., Yamaguchi, T. et al.,** Preferential recruitment of CCR6-expressing Th17 cells to inflamed joints via CCL20 in rheumatoid arthritis and its animal model. *J. Exp. Med.* 2007. **204**: 2803–2812.

714 **Breitfeld, D., Ohl, L., Kremmer, E., Ellwart, J., Sallusto, F., Lipp, M. and Forster, R.,** Follicular B helper T cells express CXC chemokine receptor 5, localize to B cell follicles, and support immunoglobulin production. *J. Exp. Med.* 2000. **192**: 1545–1552.

715 **Hsieh, C. S., Macatonia, S. E., Tripp, C. S., Wolf, S. F., O'Garra, A. and Murphy, K. M.,** Development of TH1 CD4+ T cells through IL-12 produced by Listeria-induced macrophages. *Science* 1993. **260**: 547–549.

716 **Lighvani, A. A., Frucht, D. M., Jankovic, D., Yamane, H., Aliberti, J., Hissong, B. D., Nguyen, B. V. et al.,** T-bet is rapidly induced by

interferon-gamma in lymphoid and myeloid cells. *Proc. Natl. Acad. Sci. U S A* 2001. **98**: 15137–15142.

717 **Szabo, S. J., Kim, S. T., Costa, G. L., Zhang, X., Fathman, C. G. and Glimcher, L. H.**, A novel transcription factor, T-bet, directs Th1 lineage commitment. *Cell* 2000. **100**: 655–669.

718 **Le Gros, G., Ben-Sasson, S. Z., Seder, R., Finkelman, F. D. and Paul, W. E.**, Generation of interleukin 4 (IL-4)-producing cells in vivo and in vitro: IL-2 and IL-4 are required for in vitro generation of IL-4-producing cells. *J. Exp. Med.* 1990. **172**: 921–929.

719 **Swain, S. L., Weinberg, A. D., English, M. and Huston, G.**, IL-4 directs the development of Th2-like helper effectors. *J. Immunol.* 1990. **145**: 3796–3806.

720 **Zheng, W. and Flavell, R. A.**, The transcription factor GATA-3 is necessary and sufficient for Th2 cytokine gene expression in CD4 T cells. *Cell* 1997. **89**: 587–596.

721 **Ivanov, I. I., McKenzie, B. S., Zhou, L., Tadokoro, C. E., Lepelley, A., Lafaille, J. J., Cua, D. J. et al.**, The orphan nuclear receptor RORgammat directs the differentiation program of proinflammatory IL-17+ T helper cells. *Cell* 2006. **126**: 1121–1133.

722 **Baba, N., Rubio, M., Kenins, L., Regairaz, C., Woisetschlager, M., Carballido, J. M. and Sarfati, M.**, The aryl hydrocarbon receptor (AhR) ligand VAF347 selectively acts on monocytes and naive CD4(+) Th cells to promote the development of IL-22-secreting Th cells. *Hum. Immunol.* 2012. **73**: 795–800.

723 **Gerlach, K., Hwang, Y., Nikolaev, A., Atreya, R., Dornhoff, H., Steiner, S., Lehr, H. A. et al.**, TH9 cells that express the transcription factor PU.1 drive T cell-mediated colitis via IL-9 receptor signaling in intestinal epithelial cells. *Nat. Immunol.* 2014. **15**: 676–686.

724 **Chtanova, T., Tangye, S. G., Newton, R., Frank, N., Hodge, M. R., Rolph, M. S. and Mackay, C. R.**, T follicular helper cells express a distinctive transcriptional profile, reflecting their role as non-Th1/Th2 effector cells that provide help for B cells. *J. Immunol.* 2004. **173**: 68–78.

725 **Zhu, J., Jankovic, D., Oler, A. J., Wei, G., Sharma, S., Hu, G., Guo, L. et al.**, The transcription factor T-bet is induced by multiple pathways and prevents an endogenous Th2 cell program during Th1 cell responses. *Immunity* 2012. **37**: 660–673.

726 **Mosmann, T. R., Cherwinski, H., Bond, M. W., Giedlin, M. A. and Coffman, R. L.**, Two types of murine helper T cell clone. I. Definition according to profiles of lymphokine activities and secreted proteins. *J. Immunol.* 1986. **136**: 2348–2357.

727 **Harrington, L. E., Hatton, R. D., Mangan, P. R., Turner, H., Murphy, T. L., Murphy, K. M. and Weaver, C. T.**, Interleukin 17-producing CD4+ effector T cells develop via a lineage distinct from the T helper type 1 and 2 lineages. *Nat. Immunol.* 2005. **6**: 1123–1132.

728 **Grewal, I. S., Xu, J. and Flavell, R. A.**, Impairment of antigen-specific T-cell priming in mice lacking CD40 ligand. *Nature* 1995. **378**: 617–620.

729 **Liu, F. and Whitton, J. L.**, Cutting edge: re-evaluating the in vivo cytokine responses of CD8+ T cells during primary and secondary viral infections. *J. Immunol.* 2005. 5936–5940.

730 **Kirchhoff, D., Frentsch, M., Leclerk, P., Bumann, D., Rausch, S., Hartmann, S., Thiel, A. et al.**, Identification and isolation of murine antigen-reactive T cells according to CD154 expression. *Eur J Immunol* 2007. **37**: 2370–2377.

731 **Shore, D. A., Issafras, H., Landais, E., Teyton, L. and Wilson, I. A.**, The crystal structure of CD8 in complex with YTS156.7.7 Fab and interaction with other CD8 antibodies define the binding mode of CD8 alpha-beta to MHC class I. *J. Mol. Biol.* 2008. **384**: 1190–1202.

732 **Joshi, N. S., Cui, W., Chandele, A., Lee, H. K., Urso, D. R., Hagman, J., Gapin, L. et al.**, Inflammation directs memory precursor and short-lived effector CD8(+) T cell fates via the graded expression of T-bet transcription factor. *Immunity* 2007. **27**: 281–295.

733 **Kaech, S. M., Tan, J. T., Wherry, E. J., Konieczny, B. T., Surh, C. D. and Ahmed, R.**, Selective expression of the interleukin 7 receptor identifies effector CD8 T cells that give rise to long-lived memory cells. *Nat. Immunol.* 2003. 1191–1198.

734 **Obar, J. J., Jellison, E. R., Sheridan, B. S., Blair, D. A., Pham, Q. M., Zickovich, J. M. and Lefrancois, L.**, Pathogen-induced inflammatory environment controls effector and memory CD8+ T cell differentiation. *J. Immunol.* 2011. 4967–4978.

735 **Gerlach, C., Moseman, E. A., Loughhead, S. M., Alvarez, D., Zwijnenburg, A. J., Waanders, L., Garg, R. et al.**, The chemokine receptor CX3CR1 defines three antigen-experienced CD8 T cell subsets with distinct roles in immune surveillance and homeostasis. *Immunity* 2016. **45**: 1270–1284.

736 **Sosinowski, T., White, J. T., Cross, E. W., Haluszczak, C., Marrack, P., Gapin, L. and Kedl, R. M.**, CD8α+ dendritic cell trans presentation of IL-15 to naive CD8+ T cells produces antigen-inexperienced T cells in the periphery with memory phenotype and function. *J. Immunol.* 2013. **190**: 1936–1947.

737 **White, J. T., Cross, E. W. and Kedl, R. M.**, Antigen-inexperienced memory CD8(+) T cells: where they come from and why we need them. *Nat. Rev. Immunol.* 2017. **17**: 391–400.

738 **Chiu, B. C., Martin, B. E., Stolberg, V. R. and Chensue, S. W.**, Cutting edge: central memory CD8 T cells in aged mice are virtual memory cells. *J. Immunol.* 2013. **191**: 5793–5796.

739 **Quinn, K. M., Fox, A., Harland, K. L., Russ, B. E., Li, J., Nguyen, T. H. O., Loh, L. et al.**, Age-related decline in primary CD8(+) T cell responses is associated with the development of senescence in virtual memory CD8(+) T cells. *Cell Rep* 2018. **23**: 3512–3524.

740 **Tsukumo, S.-i., Unno, M., Muto, A., Takeuchi, A., Kometani, K., Kurosaki, T., Igarashi, K. et al.**, Bach2 maintains T cells in a naive state by suppressing effector memory-related genes. *Proc. Natl. Acad. Sci. USA* 2013. 10735–10740.

741 **Kaech, S. M. and Cui, W.**, Transcriptional control of effector and memory CD8+ T cell differentiation. *Nat. Rev. Immunol.* 2012. **12**: 749–761.

742 **Mackay, L. K., Minnich, M., Kragten, N. A., Liao, Y., Nota, B., Seillet, C., Zaid, A. et al.**, Hobit and Blimp1 instruct a universal transcriptional program of tissue residency in lymphocytes. *Science* 2016. **352**: 459–463.

743 **Mittrucker, H. W., Visekruna, A. and Huber, M.**, Heterogeneity in the differentiation and function of CD8(+) T cells. *Arch. Immunol. Ther. Exp.* 2014. **62**: 449–458.

744 **Frentsch, M., Stark, R., Matzmohr, N., Meier, S., Durlanik, S., Schulz, A. R., Stervbo, U. et al.**, CD40L expression permits CD8+ T cells to execute immunologic helper functions. *Blood* 2013. **122**: 405–412.

745 **van Stipdonk, M. J., Hardenberg, G., Bijker, M. S., Lemmens, E. E., Droin, N. M., Green, D. R. and Schoenberger, S. P.**, Dynamic programming of CD8+ T lymphocyte responses. *Nat. Immunol.* 2003. **4**: 361–365.

746 **Masopust, D., Murali-Krishna, K. and Ahmed, R.**, Quantitating the magnitude of the lymphocytic choriomeningitis virus-specific CD8 T-cell response: it is even bigger than we thought. *J. Virol.* 2007. **81**: 2002–2011.

747 **Mueller, S. N. and Mackay, L. K.**, Tissue-resident memory T cells: local specialists in immune defence. *Nat. Rev. Immunol.* 2016. **16**: 79–89.

748 **Behr, F. M., Chuwonpad, A., Stark, R. and van Gisbergen, K.**, Armed and ready: transcriptional regulation of tissue-resident memory CD8 T cells. *Front. Immunol.* 2018. **9**: 1770.

749 **Beura, L. K., Fares-Frederickson, N. J., Steinert, E. M., Scott, M. C., Thompson, E. A., Fraser, K. A., Schenkel, J. M. et al.**, CD4(+) resident

memory T cells dominate immunosurveillance and orchestrate local recall responses. *J. Exp. Med.* 2019.

750 **Autengruber, A., Gereke, M., Hansen, G., Hennig, C. and Bruder, D.,** Impact of enzymatic tissue disintegration on the level of surface molecule expression and immune cell function. *Eur. J. Microbiol. Immunol.* 2012. **2**: 112–120.

751 **Rissiek, B., Haag, F., Boyer, O., Koch-Nolte, F. and Adriouch, S.,** P2X7 on mouse T cells: one channel, many functions. *Front. Immunol.* 2015. **6**: 204.

752 **Rissiek, B., Lukowiak, M., Raczkowski, F., Magnus, T., Mittrucker, H. W. and Koch-Nolte, F.,** In vivo blockade of murine ARTC2.2 during cell preparation preserves the vitality and function of liver tissue-resident memory T cells. *Front. Immunol.* 2018. **9**: 1580.

753 **Stark, R., Wesselink, T. H., Behr, F. M., Kragten, N. A. M., Arens, R., Koch-Nolte, F., van Gisbergen, K. and van Lier, R. A. W.,** T RM maintenance is regulated by tissue damage via P2RX7. *Sci. Immunol.* 2018. **3**: eaau1022.

754 **Steinert, E. M., Schenkel, J. M., Fraser, K. A., Beura, L. K., Manlove, L. S., Igyarto, B. Z., Southern, P. J. et al.,** Quantifying memory CD8 T cells reveals regionalization of immunosurveillance. *Cell* 2015. **161**: 737–749.

755 **Anderson, K. G., Mayer-Barber, K., Sung, H., Beura, L., James, B. R., Taylor, J. J., Qunaj, L. et al.,** Intravascular staining for discrimination of vascular and tissue leukocytes. *Nat. Protoc.* 2014. **9**: 209–222.

756 **Nikolich-Žugich, J. and Čičin-Šain, L.,** Aging of the Immune System Across Different Species. In N. S. Wolf (Ed.), *The comparative biology of aging*, Springer Netherlands, Dordrecht, the Netherlands, 2010. pp. 353–376.

757 **Calado, R. T. and Dumitriu, B.,** Telomere dynamics in mice and humans. *Semin. Hematol.* 2013. **50**: 165–174.

758 **Cicin-Sain, L., Brien, J. D., Uhrlaub, J. L., Drabig, A., Marandu, T. F. and Nikolich-Zugich, J.,** Cytomegalovirus infection impairs immune responses and accentuates T-cell pool changes observed in mice with aging. *PLoS Pathog.* 2012. **8**: e1002849.

759 **Reese, T. A., Bi, K., Kambal, A., Filali-Mouhim, A., Beura, L. K., Burger, M. C., Pulendran, B. et al.,** Sequential infection with common pathogens promotes human-like immune gene expression and altered vaccine response. *Cell Host Microbe* 2016. **19**: 713–719.

760 **Pinchuk, L. M. and Filipov, N. M.,** Differential effects of age on circulating and splenic leukocyte populations in C57BL/6 and BALB/c male mice. *Immun. Ageing: I&A* 2008. **5**: 1–1.

761 **Yuan, R., Meng, Q., Nautiyal, J., Flurkey, K., Tsaih, S. W., Krier, R., Parker, M. G. et al.,** Genetic coregulation of age of female sexual maturation and lifespan through circulating IGF1 among inbred mouse strains. *Proc. Natl. Acad. Sci. USA* 2012. **109**: 8224–8229.

762 **Xu, W. and Larbi, A.,** Markers of T cell senescence in humans. *Int. J. Mol. Sci.* 2017. **18**: 1742.

763 **Lanna, A., Gomes, D. C., Muller-Durovic, B., McDonnell, T., Escors, D., Gilroy, D. W., Lee, J. H. et al.,** A sestrin-dependent Erk-Jnk-p38 MAPK activation complex inhibits immunity during aging. *Nat. Immunol.* 2017. **18**: 354–363.

764 **White, J. T., Cross, E. W., Burchill, M. A., Danhorn, T., McCarter, M. D., Rosen, H. R., O'Connor, B. et al.,** Virtual memory T cells develop and mediate bystander protective immunity in an IL-15-dependent manner. *Nat. Commun.* 2016. **7**: 11291.

765 **Marandu, T. F., Oduro, J. D., Borkner, L., Dekhtiarenko, I., Uhrlaub, J. L., Drabig, A., Kroger, A. et al.,** Immune protection against virus challenge in aging mice is not affected by latent herpesviral infections. *J. Virol.* 2015. **89**: 11715–11717.

766 **Sakaguchi, S., Sakaguchi, N., Asano, M., Itoh, M. and Toda, M.,** Immunologic self-tolerance maintained by activated T cells expressing IL-2 receptor alpha-chains (CD25). Breakdown of a single mechanism of self-tolerance causes various autoimmune diseases. *J. Immunol.* 1995. **155**: 1151–1164.

767 **Hori, S., Nomura, T. and Sakaguchi, S.,** Control of regulatory T cell development by the transcription factor Foxp3. *Science* 2003. **299**: 1057–1061.

768 **Fontenot, J. D., Gavin, M. A. and Rudensky, A. Y.,** Foxp3 programs the development and function of CD4$^+$CD25$^+$ regulatory T cells. *Nat. Immunol.* 2003. **4**: 330–336.

769 **Hill, J. A., Feuerer, M., Tash, K., Haxhinasto, S., Perez, J., Melamed, R., Mathis, D. et al.,** Foxp3 transcription-factor-dependent and -independent regulation of the regulatory T cell transcriptional signature. *Immunity* 2007. **27**: 786–800.

770 **Bennett, C. L., Christie, J., Ramsdell, F., Brunkow, M. E., Ferguson, P. J., Whitesell, L., Kelly, T. E. et al.,** The immune dysregulation, polyendocrinopathy, enteropathy, X-linked syndrome (IPEX) is caused by mutations of FOXP3. *Nat. Genet.* 2001. **27**: 20–21.

771 **Brunkow, M. E., Jeffery, E. W., Hjerrild, K. A., Paeper, B., Clark, L. B., Yasayko, S. A., Wilkinson, J. E. et al.,** Disruption of a new forkhead/winged-helix protein, scurfin, results in the fatal lymphoproliferative disorder of the scurfy mouse. *Nat. Genet.* 2001. **27**: 68–73.

772 **Bacchetta, R., Passerini, L., Gambineri, E., Dai, M., Allan, S. E., Perroni, L., Dagna-Bricarelli, F. et al.,** Defective regulatory and effector T cell functions in patients with FOXP3 mutations. *J. Clin. Invest.* 2006. **116**: 1713–1722.

773 **Klein, L., Robey, E. A. and Hsieh, C. S.,** Central CD4+ T cell tolerance: deletion versus regulatory T cell differentiation. *Nat. Rev. Immunol.* 2019. **19**: 7–18.

774 **Tanoue, T., Atarashi, K. and Honda, K.,** Development and maintenance of intestinal regulatory T cells. *Nat. Rev. Immunol.* 2016. **16**: 295–309.

775 **Thornton, A. M., Korty, P. E., Tran, D. Q., Wohlfert, E. A., Murray, P. E., Belkaid, Y. and Shevach, E. M.,** Expression of Helios, an Ikaros transcription factor family member, differentiates thymic-derived from peripherally induced Foxp3+ T regulatory cells. *J. Immunol.* 2010. **184**: 3433–3441.

776 **Weiss, J. M., Bilate, A. M., Gobert, M., Ding, Y., Curotto de Lafaille, M. A., Parkhust, C. N., Xiong, H. et al.,** Neuropilin-1 is expressed on thymus-derived natural regulatory T cells, but not mucosa-generated induced Foxp3+ Treg cells. *J. Exp. Med.* 2012. **209**: 1723–1742.

777 **Sefik, E., Geva-Zatorsky, N., Oh, S., Konnikova, L., Zemmour, D., McGuire, A. M., Burzyn, D. et al.,** Individual intestinal symbionts induce a distinct population of RORgamma+ regulatory T cells. *Science* 2015. **349**: 993–997.

778 **Ohnmacht, C., Park, J. H., Cording, S., Wing, J. B., Atarashi, K., Obata, Y., Gaboriau-Routhiau, V. et al.,** The microbiota regulates type 2 immunity through RORgammat+ T cells. *Science* 2015. **349**: 989–993.

779 **Akimova, T., Beier, U. H., Wang, L., Levine, M. H. and Hancock, W. W.,** Helios expression is a marker of T cell activation and proliferation. *PLoS One* 2011. **6**: e24226.

780 **Kim, B.-S., Lu, H., Ichiyama, K., Chen, X., Zhang, Y.-B., Mistry, N. A., Tanaka, K. et al.,** Generation of RORγt+ Antigen-Specific T Regulatory 17 Cells from Foxp3+ Precursors in Autoimmunity. *Cell Rep.* 2017. **21**: 195–207.

781 **Yang, J., Zou, M., Pezoldt, J., Zhou, X. and Huehn, J.,** Thymus-derived Foxp3+ regulatory T cells upregulate RORgammat expression under inflammatory conditions. *J. Mol. Med. (Berl)* 2018. **96**: 1387–1394.

782 Delacher, M., Schreiber, L., Richards, D. M., Farah, C., Feuerer, M. and Huehn, J., Transcriptional Control of Regulatory T cells. *Curr. Topics Microbiol. Immunol.* 2014. **381**: 83–124.

783 Owen, D. L., Mahmud, S. A., Sjaastad, L. E., Williams, J. B., Spanier, J. A., Simeonov, D. R., Ruscher, R. et al., Thymic regulatory T cells arise via two distinct developmental programs. *Nat. Immunol.* 2019. **20**: 195–205.

784 Toker, A., Engelbert, D., Garg, G., Polansky, J. K., Floess, S., Miyao, T., Baron, U. et al., Active demethylation of the Foxp3 locus leads to the generation of stable regulatory T cells within the thymus. *J. Immunol.* 2013. **190**: 3180–3188.

785 Thiault, N., Darrigues, J., Adoue, V., Gros, M., Binet, B., Perals, C., Leobon, B. et al., Peripheral regulatory T lymphocytes recirculating to the thymus suppress the development of their precursors. *Nat. Immunol.* 2015. **16**: 628–634.

786 Cowan, J. E., McCarthy, N. I. and Anderson, G., CCR7 controls thymus recirculation, but not production and emigration, of Foxp3+ T cells. *Cell Rep.* 2016. **14**: 1041–1048.

787 Panduro, M., Benoist, C. and Mathis, D., Tissue Tregs. *Annu. Rev. Immunol.* 2016. **34**: 609–633.

788 Feuerer, M., Herrero, L., Cipolletta, D., Naaz, A., Wong, J., Nayer, A., Lee, J. et al., Lean, but not obese, fat is enriched for a unique population of regulatory T cells that affect metabolic parameters. *Nat. Med.* 2009. **15**: 930–939.

789 Cipolletta, D., Feuerer, M., Li, A., Kamei, N., Lee, J., Shoelson, S. E., Benoist, C. et al., PPAR-gamma is a major driver of the accumulation and phenotype of adipose tissue Treg cells. *Nature* 2012. **486**: 549–553.

790 Kolodin, D., van Panhuys, N., Li, C., Magnuson, A. M., Cipolletta, D., Miller, C. M., Wagers, A., Germain, R. N. et al., Antigen- and cytokine-driven accumulation of regulatory T cells in visceral adipose tissue of lean mice. *Cell Metab.* 2015. **21**: 543–557.

791 Burzyn, D., Kuswanto, W., Kolodin, D., Shadrach, J. L., Cerletti, M., Jang, Y., Sefik, E. et al., A special population of regulatory T cells potentiates muscle repair. *Cell* 2013. **155**: 1282–1295.

792 Arpaia, N., Green, J. A., Moltedo, B., Arvey, A., Hemmers, S., Yuan, S., Treuting, P. M. et al., A distinct function of regulatory T cells in tissue protection. *Cell* 2015. **162**: 1078–1089.

793 Dombrowski, Y., O'Hagan, T., Dittmer, M., Penalva, R., Mayoral, S. R., Bankhead, P., Fleville, S. et al., Regulatory T cells promote myelin regeneration in the central nervous system. *Nat Neurosci* 2017. **20**: 674–680.

794 Ali, N., Zirak, B., Rodriguez, R. S., Pauli, M. L., Truong, H. A., Lai, K., Ahn, R. et al., Regulatory T cells in skin facilitate epithelial stem cell differentiation. *Cell* 2017. **169**: 1119–1129 e1111.

795 Delacher, M., Imbusch, C. D., Weichenhan, D., Breiling, A., Hotz-Wagenblatt, A., Trager, U., Hofer, A. C. et al., Genome-wide DNA-methylation landscape defines specialization of regulatory T cells in tissues. *Nat. Immunol.* 2017.

796 Delacher, M., Schmidl, C., Herzig, Y., Breloer, M., Hartmann, W., Brunk, F., Kägebein, D. et al., Rbpj expression in regulatory T cells is critical for restraining TH2 responses. *Nat. Commun.* 2019. **10**: 1621.

797 Carding, S. R. and Egan, P. J., Gammadelta T cells: functional plasticity and heterogeneity. *Nat. Rev. Immunol.* 2002. **2**: 336–345.

798 Bonneville, M., O'Brien, R. L. and Born, W. K., γδ T cell effector functions: a blend of innate programming and acquired plasticity. *Nat. Rev. Immunol.* 2010. **10**: 467–478.

799 Prinz, I., Silva-Santos, B. and Pennington, D. J., Functional development of gammadelta T cells. *Eur. J. Immunol.* 2013. **43**: 1988–1994.

800 Heilig, J. S. and Tonegawa, S., Diversity of murine gamma genes and expression in fetal and adult T lymphocytes. *Nature* 1986. **322**: 836–840.

801 Garman, R. D., Doherty, P. J. and Raulet, D. H., Diversity, rearrangement, and expression of murine T cell gamma genes. *Cell* 1986. **45**: 733–742.

802 Pereira, P., Hermitte, V., Lembezat, M. P., Boucontet, L., Azuara, V. and Grigoriadou, K., Developmentally regulated and lineage-specific rearrangement of T cell receptor Valpha/delta gene segments. *Eur. J. Immunol.* 2000. **30**: 1988–1997.

803 Mallick-Wood, C. A., Lewis, J. M., Richie, L. I., Owen, M. J., Tigelaar, R. E. and Hayday, A. C., Conservation of T cell receptor conformation in epidermal gammadelta cells with disrupted primary Vgamma gene usage. *Science* 1998. **279**: 1729–1733.

804 Roark, C. L., Aydintug, M. K., Lewis, J., Yin, X., Lahn, M., Hahn, Y. S., Born, W. K. et al., Subset-specific, uniform activation among V gamma 6/V delta 1+ gamma delta T cells elicited by inflammation. *J. Leukoc. Biol.* 2004. **75**: 68–75.

805 Goodman, T. and Lefrancois, L., Intraepithelial lymphocytes. Anatomical site, not T cell receptor form, dictates phenotype and function. *J. Exp. Med.* 1989. **170**: 1569–1581.

806 Prinz, I., Sansoni, A., Kissenpfennig, A., Ardouin, L., Malissen, M. and Malissen, B., Visualization of the earliest steps of gammadelta T cell development in the adult thymus. *Nat. Immunol.* 2006. **7**: 995–1003.

807 Koenecke, C., Chennupati, V., Schmitz, S., Malissen, B., Forster, R. and Prinz, I., In vivo application of mAb directed against the gammadelta TCR does not deplete but generates "invisible" gammadelta T cells. *Eur. J. Immunol.* 2009. **39**: 372–379.

808 Sandrock, I., Reinhardt, A., Ravens, S., Binz, C., Wilharm, A., Martins, J., Oberdorfer, L. et al., Genetic models reveal origin, persistence and non-redundant functions of IL-17-producing gammadelta T cells. *J. Exp. Med.* 2018. **215**: 3006–3018.

809 Ribot, J. C., deBarros, A., Pang, D. J., Neves, J. F., Peperzak, V., Roberts, S. J., Girardi, M. et al., CD27 is a thymic determinant of the balance between interferon-gamma- and interleukin 17-producing gammadelta T cell subsets. *Nat. Immunol.* 2009. **10**: 427–436.

810 Haas, J. D., Gonzalez, F. H., Schmitz, S., Chennupati, V., Fohse, L., Kremmer, E., Forster, R. et al., CCR6 and NK1.1 distinguish between IL-17A and IFN-gamma-producing gammadelta effector T cells. *Eur. J. Immunol.* 2009. **39**: 3488–3497.

811 Lombes, A., Durand, A., Charvet, C., Riviere, M., Bonilla, N., Auffray, C., Lucas, B. et al., Adaptive Immune-like gamma/delta T Lymphocytes Share Many Common Features with Their alpha/beta T Cell Counterparts. *J. Immunol.* 2015. **195**: 1449–1458.

812 Itohara, S., Farr, A. G., Lafaille, J. J., Bonneville, M., Takagaki, Y., Haas, W. and Tonegawa, S., Homing of a gamma delta thymocyte subset with homogeneous T-cell receptors to mucosal epithelia. *Nature* 1990. **343**: 754–757.

813 Shibata, K., Yamada, H., Hara, H., Kishihara, K. and Yoshikai, Y., Resident Vdelta1+ gammadelta T cells control early infiltration of neutrophils after Escherichia coli infection via IL-17 production. *J. Immunol.* 2007. **178**: 4466–4472.

814 Papotto, P. H., Reinhardt, A., Prinz, I. and Silva-Santos, B., Innately versatile: gammadelta17 T cells in inflammatory and autoimmune diseases. *J. Autoimmun.* 2018. **87**: 26–37.

815 Ohteki, T. and MacDonald, H. R., Major histocompatibility complex class I related molecules control the development of CD4+8- and CD4-8- subsets of natural killer 1.1+ T cell receptor-alpha/beta+ cells in the liver of mice. *J. Exp. Med.* 1994. **180**: 699–704.

816 **Makino, Y., Kanno, R., Ito, T., Higashino, K. and Taniguchi, M.**, Predominant expression of invariant V alpha 14+ TCR alpha chain in NK1.1+ T cell populations. *Int. Immunol.* 1995. **7**: 1157–1161.

817 **Wei, D. G., Curran, S. A., Savage, P. B., Teyton, L. and Bendelac, A.**, Mechanisms imposing the Vbeta bias of Valpha14 natural killer T cells and consequences for microbial glycolipid recognition. *J. Exp. Med.* 2006. **203**: 1197–1207.

818 **Lantz, O. and Bendelac, A.**, An invariant T cell receptor alpha chain is used by a unique subset of major histocompatibility complex class I-specific CD4+ and CD4-8- T cells in mice and humans. *J. Exp. Med.* 1994. **180**: 1097–1106.

819 **Bendelac, A., Lantz, O., Quimby, M. E., Yewdell, J. W., Bennink, J. R. and Brutkiewicz, R. R.**, CD1 recognition by mouse NK1+ T lymphocytes. *Science.* 1995. **268**: 863–865.

820 **Benlagha, K., Weiss, A., Beavis, A., Teyton, L. and Bendelac, A.**, In vivo identification of glycolipid antigen–specific T cells using fluorescent Cd1d tetramers. *J. Exp. Med.* 2000. **191**: 1895–1904.

821 **Matsuda, J. L., Naidenko, O. V., Gapin, L., Nakayama, T., Taniguchi, M., Wang, C. R., Koezuka, Y. et al.**, Tracking the response of natural killer T cells to a glycolipid antigen using CD1d tetramers. *J. Exp. Med.* 2000. **192**: 741–754.

822 **Moran, A. E., Holzapfel, K. L., Xing, Y., Cunningham, N. R., Maltzman, J. S., Punt, J. and Hogquist, K. A.**, T cell receptor signal strength in Treg and iNKT cell development demonstrated by a novel fluorescent reporter mouse. *J. Exp. Med.* 2011. **208**: 1279–1289.

823 **Savage, A. K., Constantinides, M. G., Han, J., Picard, D., Martin, E., Li, B., Lantz, O. et al.**, The transcription factor PLZF directs the effector program of the NKT cell lineage. *Immunity* 2008. **29**: 391–403.

824 **Kovalovsky, D., Uche, O. U., Eladad, S., Hobbs, R. M., Yi, W., Alonzo, E., Chua, K. et al.**, The BTB-zinc finger transcriptional regulator PLZF controls the development of invariant natural killer T cell effector functions. *Nat. Immunol.* 2008. **9**: 1055–1064.

825 **Benlagha, K., Kyin, T., Beavis, A., Teyton, L. and Bendelac, A.**, A thymic precursor to the NK T cell lineage. *Science* 2002. **296**: 553–555.

826 **Benlagha, K., Wei, D. G., Veiga, J., Teyton, L. and Bendelac, A.**, Characterization of the early stages of thymic NKT cell development. *J. Exp. Med.* 2005. **202**: 485–492.

827 **Pellicci, D. G., Hammond, K. J. L., Uldrich, A. P., Baxter, A. G., Smyth, M. J. and Godfrey, D. I.**, A natural killer T (NKT) cell developmental pathway iInvolving a thymus-dependent NK1.1(-)CD4(+) CD1d-dependent precursor stage. *J. Exp. Med.* 2002. **195**: 835–844.

828 **Wang, H. and Hogquist, K. A.**, CCR7 defines a precursor for murine iNKT cells in thymus and periphery. *Elife* 2018. **7**.

829 **Berzins, S. P., McNab, F. W., Jones, C. M., Smyth, M. J. and Godfrey, D. I.**, Long-term retention of mature NK1.1+ NKT cells in the thymus. *J. Immunol.* 2006. **176**: 4059–4065.

830 **Lee, Y. J., Holzapfel, K. L., Zhu, J., Jameson, S. C. and Hogquist, K. A.**, Steady-state production of IL-4 modulates immunity in mouse strains and is determined by lineage diversity of iNKT cells. *Nat. Immunol.* 2013. **14**: 1146–1154.

831 **Crosby, C. M. and Kronenberg, M.**, Tissue-specific functions of invariant natural killer T cells. *Nat. Rev. Immunol.* 2018. **18**: 559–574.

832 **Salou, M., Legoux, F., Gilet, J., Darbois, A., Du Halgouet, A., Alonso, R., Richer, W. et al.**, A common transcriptomic program acquired in the thymus defines tissue residency of MAIT and NKT subsets. *J. Exp. Med.* 2019. **216**: 133–151.

833 **Brigl, M., Tatituri, R. V. V., Watts, G. F. M., Bhowruth, V., Leadbetter, E. A., Barton, N., Cohen, N. R. et al.**, Innate and cytokine-driven signals, rather than microbial antigens, dominate in natural killer T cell activation during microbial infection. *J. Exp. Med.* 2011. **208**: 1163–1177.

834 **Velazquez, P., Cameron, T. O., Kinjo, Y., Nagarajan, N., Kronenberg, M. and Dustin, M. L.**, Cutting edge: activation by innate cytokines or microbial antigens can cause arrest of natural killer T cell patrolling of liver sinusoids. *J. Immunol.* 2008. **180**: 2024–2028.

835 **Salio, M., Silk, J. D., Jones, E. Y. and Cerundolo, V.**, Biology of CD1- and MR1-restricted T cells. *Annu. Rev. Immunol.* 2014. **32**: 323–366.

836 **Wang, H. and Hogquist, K. A.**, How lipid-specific T cells become effectors: the differentiation of iNKT subsets. *Front. Immunol.* 2018. **9**: 1450.

837 **Jungblut, M., Oeltze, K., Zehnter, I., Hasselmann, D. and Bosio, A.**, Standardized preparation of single-cell suspensions from mouse lung tissue using the gentleMACS dissociator. *J. Vis. Exp.* 2009.

838 **Liu, Y., Goff, R. D., Zhou, D., Mattner, J., Sullivan, B. A., Khurana, A., Cantu, C. et al.**, A modified alpha-galactosyl ceramide for staining and stimulating natural killer T cells. *J. Immunol. Methods* 2006. **312**: 34–39.

839 **Lee, Y. J., Wang, H., Starrett, G. J., Phuong, V., Jameson, S. C. and Hogquist, K. A.**, Tissue-specific distribution of iNKT cells impacts their cytokine response. *Immunity* 2015. **43**: 566–578.

840 **Ziętara, N., Łyszkiewicz, M., Witzlau, K., Naumann, R., Hurwitz, R., Langemeier, J., Bohne, J. et al.**, Critical role for miR-181a/b-1 in agonist selection of invariant natural killer T cells. *Proc. Natl. Acad. Sci. U S A.* 2013. **110**: 7407–7412.

841 **Winter, S. J., Kunze-Schumacher, H., Imelmann, E., Grewers, Z., Osthues, T. and Krueger, A.**, MicroRNA miR-181a/b-1 controls MAIT cell development. *Immunol. Cell. Biol.* 2019. **97**: 190–202.

842 **Treiner, E., Duban, L., Bahram, S., Radosavljevic, M., Wanner, V., Tilloy, F., Affaticati, P. et al.**, Selection of evolutionarily conserved mucosal-associated invariant T cells by MR1. *Nature* 2003. **422**: 164–169.

843 **Porcelli, S., Yockey, C. E., Brenner, M. B. and Balk, S. P.**, Analysis of T cell antigen receptor (TCR) expression by human peripheral blood CD4-8- alpha/beta T cells demonstrates preferential use of several V beta genes and an invariant TCR alpha chain. *J. Exp. Med.* 1993. **178**: 1–16.

844 **Tilloy, F., Treiner, E., Park, S. H., Garcia, C., Lemonnier, F., La Salle, H. de, Bendelac, A., Bonneville, M. et al.**, An invariant T cell receptor alpha chain defines a novel TAP-independent major histocompatibility complex class Ib-restricted alpha/beta T cell subpopulation in mammals. *J. Exp. Med.* 1999. **189**: 1907–1921.

845 **Rahimpour, A., Koay, H. F., Enders, A., Clanchy, R., Eckle, S. B. G., Meehan, B., Chen, Z. et al.**, Identification of phenotypically and functionally heterogeneous mouse mucosal-associated invariant T cells using MR1 tetramers. *J. Exp. Med.* 2015. **212**: 1095–1108.

846 **Reantragoon, R., Corbett, A. J., Sakala, I. G., Gherardin, N. A., Furness, J. B., Chen, Z., Eckle, S. B. G. et al.**, Antigen-loaded MR1 tetramers define T cell receptor heterogeneity in mucosal-associated invariant T cells. *J. Exp. Med.* 2013. **210**: 2305–2320.

847 **Koay, H. F., Gherardin, N. A., Enders, A., Loh, L., Mackay, L. K., Almeida, C. F., Russ, B. E. et al.**, A three-stage intrathymic development pathway for the mucosal-associated invariant T cell lineage. *Nat. Immunol.* 2016. **17**: 1300–1311.

848 **Cui, Y., Franciszkiewicz, K., Mburu, Y. K., Mondot, S., Le Bourhis, L., Premel, V., Martin, E. et al.**, Mucosal-associated invariant T cell-rich congenic mouse strain allows functional evaluation. *J. Clin. Invest.* 2015. **125**: 4171–4185.

849 **Salou, M., Franciszkiewicz, K. and Lantz, O.**, MAIT cells in infectious diseases. *Curr. Opin. Immunol.* 2017. **48**: 7–14.

850 **Corbett, A. J.**, **Eckle, S. B.**, **Birkinshaw, R. W.**, **Liu, L.**, **Patel, O.**, **Mahony, J.**, **Chen, Z. et al.**, T-cell activation by transitory neo-antigens derived from distinct microbial pathways. *Nature* 2014. **509**: 361–365.

851 **Olivares-Villagomez, D.** and **Van Kaer, L.**, Intestinal Intraepithelial Lymphocytes: Sentinels of the Mucosal Barrier. *Trends Immunol.* 2018. **39**: 264–275.

852 **Ma, H.**, **Tao, W.** and **Zhu, S.**, T lymphocytes in the intestinal mucosa: defense and tolerance. *Cell Mol. Immunol.* 2019.

853 **Cheroutre, H.**, **Lambolez, F.** and **Mucida, D.**, The light and dark sides of intestinal intraepithelial lymphocytes. *Nat. Rev. Immunol.* 2011. **11**: 445–456.

854 **Georgiev, H.**, **Ravens, I.**, **Papadogianni, G.**, **Malissen, B.**, **Forster, R.** and **Bernhardt, G.**, Blocking the ART2.2/P2X7-system is essential to avoid a detrimental bias in functional CD4 T cell studies. *Eur. J. Immunol.* 2018. **48**: 1078–1081.

855 **Konjar, S.**, **Ferreira, C.**, **Blankenhaus, B.** and **Veldhoen, M.**, Intestinal Barrier Interactions with Specialized CD8 T Cells. *Front. Immunol.* 2017. **8**: 1281.

856 **Chennupati, V.**, **Worbs, T.**, **Liu, X.**, **Malinarich, F. H.**, **Schmitz, S.**, **Haas, J. D.**, **Malissen, B. et al.**, Intra- and intercompartmental movement of gammadelta T cells: intestinal intraepithelial and peripheral gammadelta T cells represent exclusive nonoverlapping populations with distinct migration characteristics. *J. Immunol.* 2010. **185**: 5160–5168.

857 **Malinarich, F. H.**, **Grabski, E.**, **Worbs, T.**, **Chennupati, V.**, **Haas, J. D.**, **Schmitz, S.**, **Candia, E. et al.**, Constant TCR triggering suggests that the TCR expressed on intestinal intraepithelial gammadelta T cells is functional in vivo. *Eur. J. Immunol.* 2010. **40**: 3378–3388.

858 **Martina, M. N.**, **Noel, S.**, **Saxena, A.**, **Rabb, H.** and **Hamad, A. R.**, Double negative (DN) alphabeta T cells: misperception and overdue recognition. *Immunol. Cell Biol.* 2015. **93**: 305–310.

859 **Gerlach, C.**, **van Heijst, J. W.**, **Swart, E.**, **Sie, D.**, **Armstrong, N.**, **Kerkhoven, R. M.**, **Zehn, D. et al.**, One naive T cell, multiple fates in CD8+ T cell differentiation. *J. Exp. Med.* 2010. **207**: 1235–1246.

860 **Appay, V.**, **van Lier, R. A.**, **Sallusto, F.** and **Roederer, M.**, Phenotype and function of human T lymphocyte subsets: consensus and issues. *Cytometry A* 2008. **73**: 975–983.

861 **Costantini, A.**, **Mancini, S.**, **Giuliodoro, S.**, **Butini, L.**, **Regnery, C. M.**, **Silvestri, G.** and **Montroni, M.**, Effects of cryopreservation on lymphocyte immunophenotype and function. *J. Immunol. Methods* 2003. **278**: 145–155.

862 **van den Broek, T.**, **Borghans, J. A. M.** and **van Wijk, F.**, The full spectrum of human naive T cells. *Nat. Rev. Immunol.* 2018. **18**: 363–373.

863 **Sallusto, F.**, **Lenig, D.**, **Mackay, C. R.** and **Lanzavecchia, A.**, Flexible programs of chemokine receptor expression on human polarized T helper 1 and 2 lymphocytes. *J. Exp. Med.* 1998. **187**: 875–883.

864 **Cosmi, L.**, **Annunziato, F.**, **Galli, M. I. G.**, **Maggi, R. M. E.**, **Nagata, K.** and **Romagnani, S.**, CRTH2 is the most reliable marker for the detection of circulating human type 2 Th and type 2 T cytotoxic cells in health and disease. *Eur. J. Immunol.* 2000. **30**: 2972–2979.

865 **Mahnke, Y. D.**, **Beddall, M. H.** and **Roederer, M.**, OMIP-017: human CD4(+) helper T-cell subsets including follicular helper cells. *Cytometry A* 2013. **83**: 439–440.

866 **Ouyang, W.**, **Ranganath, S. H.**, **Weindel, K.**, **Bhattacharya, D.**, **Murphy, T. L.**, **Sha, W. C.** and **Murphy, K. M.**, Inhibition of Th1 development mediated by GATA-3 through an IL-4-independent mechanism. *Immunity* 1998. **9**: 745–755.

867 **Kanhere, A.**, **Hertweck, A.**, **Bhatia, U.**, **Gokmen, M. R.**, **Perucha, E.**, **Jackson, I.**, **Lord, G. M. et al.**, T-bet and GATA3 orchestrate Th1 and Th2 differentiation through lineage-specific targeting of distal regulatory elements. *Nat. Commun.* 2012. **3**: 1268.

868 **Staudt, V.**, **Bothur, E.**, **Klein, M.**, **Lingnau, K.**, **Reuter, S.**, **Grebe, N.**, **Gerlitzki, B. et al.**, Interferon-regulatory factor 4 is essential for the developmental program of T helper 9 cells. *Immunity* 2010. **33**: 192–202.

869 **Maggi, L.**, **Santarlasci, V.**, **Capone, M.**, **Peired, A.**, **Frosali, F.**, **Crome, S. Q.**, **Querci, V. et al.**, CD161 is a marker of all human IL-17-producing T-cell subsets and is induced by RORC. *Eur. J. Immunol.* 2010. **40**: 2174–2181.

870 **Zielinski, C. E.**, **Mele, F.**, **Aschenbrenner, D.**, **Jarrossay, D.**, **Ronchi, F.**, **Gattorno, M.**, **Monticelli, S. et al.**, Pathogen-induced human TH17 cells produce IFN-gamma or IL-10 and are regulated by IL-1beta. *Nature* 2012. **484**: 514–518.

871 **Cosmi, L.**, **Maggi, L.**, **Santarlasci, V.**, **Liotta, F.** and **Annunziato, F.**, T helper cells plasticity in inflammation. *Cytometry A* 2014. **85**: 36–42.

872 **Acosta-Rodriguez, E. V.**, **Rivino, L.**, **Geginat, J.**, **Jarrossay, D.**, **Gattorno, M.**, **Lanzavecchia, A.**, **Sallusto, F. et al.**, Surface phenotype and antigenic specificity of human interleukin 17-producing T helper memory cells. *Nat. Immunol.* 2007. **8**: 639–646.

873 **Gagliani, N.**, **Amezcua Vesely, M. C.**, **Iseppon, A.**, **Brockmann, L.**, **Xu, H.**, **Palm, N. W.**, **de Zoete, M. R.**, **Licona-Limon, P. et al.**, Th17 cells transdifferentiate into regulatory T cells during resolution of inflammation. *Nature* 2015. **523**: 221–225.

874 **Jankovic, D.**, **Kugler, D. G.** and **Sher, A.**, IL-10 production by CD4+ effector T cells: a mechanism for self-regulation. *Mucosal Immunol.* 2010. **3**: 239–246.

875 **Zhang, P.**, **Lee, J. S.**, **Gartlan, K. H.**, **Schuster, I. S.**, **Comerford, I.**, **Varelias, A.**, **Ullah, M. A. et al.**, Eomesodermin promotes the development of type 1 regulatory T (TR1) cells. *Sci. Immunol.* 2017. **2**: eaah7152.

876 **Gruarin, P.**, **Maglie, S.**, **De Simone, M.**, **Haringer, B.**, **Vasco, C.**, **Ranzani, V.**, **Bosotti, R.**, **Noddings, J. S. et al.**, Eomesodermin controls a unique differentiation program in human IL-10 and IFN-gamma coproducing regulatory T cells. *Eur. J. Immunol.* 2019. **49**: 96–111.

877 **Basu, R.**, **O'Quinn, D. B.**, **Silberger, D. J.**, **Schoeb, T. R.**, **Fouser, L.**, **Ouyang, W.**, **Hatton, R. D. et al.**, Th22 cells are an important source of IL-22 for host protection against enteropathogenic bacteria. *Immunity* 2012. **37**: 1061–1075.

878 **Duhen, T.**, **Geiger, R.**, **Jarrossay, D.**, **Lanzavecchia, A.** and **Sallusto, F.**, Production of interleukin 22 but not interleukin 17 by a subset of human skin-homing memory T cells. *Nat. Immunol.* 2009. **10**: 857–863.

879 **Morita, R.**, **Schmitt, N.**, **Bentebibel, S. E.**, **Ranganathan, R.**, **Bourdery, L.**, **Zurawski, G.**, **Foucat, E. et al.**, Human blood CXCR5(+)CD4(+) T cells are counterparts of T follicular cells and contain specific subsets that differentially support antibody secretion. *Immunity* 2011. **34**: 108–121.

880 **Glatman Zaretsky, A.**, **Taylor, J. J.**, **King, I. L.**, **Marshall, F. A.**, **Mohrs, M.** and **Pearce, E. J.**, T follicular helper cells differentiate from Th2 cells in response to helminth antigens. *J. Exp. Med.* 2009. **206**: 991–999.

881 **Oja, A. E.**, **Vieira Braga, F. A.**, **Remmerswaal, E. B.**, **Kragten, N. A.**, **Hertoghs, K. M.**, **Zuo, J.**, **Moss, P. A.**, **van Lier, R. A.**, **van Gisbergen, K. P. et al.**, The transcription factor Hobit identifies human cytotoxic CD4(+) T cells. *Front. Immunol.* 2017. **8**: 325.

882 **Hamann, D.**, **Baars, P. A.**, **Rep, M. H.**, **Hooibrink, B.**, **Kerkhof-Garde, S. R.**, **Klein, M. R.** and **van Lier, R. A.**, Phenotypic and functional separation of memory and effector human CD8+ T cells. *J. Exp. Med.* 1997. **186**: 1407–1418.

883 **Appay, V.**, **Dunbar, P. R.**, **Callan, M.**, **Klenerman, P.**, **Gillespie, G. M.**, **Papagno, L.**, **Ogg, G. S. et al.**, Memory CD8+ T cells vary in differentiation phenotype in different persistent virus infections. *Nat. Med.* 2002. **8**: 379–385.

884 Sallusto, F., Lenig, D., Forster, R., Lipp, M. and Lanzavecchia, A., Two subsets of memory T lymphocytes with distinct homing potentials and effector functions. *Nature* 1999. **401**: 708–712.

885 van Aalderen, M. C., Remmerswaal, E. B., Verstegen, N. J., Hombrink, P., ten Brinke, A., Pircher, H., Kootstra, N. A., ten Berge, I. J. et al., Infection history determines the differentiation state of human CD8+ T cells. *J. Virol.* 2015. **89**: 5110–5123.

886 van Leeuwen, E. M., Remmerswaal, E. B., Vossen, M. T., Rowshani, A. T., Wertheim-van Dillen, P. M., van Lier, R. A. and ten Berge, I. J., Emergence of a CD4+CD28- granzyme B+, cytomegalovirus-specific T cell subset after recovery of primary cytomegalovirus infection. *J. Immunol.* 2004. **173**: 1834–1841.

887 Huster, K. M., Busch, V., Schiemann, M., Linkemann, K., Kerksiek, K. M., Wagner, H. and Busch, D. H., Selective expression of IL-7 receptor on memory T cells identifies early CD40L-dependent generation of distinct CD8+ memory T cell subsets. *Proc. Natl. Acad. Sci. U. S. A.* 2004. **101**: 5610–5615.

888 Hand, T. W., Morre, M. and Kaech, S. M., Expression of IL-7 receptor alpha is necessary but not sufficient for the formation of memory CD8 T cells during viral infection. *Proc. Natl. Acad. Sci. USA* 2007. **104**: 11730–11735.

889 Shay, T., Jojic, V., Zuk, O., Rothamel, K., Puyraimond-Zemmour, D., Feng, T., Wakamatsu, E. et al., Conservation and divergence in the transcriptional programs of the human and mouse immune systems. *Proc. Natl. Acad. Sci. USA* 2013. **110**: 2946–2951.

890 Remmerswaal, E. B. M., Hombrink, P., Nota, B., Pircher, H., Ten Berge, I. J. M., van Lier, R. A. W. and van Aalderen, M. C., Expression of IL-7Ralpha and KLRG1 defines functionally distinct CD8(+) T-cell populations in humans. *Eur. J. Immunol.* 2019. **49**: 694–708.

891 Intlekofer, A. M., Takemoto, N., Wherry, E. J., Longworth, S. A., Northrup, J. T., Palanivel, V. R., Mullen, A. C. et al., Effector and memory CD8+ T cell fate coupled by T-bet and eomesodermin. *Nat. Immunol.* 2005. **6**: 1236–1244.

892 Kragten, N. A. M., Behr, F. M., Vieira Braga, F. A., Remmerswaal, E. B. M., Wesselink, T. H., Oja, A. E., Hombrink, P. et al., Blimp-1 induces and Hobit maintains the cytotoxic mediator granzyme B in CD8 T cells. *Eur. J. Immunol.* 2018. **48**: 1644–1662.

893 Vieira Braga, F. A., Hertoghs, K. M., Kragten, N. A., Doody, G. M., Barnes, N. A., Remmerswaal, E. B., Hsiao, C. C. et al., Blimp-1 homolog Hobit identifies effector-type lymphocytes in humans. *Eur. J. Immunol.* 2015. **45**: 2945–2958.

894 Kim, H. J., Barnitz, R. A., Kreslavsky, T., Brown, F. D., Moffett, H., Lemieux, M. E., Kaygusuz, Y. et al., Stable inhibitory activity of regulatory T cells requires the transcription factor Helios. *Science* 2015. **350**: 334–339.

895 Sathaliyawala, T., Kubota, M., Yudanin, N., Turner, D., Camp, P., Thome, J. J., Bickham, K. L. et al., Distribution and compartmentalization of human circulating and tissue-resident memory T cell subsets. *Immunity* 2013. **38**: 187–197.

896 Thome, J. J. C., Yudanin, N., Ohmura, Y., Kubota, M., Grinshpun, B., Sathaliyawala, T., Kato, T. et al., Spatial map of human t cell compartmentalization and maintenance over decades of life. *Cell* 2014. **159**: 814–828.

897 Okhrimenko, A., Grün, J. R., Westendorf, K., Fang, Z., Reinke, S., von Roth, P., Wassilew, G. et al., Human memory T cells from the bone marrow are resting and maintain long-lasting systemic memory. 2014. **111**: 9229–9234.

898 Watanabe, R., Gehad, A., Yang, C., Scott, L. L., Teague, J. E., Schlapbach, C., Elco, C. P. et al., Human skin is protected by four functionally and phenotypically discrete populations of resident and recirculating memory T cells. *Sci. Transl. Med.* 2015. **7**: 279ra39.

899 Hombrink, P., Helbig, C., Backer, R. A., Piet, B., Oja, A. E., Stark, R., Brasser, G., Jongejan, A., Jonkers, R. E., Nota, B., Basak, O., Clevers, H. C., Moerland, P. D., Amsen, D., van Lier, R. A. Programs for the persistence, vigilance and control of human CD8+ lung-resident memory T cells. *Nat. Immunol.* 2016. **17**: 1467–1478.

900 Kumar, B. V., Ma, W., Miron, M., Granot, T., Guyer, R. S., Carpenter, D. J., Senda, T. et al., Human tissue-resident memory T cells are defined by core transcriptional and functional signatures in lymphoid and mucosal sites. *Cell Rep.* 2017. **20**: 2921–2934.

901 Oja, A. E., Piet, B., Helbig, C., Stark, R., van der Zwan, D., Blaauwgeers, H., Remmerswaal, E. B. M. et al., Trigger-happy resident memory CD4+ T cells inhabit the human lungs. *Mucosal Immunol.* 2018. **11**: 654–667.

902 Smolders, J., Heutinck, K. M., Fransen, N. L., Remmerswaal, E. B. M., Hombrink, P., Ten Berge, I. J. M., van Lier, R. A. W. et al., Tissue-resident memory T cells populate the human brain. *Nat. Commun.* 2018. **9**: 4593.

903 Pascutti, M. F., Geerman, S., Collins, N., Brasser, G., Nota, B., Stark, R., Behr, F. et al., Peripheral and systemic antigens elicit an expandable pool of resident memory CD8+ T cells in the bone marrow. *Eur. J. Immunol.* 2019. **49**: 853–872.

904 Snyder, M. E., Finlayson, M. O., Connors, T. J., Dogra, P., Senda, T., Bush, E., Carpenter, D. et al., Generation and persistence of human tissue-resident memory T cells in lung transplantation. *Sci. Immunol.* 2019. **4**: eaav5581.

905 Skon, C. N., Lee, J. Y., Anderson, K. G., Masopust, D., Hogquist, K. A. and Jameson, S. C., Transcriptional downregulation of S1pr1 is required for the establishment of resident memory CD8+ T cells. *Nat. Immunol.* 2013. **14**: 1285–1293.

906 Steinert, E. M. et al., Quantifying memory CD8 T cells reveals regionalization of immunosurveillance. *Cell* 2015. **161**: 737–749.

907 Kumar, B. V., Connors, T. J. and Farber, D. L., Human T Cell Development, Localization, and Function throughout Life. *Immunity* 2018. **48**: 202–213.

908 Cepek, K. L. et al., Adhesion between epithelial cells and T lymphocytes mediated by E-cadherin and the alpha E beta 7 integrin. *Nature* 1994. **372**: 190–193.

909 Cheuk, S., Schlums, H., Bryceson, Y. T., Eidsmo, L. and Tjernlund, A., CD49a Expression Defines Tissue-Resident CD8 + T Cells Poised for Cytotoxic Function in Human Skin. *Immunity* 2017. 1–14. https://doi.org/10.1016/j.immuni.2017.01.009

910 Webb, J. R., Milne, K., Watson, P., DeLeeuw, R. J. and Nelson, B. H., Tumor-infiltrating lymphocytes expressing the tissue resident memory marker cd103 are associated with increased survival in high-grade serous ovarian cancer. *Clin. Cancer Res.* 2014. **20**: 434–444.

911 Djenidi, F., Adam, J., Goubar, A., Durgeau, A., Meurice, G., de Montpréville, V., Validire, P. et al., CD8 + CD103 + Tumor–Infiltrating Lymphocytes Are Tumor-Specific Tissue-Resident Memory T Cells and a Prognostic Factor for Survival in Lung Cancer Patients. *J. Immunol.* 2015. **194**: 3475–3486.

912 Koh, J., Kim, S., Kim, M. Y., Go, H., Jeon, Y. K. and Chung, D. H., Prognostic implications of intratumoral CD103+ tumor-infiltrating lymphocytes in pulmonary squamous cell carcinoma. *Oncotarget* 2017. **8**: 13762–13769.

913 Ganesan, A.-P., Clarke, J., Wood, O., Garrido-Martin, E. M., Chee, S. J., Mellows, T., Samaniego-Castruita, D., Singh, D. et al., Tissue-resident memory features are linked to the magnitude of cytotoxic

T cell responses in human lung cancer. *Nat. Immunol.* 2017. **18**: 940–950.

914 Oja, A. E., Piet, B., van der Zwan, D., Blaauwgeers, H., Mensink, M., de Kivit, S., Borst, J. et al., Functional heterogeneity of CD4+ tumor-infiltrating lymphocytes with a resident memory phenotype in NSCLC. *Front. Immunol.* 2018. **9**: 2654.

915 Gu-Trantien, C. et al., CXCL13-producing T FH cells link immune suppression and adaptive memory in human breast cancer. *JCI Insight* 2017. **2**: 1–17.

916 Thommen, D. D., Koelzer, V. H., Herzig, P., Roller, A., Trefny, M., Dimeloe, S., Kiialainen, A. et al., A transcriptionally and functionally distinct PD-1 + CD8 + T cell pool with predictive potential in non-small cell lung cancer treated with PD-1 blockade. *Nat. Med.* 2018.**24**.

917 Simoni, Y. et al., Bystander CD8+ T cells are abundant and phenotypically distinct in human tumour infiltrates. *Nature* 2018. **557**: 575–579.

918 Holt, P. G., Robinson, B. W., Reid, M., Kees, U. R., Warton, A., Dawson, V. H., Rose, A., Schon-Hegrad, M. et al., Extraction of immune and inflammatory cells from human lung parenchyma: evaluation of an enzymatic digestion procedure. *Clin. Exp. Immunol.* 1986. **66**: 188–200.

919 Piet, B., de Bree, G. J., Smids-Dierdorp, B. S., van der Loos, C. M., Remmerswaal, E. B., von der Thüsen, J. H., van Haarst, J. M. et al., CD8+ T cells with an intraepithelial phenotype upregulate cytotoxic function upon influenza infection in human lung. *J. Clin. Invest.* 2011. **121**: 2254–2263.

920 Clark, R. A., Chong, B., Mirchandani, N., Brinster, N. K., Yamanaka, K., Dowgiert, R. K. and Kupper, T. S., The Vast Majority of CLA + T Cells Are Resident in Normal Skin. *J. Immunol.* 2006. **176**: 4431–4439.

921 Bektas, A., Schurman, S. H., Sen, R. and Ferrucci, L., Human T cell immunosenescence and inflammation in aging. *J. Leukoc. Biol.* 2017. **102**: 977–988.

922 Costantini, E., D'Angelo, C. and Reale, M., The role of immunosenescence in neurodegenerative diseases. *Mediators Inflamm.* 2018. **2018**: 6039171.

923 Franceschi, C., Capri, M., Monti, D., Giunta, S., Olivieri, F., Sevini, F., Panourgia, M. P. et al., Inflammaging and anti-inflammaging: a systemic perspective on aging and longevity emerged from studies in humans. *Mech. Ageing Dev.* 2007. **128**: 92–105.

924 Derhovanessian, E., Maier, A. B., Hahnel, K., Zelba, H., de Craen, A. J., Roelofs, H., Slagboom, E. P. et al., Lower proportion of naive peripheral CD8+ T cells and an unopposed pro-inflammatory response to human Cytomegalovirus proteins in vitro are associated with longer survival in very elderly people. *Age (Dordr)* 2013. **35**: 1387–1399.

925 Naylor, K., Li, G., Vallejo, A. N., Lee, W. W., Koetz, K., Bryl, E., Witkowski, J. et al., The influence of age on T cell generation and TCR diversity. *J. Immunol.* 2005. **174**: 7446–7452.

926 Olsson, J., Wikby, A., Johansson, B., Lofgren, S., Nilsson, B. O. and Ferguson, F. G., Age-related change in peripheral blood T-lymphocyte subpopulations and cytomegalovirus infection in the very old: the Swedish longitudinal OCTO immune study. *Mech. Ageing Dev.* 2000. **121**: 187–201.

927 Rubino, G., Bulati, M., Aiello, A., Aprile, S., Gambino, C. M., Gervasi, F., Caruso, C. et al., Sicilian centenarian offspring are more resistant to immune ageing. *Aging Clin. Exp. Res.* 2019. **31**: 125–133.

928 Sanderson, S. L. and Simon, A. K., In aged primary T cells, mitochondrial stress contributes to telomere attrition measured by a novel imaging flow cytometry assay. *Aging Cell* 2017. **16**: 1234–1243.

929 Arnold, C. R., Pritz, T., Brunner, S., Knabb, C., Salvenmoser, W., Holzwarth, B., Thedieck, K. et al., T cell receptor-mediated activation is a potent inducer of macroautophagy in human CD8(+)CD28(+) T cells but not in CD8(+)CD28(-) T cells. *Exp. Gerontol.* 2014. **54**: 75–83.

930 Pellicano, M., Buffa, S., Goldeck, D., Bulati, M., Martorana, A., Caruso, C., Colonna-Romano, G. et al., Evidence for less marked potential signs of T-cell immunosenescence in centenarian offspring than in the general age-matched population. *J. Gerontol. A Biol. Sci. Med. Sci.* 2014. **69**: 495–504.

931 Derhovanessian, E., Maier, A. B., Beck, R., Jahn, G., Hahnel, K., Slagboom, P. E., de Craen, A. J. et al., Hallmark features of immunosenescence are absent in familial longevity. *J. Immunol.* 2010. **185**: 4618–4624.

932 Raz, Y., Guerrero-Ros, I., Maier, A., Slagboom, P. E., Atzmon, G., Barzilai, N. and Macian, F., Activation-induced autophagy is preserved in CD4+ T-cells in familial longevity. *J. Gerontol. A Biol. Sci. Med. Sci.* 2017. **72**: 1201–1206.

933 Duggal, N. A., Pollock, R. D., Lazarus, N. R., Harridge, S. and Lord, J. M., Major features of immunesenescence, including reduced thymic output, are ameliorated by high levels of physical activity in adulthood. *Aging Cell* 2018. **17**.

934 Senda, T., Dogra, P., Granot, T., Furuhashi, K., Snyder, M. E., Carpenter, D. J., Szabo, P. A. et al., Microanatomical dissection of human intestinal T-cell immunity reveals site-specific changes in gut-associated lymphoid tissues over life. *Mucosal Immunol.* 2019. **12**(2): 378–389.

935 Thome, J. J., Bickham, K. L., Ohmura, Y., Kubota, M., Matsuoka, N., Gordon, C., Granot, T. et al., Early-life compartmentalization of human T cell differentiation and regulatory function in mucosal and lymphoid tissues. *Nat. Med.* 2016. **22**(1): 72–77.

936 Seddiki, N., Santner-Nanan, B., Martinson, J., Zaunders, J., Sasson, S., Landay, A., Solomon, M. et al., Expression of interleukin (IL)-2 and IL-7 receptors discriminates between human regulatory and activated T cells. *J. Exp. Med.* 2006. **203**(7): 1693–1700.

937 Kverneland, A. H., Streitz, M., Geissler, E., Hutchinson, J., Vogt, K., Boes, D., Niemann, N. et al., Age and gender leucocytes variances and references values generated using the standardized ONE-Study protocol. *Cytometry A* 2016. **89**(6): 543–564.

938 Abbas, A. K., Benoist, C., Bluestone, J. A., Campbell, D. J., Ghosh, S., Hori, S., Jiang, S. et al., Regulatory T cells: recommendations to simplify the nomenclature. *Nat. Immunol.* 2013. **14**(4): 307–308.

939 Himmel, M. E., MacDonald, K. G., Garcia, R. V., Steiner, T. S. and Levings, M. K., Helios+ and Helios- cells coexist within the natural FOXP3+ T regulatory cell subset in humans. *J. Immunol.* 2013. **190**(5): 2001–2008.

940 Bin Dhuban, K., d'Hennezel, E., Nashi, E., Bar-Or, A., Rieder, S., Shevach, E. M., Nagata, S. et al., Coexpression of TIGIT and FCRL3 identifies Helios+ human memory regulatory T cells. *J. Immunol.* 2015. **194**(8): 3687–3696.

941 Milpied, P., Renand, A., Bruneau, J., Mendes-da-Cruz, D. A., Jacquelin, S., Asnafi, V., Rubio, M. T. et al., Neuropilin-1 is not a marker of human Foxp3+ Treg. *Eur. J. Immunol.* 2009. **39**(6): 1466–1471.

942 Duhen, T., Duhen, R., Lanzavecchia, A., Sallusto, F. and Campbell, D. J., Functionally distinct subsets of human FOXP3+ Treg cells that phenotypically mirror effector Th cells. *Blood* 2012. **119**(19): 4430–4440.

943 MacDonald, K. G., Dawson, N. A., Huang, Q., Dunne, J. V., Levings, M. K. and Broady, R., Regulatory T cells produce profibrotic cytokines in the skin of patients with systemic sclerosis. *J. Allergy Clin. Immunol.* 2015. **135**(4): e946–e949.

944 Pesenacker, A. M., Bending, D., Ursu, S., Wu, Q., Nistala, K. and Wedderburn, L. R., CD161 defines the subset of FoxP3+ T cells capable of producing proinflammatory cytokines. *Blood* 2013. **121**(14): 2647–2658.

945 Ferreira, R. C., Rainbow, D. B., Rubio Garcia, A., Pekalski, M. L., Porter, L., Oliveira, J. J., Waldron-Lynch, F. et al., Human IL-6R(hi)TIGIT(-)

CD4(+)CD127(low)CD25(+) T cells display potent in vitro suppressive capacity and a distinct Th17 profile. *Clin. Immunol.* 2017. **179**: 25–39.

946 Hoeppli, R. E., MacDonald, K. N., Leclair, P., Fung, V. C. W., Mojibian, M., Gillies, J., Rahavi, S. M. R. et al., Tailoring the homing capacity of human Tregs for directed migration to sites of Th1-inflammation or intestinal regions. *Am. J. Transplant* 2019. **19**: 62–76.

947 Allan, S. E., Crome, S. Q., Crellin, N. K., Passerini, L., Steiner, T. S., Bacchetta, R., Roncarolo, M. G. et al., Activation-induced FOXP3 in human T effector cells does not suppress proliferation or cytokine production. *Int. Immunol.* 2007. **19**(4): 345–354.

948 Pesenacker, A. M., Wang, A. Y., Singh, A., Gillies, J., Kim, Y., Piccirillo, C. A., Nguyen, D. et al., A regulatory T-cell gene signature is a specific and sensitive biomarker to identify children with new-onset type 1 diabetes. *Diabetes* 2016. **65**(4): 1031–1039.

949 Spreafico, R., Rossetti, M., van den Broek, T., Jansen, N. J., Zhang, H., Moshref, M., Prakken, B., van Loosdregt, J., van Wijk, F. and Albani, S., A sensitive protocol for FOXP3 epigenetic analysis in scarce human samples. *Eur. J. Immunol.* 2014. **44**(10): 3141–3143.

950 Rainbow, D. B., Yang, X., Burren, O., Pekalski, M. L., Smyth, D. J., Klarqvist, M. D., Penkett, C. J. et al., Epigenetic analysis of regulatory T cells using multiplex bisulfite sequencing. *Eur. J. Immunol.* 2015. **45**(11): 3200–3203.

951 Liu, W., Putnam, A. L., Xu-Yu, Z., Szot, G. L., Lee, M. R., Zhu, S., Gottlieb, P. A. et al., CD127 expression inversely correlates with FoxP3 and suppressive function of human CD4+ T reg cells. *J. Exp. Med.* 2006. **203**(7): 1701–1711.

952 Wang, J., Ioan-Facsinay, A., van der Voort, E. I., Huizinga, T. W. and Toes, R. E., Transient expression of FOXP3 in human activated non-regulatory CD4+ T cells. *Eur. J. Immunol.* 2007. **37**(1): 129–138.

953 Wu, D., Han, J. M., Yu, X., Lam, A. J., Hoeppli, R. E., Pesenacker, A. M., Huang, Q. et al., Characterization of regulatory T cells in obese omental adipose tissue in humans. *Eur. J. Immunol.* 2019. **49**(2): 336–347.

954 Dijke, I. E., Hoeppli, R. E., Ellis, T., Pearcey, J., Huang, Q., McMurchy, A. N., Boer, K. et al., Discarded human thymus is a novel source of stable and long-lived therapeutic regulatory T cells. *Am. J. Transplant* 2016. **16**(1): 58–71.

955 Mason, G. M., Lowe, K., Melchiotti, R., Ellis, R., de Rinaldis, E., Peakman, M., Heck, S., Lombardi, G. et al., Phenotypic complexity of the human regulatory T cell compartment revealed by mass cytometry. *J. Immunol.* 2015. **195**(5): 2030–2037.

956 Dawson, N. A. J., Lam, A. J., Cook, L., Hoeppli, R. E., Broady, R., Pesenacker, A. M. and Levings, M. K., An optimized method to measure human FOXP3(+) regulatory T cells from multiple tissue types using mass cytometry. *Eur. J. Immunol.* 2018. **48**(8): 1415–1419.

957 Chen, X. and Oppenheim, J. J., Resolving the identity myth: key markers of functional CD4+FoxP3+ regulatory T cells. *Int. Immunopharmacol.* 2011. **11**(10): 1489–1496.

958 Ward-Hartstonge, K. A. and Kemp, R. A., Regulatory T-cell heterogeneity and the cancer immune response. *Clin. Transl. Immunol.* 2017. **6**(9): e154.

959 Groux, H., O'Garra, A., Bigler, M., Rouleau, M., Antonenko, S., de Vries, J. E. and Roncarolo, M. G., A CD4+ T-cell subset inhibits antigen-specific T-cell responses and prevents colitis. *Nature* 1997. **389**(6652): 737–742.

960 Jeurink, P. V., Vissers, Y. M., Rappard, B. and Savelkoul, H. F., T cell responses in fresh and cryopreserved peripheral blood mononuclear cells: kinetics of cell viability, cellular subsets, proliferation, and cytokine production. *Cryobiology* 2008. **57**(2): 91–103.

961 White, A. M. and Wraith, D. C., Tr1-like T cells—an enigmatic regulatory T cell lineage. *Front. Immunol.* 2016. **7**: 355.

962 Tran, D. Q., Andersson, J., Wang, R., Ramsey, H., Unutmaz, D. and Shevach, E. M., GARP (LRRC32) is essential for the surface expression of latent TGF-beta on platelets and activated FOXP3+ regulatory T cells. *Proc. Natl. Acad. Sci. USA* 2009. **106**(32): 13445–13450.

963 Wang, R., Kozhaya, L., Mercer, F., Khaitan, A., Fujii, H. and Unutmaz, D., Expression of GARP selectively identifies activated human FOXP3+ regulatory T cells. *Proc. Natl. Acad. Sci. USA* 2009. **106**(32): 13439–13444.

964 Camisaschi, C., Casati, C., Rini, F., Perego, M., De Filippo, A., Triebel, F., Parmiani, G. et al., LAG-3 expression defines a subset of CD4(+)CD25(high)Foxp3(+) regulatory T cells that are expanded at tumor sites. *J. Immunol.* 2010. **184**(11): 6545–6551.

965 Gagliani, N., Magnani, C. F., Huber, S., Gianolini, M. E., Pala, M., Licona-Limon, P., Guo, B. et al., Coexpression of CD49b and LAG-3 identifies human and mouse T regulatory type 1 cells. *Nat. Med.* 2013. **19**(6): 739–746.

966 Raimondi, G., Shufesky, W. J., Tokita, D., Morelli, A. E. and Thomson, A. W., Regulated compartmentalization of programmed cell death-1 discriminates CD4+CD25+ resting regulatory T cells from activated T cells. *J. Immunol.* 2006. **176**(5): 2808–2816.

967 Lam, A., MacDonald, J. K. N., Pesenacker, A. M., Juvet, S. C., Morishita, K. A., Bressler, B., iGenoMed, C. et al., Innate control of tissue-reparative human regulatory T cells. *J. Immunol.* 2019. **202**: 2195–2209.

968 Borsellino, G., Kleinewietfeld, M., Di Mitri, D., Sternjak, A., Diamantini, A., Giometto, R., Hopner, S. et al., Expression of ectonucleotidase CD39 by Foxp3+ Treg cells: hydrolysis of extracellular ATP and immune suppression. *Blood* 2007. **110**(4): 1225–1232.

969 Deaglio, S., Dwyer, K. M., Gao, W., Friedman, D., Usheva, A., Erat, A., Chen, J. F. et al., Adenosine generation catalyzed by CD39 and CD73 expressed on regulatory T cells mediates immune suppression. *J. Exp. Med.* 2007. **204**(6): 1257–1265.

970 Rissiek, A., Baumann, I., Cuapio, A., Mautner, A., Kolster, M., Arck, P. C., Dodge-Khatami, A. et al., The expression of CD39 on regulatory T cells is genetically driven and further upregulated at sites of inflammation. *J. Autoimmun.* 2015. **58**: 12–20.

971 Baecher-Allan, C., Wolf, E. and Hafler, D. A., MHC class II expression identifies functionally distinct human regulatory T cells. *J. Immunol.* 2006. **176**(8): 4622–4631.

972 Linsley, P. S., Brady, W., Urnes, M., Grosmaire, L. S., Damle, N. K. and Ledbetter, J. A., CTLA-4 is a second receptor for the B cell activation antigen B7. *J. Exp. Med.* 1991. **174**(3): 561–569.

973 Qureshi, O. S., Zheng, Y., Nakamura, K., Attridge, K., Manzotti, C., Schmidt, E. M., Baker, J. et al., Trans-endocytosis of CD80 and CD86: a molecular basis for the cell-extrinsic function of CTLA-4. *Science* 2011. **332**(6029): 600–603.

974 Norton, S. E., Ward-Hartstonge, K. A., McCall, J. L., Leman, J. K. H., Taylor, E. S., Munro, F., Black, M. A. et al., High-dimensional mass cytometric analysis reveals an increase in effector regulatory T cells as a distinguishing feature of colorectal tumors. *J. Immunol.* 2019. **202**: 1871–1884.

975 Kleinewietfeld, M., Starke, M., Di Mitri, D., Borsellino, G., Battistini, L., Rotzschke, O. and Falk, K., CD49d provides access to "untouched" human Foxp3+ Treg free of contaminating effector cells. *Blood* 2009. **113**(4): 827–836.

976 Santegoets, S. J., Dijkgraaf, E. M., Battaglia, A., Beckhove, P., Britten, C. M., Gallimore, A., Godkin, A. et al., Monitoring regulatory T cells in clinical samples: consensus on an essential marker set and gat-

ing strategy for regulatory T cell analysis by flow cytometry. *Cancer Immunol. Immunother.* 2015. **64**(10): 1271–1286.

977 Dwyer, K. M., Hanidziar, D., Putheti, P., Hill, P. A., Pommey, S., McRae, J. L., Winterhalter, A. et al., Expression of CD39 by human peripheral blood CD4+ CD25+ T cells denotes a regulatory memory phenotype. *Am. J. Transplant* 2010. **10**(11): 2410–2420.

978 Schuler, P. J., Schilling, B., Harasymczuk, M., Hoffmann, T. K., Johnson, J., Lang, S. and Whiteside, T. L., Phenotypic and functional characteristics of CD4+ CD39+ FOXP3+ and CD4+ CD39+ FOXP3neg T-cell subsets in cancer patients. *Eur. J. Immunol.* 2012. **42**(7): 1876–1885.

979 Iellem, A., Colantonio, L. and D'Ambrosio, D., Skin-versus gut-skewed homing receptor expression and intrinsic CCR4 expression on human peripheral blood CD4+CD25+ suppressor T cells. *Eur. J. Immunol.* 2003. **33**(6): 1488–1496.

980 Battaglia, A., Buzzonetti, A., Monego, G., Peri, L., Ferrandina, G., Fanfani, F., Scambia, G. et al., Neuropilin-1 expression identifies a subset of regulatory T cells in human lymph nodes that is modulated by preoperative chemoradiation therapy in cervical cancer. *Immunology* 2008. **123**(1): 129–138.

981 Griseri, T., Asquith, M., Thompson, C. and Powrie, F., OX40 is required for regulatory T cell-mediated control of colitis. *J. Exp. Med.* 2010. **207**(4): 699–709.

982 Seddiki, N., Cook, L., Hsu, D. C., Phetsouphanh, C., Brown, K., Xu, Y., Kerr, S. J. et al., Human antigen-specific CD4(+) CD25(+) CD134(+) CD39(+) T cells are enriched for regulatory T cells and comprise a substantial proportion of recall responses. *Eur. J. Immunol.* 2014. **44**(6): 1644–1661.

983 Ivison, S., Malek, M., Garcia, R. V., Broady, R., Halpin, A., Richaud, M., Brant, R. F. et al., A standardized immune phenotyping and automated data analysis platform for multicenter biomarker studies. *JCI Insight* 2018. **3**(23).

984 Fox, B. C., Bignone, P. A., Brown, P. J. and Banham, A. H., Defense of the clone: antibody 259D effectively labels human FOXP3 in a variety of applications. *Blood* 2008. **111**(7): 3897–3899.

985 Pillai, V. and Karandikar, N. J., Attack on the clones? Human FOXP3 detection by PCH101, 236A/E7, 206D, and 259D reveals 259D as the outlier with lower sensitivity. *Blood* 2008. **111**(1): 463–464; author reply 464–466.

986 Law, J. P., Hirschkorn, D. F., Owen, R. E., Biswas, H. H., Norris, P. J. and Lanteri, M. C., The importance of Foxp3 antibody and fixation/permeabilization buffer combinations in identifying CD4+CD25+Foxp3+ regulatory T cells. *Cytometry A* 2009. **75**(12): 1040–1050.

987 Kaur, G., Goodall, J. C., Jarvis, L. B. and Hill Gaston, J. S., Characterisation of Foxp3 splice variants in human CD4+ and CD8+ T cells–identification of Foxp3Delta7 in human regulatory T cells. *Mol. Immunol.* 2010. **48**(1-3): 321–332.

988 Mahnke, Y. D., Beddall, M. H. and Roederer, M., OMIP-015: human regulatory and activated T-cells without intracellular staining. *Cytometry A* 2013. **83**(2): 179–181.

989 Terstappen, L. W., Meiners, H. and Loken, M. R., A rapid sample preparation technique for flow cytometric analysis of immunofluorescence allowing absolute enumeration of cell subpopulations. *J. Immunol. Methods* 1989. **123**(1): 103–112.

990 Bonecchi, R., Bianchi, G., Bordignon, P. P., D'Ambrosio, D., Lang, R., Borsatti, A., Sozzani, S. et al., Differential expression of chemokine receptors and chemotactic responsiveness of type 1 T helper cells (Th1s) and Th2s. *J. Exp. Med.* 1998. **187**(1): 129–134.

991 Gosselin, A., Monteiro, P., Chomont, N., Diaz-Griffero, F., Said, E. A., Fonseca, S., Wacleche, V. et al., Peripheral blood CCR4+CCR6+ and CXCR3+CCR6+CD4+ T cells are highly permissive to HIV-1 infection. *J. Immunol.* 2010. **184**(3): 1604–1616.

992 Halim, L., Romano, M., McGregor, R., Correa, I., Pavlidis, P., Grageda, N., Hoong, S. J. et al., An atlas of human regulatory T helper-like cells reveals features of Th2-like Tregs that support a tumorigenic environment. *Cell Rep.* 2017. **20**(3): 757–770.

993 Bowcutt, R., Malter, L. B., Chen, L. A., Wolff, M. J., Robertson, I., Rifkin, D. B., Poles, M. et al., Isolation and cytokine analysis of lamina propria lymphocytes from mucosal biopsies of the human colon. *J. Immunol. Methods* 2015. **421**: 27–35.

994 Zheng, J., Liu, Y., Lau, Y. L. and Tu, W., γδ-T cells: An unpolished sword in human anti-infection immunity. *Cell. Mol. Immunol.* 2013. **10**: 50–57.

995 Silva-Santos, B., Serre, K. and Norell, H., γδ T cells in cancer. *Nat. Rev. Immunol.* 2015. **15**: 23–38.

996 Tanaka, Y., Sano, S., Nieves, E., De Libero, G., Rosa, D., Modlin, R. L., Brenner, M. B. et al., Nonpeptide ligands for γδ T cells. *Proc. Natl. Acad. Sci. USA* 1994. **91**: 8175–8179.

997 Godfrey, D. I., Uldrich, A. P., McCluskey, J., Rossjohn, J. and Moody, D. B., The burgeoning family of unconventional T cells. *Nat. Immunol.* 2015. **16**: 1114–1123.

998 Halary, F., Pitard, V., Dlubek, D., Krzysiek, R., de la Salle, H., Merville, P., Dromer, C. et al., Shared reactivity of Vδ2neg γδ T cells against cytomegalovirus-infected cells and tumor intestinal epithelial cells. *J. Exp. Med.* 2005. **201**: 1567–1578.

999 Morita, C. T., Chenggang, J., Sarikonda, G. and Wong, H., Nonpeptide antigens, presentation mechanisms, and immunological memory of human Vγ2Vδ2 T cells: discriminating friend from foe through the recognition of prenyl pyrophosphate antigens. *Immunol. Rev.* 2007. **215**: 59–76.

1000 Davey, M. S., Willcox, C. R., Hunter, S., Kasatskaya, S. A., Remmerswaal, E. B. M., Salim, M., Mohammed, F. et al., The human Vδ2+ T-cell compartment comprises distinct innate-like Vγ9+ and adaptive Vγ9- subsets. *Nat. Commun.* 2018. **9**: 1–14.

1001 Riganti, C., Massaia, M., Davey, M. S. and Eberl, M., Human gammadelta T-cell responses in infection and immunotherapy: common mechanisms, common mediators? *Eur. J. Immunol.* 2012. **42**: 1668–1676.

1002 Chien, Y. H., Meyer, C. and Bonneville, M., γδ T cells: first line of defense and beyond. *Annu. Rev. Immunol.* 2014. **32**: 121–155.

1003 Davodeau, F., Peyrat, M. A., Hallet, M. M., Houde, I., And, H. V. and Bonneville, M., Peripheral selection of antigen receptor junctional features in a major human γδ subset. *Eur. J. Immunol.* 1993. **23**: 804–808.

1004 Parker, C. M., Groh, V., Band, H., Porcelli, S. A., Morita, C., Fabbi, M., Glass, D. et al., Evidence for extrathymic changes in the T cell receptor gamma/delta repertoire. *J. Exp. Med.* 1990. **171**: 1597–1612.

1005 Dimova, T., Brouwer, M., Gosselin, F., Tassignon, J., Leo, O., Donner, C., Marchant, A. et al., Effector Vγ9Vδ2 T cells dominate the human fetal γδ T-cell repertoire. *Proc. Natl. Acad. Sci. USA* 2015. **112**: E556–E565.

1006 Willcox, C. R., Davey, M. S. and Willcox, B. E., Development and selection of the human Vγ9Vδ2+ T-cell repertoire. *Front. Immunol.* 2018. **9**: 1501.

1007 Hunter, S., Willcox, C. R., Davey, M. S., Kasatskaya, Sofya, A., Jeffery, H. C., Chudakov, D. M. et al., Human liver infiltrating γδ T cells are composed of clonally expanded circulating and tissue-resident populations. *J. Hepatol.* 2018. **69**: 654–665.

1008 Davey, M. S., Willcox, C. R., Baker, A. T., Hunter, S. and Willcox, B. E., Recasting human Vδ1 lymphocytes in an adaptive role. *Trends Immunol.* 2018. **39**: 446–459.

1009　Davey, M. S., Willcox, C. R., Joyce, S. P., Ladell, K., Kasatskaya, S. A., McLaren, J. E., Hunter, S. et al., Clonal selection in the human Vδ1 T cell repertoire indicates γδ TCR-dependent adaptive immune surveillance. Nat. Commun. 2017. 8: 1–15.

1010　Ravens, S., Schultze-Florey, C., Raha, S., Sandrock, I., Drenker, M., Oberdörfer, L., Reinhardt, A. et al., Human γδ T cells are quickly reconstituted after stem-cell transplantation and show adaptive clonal expansion in response to viral infection. Nat. Immunol. 2017. 18: 393–401.

1011　Correia, D., Fogli, M., Hudspeth, K., Gomes da Silva, M., Mavilio, D. and Silva-Santos, B., Differentiation of human peripheral blood Vδ1+ T cell expressing the natural cytotoxicity receptor NKp30 for recognition of lymphoid leukemia cells. Blood 2011. 118: 992–1001.

1012　Bouet-Toussaint, F., Cabillic, F., Toutirais, O., Le Gallo, M., Thomas de la Pintiere, C., Genetet, N., Meunier, B. et al., Vγ9Vδ2 T cell-mediated recognition of human solid tumors. Potential for immunotherapy of hepatocellular and colorectal carcinomas. Cancer Immunol. Immunother. 2008. 57: 531–539.

1013　Mattarollo, S. R., Kenna, T., Nieda, M. and Nicol, A. J., Chemotherapy and zoledronate sensitize solid tumour cells to Vγ9Vδ2 T cell cytotoxicity. Cancer Immunol. Immunother. 2007. 56: 1285–1297.

1014　Almeida, A. R. M., Correia, D. V., Fernandes-Platzgummer, A., da Silva, C. L., Gomes da Silva, M., Anjos, D. R. and Silva-Santos, B., Delta one T cells for immunotherapy of chronic lymphocytic leukemia: clinical-grade expansion/differentiation and preclinical proof-of-concept. Clin. Cancer Res. 2016. 22: 5795–5804.

1015　Ryan, P. L., Sumaria, N., Holland, C. J., Bradford, C. M., Izotova, N., Grandjean, C. L., Jawad, A. S. et al., Heterogeneous yet stable Vδ2(+) T-cell profiles define distinct cytotoxic effector potentials in healthy human individuals. Proc. Natl. Acad. Sci. USA 2016. 113: 14378–14383.

1016　Kinjo, Y. and Ueno, K., iNKT cells in microbial immunity: recognition of microbial glycolipids. Microbiol. Immunol. 2011. 55: 472–482.

1017　Shissler, S. C., Bollino, D. R., Tiper, I. V., Bates, J. P., Derakhshandeh, R. and Webb, T. J., Immunotherapeutic strategies targeting natural killer T cell responses in cancer. Immunogenetics 2016. 68: 623–638.

1018　Godfrey, D. I., Le Nours, J., Andrews, D. M., Uldrich, A. P. and Rossjohn, J., Unconventional T cell targets for cancer immunotherapy. Immunity 2018. 48: 453–473.

1019　Pellicci, D. G. and Uldrich, A. P., Unappreciated diversity within the pool of CD1d-restricted T cells. Semin. Cell. Dev. Biol. 2018. 84: 42–47.

1020　Godfrey, D. I., MacDonald, H. R., Kronenberg, M., Smyth, M. J. and Van Kaer, L., NKT cells: what's in a name? Nat. Rev. Immunol. 2004. 4: 231–237.

1021　Thierry, A., Robin, A., Giraud, S., Minouflet, S., Barra, A., Bridoux, F., Hauet, T. et al., Identification of invariant natural killer T cells in porcine peripheral blood. Vet. Immunol. Immunopathol. 2012. 149: 272–279.

1022　Monzon-Casanova, E., Paletta, D., Starick, L., Muller, I., Sant'Angelo, D. B., Pyz, E. and Herrmann, T., Direct identification of rat iNKT cells reveals remarkable similarities to human iNKT cells and a profound deficiency in LEW rats. Eur. J. Immunol. 2013. 43: 404–415.

1023　Gansuvd, B., Hubbard, W. J., Hutchings, A., Thomas, F. T., Goodwin, J., Wilson, S. B., Exley, M. A. et al., Phenotypic and functional characterization of long-term cultured rhesus macaque spleen-derived NKT cells. J. Immunol. 2003. 171: 2904–2911.

1024　Yasuda, N., Masuda, K., Tsukui, T., Teng, A. and Ishii, Y., Identification of canine natural CD3-positive T cells expressing an invariant T-cell receptor alpha chain. Vet. Immunol. Immunopathol. 2009. 132: 224–231.

1025　Kawano, T., Cui, J., Koezuka, Y., Toura, I., Kaneko, Y., Motoki, K., Ueno, H. et al., CD1d-restricted and TCR-mediated activation of valpha14 NKT cells by glycosylceramides. Science 1997. 278: 1626–1629.

1026　Lopez-Sagaseta, J., Kung, J. E., Savage, P. B., Gumperz, J. and Adams, E. J., The molecular basis for recognition of CD1d/alpha-galactosylceramide by a human non-Valpha24 T cell receptor. PLoS Biol. 2012. 10: e1001412.

1027　Gadola, S. D., Dulphy, N., Salio, M. and Cerundolo, V., Valpha24-JalphaQ-independent, CD1d-restricted recognition of alpha-galactosylceramide by human CD4(+) and CD8alphabeta(+) T lymphocytes. J. Immunol. 2002. 168: 5514–5520.

1028　Le Nours, J., Praveena, T., Pellicci, D. G., Gherardin, N. A., Ross, F. J., Lim, R. T., Besra, G. S., Keshipeddy, S. et al., Atypical natural killer T-cell receptor recognition of CD1d-lipid antigens. Nat. Commun. 2016. 7: 10570.

1029　Gadola, S. D., Koch, M., Marles-Wright, J., Lissin, N. M., Shepherd, D., Matulis, G., Harlos, K. et al., Structure and binding kinetics of three different human CD1d-alpha-galactosylceramide-specific T cell receptors. J. Exp. Med. 2006. 203: 699–710.

1030　Brigl, M., van den Elzen, P., Chen, X., Meyers, J. H., Wu, D., Wong, C. H., Reddington, F. et al., Conserved and heterogeneous lipid antigen specificities of CD1d-restricted NKT cell receptors. J. Immunol. 2006. 176: 3625–3634.

1031　Uldrich, A. P., Le Nours, J., Pellicci, D. G., Gherardin, N. A., McPherson, K. G., Lim, R. T., Patel, O., Beddoe, T. et al., CD1d-lipid antigen recognition by the gammadelta TCR. Nat. Immunol. 2013. 14: 1137–1145.

1032　Kobayashi, E., Motoki, K., Uchida, T., Fukushima, H. and Koezuka, Y., KRN7000, a novel immunomodulator, and its antitumor activities. Oncol. Res. 1995. 7: 529–534.

1033　Morita, M., Motoki, K., Akimoto, K., Natori, T., Sakai, T., Sawa, E., Yamaji, K. et al., Structure-activity relationship of alpha-galactosylceramides against B16-bearing mice. J. Med. Chem. 1995. 38: 2176–2187.

1034　Nair, S. and Dhodapkar, M. V., Natural killer T cells in cancer immunotherapy. Front. Immunol. 2017. 8: 1178.

1035　Rossjohn, J., Pellicci, D. G., Patel, O., Gapin, L. and Godfrey, D. I., Recognition of CD1d-restricted antigens by natural killer T cells. Nat. Rev. Immunol. 2012. 12: 845–857.

1036　Miyamoto, K., Miyake, S. and Yamamura, T., A synthetic glycolipid prevents autoimmune encephalomyelitis by inducing TH2 bias of natural killer T cells. Nature 2001. 413: 531–534.

1037　Yu, K. O., Im, J. S., Molano, A., Dutronc, Y., Illarionov, P. A., Forestier, C., Fujiwara, N. et al., Modulation of CD1d-restricted NKT cell responses by using N-acyl variants of alpha-galactosylceramides. Proc. Natl. Acad. Sci. USA 2005. 102: 3383–3388.

1038　Schmieg, J., Yang, G., Franck, R. W. and Tsuji, M., Superior protection against malaria and melanoma metastases by a C-glycoside analogue of the natural killer T cell ligand alpha-Galactosylceramide. J. Exp. Med. 2003. 198: 1631–1641.

1039　Wun, K. S., Cameron, G., Patel, O., Pang, S. S., Pellicci, D. G., Sullivan, L. C., Keshipeddy, S. et al., A molecular basis for the exquisite CD1d-restricted antigen specificity and functional responses of natural killer T cells. Immunity 2011. 34: 327–339.

1040　Wun, K. S., Ross, F., Patel, O., Besra, G. S., Porcelli, S. A., Richardson, S. K., Keshipeddy, S. et al., Human and mouse type I natural killer T cell antigen receptors exhibit different fine specificities for CD1d-antigen complex. J. Biol. Chem. 2012. 287: 39139–39148.

1041 **Freigang, S., Landais, E., Zadorozhny, V., Kain, L., Yoshida, K., Liu, Y., Deng, S. et al.**, Scavenger receptors target glycolipids for natural killer T cell activation. *J. Clin. Invest.* 2012. **122**: 3943–3954.

1042 http://tetramer.yerkes.emory.edu/reagents/cd1

1043 **Gumperz, J. E., Miyake, S., Yamamura, T. and Brenner, M. B.**, Functionally distinct subsets of CD1d-restricted natural killer T cells revealed by CD1d tetramer staining. *J. Exp. Med.* 2002. **195**: 625–636.

1044 **Sidobre, S. and Kronenberg, M.**, CD1 tetramers: a powerful tool for the analysis of glycolipid-reactive T cells. *J. Immunol. Methods* 2002. **268**: 107–121.

1045 **Boyson, J. E., Rybalov, B., Koopman, L. A., Exley, M., Balk, S. P., Racke, F. K., Schatz, F. et al.**, CD1d and invariant NKT cells at the human maternal-fetal interface. *Proc. Natl. Acad. Sci. USA* 2002. **99**: 13741–13746.

1046 **Thomas, S. Y., Hou, R., Boyson, J. E., Means, T. K., Hess, C., Olson, D. P., Strominger, J. L. et al.**, CD1d-restricted NKT cells express a chemokine receptor profile indicative of Th1-type inflammatory homing cells. *J. Immunol.* 2003. **171**: 2571–2580.

1047 **Aricescu, A. R., Lu, W. and Jones, E. Y.**, A time- and cost-efficient system for high-level protein production in mammalian cells. *Acta Crystallogr. D Biol. Crystallogr.* 2006. **62**: 1243–1250.

1048 **Ng, S. S., Souza-Fonseca-Guimaraes, F., Rivera, F. L., Amante, F. H., Kumar, R., Gao, Y., Sheel, M. et al.**, Rapid loss of group 1 innate lymphoid cells during blood stage Plasmodium infection. *Clin. Transl. Immunol.* 2018. **7**: e1003.

1049 http://www.enzolifesciences.com/BML-SL232/krn7000/

1050 https://avantilipids.com/product/867000

1051 **Boyum, A.**, Separation of leukocytes from blood and bone marrow. Introduction. *Scand. J. Clin. Lab. Invest. Suppl.* 1968. **97**: 7.

1052 **Lee, P. T., Benlagha, K., Teyton, L. and Bendelac, A.**, Distinct functional lineages of human V(alpha)24 natural killer T cells. *J. Exp. Med.* 2002. **195**: 637–641.

1053 **Montoya, C. J., Pollard, D., Martinson, J., Kumari, K., Wasserfall, C., Mulder, C. B., Rugeles, M. T. et al.**, Characterization of human invariant natural killer T subsets in health and disease using a novel invariant natural killer T cell-clonotypic monoclonal antibody, 6B11. *Immunology* 2007. **122**: 1–14.

1054 **Cameron, G., Pellicci, D. G., Uldrich, A. P., Besra, G. S., Illarionov, P., Williams, S. J., La Gruta, N. L. et al.**, Antigen Specificity of Type I NKT Cells Is Governed by TCR beta-Chain Diversity. *J Immunol* 2015. **195**: 4604–4614.

1055 https://www.miltenyibiotec.com/AU-en/products/macs-cell-separation/cell-separation-reagents/microbeads-and-isolation-kits/any-cell-type/anti-pe-microbeads.html

1056 **Rossjohn, J., Gras, S., Miles, J. J., Turner, S. J., Godfrey, D. I. and McCluskey, J.**, T cell antigen receptor recognition of antigen-presenting molecules. *Annu. Rev. Immunol.* 2015. **33**: 169–200.

1057 **Kjer-Nielsen, L., Patel, O., Corbett, A. J., Le Nours, J., Meehan, B., Liu, L., Bhati, M., Chen, Z. et al.**, MR1 presents microbial vitamin B metabolites to MAIT cells. *Nature* 2012. **491**: 717–723.

1058 **Kjer-Nielsen, L., Corbett, A. J., Chen, Z., Liu, L., Mak, J. Y., Godfrey, D. I., Rossjohn, J. et al.**, An overview on the identification of MAIT cell antigens. *Immunol. Cell. Biol.* 2018. **96**: 573–587.

1059 **Koay, H. F., Godfrey, D. I. and Pellicci, D. G.**, Development of mucosal-associated invariant T cells. *Immunol. Cell. Biol.* 2018.

1060 **Gherardin, N. A., Souter, M. N., Koay, H. F., Mangas, K. M., Seemann, T., Stinear, T. P., Eckle, S. B. et al.**, Human blood MAIT cell subsets defined using MR1 tetramers. *Immunol. Cell. Biol.* 2018. **96**: 507–525.

1061 **Le Bourhis, L., Martin, E., Peguillet, I., Guihot, A., Froux, N., Core, M., Levy, E., Dusseaux, M. et al.**, Antimicrobial activity of mucosal-associated invariant T cells. *Nat. Immunol.* 2010. **11**: 701–708.

1062 **Tang, X. Z., Jo, J., Tan, A. T., Sandalova, E., Chia, A., Tan, K. C., Lee, K. H. et al.**, IL-7 licenses activation of human liver intrasinusoidal mucosal-associated invariant T cells. *J. Immunol.* 2013. **190**: 3142–3152.

1063 **Dusseaux, M., Martin, E., Serriari, N., Peguillet, I., Premel, V., Louis, D., Milder, M. et al.**, Human MAIT cells are xenobiotic-resistant, tissue-targeted, CD161hi IL-17-secreting T cells. *Blood* 2011. **117**: 1250–1259.

1064 **Walker, L. J., Kang, Y. H., Smith, M. O., Tharmalingham, H., Ramamurthy, N., Fleming, V. M., Sahgal, N. et al.**, Human MAIT and CD8alphaalpha cells develop from a pool of type-17 precommitted CD8+ T cells. *Blood* 2012. **119**: 422–433.

1065 **Le Bourhis, L., Dusseaux, M., Bohineust, A., Bessoles, S., Martin, E., Premel, V., Core, M., Sleurs, D. et al.**, MAIT cells detect and efficiently lyse bacterially-infected epithelial cells. *PLoS Pathog.* 2013. **9**: e1003681.

1066 **Meermeier, E. W., Harriff, M. J., Karamooz, E. and Lewinsohn, D. M.**, MAIT cells and microbial immunity. *Immunol. Cell. Biol.* 2018.

1067 **Wang, H., D'Souza, C., Lim, X. Y., Kostenko, L., Pediongco, T. J., Eckle, S. B. G., Meehan, B. S. et al.**, MAIT cells protect against pulmonary Legionella longbeachae infection. *Nat. Commun.* 2018. **9**: 3350.

1068 **D'Souza, C., Chen, Z. and Corbett, A. J.**, Revealing the protective and pathogenic potential of MAIT cells. *Mol. Immunol.* 2018. **103**: 46–54.

1069 **Ussher, J. E., Bilton, M., Attwod, E., Shadwell, J., Richardson, R., de Lara, C., Mettke, E., Kurioka, A. et al.**, CD161++ CD8+ T cells, including the MAIT cell subset, are specifically activated by IL-12+IL-18 in a TCR-independent manner. *Eur. J. Immunol.* 2014. **44**: 195–203.

1070 **Ussher, J. E., Willberg, C. B. and Klenerman, P.**, MAIT cells and viruses. *Immunol. Cell. Biol.* 2018. **96**: 630–641.

1071 **van Wilgenburg, B., Scherwitzl, I., Hutchinson, E. C., Leng, T., Kurioka, A., Kulicke, C., de Lara, C., Cole, S., Vasanawathana, S. et al.**, MAIT cells are activated during human viral infections. *Nat. Commun.* 2016. **7**: 11653.

1072 **Loh, L., Wang, Z., Sant, S., Koutsakos, M., Jegaskanda, S., Corbett, A. J., Liu, L. et al.**, Human mucosal-associated invariant T cells contribute to antiviral influenza immunity via IL-18-dependent activation. *Proc. Natl. Acad. Sci. USA* 2016. **113**: 10133–10138.

1073 **Rouxel, O. and Lehuen, A.**, Mucosal-associated invariant T cells in autoimmune and immune-mediated diseases. *Immunol. Cell. Biol.* 2018. **96**: 618–629.

1074 **Gibbs, A., Leeansyah, E., Introini, A., Paquin-Proulx, D., Hasselrot, K., Andersson, E., Broliden, K. et al.**, MAIT cells reside in the female genital mucosa and are biased towards IL-17 and IL-22 production in response to bacterial stimulation. *Mucosal Immunol.* 2017. **10**: 35–45.

1075 **Dias, J., Boulouis, C., Gorin, J. B., van den Biggelaar, R., Lal, K. G., Gibbs, A., Loh, L. et al.**, The CD4(-)CD8(-) MAIT cell subpopulation is a functionally distinct subset developmentally related to the main CD8(+) MAIT cell pool. *Proc. Natl. Acad. Sci. USA* 2018. **115**: E11513–E11522.

1076 **Brozova, J., Karlova, I. and Novak, J.**, Analysis of the phenotype and function of the subpopulations of mucosal-associated invariant T cells. *Scand. J. Immunol.* 2016. **84**: 245–251.

1077 **Davanian, H., Gaiser, R. A., Silfverberg, M., Hugerth, L. W., Sobkowiak, M. J., Lu, L., Healy, K. et al.**, Mucosal-associated invariant T cells and oral microbiome in persistent apical periodontitis. *Int. J. Oral. Sci.* 2019. **11**: 16.

1078 **Mori, L., Lepore, M. and De Libero, G.**, The immunology of CD1- and MR1-restricted T cells. *Annu. Rev. Immunol.* 2016. **34**: 479–510.

1079 **Gherardin, N. A., McCluskey, J., Rossjohn, J. and Godfrey, D. I.**, The diverse family of MR1-restricted T cells. *J. Immunol.* 2018. **201**: 2862–2871.

1080 **Martin, E., Treiner, E., Duban, L., Guerri, L., Laude, H., Toly, C., Premel, V. et al.**, Stepwise development of MAIT cells in mouse and human. *PLoS Biol.* 2009. **7**: e54.

1081 **Sharma, P. K., Wong, E. B., Napier, R. J., Bishai, W. R., Ndung'u, T., Kasprowicz, V. O., Lewinsohn, D. A. et al.**, High expression of CD26 accurately identifies human bacteria-reactive MR1-restricted MAIT cells. *Immunology* 2015. **145**: 443–453.

1082 **Gold, M. C., Eid, T., Smyk-Pearson, S., Eberling, Y., Swarbrick, G. M., Langley, S. M., Streeter, P. R. et al.**, Human thymic MR1-restricted MAIT cells are innate pathogen-reactive effectors that adapt following thymic egress. *Mucosal Immunol.* 2013. **6**: 35–44.

1083 **Leeansyah, E., Ganesh, A., Quigley, M. F., Sonnerborg, A., Andersson, J., Hunt, P. W., Somsouk, M. et al.**, Activation, exhaustion, and persistent decline of the antimicrobial MR1-restricted MAIT-cell population in chronic HIV-1 infection. *Blood* 2013. **121**: 1124–1135.

1084 **Koppejan, H., Jansen, D., Hameetman, M., Thomas, R., Toes, R. E. M. and van Gaalen, F. A.**, Altered composition and phenotype of mucosal-associated invariant T cells in early untreated rheumatoid arthritis. *Arthritis Res. Ther.* 2019. **21**: 3.

1085 **Eckle, S. B., Birkinshaw, R. W., Kostenko, L., Corbett, A. J., McWilliam, H. E., Reantragoon, R., Chen, Z. et al.**, A molecular basis underpinning the T cell receptor heterogeneity of mucosal-associated invariant T cells. *J. Exp. Med.* 2014. **211**: 1585–1600.

1086 **Kurioka, A., Jahun, A. S., Hannaway, R. F., Walker, L. J., Fergusson, J. R., Sverremark-Ekstrom, E., Corbett, A. J. et al.**, Shared and distinct phenotypes and functions of human CD161++ Valpha7.2+ T cell subsets. *Front. Immunol.* 2017. **8**: 1031.

1087 **Ben Youssef, G., Tourret, M., Salou, M., Ghazarian, L., Houdouin, V., Mondot, S., Mburu, Y. et al.**, Ontogeny of human mucosal-associated invariant T cells and related T cell subsets. *J. Exp. Med.* 2018. **215**: 459–479.

1088 **Koay, H. F., Gherardin, N. A., Xu, C., Seneviratna, R., Zhao, Z., Chen, Z., Fairlie, D. P. et al.**, Diverse MR1-restricted T cells in mice and humans. *Nat. Commun.* 2019. **10**: 2243.

1089 NTCF, NIH Tetramer Core Facility: Human MR1 Tetramer Staining 2016. https://tetramer.yerkes.emory.edu/sites/default/files/shared/human_mr1_tetramer_staining.pdf

1090 NTCF, NIH Tetramer Core Facility: Tetramer Preparation - Addition of streptavidin, emory.edu 2010. https://tetramer.yerkes.emory.edu/support/protocols#10

1091 **Gherardin, N. A., Keller, A. N., Woolley, R. E., Le Nours, J., Ritchie, D. S., Neeson, P. J., Birkinshaw, R. W. et al.**, Diversity of T cells restricted by the MHC class I-related molecule MR1 facilitates differential antigen recognition. *Immunity* 2016. **44**: 32–45.

1092 **Dias, J., Leeansyah, E. and Sandberg, J. K.**, Multiple layers of heterogeneity and subset diversity in human MAIT cell responses to distinct microorganisms and to innate cytokines. *Proc. Natl. Acad. Sci. USA* 2017. **114**: E5434–E5443.

1093 **Lissina, A., Ladell, K., Skowera, A., Clement, M., Edwards, E., Seggewiss, R., van den Berg, H. A., Gostick, E. et al.**, Protein kinase inhibitors substantially improve the physical detection of T-cells with peptide-MHC tetramers. *J. Immunol. Methods* 2009. **340**: 11–24.

1094 **Wood, G. S. and Warnke, R.**, Suppression of endogenous avidin-binding activity in tissues and its relevance to biotin-avidin detection systems. *J. Histochem. Cytochem.* 1981. **29**: 1196–1204.

1095 **Harriff, M. J., McMurtrey, C., Froyd, C. A., Jin, H., Cansler, M., Null, M., Worley, A. et al.**, MR1 displays the microbial metabolome driving selective MR1-restricted T cell receptor usage. *Sci. Immunol.* 2018. **3**.

1096 **Lepore, M., Kalinichenko, A., Calogero, S., Kumar, P., Paleja, B., Schmaler, M., Narang, V. et al.**, Functionally diverse human T cells recognize non-microbial antigens presented by MR1. *Elife* 2017. **6**.

1097 **Tung, J. W., Mrazek, M. D., Yang, Y., Herzenberg, L. A. and Herzenberg, L. A.**, Phenotypically distinct B cell development pathways map to the three B cell lineages in the mouse. *Proc. Natl. Acad. Sci. USA* 2006. **103**: 6293–6298.

1098 **Manz, R. A., Hauser, A. E., Hiepe, F. and Radbruch, A.**, Maintenance of serum antibody levels. *Annu. Rev. Immunol.* 2005. **23**: 367–386.

1099 **Wen, L., Brill-Dashoff, J., Shinton, S. A., Asano, M., Hardy, R. R. and Hayakawa, K.**, Evidence of marginal-zone B cell-positive selection in spleen. *Immunity* 2005. **23**: 297–308.

1100 **Fillatreau, S. and Manz, R. A.**, Tolls for B cells. *Eur. J. Immunol.* 2006. **36**: 798–801.

1101 **Tornberg, U. C. and Holmberg, D.**, B-1a, B-1b and B-2 B cells display unique VHDJH repertoires formed at different stages of ontogeny and under different selection pressures. *EMBO J.* 1995. **14**: 1680–1689.

1102 **Ochsenbein, A. F., Fehr, T., Lutz, C., Suter, M., Brombacher, F., Hengartner, H. and Zinkernagel, R. M.**, Control of early viral and bacterial distribution and disease by natural antibodies. *Science* 1999. **286**: 2156–2159.

1103 **Stall, A. M., Adams, S., Herzenberg, L. A. and Kantor, A. B.**, Characteristics and development of the murine B-1b (Ly-1 B sister) cell population. *Ann. N. Y. Acad. Sci.* 1992. **651**: 33–43.

1104 **Kristiansen, T. A., Jaensson Gyllenbäck, E., Zriwil, A., Björklund, T., Daniel, J. A., Sitnicka, E., Soneji, S. et al.**, Cellular barcoding links B-1a B cell potential to a fetal hematopoietic stem cell state at the single-cell level. *Immunity* 2016. **45**: 346–357.

1105 **Pedersen, G. K., Li, X., Khoenkhoen, S., Ádori, M., Beutler, B. and Karlsson Hedestam, G. B.**, B-1a cell development in splenectomized neonatal mice. *Front. Immunol.* 2018. **9**: 1738.

1106 **Melchers, F., ten Boekel, E., Seidl, T., Kong, X. C., Yamagami, T., Onishi, K., Shimizu, T. et al.**, Repertoire selection by pre-B-cell receptors and B-cell receptors, and genetic control of B-cell development from immature to mature B cells. *Immunol. Rev.* 2000. **175**: 33–46.

1107 **Montecino-Rodriguez, E., Leathers, H. and Dorshkind, K.**, Identification of a B-1 B cell-specified progenitor. *Nat. Immunol.* 2006. **7**: 293–301.

1108 **Rajewsky, K.**, Early and late B-cell development in the mouse. *Curr. Opin. Immunol.* 1992. **4**: 171–176.

1109 **ten Boekel, E., Melchers, F. and Rolink, A.**, The status of Ig loci rearrangements in single cells from different stages of B cell development. *Int. Immunol.* 1995. **7**: 1013–1019.

1110 **Grawunder, U., Leu, T. M., Schatz, D. G., Werner, A., Rolink, A. G., Melchers, F. and Winkler, T. H.**, Down-regulation of RAG1 and RAG2 gene expression in preB cells after functional immunoglobulin heavy chain rearrangement. *Immunity* 1995. **3**: 601–608.

1111 **Rolink, A. and Melchers, F.**, Molecular and cellular origins of B lymphocyte diversity. *Cell* 1991. **66**: 1081–1094.

1112 **Lu, L., Smithson, G., Kincade, P. W. and Osmond, D. G.**, Two models of murine B lymphopoiesis: a correlation. *Eur. J. Immunol.* 1998. **28**: 1755–1761.

1113 **Hardy, R. R., Carmack, C. E., Shinton, S. A., Kemp, J. D. and Hayakawa, K.**, Resolution and characterization of pro-B and pre-pro-B cell stages in normal mouse bone marrow. *J. Exp. Med.* 1991. **173**: 1213–1225.

1114 **Melchers, F., Rolink, A., Grawunder, U., Winkler, T. H., Karasuyama, H., Ghia, P. and Andersson, J.,** Positive and negative selection events during B lymphopoiesis. *Curr. Opin. Immunol.* 1995. **7**: 214–227.

1115 **Ghia, P., ten Boekel, E., Sanz, E., de la Hera, A., Rolink, A. and Melchers, F.,** Ordering of human bone marrow B lymphocyte precursors by single-cell polymerase chain reaction analyses of the rearrangement status of the immunoglobulin H and L chain gene loci. *J. Exp. Med.* 1996. **184**: 2217–2229.

1116 **Allman, D., Lindsley, R. C., DeMuth, W., Rudd, K., Shinton, S. A. and Hardy, R. R.,** Resolution of three nonproliferative immature splenic B cell subsets reveals multiple selection points during peripheral B cell maturation. *J. Immunol.* 2001. **167**: 6834–6840.

1117 **Hao, Z. and Rajewsky, K.,** Homeostasis of peripheral B cells in the absence of B cell influx from the bone marrow. *J. Exp. Med.* 2001. **194**: 1151–1164.

1118 **Wells, S. M., Kantor, A. B. and Stall, A. M.,** CD43 (S7) expression identifies peripheral B cell subsets. *J. Immunol.* 1994. **153**: 5503–5515.

1119 **Hart, G., Flaishon, L., Becker-Herman, S. and Shachar, I.,** Ly49D receptor expressed on immature B cells regulates their IFN-gamma secretion, actin polymerization, and homing. *J. Immunol.* 2003. **171**: 4630–4638.

1120 **Kozmik, Z., Wang, S., Dörfler, P., Adams, B. and Busslinger, M.,** The promoter of the CD19 gene is a target for the B-cell-specific transcription factor BSAP. *Mol. Cell. Biol.* 1992. **12**: 2662–2672.

1121 **Li, Y. S., Wasserman, R., Hayakawa, K. and Hardy, R. R.,** Identification of the earliest B lineage stage in mouse bone marrow. *Immunity* 1996. **5**: 527–535.

1122 **Koni, P. A., Joshi, S. K., Temann, U.-A., Olson, D., Burkly, L. and Flavell, R. A.,** Conditional Vascular Cell Adhesion Molecule 1 Deletion in Mice: Impaired Lymphocyte Migration to Bone Marrow. *J. Exp. Med.* 2001. **193**: 741–754.

1123 **Kikuchi, K., Lai, A. Y., Hsu, C.-L. and Kondo, M.,** IL-7 receptor signaling is necessary for stage transition in adult B cell development through up-regulation of EBF. *J. Exp. Med.* 2005. **201**: 1197–1203.

1124 **Rolink, A., ten Boekel, E., Melchers, F., Fearon, D. T., Krop, I. and Andersson, J.,** A subpopulation of B220+ cells in murine bone marrow does not express CD19 and contains natural killer cell progenitors. *J. Exp. Med.* 1996. **183**: 187–194.

1125 **Osmond, D. G., Rolink, A. and Melchers, F.,** Murine B lymphopoiesis: towards a unified model. *Immunol. Today* 1998. **19**: 65–68.

1126 **Melchers, F., Haasner, D., Grawunder, U., Kalberer, C., Karasuyama, H., Winkler, T. and Rolink, A. G.,** Roles of IgH and L chains and of surrogate H and L chains in the development of cells of the B lymphocyte lineage. *Annu. Rev. Immunol.* 1994. **12**: 209–225.

1127 **Rolink, A., Streb, M., Nishikawa, S. and Melchers, F.,** The c-kit-encoded tyrosine kinase regulates the proliferation of early pre-B cells. *Eur. J. Immunol.* 1991. **21**: 2609–2612.

1128 **Tonegawa, S.,** Somatic generation of antibody diversity. *Nature* 1983. **302**: 575–581.

1129 **ten Boekel, E., Melchers, F. and Rolink, A. G.,** Precursor B cells showing H chain allelic inclusion display allelic exclusion at the level of pre-B cell receptor surface expression. *Immunity* 1998. **8**: 199–207.

1130 **Rumfelt, L. L., Zhou, Y., Rowley, B. M., Shinton, S. A. and Hardy, R. R.,** Lineage specification and plasticity in CD19- early B cell precursors. *J. Exp. Med.* 2006. **203**: 675–687.

1131 **Osmond, D. G.,** B cell development in the bone marrow. *Semin. Immunol.* 1990. **2**: 173–180.

1132 **Cancro, M. P.,** Peripheral B-cell maturation: the intersection of selection and homeostasis. *Immunol. Rev.* 2004. **197**: 89–101.

1133 **Oliver, A. M., Martin, F., Gartland, G. L., Carter, R. H. and Kearney, J. F.,** Marginal zone B cells exhibit unique activation, proliferative and immunoglobulin secretory responses. *Eur. J. Immunol.* 1997. **27**: 2366–2374.

1134 **Krzyzak, L., Seitz, C., Urbat, A., Hutzler, S., Ostalecki, C., Gläsner, J., Hiergeist, A. et al.,** CD83 modulates B cell activation and germinal center responses. *J. Immunol.* 2016. **196**: 3581–3594.

1135 **Dogan, I., Bertocci, B., Vilmont, V., Delbos, F., Mégret, J., Storck, S., Reynaud, C.-A. et al.,** Multiple layers of B cell memory with different effector functions. *Nat. Immunol.* 2009. **10**: 1292–1299.

1136 **Bell, J. and Gray, D.,** Antigen-capturing cells can masquerade as memory B cells. *J. Exp. Med.* 2003. **197**: 1233–1244.

1137 **Schittek, B. and Rajewsky, K.,** Maintenance of B-cell memory by long-lived cells generated from proliferating precursors. *Nature* 1990. **346**: 749–751.

1138 **Anderson, S. M., Tomayko, M. M., Ahuja, A., Haberman, A. M. and Shlomchik, M. J.,** New markers for murine memory B cells that define mutated and unmutated subsets. *J. Exp. Med.* 2007. **204**: 2103–2114.

1139 **Good-Jacobson, K. L., Song, E., Anderson, S., Sharpe, A. H. and Shlomchik, M. J.,** CD80 expression on B cells regulates murine T follicular helper development, germinal center B cell survival, and plasma cell generation. *J. Immunol.* 2012. **188**: 4217–4225.

1140 **Zuccarino-Catania, G. V., Sadanand, S., Weisel, F. J., Tomayko, M. M., Meng, H., Kleinstein, S. H., Good-Jacobson, K. L. et al.,** CD80 and PD-L2 define functionally distinct memory B cell subsets that are independent of antibody isotype. *Nat. Immunol.* 2014. **15**: 631–637.

1141 **Tomayko, M. M., Steinel, N. C., Anderson, S. M. and Shlomchik, M. J.,** Cutting edge: Hierarchy of maturity of murine memory B cell subsets. *J. Immunol.* 2010. **185**: 7146–7150.

1142 **Weisel, F. J., Zuccarino-Catania, G. V., Chikina, M. and Shlomchik, M. J.,** A temporal switch in the germinal center determines differential output of memory B and plasma cells. *Immunity* 2016. **44**: 116–130.

1143 **Weisel, F. and Shlomchik, M.,** Memory B cells of mice and humans. *Annu. Rev. Immunol.* 2017. **35**: 255–284.

1144 **Loder, F., Mutschler, B., Ray, R. J., Paige, C. J., Sideras, P., Torres, R., Lamers, M. C. et al.,** B cell development in the spleen takes place in discrete steps and is determined by the quality of B cell receptor-derived signals. *J. Exp. Med.* 1999. **190**: 75–89.

1145 **Carsetti, R., Köhler, G. and Lamers, M. C.,** Transitional B cells are the target of negative selection in the B cell compartment. *J. Exp. Med.* 1995. **181**: 2129–2140.

1146 **Baumgarth, N.,** The double life of a B-1 cell: self-reactivity selects for protective effector functions. *Nat. Rev. Immunol.* 2011. **11**: 34–46.

1147 **Haas, K. M., Poe, J. C., Steeber, D. A. and Tedder, T. F.,** B-1a and B-1b cells exhibit distinct developmental requirements and have unique functional roles in innate and adaptive immunity to S. pneumoniae. *Immunity* 2005. **23**: 7–18.

1148 **Hardy, R. R., Hayakawa, K., Parks, D. R., Herzenberg, L. A. and Herzenberg, L. A.,** Murine B cell differentiation lineages. *J. Exp. Med.* 1984. **159**: 1169–1188.

1149 **Pedersen, G. K., Àdori, M., Khoenkhoen, S., Dosenovic, P., Beutler, B. and Karlsson Hedestam, G. B.,** B-1a transitional cells are phenotypically distinct and are lacking in mice deficient in IκBNS. *Proc. Natl. Acad. Sci. USA* 2014. **111**: E4119–4126.

1150 **Herzenberg, L. A., Stall, A. M., Braun, J., Weaver, D., Baltimore, D., Herzenberg, L. A. and Grosschedl, R.,** Depletion of the predominant B-

cell population in immunoglobulin mu heavy-chain transgenic mice. *Nature* 1987. **329**: 71–73.

1151 Shinall, S. M., Gonzalez-Fernandez, M., Noelle, R. J. and Waldschmidt, T. J., Identification of murine germinal center B cell subsets defined by the expression of surface isotypes and differentiation antigens. *J. Immunol.* 2000. **164**: 5729–5738.

1152 Naito, Y., Takematsu, H., Koyama, S., Miyake, S., Yamamoto, H., Fujinawa, R., Sugai, M. et al., Germinal center marker GL7 probes activation-dependent repression of N-glycolylneuraminic acid, a sialic acid species involved in the negative modulation of B-cell activation. *Mol. Cell. Biol.* 2007. **27**: 3008–3022.

1153 Grötsch, B., Brachs, S., Lang, C., Luther, J., Derer, A., Schlötzer-Schrehardt, U., Bozec, A. et al., The AP-1 transcription factor Fra1 inhibits follicular B cell differentiation into plasma cells. *J. Exp. Med.* 2014. **211**: 2199–2212.

1154 Arnold, L. W., Pennell, C. A., McCray, S. K. and Clarke, S. H., Development of B-1 cells: segregation of phosphatidyl choline-specific B cells to the B-1 population occurs after immunoglobulin gene expression. *J. Exp. Med.* 1994. **179**: 1585–1595.

1155 Rauch, P. J., Chudnovskiy, A., Robbins, C. S., Weber, G. F., Etzrodt, M., Hilgendorf, I., Tiglao, E. et al., Innate response activator B cells protect against microbial sepsis. *Science* 2012. **335**: 597–601.

1156 Bouaziz, J.-D., Yanaba, K. and Tedder, T. F., Regulatory B cells as inhibitors of immune responses and inflammation. *Immunol. Rev.* 2008. **224**: 201–214.

1157 Shen, P. and Fillatreau, S., Antibody-independent functions of B cells: a focus on cytokines. *Nat. Rev. Immunol.* 2015. **15**: 441–451.

1158 Bermejo, D. A., Jackson, S. W., Gorosito-Serran, M., Acosta-Rodriguez, E. V., Amezcua-Vesely, M. C., Sather, B. D., Singh, A. K. et al., Trypanosoma cruzi trans-sialidase initiates a program independent of the transcription factors RORγt and Ahr that leads to IL-17 production by activated B cells. *Nat. Immunol.* 2013. **14**: 514–522.

1159 Shen, P., Roch, T., Lampropoulou, V., O'Connor, R. A., Stervbo, U., Hilgenberg, E., Ries, S. et al., IL-35-producing B cells are critical regulators of immunity during autoimmune and infectious diseases. *Nature* 2014. **507**: 366–370.

1160 Fillatreau, S., Pathogenic functions of B cells in autoimmune diseases: IFN-γ production joins the criminal gang. *Eur. J. Immunol.* 2015. **45**: 966–970.

1161 Mizoguchi, A. and Bhan, A. K., A case for regulatory B cells. *J. Immunol.* 2006. **176**: 705–710.

1162 Rosser, E. C. and Mauri, C., Regulatory B cells: origin, phenotype, and function. *Immunity* 2015. **42**: 607–612.

1163 Maseda, D., Smith, S. H., DiLillo, D. J., Bryant, J. M., Candando, K. M., Weaver, C. T. and Tedder, T. F., Regulatory B10 cells differentiate into antibody-secreting cells after transient IL-10 production in vivo. *J. Immunol.* 2012. **188**: 1036–1048.

1164 Kulkarni, U., Karsten, C. M., Kohler, T., Hammerschmidt, S., Bommert, K., Tiburzy, B., Meng, L. et al., IL-10 mediates plasmacytosis-associated immunodeficiency by inhibiting complement-mediated neutrophil migration. *J. Allergy Clin. Immunol.* 2016. **137**: 1487–1497.e6.

1165 Matsumoto, M., Baba, A., Yokota, T., Nishikawa, H., Ohkawa, Y., Kayama, H., Kallies, A. et al., Interleukin-10-producing plasmablasts exert regulatory function in autoimmune inflammation. *Immunity* 2014. **41**: 1040–1051.

1166 Blanc, P., Moro-Sibilot, L., Barthly, L., Jagot, F., This, S., de Bernard, S., Buffat, L. et al., Mature IgM-expressing plasma cells sense antigen and develop competence for cytokine production upon antigenic challenge. *Nat. Commun.* 2016. **7**: 13600.

1167 Lino, A. C., Dang, V. D., Lampropoulou, V., Welle, A., Joedicke, J., Pohar, J., Simon, Q. et al., LAG-3 inhibitory receptor expression identifies immunosuppressive natural regulatory plasma cells. *Immunity* 2018. **49**: 120–133.e129.

1168 Evans, J. G., Chavez-Rueda, K. A., Eddaoudi, A., Meyer-Bahlburg, A., Rawlings, D. J., Ehrenstein, M. R. and Mauri, C., Novel suppressive function of transitional 2 B cells in experimental arthritis. *J. Immunol.* 2007. **178**: 7868–7878.

1169 Blair, P. A., Chavez-Rueda, K. A., Evans, J. G., Shlomchik, M. J., Eddaoudi, A., Isenberg, D. A., Ehrenstein, M. R. et al., Selective targeting of B cells with agonistic anti-CD40 is an efficacious strategy for the generation of induced regulatory T2-like B cells and for the suppression of lupus in MRL/lpr mice. *J. Immunol.* 2009. **182**: 3492–3502.

1170 Miles, K., Heaney, J., Sibinska, Z., Salter, D., Savill, J., Gray, D. and Gray, M., A tolerogenic role for Toll-like receptor 9 is revealed by B-cell interaction with DNA complexes expressed on apoptotic cells. *Proc. Natl. Acad. Sci. USA* 2012. **109**: 887–892.

1171 Bankoti, R., Gupta, K., Levchenko, A. and Stäger, S., Marginal zone B cells regulate antigen-specific T cell responses during infection. *J. Immunol.* 2012. **188**: 3961–3971.

1172 Tedder, T. F., B10 cells: a functionally defined regulatory B cell subset. *J. Immunol.* 2015. **194**: 1395–1401.

1173 Ding, Q., Yeung, M., Camirand, G., Zeng, Q., Akiba, H., Yagita, H., Chalasani, G. et al., Regulatory B cells are identified by expression of TIM-1 and can be induced through TIM-1 ligation to promote tolerance in mice. *J. Clin. Invest.* 2011. **121**: 3645–3656.

1174 Xiao, S., Brooks, C. R., Sobel, R. A. and Kuchroo, V. K., Tim-1 is essential for induction and maintenance of IL-10 in regulatory B cells and their regulation of tissue inflammation. *J. Immunol.* 2015. **194**: 1602–1608.

1175 Fillatreau, S., Natural regulatory plasma cells. *Curr. Opin. Immunol.* 2018. **55**: 62–66.

1176 Mills, D. M. and Cambier, J. C., B lymphocyte activation during cognate interactions with CD4+ T lymphocytes: molecular dynamics and immunologic consequences. *Semin. Immunol.* 2003. **15**: 325–329.

1177 Okada, T., Miller, M., Parker, I., Krummel, M. F., Neighbors, M., Hartley, S. B., O'Garra, A. et al., Antigen-engaged B cells undergo chemotaxis toward the T zone and form motile conjugates with helper T cells. *PLoS Biol.* 2005. **3**: e150.

1178 MacLennan, I., Germinal centers. *Annu. Rev. Immunol.* 1994. **12**: 117–139.

1179 Victora, G. D. and Nussenzweig, M. C., Germinal centers. *Annu. Rev. Immunol.* 2012. **30**: 429–457.

1180 Nieuwenhuis, P. and Opstelten, D., Functional anatomy of germinal centers. *Am. J. Anat.* 1984. **170**: 421–435.

1181 Wagner, S. and Neuberger, Somatic hypermutation of immunoglobulin genes. *Annu. Rev. Immunol.* 1996. **14**: 441–457.

1182 Li, Z., Woo, C. J., Iglesias-Ussel, M. D., Ronai, D. and Scharff, M. D., The generation of antibody diversity through somatic hypermutation and class switch recombination. *Genes Dev.* 2004. **18**: 1–11.

1183 Wu, J., Qin, D., Burton, G., Szakal, A. and Tew, J., Follicular dendritic cell-derived antigen and accessory activity in initiation of memory IgG responses in vitro. *J. Immunol.* 1996. **157**: 3404–3411.

1184 Yeh, C.-H. H., Nojima, T., Kuraoka, M. and Kelsoe, G., Germinal center entry not selection of B cells is controlled by peptide-MHCII complex density. *Nat. Commun.* 2018. **9**: 928.

1185 Klaus, G., Humphrey, J., Kunkl, A. and Dongworth, D., The follicular dendritic cell: its role in antigen presentation in the generation of immunological memory. *Immunol. Rev.* 1980. **53**: 3–28.

1186 **Coico, R., Bhogal, B. and Thorbecke, G.**, Relationship of germinal centers in lymphoid tissue to immunologic memory. VI. Transfer of B cell memory with lymph node cells fractionated according to their receptors for peanut agglutinin. *J. Immunol.* 1983. **131**: 2254–2257.

1187 **Benner, R., Hijmans, W. and Haaijman, J.**, The bone marrow: the major source of serum immunoglobulins, but still a neglected site of antibody formation. *Clin. Exp. Immunol.* 1981. **46**: 1–8.

1188 **Dilosa, R., Maeda, K., Masuda, A., Szakal, A. and Tew, J.**, Germinal center B cells and antibody production in the bone marrow. *J. Immunol.* 1991. **146**: 4071–4077.

1189 **Meyer-Hermann, M., Deutsch, A. and Or-Guil, M.**, Recycling probability and dynamical properties of germinal center reactions. *J. Theor. Biol.* 2001. **210**: 265–285.

1190 **Oprea, M. and Perelson, A.**, Somatic mutation leads to efficient affinity maturation when centrocytes recycle back to centroblasts. *J. Immunol.* 1997. **158**: 5155–5162.

1191 **Oliver, A., Martin, F. and Kearney, J.**, Mouse CD38 is down-regulated on germinal center B cells and mature plasma cells. *J. Immunol.* 1997. **158**: 1108–1115.

1192 **Laszlo, G., Hathcock, K., Dickler, H. and Hodes, R.**, Characterization of a novel cell-surface molecule expressed on subpopulations of activated T and B cells. *J. Immunol.* 1993. **150**: 5252–5262.

1193 **Reichert, R., Gallatin, W., Weissman, I. and Butcher, E.**, Germinal center B cells lack homing receptors necessary for normal lymphocyte recirculation. *J Exp. Med.* 1983. **157**: 813–827.

1194 **Butcher, E. et al.**, Surface phenotype of Peyer's patch germinal center cells: implications for the role of germinal centers in B cell differentiation. *J. Immunol.* 1982. **129**: 2698–2707.

1195 **Davies, A., Forrester, J., Rose, M., Birbeck and Wallis, V.**, Peanut lectin binding properties of germinal centers of mouse lymphoid tissue. *Nature* 1980. **284**: 364.

1196 **Kraal, G., Weissman, I. and Butcher, E.**, Germinal centre B cells: antigen specificity and changes in heavy chain class expression. *Nature* 1982. **298**: 377–379.

1197 **Smith, K., Nossal, G. and Tarlinton, D.**, FAS is highly expressed in the germinal center but is not required for regulation of the B-cell response to antigen. *Proc. Natl. Acad. Sci. USA* 1995. **92**: 11628–11632.

1198 **Bourgois, A., Kitajima, K., Hunter, I. and Askonas**, Surface immunoglobulins of lipopolysaccharide-stimulated spleen cells. The behavior of IgM, IgD and IgG. *Eur. J. Immunol.* 1977. **7**: 151–153.

1199 **Monroe, J., Havran, W. and Cambier, J.**, B lymphocyte activation: entry into cell cycle is accompanied by decreased expression of IgD but not IgM. *Eur. J. Immunol.* 1983. **13**: 208–213.

1200 **Hathcock, K. et al.**, Identification of an alternative CTLA-4 ligand costimulatory for T cell activation. *Science* 1993. **262**: 905–907.

1201 **Freeman, G., Borriello, F., Hodes, R. J., Reiser, H., Hathcock, K. S., Laszlo, G., McKnight, A. J. et al.**, Uncovering of functional alternative CTLA-4 counter-receptor in B7-deficient mice. *Science (New York, N.Y.)* 1993. **262**: 907–909.

1202 **Freeman, G., Borriello, F., Hodes, R. J., Reiser, H., Gribben, J. G., Ng, J. W., Kim, J. et al.**, Murine B7-2, an alternative CTLA4 counter-receptor that costimulates T cell proliferation and interleukin 2 production. *J. Exp. Med.* 1993. **178**: 2185–2192.

1203 **Allen, C. D., Ansel, K. M., Low, C., Lesley, R., Tamamura, H., Fujii, N. and Cyster, J. G.**, Germinal center dark and light zone organization is mediated by CXCR4 and CXCR5. *Nat. Immunol.* 2004. **5**: 943–952.

1204 **Victora, G. D., Schwickert, T. A., Fooksman, D. R., Kamphorst, A. O., Meyer-Hermann, M., Dustin, M. L., Nussenzweig, M. C. et al.**, Germinal center dynamics revealed by multiphoton microscopy with a photoactivatable fluorescent reporter. *Cell* 2010. **143**: 592–605.

1205 **Anderson, K. C., Bates, M. P., Slaughenhoupt, B. L., Pinkus, G. S., Schlossman, S. F. and Nadler, L. M.**, Expression of human B cell-associated antigens on leukemias and lymphomas: a model of human B cell differentiation. *Blood* 1984. **63**: 1424–1433.

1206 **Stashenko, P., Nadler, L. M., Hardy, R. and Schlossman, S. F.**, Characterization of a human B lymphocyte-specific antigen. *J. Immunol.* 1980. **125**: 1678–1685.

1207 **LeBien, T. W. and Tedder, T. F.**, B lymphocytes: how they develop and function. *Blood* 2008. **112**: 1570–1580.

1208 **Sims, G. P., Ettinger, R., Shirota, Y., Yarboro, C. H., Illei, G. G. and Lipsky, P. E.**, Identification and characterization of circulating human transitional B cells. *Blood* 2005. **105**: 4390–4398.

1209 **Klein, U., Rajewsky, K. and Kuppers, R.**, Human immunoglobulin (Ig)M+IgD+ peripheral blood B cells expressing the CD27 cell surface antigen carry somatically mutated variable region genes: CD27 as a general marker for somatically mutated (memory) B cells. *J. Exp. Med.* 1998. **188**: 1679–1689.

1210 **Kuppers, R., Klein, U., Hansmann, M. L. and Rajewsky, K.**, Cellular origin of human B-cell lymphomas. *N. Engl. J. Med.* 1999. **341**: 1520–1529.

1211 **Agematsu, K., Hokibara, S., Nagumo, H. and Komiyama, A.**, CD27: a memory B-cell marker. *Immunol. Today* 2000. **21**: 204–206.

1212 **Agematsu, K., Nagumo, H., Yang, F. C., Nakazawa, T., Fukushima, K., Ito, S., Sugita, K. et al.**, B cell subpopulations separated by CD27 and crucial collaboration of CD27+ B cells and helper T cells in immunoglobulin production. *Eur. J. Immunol.* 1997. **27**: 2073–2079.

1213 **Odendahl, M., Jacobi, A., Hansen, A., Feist, E., Hiepe, F., Burmester, G. R., Lipsky, P. E. et al.**, Disturbed peripheral B lymphocyte homeostasis in systemic lupus erythematosus. *J. Immunol.* 2000. **165**: 5970–5979.

1214 **Mei, H. E., Wirries, I., Frolich, D., Brisslert, M., Giesecke, C., Grun, J. R. et al.**, A unique population of IgG-expressing plasma cells lacking CD19 is enriched in human bone marrow. *Blood* 2015. **125**: 1739–1748.

1215 **Pascual, V., Liu, Y. J., Magalski, A., de Bouteiller, O., Banchereau, J. and Capra, J. D.**, Analysis of somatic mutation in five B cell subsets of human tonsil. *J. Exp. Med.* 1994. **180**: 329–339.

1216 **Kikutani, H., Suemura, M., Owaki, H., Nakamura, H., Sato, R., Yamasaki, K., Barsumian, E. L. et al.**, Fc epsilon receptor, a specific differentiation marker transiently expressed on mature B cells before isotype switching. *J. Exp. Med.* 1986. **164**: 1455–1469.

1217 **Clark, E. A. and Lane, P. J.**, Regulation of human B-cell activation and adhesion. *Annu. Rev. Immunol.* 1991. **9**: 97–127.

1218 **Wu, Y. C., Kipling, D. and Dunn-Walters, D. K.**, The relationship between CD27 negative and positive B cell populations in human peripheral blood. *Front. Immunol.* 2011. **2**: 81.

1219 **Wei, C., Anolik, J., Cappione, A., Zheng, B., Pugh-Bernard, A., Brooks, J., Lee, E. H. et al.**, A new population of cells lacking expression of CD27 represents a notable component of the B cell memory compartment in systemic lupus erythematosus. *J. Immunol.* 2007. **178**: 6624–6633.

1220 **Jacobi, A. M., Reiter, K., Mackay, M., Aranow, C., Hiepe, F., Radbruch, A., Hansen, A. et al.**, Activated memory B cell subsets correlate with disease activity in systemic lupus erythematosus: delineation by expression of CD27, IgD, and CD95. *Arthritis Rheum.* 2008. **58**: 1762–1773.

1221 **Wehr, C., Eibel, H., Masilamani, M., Illges, H., Schlesier, M., Peter, H. H. and Warnatz, K.**, A new CD21low B cell population in the peripheral blood of patients with SLE. *Clin. Immunol.* 2004. **113**: 161–171.

1222 **Tedder, T. F., Zhou, L. J. and Engel, P.**, The CD19/CD21 signal transduction complex of B lymphocytes. *Immunol. Today* 1994. **15**: 437–442.

1223 **Jacobi, A. M. and Dorner, T.**, B-cell-directed therapy in patients with connective tissue diseases. *Dtsch. Med. Wochenschr.* 2012. **137**: 1755–1757.

1224 **Polikowsky, H. G., Wogsland, C. E., Diggins, K. E., Huse, K. and Irish, J. M.**, Cutting edge: redox signaling hypersensitivity distinguishes human germinal center B Cells. *J. Immunol.* 2015. **195**: 1364–1367.

1225 **Carrion, C., Guerin, E., Gachard, N., le Guyader, A., Giraut, S. and Feuillard, J.**, Adult bone marrow three-dimensional phenotypic landscape of B-cell differentiation. *Cytometry B Clin. Cytom.* 2019. **96**: 30–38.

1226 **Bernasconi, N. L., Traggiai, E. and Lanzavecchia, A.**, Maintenance of serological memory by polyclonal activation of human memory B cells. *Science* 2002. **298**: 2199–2202.

1227 **Giesecke, C., Meyer, T., Durek, P., Maul, J., Preiss, J., Jacobs, J. F. M. et al.**, simultaneous presence of non- and highly mutated keyhole limpet hemocyanin (KLH)-specific plasmablasts early after primary KLH immunization suggests cross-reactive memory B cell activation. *J. Immunol.* 2018. **200**(12): 3981–3992.

1228 **Liao, H. Y., Tao, L., Zhao, J., Qin, J., Zeng, G. C., Cai, S. W. et al.**, Clostridium butyricum in combination with specific immunotherapy converts antigen-specific B cells to regulatory B cells in asthmatic patients. *Sci. Rep.* 2016. **6**: 20481.

1229 **Ellebedy, A. H., Jackson, K. J., Kissick, H. T., Nakaya, H. I., Davis, C. W., Roskin, K. M. et al.**, Defining antigen-specific plasmablast and memory B cell subsets in human blood after viral infection or vaccination. *Nat. Immunol.* 2016. **17**(10): 1226–1234.

1230 **Kerkman, P. F., Fabre, E., van der Voort, E. I., Zaldumbide, A., Rombouts, Y., Rispens, T. et al.**, Identification and characterisation of citrullinated antigen-specific B cells in peripheral blood of patients with rheumatoid arthritis. *Ann. Rheum. Dis.* 2016. **75**: 1170–1176.

1231 **Murugan, R., Buchauer, L., Triller, G., Kreschel, C., Costa, G., Pidelaserra Marti, G. et al.**, Clonal selection drives protective memory B cell responses in controlled human malaria infection. *Sci. Immunol.* 2018. **3**(20): eaap8029.

1232 **Germar, K., Fehres, C. M., Scherer, H. U., van Uden, N., Pollastro, S., Yeremenko, N. et al.**, Generation and characterization of anti-citrullinated protein antibody-producing B-cell clones from rheumatoid arthritis patients. *Arthritis Rheumatol.* 2019. **71**: 340–350.

1233 **Kwakkenbos, M. J., Diehl, S. A., Yasuda, E., Bakker, A. Q., van Geelen, C. M., Lukens, M. V. et al.**, Generation of stable monoclonal antibody-producing B cell receptor-positive human memory B cells by genetic programming. *Nat. Med.* 2010. **16**(1): 123–128.

1234 **Giesecke, C., Frolich, D., Reiter, K., Mei, H. E., Wirries, I., Kuhly, R. et al.**, Tissue distribution and dependence of responsiveness of human antigen-specific memory B cells. *J. Immunol.* 2014. **192**(7): 3091–3100.

1235 **Kerkman, P. F., Kempers, A. C., van der Voort, E. I., van Oosterhout, M., Huizinga, T. W., Toes, R. E. et al.**, Synovial fluid mononuclear cells provide an environment for long-term survival of antibody-secreting cells and promote the spontaneous production of anti-citrullinated protein antibodies. *Ann. Rheum. Dis.* 2016. **75**(12): 2201–2207.

1236 **Kerkman, P. F., Rombouts, Y., van der Voort, E. I., Trouw, L. A., Huizinga, T. W., Toes, R. E. et al.**, Circulating plasmablasts/plasmacells as a source of anticitrullinated protein antibodies in patients with rheumatoid arthritis. *Ann. Rheum. Dis.* 2013. **72**(7): 1259–1263.

1237 **Hansen, A., Reiter, K., Dorner, T. and Pruss, A.**, Cryopreserved human B cells as an alternative source for single cell mRNA analysis. *Cell Tissue Bank* 2005. **6**(4): 299–308.

1238 **Townsend, S. E., Goodnow, C. C. and Cornall, R. J.**, Single epitope multiple staining to detect ultralow frequency B cells. *J. Immunol. Methods* 2001. **249**(1-2): 137–146.

1239 **Brooks, J. F., Liu, X., Davies, J. M., Wells, J. W. and Steptoe, R. J.**, Tetramer-based identification of naive antigen-specific B cells within a polyclonal repertoire. *Eur. J. Immunol.* 2018. **48**(7): 1251–1254.

1240 **Cornec, D., Berti, A., Hummel, A., Peikert, T., Pers, J. O. and Specks, U.**, Identification and phenotyping of circulating autoreactive proteinase 3-specific B cells in patients with PR3-ANCA associated vasculitis and healthy controls. *J. Autoimmun.* 2017. **84**: 122–131.

1241 **Frolich, D., Giesecke, C., Mei, H. E., Reiter, K., Daridon, C., Lipsky, P. E. and Dorner, T.**, Secondary immunization generates clonally related antigen-specific plasma cells and memory B cells. *J. Immunol.* 2010. **185**: 3103–3110.

1242 **Lighaam, L. C., Vermeulen, E., Bleker, T., Meijlink, K. J., Aalberse, R. C., Barnes, E. et al.**, Phenotypic differences between IgG4+ and IgG1+ B cells point to distinct regulation of the IgG4 response. *J. Allergy Clin. Immunol.* 2014. **133**(1): 267–270 e1-6.

1243 **Koning, M. T., Kielbasa, S. M., Boersma, V., Buermans, H. P. J., van der Zeeuw, S. A. J., van Bergen, C. A. M. et al.**, ARTISAN PCR: rapid identification of full-length immunoglobulin rearrangements without primer binding bias. *Br. J. Haematol.* 2017. **178**(6): 983–986.

1244 **Gatto, M., Wiedemann, A., Nomovi, N., Reiter, K., Schrezenmeier, E., Rose, T. et al.**, Circulating Pentraxin3-Specific B Cells Are Decreased in Lupus Nephritis. *Front. Immunol.* 2019. **10**: 29.

1245 **Odendahl, M., Mei, H., Hoyer, B. F., Jacobi, A. M., Hansen, A., Muehlinghaus, G., Berek, C. et al.**, Generation of migratory antigen-specific plasma blasts and mobilization of resident plasma cells in a secondary immune response. *Blood* 2005. **105**: 1614–1621.

1246 **Mei, H. E., Hahne, S., Redlin, A., Hoyer, B. F., Wu, K., Baganz, L. et al.**, Plasmablasts With a Mucosal Phenotype Contribute to Plasmacytosis in Systemic Lupus Erythematosus. *Arthritis Rheumatol.* 2017. **69**: 2018–2028.

1247 **Willemze, A., Trouw, L. A., Toes, R. E. and Huizinga, T. W.**, The influence of ACPA status and characteristics on the course of RA. *Nat. Rev. Rheumatol.* 2012. **8**(3): 144–152.

1248 **Katz, S. I., Parker, D. and Turk, J. L.**, B-cell suppression of delayed hypersensitivity reactions. *Nature* 1974. **251**: 550–551.

1249 **Neta, R. and Salvin, S. B.**, Specific suppression of delayed hypersensitivity: the possible presence of a suppressor B cell in the regulation of delayed hypersensitivity. *J. Immunol.* 1974. **113**: 1716–1725.

1250 **Wolf, S. D., Dittel, B. N., Hardardottir, F. and Janeway, C. A., Jr.**, Experimental autoimmune encephalomyelitis induction in genetically B cell-deficient mice. *J. Exp. Med.* 1996. **184**: 2271–2278.

1251 **Mizoguchi, A., Mizoguchi, E., Takedatsu, H., Blumberg, R. S. and Bhan, A. K.**, Chronic intestinal inflammatory condition generates IL-10-producing regulatory B cell subset characterized by CD1d upregulation. *Immunity* 2002. **16**: 219–230.

1252 **Fillatreau, S., Sweenie, C. H., McGeachy, M. J., Gray, D. and Anderton, S. M.**, B cells regulate autoimmunity by provision of IL-10. *Nat. Immunol.* 2002. **3**: 944–950.

1253 **van de Veen, W., Stanic, B., Wirz, O. F., Jansen, K., Globinska, A. and Akdis, M.**, Role of regulatory B cells in immune tolerance to allergens and beyond. *J. Allergy Clin. Immunol.* 2016. **138**: 654–665.

1254 **Wirz, O. F., Globinska, A., Ochsner, U., van de Veen, W., Eller, E., Christiansen, E. S., Halken, S. et al.**, Comparison of regulatory B cells in asthma and allergic rhinitis. *Allergy* 2019. **74**: 815–818.

1255 **van de Veen, W., Stanic, B., Yaman, G., Wawrzyniak, M., Sollner, S., Akdis, D. G., Ruckert, B. et al.**, IgG4 production is confined to human IL-

10-producing regulatory B cells that suppress antigen-specific immune responses. *J. Allergy Clin. Immunol.* 2013. **131**: 1204–1212.

1256 Kaminski, D. A., Wei, C., Qian, Y., Rosenberg, A. F. and Sanz, I., Advances in human B cell phenotypic profiling. *Front. Immunol.* 2012. **3**: 302.

1257 Carter, N. A., Rosser, E. C. and Mauri, C., Interleukin-10 produced by B cells is crucial for the suppression of Th17/Th1 responses, induction of T regulatory type 1 cells and reduction of collagen-induced arthritis. *Arthritis Res. Ther.* 2012. **14**: R32.

1258 Parekh, V. V., Prasad, D. V., Banerjee, P. P., Joshi, B. N., Kumar, A. and Mishra, G. C., B cells activated by lipopolysaccharide, but not by anti-Ig and anti-CD40 antibody, induce anergy in CD8+ T cells: role of TGF-beta 1. *J. Immunol.* 2003. **170**: 5897–5911.

1259 Tian, J., Zekzer, D., Hanssen, L., Lu, Y., Olcott, A. and Kaufman, D. L., Lipopolysaccharide-activated B cells down-regulate Th1 immunity and prevent autoimmune diabetes in nonobese diabetic mice. *J. Immunol.* 2001. **167**: 1081–1089.

1260 Carter, N. A., Vasconcellos, R., Rosser, E. C., Tulone, C., Munoz-Suano, A., Kamanaka, M., Ehrenstein, M. R. et al., Mice lacking endogenous IL-10-producing regulatory B cells develop exacerbated disease and present with an increased frequency of Th1/Th17 but a decrease in regulatory T cells. *J. Immunol.* 2011. **186**: 5569–5579.

1261 Schioppa, T., Moore, R., Thompson, R. G., Rosser, E. C., Kulbe, H., Nedospasov, S., Mauri, C. et al., B regulatory cells and the tumor-promoting actions of TNF-alpha during squamous carcinogenesis. *Proc. Natl. Acad. Sci. USA* 2011. **108**: 10662–10667.

1262 Gray, M., Miles, K., Salter, D., Gray, D. and Savill, J., Apoptotic cells protect mice from autoimmune inflammation by the induction of regulatory B cells. *Proc. Natl. Acad. Sci. USA* 2007. **104**: 14080–14085.

1263 Bankoti, R., Gupta, K., Levchenko, A. and Stager, S., Marginal zone B cells regulate antigen-specific T cell responses during infection. *J. Immunol.* 2012. **188**: 3961–3971.

1264 Matsushita, T., Horikawa, M., Iwata, Y. and Tedder, T. F., Regulatory B cells (B10 cells) and regulatory T cells have independent roles in controlling experimental autoimmune encephalomyelitis initiation and late-phase immunopathogenesis. *J. Immunol.* 2010. **185**: 2240–2252.

1265 Kalampokis, I., Yoshizaki, A. and Tedder, T. F., IL-10-producing regulatory B cells (B10 cells) in autoimmune disease. *Arthritis Res. Ther.* 2013. **15** (Suppl 1): S1.

1266 Watanabe, R., Ishiura, N., Nakashima, H., Kuwano, Y., Okochi, H., Tamaki, K., Sato, S. et al., Regulatory B cells (B10 cells) have a suppressive role in murine lupus: CD19 and B10 cell deficiency exacerbates systemic autoimmunity. *J. Immunol.* 2010. **184**: 4801–4809.

1267 Sheng, J. R., Quan, S. and Soliven, B., CD1d(hi)CD5+ B cells expanded by GM-CSF in vivo suppress experimental autoimmune myasthenia gravis. *J. Immunol.* 2014. **193**: 2669–2677.

1268 Yang, M., Deng, J., Liu, Y., Ko, K. H., Wang, X., Jiao, Z., Wang, S. et al., IL-10-producing regulatory B10 cells ameliorate collagen-induced arthritis via suppressing Th17 cell generation. *Am. J. Pathol.* 2012. **180**: 2375–2385.

1269 Yanaba, K., Yoshizaki, A., Asano, Y., Kadono, T., Tedder, T. F. and Sato, S., IL-10-producing regulatory B10 cells inhibit intestinal injury in a mouse model. *Am. J. Pathol.* 2011. **178**: 735–743.

1270 Khan, A. R., Amu, S., Saunders, S. P., Hams, E., Blackshields, G., Leonard, M. O., Weaver, C. T. et al., Ligation of TLR7 on CD19(+) CD1d(hi) B cells suppresses allergic lung inflammation via regulatory T cells. *Eur. J. Immunol.* 2015. **45**: 1842–1854.

1271 Amu, S., Saunders, S. P., Kronenberg, M., Mangan, N. E., Atzberger, A. and Fallon, P. G., Regulatory B cells prevent and reverse allergic airway

inflammation via FoxP3-positive T regulatory cells in a murine model. *J. Allergy Clin. Immunol.* 2010. **125**: 1114–1124.e1118.

1272 Yanaba, K., Bouaziz, J. D., Haas, K. M., Poe, J. C., Fujimoto, M. and Tedder, T. F., A regulatory B cell subset with a unique CD1dhiCD5+ phenotype controls T cell-dependent inflammatory responses. *Immunity* 2008. **28**: 639–650.

1273 Xiao, S., Brooks, C. R., Zhu, C., Wu, C., Sweere, J. M., Petecka, S., Yeste, A. et al., Defect in regulatory B-cell function and development of systemic autoimmunity in T-cell Ig mucin 1 (Tim-1) mucin domain-mutant mice. *Proc. Natl. Acad. Sci. USA* 2012. **109**: 12105–12110.

1274 Neves, P., Lampropoulou, V., Calderon-Gomez, E., Roch, T., Stervbo, U., Shen, P., Kuhl, A. A. et al., Signaling via the MyD88 adaptor protein in B cells suppresses protective immunity during Salmonella typhimurium infection. *Immunity* 2010. **33**: 777–790.

1275 Dass, S., Vital, E. M. and Emery, P., Development of psoriasis after B cell depletion with rituximab. *Arthritis Rheum.* 2007. **56**: 2715–2718.

1276 Goetz, M., Atreya, R., Ghalibafian, M., Galle, P. R. and Neurath, M. F., Exacerbation of ulcerative colitis after rituximab salvage therapy. *Inflamm. Bowel Dis.* 2007. **13**: 1365–1368.

1277 Blair, P. A., Norena, L. Y., Flores-Borja, F., Rawlings, D. J., Isenberg, D. A., Ehrenstein, M. R. and Mauri, C., CD19(+)CD24(hi)CD38(hi) B cells exhibit regulatory capacity in healthy individuals but are functionally impaired in systemic Lupus Erythematosus patients. *Immunity* 2010. **32**: 129–140.

1278 Das, A., Ellis, G., Pallant, C., Lopes, A. R., Khanna, P., Peppa, D., Chen, A. et al., IL-10-producing regulatory B cells in the pathogenesis of chronic hepatitis B virus infection. *J. Immunol.* 2012. **189**: 3925–3935.

1279 Flores-Borja, F., Bosma, A., Ng, D., Reddy, V., Ehrenstein, M. R., Isenberg, D. A. and Mauri, C., CD19+CD24hiCD38hi B cells maintain regulatory T cells while limiting TH1 and TH17 differentiation. *Sci. Transl. Med.* 2013. **5**: 173ra123.

1280 Iwata, Y., Matsushita, T., Horikawa, M., Dilillo, D. J., Yanaba, K., Venturi, G. M., Szabolcs, P. M. et al., Characterization of a rare IL-10-competent B-cell subset in humans that parallels mouse regulatory B10 cells. *Blood* 2011. **117**: 530–541.

1281 Machado-Santos, J., Saji, E., Troscher, A. R., Paunovic, M., Liblau, R., Gabriely, G., Bien, C. G. et al., The compartmentalized inflammatory response in the multiple sclerosis brain is composed of tissue-resident CD8+ T lymphocytes and B cells. *Brain* 2018. **141**: 2066–2082.

1282 Horikawa, M., Weimer, E. T., DiLillo, D. J., Venturi, G. M., Spolski, R., Leonard, W. J., Heise, M. T. et al., Regulatory B cell (B10 Cell) expansion during Listeria infection governs innate and cellular immune responses in mice. *J Immunol* 2013. **190**: 1158–1168.

1283 Menon, M., Blair, P. A., Isenberg, D. A. and Mauri, C., A regulatory feedback between plasmacytoid dendritic cells and regulatory B cells is aberrant in systemic lupus erythematosus. *Immunity* 2016. **44**: 683–697.

1284 Ramirez, J., Lukin, K. and Hagman, J., From hematopoietic progenitors to B cells: mechanisms of lineage restriction and commitment. *Curr. Opin. Immunol.* 2010. **22**: 177–184.

1285 Hardy, R. R., Kincade, P. W. and Dorshkind, K., The protean nature of cells in the B lymphocyte lineage. *Immunity* 2007. **26**: 703–714.

1286 Cerutti, A., Puga, I. and Cols, M., New helping friends for B cells. *Eur. J. Immunol.* 2012. **42**: 1956–1968.

1287 Xu, Z., Zan, H., Pone, E. J., Mai, T. and Casali, P., Immunoglobulin class-switch DNA recombination: induction, targeting and beyond. *Nat. Rev. Immunol.* 2012. **12**: 517–531.

1288 **King, C., Tangye, S. G. and Mackay, C. R.**, T follicular helper (TFH) cells in normal and dysregulated immune responses. *Annu. Rev. Immunol.* 2008. **26**: 741–766.

1289 **Papavasiliou, F. N. and Schatz, D. G.**, Somatic hypermutation of immunoglobulin genes: merging mechanisms for genetic diversity. *Cell* 2002. **109** Suppl: S35–4.

1290 **Radbruch, A., Muehlinghaus, G., Luger, E. O., Inamine, A., Smith, K. G., Dorner, T. and Hiepe, F.**, Competence and competition: the challenge of becoming a long-lived plasma cell. *Nat. Rev. Immunol.* 2006. **6**: 741–750.

1291 **Honjo, T.**, Immunoglobulin genes. *Annu. Rev. Immunol.* 1983. **1**: 499–528.

1292 **Schatz, D. G. and Ji, Y.**, Recombination centres and the orchestration of V(D)J recombination. *Nat. Rev. Immunol.* 2011. **11**: 251–263.

1293 **Shan, M., Carrillo, J., Yeste, A., Gutzeit, C., Segura-Garzon, D., Walland, A. C., Pybus, M. et al.**, Secreted IgD amplifies humoral T helper 2 cell responses by binding basophils via galectin-9 and CD44. *Immunity* 2018. **49**: 709–724 e708.

1294 **Boonpiyathad, T., Meyer, N., Moniuszko, M., Sokolowska, M., Eljaszewicz, A., Wirz, O. F., Tomasiak-Lozowska, M. M. et al.**, High-dose bee venom exposure induces similar tolerogenic B-cell responses in allergic patients and healthy beekeepers. *Allergy* 2017. **72**: 407–415.

1295 **Kallies, A., Hasbold, J., Tarlinton, D. M., Dietrich, W., Corcoran, L. M., Hodgkin, P. D. and Nutt, S. L.**, Plasma cell ontogeny defined by quantitative changes in blimp-1 expression. *J. Exp. Med.* 2004. **200**: 967–977.

1296 **Nutt, S. L., Hodgkin, P. D., Tarlinton, D. M. and Corcoran, L. M.**, The generation of antibody-secreting plasma cells. *Nat. Rev. Immunol.* 2015. **15**: 160–171.

1297 **Bankoti, R., Ogawa, C., Nguyen, T., Emadi, L., Couse, M., Salehi, S., Fan, X. et al.**, Differential regulation of Effector and Regulatory T cell function by Blimp1. *Sci. Rep.* 2017. **7**: 12078.

1298 **Fukushima, P. I., Nguyen, P. K. T., O'Grady, P. and Stetler-Stevenson, M.**, Flow cytometric analysis of kappa and lambda light chain expression in evaluation of specimens for B-cell neoplasia. *Cytometry* 1996. **26**: 243–252.

1299 **Pelz, A., Schaffert, H., Diallo, R., Hiepe, F., Meisel, A. and Kohler, S.**, S1P receptor antagonists fingolimod and siponimod do not improve the outcome of experimental autoimmune myasthenia gravis mice after disease onset. *Eur. J. Immunol.* 2018. **48**: 498–508.

1300 **Chu, V. T., Fröhlich, A., Steinhauser, G., Scheel, T., Roch, T., Fillatreau, S., Lee, J. J. et al.**, Eosinophils are required for the maintenance of plasma cells in the bone marrow. *Nat. Immunol.* 2011. **12**: 151–159.

1301 **Wilmore, J. R., Jones, D. D. and Allman, D.**, Protocol for improved resolution of plasma cell subpopulations by flow cytometry. *Eur. J. Immunol.* 2017. **47**: 1386–1388.

1302 **Cantor, J., Browne, C. D., Ruppert, R., Féral, C. C., Fässler, R., Rickert, R. C. and Ginsberg, M. H.**, CD98hc facilitates B cell proliferation and adaptive humoral immunity. *Nat. Immunol.* 2009. **10**: 412–419.

1303 **Wrammert, J., Källberg, E., Agace, W. W. and Leanderson, T.**, Ly6C expression differentiates plasma cells from other B cell subsets in mice. *Eur. J. Immunol.* 2002. **32**: 97–103.

1304 **Smith, K. G. C., Hewitson, T. D., Nossal, G. J. V. and Tarlinton, D. M.**, The phenotype and fate of the antibody-forming cells of the splenic foci. *Eur. J. Immunol.* 1996. **26**: 444–448.

1305 **Manz, R. A., Thiel, A. and Radbruch, A.**, Lifetime of plasma cells in the bone marrow. *Nature* 1997. **388**: 133–134.

1306 **Zehentmeier, S., Roth, K., Cseresnyes, Z., Sercan, Ö., Horn, K., Niesner, R. A., Chang, H.-D. et al.**, Static and dynamic components synergize to form a stable survival niche for bone marrow plasma cells: cellular immune response. *Eur. J. Immunol.* 2014. **44**: 2306–2317.

1307 **Sanderson, R. D., Lalor, P. and Bernfield, M.**, B lymphocytes express and lose syndecan at specific stages of differentiation. *Cell Regul.* 1989. **1**: 27–35.

1308 **Arumugakani, G., Stephenson, S. J., Newton, D. J., Rawstron, A., Emery, P., Doody, G. M., McGonagle, D. et al.**, Early emergence of CD19-negative human antibody-secreting cells at the plasmablast to plasma cell transition. *J. Immunol.* 2017. **198**: 4618–4628.

1309 **Racine, R., Chatterjee, M. and Winslow, G. M.**, CD11c expression identifies a population of extrafollicular antigen-specific splenic plasmablasts responsible for CD4 T-independent antibody responses during intracellular bacterial infection. *J. Immunol.* 2008. **181**: 1375–1385.

1310 **Van Camp, B., Durie, B. G., Spier, C., De Waele, M., Van Riet, I., Vela, E., Frutiger, Y. et al.**, Plasma cells in multiple myeloma express a natural killer cell-associated antigen: CD56 (NKH-1; Leu-19). *Blood* 1990. **76**: 377–382.

1311 **Hoffmann, F. S., Kuhn, P.-H., Laurent, S. A., Hauck, S. M., Berer, K., Wendlinger, S. A., Krumbholz, M. et al.**, The immunoregulator soluble TACI is released by ADAM10 and reflects B cell activation in autoimmunity. *J. Immunol.* 2015. **194**: 542–552.

1312 **Pinto, D., Montani, E., Bolli, M., Garavaglia, G., Sallusto, F., Lanzavecchia, A. and Jarrossay, D.**, A functional BCR in human IgA and IgM plasma cells. *Blood* 2013. **121**: 4110–4114.

1313 **Yoshida, T., Mei, H., Dörner, T., Hiepe, F., Radbruch, A., Fillatreau, S. and Hoyer, B. F.**, Memory B and memory plasma cells. *Immunol. Rev.* 2010. **237**: 117–139.

1314 **Slifka, M. K., Antia, R., Whitmire, J. K. and Ahmed, R.**, Humoral immunity due to long-lived plasma cells. *Immunity* 1998. **8**: 363–372.

1315 **Jacobi, A. M., Mei, H., Hoyer, B. F., Mumtaz, I. M., Thiele, K., Radbruch, A., Burmester, G. R. et al.**, HLA-DRhigh/CD27high plasmablasts indicate active disease in patients with systemic lupus erythematosus. *Ann. Rheum. Dis.* 2010. **69**: 305–308.

1316 **Hoyer, B. F., Mumtaz, I. M., Loddenkemper, K., Bruns, A., Sengler, C., Hermann, K. G., Maza, S. et al.**, Takayasu arteritis is characterised by disturbances of B cell homeostasis and responds to B cell depletion therapy with rituximab. *Ann. Rheum. Dis.* 2012. **71**: 75–79.

1317 **Sarkander, J., Hojyo, S. and Tokoyoda, K.**, Vaccination to gain humoral immune memory. *Clin. Transl. Immunol.* 2016. **5**: e120.

1318 **Wrammert, J., Onlamoon, N., Akondy, R. S., Perng, G. C., Polsrila, K., Chandele, A., Kwissa, M. et al.**, Rapid and massive virus-specific plasmablast responses during acute dengue virus infection in humans. *J. Virol.* 2012. **86**: 2911–2918.

1319 **Mei, H. E., Frolich, D., Giesecke, C., Loddenkemper, C., Reiter, K., Schmidt, S., Feist, E. et al.**, Steady-state generation of mucosal IgA+ plasmablasts is not abrogated by B-cell depletion therapy with rituximab. *Blood* 2010. **116**: 5181–5190.

1320 **Huggins, J., Pellegrin, T., Felgar, R. E., Wei, C., Brown, M., Zheng, B., Milner, E. C. et al.**, CpG DNA activation and plasma-cell differentiation of CD27- naive human B cells. *Blood* 2007. **109**: 1611–1619.

1321 **Cocco, M., Stephenson, S., Care, M. A., Newton, D., Barnes, N. A., Davison, A., Rawstron, A. et al.**, In vitro generation of long-lived human plasma cells. *J. Immunol.* 2012. **189**: 5773–5785.

1322 **Mei, H. E., Yoshida, T., Sime, W., Hiepe, F., Thiele, K., Manz, R. A., Radbruch, A. et al.**, Blood-borne human plasma cells in steady state are derived from mucosal immune responses. *Blood* 2009. **113**: 2461–2469.

1323 **Kantele, A., Hakkinen, M., Moldoveanu, Z., Lu, A., Savilahti, E., Alvarez, R. D., Michalek, S. et al.**, Differences in immune responses

induced by oral and rectal immunizations with Salmonella typhi Ty21a: evidence for compartmentalization within the common mucosal immune system in humans. *Infect. Immun.* 1998. **66**: 5630–5635.

1324 Medina, F., Segundo, C., Campos-Caro, A., Gonzalez-Garcia, I. and Brieva, J. A., The heterogeneity shown by human plasma cells from tonsil, blood, and bone marrow reveals graded stages of increasing maturity, but local profiles of adhesion molecule expression. *Blood* 2002. **99**: 2154–2161.

1325 Caraux, A., Klein, B., Paiva, B., Bret, C., Schmitz, A., Fuhler, G. M., Bos, N. A. et al., Circulating human B and plasma cells. Age-associated changes in counts and detailed characterization of circulating normal CD138− and CD138+ plasma cells. *Haematologica* 2010. **95**: 1016–1020.

1326 Arce, S., Luger, E., Muehlinghaus, G., Cassese, G., Hauser, A., Horst, A., Lehnert, K. et al., CD38 low IgG-secreting cells are precursors of various CD38 high-expressing plasma cell populations. *J. Leukoc. Biol.* 2004. **75**: 1022–1028.

1327 Jourdan, M., Caraux, A., Caron, G., Robert, N., Fiol, G., Reme, T., Bollore, K. et al., Characterization of a transitional preplasmablast population in the process of human B cell to plasma cell differentiation. *J. Immunol.* 2011. **187**: 3931–3941.

1328 Mei, H. E., Schmidt, S. and Dorner, T., Rationale of anti-CD19 immunotherapy: an option to target autoreactive plasma cells in autoimmunity. *Arthritis Res. Ther.* 2012. **14** Suppl 5: S1.

1329 Lokhorst, H. M., Plesner, T., Laubach, J. P., Nahi, H., Gimsing, P., Hansson, M., Minnema, M. C. et al., Targeting CD38 with daratumumab monotherapy in multiple myeloma. *N Engl J Med* 2015. **373**: 1207–1219.

1330 Halliley, J. L., Tipton, C. M., Liesveld, J., Rosenberg, A. F., Darce, J., Gregoretti, I. V., Popova, L. et al., Long-lived plasma cells are contained within the CD19(-)CD38(hi)CD138(+) subset in human bone marrow. *Immunity* 2015. **43**: 132–145.

1331 Landsverk, O. J., Snir, O., Casado, R. B., Richter, L., Mold, J. E., Reu, P., Horneland, R. et al., Antibody-secreting plasma cells persist for decades in human intestine. *J. Exp. Med.* 2017. **214**: 309–317.

1332 Hacbarth, E. and Kajdacsy-Balla, A., Low density neutrophils in patients with systemic lupus erythematosus, rheumatoid arthritis, and acute rheumatic fever. *Arthritis Rheum.* 1986. **29**: 1334–1342.

1333 Sato, S., Fujimoto, M., Hasegawa, M. and Takehara, K., Altered blood B lymphocyte homeostasis in systemic sclerosis: expanded naive B cells and diminished but activated memory B cells. *Arthritis Rheum.* 2004. **50**: 1918–1927.

1334 Carrell, J. and Groves, C. J., OMIP-043: Identification of human antibody secreting cell subsets. *Cytometry A* 2018. **93**: 190–193.

1335 Mesin, L., Di Niro, R., Thompson, K. M., Lundin, K. E. and Sollid, L. M., Long-lived plasma cells from human small intestine biopsies secrete immunoglobulins for many weeks in vitro. *J. Immunol.* 2011. **187**: 2867–2874.

1336 Laurent, S. A., Hoffmann, F. S., Kuhn, P.-H., Cheng, Q., Chu, Y., Schmidt-Supprian, M., Hauck, S. M. et al., γ-Secretase directly sheds the survival receptor BCMA from plasma cells. *Nat. Commun.* 2015. **6**: 7333.

1337 Kunkel, E. J. and Butcher, E. C., Plasma-cell homing. *Nat. Rev. Immunol.* 2003. **3**: 822–829.

1338 Delogu, A., Schebesta, A., Sun, Q., Aschenbrenner, K., Perlot, T. and Busslinger, M., Gene repression by Pax5 in B cells is essential for blood cell homeostasis and is reversed in plasma cells. *Immunity* 2006. **24**: 269–281.

1339 Medina, F., Segundo, C., Jimenez-Gomez, G., Gonzalez-Garcia, I., Campos-Caro, A. and Brieva, J. A., Higher maturity and connective tis-sue association distinguish resident from recently generated human tonsil plasma cells. *J. Leukoc. Biol.* 2007. **82**: 1430–1436.

1340 Frigyesi, I., Adolfsson, J., Ali, M., Christophersen, M. K., Johnsson, E., Turesson, I., Gullberg, U. et al., Robust isolation of malignant plasma cells in multiple myeloma. *Blood* 2014. **123**: 1336–1340.

1341 Spits, H., Artis, D., Colonna, M., Diefenbach, A., Di Santo, J. P., Eberl, G., Koyasu, S. et al., Innate lymphoid cells—a proposal for uniform nomenclature. *Nat. Rev. Immunol.* 2013. **13**: 145–149.

1342 Vivier, E., Artis, D., Colonna, M., Diefenbach, A., Di Santo, J. P., Eberl, G., Koyasu, S. et al., Innate lymphoid cells: 10 years on. *Cell* 2018. **174**: 1054–1066.

1343 Biron, C. A., Nguyen, K. B., Pien, G. C., Cousens, L. P. and Salazar-Mather, T. P., Natural killer cells in antiviral defense: function and regulation by innate cytokines. *Annu. Rev. Immunol.* 1999. **17**: 189–220.

1344 Daussy, C., Faure, F., Mayol, K., Viel, S., Gasteiger, G., Charrier, E., Bienvenu, J. et al., T-bet and Eomes instruct the development of two distinct natural killer cell lineages in the liver and in the bone marrow. *J. Exp. Med.* 2014. **211**: 563–577.

1345 Klose, C. S., Flach, M., Mohle, L., Rogell, L., Hoyler, T., Ebert, K., Fabiunke, C. et al., Differentiation of type 1 ILCs from a common progenitor to all helper-like innate lymphoid cell lineages. *Cell* 2014. **157**: 340–356.

1346 Sojka, D. K., Plougastel-Douglas, B., Yang, L., Pak-Wittel, M. A., Artyomov, M. N., Ivanova, Y., Zhong, C. et al., Tissue-resident natural killer (NK) cells are cell lineages distinct from thymic and conventional splenic NK cells. *Elife* 2014. **3**: e01659.

1347 Walker, J. A. and McKenzie, A. N., Development and function of group 2 innate lymphoid cells. *Curr. Opin. Immunol.* 2013. **25**: 148–155.

1348 Montaldo, E., Juelke, K. and Romagnani, C., Group 3 innate lymphoid cells (ILC3s): origin, differentiation, and plasticity in humans and mice. *Eur. J. Immunol.* 2015. **45**: 2171–2182.

1349 Spits, H. and Cupedo, T., Innate lymphoid cells: emerging insights in development, lineage relationships, and function. *Annu. Rev. Immunol.* 2012. **30**: 647–675.

1350 Paclik, D., Stehle, C., Lahmann, A., Hutloff, A. and Romagnani, C., ICOS regulates the pool of group 2 innate lymphoid cells under homeostatic and inflammatory conditions in mice. *Eur. J. Immunol.* 2015. **45**: 2766–2772.

1351 Ryon, J. J., Isolation of mononuclear cells from tonsillar tissue. *Curr. Protoc. Immunol.* 2001. Chapter 7: Unit 7 8.

1352 Gasteiger, G., Fan, X., Dikiy, S., Lee, S. Y. and Rudensky, A. Y., Tissue residency of innate lymphoid cells in lymphoid and nonlymphoid organs. *Science* 2015. **350**: 981–985.

1353 Hoyler, T., Klose, C. S., Souabni, A., Turqueti-Neves, A., Pfeifer, D., Rawlins, E. L., Voehringer, D. et al., The transcription factor GATA-3 controls cell fate and maintenance of type 2 innate lymphoid cells. *Immunity* 2012. **37**: 634–648.

1354 Fuchs, A., Vermi, W., Lee, J. S., Lonardi, S., Gilfillan, S., Newberry, R. D., Cella, M. et al., Intraepithelial type 1 innate lymphoid cells are a unique subset of IL-12- and IL-15-responsive IFN-gamma-producing cells. *Immunity* 2013. **38**: 769–781.

1355 Robinette, M. L., Fuchs, A., Cortez, V. S., Lee, J. S., Wang, Y., Durum, S. K., Gilfillan, S. et al., Transcriptional programs define molecular characteristics of innate lymphoid cell classes and subsets. *Nat. Immunol.* 2015. **16**: 306–317.

1356 Serafini, N., Klein Wolterink, R. G., Satoh-Takayama, N., Xu, W., Vosshenrich, C. A., Hendriks, R. W. and Di Santo, J. P., Gata3 drives development of RORgammat+ group 3 innate lymphoid cells. *J. Exp. Med.* 2014. **211**: 199–208.

1357 **Moro, K., Yamada, T., Tanabe, M., Takeuchi, T., Ikawa, T., Kawamoto, H., Furusawa, J. et al.**, Innate production of T(H)2 cytokines by adipose tissue-associated c-Kit(+)Sca-1(+) lymphoid cells. *Nature* 2010. **463**: 540–544.

1358 **Neill, D. R., Wong, S. H., Bellosi, A., Flynn, R. J., Daly, M., Langford, T. K., Bucks, C. et al.**, Nuocytes represent a new innate effector leukocyte that mediates type-2 immunity. *Nature* 2010. **464**: 1367–1370.

1359 **Sawa, S., Cherrier, M., Lochner, M., Satoh-Takayama, N., Fehling, H. J., Langa, F. et al.**, Lineage relationship analysis of RORgammat+ innate lymphoid cells. *Science* 2010. **330**: 665–669.

1360 **Rankin, L. C., Groom, J. R., Chopin, M., Herold, M. J., Walker, J. A., Mielke, L. A. et al.**, The transcription factor T-bet is essential for the development of NKp46+ innate lymphocytes via the Notch pathway. *Nat. Immunol.* 2013. **14**: 389–395.

1361 **Klose, C. S., Kiss, E. A., Schwierzeck, V., Ebert, K., Hoyler, T., d'Hargues, Y., Goppert, N. et al.**, A T-bet gradient controls the fate and function of CCR6-RORgammat+ innate lymphoid cells. *Nature* 2013. **494**: 261–265.

1362 **Vonarbourg, C., Mortha, A., Bui, V. L., Hernandez, P. P., Kiss, E. A., Hoyler, T., Flach, M. et al.**, Regulated expression of nuclear receptor RORgammat confers distinct functional fates to NK cell receptor-expressing RORgammat(+) innate lymphocytes. *Immunity* 2010. **33**: 736–751.

1363 **Cella, M., Fuchs, A., Vermi, W., Facchetti, F., Otero, K., Lennerz, J. K. M., Doherty, J. M. et al.**, A human natural killer cell subset provides an innate source of IL-22 for mucosal immunity. *Nature* 2009. **457**: 722–725.

1364 **Mjosberg, J. M., Trifari, S., Crellin, N. K., Peters, C. P., van Drunen, C. M., Piet, B., Fokkens, W. J. et al.**, Human IL-25- and IL-33-responsive type 2 innate lymphoid cells are defined by expression of CRTH2 and CD161. *Nat. Immunol.* 2011. **12**: 1055–1062.

1365 **Bernink, J. H., Peters, C. P., Munneke, M., te Velde, A. A., Meijer, S. L., Weijer, K., Hreggvidsdottir, H. S. et al.**, Human type 1 innate lymphoid cells accumulate in inflamed mucosal tissues. *Nat. Immunol.* 2013. **14**: 221–229.

1366 **Hazenberg, M. D. and Spits, H.**, Human innate lymphoid cells. *Blood* 2014. **124**: 700–709.

1367 **Cupedo, T., Crellin, N. K., Papazian, N., Rombouts, E. J., Weijer, K., Grogan, J. L., Fibbe, W. E. et al.**, Human fetal lymphoid tissue-inducer cells are interleukin 17-producing precursors to RORC+ CD127+ natural killer-like cells. *Nat. Immunol.* 2009. **10**: 66–74.

1368 **Marquardt, N., Beziat, V., Nystrom, S., Hengst, J., Ivarsson, M. A., Kekalainen, E., Johansson, H. et al.**, Cutting edge: identification and characterization of human intrahepatic CD49a+ NK cells. *J. Immunol.* 2015. **194**: 2467–2471.

1369 **Vacca, P., Montaldo, E., Croxatto, D., Loiacono, F., Canegallo, F., Venturini, P. L., Moretta, L. et al.**, Identification of diverse innate lymphoid cells in human decidua. *Mucosal Immunol.* 2015. **8**: 254–264.

1370 **Montaldo, E., Vacca, P., Chiossone, L., Croxatto, D., Loiacono, F., Martini, S., Ferrero, S. et al.**, Unique eomes(+) NK cell subsets are present in uterus and decidua during early pregnancy. *Front. Immunol.* 2015. **6**: 646.

1371 **Teunissen, M. B., Munneke, J. M., Bernink, J. H., Spuls, P. I., Res, P. C., Te Velde, A., Cheuk, S. et al.**, Composition of innate lymphoid cell subsets in the human skin: enrichment of NCR(+) ILC3 in lesional skin and blood of psoriasis patients. *J. Invest. Dermatol.* 2014. **134**: 2351–2360.

1372 **Lim, A. I., Li, Y., Lopez-Lastra, S., Stadhouders, R., Paul, F., Casrouge, A., Serafini, N. et al.**, Systemic human ILC precursors provide a substrate for tissue ILC differentiation. *Cell* 2017. **168**: 1086–1100 e1010.

1373 **Wojno, E. D., Monticelli, L. A., Tran, S. V., Alenghat, T., Osborne, L. C., Thome, J. J., Willis, C. et al.**, The prostaglandin D(2) receptor CRTH2 reg-ulates accumulation of group 2 innate lymphoid cells in the inflamed lung. *Mucosal Immunol.* 2015. **8**: 1313–1323.

1374 **Kim, S., Iizuka, K., Kang, H. S., Dokun, A., French, A. R., Greco, S. and Yokoyama, W. M.**, In vivo developmental stages in murine natural killer cell maturation. *Nat. Immunol.* 2002. **3**: 523–528.

1375 **Hayakawa, Y. and Smyth, M. J.**, CD27 dissects mature NK cells into two subsets with distinct responsiveness and migratory capacity. *J. Immunol.* 2006. **176**: 1517–1524.

1376 **Chiossone, L., Chaix, J., Fuseri, N., Roth, C., Vivier, E. and Walzer, T.**, Maturation of mouse NK cells is a 4-stage developmental program. *Blood* 2009. **113**: 5488–5496.

1377 **Bjorkstrom, N. K., Riese, P., Heuts, F., Andersson, S., Fauriat, C., Ivarsson, M. A., Bjorklund, A. T. et al.**, Expression patterns of NKG2A, KIR, and CD57 define a process of CD56dim NK-cell differentiation uncoupled from NK-cell education. *Blood* 2010. **116**: 3853–3864.

1378 **Lopez-Verges, S., Milush, J. M., Pandey, S., York, V. A., Arakawa-Hoyt, J., Pircher, H., Norris, P. J. et al.**, CD57 defines a functionally distinct population of mature NK cells in the human CD56dimCD16+ NK-cell subset. *Blood* 2010. **116**: 3865–3874.

1379 **Juelke, K., Killig, M., Luetke-Eversloh, M., Parente, E., Gruen, J., Morandi, B., Ferlazzo, G. et al.**, CD62L expression identifies a unique subset of polyfunctional CD56dim NK cells. *Blood* 2010. **116**: 1299–1307.

1380 **Sanos, S. L., Bui, V. L., Mortha, A., Oberle, K., Heners, C., Johner, C. and Diefenbach, A.**, ROR gamma t and commensal microflora are required for the differentiation of mucosal interleukin 22-producing NKp46(+) cells. *Nat. Immunol.* 2009. **10**: 83–91.

1381 **Satoh-Takayama, N., Vosshenrich, C. A. J., Lesjean-Pottier, S., Sawa, S., Lochner, M., Rattis, F., Mention, J. J. et al.**, Microbial flora drives interleukin 22 production in intestinal NKp46(+) cells that provide innate mucosal immune defense. *Immunity* 2008. **29**: 958–970.

1382 **Luci, C., Reynders, A., Ivanov, I. I., Cognet, C., Chiche, L., Chasson, L., Hardwigsen, J. et al.**, Influence of the transcription factor ROR gamma t on the development of NKp46(+) cell populations in gut and skin. *Nat. Immunol.* 2009. **10**: 75–82.

1383 **Fort, M. M., Cheung, J., Yen, D., Li, J., Zurawski, S. M., Lo, S., Menon, S. et al.**, IL-25 induces IL-4, IL-5, and IL-13 and Th2-associated pathologies in vivo. *Immunity* 2001. **15**: 985–995.

1384 **Price, A. E., Liang, H. E., Sullivan, B. M., Reinhardt, R. L., Eisley, C. J., Erle, D. J. and Locksley, R. M.**, Systemically dispersed innate IL-13-expressing cells in type 2 immunity. *Proc. Natl. Acad. Sci. USA* 2010. **107**: 11489–11494.

1385 **Walzer, T., Blery, M., Chaix, J., Fuseri, N., Chasson, L., Robbins, S. H., Jaeger, S. et al.**, Identification, activation, and selective in vivo ablation of mouse NK cells via NKp46. *Proc. Natl. Acad. Sci. USA* 2007. **104**: 3384–3389.

1386 **Carlyle, J. R., Mesci, A., Ljutic, B., Belanger, S., Tai, L. H., Rousselle, E., Troke, A. D. et al.**, Molecular and genetic basis for strain-dependent NK1.1 alloreactivity of mouse NK cells. *J. Immunol.* 2006. **176**: 7511–7524.

1387 **Del Zotto, G., Marcenaro, E., Vacca, P., Sivori, S., Pende, D., Della Chiesa, M., Moretta, F. et al.**, Markers and function of human NK cells in normal and pathological conditions. *Cytom. B Clin. Cytom.* 2017. **92**: 100–114.

1388 **Crinier, A., Milpied, P., Escaliere, B., Piperoglou, C., Galluso, J., Balsamo, A., Spinelli, L. et al.**, High-dimensional single-cell analysis identifies organ-specific signatures and conserved nk cell subsets in humans and mice. *Immunity* 2018. **49**: 971–986 e975.

1389 **Weizman, O. E., Adams, N. M., Schuster, I. S., Krishna, C., Pritykin, Y., Lau, C., Degli-Esposti, M. A. et al.**, ILC1 confer early host protection at initial sites of viral infection. *Cell* 2017. **171**: 795–808 e712.

1390 **Huntington, N. D., Tabarias, H., Fairfax, K., Brady, J., Hayakawa, Y., Degli-Esposti, M. A., Smyth, M. J. et al.**, NK cell maturation and peripheral homeostasis is associated with KLRG1 up-regulation. *J. Immunol.* 2007. **178**: 4764–4770.

1391 **Sciume, G., Hirahara, K., Takahashi, H., Laurence, A., Villarino, A. V., Singleton, K. L., Spencer, S. P. et al.**, Distinct requirements for T-bet in gut innate lymphoid cells. *J. Exp. Med.* 2012. **209**: 2331–2338.

1392 **Quatrini, L., Wieduwild, E., Escaliere, B., Filtjens, J., Chasson, L., Laprie, C., Vivier, E. et al.**, Endogenous glucocorticoids control host resistance to viral infection through the tissue-specific regulation of PD-1 expression on NK cells. *Nat. Immunol.* 2018. **19**: 954–962.

1393 **Herberman, R. B., Nunn, M. E., Holden, H. T. and Lavrin, D. H.**, Natural cytotoxic reactivity of mouse lymphoid cells against syngeneic and allogeneic tumors. II. Characterization of effector cells. *Int. J. Cancer* 1975. **16**: 230–239.

1394 **Herberman, R. B., Nunn, M. E. and Lavrin, D. H.**, Natural cytotoxic reactivity of mouse lymphoid cells against syngeneic acid allogeneic tumors. I. Distribution of reactivity and specificity. *Int. J. Cancer* 1975. **16**: 216–229.

1395 **Ljunggren, H. G. and Karre, K.**, In search of the 'missing self': MHC molecules and NK cell recognition. *Immunol. Today* 1990. **11**: 237–244.

1396 **Moretta, A., Bottino, C., Mingari, M. C., Biassoni, R. and Moretta, L.**, What is a natural killer cell? *Nat. Immunol.* 2002. **3**: 6–8.

1397 **Vivier, E., Tomasello, E., Baratin, M., Walzer, T. and Ugolini, S.**, Functions of natural killer cells. *Nat. Immunol.* 2008. **9**: 503–510.

1398 **Lopez-Botet, M., Perez-Villar, J. J., Carretero, M., Rodriguez, A., Melero, I., Bellon, T., Llano, M. et al.**, Structure and function of the CD94 C-type lectin receptor complex involved in recognition of HLA class I molecules. *Immunol. Rev.* 1997. **155**: 165–174.

1399 **Braud, V. M., Allan, D. S., O'Callaghan, C. A., Soderstrom, K., D'Andrea, A., Ogg, G. S., Lazetic, S. et al.**, HLA-E binds to natural killer cell receptors CD94/NKG2A, B and C. *Nature* 1998. **391**: 795–799.

1400 **Moretta, A., Bottino, C., Vitale, M., Pende, D., Biassoni, R., Mingari, M. C. and Moretta, L.**, Receptors for HLA class-I molecules in human natural killer cells. *Annu. Rev. Immunol.* 1996. **14**: 619–648.

1401 **Parham, P.**, MHC class I molecules and KIRs in human history, health and survival. *Nat. Rev. Immunol.* 2005. **5**: 201–214.

1402 **Moretta, A., Bottino, C., Vitale, M., Pende, D., Cantoni, C., Mingari, M. C., Biassoni, R. et al.**, Activating receptors and coreceptors involved in human natural killer cell-mediated cytolysis. *Annu. Rev. Immunol.* 2001. **19**: 197–223.

1403 **Vivier, E., Raulet, D. H., Moretta, A., Caligiuri, M. A., Zitvogel, L., Lanier, L. L., Yokoyama, W. M. et al.**, Innate or adaptive immunity? The example of natural killer cells. *Science* 2011. **331**: 44–49.

1404 **Raulet, D. H.**, Roles of the NKG2D immunoreceptor and its ligands. *Nat. Rev. Immunol.* 2003. **3**: 781–790.

1405 **Moretta, A., Sivori, S., Vitale, M., Pende, D., Morelli, L., Augugliaro, R., Bottino, C. et al.**, Existence of both inhibitory (p58) and activatory (p50) receptors for HLA-C molecules in human natural killer cells. *J. Exp. Med.* 1995. **182**: 875–884.

1406 **Wagtmann, N., Biassoni, R., Cantoni, C., Verdiani, S., Malnati, M. S., Vitale, M., Bottino, C. et al.**, Molecular clones of the p58 NK cell receptor reveal immunoglobulin-related molecules with diversity in both the extra- and intracellular domains. *Immunity* 1995. **2**: 439–449.

1407 **Sivori, S., Cantoni, C., Parolini, S., Marcenaro, E., Conte, R., Moretta, L. and Moretta, A.**, IL-21 induces both rapid maturation of human CD34+ cell precursors towards NK cells and acquisition of surface killer Ig-like receptors. *Eur. J. Immunol.* 2003. **33**: 3439–3447.

1408 **Freud, A. G. and Caligiuri, M. A.**, Human natural killer cell development. *Immunol. Rev.* 2006. **214**: 56–72.

1409 **Hu, P. F., Hultin, L. E., Hultin, P., Hausner, M. A., Hirji, K., Jewett, A., Bonavida, B. et al.**, Natural killer cell immunodeficiency in HIV disease is manifest by profoundly decreased numbers of CD16+CD56+ cells and expansion of a population of CD16dimCD56- cells with low lytic activity. *J. Acquir. Immune Defic. Syndr. Hum. Retrovirol.* 1995. **10**: 331–340.

1410 **Mavilio, D., Lombardo, G., Benjamin, J., Kim, D., Follman, D., Marcenaro, E., O'Shea, M. A. et al.**, Characterization of CD56-/CD16+ natural killer (NK) cells: a highly dysfunctional NK subset expanded in HIV-infected viremic individuals. *Proc. Natl. Acad. Sci. U. S. A.* 2005. **102**: 2886–2891.

1411 **Della Chiesa, M., Falco, M., Podesta, M., Locatelli, F., Moretta, L., Frassoni, F. and Moretta, A.**, Phenotypic and functional heterogeneity of human NK cells developing after umbilical cord blood transplantation: a role for human cytomegalovirus? *Blood* 2012. **119**: 399–410.

1412 **Pesce, S., Greppi, M., Tabellini, G., Rampinelli, F., Parolini, S., Olive, D., Moretta, L. et al.**, Identification of a subset of human natural killer cells expressing high levels of programmed death 1: a phenotypic and functional characterization. *J. Allergy Clin. Immunol.* 2017.**139**: 335–346 e333.

1413 **Caligiuri, M. A., Zmuidzinas, A., Manley, T. J., Levine, H., Smith, K. A. and Ritz, J.**, Functional consequences of interleukin 2 receptor expression on resting human lymphocytes. Identification of a novel natural killer cell subset with high affinity receptors. *J. Exp. Med.* 1990. **171**: 1509–1526.

1414 **Carson, W. E., Fehniger, T. A. and Caligiuri, M. A.**, CD56bright natural killer cell subsets: characterization of distinct functional responses to interleukin-2 and the c-kit ligand. *Eur. J. Immunol.* 1997. **27**: 354–360.

1415 **Frey, M., Packianathan, N. B., Fehniger, T. A., Ross, M. E., Wang, W. C., Stewart, C. C., Caligiuri, M. A. et al.**, Differential expression and function of L-selectin on CD56bright and CD56dim natural killer cell subsets. *J. Immunol.* 1998. **161**: 400–408.

1416 **Campbell, J. J., Qin, S., Unutmaz, D., Soler, D., Murphy, K. E., Hodge, M. R., Wu, L. et al.**, Unique subpopulations of CD56+ NK and NK-T peripheral blood lymphocytes identified by chemokine receptor expression repertoire. *J. Immunol.* 2001. **166**: 6477–6482.

1417 **Robertson, M. J.**, Role of chemokines in the biology of natural killer cells. *J. Leukoc. Biol.* 2002. **71**: 173–183.

1418 **Lima, M., Leander, M., Santos, M., Santos, A. H., Lau, C., Queiros, M. L., Goncalves, M. et al.**, Chemokine receptor expression on normal blood CD56(+) NK-cells elucidates cell partners that comigrate during the innate and adaptive immune responses and identifies a transitional NK-cell population. *J. Immunol. Res.* 2015. **2015**: 839684.

1419 **De Maria, A., Bozzano, F., Cantoni, C. and Moretta, L.**, Revisiting human natural killer cell subset function revealed cytolytic CD56(dim)CD16+ NK cells as rapid producers of abundant IFN-gamma on activation. *Proc. Natl. Acad. Sci. USA* 2011. **108**: 728–732.

1420 **Fauriat, C., Long, E. O., Ljunggren, H. G. and Bryceson, Y. T.**, Regulation of human NK-cell cytokine and chemokine production by target cell recognition. *Blood* 2010. **115**: 2167–2176.

1421 **Guma, M., Angulo, A., Vilches, C., Gomez-Lozano, N., Malats, N. and Lopez-Botet, M.**, Imprint of human cytomegalovirus infection on the NK cell receptor repertoire. *Blood* 2004. **104**: 3664–3671.

1422 **Malmberg, K. J., Beziat, V. and Ljunggren, H. G.**, Spotlight on NKG2C and the human NK-cell response to CMV infection. *Eur. J. Immunol.* 2012. **42**: 3141–3145.

1423 **Muccio, L., Bertaina, A., Falco, M., Pende, D., Meazza, R., Lopez-Botet, M., Moretta, L. et al.**, Analysis of memory-like natural killer cells in

human cytomegalovirus-infected children undergoing alphabeta+T and B cell-depleted hematopoietic stem cell transplantation for hematological malignancies. *Haematologica* 2016. **101**: 371–381.

1424 Sivori, S., Falco, M., Marcenaro, E., Parolini, S., Biassoni, R., Bottino, C., Moretta, L. et al., Early expression of triggering receptors and regulatory role of 2B4 in human natural killer cell precursors undergoing in vitro differentiation. *Proc. Natl. Acad. Sci. USA* 2002. **99**: 4526–4531.

1425 Vacca, P., Pietra, G., Falco, M., Romeo, E., Bottino, C., Bellora, F., Prefumo, F. et al., Analysis of natural killer cells isolated from human decidua: Evidence that 2B4 (CD244) functions as an inhibitory receptor and blocks NK-cell function. *Blood* 2006. **108**: 4078–4085.

1426 Vacca, P., Vitale, C., Montaldo, E., Conte, R., Cantoni, C., Fulcheri, E., Darretta, V. et al., CD34+ hematopoietic precursors are present in human decidua and differentiate into natural killer cells upon interaction with stromal cells. *Proc. Natl. Acad. Sci. USA* 2011. **108**: 2402–2407.

1427 Hanna, J., Goldman-Wohl, D., Hamani, Y., Avraham, I., Greenfield, C., Natanson-Yaron, S., Prus, D. et al., Decidual NK cells regulate key developmental processes at the human fetal-maternal interface. *Nat. Med.* 2006. **12**: 1065–1074.

1428 Fehniger, T. A., Cooper, M. A., Nuovo, G. J., Cella, M., Facchetti, F., Colonna, M. and Caligiuri, M. A., CD56bright natural killer cells are present in human lymph nodes and are activated by T cell-derived IL-2: a potential new link between adaptive and innate immunity. *Blood* 2003. **101**: 3052–3057.

1429 Ferlazzo, G., Thomas, D., Lin, S. L., Goodman, K., Morandi, B., Muller, W. A., Moretta, A. et al., The abundant NK cells in human secondary lymphoid tissues require activation to express killer cell Ig-like receptors and become cytolytic. *J. Immunol.* 2004. **172**: 1455–1462.

1430 Merad, M., Sathe, P., Helft, J., Miller, J. and Mortha, A., The dendritic cell lineage: ontogeny and function of dendritic cells and their subsets in the steady state and the inflamed setting. *Annu. Rev. Immunol.* 2013. **31**: 563–604.

1431 Ginhoux, F. and Guilliams, M., Tissue-resident macrophage ontogeny and homeostasis. *Immunity* 2016. **44**: 439–449.

1432 Heidkamp, G. F. et al., Functional specialization of Dendritic cell subsets. *Encyclopedia of Cell Biology*, (Elsevier) 2016. 588–604.

1433 Dress, R. J., Wong, A. Y. and Ginhoux, F., Homeostatic control of dendritic cell numbers and differentiation. *Immunol. Cell Biol.* 2018. **96**: 463–476.

1434 Hoeffel, G. and Ginhoux, F., Fetal monocytes and the origins of tissue-resident macrophages. *Cell. Immunol.* 2018. **330**: 5–15.

1435 Collin, M. and Ginhoux, F., Human dendritic cells. *Semin. Cell Dev. Biol.* 2019. **86**: 1–2.

1436 Schlitzer, A., Sivakamasundari, V., Chen, J., Sumatoh, H. R., Schreuder, J., Lum, J., Malleret, B. et al., Identification of cDC1- and cDC2-committed DC progenitors reveals early lineage priming at the common DC progenitor stage in the bone marrow. *Nat. Immunol.* 2015. **16**: 718–728.

1437 Guilliams, M., Dutertre, C. A., Scott, C. L., McGovern, N., Sichien, D., Chakarov, S., Van Gassen, S. et al., Unsupervised high-dimensional analysis aligns dendritic cells across tissues and species. *Immunity* 2016. **45**: 669–684.;

1438 Dress, R. J., Dutertre, C. A., Giladi, A., Schlitzer, A., Low, I., Shadan, N. B., Tay, A. et al., Plasmacytoid dendritic cells develop from Ly6D+ lymphoid progenitors distinct from the myeloid lineage. *Nat. Immunol.* 2019. **20**: 852–864.

1439 Rodrigues, P. F., Alberti-Servera, L., Eremin, A., Grajales-Reyes, G. E., Ivanek, R. and Tussiwand, R., Distinct progenitor lineages contribute

to the heterogeneity of plasmacytoid dendritic cells. *Nat. Immunol.* 2018. **19**: 711–722.

1440 Herman, J. S., Sagar and Grun, D., FateID infers cell fate bias in multipotent progenitors from single-cell RNA-seq data. *Nat. Methods* 2018. **15**: 379–386.

1441 Hoeffel, G., Wang, Y., Greter, M., See, P., Teo, P., Malleret, B., Leboeuf, M. et al., Adult Langerhans cells derive predominantly from embryonic fetal liver monocytes with a minor contribution of yolk sac-derived macrophages. *J. Exp. Med.* 2012. **209**: 1167–1181.

1442 Ginhoux, F., Tacke, F., Angeli, V., Bogunovic, M., Loubeau, M., Dai, X. M., Stanley, E. R. et al., Langerhans cells arise from monocytes in vivo. *Nat. Immunol.* 2006. **7**: 265–273.

1443 Doebel, T., Voisin, B. and Nagao, K., Langerhans Cells - The Macrophage in Dendritic Cell Clothing. *Trends Immunol.* 2017. **38**: 817–828.

1444 Ginhoux, F. and Jung, S., Monocytes and macrophages: developmental pathways and tissue homeostasis. *Nat. Rev. Immunol.* 2014. **14**: 392–404.

1445 Geissmann, F., Jung, S. and Littman, D. R., Blood monocytes consist of two principal subsets with distinct migratory properties. *Immunity* 2003. **19**: 71–82.

1446 Tamoutounour, S., Henri, S., Lelouard, H., de Bovis, B., de Haar, C., van der Woude, C. J., Woltman, A. M. et al., CD64 distinguishes macrophages from dendritic cells in the gut and reveals the Th1-inducing role of mesenteric lymph node macrophages during colitis. *Eur. J. Immunol.* 2012. **42**: 3150–3166.

1447 Bain, C. C., Scott, C. L., Uronen-Hansson, H., Gudjonsson, S., Jansson, O., Grip, O., Guilliams, M. et al., Resident and pro-inflammatory macrophages in the colon represent alternative context-dependent fates of the same Ly6Chi monocyte precursors. *Mucosal Immunol* 2013. **6**: 498–510.

1448 Heidkamp, G. F., Sander, J., Lehmann, C. H. K., Heger, L., Eissing, N., Heger, L., Baranska, A. et al., Human lymphoid organ dendritic cell identity is predominantly dictated by ontogeny, not tissue microenvironment. *Sci. Immunol.* 2016. **1**: pii: eaai7677.

1449 Alcántara-Hernández, M., Leylek, R., Wagar, L. E., Engleman, E. G., Keler, T., Marinkovich, M. P., Davis, M. M. et al., High-Dimensional Phenotypic Mapping of Human Dendritic Cells Reveals Interindividual Variation and Tissue Specialization. *Immunity.* 2017. **47**: 1037–1050.e6.

1450 See, P., Dutertre, C. A., Chen, J., Gunther, P., McGovern, N., Irac, S. E., Gunawan, M. et al., Mapping the human DC lineage through the integration of high-dimensional techniques. *Science* 2017. **356**: eaag3009.

1451 Ziegler-Heitbrock, L., Ancuta, P., Crowe, S., Dalod, M., Grau, V., Hart, D. N., Leenen, P. J. et al., Nomenclature of monocytes and dendritic cells in blood. *Blood* 2010. **116**: e74–80.

1452 Briseno, C. G., Haldar, M., Kretzer, N. M., Wu, X., Theisen, D. J., Kc, W., Durai, V. et al., Distinct transcriptional programs control cross-priming in classical and monocyte-derived dendritic cells. *Cell Rep* 2016. **15**: 2462–2474.

1453 Fujiyama, S., Nakahashi-Oda, C., Abe, F., Wang, Y., Sato, K. and Shibuya, A., Identification and isolation of splenic tissue-resident macrophage sub-populations by flow cytometry. *Int. Immunol.* 2019. **31**: 51–56.

1454 Crozat, K., Guiton, R., Contreras, V., Feuillet, V., Dutertre, C. A., Ventre, E., Vu Manh, T. P. et al., The XC chemokine receptor 1 is a conserved selective marker of mammalian cells homologous to mouse CD8alpha+ dendritic cells. *J. Exp. Med.* 2010. **207**: 1283–1292.

1455 Gurka, S., Hartung, E., Becker, M. and Kroczek, R. A., Mouse conventional dendritic cells can be universally classified based on the mutu-

ally exclusive expression of XCR1 and SIRPalpha. *Front Immunol* 2015. **6**: 35.

1456 Misharin, A. V., Morales-Nebreda, L., Mutlu, G. M., Budinger, G. R. and Perlman, H., Flow cytometric analysis of macrophages and dendritic cell subsets in the mouse lung. *Am. J. Respir. Cell Mol. Biol.* 2013. **49**: 503–510.

1457 Chakarov, S., Lim, H. Y., Tan, L., Lim, S. Y., See, P., Lum, J., Zhang, X. M. et al., Two distinct interstitial macrophage populations coexist across tissues in specific subtissular niches. *Science* 2019. **363**.

1458 Schlitzer, A., McGovern, N., Teo, P., Zelante, T., Atarashi, K., Low, D., Ho, A. W. et al., IRF4 transcription factor-dependent CD11b+ dendritic cells in human and mouse control mucosal IL-17 cytokine responses. *Immunity* 2013. **38**: 970–983.

1459 Shaw, T. N., Houston, S. A., Wemyss, K., Bridgeman, H. M., Barbera, T. A., Zangerle-Murray, T., Strangward, P. et al., Tissue-resident macrophages in the intestine are long lived and defined by Tim-4 and CD4 expression. *J. Exp. Med.* 2018. **215**: 1507–1518.

1460 Takenaka, S., Safroneeva, E., Xing, Z. and Gauldie, J., Dendritic cells derived from murine colonic mucosa have unique functional and phenotypic characteristics. *J. Immunol.* 2007. **178**: 7984–7993.

1461 Johansson-Lindbom, B., Svensson, M., Pabst, O., Palmqvist, C., Marquez, G., Forster, R. and Agace, W. W., Functional specialization of gut CD103+ dendritic cells in the regulation of tissue-selective T cell homing. *J. Exp. Med.* 2005. **202**: 1063–1073.

1462 Harusato, A., Geem, D. and Denning, T. L., Macrophage isolation from the mouse small and large intestine. *Methods Mol. Biol.* 2016. **1422**: 171–180.

1463 Gross, M., Salame, T. M. and Jung, S., Guardians of the gut—murine intestinal macrophages and dendritic cells. *Front Immunol* 2015. **6**: 254.

1464 Helft, J. and Merad, M., Isolation of cutaneous dendritic cells. *Methods Mol. Biol.* 2010. **595**: 231–233.

1465 Benck, C. J., Martinov, T., Fife, B. T. and Chatterjea, D., Isolation of infiltrating leukocytes from mouse skin using enzymatic digest and gradient separation. *J Vis Exp* 2016: e53638.

1466 Forni, M. F., Ramos Maia Lobba, A., Pereira Ferreira, A. H. and Sogayar, M. C., Simultaneous isolation of three different stem cell populations from murine skin. *PLoS One* 2015. **10**: e0140143.

1467 Merad, M., Ginhoux, F. and Collin, M., Origin, homeostasis and function of Langerhans cells and other langerin-expressing dendritic cells. *Nat. Rev. Immunol.* 2008. **8**: 935–947.

1468 Stutte, S., Jux, B., Esser, C. and Forster, I., CD24a expression levels discriminate Langerhans cells from dermal dendritic cells in murine skin and lymph nodes. *J. Invest. Dermatol.* 2008. **128**: 1470–1475.

1469 Malissen, B., Tamoutounour, S. and Henri, S., The origins and functions of dendritic cells and macrophages in the skin. *Nat. Rev. Immunol.* 2014. **14**: 417–428.

1470 Becht, E., McInnes, L., Healy, J., Dutertre, C. A., Kwok, I. W. H., Ng, L. G., Ginhoux, F. et al., Dimensionality reduction for visualizing single-cell data using UMAP. *Nat. Biotechnol.* 2019. **37**: 38–44.

1471 McInnes, L., Healy, J., Saul, N. and Großberger, L., UMAP: uniform manifold approximation and projection. *J. Open Source Softw.* 2018. **3**: 861.

1472 Ester, M., Kriegel, H. P., Sander, J. and Xu, X., A density-based algorithm for discovering clusters in large spatial databases with noise. In KDD'96 Proceedings of the Second International Conference on Knowledge Discovery and Data Mining. Portland, OR, 1996, pp. 226–231.

1473 Levine, J. H., Simonds, E. F., Bendall, S. C., Davis, K. L., Amir el, A. D., Tadmor, M. D., Litvin, O. et al., Data-driven phenotypic dissection

of AML reveals progenitor-like cells that correlate with prognosis. *Cell* 2015. **162**: 184–197.

1474 Villani, A. C., Satija, R., Reynolds, G., Sarkizova, S., Shekhar, K., Fletcher, J., Griesbeck, M. et al., Single-cell RNA-seq reveals new types of human blood dendritic cells, monocytes, and progenitors. *Science* 2017. **356**: eaaah4573.

1475 Dutertre, C.-A., Becht, E., Irac, S. E., Khalilnezhad, A., Narang, V., Khalilnezhad, S., Ng, P. Y. et al., Single-cell analysis of human mononuclear phagocytes reveals subset-defining markers and identifies circulating inflammatory dendritic cells. *Immunity* 2019. **51**: 573–589.e8.

1476 Casanova-Acebes, M., Pitaval, C., Weiss, L. A., Nombela-Arrieta, C., Chevre, R., N, A. G., Kunisaki, Y., Zhang, D. et al., Rhythmic modulation of the hematopoietic niche through neutrophil clearance. *Cell* 2013. **153**: 1025–1035.

1477 Maueroder, C., Mahajan, A., Paulus, S., Gosswein, S., Hahn, J., Kienhofer, D., Biermann, M. H. et al., Menage-a-Trois: the ratio of bicarbonate to CO_2 and the pH regulate the capacity of neutrophils to form NETs. *Front. Immunol.* 2016. **7**: 583.

1478 Evrard, M., Kwok, I. W. H., Chong, S. Z., Teng, K. W. W., Becht, E., Chen, J., Sieow, J. L. et al., Developmental analysis of bone marrow neutrophils reveals populations specialized in expansion, trafficking, and effector functions. *Immunity* 2018. **48**: 364–379 e368.

1479 Kim, M. H., Yang, D., Kim, M., Kim, S. Y., Kim, D. and Kang, S. J., A late-lineage murine neutrophil precursor population exhibits dynamic changes during demand-adapted granulopoiesis. *Sci. Rep.* 2017. **7**: 39804.

1480 Zhu, Y. P., Padgett, L., Dinh, H. Q., Marcovecchio, P., Blatchley, A., Wu, R., Ehinger, E. et al., Identification of an early unipotent neutrophil progenitor with pro-tumoral activity in mouse and human bone marrow. *Cell Rep.* 2018. **24**: 2329–2341 e2328.

1481 Geering, B., Stoeckle, C., Conus, S. and Simon, H. U., Living and dying for inflammation: neutrophils, eosinophils, basophils. *Trends Immunol.* 2013. **34**: 398–409.

1482 Borregaard, N., Neutrophils, from marrow to microbes. *Immunity* 2010. **33**: 657–670.

1483 Ley, K., Hoffman, H. M., Kubes, P., Cassatella, M. A., Zychlinsky, A., Hedrick, C. C. and Catz, S. D., Neutrophils: new insights and open questions. *Sci. Immunol.* 2018. **3**.

1484 Ng, L. G., Ostuni, R. and Hidalgo, A., Heterogeneity of neutrophils. *Nat. Rev. Immunol.* 2019. **19**: 255–265.

1485 Terstappen, L. W., Safford, M. and Loken, M. R., Flow cytometric analysis of human bone marrow. III. Neutrophil maturation. *Leukemia* 1990. **4**: 657–663.

1486 Satake, S., Hirai, H., Hayashi, Y., Shime, N., Tamura, A., Yao, H., Yoshioka, S. et al., C/EBPbeta is involved in the amplification of early granulocyte precursors during candidemia-induced "emergency" granulopoiesis. *J. Immunol.* 2012. **189**: 4546–4555.

1487 Theilgaard-Monch, K., Jacobsen, L. C., Borup, R., Rasmussen, T., Bjerregaard, M. D., Nielsen, F. C., Cowland, J. B. et al., The transcriptional program of terminal granulocytic differentiation. *Blood* 2005. **105**: 1785–1796.

1488 Garley, M. and Jablonska, E., Heterogeneity among neutrophils. *Arch. Immunol. Ther. Exp.* 2018. **66**: 21–30.

1489 Scapini, P., Marini, O., Tecchio, C. and Cassatella, M. A., Human neutrophils in the saga of cellular heterogeneity: insights and open questions. *Immunol. Rev.* 2016. **273**: 48–60.

1490 Coffelt, S. B., Kersten, K., Doornebal, C. W., Weiden, J., Vrijland, K., Hau, C. S., Verstegen, N. J. M. et al., IL-17-producing gammadelta

T cells and neutrophils conspire to promote breast cancer metasta-sis. *Nature* 2015. **522**: 345–348.

1491 Engblom, C., Pfirschke, C., Zilionis, R., Da Silva Martins, J., Bos, S. A., Courties, G., Rickelt, S. et al., Osteoblasts remotely supply lung tumors with cancer-promoting SiglecF(high) neutrophils. *Science* 2017. **358**: eaal5081.

1492 Youn, J. I., Collazo, M., Shalova, I. N., Biswas, S. K. and Gabrilovich, D. I., Characterization of the nature of granulocytic myeloid-derived suppressor cells in tumor-bearing mice. *J. Leukoc. Biol.* 2012. **91**: 167–181.

1493 McAlpine, C. S., Kiss, M. G., Rattik, S., He, S., Vassalli, A., Valet, C., Anzai, A. et al., Sleep modulates haematopoiesis and protects against atherosclerosis. *Nature* 2019. **566**: 383–387.

1494 Grassi, L., Pourfarzad, F., Ullrich, S., Merkel, A., Were, F., Carrillo-de-Santa-Pau, E., Yi, G. et al., Dynamics of transcription regulation in human bone marrow myeloid differentiation to mature blood neu-trophils. *Cell Rep.* 2018. **24**: 2784–2794.

1495 Friedenstein, A. J., Chailakhjan, R. K. and Lalykina, K. S., The develop-ment of fibroblast colonies in monolayer cultures of guinea-pig bone marrow and spleen cells. *Cell Tissue Kinet.* 1970. **3**: 393–403.

1496 Friedenstein, A. J., Chailakhyan, R. K., Latsinik, N. V., Panasyuk, A. F. and Keiliss-Borok, I. V., Stromal cells responsible for transferring the microenvironment of the hemopoietic tissues. Cloning in vitro and retransplantation in vivo. *Transplantation* 1974. **17**: 331–340.

1497 Frenette, P. S., Pinho, S., Lucas, D. and Scheiermann, C., Mesenchy-mal stem cell: keystone of the hematopoietic stem cell niche and a stepping-stone for regenerative medicine. *Annu. Rev. Immunol.* 2013. **31**: 285–316.

1498 Pinho, S. and Frenette, P. S., Haematopoietic stem cell activity and interactions with the niche. *Nat. Rev. Mol. Cell Biol.* 2019.

1499 Chan, C. K., Chen, C. C., Luppen, C. A., Kim, J. B., DeBoer, A. T., Wei, K., Helms, J. A. et al., Endochondral ossification is required for haematopoietic stem-cell niche formation. *Nature* 2009. **457**: 490–494.

1500 Mendez-Ferrer, S., Michurina, T. V., Ferraro, F., Mazloom, A. R., Macarthur, B. D., Lira, S. A., Scadden, D. T. et al., Mesenchymal and haematopoietic stem cells form a unique bone marrow niche. *Nature* 2010. **466**: 829–834.

1501 Kunisaki, Y., Bruns, I., Scheiermann, C., Ahmed, J., Pinho, S., Zhang, D., Mizoguchi, T. et al., Arteriolar niches maintain haematopoietic stem cell quiescence. *Nature* 2013. **502**: 637–643.

1502 Zhou, B. O., Yue, R., Murphy, M. M., Peyer, J. G. and Morrison, S. J., Leptin-receptor-expressing mesenchymal stromal cells represent the main source of bone formed by adult bone marrow. *Cell Stem Cell* 2014. **15**: 154–168.

1503 Omatsu, Y., Sugiyama, T., Kohara, H., Kondoh, G., Fujii, N., Kohno, K. and Nagasawa, T., The essential functions of adipo-osteogenic pro-genitors as the hematopoietic stem and progenitor cell niche. *Immunity* 2010. **33**: 387–399.

1504 Greenbaum, A., Hsu, Y. M., Day, R. B., Schuettpelz, L. G., Christopher, M. J., Borgerding, J. N., Nagasawa, T. et al., CXCL12 in early mesenchy-mal progenitors is required for haematopoietic stem-cell maintenance. *Nature* 2013. **495**: 227–230.

1505 Mizoguchi, T., Pinho, S., Ahmed, J., Kunisaki, Y., Hanoun, M., Mendel-son, A., Ono, N. et al., Osterix marks distinct waves of primitive and definitive stromal progenitors during bone marrow development. *Dev. Cell* 2014. **29**: 340–349.

1506 Chan, C. K., Seo, E. Y., Chen, J. Y., Lo, D., McArdle, A., Sinha, R., Tevlin, R. et al., Identification and specification of the mouse skeletal stem cell. *Cell* 2015. **160**: 285–298.

1507 Marecic, O., Tevlin, R., McArdle, A., Seo, E. Y., Wearda, T., Duldulao, C., Walmsley, G. G. et al., Identification and characterization of an injury-induced skeletal progenitor. *Proc Natl Acad Sci USA* 2015. **112**: 9920–9925.

1508 Debnath, S., Yallowitz, A. R., McCormick, J., Lalani, S., Zhang, T., Xu, R., Li, N. et al., Discovery of a periosteal stem cell mediating intramem-branous bone formation. *Nature* 2018. **562**: 133–139.

1509 Dominici, M., Le Blanc, K., Mueller, I., Slaper-Cortenbach, I., Marini, F., Krause, D., Deans, R. et al., Minimal criteria for defining multipo-tent mesenchymal stromal cells. The International Society for Cellular Therapy position statement. *Cytotherapy* 2006. **8**: 315–317.

1510 Suire, C., Brouard, N., Hirschi, K. and Simmons, P. J., Isolation of the stromal-vascular fraction of mouse bone marrow markedly enhances the yield of clonogenic stromal progenitors. *Blood* 2012. **119**: e86–95.

1511 Pinho, S., Lacombe, J., Hanoun, M., Mizoguchi, T., Bruns, I., Kunisaki, Y. and Frenette, P. S., PDGFRalpha and CD51 mark human nestin+ sphere-forming mesenchymal stem cells capable of hematopoietic progenitor cell expansion. *J. Exp. Med.* 2013. **210**: 1351–1367.

1512 Morikawa, S., Mabuchi, Y., Kubota, Y., Nagai, Y., Niibe, K., Hiratsu, E., Suzuki, S. et al., Prospective identification, isolation, and systemic transplantation of multipotent mesenchymal stem cells in murine bone marrow. *J. Exp. Med.* 2009. **206**: 2483–2496.

1513 Houlihan, D. D., Mabuchi, Y., Morikawa, S., Niibe, K., Araki, D., Suzuki, S., Okano, H. et al., Isolation of mouse mesenchymal stem cells on the basis of expression of Sca-1 and PDGFR-alpha. *Nat. Protoc.* 2012. **7**: 2103–2111.

1514 Worthley, D. L., Churchill, M., Compton, J. T., Tailor, Y., Rao, M., Si, Y., Levin, D. et al., Gremlin 1 identifies a skeletal stem cell with bone, cartilage, and reticular stromal potential. *Cell* 2015. **160**: 269–284.

1515 Boulais, P. E., Mizoguchi, T., Zimmerman, S., Nakahara, F., Vivie, J., Mar, J. C., van Oudenaarden, A. et al., The majority of CD45(-) Ter119(-) CD31(-) bone marrow cell fraction is of hematopoietic origin and con-tains erythroid and lymphoid progenitors. *Immunity* 2018. **49**: 627–639, e626.

1516 Morrison, S. J., Uchida, N. and Weissman, I. L., The biology of hematopoietic stem cells. *Annu. Rev. Cell. Dev. Biol.* 1995. **11**: 35–71.

1517 Spangrude, G. J., Brooks, D. M. and Tumas, D. B., Long-term repopula-tion of irradiated mice with limiting numbers of purified hematopoietic stem cells: in vivo expansion of stem cell phenotype but not function. *Blood* 1995. **85**(4): 1006–1016.

1518 Cheshier, S. H., Morrison, S. J., Liao, X. and Weissman, I. L., In vivo proliferation and cell cycle kinetics of long-term self-renewing hematopoietic stem cells. *Proc. Natl. Acad. Sci. USA* 1999. **96**(6): 3120–3125.

1519 Calvi, L. M., Adams, G. B., Weibrecht, K. W., Weber, J. M., Olson, D. P., Knight, M. C., Martin, R. P. et al., Osteoblastic cells regulate the haematopoietic stem cell niche. *Nature* 2003. **425**(6960): 841–846.

1520 Arai, F., Hirao, A., Ohmura, M., Sato, H., Matsuoka, S., Takubo, K., Ito, K. et al., Tie2/angiopoietin-1 signaling regulates hematopoietic stem cell quiescence in the bone marrow niche. *Cell* 2004. **118**(2): 149–161.

1521 Zhang, J., Niu, C., Ye, L., Huang, H., He, X., Tong, W. G., Ross, J. et al., Identification of the haematopoietic stem cell niche and control of the niche size. *Nature* 2003. **425**(6960): 836–841.

1522 Hofer, T., Busch, K., Klapproth, K. and Rodewald, H. R., Fate mapping and quantitation of hematopoiesis in vivo. *Annu. Rev. Immunol.* 2016. **34**: 449–478.

1523 Carrelha, J., Meng, Y., Kettyle, L. M., Luis, T. C., Norfo, R., Alcolea, V., Boukarabila, H. et al., Hierarchically related lineage-restricted fates of

multipotent haematopoietic stem cells. *Nature* 2018. **554**(7690): 106–111.

1524 Haas, S., Hansson, J., Klimmeck, D., Loeffler, D., Velten, L., Uckelmann, H., Wurzer, S. et al., Inflammation-induced emergency megakaryopoiesis driven by hematopoietic stem cell-like megakaryocyte progenitors. *Cell Stem Cell* 2015. **17**(4): 422–434.

1525 Medvinsky, A., Rybtsov, S. and Taoudi, S., Embryonic origin of the adult hematopoietic system: advances and questions. *Development* 2011. **138**(6): 1017–1031.

1526 Kajikhina, K., Melchers, F. and Tsuneto, M., Chemokine polyreactivity of IL7Ralpha+CSF-1R+ lympho-myeloid progenitors in the developing fetal liver. *Sci. Rep.* 2015. **5**: 12817.

1527 Mikkola, H. K. and Orkin, S. H., The journey of developing hematopoietic stem cells. *Development* 2006. **133**(19): 3733–3744.

1528 Majeti, R., Park, C. Y., Weissman, I. L., Identification of a hierarchy of multipotent hematopoietic progenitors in human cord blood. *Cell Stem Cell* 2007. **1**(6): 635–645.

1529 Notta, F., Zandi, S., Takayama, N., Dobson, S., Gan, O. I., Wilson, G., Kaufmann, K. B. et al., Distinct routes of lineage development reshape the human blood hierarchy across ontogeny. *Science* 2016. **351**(6269): aab2116.

1530 Cosgun, K. N., Rahmig, S., Mende, N., Reinke, S., Hauber, I., Schafer, C., Petzold, A. et al., Kit regulates HSC engraftment across the human-mouse species barrier. *Cell Stem Cell* 2014. **15**(2): 227–238.

1531 Kiel, M. J., Yilmaz, O. H., Iwashita, T., Yilmaz, O. H., Terhorst, C. and Morrison, S. J., SLAM family receptors distinguish hematopoietic stem and progenitor cells and reveal endothelial niches for stem cells. *Cell* 2005. **121**(7): 1109–1121.

1532 Papathanasiou, P., Attema, J. L., Karsunky, H., Xu, J., Smale, S. T. and Weissman, I. L., Evaluation of the long-term reconstituting subset of hematopoietic stem cells with CD150. *Stem Cells* 2009. **27**(10): 2498–2508.

1533 Yilmaz, O. H., Kiel, M. J. and Morrison, S. J., SLAM family markers are conserved among hematopoietic stem cells from old and reconstituted mice and markedly increase their purity. *Blood* 2006. **107**(3): 924–930.

1534 Pei, W., Feyerabend, T. B., Rossler, J., Wang, X., Postrach, D., Busch, K., Rode, I. et al., Polylox barcoding reveals haematopoietic stem cell fates realized in vivo. *Nature* 2017. **548**(7668): 456–460.

1535 Busch, K., Klapproth, K., Barile, M., Flossdorf, M., Holland-Letz, T., Schlenner, S. M., Reth, M. et al., Fundamental properties of unperturbed haematopoiesis from stem cells in vivo. *Nature* 2015. **518**(7540): 542–546.

1536 Gomez Perdiguero, E., Klapproth, K., Schulz, C., Busch, K., Azzoni, E., Crozet, L., Garner, H. et al., Tissue-resident macrophages originate from yolk-sac-derived erythro-myeloid progenitors. *Nature* 2015. **518**(7540): 547–551.

1537 Tornack, J., Reece, S. T., Bauer, W. M., Vogelzang, A., Bandermann, S., Zedler, U., Stingl, G. et al., Human and Mouse Hematopoietic Stem Cells Are a Depot for Dormant Mycobacterium tuberculosis. *PLoS One* 2017. **12**(1): e0169119.

1538 Spangrude, G. J., Heimfeld, S. and Weissman, I. L., Purification and characterization of mouse hematopoietic stem cells. *Science* 1988. **241**(4861): 58–62.

1539 Ikuta, K. and Weissman, I. L., Evidence that hematopoietic stem cells express mouse c-kit but do not depend on steel factor for their generation. *Proc. Natl. Acad. Sci. USA* 1992. **89**(4): 1502–1506.

1540 Morrison, S. J. and Weissman, I. L., The long-term repopulating subset of hematopoietic stem cells is deterministic and isolatable by phenotype. *Immunity* 1994. **1**(8): 661–673.

1541 Okada, S., Nakauchi, H., Nagayoshi, K., Nishikawa, S., Miura, Y. and Suda, T., In vivo and in vitro stem cell function of c-kit- and Sca-1-positive murine hematopoietic cells. *Blood* 1992. **80**: 3044–3050.

1542 Balazs, A. B., Fabian, A. J., Esmon, C. T. and Mulligan, R. C., Endothelial protein C receptor (CD201) explicitly identifies hematopoietic stem cells in murine bone marrow. *Blood* 2006. **107**: 2317–2321.

1543 Osawa, M., Hanada, K., Hamada, H. and Nakauchi, H., Long-term lymphohematopoietic reconstitution by a single CD34-low/negative hematopoietic stem cell. *Science* 1996. **273**: 242–245.

1544 Tornack, J., Kawano, Y., Garbi, N., Hammerling, G. J., Melchers, F. and Tsuneto, M., Flt3 ligand-eGFP-reporter expression characterizes functionally distinct subpopulations of CD150(+) long-term repopulating murine hematopoietic stem cells. *Eur. J. Immunol.* 2017. **47**: 1477–1487.

1545 Zhou, S., Schuetz, J. D., Bunting, K. D., Colapietro, A. M., Sampath, J., Morris, J. J., Lagutina, I. et al., The ABC transporter Bcrp1/ABCG2 is expressed in a wide variety of stem cells and is a molecular determinant of the side-population phenotype. *Nat. Med.* 2001. **7**: 1028–1034.

1546 Ergen, A. V., Jeong, M., Lin, K. K., Challen, G. A., Goodell, M. A., Isolation and characterization of mouse side population cells. *Methods Mol. Biol.* 2013. **946**: 151–162.

1547 Lu, R., Neff, N. F., Quake, S. R. and Weissman, I. L., Tracking single hematopoietic stem cells in vivo using high-throughput sequencing in conjunction with viral genetic barcoding. *Nat. Biotechnol.* 2011. **29**: 928–933.

1548 Bystrykh, L. V., de Haan, G. and Verovskaya, E., Barcoded vector libraries and retroviral or lentiviral barcoding of hematopoietic stem cells. *Methods Mol. Biol.* 2014. **1185**: 345–360.

1549 Kawano, Y., Petkau, G., Stehle, C., Durek, P., Heinz, G. A., Tanimoto, K., Karasuyama, H. et al., Stable lines and clones of long-term proliferating normal, genetically unmodified murine common lymphoid progenitors. *Blood* 2018. **131**(18): 2026–2035.

1550 Knapp, D. J., Hammond, C. A., Miller, P. H., Rabu, G. M., Beer, P. A., Ricicova, M., Lecault, V. et al., Dissociation of survival, proliferation, and state control in human hematopoietic stem cells. *Stem Cell Rep.* 2017. **8**(1): 152–162.

1551 Yamamoto, R., Morita, Y., Ooehara, J., Hamanaka, S., Onodera, M., Rudolph, K. L., Ema, H. et al., Clonal analysis unveils self-renewing lineage-restricted progenitors generated directly from hematopoietic stem cells. *Cell* 2013. **154**(5): 1112–1126.

1552 Uchida, N. and Weissman, I. L., Searching for hematopoietic stem cells: evidence that Thy-1.1lo Lin- Sca-1+ cells are the only stem cells in C57BL/Ka-Thy-1.1 bone marrow. *J. Exp. Med.* 1992. **175**(1): 175–184.

1553 Murray, L., Chen, B., Galy, A., Chen, S., Tushinski, R., Uchida, N., Negrin, R. et al., Enrichment of human hematopoietic stem cell activity in the CD34+Thy-1+Lin- subpopulation from mobilized peripheral blood. *Blood* 1995. **85**(2): 368–378.

1554 Civin, C. I., Strauss, L. C., Brovall, C., Fackler, M. J., Schwartz, J. F. and Shaper, J. H., Antigenic analysis of hematopoiesis. III. A hematopoietic progenitor cell surface antigen defined by a monoclonal antibody raised against KG-1a cells. *J. Immunol.* 1984. **133**(1): 157–165.

1555 Goodell, M. A., Rosenzweig, M., Kim, H., Marks, D. F., DeMaria, M., Paradis, G., Grupp, S. A. et al., Dye efflux studies suggest that hematopoietic stem cells expressing low or undetectable levels of CD34 antigen exist in multiple species. *Nat. Med.* 1997. **3**(12): 1337–1345.

1556 Kang, Y., Chao, N. J., Aversa, F., Unmanipulated or CD34 selected haplotype mismatched transplants. *Curr. Opin. Hematol.* 2008. **15**(6): 561–567.

1557 Wang, J., Kimura, T., Asada, R., Harada, S., Yokota, S., Kawamoto, Y., Fujimura, Y. et al., SCID-repopulating cell activity of human cord

blood-derived CD34- cells assured by intra-bone marrow injection. *Blood* 2003. **101**(8): 2924–2931.

1558　Bhatia, M., Bonnet, D., Murdoch, B., Gan, O. I. and Dick, J. E., A newly discovered class of human hematopoietic cells with SCID-repopulating activity. *Nat. Med.* 1998. **4**(9): 1038–1045.

1559　Danet, G. H., Luongo, J. L., Butler, G., Lu, M. M., Tenner, A. J., Simon, M. C. and Bonnet, D. A., C1qRp defines a new human stem cell population with hematopoietic and hepatic potential. *Proc. Natl. Acad. Sci. USA* 2002. **99**(16): 10441–10445.

1560　Herbein, G., Sovalat, H., Wunder, E., Baerenzung, M., Bachorz, J., Lewandowski, H., Schweitzer, C. et al., Isolation and identification of two CD34+ cell subpopulations from normal human peripheral blood. *Stem Cells* 1994. **12**: 187–197.

1561　Bhatia, M., Wang, J. C., Kapp, U., Bonnet, D. and Dick, J. E., Purification of primitive human hematopoietic cells capable of repopulating immune-deficient mice. *Proc. Natl. Acad. Sci. USA* 1997. **94**(10): 5320–5325.

1562　Notta, F., Doulatov, S., Laurenti, E., Poeppl, A., Jurisica, I. and Dick, J. E., Isolation of single human hematopoietic stem cells capable of long-term multilineage engraftment. *Science* 2011. **333**(6039): 218–221.

1563　Fares, I., Chagraoui, J., Lehnertz, B., MacRae, T., Mayotte, N., Tomellini, E., Aubert, L. et al., EPCR expression marks UM171-expanded CD34(+) cord blood stem cells. *Blood* 2017. **129**(25): 3344–3351.

1564　Iwasaki, H., Arai, F., Kubota, Y., Dahl, M., Suda, T., Endothelial protein C receptor-expressing hematopoietic stem cells reside in the perisinusoidal niche in fetal liver. *Blood* 2010. **116**(4): 544–553.

1565　Galuzzi, L., Vacchelli, E., Bravo-San Pedro, J. M., Buqué, A., Senovilla, L., Baracco, E. E., Bloy, N. et al., Classification of current anticancer immunotherapies. *Oncotarget* 2015. **5**(24): 12472–12508.

1566　Hanahan, D. and Weinberg, R. A., Hallmarks of cancer – the next generation. *Cell* 2011. **144**: 646–674. https://doi.org/10.1016/j.cell.2011.02.013

1567　Lansdorp, P. M., Sutherland, H. J. and Eaves, C. J., Selective expression of CD45 isoforms on functional subpopulations of CD34+ hemopoietic cells from human bone marrow. *J. Exp. Med.* 1990. **172**: 363–366. https://doi.org/363-3660022-1007/90/07/0363/04

1568　van Dongen, J. J. M., Lhermitte, L., Böttcher, S., Almeida, J., van der Velden, J. V. H., Flores-Montero, J., Rawstron, A. et al., on behalf of the EuroFlow Consortium (EU-FP6, LSHB-CT-2006-018708). EuroFlow antibody panels for standardized n-dimensional flow cytometric immunophenotyping of normal, reactive and malignant leukocytes. *Leukemia* 2012. **26**: 1908–1975.

1569　Streitz, M., Miloud, T., Kapinsky, M., Reed, M. R., Magari, R., Geissler, E. K., Hutchinson, J. A. et al., Standardization of whole blood immune phenotype monitoring for clinical trials: panels and methods from the ONE study. *Transplant Res.* 2013. **2**(1): 17.

1570　Alix-Panabières, C. and Pantel, K., Challenges in circulating tumour cell research. *Nat. Rev. Cancer* 2014. **14**: 623–631. https://doi.org/10.1038/nrc3820

1571　Lopresti, A., Malergue, F., Bertucci, F., Liberatoscioli, M. L., Garnier, S., DaCosta, Q., Finetti, P. et al., Sensitive and easy screening for circulating tumor cells by flow cytometry. *JCI Insight* 2019. 5: 128180. https://doi.org/10.1172/jci.insight.128180

1572　Schumacher, T. and Schreiber, R. D., Neoantigens in cancer immunotherapy. *Science* 2015. **348**(6230): 69–74.

1573　Grizzi, F., Mirandola, L., Qehajaj, D., Cobos, E., Figueroa, J. A. and Chiriva-Internati, M., Cancer-testis antigens and immunotherapy in the light of cancer complexity. *Int. Rev. Immunol.* 2015. **34**: 143–153. https://doi.org/10.3109/08830185.2015.1018418

1574　Garrido, F., Aptsiauri, N., Doorduijn, E. M., Garcia Lora, A. M. and van Hall, T., The urgent need to recover MHC class I in cancers for effective immunotherapy. *Curr. Opin. Immunol.* 2016. **39**: 44–51. https://doi.org/10.1016/j.coi.2015.12.007

1575　Raulet, D. H., Gasser, S., Gowen, B. G., Deng, W. and Jung, H., Regulation of ligands for the NKG2D activating receptor. *Annu. Rev. Immunol.* 2013. **31**: 413–441.

1576　Sers, C., Kuner, R., Fak, C. S., Lund, P., Sueltmann, H., Braun, M., Buness, A. et al., Down-regulation of HLA Class I and NKG2D ligands through a concerted action of MAPK and DNA methyltransferases in colorectal cancer cells. *Int. J. Cancer* 2009. **125**(7): 1626–1639.

1577　Luo, Z., Wu, R. R., Lv, L., Li, P., Zhang, L. Y., Hao, Q. L. and Li, W., Prognostic value of CD44 expression in non-small cell lung cancer: a systematic review. *Int. J. Clin. Exp. Pathol.* 2014. **7**(7): 3632–3646.

1578　Paulis, Y. W., Huijbers, E. J., van der Schaft, D. W., Soetekouw, P. M., Pauwels, P., Tjan-Heijnen, V. C. and Griffioen, A. W., CD44 enhances tumor aggressiveness by promoting tumor cell plasticity. *Oncotarget* 2015. **6**(23): 19634–19646.

1579　http://www.cancerresearchuk.org/about-cancer/what-is-cancer/how-cancer-starts/types-of-cancer#carcinomas

1580　Weng, Y. R., Cui, Y. and Fang, J. Y., Biological functions of cytokeratin 18 in cancer. *Mol. Cancer Res.* 2012. **10**(4): 485–493.

1581　Appert-Collin, A., Hubert, P., Crémel, G. and Bennasroune, A., Role of ErbB receptors in cancer cell migration and invasion. *Front. Pharmacol.* 2015. https://doi.org/10.3389/fphar.2015.00283

1582　http://www.cancer.org/cancer/breastcancer/detailedguide/breast-cancer-breast-cancer-types

1583　Park, J. W., Lee, J. K., Phillips, J. W., Huang, P., Cheng, D., Huang, J. and Witte, O. N., Prostate epithelial cell of origin determines cancer differentiation state in an organoid transformation assay. *Proc. Natl. Acad. Sci. USA* 2016. **113**: 4482–4487.

1584　http://screening.iarc.fr/colpochap.php?chap=2

1585　https://www.iarc.fr/en/publications/pdfs-online/pat-gen/bb2/bb2-chap1.pdf

1586　http://www.cancer.org/cancer/bladdercancer/detailedguide/bladder-cancer-what-is-bladder-cancer

1587　Hruban, R. H. and Fukushima, N., Pancreatic adenocarcinoma: update on the surgical pathology of carcinomas of ductal origin and PanINs. *Modern Pathol.* 2007. **20**: 61–70.

1588　DuBois, S. G., Epling, C. L., Teague, J., Matthay, K. K. and Sinclair, E., Flow cytometric detection of ewing sarcoma cells in peripheral blood and bone marrow. *Pediatr. Blood Cancer* 2010. **54**(1): 13–18. https://doi.org/10.1002/pbc.22245

1589　Avey, D., Brewers, B. and Zhu, F., Recent advances in the study of Kaposi's sarcoma-associated herpesvirus replication and athogenesis. *Virol Sin.* 2015. **30**(2): 130-145. https://doi.org/10.1007/s12250-015-3595-2

1590　Deel, M. D., Li, J. J., Crose, L. E. and Linardic, C. M., A Review: molecular aberrations within hippo signaling in bone and soft-tissue sarcomas. *Front Oncol.* 2015. **5**: 190. https://doi.org/10.3389/fonc.2015.00190

1591　Sullivan, R. J., The role of mitogen-activated protein targeting in melanoma beyond BRAFV600. *Curr. Opin. Oncol.* 2016. **28**(2): 185–191.

1592　Sucker, A., Zhao, F., Real, B., Heeke, C., Bielefeld, N., Maßen, S., Horn, S. et al., Genetic evolution of T cell resistance in the course of melanoma progression. *Clin. Canc. Res.* 2014. **20**(24): 6593–6604.

1593　Lakshmikanth, T., Burke, S., Ali, T. H., Kimpfler, S., Ursini, F., Ruggeri, L., Capanni, M. et al., NCRs and DNAM-1 mediate NK cell recognition

and lysis of human and mouse melanoma cell lines in vitro and in vivo. *J. Clin. Invest.* 2009. **119**(5): 1251–1263. https://doi.org/10.1172/JCI36022

1594 Binder, D. C., Davis, A. A. and Wainwright, D. A., Immunotherapy for cancer in the central nervous system: Current and future directions. *Oncoimmunology* 2015. **5**(2): e1082027.

1595 Razavi, S. M., Lee, K. E., Jin, B. E., Aujla, P. S., Gholamin, S. and Li, G., Immune Evasion Strategies of Glioblastoma. *Frnt. Surg.* 2016. **3**: 11.

1596 Seifert, M., Garbe, M., Friedrich, B., Mittelbronn, M. and Klink, B., Comparative transcriptomics reveals similarities and differences between astrocytoma grades. *BMC Cancer* 2015. **15**: 952.

1597 Dranoff, G., Experimental mouse tumour models: what can be learnt about human cancer immunology? *Nat. Rev. Immunol.* 2012. **12**: 61–66. https://doi.org/10.1038/nri3129

1598 Morton, J. J., Bird, G., Fefaeli, Y. and Jimeno, A., Humanized mouse xenograft models: narrowing the tumor-microenvironment gap. *Canc. Res.* 2016. **76**: 6153–6158.

1599 Huntington, N. D., Xu, Y., Puthalakath, H., Light, A., Willis, S. N., Strasser, A. et al., CD45 links the B cell receptor with cell survival and is required for the persistence of germinal centers. *Nat. Immunol.* 2006. **7**(2): 190–198.

1600 Oracki, S. A., Walker, J. A., Hibbs, M. L., Corcoran, L. M. and Tarlinton, D. M., Plasma cell development and survival. *Immunol. Rev.* 2010. **237**(1): 140–159.

1601 Brynjolfsson, S. F., Persson Berg, L., Olsen Ekerhult, T., Rimkute, I., Wick, M. J., Martensson, I. L. et al., Long-lived plasma cells in mice and men. *Front. Immunol.* 2018. **9**: 2673.

1602 Steensma, D. P., Gertz, M. A., Greipp, P. R., Kyle, R. A., Lacy, M. Q., Lust, J. A. et al., A high bone marrow plasma cell labeling index in stable plateau-phase multiple myeloma is a marker for early disease progression and death. *Blood* 2001. **97**(8): 2522–2523.

1603 Bakkus, M. H., Heirman, C., Van Riet, I., Van Camp, B. and Thielemans, K., Evidence that multiple myeloma Ig heavy chain VDJ genes contain somatic mutations but show no intraclonal variation. *Blood* 1992. **80**(9): 2326–2335.

1604 Kosmas, C., Stamatopoulos, K., Stavroyianni, N., Zoi, K., Belessi, C., Viniou, N. et al., Origin and diversification of the clonogenic cell in multiple myeloma: lessons from the immunoglobulin repertoire. *Leukemia* 2000. **14**(10): 1718–1726.

1605 Pfeifer, S., Perez-Andres, M., Ludwig, H., Sahota, S. S. and Zojer, N., Evaluating the clonal hierarchy in light-chain multiple myeloma: implications against the myeloma stem cell hypothesis. *Leukemia* 2011. **25**(7): 1213–1216.

1606 Hansmann, L., Han, A., Penter, L., Liedtke, M. and Davis, M. M., Clonal expansion and interrelatedness of distinct B-lineage compartments in multiple myeloma bone marrow. *Cancer Immunol. Res.* 2017. **5**: 744–754.

1607 Hideshima, T., Nakamura, N., Chauhan, D. and Anderson, K. C., Biologic sequelae of interleukin-6 induced PI3-K/Akt signaling in multiple myeloma. *Oncogene* 2001. **20**(42): 5991–6000.

1608 de Haart, S. J., van der Donk, N. W., Minnema, M. C., Huang, J. H., Aarts-Riemens, T., Bovenschen, N. et al., Accessory cells of the microenvironment protect multiple myeloma from T-cell cytotoxicity through cell adhesion-mediated immune resistance. *Clin. Cancer Res.* 2013. **19**(20): 5591–5601.

1609 Hideshima, T., Bergsagel, P. L., Kuehl, W. M. and Anderson, K. C., Advances in biology of multiple myeloma: clinical applications. *Blood* 2004. **104**: 607–618.

1610 Mitsiades, C. S., Mitsiades, N., Munshi, N. C. and Anderson, K. C., Focus on multiple myeloma. *Cancer Cell* 2004. **6**(5): 439–444.

1611 Mitsiades, C. S., Mitsiades, N. S., Richardson, P. G., Munshi, N. C. and Anderson, K. C., Multiple myeloma: a prototypic disease model for the characterization and therapeutic targeting of interactions between tumor cells and their local microenvironment. *J. Cell. Biochem.* 2007. **101**(4): 950–968.

1612 Bianchi, G. and Munshi, N. C., Pathogenesis beyond the cancer clone(s) in multiple myeloma. *Blood* 2015. **125**(20): 3049–3058.

1613 Keats, J. J., Chesi, M., Egan, J. B., Garbitt, V. M., Palmer, S. E., Braggio, E. et al., Clonal competition with alternating dominance in multiple myeloma. *Blood* 2012. **120**(5): 1067–1076.

1614 Lohr, J. G., Kim, S., Gould, J., Knoechel, B., Drier, Y., Cotton, M. J. et al., Genetic interrogation of circulating multiple myeloma cells at single-cell resolution. *Sci. Transl. Med.* 2016. **8**(363): 363ra147.

1615 Lohr, J. G., Stojanov, P., Carter, S. L., Cruz-Gordillo, P., Lawrence, M. S., Auclair, D. et al., Widespread genetic heterogeneity in multiple myeloma: implications for targeted therapy. *Cancer Cell* 2014. **25**(1): 91–101.

1616 Paino, T., Paiva, B., Sayagues, J. M., Mota, I., Carvalheiro, T., Corchete, L. A. et al., Phenotypic identification of subclones in multiple myeloma with different chemoresistant, cytogenetic and clonogenic potential. *Leukemia* 2015. **29**(5): 1186–1194.

1617 Arroz, M., Came, N., Lin, P., Chen, W., Yuan, C., Lagoo, A. et al., Consensus guidelines on plasma cell myeloma minimal residual disease analysis and reporting. *Cytom. B Clin. Cytom.* 2016. **90**(1): 31–39.

1618 Flores-Montero, J., de Tute, R., Paiva, B., Perez, J. J., Bottcher, S., Wind, H. et al., Immunophenotype of normal vs. myeloma plasma cells: Toward antibody panel specifications for MRD detection in multiple myeloma. *Cytom. B Clin. Cytom.* 2016. **90**(1): 61–72.

1619 Jelinek, T. and Hajek, R., Monoclonal antibodies—a new era in the treatment of multiple myeloma. *Blood Rev.* 2016. **30**(2): 101–110.

1620 Paiva, B., Puig, N., Cedena, M. T., de Jong, B. G., Ruiz, Y., Rapado, I. et al., Differentiation stage of myeloma plasma cells: biological and clinical significance. *Leukemia* 2017. **31**(2): 382–392.

1621 Lisenko, K., Schonland, S., Hegenbart, U., Wallenwein, K., Braun, U., Mai, E. K. et al., Potential therapeutic targets in plasma cell disorders: a flow cytometry study. *Cytom. B Clin. Cytom.* 2017. **92**(2): 145–152.

1622 Berliner, N., Ault, K. A., Martin, P. and Weinberg, D. S., Detection of clonal excess in lymphoproliferative disease by kappa/lambda analysis: correlation with immunoglobulin gene DNA rearrangement. *Blood* 1986. **67**(1): 80–85.

1623 Smock, K. J., Perkins, S. L. and Bahler, D. W., Quantitation of plasma cells in bone marrow aspirates by flow cytometric analysis compared with morphologic assessment. *Arch. Pathol. Lab. Med.* 2007. **131**(6): 951–955.

1624 Lokhorst, H. M., Laubach, J. and Nahi, H., Dose-dependent efficacy of daratumumab (DARA) as monotherapy in patients with relapsed or refractory multiple myeloma (RR MM). *J Clin. Oncol.* 2014. 32: abstract 8513.

1625 Lammerts van Bueren, J., Jakobs, D. and Kaldenhoven, N., Direct in vitro comparison of daratumumab with surrogate analogs of CD38 antibodies MOR03087, SAR650984 and Ab79. In: 56*th ASH Annual Meeting & Exposition*: Oral and Poster Abstracts, 2014.

1626 Oberle, A., Brandt, A., Alawi, M., Langebrake, C., Janjetovic, S., Wolschke, C. et al., Long-term CD38 saturation by daratumumab interferes with diagnostic myeloma cell detection. *Haematologica* 2017. **102**(9): e368–e370.

1627 Perincheri, S., Torres, R., Tormey, C. A., Smith, B. R., Rinder, H. M. and Siddon, A. J., Daratumumab interferes with flow cytometric evaluation of multiple myeloma. 2016. **128**(22): 5630–5630.

1628 **Malaer, J. D. and Mathew, P. A.**, CS1 (SLAMF7, CD319) is an effective immunotherapeutic target for multiple myeloma. *Am. J. Cancer Res.* 2017. **7**(8): 1637–1641.

1629 **Tellier, J., Shi, W., Minnich, M., Liao, Y., Crawford, S., Smyth, G. K. et al.**, Blimp-1 controls plasma cell function through the regulation of immunoglobulin secretion and the unfolded protein response. *Nat. Immunol.* 2016. **17**(3): 323–330.

1630 **Rawstron, A. C., Orfao, A., Beksac, M., Bezdickova, L., Brooimans, R. A., Bumbea, H. et al.**, Report of the European Myeloma Network on multiparametric flow cytometry in multiple myeloma and related disorders. *Haematologica* 2008. **93**(3): 431–438.

1631 **Paiva, B., Garcia-Sanz, R. and San Miguel, J. F.**, Multiple myeloma minimal residual disease. *Cancer Treat. Res.* 2016. **169**: 103–122.

1632 **Paiva, B., van Dongen, J. J. and Orfao, A.**, New criteria for response assessment: role of minimal residual disease in multiple myeloma. *Blood* 2015. **125**(20): 3059–3068.

1633 **Flores-Montero, J., Sanoja-Flores, L., Paiva, B., Puig, N., Garcia-Sanchez, O., Bottcher, S. et al.**, Next Generation Flow for highly sensitive and standardized detection of minimal residual disease in multiple myeloma. *Leukemia* 2017. **31**(10): 2094–2103.

1634 **Roschewski, M., Stetler-Stevenson, M., Yuan, C., Mailankody, S., Korde, N. and Landgren, O.**, Minimal residual disease: what are the minimum requirements? *J. Clin. Oncol.* 2014. **32**(5): 475–476.

1635 **Cahoy, J. D., Emery, B., Kaushal, A., Foo, L. C., Zamanian, J. L., Christopherson, K. S., Xing, Y. et al.**, A Transcriptome Database for Astrocytes, Neurons, and Oligodendrocytes: A New Resource for Understanding Brain Development and Function. *J. Neurosci.* 2008. **28**: 264–278.

1636 **Hawrylycz, M. J., Lein, E. S., Guillozet-Bongaarts, A. L., Shen, E. H., Ng, L., Miller, J. A., Van De Lagemaat, L. N. et al.**, An anatomically comprehensive atlas of the adult human brain transcriptome. *Nature* 2012. **489**: 391.

1637 **Mink, J. W., Blumenschine, R. J. and Adams, D. B.**, Ratio of central nervous system to body metabolism in vertebrates: its constancy and functional basis. *Am. J. Physiol. Regul. Integr. Comp. Physiol.* 1981. **241**: R203–R212.

1638 **Lake, B. B., Ai, R., Kaeser, G. E., Salathia, N. S., Yung, Y. C., Liu, R., Wildberg, A. et al.**, Neuronal subtypes and diversity revealed by single-nucleus RNA sequencing of the human brain. *Science* 2016. **352**: 1586–1590.

1639 **Bradl, M. and Lassmann, H.**, Oligodendrocytes: biology and pathology. *Acta Neuropathol.* 2010. **119**: 37–53.

1640 **Sofroniew, M. V. and Vinters, H. V.**, Astrocytes: biology and pathology. *Acta Neuropathol.* 2010. **119**: 7–35.

1641 **Bergström, T. and Forsberg-Nilsson, K.**, Neural stem cells: brain building blocks and beyond. *Ups. J. Med. Sci.* 2012. **117**: 132–142.

1642 **Ginhoux, F., Greter, M., Leboeuf, M., Nandi, S., See, P., Gokhan, S., Mehler, M. F. et al.**, Fate mapping analysis reveals that adult microglia derive from primitive macrophages. *Science* 2010. **330**: 841–845.

1643 **Goldmann, T., Wieghofer, P., Jordão, M. J. C., Prutek, F., Hagemeyer, N., Frenzel, K., Amann, L. et al.**, Origin, fate and dynamics of macrophages at central nervous system interfaces. *Nat. Immunol.* 2016. **17**: 797–805.

1644 **Kantzer, C. G., Boutin, C., Herzig, I. D., Wittwer, C., Reiß, S., Tiveron, M. C., Drewes, J. et al.**, Anti-ACSA-2 defines a novel monoclonal antibody for prospective isolation of living neonatal and adult astrocytes. *Glia* 2017. **65**: 990–1004.

1645 **Batiuk, M. Y., De Vin, F., Duque, S. I., Li, C., Saito, T., Saido, T., Fiers, M. et al.**, An immunoaffinity-based method for isolating ultrapure adult astrocytes based on ATP1B2 targeting by the ACSA-2 antibody. *J. Biol. Chem.* 2017. **292**: 8874–8891.

1646 **Lin, C.-C. J., Yu, K., Hatcher, A., Huang, T.-W., Lee, H. K., Carlson, J., Weston, M. C. et al.**, Identification of diverse astrocyte populations and their malignant analogs. *Nat. Neurosci.* 2017. **20**: 396.

1647 **Tsai, H.-H., Li, H., Fuentealba, L. C., Molofsky, A. V., Taveira-Marques, R., Zhuang, H., Tenney, A. et al.**, Regional astrocyte allocation regulates CNS synaptogenesis and repair. *Science* 2012. **337**: 358–362.

1648 **Guttenplan, K. A. and Liddelow, S. A.**, Astrocytes and microglia: models and tools. *J. Exp. Med.* 2018. **216**: 71–83.

1649 **Zhuo, L., Sun, B., Zhang, C. L., Fine, A., Chiu, S. Y. and Messing, A.**, Live astrocytes visualized by green fluorescent protein in transgenic mice. *Dev. Biol.* 1997. **187**: 36–42.

1650 **Nolte, C., Matyash, M., Pivneva, T., Schipke, C. G., Ohlemeyer, C., Hanisch, U.-K., Kirchhoff, F. et al.**, GFAP promoter-controlled EGFP-expressing transgenic mice: a tool to visualize astrocytes and astrogliosis in living brain tissue. *Glia* 2001. **33**: 72–86.

1651 **Kuzmanovic, M., Dudley, V. J. and Sarthy, V. P.**, GFAP promoter drives Muller cell-specific expression in transgenic mice. Invest. *Ophthalmol. Vis. Sci.* 2003. **44**: 3606–3613.

1652 **Cho, W., Hagemann, T. L., Johnson, D. A., Johnson, J. A. and Messing, A.**, Dual transgenic reporter mice as a tool for monitoring expression of glial fibrillary acidic protein. *J. Neurochem.* 2009. **110**: 343–351.

1653 **Regan, M. R., Huang, Y. H., Kim, Y. S., Dykes-Hoberg, M. I., Jin, L., Watkins, A. M., Bergles, D. E. et al.**, Variations in promoter activity reveal a differential expression and physiology of glutamate transporters by glia in the developing and mature CNS. *J. Neurosci.* 2007. **27**: 6607–6619.

1654 **Bardehle, S., Kruger, M., Buggenthin, F., Schwausch, J., Ninkovic, J., Clevers, H., Snippert, H. J. et al.**, Live imaging of astrocyte responses to acute injury reveals selective juxtavascular proliferation. *Nat. Neurosci.* 2013. **16**: 580–586.

1655 **Yang, Y., Vidensky, S., Jin, L., Jie, C., Lorenzini, I., Frankl, M. and Rothstein, J. D.**, Molecular comparison of GLT1+ and ALDH1L1+ astrocytes in vivo in astroglial reporter mice. *Glia* 2011. **59**: 200–207.

1656 **Gong, S., Zheng, C., Doughty, M. L., Losos, K., Didkovsky, N., Schambra, U. B., Nowak, N. J. et al.**, A gene expression atlas of the central nervous system based on bacterial artificial chromosomes. *Nature* 2003. **425**: 917–925.

1657 **Jung, S., Aliberti, J., Graemmel, P., Sunshine, M. J., Kreutzberg, G. W., Sher, A. and Littman, D. R.**, Analysis of fractalkine receptor CX(3)CR1 function by targeted deletion and green fluorescent protein reporter gene insertion. *Mol. Cell Biol.* 2000. **20**: 4106–4114.

1658 **Yona, S., Kim, K. W., Wolf, Y., Mildner, A., Varol, D., Breker, M., Strauss-Ayali, D. et al.**, Fate mapping reveals origins and dynamics of monocytes and tissue macrophages under homeostasis. *Immunity* 2013. **38**: 79–91.

1659 **Buttgereit, A., Lelios, I., Yu, X., Vrohlings, M., Krakoski, N. R., Gautier, E. L., Nishinakamura, R. et al.**, Sall1 is a transcriptional regulator defining microglia identity and function. *Nat. Immunol.* 2016. **17**: 1397–1406.

1660 **Hirasawa, T., Ohsawa, K., Imai, Y., Ondo, Y., Akazawa, C., Uchino, S. and Kohsaka, S.**, Visualization of microglia in living tissues using Iba1-EGFP transgenic mice. *J. Neurosci. Res.* 2005. **81**: 357–362.

1661 **Sasmono, R. T., Oceandy, D., Pollard, J. W., Tong, W., Pavli, P., Wainwright, B. J., Ostrowski, M. C. et al.**, A macrophage colony-stimulating factor receptor-green fluorescent protein transgene is expressed throughout the mononuclear phagocyte system of the mouse. *Blood* 2003. **101**: 1155–1163.

1662 **Dziennis, S., Van Etten, R. A., Pahl, H. L., Morris, D. L., Rothstein, T. L., Blosch, C. M., Perlmutter, R. M. et al.**, The CD11b promoter directs

high-level expression of reporter genes in macrophages in transgenic mice. *Blood* 1995. **85**: 319–329.

1663 Yang, J., Hills, D., Taylor, E., Pfeffer, K., Ure, J. and Medvinsky, A., Transgenic tools for analysis of the haematopoietic system: knock-in CD45 reporter and deletor mice. *J. Immunol. Methods* 2008. **337**: 81–87.

1664 Pillai, M. M., Hayes, B. and Torok-Storb, B., Inducible transgenes under the control of the hCD68 promoter identifies mouse macrophages with a distribution that differs from the F4/80 - and CSF-1R-expressing populations. *Exp. Hematol.* 2009. **37**: 1387–1392.

1665 Iqbal, A. J., Mcneill, E., Kapellos, T. S., Regan-Komito, D., Norman, S., Burd, S., Smart, N. et al., Human CD68 promoter GFP transgenic mice allow analysis of monocyte to macrophage differentiation in vivo. *Blood* 2014. **124**: e33–e44.

1666 Hägglund, M., Borgius, L., Dougherty, K. J. and Kiehn, O., Activation of groups of excitatory neurons in the mammalian spinal cord or hindbrain evokes locomotion. *Nat. Neurosci.* 2010. **13**: 246–252.

1667 Blanco-Centurion, C., Bendell, E., Zou, B., Sun, Y., Shiromani, P. J. and Liu, M., VGAT and VGLUT2 expression in MCH and orexin neurons in double transgenic reporter mice. *IBRO Rep.* 2018. **4**: 44–49.

1668 Daigle, T. L., Madisen, L., Hage, T. A., Valley, M. T., Knoblich, U., Larsen, R. S., Takeno, M. M. et al., A suite of transgenic driver and reporter mouse lines with enhanced brain-cell-type targeting and functionality. *Cell* 2018. **174**: 465–480.e422.

1669 Martin, D., Xu, J., Porretta, C. and Nichols, C. D., Neurocytometry: flow cytometric sorting of specific neuronal populations from human and rodent brain. *ACS Chem. Neurosci.* 2017. **8**: 356–367.

1670 Evrony, G. D., Cai, X., Lee, E., Hills, L. B., Elhosary, P. C., Lehmann, H. S., Parker, J. J. et al., Single-neuron sequencing analysis of L1 retrotransposition and somatic mutation in the human brain. *Cell* 2012. **151**: 483–496.

1671 Cai, X., Evrony, G. D., Lehmann, H. S., Elhosary, P. C., Mehta, B. K., Poduri, A. and Walsh, C. A., Single-cell, genome-wide sequencing identifies clonal somatic copy-number variation in the human brain. *Cell Rep.* 2014. **8**: 1280–1289.

1672 Girdhar, K., Hoffman, G. E., Jiang, Y., Brown, L., Kundakovic, M., Hauberg, M. E., Francoeur, N. J. et al., Cell-specific histone modification maps in the human frontal lobe link schizophrenia risk to the neuronal epigenome. *Nat. Neurosci.* 2018. **21**: 1126–1136.

1673 Matevossian, A. and Akbarian, S., Neuronal nuclei isolation from human postmortem brain tissue. *J. Vis. Exp.* 2008. **1**: 914.

1674 McCarthy, K. D. and De Vellis, J., Preparation of separate astroglial and oligodendroglial cell cultures from rat cerebral tissue. *J. Cell. Biol.* 1980. **85**: 890–902.

1675 Barres, B. A., Hart, I. K., Coles, H. S. R., Burne, J. F., Voyvodic, J. T., Richardson, W. D. and Raff, M. C., Cell death and control of cell survival in the oligodendrocyte lineage. *Cell* 1992. **70**: 31–46.

1676 Seiwa, C., Kojima-Aikawa, K., Matsumoto, I. and Asou, H., CNS myelinogenesis in vitro: myelin basic protein deficient shiverer oligodendrocytes. *J. Neurosci. Res.* 2002. **69**: 305–317.

1677 Yang, Z., Watanabe, M. and Nishiyama, A., Optimization of oligodendrocyte progenitor cell culture method for enhanced survival. *J. Neurosci. Meth.* 2005. **149**: 50–56.

1678 Robinson, A. P., Rodgers, J. M., Goings, G. E. and Miller, S. D., Characterization of oligodendroglial populations in mouse demyelinating disease using flow cytometry: clues for MS pathogenesis. *PLoS ONE* 2014. **9**: e107649.

1679 Zhang, Y., Sloan, S. A., Clarke, L. E., Caneda, C., Plaza, C. A., Blumenthal, P. D., Vogel, H. et al., Purification and Characterization of

Progenitor and Mature Human Astrocytes Reveals Transcriptional and Functional Differences with Mouse. *Neuron* 2016. **89**: 37–53.

1680 Deng, Y., Kim, B., He, X., Kim, S., Lu, C., Wang, H., Cho, S. G. et al., Direct visualization of membrane architecture of myelinating cells in transgenic mice expressing membrane-anchored EGFP. *Genesis* 2014. **52**: 341–349.

1681 Hughes, E. G., Kang, S. H., Fukaya, M. and Bergles, D. E., Oligodendrocyte progenitors balance growth with self-repulsion to achieve homeostasis in the adult brain. *Nat. Neurosci.* 2013. **16**: 668–676.

1682 Sedgwick, J. D., Schwender, S., Imrich, H., Dörries, R., Butcher, G. W. and Ter Meulen, V., Isolation and direct characterization of resident microglial cells from the normal and inflamed central nervous system. *Proc. Natl. Acad. Sci. USA* 1991. **88**: 7438–7442.

1683 Bennett, M. L., Bennett, F. C., Liddelow, S. A., Ajami, B., Zamanian, J. L., Fernhoff, N. B., Mulinyawe, S. B. et al., New tools for studying microglia in the mouse and human CNS. *Proc. Natl. Acad. Sci. USA* 2016. **113**: E1738–E1746.

1684 Korin, B., Ben-Shaanan, T. L., Schiller, M., Dubovik, T., Azulay-Debby, H., Boshnak, N. T., Koren, T. et al., High-dimensional, single-cell characterization of the brain's immune compartment. *Nat. Neurosci.* 2017. **20**: 1300–1309.

1685 Mrdjen, D., Hartmann, F. J. and Becher, B., High dimensional cytometry of central nervous system leukocytes during neuroinflammation. *Methods Mol. Biol.* 2017. **1559**: 321–332.

1686 Ajami, B., Samusik, N., Wieghofer, P., Ho, P. P., Crotti, A., Bjornson, Z., Prinz, M. et al., Single-cell mass cytometry reveals distinct populations of brain myeloid cells in mouse neuroinflammation and neurodegeneration models. *Nat. Neurosci.* 2018. **21**: 541–551.

1687 Mrdjen, D., Pavlovic, A., Hartmann, F. J., Schreiner, B., Utz, S. G., Leung, B. P., Lelios, I. et al., High-dimensional single-cell mapping of central nervous system immune cells reveals distinct myeloid subsets in health, aging, and disease. *Immunity* 2018. **48**: 599.

1688 Böttcher, C., Schlickeiser, S., Sneeboer, M. a. M., Kunkel, D., Knop, A., Paza, E., Fidzinski, P. et al., Human microglia regional heterogeneity and phenotypes determined by multiplexed single-cell mass cytometry. *Nat. Neurosci.* 2019. **22**: 78–90.

1689 Ecker, J. R., Geschwind, D. H., Kriegstein, A. R., Ngai, J., Osten, P., Polioudakis, D., Regev, A. et al., The BRAIN Initiative Cell Census Consortium: lessons learned toward generating a comprehensive brain cell atlas. *Neuron* 2017. **96**: 542–557.

1690 Tham, C. S., Lin, F. F., Rao, T. S., Yu, N. and Webb, M., Microglial activation state and lysophospholipid acid receptor expression. *Int. J. Dev. Neurosci.* 2003. **21**: 431–443.

1691 Pfenninger, C. V., Roschupkina, T., Hertwig, F., Kottwitz, D., Englund, E., Bengzon, J., Jacobsen, S. E. et al., CD133 is not present on neurogenic astrocytes in the adult subventricular zone, but on embryonic neural stem cells, ependymal cells, and glioblastoma cells. *Cancer Res.* 2007. **67**: 5727–5736.

1692 Moussaud, S. and Draheim, H. J., A new method to isolate microglia from adult mice and culture them for an extended period of time. *J. Neurosci. Methods* 2010. **187**: 243–253.

1693 Foo, L. C., Allen, N. J., Bushong, E. A., Ventura, P. B., Chung, W.-S., Zhou, L., Cahoy, J. D. et al., Development of a Method for the Purification and Culture of Rodent Astrocytes. *Neuron* 2011. **71**: 799–811.

1694 Horst, A. K., Neumann, K., Diehl, L. and Tiegs, G., Modulation of liver tolerance by conventional and nonconventional antigen-presenting cells and regulatory immune cells. *Cell. Mol. Immunol.* 2016. **13**: 277–292.

1695 **Jenne, C. N. and Kubes, P.**, Immune surveillance by the liver. *Nat. Immunol.* 2013. **14**: 996–1006.

1696 **Thomson, A. W. and Knolle, P. A.**, Antigen-presenting cell function in the tolerogenic liver environment. *Nat. Rev. Immunol.* 2010. **10**: 753–766.

1697 **Crispe, I. N.**, Immune tolerance in liver disease. *Hepatology* 2014. **60**: 2109–2117.

1698 **Racanelli, V. and Rehermann, B.**, The liver as an immunological organ. *Hepatology.* 2006. **43**: S54–62.

1699 **Blom, K. G., Qazi, M. R., Matos, J. B., Nelson, B. D., DePierre, J. W. and Abedi-Valugerdi, M.**, Isolation of murine intrahepatic immune cells employing a modified procedure for mechanical disruption and functional characterization of the B, T and natural killer T cells obtained. *Clin. Exp. Immunol.* 2009. **155**: 320–329.

1700 **Gao, B., Radaeva, S. and Park, O.**, Liver natural killer and natural killer T cells: immunobiology and emerging roles in liver diseases. *J. Leukoc. Biol.* 2009. **86**: 513–528.

1701 **Niemeyer, M., Darmoise, A., Mollenkopf, H. J., Hahnke, K., Hurwitz, R., Besra, G. S., Schaible, U. E. et al.**, Natural killer T-cell characterization through gene expression profiling: an account of versatility bridging T helper type 1 (Th1), Th2 and Th17 immune responses. *Immunology* 2008. **123**: 45–56.

1702 **Pang, D. J., Neves, J. F., Sumaria, N. and Pennington, D. J.**, Understanding the complexity of γδ T-cell subsets in mouse and human. *Immunology* 2012. **136**: 283–290.

1703 **Golubovskaya, V. and Wu, L.**, Different subsets of T cells, memory, effector functions, and CAR-T immunotherapy. *Cancers* 2016. **8**(3): E36.

1704 **Davies, L. C., Jenkins, S. J., Allen, J. E. and Taylor, P. R.**, Tissue-resident macrophages. *Nat. Immunol.* 2013. **14**: 986–995.

1705 **Gordon, S. and Plüddemann, A.**, Tissue macrophages: Heterogeneity and functions. *BMC. Biol.* 2017. **15**: 53.

1706 **Gordon, S. and Taylor, P. R.**, Monocyte and macrophage heterogeneity. *Nat. Rev. Immunol.* 2005. **5**: 953–964.

1707 **Shortman, K. and Liu, Y. J.**, Mouse and human dendritic cell subtypes. *Nat. Rev. Immunol.* 2002. **2**: 151–161.

1708 **Meurens, F., Summerfield, A., Nauwynck, H., Saif, L. and Gerdts, V.**, The pig: a model for human infectious diseases. *Trends Microbiol.* 2012. **20**: 50–57.

1709 **Piriou-Guzylack, L. and Salmon, H.**, Membrane markers of the immune cells in swine: an update. *Vet. Res.* 2008. **39**: 54.

1710 **Dawson, H. D. and Lunney, J. K.**, Porcine cluster of differentiation (CD) markers 2018 update. *Res. Vet. Sci.* 2018. **118**: 199–246.

1711 **Saalmüller, A., Reddehase, M. J., Bühring, H.-J., Jonjić, S. and Koszinowski, U. H.**, Simultaneous expression of CD4 and CD8 antigens by a substantial proportion of resting porcine T lymphocytes. *Eur. J. Immunol.* 1987. **17**(9): 1297–1301.

1712 **Saalmüller, A., Weiland, F. and Reddehase, M. J.**, Resting porcine T lymphocytes expressing class II major histocompatibility antigen. *Immunobiology* 1991. **183**: 102–114.

1713 **Reutner, K., Leitner, J., Mullebner, A., Ladinig, A., Essler, S. E., Duvigneau, J. C., Ritzmann, M. et al.**, CD27 expression discriminates porcine T helper cells with functionally distinct properties. *Vet. Res.* 2013. **44**(1): 18.

1714 **Mair, K. H., Essler, S. E., Patzl, M., Storset, A. K., Saalmüller, A. and Gerner, W.**, NKp46 expression discriminates porcine NK cells with different functional properties. *Eur. J. Immunol.* 2012. **42**(5): 1261–1271.

1715 **Álvarez, B., Escalona, Z., Uenishi, H., Toki, D., Revilla, C., Yuste, M., Gómez del Moral, M. et al.**, Molecular and functional characterization of porcine Siglec-3/CD33 and analysis of its expression in blood and tissues. *Dev. Comp. Immunol.* 2015. **51**(2): 238–250.

1716 **Summerfield, A., Guzylack-Piriou, L., Schaub, A., Carrasco, C. P., Tâche, V., Charley, B. and McCullough, K. C.**, Porcine peripheral blood dendritic cells and natural interferon-producing cells. *Immunology* 2003. **110**(4): 440–449.

1717 **Escalona, Z., Álvarez, B., Uenishi, H., Toki, D., Yuste, M., Revilla, C., Gómez del Moral, M. et al.**, Molecular characterization of porcine Siglec-10 and analysis of its expression in blood and tissues. *Dev. Comp. Immunol.* 2015. **48**(1): 116–123. https://doi.org/10.1016/j.dci.2014.09.011

1718 **Sedlak, C., Patzl, M., Saalmüller, A. and Gerner, W.**, IL-12 and IL-18 induce interferon-γ production and de novo CD2 expression in porcine γδ T cells. *Dev. Comp. Immunol.* 2014b. **47**(1): 115–122. https://doi.org/10.1016/j.dci.2014.07.007

1719 **Yang, H. and Parkhouse, R. M.**, Phenotypic classification of porcine lymphocyte subpopulations in blood and lymphoid tissues. *Immunology* 1996. **89**(1): 76–83.

1720 **Saalmüller, A., Hirt, W. and Reddehase, M. J.**, Porcine γ/δ T lymphocyte subsets differing in their propensity to home to lymphoid tissue. *Eur. J. Immunol.* 1990. **20**(10): 2343–2346.

1721 **Sinkora, M., Šinkorová, J. and Holtmeier, W.**, Development of γδ thymocyte subsets during prenatal and postnatal ontogeny. *Immunology* 2005. **115**(4): 544–555.

1722 **Wen, K., Bui, T., Li, G., Liu, F., Li, Y., Kocher, J. and Yuan, L.**, Characterization of immune modulating functions of γδ T cell subsets in a gnotobiotic pig model of human rotavirus infection. *Comp. Immunol. Microbiol. Infect. Dis.* 2012. **35**(4): 289–301.

1723 **Lee, J., Choi, K., Olin, M. R., Cho, S.-N. and Molitor, T. W.**, Γδ T cells in immunity induced by *Mycobacterium bovis* Bacillus Calmette-Guérin vaccination. *Infect. Immun.* 2004. **72**(3): 1504–1511.

1724 **Sedlak, C., Patzl, M., Saalmüller, A. and Gerner, W.**, CD2 and CD8α define porcine γδ T cells with distinct cytokine production profiles. *Dev. Comp. Immunol.* 2014. **45**: 97–106.

1725 **Yang, H. and Parkhouse, R. M.**, Differential expression of CD8 epitopes amongst porcine CD8-positive functional lymphocyte subsets. *Immunology* 1997. **92**(1): 45–52.

1726 **Olin, M. R., Choi, K. H., Lee, J. and Molitor, T. W.**, Γδ T-lymphocyte cytotoxic activity against *Mycobacterium bovis* analyzed by flow cytometry. *J. Immunol. Methods* 2005. **297**: 1–11.

1727 **Rodríguez-Gómez, I. M., Talker, S. C., Käser, T., Stadler, M., Reiter, L., Ladinig, A., Milburn, J. V. et al.**, Expression of T-Bet, eomesodermin, and GATA-3 correlates with distinct phenotypes and functional properties in porcine γδ T cells. *Front. Immunol.* 2019. **10**. https://doi.org/10.3389/fimmu.2019.00396

1728 **Summerfield, A., Rziha, H.-J. and Saalmüller, A.**, Functional characterization of porcine CD4+CD8+extrathymic T lymphocytes. *Cell. Immunol.* 1996. **168**(2): 291–296. https://doi.org/10.1006/cimm.1996.0078

1729 **Rodríguez-Gómez, I. M., Talker, S. C., Käser, T., Stadler, M., Hammer, S. E., Saalmüller, A. and Gerner, W.**, Expression of T-bet, eomesodermin and GATA-3 in porcine αβ T cells. *Dev. Comp. Immunol.* 2016. **60**: 115–126.

1730 **Talker, S. C., Käser, T., Reutner, K., Sedlak, C., Mair, K. H., Koinig, H., Graage, R. et al.**, Phenotypic maturation of porcine NK- and T-cell subsets. *Dev. Comp. Immunol.* 2013. **40**(1): 51–68.

1731 **Käser, T., Gerner, W., Hammer, S. E., Patzl, M. and Saalmüller, A.**, Detection of Foxp3 protein expression in porcine T lymphocytes. *Vet. Immunol. Immunopathol.* 2008. **125**(1–2): 92–101. https://doi.org/10.1016/j.vetimm.2008.05.007

1732 **Ebner, F., Rausch, S., Scharek-Tedin, L., Pieper, R., Burwinkel, M., Zentek, J. and Hartmann, S.**, A novel lineage transcription factor based

analysis reveals differences in T helper cell subpopulation development in infected and intrauterine growth restricted (IUGR) piglets. *Dev. Comp. Immunol.* 2014. **46**: 333–340.

1733 Gerner, W., Denyer, M. S., Takamatsu, H.-H., Wileman, T. E., Wiesmüller, K.-H., Pfaff, E. and Saalmüller, A., Identification of novel foot-and-mouth disease virus specific T-cell epitopes in c/c and d/d haplotype miniature swine. *Virus Res.* 2006. **121**(2): 223–228.

1734 Ebner, F., Schwiertz, P., Steinfelder, S., Pieper, R., Zentek, J., Schütze, N., Baums, C. G. et al., Pathogen-reactive T helper cell analysis in the pig. *Front. Immunol.* 2017. **8**: 565. https://doi.org/10.3389/fimmu.2017.00565

1735 Stepanova, K. and Sinkora, M., Porcine γδ T lymphocytes can be categorized into two functionally and developmentally distinct subsets according to expression of CD2 and level of TCR. *J. Immunol.* 2013. **190**(5): 2111–2120. https://doi.org/10.4049/jimmunol.1202890

1736 Gerner, W., Talker, S. C., Koinig, H. C., Sedlak, C., Mair, K. H. and Saalmüller, A., Phenotypic and functional differentiation of porcine Aβ T cells: current knowledge and available tools. *Mol. Immunol.* 2015. **66**(1): 3–13. https://doi.org/10.1016/j.molimm.2014.10.025

1737 Holzer, B., Morgan, S. B., Matsuoka, Y., Edmans, M., Salguero, F. J., Everett, H., Brookes, S. M. et al., Comparison of heterosubtypic protection in ferrets and pigs induced by a single-cycle influenza vaccine. *J. Immunol.* 2018. **200**: 4068–4077.

1738 Hayashi, Y., Okutani, M., Ogawa, S., Tsukahara, T. and Inoue, R., Generation of anti-porcine CD69 monoclonal antibodies and their usefulness to evaluate early activation of cellular immunity by flow cytometric analysis. *Anim. Sci. J.* 2018. **89**: 825–832.

1739 Yang, W. C., Schultz, R. D. and Spano, J. S., Isolation and characterization of porcine natural killer (NK) cells. *Vet. Immunol. Immunopathol.* 1987. **14**(4): 345–356.

1740 Denyer, M. S., Wileman, T. E., Stirling, C. M., Zuber, B. and Takamatsu, H. H., Perforin expression can define CD8 positive lymphocyte subsets in pigs allowing phenotypic and functional analysis of natural killer, cytotoxic T, natural killer T and MHC un-restricted cytotoxic T-cells. *Vet. Immunol. Immunopathol.* 2006. **110**: 279–292.

1741 Walzer, T., Jaeger, S., Chaix, J. and Vivier, E., Natural Killer Cells: From CD3(-)NKp46(+) to post-genomics meta-analyses. *Curr. Opin. Immunol.* 2007. **19**(3): 365–372.

1742 Mair, K. H., Müllebner, A., Essler, S. E., Duvigneau, J. C., Storset, A. K., Saalmüller, A. and Gerner, W., Porcine CD8αdim/-NKp46high NK cells are in a highly activated state. *Vet. Res.* 2013. **44** (March): 13. https://doi.org/10.1186/1297-9716-44-13

1743 Forberg, H., Hauge, A. G., Valheim, M., Garcon, F., Nunez, A., Gerner, W., Mair, K. H. et al., Early responses of natural killer cells in pigs experimentally infected with 2009 pandemic H1N1 influenza A virus. *PLoS One* 2014. **9**(6): e100619. https://doi.org/10.1371/journal.pone.0100619

1744 Jones, M., Cordell, J. L., Beyers, A. D., Tse, A. G. and Mason, D. Y., Detection of T and B cells in many animal species using cross-reactive anti-peptide antibodies. *J. Immunol.* 1993. **150**: 5429–5435.

1745 Reutner, K., Leitner, J., Essler, S. E., Witter, K., Patzl, M., Steinberger, P., Saalmüller, A. et al., Porcine CD27: identification, expression and functional aspects in lymphocyte subsets in swine. *Dev. Comp. Immunol.* 2012. **38**(2): 321–331.

1746 Sinkora, M., Stepanova, K. and Sinkorova, J., Different Anti-CD21 antibodies can be used to discriminate developmentally and functionally different subsets of B lymphocytes in circulation of pigs. *Dev. Comp. Immunol.* 2013. **39**(4): 409–418.

1747 Kandasamy, S., Chattha, K. S., Vlasova, A. N., Rajashekara, G. and Saif, L. J., Lactobacilli and Bifidobacteria enhance mucosal

B cell responses and differentially modulate systemic antibody responses to an oral human rotavirus vaccine in a neonatal gnotobiotic pig disease model. *Gut Microbes* 2014. **5**(5): 639–651. https://doi.org/10.4161/19490976.2014.969972

1748 Braun, R. O., Python, S. and Summerfield, A., Porcine B cell subset responses to toll-like receptor ligands. *Front. Immunol.* 2017. **8**: 1044. https://doi.org/10.3389/fimmu.2017.01044

1749 Summerfield, A., Auray, G. and Ricklin, M., Comparative dendritic cell biology of veterinary mammals. *Annu. Rev. Anim. Biosci.* 2015. **3**: 533–557.

1750 Vu Manh, T.-P., Elhmouzi-Younes, J., Urien, C., Ruscanu, S., Jouneau, L., Bourge, M., Moroldo, M. et al., Defining mononuclear phagocyte subset homology across several distant warm-blooded vertebrates through comparative transcriptomics. *Front. Immunol.* 2015. **6**: 299.

1751 Soldevila, F., Edwards, J. C., Graham, S. P., Stevens, L. M., Crudgington, B., Crooke, H. R., Werling, D. et al., Characterization of the myeloid cell populations' resident in the porcine palatine tonsil. *Front. Immunol.* 2018. **9**: 1800.

1752 Auray, G., Keller, I., Python, S., Gerber, M., Bruggmann, R., Ruggli, N. and Summerfield, A., Characterization and transcriptomic analysis of porcine blood conventional and plasmacytoid dendritic cells reveals striking species-specific differences. *J. Immunol.* 2016. **197**(12): 4791–4806.

1753 Maisonnasse, P., Bouguyon, E., Piton, G., Ezquerra, A., Urien, C., Deloizy, C., Bourge, M. et al., The respiratory DC/macrophage network at steady-state and upon influenza infection in the swine biomedical model. *Mucosal Immunol.* 2016a. **9**(4): 835–849. https://doi.org/10.1038/mi.2015.105

1754 Chun, T., Wang, K., Zuckermann, F. A. and Rex Gaskins, H., Molecular cloning and characterization of a novel CD1 gene from the pig. *J. Immunol.* 1999. **162**(11): 6562–6571.

1755 Nestle, F. O., Zheng, X. G., Thompson, C. B., Turka, L. A. and Nickoloff, B. J., Characterization of dermal dendritic cells obtained from normal human skin reveals phenotypic and functionally distinctive subsets. *J. Immunol.* 1993. **151**(11): 6535–6545.

1756 Dutertre, C.-A., Wang, L.-F. and Ginhoux, F., Aligning bona fide dendritic cell populations across species. *Cell. Immunol.* 2014. **291**(1): 3–10. https://doi.org/10.1016/j.cellimm.2014.08.006

1757 Chamorro, S., Revilla, C., Alvarez, B., Alonso, F., Ezquerra, A. and Domínguez, J., Phenotypic and functional heterogeneity of porcine blood monocytes and its relation with maturation. *Immunology* 2005. **114**(1): 63–71.

1758 Ondrackova, P., Nechvatalova, K., Kucerova, Z., Leva, L., Dominguez, J. and Faldyna, M., Porcine mononuclear phagocyte subpopulations in the lung, blood and bone marrow: dynamics during inflammation induced by actinobacillus pleuropneumoniae. *Vet. Res.* 2010. **41**: 64.

1759 Fairbairn, L., Kapetanovic, R., Beraldi, D., Sester, D. P., Tuggle, C. K., Archibald, A. L. and Hume, D. A., Comparative analysis of monocyte subsets in the pig. *J. Immunol.* 2013. **190**(12): 6389–6396. https://doi.org/10.4049/jimmunol.1300365

1760 Ondrackova, P., Leva, L., Kucerova, Z., Vicenova, M., Mensikova, M. and Faldyna, M., Distribution of porcine monocytes in different lymphoid tissues and the lungs during experimental actinobacillus pleuropneumoniae infection and the role of chemokines. *Vet. Res.* 2013. **44**: 98.

1761 Moreno, S., Alvarez, B., Poderoso, T., Revilla, C.Ezquerra, A., Alonso, F. and Dominguez, J., Porcine monocyte subsets differ in the expression of CCR2 and in their responsiveness to CCL2. *Vet Res.* 2010. **41**: 76.

1762 Ezquerra, A., Revilla, C., Alvarez, B., Pérez, C., Alonso, F. and Domínguez, J., Porcine myelomonocytic markers and cell populations. *Dev. Comp. Immunol.* 2009. **33**(3): 284–298. https://doi.org/10.1016/j.dci.2008.06.002

1763 Fernández-Caballero, T., Álvarez, B., Revilla, C., Zaldívar-López, S., Alonso, F., Garrido, J. J., Ezquerra, Á. et al., Phenotypic and functional characterization of porcine bone marrow monocyte subsets. *Dev. Comp. Immunol.* 2018. **81**: 95–104. https://doi.org/10.1016/j.dci.2017.11.012

1764 Talker, S. C., Baumann, A., Tuba Barut, G., Keller, I., Bruggmann, R. and Summerfield, A., Precise delineation and transcriptional characterization of bovine blood dendritic-cell and monocyte subsets. *Front. Immunol.* 2018. **9**: 2505.

1765 Sinkora, M. and Sinkorova, J., B cell lymphogenesis in swine is located in the bone marrow. *J. Immunol.* 2014. **193**(10): 5023–5032.

1766 Maisonnasse, P., Bordet, E., Bouguyon, E. and Bertho, N., Broncho alveolar dendritic cells and macrophages are highly similar to their interstitial counterparts. *PLoS One* 2016b. **11**(12): e0167315. https://doi.org/10.1371/journal.pone.0167315

1767 Bordet, E., Maisonnasse, P., Renson, P., Bouguyon, E., Crisci, E., Tiret, M., Descamps, D. et al., Porcine alveolar macrophage-like cells are pro-inflammatory pulmonary intravascular macrophages that produce large titers of porcine reproductive and respiratory syndrome virus. *Sci. Rep.* 2018. **8**(1): 10172. https://doi.org/10.1038/s41598-018-28234-y

1768 Guilliams, M., Ginhoux, F., Jakubzick, C., Naik, S. H., Onai, N., Schraml, B. U., Segura, E. et al., Dendritic cells, monocytes and macrophages: a unified nomenclature based on ontogeny. *Nat. Rev. Immunol.* 2014. **14**: 571–578.

1769 Bharat, A., Bhorade, S. M., Morales-Nebreda, L., McQuattie-Pimentel, A. C., Soberanes, S., Ridge, K., DeCamp, M. M. et al., Flow cytometry reveals similarities between lung macrophages in humans and mice. *Am. J. Respir Cell Mol Biol* 2016 **54**(1): 147–149. https://doi.org/10.1165/rcmb.2015-0147LE

1770 Cai, Y., Sugimoto, C., Arainga, M., Alvarez, X., Didier, E. S. and Kuroda, M. J., In vivo characterization of alveolar and interstitial lung macrophages in rhesus macaques: implications for understanding lung disease in humans. *J. Immunol. (Baltimore, Md.: 1950)* 2014. **192**(6): 2821–2829. https://doi.org/10.4049/jimmunol.1302269

1771 Yu, Y.-R. A., Hotten, D. F., Malakhau, Y., Volker, E., Ghio, A. J., Noble, P. W., Kraft, M. et al., Flow cytometric analysis of myeloid cells in human blood, bronchoalveolar lavage, and lung tissues. *Am. J. Respir. Cell Mol. Biol.* 2016. **54**(1): 13–24.

1772 Marquet, F., Vu Manh, T.-P., Maisonnasse, P., Elhmouzi-Younes, J., Urien, C., Bouguyon, E., Jouneau, L. et al., Pig skin includes dendritic cell subsets transcriptomically related to human CD1a and CD14 dendritic cells presenting different migrating behaviors and T cell activation capacities. *J. Immunol.* 2014. **193**(12): 5883–5893.

1773 Parra-Sánchez, H., Puebla-Clark, L., Reséndiz, M., Valenzuela, O. and Hernández, J., Characterization and expression of DEC205 in the CDC1 and CDC2 subsets of porcine dendritic cells from spleen, tonsil, and submaxillary and mesenteric lymph nodes. *Mol. Immunol.* 2018. **96**: 1–7.

1774 Saalmüller, A., Pauly, T., Lunney, J. K., Boyd, P., Aasted, B., Sachs, D. H., Arn, S. et al., Overview of the second international workshop to define swine cluster of differentiation (CD) antigens. *Vet. Immunol. Immunopathol.* 1998. **60**(3–4): 207–228.

1775 Leitner, J., Reutner, K., Essler, S. E., Popow, I., Gerner, W., Steinberger, P. and Saalmüller, A., Porcine SWC1 Is CD52—final determination by the use of a retroviral CDNA expression library. *Vet. Immunol. Immunopathol.* 2012. **146**(1): 27–34.

1776 Pérez, C., Revilla, C., Alvarez, B., Chamorro, S., Correa, C., Domenech, N., Alonso, F. et al., Phenotypic and functional characterization of porcine granulocyte developmental stages using two new markers. *Dev. Comp. Immunol.* 2007. **31**(3): 296–306.

1777 Saalmüller, A. and Aasted, B., Summary of the animal homologue section of HLDA8. *Vet. Immunol. Immunopathol.* 2007. **119**: 2–13.

1778 Saalmüller, A., Lunney, J. K., Daubenberger, C., Davis, W., Fischer, U., Göbel, T. W. and Griebel, P. et al., Summary of the animal homologue section of HLDA8. *Cell. Immunol.* 2005. **236**: 51–58.

1779 Cobaleda, C., Schebesta, A., Delogu, A. and Busslinger, M., Pax5: the guardian of B cell identity and function. *Nat. Immunol.* 2007. **8**: 463–470.

1780 Brodie, T., Brenna, E. and Sallusto, F., OMIP-018: chemokine receptor expression on human T helper cells. *Cytometry A* 2013. **83**: 530–532.

1781 Shaffer, A. L., Lin, K.-I., Kuo, T. C., Yu, X., Hurt, E. M., Rosenwald, A. and Giltnane, J. M. et al., Blimp-1 orchestrates plasma cell differentiation by extinguishing the mature B cell gene expression program. *Immunity* 2002. **17**: 51–62.

1782 Bekeredjian-Ding, I. and Jego, G., Toll-like receptors—sentries in the B-cell response. *Immunology* 2009. **128**: 311–323.

1783 Calame, K., Activation-dependent induction of Blimp-1. *Curr. Opin. Immunol.* 2008. **20**: 259–264.

1784 Gerner, W., Käser, T. and Saalmüller, A., Porcine T lymphocytes and NK cells - an update. *Dev. Comp. Immunol.* 2009. **33**: 310–320.

1785 Saalmüller, A., Werner, T. and Fachinger, V., T-helper cells from naive to committed. *Vet. Immunol. Immunopathol.* 2002. **87**: 137–145.

1786 Bolzer, K., Käser, T., Saalmüller, A. and Hammer, S. E., Molecular characterisation of porcine Forkhead-box p3 (Foxp3). *Vet. Immunol. Immunopathol.* 2009. **132**: 275–281.

1787 Rocchi, M. S., Wattegedera, S. R., Frew, D., Entrican, G., Huntley, J. F. and McNeilly, T. N., Identification of CD4$^+$CD25^{high} Foxp3$^+$ T cells in ovine peripheral blood. *Vet. Immunol. Immunopathol.* 2011. **144**: 172–177.

1788 Käser, T., Mair, K. H., Hammer, S. E., Gerner, W. and Saalmüller, A., Natural and inducible Tregs in swine: helios expression and functional properties. *Dev. Comp. Immunol.* 2015. **49**: 323–331.

1789 Kwong, L. S., Thom, M., Sopp, P., Rocchi, M., Wattegedera, S., Entrican, G. and Hope, J. C., Production and characterization of two monoclonal antibodies to bovine tumour necrosis factor alpha (TNF-alpha) and their cross-reactivity with ovine TNF-alpha. *Vet. Immunol. Immunopathol.* 2010. **135**: 320–324.

1790 Wattegedera, S. R., Corripio-Miyar, Y., Pang, Y., Frew, D., McNeilly, T. N., Palarea-Albaladejo, J. and McInnes, C. J. et al., Enhancing the toolbox to study IL-17A in cattle and sheep. *Vet. Res.* 2017. **48**: 20.

1791 Pedersen, L. G., Castelruiz, Y., Jacobsen, S. and Aasted, B., Identification of monoclonal antibodies that cross-react with cytokines from different animal species. *Vet. Immunol. Immunopathol.* 2002. **88**: 111–122.

1792 Franzoni, G., Kurkure, N. V., Edgar, D. S., Everett, H. E., Gerner, W., Bodman-Smith, K. B., Crooke, H. R et al., Assessment of the phenotype and functionality of porcine CD8 T cell responses following vaccination with live attenuated classical swine fever virus (CSFV) and virulent CSFV challenge. *Clin. Vaccine Immunol.* 2013. **20**: 1604–1616.

1793 Takamatsu, H. H., Denyer, M. S., Stirling, C., Cox, S., Aggarwal, N., Dash, P., Wileman, T. E. et al., Porcine γδ T cells: possible roles on the innate and adaptive immune responses following virus infection. *Vet. Immunol. Immunopathol.* 2006. **112**: 49–61.

1794 Saeys, Y., Gassen, S. V. and Lambrecht, B. N., Computational flow cytometry: helping to make sense of high-dimensional immunology data. *Nat. Rev. Immunol.* 2016. **16**: 449–462.

1795 Aghaeepour, N., Finak, G., The FlowCAP Consortium, The DREAM Consortium, Hoos, H., Mosmann, T. R., Brinkman, R. et al., Critical assessment of automated flow cytometry data analysis techniques. *Nat. Methods* 2013. **10**: 228–238.

1796 Bashashati, A. and Brinkman, R. R., A survey of flow cytometry data analysis methods. *Adv. Bioinformatics* 2009. **2009**: 584603

1797 O'Neill, K., Aghaeepour, N., Spidlen, J. and Brinkman, R. R., Flow cytometry bioinformatics. *PLoS Comput. Biol.* 2013. **9**: e1003365.

1798 Aghaeepour, N., Chattopadhyay, P. K., Ganesan, A., O'Neill, K., Zare, H., Jalali, A., Hoos, H. et al., Early immunologic correlates of HIV protection can be identified from computational analysis of complex multivariate T-cell flow cytometry assays. *Bioinformatics* 2012. **28**: 1009–1016.

1799 Aghaeepour, N., Nikolic, R., Hoos, H. H., and Brinkman, R. R. Rapid cell population identification in flow cytometry data. *Cytometry Part A* 2011. **79A**: 6–13.

1800 Finak, G., Bashashati, A., Brinkman, R. and Gottardo, R., Merging mixture components for cell population identification in flow cytometry. *Adv. Bioinformatics* 2009, 247646.

1801 Mosmann, T. R., Naim, I., Rebhahn, J., Rebhahn, J., Datta, S., Cavenaugh, J. S., Weaver, J. M. and Sharma, G., SWIFT-scalable clustering for automated identification of rare cell populations in large, high-dimensional flow cytometry datasets, Part 2: Biological evaluation. *Cytometry A* 2014. **85**: 422–433.

1802 Finak, G., Langweiler, M., Jaimes, M., Malek, M., Taghiyar, J., Korin, Y., Raddassi, K. et al., Standardizing flow cytometry immunophenotyping analysis from the human immunophenotyping consortium. *Sci. Rep.* 2016. **6**: 20686.

1803 Qian, Y., Wei, C., Eun-Hyung Lee, F., Campbell, J., Halliley, J., Lee, J. A., Cai, J. et al., Elucidation of seventeen human peripheral blood B-cell subsets and quantification of the tetanus response using a density-based method for the automated identification of cell populations in multidimensional flow cytometry data. *Cytometry B Clin. Cytom.* 2010. **78**(Suppl 1): S69–S82.

1804 Qiu, P., Simonds, E. F., Bendall, S. C., Gibbs, K. D., Bruggner, R. V., Linderman, M. D., Sachs, K. et al., Extracting a cellular hierarchy from high-dimensional cytometry data with SPADE. *Nat. Biotechnol.* 2011. **29**: 886–891.

1805 Naim, I., Datta, S., Cavenaugh, J. S., Mosmann, T. R. and Sharma, G., SWIFT-scalable clustering for automated identification of rare cell populations in large, high-dimensional flow cytometry datasets, Part 1: Algorithm design, *Cytometry A* 2014. **85**: 408–421.

1806 Leipold, M. D. and Maecker, H. T., Mass cytometry: protocol for daily tuning and running cell samples on a CyTOF mass cytometer. *J. Vis. Exp.* 2012. e4398.

1807 Fletez-Brant, K., Spidlen, J., Brinkman, R. R., Roederer, M. and Chattopadhyay, P. K., flowClean: Automated identification and removal of fluorescence anomalies in flow cytometry data. *Cytometry A* 2016. **89**: 461–471.

1808 Finak, G., Perez, J. M., Weng, A. and Gottardo, R., Optimizing transformations for automated, high throughput analysis of flow cytometry data. *BMC Bioinformatics.* 2010. **11**: 546.

1809 Finak, G., Perez, J. M. and Gottardo, R., flowTrans: Parameter Optimization for Flow Cytometry Data Transformation. *R package version* 1.24.0. 2010.

1810 Hahne, F., Khodabakhshi, A. H., Bashashati, A., Wong, C. J., Gascoyne, R. D., Weng, A. P., Seyfert-Margolis, V. et al., Per-channel basis normalization methods for flow cytometry data. *Cytometry A* 2010. **77**: 121–131.

1811 Finak, G., Jiang, W., Krouse, K., Wei, C., Sanz, I., Phippard, D., Asare, A. et al., High–throughput flow cytometry data normalization for clinical trials. *Cytometry A* 2014. **85**: 277–286

1812 Mair, F., Gate to the future: computational analysis of immunophenotyping data. *Cytometry A* 2019. **95**: 147–149.

1813 Aghaeepour, N., Chattopadhyay, P., Chikina, M., Dhaene, T., Van Gassen, S., Kursa, M., Lambrecht, B. N. et al., A benchmark for evaluation of algorithms for identification of cellular correlates of clinical outcomes. *Cytometry* 2016. **89**: 16–21.

1814 Weber, L. M. and Robinson, M. D., Comparison of clustering methods for high-dimensional single-cell flow and mass cytometry data. *Cytometry A* 2016. **89**: 1084–1096.

1815 Li, H., Shaham, U., Stanton, K. P., Yao, Y., Montgomery, R. R. and Kluger, Y., Gating mass cytometry data by deep learning. *Bioinformatics* 2017. **33**: 3423–3430.

1816 Ko, B. S., Wang, Y. F., Li, J. L., Li, C. C., Weng, P. F., Hsu, S. C., Hou, H. A. et al., Clinically validated machine learning algorithm for detecting residual diseases with multicolor flow cytometry analysis in acute myeloid leukemia and myelodysplastic syndrome. *EBioMedicine* 2018. **37**: 91–100.

1817 Azad, A., Rajwa, B. and Pothen, A., Immunophenotype discovery, hierarchical organization, and template-based classification of flow cytometry samples. *Front. Oncol.* 2016. **6**: 188.

1818 Finak, G., Frelinger, J., Jiang, W., Newell, E. W., Ramey, J., Davis, M. M., Kalams, S. A. et al., OpenCyto: An open source infrastructure for scalable, robust, reproducible, and automated, end-to-end flow cytometry data analysis. *PLoS Comput. Biol.* 2014. **10**: e1003806.

1819 Malek, M., Taghiyar, M. J., Chong, L., Finak, G., Gottardo, R. and Brinkman, R. R., flowDensity: Reproducing manual gating of flow cytometry data by automated density-based cell population identification. *Bioinformatics* 2015. **31**: 606–607.

1820 Lux, M., Brinkman, R. R., Chauve, C., Laing, A., Lorenc, A., Abeler-Dörner, L., Hammer, B. et al., flowLearn: fast and precise identification and quality checking of cell populations in flow cytometry. *Bioinformatics* 2018. **1**: 9.

1821 Kalina, T., Flores-Montero, J., Lecrevisse, Q., Pedreira, C. E., van der Velden, V. H., Novakova, M., Mejstrikova, E., Hrusak, O. et al., Quality assessment program for Euro Flow protocols: Summary results of four-year (2010–2013) quality assurance rounds. *Cytometry A* 2015. **87**(2): 145–156.

1822 Aghaeepour, N., FlowMeans: non-parametric flow cytometry data gating. R package version. 2010. 1(0).

1823 Aghaeepour, N. and Simonds, E. F., GateFinder: projection-based gating strategy optimization for polychromatic and mass flow cytometry data. *Bioinformatics* 2018. **34**: 4131–4133.

1824 Amir, E.-A. D., Davis, K. L., Tadmor, M. D., Simonds, E. F., Levine, J. H., Bendall, S. C., Shenfeld, D. K. et al., viSNE enables visualization of high dimensional single-cell data and reveals phenotypic heterogeneity of leukemia. *Nat. Biotechnol.* 2013. **31**: 545–552.

1825 Samani, F. S., Moore, J. K., Khosravani, P. and Ebrahimi, M., Features of free software packages in flow cytometry: a comparison between four non-commercial software sources. *Cytotechnology.* 2014. **66**(4): 555–559.

1826 Chen, T. J. and Kotecha, N., Cytobank: providing an analytics platform for community cytometry data analysis and collaboration. *Curr. Top. Microbiol. Immunol.* 2014. **377**: 127–157.

1827 Roederer, M., Nozzi, J. L. and Nason, M. C., SPICE: Exploration and analysis of post-cytometric complex multivariate datasets. *Cytometry A.* 2011. **79**: 167–174.

1828 **Spidlen, J., Barsky, A., Breuer, K., Carr, P., Nazaire, M. D., Hill, B. A., Qian, Y. et al.**, GenePattern flow cytometry suite. *Source Code Biol. Med.* 2013. **8**: 14.

1829 **Brinkman, R. R., Aghaeepour, N., Finak, G., Gottardo, R., Mosmann, T. and Scheuermann, R. H.**, Automated analysis of flow cytometry data comes of age. *Cytometry A* 2016. **89**: 16–21.

1830 **Benjamini, Y. and Hochberg, Y.**, Controlling the False Discovery Rate - a Practical and Powerful Approach to Multiple Testing. *Journal of the Royal Statistical Society Series B-Methodological* 1995. **57**: 289–300.

1831 **Almudevar, A.**, Multiple hypothesis testing: a methodological overview. *Methods Mol. Biol.* 2013. **972**: 37–55.

1832 **Rebhahn, J. A., Roumanes, D. R., Qi, Y., Khan, A., Thakar, J., Rosenberg, A., Lee, F. E. et al.**, Competitive SWIFT cluster templates enhance detection of aging changes. *Cytometry A* 2016. **89**: 59–70.

1833 **Maaten, L. V. D. and Hinton, G.**, Visualizing data using t-SNE. *J. Mach. Learn. Res.* 2008. **9**: 2579–2605.

1834 **Aghaeepour, N., Jalali, A., O'Neill, K., Chattopadhyay, P. K., Roederer, M., Hoos, H. H. and Brinkman, R. R.**, RchyOptimyx: Cellular hierarchy optimization for flow cytometry. *Cytometry A* 2012. **81**: 1022–1030.

1835 **O'Neill, K., Jalali, A., Aghaeepour, N., Hoos, H. and Brinkman, R. R.**, Enhanced flowType/RchyOptimyx: a bioconductor pipeline for discovery in high-dimensional cytometry data. *Bioinformatics* 2014. **30**: 1329–1330.

1836 **Tong, D. L., Ball, G. R. and Pockley, A. G.**, gEM/GANN: a multivariate computational strategy for auto-characterizing relationships between cellular and clinical phenotypes and predicting disease progression time using high-dimensional flow cytometry data. *Cytometry* 2015. **87**: 616–623.

1837 **Gassen, S. V., Vens, C., Dhaene, T., Lambrecht, B. N. and Saeys, Y.**, Flo-ReMi: flow density survival regression using minimal feature redundancy. *Cytometry A* 2015. **89**: 22–29.

1838 **Mair, F., Hartmann, F. J., Mrdjen, D., Tosevski, V., Krieg, C. and Becher, B.**, The end of gating? An introduction to automated analysis of high dimensional cytometry data. *Eur. J. Immunol.* 2016. **46**: 34–43.

1839 **LeCun, Y., Bengio, Y. and Hinton, G.**, Deep learning. *Nature* 2015. **521**: 436–444.

1840 **Rosenblatt, F.**, The Perceptron: a probabilistic model for information storage and organization in the brain. *Psychol. Rev.* 1958. **65**: 386–408.

1841 **Szegedy, C., Liu, W., Jia, Y., Sermanet, P., Reed, S. E., Anguelov, D., Erhan, D. et al.**, Going deeper with convolutions. 2015 IEEE Conference on Computer Vision and Pattern Recognition (CVPR), Boston, MA, 2015, pp. 1–9.

1842 **Gupta, P. J. Harrison, Wieslander, H., Pielawski, N., Kartasalo, K., Partel, G., Solorzano, L., Suveer, A. et al.**, Deep learning in image cytometry: a review. *Cytometry A* 2019. **95**: 366–380.

1843 **Eulenberg, P., Koehler, N., Blasi, T., Filby, A., Carpenter, A. E., Rees, P., Theis, F. J. et al.**, Reconstructing cell cycle and disease progression using deep learning. *Nat. Commun.* 2017. **8**: 463.

1844 **Behrmann, J., Etmann, C., Boskamp, T., Casadonte, R., Kriegsmann, J. and Maass, P.**, Deep learning for tumor classification in imaging mass spectrometry. *Bioinformatics* 2017. **1**: 1–10.

1845 **Arvaniti, E. and Claassen, M.**, Sensitive detection of rare disease-associated cell subsets via representation learning. *Nat. Commun.* 2017. **8**: 14825

1846 **Li, H., Shaham, U., Stanton, K. P., Yao, Y., Montgomery, R. R., Kluger, Y. et al.**, Gating mass cytometry data by deep learning. *Bioinformatics* 2017. **33**: 3423–3430.

1847 **Ornatsky, O. I., Kinach, R., Bandura, D. R., Lou, X., Tanner, S. D., Baranov, V. I., Nitz, M. and Winnik, M. A.**, Development of analytical methods for multiplex bio-assay with inductively coupled plasma mass spectrometry. *J. Anal. At. Spectrom.* 2008. **23**: 463–469.

1848 **Jolliffe, I. T.**, *Principal component analysis*, Springer Science & Business Media, Berlin, Germany 2002.

1849 **Bendall, S. C., Simonds, E. F., Qiu, P., Amir el, A. D., Krutzik, P. O., Finck, R., Bruggner, R. V. et al.**, Single-cell mass cytometry of differential immune and drug responses across a human hematopoietic continuum. *Science* 2011. **332**: 687–696.

1850 **Newell, E. W., Sigal, N., Bendall, S. C., Nolan, G. P. and Davis, M. M.**, Cytometry by time-of-flight shows combinatorial cytokine expression and virus-specific cell niches within a continuum of CD8+ T cell phenotypes. *Immunity* 2012. **36**: 142–152.

1851 **Kotecha, N., Krutzik, P. O. and Irish, J. M.**, Web-based analysis and publication of flow cytometry experiments. *Curr. Protoc. Cytom.* 2010. Chapter 10, Unit10.17.

1852 **Höllt, T. et al.**, Cytosplore: interactive immune cell phenotyping for large single-cell datasets. *Comput. Graphics Forum* 2016. **35**: 171–180.

1853 **Chen, H. et al.**, Cytofkit: a bioconductor package for an integrated mass cytometry data analysis pipeline. *PLoS Comput. Biol.* 2016. **12**: e1005112.

1854 **Kobak, D. and Berens, P.**, The art of using t-SNE for single-cell transcriptomics. *bioRxiv.* 2018. Available at: https://doi.org/10.1101/453449

1855 **Wattenberg, M., Viégas, F. and Johnson, I.**, How to use t-SNE effectively. *Distill* 2016. **1**(10). https://doi.org/10.23915/distill.00002

1856 **Belkina, A. C. et al.**, Automated optimal parameters for T-distributed stochastic neighbor embedding improve visualization and allow analysis of large datasets. *bioRxiv.* 2018.

1857 **Linderman, G. C., Rachh, M., Hoskins, J. G., Steinerberger, S. and Kluger, Y.**, Efficient Algorithms for t-distributed stochastic neighborhood embedding. *arXiv.* 2017. Available at: https://arxiv.org/abs/1712.09005

1858 **van der Maaten, L. J. P.**, Accelerating t-SNE using tree-based algorithms. *J. Mach. Learn. Res.* 2014. (15): 3221–3245.

1859 **Pezzotti, N., Lelieveldt, B. P. F., Van Der Maaten, L., Hollt, T., Eisemann, E., Vilanova, A. et al.**, Approximated and user steerable tSNE for progressive visual analytics. *IEEE Trans. Vis. Comput. Graph.* 2017. **23**: 1739–1752.

1860 **Linderman, G. C., Rachh, M., Hoskins, J. G., Steinerberger, S. and Kluger, Y.**, Fast interpolation-based t-SNE for improved visualization of single-cell RNA-seq data. *Nat. Methods* 2019. **16**(3): 243–245.

1861 **Pezzotti, N., Höll, T., Lelieveldt, T., Eisemann, E. and Vilanova, A.**, Hierarchical stochastic neighbor embedding. *Comput. Graphics Forum* 2016. **35**: 21–30.

1862 **van Unen, V., Höllt, T., Pezzotti, N., Li, N., Reinders, M. J. T., Eisemann, E., Koning, F. et al.**, Visual analysis of mass cytometry data by hierarchical stochastic neighbour embedding reveals rare cell types. *Nat. Commun.* 2017. **8**: 1740.

1863 **Linderman, G. C. and Steinerberger, S.**, Clustering with t-SNE, provably. *arXiv.* 2017. Available at: https://arxiv.org/abs/1706.02582

1864 **Shekhar, K. et al.**, Automatic classification of cellular expression by nonlinear stochastic embedding (ACCENSE). *Proc. Natl. Acad. Sci. USA* 2014. **111**: 202–207.

1865 **Murphy, R. F.**, Automated identification of subpopulations in flow cytometric list mode data using cluster analysis. *Cytometry.* 1985. **6**: 302–309.

1866 **Diggins, K. E., Gandelman, J. S., Roe, C. E. and Irish, J. M.**, Generating quantitative cell identity labels with marker enrichment modeling (MEM). *Curr. Protoc. Cytom.* 2018. **83**: 10.21.1–10.21.28.

1867 **Schadt, E. E., Lamb, J., Yang, X., Zhu, J., Edwards, S., Guhathakurta, D., Sieberts, S. K. et al.**, An integrative genomics approach to infer causal associations between gene expression and disease. *Nat. Genet.* 2005. **37**: 710–717.

1868 **Emilsson, V., Thorleifsson, G., Zhang, B., Leonardson, A. S., Zink, F., Zhu, J., Carlson, S. et al.**, Genetics of gene expression and its effect on disease. *Nature* 2008. **452**: 423–428.

1869 **Stegle, O., Teichmann, S. A. and Marioni, J. C.**, Computational and analytical challenges in single-cell transcriptomics. *Nat. Rev. Genet.* 2015; **16**: 133–145.

1870 **Bantscheff, M., Schirle, M., Sweetman, G., Rick, J. and Kuster, B.**, Quantitative mass spectrometry in proteomics: a critical review. *Anal. Bioanal. Chem.* 2007. **389**: 1017–1031.

1871 **Weston, A. D. and Hood, L.**, Systems biology, proteomics, and the future of health care: toward predictive, preventative, and personalized medicine. *J. Proteome Res.* 2004. **3**: 179–196.

1872 **Aghaeepour, N., Lehallier, B., Baca, Q., Ganio, E. A., Wong, R. J., Ghaemi, M. S., Culos, A. et al.**, A proteomic clock of human pregnancy. *Am. J. Obstet. Gynecol.* 2018. **218**: 347.e1–347.e14.

1873 **Patterson, A. D., Maurhofer, O., Beyoglu, D., Lanz, C., Krausz, K. W., Pabst, T., Gonzalez, F. J. et al.**, Aberrant lipid metabolism in hepatocellular carcinoma revealed by plasma metabolomics and lipid profiling. *Cancer Res.* 2011. **71**: 6590–6600.

1874 **Zhao, Y., Fu, L., Li, R., Wang, L. N., Yang, Y., Liu, N. N., Zhang, C. M. et al.**, Metabolic profiles characterizing different phenotypes of polycystic ovary syndrome: plasma metabolomics analysis. *BMC Med.* 2012. **10**: 153.

1875 **Chen, X., Liu, L., Palacios, G., Gao, J., Zhang, N., Li, G., Lu, J. et al.**, Plasma metabolomics reveals biomarkers of the atherosclerosis. *J. Sep. Sci.* 2010. **33**: 2776–2783.

1876 **Psychogios, N., Hau, D. D., Peng, J., Guo, A. C., Mandal, R., Bouatra, S., Sinelnikov, I. et al.**, The human serum metabolome. *PLoS One* 2011. **6**: e16957.

1877 **Bathe, O. F. et al.**, Feasibility of identifying pancreatic cancer based on serum metabolomics. *Cancer Epidemiol. Biomarkers Prev.* 2011. **20**: 140–147.

1878 **Zhang, A., Sun, H. and Wang, X.**, Serum metabolomics as a novel diagnostic approach for disease: a systematic review. *Anal. Bioanal. Chem.* 2012. **404**: 1239–1245.

1879 **Bouatra, S., Aziat, F., Mandal, R., Guo, A. C., Wilson, M. R., Knox, C., Bjorndahl, T. C. et al.**, The human urine metabolome. *PLoS One* 2013. **8**: e73076.

1880 **Kim, Y., Koo, I., Jung, B. H., Chung, B. C. and Lee, D.**, Multivariate classification of urine metabolome profiles for breast cancer diagnosis. *BMC Bioinformatics* 2010. **11**: S4.

1881 **Dethlefsen, L., McFall-Ngai, M. and Relman, D. A.**, An ecological and evolutionary perspective on human-microbe mutualism and disease. *Nature* 2007. **449**: 811–818.

1882 **Woodward, L. J., Anderson, P. J., Austin, N. C., Howard, K. and Inder, T. E.**, Neonatal MRI to predict neurodevelopmental outcomes in preterm infants. *N. Engl. J. Med.* 2006. **355**: 685–694.

1883 **Giesen, C., Wang, H. A., Schapiro, D., Zivanovic, N., Jacobs, A., Hattendorf, B., Schuffler, P. J. et al.**, Highly multiplexed imaging of tumor tissues with subcellular resolution by mass cytometry. *Nat. Methods* 2014. **11**: 417–422.

1884 **Halilaj, E., Hastie, T. J., Gold, G. E. and Delp, S. L.**, Physical activity is associated with changes in knee cartilage microstructure. *Osteoarthr. Cartil.* 2018. **26**: 770–774.

1885 **Jensen, P. B., Jensen, L. J. and Brunak, S.**, Mining electronic health records: towards better research applications and clinical care. *Nat. Rev. Genet.* 2012. **13**: 395–405.

1886 **Marbach, D., Costello, J. C., Küffner, R., Vega, N. M., Prill, R. J., Camacho, D. M., Allison, K. R. et al.**, Wisdom of crowds for robust gene network inference. *Nat. Methods* 2012. **9**: 796–804.

1887 **Elhalawani, H. et al.**, Machine Learning Applications in Head and Neck Radiation Oncology: Lessons From Open-Source Radiomics Challenges. *Front. Oncol.* 2018. **8**: 294.

1888 **Ritchie, M. D., Holzinger, E. R., Li, R., Pendergrass, S. A. and Kim, D.**, Methods of integrating data to uncover genotype-phenotype interactions. *Nat. Rev. Genet.* 2015. **16**: 85–97.

1889 **Feinberg, A. P.**, Epigenomics reveals a functional genome anatomy and a new approach to common disease. *Nat. Biotechnol.* 2010. **28**: 1049–1052.

1890 **Huang, S., Chaudhary, K. and Garmire, L. X.**, More Is Better: Recent Progress in Multi-Omics Data Integration Methods. *Front. Genet.* 2017. **8**: 84.

1891 **Bersanelli, M. et al.**, Methods for the integration of multi-omics data: mathematical aspects. *BMC Bioinformatics* 2016. **17**(Suppl 2): 15.

1892 **Li, Y., Wu, F-X. and Ngom, A.**, A review on machine learning principles for multi-view biological data integration. *Brief. Bioinformatics* 2018. **19**: 325–340.

1893 **Tini, G., Marchetti, L., Priami, C. and Scott-Boyer, M-P.**, Multi-omics integration-a comparison of unsupervised clustering methodologies. *Brief. Bioinformatics* 2017. bbx167

1894 **Shen, R., Olshen, A. B. and Ladanyi, M.**, Integrative clustering of multiple genomic data types using a joint latent variable model with application to breast and lung cancer subtype analysis. *Bioinformatics* 2009. **25**: 2906–2912.

1895 **Lock, E. F., Hoadley, K. A., Marron, J. S. and Nobel, A. B.**, Joint and individual variation explained (jive) for integrated analysis of multiple data types. *Ann. Appl. Stat.* 2013. **7**: 523–542.

1896 **Wang, B. et al.**, Similarity network fusion for aggregating data types on a genomic scale. *Nat. Methods* 2014. **11**: 333–337.

1897 **Nassar, H. and Gleich, D. F.**, in *Proceedings of the 2017 SIAM international conference on data mining*, In N. Chawla, W. Wang, (Eds) Society for Industrial and Applied Mathematics, Philadelphia, PA, 2017. pp. 615–623.

1898 **Lock, E. F., Dunson, D. B.**, Bayesian consensus clustering. *Bioinformatics* 2013. **29**: 2610–2616.

1899 **Lin, D., Zhang, J., Li, J., Calhoun, V. D., Deng, H. W. and Wang, Y. P.**, Group sparse canonical correlation analysis for genomic data integration. *BMC Bioinformatics* 2013. **14**: 245.

1900 **Holzinger, E. R., Dudek, S. M., Frase, A. T., Pendergrass, S. A. and Ritchie, M. D.**, ATHENA: the analysis tool for heritable and environmental network associations. *Bioinformatics* 2014. **30**: 698–705.

1901 **Ghaemi, M. S. et al.**, Multiomics modeling of the immunome, transcriptome, microbiome, proteome and metabolome adaptations during human pregnancy. *Bioinformatics* 2019. **35**: 95–103.

1902 **Singh, A. et al.**, DIABLO: an integrative approach for identifying key molecular drivers from multi-omic assays. *Bioinformatics* 2019. https://doi.org/10.1093/bioinformatics/bty1054

1903 **He, L.**, **Yang, Z.**, **Zhao, Z.**, **Lin, H. and Li, Y.**, Extracting drug-drug interaction from the biomedical literature using a stacked generalization-based approach. *PLoS One* 2013. **8**: e65814.

1904 **Bendall, S. C.**, **Davis, K. L.**, **Amir, E.-A. D.**, **Tadmor, M. D.**, **Simonds, E. F.**, **Chen, T. J.**, **Shenfeld, D. K. et al.**, Single-cell trajectory detection uncovers progression and regulatory coordination in human B cell development. *Cell* 2014. **157**: 714–725.

1905 **Saelens, W.**, **Cannoodt, R.**, **Todorov, H. and Saeys, Y.**, A comparison of single-cell trajectory inference methods. *Nat. Biotechnol.* 2019. **37**: 547–554.

1906 **Treutlein, B.**, **Lee, Q. Y.**, **Camp, J. G.**, **Mall, M.**, **Koh, W.**, **Shariati, S. A. M.**, **Sim, S. et al.**, Dissecting direct reprogramming from fibroblast to neuron using single-cell RNA-seq. *Nature* 2016. **534**: 391–395.

1907 **Cannoodt, R.**, **Saelens, W. and Saeys, Y.**, Computational methods for trajectory inference from single cell transcriptomics. *Eur. J. Immunol.* 2016. **46**: 2496–2506.

1908 **Rebhahn, J. A.**, **Deng, N.**, **Sharma, G.**, **Livingstone, A. M.**, **Huang, S. and Mosmann, T. R.**, An animated landscape representation of CD4+ T-cell differentiation, variability, and plasticity: insights into the behavior of populations versus cells. *Eur. J. Immunol.* 2014. **44**: 2216–2229.

1909 **Dean, P. N. and Jett, J. J.**, Mathematical analysis of DNA distributions derived from flow microfluorometry. *J. Cell. Biol.* 1974. **60**: 523–527.

1910 **Gray, J. W.**, Cell cycle analysis from computer synthesis of deoxyribonucleic acid histograms. *J. Histochem. Cytochem.* 1974. **22**: 642–650.

1911 **Watson, J. V.**, The application of age distribution theory in the analysis of cytofluorimetric DNA-histogram data. *Cell Tissue Kinet.* 1977. **10**: 157–169.

1912 **Watson, J. V.**, **Chambers, S. H. and Smith, P. J.**, A pragmatic approach to the analysis of DNA histograms with a definable G1 peak. *Cytometry* 1987. **8**: 1–8.

1913 **Rosenblatt, J. I.**, **Hokanson, J. A.**, **McLaughlin, S. R. and Leary, J. F.**, Theoretical basis for sampling statistics useful for detecting and isolating rare cells using flow cytometry and cell sorting. *Cytometry* 1997. **27**: 233–238.

1914 **Poisson, S. D.**, *Recherches sur la probabilité des jugements en matière criminelle et en matière civile: précédées des règles générales du calcul des probabilités*. Bachelier, Paris, France, 1837.

1915 **Gosset, W. S.**, The probable error of a mean. *Biometrica* 1908. **6**: 1–25.

1916 **Fisher, R. A.**, *Statistical methods for research workers*. Oliver & Boyd, Edinburgh, U.K., 1925.

1917 **Watson, J. V.**, *Flow cytometry data analysis: basic concepts and statistics*, Cambridge University Press, Cambridge, UK, 2005.

1918 **Fisher, R. A. and Yates, F.**, *Statistical tables for biological, medical and agricultural research*. Oliver and Boyd, Edinburgh, UK, 1963. p. 86.

1919 **Snedecor, G. W.**, *Statistical methods* 4th ed., Iowa State College Press, Ames, Iowa, 1946.

1920 **Wilcoxon, F.**, Individual comparisons by ranking methods. *Biometrics Bull.* 1945. **1**: 80–83.

1921 **Mann, H. B. and Whitney, D. R.**, On a test of whether one of two random variables is stochastically larger than the other. *Ann. Math. Stat.* 1947. **18**: 50–60.

1922 **Siegel, S. and Castellón, N. J.**, *Non-parametric statistics for the behavioral sciences*, 2nd ed., McGraw-Hill, New York, NY, 1988, Chapter 6.

1923 **Young, I. T.**, Proof without prejudice: use of the Kolmogorov–Smirnov test for the analysis of histograms from flow systems and other sources. *J. Histochem. Cytochem.* 1977. **25**: 935–941.

1924 **Kendall, M. G.**, Rank and product-moment correlation. *Biometrika* 1949. **36**: 177–193.

1925 **Watson, J. V.**, Proof without prejudice revisited: Immunofluorescence histogram analysis using cumulative frequency subtraction plus ratio analysis of means. *Cytometry* 2001. **43**: 55–68.

1926 **Bocsi, J.**, **Melzer, S.**, **Dähnert, I. and Tárnok, A.**, OMIP-023: 10-color, 13 antibody panel for in-depth phenotyping of human peripheral blood leukocytes. *Cytometry A* 2014. **85**: 781–784.

1927 **Melzer, S.**, **Zachariae, S.**, **Bocsi, J.**, **Engel, C.**, **Löffler, M. and Tárnok, A.**, Reference intervals for leukocyte subsets in adults: Results from a population-based study using 10-color flow cytometry. *Cytometry B Clin. Cytom.* 2015. **88**: 270–281.

1928 **Nettey, L.**, **Giles, A. J. and Chattopadhyay, P. K.**, OMIP-050: a 28-color/30-parameter fluorescence flow cytometry panel to enumerate and characterize cells expressing a wide array of immune checkpoint molecules. *Cytometry A* 2018. **93**:1094–1096.

1929 **Mazza, E. M. C.**, **Brummelman, J.**, **Alvisi, G.**, **Roberto, A.**, **De Paoli, F.**, **Zanon, V**, **Colombo, F.**, **Roederer, M. et al.**, Background fluorescence and spreading error are major contributors of variability in high-dimensional flow cytometry data visualization by t-distributed stochastic neighboring embedding. *Cytometry A* 2018. **93**:785–792.

1930 **Diggins, K. E.**, **Ferrell, P. B. and Irish, J. M.**, Methods for discovery and characterization of cell subsets in high dimensional mass cytometry data. *Methods* 2015. **82**: 55–63.

1931 **Pierzchalski, A.**, **Robitzki, A.**, **Mittag, A.**, **Emmrich, F.**, **Sack, U.**, **O'Connor, J. E.**, **Bocsi, J. et al.**, Cytomics and nanobioengineering. *Cytometry B Clin. Cytom.* 2008. **74**:416–426.

1932 **Van Gassen, S.**, **Callebaut, B.**, **Van Helden, M. J.**, **Lambrecht, B. N.**, **Demeester, P.**, **Dhaene, T. and Saeys, Y.**, FlowSOM: using self-organizing maps for visualization and interpretation of cytometry data. *Cytometry A* 2015. **87**: 636–645.

1933 **Elhmouzi-Younes, J.**, **Palgen, J. L.**, **Tchitchek, N.**, **Delandre, S.**, **Namet, I.**, **Bodinham, C. L.**, **Pizzoferro, K. et al.**, In depth comparative phenotyping of blood innate myeloid leukocytes from healthy humans and macaques using mass cytometry. *Cytometry A* 2017. **91**:969–982.

1934 **Loeffler, M.**, **Engel, C.**, **Ahnert, P.**, **Alfermann, D.**, **Arelin, K.**, **Baber, R.**, **Beutner, F. et al.**, The LIFE-Adult-Study: objectives and design of a population-based cohort study with 10 000 deeply phenotyped adults in Germany. *BMC Public Health* 2015. **15**: 691.

1935 **Moher, D.**, **Glasziou, P.**, **Chalmers, I.**, **Nasser, M.**, **Bossuyt, P. M.**, **Korevaar, D. A.**, **Graham, I. D. et al.**, Increasing value and reducing waste in biomedical research: who's listening? *Lancet* 2015. **387**: 1573–1586.

1936 **Taylor, C. F.**, **Field, D.**, **Sansone, S. A.**, **Aerts, J.**, **Apweiler, R.**, **Ashburner, M.**, **Ball, C. A. et al.**, Promoting coherent minimum reporting guidelines for biological and biomedical investigations: the MIBBI project. *Nat. Biotechnol.* 2008. **26**: 889–896.

1937 **Nies, K. P. H.**, **Kraaijvanger, R.**, **Lindelauf, K. H. K.**, **Drent, R. J. M. R.**, **Rutten, R. M. J.**, **Ramaekers, F. C. S. and Leers, M. P. G.**, Determination of the proliferative fractions in differentiating hematopoietic cell lineages of normal bone marrow. *Cytometry A.* 2018. **93**:1097–1105.

1938 **Parks, D. R.**, **Moore, W. A.**, **Brinkman, R. R.**, **Chen, Y.**, **Condello, D.**, **El Khettabi, F.**, **Nolan, J. P. et al.**, Methodology for evaluating and comparing flow cytometers: a multisite study of 23 instruments. *Cytometry A* 2018. **93**:1087–1091.

1939 **Jaracz-Ros, A.**, **Hémon, P.**, **Krzysiek, R.**, **Bachelerie, F.**, **Schlecht-Louf, G. and Gary-Gouy, H.**, OMIP-048 MC: quantification of calcium sensors and channels expression in lymphocyte subsets by mass cytometry. *Cytometry A* 2018. **93**:681–684.

1940 **Leavesley, S. and Tárnok, A.**, Tycho Brahe's way to precision. *Cytometry A.* 2018. **93**:977–979.

1941 **Spidlen, J., Breuer, K. and Brinkman, R.**, Preparing a Minimum Information about a Flow Cytometry Experiment (MIFlowCyt) compliant manuscript using the International Society for Advancement of Cytometry (ISAC) FCS file repository (FlowRepository.org). *Curr. Protoc. Cytom.* 2012. Chapter 10: Unit 10.18.

1942 **Holzwarth, K., Köhler, R., Philipsen, L., Tokoyoda, K., Ladyhina, V., Wählby, C., Niesner, R. A.** et al., Multiplexed fluorescence microscopy reveals heterogeneity among stromal cells in mouse bone marrow sections. *Cytometry A* 2018. **93**:876–888.

1943 **Roederer, M. and Tárnok, A.**, OMIPs–Orchestrating multiplexity in polychromatic science. *Cytometry A* 2010. **77**: 811–812.

1944 **Finak, G., Jiang, W. and Gottardo, R.**, CytoML for cross-platform cytometry data sharing. *Cytometry A* 2018. **93**: 1189–1196

1945 **O'Neill, K. and Brinkman, R. R.**, Publishing code is essential for reproducible flow cytometry bioinformatics. *Cytometry A* 2016. **89**: 10–11.

1946 Thomson Reuters. Collaborative Science - Solving the Issues of Discovery, Attribution and Measurement in Data Sharing. 2012. http://wokinfo.com/products_tools/multidisciplinary/dci/collaborative_science_essay.pdf

1947 **Piwowar, H. A. and Chapman, W. W.**, A review of journal policies for sharing research data. Proceedings ELPUB 2008 Conference on Electronic Publishing, 2008, http://elpub.scix.net/data/works/att/001_elpub2008.content.pdf

1948 **Fecher, B., Friesike, S. and Hebing, M.**, What drives academic data sharing? *PLoS One* 2015. **10**: e0118053.

1949 **Nicol, A., Caruso, J. and Archambault, É.**, Open Data Access Policies and Strategies in the European Research Area and Beyond. Science-Metrix, Inc. Produced for the European Commission DG Research & Innovation, 2013, http://www.science-metrix.com/pdf/SM_EC_OA_Data.pdf

1950 National Institute of Health. NIH Data Sharing Policy. http://grants.nih.gov/grants/policy/data_sharing/

1951 PLOS. PLOS' New Data Policy: Public Access to Data. http://blogs.plos.org/everyone/2014/02/24/plos-new-data-policy-public-access-data-2/

1952 **Spidlen, J., Breuer, K., Rosenberg, C., Kotecha, N. and Brinkman, R. R.**, FlowRepository: a resource of annotated flow cytometry datasets associated with peer-reviewed publications. *Cytometry A* 2012. **81**: 727–731.

1953 **Kong, Y. M., Dahlke, C., Xiang, Q., Qian, Y., Karp, D. and Scheuermann, R. H.**, Toward an ontology-based framework for clinical research databases. *J. Biomed. Inform.* 2011. **44**: 48–58.

1954 **Bhattacharya, S., Andorf, S., Gomes, L., Dunn, P., Schaefer, H., Pontius, J., Berger, P.** et al., ImmPort: disseminating data to the public for the future of immunology. *Immunol. Res.* 2014. **58**: 234–239.

1955 **Brusic, V., Gottardo, R., Kleinstein, S. H., Davis, M. M.; HIPC steering committee**, Computational resources for high-dimensional immune analysis from the Human Immunology Project Consortium. *Nat. Biotechnol.* 2014. **32**(2): 146–148.

1956 U.S. Department of Health & Human Services. Summary of the HIPAA Privacy Rule. http://www.hhs.gov/sites/default/files/privacysummary.pdf

1957 **Vasilevsky, N. A., Minnier, J., Haendel, M. A. and Champieux, R. E.**, Reproducible and reusable research: are journal data sharing policies meeting the mark? *Peer J.* 2017. **5**: e3208.

1958 **Kay, D. B., Cambier, J. L. and Wheeless, L. L., Jr.**, Imaging in flow. *J. Histochem. Cytochem.* 1979. **27**: 329–334.

1959 **George, T. C., Basiji, D. A., Hall, B. E., Lynch, D. H., Ortyn, W. E., Perry, D. J., Seo, M. J.** et al., Distinguishing modes of cell death using the ImageStream multispectral imaging flow cytometer. *Cytometry A* 2004. **59**: 237–245.

1960 **Pozarowski, P., Holden, E. and Darzynkiewicz, Z.**, Laser scanning cytometry: principles and applications-an update. *Methods Mol. Biol.* 2013. **931**: 187–212.

1961 **Stavrakis, S., Holzner, G., Choo, J. and deMello, A.**, High-throughput microfluidic imaging flow cytometry. *Curr. Opin. Biotechnol.* 2019. **55**: 36–43.

1962 **Nitta, N., Sugimura, T., Isozaki, A., Mikami, H., Hiraki, K., Sakuma, S., Iino, T.** et al., Intelligent image-activated cell sorting. *Cell* 2018. **175**: 266–276.

1963 **Hritzo, M. K., Courneya, J. P. and Golding, A.**, Imaging flow cytometry: a method for examining dynamic native FOXO1 localization in human lymphocytes. *J. Immunol. Methods* 2018. **454**: 59–70.

1964 **Maguire, O., Collins, C., O'Loughlin, K., Miecznikowski, J. and Minderman, H.**, Quantifying nuclear p65 as a parameter for NF-kappaB activation: Correlation between ImageStream cytometry, microscopy, and Western blot. *Cytometry A* 2011. **79**: 461–469.

1965 **Maguire, O., Tornatore, K. M., O'Loughlin, K. L., Venuto, R. C. and Minderman, H.**, Nuclear translocation of nuclear factor of activated T cells (NFAT) as a quantitative pharmacodynamic parameter for tacrolimus. *Cytometry A* 2013. **83**: 1096–1104.

1966 **Stone, R. C., Feng, D., Deng, J., Singh, S., Yang, L., Fitzgerald-Bocarsly, P., Eloranta, M. L.** et al., Interferon regulatory factor 5 activation in monocytes of systemic lupus erythematosus patients is triggered by circulating autoantigens independent of type I interferons. *Arthritis Rheum.* 2012. **64**: 788–798.

1967 **Trifonova, R. T. and Barteneva, N. S.**, Quantitation of IRF3 nuclear translocation in heterogeneous cellular populations from cervical tissue using imaging flow cytometry. *Methods Mol. Biol.* 2018. **1745**: 125–153.

1968 **Volk, A., Li, J., Xin, J., You, D., Zhang, J., Liu, X., Xiao, Y.** et al., Co-inhibition of NF-kappaB and JNK is synergistic in TNF-expressing human AML. *J. Exp. Med.* 2014. **211**: 1093–1108.

1969 **Wan, C. K., Andraski, A. B., Spolski, R., Li, P., Kazemian, M., Oh, J., Samsel, L.** et al., Opposing roles of STAT1 and STAT3 in IL-21 function in CD4+ T cells. *Proc. Natl. Acad. Sci. USA* 2015. **112**: 9394–9399.

1970 **Haridas, V., Ranjbar, S., Vorobjev, I. A., Goldfeld, A. E. and Barteneva, N. S.**, Imaging flow cytometry analysis of intracellular pathogens. *Methods* 2017. **112**: 91–104.

1971 **Pugsley, H. R.**, Quantifying autophagy: Measuring LC3 puncta and autolysosome formation in cells using multispectral imaging flow cytometry. *Methods* 2017. **112**: 147–156.

1972 **Lannigan, J. and Erdbruegger, U.**, Imaging flow cytometry for the characterization of extracellular vesicles. *Methods* 2017. **112**: 55–67.

1973 **Shenoy, G. N., Loyall, J., Maguire, O., Iyer, V., Kelleher, R. J., Jr., Minderman, H., Wallace, P. K.** et al., Exosomes associated with human ovarian tumors harbor a reversible checkpoint of T-cell responses. *Cancer Immunol. Res.* 2018. **6**: 236–247.

1974 **Ploppa, A., George, T. C., Unertl, K. E., Nohe, B. and Durieux, M. E.**, ImageStream cytometry extends the analysis of phagocytosis and oxidative burst. *Scand J. Clin. Lab. Invest.* 2011. **71**: 362–369.

1975 **Henery, S., George, T., Hall, B., Basiji, D., Ortyn, W. and Morrissey, P.**, Quantitative image based apoptotic index measurement using multi-

spectral imaging flow cytometry: a comparison with standard photo-metric methods. *Apoptosis* 2008. **13**: 1054–1063.

1976 Poh, S. E. P., Png, E. and Tong, L., Quantitative image analysis of cellular morphology using Amnis® ImageStreamX Mark II imaging flow cytometer: a comparison against conventional methods. *Single Cell Biol.* 2015. **4**: s1.

1977 Balta, E., Stopp, J., Castelletti, L., Kirchgessner, H., Samstag, Y. and Wabnitz, G. H., Qualitative and quantitative analysis of PMN/T-cell interactions by InFlow and super-resolution microscopy. *Methods* 2017. **112**: 25–38.

1978 Mace, T. A., Zhong, L., Kilpatrick, C., Zynda, E., Lee, C. T., Capitano, M., Minderman, H. et al., Differentiation of CD8+ T cells into effector cells is enhanced by physiological range hyperthermia. *J. Leukoc. Biol.* 2011. **90**: 951–962.

1979 Maguire, O., Wallace, P. K. and Minderman, H., Fluorescent in situ hybridization in suspension by imaging flow cytometry. *Methods Mol. Biol.* 2016. **1389**: 111–126.

1980 Blasi, T., Hennig, H., Summers, H. D., Theis, F. J., Cerveira, J., Patterson, J. O., Davies, D. et al., Label-free cell cycle analysis for high-throughput imaging flow cytometry. *Nat. Commun.* 2016. **7**: 10256.

1981 Ortyn, W. E., Perry, D. J., Venkatachalam, V., Liang, L., Hall, B. E., Frost, K. and Basiji, D. A., Extended depth of field imaging for high speed cell analysis. *Cytometry A* 2007. **71**: 215–231.

1982 Ortyn, W. E., Hall, B. E., George, T. C., Frost, K., Basiji, D. A., Perry, D. J., Zimmerman, C. A. et al., Sensitivity measurement and compensation in spectral imaging. *Cytometry A* 2006. **69**: 852–862.

1983 Chester, C. and Maecker, H. T., Algorithmic tools for mining high-dimensional cytometry data. *J. Immunol.* 2015. **195**: 773–779.

1984 Krutzik, P. O. and Nolan, G. P., Fluorescent cell barcoding in flow cytometry allows high-throughput drug screening and signaling profiling. *Nat. Methods* 2006. **3**: 361–368.

1985 Bodenmiller, B., Zunder, E. R., Finck, R., Chen, T. J., Savig, E. S., Bruggner, R. V., Simonds, E. F. et al., Multiplexed mass cytometry profiling of cellular states perturbed by small-molecule regulators. *Nat. Biotechnol.* 2012. **30**: 858–867.

1986 Behbehani, G. K., Thom, C., Zunder, E. R., Finck, R., Gaudilliere, B., Fragiadakis, G. K., Fantl, W. J. et al., Transient partial permeabilization with saponin enables cellular barcoding prior to surface marker staining. *Cytometry A* 2014. **85**: 1011-1019.

1987 Mei, H. E., Leipold, M. D. and Maecker, H. T., Platinum-conjugated antibodies for application in mass cytometry. *Cytometry A* 2016. **89**: 292–300.

1988 Mei, H. E., Leipold, M. D., Schulz, A. R., Chester, C. and Maecker, H. T., Barcoding of live human peripheral blood mononuclear cells for multiplexed mass cytometry. *J. Immunol.* 2015. **194**: 2022–2031.

1989 Lai, L., Ong, R., Li, J. and Albani, S., A CD45-based barcoding approach to multiplex mass-cytometry (CyTOF). *Cytometry A* 2015. **87**: 369–374.

1990 Akkaya, B., Miozzo, P., Holstein, A. H., Shevach, E. M., Pierce, S. K. and Akkaya, M., A simple, versatile antibody-based barcoding method for flow cytometry. *J. Immunol.* 2016.

1991 Nassar, A. F., Wisnewski, A. V. and Raddassi, K., Automation of sample preparation for mass cytometry barcoding in support of clinical research: protocol optimization. *Anal. Bioanal. Chem.* 2017. **409**: 2363–2372.

1992 Zunder, E. R., Finck, R., Behbehani, G. K., Amir el, A. D., Krishnaswamy, S., Gonzalez, V. D., Lorang, C. G. et al., Palladium-based mass tag cell barcoding with a doublet-filtering scheme and single-cell deconvolution algorithm. *Nat. Protoc.* 2015. **10**: 316–333.

1993 Catena, R., Ozcan, A., Zivanovic, N. and Bodenmiller, B., Enhanced multiplexing in mass cytometry using osmium and ruthenium tetroxide species. *Cytometry A* 2016. **89**: 491–497.

1994 Chevrier, S., Crowell, H. L., Zanotelli, V. R. T., Engler, S., Robinson, M. D. and Bodenmiller, B., Compensation of signal spillover in suspension and imaging mass cytometry. *Cell Syst.* 2018. **6**: 612–620.e615.

1995 Fread, K. I., Strickland, W. D., Nolan, G. P. and Zunder, E. R., An updated debarcoding tool for mass cytometry with cell type-specific and cell sample-specific stringency adjustment. *Pac. Symp. Biocomput.* 2017. **22**: 588–598.

1996 Zivanovic, N., Jacobs, A. and Bodenmiller, B., A practical guide to multiplexed mass cytometry. *Curr. Top. Microbiol. Immunol.* 2013.

1997 Hartmann, F. J., Simonds, E. F. and Bendall, S. C., A universal live cell barcoding-platform for multiplexed human single cell analysis. *Sci. Rep.* 2018. **8**: 10770.

1998 Yamanaka, Y. J., Szeto, G. L., Gierahn, T. M., Forcier, T. L., Benedict, K. F., Brefo, M. S., Lauffenburger, D. A. et al., Cellular barcodes for efficiently profiling single-cell secretory responses by microengraving. *Anal. Chem.* 2012. **84**: 10531–10536.

1999 Schulz, A. R. and Mei, H. E., Surface barcoding of live PBMC for multiplexed mass cytometry. *Methods Mol. Biol.* 2019. **1989**: 93–108.

2000 Simard, C., Cloutier, M. and Neron, S., Rapid determination of IL-6 specific activity by flow cytometry. *J. Immunol. Methods* 2014. **415**: 63–65.

2001 Simard, C., Cloutier, M. and Neron, S., Feasibility study: phosphospecific flow cytometry enabling rapid functional analysis of bone marrow samples from patients with multiple myeloma. *Cytometry B Clin. Cytom.* 2014. **86**: 139–144.

2002 Krutzik, P. O., Clutter, M. R., Trejo, A. and Nolan, G. P., Fluorescent cell barcoding for multiplex flow cytometry. *Curr. Protoc. Cytom.* 2011. Chapter 6: Unit 6 31.

2003 Krutzik, P. O., Crane, J. M., Clutter, M. R. and Nolan, G. P., High-content single-cell drug screening with phosphospecific flow cytometry. *Nat. Chem. Biol.* 2008. **4**: 132–142.

2004 Frischbutter, S., Schultheis, K., Patzel, M., Radbruch, A. and Baumgrass, R., Evaluation of calcineurin/NFAT inhibitor selectivity in primary human Th cells using bar-coding and phospho-flow cytometry. *Cytometry A* 2012. **81**: 1005–1011.

2005 Bernardo, S. M., Allen, C. P., Waller, A., Young, S. M., Oprea, T., Sklar, L. A. and Lee, S. A., An automated high-throughput cell-based multiplexed flow cytometry assay to identify novel compounds to target Candida albicans virulence-related proteins. *PLoS One* 2014. **9**: e110354.

2006 Spurgeon, B. E., Aburima, A., Oberprieler, N. G., Tasken, K. and Naseem, K. M., Multiplexed phosphospecific flow cytometry enables large-scale signaling profiling and drug screening in blood platelets. *J. Thromb. Haemost.* 2014. **12**: 1733–1743.

2007 Clark, M. A., Goheen, M. M., Spidale, N. A., Kasthuri, R. S., Fulford, A. and Cerami, C., RBC barcoding allows for the study of erythrocyte population dynamics and P. falciparum merozoite invasion. *PLoS One* 2014. **9**: e101041.

2008 Becher, B., Schlitzer, A., Chen, J., Mair, F., Sumatoh, H. R., Teng, K. W. et al., High-dimensional analysis of the murine myeloid cell system. *Nat. Immunol.* 2014. **15**: 1181–1189.

2009 McCarthy, R. L., Mak, D. H., Burks, J. K. and Barton, M. C., Rapid monoisotopic cisplatin based barcoding for multiplexed mass cytometry. *Sci. Rep.* 2017. **7**: 3779.

2010 Schulz, A. R. and Mei, H. E., Cell-surface barcoding of live PBMC for multiplexed mass cytometry. In McGuire, H. and Ashhurst, T. (Eds.) *Methods in molecular biology*. Springer Nature, Basingstoke, UK 2019.

2011 **Willis, L. M., Park, H., Watson, M. W. L., Majonis, D., Watson, J. L. and Nitz, M.,** Tellurium-based mass cytometry barcode for live and fixed cells. *Cytometry A* 2018. **93**: 685–694.

2012 **Wu, X., DeGottardi, Q., Wu, I. C., Wu, L., Yu, J., Kwok, W. W. and Chiu, D. T.,** Ratiometric Barcoding for Mass Cytometry. *Anal. Chem.* 2018. **90**: 10688–10694.

2013 **Meng, H., Warden, A., Zhang, L., Zhang, T., Li, Y., Tan, Z., Wang, B. et al.,** A mass-ratiometry-based CD45 barcoding method for mass cytometry detection. *SLAS Technol.* 2019. 2472630319834057.

2014 **Irish, J. M., Myklebust, J. H., Alizadeh, A. A., Houot, R., Sharman, J. P., Czerwinski, D. K., Nolan, G. P. et al.,** B-cell signaling networks reveal a negative prognostic human lymphoma cell subset that emerges during tumor progression. *Proc. Natl. Acad. Sci. USA* 2010. **107**: 12747–12754.

2015 **Gaudillière, B., Fragiadakis, G. K., Bruggner, R. V., Nicolau, M., Finck, R., Tingle, M., Silva, J. et al.,** Clinical recovery from surgery correlates with single-cell immune signatures. *Sci. Transl. Med.* 2014. **6**: 255ra131.

2016 **Bandura, D. R., Baranov, V. I., Ornatsky, O. I., Antonov, A., Kinach, R., Lou, X., Pavlov, S. et al.,** Mass cytometry: technique for real time single cell multitarget immunoassay based on inductively coupled plasma time-of-flight mass spectrometry. *Anal. Chem.* 2009. **81**: 6813–6822.

2017 **Bendall, S. C., Nolan, G. P., Roederer, M. and Chattopadhyay, P. K.,** A deep profiler's guide to cytometry. *Trends Immunol.* 2012. **33**: 323–332.

2018 **Tanner, S. D., Baranov, V. I., Ornatsky, O. I., Bandura, D. R. and George, T. C.,** An introduction to mass cytometry: fundamentals and applications. *Cancer Immunol. Immunother.* 2013. **62**: 955–965.

2019 **Wong, M. T., Ong, D. E., Lim, F. S., Teng, K. W., McGovern, N., Narayanan, S., Ho, W. Q. et al.,** A high-dimensional atlas of human T cell diversity reveals tissue-specific trafficking and cytokine signatures. *Immunity* 2016. **45**: 442–456.

2020 **Zunder, E. R., Lujan, E., Goltsev, Y., Wernig, M. and Nolan, G. P.,** A continuous molecular roadmap to iPSC reprogramming through progression analysis of single-cell mass cytometry. *Cell Stem Cell* 2015. **16**: 323–337.

2021 **Nair, N., Mei, H. E., Chen, S. Y., Hale, M., Nolan, G. P., Maecker, H. T., Genovese, M. et al.,** Mass cytometry as a platform for the discovery of cellular biomarkers to guide effective rheumatic disease therapy. *Arthritis Res. Ther.* 2015. **17**: 127.

2022 **Mingueneau, M., Boudaoud, S., Haskett, S., Reynolds, T. L., Nocturne, G., Norton, E., Zhang, X. et al.,** Cytometry by time-of-flight immunophenotyping identifies a blood Sjogren's signature correlating with disease activity and glandular inflammation. *J. Allergy Clin. Immunol.* 2016. **137**: 1809–1821 e1812.

2023 **Olin, A., Henckel, E., Chen, Y., Lakshmikanth, T., Pou, C., Mikes, J., Gustafsson, A. et al.,** Stereotypic immune system development in newborn children. *Cell* 2018. **174**: 1277–1292.

2024 **Brodin, P., Jojic, V., Gao, T., Bhattacharya, S., Angel, C. J., Furman, D., Shen-Orr, S. et al.,** Variation in the human immune system is largely driven by non-heritable influences. *Cell* 2015. **160**: 37–47.

2025 **Pejoski, D., Tchitchek, N., Rodriguez Pozo, A., Elhmouzi-Younes, J., Yousfi-Bogniaho, R., Rogez-Kreuz, C., Clayette, P. et al.,** Identification of vaccine-altered circulating b cell phenotypes using mass cytometry and a two-step clustering analysis. *J. Immunol.* 2016. **196**: 4814–4831.

2026 **Leipold, M. D., Ornatsky, O., Baranov, V., Whitfield, C. and Nitz, M.,** Development of mass cytometry methods for bacterial discrimination. *Anal. Biochem.* 2011. **419**: 1–8.

2027 **Guo, Y., Baumgart, S., Stark, H. J., Harms, H. and Muller, S.,** Mass cytometry for detection of silver at the bacterial single cell level. *Front Microbiol.* 2017. **8**: 1326.

2028 **Yang, Y. S., Atukorale, P. U., Moynihan, K. D., Bekdemir, A., Rakhra, K., Tang, L., Stellacci, F. et al.,** High-throughput quantitation of inorganic nanoparticle biodistribution at the single-cell level using mass cytometry. *Nat. Commun.* 2017. **8**: 14069.

2029 **Abdelrahman, A. I., Ornatsky, O., Bandura, D., Baranov, V., Kinach, R., Dai, S., Thickett, S. C. et al.,** Metal-containing polystyrene beads as standards for mass cytometry. *J. Anal. At Spectrom.* 2010. **25**: 260–268.

2030 **Galli, E., Friebel, E., Ingelfinger, F., Unger, S., Nunez, N. G. and Becher, B.,** The end of omics? High dimensional single cell analysis in precision medicine. *Eur. J. Immunol.* 2019. **49**: 212–220.

2031 **Kimball, A. K., Oko, L. M., Bullock, B. L., Nemenoff, R. A., van Dyk, L. F. and Clambey, E. T.,** A beginner's guide to analyzing and visualizing mass cytometry data. *J. Immunol.* 2018. **200**: 3–22.

2032 **Cosma, A.,** A time to amaze, a time to settle down, and a time to discover. *Cytometry A* 2015. **87**: 795–796.

2033 **Chang, Q., Ornatsky, O. I., Siddiqui, I., Loboda, A., Baranov, V. I. and Hedley, D. W.,** Imaging mass cytometry. *Cytometry A* 2017. **91**: 160–169.

2034 **Zhao, Y., Uduman, M., Siu, J. H. Y., Tull, T. J., Sanderson, J. D., Wu, Y. B., Zhou, J. Q. et al.,** Spatiotemporal segregation of human marginal zone and memory B cell populations in lymphoid tissue. *Nat. Commun.* 2018. **9**: 3857.

2035 **Keren, L., Bosse, M., Marquez, D., Angoshtari, R., Jain, S., Varma, S., Yang, S. R. et al.,** A structured tumor-immune microenvironment in triple negative breast cancer revealed by multiplexed ion beam imaging. *Cell* 2018. **174**: 1373–1387 e1319.

2036 **Tricot, S., Meyrand, M., Sammicheli, C., Elhmouzi-Younes, J., Corneau, A., Bertholet, S., Malissen, M., Le Grand, R. et al.,** Evaluating the efficiency of isotope transmission for improved panel design and a comparison of the detection sensitivities of mass cytometer instruments. *Cytometry A* 2015. **87**: 357–368.

2037 **Rahman, A. H., Tordesillas, L. and Berin, M. C.,** Heparin reduces nonspecific eosinophil staining artifacts in mass cytometry experiments. *Cytometry A* 2016. **89**: 601–607.

2038 **Schulz, A. R., Stanislawiak, S., Baumgart, S., Grutzkau, A. and Mei, H. E.,** Silver nanoparticles for the detection of cell surface antigens in mass cytometry. *Cytometry A* 2017. **91**: 25–33.

2039 **Lin, W., Hou, Y., Lu, Y., Abdelrahman, A. I., Cao, P., Zhao, G., Tong, L. et al.,** A high-sensitivity lanthanide nanoparticle reporter for mass cytometry: tests on microgels as a proxy for cells. *Langmuir* 2014. **30**: 3142–3153.

2040 **Tong, L., Lu, E., Pichaandi, J., Zhao, G. and Winnik, M. A.,** Synthesis of uniform NaLnF4 (Ln: Sm to Ho) nanoparticles for mass cytometry. *J. Phys. Chem. C* 2016. **120**: 6269–6280.

2041 **Baumgart, S., Schulz, A. R., Peddinghaus, A., Stanislawiak, S., Gillert, S., Hirseland, H., Krauthauser, S. et al.,** Dual-labelled antibodies for flow and mass cytometry: a new tool for cross-platform comparison and enrichment of target cells for mass cytometry. *Eur. J. Immunol.* 2017.

2042 **Finck, R., Simonds, E. F., Jager, A., Krishnaswamy, S., Sachs, K., Fantl, W., Pe'er, D. et al.,** Normalization of mass cytometry data with bead standards. *Cytometry A* 2013. **83**: 483–494.

2043 **Schulz, A. R., Baumgart, S., Schulze, J., Urbicht, M., Grutzkau, A. and Mei, H. E.,** Stabilizing antibody cocktails for mass cytometry. *Cytometry A* 2019.

2044 **Kadic, E., Moniz, R. J., Huo, Y., Chi, A. and Kariv, I.,** Effect of cryopreservation on delineation of immune cell subpopulations in tumor specimens as determined by multiparametric single cell mass cytometry analysis. *BMC Immunol.* 2017. **18**: 6.

2045 **Kleinsteuber, K., Corleis, B., Rashidi, N., Nchinda, N., Lisanti, A., Cho, J. L., Medoff, B. D. et al.**, Standardization and quality control for high-dimensional mass cytometry studies of human samples. *Cytometry A* 2016. **89**: 903–913.

2046 **Leipold, M. D., Obermoser, G., Fenwick, C., Kleinstuber, K., Rashidi, N., McNevin, J. P., Nau, A. N. et al.**, Comparison of CyTOF assays across sites: Results of a six-center pilot study. *J. Immunol. Methods* 2018. **453**: 37–43.

2047 **Sumatoh, H. R., Teng, K. W., Cheng, Y. and Newell, E. W.**, Optimization of mass cytometry sample cryopreservation after staining. *Cytometry A* 2017. **91**: 48–61.

2048 **Nicholas, K. J., Greenplate, A. R., Flaherty, D. K., Matlock, B. K., Juan, J. S., Smith, R. M., Irish, J. M. et al.**, Multiparameter analysis of stimulated human peripheral blood mononuclear cells: a comparison of mass and fluorescence cytometry. *Cytometry A* 2016. **89**: 271–280.

2049 **Baumgart, S., Peddinghaus, A., Schulte-Wrede, U., Mei, H. E. and Grutzkau, A.**, OMIP-034: comprehensive immune phenotyping of human peripheral leukocytes by mass cytometry for monitoring immunomodulatory therapies. *Cytometry A* 2017. **91**: 34–38.

2050 **Behbehani, G. K., Bendall, S. C., Clutter, M. R., Fantl, W. J. et al.**, Single-cell mass cytometry adapted to measurements of the cell cycle. *Cytometry A* 2012. **81**: 552–566.

2051 **Frei, A. P., Bava, F. A., Zunder, E. R., Hsieh, E. W., Chen, S. Y., Nolan, G. P. and Gherardini, P. F.**, Highly multiplexed simultaneous detection of RNAs and proteins in single cells. *Nat. Methods* 2016. **13**: 269–275.

2052 **Mavropoulos, A., Allo, B., He, M., Park, E., Majonis, D. and Ornatsky, O.**, Simultaneous detection of protein and mRNA in Jurkat and KG-1a cells by mass cytometry. *Cytometry A* 2017. **91**: 1200–1208.

2053 **Cheung, P., Vallania, F., Warsinske, H. C., Donato, M., Schaffert, S., Chang, S. E., Dvorak, M. et al.**, Single-cell chromatin modification profiling reveals increased epigenetic variations with aging. *Cell* 2018. **173**: 1385–1397 e1314.

2054 **Lumba, M. A., Willis, L. M., Santra, S., Rana, R., Schito, L., Rey, S., Wouters, B. G. et al.**, A beta-galactosidase probe for the detection of cellular senescence by mass cytometry. *Org. Biomol. Chem.* 2017. **15**: 6388–6392.

2055 **Edgar, L. J., Vellanki, R. N., Halupa, A., Hedley, D., Wouters, B. G. and Nitz, M.**, Identification of hypoxic cells using an organotellurium tag compatible with mass cytometry. *Angew Chem. Int. Ed. Engl.* 2014. **53**: 11473–11477.

2056 **Stern, A. D., Rahman, A. H. and Birtwistle, M. R.**, Cell size assays for mass cytometry. *Cytometry A* 2017. **91**: 14–24.

2057 **Rapsomaniki, M. A., Lun, X. K., Woerner, S., Laumanns, M., Bodenmiller, B. and Martinez, M. R.**, CellCycleTRACER accounts for cell cycle and volume in mass cytometry data. *Nat. Commun.* 2018. **9**: 632.

2058 **Budzinski, L., Schulz, A. R., Baumgart, S., Burns, T., Rose, T., Hirseland, H. and Mei, H. E.**, Osmium-labeled microspheres for bead-based assays in mass cytometry. *J. Immunol.* 2019. **202**: 3103–3112.

2059 **Bringeland, G. H., Bader, L., Blaser, N., Budzinski, L., Schulz, A. R., Mei, H. E., Myhr, K. M. et al.**, Optimization of receptor occupancy assays in mass cytometry: standardization across channels with QSC beads. *Cytometry A* 2019. **95**: 314–322.

2060 **Ornatsky, O. I., Lou, X., Nitz, M., Schafer, S., Sheldrick, W. S., Baranov, V. I., Bandura, D. R. et al.**, Study of cell antigens and intracellular DNA by identification of element-containing labels and metallointercalators using inductively coupled plasma mass spectrometry. *Anal. Chem.* 2008. **80**: 2539–2547.

2061 **Blair, T. A., Michelson, A. D. and Frelinger, A. L., 3rd**, Mass cytometry reveals distinct platelet subtypes in healthy subjects and novel alter-ations in surface glycoproteins in Glanzmann thrombasthenia. *Sci. Rep.* 2018. **8**: 10300.

2062 **Lee, B. H. and Rahman, A. H.**, Acquisition, Processing, and Quality Control of Mass Cytometry Data. *Methods Mol. Biol.* 2019. **1989**: 13–31.

2063 **Fienberg, H. G., Simonds, E. F., Fantl, W. J., Nolan, G. P. and Bodenmiller, B.**, A platinum-based covalent viability reagent for single-cell mass cytometry. *Cytometry A* 2012. **81**: 467–475.

2064 **Leipold, M. D. and Maecker, H. T.**, Phenotyping of live human PBMC using CyTOFTM mass cytometry. *bio-protocol* 2015. **5**: e1382.

2065 **Han, G., Spitzer, M. H., Bendall, S. C., Fantl, W. J. and Nolan, G. P.**, Metal-isotope-tagged monoclonal antibodies for high-dimensional mass cytometry. *Nat. Protoc.* 2018. **13**: 2121–2148.

2066 **Han, G., Chen, S. Y., Gonzalez, V. D., Zunder, E. R., Fantl, W. J. and Nolan, G. P.**, Atomic mass tag of bismuth-209 for increasing the immunoassay multiplexing capacity of mass cytometry. *Cytometry A* 2017. **91**: 1150–1163.

2067 **Horowitz, A., Strauss-Albee, D. M., Leipold, M., Kubo, J., Nemat-Gorgani, N., Dogan, O. C., Dekker, C. L. et al.**, Genetic and environmental determinants of human NK cell diversity revealed by mass cytometry. *Sci. Transl. Med.* 2013. **5**: 208ra145.

2068 **Leipold, M. D., Newell, E. W. and Maecker, H. T.**, Multiparameter phenotyping of human PBMCs using mass cytometry. *Methods Mol. Biol.* 2015. **1343**: 81–95.

2069 **Olsen, L. R., Leipold, M. D., Pedersen, C. B. and Maecker, H. T.**, The anatomy of single cell mass cytometry data. *Cytometry A* 2018.

2070 **Robinson, J. P., Patsekin, V., Holdman, C., Ragheb, K., Sturgis, J., Fatig, R., Avramova, L. V. et al.**, High-throughput secondary screening at the single-cell level. *J. Lab. Automat.* 2012. **18**: 85–98.

2071 **Robinson, J. P., Durack, G. and Kelley, S.**, An innovation in flow cytometry data collection & analysis producing a correlated multiple sample analysis in a single file. *Cytometry* 1991. **12**: 82–90.

2072 **Newell, E., Bendall, S., Hong, D., Lewis, D., Nolan, G. and Davis, M.**, Surveying the influenza-specific cytotoxic T cell response in humans and mice using mass-cytometry (CyTOF) and combinatorial tetramer staining. *Clin. Immunol.* 2010. **135**: S104–S104.

2073 **Rajwa, B., Venkatapathi, M., Ragheb, K., Banada, P. P., Hirleman, E. D., Lary, T. and Robinson, J. P.** Automated classification of bacterial particles in flow by multiangle scatter measurement and a support vector machine classifier. *Cytometry Part A* 2008. **73A**: 369–379.

2074 **Costa, E. S., Pedreira, C. E., Barrena, S., Lecrevisse, Q., Flores, J., Quijano, S., Almeida, J. et al.**, Automated pattern-guided principal component analysis vs expert-based immunophenotypic classification of B-cell chronic lymphoproliferative disorders: A step forward in the standardization of clinical immunophenotyping. *Leukemia* 2010. **24**: 1927–1933.

2075 **Dundar, M., Akova, F., Yerebakan, H. Z. and Rajwa, B.**, A non-parametric Bayesian model for joint cell clustering and cluster matching: identification of anomalous sample phenotypes with random effects. *BMC Bioinformatics* 2014. **15**: 314.

2076 **Bagwell, C. B., Hunsberger, B. C., Herbert, D. J., Munson, M. E., Hill, B. L., Bray, C. M. and Preffer, F. I.**, Probability state modeling theory. *Cytometry A* 2015. **87**: 646–660.

2077 **Robinson, J. P., Rajwa, B., Patsekin, V. and Davisson, V. J.**, Computational analysis of high throughput flow cytometry data. *Expert Opin. Drug Deliv.* 2012. **7**: 679–693.

2078 **Fulton, R. J., McDade, R. L., Smith, P. L., Kienker, L. J. and Kettman, J. R.** Advanced multiplexed analysis with the FlowMetrix system. *Clin. Chem.* 1997. **43**: 1749–1756.

2079 **Robinson, J. P.**, **Patsekin, V.**, **Gregori, G.**, **Rajwa, B. and Jones, J.**, Multi-spectral flow cytometry: next generation tools for automated classification. *Microsc. Microanal.* 2005. **11**: 2–3.

2080 **Mair, F. and Prlic, M.**, OMIP-044: 28-color immunophenotyping of the human dendritic cell compartment. *Cytometry A.* 2018. **106**: 255.

2081 **Nolan, J. P. and Condello, D.**, Spectral flow cytometry. *Curr. Protoc. Cytom.* 2013. Chapter 1:Unit1.27–1.27.13.

2082 **Bagwell, C. B. and Adams, E. G.**, Fluorescence spectral overlap compensation for any number of flow cytometry parameters. *Ann. N. Y. Acad. Sci.* 1993. **677**: 167–184.

2083 **Roederer, M.**, Compensation is not dependent on signal intensity or on number of parameters. *Cytometry.* 2001. **46**: 357–359.

2084 **Perfetto, S. P.**, **Chattopadhyay, P. K. and Roederer, M.**, Seventeen-colour flow cytometry: unravelling the immune system. *Nat. Rev. Immunol.* 2004. **4**: 648–655.

2085 **Mahnke, Y. D.**, **Brodie, T. M.**, **Sallusto, F.**, **Roederer, M.**, **Lugli, E.**, The who's who of T-cell differentiation: human memory T-cell subsets. *Eur. J. Immunol.* 2013. **43**: 2797–2809.

2086 **Herzenberg, L. A.**, **Tung, J.**, **Moore, W. A.**, **Herzenberg, L. A. and Parks, D. R.**, Interpreting flow cytometry data: a guide for the perplexed. *Nat. Immunol.* 2006. **7**: 681–685.

2087 **Gerner, M. Y.**, **Kastenmüller, W.**, **Ifrim, I.**, **Kabat, J. and Germain, R. N.**, Histo-cytometry: a method for highly multiplex quantitative tissue imaging analysis applied to dendritic cell subset microanatomy in lymph nodes. *Immunity.* 2012. **37**: 364–376.

2088 **Ashhurst, T. M.**, **Smith, A. L. and King, N. J. C.**, *High-dimensional fluorescence cytometry.* John Wiley & Sons, Inc., Hoboken, NJ 2017. 5.8.1–5.8.38.

2089 **Picelli, S.**, **Faridani, O. R.**, **Björklund, A. K.**, **Winberg, G.**, **Sagasser, S. and Sandberg, R.**, Full-length RNA-seq from single cells using Smart-seq2. *Nat. Protoc.* 2014. **9**: 171–181.

2090 **Lafzi, A.**, **Moutinho, C.**, **Picelli, S. and Heyn, H.**, Tutorial: guidelines for the experimental design of single-cell RNA sequencing studies. *Nat. Protoc.* 2018. **13**: 2742–2757.

2091 **Macosko, E. Z.**, **Basu, A.**, **Satija, R.**, **Nemesh, J.**, **Shekhar, K.**, **Goldman, M.**, **Tirosh, I.** et al., Highly parallel genome-wide expression profiling of individual cells using nanoliter droplets. *Cell.* 2015. **161**: 1202–1214.

2092 **Klein, A. M.**, **Mazutis, L.**, **Akartuna, I.**, **Tallapragada, N.**, **Veres, A.**, **Li, V.**, **Peshkin, L.** et al., Droplet barcoding for single-cell transcriptomics applied to embryonic stem cells. *Cell.* 2015. **161**: 1187–1201.

2093 **Valihrach, L.**, **Androvic, P. and Kubista, M.**, Platforms for single-cell collection and analysis. *Int. J. Mol. Sci.* 2018. **19**: 807.

2094 **Cao, J.**, **Packer, J. S.**, **Ramani, V.**, **Cusanovich, D. A.**, **Huynh, C.**, **Daza, R.**, **Qiu, X.** et al., Comprehensive single-cell transcriptional profiling of a multicellular organism. *Science.* 2017. **357**: 661–667.

2095 **Bucevičius, J.**, **Lukinavičius, G. and Gerasimaitė, R.**, The use of Hoechst dyes for DNA staining and beyond. *Chemosensors.* 2018. **6**: 18.

2096 **Smith, P. J.**, **Blunt, N.**, **Wiltshire, M.**, **Hoy, T.**, **Teesdale-Spittle, P.**, **Craven, M. R.**, **Watson, J. V.** et al., Characteristics of a novel deep red/infrared fluorescent cell-permeant DNA probe, DRAQ5, in intact human cells analyzed by flow cytometry, confocal and multiphoton microscopy. *Cytometry.* 2000. **40**: 280–291.

2097 **Wlodkowic, D.**, **Skommer, J. and Darzynkiewicz, Z.**, Flow cytometry-based apoptosis detection. *Methods Mol. Biol.* 2009. **559**: 19–32.

2098 **Belloc, F.**, **Belaud-Rotureau, M. A.**, **Lavignolle, V.**, **Bascans, E.**, **Braz-Pereira, E.**, **Durrieu, F. and Lacombe, F.**, Flow cytometry detection of caspase 3 activation in preapoptotic leukemic cells. *Cytometry.* 2000. **40**: 151–160.

2099 **Shapiro, H. M.**, *Practical flow cytometry.* Wiley-Liss, Hoboken, NJ 2003.

2100 **Riddell, A.**, **Gardner, R.**, **Perez-Gonzalez, A.**, **Lopes, T. and Martinez, L.**, Rmax: a systematic approach to evaluate instrument sort performance using center stream catch. *Methods.* 2015. **82**: 64–73.

2101 **Ziegenhain, C.**, **Vieth, B.**, **Parekh, S.**, **Reinius, B.**, **Guillaumet-Adkins, A.**, **Smets, M.**, **Leonhardt, H.** et al., Comparative analysis of single-cell RNA sequencing methods. *Mol. Cell.* 2017. **65**: 631–643.

2102 **Semrau, S.**, **Goldmann, J. E.**, **Soumillon, M.**, **Mikkelsen, T. S.**, **Jaenisch, R. and van Oudenaarden, A.**, Dynamics of lineage commitment revealed by single-cell transcriptomics of differentiating embryonic stem cells. *Nat. Commun.* 2017. **8**: 243.

2103 **Patel, A. P.**, **Tirosh, I.**, **Trombetta, J. J.**, **Shalek, A. K.**, **Gillespie, S. M.**, **Wakimoto, H.**, **Cahill, D. P.** et al., Single-cell RNA-seq highlights intratumoral heterogeneity in primary glioblastoma. *Science.* 2014. **344**: 1396–1401.

2104 **Lopez, R.**, **Regier, J.**, **Cole, M. B.**, **Jordan, M. I. and Yosef, N.**, Deep generative modeling for single-cell transcriptomics. *Nat. Methods.* 2018. **15**: 1053–1058.

2105 **Bacher, R. and Kendziorski, C.**, Design and computational analysis of single-cell RNA-sequencing experiments. *Genome Biol.* 2016. **17**: 63.

2106 **Vallejos, C. A.**, **Marioni, J. C. and Richardson, S.**, BASiCS: Bayesian analysis of single-cell sequencing data *PLoS Comput. Biol.* 2015. **11**: e1004333.

2107 **Anders, S. and Huber, W.**, Differential expression analysis for sequence count data. *Genome Biol.* 2010. **11**: R106.

2108 **Robinson, M. D. and Oshlack, A.**, A scaling normalization method for differential expression analysis of RNA-seq data. *Genome Biol.* 2010. **11**: R25.

2109 **Bullard, J. H.**, **Purdom, E.**, **Hansen, K. D. and Dudoit, S.**, Evaluation of statistical methods for normalization and differential expression in mRNA-Seq experiments. *BMC Bioinformatics.* 2010. **11**: 94.

2110 **Bacher, R.**, **Chu, L-F**, **Leng, N.**, **Gasch, A. P.**, **Thomson, J. A.**, **Stewart, R. M.**, **Newton, M.** et al., SCnorm: robust normalization of single-cell RNA-seq data. *Nat. Methods.* 2017. **14**: 584–586.

2111 **Lun, A. T. L.**, **Bach, K. and Marioni, J. C.**, Pooling across cells to normalize single-cell RNA sequencing data with many zero counts. *Genome Biol.* 2016. **17**: 75.

2112 **Butler, A.**, **Hoffman, P.**, **Smibert, P.**, **Papalexi, E. and Satija, R.**, Integrating single-cell transcriptomic data across different conditions, technologies, and species. *Nat. Biotechnol.* 2018. **36**: 411–420.

2113 **Abdi, H. and Williams, L. J.**, Principal component analysis. *Wiley Interdiscip. Rev. Comput. Stat.* 2010. **2**: 433–459.

2114 **Ståhlberg, A. and Bengtsson, M.**, Single-cell gene expression profiling using reverse transcription quantitative real-time PCR. *Methods.* 2010. **50**: 282–288.

2115 **Ståhlberg, A.**, **Bengtsson, M.**, **Hemberg, M. and Semb, H.**, Quantitative transcription factor analysis of undifferentiated single human embryonic stem cells. *Clin. Chem.* 2009. **55**: 2162–2170.

2116 **Kiselev, V. Y.**, **Kirschner, K.**, **Schaub, M. T.**, **Andrews, T.**, **Yiu, A.**, **Chandra, T.**, **Natarajan, K. N.** et al., SC3: consensus clustering of single-cell RNA-seq data. *Nat. Methods.* 2017. **14**: 483–486.

2117 **Soneson, C. and Robinson, M. D.**, Bias, robustness and scalability in single-cell differential expression analysis. *Nat. Methods.* 2018. **15**: 255–261.

2118 **Koch, C. and Muller, S.**, Personalized microbiome dynamics—cytometric fingerprints for routine diagnostics. *Mol. Aspects Med.* 2018. **59**: 123–134.

2119 **Muller, S.**, Modes of cytometric bacterial DNA pattern: a tool for pursuing growth. *Cell Prolif.* 2007. **40**: 621–639.

2120 **Delgado-Baquerizo, M., Oliverio, A. M., Brewer, T. E., Benavent-Gonzalez, A., Eldridge, D. J., Bardgett, R. D., Maestre, F. T. et al.**, A global atlas of the dominant bacteria found in soil. *Science* 2018. **359**: 320–325.

2121 **Koch, C., Harnisch, F., Schroder, U. and Muller, S.**, Cytometric fingerprints: evaluation of new tools for analyzing microbial community dynamics. *Front Microbiol.* 2014. **5**: 273.

2122 **Zimmermann, J., Hubschmann, T., Schattenberg, F., Schumann, J., Durek, P., Riedel, R., Friedrich, M. et al.**, High-resolution microbiota flow cytometry reveals dynamic colitis-associated changes in fecal bacterial composition. *Eur. J. Immunol.* 2016. **46**: 1300–1303.

2123 **Vandeputte, D., Kathagen, G., D'Hoe, K., Vieira-Silva, S., Valles-Colomer, M., Sabino, J., Wang, J. et al.**, Quantitative microbiome profiling links gut community variation to microbial load. *Nature* 2017. **551**: 507–511.

2124 **Muller, S. and Nebe-von-Caron, G.**, Functional single-cell analyses: flow cytometry and cell sorting of microbial populations and communities. *FEMS Microbiol. Rev.* 2010. **34**: 554–587.

2125 **Lambrecht, J., Schattenberg, F., Harms, H. and Mueller, S.**, Characterizing microbiome dynamics—flow cytometry based workflows from pure cultures to natural communities. *J. Vis. Exp.* 2018.

2126 **Gunther, S., Hubschmann, T., Rudolf, M., Eschenhagen, M., Roske, I., Harms, H. and Muller, S.**, Fixation procedures for flow cytometric analysis of environmental bacteria. *J. Microbiol. Methods* 2008. **75**: 127–134.

2127 **Shi, L., Gunther, S., Hubschmann, T., Wick, L. Y., Harms, H. and Muller, S.**, Limits of propidium iodide as a cell viability indicator for environmental bacteria. *Cytometry A* 2007. **71**: 592–598.

2128 **Props, R., Rubbens, P., Besmer, M., Buysschaert, B., Sigrist, J., Weilenmann, H., Waegeman, W. et al.**, Detection of microbial disturbances in a drinking water microbial community through continuous acquisition and advanced analysis of flow cytometry data. *Water Res.* 2018. **145**: 73–82.

2129 **Stepanauskas, R., Fergusson, E. A., Brown, J., Poulton, N. J., Tupper, B., Labonte, J. M., Becraft, E. D. et al.**, Improved genome recovery and integrated cell-size analyses of individual uncultured microbial cells and viral particles. *Nat. Commun.* 2017. **8**: 84.

2130 **Jahn, M., Seifert, J., von Bergen, M., Schmid, A., Buhler, B. and Muller, S.**, Subpopulation-proteomics in prokaryotic populations. *Curr. Opin. Biotechnol.* 2013. **24**: 79–87.

2131 **Liu, Z., Cichocki, N., Hubschmann, T., Suring, C., Ofiteru, I. D., Sloan, W. T., Grimm, V. et al.**, Neutral mechanisms and niche differentiation in steady-state insular microbial communities revealed by single cell analysis. *Environ. Microbiol.* 2019. **21**: 164–181.

2132 **Koch, C., Gunther, S., Desta, A. F., Hubschmann, T. and Muller, S.**, Cytometric fingerprinting for analyzing microbial intracommunity structure variation and identifying subcommunity function. *Nat. Protoc.* 2013. **8**: 190–202.

2133 **Rogers, W. T. and Holyst, H. A.**, FlowFP: A Bioconductor Package for Fingerprinting Flow Cytometric Data. *Adv. Bioinformatics* 2009. 193947.

2134 **De Roy, K., Clement, L., Thas, O., Wang, Y. and Boon, N.**, Flow cytometry for fast microbial community fingerprinting. *Water Res.* 2012. **46**: 907–919.

2135 **Koch, C., Fetzer, I., Harms, H. and Muller, S.**, CHIC-an automated approach for the detection of dynamic variations in complex microbial communities. *Cytometry A* 2013. **83**: 561–567.

2136 **Schroder, K. and Tschopp, J.**, The inflammosomes. *Cell* 2010. **140**: 821–832.

2137 **Aachoui, Y., Sagulenko, V., Miao, E. A. and Stacey, K. J.**, Inflammasomemediated pyroptotic and apoptotic cell death, and defense against infection. *Curr. Opin. Microbiol.* 2013. **16**: 319–326.

2138 **Miao, E. A., Rajan, J. V. and Aderem, A.**, Caspase-1-induced pyroptotic cell death. *Immunol. Rev.* 2011. **243**: 206–214.

2139 **Jin, C. and Flavell, R.A.**, Molecular mechanism of NLRP3 inflammasome activation. *J. Clin. Immunol.* 2010. **30**: 628–631.

2140 **Lamkanfi, M.**, Emerging inflammasome effector mechanisms. *Nat. Rev. Immunol.* 2011. **11**: 213–220.

2141 **Vajjhala, P. R., Lu, A., Brown, D. L., Pang, S. W., Sagulenko, V., Sester, D. P., Cridland, S. O. et al.**, The inflammasome adaptor ASC induces procaspase-8 death effector domain filaments. *J. Biol. Chem.* 2015. 4;**290**: 29217–29230.

2142 **Man, S. M., Tourlomousis, P., Hopkins, L., Monie, T. P., Fitzgerald, K. A. and Bryant, C. E.**, Salmonella infection induces recruitment of Caspase-8 to the inflammasome to modulate IL-1beta production. *J. Immunol.* 2013. **191**: 5239–5246.

2143 **Agostini, L., Martinon, F., Burns, K., McDermott, M. F., Hawkins, P. N. and Tschopp, J.**, NALP3 forms an IL-1beta-processing inflammasome with increased activity in Muckle-Wells autoinflammatory disorder. *Immunity* 2004. **20**: 319–325.

2144 **Martinon, F., Agostini, L., Meylan, E. and Tschopp, J.**, Identification of bacterial muramyl dipeptide as activator of the NALP3/cryopyrin inflammasome. *Curr. Biol.* 2004. **14**: 1929–1934.

2145 **Sagulenko, V., Thygesen, S. J., Sester, D. P., Idris, A., Cridland, J. A., Vajjhala, P. R., Roberts, T. L., Schroder, K., Vince, J. E., Hill, J. M. Silke, J. and Stacey K. J.**, AIM2 and NLRP3 inflammasomes activate both apoptotic and pyroptotic death pathways via ASC. *Cell Death Differ.* 2013. **20**: 1149–1160.

2146 **Masumoto, J., Taniguchi, S., Ayukawa, K., Sarvotham, H., Kishino, T., Niikawa, N., Hidaka, E. et al.**, ASC, a novel 22-kDa protein, aggregates during apoptosis of human promyelocytic leukemia HL-60 cells. *J. Biol. Chem.* 1999. **274**: 33835–33838.

2147 **Franklin, B. S., Bossaller, L., De Nardo, D., Ratter, J. M., Stutz, A., Engels, G., Brenker, C. et al.**, The adaptor ASC has extracellular and 'prionoid' activities that propagate inflammation. *Nat. Immunol.* 2014. **15**: 727–737.

2148 **Baroja-Mazo, A., Martín-Sánchez, F., Gomez, A. I., Martínez, C. M., Amores-Iniesta, J., Compan, V., Barberà-Cremades, M. et al.**, The NLRP3 inflammasome is released as a particulate danger signal that amplifies the inflammatory response. *Nat. Immunol.* 2014. **15**: 738–748.

2149 **Venegas, C., Kumar, S., Franklin, B. S., Dierkes, T., Brinkschulte, R., Tejera, D., Vieira-Saecker, A. et al.**, Microglia-derived ASC specks cross-seed amyloid-β in Alzheimer's disease. *Nature* 2017. **552**: 355–361.

2150 **Pollard, K. M. and Kono, D. H.**, Requirements for innate immune pathways in environmentally induced autoimmunity. *BMC Med.* 2013. **11**: 100.

2151 **Master, S. L.**, Specific inflammasomes in complex diseases. *Clin. Immunol.* 2013. **143**: 223–228.

2152 **Rubartelli, A.**, Redox control of NLRP3 inflammasome activation in health and disease. *J. Leukoc. Biol.* 2012. **92**: 951–958.

2153 **Heneka, M. T., Kummer, M. P., Stutz, A., Delekate, A., Schwartz, S., Vieira-Saecker, A., Griep, A. et al.**, NLRP3 is activated in Alzheimer's disease and contributes to pathology in APP/PS1 mice. *Nature* 2013. **493**: 674–678.

2154 Saresella, M., La Rosa, F., Piancone, F., Zoppis, M., Marventano, I., Calabrese, E., Rainone, V., Nemni, R. et al., The NLRP3 and NLRP1 inflammasomes are activated in Alzheimer's disease. Mol. Neurodegener 2016. 11(1): 23.

2155 Saresella, M., Piancone, F., Marventano, I., Zoppis, M., Hernis, A., Zanette, M., Trabattoni, D. et al., Multiple Inflammasome Complexes are Activated in Autistic Spectrum Disorders. Brain Behav. Immun. 2016. 57: 125–133.

2156 Piancone, F., Saresella, M., Marventano, I., La Rosa, F., Santangelo, M. A., Caputo, D., Mendozzi, L., Rovaris, M. et al., Monosodium urate crystals activate the inflammasome in primary progressive multiple sclerosis. Front. Immunol. 2018. 9: 983.

2157 Bandera, A., Masetti, M., Fabbiani, M., Biasin, M., Muscatello, A., Squillace, N., Clerici, M. et al., The NLRP3 Inflammasome is Upregulated in HIV-Infected ART-treated Individuals with Defective Immune Recovery. Front. Immunol. 2018. 9: 214.

2158 Nagar, A., DeMarco, R. A. and Harton, J. A., Inflammasome and caspase-1 activity characterization and evaluation: An imaging flow cytometer-based detection and assessment of inflammasome specks and caspase-1 activation. J. Immunol. 2019. 202: 1003–1015.

2159 Hooijberg, J. H. Broxterman H. J., Kool M., Assaraf Y. G., Peters G. J., Noordhuis P. and Scheper R. J., Antifolate resistance mediated by the multidrug resistance proteins MRP1 and MRP2. Cancer Res. 1999. 59: 2532–2535.

2160 Zeng, H. et al., Transport of methotrexate (MTX) and folates by multidrug resistance protein (MRP) 3 and MRP1: effect of polyglutamylation on MTX transport. Cancer Res. 2001. 61: 7225–7232.

2161 Volk, E. L., Farley, K. M., Wu, Y., Li, F., Robey, R. W. and Schneider, E., Overexpression of wild-type breast cancer resistance protein mediates methotrexate resistance. Cancer Res. 2002. 62: 5035–5040.

2162 Sarkadi, B. et al., Human multidrug resistance ABCB and ABCG transporters: participation in a chemoimmunity defense system. Physiol Rev. 2006. 86: 1179–1236.

2163 Lee, N. H., Pharmacogenetics of drug metabolizing enzymes and transporters: effects on pharmacokinetics and pharmacodynamics of anticancer agents. Anticancer Agents Med. Chem. 2010. 10: 583–592.

2164 Porcelli, L., Lemos, C., Peters, G. J., Paradiso, A. and Azzariti, A., Intracellular trafficking of MDR transporters and relevance of SNPs. Curr. Top. Med. Chem. 2009. 9: 197–208.

2165 Damiani, D. et al., The prognostic value of P-glycoprotein (ABCB) and breast cancer resistance protein (ABCG2) in adults with de novo acute myeloid leukemia with normal karyotype. Haematologica 2006. 91: 825–828.

2166 Georges, E., Tsuruo, T. and Ling, V., Topology of P-glycoprotein as determined by epitope mapping of MRK-16 monoclonal antibody. J. Biol. Chem. 1993. 268: 1792–1798.

2167 Vasudevan, S., Tsuruo, T. and Rose, D. R., Mode of binding of anti-P-glycoprotein antibody MRK-16 to its antigen. A crystallographic and molecular modeling study. J. Biol. Chem. 1998. 273: 25413–25419.

2168 Telbisz, A., Hegedüs, C., Özvegy-Laczka, C., Goda, K., Várady, G., Takáts, Z., Szabó, E. et al., Antibody binding shift assay for rapid screening of drug interactions with the human ABCG2 multidrug transporter. Eur. J. Pharm. Sci. 2012. 45: 101–109.

2169 Toldi, G. et al., Peripheral lymphocyte multidrug resistance activity as a predictive tool of biological therapeutic response in rheumatoid arthritis. J. Rheumatol. 2019. 46: 572–578.

2170 Micsik, T. et al., MDR-1 and MRP-1 activity in peripheral blood leukocytes of rheumatoid arthritis patients. Diagn. Pathol. 2015. 10: 216.

2171 Homolya, L., Holló, Z., Germann, U. A., Pastan, I., Gottesman, M. M., Sarkadi, B. Fluorescent cellular indicators are extruded by the multidrug resistance protein. J. Biol. Chem. 1993. 268: 21493–21496.

2172 Cortada, C. M. et al., Lymphocyte P-glycoprotein variability in healthy individuals. Medicina 2009. 69: 619–624.

2173 Szerémy, P., Tauberné Jakab, K., Baráth, S., Apjok, A., Filkor, K., Holló, Z., Márki-Zay, J., Kappelmayer, J., Sipka, S., Krajcsi, P., Toldi, G. Determination of reference values of MDR-ABC transporter activities in CD3+ lymphocytes of healthy volunteers using a flow cytometry based method. Cytometry B Clin. Cytom. 2018 https://doi.org/10.1002/cyto.b.21729. [Epub ahead of print].

2174 Yu, L., Sa, S., Wang, L., Dulmage, K., Bhagwat, N., Yee, S. S., Sen, M. et al., An integrated enrichment system to facilitate isolation and molecular characterization of single cancer cells from whole blood. Cytometry A 2018. 93: 1226–1233.

2175 Hayashi, T., Shibata, N., Okumura, R., Kudome, T., Nishimura, O., Tarui, H. and Agata, K., Single-cell gene profiling of planarian stem cells using fluorescent activated cell sorting and its "index sorting" function for stem cell research. Dev. Growth Differ. 2010. 52: 131–144.

2176 Schulte, R., Wilson, N. K., Prick, J. C., Cossetti, C., Maj, M. K., Gottgens, B. and Kent, D. G., Index sorting resolves heterogeneous murine hematopoietic stem cell populations. Exp. Hematol. 2015. 43: 803–811.

2177 Wilson, N. K., Kent, D. G., Buettner, F., Shehata, M., Macaulay, I. C., Calero-Nieto, F. J., Sanchez Castillo, M. et al., Combined single-cell functional and gene expression analysis resolves heterogeneity within stem cell populations. Cell Stem Cell 2015. 16: 712–724.

2178 Busse, C. E., Czogiel, I., Braun, P., Arndt, P. F. and Wardemann, H., Single-cell based high-throughput sequencing of full-length immunoglobulin heavy and light chain genes. Eur. J. Immunol. 2014. 44: 597–603.

2179 Gee, M. H., Han, A., Lofgren, S. M., Beausang, J. F., Mendoza, J. L., Birnbaum, M. E., Bethune, M. T. et al., Antigen identification for orphan T cell receptors expressed on tumor-infiltrating lymphocytes. Cell 2018. 172: 549–563.

2180 Penter, L., Dietze, K., Bullinger, L., Westermann, J., Rahn, H. P. and Hansmann, L., FACS single cell index sorting is highly reliable and determines immune phenotypes of clonally expanded T cells. Eur. J. Immunol. 2018. 48: 1248–1250.

2181 Penter, L., Dietze, K., Ritter, J., Lammoglia-Cobo, M. F., Garmshausen, J., Aigner, F., Bullinger, L. et al., Localization-associated immune phenotypes of clonally expanded tumor-infiltrating T cells and distribution of their target antigens in rectal cancer. Oncoimmunology 2019. 8: e1586409.

2182 Higdon, L. E., Cain, C. J., Colden, M. A. and Maltzman, J. S. Optimization of single-cell plate sorting for high throughput sequencing applications. J. Immunol. Methods 2019. 466: 17–23.

2183 Kleeberger, C. A., Lyles, R. H., Margolick, J. B., Rinaldo, C. R., Phair, J. P. and Giorgi, J. V., Viability and recovery of peripheral blood mononuclear cells cryopreserved for up to 12 years in a multicenter study. Clin. Diagn. Lab. Immunol. 1999. 6: 14–19.

2184 Ruitenberg, J. J., Mulder, C. B., Maino, V. C., Landay, A. L. and Ghanekar, S. A., VACUTAINER CPT and Ficoll density gradient separation perform equivalently in maintaining the quality and function of PBMC from HIV seropositive blood samples. BMC Immunol. 2006. 7: 11.

2185 Grievink, H. W., Luisman, T., Kluft, C., Moerland, M. and Malone, K. E., Comparison of three isolation techniques for human peripheral blood mononuclear cells: cell recovery and viability, population composition, and cell functionality. Biopreserv. Biobank. 2016. 14: 410–415.

2186 **Disis, M. L.**, **dela Rosa, C.**, **Goodell, V.**, **Kuan, L-Y**, **Chang, JCC**, **Kuus-Reichel, K.**, **Clay, T. M. et al.**, Maximizing the retention of antigen specific lymphocyte function after cryopreservation. *J. Immunol. Methods* 2006. **308**: 13–18.

2187 **Weinberg, A.**, **Song, L-Y**, **Wilkening, C.**, **Sevin, A.**, **Blais, B.**, **Louzao, R.**, **Stein, D. et al.**, Optimization and limitations of use of cryopreserved peripheral blood mononuclear cells for functional and phenotypic T-cell characterization. *Clin. Vaccine Immunol.* 2009. **16**: 1176–1186.

2188 **Bull, M.**, **Lee, D.**, **Stucky, J.**, **Chiu, Y-L**, **Rubin, A.**, **Horton, H. and McElrath, M. J.**, Defining blood processing parameters for optimal detection of cryopreserved antigen-specific responses for HIV vaccine trials. *J. Immunol. Methods.* 2007. **322**: 57–69.

2189 **Scheiermann, C.**, **Kunisaki, Y. and Frenette, P. S.**, Circadian control of the immune system. *Nat. Rev. Immunol.* 2013. **13**: 190–198.

2190 **Tompa, A.**, **Nilsson-Bowers, A. and Faresjö, M.**, Subsets of CD4+, CD8+, and CD25hi lymphocytes are in general not influenced by isolation and long-term cryopreservation. *J. Immunol.* 2018. **201**: 1799–1809.

2191 **Seale, A. C.**, **de Jong, B. C.**, **Zaidi, I.**, **Duvall, M.**, **Whittle, H.**, **Rowland-Jones, S. and Jaye, A.**, Effects of cryopreservation on CD4+ CD25+ T cells of HIV-1 infected individuals. *J. Clin. Lab. Anal.* 2008. **22**: 153–158.

2192 **AssumpcióRomeu, M.**, **Mestre, M.**, **González, L.**, **Valls, A.**, **Verdaguer, J.**, **Corominas, M.**, **Bas, J. et al.**, Lymphocyte immunophenotyping by flow cytometry in normal adults. *J. Immunol. Methods* 1992. **154**: 7–10.

2193 **Lemieux, J.**, **Jobin, C.**, **Simard, C. and Néron, S.**, A global look into human T cell subsets before and after cryopreservation using multiparametric flow cytometry and two-dimensional visualization analysis. *J. Immunol. Methods* 2016. **434**: 73–82.

2194 **Wang, L.**, **Hückelhoven, A.**, **Hong, J.**, **Jin, N.**, **Mani, J.**, **Chen, B.**, **Schmitt, M. et al.**, Standardization of cryopreserved peripheral blood mononuclear cells through a resting process for clinical immunomonitoring—development of an algorithm. *Cytometry A.* 2016. **89**: 246–258.

2195 **Holland, M.**, **Cunningham, R.**, **Seymour, L.**, **Kleinsteuber, K.**, **Cunningham, A.**, **Patel, T.**, **Manos, M. et al.**, Separation, banking, and quality control of peripheral blood mononuclear cells from whole blood of melanoma patients. *Cell Tissue Bank.* 2018. **19**: 783–790.

2196 **De Boer, F.**, **Dräger, A. M.**, **Van der Wall, E.**, **Pinedo, H. M. and Schuurhuis, G. J.**, Changes in L-selectin expression on CD34-positive cells upon cryopreservation of peripheral blood stem cell transplants. *Bone Marrow Transplant.* 1998. **22**: 1103–1110.

2197 **Campbell, D. E.**, **Tustin, N. B.**, **Riedel, E.**, **Tustin, R.**, **Taylor, J.**, **Murray, J. and Douglas, S. D.**, Cryopreservation decreases receptor PD-1 and ligand PD-L1 coinhibitory expression on peripheral blood mononuclear cell-derived T cells and monocytes. *Clin. Vaccine Immunol.* 2009. **16**: 1648–1653.

2198 **Zhang, W.**, **Nilles, T. L.**, **Johnson, J. R. and Margolick, J. B.**, The effect of cellular isolation and cryopreservation on the expression of markers identifying subsets of regulatory T cells. *J. Immunol. Methods.* 2016. **431**: 31–37.

2199 **Posevitz-Fejfár, A.**, **Posevitz, V.**, **Gross, C. C.**, **Bhatia, U.**, **Kurth, F.**, **Schütte, V.**, **Bar-Or, A. et al.**, Effects of blood transportation on human peripheral mononuclear cell yield, phenotype and function: implications for immune cell biobanking. *PLoS One.* 2014. **9**: e115920.

2200 **Nemes, E.**, **Kagina, B. M. N.**, **Smit, E.**, **Africa, H.**, **Steyn, M.**, **Hanekom, W. A. and Scriba, T. J.**, Differential leukocyte counting and immunophenotyping in cryopreserved ex vivo whole blood. *Cytometry A.* 2015. **87**: 157–165.

2201 **Maecker, H. T.**, **McCoy, J. P.**, **FOCIS Human Immunophenotyping Consortium**, **Amos, M.**, **Elliott, J.**, **Gaigalas, A.**, **Wang, L. et al.**, A model for harmonizing flow cytometry in clinical trials. *Nat. Immunol.* 2010. **11**: 975–978.

2202 **Burel, J. G.**, **Qian, Y.**, **Lindestam Arlehamn, C.**, **Weiskopf, D.**, **Zapardiel-Gonzalo, J.**, **Taplitz, R.**, **Gilman, R. H. et al.**, An integrated workflow to assess technical and biological variability of cell population frequencies in human peripheral blood by flow cytometry. *J. Immunol.* 2017. **198**: 1748–1758.

2203 **Bernemann, I.**, **Kersting, M.**, **Prokein, J.**, **Hummel, M.**, **Klopp, N. and Illig, T.**, [Centralized biobanks: a basis for medical research]. *Bundesgesundheitsblatt. Gesundheitsforschung. Gesundheitsschutz.* 2016. **59**: 336–343.

2204 **Labarga, A.**, **Beloqui, I. and Martin, A. G.**, Information Management. *Methods Mol. Biol.* 2017. **1590**: 29–39.

2205 **Bendou, H.**, **Sizani, L.**, **Reid, T.**, **Swanepoel, C.**, **Ademuyiwa, T.**, **Merino-Martinez, R.**, **Meuller, H. et al.**, Baobab laboratory information management system: development of an open-source laboratory information management system for biobanking. *Biopreserv. Biobank.* 2017. **15**: 116–120.

2206 **Mate, S.**, **Kadioglu, D.**, **Majeed, R. W.**, **Stöhr, M. R.**, **Folz, M.**, **Vormstein, P.**, **Storf, H. et al.**, Proof-of-concept integration of heterogeneous biobank IT infrastructures into a hybrid biobanking network. *Stud. Health Technol. Inform.* 2017. **243**: 100–104.

2207 **Consuegra, I.**, **Rodríguez-Aierbe, C.**, **Santiuste, I.**, **Bosch, A.**, **Martínez-Marín, R.**, **Fortuto, M. A.**, **Díaz, T. et al.**, Isolation methods of peripheral blood mononuclear cells in spanish biobanks: an overview. *Biopreserv. Biobank.* 2017. **15**: 305–309.

2208 **Aziz, N.**, **Margolick, J. B.**, **Detels, R.**, **Rinaldo, C. R.**, **Phair, J.**, **Jamieson, B. D. and Butch, A. W.**, Value of a quality assessment program in optimizing cryopreservation of peripheral blood mononuclear cells in a multicenter study. *Clin. Vaccine Immunol.* 2013. **20**: 590–595.

2209 **Ramos, T. V.**, **Mathew, A. J.**, **Thompson, M. L. and Ehrhardt, R. O.**, Standardized cryopreservation of human primary cells. *Curr. Protoc. Cell Biol.* 2014. **64**: A.3I.1-8.

2210 **Xiao, D.**, **Ling, K. H. J.**, **Custodio, J.**, **Majeed, S. R. and Tarnowski, T.**, Quantitation of intracellular triphosphate metabolites of antiretroviral agents in peripheral blood mononuclear cells (PBMCs) and corresponding cell count determinations: review of current methods and challenges. *Expert Opin. Drug Metab. Toxicol.* 2018. **14**: 781–802.

2211 **Becher, F.**, **Pruvost, A. G.**, **Schlemmer, D. D.**, **Créminon, C. A.**, **Goujard, C. M.**, **Delfraissy, J. F.**, **Benech, H. C. et al.**, Significant levels of intracellular stavudine triphosphate are found in HIV-infected zidovudine-treated patients. *AIDS.* 2003. **17**: 555–561.

2212 **Corkum, C. P.**, **Ings, D. P.**, **Burgess, C.**, **Karwowska, S.**, **Kroll, W. and Michalak, T. I.**, Immune cell subsets and their gene expression profiles from human PBMC isolated by Vacutainer Cell Preparation Tube (CPT™) and standard density gradient. *BMC Immunol.* 2015. **16**: 48.

2213 **Angel, S.**, **von Briesen, H.**, **Oh, Y.-J.**, **Baller, M. K.**, **Zimmermann, H. and Germann, A.**, Toward optimal cryopreservation and storage for achievement of high cell recovery and maintenance of cell viability and T cell functionality. *Biopreserv. Biobank.* 2016. **14**: 539–547.

2214 **Angelo, M.**, **Bendall, S. C.**, **Finck, R.**, **Hale, M. B.**, **Hitzman, C.**, **Borowsky, A. D.**, **Levenson, R. M. et al.**, Multiplexed ion beam imaging of human breast tumors. *Nat. Med.* 2014. **20**: 436–442.

2215 **Smets, T.**, **Stevenaert, F.**, **Adams, H. and Vanhoof, G.**, Deep profiling of the immune system of multiple myeloma patients using cytometry by time-of-flight (CyTOF). *Methods Mol. Biol.* 2018. **1792**: 47–54.

2216 **Edwards, B. S. and Sklar, L. A.**, Flow cytometry: impact on early drug discovery. *J. Biomol. Screen* 2015. **20**: 689–707.

2217 **Moffat, J. G.**, **Vincent, F.**, **Lee, J. A.**, **Eder, J.** and **Prunotto, M.**, Opportunities and challenges in phenotypic drug discovery: an industry perspective. *Nat. Rev. Drug Discov.* 2017. **16**: 531–543.

2218 **Vignali, D. A.**, Multiplexed particle-based flow cytometric assays. *J. Immunol. Methods* 2000. **243**: 243–255.

2219 **Joslin, J.**, **Gilligan, J.**, **Anderson, P.**, **Garcia, C.**, **Sharif, O.**, **Hampton, J.**, **Cohen, S. et al.**, A Fully automated high-throughput flow cytometry screening system enabling phenotypic drug discovery. *SLAS Discov.* 2018. **23**: 697–707.

2220 **Bredemeyer, A. L.**, **Edwards, B. S.**, **Haynes, M. K.**, **Morales, A. J.**, **Wang, Y.**, **Ursu, O.**, **Waller, A. et al.**, High-throughput screening approach for identifying compounds that inhibit nonhomologous end joining. *SLAS Discov.* 2018. **23**: 624–633.

2221 **Buranda, T.**, **Gineste, C.**, **Wu, Y.**, **Bondu, V.**, **Perez, D.**, **Lake, K. R.**, **Edwards, B. S. et al.**, A high-throughput flow cytometry screen identifies molecules that inhibit hantavirus cell entry. *SLAS Discov.* 2018. **23**: 634–645.

2222 **Wang, Y.**, **Yoshihara, T.**, **King, S.**, **Le, T.**, **Leroy, P.**, **Zhao, X.**, **Chan, C. K. et al.**, Automated high-throughput flow cytometry for high-content screening in antibody development. *SLAS Discov.* 2018. **23**: 656–666.

2223 **Martinez, E. M.**, **Klebanoff, S. D.**, **Secrest, S.**, **Romain, G.**, **Haile, S. T.**, **Emtage, P. C. R.** and **Gilbert, A. E.**, High-throughput flow cytometric method for the simultaneous measurement of CAR-T cell characterization and cytotoxicity against solid tumor cell lines. *SLAS Discov.* 2018. **23**: 603–612.

2224 **Kaur, M.** and **Esau, L.**, Two-step protocol for preparing adherent cells for high-throughput flow cytometry. *Biotechniques* 2015. **59**: 119–126.

2225 **Chan, B. M.**, **Badh, A.**, **Berry, K. A.**, **Grauer, S. A.** and **King, C. T.**, Flow cytometry-based epitope binning using competitive binding profiles for the characterization of monoclonal antibodies against cellular and soluble protein targets. *SLAS Discov.* 2018. **23**: 613–623.

2226 **Virginia Litwin, P. M.**, *Flow cytometry in drug discovery and development.* Wiley, Hoboken, NJ 2011.

2227 **Goni-de-Cerio, F.**, **Mariani, V.**, **Cohen, D.**, **Madi, L.**, **Thevenot, J.**, **Oliveira, H.**, **Uboldi, C. et al.**, Biocompatibility study of two diblock copolymeric nanoparticles for biomedical applications by in vitro toxicity testing. *J. Nanopart. Res.* 2013. **15**: 1–17.

2228 **Buenz, E. J.**, **Limburg, P. J.** and **Howe, C. L.**, A high-throughput 3-parameter flow cytometry-based cell death assay. *Cytometry A* 2007. **71**: 170–173.

2229 **Boitano, A. E.**, **Wang, J.**, **Romeo, R.**, **Bouchez, L. C.**, **Parker, A. E.**, **Sutton, S. E.**, **Walker, J. R. et al.**, Aryl hydrocarbon receptor antagonists promote the expansion of human hematopoietic stem cells. *Science* 2010. **329**: 1345–1348.

2230 **Zhao, Z.**, **Henowitz, L.** and **Zweifach, A.**, A multiplexed assay that monitors effects of multiple compound treatment times reveals candidate immune-enhancing compounds. *SLAS Discov.* 2018. **23**: 646–655.

2231 **Ding, M.**, **Kaspersson, K.**, **Murray, D.** and **Bardelle, C.**, High-throughput flow cytometry for drug discovery: principles, applications, and case studies. *Drug Discov. Today* 2017. **22**: 1844–1850.

2232 **Javarappa, K. K.**, **Tsallos, D.** and **Heckman, C. A.**, A multiplexed screening assay to evaluate chemotherapy-induced myelosuppression using healthy peripheral blood and bone marrow. *SLAS Discov.* 2018. **23**: 687–696.

2233 **Nolan, J. P.** and **Mandy, F.**, Multiplexed and microparticle-based analyses: quantitative tools for the large-scale analysis of biological systems. *Cytometry A* 2006. **69**: 318–325.

2234 **Moeller, T.**, **Brown, C.**, **Muchow, M.** and **Yee, B.**, Transcript regulation of 18 ADME genes by prototypical inducers in human hepatocytes. *Drug Metab. Rev.* 2012. **44**: 79–80.

2235 **Liu, Z.** and **O'Rourke, J.**, Expediting antibody discovery with a cell and bead multiplexed competition assay. *SLAS Discov.* 2018. **23**: 667–675.

2236 **Young, S. M.**, **Bologa, C.**, **Prossnitz, E. R.**, **Oprea, T. I.**, **Sklar, L. A.** and **Edwards, B. S.**, High-throughput screening with HyperCyt flow cytometry to detect small molecule formylpeptide receptor ligands. *J. Biomol. Screen* 2005. **10**: 374–382.

2237 **Lahl, K.**, **Loddenkemper, C.**, **Drouin, C.**, **Freyer, J.**, **Arnason, J.**, **Eberl, G.**, **Hamann, A. et al.**, Selective depletion of Foxp3+ regulatory T cells induces a scurfy-like disease. *J. Exp. Med.* 2007. **204**: 57–63.

2238 **Zhang, J. H.**, **Chung, T. D.** and **Oldenburg, K. R.**, A simple statistical parameter for use in evaluation and validation of high throughput screening assays. *J. Biomol. Screen* 1999. **4**: 67–73.

2239 **Moore, J.** and **Roederer, M.**, The flow cytometry shared resource laboratory: best practices to assure a high-quality, cost-effective partnership with biomedical research laboratories. *Cytometry A* 2009. **75**: 643–649.

2240 **Meder, D. et al.**, Institutional core facilities: prerequisite for breakthroughs in the life sciences: core facilities play an increasingly important role in biomedical research by providing scientists access to sophisticated technology and expertise. *EMBO Rep.* 2016. **17**: 1088–1093.

2241 **Barsky, L. W. et al.**, International Society for Advancement of Cytometry (ISAC) flow cytometry shared resource laboratory (SRL) best practices. *Cytometry A* 2016. **89**: 1017–1030.

2242 **Ferrando-May, E. et al.**, Advanced light microscopy core facilities: Balancing service, science and career. *Microsc. Res. Tech.* 2016. **79**: 463–479.

2243 **Brown, C. M.**, Careers in core facility management. *Cold Spring Harb. Perspect. Biol.* 2018. **10**(8).

2244 **Davies, D.**, **Filby, A.** and **Lannigan, J.**, Shared Resource Laboratory (SRL) Communications—a new journal type. *Cytometry A* 2018.

2245 **Box, A. C.**, **Park, J.**, **Semerad, C. L.**, **Konnesky, J.** and **Haug, J. S.**, Cost accounting method for cytometry facilities. *Cytometry A* 2012. **81**: 439–444.

2246 **Petrunkina, A. M.**, Algorithm and metrics for a standardized evaluation of cell sorting service delivery. *Cytometry A* 2013. **83**: 602–607.

2247 **Lennartz, K.**, **Lu, M.**, **Flasshove, M.**, **Moritz, T.** and **Kirstein, U.**, Improving the biosafety of cell sorting by adaptation of a cell sorting system to a biosafety cabinet. *Cytometry A* 2005. **66**: 119–127.

2248 **Mische, S.** and **Wilkerson, A.**, Disaster and Contingency Planning for Scientific Shared Resource Cores. *J. Biomol. Tech.* 2016. **27**: 4–17.

2249 **Antal-Szalmás, P.**, **Nagy, B. Jr**, **Debreceni, I. B.** and **Kappelmayer, J.**, Measurement of soluble biomarkers by flow cytometry. *EJIFCC* 2013. **23**: 135–142.

2250 **Commenges, D.**, **Alkhassim, C.**, **Gottardo, R.**, **Hejblum, B.** and **Thiebaut, R.**, cytometree: a binary tree algorithm for automatic gating in cytometry analysis. *bioRxiv.* 2018 1:335554.

2251 **de Jager, W.**, **te Velthuis, H.**, **Prakken, B. J.**, **Kuis, W.** and **Rijkers, G. T.**, Simultaneous detection of 15 human cytokines in a single sample of stimulated peripheral blood mononuclear cells. *Clin. Diagn. Lab. Immunol.* 2003. **10**: 133–139.

2252 **DiGiuseppe, J. A.**, **Cardinali, J. L.**, **Rezuke, W. N.** and **Pe'er, D.**, PhenoGraph and viSNE facilitate the identification of abnormal T-cell populations in routine clinical flow cytometric data. *Cytometry B Clin. Cytom.* 2018. **94**: 744–757.

2253 **Gomaa, A.** and **Boye, J.**, Simultaneous detection of multi-allergens in an incurred food matrix using ELISA, multiplex flow cytometry and liquid chromatography mass spectrometry (LC–MS). *Food Chem.* 2015. **175**: 585–592.

2254   http://www.cancer.net/cancer-types/sarcoma-soft-tissue/overview

2255   **Maggi, L., Cimaz, R., Capone, M., Santarlasci, V., Rossi, M. C., Mazzoni, A., Montaini, G. et al.**, Immunosuppressive activity of abatacept on circulating T helper lymphocytes from juvenile idiopathic arthritis patients. *Int. Arch. Allergy Immunol.* 2016. **171**: 45–53.

2256   **Maueröder, C., Chaurio, R. A., Dumych, T., Podolska, M., Lootsik, M. D., Culemann, S., Friedrich, R. P. et al.**, A blast without power—cell death induced by the tuberculosis-necrotizing toxin fails to elicit adequate immune responses. *Cell Death Differ.* 2016. **23**: 1016–1025.

2257   **Munoz, L. E., Maueroder, C., Chaurio, R., Berens, C., Herrmann, M. and Janko, C.**, Colourful death: six-parameter classification of cell death by flow cytometry–dead cells tell tales. *Autoimmunity* 2013. **46**: 336–341.

2258   **Salvioli, S., Ardizzoni, A., Franceschi, C. and Cossarizza, A.**, JC-1, but not DiOC6(3) or rhodamine 123, is a reliable fluorescent probe to assess AW changes in intact cells: implications for studies on mitochondrial functionality during apoptosis. *FEBS Lett.* 1997. **411**: 77–82.

Abbreviations: **7AAD**: 7-aminoactinomycin D · **ab**: antibody · **ADC**: analog-to-digital conversion · **ADCC**: antibody dependent cellular cytotoxicity · **AHR**: aryl hydrocarbon receptor · **AM**: acetoxymethyl · **AMPK**: 5AMP-activated protein kinase · **ANX-V**: annexin-V · **AO**: acridine orange · **APC**: allophycocyanin · **APD**: avalanche photodiodes · **APS**: ammonium peroxodisulfate · **ASCs**: antibody-secreting cells · **ATCC**: American type tissue collection · **ATGs**: autophagy related genes · **AxA5**: fluorophore-conjugated annexin A5 · **BafA**: bafilomycin A1 · **BAFF**: Bcell activating factor · **BCL6**: B-cell lymphoma 6 · **BD**: Becton Dickinson · **bDNA**: branched DNA technology · **BDS**: bright detail similarity · **BF**: brightfield · **BFA**: brefeldin A · **BISC**: Bioinformatics Integration Support Contract · **BM**: bone marrow · **BP**: band pass · **BrdU**: 5-bromo-2-deoxyuridine · **BSA**: bovine serum albumin · **BV**: brilliant violet · **CCCP**: carbonyl cyanide 3-chloro phenyl hydrazine · **CCDs**: charge-coupled devices · **CLL**: chronic lymphocytic leukemia · **cDCs**: classical DCs · **CDR**: complementarity determining regions · **CEA**: carcinoembryonal · **CECs**: circulating endothelial cells · **CFSE**: carboxyfluorescein succinimidyl ester · **CFU-F**: colony-forming units-fibroblasts · **CIMT**: cancer immunotherapy consortium · **CIP**: CIMT immunoguiding program · **CK**: cytokeratin 18 · **CM**: central memory · **cMOP**: common monocyte precursors · **CMV**: cytomegalovirus · **CS&T**: cytometer setup and tracking · **CSF**: cerebrospinal fluid · **CT**: cancer-testis · **CTCs**: circulating tumor cells · **CTL**: cytolytic cells · **CV**: coefficient of variation · **CW**: continuous wave · **Cy**: cyanine · **CyTOF**: Cytometry by Time-Of-Flight · **DAIT**: Division of Allergy, Immunology, and Transplantation · **DAMP**: danger-associated molecular patterns · **DAPI**: 4,6-diamidine-2-phenylindole · **DCF**: 2,7-dichlorofluorescein · **DCFDA**: 2-7-dichlorodihydrofluorescein diacetate · **DCs**: dendritic cells · **DCV**: dyecycle violet · **DHR**: dihydrorhodamine · **DIOC6**: 3,3-dihexyloxacarbocyanine iodide · **DLD**: deterministic lateral displacement · **DLP**: dichroic longpass · **DMSO**: dimethyl sulfoxide · **DNase**: deoxyribonuclease · **DNR**: dynamic detection range · **DPBS**: Dulbecco's phosphate buffered saline · **DPEC**: double positive effector cells · **E:T**: effector-to-target cell · **ECI 2015**: European Congress of Immunology ECI 2015 · **EdU**: 5-ethynyl-2-deoxyuridine · **EGFR**: epidermal growth factor receptor · **EM**: effector memory cells · **ENOBs**: effective number of bits · **ERK pathway**: extracellular-signal regulated kinase pathway · **ESCCA**: European Society for Clinical Cell Analysis · **FACS**: fluorescence activated cell sorting · **FBS**: fetal bovine serum · **Fc**: fragment of immunoglobulins · **FCCP**: carbonyl cyanide-4- (trifluoromethoxy)phenylhydrazone · **FCM**: flow cytometry · **FCS**: fetal calf serum · **FCS**: flow cytometry standard · **FDA**: fluorescein-diacetate · **FGFR**: fibroblast growth factor receptor · **FISH**: fluorescent in situ hybridization · **FITC**: fluorescein isothiocyanate · **FL1-10**: fluorescence channels · **FLIMs**: fluorescent life time measurements · **FMK**: fluoromethyl ketone · **FMO**: fluorescence minus one · **FOCIS**: Federation of Clinical Immunology Societies · **FOXP3**: forkhead box P3 · **FSC**: forward scatter · **GATA3**: GATA binding protein-3 · **GFP**: green fluorescent protein · **GUIs**: graphical user interfaces · **GZMB**: granzyme B · **HBSS**: Hank's balanced saline solution · **HCC**: hepatocellular carcinoma · **HCS**: hematopoietic progenitor cells · **HHV8**: human herpesvirus 8 · **HIPAA**: Health Insurance Portability and Accountability Act · **HIPC**: Human Immunology Project Consortium · **HIV**: Human immunodeficiency virus · **HLA**: human leukocyte antigen · **HSC**: hematopoietic stem cell · **HTS**: high throughput system · **IBD**: inflammatory bowel disease · **ICCS**: International Clinical Cytometry Society · **ICPC TOF-MS**: inductively-coupled plasma time of flight mass spectrometry · **IdU**: Iodo-2-deoxyuridine · **IFN**: interferon · **Ig**: immunoglobulin · **IL**: interleukin · **ILCs**: innate lymphoid cells · **ImmPort**: immunology database and analysis portal · **iono**: ionomycin · **IRF4**: interferon regulatory factor 4 · **ISAC**: International Society for Analytical Cytology · **ISR**: internal store release · **ITAM**: immune-receptor tyrosinebased activating motifs · **ITIM**: immune-receptor tyrosine-based inhibition motif · **KIRs**: killer Ig-like receptors · **KLH**: keyhole limpet hemocyanin · **KLRG1**: killer cell lectin-like receptor G1 · **K-S**: Kolmogorov-Smirnov statistic · **L/D**: live dead · **LCA**: leukocyte common antigen · **Lin**: lineage markers · **Lin−**: lineage-negative · **lncRNA**: long non-coding RNA · **LmP**: lamina propria · **LP**: long pass · **LPS**: lipopolysaccharide · **LRR**: leucine-rich repeat · **LRR-CT**: LRR C-terminal capping · **LRR-NT**: LRR N-terminal · **LTi**: lymphoid tissue-inducer cells · **mAb**: monoclonal antibody · **MAP kinase**: membrane activated protein kinase · **MARS-seq**: massive parallel single-cell RNA-seq · **mBCs**: memory B cells · **MCs**: mononuclear cells · **MdFI**: median fluorescence intensity · **MDP**: monocyte/macrophage-DC precursors · **MFI**: mean fluorescence intensity · **MHC**: major histocompatibility complex · **MIBBI**: minimum information for biological and biomedical investigations · **MIBI**: multiplexed ion beam imaging · **MIFloCyt**: minimum information about a flow cytometry experiment · **mitoPY**: mitochondria peroxy yellow-1 · **MitoSOX**: mitochondrial superoxide indicator · **MMM**: metal-minusmany · **MN**: monensin · **MoDC**: monocyte-derived DC · **MPEC**: memoryprecursor effector cells · **mRNA**: messenger RNA · **MSPCs**: mesenchymal stem and progenitor cells · **mt**: mitochondrial · **mtmP**: mitochondrial membrane potential · **mTOR**: mammalian target of rapamycin complex 1 · **NAO**: nonyl acridine orange · **NIAID**: National Institute of Allergy and Infectious Diseases · **NIH**: National Institutes of Health · **NIR**: near infrared · **NK**: natural killer · **NLOs**: non-lymphoid organs · **NSCLC**: non-small cell lung cancer · **NYSTEM Program**: New York State Department of Health Program · **OH**: hydroxyl radicals · **OMIP**: optimized multicolor immunofluorescence panels · **OVA**: ovalbumin · **OxPhos**: oxidative phosphorylation · **PI3K**: Phosphatidylinositol-4,5- bisphosphate 3-kinase · **PAMPs**: pathogen-associated molecular patterns · **PB**: peripheral blood · **PBMC**: peripheral blood mononuclear cells · **PBPC**: peripheral blood progenitor cell · **PBS**: phosphate buffered saline · **PD-1**: programmed cell death protein 1 · **PDGFR**: platelet-derived growth factor receptor · **PEA**: phosphatidylethanolamine · **PE**: phycoerythrin · **PerCP**: peridinin-chlorophyll · **PI**: propidium iodide · **PMA**: phorbol 12-myristate 13-acetate · **PMT**: photomultiplier tube · **PP**: phagocytosis product · **PS**: phosphatidylserine · **PVP**: polyvinylpyrrolidone · **PY(G)**: pyronin Y(G) · **RAR**: retinoic acid receptor · **RCC**: renal cell carcinoma · **Rho123**: rhodamine-123 · **RNase**: ribonuclease · **ROR-γt**: retinoic acid receptor-related orphan receptor gamma t · **RORγtfm**: RORγt fate mapping · **ROS**: reactive oxygen species · **RPMI 1640**: Roswell Park Memorial Institute 1640 · **RT**: room temperature · **SAPK/JNK pathway**: stress-activated protein kinase/c-jun n-terminal kinase · **SAW**: surface acoustic waves · **SB**: staining buffer · **SD**: standard deviation · **SE**: standard error · **SEB**: Staphylococcus enterotoxin B · **SERS**: surface enhanced Raman scattering · **SI**: small intestinal · **SIP**: sample injection port · **SLE**: systemic lupus erythematosus · **SLEC**: short-lived effector cells · **SLOs**: secondary lymphoid organs · **SMO**: signal-minus-one · **SNRs**: signal-tonoise ratios · **SOCE**: store-operated Ca2+ entry · **SOV**: spillover

value · **SP**: short pass · **SPADE**: Spanning-tree progression analysis of densitynormalized data · **β2m**: beta-2-microglobulin · **SSC**: side scatter · **SSM**: spillover-spreading matrix · **TAA**: tumor-associates antigens · **Tcon**: conventional T cells · **TCR**: T cell receptor · **TCRtg**: TCR-transgenic · **TdT**: terminal deoxynucleotidyltransferase · **Th cells**: T helper cells · **TIA**: transimpedance · **TM**: memory T lymphocytes · **TMRE**: tetramethylrhodamine · **TNF**: tumor necrosis factor · **TOF**: time-of-flight · **Treg**: regulatory T cells · **TRAIL**: TNF-related apoptosis-inducing ligand · **TSLP**: thymic stromal lymphopoietin · **t-SNE**: t-distributed stochastic neighbor embedding · **TUNEL**: TdT-mediated dUTP nick end labelling · **VA**: voltage · **ULK1**: Serine/threonine-protein kinase ULK1 · **UV**: ultraviolet · **Var**: variance · **VLR**: variable lymphocyte receptor · **Vps34**: vacuolar protein sorting34 · **WDM**: wavelength division multiplexer

Full correspondence: Prof. Andrea Cossarizza and Dr. Hyun-Dong Chang
e-mail: andrea.cossarizza@unimore.it; chang@drfz.de